



Dipl.-Ing. Andreas Ringhofer, BSc.

Axially Loaded Self-Tapping Screws in Solid Timber and Laminated Timber Products

DOCTORAL THESIS

To achieve the university degree of
Doktor der technischen Wissenschaften

Submitted to
Graz University of Technology

Supervisors

Univ.-Prof. Dipl.-Ing. Dr.techn. Gerhard Schickhofer
Institute of Timber Engineering and Wood Technology,
Graz University of Technology

Univ.-Prof. Dr.-Ing. Hans Joachim Blaß
Research Center for Steel, Timber and Masonry
Karlsruhe Institute of Technology (KIT)

Graz, June 2017

EIDESSTATTLICHE ERKLÄRUNG

AFFIDAVIT

Ich erkläre an Eides statt, dass ich die vorliegende Arbeit selbstständig verfasst, andere als die angegebenen Quellen/Hilfsmittel nicht benutzt, und die den benutzten Quellen wörtlich und inhaltlich entnommenen Stellen als solche kenntlich gemacht habe. Das in TUGRAZonline hochgeladene Textdokument ist mit der vorliegenden Doktorarbeit identisch.

I declare that I have authored this thesis independently, that I have not used other than the declared sources/resources, and that I have explicitly indicated all material which has been quoted either literally or by content from the sources used. The text document uploaded to TUGRAZonline is identical to the present doctoral thesis.

Datum / Date

Unterschrift / Signature

Danksagung

Die vorliegende Arbeit entstand in den Jahren 2012 bis 2017 während meiner Tätigkeit als Universitätsassistent am Institut für Holzbau und Holztechnologie der Technischen Universität Graz.

Zu Beginn möchte ich mich herzlich bei Univ.-Prof. Dr.-Ing. Hans Joachim Blaß, Leiter der Abteilung / des Lehrstuhls für Holzbau und Baukonstruktion der Versuchsanstalt für Stahl, Holz und Steine am Karlsruher Institut für Technologie (KIT), bedanken, welcher nicht nur so freundlich war, meine Arbeit zu begutachten sondern mich auch im Rahmen einer Short Term Scientific Mission (STSM) als Teil der COST Action FP1402 zu sich an das KIT einzuladen, um gemeinsam mit ihm und seinem Team an den selbstbohrenden Holzbauschrauben zu arbeiten.

Besonderer Dank gebührt Univ.-Prof. Dipl.-Ing. Dr.techn. Gerhard Schickhofer, Leiter des Instituts für Holzbau und Holztechnologie der Technischen Universität Graz, für das Wecken meines Interesses am wissenschaftlichen Arbeiten (insbesondere an der Thematik der selbstbohrenden Holzbauschrauben), für die freundliche Aufnahme in sein Team am Institut, für die langjährige und freundliche Unterstützung meiner Person, was mir insbesondere in so manch harten Zeiten eine große Hilfe war, sowie natürlich auch für die wissenschaftliche Betreuung und Begutachtung der vorliegenden Arbeit.

Es sei allen ehemaligen und aktuellen Kolleginnen und Kollegen am Institut für Holzbau und Holztechnologie und an der holz.bau forschungs gmbh für das gute Arbeitsklima, die gegenseitige Unterstützung sowie für die schönen gemeinsamen Erlebnisse gedankt.

Speziell möchte ich mich bei Manfred Augustin, Thomas Bogensperger sowie Reinhard Brandner bedanken, welche ihre umfangreichen Fachkenntnisse mit mir teilten, immer ein offenes Ohr für mich hatten und damit zum vorliegenden Inhalt der Arbeit zweifellos einen hohen Beitrag leisteten. Auch meinem ehemaligen Kollegen Gernot Pirnbacher sei gedankt, welcher mich bereits im Rahmen meiner Bakkalaureatsarbeit mit der vorliegenden Themenstellung vertraut machte.

Ein besonderer Dank gebührt meinem Leidensgenossen, Kollegen, Bergkameraden und Freund, Georg Flatscher, nicht nur für die schöne Zusammenarbeit und gegenseitige Unterstützung als Universitätsassistenten sondern auch ob der vielen bereichernden (und manchmal sogar geistreichen) Diskussionen beruflicher und privater Natur.

Ich möchte mich auch bei Bernd Heissenberger bedanken, welcher mir durch seine Expertise in der Abwicklung von Laboruntersuchungen sowie bei der Umsetzung sämtlicher nachfolgend

genannter Studentenprojekte eine große Hilfe war. Dies gilt sinngemäß auch für meinen ehemaligen Kollegen Thomas Kröpfl, welcher in der Anzahl an durchgeführten Ausziehprüfungen von selbstbohrenden Holzbauschrauben wahrscheinlich den Weltrekord innehat. Herzlichen Dank auch an Hildegard Weißnar für ihre Unterstützung in sämtlichen administrativen Angelegenheiten.

Viel lernen konnte ich von Ulrich Müller, Mitarbeiter des Instituts für Holztechnologie und Nachwachsende Rohstoffe an der Universität für Bodenkultur Wien, sowie von Rudolf Vallant, Mitarbeiter des Instituts für Werkstoffkunde, Fügetechnik und Umformtechnik der Technischen Universität Graz, bei welchen ich mich für die tolle Zusammenarbeit im Rahmen unserer gemeinsamen Forschungsprojekte herzlich bedanken will.

Dies gilt auch für Philipp Dietsch, Teamleiter Holzbau des Lehrstuhls für Holzbau und Baukonstruktionen der Technischen Universität München, sowie meinem ehemaligen Kollegen Ulrich Hübner, welche zudem die Entwicklung meiner Dissertation mit freundschaftlichem Rat unterstützten.

Ein Großteil der folglich vorgestellten Prüfergebnisse ist auf die unermüdliche Arbeit einer Vielzahl von Studierenden zurückzuführen, die ich bei diversen Projekten (mit)betreuen durfte. Ohne die Leistungen von Laura Brandl, Katarina Bratulić, Blazenka Jelec, Irene Obermayr, Birgit Reichelt, Catarina Silva, Alexander Beisl, Florian De Monte, Thomas Ehrhart, Reinhard Fleißner, Daniel Gasser, Rainer Hauptmann, Anel Imsirovic, Markus Laggner, Matthias Pöll, Florian Prettnner, Matthias Rebhan, Lukas Toblier, Markus Tripolt und speziell meinem Kollegen und Freund Markus Grabner wäre die vorliegende Arbeit in dieser Form nicht realisierbar gewesen.

Für die aufopfernde Korrektur meines englischen Elaborats will ich mich zudem herzlich bei Sigrid Deutsch bedanken sowie bei meinem Kollegen, Raimund Sieder für viele nützliche Tipps in der Softwareanwendung.

Großer Dank gebührt meinem gesamtem Umfeld, besonders meinen Eltern, Gertrude und Andreas (†) Ringhofer, meinen näheren Verwandten sowie meinen Freundinnen und Freunden. Speziell möchte ich mich bei meiner Partnerin Daniela Kneißl bedanken, welche bereits seit mehr als 11 Jahren an meiner Seite steht und mich in allen Lebenslagen unglaublich unterstützt und motiviert. Ihr sei diese Arbeit gewidmet.

Teile der vorliegenden Arbeit wurden im Rahmen des Projektes ‚focus_sts‘ vom Kompetenzzentrum holz.bau forschungs gmbh finanziert und in Kooperation mit dem Institut für Holzbau und Holztechnologie der TU Graz bearbeitet.

Das Projekt wird aus Mitteln des Bundesministeriums für Wissenschaft, Forschung und Wirtschaft (BMWFW), des Bundesministeriums für Verkehr, Innovation und Technologie (BMVIT), der Steirischen Wirtschaftsförderungs-gesellschaft mbH (SFG), des Landes Steiermark (A12), des Kärntner Wirtschaftsförderungs Fonds (KWF), des Landes Niederösterreich Abteilung Wirtschaft, Tourismus und Technologie und der Standortagentur Tirol gefördert.

In diesem Zusammenhang möchte ich die langjährige und gute Zusammenarbeit mit der Firma Schmid Schrauben Hainfeld GmbH hervorstreichen. Speziell sei hier Erwin Reischer, Leiter Forschung und Entwicklung, gedankt, von dem ich viel über die Natur der Schraube lernen konnte und welcher mich bei vielen Untersuchungen mit seinem Einsatz unterstützte.

Abstract

Axially Loaded Self-Tapping Screws in Solid Timber and Laminated Timber Products

Within the last 25 years, self-tapping screws have become probably the most relevant fasteners in contemporary timber engineering. The main reasons for their success are their simple and economic installation without pre-drilling, as well as their flexible geometry, enabling the use for various different design situations, separated into connections and reinforcements. Restricting the scope to axial loading, as most efficient way of application, the present thesis aims on gaining a fundamental knowledge concerning the specifics of this kind of dowel-type fastener. Thereby, the related considerations are divided into the two main topics, namely (a), the (steel) product “self-tapping screw” itself and (b), the withdrawal behaviour, defined as the axial composite interaction with the timber material where it is inserted into.

With regard to (a), the main outcomes are the derivation and verification of a mechanical approach, describing the relationships of the relevant design properties f_{tens} , f_{tor} and M_y in dependence of a geometrically varying screw thread profile, as well as some fundamental findings in terms of fatigue-relevant loading and hydrogen-induced stress corrosion cracking (HISCC), both assignable to the field of material science.

In case of (b), based on comprehensive experimental campaigns comprising about 14,000 single test results, the impact of several influencing parameters (classified into “screw”, “timber product”, “application” and “loading”) on the withdrawal behaviour of self-tapping screws is determined, discussed and described by means of empirical, stochastic and mechanical modelling.

Those parameters, where a significant influence can be observed, are finally included in the determination of a universal approach for the empirical prediction of the screw’s mean and characteristic (5 %-) withdrawal strength f_{ax} , irrespective the timber product used (solid timber and the board-based, laminated timber products glued and cross laminated timber) and the position the screw is inserted into.

Kurzfassung

Axial beanspruchte, selbstbohrende Holzbauschrauben in Vollholz und geschichteten Holzwerkstoffen

Im Zuge der letzten 25 Jahre sind selbstbohrende Holzbauschrauben die wahrscheinlich bedeutendsten Verbindungsmittel im modernen Ingenieurholzbau geworden. Als wesentlichste Gründe für ihren verbreiteten Einsatz sind ihre einfache und wirtschaftliche Montage ohne Vorbohren sowie ihre flexible Geometrie zu nennen, die ihre Anwendung für eine ganze Reihe unterschiedlicher Einsatzbereiche, gliederbar in Verbindungen und Verstärkungen, ermöglicht. Unter Einschränkung des Betrachtungsbereiches auf die axiale Beanspruchung, zufolge welcher die Schrauben wohl am Wirksamsten eingesetzt werden können, konzentriert sich die vorliegende Arbeit auf das Schaffen von Grundlagenwissen hinsichtlich der Besonderheiten dieses stiftförmigen Verbindungsmittels. Dies aufgeteilt in zwei Teilbereiche, welche sich einerseits mit dem Produkt „selbstbohrende Holzschraube“ und andererseits mit dessen Ausziehverhalten, der axialen Verbundwirkung der Schraube mit dem umgebenden Holzwerkstoff, beschäftigen.

Im Rahmen des ersten Teilbereichs ist als wesentlichstes Ergebnis der Arbeit die Herleitung und Verifizierung eines mechanischen Modells, welches die Beziehung der relevanten Bemessungskenngrößen f_{tens} , f_{tor} und M_y in Abhängigkeit einer variierenden Gewindegeometrie beschreibt, zu nennen. Ferner werden eine Reihe grundlegender Erkenntnisse zum Ermüdungstragverhalten sowie zur wasserstoffinduzierten Spannungsrisskorrosion bei axialer Beanspruchung, welche dem Themenbereich der Werkstoffkunde zuzuordnen sind, diskutiert.

Der zweite Teilbereich der Arbeit beinhaltet die Untersuchung, Diskussion und Beschreibung (mittels empirischer, stochastischer und mechanischer Ansätze) der Auswirkungen einer Variation unterschiedlicher Einflussparameter (eingeteilt in die Hauptgruppen „Schraube“, „Holz“, „Applikation“ und „Beanspruchung“) auf das Ausziehtragverhalten der axial beanspruchten, selbstbohrenden Holzbauschrauben. Dem zugrunde liegen rund 14.000 Einzelergebnisse aus einer umfangreichen Reihe an experimentellen Prüfserien.

Jene Parameter, welche das Tragverhalten der Schrauben signifikant beeinflussen, werden in weiterer Folge für die Herleitung eines universellen Ansatzes zur empirischen Vorhersage des Mittelwertes und charakteristischen (5 %-) Wertes der Ausziehfestigkeit f_{ax} der Holzbauschrauben berücksichtigt. Das Modell ermöglicht letztendlich die Bestimmung von f_{ax} , unabhängig des verwendeten Holzwerkstoffes (Vollholz sowie die brettbasierenden, geschichteten Holzwerkstoffe Brettschichtholz und Brettsperrholz) und der Lage der Verschraubung im Holz.

Contents

CHAPTER 1 MOTIVATION AND SCOPE OF THIS THESIS	1
CHAPTER 2 APPLICATION OF SELF-TAPPING SCREWS IN MODERN TIMBER ENGINEERING	5
2-1 Introduction	5
2-1.1 Design principles for an optimised connection	5
2-1.2 Historical background of modern screw application	7
2-1.3 Intermediate conclusions	13
2-2 Development of approvals and standardisation with focus on screws	15
2-2.1 Standardisation in Austria	16
2-2.2 Standardisation in Germany	26
2-2.3 Standardisation in Switzerland	30
2-2.4 Judicial background from 1990 – 2015	33
2-2.5 Development process based on technical approvals	42
2-2.6 Intermediate conclusions	54
2-3 Active application as connection	56
2-3.1 Normal joints	56
2-3.2 Transversal joints	71
2-3.3 Moment joints	75
2-3.4 Screwed connections in solid timber constructions	78
2-4 Passive application as reinforcement	83
2-4.1 Reinforcement against compression perpendicular to grain	83
2-4.2 Reinforcement against tension perpendicular to grain	88
2-4.3 Reinforcement against shear	99
2-4.4 Reinforcement of laterally loaded dowel-type connections	106
2-4.5 Further reinforcement applications and general works	111
2-5 Concluding remarks to Chapter 2	114
CHAPTER 3 COMPONENTS, PRODUCTION AND MAIN MATERIAL PROPERTIES OF SELF-TAPPING SCREWS	115
3-1 Introduction	115
3-2 Geometry of self-tapping screws	116
3-2.1 Screw drive characteristics	116
3-2.2 Screw head characteristics	117
3-2.3 Screw shank characteristics	119
3-2.4 Screw thread characteristics	119
3-2.5 Screw tip characteristics	121

3-2.6	Summary of geometrical screw characteristics	122
3-3	Production process of self-tapping screws	123
3-3.1	Properties and pre-treatment of raw material	123
3-3.2	Forming the screw geometry	124
3-3.3	Screw hardening process	125
3-3.4	Adding protective coats	127
3-3.5	Final treatment	130
3-4	Geometrical and mechanical properties of self-tapping screws	131
3-4.1	Motivation	131
3-4.2	Mathematical description of the screw 3D surface	132
3-4.3	Cross-sectional screw properties	136
3-4.4	Experimental programme	158
3-4.5	Mechanical screw properties	167
3-4.6	Concluding remarks to section 3-4	182
3-5	Influencing parameters on screw tensile capacity	185
3-5.1	Introduction and overview	185
3-5.2	Production process	185
3-5.3	Loading	194
3-5.4	Environment	208
3-5.5	Concluding remarks to section 3-5	238

CHAPTER 4 DEFINITION AND LAY-UP OF SOLID TIMBER AND LAMINATED TIMBER PRODUCTS WITH FOCUS ON SCREW APPLICATION... 243

4-1	Introduction	243
4-2	Definition of timber specimen applied for screw investigations	243
4-3	Main mechanical constitutions of clear wood	248
4-4	Definition and lay-up of laminated timber products	252

CHAPTER 5 INFLUENCING PARAMETERS ON WITHDRAWAL PROPERTIES 255

5-1	Introduction and overview	255
5-1.1	The definition of withdrawal failure	256
5-1.2	General considerations regarding the experimental determination of withdrawal properties	259
5-1.3	A brief discussion of main literature sources	269
5-1.4	Overview and classification of parameters influencing withdrawal properties	272
5-2	Screw	273
5-2.1	Thread geometry	273
5-2.2	Thread surface condition	281
5-3	Timber product	282
5-3.1	Clear wood properties	282

5-3.2	Environmental conditions.....	301
5-3.3	Lamination – general lay-up parameters	315
5-3.4	Lamination – CLT production specifics.....	334
5-4	Application	348
5-4.1	Spacings	348
5-4.2	Pre-drilling	363
5-4.3	Axis-to-grain angle α	375
5-4.4	Position to annual ring structure.....	389
5-4.5	Effective inserted thread length l_{ef}	395
5-4.6	Embedment length l_{emb}	404
5-5	Loading.....	407
5-5.1	Load introduction and supporting conditions.....	407
5-5.2	Loading velocity.....	415
5-5.3	Duration of load	421
5-5.4	Type of loading	424
5-6	Summary and conclusions.....	427
5-6.1	Screw.....	427
5-6.2	Timber product.....	428
5-6.3	Application.....	430
5-6.4	Loading	433
5-6.5	Final comments to the ductility of axially loaded self-tapping screws failing in withdrawal .	434
CHAPTER 6 EMPIRICAL MODELLING OF WITHDRAWAL STRENGTH		437
6-1	Introduction	437
6-2	Overview of considered test results and property correction	438
6-3	Discussion of model components.....	440
6-3.1	Variable exponent k_p considering the density impact in case of $N = 1$	440
6-3.2	Function k_{ax} considering the influence of angle and gap variation.....	442
6-4	Approach for reference withdrawal strength.....	448
6-5	Model verification	451
6-6	Derivation and verification of a characteristic approach.....	454
6-7	Summary and conclusion	456
CHAPTER 7 SUMMARY, PRACTICAL RECOMMENDATIONS AND OUTLOOK		459
7-1	Summary	459
7-2	Practical recommendations.....	461
7-3	Outlook.....	462

ANNEX A	REGISTER	464
A-1	References.....	464
ANNEX B	ADDITIONAL INFORMATION.....	492
B-1	Supplementary material to chapter 2	492
B-2	Supplementary material to chapter 3	500
B-2.1	Supplementary figures	500
B-2.2	Supplementary test results.....	504
B-3	Supplementary material to chapter 5	507
B-3.1	Supplementary figures	507
B-3.2	Supplementary test results.....	544
B-4	Supplementary material to chapter 6	579
B-4.1	Supplementary figures	579
B-4.2	Supplementary test results.....	583

CHAPTER 1

MOTIVATION AND SCOPE OF THIS THESIS

The application of screws for various purposes in everyday life accompanied the human development from ancient times on. About 2,500 years ago, the main function of the first known “screw pumps” (note: the theoretical principle was originally derived by Archimedes of Syracuse, 287 ÷ 212 BC), commonly consisting of a heavy wooden pole, a double or triple helix, built of wood strips (or bronze sheeting), and a board coating, waterproofed with pitch, was to lift the water from a lower to an upper level of plantation, c. f. Dalley and Oleson (2003). Even though this form of conveying technique is still applied, e. g. in agriculture or heat technology, the modern screw application predominately aims on transmitting axial or lateral forces between two components in the frame of joining technology. In detail, this concerns a huge variety of different technical fields such as astronautics, aeronautics, shipping, optics and fine mechanics, as well as automotive, medical and environmental engineering. Therefore applied screw diameters range from less than one millimetre to more than half of a metre, combined with a total length of several metres, c. f. Strassmann (2005). Apart from steel, as probably the main material for manufacturing, not only further metals such as titan and aluminium, but also magnesium or various synthetics are frequently applied for their production.

Concentrating on their use for connecting wooden components, the application of first (metallic) screws with cut or rolled threads dates back to the 18th century, c. f. Hübner (2013a). For a long period of time, ending in the late 1990s, this predominately comprised furniture, or – with respect to timber engineered structures – laterally loaded joints as the common method of assembling the connections at that time. In fact, the last 20 ÷ 25 years of Central European research and development in timber engineering changed a lot. The trussed systems for the hall constructions, as well as the post and beam or frame constructions for the residential buildings, both parts of the timber lightweight construction technique, were gradually replaced by solid-web girder systems and solid timber constructions, realised with laminar elements. Consequently, solid timber (ST), as the primary building product in the past, lost its former relevance in favour of glued laminated timber (GLT) or cross laminated timber (CLT), as board-based laminated products, with cross-sectional dimensions, fulfilling the demands on the new construction types. Nevertheless, structural systems, composed by these new and/or improved timber components, required new solutions for specific details i. e. the normal and the transversal joints with high force components, the (CLT) edge joints with comparatively high member thicknesses, as well as the weak timber areas, stressed perpendicular to grain.

The parallel ongoing development of the self-tapping screws, optimised for an insertion without pre-drilling, combined with the idea of situating them in a way, they are loaded predominately in axial direction, established several opportunities for applying them to fulfil the aforementioned demands. A huge variety in geometry, currently limited by the outer thread diameters up to 14 mm and the thread lengths up to 2000 mm, c. f. ETA-11/0190 (2013), enables the design and the realisation of powerful and efficient timber- or metal-to-timber connections in one- or two-dimensional loadbearing structures. The butt joints, transmitting several MN of tensile forces, or the pre-fabricated (transversal) system connectors, optimised for a fast assembly on site, are just two well-known examples related. With regard to timber components, stressed in perpendicular to grain or by shear, especially the aforementioned upper limits of the outer thread diameter and the thread length enable a flexible and particularly invisible reinforcement of the related member areas. If compared to the glued-in rods, as second alternative, covering a similar bandwidth of application, the screws benefit from a fast and economic assembling and a less effort in quality control. It has to be pointed out, that they consequently fulfil the aforementioned demands in probably the most powerful way and thus have become indispensable in modern timber engineering.

With regard to the design of the self-tapping screws, loaded in axial direction, focusing on the single fastener performance, two main failure modes, namely the steel failure in tension, as well as the withdrawal failure, are not only predominately considered for the structural design, but also govern the suitability of this kind of fastener. The former one, reached by exceeding the material's steel tensile capacity, represents the maximum force, which is bearable by one screw, as the upper limit to be achieved for realising an efficient connection or reinforcement. The latter one, describing the response of the local timber surrounding the screw, is not less important, since it includes all the timber-relevant boundary conditions for a related design and optimisation process.

It is worth pointing out, that both failure scenarios depend on and are influenced by several different parameters, whose impact is not entirely known so far. With regard to the mechanical performance of the screw itself, this especially concerns the quantitative influence of the production process, the thread geometry, the loading and the environmental exposure on its (steel) tensile capacity. For simplifying their development, testing and design process, a mechanical approximation of the relationship between the screw tensile, bending and torsional properties would be a valuable contribution as well. In case of withdrawal, the given lack of knowledge does more specifically comprise the interrelationships between the main influencing parameters (the outer thread diameter, the axis-to-grain angle, the timber density), as well as the lamination effects (of screws situated in GLT or CLT) and, again, the environmental exposure. Especially concentrating on determining and describing these impacts for both failure scenarios, the present thesis aims to summarise and supplement the fundamental know-how, regarding the axial loadbearing behaviour of modern self-tapping screws, applied in solid timber and in the laminated timber

products GLT and CLT. Worth pointing out, that this not only concerns their bearing resistance, but also their stiffness and their ductility, as both are supplemental information for describing their force-displacement relationship. The related content is separated into chapters 2 ÷ 6, which shall be summarised as follows:

Chapter 2 represents a general introduction to the topic self-tapping screws and their relevance in timber engineering. Beginning with and basing on a general definition of the most important principles for the design of timber connections, the historical background of the modern screw application from the early 1990s on is summarised in brief. Furthermore, the development process of the self-tapping screws, as mirrored by and depending on the product and design standards, the judicial documents, such as building laws, directives and regulations, as well as on the technical product assessments, is illustrated and discussed. The third and final part of chapter 2 deals with a comprehensive literature survey regarding the previously conducted works in this field, thematically separated into the active (connections) and the passive (reinforcements) application of the self-tapping screws.

The content of chapter 3 is about the first core topic of this thesis, namely the mechanical material behaviour of the self-tapping screws and consists of a comprehensive summary, regarding their geometrical properties, as well as their production process, which especially concerns the thread rolling and the steel hardening as production steps, governing the related properties. Furthermore, a mechanical approach, basing on the Euler-Bernoulli's beam theory, a geometrical 3D-model of the screw thread surface, as well as on an ideal plastic material behaviour, is formulated to determine the main steel product characteristics, i. e. the tensile capacity f_{tens} , the yield moment M_y and the torsional capacity f_{tor} . The related model verification comprises a comparison with the results, gained from several experimental programmes and numerical (FE-) calculations. This knowledge is further applied for determining the performance of the screws if loaded in axial tension. This not only covers an ideal screw thread geometry, statically loaded in tension, but also the impact of further parameters, such as the production inaccuracies, the type of loading (static vs. cyclic/fatigue), as well as the varying environmental conditions, the latter provoking the phenomenon of hydrogen-induced stress corrosion cracking (HISCC).

In the frame of chapters 4 to 6, the focus is on the composite interaction between the screw thread and the local timber area around, limited by the withdrawal failure in case of the axial loading. Thereby, chapter 4 describes the relevant scale of the timber material, as characterised by its size and local defects, as well as by its main physical and mechanical parameters, the latter for the assumption of orthotropic material behaviour. Furthermore, the term "layered clear wood" is introduced and defined by the lamination parameters, specifically given for the screw insertion in GLT and CLT.

As the second core topic of this thesis, chapter 5 comprehensively summarises, evaluates and describes the impact of several parameters on the axial load carrying capacity of the self-tapping screws failing in withdrawal. The related classification comprises four main categories, denoted as “screw”, “timber product”, “application” and “loading”. The considerations mainly base on several experimental campaigns, carried out at Graz University of Technology during the last 10 years and not only include the property withdrawal strength, but also the stiffness and the ductility. Furthermore, the outcomes are compared with the findings made so far, and in cases, where new effects are observed (interrelationship of the timber density with further main parameters; impact of the number of the penetrated layers, the moisture content variation, the gaps, etc.) subsequently described by specifically chosen approaches (empirical, stochastic, mechanical).

Within chapter 6, results of chapter 5 are applied to derive a new model, determining the withdrawal strength of the self-tapping screws, situated in solid timber and the laminated timber products GLT and CLT. This multiplicative, universal approach consists of a reference withdrawal strength model, modification factors covering the interrelationship between more than one influencing parameter, as well as of single parameter impact models. While the latter are adopted from chapter 5, both former are derived and discussed in this chapter. After a successful verification, an additional approach is derived for determining the characteristic (5 %-) withdrawal strength, as this property is required for the ULS design, according to ON EN 1990 (2013).

Finally, all relevant findings, made in this thesis, are summarised in chapter 7, leading to practical recommendations, not only for the design of and the construction with axially loaded self-tapping screws, but also for the testing issues and the fastener optimisation.

CHAPTER 2

APPLICATION OF SELF-TAPPING SCREWS IN MODERN TIMBER ENGINEERING

2-1 INTRODUCTION

Within this first introductory chapter, the way and background of how self-tapping screws are applied in modern timber engineering nowadays, is described and discussed. In line with the overall aim of this thesis, the focus is mainly on their performance if stressed predominately in axial direction. Thus, the time frame analysed begins with the early 1990s, when first measures were set, enabling this form of application (as explained later on). It is worth mentioning that a more historical view on this topic, especially concerning the development and production of (timber) screws in general, can be found elsewhere, see e. g. Hübner (2013a). In order to start this introduction with a structural performance related comparison of self-tapping screws in dependence of their load-to-axis orientation (either axially or laterally loaded or something in between), three main design criteria have to be considered when planning a timber connection and are discussed as follows.

2-1.1 Design principles for an optimised connection

Gehri (1993) mentions the joint's ductility D as the dominating principle, essentially influencing the connection's loadbearing behaviour. According to ON EN 12512 (2001), D is defined as a ratio between the joint's deformation at the ultimate load bearable, F_u (which is in major cases 80 % of the maximum load F_{max} after reaching this value, their definition is illustrated in Figure 2.1) and that at the yielding load F_y . There are two main reasons for its major importance: first, a high ductility of the single fastener goes along with a high 'plastic' deformation at load levels close to F_{max} and thus allows a load redistribution of the fasteners in the connection. The consequences are (i) a joint's bearing resistance $F_{max,n}$ as the sum of all single fasteners' bearing resistances $F_{max,i}$ in average (which means, that the effective number of fasteners, n_{ef} is equal to n as the total number of fasteners) and (b) a decreased variability of $F_{max,n}$ if compared to that of $F_{max,i}$ due to homogenisation effects. Second, a high ductility of the connection itself enables a load redistribution of the total system (if overdetermined), useful in case of timber members applied as bearing components, commonly failing by brittle modes; c. f. Schickhofer (2006b).

The second relevant design criteria is defined by Gehri (1993) as the joint's total bearing resistance, $F_{max,n}$, widely classified by the efficiency η_{max} as the ratio between $F_{max,n}$ and the unjointed resistance of

the structural members to be connected. High values of η_{\max} enable a high utilisation of the structure's bearing components increasing its economic feasibility. In contrast, connections with a pronounced ductile failure behaviour and low η_{\max} are advantageous for structures exposed to seismic actions. Due to their minor resistance if compared to the timber component failing by brittle mode, they are certainly the weakest points in the structure dissipating energy in case of an earthquake. Commonly used capacity design methods in seismic engineering are applied to ensure this typical behaviour, see Priestley et al. (2007).

Finally, Gehri (1993) denotes the joint stiffness K_{ser} as the ratio between force F and deformation v in the linear elastic part of the force-deformation-relationship as the third principle regarding the compilation of connections. In terms of serviceability limit state (SLS) design, timber structures, especially those with a high number of joints such as trussed systems, benefit from stiff connections significantly decreasing vertical displacements to be limited. Furthermore, certain ultimate limit state (ULS) design situations, e. g. buckling of columns or bending of beams, composed by flexibly bonded composites also advantage from rigid joints and joint lines improving their structural performance. In contrast, there are cases high K_{ser} may negatively affect the timber structures' loadbearing behaviour, especially in form of partially restrained hinges, originally designed as moment-free joints.

Briefly-worded: for major fields of application all three criteria introduced, namely ductility, bearing resistance, as well as stiffness of a timber connection should be increased as far as possible, optimising the joint's structural performance and cost-efficiency. Based on mentioned requirements a qualitative joint behaviour, similar to the typical bilinear force-deformation relationship of low carbon steel (high stiffness in the linear elastic part followed by pronounced plastic deformation until failure occurs at a high load level), seems to be the ideal solution of this matter.

Nevertheless, the behaviour of commonly applied connections in timber engineering deviates from this ideal conception. In Figure 2.1, not only the force-deformation diagrams of different kinds of connections but also those of the two main directions self-tapping screws are commonly loaded are illustrated (lateral and axial; both experimental curves (referred to $n = 1$) were determined by Bratulic et al. (2014) in cross-laminated timber, CLT). The different timber products and the fastener dimensions disable a quantitative comparison of absolute values. Nevertheless, from a qualitative point of view, clear dependencies between ductility, resistance and stiffness can be observed. They indicate an almost rigid behaviour of connections with a rather high bearing resistance but minor ductility, such as glued joints or axially loaded self-tapping screws. In contrast, shear plane connections, where dowels, bolts or self-tapping screws are stressed perpendicular to their axis, reach high ultimate deformations (thus high values of ductility), but are significantly weaker in terms of bearing resistance and stiffness. Although, all various forms of connections applied in modern timber engineering cannot be represented by those given in

Figure 2.1. The fact, that all three criteria are hardly fulfilled by one type of connection remains obviously.

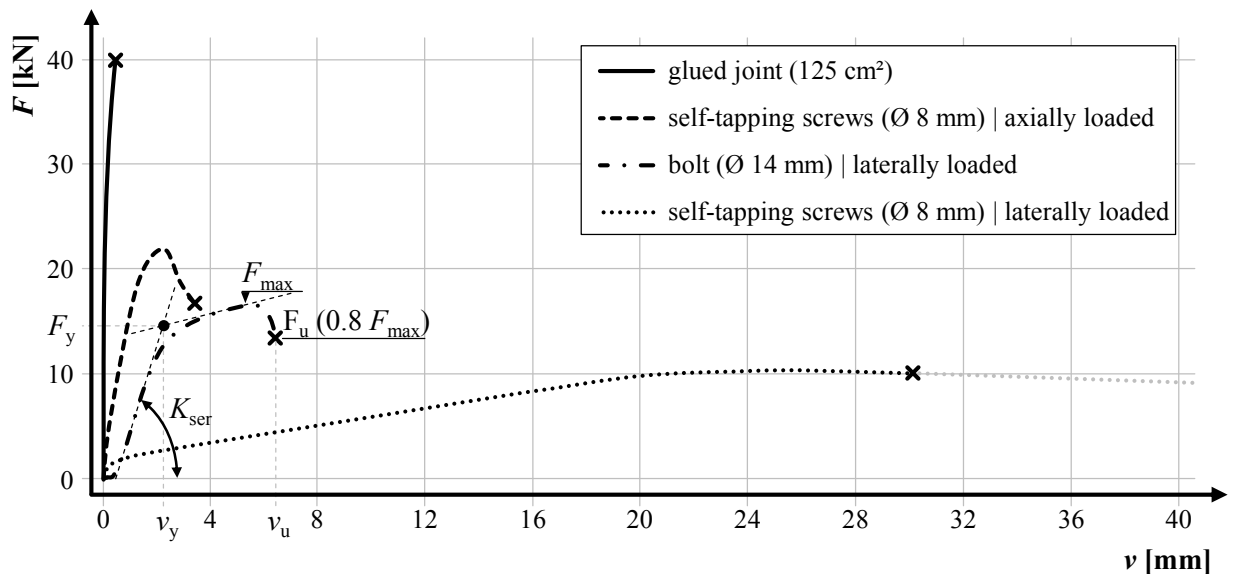


Figure 2.1: Force-deformation relationships of different timber connections and fasteners, according to Schickhofer (2006b) and Bratulic et al. (2014)

With special regard to both experimental curves related to differently applied self-tapping screws, the angle between screw and load axis, ε balances their structural behaviour: in case of lateral loading ($\varepsilon = 90^\circ$), the comparatively smallest failure loads appear at maximal deformations (maximal ductility). Consequently, decreasing ε increases bearing resistance and stiffness, while ultimate deformation and ductility are reduced. Extreme values are reached again at total axial load conditions ($\varepsilon = 0^\circ$). Bratulic et al. (2014) detected the joint stiffness K_{ser} as a parameter mainly affected by varying ε , extreme differences between axial and lateral stiffness reach ratios even up to 35.

2-1.2 Historical background of modern screw application

Based on a literature survey (in Europe) concerning modern screw application, KÜng (1987) can be seen as one of the first recognizing this favourable opportunity to benefit from axial load condition in terms of stiffness and resistance. In order to rehabilitate timber floors with reinforced concrete (RFC) slabs acting as a composite system, KÜng (1987) experimentally evaluated the suitability of traditional wood screws (standardised e. g. according to DIN 571 (1986) at this time) as mechanical fasteners connecting both components. It is worth mentioning, that those structural systems need very rigid connections in order to activate the total bearing potential of timber and concrete. Part of his examinations was, that he tested two values of α as an inclination angle between screw axis and fibre orientation, namely 60° and 90° . Although 60° describe a rather high inclination, KÜng observed remarkably increased strength and

stiffness values of the connection line as a consequence of mainly axially loaded fasteners if compared to those with $\alpha = 90^\circ$ predominately stressed in bending. The only but essential disadvantage of this system was the necessity of pre-drilling the timber component when using traditional wood screws, which in fact causes high installation efforts.

Only a few years later, the Swiss company “SFS Group AG” firstly developed a timber-concrete composite screw, c. f. Z-9.1-342 (2010), which has been geometrically optimised for this specific kind of application. As given in Figure 2.2, this fastener, designed as a partially threaded timber screw, has to transmit horizontal shear forces from the timber beam (threaded part) to the concrete slab (shanked part, acts as common shear stud). Due to inclined positioning ($\alpha = 45^\circ$) and the significant differences between axial and lateral stiffness mentioned, the screw is again mainly loaded in withdrawal activating its maximal bearing performance. Meierhofer (1993) summarises the first experiences made with this innovative system and recommends fastener design by assuming truss-like load distribution as explained later on. Furthermore, he reports test results carried out at the Swiss Federal Laboratories for Materials Testing and Research (EMPA), indicating a roughly 15 times higher horizontal shear stiffness of the inclined connection line if compared to perpendicular arrangement. It is worth mentioning, that they were now able to install the fasteners without prior pre-drilling, significantly increasing the system’s cost-efficiency.

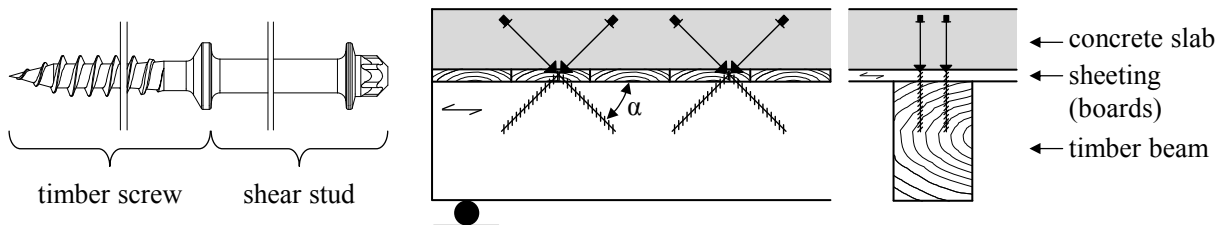


Figure 2.2: Left: SFS timber-concrete composite screw according to Z-9.1-342 (2010); right: schematic illustration of a timber-concrete composite connection

Additional experimental and numerical investigations, concerning the loadbearing behaviour of timber-concrete composite structures with timber screws, carried out by e. g. Blaß and Schlager (1996), Blaß et al. (1996) (investigated short- and long-time behaviour) and Frangi (2001) (investigated general conditions and fire exposure) were improving the suitability of this system.

At this time timber-concrete composite systems were just one application field of self-tapping screws. Between 1990 and 2000 especially partially threaded screws were often used to fasten thermal insulation material on top of rafters, see Figure 2.3. As discussed in Blaß (2000a), screws are again positioned inclined and thus aimed to transmit the roof loads’ shear components by withdrawal instead of bending. Due to the growing material thickness, caused by increasing requirements in terms of thermal building insulation, the screws used therefore were produced with nominal (thread) diameters d up to 12 mm and

total lengths l_{screw} of even 500 mm. Compared to traditional wood screws according to DIN 571 (1986), their advantages were again a simple installation without pre-drilling as well as their geometry especially modified for this form of application.

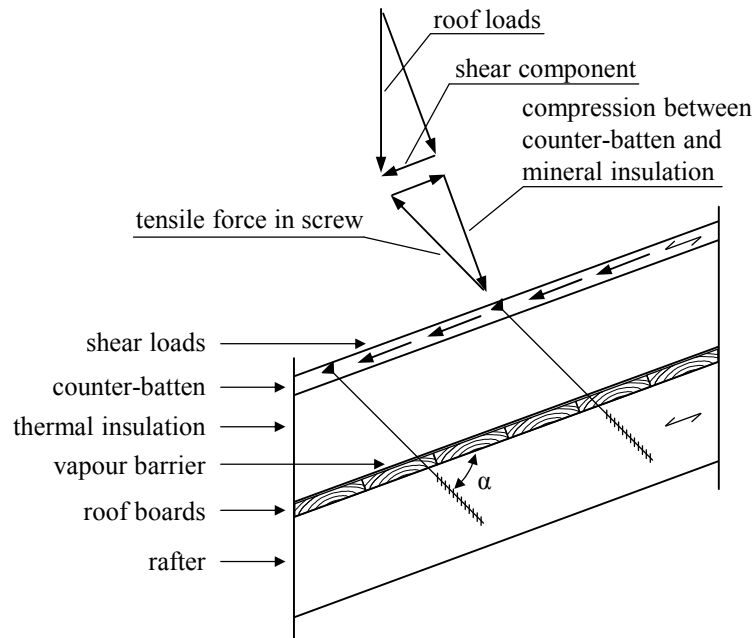


Figure 2.3: *Fastening of thermal insulation material on top of rafters – detail and loadbearing model; according to Blaß (2000b) and ETA-11/0190 (2013)*

Figure 2.3 also illustrates the former mentioned truss-like loadbearing model assumption. Thereby, the roof loads' shear components, acting in parallel to the rafter's system axis, are transmitted by the horizontal (tensile) resistance component of the inclined positioned self-tapping screws. The equilibrium is fulfilled by considering the tensile force in the screw and the compressive force between counter-batten and insulation. Thus, the latter mentioned component applies additional compressive loads on the insulation material.

In addition to the increasing use of partially threaded self-tapping timber screws with thread lengths, equal or smaller than the traditional ones according to DIN 571 (1986), new types with continuous threads over the whole length and diameters relevant for timber engineered structures (6 to 12 mm) were first produced in the late 1990s, c. f. Blaß (1998). The idea behind was to connect two timber components together, e. g. in form of combined purlins, joints between main and secondary beams, as well as butt joints, see Figure 2.4. If compared to partially threaded screws, also generally suitable for this purpose, their main advantages are (i) an equal force transmission in tension and compression, see e. g. Bejtka (2003), and (ii) threaded parts situated in both timber components, both failing in withdrawal, instead of head pull-through as the weaker resistance governing the design of partially threaded screws.

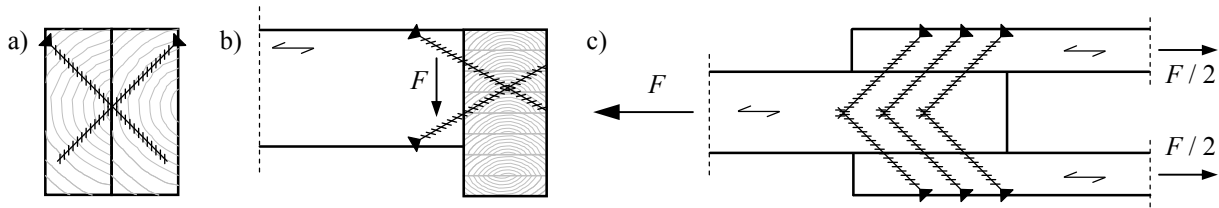


Figure 2.4: Application examples of fully threaded inclined self-tapping screws applied in timber connections; according to Blaß (1998) and Blaß and Bejtka (2004b);

a) combined purlins; b) joint between main and secondary beam; c) tensile butt joint

Another very important (or maybe the even more important) reason for the vast development of fully threaded self-tapping screws is seen in their suitability for various kinds of reinforcement measures. A trend, beginning in the 2nd half of the 20th century is preferring laminated products such as glued laminated timber (GLT, glulam) instead of solid timber (ST) as the primary timber building product in the past. While geometrically limited ST was mainly applied in form of lightweight structures, such as truss systems, the lamellar composed GLT allowed the production of solid web girders with hardly any restriction regarding size and form. Consequently, (mainly) the geometrical conditions at specific locations of tapered and/or curved GLT beams, e. g. supports (with or without notches), cut-outs, holes, transversely loaded dowel-type connections and apex areas in combination with the well-known weakness of timber if stressed perpendicular to grain, led to a significantly increasing demand for solutions strengthening these zones. Due to their high load-carrying capacity in axial direction, as well as their simplicity in terms of installation, fully threaded self-tapping screws are, in fact, an economical alternative to commonly used glued-in rods or glued-on wood-based panels for this purpose (see Figure 2.5 and Figure 2.6). The first main related research was done at the Karlsruhe Institute of Technology (KIT), see e. g. Blaß and Schmid (2001), Blaß and Bejtka (2004a), Bejtka and Blaß (2005), Bejtka (2005) and Bejtka and Blaß (2006).

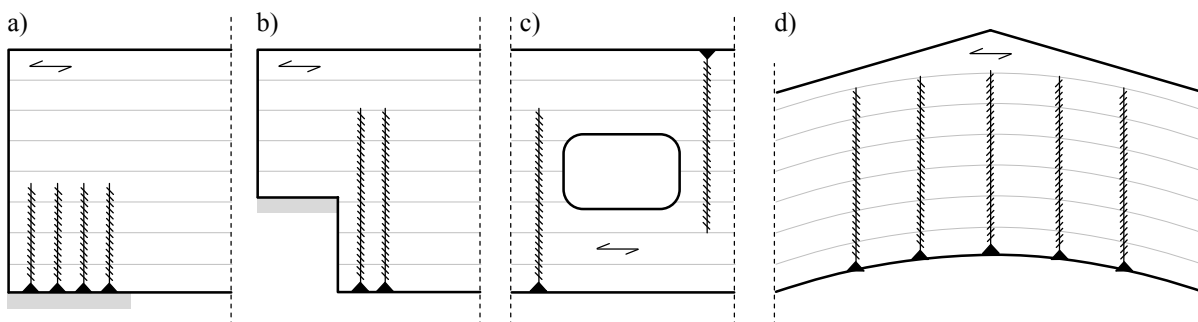


Figure 2.5: Fully threaded self-tapping screws applied as beam reinforcements; according to Blaß and Bejtka (2004a); a) compression perpendicular to grain at supporting; b) tension perpendicular to grain at notched supporting; c) tension perpendicular to grain at hole; d) tension perpendicular to grain in apex area

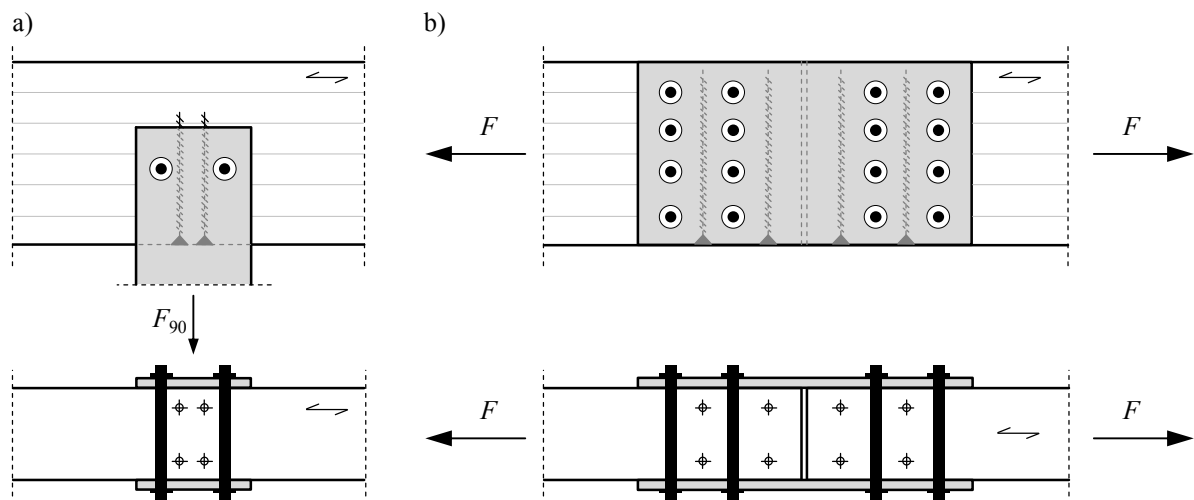


Figure 2.6: Fully threaded self-tapping screws applied as reinforcements of dowel-type connections; according to Blaß and Bejtka (2004a) and Blaß and Schmid (2001);
 a) transversely (perpendicular to grain) loaded connection; b) longitudinally loaded butt joint

Back to screw application in form of connections. With special focus on the timber-to-timber butt joint, illustrated in Figure 2.4, one main fact, concerning the activated screws' loadbearing potential, has to be discussed. Due to their application without pre-drilling, especially fully threaded self-tapping screws require torsional resistances in a dimension only being achieved by steel hardening after rolling the thread (c. f. section 3-3). Direct proportional to increasing torsional strengths f_{tor} , steel tensile strengths f_u reach thus values above 1,000 N/mm². As a consequence of connecting two timber elements, the total thread length is divided into two penetration lengths $l_{ef,i}$ being far too short reaching withdrawal resistances up to steel tensile capacities in major cases. To sum up: the fastener's total bearing resistance can hardly be activated by one of the joint details shown in Figure 2.4.

In order to achieve more powerful and economic connections, further developments regarding the application of (especially) fully threaded self-tapping screws (with $d \leq 12$ mm and $l_{screw} \leq 600$ mm) concentrated on solutions with steel plates as outer members; see Figure 2.7 (a). This measure enables the arrangement of the nearly whole screw thread in just one timber component controlling the failure mode desired (either withdrawal or tensile steel) by varying its penetration depth. Between 2000 ÷ 2010, this optimisation procedure finally led to steel-to-timber butt joints with several hundreds of inclined positioned self-tapping screws transmitting normal forces up to 10 MN (or even more), c. f. Krenn and Schickhofer (2007), Krenn and Schickhofer (2009) and Brunauer (2009). It should be pointed out, that such details demand strict regulations in terms of production accuracy and quality control.

In a more simple form, this efficient combination of inclined positioned self-tapping screws and metal plates as outer members was also recognized and applied in form of system connectors, designated for joining main and secondary beams. In contrast to formerly known solutions with screws, dowels or nails,

perpendicular arranged to force direction and thus mainly loaded by shear, first connectors with inclined positioned and predominately axially loaded self-tapping screws were developed in the early 2000s, c. f. Z-9.1-550 (2007) and Figure 2.7 (b). As compared in section 2-1.1, the significantly increased bearing resistances per fastener stressed in axial direction reduced their total number necessary by far, improving the cost-efficiency of the system. Furthermore, the maximum number of fasteners, arrangeable in one end-grain system connector, depends on the cross-section dimensions of the secondary beam. The only measure, remarkably increasing the connector's resistance, is to achieve each single fastener's total loadbearing potential, c. f. Hude (2005). Thus, inclined positioning of self-tapping screws, combined with their optimised arrangement, led to the development of a high performing connection system reaching total (vertical) resistances of more than 600 kN nowadays, c. f. ETA-11/0295 (2013). One related example is shown in Figure 2.7 (c).

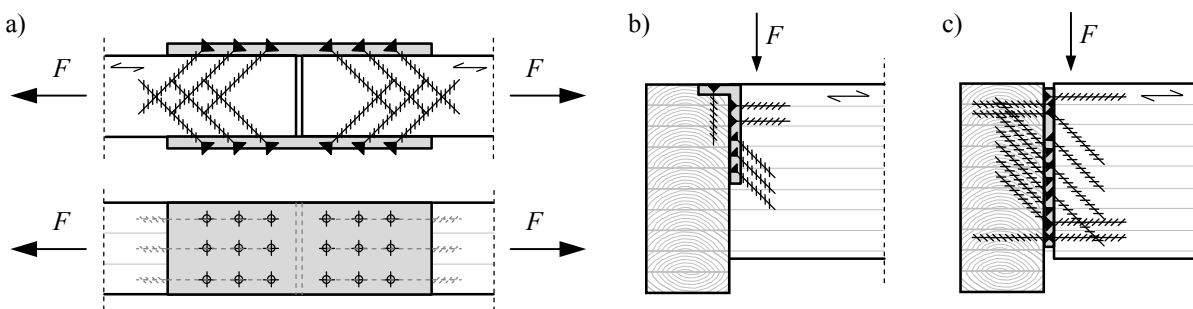


Figure 2.7: Examples of screwed connections with metal plates as outer members; a) tensile loaded high stressed steel-to-timber butt joint; b) system connector “EL” illustrated in Blaß (2004); c) system connector “SHERPA connector” according to Flatscher and Augustin (2010);

More or less parallel to the successful development of self-tapping screws beginning in the 1990s, the two-dimensional orthogonally laminated timber product CLT has raised up to one of the most commonly used building materials in modern timber engineering, see Brandner et al. (2016a). In form of the so-called “Solid Timber Construction Technique (STC)”, CLT panels, with dimensions up to roughly $18 \times 3.0 \times 0.4 \text{ m}^3$, are applied as wall and floor elements, especially aiming to erect single family houses and multi-storey residential or office buildings. In contrast to timber frame systems, using predominately nails (in form of angle brackets and hold-downs) and clamps for joining horizontal and vertical members, as well as planking material, CLT has higher requirements on the connection technique applied.

The main reasons therefore are (i) panel dimensions with thicknesses up to 400 mm, demanding fastener lengths in the size of self-tapping screws and (ii) the ongoing trend of increasing storey numbers necessitates connections being able to transmit especially high horizontal wind and earthquake loads, see Figure 2.8 (c). Several thousands of screws are thus applied in just one CLT housing project, c. f. Bernasconi (2012) and Jacob-Freitag (2013), which significantly contributes to their fast growing sales market.

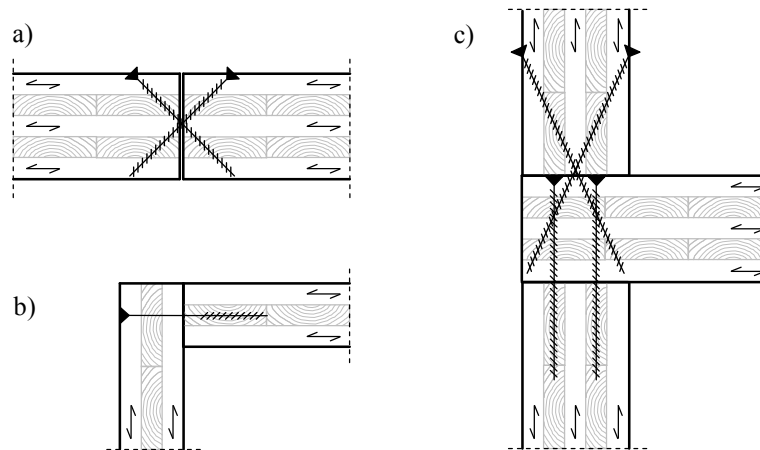


Figure 2.8: Fully and partially threaded self-tapping screws applied in CLT structures; a) floor-to-floor joint; b) wall-to-wall joint; c) wall-to-floor-to-wall joint according to Bernasconi (2012)

In the last decades an increasing growth rate of deciduous trees has been observed in Central Europe; c. f. Hübner (2013a). Consequently, boards or veneers out of hardwood species, such as European beech (*Fagus sylvatica* L.), European ash (*Fraxinus excelsior* L.) or birch (*Betula Pendula*) will gain significant relevance as a competitive alternative to the predominately used softwood species Norway spruce (*Picea abies*) or larch (*Larix decidua* Mill.) for composing laminated timber products. Due to their comparatively higher strength and stiffness values, especially in tension and compression parallel to grain direction, hardwood applications enable a remarkable reduction of cross-sectional areas. Since the axial loadbearing capacity of self-tapping screws is mainly influenced by thread lengths inserted, application concepts, where the screw is oriented in parallel to the member's axis, seem to be the logical consequence of this development. These steel-to-timber end-grain joints, schematically given in Figure 2.9, are focused by recent investigations and can be regarded as one of the main research activities concerning self-tapping screws in the near future; c. f. Gehri (2009), Gehri (2010), Grabner and Ringhofer (2014) and Meyer (2016) for instance.

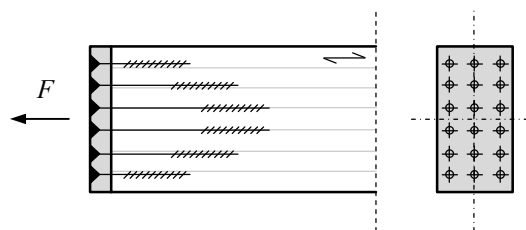


Figure 2.9: Steel-to-timber end-grain joint connecting hardwood components

2-1.3 Intermediate conclusions

As discussed in section 2-1.2, self-tapping screws have been frequently used in timber engineered structures for about 25 years. Starting with the first application fields as timber concrete composite

connectors or special fasteners for thermal insulation on top of rafters, they gained significant relevance as their huge potential as economical solutions in terms of timber-to-timber connections and various kinds of reinforcement measures was recognised. A further optimisation enabled the arrangement of numerous screws in highly stressed steel-to-timber joints or efficient system connectors. Especially in case of the prior mentioned connections, their total loadbearing potential is activated by inserting the screw thread in just one timber component, reaching steel tensile capacity as upper limit. The parallel and successful development of cross-laminated timber, nowadays a building material of global interest, offered further favourable opportunities for their copious application in form of point and line connections. The current research and development (R&D) activities mainly concentrate on screw application in engineered hardwood products, especially regarding the loadbearing behaviour and potential of steel-to-timber end-grain joints.

With regard to the examples, described in section 2-1.2, modern structural timber design always aims to arrange self-tapping screws in a way they are predominately loaded in axial direction. Furthermore, the mentioned various application types can be divided in two main fields, namely in “connection” and “reinforcement”, see Figure 2.10.

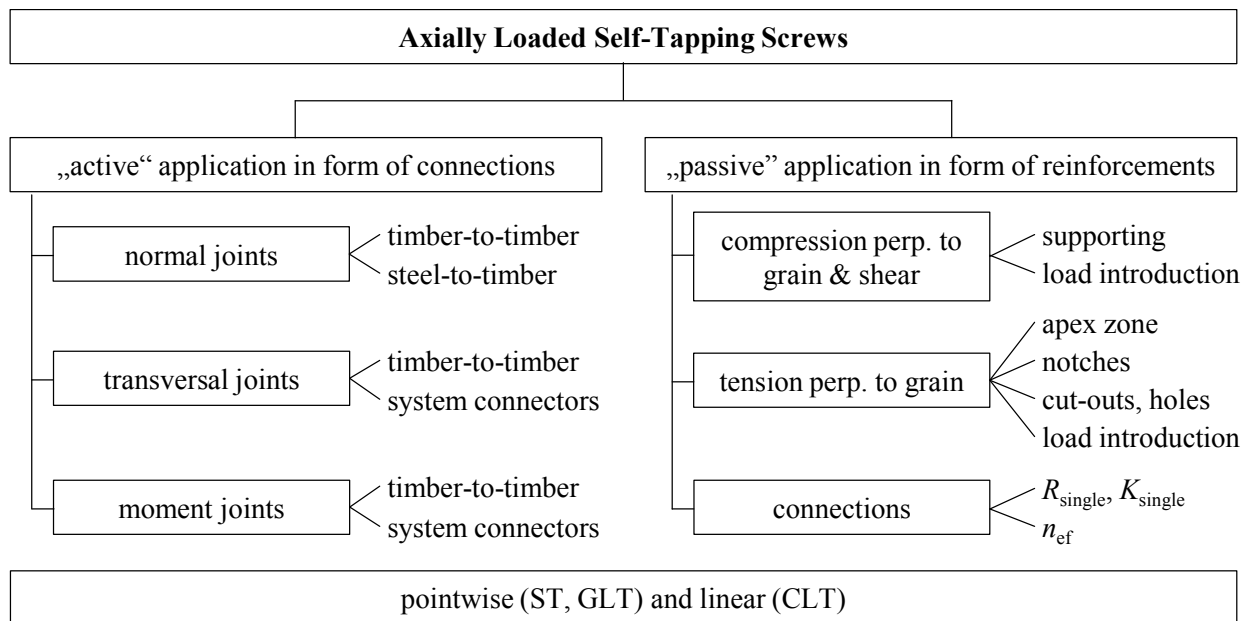


Figure 2.10: Classification of axially loaded self-tapping screws in modern timber engineering; according to Ringhofer et al. (2014a)

One possibility differing between both fields can be seen in their function regarding the construction’s structural performance: in those cases, where screws connect two bearing components, they “actively” contribute to the system’s loadbearing behaviour. In contrast, if they are applied as reinforcements, they are arranged in just one component, “passively” improving its bearing resistance at selected detail points.

Consequently, the main research activities, done so far, will be discussed in two separate sections 2-3 (connections) and 2-4 (reinforcements).

If compared to other commonly used mechanical fastening systems in timber engineering, the main advantages of screws are their simple installation without pre-drilling and a flexible geometry being adaptable for many different purposes. Especially the latter mentioned fact requires product's technical guidelines for application and design, being suitable for dynamical adaptations as a consequence of permanently growing application fields. This is also a main reason why self-tapping screws are ruled in technical assessments (or approvals), able to cover the latest findings and developments (state-of-knowledge), instead of product and design standards subjected to much longer actualisation rates, mirroring state-of-art, c. f. Jöbstl (2010). As a consequence, beginning in the early 1990s, the study of these documents not only provides a deeper insight into the development of the product "self-tapping screw" itself within this timeframe, but also enables the illustration and comparison of selected product characteristics between different manufactures, application fields and issue dates. In section 2-2, the development of product and design regulations regarding self-tapping screws during the last 25 years is thus treated more in detail. The geographical focus is thereby set on Central Europe, which especially includes the so-called D-A-CH countries (Germany, Austria and Switzerland).

2-2 DEVELOPMENT OF APPROVALS AND STANDARDISATION WITH FOCUS ON SCREWS

As mentioned in section 2-1.3, considered as a common circumstance for innovative fasteners and connection systems (at least in Europe), the application and design of self-tapping screws, as well as their geometrical characteristics, are ruled in so-called European Technical Assessments (ETAs, formerly known as European Technical Approvals) nowadays. The corresponding judicial background, based on EU Regulation No 305/2011, c. f. European Union (2011), is together with the regulations being valid before this document was published discussed in section 2-2.4. When designing timber connections by using self-tapping screws, the somewhat complex interaction of design standards and technical assessments/approvals has to be focused more in detail. Thus, sections 2-2.1 to 2-2.3 summarise the development process regarding standardisation of design standards in Austria, Germany and Switzerland from the early 1990s on, as well as the current situation in Europe. The concentration is thereby on chapters related to the application and design of screwed connections predominately loaded in axial direction.

2-2.1 Standardisation in Austria

2-2.1.1 General comments

Regarding the development of Austrian timber design standards during the last 25 years, three main periods have to be pointed out and separately discussed:

Between 1990 and 2006, all in all six different versions of the document ON B 4100-2 (2008) “Timber Structures – Part 2: Design and construction” were published by the Austrian Standards Institute. Similar to the standardisation in Germany and Switzerland, valid at least until 2003, this design guideline principally bases on a global (deterministic) safety concept, where verification process has to be done as follows:

$$S_m \leq \frac{R_m}{\gamma_0} \text{ and } \sigma_{\text{ex}} \leq \sigma_{\text{per}}, \quad (2.1)$$

where S_m is the nominal (mean) value of the action, R_m the nominal (mean) value of the resistance, γ_0 the global safety factor, σ_{ex} the existing stress and σ_{per} the permissible stress. As given in eq. (2.1), the action S_m has to be less than, or equal to, the resistance R_m divided by a *global* safety factor namely γ_0 , considering both uncertainties in terms of action and resistance.

On January 1, 2006, the standard ON EN 1995-1-1 (2006), the first official version of Eurocode 5 (European design standard for timber structures), was published in Austria. From that time on, the document ONR 21990 (2008) allowed the parallel application of the codes ON B 4100-2 (2004) and ON EN 1995-1-1 (2006) for timber design purposes. This so-called “coexistence period” lasted roughly three years and ended at May 31, 2009. In contrast to the ON B 4100-2 series, Eurocodes base on a semi-probabilistic safety concept, where *partial* multiplicative safety factors namely γ_i increase actions on the one hand and decrease resistances on the other hand. Furthermore, the characteristic (k) values, instead of nominal (mean) values, for actions and resistances are applied, see eq. (2.2).

$$\frac{R_k}{\gamma_R} \geq \gamma_S \cdot S_k, \quad (2.2)$$

where S_k is the characteristic value of the action, R_k the characteristic value of the resistance, γ_R the partial safety factor of the resistance and γ_S the partial safety factor of the action. Since July 1, 2009, ON EN 1995-1-1 (2009), its replacement documents and their national appendices (“B-documents”) have to be solely considered for the structural design of timber buildings.

2-2.1.2 Regulations in ON B 4100-2 series

This subsection includes a discussion of the documents ON B 4100-2 (1981), ON B 4100-2 (1997), ON B 4100-2 (2003a), ON B 4100-2 (2003b), ON B 4100-2 (2004) and ON B 4100-2 (2008).

- *ON B 4100-2 (1981)*

In the first document of this series, ON B 4100-2 (1981), regarding the analysed timeframe, the design of connections is declared within section 2.3.2. The regulations, concerning the determination of permissible forces R_{per} of “novel connections” (which corresponds to self-tapping screws at this time), basing on laboratory examinations are given in subsection 2.3.2.1 (3), see

$$R_{\text{per}} \leq \frac{R_{\text{m}}}{2.75}. \quad (2.3)$$

Furthermore, subsection 2.3.2.5 of ON B 4100-2 (1981) covers the application and design of screwed connections. Three main facts are worth to be pointed out: (i) the minimum *shank* diameter d_{sh} had to be at least 5 mm, (ii) pre-drilling was mandatory and (iii) the consideration of screws situated in end-grain joints ($\alpha = 0^\circ$) for structural purposes was not allowed. Although it is not explicitly mentioned within section 2.3.2.5, especially point (i) and (ii), as well as the issue date of this standard indicate the exclusive consideration of traditional wood screws for structural purposes in ON B 4100-2 (1981). Their permissible force in axial direction $N_{z,\text{per}}$ (in N) in “dry wood” (irrespective the species) had to be determined according to 2.3.2.5 (4):

$$N_{z,\text{per}} = 300 \cdot s_{\text{g}} \cdot d_{\text{sh}} \quad \text{and} \quad 4d_{\text{sh}} \leq s_{\text{g}} \leq 7d_{\text{sh}}, \quad (2.4)$$

with s_{g} as the inserted threaded part (including the screw tip) and d_{sh} as the already mentioned shank diameter – both in cm. The minimum spacing requirements were equal to those of dowels, see Table 2.1. For reasons of a better comparability of all documents, discussed in section 2-2, the minimum spacings given are notated according to the latest version of ON EN 1995-1-1 (2015), see Figure 2.11. Thereby, a_1 and a_2 are the distances between two fasteners in and perpendicular to grain direction, $a_{1,\text{CG}}$ as *unloaded* end and $a_{2,\text{CG}}$ as *unloaded* edge distance (as a consequence of pure axial loading considered).

- *ON B 4100-2 (1997)*

In ON B 4100-2 (1997), as replacement document of ON B 4100-2 (1981), now the structural design of connections was ruled in section 4.2. Again, the general subsection 4.2.1 (5) of ON B 4100-2 (1997) contains the regulations concerning the (experimental) determination of permissible forces R_{per} of *mechanical* connections, which were not ruled within this standard. As given in the therein referred section 6 “New Products and Building Techniques”, this process had to be done according to eq. (2.5):

$$R_{\text{per}} = \min \left\{ \begin{array}{l} \frac{R_m}{3.00} \\ \frac{R_{\text{min}}}{2.50} \end{array} \right., \quad (2.5)$$

whereat R_{min} is the minimum value of a series, containing at least five tests with specimen of equal dimension. While the way determining $N_{z,\text{per}}$, has not been remarkably changed (c. f. eq. (2.6), s_g and d_{sh} now in mm), now the minimum spacing requirements were equal to nails with pre-drilled holes (section 4.2.5.3), see Table 2.1. Moreover, the necessity of pre-drilling for $d_{\text{sh}} > 6$ mm was ruled in section 5.4.5.

$$N_{z,\text{per}} = 3 \cdot s_g \cdot d_{\text{sh}} \text{ and } 4d_{\text{sh}} \leq s_g \leq 12d_{\text{sh}} \text{ with } d_{\text{sh}} \geq 4 \text{ mm.} \quad (2.6)$$

- *ON B 4100-2 (2003a), ON B 4100-2 (2003b), ON B 4100-2 (2004) and ON B 4100-2 (2008)*

Compared to ON B 4100-2 (1997) in the above listed documents no relevant changes have been made concerning design and application of screws in timber connections. The only exceptions are the increase of $a_{2,\text{CG}}$ to 5 times d_{sh} (c. f. Table 2.1) and the fact, that the fastener design is ruled in section 5.2 now. The aforementioned assumption, ON B 4100-2 series only cover traditional wood screws in the relevant sections, still remains. Furthermore, it is worth mentioning that the documents analysed do not consider any limitations regarding the angle between screw axis to grain direction α in the frame of screw application and design. Note: sole exception is the permission of screws applied in end-grain joints acc. to ON B 4100-2 (1981).

Table 2.1: *Minimum spacings of screws according to ON B 4100-2 series, notation according to ON EN 1995-1-1 (2015)*

standard	a_1	a_2	$a_{1,\text{CG}}$	$a_{2,\text{CG}}$
ON B 4100-2 (1981)	$5 d_{\text{sh}}$	$3 d_{\text{sh}}$	$3 d_{\text{sh}}$	$3 d_{\text{sh}}$
ON B 4100-2 (1997)	$5 d_{\text{sh}}$	$5 d_{\text{sh}}$	$5 d_{\text{sh}}$	$3 d_{\text{sh}}$
ON B 4100-2 (2003a), ON B 4100-2 (2008)	$5 d_{\text{sh}}$	$5 d_{\text{sh}}$	$5 d_{\text{sh}}$	$5 d_{\text{sh}}$

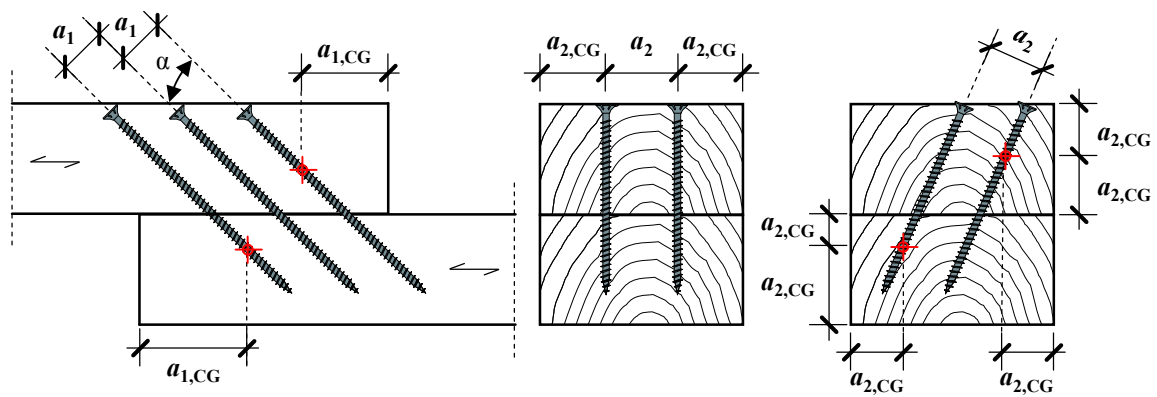


Figure 2.11: Minimum distances of predominately axially loaded screws according to ON EN 1995-1-1 (2015)

2-2.1.3 Regulations in ON EN 1995-1-1 series

As mentioned in section 2-2.1.1, the first official version of Eurocode 5 has been published in Austria on January 1, 2006. In order to describe the development of EN 1995-1-1, regarding the regulations of screwed connections from the early stage of this standard on, this subsection not only includes a discussion of the documents ON EN 1995-1-1 (2006), ON EN 1995-1-1 (2009), ON EN 1995-1-1 (2014), ON EN 1995-1-1 (2015), but also of their forerunners ON ENV 1995-1-1 (1992), ON ENV 1995-1-1 (1995) and prEN 1995-1-1 (1999). All related national appendices such as ON B 1995-1-1 (2006), ON B 1995-1-1 (2009), ON B 1995-1-1 (2014) and ON B 1995-1-1 (2015) are considered, too.

- *ON ENV 1995-1-1 (1992)*

The document ON ENV 1995-1-1 (1992) was the first (draft) issue of Eurocode 5 published for the application in Austria, c. f. Austrian Standards (2015). Therein, connections are regulated in its section 6, screwed joints consequently in subsection 6.7. The design withdrawal capacity for axially loaded screws (at $\alpha = 90^\circ$), R_d (in N) had to be determined according to equations 6.7.2a and b, see

$$R_d = f_{b,d} \cdot (l_{ef} - d_{sh}) \quad \text{and} \quad f_{b,k} = (1.5 + 0.6 d_{sh}) \cdot \sqrt{\rho_k}, \quad (2.7)$$

where $f_{b,d}$ is seen as the withdrawal parameter (own assumption, not mentioned by name in this document) in N/mm, l_{ef} the threaded length in the member *receiving the screw* (including its tip), d_{sh} the *shank* diameter (denoted as d in this document), both in mm, and ρ_k the characteristic density of the wood product in kg/m^3 . The latter mentioned parameter is commonly used as a material indicator, describing shear and embedment strength of dowel-type fasteners in modern design codes, c. f. ON EN 1995-1-1 (2015). In contrast to eq. (2.6), implemented in ON B 4100-2 series where no material parameter considers the inherent strength variability of timber products, the density in eq. (2.7) enables the consideration of different withdrawal properties, caused by different strength classes of one wood species

applied, as well as those of different wood species in general. Furthermore, also deviating from ON B 4100, l_{ef} is reduced by one times the diameter, maybe taking the screw tip barely contributing to axial loadbearing performance into account. Similar to ON B 4100-2, the minimum penetration depth is limited to $4 d_{sh}$. With regard to the screw application in form of an axially loaded connection, minimum distances should be chosen equally to lateral loading; see Table 2.2. As given in section 7.4(9) of this standard, all screws with $d_{sh} > 5$ mm should be pre-drilled.

Table 2.2: Minimum spacings of screws according to ON ENV 1995-1-1 (1992), notation according to ON EN 1995-1-1 (2015)

minimum spacings	$d_{sh} < 8$ mm		$d_{sh} \geq 8$ mm	
	without pre-drilling		with pre-drilling	
	$\rho_k \leq 420$ kg/m ³	$420 \leq \rho_k \leq 500$ kg/m ³		
a_1	$d_{sh} < 5$ mm: $10 d_{sh}$ $d_{sh} \geq 5$ mm: $12 d_{sh}$	$15 d_{sh}$	$7 d_{sh}$	$4 d_{sh}$
a_2	$5 d_{sh}$	$5 d_{sh}$	$3 d_{sh}$	$4 d_{sh}$
$a_{1,CG}$	$10 d_{sh}$	$15 d_{sh}$	$7 d_{sh}$	$4 d_{sh}$
$a_{2,CG}$	$5 d_{sh}$	$7 d_{sh}$	$3 d_{sh}$	$3 d_{sh}$

Note: in Table 2.2, each cos- or sin-components increasing the specific distance a_i are neglected.

- ON ENV 1995-1-1 (1995)

The regulations, concerning axially loaded screwed connections in the second draft version of Eurocode 5 published on February 1, 1995 in Austria, do not differ remarkably from the document discussed before. The sole exceptions are the requirements on minimum distances between two screws and $d_{sh} < 8$ mm, see Table 2.3.

Table 2.3: Minimum spacings of screws in ON ENV 1995-1-1 (1995), only those deviating from ON ENV 1995-1-1 (1992); notation according to ON EN 1995-1-1 (2015)

minimum spacings	$d_{sh} < 8$ mm		
	without pre-drilling		with pre-drilling
	$\rho_k \leq 420$ kg/m ³	$420 \leq \rho_k \leq 500$ kg/m ³	
a_1	$5 d_{sh}$	$7 d_{sh}$	$4 d_{sh}$
a_2	$5 d_{sh}$	$7 d_{sh}$	$3 d_{sh}$

Note: in Table 2.3, each cos- or sin-components increasing the specific distance a_i are neglected.

- *prEN 1995-1-1 (1999)*

prEN 1995-1-1 (1999) is identified as the first working draft for EN 1995-1-1 (2004) (general European version) and has not been published as Austrian draft standard. Its specific regulations on screwed connections significantly differ from the aforementioned codes and are majorly influencing the following documents. Thus, it needs to be discussed in this section. Now the connections are ruled in section 8, whereat subsection 8.7.2 especially concentrates on axially loaded screws. Therein, point 8.7.2(1) firstly mentions different failure mechanism of such connections: (i) withdrawal, (ii) head pull-through and (iii) a so-called pull-out failure of a whole timber block with a group of screws (denoted as plug shear). Furthermore, equal to modern standards and approvals/assessments, d is denoted as the outer thread diameter and applied for determining the characteristic withdrawal capacity R_k instead of the formerly used shank diameter d_{sh} , which additionally should be less than d ; according to prEN 1995-1-1 (1999), see

$$R_k = f_{v,k} (\pi \cdot d \cdot l_{ef}) \quad \text{with} \quad f_{v,k} = \frac{f_{v,90,k}}{\sin^2 \alpha + \frac{4}{3} \cos^2 \alpha} \quad \text{and} \quad f_{v,90,k} = 1.2 \cdot 10^{-3} \cdot \rho_k^{1.5} \cdot d^{-0.2}. \quad (2.8)$$

In eq. (2.8), determination bases on $f_{v,k}$ as the characteristic withdrawal strength in N/mm², firstly considering the significant influence of α on withdrawal properties. Since no related limitations were given, prEN 1995-1-1 (1999) allowed the application of screwed connections *irrespective* their arrangement in the timber product. Furthermore, the so-called group effect, reducing the resistance of a connection with more than one fastener, is given in prEN 1995-1-1 (1999) for the first time, see

$$n_{ef} = 2 \cdot \left(\frac{n}{2} \right)^{0.8} \quad \text{for } n \geq 2, \quad (2.9)$$

with n_{ef} as the effective number of screws and n as the total number of screws acting together in a connection. Similar to the aforementioned standards, the minimum penetration depth of the threaded part of the screw, $l_{ef,min}$ (including its tip) had to be at least $4d$. Now the minimum spacings were treated separately from the ones of laterally loaded screwed connections, see Table 2.4. The therein made differentiations in dependence of α are especially worth to be pointed out. Similar to the documents discussed so far, screws with diameters > 5 mm should be pre-drilled.

- *ON EN 1995-1-1 (2006) and ON B 1995-1-1 (2006)*

ON EN 1995-1-1 (2006), as the first official version of Eurocode 5 published in Austria, is identical with the general European version EN 1995-1-1 (2004). Thus, both documents are not discussed separately. If compared to prEN 1995-1-1 (1999), some remarkable changes have been made regarding the axial

loadbearing design: (a) the screw failure in tension (including screw head tear-off) has been added to the failure modes (i) to (iii) as listed before, and (b) determining the withdrawal capacity $F_{ax,\alpha,Rk}$ had to be executed as follows:

$$F_{ax,\alpha,Rk} = n_{ef} \cdot (\pi \cdot d \cdot l_{ef})^{0.8} \cdot f_{ax,\alpha,k}, \quad f_{ax,\alpha,k} = \frac{f_{ax,k}}{\sin^2 \alpha + 1.5 \cos^2 \alpha} \text{ and } f_{ax,k} = 3.6 \cdot 10^{-3} \cdot \rho_k^{1.5}. \quad (2.10)$$

Furthermore, the method calculating the effective number of screws acting together in one connection, n_{ef} has been simplified as given in eq. (2.11):

$$n_{ef} = n^{0.9}. \quad (2.11)$$

With regard to the requirements concerning screw application, $l_{ef,min}$ (now without the tip, considered as a reduction of one d) was increased to $6d$, while the minimum spacings have been kept the same. Furthermore, the minimal diameter, where no pre-drilling was necessary, was also increased to 6 mm. Within the national appendix ON B 1995-1-1 (2006) no specifications have been made regarding axially loaded screwed connections.

- *ON EN 1995-1-1 (2009) and ON B 1995-1-1 (2009)*

As mentioned in section 2-2.1.1, ON EN 1995-1-1 (2009) together with its national appendix ON B 1995-1-1 (2009) were the first versions of Eurocode 5 exclusively ruling the construction and design of timber buildings in Austria. Both differ significantly from older versions in terms of content and volume. With regard to screwed connections, especially the amendment document EN 1995-1-1:2004/A1 (2008), published during the Austrian coexistence period (2006 – 2009) and considered in these new versions of Eurocode 5, influenced the related sections 8.7.2 and 10.4.5 of ON EN 1995-1-1 (2009) in a major way. With regard to the axial loadbearing design, buckling of screws loaded in compression (e. g. in form of reinforcement measures, see section 2-1.2), has been added to the list of failure mechanisms. Furthermore, the method $F_{ax,\alpha,Rk}$ is determined, has been changed remarkably:

$$F_{ax,\alpha,Rk} = \frac{n_{ef} \cdot f_{ax,k} \cdot d \cdot l_{ef} \cdot k_d}{1.2 \cdot \cos^2 \alpha + \sin^2 \alpha} \text{ with } f_{ax,k} = 0.52 \cdot d^{-0.5} \cdot l_{ef}^{-0.1} \cdot \rho_k^{0.8} \text{ and } k_d = \min \left\{ \frac{d}{8}, 1 \right\}. \quad (2.12)$$

While *new* parameters, such as k_d as a correction factor for diameters less than 8 mm, are rare, the regression function determining $f_{ax,k}$ (the value now included the circle constant π , but again denoted as “strength”), as well as the term considering the influence of α on withdrawal capacity were significantly modified. In clear contrast to eq. (2.8), given in prEN 1995-1-1 (1999), a lower limit of 30° between screw axis and grain direction was established.

In terms of the screw application the minimum spacings have been increased by far (see Table 2.4) while the requirement of $l_{ef,min} = 6 d$, equal to the minimal thread length according to ON EN 14592 (2009), has been adopted. In addition, new criteria were introduced: on the one hand, a minimum thickness t of the timber product, where the screw is inserted into, was set to $12 d$ and on the other hand the following requirements on screw geometry were defined in accordance with ON EN 14592 (2009):

- $6 \text{ mm} \leq d \leq 12 \text{ mm}$, and
- $0.60 \leq d_c / d \leq 0.75$,

where d_c is the inner thread diameter of the screw. The latter mentioned standard ON EN 14592 (2009) as well as its currently valid replacement document ON EN 14592 (2012) influenced the test procedure of several screw design parameters and CE-labelling of the product itself in a major way, and are thus separately discussed in section 2-2.4. In those cases when these geometrical conditions are not fulfilled, the characteristic withdrawal strength $f_{ax,k}$ in eq. (2.12) has to be experimentally determined according to ON EN 14592 (2009). This, together with eq. (2.12), multiplied by the factor $(\rho_k / \rho_a)^{0.8}$, where ρ_a considers the density of the timber material used for these tests.

Table 2.4: Minimum spacings of screws according to Eurocode 5 series, beginning with prEN 1995-1-1 (1999); notation according to ON EN 1995-1-1 (2015)

standard		a_1	a_2	$a_{1,CG}$	$a_{2,CG}$
prEN 1995-1-1 (1999), ON EN 1995-1-1 (2006)	at right angle to the grain	$4 d$	$4 d$	$4 d$	$4 d$
	in end grain face		$4 d$		$2.5 d$
ON EN 1995-1-1 (2009) to ON EN 1995-1-1 (2015)		$7 d$	$5 d$	$10 d$	$4 d$

With regard to section 10.4.5 in ON EN 1995-1-1 (2009), the pre-drilling requirement for screws with $d > 6 \text{ mm}$ (in softwood) did not concern the modern self-tapping timber screws any more, while the hardwood application of screws necessitates this procedure in principle.

In contrast to older versions, the Austrian appendix ON B 1995-1-1 (2009) included comments concerning both relevant sections, 8.7 and 10.4.5 in ON EN 1995-1-1 (2009). Therein, the application and design of screws, according to their European Technical Approvals (ETAs), is explicitly recommended in cases, where the regulations deviate from those given in ON EN 14592 (2009). It should be pointed out, that on the issue date of these documents no ETA concerning self-tapping screws was existing, c. f. section 2-2.5.

- *ON EN 1995-1-1 (2014) and ON B 1995-1-1 (2014)*

Both documents were published on November 15, 2014. While the regulations concerning the screwed connections have not been changed in the EN part, ON B 1995-1-1 (2014) includes several related national specifications. The already mentioned recommendation, designing screws according to ETAs as alternative to the regulations given in section 8.7, has been adopted. Furthermore, a new Annex K, firstly including design rules for CLT as a structural building material, has been provided. Due to its cross-layered inhomogeneous lay-up, the regulations regarding the position of screws and their design in ON EN 1995-1-1 (2014), section 8.7.2 are not sufficient to cover all application possibilities in CLT side and narrow faces (definition shown in Figure 2.12). Consequently, Annex K specifies this form of application as follows: In contrast to ON EN 1995-1-1 (2014), $l_{ef,min}$ is generally reduced to $4d$. When positioned in the CLT panels' narrow faces, section K.8.7.2 introduces three further geometrical requirements, depending on the outer thread diameter to be fulfilled; namely $t_{CLT,min}$ as minimal panel thickness, $t_{l,min}$ as minimal layer thickness, where the screw is placed into, and l_{min} as minimal insertion length, see Table 2.5. Furthermore, the lower limits for d , as well as the minimum spacings between two fasteners with respect to the panel's ends and edges – indices “3” and “4” instead of “1” and “2” according to ON EN 1995-1-1 (2014) – both again depending on the screw position, are outlined. The comparatively higher d -value for the narrow face application is caused by the possibility of gaps, which are currently limited to $w_{gap} \leq 6$ mm, c. f. Brandner (2013a), between two wooden boards in one panel layer, significantly decreasing the withdrawal resistance if the screw is placed into, see Grabner (2013). While the withdrawal capacity $F_{ax,\alpha,Rk}$ of screws in CLT side faces may be determined according to eq. (2.12), the narrow face application again requires a special treatment:

$$F_{ax,Rk} = 20 \cdot d^{0.8} \cdot l_{ef}^{0.9}. \quad (2.13)$$

As a consequence of different axis-to-grain angles α in CLT narrow faces, ON B 1995-1-1 (2014) suggests to situate the screws in layers with $\alpha = 90^\circ$, if possible. If not, only partially threaded screws should be used, including the boundary condition

$$l_{min} = 3d + l_{ef}. \quad (2.14)$$

In case of $\alpha \geq 45^\circ$ and screws are arranged in just one layer, $F_{ax,Rk}$ determined according to eq. (2.13) can be increased by multiplying it with the factor 1.25.

Table 2.5: Minimum spacings and other geometrical requirements of screws in CLT side and narrow faces; according to ON B 1995-1-1 (2014)

position	a_1	a_2	$a_{3,c}$	$a_{4,c}$	$t_{CLT,min}$	$t_{l,min}$	l_{min}	d_{min}
side face	$4 d$	$2.5 d$	$6 d$	$2.5 d$				6 mm
narrow face	$10 d$	$3 d$	$7 d$	$5 d$	$10 d$	$d < 8 \text{ mm}: 3 d$ $d \geq 8 \text{ mm}: 2 d$	$10 d$	8 mm

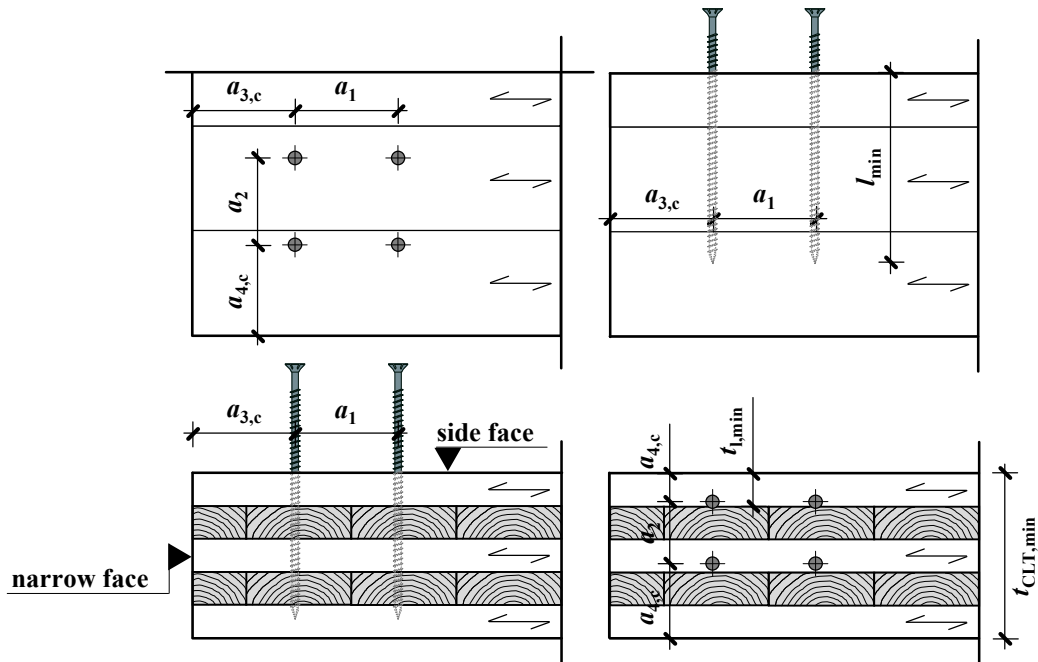


Figure 2.12: Minimum distances of predominately axially loaded screws in CLT side and narrow faces; according to ON B 1995-1-1 (2014)

Finally, and as a consequence of the linear (one dimensional) character of typical CLT connections, section K.10 in ON B 1995-1-1 (2014) also provides different kinds of maximum distances $e_{max,i}$ between two fasteners/connectors to be kept. With regard to screws, they are

- line connection CLT with CLT: $e_{max} = 500 \text{ mm}$
- line connection CLT with GLT: $e_{max} = 500 \text{ mm}$
- line connection CLT with steel beams: $e_{max} = 750 \text{ mm}$.

The outer thread diameter d should be at least 8 mm for loadbearing CLT connections, excluding the aforementioned $d = 6 \text{ mm}$ side face criteria, being only applicable for stepped joints. Furthermore l_{screw} as the total length of the screw, should be at least 1.5 times the thickness of the CLT panel where its head is placed into. In case of stepped joints, l_{screw} is limited to $\geq 0.8 t_{CLT}$.

- *ON EN 1995-1-1 (2015) and ON B 1995-1-1 (2015)*

The current Austrian version of Eurocode 5 was issued on June 16, 2015. Regulations concerning axially loaded self-tapping screws were majorily adopted from the forerunner documents. Sole exception is the minimum layer thickness requirement expressed in Table 2.5, which was corrected as follows:

$$t_{l,\min} = \begin{cases} 3d & \text{for } d > 8 \text{ mm} \\ 2d & \text{for } d \leq 8 \text{ mm} \end{cases} \quad (2.15)$$

2-2.2 Standardisation in Germany

2-2.2.1 General comments

Similar to Austrian history, regarding the development of timber design standards introduced in section 2-2.1.1, there are also three different periods of German standardisation worth to be separately discussed. Between 1990 and 2004, national DIN standards DIN 1052 P1 (1988) (design and calculation), DIN 1052 P2 (1988) (mechanical joints) and DIN 1052 P3 (1988) (buildings constructed from timber panels), including a corrigendum published in 1996, were provided by the German Institute for Standardisation in order to design timber structures.

Equal to ON B 4100-2 series, these documents ruled the design process by a deterministic safety concept. Unlike Austria, where the safety concept in ON B 4100-2 has never been changed within the document's validity period, the German replacement document DIN 1052 (2004) already contained a semi-probabilistic safety concept comparable to Eurocode 5. Between 2004 and 2010, DIN 1052 (2004), later DIN 1052 (2008) and DIN 1052 C1 (2010) (corrigendum) had to be solely considered for design purposes. The German coexistence period, regulated by the so-called Model List of Technical Building Rules (MLTB), c. f. IS-ARGEBAU (2014), started in December 2011 and lasted till July 1, 2012 (December 31, 2013 in the countries Hesse and Bavaria). Within this time period, DIN EN 1995-1-1 (2010), together with its national appendix DIN EN 1995-1-1/NA (2010) as the first official German Eurocode 5 versions, were applicable in parallel to DIN 1052.

Since January 1, 2014 at latest, the European standardisation in form of DIN EN 1995-1-1 (2010) and the current national version DIN EN 1995-1-1/NA (2013) are valid. In strict contrast to Austrian conditions, the national standard DIN 1052-10 (2012) still supplements both Eurocode 5 documents in terms of specific design situations.

2-2.2.2 Regulations in DIN 1052 series

This subsection includes a discussion of the documents DIN 1052 P2 (1988), DIN 1052 (2004), DIN 1052 (2008) and DIN 1052 C1 (2010).

- *DIN 1052 P2 (1988)*

Published in 1988 the DIN 1052 document contained three parts overall, each treating specific topics, such as mechanical fasteners specified in DIN 1052 P2 (1988). Therein, section 9 rules the design of screwed connections, confined to the exclusive application of pre-drilled traditional wood screws, according to DIN 96 (1986), DIN 97 (1986) and DIN 571 (1986), in subsection 9.1. The permissible bearing capacity in terms of axial loading, as well as the boundary conditions concerning the minimum shank diameter, effective length and minimum spacings are equal to ON B 4100-2 (1997), as discussed in 2-2.1.2, see eq. (2.6) and Table 2.1. Furthermore, general notes, given in section 3.4 of DIN 1052 P2 (1988), forbid the arrangement of screws as a loadbearing connection in end-grain joints. There are no additional comments limiting α .

- *DIN 1052 (2004)*

As already mentioned in section 2-2.2.1, DIN 1052 (2004) as a replacement document of DIN 1052 P2 (1988), regarding the design of fasteners, already contained a semi-probabilistic safety concept. Furthermore, this document explicitly mentions the application of *non-predrilled* (except ρ_k exceeds 500 kg/m^3 and/or Douglas fir is used) self-tapping screws within section 12.6 as an alternative to traditional wood screws with threads according to DIN 7998 (1975). As a consequence of product characteristics, deviating from the mentioned standards related, predominately in terms of geometry, the suitability of self-tapping screws as loadbearing fasteners for timber engineered structures had to be verified in national technical approvals (NTAs, c. f. section 2-2.4). $R_{ax,k}$, as the withdrawal screw capacity (in softwood), had to be determined as minimum of both failure mechanisms “withdrawal” and “head pull-through”, see

$$R_{ax,k} = \min \left\{ \frac{f_{1,k} \cdot d \cdot l_{ef}}{\sin^2 \alpha + \frac{4}{3} \cos^2 \alpha}; f_{2,k} \cdot d_{head}^2 \right\}. \quad (2.16)$$

Hereby, $f_{1,k}$ and $f_{2,k}$ are denoted as the characteristic withdrawal (including π) and head pull-through parameters, both in N/mm^2 , divided into three loadbearing classes 1, 2, 3 and A, B, C, see Table 2.6. Furthermore, d_{head} is the diameter of the screw head or the washer (in original form with the index k) and l_{ef} the inserted threaded part of the screw including its tip. For traditional wood screws the loadbearing class 2A may have been applied, while in terms of self-tapping screws, the related values published in NTAs had to be used. In clear contrast to the similar formulation for determining $R_{ax,k}$ according to prEN 1995-1-1 (1999), given in eq. (2.8), α is limited to $45^\circ \leq \alpha \leq 90^\circ$. In case of “steel failure in tension”,

also mentioned as mechanism to be verified, section 12.8.2(7) regulates the determination of $R_{ax,k}$ for traditional wood screws, see eq. (2.16).

$$R_{ax,k} = 75 \cdot \pi \cdot (0.9 \cdot d)^2, \quad (2.17)$$

which bases on a steel tensile strength $f_{u,k}$ of 300 N/mm² far below that of self-tapping screws, again given in the related NTA. As a consequence that no related regulations are given in DIN 1052 (2004) and deviating from Eurocode 5 series, beginning with prEN 1995-1-1 (1999), the effective number of fasteners in one connection, n_{ef} was set equal to its total number n .

Table 2.6: Classification of screw strength parameters according to DIN 1052 (2004)

loadbearing class	$f_{1,k}$	loadbearing class	$f_{2,k}$
1	$60 \cdot 10^{-6} \cdot \rho_k^2$	A	$60 \cdot 10^{-6} \cdot \rho_k^2$
2	$70 \cdot 10^{-6} \cdot \rho_k^2$	B	$80 \cdot 10^{-6} \cdot \rho_k^2$
3	$80 \cdot 10^{-6} \cdot \rho_k^2$	C	$100 \cdot 10^{-6} \cdot \rho_k^2$

With regard to the minimum spacings between two screws and to the timber product's ends and edges, DIN 1052 (2004), section 12.8.2(8) regulates their application irrespective of the angle between load and screw axis. Furthermore, similar to ON ENV 1995-1-1 (1992) and ON ENV 1995-1-1 (1995) (c. f. Table 2.2 and Table 2.3), but without the differentiation in dependence of d smaller or bigger than 8 mm, screws should be treated equally to nails, see Table 2.7.

Table 2.7: Minimum spacings of screws according to DIN 1052 (2004)

minimum spacings	without pre-drilling		with pre-drilling
	$\rho_k \leq 420 \text{ kg/m}^3$	$420 \leq \rho_k \leq 500 \text{ kg/m}^3$	
a_1	$5 d$	$7 d$	$3 d$
a_2	$5 d$	$7 d$	$3 d$
$a_{1,CG}$	$d < 5 \text{ mm}: 7 d$ $d \geq 5 \text{ mm}: 10 d$	$15 d$	$7 d$
$a_{2,CG}$	$5 d$	$7 d$	$3 d$

Note: in Table 2.7, each cos- or sin-components increasing the specific distance a_i are neglected.

Similar to ON EN 1995-1-1 (2009) and to avoid splitting failure, a minimum thickness t of the timber product applied was introduced and determined as follows:

Timber in general:
$$t = \max \left\{ 14 \cdot d; (13 \cdot d - 30) \cdot \frac{\rho_k}{200} \right\}. \quad (2.18)$$

Pine softwood and components made of other softwoods if $a_{2,CG} \geq 10 d$ (14 d) and $\rho_k \leq 420 \text{ kg/m}^3$ (500 kg/m^3):

$$t = \max \left\{ 7 \cdot d; (13 \cdot d - 30) \cdot \frac{\rho_k}{400} \right\}. \quad (2.19)$$

- *DIN 1052 (2008) and DIN 1052 C1 (2010)*

Compared to the previously discussed DIN 1052 (2004), no remarkable changes, regarding the design and application of axially loaded self-tapping screws, have been made in DIN 1052 (2008) and later in DIN 1052 C1 (2010). The only exception is found in the diameter used for determining the steel tensile capacity according to eq. (2.17). Therein, the product $0.9 \cdot d$ has been replaced by the inner thread diameter d_c .

2-2.2.3 Regulations in DIN EN 1995-1-1 series

In addition to a discussion of DIN EN 1995-1-1 (2010), together with DIN EN 1995-1-1/NA (2010) and subsequently DIN EN 1995-1-1/NA (2013) the first official version of Eurocode 5 applied in Germany, this section also includes some short comments on DIN V ENV 1995-1-1 (1994) and DIN V ENV 1995-1-1 NAD (1995). This, due to the fact, that both latter mentioned standards are referred in several NTAs as an alternative to the also valid version of DIN 1052.

- *DIN V ENV 1995-1-1 (1994) and DIN V ENV 1995-1-1 NAD (1995)*

While DIN V ENV 1995-1-1 (1994) is widely identical with the Austrian equivalent ON ENV 1995-1-1 (1995), discussed in section 2-2.1.3, the additionally published national application document DIN V ENV 1995-1-1 NAD (1995) contains some supplements regarding the specific design situations. In case of screwed connections, equal to DIN 1052 P2 (1988), the screw geometries applied have to coincide with the product standards mentioned in section 2-2.2.2. Furthermore, the characteristic steel tensile strength $f_{u,k}$ was set to 300 N/mm^2 , when introducing eq. (2.17) as additional failure mechanism to be considered for design purposes. It has to be mentioned, that the characteristic properties, determined by experiments and provided for the design process, had to be regulated in accordance to the responsible building authority.

- *DIN EN 1995-1-1 (2010), DIN EN 1995-1-1/NA (2010), DIN EN 1995-1-1/NA (2013) and DIN 1052-10 (2012)*

The document DIN EN 1995-1-1 (2010), currently applied in Germany for designing screwed connections, is generally equal to the latest Austrian EN document discussed in section 2-2.1.3. Furthermore, both national appendices, published between 2010 and nowadays, do not include any deviating modifications concerning the axial loadbearing design and application of self-tapping screws.

This also concerns supplemental information given in DIN 1052-10 (2012), wherein no self-tapping screw related specifics were found.

2-2.3 Standardisation in Switzerland

2-2.3.1 General comments

In contrast to the situation in Austria and Germany (discussed in sections 2-2.1 and 2-2.2), the Swiss standardisation predominately contained and contains exclusively applied national documents. In terms of structural timber design, again two main periods with different safety concepts are worth to be pointed out. Between 1992 and 2003 SIA 164 (1992), containing a deterministic safety concept, was provided for timber design purposes. With the issue date of SIA 265 (2003) on March 2003, the concerning situation has been changed and a semi-probabilistic safety concept, comparable to Eurocode series, has been introduced in Switzerland. Since the country (or better the Swiss Association for Standardisation, SNV) is a member of the European Committee for Standardisation (CEN), it confirmed adopting Eurocode 5 as a timber structures' related regulation, see also SIA (2015). Following the principle of Eurocode standardisation, the national appendices, including specific federal regulations, should supplement the main documents in order to provide a reasonable background for practical application. On May 1, 2014, SN EN 1995-1-1/NA (2014) as the first national Annex of Eurocode 5, containing "Nationally Determined Parameters (NDP)", has been published in Switzerland, c. f. Fischer (2015). Thus, it is assumed that both standards SIA 265 (2012) replacing SIA 265 (2003) as well as Eurocode 5 are currently applicable regarding the design of timber structures.

2-2.3.2 Regulations in SIA 164 (1992)

The comments, given in section 3.23.5 of SIA 164 (1992), concerning application and design of axially loaded screwed connections, are equal to those found in ON B 4100-2 (1981), regarding the determination of $N_{z,per}$ (see eq. (2.4)), and to those given in DIN 1052 P2 (1988), where the screw geometries are ruled in accordance to certain product standards in form of VSM 12 800 (1942), VSM 12 801 (1942), VSM 12 802 (1942) and VSM 12 803 (1942). Deviations from Austrian and German documents are seen in the determination of permissible resistances by tests (see eq. (2.20)) and in specific boundary conditions: neither a minimum (shank) diameter nor a limit depending on axis to grain angles (e. g. the prohibition of end-grain joints as loadbearing connections) are found in SIA 164 (1992). The minimum spacings were ruled equally to pre-drilled nails, see Table 2.8.

$$R_{per} = \begin{cases} \frac{R_m}{3.00} & R_{min} \geq 0.75 R_m \\ \frac{R_{min}}{2.25} & R_{min} < 0.75 R_m \end{cases} \quad (2.20)$$

Table 2.8: Minimum spacings of screws according to SIA 164 (1992); notation according to ON EN 1995-1-1 (2015)

standard	a_1	a_2	$a_{1,CG}$	$a_{2,CG}$
SIA 164 (1992)	$7 d_{sh}$	$4 d_{sh}$	$7 d_{sh}$	$4 d_{sh}$

2-2.3.3 Regulations in SIA 265 series

This subsection contains a discussion of the documents SIA 265 (2003) and SIA 265 (2012), together with their supplements for wood based products SIA 265/1 (2003) and SIA 265/1 (2009); the corrigenda SIA 265-C1 (2008) and SIA 265/1-C1 (2012) are also considered.

- SIA 265 (2003) and SIA 265/1 (2003)

In addition to modifications regarding the safety concept applied (see section 2-2.3.1), essentially influencing the general design process, significant changes compared to SIA 164 (1992) have also been made in terms of screwed connections. Similar to DIN 1052 (2004), SIA 265 (2003), section 6.5.1 explicitly denotes “self-cutting” screws (equal to self-tapping; pre-drilling was ruled according to technical regulations provided by screw manufacturers) as an alternative to traditional wood screws and also defines them by $d_c \geq 0.6 d$ (d was originally denoted as d_a), providing design equations in case of $4 \text{ mm} \leq d \leq 10 \text{ mm}$ (for traditional wood screws: $4 \text{ mm} \leq d_{sh} \leq 16 \text{ mm}$ and $f_{u,min} = 800 \text{ N/mm}^2$). No further comments about the necessity of technical approvals for self-tapping screws could be found.

With regard to axial loadbearing design, regulations given in SIA 265 (2003), section 6.5.3 correspond to different Eurocode 5 versions discussed in section 2-2.1.3: The *design* (instead of *characteristic* as given in Eurocode 5) withdrawal capacity had to be determined according to eq. (2.21), which is quite similar to ON EN 1995-1-1 (2006), see

$$R_{ax,d} = n^{0.9} (\pi \cdot d \cdot l_{ef}) f_{v,\alpha,d}, \quad f_{v,\alpha,d} = \frac{f_{v,90,d}}{\sin^2 \alpha + 1.5 \cos^2 \alpha} \quad \text{and} \quad f_{v,90,d} = 30 \cdot 10^{-3} (\pi \cdot d \cdot l_{ef})^{-0.2} \rho_k, \quad (2.21)$$

where $f_{v,90,d}$ is denoted as shear strength against withdrawal (at $\alpha = 90^\circ$), also found in prEN 1995-1-1 (1999). Furthermore, SIA 265 (2003) contains the same regulations with respect to minimum spacings as given in ON EN 1995-1-1 (2006), see Table 2.4, while specifications regarding the minimum insertion length l_{min} (originally denoted as l) were treated more accurately:

- traditional wood screws: $l_{min} = 6 d$
- self-tapping screws: $l_{min} = 8 d$
- self-tapping screws (exclusively applied in end-grain joints): $l_{min} = 100 \text{ mm}$

The latter mentioned form of application was only allowed for moisture classes 1 and 2 (similar to service class definition given in Eurocode 5). Finally, failure mechanisms, which had to be verified, are again identical with the comments given in ON EN 1995-1-1 (2006). Within the supplementary document SIA 265/1 (2003), no specifications regarding screwed connections are found.

- *SIA 265 (2012) and SIA 265/1 (2009)*

On January 1, 2012 the latest and currently valid issue of SIA 265 (2012) has been published in Switzerland. In contrast to its forerunner document, SIA 265 (2012), section 6.5.1 clearly differs between (i) traditional wood screws and (ii) modern self-tapping timber screws in terms of definition and application: in case (i), thread geometries are regulated in accordance to DIN 7998 (1975), whereby $d_{sh} = \max[d]$. Furthermore, pre-drilling is mandatory. In case (ii), self-tapping screws (fully and partially threaded) are defined by $d_{sh} < \max[d]$. Both pre-drilling (where $d_{pD} = d_c$) and non-pre-drilling is possible, except for characteristic densities $\rho_k > 420 \text{ kg/m}^3$ necessitating the prior mentioned form of preparation. For both different types of screws, SN EN 14592+A1 (2012) is referred as a basis document. This also concerns the geometrical limits in terms of the outer thread diameter and its relationship to the inner thread diameter, c. f. section 2-2.1.3.

With regard to screwed connections applied as end-grain joints ($\alpha = 0^\circ$), regulations given in SIA 265 (2003) have been supplemented by $l_{ef} \text{ (tip included)} \geq 8d$ and the condition, that no cracks are allowed in the timber member while failure mechanisms, as well as minimal spacings and insertion depths, are ruled according to ON EN 1995-1-1 (2015) now, see Table 2.4. A modification of the latter mentioned geometrical requirements, deviating from those given in SIA 265 (2003), was done in SIA 265-C1 (2008) and adopted in SIA 265 (2012). In addition, SIA 265 (2012) includes the possibility of decreasing a_2 to $3d$ in cases, screws are pre-drilled and $R_{ax,d}$ is reduced by

$$k_{red} = \left(\frac{a_2}{5d} \right)^{0.35}, \quad (2.22)$$

Focusing on the withdrawal resistance, the general determination of $R_{ax,d}$ has not been changed, compared to SIA 265 (2003), while the prior mentioned harmonisation process to Eurocode 5 significantly influenced the procedure calculating the *design* shear strength $f_{v,\alpha,d}$ as a basis input value, see

$$f_{v,\alpha,d} = \begin{cases} \frac{k_\alpha \cdot f_{ax,k}}{\pi \cdot (\sin^2 \alpha + 1.2 \cdot \cos^2 \alpha)} & \alpha \geq 30^\circ \\ 20 \cdot 10^{-3} \cdot [\pi \cdot d \cdot (l_{ef} - d)]^{-0.2} \cdot \rho_k & 0^\circ \leq \alpha < 30^\circ \end{cases}, \quad (2.23)$$

and

$$f_{ax,k} = 0.52 \cdot d^{-0.5} \cdot l_{ef}^{-0.1} \cdot \rho_k^{0.8} \cdot k_d, \quad (2.24)$$

where $k_\alpha (= 0.62)$ is a factor, converting the *characteristic* value given in Eurocode 5 to the *design* value used in SIA 265 (2012), and $f_{ax,k}$ is the characteristic withdrawal strength determined according to Eurocode 5. With respect to eq. (2.23), the size of α designates the way $f_{v,\alpha,d}$ has to be determined. In case of $\alpha \geq 30^\circ$, the Eurocode 5 procedure, denoted in ON EN 1995-1-1 (2009), is applied. In case of lower α , SIA 265 (2003) formula (see eq. (2.21)) is used for setting α constantly to zero. Thereby noticed irritations, predominately caused by different approaches regarding the way the screw tip is considered (at $\alpha \geq 30^\circ$ tip is included, at $\alpha < 30^\circ$ tip is excluded) have already been discussed in Hübner (2013a). Within the supplementary document SIA 265/1 (2009), again no specifications regarding the axially loaded screwed connections are found. Thereby the only exception is the modification, provided in SIA 265/1-C1 (2012), that in cases, when the timber members are connected with wood based materials, traditional wood screws with threads according to DIN 7998 (1975) are not allowed.

2-2.3.4 Short comments on SN EN 1995-1-1 series

Specific regulations, concerning the design and application of axially loaded self-tapping screws, were not found in SN EN 1995-1-1/NA (2014) as the first (and still valid) Swiss national Annex of Eurocode 5. Thus, the related content given in the European document can be applied without any constraints.

2-2.4 Judicial background from 1990 – 2015

2-2.4.1 Introduction

This section deals with the context between the D-A-CH standards, discussed in section 2-2.1 to 2-2.3, and both different types of national and European Technical Approvals (Assessments, ETAs) regarding the application and design of axially loaded screwed connections. Not only the relationship between those types of specifications (standards and approvals), but also the judicial background of screw application in general is influenced by national, European and international guidelines, regulations and laws. Consequently, these legal documents and their impact on self-tapping screws' design process in D-A-CH countries are also explained and discussed.

2-2.4.2 European Construction Products Directive

In order to support the free movement of goods, produced by the construction industry within the European Economic Area (EEA) in form of an easily accessible and transparent internal market, the European Economic Community (EEC) published the council directive (89/106/EEC) on February 11, 1989, c. f. European Union (1989). Doing so, various kinds of *national* requirements, which are subjected to provisions, regulations or administrative actions – directly influencing the nature of construction products – should be replaced by *harmonised* technical specifications (in order of relevance: product

standards, European Technical Approvals and non-harmonised documents recognized at Community level). They base on and include essential requirements ruled in so-called interpretative documents, e. g. in Austria the OIB guidelines, c. f. OIB (2015c), related products have to fulfil (in major cases):

- mechanical resistance and stability
- safety in case of fire
- hygiene, health and the environment
- safety in use
- protection against noise
- energy economy and heat retention

The construction products (e. g. self-tapping screws), performing in accordance to these technical specifications, are identified as “fit for use”, enabling free movement and use within the EEA and without any national restrictions. For a better recognition, they are consequently labelled by the EC-mark (better known as CE label). In order to obtain the CE labelling for a construction product, conformity to the aforementioned harmonised specifications has to be declared by an approved certification body or by the manufacturer itself. Details concerning the conformity attestation and surveillance during the production can be found in European Union (1989).

Back to product standards and ETAs denoted as technical specifications. The overall aim of the document is to regulate the CE labelled construction products according to product standards such as ON EN 14592 (2012) for self-tapping screws. In case (a), product standards are not available and cannot be produced or foreseen within a reasonable period of time or (b), products substantially deviate from these standards, the fitness for their use should be proved by ETAs issued for a five-year period with an option for extension; c. f. European Union (1989). These approvals base on investigations and (laboratory) tests being regulated by the aforementioned interpretative documents and so-called European Technical Approval Guidelines (ETAGs), which were published for this reason. If ETAGs for the specific purpose do not exist (this was the situation for self-tapping screws), an individual ETA can be issued in accordance to the relevant essential requirements and interpretative documents. Furthermore, the assessment of the product will be consensually adopted by the approved certification bodies in form of Common Understanding of Assessment Procedure (CUAP) documents; see also Jöbstl (2010). In case of self-tapping screws, CUAP 06.03/08 (2010), discussed in section 2-2.4.5, was published to regulate this approval process.

2-2.4.3 European Construction Products Regulation

On April 4, 2011 and twenty-two years after publishing the council directive (89/106/EEC), the document has been replaced by regulation (EU) No 305/2011, considering a transitional period until July 1, 2013, see European Union (2011). By the latter mentioned date at the latest, regulation (EU) No 305/2011

repealed the formerly discussed directive in order to simplify and precise the valid conditions. Furthermore, it aimed to improve transparency and effectualness of the existing measures associated with making construction products being available on the market. Compared to the European Construction Products Directive significant modifications are as follows:

Firstly, the essential requirements, discussed in section 2-2.4.2, have been renamed in “basic requirements” and expanded by a seventh clause to be considered and denoted as “sustainable use of natural resources”.

Secondly, CE labelling should exclusively indicate the product’s conformity with its declared performance and compliance with requirements related to the Union harmonisation legislation.

Thirdly, products, covered by a harmonised specification (product standard or European Technical Assessment, again abbreviated as ETA) should own a declaration of performance (DoP) fulfilling specifically defined essential characteristics related to the mentioned basic requirements. In cases, when the harmonised product standards may not sufficiently enable a declaration of performance (the product does not fall within the standard’s scope or one of the standard’s assessment methods is inappropriate or even missing for at least one essential characteristic), the European Technical Assessments, which replace the aforementioned European Technical Approvals (note: still valid Approvals can be used as Assessments), have to be issued for related products.

Finally, the ETA’s compilation process, graphically explained in Figure 2.13, is covered by European Assessment documents (EADs) replacing the formerly used ETAGs and CUAPs.

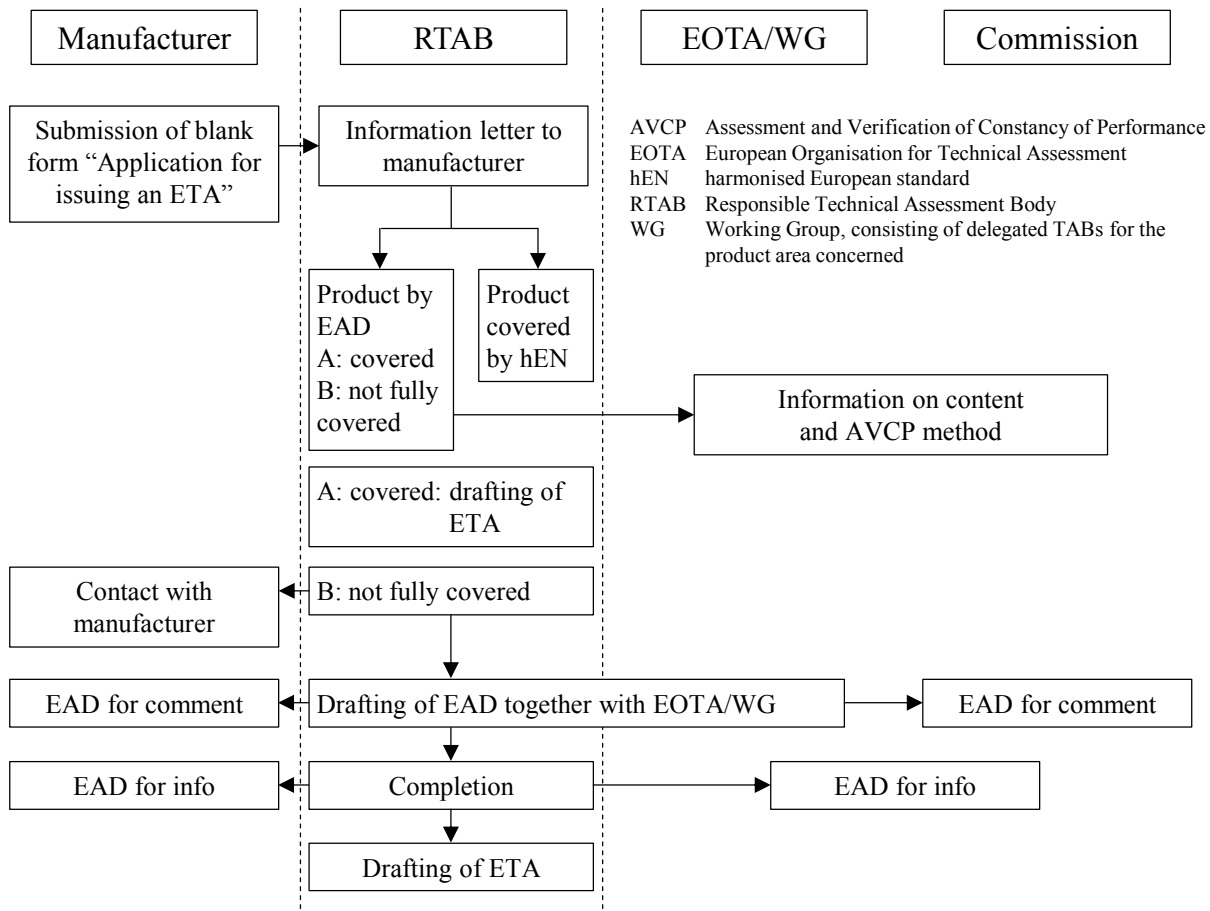


Figure 2.13: Procedure for drafting a European Assessment Document, according to DIBt (2015c)

2-2.4.4 Harmonised product standard EN 14592 for dowel-type fasteners

ON EN 14592 (2009), as well as its currently valid replacement document ON EN 14592 (2012), are defined as product standards for dowel-type fasteners used in timber structures, thus also including traditional wood and modern self-tapping timber screws. As mentioned in section 2-2.1.3, they influence the application and design process of screwed connections, given in design standards such as Eurocode 5. In addition, according to European Union (1989), both documents have been listed in European Union (2009) and European Union (2013) respectively. Consequently, they are harmonised specifications, CE-labelled dowel-type fasteners traded in Europe and used in timber structures have to conform. Covering the essential requirements explained in section 2-2.4.2, section 6 of both ON EN 14592 (2009) and ON EN 14592 (2012) provides specific minimum demands on those fasteners regarding (i) the (basis) material, (ii) the geometry ($2.4 \text{ mm} \leq d \leq 24 \text{ mm}$, $0.60 \leq d_c / d \leq 0.90$), (iii) the mechanical strength and stiffness and (iv) the protection against corrosion. In order to verify the product's conformity with the harmonised standard, enabling its CE-labelling and fitness-for-use, both Initial Type Testing (ITT) and Factory Production Control (FPC) procedures have to be executed. Regarding ITT, requirements (i) to (iv), according to section 6 of these standards, have to be controlled by an approved laboratory.

Focusing on self-tapping screws, the requirements (ii) to (iv) can easily be fulfilled, while ON EN 14592 (2009) regulated the basis material (i), they have to be produced according to ON EN 10016-1 (1995), ON EN 10016-2 (1995), ON EN 10016-3 (1995), ON EN 10016-4 (1995) and ON EN 10083-2 (2006) for carbon steels, as well as ON EN 10083-1 (2006) and ON EN 10088-2 (2005) for stainless steels. None of these standards includes basis material, sufficiently enabling the production of modern self-tapping timber screws, especially with regard to their tensile strengths above 1,000 N/mm², caused by steel hardening, c. f. Jöbstl (2010). Consequently, self-tapping screws substantially deviated from ON EN 14592 (2009) and necessitated the proof of fitness-for-use according to European Technical Approvals, basing on CUAP 06.03/08 (2010), c. f. section 2-2.4.5.

On March 1, 2013, ON EN 14592 (2012) obtained the official denotation as a harmonised standard in accordance to the council directive (89/106/EEC); see European Union (2013). With regard to screw production, two essential points were modified – if compared to ON EN 14592 (2009): first, the minimum thread length has been reduced to 4 *d*. Second, the requirement (i) concerning the basis material was modified, including the clause that steel grades, which are not listed in the mentioned standards are also suitable for screw production – if the mechanical product characteristics (to be verified in the frame of ITT) correspond to the standards.

The latter mentioned flexibility in choosing different steel grades enabled the proof of fitness-for-use according to the council directive (89/106/EEC) (for the timeframe between March 1 to July 1, 2013), as well as the declaration of performance according to regulation (EU) No 305/2011 on the basis of ON EN 14592 (2012). Nevertheless, 27 European Technical Approvals, concerning self-tapping screws, have been issued within the mentioned timeframe, see OIB (2015b). The reason therefore can be seen in the assessment method determining the fastener's stiffness $K_{ser,ax}$ (affecting basis requirement “mechanical resistance and stability”), not declared in ON EN 14592 (2012), which may disables the sufficient assessment of self-tapping screws. Furthermore, an EAD offers the favourable opportunity to define and assess certain characteristics related to screw application deviating from Eurocode 5, such as the necessity of pre-drilling (maximum density without pre-drilling, specific values for d_{PD}) or minimum spacings between two screws and the timber member's end and edge distances.

2-2.4.5 Common Understanding of Assessment Procedure for self-tapping screws

Due to the circumstance, that no ETAG existed for self-tapping screws, CUAP 06.03/08 (2010) has been issued in December 2010 and served as a guideline for the development of European Technical Approvals in accordance to the council directive (89/106/EEC) until the end of the transition period on July 1, 2013. All in all 65 ETAs related to self-tapping screws, according to this guideline, have been published in this timeframe; c. f. OIB (2015b). Especially in comparison with ON EN 14592 (2009), CUAP 06.03/08 (2010) enables more flexibility with respect to fastener design ($0.50 \leq d_c / d \leq 0.90$) and steel material

used for screw production. Furthermore, the document provides assessment methods of tensile yield strength f_y and axial stiffness, which are missing in EN 14592, as well as additional regulations concerning minimum spacings and timber thickness. The latter may decrease corresponding values currently given in ON EN 1995-1-1 (2015) – if positively evaluated.

2-2.4.6 European Assessment Document (EAD) for self-tapping screws

After a comparatively long time period, within manufacturers could only declare their screw product's performance according to ON EN 14592 (2012), EAD 130118-00-0603 (2016) as the assessment document for “screws for use in timber constructions” was issued on April 7, 2016. Even though several specific regulations regarding the determination of the fasteners' main mechanical properties were modified, content of EAD 130118-00-0603 (2016) is quite comparable to that of CUAP 06.03/08 (2010). The probably most significant change worth pointing out in this context concerns the lower limit of l_{ef} , which now depends on the axis-to-grain angle applied, see eq. (2.25) and Figure 2.14.

$$l_{ef} = \min \left\{ \begin{array}{l} 4d \\ \sin \alpha \cdot 20d \end{array} \right. \quad (2.25)$$

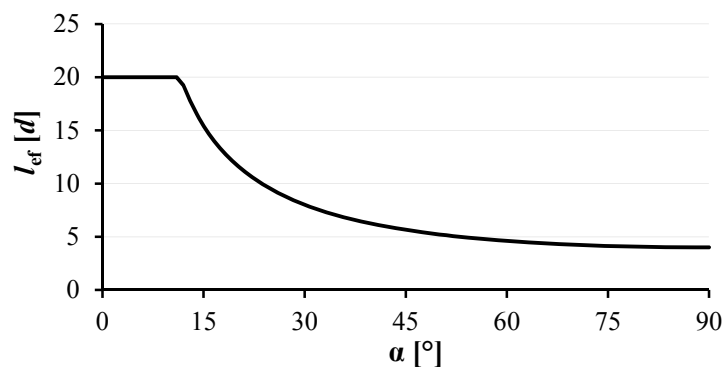


Figure 2.14: Effective inserted thread length (including the tip) as function of α ; according to EAD 130118-00-0603 (2016)

As pointed out in EAD 130118-00-0603 (2016), this especially concerns manufacturers intending to allow parallel-to-grain screw insertion in their ETAs. In this case ($\alpha < 15^\circ$), three further conditions have to be fulfilled as well:

- the timber material is restricted to solid softwood according to ON EN 14081-1 (2016) and glued laminated timber made from softwood according to ON EN 14080 (2013),
- $f_{ax,\alpha=0^\circ,k} / f_{ax,\alpha=0^\circ,k} \geq 0.6$, with $f_{ax,\alpha=i,k}$ as short-term characteristic withdrawal strength, and
- the number of screws in the connection, n shall be at least four.

2-2.4.7 Judicial situation in Germany

In Germany, the design and construction of timber engineered supernatural buildings is ruled in so-called federal building codes being specifically valid in and issued by the 16 constituent states of the federal republic. All federal documents generally base on the Model Building Regulation (MBR), administrated by the conference of Ministers of Construction (IS-ARGEBAU). Thus, the currently valid MBR (version November 2002, modified on September 2012), c. f IS-ARGEBAU (2012), is discussed in this section. Therein, both paragraphs, §3 and §17, especially concern the design and application of screwed connections and are worth to be focused in detail:

First, §3 “General Requirements” refers in section (3) to (more or less) annually published Technical Building Rules, which have to be considered in the frame of design and construction process. The currently valid List of Technical Building Rules consists of three parts (part I: Model List of Technical Building Rules (MLTB), issued in June 2015, part II and III issued in November 2014), see IS-ARGEBAU (2015) and DIBt (2014), wherein part I includes certain standards/documents, which have to be considered for the design of building structures. In case of screwed connections, applied in timber buildings, MLTB refers to Eurocode 5, to DIN 1052-10 (2012), as well as to DIN 20000-6 (2015) (note: enclosure 2.5/1 E, point 6). The latter mentioned document contains German national application rules of dowel-type fasteners according to EN 14592 in this context. This subsequently leads to the fact, that dowel-type fasteners regulated in EN 14592 (excluding bolts and dowels with circular cross-sections and smooth shanked nails, but definitively including self-tapping screws) had to be applied according to other technical regulations such as National Technical Approvals (NTAs) until DIN 20000-6 (2013) as the forerunner document of DIN 20000-6 (2015) was issued, referred in the MLTB (which was firstly done within version 03/2014) and adopted in the federal building codes.

Second, §17 “Building products” differs between three types of products being applicable for the German building market. These are: (i) so-called “regulated products” in accordance to the technical regulations given in Construction Products List A (traditional wood screws with threads according to DIN 7998 (1975) are e. g. regulated by DIN 1052 (2008) and DIN 1052 C1 (2010); see DIBt (2015a)), (ii) products sufficiently deviating from these technical regulations, or where such regulations are missing (“non-regulated products”), and (iii) CE-labelled products according to the regulation (EU) No 305/2011 (before: council directive, 89/106/EEC), where related harmonised standards (EN 14592) and guidelines (ETAG, CUAP or EAD) are referred in Construction Products List B, c. f. DIBt (2015a). In case (ii), including modern self-tapping timber screws, *before* EN 14592 and DIN 20000-6 (2013) were referred in Construction Products List B and MLTB respectively (including the adoption in federal building codes), all application was exclusively done in accordance to National Technical Approvals (§18 MBR). It has to be mentioned that option (iii) is also possible in cases when self-tapping screws are CE-labelled according to EN 14592.

As a consequence of their dynamical adaption process, NTAs, issued by the “Centre of Competence in Civil Engineering (DIBt)”, essentially influenced and mirrored the development of self-tapping screws at least in D-A-CH countries (see the comment in section 2-1.3 and the related discussion in section 2-2.5) during the analysed timeframe. As given in Figure 2.15, the process for obtaining an approval deviates from that explained in section 2-2.4.3 for ETAs, especially with regard to an occasionally differing test programme determined by the DIBt in agreement with an expert committee and not regulated in specific guidelines such as CUAP 06.03/08 (2010) or EAD 130118-00-0603 (2016).

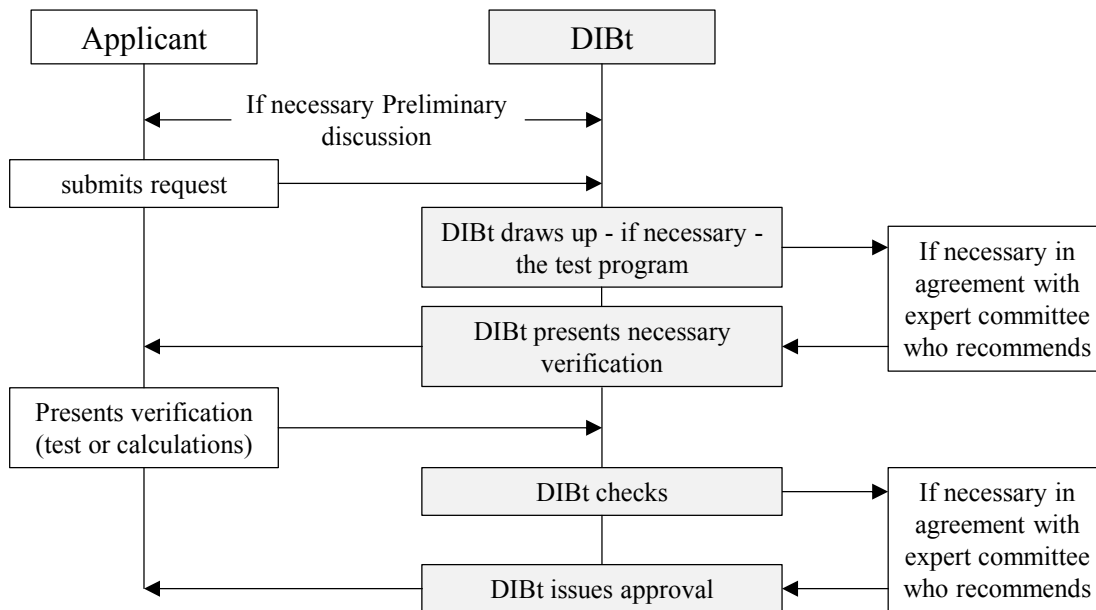


Figure 2.15: Procedure for obtaining a National Technical Approval, according to DIBt (2015d)

2-2.4.8 Judicial situation in Austria

Similar to the situation in Germany, discussed in section 2-2.4.7, in Austria the design and construction of timber engineered supernatural buildings is also regulated by nine different federal state building codes. In contrast, Austrian building codes do not base on a fundamental document (such as MBR in DE) and thus significantly differ regarding the treatment of specific topics. Avoiding to overextend the scope of this introductory chapter, the *Styrian Building Code (SBC)*, together with the *Styrian Building Products and Market Surveillance Act (SBPMSA)*, are representatively discussed within this section.

Within this document – and deviating from the German building law where specific technical regulations are explicitly denoted – basic requirements for the design and construction of buildings, given in regulation (EU) No 305/2011 and adopted in §43 SBC, especially those concerning their mechanical resistance and stability, have to be fulfilled by generally applying the “state-of-art”. This means, that structural design, according to the current version of Eurocode 5, is possible and reasonable but not mandatory in Styria (Austria). With regard to the application of building products, the currently valid

Styrian building code refers to the Styrian Building Products and Market Surveillance Act from 2013, c. f. Federal State of Styria (2013). Therein, three types of building products are differentiated: (i) products not underlying harmonised technical specifications, (ii) products underlying harmonised technical specifications and (iii) other products. Since ON EN 14592 (2012) and ETAs are defined as harmonised technical specifications, see section 2-2.4.2, self-tapping timber screws, CE-labelled according to ETAs or ON EN 14592 (2012), are part of group (ii).

The requirements on products as parts of group (ii) are treated in section 4, §10 and §11 SBPMSA indicating their registration in the so-called Building Products List ÖE; c. f. OIB (2015a). This list specifies the regulations concerning the application and performance of such products, which require a detailed specification (from the opinion of the Austrian Institute of Construction Engineering, in short: OIB). Due to the fact, that none of the plenty CE-labelled screw products is mentioned in the current Building Products List ÖE, c. f. OIB (2013), self-tapping screws obviously need no specific treatment.

Before CUAP 06.03/08 (2010) was published and self-tapping screws were applied without CE-labelling in Austria, different versions of the Styrian Building Code (together with Styrian Building Products Acts, SBPA, as forerunners of SBPMSA) were existing and classified the screws as products, not underlying harmonised standards. Their application was generally possible, providing that they correspond to §43 SBC (fitness-for-use in accordance to “state-of-art”). Further product specifications, such as an Austrian Technical Approval or an OIB expertise, proved this circumstance but were not mandatory. In fact, the majority of people, involved in the Austrian building process, designed and realised screwed timber connections in accordance to product-related German NTAs, also representing state-of-art at this time rather than according to the aforementioned Austrian documents, see e. g. Pirnbacher and Schickhofer (2007).

2-2.4.9 Judicial situation in Switzerland

Unlike Germany (section 2-2.4.7) and similar to Austria (section 2-2.4.8), design and construction of supernatural timber engineered buildings in Switzerland allows certain flexibility regarding the application of standards and guidelines within this process. As described in section 0, SIA 265 (2012) currently represents the state-of-art of Swiss timber building standardisation and is also part of the building contract between the customer and the contractor, according to SIA 118/265 (2004). Note: this document is currently under modification, c. f. prSIA 118/265 (2015). Within the latter mentioned (draft) document, the requirements on building products applied in timber structures should correspond to the regulations given in SIA 265 (2012). It is worth mentioning that section 0.4 allows deviations from those regulations, if reasonably proved by theoretical and experimental investigations or if legitimated by new developments and findings, actualising the “state-of-art”. Note: this clause is also included in the forerunner documents SIA 265 (2003) and SIA 164 (1992).

Further regulations, concerning the placement and application of building products on the Swiss market, are found in both (i) Swiss Federal Construction Product Law and (ii) Swiss Federal Construction Product Regulation – see Swiss Federal Authorities (2014a) and Swiss Federal Authorities (2014b). Document (i) thereby denotes essential characteristics building products have to fulfil. They correspond to those included in regulation (EU) No 305/2011, indicating an adaption to the latter mentioned document by the Swiss Federal Legislation. Consequently, CE-labelled products, according to harmonised specifications such as EN 14592 (included in the related Swiss list) and including a declaration of performance, are seen as “fit-for-use” within the Swiss building market. Prior to the issue date of CUAP 06.03/08 (2010), the forerunner documents of (i) regulated their application as “fit-for-use” by providing two options: clause (a) (article 3, section 5) included building products deviating from technical specifications and allowed their application when produced in accordance to state-of-art and fulfilled requirements given in other federal regulations (not explicitly cited and thus not analysed within this section). Clause (b) (article 5, section 6) allowed the proof of fitness-for-use according to foreign technical approvals if the notified bodies publishing those documents fulfilled the requirements given in the Swiss Federal Law on Technical Barriers to Trade, article 18, sections 2 and 3; c. f. Swiss Federal Authorities (2010a) and Swiss Federal Authorities (2010b). Assuming that the DIBt fulfilled these requirements, the German NTAs served as alternative documents, proved fitness-for-use and enabled the application of self-tapping screws in Switzerland.

2-2.5 Development process based on technical approvals

2-2.5.1 General comments

Summarising the conclusions made in section 2-2.1 to 2-2.4, the technical approvals governed the design and application process of timber connections composed by self-tapping screws over the whole analysed timeframe. Prior to the issue date of CUAP 06.03/08 (2010) on December, 2010, German National Technical Approvals (NTAs), not only used in Germany, but also in Austria and Switzerland, were fulfilling this purpose. From December, 2010 on, the European Technical Approvals/Assessments (ETAs) replaced the national ones and are seen as background documents, CE-labelling and declaration of performance of self-tapping screws are basing on them. Consequently, NTAs and ETAs include essential information, not only regarding the market development, but also the one of the screw product itself and thus mirror the relevant research activities done so far within this scientific field. Section 2-2.5.2 to 2-2.5.6 illustrate this process by comparing selected market parameters and product characteristics between different approval holders (geometry, design process, application, referenced standards, etc.). Worth mentioning, related timeframe analysed covers the years 1986 ÷ 2014. Such ETAs published according to EAD 130118-00-0603 (2016) are thus excluded from the following considerations.

2-2.5.2 General facts and figures

As discussed in section 2-2.4.7, the DIBt is responsible for issuing the German National Technical Approvals. All documents related to self-tapping screws contain the denotation Z-9.1-XXX, see DIBt (2015b), wherein “9” stands for “Timber construction and derived timber products”, subitem “1” for “Timber construction” and “XXX” for a sequential number. Beginning with Z-9.1-175 (1986) and ending with Z-9.1-845 (2014), 73 approval numbers have been issued between 1986 and 2014. The documents have been dynamically adapted, predominantly before reaching their maximum validity period of five years. The main reasons were geometrical modifications (or better extensions) on the one hand and adaptations including latest research findings related to self-tapping screws on the other hand. Thus, all in all 220 documents have been analysed and considered within this section, c. f. Annex B-1, Table B.1 to Table B.4.

With regard to the European Technical Approvals, deviating from German NTAs, their denotation ETA-YY/XXXX consists of “YY” as year specification (when the approval was firstly issued) and “XXXX” as sequential number. Between 2011, after CUAP 06.03/08 (2010) was published, and 2014, 42 numbers have been assigned, including 65 documents all in all, c. f. Annex B-1, Table B.5 and Table B.6.

In Figure 2.16, the number of simultaneously valid documents, including NTAs and ETAs, is illustrated for the timeframe between 1990 and 2014. Furthermore, Figure 2.17 and Figure 2.18 classify the number of the approval holders (motivated by the fact, that several companies hold more than one NTA or ETA) in dependence of their nationality. With regard to German National Technical Approvals, three main periods are worth to focus on. Between 1990 and 1997 less than ten approvals have been valid at the same time, confirming the conclusions made in section 2-1.3, concerning the minor relevance of self-tapping screws as connection solutions in timber engineering of the 1990s. Between 1997 and 2000, as well as between 2005 and 2010, the number of approvals (and their holders) significantly increased. The reasons therefore are definitively seen in an increasing focus of research and development activities on these fastener types emerging several new possibilities of their application as discussed in section 2-1.2. Especially both surges, 1998 and 2005, may be directly related to research activities detailed in sections 2-3 and 2-4.

Simultaneously to the significant increase of European Technical Approvals starting in 2011, a continuous decrease of German NTAs, provoked by the possibility to use ETAs as an alternative (see section 2-2.4), can be observed. A further reason is found in the circumstance, that additional application forms of self-tapping screws, such as the fastening of insulation on top of rafters, which were formerly ruled in separated documents, are unified in the manufacturers “main” approvals now. A main argument confirming the second reason is found in Figure 2.17, where the number of approval holders remains more or less constant since 2009. Here, a decreasing trend can not be observed.

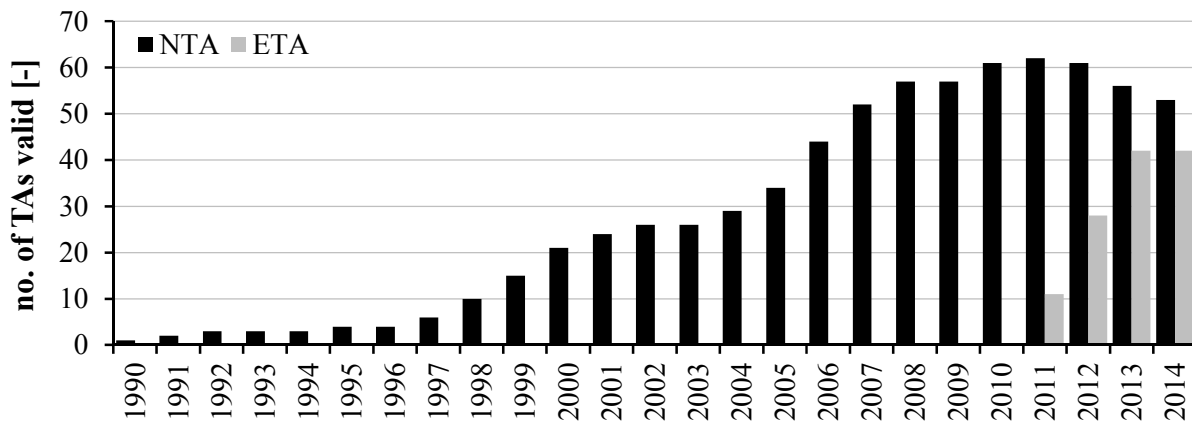


Figure 2.16: Number of Technical Approvals valid at the same time

One reason why section 2-2 treats standardisation and judicial background exclusively for D-A-CH countries is seen in the distribution of approval holders in dependence of their nationalities, as given in Figure 2.17 and Figure 2.18. Focusing on NTAs (Figure 2.17), especially between 1990 and 2005, the vast majority of approvals corresponds to German holders (in average 81 %). Further Central European countries such as Switzerland, Austria and Hungary only share minor parts in this market distribution. From 2006 to 2014, the number of German approval holders did not change remarkably, while the total increase was mainly influenced by that of foreign approval holders, including Italy and Taiwan, too. Nevertheless, the share of German companies is still about two thirds of the total sum. With regard to the ETA related development, given in Figure 2.18, market relations similar to those of NTAs between 2006 and 2014 can be found. Although further countries such as Spain, Czech Republic and Liechtenstein also contribute to the total number, the German share (61 %) and that of the D-A-CH countries (74 %) still significantly prevails. It is worth mentioning, that the Austrian and Swiss parts together currently are about 20 % (ETA) to 30 % (NTA) of that of D-A-CH, which directly mirrors the relation of size and population between Austria, Germany and Switzerland.

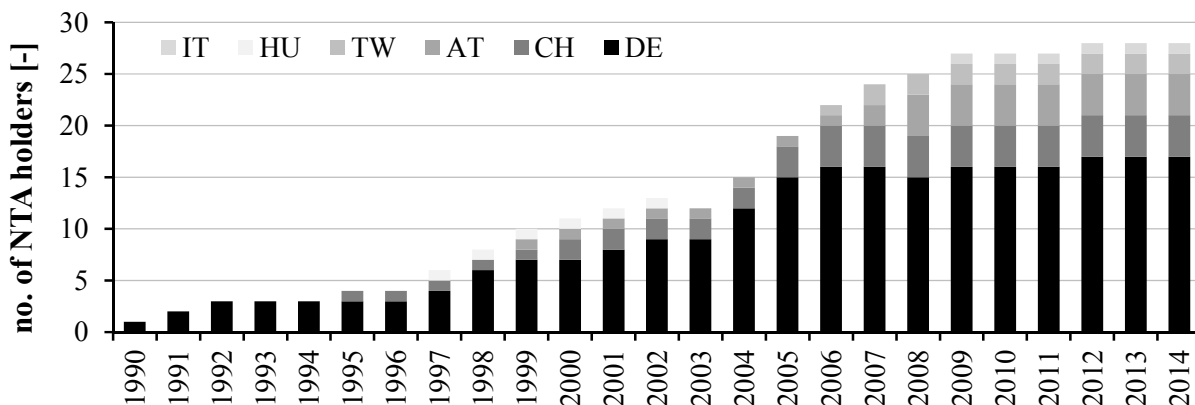


Figure 2.17: Number of holders of National Technical Approvals valid at the same time

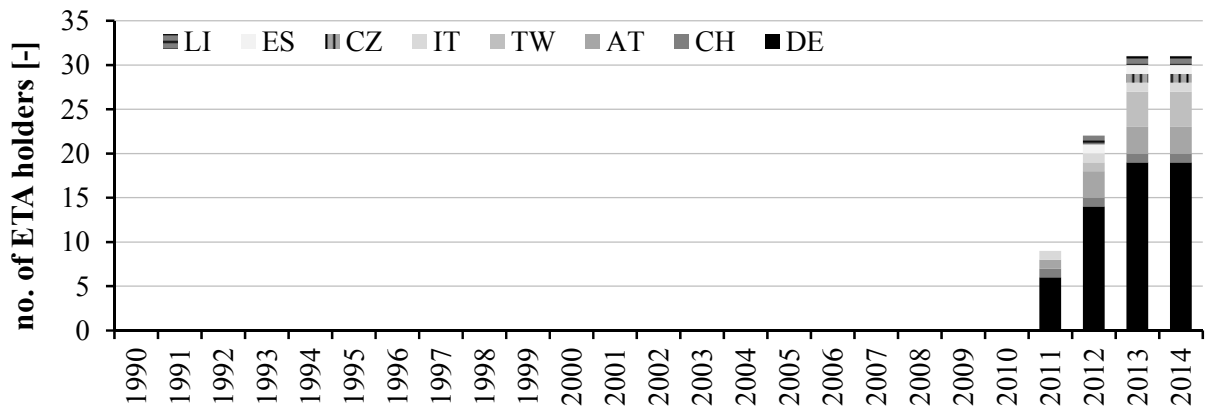


Figure 2.18: Number of holders of European Technical Approvals valid at the same time

Deviating from German NTAs, exclusively issued by the DIBt, European Technical Approvals can be generally published by certain notified bodies according to regulation (EU) No 305/2011, as members of the European Organisation for Technical Assessment (EOTA). In case of ETAs related to self-tapping screws, Figure 2.19 illustrates the distribution of these institutions regarding the number of specifications they have already issued. Therein, it can be clearly seen, that (a) only four institutions are part of this process and (b) both DIBt and ETA Danmark dominate this development while further ones, such as the Austrian OIB or the Czech Technical and Test Institute for Construction (TZUS), only amount a negligible part.

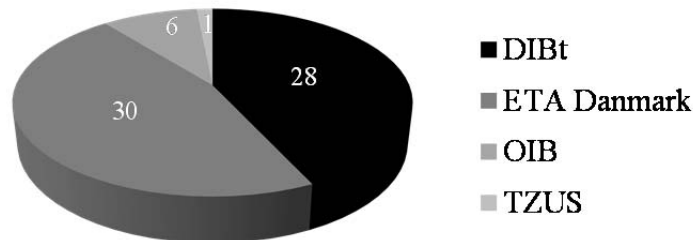


Figure 2.19: Overview of notified bodies regarding the number of issued ETAs

2-2.5.3 Screw types and geometrical characteristics

As summarised in section 2-1.2, the screw development led to three main different types of screw products during the last 25 years, each related to a specific form of application. These are: (i) partially threaded screws (PT), (ii) fully threaded screws (FT) and (iii) screws used as timber-concrete composite connectors (TCC). With regard to the technical approvals analysed, (iv) double threaded screws (DT) as hybrid forms of (i) and (ii) are worth to be additionally considered. Figure 2.20 (NTAs) and Figure 2.21 (ETAs) consequently overview the development of these four different screw types between 1990 and 2014. Focusing on partially and fully threaded screws (all diameters d) ruled in NTAs, a behaviour

similar to the approval number's development, given in Figure 2.16 (poor between 1991 and 1997, followed by two surges in 1998 and 2005), can be observed. Both discussed figures also show the number of approvals containing fully threaded screws with outer thread diameters d bigger than 7 mm. This value is seen as a lower limit for practical use in high stressed timber connections or reinforcement measures. As given in Figure 2.20, the first related NTA was issued in 2002, which may be again caused by research findings recommending self-tapping screws as suitable fasteners for both application fields, c. f. sections 2-3 and 2-4. Finally, with focus on double threaded and TCC screws: although the number of approvals, including one of both types steadily increases from 1995 to 2014, their market impact is comparatively small if compared to fully or partially threaded screws.

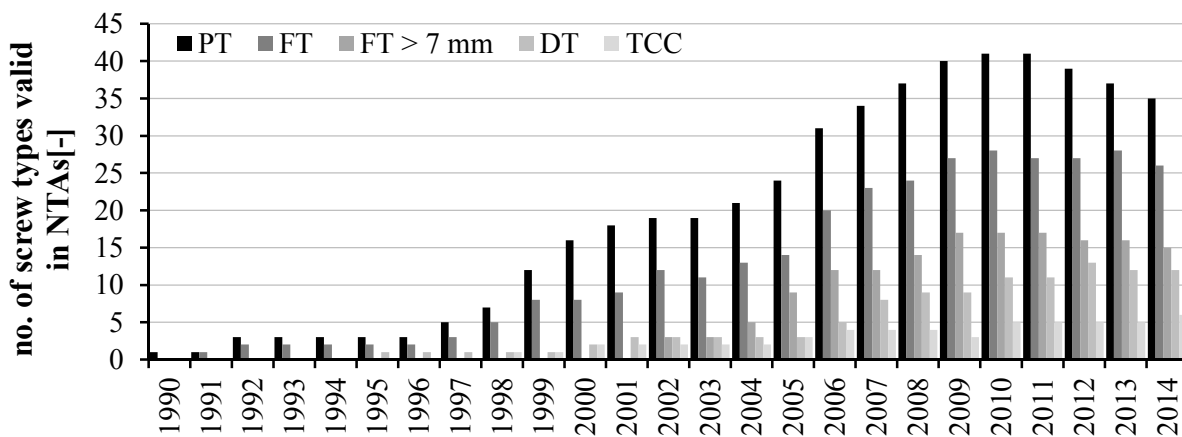


Figure 2.20: Number of different screw types given in National Technical Approvals valid at the same time

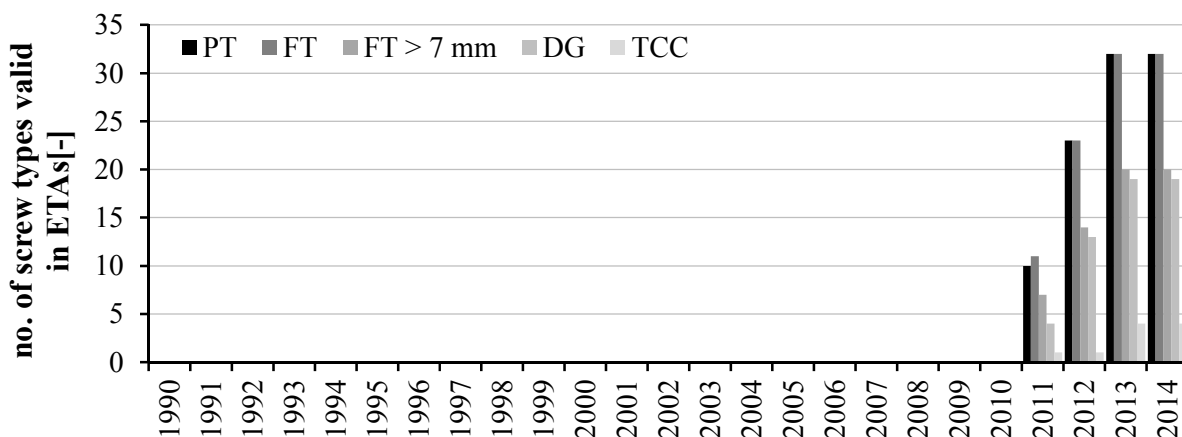


Figure 2.21: Number of different screw types given in European Technical Approvals valid at the same time

Geometrical properties, such as the outer thread diameter d and the thread length l_{thread} , as well as the properties directly related to screw application, hereby especially the insertion angle α , are seen as reasonable indicators how the specific screw product can be valuably used in certain detail solutions.

Thus, Figure 2.22 illustrates the NTA development trend of these mentioned parameters (each annual maximum in case of d and l_{thread} , each annual minimum in case of α) for the period between 1990 and 2014.

Focusing on self-tapping screws suitable for (a) high stressed timber connections and (b) reinforcement measures, both in GLT or CLT components: in order to enable an optimal loadbearing behaviour, comparatively long thread lengths caused by geometrical and mechanical conditions are required. Reason therefore is steel failure in tension as maximum load bearable per fastener occurring at $l_{\text{thread}} > 15 \div 20 d$; see e. g. Gaich et al. (2008). As shown in Figure 2.22, the screw development firstly enabled both application forms (a) and (b) between 2002 and 2003. Again, the hereby observed surge, especially concerning l_{thread} can be directly referred to related research activities, see sections 2-3 and 2-4. Thread lengths, equal or below 116 mm as upper limit between 1990 and 2001 (see Figure 2.22), indicate the predominate use of partially threaded screws for fixing the insulation on top of the rafters or very short fully threaded screws for minor loadbearing tasks and/or as TCC connectors at this time. Currently, the latest screw development led to outer thread diameters up to 14 mm and thread lengths up to even 2,000 mm (e. g. declared in ETA-11/0190 (2013), not published in NTAs and illustrated in Figure 2.22). Note: the latter mentioned geometrical maximums are only applied as reinforcements of GLT beams with extraordinary dimensions and can be seen as a self-tapping alternative to threaded rods.

With regard to the insertion angle's development, a steady trend of minimising α with a remarkable surge from 45° to 15° in 2006 can be observed. Currently, the whole spectrum between 0° and 90° is applicable, considering the significant restrictions if screw axes are arranged parallel to grain as a consequence of poor long-time loadbearing behaviour as described in Pirnbacher and Schickhofer (2012) or Hübner (2013b) for instance.

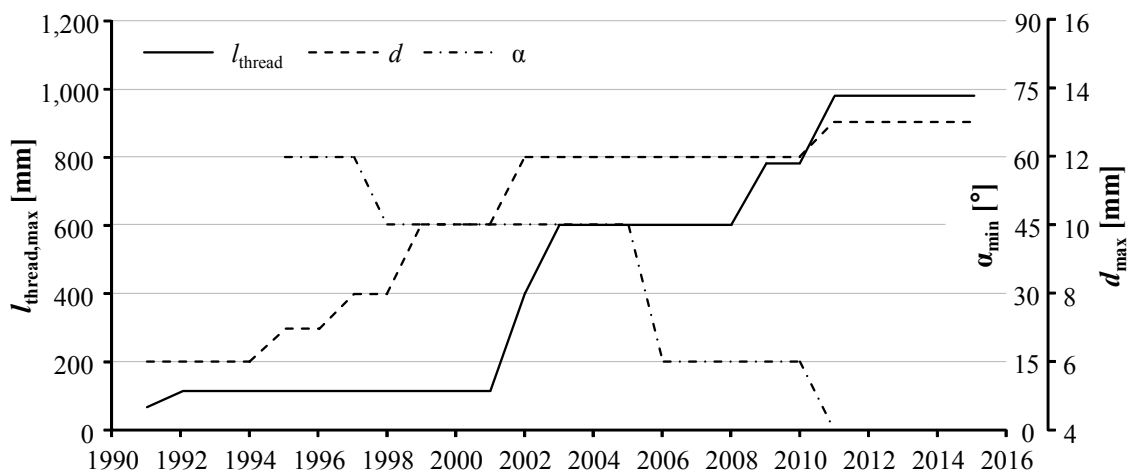


Figure 2.22: Development of thread length, outer thread diameter and minimum insertion angle between 1990 and 2014; only NTAs considered

In addition, Figure B.1 and Figure B.2, given in Annex B-1, overview the outer thread diameter bandwidth of all analysed NTAs and ETAs. Therein, a clear concentration of d between 6 and 10 mm can be observed.

2-2.5.4 Minimum distances and insertion depths

The arrangement of fasteners plays an important role for designing competitive connections in terms of mechanical strength and stiffness, cost effectiveness and optical visibility. With regard to axially loaded screwed connections, standards, discussed in section 2-2.1 to 2-2.3, include the minimum spacings between two screws (a_1 parallel and a_2 perpendicular to grain direction), the timber member's end and edge distances ($a_{1,CG}$ to the ends and $a_{2,CG}$ to the edges), as well as the minimum member thickness t_{min} , as the related geometrical boundary conditions. As discussed in section 2-2.4.4, NTAs and ETAs offer the favourable opportunity of modifying these conditions by adopting the current state-of-knowledge. In 2003, two NTAs Z-9.1-449 (2003) and Z-9.1-519 (2003) related to self-taping screws being applicable for high stressed connections and reinforcements (TCC screws are again excluded), firstly introduced the specific regulations deviating from DIN standardisation (valid at this time) concerning minimum spacings and dimensions. Similar to the minimum values found in all analysed approvals, compared in Table 2.9, they were quite equal to those for pre-drilled traditional wood screws published in DIN 1052 P2 (1988). This fact (similar values for pre-drilling and self-tapping) already indicates a certain trend, especially minimising the spacings a_1 , a_2 and $a_{1,CG}$, which is seen as a competitive process between approval holders from this time on. Consequently, the majority of Technical Approvals (TAs), valid in 2014, contained the specifications given in Table 2.9, line 2.

The current test procedure, these spacings and dimensions are determined with, was originally developed by Uibel (2012) and is published in CUAP 06.03/08 (2010) and EAD 130118-00-0603 (2016). It should be pointed out, that it generally bases on drilling-in tests, not being able to cover the group loadbearing behaviour. In case of certain conditions, regarding the connection geometry (spacings according to modern TAs) and loading, Mahlkecht et al. (2014) observed block shear failure of screwed groups, which were designed to fail in withdrawal or steel tensile. This failure mode, with lower bearing resistance if compared to withdrawal or steel tensile, is currently not ruled in approvals and/or standardisation and significantly depends on the size of the timber volume stressed by the connection, see section 2-3. Consequently, there is a certain demand in clarifying this situation, either by increasing the minimum values given and/or by introducing a design background covering this additional failure mode.

Table 2.9: Comparison of minimum spacings and timber dimensions given in Eurocode 5 and Technical Approvals (TCC screw approvals excluded)

source	a_1	a_2	$\min(a_1 \cdot a_2)$	$a_{1,CG}$	$a_{2,CG}$	t_{\min}
ON EN 1995-1-1 (2009) to ON EN 1995-1-1 (2015)	7 d	5 d	35 d ²	10 d	4 d	12 d
minimum values currently given in Technical Approvals	5 d	2.5 d	25 d ²	5 d	3 d	10 d

2-2.5.5 Design background and mechanical properties

Due to their dynamical character, enabling the content modification whenever necessary, Technical Approvals generally cover the currently applicable state-of-knowledge – in contrast to product and design standards subjected to much longer actualisation rates (c. f. section 2-1.3). Nevertheless, the latter mentioned guidelines always serve as background documents for NTAs and ETAs, especially concerning the way certain material properties have to be determined and the design process has to be executed. In case of European Technical Approvals, EN 1995-1-1:2004/A1 (2008) is referred by all documents published so far. In case of National Technical Approvals, the German standardisation process, discussed in section 2-2.2, significantly influenced related information given in the documents. Figure 2.23 consequently illustrates the number of NTAs valid per year in dependence of the standards they are referring to. The only exception, not treated in Figure 2.23, is Z-9.1-251 (2004), bases on DIN 18168-1 (2007) as German standard, ruling the application of suspended ceilings with gypsum plasterboards. The comparison given in Figure 2.23 shall underline the fact, that approvals often referred to standards, which were not valid at this time; c. f. section 2-2.2. For example, information concerning design and application of self-tapping screws, according to a semi-probabilistic safety concept as given in DIN V ENV 1995-1-1 (1994), was firstly provided in 1998, four years before DIN 1052 (2004) (also semi-probabilistic) has been published in Germany. Furthermore, in 2014, ten approvals still provided design properties for application of the deterministic safety concept according to DIN 1052 P2 (1988) as a standard published 26 years ago and valid until 2004.

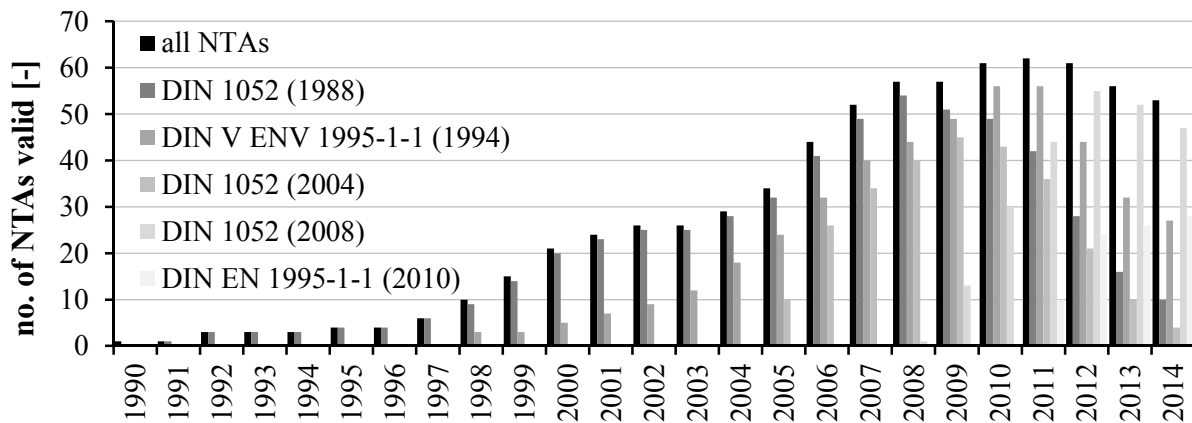


Figure 2.23: Number of NTAs valid at the same time and classified by the standards the design and application process has been done in accordance to

With regard to the design process of screwed connections, the main mechanical properties used therefore are one of the essential contents provided in Technical Approvals. In terms of axial loadbearing conditions, as the main topic of this thesis, both withdrawal ($f_{ax,k}$) and head pull-through ($f_{head,k}$) parameters, as well as the screw's steel tensile capacity $f_{tens,k}$ are needed for failure mechanism verification, as discussed in section 2-2.1.3. Based on a statistical evaluation of the vast majority of currently valid ETAs (at the beginning of 2015) and related to self-tapping screws (TCC screw approvals contain system resistances and are thus excluded), Table 2.10 summarises mean values, coefficients of variation $CV[X]$, minima and maxima of both properties $f_{ax,k}$ and $f_{tens,i,k}$ for a reference outer thread diameter $d = 8$ mm. Since the head pull-through failure mechanism is only of minor relevance when focusing on high stressed screwed connections (c. f. section 2-1.2), its parameter related is not treated within this consideration. In case of $f_{ax,k}$, the given value belongs to the reference density $\rho_k = 350$ kg/m³ and the insertion angle $\alpha = 90^\circ$. With regard to $f_{tens,i,k}$, the index “i” classifies the screw product used as hardened carbon steel (index 1) and unhardened carbon or stainless steel (index 2).

It is well known, that the steel tensile strength of self-tapping screws principally shows a much smaller variability (especially if one charge of fasteners is tested), than those of timber properties in general. Nevertheless, different basic steel material, hardening procedures and further treatments, discussed in section 3-3 in detail, lead to comparatively high deviations of this property in dependence of the screw manufacturer or approval holder (difference of 47 % (1) | 36 % (2) between minimum (reference) and maximum value issued!), even bigger than that of the withdrawal parameter (at least in case of $f_{tens,1,k}$). Although the procedure (timber material, density, moisture content, test set-up etc.) determining the latter mentioned value was clearly ruled in CUAP 06.03/08 (2010), and any further differentiations regarding the thread geometry (e. g. described by the ratio d_c / d) do not really influence the withdrawal properties

of self-tapping screws in a major way, c. f. Pirnbacher and Schickhofer (2007) or Frese et al. (2010) for instance, an unexpected high difference between $f_{ax,k,min}$ (reference) and $f_{ax,k,max}$ of 37 % can be observed.

Table 2.10: Main statistics of withdrawal and steel strength properties issued in currently valid ETAs (TCC screw approvals excluded)

property		mean[X]	CV[X]	min[X]	max[X]
$f_{ax,k}$	[N/mm ²]	11.7	8.52%	10.0	13.7
$f_{tens,1,k}$	[N]	20,477	9.01%	17,000	25,000
$f_{tens,2,k}$	[N]	12,736	8.13%	11,000	15,000

1 = carbon steel screws, 2 = stainless steel screws

As discussed in section 2-2.2.1, DIN 1052 (2004) was the first German standard, when published already containing a semi-probabilistic safety concept. Thus, approvals issued until 2004 exclusively provided the equations for determining the permissible withdrawal resistance $N_{Z,per}$ similar to that given in DIN 1052 P2 (1988), see eq. (2.6). The deviations to eq. (2.6) are: (a) NTAs use the outer thread diameter d instead of the shank diameter d_{sh} and (b) several documents contained pre-factors up to 5, instead of 3 as a fixed value given in eq. (2.6). Worth mentioning, the ratio between $N_{Z,per}$ and $F_{ax,k}$ if $\rho_k = 350 \text{ kg/m}^3$, $d = 8 \text{ mm}$, $l_{ef}(s_g) = 10 d$ and $\alpha = 90^\circ$ of all NTAs analysed results to roughly 2.0, which was also found between the permissible and characteristic steel tensile capacities.

The modern standardisation of timber engineered structures, such as ON EN 1995-1-1 (2015), explicitly mentions the connection stiffness $K_{ser,ax}$ do be considered for ultimate and serviceability limit state (ULS and SLS) design process. Furthermore, also discussed in section 2-2.4.4, this mechanical property concerns the basis requirement “mechanical resistance and stability” according to regulation (EU) No 305/2011 and thus should be provided within the declaration of performance when basing on Technical Approvals. Consequently, first approaches determining the axial fastener stiffness have been published in German NTAs in the early 2000s, see Figure 2.24. Therein, both numbers of simultaneously valid NTAs and ETAs containing withdrawal stiffness specifications are given for the timeframe analysed, approvals treating TCC screws and thus providing system values are again excluded. As shown in Figure 2.24, only a small number of NTAs specifies this property at all, while $K_{ser,ax}$ is included in most of the ETAs related. A significant surge can be observed between 2006 and 2007, which is once again caused by research findings discussed in sections 2-3 and 2-4.

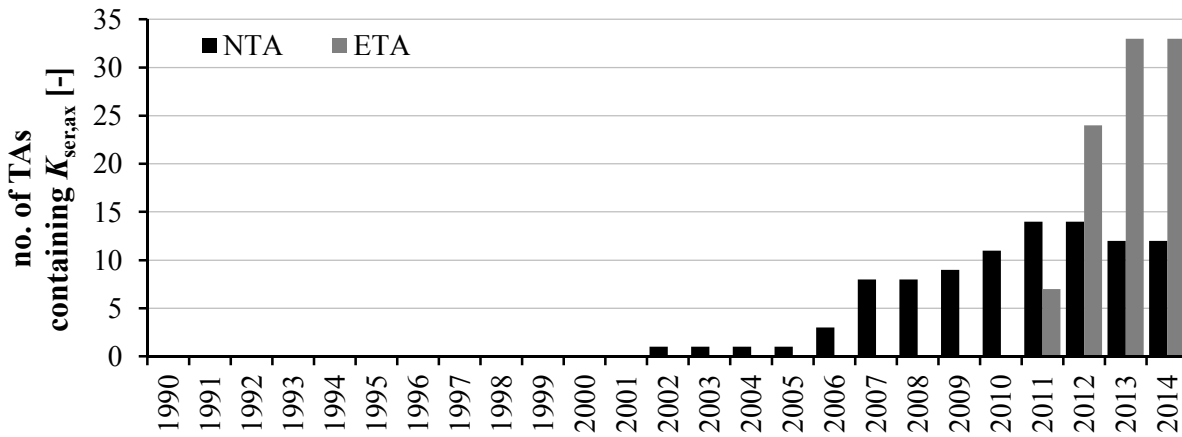


Figure 2.24: Number of Technical Approvals providing withdrawal stiffness specifications (TCC screw approvals excluded)

In contrast to the withdrawal strength predominately provided as a constant value in dependence of a reference diameter and density, the information regarding $K_{ser,ax}$ is consistently given in form of certain equations, which can be applied for value determination. Although different formulas are provided, two main approaches remain as worth being discussed; see

$$(Ia) K_{ser,ax} = d^{0.2} \cdot l_{ef}^{0.4} \cdot \begin{cases} 780 \text{ softwood} \\ 870 \text{ hardwood} \end{cases}; (Ib) K_{ser,ax} = \frac{234 \cdot (\rho \cdot d)^{0.2}}{\frac{1}{l_{ef,1}^{0.4}} + \frac{1}{l_{ef,2}^{0.4}}}; (Ic) K_{ser,ax} = \frac{1120}{\frac{1}{l_{ef,1}^{0.4}} + \frac{1}{l_{ef,2}^{0.4}}}, \quad (2.26)$$

$$(IIa) K_{ser,ax} = 25 \cdot l_{ef} \cdot d; (IIb) K_{ser,ax} (\alpha = 45^\circ) = \frac{16 \cdot d}{\frac{1}{l_{ef,1}} + \frac{1}{l_{ef,2}}}, \quad (2.27)$$

with indices 1 and 2 in cases, two timber members are penetrated by one screw acting as serial system. As shown in eq. (2.26) and (2.27), both approaches (I) and (II) significantly differ in the way, their main influencing parameters ρ , d and l_{ef} are considered. Furthermore, the specifications concerning a varying insertion angle are missing. Thus, $K_{ser,ax}$ values, determined with all approaches shown, except of (IIb), are equal for the whole bandwidth of α . Due to the fact, that equations (Ia,b,c) show no remarkable differences for the diameter bandwidth $d = 8 \div 12$ mm considered, Figure 2.25 solely compares $K_{ser,ax}$ values determined by both approaches (Ia) and (IIa) in dependence of the screw's effective length and a constant $\rho_k = 350$ kg/m³. Therein, significant deviations up to 720 % between (Ia) and (IIb) can be observed, indicating the fact, that different opinions concerning the determination of this parameter exist.

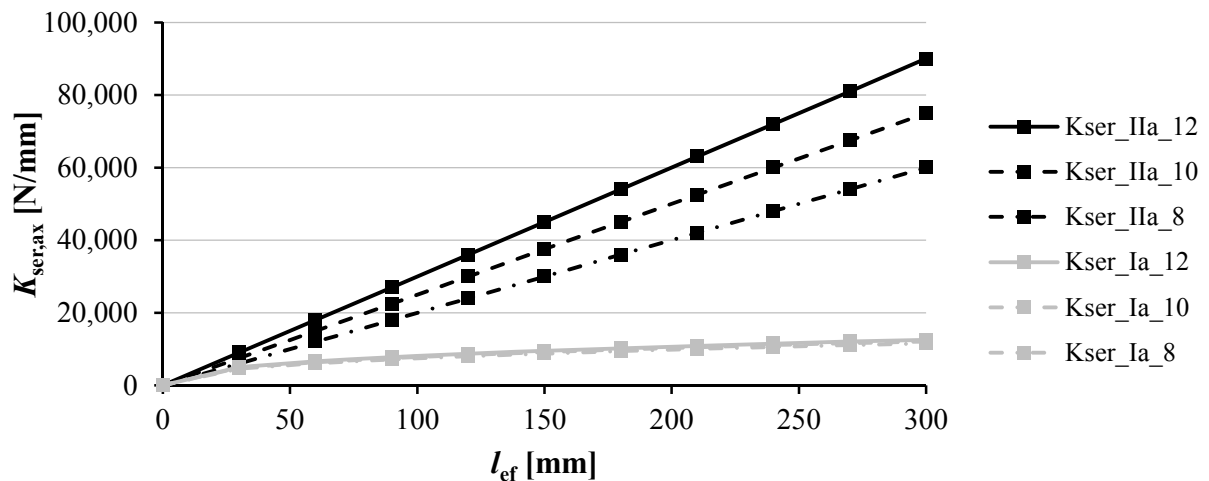


Figure 2.25: Comparison of different specifications regarding the withdrawal stiffness provided in Technical Approvals (TCC screw approvals excluded)

2-2.5.6 Approved laminated timber products and wood species

As introduced in chapter 1, this thesis concentrates on examinations of axially loaded screwed connections, situated in laminated timber products, which are composed of N single boards as a basis material. This definition contains unidirectional and orthogonal oriented glued and cross laminated timber (GLT and CLT), as well as solid timber (ST; $N=1$) as the lower limit in both cases. Thus, the information regarding the applicability of these products, approved in NTAs and ETAs, is a further topic of interest to be treated within this section 2-2.5. While all NTAs and ETAs approve the application of self-tapping screws in solid timber and in addition all documents apart from Z-9.1-175 (1986) in GLT, the National Technical Approvals allowing the same in CLT are rare. The first NTA considering CLT was published in 2005; c. f. Z-9.1-279 (2005). This document, as well as the majority of further ones, issued between 2005 and 2014 and regulating this timber product, predominately approved self-tapping screws exclusively applied as fasteners for the insulation on top of rafters or as TCC connectors. In both mentioned application fields, screws are mainly used in form of line connections, situated in the side face of CLT panels. The requirements concerning the minimum spacings in both, side and narrow face, especially necessary for high-stressed punctual connections, are not ruled therein. In 2014, 11 out of 40 NTAs valid, allow the use in CLT, whereof only two documents detail their application in form of specific minimum spacings and thicknesses. The situation for European Technical Approvals is in contrast: here, only two out of 40 analysed ETAs (valid in 2014) do not contain the applicability in CLT. Nevertheless, the number of documents, clearly specifying this form of application, is rare again.

As mentioned in section 2-1.2, contemporary research activities mainly focus on screwed connections in timber products made of hardwood species. In this context, only seven approvals (three NTAs, all of the same approval holder, and four ETAs) allow screw application in these materials. The wood

species/products, mentioned in these six documents, are ST and GLT in beech and oak (6 times) and GLT in ash (3 times).

2-2.6 Intermediate conclusions

Focusing on axially loaded screwed connection, the development of standardisation and approvals (between 1990 and 2014) has been analysed within section 2-2. Based on the findings, the following intermediate conclusions are worth to be shortly summarised.

Firstly, based on the study of Central European (D-A-CH countries) design standards related to timber engineering, none of them exclusively enables the design and the application of self-tapping screws without any further documents, e. g. considering Technical Approvals. The reasons therefore are on the one hand that older documents, namely ON B 4100-2 series, DIN 1052 P2 (1988) or SIA 164 (1992) solely rule traditional wood screws, and on the other hand that, beginning with SIA 265 (2003) and DIN 1052 (2004) respectively, modern design codes only provide insufficient information concerning specific screw parameters (e. g. axial stiffness) and application forms (CLT, hardwood products). In addition to these technical barriers, the publication of council directive (89/106/EEC) and regulation (EU) No 305/2011 in combination with EN 14592 enable the CE labelling of self-tapping screws, which currently also necessitates European Technical Approvals as basis documents.

Secondly, with regard to the development process of self-tapping screws based on Technical Approvals, German NTAs, not only applied nationally, but also in Austria and Switzerland, and later ETAs, clearly mirror the main research findings made in this specific field within the timeframe analysed. Due to the fact, that these documents still govern the design and application process of self-tapping screws, related statistics of Technical Approvals also serve as good market indicators of this specific fastener product. The main development steps regarding standards, building and building product laws as well as technical approvals, discussed in section 2-2, are illustrated in Figure 2.26.

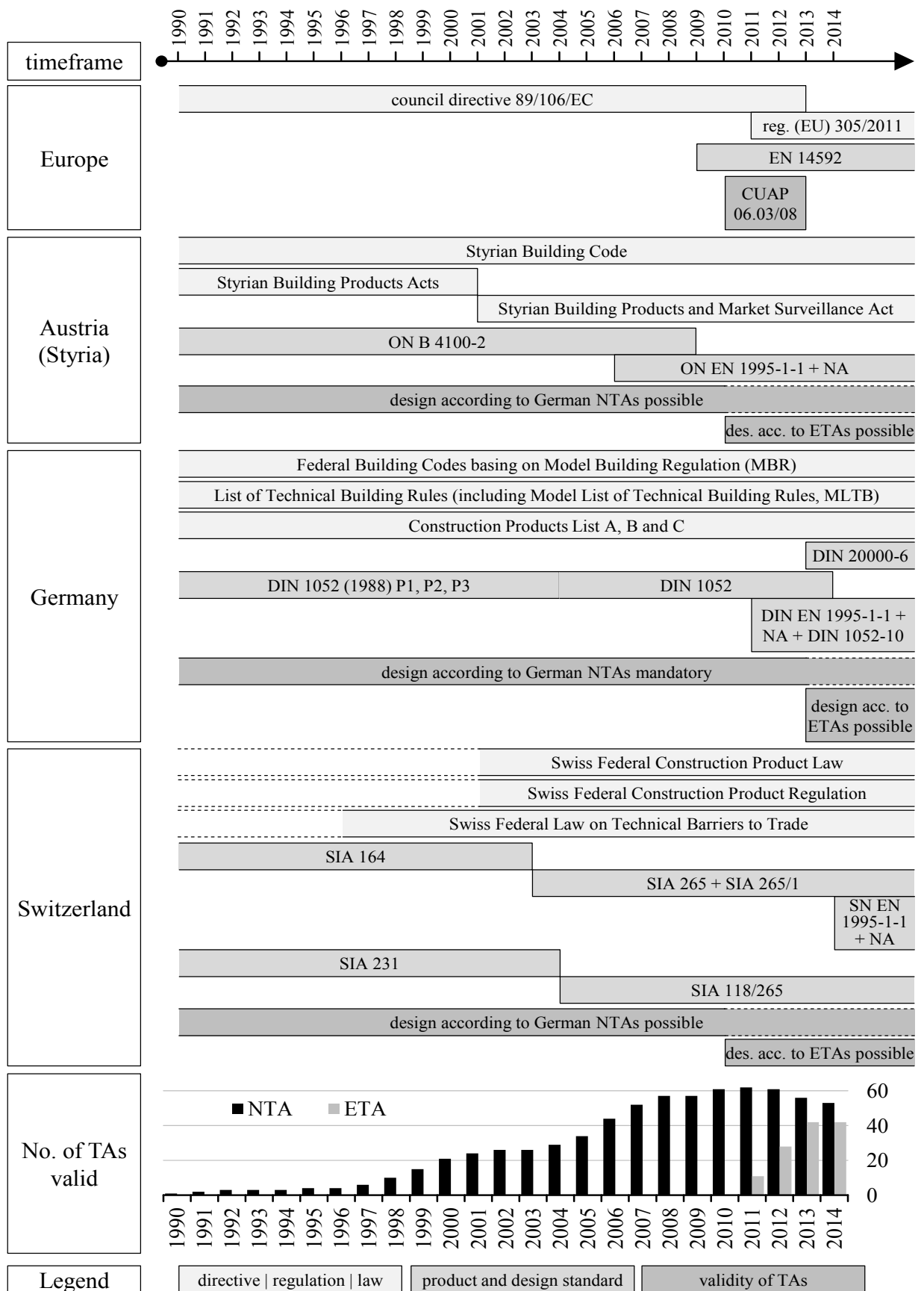


Figure 2.26: Illustration of the development of standards and approvals analysed in section 2-2

2-3 ACTIVE APPLICATION AS CONNECTION

As previously introduced, this section 2-3 summarises the main research activities done so far, concerning the *active* application of self-tapping screws in form of *predominately axially* loaded timber connections. Subsections 2-3.1 to 2-3.3, structured in accordance to Figure 2.10, consequently focus on normal, transversal and moment joints, wherein screws are responsible for transferring structural loads between two loadbearing members in timber and/or steel. Due to the fact that fasteners, line-wisely connecting CLT elements, are mostly stressed by load combinations (normal and transversal forces and/or moments), the concerning literature is separately discussed in section 2-3.4.

The documents, regulating screws applied as TCC connectors, only have a minor relevance with regard to the total number of related approvals published so far, c. f. section 2-2.5.3. In addition, their loadbearing behaviour is influenced to a large extent by that of the concrete member, not thematically treated within this thesis. Thus, research works already done concerning this subject are not taken into consideration. This also concerns predominately partially threaded and comparatively minor stressed self-tapping screws applied to fix insulation material on top of rafters.

It is worth mentioning, that research activities exclusively concentrating on influencing parameters and their application in the frame of different prediction models of axially loaded single screws, mostly failing by withdrawal, are not discussed within section 2-3. In fact, their essential impact on the current state-of-knowledge, especially concerning self-tapping screws' withdrawal behaviour as one of the core topics of this thesis, is discussed in chapter 5 in detail.

2-3.1 Normal joints

2-3.1.1 Timber-to-timber normal joints

In Figure 2.27, a commonly applied timber-to-timber tensile connection with inclined positioned self-tapping screws is shown. This so-called butt joint can either be composed by equally orientated screws loaded in tension (Figure 2.27, left) or oppositional oriented crossed screws, loaded either in tension or in compression. The joint's main design parameters are (a) the screw's length l_{screw} (and thread length l_{thread} in case of partially threaded screws) and outer thread diameter d , (b) thicknesses t_i and the material properties (commonly represented by ρ_i) of the outer and inner timber members and (c) the inclination angle α as a parameter depending on the joint's application. Worth mentioning, that the distances a_i and $a_{i,CG}$ between two screws and to the timber members ends and edges, introduced in section 2-2 but not illustrated in Figure 2.27, have to be considered in the design process as well.

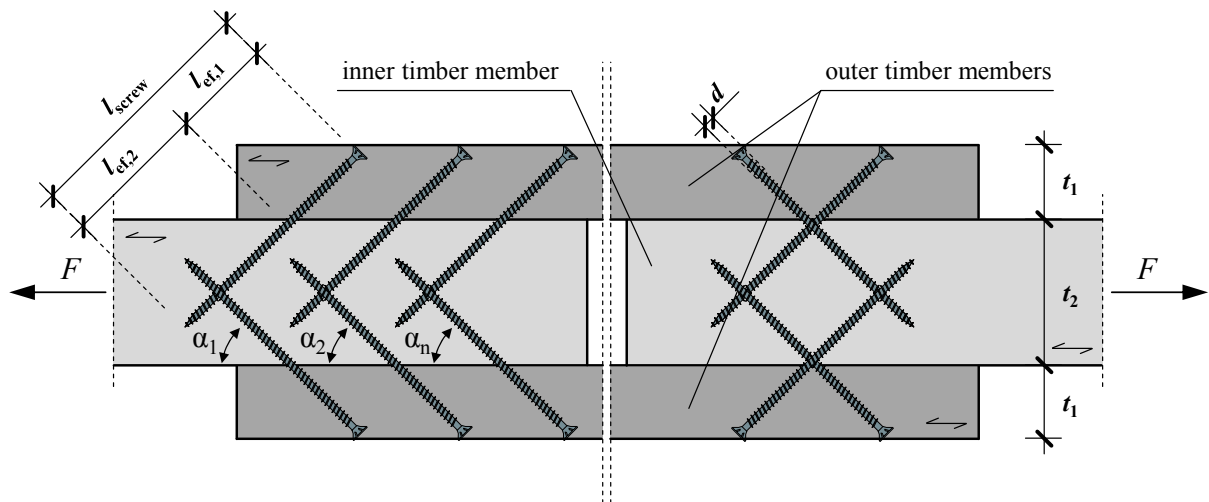


Figure 2.27: Cross-section of a typical timber-to-timber tensile connection with inclined positioned self-tapping screws; left: tensioned screw joint; right: crossed screw joint

As already discussed in Blaß (1998) and demonstrated in section 2-2.5.3, the development of fully threaded screws with $d > 7$ mm, and lengths being relevant for the corresponding geometrical conditions, firstly enabled this form of application in the early 2000s. Due to their comparatively smaller thread lengths, leading to smaller withdrawal capacities and the fact, that their axial resistance is governed by their head pull-through capacities in the outer timber members, the use of inclined positioned partially threaded screws results in a significantly reduced joint capacity. Thus, they are barely applied for this purpose and not treated in the literature discussed within this section.

Focusing on the application of former mentioned fully threaded screws, Blaß and Bejtka (2001), Bejtka and Blaß (2002), Blaß and Bejtka (2003b), Blaß and Bejtka (2004b) and finally Blaß et al. (2006) carried out several investigations to describe the loadbearing behaviour of this specific joint detail. Due to inclined positioning, the screw axis' directions, shown in Figure 2.27, deviate from the direction of the joint load F . Since screws are stressed in axial and lateral direction, their loadbearing behaviour is influenced by screw withdrawal and bending, as well as the timber members' embedment strength $f_{h,i}$. Both latter mentioned failure modes are commonly used for determining the lateral bearing capacity of dowel-type fasteners loaded perpendicular to their axis. In Blaß and Bejtka (2001), they adapted this calculation method basing on Johansen's yield theory (in particular failure mode 3 where one plastic hinge occurs in each timber component, c. f. Johansen (1949), see Figure 2.28, left) by introducing an additional term in form of the horizontal component (parallel to the direction of F , see Figure 2.28 right) of the previously mentioned fastener's withdrawal capacity $R_{ax,i}$. In Bejtka and Blaß (2002), they extended this design approach for all possible Johansen's failure modes, and also considered the positive effect of friction caused by the vertical component of $R_{ax,i}$ (perpendicular to F) compressing the gap between the timber members.

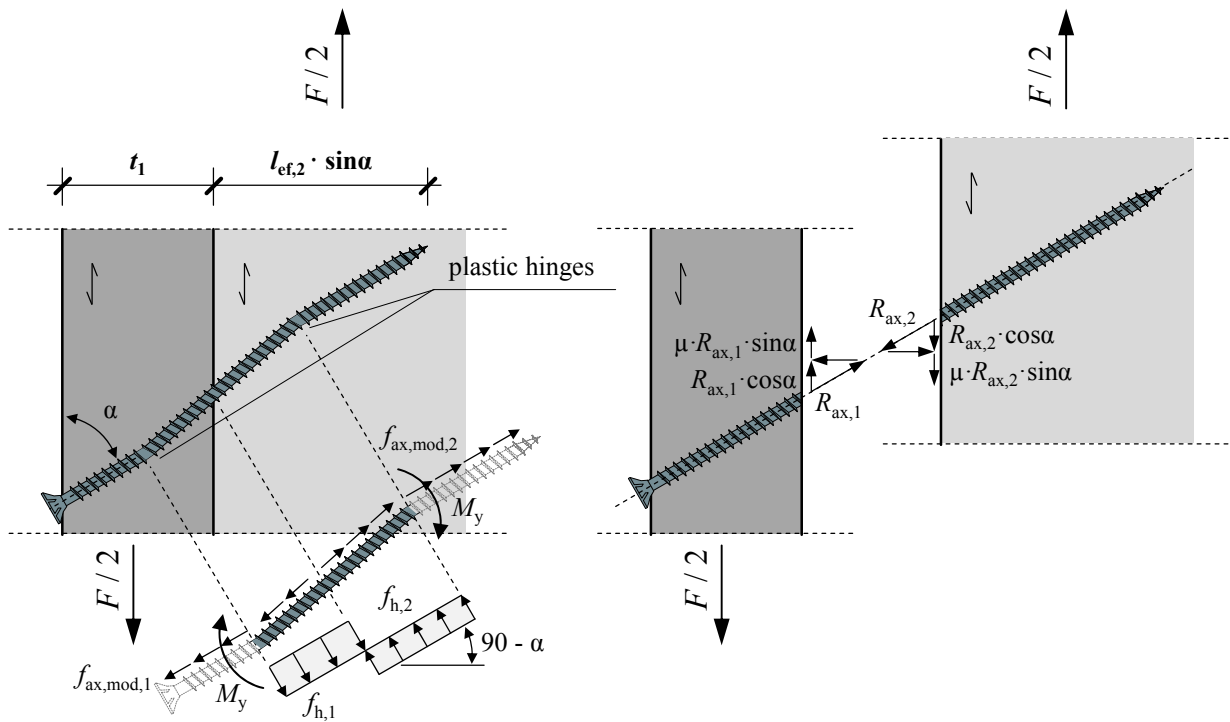


Figure 2.28: *Left: schematic illustration of forces and stress distributions in an inclined screwed timber-to-timber connection for Johansen's failure mode 3; according to Blaß and Bejtka (2001) and Bejtka and Blaß (2002); right: truss-like force system exclusively considering axial screw capacity; according to Blaß and Bejtka (2003b)*

Furthermore, they reduced the withdrawal strength f_{ax} (in original form the withdrawal parameter f_1) in dependence of the lateral displacement δ , negatively affecting the composite behaviour between timber and screw. Eq. (2.28) exemplarily shows the determination of the load-carrying capacity of one screw, R in case of Johansen's extended failure mode 3:

$$R_{\text{mech}3} = R_{\text{ax,mech}3} \cdot (\cos \alpha + \mu \sin \alpha) + (1 - \mu \cot \alpha) \cdot \sqrt{\frac{2\beta}{1+\beta}} \cdot \sqrt{2 \cdot M_y \cdot d \cdot f_{h,1} \cdot \sin^2 \alpha}, \quad (2.28)$$

with

$$R_{\text{ax,mech}3} = \min \left\{ \begin{array}{l} R_{\text{ax},1} \\ R_{\text{ax},2} \end{array} \right. = \min \left\{ \begin{array}{l} f_{\text{ax,mod},1} \cdot d \cdot \pi \cdot l_{\text{ef},1} \\ f_{\text{ax,mod},2} \cdot d \cdot \pi \cdot l_{\text{ef},2} \end{array} \right. \text{ and } \min [f_{\text{ax,mod},i}] = 0.7 \cdot f_{\text{ax},i}, \quad (2.29)$$

where μ is the friction coefficient between the two timber members (assumed between 0.25 and 0.35), M_y the yield moment of the screw and $f_{\text{ax,mod},i}$ the modified (= reduced) withdrawal strength of the timber member i . A detailed derivation of further Johansen's extended failure modes 1a to 2b, as well as the relationship between $f_{\text{ax,mod},i}$ and δ , can be found in Bejtka and Blaß (2002).

In Blaß et al. (2006) they finally summarised the results of their research so far. Thereby, they not only concentrated on the formerly mentioned design approach and its experimental evaluation but also on the determination of prediction models describing the lateral (f_h and M_y) and axial (f_{ax} , $f_{ax,mod}$, $K_{ser,ax}$) screw basic properties. Focusing on axial (withdrawal) loadbearing behaviour, they recommend determining R_{ax} as follows:

$$R_{ax} = \frac{0.6 \cdot \sqrt{d} \cdot l_{ef}^{0.9} \cdot \rho^{0.8}}{1.2 \cdot \cos^2 \alpha + \sin^2 \alpha} \quad (2.30)$$

Eq. (2.30) bases on the regression model published in Bejtka (2005). Furthermore, the characteristic withdrawal capacities were determined by decreasing the pre-factor 0.6 to 0.52 and considering ρ_k instead of ρ . Issuing EN 1995-1-1:2004/A1 (2008), eq. (2.30) as the currently valid European approach of determining the characteristic withdrawal capacity of axially loaded self-tapping screws, has firstly been applied for Eurocode 5 series, c. f. section 2-2.1.3. In terms of withdrawal stiffness $K_{ser,ax}$ (in original form K_{ax}), they also provide a model approach in form of

$$K_{ser,ax} = 234 \cdot (\rho \cdot d)^{0.2} \cdot l_{ef}^{0.4}, \quad (2.31)$$

again on the basis of Bejtka (2005). The majority of technical approvals, which contain information regarding the withdrawal stiffness, therefore provide at least a modified form of eq. (2.31); c. f. section 2-2.5.5. Thus, eq. (2.31) significantly influenced the design process of self-tapping screws in the last years.

Back to the experimental investigations concerning timber-to-timber normal joints, composed by several inclined screws. For the majority of practical cases, where α as the angle between screw axis and fibre direction does not exceed 45 °, eq. (2.28) can be simplified to

$$R = R_{ax} \cdot (\cos \alpha + \mu \sin \alpha), \quad (2.32)$$

solely considering the axial loadbearing component of the screw. This is due to the fact, that no plastic screw deformations were observed for specimen, which were opened after tests had been finished. Since the group effect was not negatively influencing the loadbearing capacity of a group of n fasteners, compared to that of $n = 1$ (this means $n = n_{ef}$, deviating from recommendations published in Eurocode 5), eq. (2.32), multiplied by n , showed a good overall agreement with test results. In case of connections where screw pairs are crosswise applied, one loaded in tension and one in compression, no detailed approach similar to that given in eq. (2.28) had been determined so far. Thus, Blaß et al. (2006) applied a simplified model for determining R_X as the withdrawal resistance of one screw pair originally reported by Kevarinmäki (2002) in form of

$$R_x = 2 \cdot R_{ax} \cdot \cos \alpha . \quad (2.33)$$

As there is no significant difference between tension and compression, c. f. Bejtka (2005), the withdrawal capacity of one screw can be doubled, while any friction between the two timber members remains zero. In fact, friction depended components $\mu \cdot R_{ax,i} \cdot \sin \alpha$ balance each other. Again, the model assumptions (this time multiplied by the number of screw pairs) corresponded very well to related test results. Now focusing on the lateral (parallel to force axis) stiffness of these connections, two important matters have to be outlined:

Firstly, test results with 11 single screws or 7 screw pairs (both per gap), compared to those with one screw or one screw pair, showed significantly reduced connection stiffness (about 86 % and 82 % of one screw or screw pair multiplied by their number). Thus, a certain group effect has to be considered when estimating the specific joint stiffness. This was done in Blaß et al. (2006) by applying the theory of Lantos (1969) in form of a declining behaviour of $K_{ser,n}$ with increasing n .

Secondly, Blaß et al. (2006) recommend to determine the single fastener's (or pairs') lateral stiffness K_{ser} as a serial system of the two inserted screw threads' axial stiffness as follows (note: exclusively for $0^\circ \leq \alpha \leq 45^\circ$):

$$\text{Tensioned screw joint (one screw):} \quad K_{ser} = \frac{1 + \mu \cdot \tan \alpha}{\frac{1}{K_{ser,ax,1}} + \frac{1}{K_{ser,ax,2}}} \quad (2.34)$$

$$\text{Crossed screw joint (one pair):} \quad K_{ser} = \frac{2}{\frac{1}{K_{ser,ax,1}} + \frac{1}{K_{ser,ax,2}}} \quad (2.35)$$

Nevertheless, the estimated connection stiffness in form of single values according to eqs. (2.34) and (2.35) multiplied by a reduced n_{ef} according to Lantos (1969) clearly underestimated the experimental results. The main reason therefore was seen by Blaß et al. (2006) in the application of eq. (2.31) for estimating $K_{ser,ax,i}$ of screw types (thread geometries) applied in the connection tests, which differ from those screw types eq. (2.31) was derived with.

Basing on the previously discussed publications, Tomasi et al. (2010) carried out an extensive experimental campaign related to this topic. Thereby, they extended the possibilities of screw application, given in Figure 2.27, by one further configuration covering the case of screws, which are exclusively stressed in compression. An overview of their programme, which also contains a comparison between one and two rows of screws (including two values of $a_1 = \{70, 160\}$ mm and three of $\alpha = \{45, 60, 75, 90\}^\circ$, is shown in Figure 2.29.

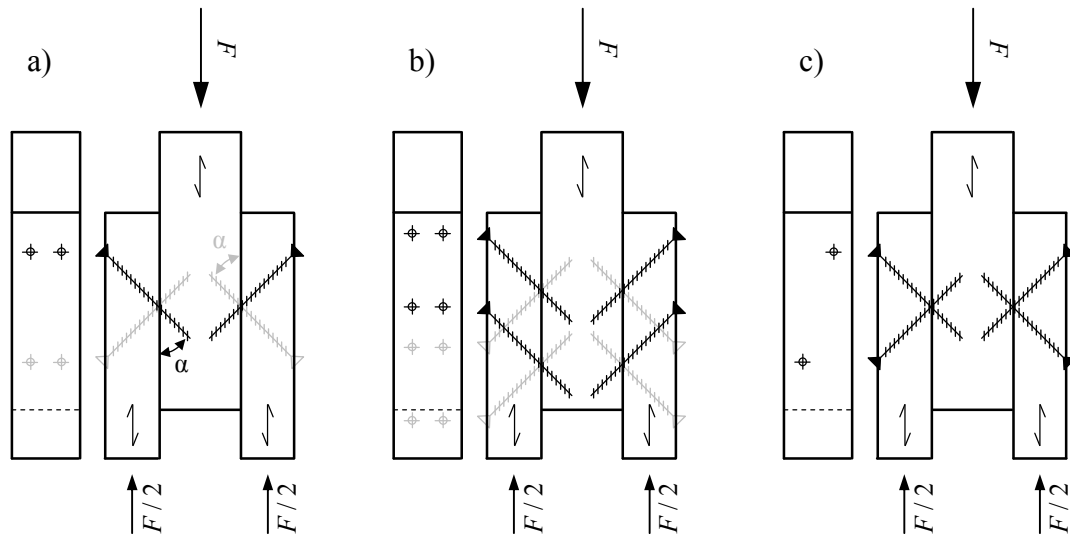


Figure 2.29: Screw configurations tested by Tomasi et al. (2010); a) single row and b) double row (a_1 varied) joint with tensioned or compressed screws, c) joint with crossed screws

As discussed in section 2-1.1, not only strength and stiffness properties but also its ductility D governs the joint's design process and classification. Thus, Tomasi et al. (2010) determined this parameter “static” ductility D_s according to ON EN 12512 (2001) increasing from $\min[D_s] = 4$ for low α (predominately axially loaded joints) to $\max[D_s] = 30$ for $\alpha = 90^\circ$ (predominately laterally loaded joints). The verification of the bearing capacities $F_{\max,i}$ was done by applying the design approach recommended in the Eurocode 5 version (valid at this time), and the functions derived by Bejtka and Blaß (2002), exemplarily given in eq. (2.28). In case of an inclined screw positioning (tensioned and crossed), the latter mentioned model again shows a good agreement with test results, while the one according to Eurocode 5 significantly underestimates the real load-carrying capacity. Higher deviations (underestimations) between eq. (2.28) and tests results were found for both, compressed and laterally loaded, screws ($\alpha = 90^\circ$), which were quite equal in the size of F_{\max} . Worth mentioning, Tomasi et al. (2010) applied eq. (2.28) for all screw positions tested and used the total withdrawal strength instead of a reduced one, as recommended in Bejtka and Blaß (2002).

In contrast to the estimation of the loadbearing capacities and alternative to Blaß et al. (2006), Tomasi et al. (2010) derived a new approach, estimating the stiffness K_{ser} (parallel to force axis) of the screwed connection. Based on the relationship between the displacements δ_i shown in Figure 2.30 (left) and Hooke's law $\delta_i = F_i / K_i$, they recommend to apply eq. (2.36) for this purpose.

$$K_{\text{ser}} = K_{\text{ser,lat}} \cdot \sin \alpha \cdot (\sin \alpha - \mu \cdot \cos \alpha) + K_{\text{ser,ax}} \cdot \cos \alpha \cdot (\cos \alpha + \mu \cdot \sin \alpha), \quad (2.36)$$

$$\text{with } K_{\text{ser,lat}} = \frac{\rho_{\text{mean}}^{1.5} \cdot d}{23}, \quad K_{\text{ser,ax}} = \frac{1}{\frac{1}{K_{\text{ser,ax},1}} + \frac{1}{K_{\text{ser,ax},2}}} \quad \text{and} \quad K_{\text{ser,ax},i} = 30 \cdot l_{\text{ef},i} \cdot d, \quad (2.37)$$

as lateral and axial stiffness of both parts of the screw thread situated in the timber members 1 and 2. While the former mentioned has been adopted from Eurocode 5 for laterally loaded dowel-type connections (ρ_{mean} as average density of both timber members), the latter one again bases on the assumption of a serial system with $K_{\text{ser,ax},i}$ determined according to Z-9.1-472 (2006), which was the technical approval of the applied screws' manufacturer. As demonstrated in section 2-2.5.5, the application of this approach (eq.(2.37), right) for determining $K_{\text{ser,ax},i}$ results in stiffness values significantly higher than those estimated with eq. (2.31). A comparison of both approaches (eq. (2.34) and eq. (2.36)) is illustrated in Figure 2.30 (right). The parameters were set to tensioned screws, $30^\circ \leq \alpha \leq 90^\circ$, $\mu = 0.30$ and a ratio between $K_{\text{ser,ax}}$ and $K_{\text{ser,lat}}$ of 35:1, as published in Bratulic et al. (2014), ignoring the previously discussed deviations between $K_{\text{ser,ax,eq.}(2.34)}$ and $K_{\text{ser,ax,eq.}(2.36)}$. While the estimations, determined with eq. (2.34), slightly decrease with decreasing α (as a consequence of δ as the cos component of δ_{ax}), those determined with eq. (2.36) show a clear oppositional behaviour in dependence from the inclination angle. Hence Blaß and Bejtka (2001) experimentally determined a ratio between $K_{\text{ser},\alpha=45^\circ}$ and $K_{\text{ser},\alpha=90^\circ}$ of roughly 12:1, a high predictive quality, concerning not only the stiffness values, but also the course of $K_{\text{ser}}(\alpha)$, can be addressed to the approach published by Tomasi et al. (2010).

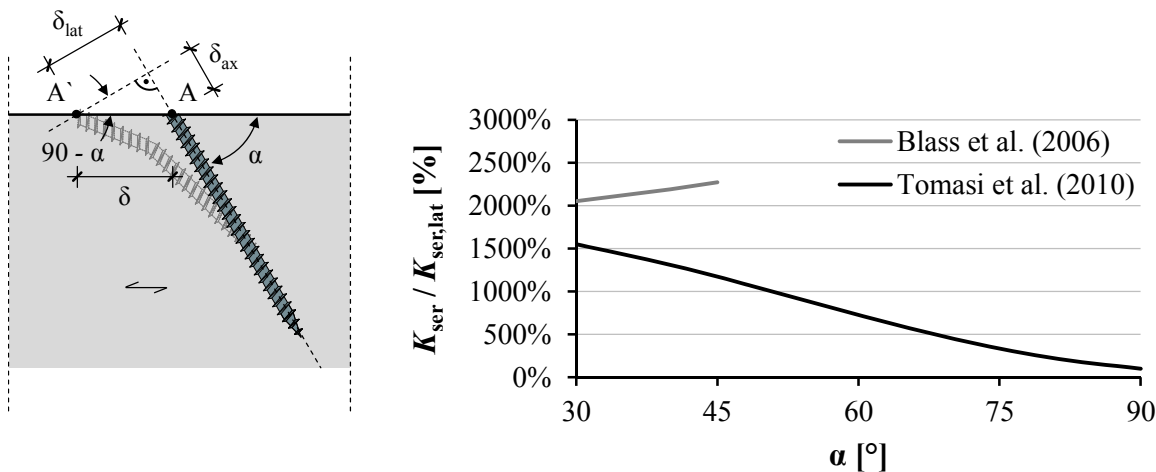


Figure 2.30: Left: lateral and axial displacement components of inclined screw joints; according to Tomasi et al. (2010); right: comparison of connection stiffness K_{ser} (referred to $K_{\text{ser,lat}}$) between the models of Blaß et al. (2006) and Tomasi et al. (2010)

Nevertheless, expectations of K_{ser} again significantly underestimated experimental results, especially for low α and predominately axially loaded screws. Based on optical examinations of tested connections,

where the (remarkable) screw displacements mostly occurred in only one of both timber members, Tomasi et al. (2010) consequently assumed $K_{ser,ax} = \min(K_{ser,ax,i})$. This measure increases the connection stiffness by far and led to a much better compliance with experiments. Since K_{ser} describes the *linear* elastic force-deformation relationship at minor values of δ_i , this assumption, basing on *nonlinear* deformations after connection failure observed, seems questionable. With regard to the effective number of fasteners n_{ef} , compared to their total number n , possibly influenced by different $a_{1,i} = \{70, 160\}$ mm, no remarkable difference was found as a consequence of the parameter variation. Moreover, the general assumption of $n_{ef} = n$, published by Blaß et al. (2006), could be confirmed.

All models discussed so far allow a determination of resistance and stiffness solely for joints loaded in parallel to the timber members' surface. For screwed connections with a load-to-surface angle of 90° , Jockwer et al. (2014) derived a further approach, which enables the determination of both properties in this case. As illustrated in Figure 2.31 (left), their considerations again base on Johansen's theory, taking the timber member's resistance against the force component F_v acting perpendicular to the screw axis into account. As the screw is hereby torn out of the timber member, the embedment strength at its surface has to be zero. According to Jockwer et al. (2014), the length x_1 , along the embedment strength has to be reduced, mainly depends on the timber's rolling shear strength f_r and can be determined as follows:

$$x_1 = \frac{f_h \cdot d_{ef}}{2 \cdot \tan \alpha \cdot f_r}, \quad (2.38)$$

with $d_{ef} = 1.1 \cdot d_c$ as the effective diameter of the screw according to ON EN 1995-1-1 (2015) and presupposing that the screw is inclined in fibre direction. Further assuming zero embedment strength along x_1 , Jockwer et al. (2014) propose the determination of R_v defined as the screw's lateral resistance according to eq. (2.39), see

$$R_v = -f_h \cdot x_1 \cdot d_{ef} + \sqrt{(2 \cdot M_y + f_h \cdot x_1^2 \cdot d_{ef}) \cdot f_h \cdot d_{ef}}. \quad (2.39)$$

R_{90} as the screw's resistance against a load direction perpendicular to the timber member's surface can be finally determined according to eq. (2.40):

$$R_{90} = R_{ax} \cdot \sin \alpha + R_v \cdot \cos \alpha. \quad (2.40)$$

With regard to the joint stiffness, Jockwer et al. (2014) recommend to treat both stiffness components $K_{ser,ax}$ and $K_{ser,v}$ as serial system, see:

$$\frac{1}{K_{ser,90}} = \frac{1}{K_{ser,v}} + \frac{1}{K_{ser,ax}} \quad \text{with} \quad K_{ser,lat} = \frac{3 \cdot E_s \cdot \pi \cdot d_c^4}{64 \cdot x_1^3}, \quad (2.41)$$

assumed as bending stiffness of a cantilever beam with length x_1 , see Figure 2.31 (right). A comparison of the model approach with results of an experimental campaign on screwed connections with varying inclination angles, also presented in Jockwer et al. (2014), showed a high agreement. Worth mentioning, that Jockwer et al. (2014) used a modified form of of eq. (2.27) (pre-factor 25 replaced by 40) for estimating $K_{ser,ax}$ in this case.

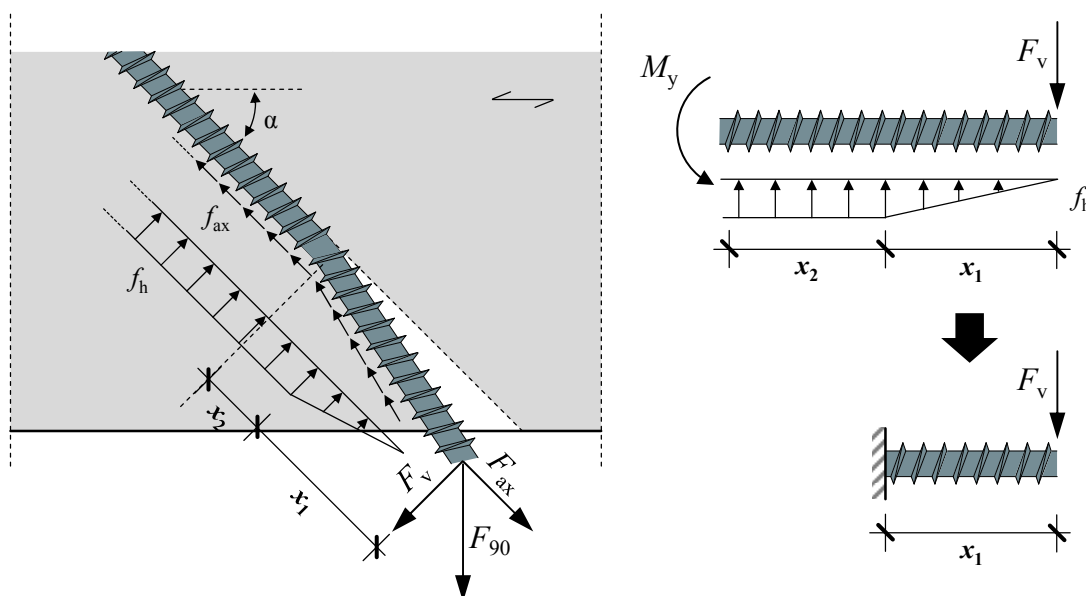


Figure 2.31: Left: schematic illustration of forces and stress distributions in an inclined screwed timber-to-timber connection loaded perpendicular to grain; right: stiffness model simplification with reduced embedment strength; according to Jockwer et al. (2014)

Finally, four further works done by Kevarinmäki (2002), Tomasi et al. (2006), Gehri (2010) and Piazza et al. (2011) are worth to be highlighted within this section. Similar to Bejtka and Blaß (2002), Kevarinmäki (2002) focused on determining strength and stiffness properties of (i) tensioned and (ii) crossed screw connections in solid timber and laminated veneer lumber (LVL). His already mentioned model approach, given in eq. (2.33), estimating the joint's bearing resistance in case (ii), has to be pointed out again. Concentrating on their behaviour in case of seismic actions (earthquakes), Tomasi et al. (2006) and Piazza et al. (2011) conducted several experimental investigations on screwed connections under monotonic and cyclic loading according to ON EN 12512 (2001). In addition, they confirmed the monotonic test results with the approach developed by Bejtka and Blaß (2002), as well as by means of numerical methods. In terms of seismic behaviour, they classified the connections as L (low ductility, small values of α , predominately axially loaded screws) to H (high ductility, $\alpha \rightarrow 90^\circ$, predominately laterally loaded screws) according to ON EN 1998-1 (2013). Furthermore, tests on connections with varying α_i (within one specimen) showed, that the total joint capacity R may be easily composed by summing up all single capacities $R_i(\alpha_i)$; even in cases, α_i significantly differed. According to Tomasi et al.

(2006) and Gehri (2010), it would be possible to control the shape of the joint's force-deformation relationship by applying differently inclined screws within one connection.

2-3.1.2 Steel-to-timber normal joints

As discussed in section 2-1.2, further investigations, aiming to maximise the loadbearing capacity of predominately axially loaded screwed connections, led to the development of two different kinds of steel-to-timber joint designs. The first possibility, given in Figure 2.32 (left), simply replaces both outer timber components by steel plates, while the inclined screw configuration, shown in Figure 2.27, has been adopted. In the second case (Figure 2.32, right), analogies found between glued-in rods and screws regarding their loadbearing behaviour resulted in screw arrangement parallel to grain (end-grain joints). Due to the fact, that almost the whole screw thread ($l_{ef} = \{l_{screw} - t_{st} / \cos\alpha, l_{screw} - (t_{add} + t_{st})\}$) is situated in just one timber component, the steel tensile failure as the maximum loadbearing capacity per screw in axial direction may be reached by both possibilities. With regard to joint design, the input parameters are similar to those mentioned in section 2-3.1.1.

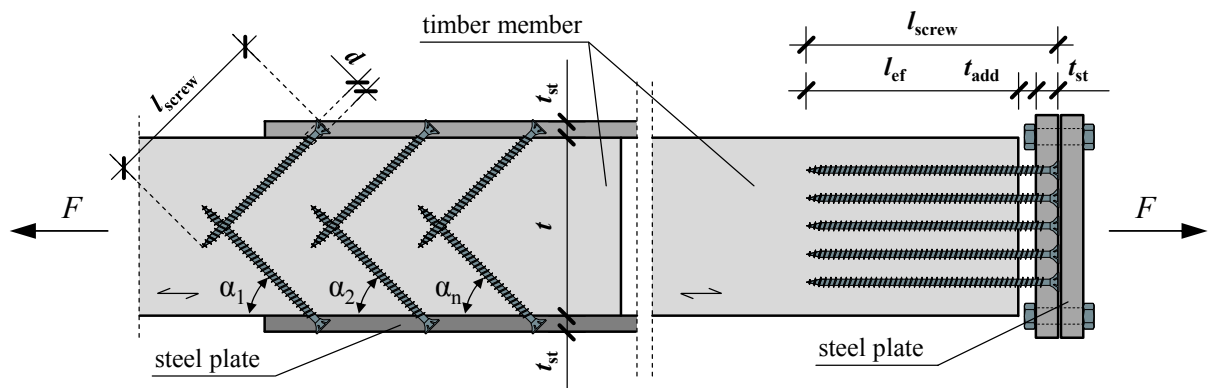


Figure 2.32: Cross-section of two types of steel-to-timber connections with predominately axially loaded self-tapping screws; left: inclined screw butt joint; right: end-grain joint with screws inserted parallel to grain direction

Focusing on steel-to-timber butt joints with inclined positioned self-tapping screws, major investigations related have been conducted by Krenn and Schickhofer (2007), Krenn (2009), Krenn and Schickhofer (2009) and Krenn (2010). Therein, they carried out a huge experimental campaign with up to 600 tests on single and multiple row joints with one to eight screws per gap. The overall aim of this research programme was to determine whether a negative group effect for this type of connection exists or not. Further parameters varied were: $\alpha_i = \{30^\circ, 45^\circ\}$, the effect of friction (for a certain number of tests, Teflon stripes ($\mu \rightarrow 0$) have been used) and screw thread length (fully and partially threaded screws were applied), the latter consequently leads to different failure mechanisms (withdrawal instead of head tear-off).

Based on the conclusions made in Krenn and Schickhofer (2009), a slightly reduced n_{ef} with increasing n results for screws failing in withdrawal, while in case of head tear-off (steel tensile) failure no influence of n on R has been observed. In fact, the average loadbearing capacity (referred to one screw) of the latter mentioned failure mode slightly increased with n , probably being influenced by a certain screw ductility, enabling a load redistribution within the connection to a small degree. In terms of withdrawal failure, their observations differ from those made by Blaß et al. (2006), which may be caused by outer steel plates allowing minor deformations (and thus minor load redistribution) if compared to the timber components they replace. Nevertheless, in order to avoid differing between the two failure mechanism observed, and to cover practical uncertainty (as mentioned in section 2-1.2, steel-to-timber connections require far more production accuracy and quality control), Krenn and Schickhofer (2009) recommend determining n_{ef} as the product of n multiplied by 0.9.

With regard to the loadbearing capacity of steel-to-timber joints, composed by inclined positioned self-tapping screws, Krenn and Schickhofer (2009) confirmed the simplified approach from Blaß et al. (2006) (and Kevarinmäki (2002) respectively) of solely considering the screw's axial resistance (including both \cos and $\mu \cdot \sin$ components) in form of a truss-like force system. Thereby, they recommend approximating the friction coefficient to $\mu = 0.25$. Focusing on serviceability limit state (SLS), the determined connection stiffness $K_{ser,n}$ showed a clear regressive behaviour by increasing n , similar to the findings for timber-to-timber joints made by Blaß et al. (2006). For instance, $K_{ser,8}$ of tests with eight screws per gap (head tear-off failure) was roughly 70 % of $K_{ser,1}$ multiplied by $n = 8$. Consequently, $n_{ef,ser}$ should be assumed by $n^{0.8}$. Concerning the structural detailing, Krenn and Schickhofer (2009) recommend overlapping the screws at least $4d$ at the timber member's system axis, in order to avoid its splitting caused by remarkable tensile stresses perpendicular to grain occurring in this zone (observed and numerically verified).

Concluding the findings made by Krenn and Schickhofer (2009), steel tensile failure always occurred as a head tear-off rupture at the transition zone between timber member and outer steel plate. This due to an assumed tensile (axial tension and bending) and shear stress interaction, caused by the contact of the thread flanks with the steel plate's borehole wall at minor deformations parallel to force direction. Consequently, the investigations done by Ringhofer et al. (2014b) focused on the development of an optimised screw geometry, which based on an idea from Pirnbacher et al. (2009), for this type of connection. The main differences between the modified and standard screw geometry are some kind of a bunch with diameter equal to d (centring the screw in the borehole), followed by a thinner thread-free area in order to start with the thread at least $2d$ below the timber's surface; see Figure 2.33.

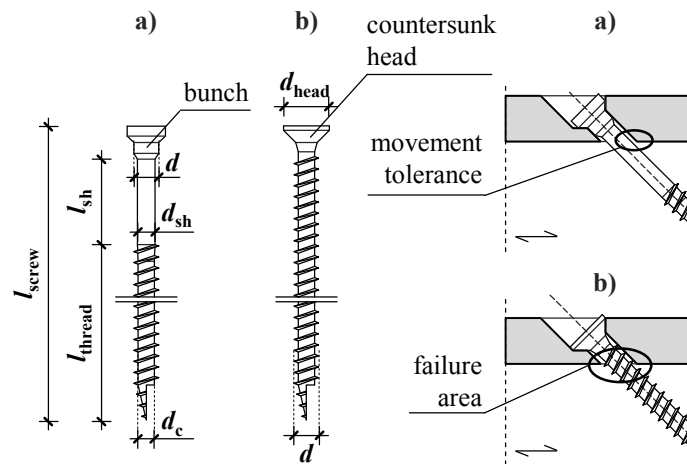


Figure 2.33: Comparison: (a) modified with (b) standard screw geometry; according to Ringhofer et al. (2014b)

The results of an experimental programme, wherein the new prototypes in form of a steel-to-timber tensile connection have been applied (test configuration according to Krenn and Schickhofer (2009), eight screws per gap), assigned them a bearing capacity roughly 5 % higher if compared to a standard screw model commonly used for this purpose. Furthermore, a tentative assembly of two test specimen with 20 screws per gap led to a net cross-section failure of the GLT timber specimen with a characteristic V-shaped crack formation occurring along the inclined screw axis. Due to the fact, that common design approaches only consider a cross-sectional weakening by subtracting all $A_{Q,i}$ situated within, c. f. Colling (2012) and Figure 2.34 (middle), Ringhofer et al. (2014b) recommend determining the net cross-sectional area as follows:

$$A_{\text{net}} = h \cdot w - 2 \cdot m \cdot d \cdot l_{\text{ef}} \cdot \sin \alpha, \tag{2.42}$$

where m is the number of the screw rows within the connection, see Figure 2.34 (right).

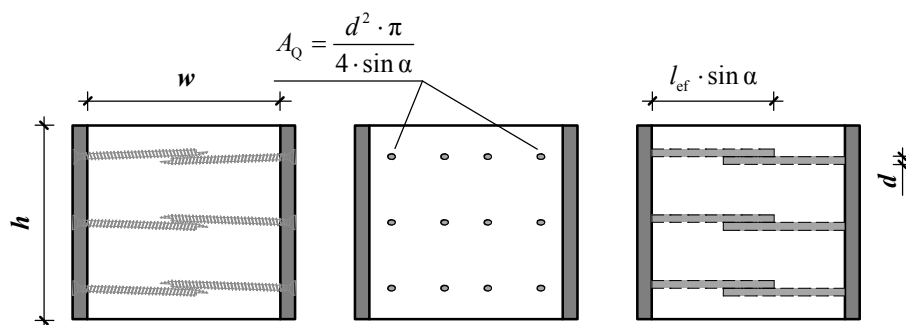


Figure 2.34: Different possibilities of determining the reduced cross-sectional area; left: cross-section of the screwed connection; middle: cut surfaces of screw axis; right: projection of screws' outer thread surfaces; according to Ringhofer et al. (2014b)

Since the approach given in eq. (2.42) only bases on a qualitative evaluation of crack formation, Brandl (2015) carried out an experimental campaign determining the quantitative decrease of timber tensile resistance caused by its weakened cross-section. The conclusion of her findings is, that the function given in eq. (2.42) underestimates the net cross-section's loadbearing capacity. Thus, she recommends a modified version to be applied as follows:

$$A_{\text{net}} = w \cdot (h - m \cdot d), \quad (2.43)$$

which solely deviates from eq. (2.42) concerning the length used for determining the screw's projected outer thread surface.

As discussed in section 2-1.2, the increasing application of timber members – composed by boards and veneers out of hardwood species in the near future – reduces their necessary cross-sections by far. Consequently, the dowel-type connection technique, especially if the activated axial loadbearing capacity is governed by the fastener's inserted length (the thread length in case of self-tapping screws), needs new solutions regarding a significantly reduced space the joint has to be arranged in. Since the maximum thread length increases by decreasing α (nearly unlimited $l_{\text{thread},i}$ are reached in case of $\alpha = 0^\circ$, parallel to the member axis), end-grain joints with screws arranged parallel to grain are the logical consequence of this development process. Due to their similarities to glued-in rods, but with big advantages in terms of application, Gehri (2007), Gehri (2009) and Gehri (2010) concentrated on the realisation of this kind of screwed connection by generally basing on approaches developed for the before mentioned fastener types. While basic properties of axially loaded self-tapping screws applied in hardwood have been investigated elsewhere, see e. g. Hübner (2009), Hübner et al. (2010), Hübner (2013a) and Hübner (2013b), Gehri (2009) focused on the group effect of end-grain connections by comparing the joint's loadbearing capacity ($n_{\text{max}} = 16$) with that of $n = 1$. In contrast to the previously discussed works, done by Blaß et al. (2006) and Krenn and Schickhofer (2009), who were interested in group behaviour at sufficient in-between spacings applied, Gehri (2009) describes the varying joint capacities by varying ratios a / d (a as side length of a virtual quadratic minimum area per screw) as follows:

$$k_{\text{red}} = \frac{n_{\text{ef}}}{n} = n^{-\zeta} \cdot \left(\frac{a}{a_{\text{threshold}}} \right)^\xi, \quad (2.44)$$

where ζ is an inverse power parameter, covering the possibility of the load redistribution of fasteners in a row parallel to grain, $a_{\text{threshold}}$ is an upper limit, above the screw spacings have no influence on loadbearing behaviour and ξ is the power parameter covering the impact of $a / a_{\text{threshold}}$ on k_{red} . In case of screwed end-grain joints, Gehri (2009) assumes $\zeta = 0$ (which means $n = n_{\text{ef}}$ at sufficient spacings), $a_{\text{threshold}} = 5d$ and $\xi = 0.35$. A comparison of eq. (2.44) with the test results ($a_i = \{3, 4, 6 \text{ and } 12.5\}d$) confirmed the data

trend, while the absolute values were slightly underestimated, indicating a conservative approach. Noteworthy to mention, all tests failed in withdrawal, while the steel failure in tension or splitting of the timber member (tension perpendicular to grain), as an additional mode occurring in such connections, were not treated in detail. In Gehri (2010), two further aspects concerning the screwed end-grain joints are pointed out:

First, and similar to the conclusions made in section 2-1.1, the ductility D significantly decreases by decreasing α , end-grain joints are thus concluded to show only brittle failure modes.

Second, tests on connections ($n = 8$, European ash) with thread lengths reaching the screws' steel failure in tension (as maximum loadbearing capacity per fastener), showed a reduced loadbearing capacity of roughly $10 \div 15 \%$ if compared to the product of the single screw's steel tensile capacity, $f_{\text{tens},1}$ and n . Applying eq. (2.44) for the specific detail tested ($a = \{3.46, 4.33\} d$), the model results slightly overestimate the real decrease mentioned – data trend is again well represented.

Obermayr (2014) applied a similar test configuration determining the loadbearing behaviour of screwed end-grain connections in GLT made of birch. Thereby, she not only varied the number of screws ($n = \{9, 13\}$), which consequences $a_i = \{3.33, 2.77\} d$, but also their inserted thread lengths in order to differ between withdrawal and steel failure in tension. Her results gained indicate (a) confirmation with eq. (2.44) in case of $n = 9$ and steel failure in tension (two tests considered, $a = 3.33 d$: $F_{\text{max,mean,exp}} / f_{\text{tens},1} = 0.90$, $k_{\text{red,eq. (2.44)}} = 0.87$) and (b) splitting of the timber member nearly for all tests where $n = 13$ and $a = 2.77 d$ respectively. Worth mentioning, that in principle the screws applied in case (b) were aimed to reach the steel failure in tension, the lower limit of $a = 2.50 d$ to prevent splitting failure, as mentioned in Gehri (2009), could thus not be confirmed.

Also focusing on this specific type of screwed connection, Grabner and Ringhofer (2014) experimentally determined its loadbearing capacity in case of steel failure in tension, $n = 13$ and $a = 3.19 d$. As a consequence of the slight increase in a and the application of screws with lower f_{tens} , the splitting failure of the timber member could be prevented in ten of eleven cases, while results are slightly underestimated by eq. (2.44) (ten tests considered, $a = 3.19 d$: $F_{\text{max,mean,exp}} / f_{\text{tens},1} = 0.92$, $k_{\text{red,eq. (2.44)}} = 0.85$).

Quite recent examinations regarding this topic are reported by Meyer (2016), who experimentally determined the bearing resistance of this joint configuration ($n = 4$, $d = 10 \text{ mm}$, $a = 2.75 d$) in LVL made of beech. Interestingly, four out of five specimen failed by exceeding the screws' steel tensile capacity, one by shear failure of the LVL specimen (explained by production inaccuracies) but none by splitting. Even though this specific product is known for a comparatively weak performance in tension perpendicular to grain, c. f. ETA-14/0354 (2015), it is obviously possible to develop such a joint detail avoiding the latter mentioned, unfavourable failure mode even at $a < 3 d$.

In cases, spacings a_i are high enough to prevent a splitting failure of the timber member (presupposing that screws are pre-drilled) and the steel failure in tension is reached as maximum loadbearing capacity per fastener, n_{ef} may be conservatively assumed to $0.9 \cdot n$, as also recommended in Krenn and Schickhofer (2009), for inclined screwed steel-to-timber connections. The effect of $a_i \geq a_{\text{threshold}}$ on n_{ef} may thus converging to 1.00 has not been investigated yet. The efficiency η resulting to roughly 0.50 for the connection tested in Grabner and Ringhofer (2014) will decrease by this measure, making the discussed solution less attractive for the application in timber structures, c. f. Gehri (2007). Finally, the comparatively poor long-time loadbearing behaviour of axially loaded self-tapping screws inserted parallel to grain should be pointed out in this context, c. f. Pirnbacher and Schickhofer (2012). To avoid this effect, certain measures in structural detailing, such as the arrangement of an embedment length l_{emb} between the end-grain surface and the screw thread inserted of at least $2d$ (similar to that given in Figure 2.33, a) and/or the use of thread lengths, long enough to reach the steel failure in tension instead of withdrawal, even at $t \rightarrow \infty$, are required.

Summarising the findings made by Gehri (2009), Obermayr (2014) and Grabner and Ringhofer (2014), the splitting failure of the timber member represents a lower limit, in-between spacings of screws should not exceed. With regard to connections, where both screw axis *and* force direction are inclined positioned to the timber member's fibre orientation the screws are inserted in (see Figure 2.35, $\alpha > 0^\circ$), the occurrence of the block shear (and at certain conditions plug shear) failure mode shows a similar dependency on the size of the connection situated. Motivated by the first related observations published in Plieschounig (2010), further works reported in Mahlkecht (2011), Mahlkecht and Brandner (2013), Mahlkecht et al. (2014) and Mahlkecht et al. (2016) experimentally determined this effect in timber components made of solid timber, GLT and CLT. Thereby, not only spacings a_i between two screws, but also the inserted thread length, as well as α (here: angle between screw *and* force axis to grain direction) have been varied. The results show significant dependencies of block shear failure mechanism on all parameters mentioned and indicate, that the size of the timber volume stressed (combination of tension perpendicular to grain, shear and rolling shear; at least for $\alpha = 90^\circ$ as worst case scenario shown in Figure 2.35, right) governs the connection's resistance related.

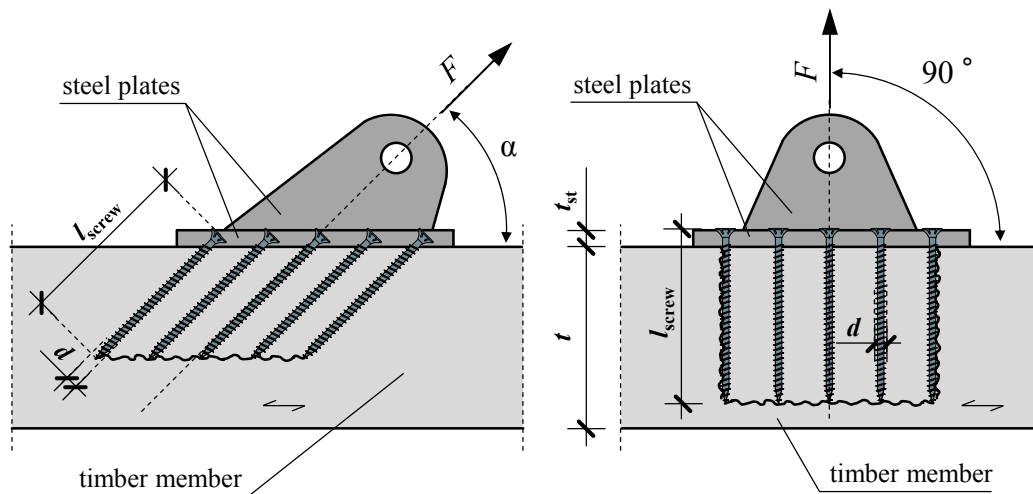


Figure 2.35: Crack formation (block shear failure) of inclined steel-to-timber joints; left: general definition with varying α ; right: worst case scenario at $\alpha = 90^\circ$

In Mahlkecht et al. (2014), a first approach determining the block shear resistance of such joints for $\alpha = 90^\circ$ and timber components in ST and GLT is given. Its adaption as a design rule to be included in standardisation as well as the consideration of varying α and further timber products, block shear may also occur in CLT side faces, see Mahlkecht and Brandner (2013), are seen as a main task for further investigations.

2-3.2 Transversal joints

2-3.2.1 Timber-to-timber transversal joints

Figure 2.36 (left) illustrates a typical timber-to-timber transversal joint transferring the shear forces ($V = F$) from a secondary to a main beam (the latter assumed supporting the former). Similar to timber-to-timber normal joints, discussed in section 2-3.1.1, the screws are applied inclined to force direction (angle ϵ) and thus are again predominately axially loaded. The deviations from normal joints are (i) different angles between screw axis and fibre direction of secondary (α) and main beam ($\alpha = 90^\circ$) and (ii) certain boundary conditions to be additionally considered in the design process as discussed as follows.

In addition to their investigations, carried out for normal joints, Blaß and Bejtka (2001) and Blaß and Bejtka (2003b) also concentrated on this kind of connection. Thereby, they experimentally determined the related loadbearing behaviour by varying the following parameters: $\alpha = \{30^\circ, 45^\circ \text{ and } 60^\circ\}$ (for secondary beam), screw positions (one tensioned screw vs. two crossed screws), as well as the way main beams are supported (fixed-end beam, see Figure 2.36, middle, vs. hinged supported beam, see Figure 2.36, right).

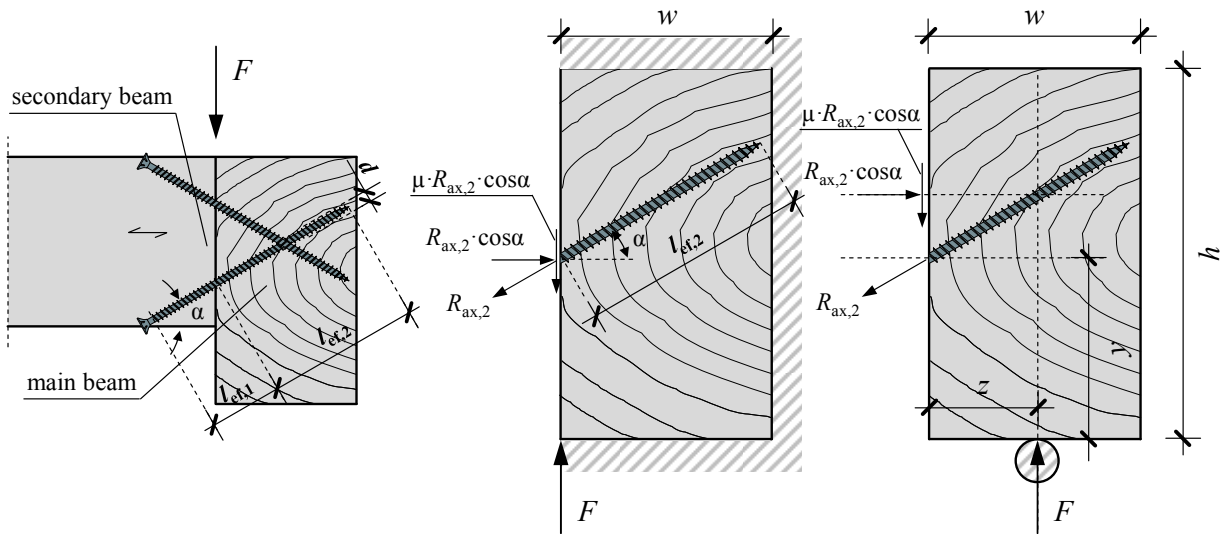


Figure 2.36: Left: main to secondary beam transversal joint with crossed screws; middle: force system at fixed-end main beam; right: force system at hinged supported main beam; according to Blaß and Bejtka (2003b)

Since the model derived for normal joints enables a simple, but comparatively accurate, design process, Blaß and Bejtka (2003b) applied the same approach for estimating the loadbearing capacity of transversal joints, shown in Figure 2.36. As previously mentioned, they derived two further boundary conditions, which – in dependence from screw positioning and main beam’s supporting – restrict the value of α . In case of both, tensioned and crossed screw configurations, and a fixed-ends main beam, eqs. (2.32) and (2.33) can be adopted. In case of the tensioned screw configuration and a hinged supported main beam, ε is limited as follows:

$$\alpha \leq \arctan\left(\frac{h-y}{z}\right), \quad (2.45)$$

with h as the main beam’s height, z as the parallel distance between the supporting force axis and the main beam’s left (or right) edge, and y as the distance between the intersection of the screw axis with the main beam’s left (or right) edge and its lower edge, c. f. Figure 2.36 (right). If α exceeds the upper limit defined in eq. (2.45), no compressive force (cos component of $R_{ax,2}$) will sustain the equilibrium in this (consequently kinematic) system. In case of a crossed screwed configuration and a hinged supported main beam, α should be chosen according to eq. (2.46), in order to avoid the transmission of an additional moment by the screws caused by an eccentric load introduction:

$$\alpha = \arctan\left(\frac{h_i}{2 \cdot z}\right), \quad (2.46)$$

where h_i is defined as the distance between the intersections of both screw axis with the main beam's left (or right) edge. A final comparison of the test results showed a good agreement with the discussed model assumptions, slightly underestimating the experimentally determined bearing capacities.

Further examinations, regarding timber-to-timber transversal joints composed with self-tapping screws, have been carried out by Prat-Vincent et al. (2010) and Yeh et al. (2014). Except of their crossing point located in the gap between main and secondary beam, both applied an inclined screw configuration, similar to that shown in Figure 2.36 (left), in their experimental campaigns. Summarising the main outcomes, Prat-Vincent et al. (2010) report a high agreement between test results and values predicted by the model approach for crossed screw joints given in eq. (2.33), again confirming its applicability for this purpose. Yeh et al. (2014) compare the experimental values of inclined screw joints, with those where screws have been laterally loaded and observe significantly higher bearing capacities as a consequence of predominately axial loading in the former case.

With regard to the fire design of such timber-to-timber transversal joints realised with inclined positioned self-tapping screws, the investigations reported in Werther et al. (2014), Hofmann et al. (2016a) and Hofmann et al. (2016b) are worth being mentioned. In particular, in Hofmann et al. (2016b), some constructive regulations concerning minimum spacings and cross-sectional dimensions for 30 and 60 minutes of fire exposure are given.

2-3.2.2 Steel (metal)-to-timber transversal joints – System connectors

Since typical timber structures consist of one-dimensional members, classified in dependence of their arrangement in main and secondary beams (sometimes also tertiary beams exist), the connections between both components are mainly transmitting shear forces (which are the supporting forces of the secondary beam) and represent the majority of joint details in such systems. Due to their similarity within one construction, but also in general as a consequence of standardised timber members' dimensions (especially the width of GLT beams), the use of high-grade pre-fabricated connection systems increases the structure's cost efficiency and saves erection time. As discussed in section 2-1.2, the efficient combination of inclined positioned self-tapping screws and steel (or general metal) plates as outer members replaced the most former applied solutions with screws, dowels and nails perpendicular arranged to force direction and thus mainly loaded by shear.

Since the early 2000s, many different forms of system connectors with inclined positioned self-tapping screws have been developed; see e. g. Blaß (2004), Hude (2005), Bogensperger and Hude (2007), Blaß (2007), Augustin (2009), Flatscher and Augustin (2010) and Augustin (2011). In general, their loadbearing capacity is governed by the one of the fasteners applied, whose design process bases on the same assumption as of a truss-like force system, as discussed in section 2-3.1 and is thus not further

treated in this section. Consequently focusing on those cases, where the main beam is weak in terms of torsional stiffness (or it is not sufficiently supported against torsion) and asymmetrical loading (different supporting loads of two secondary beams or the main beam serves as edge girder), an additional moment due to eccentricity e has to be transmitted by the screws, see Figure 2.37.

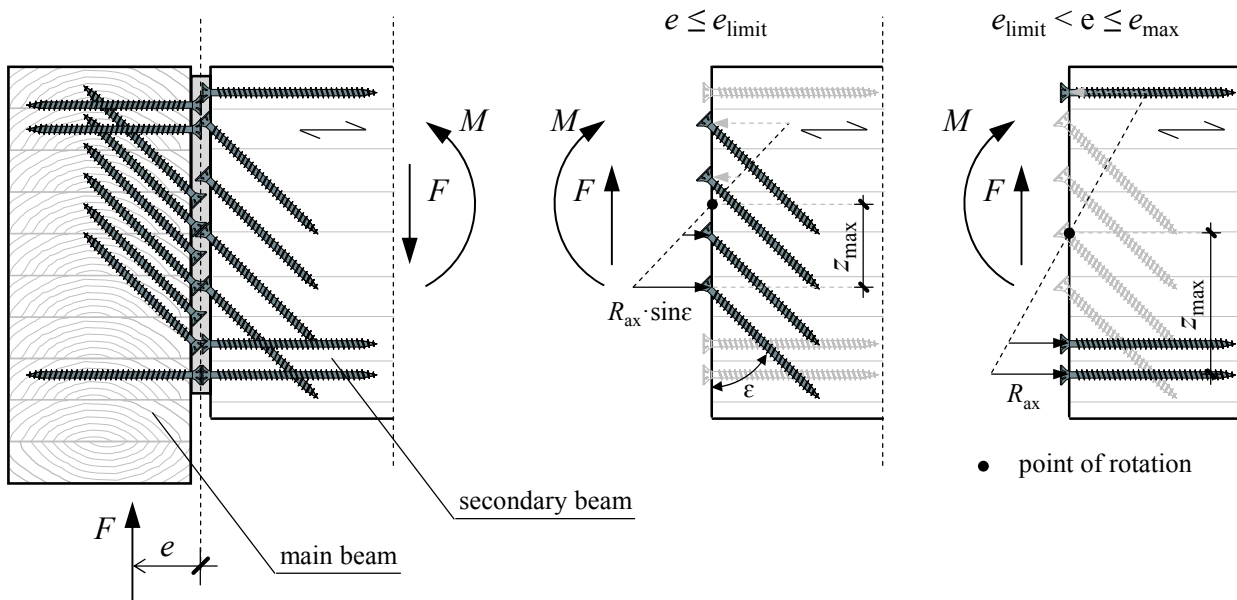


Figure 2.37: Left: cross-section of the aluminium-to-timber system connector “SHERPA”; middle and right: secondary beam force systems for an eccentric load introduction in dependence of e_{limit} ; according to Augustin (2011)

Basing on an expert report written by Blaß (2010), Augustin (2011) exemplarily provides a model approach verifying this additional moment for the dovetail system connector shown in Figure 2.37 (left). As illustrated in Figure 2.37 (middle and right), two possibilities, which depend on the relationship between e and an upper limit value e_{limit} , have to be separately discussed. In cases, e is smaller than or equal to e_{limit} , the tensile forces caused by the additional moment are covered by the compressive components ($\sin \epsilon$ component, activates friction between aluminium plate and timber surface) of the inclined positioned axially loaded screws transmitting the shear force F . In cases, e exceeds e_{limit} , supplementary “moment screws”, inserted parallel to the tensile forces’ load direction, transmit the additional moment (solely the part caused by difference $e - e_{\text{limit}}$). Assuming a cubic (originally quadratic, the power value has been increased in order to correspond with test results) interaction between shear force F and M , the connector’s bearing resistance R in case two may be determined by decreasing R_1 (bearing resistance when $e \leq e_{\text{limit}}$) in dependence of e as shown in eq. (2.47).

$$R = \begin{cases} R_1 = \frac{1.25 \cdot n \cdot R_{ax}}{\sqrt{2}} & \text{if } e \leq e_{\text{limit}} \\ \frac{R_1}{\sqrt[3]{1 + \left(\frac{e - e_{\text{limit}}}{e_{\text{max}}}\right)^3}} & \text{if } e > e_{\text{limit}} \text{ and } e_{\text{limit}} = \frac{\sum_{i=1}^n z_i^2}{n \cdot z_{\text{max}}} \end{cases}, \quad (2.47)$$

with R_1 as a result of eq. (2.32) for $\mu = 0.25$ and $\alpha = \varepsilon = 45^\circ$, e_{max} as the limit eccentricity for the maximum moment bearable and z_i (z_{max}) as the normal distance between screw tensile resistance components and the assumed centre of rotation. Worth mentioning, that both sub-connections (main and secondary beam, each to aluminium plate) have to be verified within the design process explained. For the description of further load situations of minor relevance (horizontal instead of vertical shear forces, normal forces in the secondary beam, uplift due to negative F , etc.) by adequate models, see Augustin (2011). The experimental investigations concerning the variation of all different cases of loading and eccentricity, discussed in Augustin (2011), generally confirm his model assumptions, slightly underestimating the test results.

A further examination worth mentioning in this context is reported in Laggner et al. (2016). In the frame of his master's thesis, Laggner (2016) concentrated on experimentally determining the bearing resistance of self-tapping screws exposed to combined axial and lateral loading for verifying corresponding regulations given in ON B 1995-1-1 (2015). Note: section 8.7.3 in ON B 1995-1-1 (2015) presupposes quadratic interaction for this design situation. Irrespective of the way loading was applied (sequentially vs. simultaneously), gained results indicate a possible increase of the related power parameter in form of {2.4, 3.1} for average and 5 %-quantile screw loadbearing capacities.

2-3.3 Moment joints

While inclined (or parallel) positioned, predominately axially loaded screws are frequently applied in connections transferring normal and transversal loads between two bearing members nowadays, see sections 2-3.1 and 2-3.2, similar solutions for moment rigid joints are comparatively scarce. Typical forms of latter mentioned connection details in timber engineered structures are: (a) moment rigid corner joints in frame systems and (b) clamped column bases or beam-to-column connections. While in case (b) for instance, a two-sided joint – each side detailed as a steel-to-timber connection with inclined positioned self-tapping screws transferring either the bending moment's tensile or the compressive component – can be simply regarded as the sum of two normal joints, c. f. Cloßen and Lam (2012), Kasal et al. (2014) and Gohlich and Erochko (2016) for instance, case (a) remains somewhat specific and is thus further discussed within this section.

Motivated by an increasing availability of fully threaded self-tapping screws and threaded rods with sufficient lengths and diameters for this purpose (c. f. Figure 2.22 in section 2-2.5.3), Trautz and Koj (2008), Trautz and Koj (2009), Koj and Trautz (2014) and Koj and Trautz (2016) investigated – amongst other topics discussed in section 2-4 – the feasibility of moment rigid frame corners, where both fastener types are applied for predominately transferring tensile loads (caused by the corner moment) between two GLT members. Their experimental programme contained several laboratory tests concerning these connections, whereby input parameters, such as the sign of the moment (positive and negative), the fastener arrangement and the duration of load (DoL, in combination with different load steps and climate changing) have been varied. The way, fasteners were situated in the connection (Figure 2.39), as well as the method of evaluating test results with model assumptions was derived from a simple strut-and-tie model similar to those commonly applied for structures made in reinforced concrete, see Figure 2.38.

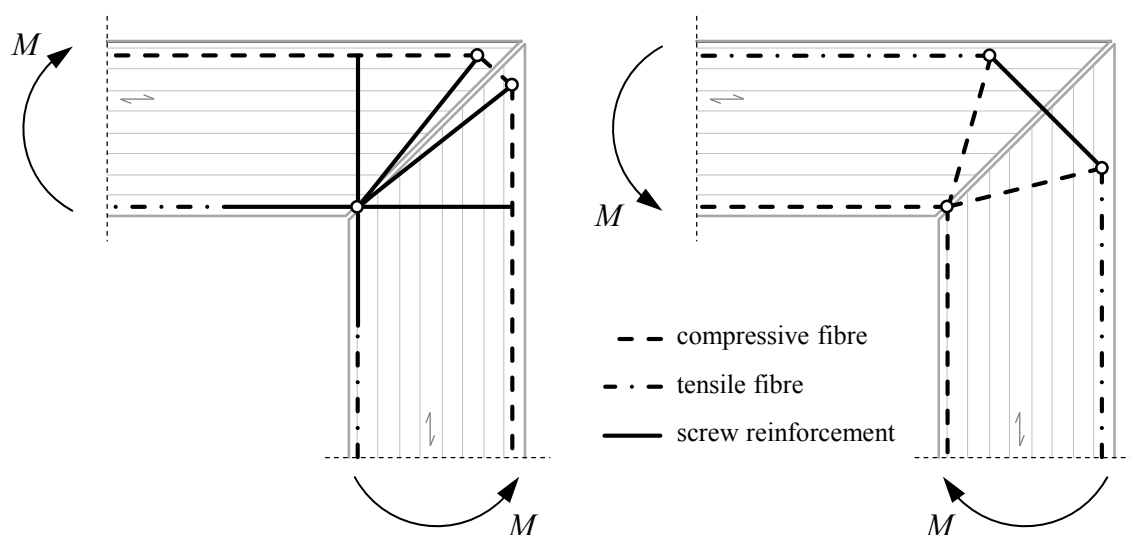


Figure 2.38: Assumed strut-and-tie models for moment rigid frame corners with axially loaded self-tapping screws; left: positive moment; right: negative moment; according to Trautz and Koj (2009)

With regard to short-time laboratory tests, determining the maximum bearing capacity M_{\max} of both connections, shown in Figure 2.39 (enhancements of a first series and published in Trautz and Koj (2009), only tensile screws are illustrated), a significantly higher 5%-quantile of M_{\max} if compared to assumed characteristic properties of alternative solutions, such as glued finger joints and doweled connections, was found. Both connection types showed favourable failure mechanisms regarding their utilisation ratio η (87.3 % for negative moment; 69.5 % for positive moment; both referred to the characteristic bending capacity of the GLT member used): the connection stressed by a positive moment (Figure 2.39, left) reached its maximum loadbearing capacity by steel failure in tension of the screws. The failure of the other type, stressed by a negative moment (Figure 2.39, right), was caused by reaching the GLT member's bending tensile strength in the reduced net cross-section. As discussed in Trautz and Koj

(2008), the test results with screws failing in tension confirmed the model assumptions determined by the mentioned strut-and-tie approach.

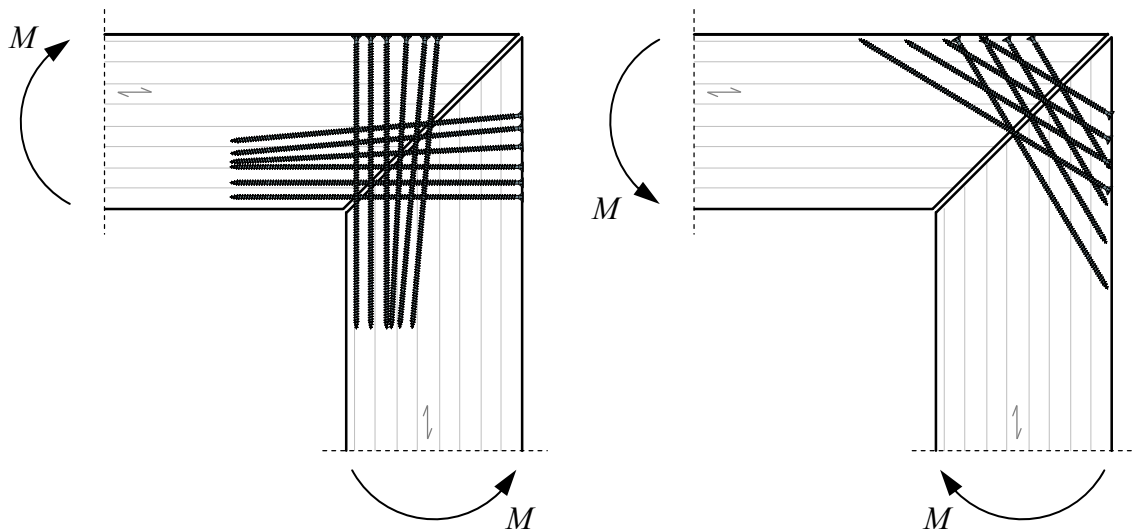


Figure 2.39: Arrangement of self-tapping screws responsible for tensile load transmission; left: positive moment; right: negative moment; according to Trautz and Koj (2009)

In order to determine DoL and creep effects, negatively influencing the long-time loadbearing behaviour of timber structures in general, the sustained loading (about 40 % to 55 % of M_{\max} , solely negative moments) was applied under service class 2 conditions according to ON EN 1995-1-1 (2015) for different joint configurations (i. a. the detail shown in Figure 2.39, right) for a period of two years, c. f. Koj and Trautz (2014). The main results were, that the creep factors $\varphi_i(t)$ were remarkably higher (between 2.9 and 3.5) than those for GLT according to Eurocode 5 ($\varphi_i(t) = 1.8$), as well as the bearing resistances (determined by short-time testing after sustained loading was finished) between 0 % and 17.5 % lower than those previously gained from short-time tests under laboratory conditions.

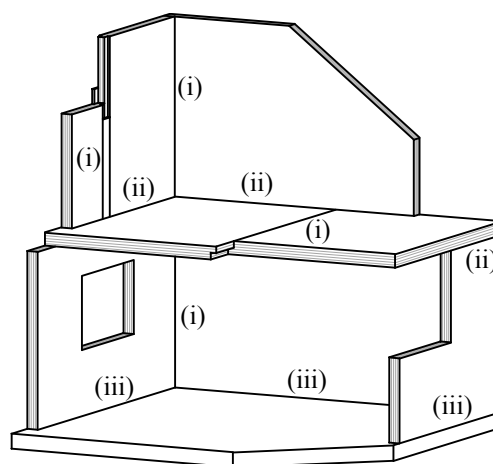
Especially the connection, where the maximum difference of 17.5 % occurred, is worth to be focused in detail. In this case, Koj and Trautz (2014) observed withdrawal failure of the outermost situated tensile screws (see Figure 2.39, right), deviating from the failure behaviour of the previously conducted short time tests. Consequently, they assume the change in failure mechanism as a consequence of DoL effects. Hence, the joints were loaded under service class 2 conditions for two years, leading to moisture contents of up to 18 % after this period. As own investigations, see Ringhofer et al. (2014c), indicate a decrease of withdrawal strength per % increasing moisture content of about 3 %, the difference between both bearing capacities (especially combined with the change of failure mechanism) may be alternatively addressed to the climatic variation. Presupposing, that the bearing capacity was determined directly after the sustained loading has been finished (without any in-between storage time at 20 °C and 65 % relative humidity).

Apart from specific the uncertainties concerning the long-time behaviour, which should be focused on by further investigations, c. f. Koj and Trautz (2014) and Koj and Trautz (2016), the moment rigid corner joints with axially loaded self-tapping screws seem to be an economical and powerful alternative to commonly applied glued finger joints and doweled connections.

2-3.4 Screwed connections in solid timber constructions

Figure 2.40 (left) illustrates the section of a typical Solid Timber Construction, whereby CLT panels applied serve as loadbearing elements for all supernatural walls and floors, which are parts of the structural system. As discussed in section 2-1.2, the size of these elements is limited by the production facilities. The current dimensions are about 18 m x 3.0 m x 0.4 m, c. f. Brandner et al. (2016a). Thus, not only walls and floors (out-of-plane joints), but also components with the same orientation (in-plane joints) have to be connected by fasteners with sufficient lengths in view of the timber product's dimensions (thickness). Since CLT panels also show high in-plane stiffness and loadbearing capacities, a weakest-link structural joint design influences the whole construction's bearing performance and cost effectiveness remarkably.

Apart from case (iii) (wall-to-foundation), nowadays self-tapping screws are commonly applied for various point and line connections, given in Figure 2.40. Hence their majority is stressed by loads, at least acting in two different directions, a classification similar to that given for one-dimensional bearing components, discussed in sections 2-3.1 to 2-3.3, is not reasonable. Especially the wall-to-floor or floor-to-wall line connections stressed by in-plane normal and shear forces, as well as the bending moments are decisive parts of the construction, especially if loaded in horizontal direction.



- (i) wall-to-wall or floor-to-floor joint
- (ii) wall-to-floor joint
- (iii) wall-to-foundation joint

Figure 2.40: Definition of joints in Solid Timber Constructions with CLT; according to Brandner et al. (2016a)

During the last years, several investigations determining the loadbearing behaviour of these connections were carried out. Focusing on axially loaded screws, the discussed publications may be classified into those concentrating on (a) single joint tests, (b) wall tests or both. Since their work served as a basis for the test result evaluation in many related publications (especially for case a), research activities done by Uibel and Blaß (2006), Blaß and Uibel (2007) and Uibel and Blaß (2007) have to be outlined. They were the first who determined (and modelled) mechanical properties (withdrawal and embedment strength) as well as minimum spacings of dowel-type fasteners (nails, screws, dowels) situated in CLT panels' side and narrow faces. A detailed discussion of their findings, focusing on the withdrawal properties of self-tapping screws, is given in sections 5-3.3 and 5-3.4.

With regard to CLT elements, connected by inclined positioned self-tapping screws, investigations carried out by Flatscher et al. (2013), Bratulic et al. (2014), Bratulic et al. (2014a), Flatscher et al. (2014a) and Flatscher et al. (2014b) are worth being discussed. In order to determine the basic properties concerning the loadbearing behaviour of line connections, their first step was to experimentally evaluate those of single joints (case a, at most four fasteners per gap), see Figure 2.41. A parameter variation not only covered the connection type (stepped joint as in-plane connection, wall-to-floor joint as out-of-plane connection) and the load direction (for instance see Figure 2.41, middle and right), but also the fastener type (partially and fully threaded screws, with different diameters and head geometries) and the loading protocol, applying monotonic loading according to ON EN 26891 (1991) and cyclic loading according to ISO 16670 (2003).

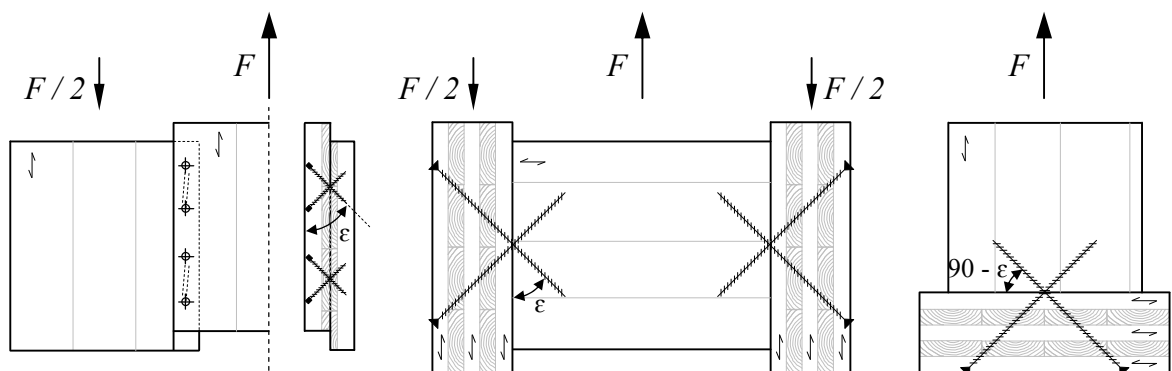


Figure 2.41: Different CLT connections with axially loaded crossed screws (exemplarily, $\varepsilon = 45^\circ$); left: stepped joint as in-plane connection; middle and right: wall-to-floor joint as out-of-plane connection; according to Bratulic et al. (2014a)

Summarising the results, the angle ε has to be seen as a main parameter influencing the loadbearing behaviour of these connection types. As generally discussed in section 2-1.1, Bratulic et al. (2014a) observed the increasing bearing resistance and stiffness by decreasing ε for all configurations tested. In contrast to the situation for the joints' ductility D : especially the results, where the head pull-through

failure of partially threaded self-tapping screws dominated the loadbearing behaviour, significantly deviated from the fundamental assumption of decreasing D with decreasing ε . Furthermore, even fully threaded screws showed higher D for $\varepsilon = 45^\circ$ (predominately axial) than for $\varepsilon = 90^\circ$ (predominately lateral) in special cases. Consequently, an overall trend of D in dependence of ε could not be declared by Bratulic et al. (2014a). With regard to a possible influence caused by varying loading protocols, no significant differences were found between monotonic and cyclic loading (1st curve envelope considered).

Subsequently, Bratulic et al. (2014) and Bratulic et al. (2014a) compared the test results with model assumptions, discussed in section 2-3.1.1 (eqs. (2.28), (2.29) and (2.33)). As mentioned above, the screw basic properties, published by Blaß and Uibel (2007), were applied as input parameters for these approaches. In case of predominately axially loaded screws ($\varepsilon \leq 45^\circ$) failing in withdrawal, experimental values confirmed the models, being also applicable for screwed CLT connections. In contrast, if partially threaded screws failed by head pull-through or predominately laterally loaded screws were applied ($\varepsilon = 90^\circ$, irrespective their thread characteristics), in major cases the model assumptions significantly underestimated the test results. The average deviations were about 50 % (test results were twice the model assumptions), which corresponds to the findings for timber-to-timber normal joints with similar screw arrangement as published by e. g. Tomasi et al. (2010), c. f. section 2-3.1.1.

In addition to the aforementioned publications, Gavric et al. (2015) also tested (monotonic and cyclic) axially loaded screwed connections in form of two out-of-plane CLT wall-to-floor configurations, see Figure 2.41 (right). The screws applied were partially threaded with some kind of modified countersunk head and $d = 10$ mm, while ε as the angle between screw and load axis was constantly set to 0° . As discussed in Gavric et al. (2015), the majority of related tests showed a typical head pull-through failure mode, in some cases combined with withdrawal. Regardless that a deviating failure mode has been observed, Gavric et al. (2015) compared the screws' axial loadbearing resistance (head pull-through) with withdrawal model assumptions according to Blaß and Uibel (2007). Interestingly, a good confirmation with test results has been found, which can be explained by a very conservative interpretation of the model. Considering different head geometries and diameters, the results (resistance, stiffness and ductility) are in the range of those determined by Bratulic et al. (2014a), using a similar configuration.

Further experimental investigations on spatially inclined fully threaded screws arranged in CLT in-plane connections were carried out by Jacquier and Girhammar (2014), Danzig et al. (2014), Hossain, Popovski and Tannert (2016), Hossain, Danzig and Tannert (2016). Avoiding to overextend the scope of this literature review, the decision was not to discuss these sources in detail. Corresponding results widely confirm findings and conclusions discussed so far in this chapter.

Focusing on (b), the mechanical performance of in-plane loaded CLT shear walls, Popovski and Karacabeyli (2011) experimentally determined the main properties of wall configurations at varying geometrical parameters and connection technique. Amongst others, their programme contained a line-wise screwed connection considering two different arrangements (18 screws at equal spacings vs. 34 screws with concentration on both edges). Deviating from the detail shown in Figure 2.40 (right), the screws ($d = 6.5$ mm, two threaded parts) were inclined inserted from the wall into the CLT floor element (see e. g. Figure 2.8, c). Concluding their findings, Popovski and Karacabeyli (2011) observed a comparatively poor bearing resistance and energy dissipation for both configurations tested. Due to these circumstances (especially energy dissipation), they recommend not using screws (placed at an angle) as fasteners for floor-to-wall connections in earthquake prone regions. Since they did not publish any quantitative test results related to the screwed connections (resistance, stiffness, ductility), a reasonable comparison with similar investigations is hardly possible.

Further experimental investigations concerning CLT shear walls were carried out by Flatscher (2012), Flatscher et al. (2014a) and Flatscher et al. (2014b). Again, different fasteners, suitable for wall-to-floor connection lines, such as angle brackets, angle brackets combined with hold-downs and self-tapping screws have been varied. Deviating from the conclusions made in Popovski and Karacabeyli (2011), the main mechanical properties, namely resistance, ductility and equivalent damping ratio v_{eq} , the latter according to Chopra (2007), resulted in a comparable range, irrespective the fastener type applied. Obviously, the screw arrangement (*inclined* insertion from the wall into the floor vs. *perpendicular* insertion from the floor into the wall) remarkably influences the wall's loadbearing behaviour. Flatscher et al. (2014b) developed a mechanical model in order to describe the nonlinear bearing behaviour of CLT shear walls with line-wisely applied screws. Thereby, single joint properties determined by Bratulic et al. (2014a) serve as input parameters for lateral and axial load conditions. Worth mentioning, the analytical description of both force-deformation relationships lateral and axial, c. f. Flatscher and Schickhofer (2014), enables a steady prediction of the shear wall behaviour under horizontal loading.

Focusing on steel-to-CLT connections predominately applied as single joints, a comparatively less effort has been made so far. Apart from research activities done by Mahlknecht and Brandner (2013), the investigations carried out by Plüss (2014) and Plüss and Brandner (2014) are worth to be outlined. As shown in Figure 2.12, group-wise arrangements of screws in CLT narrow faces often necessitate their application in different layers. Consequently, material inhomogeneity caused by different layer orientation ($0^\circ \leq \alpha \leq 90^\circ$), intermediate zones between two layers and gaps between two boards remarkably influences the loadbearing (especially withdrawal) behaviour of such connections. Basing on a comprehensive test programme, carried out by Plüss (2014), wherein CLT lay-ups, fastener numbers and positions have been varied, Plüss and Brandner (2014) provide a simplified model approach estimating the withdrawal resistance of axially loaded screwed groups in CLT narrow faces, $R_{ax,n}$, see:

$$R_{ax,n} = 0.90 \cdot \sum_{i=1}^N R_{ax,ref,i} \cdot n_i, \quad (2.48)$$

with N as the number of penetrated layers, n_i as the number of screws and $R_{ax,ref,i}$ as the reference withdrawal capacity per layer. For reasons of practical inaccuracies, similar to the approach published by Krenn and Schickhofer (2009), $R_{ax,n}$ is reduced by 0.9 in eq. (2.48) for an adoption in the design process. Hence the experimental results widely confirmed the model assumptions (eq. (2.48) without pre-factor 0.9) a combination of screws situated in layers with different orientation has no negative influence on the connection's bearing (withdrawal) capacity. Presupposing, that minimum spacings (especially a_1) according to ON B 1995-1-1 (2015) are fulfilled.

With regard to steel-to-CLT joints, applied as system connectors, the solutions discussed in section 2-3.1.2 can also be applied for CLT panels. Some CLT specific developments, presented in Kraler et al. (2014), Polastri and Angeli (2014) and Zingerle et al. (2016), are worth to be noted. Furthermore, the number of investigations focusing on the loadbearing behaviour of CLT-GLT/concrete/steel composite members, connected (or reinforced) by inclined positioned self-tapping screws, increased within the last years, c. f. Jacquier and Girhammar (2015), Yagi et al. (2016), Giongo et al. (2016) and Loss and Davison (2017). Since main principles behind were already discussed in the frame of this chapter, the decision was to discuss these sources not in detail.

2-4 PASSIVE APPLICATION AS REINFORCEMENT

Beside their *active* application, as discussed in section 2-3, nowadays self-tapping screws are also frequently applied in *passive* form, reinforcing timber members and laterally loaded dowel-type connections against stresses perpendicular to grain or shear. Again, the following subsections 2-4.1 to 2-4.4 are structured in accordance to Figure 2.10. In addition, section 2-4.5 deals with further types of screw reinforcements, where a classification into the aforementioned main fields is not reasonable.

2-4.1 Reinforcement against compression perpendicular to grain

Assumed as an orthotropic material, timber members applied for structural purpose show significantly different mechanical properties in dependence of the angle between stress and grain direction. For instance, compressive strength and corresponding E-modulus perpendicular to grain are only about 12 % and 3 % from those parallel to grain, c. f. ON EN 338 (2016). Consequently, details where such building components are exposed to high and concentrated compressive loads normal to their axis (supportings or point loading), can, in special cases, be decisive for the design process (e. g. small supporting areas for comparatively high beams). In order to avoid uneconomical member dimensions, as well as local plastic material deformation, those zones are commonly reinforced nowadays. This not only concerns practical application in realised constructions, but also enables a local introduction of high point loads being necessary for specific laboratory investigations, as e. g. described in Brandner et al. (2012) or Bogensperger and Jöbstl (2015).

Before self-tapping screws were produced in a dimension and geometry being reasonable for this purpose (see Figure 2.22), the applied alternatives were different kinds of internal (glued-in rods or glued-in hardwood dowels) and external solutions (glued-on laminar timber products or nail plates), c. f. Bejtka (2005). Nowadays, screws are (more or less) exclusively used for reinforcing structural timber products against compression perpendicular to grain. The main reasons are their simple installation without pre-drilling, as well as their invisibility regarding the timber member's optical appearance. According to Bejtka and Blaß (2006), the loadbearing capacities of reinforced beam supports can be increased up to 300 % if compared to the unreinforced detail.

Equal to the tensile timber-to-timber joints with inclined positioned self-tapping screws, discussed in section 2-3.1, the main efforts made in this field can be addressed to Karlsruhe Institute of Technology (KIT). Based on the first ideas and investigations made in Blaß (1998), Colling (2001a) and Colling (2001b), Bejtka (2003), Blaß and Bejtka (2004a), Blaß and Bejtka (2004b), Bejtka (2005) and finally Bejtka and Blaß (2006) concentrated on – amongst other topics discussed in sections 2-4.2 and 2-4.4 – the application of self-tapping screws as reinforcements against compression perpendicular to grain, as shown

in Figure 2.42. According to Bejtka (2005), the corresponding design process is separated in three different failure modes, which have to be verified:

- For screws with comparatively small lengths, a simultaneous failure occurs for both components – timber (comp. perpendicular to grain at the supported timber surface) and screw (pushing-in).
- In case of long screws or high values for slenderness λ , here as l_{screw} / d ratio, the buckling (perpendicular to grain direction) of the embedded screws replaces the former mentioned pushing-in failure mode.
- For small supporting areas, reinforced by a high number of screws with small lengths, compression perpendicular to grain may also appear at the transition zone between the unreinforced and reinforced area of the timber member as outlined in Figure 2.42.

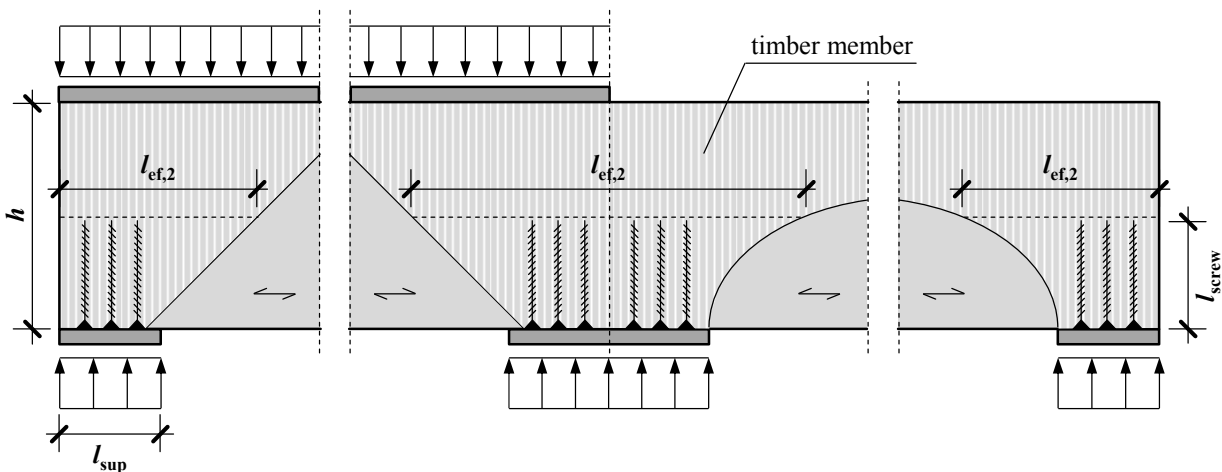


Figure 2.42: Different loading and supporting situations for beam supports reinforced with self-tapping screws: left: directly loaded end support; middle: support with both load situations; right: indirectly loaded end support; according to Bejtka and Blaß (2006)

In order to determine the pushing-in capacity of self-tapping screws, necessary for the verification of case (a), Bejtka (2005) carried out an experimental campaign varying different outer thread diameters $d = \{6.0; 7.5; 8.0; 10; 12\}$ mm and slenderness $\lambda = 3.33 \div 16.0$ for axial load conditions. Considering the given load situation, single self-tapping screws were pushed into the timber member at $\alpha = 90^\circ$ by applying a compression force. Since Bejtka (2005) reports no differences in capacity if screws are pushed into the test specimen or pulled out of it, his related findings consequently led to the proposal given in eq. (2.30) for determining the withdrawal capacity R_{ax} of axially loaded self-tapping screws – also adopted in Eurocode 5 for this purpose, c. f. section 2-2.1.3.

In case of failure mode (b), Bejtka (2005) modelled the inserted screw as an elastically bedded one-dimensional beam loaded by a single compression force N_{ki} , see Figure 2.43 (left). In addition to screw steel and geometrical parameters (E -modulus E_s , yield strength f_y , length l_{screw} , inner thread diameter d_c),

further input factors are the coefficients c_h and c_v for elastic foundation and support, as well as the support condition of the screw head in form of the spring parameter K . As shown in Figure 2.43 (right), Bejtka (2005) differed between a fixed head support, realised by clamping the screw head by an additional steel plate, and a hinged head support as assumed for the common case of screw heads situated in the timber member flush with its compressed surface.

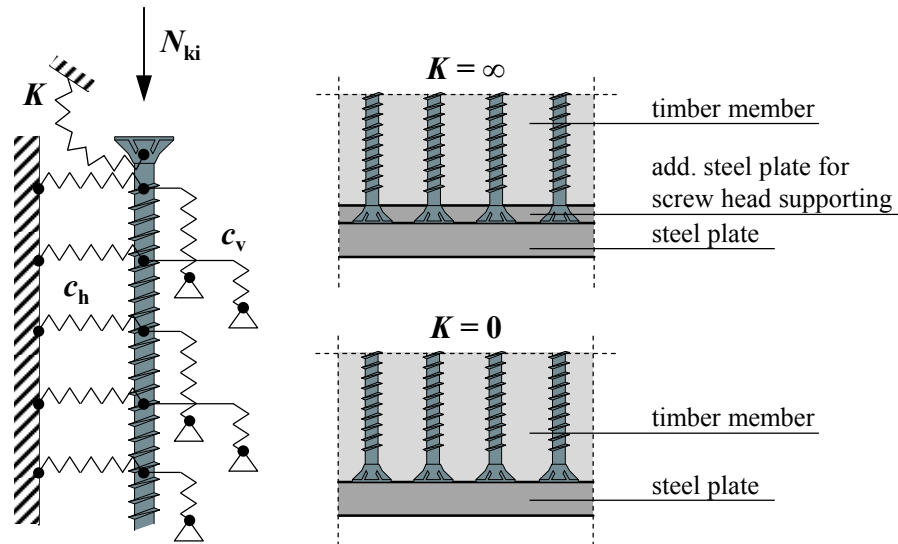


Figure 2.43: Left: assumed model for determining corresponding buckling loads; right: different forms of screw insertion as reinforcement of beam supports: screw head clamped in an additional steel plate (above); screw head placed in the timber member (below); according to Bejtka (2005)

While K was either assumed ∞ (fixed support) or 0 (hinged support), Bejtka (2005) experimentally determined both coefficients c_h (by embedment tests) and c_v (gained from the pushing-in tests mentioned before), for a varying bandwidth of parameter characteristics. In eq. (2.49), corresponding regression models for c_h and c_v are given:

$$c_h = \frac{(0.22 + 0.014 \cdot d) \cdot \rho}{1.17 \cdot \sin^2 \beta + \cos^2 \beta} \quad \text{and} \quad c_v = 234 \cdot \frac{(\rho \cdot d)^{0.2}}{l_{ef}^{0.6}}, \quad (2.49)$$

with β as the angle between the lateral force and fibre direction (for $\alpha = 90^\circ$). It is noteworthy, that the model for determining $K_{ser,ax}$ for axially loaded self-tapping screws as given in eq. (2.26) (also adopted in the majority of ETAs related, c. f. section 2-2.5.5) generally bases on the approach for estimating c_v , shown in eq. (2.49). Due to the high number of input parameters and the complex structure of the corresponding differential equation, Bejtka (2005) determined N_{ki} for the varying bandwidths of mentioned input parameters by means of a numerical (FE) calculation method. The obtained results are e. g. provided in Bejtka and Blaß (2006) in a tabular form. Therein, they also compared numerically

derived N_{ki} , with those determined by simplified approaches for elastically bedded beams without supports (approach for hinged head support) and two supports (approach for fixed head support), see eq. (2.50):

$$N_{ki} = \zeta \cdot \sqrt{c_h \cdot E_s \cdot I_s}, \quad (2.50)$$

with I_s as the moment of area of a circular screw cross section with $d = d_c$) and $\zeta = \{1, 2\}$ for {hinged, fixed} head support. Since the simplified solutions (l_{screw} , for instance, has no influence), determined according to eq. (2.50), only slightly underestimate the numerical ones in case of high λ , the majority of Technical Approvals, discussed in section 2-2.5, adopted the related approach including eqs. (2.49) and (2.50) for determining the buckling resistance of self-tapping screws, applied as reinforcements against compression perpendicular to grain.

Both failure modes, (a) and (b), general base on the assumption, that the screw failure (withdrawal, buckling) and the one of the timber member (compression perpendicular to grain) appear at the same time. Although the related force-deformation relationships remarkably differ from each other in their course, Bejtka (2005) proved by means of analytical and numerical analysis, that for the vast majority of possible screw applications the timber member's compressive strength is already reached when screw failure occurs. Consequently, both resistances can be summed up, determining the detail's bearing capacity against this loading situation.

Focusing on the failure mode (c), the timber member's capacity against compression perpendicular to grain in the transition zone between its reinforced and unreinforced area not only depends on the corresponding compressive strength, but also on specific situations in terms of loading and supporting. As shown in Figure 2.42, differentiations are made by Bejtka and Blaß (2006) if the beam's supports are directly (Figure 2.42, left) or indirectly (Figure 2.42, right) loaded, influencing the corresponding load distribution and thus the compressed area, and also if an end (single-sided load distribution) or middle support (double-sided load distribution) has to be verified. For direct loading, the linear load distribution with an angle of 45° is generally assumed. For indirect loading, a nonlinear and degressive course in load distribution was numerically derived by Bejtka and Blaß (2006), again covering a practical scope of application. Thereby the gained results for $l_{ef,2}$ as the total length of the transition plane loaded in compression perpendicular to grain are shown in eqs. (2.51) and (2.52) in form of a simplified fitted exponential equation.

single-sided load distribution:
$$l_{ef,2} = l_{sup} + 0.25 \cdot l_{screw} \cdot \exp\left(3.3 \cdot \frac{l_{screw}}{h}\right), \quad (2.51)$$

$$\text{double-sided load distribution: } l_{\text{ef},2} = l_{\text{sup}} + 0.58 \cdot l_{\text{screw}} \cdot \exp\left(3.6 \cdot \frac{l_{\text{screw}}}{h}\right), \quad (2.52)$$

Summarising their results, Bejtka and Blaß (2006) recommend the verification process of timber members reinforced by self-tapping screws against compression perpendicular to grain including the failure modes (a) to (c) in simplified form, according to eqs. (2.53) to (2.58).

$$R_{90} = \min \begin{cases} n \cdot R + k_{c,90} \cdot l_{\text{ef}} \cdot w \cdot f_{c,90} \\ w \cdot l_{\text{ef},2} \cdot f_{c,90} \end{cases}, \quad (2.53)$$

with

$$R = \min \{R_{\text{ax}}; R_c\}, \quad (2.54)$$

$$R_c = \kappa_c \cdot N_{\text{pl}}, \quad (2.55)$$

$$\kappa_c = \begin{cases} 1 & \text{for } \bar{\lambda} \leq 0.2 \\ \frac{1}{k + \sqrt{k^2 - \bar{\lambda}^2}} & \text{for } \bar{\lambda} > 0.2 \end{cases}, \quad (2.56)$$

$$k = 0.5 \cdot \left[1 + 0.49 \cdot (\bar{\lambda} - 0.2) + \bar{\lambda}^2\right], \quad (2.57)$$

$$\bar{\lambda} = \sqrt{\frac{N_{\text{pl}}}{N_{\text{ki}}}}, \quad (2.58)$$

and n as number of applied screws (deviating from Eurocode 5: $n = n_{\text{ef}}$), w as width of the beam, l_{ef} as effective length of the compressed timber surface at the supportings, $k_{c,90}$ as load distribution coefficient, $f_{c,90}$ as compressive strength perpendicular to grain, N_{pl} as plastic load-carrying capacity of the screw, and N_{ki} as well as $l_{\text{ef},2}$ as explained before. Since the comparison with experimentally determined bearing capacities showed a high agreement with model predictions, c. f. Bejtka and Blaß (2006), the verification process described was also adopted in Technical Approvals of screws applicable for this purpose. In addition, Bejtka (2005) derived an analytical approach basing on Volkersen's theory, c. f. Volkersen (1953), for determining the comparatively higher stiffness (about 2 ÷ 6 times, own comparison) of the reinforced beam support against stresses perpendicular to grain. Again, the experimental results widely confirmed the model estimations, c. f. Bejtka and Blaß (2006).

Focusing on the practical application, Bejtka (2005) also concentrated on the sensitivity of the reinforcement measure regarding the inaccuracies in terms of screw insertion. The screw heads sunken

into the timber member (max. 3 mm) and the axis-to-grain angles deviating from $\alpha = 90^\circ$ (max. 10°) did not influence the bearing capacity at all, while the corresponding stiffness significantly decreased. Consequently, Bejtka and Blaß (2006) persist on a high accuracy in installation when considering the increased stiffness caused by reinforcing the detail.

Apart from the investigations discussed so far, further works concerning the application of self-tapping screws for reinforcing timber members against compression perpendicular to grain are scarce. Thus, the efforts made by Ed and Hasselqvist (2011), Lathuilière et al. (2014), Gasparri et al. (2016) and Naderer et al. (2016) are worth to be noted in this context.

2-4.2 Reinforcement against tension perpendicular to grain

As mentioned in section 2-4.1, structural timber shows poor mechanical performance if stressed perpendicular to grain direction. In case of timber members loaded in tension perpendicular to grain, their corresponding resistance is even weaker, than the one against compression in the same direction. According to ON EN 338 (2016), the related strength value $f_{t,90,k}$ of structural timber C24 is 0.4 N/mm^2 and only about 3 % from that parallel to grain direction ($f_{t,0,k}$). Furthermore, the mechanical behaviour is expressed by a linear-elastic force-deformation relationship, followed by brittle failure without any preliminary warning. The first research work, concerning this essential topic for timber engineered structures was done in the 2nd half of the 20th century. Beside self-tapping screws, nowadays also frequently applied for this purpose, glued-in rods or glued-on laminar timber products are used to reinforce related details. In contrast to compression perpendicular to grain, which is more or less allocated to member supportings or point load introductions (see section 2-4.1), these details show a high variability regarding their character and location in the bearing structure. Thus they are separately discussed in the following subsections 2-4.2.1 to 2-4.2.4. Thereby the focus is set on special literature about the reinforcement with self-tapping screws.

2-4.2.1 Timber members loaded by connections perpendicular to grain

In case of transversal joints between main and secondary beams or between main beams and tensile bars, the corresponding design process not only comprises that of the connection itself, but also the verification of one or even both timber members against tension perpendicular to grain. These stresses, significantly influenced by the joint geometry, increase with decreasing h_e as distance between the main timber member's stressed edge and the furthest row of the dowelled connection where a possible crack formation is assumed, see Figure 2.44. Consequently, the related verification depends on the ratio between h_e and h , which defines the timber member's height. According to Schickhofer (2006b), no further measures have to be considered if h_e/h exceeds 0.70, minimising the aforementioned stress concentration. In cases, h_e/h is in between 0.20 and 0.70 the detail has to be verified regarding tension

perpendicular to grain, while $h_e / h < 0.20$ should be avoided in general. Considering the weakness of timber against this load situation, Schickhofer (2006b) recommends reinforcing the detail when $0.20 \leq h_e / h \leq 0.70$, regardless the verification is fulfilled or not. The corresponding force, the reinforcement measure has to be designed for, $F_{t,90}$, can be determined according to Ehlbeck et al. (1989), see

$$F_{t,90} = \eta \cdot F_{90} = \left[1 - 3 \cdot \left(\frac{h_e}{h} \right)^2 + 2 \cdot \left(\frac{h_e}{h} \right)^3 \right] \cdot F_{90}, \quad (2.59)$$

with F_{90} as the total force transmitted by the connection. Focusing on its reinforcement with self-tapping screws and basing on the first ideas made in Blaß (1998), Bejtka (2003) and Blaß and Bejtka (2004b) recommend the related verification as follows:

$$F_{90} \leq \frac{n \cdot R_{ax}}{\eta}, \quad (2.60)$$

with $R_{ax} = f(\min[l_{ef,1}; l_{ef,2}])$ as the single self-tapping screw's axial loadbearing capacity and n as the total number of screws applied as reinforcements. In Blaß and Bejtka (2003a), they experimentally determined the bearing resistance (F_{90}) of unreinforced and reinforced dowel-type connections ($n = 2$) similar to the detail shown in Figure 2.44. Thereby, they observed an increase of F_{90} of roughly 40 % (one screw as reinforcement) to 75 % (two screws as reinforcements), as well as a comparatively ductile failure behaviour if referred to the unreinforced connection. Comparing the experimental results with the model predictions, Blaß and Bejtka (2003a) show that eq. (2.60) adequately describes the corresponding data trend but underestimates the real bearing capacities by far. One reason therefore is a possible interaction of both resistances tension perpendicular to grain and screw withdrawal (or steel tensile) not covered by the design approach given in eq. (2.60).

With regard to the screw arrangement, Bejtka (2003) recommends situating them in direct vicinity of the laterally loaded fasteners, where the highest tensile stresses perpendicular to grain occur. As discussed in Mahlkecht and Brandner (2013), the total inserted screw length should exceed 75 % of the timber member's height, minimising the tensile stress concentration at the screw tips. Otherwise, the design should also comprise a corresponding verification in this area, c. f. Dietsch and Brandner (2015).

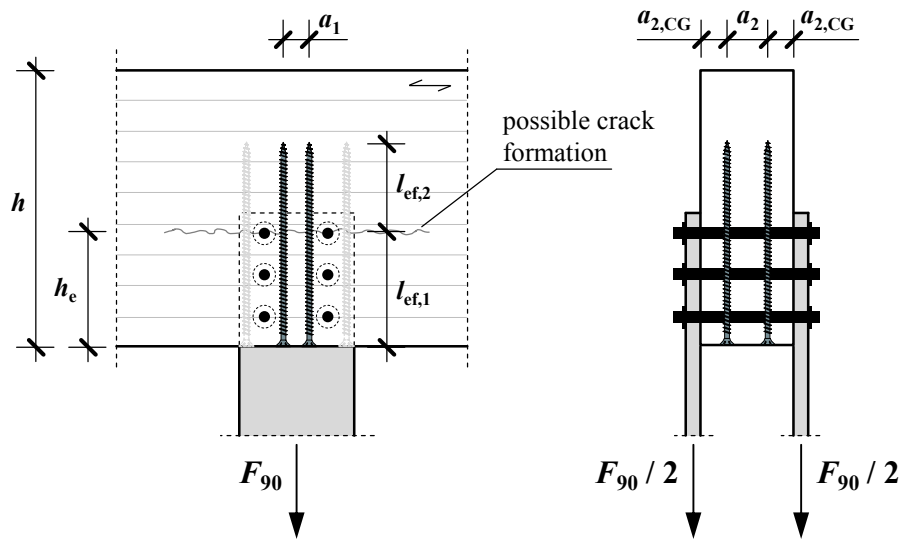


Figure 2.44: Dowel-type connection with a force component perpendicular to grain reinforced with self-tapping screws

Similar tests on dowelled connections, reinforced with self-tapping screws, were also carried out by Schoenmakers (2010). In dependence of the geometrical conditions (beam dimensions, as well as the joint configuration have been varied, while the screw length has been kept constant) increasing loadbearing capacities from 8 % to 100 % if compared to the unreinforced detail could be observed. Low load enhancements were found for screw lengths equal to h_e ($l_{ef,2} \rightarrow 0$, see Figure 2.44) and/or smaller than 75 % of h , confirming the aforementioned constructive recommendations.

2-4.2.2 Notched timber beams and dovetail connections

The arrangement of notched timber members is a favourable opportunity reducing the building's construction height or to enable the transversal connection between two timber members on the same level, and is thus often used in timber engineering. Thereby, the reduction of the timber member's height of $1 - \gamma \cdot h$ close to the supporting leads to an abrupt change in its cross-section, an unfavourable stress concentration of tension perpendicular to grain and shear and thus brittle failure of the timber member caused by crack formation in this area, c. f. Figure 2.45 (left).

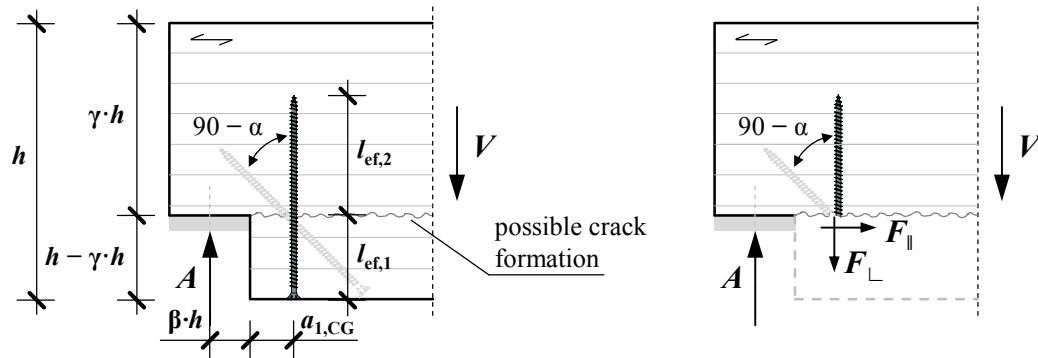


Figure 2.45: Left: supporting of a notched timber beam reinforced with self-tapping screws; right: force components parallel and perpendicular to crack formation transferred by the reinforcements, according to Jockwer (2014)

The corresponding shear verification process given in e. g. Eurocode 5, bases on a fracture mechanical approach derived by Gustafsson (1988) and limits the detail's loadbearing capacity to that one of the reduced cross-section $w \cdot \gamma \cdot h$. Since decreasing proportional factors γ and β decrease the member's shear loadbearing capacity by far, it is recommended to restrict both values to $\gamma \geq 0.5$ and $\beta \leq 0.4$, c. f. ON B 1995-1-1 (2015) or Schickhofer (2006b). In those cases, the verification itself is not fulfilled, the notched timber member has to be reinforced. In some publications it is additionally recommended to reinforce notched timber members anyway, c. f. for instance Jockwer (2014). The corresponding measures are similar to those mentioned in section 2-4.2.1 and comprise self-tapping screws nowadays. Related chapters in currently valid national appendices, see ON B 1995-1-1 (2015) or DIN EN 1995-1-1/NA (2013) base on the work done by Henrici (1984) and recommend determining the force $F_{t,90}$, the reinforcement has to be designed for, as follows:

$$F_{t,90} = \eta \cdot V = 1.3 \cdot \left[3 \cdot (1 - \gamma)^2 - 2 \cdot (1 - \gamma)^3 \right] \cdot V, \quad (2.61)$$

with 1.3 as a factor considering the orthotropic material and the influence of β restricted to $\beta \leq 1/3$. The verification is consequently done according to eq. (2.60) ($F_{90} = V$, η according to eq. (2.61)) with the boundary condition, that only the fastener row next to the notch in fibre direction can be counted for n .

A first experimental campaign determining the mechanical behaviour of notched beam supports reinforced with self-tapping screws was carried out by Blaß and Bejtka (2003a). The parameter variation comprised the existence of the reinforcement, the proportional factor γ , as well as the screw axis-to-grain angle $\alpha = \{45^\circ, 90^\circ\}$, see Figure 2.45 (left). The corresponding results indicate a significant loss of bearing resistance R with decreasing γ for unreinforced and reinforced notches. Comparing the structural performance of unreinforced and reinforced notches with equal γ , a remarkable increase of R as a consequence of the reinforcement measure has been observed, while a change of α from 90° to 45° did not show any positive effect. In addition, the bearing capacities determined with eq. (2.60) significantly

underestimated the experimental results, but again described the data trend adequately. Consequently, Blaß and Bejtka (2004a) and Blaß and Bejtka (2004b) recommend an application of eqs. (2.60) and (2.61) for the design of notched beams reinforced with self-tapping screws.

Some oppositional findings are reported in Jockwer (2014), who experimentally determined the bearing resistances R of notches reinforced with self-tapping screws inserted at varying $\alpha = \{45^\circ, 60^\circ, 90^\circ\}$: First, a slight increase of R could be observed at $\alpha = 45^\circ$ if compared to $\alpha = 60^\circ$ and 90° . Second, bearing capacities determined with eqs. (2.60) and (2.61) significantly overestimated the test results in cases where failure was governed by shear failure of the notch, c. f. also Jockwer et al. (2013). In order to optimise the design process of reinforced notched beams by means of axially loaded fasteners, Jockwer (2014) consequently derived an analytical model based on a fracture mechanical approach. Summarising his findings and deviating from the currently applied function given in eq. (2.61), Jockwer (2014) recommends to verify the corresponding reinforcement measure against two forces F_{\parallel} and F_{\perp} acting parallel (shear) and perpendicular (tension perpendicular to grain) to the surface where crack formation may occur, see Figure 2.45 (right). A conservative, but simple, way recommended by Jockwer (2014) for predicting F_{\parallel} and F_{\perp} is given in eq. (2.62):

$$F_{\parallel} = 3V \cdot (\gamma - \gamma^2) \cdot (2\beta + 1) \text{ and } F_{\perp} = V \cdot (1 - \gamma). \quad (2.62)$$

In cases, both forces F_{\parallel} and F_{\perp} have to be transmitted by the same screw, proposed to be inclined positioned, the corresponding bearing resistances can be determined according to eq. (2.28) for F_{\parallel} and eq. (2.40) for F_{\perp} . A verification is consequently done by means of quadratic interaction of thereby determined utilisation ratios η_{\parallel} and η_{\perp} . Furthermore, the reinforcement optimisation aims to achieve the shear capacity of the reduced cross-section. Therefore, Jockwer (2014) suggests designing the reinforcement, considering the boundary condition in terms of the screw's axial stiffness, according to eq. (2.63):

$$K_{\text{ser,ax}} = 10^{8.3 - 5.4\gamma + \beta(2.3\beta + 1)}. \quad (2.63)$$

Worth mentioning that Jockwer (2014) (currently) limits eq. (2.63) to beam dimensions $h = 600$ mm and $w = 140$ mm. Apart from the sources discussed so far, two further approaches, one analytical and one numerical, regarding the reinforcement of notched timber beams, were recently published by Augustin et al. (2016) and Oudjene et al. (2016).

As shown in Figure 2.46 (a), the geometry of the tenon part of a dovetail connection is quite similar to that of the notched beam. Crack formation again occurs as a consequence of the abrupt change of the secondary beam's cross-section. An experimental campaign, determining the bearing resistance of

dovetail connections reinforced with self-tapping screws, as given in Figure 2.46 (a-c), has been carried out by Tannert and Lam (2009). The varied parameters were the number of inserted screws $n = \{1, 2\}$ and the axis-to-grain angle $\alpha = \{55^\circ, 90^\circ\}$, the latter combined with different configurations screws were arranged in this type of connection (screw insertion equal to Figure 2.45, left; c. f. Figure 2.46, a; inclined screw insertion comparable to a transversal joint between main and secondary beam, c. f. Figure 2.46, b and c).

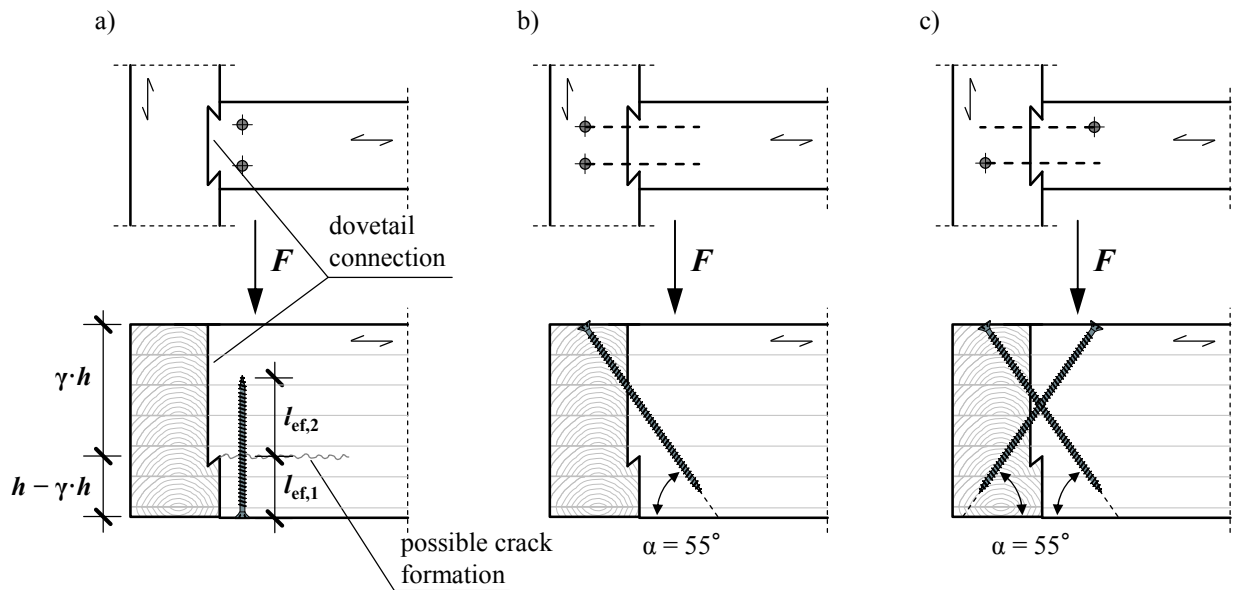


Figure 2.46: *Dovetail joints reinforced with self-tapping screws according to Tannert and Lam (2009); a) reinforcement equal to notched timber beams, b) and c) reinforcement with inclined screws, similar to a transversal joint*

Again, the results show a significant increase of the loadbearing capacity, as a consequence of the reinforcement measure, which was found to be the most effective when screws were positioned inclined, Figure 2.46 (b, c). Furthermore, Tannert and Lam (2009) compared the test results with values predicted by different model approaches. In brief: in case of a screw arrangement at $\alpha = \{90^\circ\}$, application of eqs. (2.60) and (2.61) significantly overestimates the experimental values. Replacing h_e / h by A_e / A (ratio of the reduced and total cross-sectional area) in eq. (2.61) yields to a conservative but also inaccurate bearing resistances. Nevertheless, Tannert and Lam (2009) recommend designing the reinforcement measure in this way. In case of an inclined screw arrangement at $\alpha = 55^\circ$, they assumed the screw reinforcement as a timber-to-timber connection and determined the corresponding loadbearing capacities by model approaches for tensioned and crossed screw joints, discussed in section 2-3.1.1. Thereby, a contribution of the dovetail connection itself to the loadbearing behaviour is ignored, which leads to a remarkable underestimation of the experimental results. Consequently, Tannert and Lam (2009) conclude,

that further investigations should be carried out, concentrating on this interaction in order to optimise the reinforcement with inclined positioned self-tapping screws, as well as the related design process.

More recently, Tannert (2016) published results of further investigations regarding the loadbearing behaviour of unreinforced dovetail joints and such reinforced with an adhesive layer and/or inclined positioned self-tapping screws. In contrast to the findings reported in Tannert and Lam (2009), a remarkably higher joint stiffness but no significant increase of its loadbearing capacity could be observed as a consequence of the latter mentioned measure. As also indicated in Tannert (2016), this is caused by dovetail geometry and screw outer thread diameter deviating from the ones applied in Tannert and Lam (2009).

2-4.2.3 Timber members with holes

Service installations in office buildings and commercial buildings or halls are often allocated on the same level as the floor or roof structure. The direct line run systems, pursued for optimising the building service efficiency, consequently necessitate the arrangement of holes in the structural members. In case of timber beams stressed in bending and shear, the corresponding and abrupt change of the beam's cross-section leads to a stress concentration of tension perpendicular to grain and shear and thus crack formation occurring at the edges of these openings, see Figure 2.47.

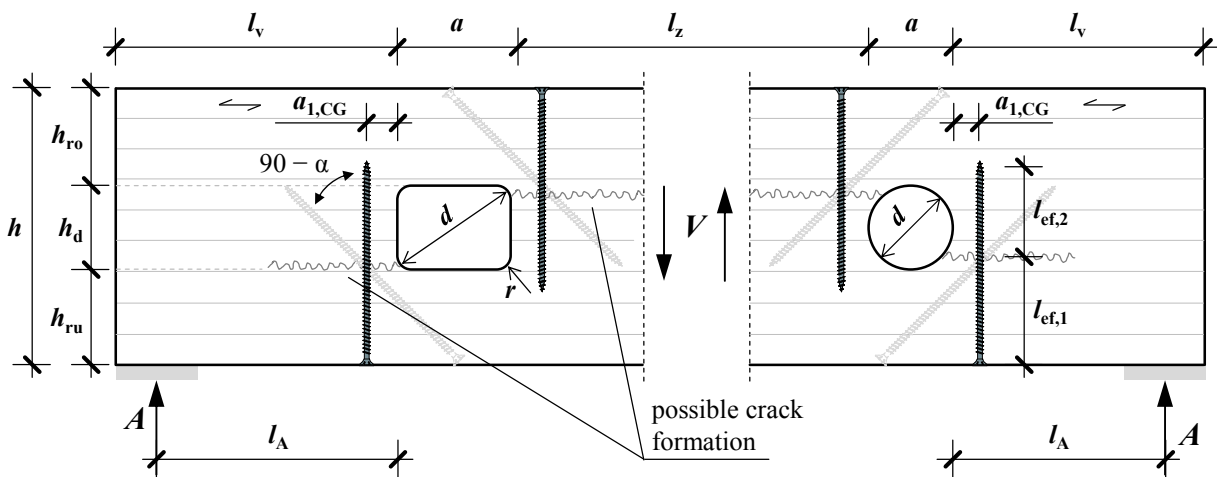


Figure 2.47: Different types of holes in timber members reinforced with self-tapping screws:
left: prismatic hole; right: round hole

Similar to notched timber beams, discussed in section 2-4.2.2, the screw reinforcement is again an appropriate way for increasing the loadbearing capacity of this detail. The related design process, as given in ON B 1995-1-1 (2015) for instance, comprises geometrical boundary conditions such as

$$l_A \geq 0.5h, l_v \geq h, l_z = \max \left\{ \begin{array}{l} h \\ 300\text{mm} \end{array} \right., a \leq 2.5h_d, \{h_{ro}, h_{ru}\} \geq 0.25h, h_d \leq 0.30h, r \geq 15\text{mm} \quad (2.64)$$

as well as the verification of the fastener against $F_{t,90}$ acting perpendicular to grain, see eq. (2.65):

$$F_{t,90} = F_{t,v} + F_{t,m} = \frac{V \cdot h_d}{4 \cdot h} \cdot \left[3 - \left(\frac{h_d}{h} \right)^2 \right] + 0.008 \cdot \frac{M}{h_r}, \text{ with} \quad (2.65)$$

$$h_r = \min \left\{ \begin{array}{l} h_{ro} \\ h_{ru} \end{array} \right. \text{ for prismatic holes, } h_r = \min \left\{ \begin{array}{l} h_{ro} \\ h_{ru} \end{array} \right. + 0.15 \cdot h_d \text{ for round holes, and} \quad (2.66)$$

$F_{t,v}$ and $F_{t,m}$ as the force components caused by the shear force and the bending moment, h_d the opening's height and h_{ro} and h_{ru} as the beam heights above and below the opening. For determining R_{ax} , the effective threaded part of screw below the opening, $l_{ef,1}$, is equal to h_r given in eq. (2.66). Worth mentioning, only the first screw row next to the opening in fibre direction can be counted as reinforcement.

Equal to the details discussed in section 2-4.2.1 and 2-4.2.2, first experiments for determining and verifying the bearing capacity of timber members with holes reinforced with self-tapping screws were carried out by Blaß and Bejtka (2003a). The corresponding parameter variation comprised the screw type (diameter $d = \{7.5, 8.0\}$ mm and thread length $l_{thread} = \{132, 182, 340\}$ mm), the axis-to-grain angle $\alpha = \{90, 45\}^\circ$, see Figure 2.47, the number of screws $n = \{1, 2\}$ on each side of the opening, their arrangement (reinforcement of two edges as given in Figure 2.47 vs. reinforcement of all edges), the ratio $a/h = \{0.33, 0.40, 0.42, 0.63 \text{ and } 1.00\}$, the beam's height $h = \{160, 240, 300\}$ mm and the type of the opening (prismatic and round), while the ratio $h_d/h = 0.4$ has been kept constant for all tests. For prismatic openings, reinforced with self-tapping screws at $\alpha = 90^\circ$, an average increase of 44 % of the member's bearing capacity if compared to the unreinforced detail could be observed. In case of round openings reinforced with the same configuration, no remarkable enhancement could be achieved. According to Blaß and Bejtka (2003a) this can be explained by different failure mechanisms observed for unreinforced prismatic and round openings. Prismatic openings failed in tension perpendicular to grain (crack opening parallel to screw axis), while round openings failed in shear and tension perpendicular to grain (crack opening parallel and perpendicular to screw axis). In the latter case, the screws were partially laterally loaded, weakening their bearing performance and stiffness and consequently their efficiency as reinforcement. In addition, Blaß and Bejtka (2003a) report higher bearing capacities of openings, which were reinforced by screws at $\alpha = 45^\circ$.

Comparing test data with values predicted by eq. (2.65) ($F_{t,90} = R_{ax,est}$), Blaß and Bejtka (2003a) show, that in specific cases the calculated resistances were significantly higher than the experimental values,

where the beams failed in shear close to the opening. Since this failure mechanism can not be covered by eq. (2.65), Blaß and Bejtka (2003a) derived, by means of FE-analysis with varying geometrical properties h , h_d and a , an additional equation to be verified in the related design process, see eq. (2.67):

$$\tau = k_\tau \cdot \frac{1.5 \cdot V}{w \cdot (h - h_d)} \leq f_v, \quad k_\tau = 1.84 \cdot \left(1 + \frac{a}{h}\right) \cdot \left(\frac{h_d}{h}\right)^{0.2}, \quad (2.67)$$

and f_v as the shear strength of the timber beam. Applying both eqs. (2.65) and (2.67) (minimum condition) for predicting the experimentally determined bearing capacities, Blaß and Bejtka (2003a) could increase the agreement between test results and calculated values by far. A summary of this approach, also adopted in modern standardisation, see e. g. ON B 1995-1-1 (2015), is given in Blaß and Bejtka (2004a).

A further experimental study determining the bearing resistance of timber members with holes, unreinforced as well as reinforced with self-tapping screws and glued-in steel rods, was carried out by Aicher and Höfflin (2009). The reinforcement design according to eq. (2.65) was thereby aimed to achieve the same timber member's bearing capacity in shear as of a beam with the same dimensions, but without openings. Focusing on the tests related to self-tapping screws, all with $d = 12$ mm, $l_{\text{thread}} = 350$ mm and applied at $\alpha = 90^\circ$, a significant increase in bearing resistance of about 54 % (if compared to the unreinforced detail) could again be observed. Nevertheless, the corresponding test results (mean value) were about 10 % smaller than the characteristic shear capacity predicted for a timber beam without any opening. Consequently, Aicher and Höfflin (2009) recommend adapting the design proposal given in eq. (2.65). Note: it is not clear if they also considered the shear verification given in eq. (2.67), possibly influencing this statement.

An additional examination regarding the structural behaviour of timber beams with round holes loaded in bending was carried out by Danzer et al. (2016): the related parameter variation comprised their number (one vs. two holes in horizontal and vertical direction), their clear distance $l_z = \{0.35, 0.70, 1.05\} h$ in horizontal direction, the ratio $d/h = \{0.25, 0.35\}$, their eccentricity to the beam's neutral axis $e = \{-0.225, -0.175, -0.100, 0.100, 0.175, 0.225\} h$ as well as if the reinforcement (self-tapping screws, $d = 10$ mm, $l_{\text{thread}} = \text{var.}$, $\alpha = 60^\circ$, one series with $\alpha = 90^\circ$) was applied or not, while material (GL28h) and cross-section ($w/h = 120/400$ mm) remained constant. Apart from confirming the positive impact of the screw reinforcement on the beam's loadbearing capacity (ultimate loads could be increased up to 100 % if compared to unreinforced beams), Danzer et al. (2016) applied a numerical approach for related estimation, achieving a good agreement between model estimation and test results. Interestingly, for verification, they used a self-tapping measurement screw, quite equal to the one developed by Wolfthaler (2015) and presented in Wolfthaler and Augustin (2016), c. f. section 2-4.4. Within a further parameter

study, worth pointing out in this context, Danzer et al. (2016) observed the distance between screw axis and hole edge significantly influencing the efficiency of this kind of reinforcement measure.

2-4.2.4 Double tapered, curved and pitched cambered beams

The occurrence of tensile stresses perpendicular to grain in linear timber members with a double tapered, curved or pitched cambered shape, frequently applied for hall constructions, is a well-known problem in timber engineering. The corresponding verification process, given in modern standards such as Eurocode 5 principally bases on the work done by Blumer (1979). Thereby, $\sigma_{t,90}$ is determined in dependence of the beam geometry and the bending moment M_{ap} given in the apex zone of the aforementioned beam types, see eq. (2.68):

$$\sigma_{t,90} = k_p \cdot \sigma_{m,ap} = k_p \cdot \frac{6 \cdot M_{ap}}{w \cdot h_{ap}^2} = \left[k_5 + k_6 \cdot \left(\frac{h_{ap}}{r} \right) + k_7 \cdot \left(\frac{h_{ap}}{r} \right)^2 \right] \cdot \frac{6 \cdot M_{ap}}{w \cdot h_{ap}^2}, \text{ with} \quad (2.68)$$

$$k_5 = 0.2 \cdot \tan \alpha_{ap}, \quad k_6 = 0.25 - 1.5 \cdot \tan \alpha_{ap} + 2.6 \cdot \tan^2 \alpha_{ap}, \quad k_7 = 2.1 \cdot \tan \alpha_{ap} - 4 \cdot \tan^2 \alpha_{ap}, \quad (2.69)$$

and h_{ap} and α_{ap} as the height and the angle of the taper in the middle of the apex zone. The verification, according to eq. (2.68), governs the size of the beam dimensions in several cases, c. f. Schickhofer (2006b). Furthermore, the timber tensile strength perpendicular to grain is known as its weakest material property with a high variability, significantly influenced by the size of the stressed timber volume, as well as changes in moisture content. The reinforcement of this detail – currently, glued-on wood-based products, glued-in rods, as well as self-tapping screws and threaded rods are applied – consequently avoids uneconomical beam dimensions combined with a hardly predictable resistance against the stress state given. The corresponding measures (the focus is again on self-tapping screws) can be separated into: those designed for carrying all stresses caused by static loading and those solely against tensile stresses perpendicular to grain, additionally caused by changes in moisture content, c. f. DIN EN 1995-1-1/NA (2013):

Against all tensile stresses perpendicular to grain caused by static loading:

$$F_{t,90} = \sigma_{t,90} \cdot \frac{w \cdot a_1}{n} \quad (2.70)$$

Against stresses caused by climatic changes:

$$F_{t,90} = \sigma_{t,90} \cdot \frac{w^2 \cdot a_1}{640 \cdot n} \quad (2.71)$$

Eqs. (2.70) and (2.71) are thereby used for the verification of the fasteners situated in both inner quarters of the zone stressed in tension perpendicular to grain. In Figure 2.48, this zone with the length c is exemplarily illustrated for pitched cambered timber beams. According to Schickhofer (2006b), c can be determined as follows:

Pitched cambered and curved beams:
$$c = 2 \cdot r_{in} \cdot \sin \beta \quad (2.72)$$

Double tapered beams:
$$c = h_{ap} \quad (2.73)$$

Thereby, β and r_{in} are the beam's inner inclination and radius. Since the tensile stresses perpendicular to grain decrease with increasing distance from the apex, both outer quarters only need to be reinforced for $2/3$ of $F_{t,90}$ according to eq. (2.70). Worth mentioning that only 50 % of the screw's axial load-carrying capacity R_{ax} should be counted for the verification, see e. g. ON B 1995-1-1 (2015). The verification given in eq. (2.71) bases on the assumption, that $1/4$ of tensile stresses perpendicular to grain (referred to $w = 160$ mm), according to eq. (2.68) have to be transmitted by the reinforcement. Since the moisture induced stresses increase with increasing member dimensions, this value, referred to $w = 160$ mm, also depends on the width of the beam, c. f. Blaß et al. (2004). With regard to the screw arrangement, it is recommended that a_1 , according to Figure 2.48, should not exceed 75 % of h_{ap} (in case of reinforcement against moisture induced stresses 100 % of h_{ap}).

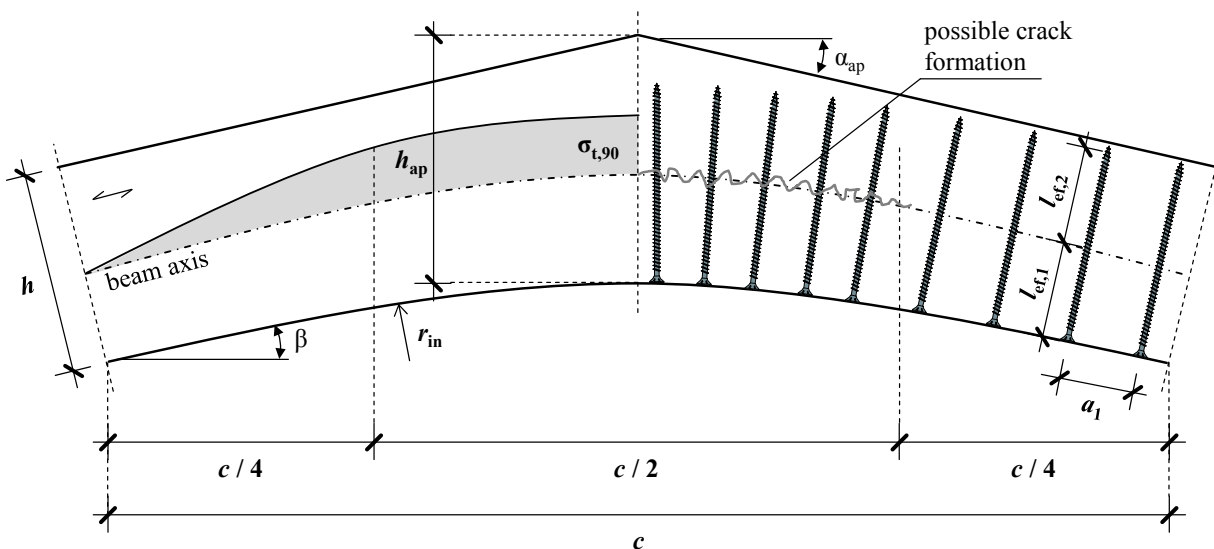


Figure 2.48: Tensile stress distribution perpendicular to grain and reinforcement with self-tapping screws of a pitched cambered beam loaded in bending

The comprehensive investigations, focusing on the loadbearing behaviour of curved timber beams reinforced with self-tapping screws, have been carried out by Jönsson and Thelandersson (2005). The related parameter variation comprised the reinforcement itself (unreinforced beams, pre-reinforced beams

and beams reinforced after failure in tension perpendicular to grain have been examined), the arrangement of screws (over the whole beam length vs. only in its curved part), as well as the climate conditions (seasoned in 40 % and 80 % relative humidity and tested in this state vs. climate change from 40 % to 80 % r. h. and reversed inducing additional internal stresses). The spacings between the screws have been kept constant at $a_1 = 0.40 h$, which resulted from an antecedent FE-study as an optimised distance recommended by Jönsson and Thelandersson (2005) in order to achieve a uniform stress distribution in the curved part of the beam.

Summarising their findings, Jönsson and Thelandersson (2005) report an increase of loadbearing capacity as a consequence of pre-reinforcement of about 50 % if compared to the unreinforced beams. For those beams, which were reinforced after their first failure in tension perpendicular to grain, only a slight increase in loadbearing capacity took place. Interestingly, the capacity was reached at significantly higher ultimate deformations. Since the reinforced beams mainly failed in shear at their ends, Jönsson and Thelandersson (2005) assume a limiting influence of the set-up and even higher bearing capacities in practice. Comparing both different screw arrangements, the insertion over the whole beam length did not show any positive effect. With regard to climatic conditions, reinforced beams almost reached the same capacities irrespective from climatic changes and the size of relative humidity, while unreinforced beams show remarkably smaller capacities as a consequence of a climate change from 40 % to 80 % r. h. (moistening phase).

Apart from this investigation, the works focusing on the loadbearing behaviour of double tapered, curved or pitched cambered beams reinforced with self-tapping screws are scarce. Those generally concentrating on the influence of moisture induced stresses on reinforcements are outlined in section 2-4.5.

2-4.3 Reinforcement against shear

Compared to reinforcement measures against stresses perpendicular to grain, discussed in section 2-4.1 and 2-4.2, the enhancement of the timber material properties against shear stresses is a new research field and was significantly influenced by the development process of self-tapping screws and threaded rods during the last years. The affected timber members are those with comparatively small span lengths and/or variable beam heights with small cross-sectional dimensions in zones where the maximum internal shear forces occur (e. g. supportings of double tapered or pitched cambered beams, see section 2-4.2.4).

First investigations were done by Trautz and Koj (2008) and Trautz and Koj (2009). Therein, they summarise an experimental campaign comprising the bending tests of GLT beams reinforced with self-tapping screws over their whole span length. Screws were arranged in form of a truss system, see Figure 2.49. Thereby, the varied parameters contained the truss type (quadrangular trusses with screws as tensile diagonals or as tensile verticals and compressive diagonals, warren trusses with screws as tensile or

tensile and compressive diagonals), as well as the screw axis-to-grain angle $\alpha = \{32.5 \text{ and } 45\}^\circ$, the latter in case of warren trusses.

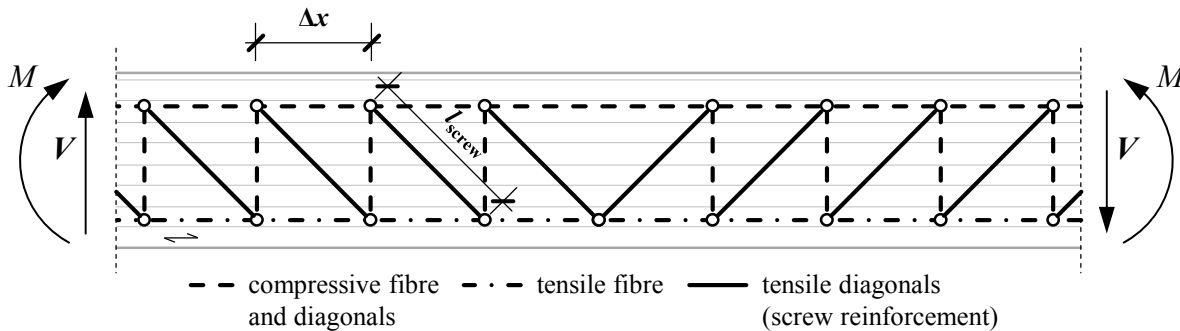


Figure 2.49: Example of a truss-like screw arrangement in GLT beams stressed in bending; according to Trautz and Koj (2009)

Since all tested beams failed when exceeding their bending tensile strength, Trautz and Koj (2008) could not observe any differences as a consequence of shear reinforcement. Focusing on the stiffness properties, a small increase of bending stiffness due to a comparatively higher shear stiffness GA (max. 10 %), which is increased by the screw reinforcement, was found. For the quadrangular truss types, with screws arranged as tensile diagonals (see Figure 2.49, experimentally determined increase of GA about 3 %), Trautz and Koj (2009) derived a model approach basing on the truss analogy for determining $(GA)_{\text{ideal}}$ as additional shear stiffness caused by the screw reinforcement, see eq. (2.74).

$$(GA)_{\text{ideal}} = \frac{1}{\frac{1}{\sin^2 \alpha \cdot \cos \alpha \cdot (EA)_s} + \frac{2}{\sin^2 \alpha \cdot \sum K_{\text{ser,ax}} \cdot \Delta x} + \frac{\sin \alpha}{\cos \alpha \cdot (EA)_{w,90}}}, \quad (2.74)$$

with $(EA)_s$ as the screw's steel tensile stiffness, $(EA)_{w,90}$ as the compressive stiffness (perpendicular to grain) of the timber vertical and Δx as the length of the truss field, c. f. Figure 2.49. Adding the predicted $(GA)_{\text{ideal}}$ to the unreinforced beams' shear stiffness $(GA)_w$, Trautz and Koj (2009) observed high agreement between modelled and experimentally determined shear stiffness of reinforced beams. Nevertheless, a remarkable enhancement of timber shear stiffness properties as a consequence of screw reinforcement could obviously not be achieved.

Further investigations, regarding the shear reinforcement of timber beams with self-tapping screws and threaded rods, have been carried out by Blaß and Krüger (2010). Their related experimental campaign comprised 4-point bending tests of unreinforced GLT beams and those with reinforcements closely situated to their supportings, as shown in Figure 2.50 (left). In order to achieve the shear failure, instead of a bending tensile one, beams were produced with an I-section according to Schickhofer and Obermayr

(1998). The parameter variation contained beam dimensions (beam type I: web width $w = 100$ mm, $h = 608$ mm; beam type II: $w = 150$ mm, $h = 200$ mm), fastener types (beam type I with threaded rods, $d = 16$ mm and beam type II with self-tapping screws, $d = 8$ mm) and their number (n), as well as their arrangement (a varying position between load introduction and supporting; an insertion as tensile diagonals, $\alpha = 135^\circ$, or as compressive diagonals, $\alpha = 45^\circ$, see Figure 2.50). Furthermore, unreinforced beams were reinforced after failure (screws, threaded rods and glued-in steel bars were applied) and tested again, verifying the efficiency of this refurbishment measure.

The determined shear capacities of beams with fasteners, arranged as tensile diagonals, indicate a more or less pronounced increase in shear strength between 6 % and 33 %, as well as a slightly positive influence of n on f_v . In contrast, the fasteners arranged as compressive diagonals did not affect the bearing capacity at all. According to Blaß and Krüger (2010) this can be explained by the truss analogy (see also section 2-3.1.1), meaning that in dependence of the fastener arrangement (loaded in tension or in compression) compressive or tensile stresses perpendicular to grain have to be transmitted in the zone, where crack formation occurs. Since the shear strength is significantly influenced by the stress-state perpendicular to grain (positively by compressive, negatively by tensile stresses), a probably positive participation of reinforcements loaded in compression is contradicted by the tensile stresses decreasing the timber shear properties, c. f. Blaß and Krüger (2010).

A comparison of the test results with capacities predicted by means of a nonlinear FE-analysis – Blaß and Krüger (2010) applied the relationship given in eq. (2.75), as well as test curves of axially loaded screws and threaded rods – indicates a high conformity of the numerical model in case of beam type I. In case of beam type II, Blaß and Krüger (2010) explain the observed deviations by inaccuracies caused due to restrictions in FE-modelling.

$$f_v = f_{v,0} - 1.15 \cdot \sigma_{\perp} - 0.13 \cdot \sigma_{\perp}^2, \quad (2.75)$$

with $f_{v,0}$ as shear strength at $\sigma_{\perp} = 0$ N/mm². With regard to the results, gained from tests of refurbished beams, similar bearing capacities, than those of the unreinforced beams, could be reached in most of the cases. Thereby, the number of fasteners, as parts of the refurbishment, was determined according to eq. (2.76).

$$n = \frac{\sqrt{2} \cdot V}{R_{ax} \cdot (1 + \mu)}. \quad (2.76)$$

For practical application of eq. (2.76), Blaß and Krüger (2010) recommend to assume μ conservatively and to fill out open cracks with adhesives before inserting the fasteners, especially if glued-in steel bars or rods are used.

In addition to the works discussed so far, comprehensive examinations on the shear reinforcement of glulam beams can be found in Dietsch (2012), Dietsch et al. (2012), Dietsch et al. (2013) and Dietsch (2014). In his dissertation and in contrast to the aforementioned sources, Dietsch (2012) applies the principle of the structural anisotropy for determining the influence of the reinforcement measure on the timber member's shear properties. Thereby, the reinforced timber beam is assumed as a composite section with stiffness matrix \mathbf{C}_0 , which can be calculated by summing up the single stiffness matrices $\mathbf{C}_{1,0}$ and $\mathbf{C}_{2,0}$ of the timber member and the reinforcement respectively, see eq. (2.77) to eq. (2.79):

$$\mathbf{C}_0 = \mathbf{C}_{1,0} + \mathbf{C}_{2,0} = \begin{bmatrix} E_0 & 0 & 0 \\ 0 & E_{90} & 0 \\ 0 & 0 & G \end{bmatrix} + \left(\frac{n_s}{w} \cdot \frac{\gamma \cdot (EA)_s}{a_{1,CG}} \right) \cdot \mathbf{T}_{C,S-0}, \text{ with} \quad (2.77)$$

$$\gamma = \frac{1}{1 + \frac{\pi^2 \cdot (EA)_s}{(2 \cdot l_{ef})^2 \cdot k}}, \quad k = \lambda^2 \cdot (EA)_s, \quad \lambda \cdot (e^{\lambda \cdot l_{ef}} - e^{-\lambda \cdot l_{ef}}) = 2 \cdot \frac{K_{ser,ax}}{(EA)_s}, \quad (2.78)$$

$$\mathbf{T}_{C,S-0} = \begin{bmatrix} \cos^4 \varphi & \sin^2 \varphi \cdot \cos^2 \varphi & -\sin \varphi \cdot \cos^3 \varphi \\ \sin^2 \varphi \cdot \cos^2 \varphi & \sin^4 \varphi & -\sin^3 \varphi \cdot \cos \varphi \\ -\sin \varphi \cdot \cos^3 \varphi & -\sin^3 \varphi \cdot \cos \varphi & \sin^2 \varphi \cdot \cos^2 \varphi \end{bmatrix}, \text{ and} \quad (2.79)$$

n_s as the number of fastener rows perpendicular to the loaded plane, γ as the factor considering the semi-rigid composite action between the axially loaded fastener and the timber element, k as embedment modulus of the corresponding composite model (differential equation of a horizontally loaded beam on elastic foundation), λ as iteratively derivable coefficient of the solution of this differential equation and $\mathbf{T}_{C,S-0}$ as transformation matrix considering the different coordinates of both, timber member and reinforcement, see Figure 2.50. Worth mentioning, that only 50 % of the inserted screw thread length should be counted for l_{ef} .

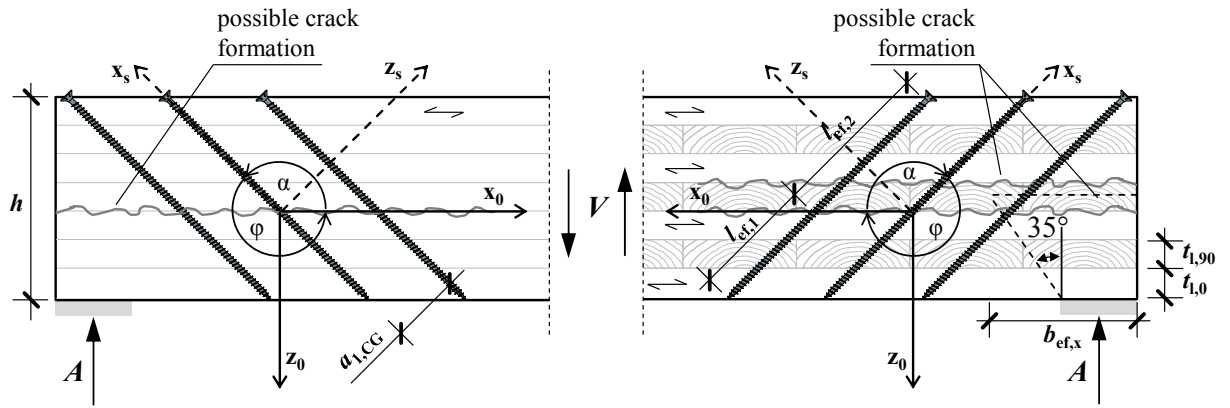


Figure 2.50: Screw reinforcement of laminated timber members against shear stresses, denotation of coordinates and angles within the structural anisotropy: left: GLT; right: CLT; according to Dietsch et al. (2012)

Taking linear-elastic stress-strain-relationship into account, the strain vector $\boldsymbol{\varepsilon}_0$ of the composite section is the product of a load (stress) vector \boldsymbol{n}_0 and the inverse of the stiffness matrix \boldsymbol{C}_0 . Since both coordinate systems of the timber member and the composite section are equal ($\rightarrow \boldsymbol{\varepsilon}_1 = \boldsymbol{\varepsilon}_0$, $\boldsymbol{\varepsilon}_1$ as the strain vector of the timber member), the stress vector in the timber member $\boldsymbol{n}_{1,0}$ results as follows:

$$\boldsymbol{n}_{1,0} = \begin{bmatrix} \sigma_{w,x_0} \\ \sigma_{w,z_0} \\ \tau_{w,xz_0} \end{bmatrix} = \boldsymbol{C}_{1,0} \cdot \boldsymbol{C}_0^{-1} \cdot \boldsymbol{n}_0 = \boldsymbol{C}_{1,0} \cdot \boldsymbol{C}_0^{-1} \cdot \begin{bmatrix} \sigma_{x_0} \\ \sigma_{z_0} \\ \tau_{xz_0} \end{bmatrix}. \quad (2.80)$$

Consequently, η_τ defined by Dietsch (2012) as the efficiency of the reinforcement (reduction of the shear stress in the timber member) can be determined according to eq. (2.81):

$$\eta_\tau = \frac{\tau_{xz_0}}{\tau_{w,xz_0}}. \quad (2.81)$$

Furthermore, the positive influence of compressive stresses perpendicular to grain on the shear strength, occurring if the reinforcement is loaded in tension, can be considered by applying eq. (2.75) with $\sigma_\perp = \sigma_{w,z_0} \cdot N_{s,xs}$ as the axial force in the reinforcement, which is relevant for the related fastener design, results through transforming $\boldsymbol{\varepsilon}_0$ into the reinforcement's local coordinate system and applying Hooke's law, see eq. (2.82):

$$N_{S,x_s} = \boldsymbol{\varepsilon}_{x_s} \cdot (EA)_s = \begin{bmatrix} \varepsilon_{x_0} \\ \varepsilon_{z_0} \\ \gamma_{xz_0} \end{bmatrix} \cdot \begin{bmatrix} \cos^2 \alpha & \sin^2 \alpha & \sin \alpha \cdot \cos \alpha \end{bmatrix} \cdot (EA)_s. \quad (2.82)$$

In Dietsch (2012), this analytical approach is compared with the already discussed experimental results given in Trautz and Koj (2009) and Blaß and Krüger (2010), as well as with the properties determined by own tests (shear modulus by bending tests, shear strength by shear tests according to ON EN 408 (2010), unreinforced and reinforced specimen with and without cracks). Thereby, the values for the embedment modulus k , gained from Mestek (2011), were applied. Overall, a high agreement between model predictions and test results could be observed, especially if the relationship between shear stresses and stresses perpendicular to grain, according to eq. (2.75), is applied.

For a practical application, the model approach derived by Dietsch (2012) has been simplified and is given in ETAs of self-tapping screws such as ETA-11/0190 (2013) for instance in the following form:

$$\frac{\tau}{f_{v,\text{mod}}} \leq 1.00, \text{ with } f_{v,\text{mod}} = \frac{f_v \cdot k_\tau}{\eta_H}, \quad (2.83)$$

$$\eta_H = \frac{G \cdot w}{G \cdot w + \frac{1}{2 \cdot \sqrt{2} \cdot \left(\frac{6}{\pi \cdot d \cdot h \cdot k_{\text{ser},\text{ax}}} + \frac{a_{1,\text{CG}}}{(EA)_s} \right)}}, \quad (2.84)$$

$$k_\tau = 1 - 0.46 \cdot \sigma_\perp - 0.052 \cdot \sigma_\perp^2, \quad (2.85)$$

$$\sigma_\perp = \frac{F_{\text{ax},\text{d}}}{\sqrt{2} \cdot w \cdot a_{1,\text{CG}}} = \frac{(1 - \eta_H) \cdot V \cdot a_{1,\text{CG}}}{h \cdot w \cdot a_{1,\text{CG}}}, \quad (2.86)$$

With regard to the reinforcement's efficiency in general a parameter study summarised in Dietsch (2014) indicates, that the shear capacity of linear timber members can be increased up to 50 % as a consequence of this measure. Since this value has only been achievable by applying threaded rods, $d = 20$ mm, situated in comparatively small beams at $a_{1,\text{CG},\text{min}} = 100$ mm, Dietsch (2014) concludes, that an average increase rate of about 20 % can be realised in practice. This comparatively low benefit can be explained with the occurrence of a shear failure at deformations too small to activate the total bearing potential of the screws, even if they are predominately axially loaded. This means, that there is still a reserve in capacity, having a beneficial effect on the structural system's robustness, since the reinforcement avoids a full separation of the beam in the fractured state, c. f. Dietsch (2012). Further investigations, focusing on the loadbearing performance of such longitudinally cracked beams reinforced with self-tapping screws, were recently published by Jockwer and Steiger (2016) and Wu et al. (2016). Both confirm the positive impact of this measure with respect to timber's ULS and SLS performance.

The cross-wise lay-up of CLT panels loaded out-of-plane consequences a shear stress distribution deviating from that of linear and unidirectional oriented timber products, such as ST or GLT. Since the product's rolling shear strength f_r is about 30 ÷ 50 % of f_v , c. f. Brandner et al. (2016a), the rolling shear failure, as illustrated in Figure 2.50 (right), governs the corresponding verification process in several cases. This, combined with comparatively higher ultimate shear deformations ($G_r \approx 10 \div 15$ % of G), may increase the efficiency of shear reinforcements with dowel-type fasteners by far. Mestek and Winter (2011) summarise a related experimental programme on uniaxial and biaxial out-of-plane bending tests of CLT panels reinforced with self-tapping screws, carried out by Mestek (2011). The results indicate the average strengthening factors η_r in the range of 1.25 to 1.64.

In case of shear reinforced CLT panels, transmitting out-of-plane loads only in uniaxial direction (1D-beams), a high agreement between test results and values predicted by the aforementioned principle of structural anisotropy was found, c. f. Dietsch et al. (2012). Note: the specific CLT lay-up has to be considered when determining the timber member's stiffness matrix $C_{1,0}$. In case of a biaxial load transmission, alternative approaches such as FE-analysis have to be applied; c. f. Mestek (2011). For a practical application, Mestek and Winter (2011) present a simplified model basing on truss-analogy for determining the increased rolling shear strength values of shear reinforced CLT panels, see eq. (2.87) to eq. (2.89).

$$\bar{f}_r = k_{r,90} + \frac{R_{ax} / \sqrt{2}}{a_{1,CG} \cdot a_{2,ef}}, \text{ with} \quad (2.87)$$

$$k_{r,90} = \min \left\{ \begin{array}{l} 1 + 0.35 \cdot \sigma_{c,90} \\ 1.20 \end{array} \right., \quad a_{2,ef} = \max \left\{ \begin{array}{l} a_{2,CG} \\ w / n_{\perp} \text{ uniaxial,} \\ w_{ef,x} / n_{\perp} \text{ biaxial} \end{array} \right. \quad (2.88)$$

$$\sigma_{c,90} = \frac{R_{ax} / \sqrt{2}}{a_{1,CG} \cdot a_{2,ef}} + \left\{ \begin{array}{l} 0 \quad \text{uniaxial} \\ F \quad \text{biaxial} \end{array} \right., \text{ and} \quad (2.89)$$

\bar{f}_r as enhanced rolling shear strength, n_{\perp} as the number of screw rows perpendicular to the loadbearing direction and $w_{ef,i}$ as effective widths illustrated in Figure 2.50 (right). A comparison between model predictions and the aforementioned results of uniaxial and biaxial bending tests indicates that eq. (2.87) underestimates the real capacities, but describes the data trend accurately.

2-4.4 Reinforcement of laterally loaded dowel-type connections

The design process of laterally loaded dowel-type connections in modern standards, such as Eurocode 5, generally bases on Johansen's yield theory, c. f. Johansen (1949). His approach comprises the determination of the single fastener's loadbearing resistance as a minimum of different failure modes (timber embedment failure, combined failure of timber embedment and steel yielding), which depend on the connection type, geometrical dimensions, such as the slenderness λ (ratio between fastener diameter and embedment depth), as well as on timber and steel material properties. In cases, n fasteners are applied parallel to the grain direction, the joint's load-carrying capacity (in this direction) was found to be lower than the single fastener resistance multiplied by n . This group effect, additionally influenced by fastener spacings and their geometry, can be covered by assuming an effective number $n_{\text{ef}} < n$, e. g. according to Jorissen (1988). His considerations take a nonlinear load distribution between the fasteners at time of failure into account, especially when splitting failure of the timber member occurs at small deformations, c. f. Blaß and Schmid (2001). Nowadays, the reinforcement of such connections with self-tapping screws follows two strategies:

First, the aforementioned splitting failure of joints with comparatively stout fasteners (small λ) can be prevented by inserting screws in-between parallel to grain spacings (screw axis perpendicular to grain direction and perpendicular to fastener axis, see Figure 2.51), enabling plastic timber deformation, load redistribution and hence higher values for n_{ef} .

Second, in addition to the aforementioned measure, a screw arrangement in direct contact to the fasteners in load direction restricts their lateral deformation and thus enhances their loadbearing behaviour with regard to stiffness and resistance.

2-4.4.1 Reinforcement to increase the effective number of fasteners

The first known examinations, concerning the screw reinforcement of laterally loaded dowel-type connections for increasing their effective number in grain direction, have been carried out by Blaß and Schmid (2001). Therein they simplify the initially cracked connection, shown in Figure 2.51, as a beam on elastic foundation (springs only in the non-cracked area, beam height equal to $h/2$) firstly applied by Jorissen (1988). The differences between their approach and the original one are the number and position of cracks (just one area of crack formation in the connection axis is assumed), as well as the consideration of a reinforcement (situated in the middle between two fasteners) in form of an additional support of this beam model. Worth mentioning, deviating from Figure 2.51, Blaß and Schmid (2001) fixed z -displacements in this support ($K_{\text{ser,ax}} \rightarrow \infty$), so the crack formation was only assumed in the area between dowel and reinforcement. The external loads V and M in dependence of F were determined as follows:

$$V = \frac{F}{5} \div \frac{F}{10} \text{ according to Jorissen (1988) and Werner (1993), and} \quad (2.90)$$

$$M = \frac{F \cdot h}{8}, \quad (2.91)$$

with F as the decisive load per shear plane according to Johansen (1949). Consequently, F_{ax} as the axial force in the screw reinforcement is determined by solving the differential equation of the beam on the (piecewise) elastic foundation with the spring coefficient K , calculated according to eq. (2.92), see

$$K = \frac{E_{90} \cdot t_1 \cdot 4}{h}. \quad (2.92)$$

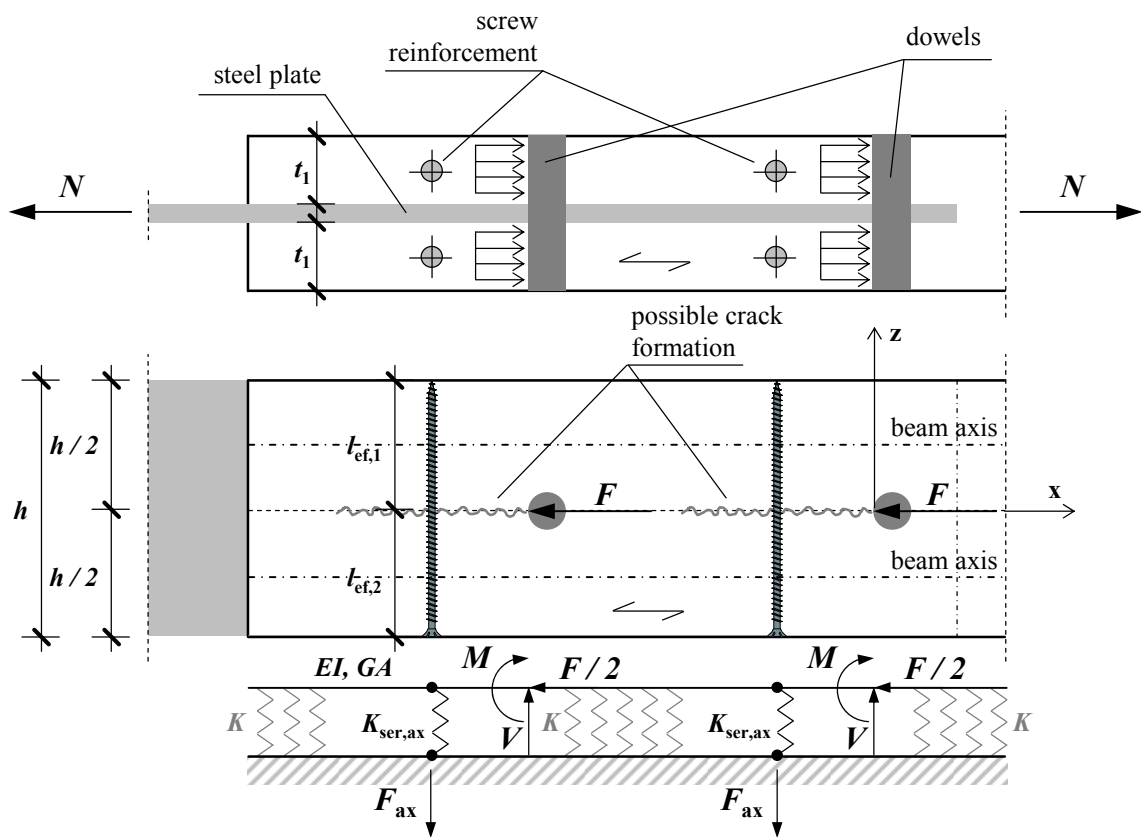


Figure 2.51: Illustration and mechanical model of a laterally loaded steel-to-timber tensile joint reinforced with self-tapping screws to increase n_{ef} , according to Schmid (2002) and Bejtka (2005)

Blaß and Schmid (2001) also summarise the results of an experimental campaign on dowelled timber-to-timber tensile joints, carried out to determine the efficiency of the screw reinforcement, expressed in form of increasing n_{ef} . Although a high plastic deformation of reinforced specimen was observed, n_{ef} increased only about 10 % in average. Thereby, the crack formation did not exceed the mentioned assumed area, indicating the withdrawal capacity of the screws applied, being significantly higher than the estimated

load. Beside other topics, Schmid (2002) enhanced the aforementioned model approach (additional consideration of the beam's shear flexibility in elastically supported zones, determination of V according to eq. (2.93)) and predicted axial screw forces occurring in different connection types (timber-to-timber, steel-to-timber) and configurations (n up to 5), as well as for varying Johansen's failure modes.

$$V = F \cdot \frac{\frac{1 - \sin^2 \varphi}{2} \cdot \cos \varphi - \left(\frac{\pi}{4} - \frac{\varphi}{2} - \frac{\sin 2\varphi}{4} \right) \cdot \sin \varphi}{2 \cdot \cos \varphi}, \quad (2.93)$$

with $\varphi = 19^\circ$ as the assumed friction angle between dowel and timber. Irrespective the given failure mode and applied dowel diameter, Schmid (2002) finally recommends to design the reinforcement with $F_{ax} \approx 0.30 \cdot F$ in order to achieve $n_{ef} = n$. Worth mentioning, this relationship has also been adopted in modern standardisation, see e. g. ON B 1995-1-1 (2015).

Bejtka (2005) also concentrated on improving the discussed model approach. In contrast to Schmid (2002), he attests the screw applied as a reinforcement with a certain flexibility in z -direction and replaces the aforementioned pinned support ($K_{ser,ax} \rightarrow \infty$) by a spring with stiffness $K_{ser,ax} < \infty$. The consequence is a crack formation beyond the reinforcement, as illustrated in Figure 2.51. Furthermore, Bejtka (2005) aims to activate the screw's total axial bearing potential, which is achieved in cases, crack opening at the spring v_{ax} is equal to $\delta_{ax} = \delta(R_{ax})$ (see eq. (2.94), determined by means of regression analysis of screw withdrawal test results), while crack formation is assumed over the whole connection length in fibre direction.

$$\delta_{ax} = 0.0016 \cdot d \cdot \sqrt{\rho \cdot l_{ef}}. \quad (2.94)$$

The beam model, given in Figure 2.51, can thus be simplified as a cantilever beam with fixed support, located at the fastener with the longest distance to the timber's end grain and solved as n -times statically indeterminate system. Deviating from Schmid (2002), the reinforcement design comprises the determination of an axial slip modulus $K_{ser,ax,min}$ (in Bejtka (2005), eq. (2.31) is applied), necessary for assuming n_{ef} equal to n . Since this property is influenced by several parameters, Bejtka (2005) provides design diagrams for different joint configurations containing isolines of $R_{1,0}$, defined as the referred maximum loadbearing capacity per fastener and shear plane at a unit displacement of the cantilever, $v = 1.0$ mm. For the joint detail given, $R_{1,0}$ can be determined as follows:

$$R_{1,0} = \frac{R_{req}}{v_{ax}} \text{ and } v_{ax} = \min \left\{ \begin{array}{l} \delta_{ax} \\ 0.05 \cdot d_1 \end{array} \right., \quad (2.95)$$

with R_{req} as the single fastener's loadbearing capacity per shear plane according to Johansen (1949) (equal to F in the beam model) and d_1 as the laterally loaded fastener's diameter. This value combined with a given spacing a_1 consequently enables the determination of $K_{\text{ser,ax,min}}$ in the diagram. Worth mentioning, that all related graphs published by Bejtka (2005) base on a screw arrangement as close as possible to the corresponding fastener as well as on $(5 d \leq a_1 \leq 10 d) \cdot n^{0.4}$. A comparison of the model approach with results of an experimental campaign on laterally loaded reinforced connections indicates a high conformity between predicted values and test results, except for joints failing in plug shear of a row of fasteners in grain direction. Since the discussed reinforcement measure is not effective in this case, Bejtka (2005) additionally derived a plug shear model, which should therefore be considered in the design process. The gained values for ductility D of reinforced and unreinforced connections are shown and discussed in Blaß and Schädle (2011).

While the aforementioned works mainly focused on analytical approaches for determining the loadbearing behaviour of reinforced dowel-type connections, Blaß and Bejtka (2008) performed the advanced FE analysis for this purpose. In doing so, they also tried to verify the relationship $F_{\text{ax}} \approx 0.30 \cdot F$ currently applied in standardisation as discussed before. The results gained from a corresponding parameter study including different diameters d_1 , densities, spacings a_1 and especially n indicate that Schmid's approach overestimates the numerically determined capacities. According to Blaß and Bejtka (2008), this is caused by the given restrictions in modelling timber by FE and the fact, that only Johansen's failure mode 1 was examined.

The relationship between Johansen's failure load and the force occurring in the screw reinforcement has also been verified by Wolfthaler (2015). Therein, he developed a self-tapping measuring screw, which records the axial force in the reinforcements when testing the connection. In the frame of a corresponding experimental campaign on steel-to-timber tensile joints he observed a hyperbolic distribution of these forces in form of two load peaks in the screws, situated at the beginning and the end of the connection. The gained values significantly deviate in their size and course from those predicted by the approaches given in Schmid (2002) and Bejtka (2005), which result in a more or less linear increase of F_{ax} with decreasing distance to the timber's end grain. Consequently, Wolfthaler (2015) recommends assuming $F_{\text{ax}} \approx 0.50 \cdot F$ for screws situated in both outer thirds and $F_{\text{ax}} \approx 0.15 \cdot F$ for those situated in the inner third of the connection.

Further investigations concerning the reinforcement of laterally loaded dowel-type connections were carried out by Mohammad et al. (2006). Therein, they summarise an experimental programme on steel-to-timber tensile joints, unreinforced and reinforced with different types of self-tapping screws, as well as with truss plates. The parameter variation further comprised the end distance $a_{3,t} = \{5 d_1, 7 d_1\}$, the number of fasteners in grain direction $n = \{1, 2\}$, the number of rows $m = \{1, 2\}$, as well as the screw

reinforcement of specimen containing an artificial split to verify the refurbishment potential of this measure. Additional test series with specimen loaded perpendicular to grain were carried out to compare the loadbearing behaviour of initially reinforced connections and those reinforced after splitting failure.

The corresponding test results indicate no valuable influence of reinforcement on the ultimate loads achieved, while plastic deformations and thus the joint's ductility (again) could be increased by far. Since just one test series was carried out with more than one fastener in a row ($n = 2$) and the spacings a_1 and $a_{3,t}$ were below standardised minimums, a quantitative statement concerning the reinforcement's influence on n_{ef} cannot be derived from their investigations. With regard to the reinforcement applied as a refurbishment, the ultimate load of reinforced connections with artificial splits was found being about 30 % lower, than that of the unreinforced connection without any splits. Further examinations and findings on screw refurbishment of single dowels as well as bolted steel-to-timber connections, stressed by normal forces and/or bending moments, can be found in Lam et al. (2008), Delahunty et al. (2014), Min-Juan and Hui-Fen (2015), Wang et al. (2015), Min-Juan et al. (2016), Zhang et al. (2016), Wrzesniak and Fragiaco (2016), Lederer et al. (2016) and Karagiannis et al. (2017).

Apart from the works discussed so far, the investigations concerning the screw reinforcement of dowelled connections with large diameters d_1 , done by Kobel (2011), have to be finally noted.

2-4.4.2 Reinforcement to increase single fastener resistance

In addition to the reinforcement measure, discussed in section 2-4.4.1, it is also possible to arrange screws in a way, they positively contribute to the single fastener's loadbearing performance in terms of increasing stiffness and resistance. Thereby, the screws should be inserted in direct contact to the laterally loaded fastener, acting as an additional but flexible support for the equivalent statical system, Johansen's approach is basing on. Consequently, the fastener's loadbearing resistance can be determined by extending Johansen's failure modes considering this additional boundary condition. Since the screw itself is predominately loaded in lateral direction (in fact, the design of the screw also follows Johansen's theory), this reinforcement measure is not discussed in detail. The summary of a corresponding model approach is given in Bejtka and Blaß (2005), basing on investigations done by Bejtka (2005). In addition, Blaß et al. (2006) present a related software application for practical use. A combination of reinforcement measures may increase the capacity of a laterally loaded connection of up to 120 %, c. f. Bejtka and Blaß (2005).

2-4.5 Further reinforcement applications and general works

2-4.5.1 Reinforcement of timber beams against bending stresses and deflections

As introduced in section 2-1.2, the high axial stiffness of self-tapping screws has been recognised very early and has been used advantageously for developing effective composite structures. With regard to the reinforcement (or better refurbishment) of timber beams overcharged in bending, not only the already discussed TCC systems, but also additional lamellas in steel or high-grade wood or fibre products, situated on the timber member's bottom side in their tensile zone, are applied for this purpose nowadays. In Trautz and Koj (2009) corresponding experiments on timber beams reinforced by an additional steel lamella connected with inclined positioned self-tapping screws are summarised. Thereby, significantly higher capacities and bending stiffness could be achieved. Failure was observed in form of steel yielding and plastic deformation in the timber compressive zone, indicating a suitable composite behaviour. Furthermore, the values predicted by the γ -method, as proposed in ON EN 1995-1-1 (2015), corresponded well with the test results.

Further work done by Giongo et al. (2013), who concentrate on the cambering of timber beams with excessive permanent mid-span deflections by self-tapping screws, has also to be mentioned.

2-4.5.2 Influence of screw reinforcement on moisture induced stresses

In general, timber material properties are well known for their significant dependency on the moisture content u . Its variation not only changes the size of timber strength and stiffness parameters, but also causes a member deformation in form of shrinkage (decreasing u) and swelling (increasing u). Thereby induced internal stresses (due to an inhomogeneous distribution of u over the member's cross-section) occur in a size, that they exceed corresponding tensile strength perpendicular to grain in specific cases. The crack formation consequently occurs and decreases the bearing performance against e. g. tension perpendicular to grain or shear. The arrangement of self-tapping screws or threaded rods, originally applied to reinforce such vulnerable areas in timber beams (c. f. sections 2-4.2 and 2-4.3), constrains the moisture induced deformations to some extent and consequently influences the internal stress distribution.

Motivated by this essential but open topic, related investigations on interactive effects between self-tapping screws or threaded rods and reinforced timber members have been carried out by Angst (2012), Angst and Malo (2012), Dietsch (2012), Wallner (2012) and Dietsch et al. (2014). Their main and similar outcomes are summarised in brief: all mentioned authors observed a very complex relationship between timber member and reinforcement at a varying moisture content, which is influenced by several geometrical and physical parameters, such as specimen dimensions (especially width and height), screw arrangement (diameter and distance), as well as the way moisture content has been varied.

First, a decrease of u in reinforced specimen prevents free shrinkage deformations, and thus increases tensile stresses perpendicular to grain exceeding the corresponding strength $f_{t,90}$ as the crack formation has partially been observed. The force equilibrium in the cross-section thus constitutes compressive stresses in the reinforcement similar to the axial loadbearing capacity of the applied fastener. This already occurs at Δu of about 4 % as commonly given in practical application, c. f. Wallner (2012).

Second, the reinforcement of specimen exposed to wetting (increasing u) results in a decrease of occurring tensile stresses perpendicular to grain, which would have been critical with respect to $f_{t,90}$ if no reinforcement had been applied. In contrast to the shrinkage process, a prevention of swelling causes tensile stresses in the reinforcement, again in a size close to the fastener's tensile capacity, c. f. Angst and Malo (2012).

Focusing on fastener arrangement, both Angst and Malo (2012) and Dietsch et al. (2014) determine a significant influence of in-between spacings on the size and distribution of internal stresses occurring in reinforced specimen. Focusing on shrinkage effects, Dietsch et al. (2014) recommend increasing distances as much as possible (prevention of an increase in $\sigma_{t,90}$), while in case of swelling, Angst and Malo (2012) determined a negative relationship between stress reduction and screw distance, concluding that small spacings are advantageous regarding the decrease of tensile stress distribution perpendicular to grain. Furthermore, Dietsch et al. (2014) report an influence of α on the size of induced stresses. The shear reinforcement (see section 2-4.3, $\alpha = 45^\circ$) thus has a minor impact on $\sigma_{t,90}$ than that against stresses perpendicular to grain ($\alpha = 90^\circ$).

2-4.5.3 Further publications and general works

The vast majority of reinforcement measures discussed in sections 2-4 is aimed to enhance the timber's bearing performance against tensile stresses perpendicular to grain. Thereby, the screw-timber interaction is enabled by the given transverse strains in the affected area, finally leading to crack formation. The pre-stressing of wood induces compressive stresses perpendicular to grain and is thus one possibility to avoid this unfavourable behaviour. In this context, Steilner and Blaß (2010) developed a screw with varying pitch along its axis, capable to fulfil this purpose. As demonstrated in Steilner (2014), its application induces a nonlinear compressive stress distribution along the screw axis. The peak values decreasing with increasing distance from the fastener thereby result in a size comparable to $f_{t,90}$. The relaxation effects, which weaken the effect of pre-stressing, were observed to decrease these stresses about 25 % during the first hours of application. Consequently, 75 % of the initially induced stresses remain and can be accounted for the design process, c. f. Steilner (2014).

The following review of literature (concerning the reinforcement of timber members with self-tapping screws) is worth to be outlined: a summary of the reinforcement of laterally loaded dowel type

connections discussed in section 2-4.4 is provided by Lathuillière et al. (2015), while in Dietsch and Brandner (2015) a comprehensive overview of screw reinforcement is given.

2-5 CONCLUDING REMARKS TO CHAPTER 2

Within this introductory chapter the current state-of-the-art concerning the application of self-tapping screws as efficient fasteners in modern timber engineering has been summarised and discussed. Thereby, the main conclusions can be drawn as follows:

- With regard to resistance, stiffness and ductility, as three main design criteria to be considered when detailing a timber connection, self-tapping screws obtain their maximum loadbearing efficiency if predominately stressed in axial direction.
- National and European Technical Assessments (formerly known as Technical Approvals) clearly mirror the current state-of-knowledge regarding this CE-labelled product. Seen as a supplementation to the rules given in standardisation, they have a significant impact on the design process. Furthermore, their developing process over the last decades indicates their role as the reasonable market indicator of this product.
- The EC-mark, also known as CE label, identifies the construction products being “fit for use” and enables their free movement and application within the European Economic Area (EEA). It shall increase their economy while ensuring a certain level of quality. At least in case of self-tapping screws, national regulations comprising the treatment of CE labelled products in the specific member states are very inhomogeneous and still show a high level of complexity, contradicting the idea behind. There is definitively a need for further harmonisation sustaining the competitiveness of European screw manufacturers in the global market.
- Based on the literature study summarised in sections 2-3 and 2-4, nowadays screws are applied as fasteners transmitting loads in connections between elements as well as reinforcements persisting the exceedance of internal resistances in timber’s weak directions. They are commonly arranged in solid timber and the laminated timber products GLT and CLT.
- Although the design process comprises a lot of different approaches derived for the specific detail examined, both application fields unify the determination of the screw’s axial load-carrying capacity as a core property governed by the main failure modes “withdrawal” and “steel failure in tension”. Furthermore, recent models more and more comprise their axial stiffness, especially with regard to the screws applied as reinforcements. In contrast, none approach was found, wherein ductility influences the related design process. Consequently, the investigations focusing on the latter mentioned parameter for axially loaded single screws and its application for estimating the same for screwed connections, are scarce.

Especially motivated by the last point, the further chapters of this thesis thus basically concentrate on both mentioned failure modes of axially loaded single screws. The main focus is thereby set on the axial resistance influenced by several physical, mechanical and geometrical parameters.

CHAPTER 3

COMPONENTS, PRODUCTION AND MAIN MATERIAL PROPERTIES OF SELF-TAPPING SCREWS

3-1 INTRODUCTION

As previously discussed in chapter 2, the product characteristics of self-tapping screws influence their efficiency as fasteners, applied for connections and reinforcements, in a major way. The main parameters, such as their tensile capacity and yield moment in case of loadbearing, or their torsional resistance relevant for screw insertion, are governed by the interrelationship of several geometrical and mechanical screw properties.

The aim of this chapter is to compile the basic knowledge regarding the product self-tapping timber screw. The corresponding considerations comprise its morphology, the screw production process, a mathematical description of the screw thread geometry, applied for modelling the aforementioned mechanical properties, as well as the structural tensile behaviour of self-tapping screws exposed to varying conditions in terms of loading and environment.

Especially in the frame of the latter mentioned topic, the impact of time-dependent effects on the endurance of self-tapping screws, e. g. restricted to tensile failure by fatigue or to hydrogen-induced stress corrosion cracking (HISCC), is discussed. Both phenomena have a major influence on the research activities in the field of material science. In case of self-tapping screws they are not considered as they should. Consequently, corresponding investigations shall expand basic knowledge regarding this fastener type.

3-2 GEOMETRY OF SELF-TAPPING SCREWS

Within the last decades, the increasing demand of self-tapping screws for numerous applications in timber engineered structures led to the development of several different fastener geometries specifically designated for varying purposes. Nevertheless, their general lay-up is more or less equal (TCC screws are herein excluded) and can be regarded as a system composed by the following five main components: “drive”, “head”, “shank”, “thread” and “tip”, which are exemplarily illustrated in Figure 3.1. Within subsections 3-2.1 to 3-2.5, their characteristics and geometrical parameters, as well as their function in the frame of insertion and loadbearing, are described and discussed.

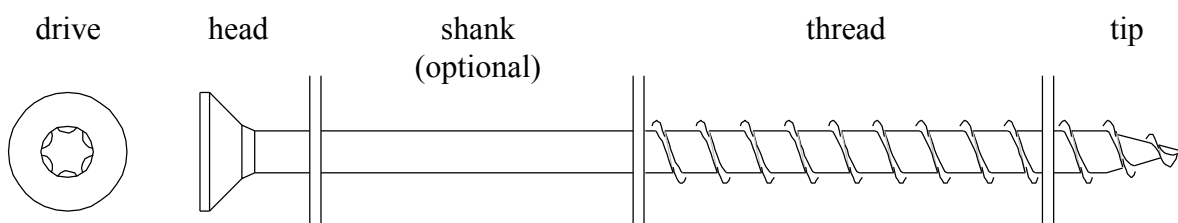


Figure 3.1: Classification of a self-tapping timber screw as composed by five main components

3-2.1 Screw drive characteristics

Focusing on the insertion process, the screw drive can be regarded as the interface between fastener and screwing device, transmitting the torsional moment being necessary for drilling the screw into the timber member. Drive geometry and manufacturing quality (precision and mechanical robustness) significantly influence the size of the force, which therefore has to be applied, as well as the level of reusability, especially when inserting long thread lengths and/or arranging the fastener in timber with high density, e. g. in hardwood species.

Nowadays screws are generally produced with a high variety of drive geometries, again developed for specific purposes, but the number of different types applied for self-tapping timber screws is comparatively small. A corresponding overview on the basis of currently valid ETAs is illustrated in Figure 3.2. Thereby, the drives are classified into internal, external and combined forms. Internal drives can be further separated into hexalobular sockets (“Torx”) and cruciform ones (“Phillips” and “Pozidriv”). External ones are commonly produced with hexagonal shape (“Hex”), while external Torx drives are minor used for fully threaded screws with long thread lengths and large diameters, demanding the transmission of high torsional moments. The combined forms with internal hexalobular sockets and external hexagonal shapes can be regarded as a useful supplement of the latter mentioned type. Worth mentioning, the drive dimensions are always given in form of wrench size classes.

The vast majority of self-tapping screws is produced with different modifications of the originally denoted Torx drive, currently regarded as the most efficient type of this kind of fastener. Further considerations regarding the historical development of timber screw drives from the 19th century on can be found in Hübner (2013a).

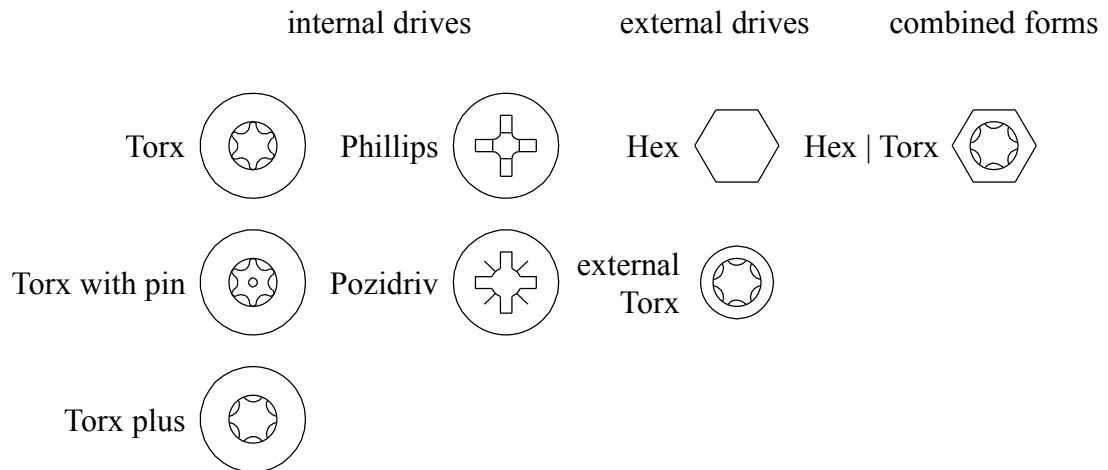


Figure 3.2: Overview and classification of screw drives declared in currently valid ETAs

3-2.2 Screw head characteristics

With regard to all heads declared in currently valid ETAs of self-tapping screws, a huge variety of different types has to be observed. Nevertheless, again they can be classified in form of Figure 3.3. Therein, five selected and representative screw heads can be separated into (a) those aimed to be sunk into and (b) those where the major part of the head is situated outside the timber member. The main parameter describing the difference between both groups is the compression force to be transmitted by the screw head into the timber member in case of axial loading (either in form of a timber-to-timber connection or if two timber components are stressed together).

Group (a) geometries are produced to minimise the timber's resistance against the screw head insertion and consequently reach the weaker head pull-through capacities R_{head} . Especially cylinder heads enable a full countersink of the screw into timber, the corresponding depth is theoretically only limited by the drill bit length of the screwing device. This is enabled by their head diameter d_{head} , rarely exceeding their outer thread diameter d (minimum d_{head} limited by the size of the internal drive), decreasing R_{head} close to zero. Consequently, the cylinder heads are exclusively applied for fully threaded screws with no need for a certain head pull-through capacity. The countersunk heads, the majority of self-tapping screws are produced with, are designated for the screw arrangement flush with the timber's surface and show a certain resistance against head pull-through. Nevertheless, an efficient timber-to-timber connection (equal resistances in both components) with the screw head (pull-through failure) situated in one part and its

thread (withdrawal failure) situated in the other part is hardly realisable with the currently available CS head geometries, c. f. section 2-1.2.

Group (b) screw heads, especially those with a washer form, are produced with significantly higher d_{head} aiming to maximise their resistance against head pull-through. In contrary to cylinder heads, they are exclusively applied for partially threaded screws. Since their head diameters are limited by the production facility to some extent, the further increase of R_{head} can be achieved by combining washers with CS heads. Both maximum ratios d_{head}/d analysed are 2.8 (washer heads) and 3.6 (CS heads with washers) respectively, the increase of R_{head} can thus be estimated to 30 %. Washers, produced with an insertion angle $\alpha = 45^\circ$, are also applied for inclined positioned screws in steel-to-timber joints, replacing the countersunk drill holes in the steel plate by more economically producible long slots. The hexagonal heads, as the last type given in Figure 3.3, are in general not designated to be sunk in the timber member and consequently also classified in group (b). Their minor relevance in application predominately comprises laterally loaded screwed steel-to-timber joints and mounting connections.

The main geometrical parameters of the screw heads are their head diameter d_{head} , as already discussed, as well as their heights h_i . The index i thereby depends on head location, $i = 1$ for head parts inside the timber member, $i = 2$ for those outside the timber member. The form of head types with partially trapezoidal shape (e. g. CS and washer head in Figure 3.3) is additionally described by the head inclination angle ϑ .

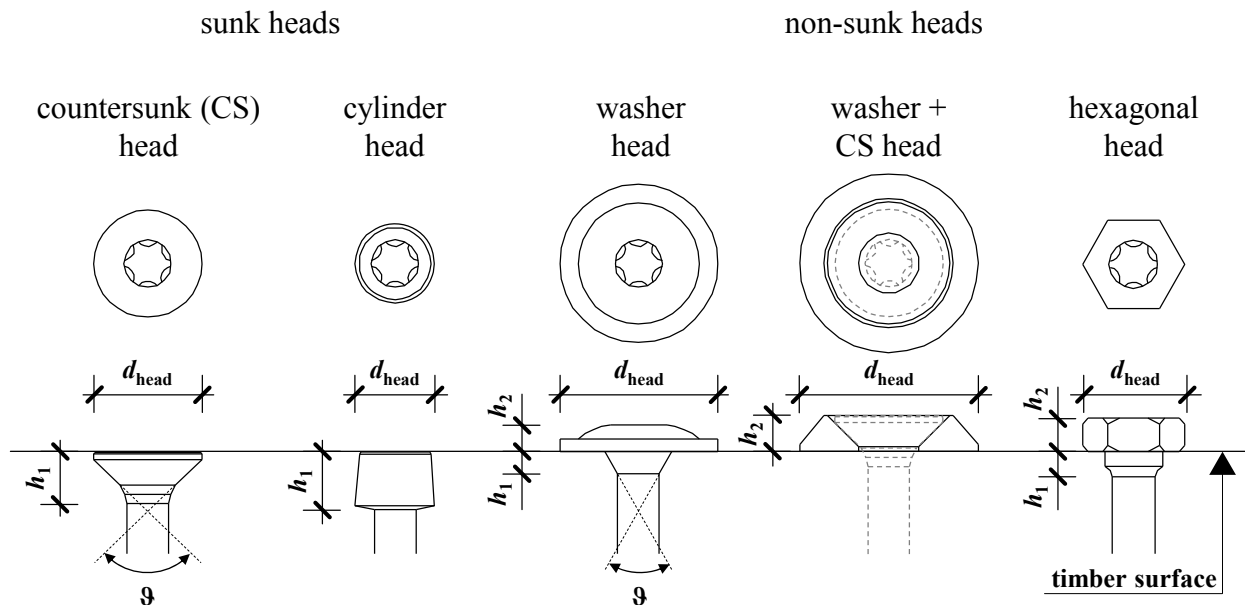


Figure 3.3: Overview and classification of screw heads declared in currently valid ETAs

3-2.3 Screw shank characteristics

The simple purpose of screw shanks, as shown in Figure 3.4, is to connect the screw head with its thread; or – as also frequently applied – two threaded parts with each other. The corresponding geometrical parameters for shank description are l_{sh} and d_{sh} , defined as the shank length and its diameter. While shank lengths solely serve as an indicator for the screw application (screws with long shanks are e. g. used for fastening thermal insulation on top of rafters) having no further mechanical relevance, shank diameters govern the mechanical screw properties axial and torsional resistance, as well as the yield moment. Common shank diameters are equal to the diameters of wire rods, screws are produced with, and thus vary between the screw's outer and inner thread diameter.

In order to decrease the screw's (empirically determined) insertion moment, see e. g. Schmid Schrauben Hainfeld GmbH (2015), especially partially threaded screws are produced with shank cutters, closely situated at the transition between screw shank and thread (in specific cases also between screw thread and tip). Figure 3.4 shows three selected cutter types, illustrating the high geometrical variability of this shank modification. Again, l_{cut} and d_{cut} , herein defined as the cutter's length and its diameter, serve to describe the corresponding dimensions. First partially threaded screws comprising shank cutters have been published in Z-9.1-427 (2000) and Z-9.1-453 (2000) respectively.

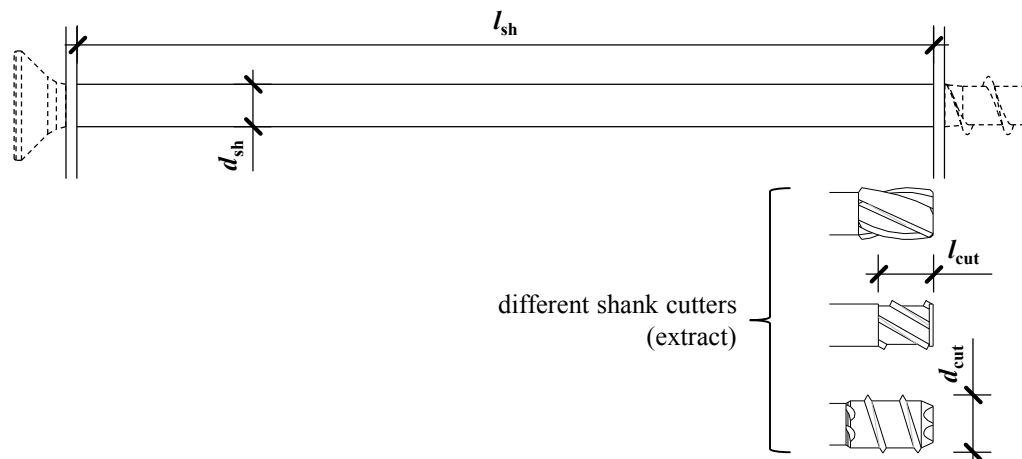


Figure 3.4: Geometrical parameters of screw shanks, including an extract of cutter geometries

3-2.4 Screw thread characteristics

Focusing on self-tapping screws applied for axial loading, their threads being responsible for load transmission into the timber member, can definitively be regarded as the core components of this fastener system. Screw threads (all produced as right-hand threads) may be classified in dependence of (a), their geometrical parameters p as the thread's pitch, d_c and d as the inner and outer thread diameter and v as the

thread's flank inclination angle, (b), the number of threads, n_{thread} screws are produced with, currently subdividing into single- and double-threaded screws ($n_{\text{thread}} = \{1, 2\}$) and (c) their length l_{thread} .

Further concentrating on (a), Figure 3.5 illustrates the aforementioned geometrical parameters p , d_c , d and v for three different thread characteristics found in currently valid ETAs. Therein, thread type (I) represents the common geometry the majority of screws is produced with. In specific cases, c. f. ETA-12/0373 (2012), the varying denotations for type (I), such as single-, double- or coarse-thread, have been found. Despite of different values for p (and consequently differences regarding the speed of screw insertion as well as in the size of the insertion moment), no geometrical variations between these types can be observed. The only exception is illustrated as type (III) and denoted as “HiLo”-thread (high-low), which can be defined as a double-start screw thread with two alternating parameter sets of p , d_c and v . While these parameters remain (alternately) constant for both thread types (I) and (III), thread type (II) is produced with a variable pitch as function of x , given in Figure 3.5. This geometry, currently declared in ETA-11/0452 (2011), has been developed in order to pre-stress the wood, when inserting the screw, c. f. section 2-4.5.3, Steilner and Blaß (2010) and Steilner (2014) respectively. Further geometrical thread modifications, such as ground serrations or cutting edges, not given in Figure 3.5, are of minor relevance in case of loading and thus not discussed in detail.

The form of ideal screw threads (ignoring process based intolerances) can generally be described by helicoids as functions of p , d , d_c and v thus influencing the cross-sectional dependent product properties, such as the screw's tensile and torsional capacity, as well as its yield moment in a major way. Findings made in this field are discussed in section 3-4, while a possible influence of thread characteristics on screw withdrawal properties is part of section 5-2.

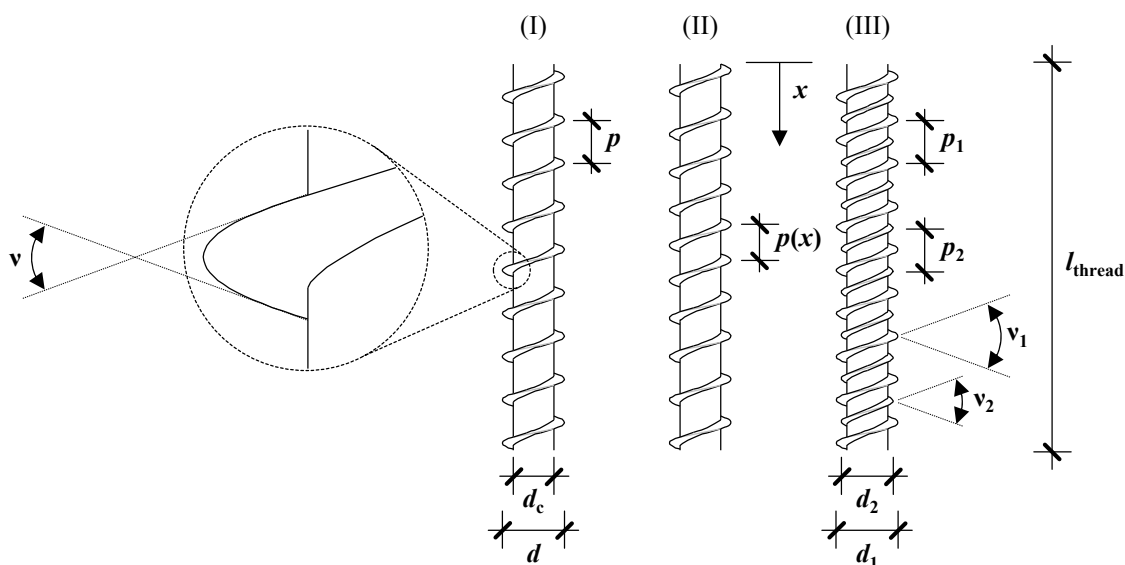


Figure 3.5: Classification and geometrical parameters of screw threads

3-2.5 Screw tip characteristics

With regard to screw tips, again a huge variety of corresponding geometries can be found in currently valid ETAs. One possibility of classifying them is shown in Figure 3.6. Therein, the screw tips are grouped into threaded and non-threaded ones. In the latter case, a differentiation is made between drill tips and cut tips, while threaded tips are subdivided into full and partial tips (tips with notches, half tips, etc.). In special cases, see e. g. ETA-12/0373 (2012), drill tips are also produced with threads. Furthermore, threaded tip geometries are frequently modified in form of additional mating threads, rips, compactors or cutters.

The exclusive function of screw tips is to place the screw on the timber member's surface. The aforementioned development of different tip geometries and their modifications are to increase the precision of screw placement and the velocity of screw insertion (due to a fast bite), as well as to decrease the insertion moment. With regard to the load situation, only the tip length, herein denoted as l_{tip} , can be defined as relevant parameter decreasing the effective thread length being responsible for load transmission, c. f. section 5-4.

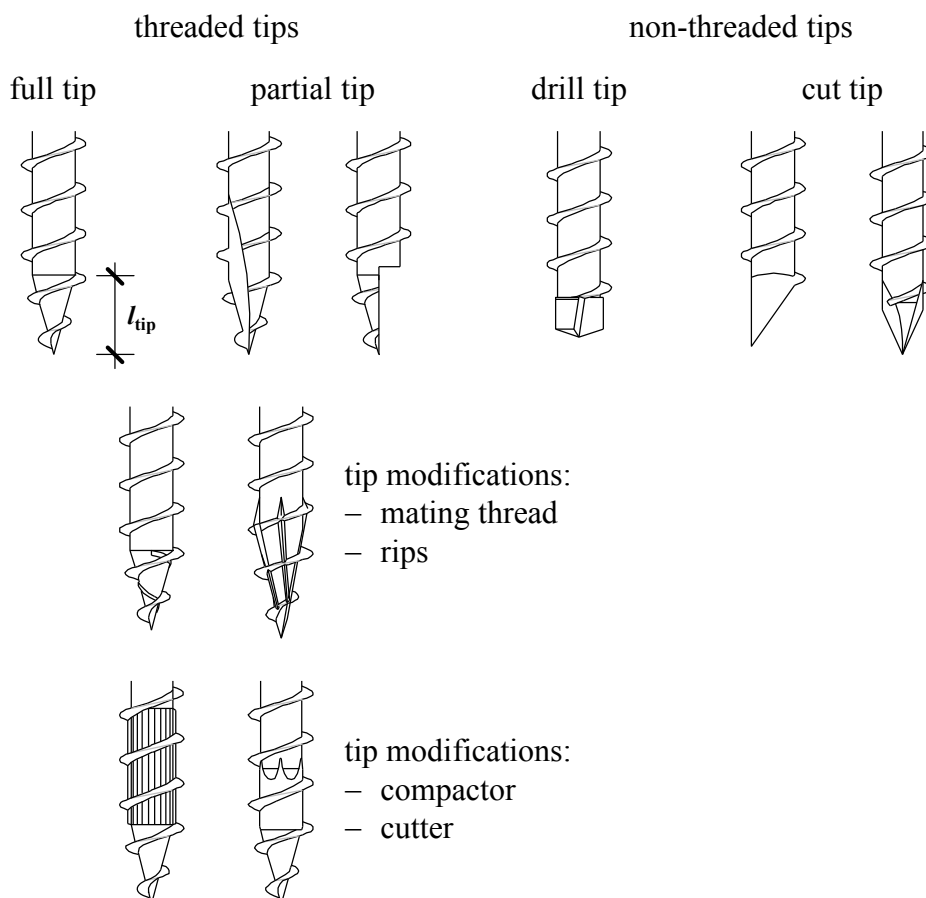


Figure 3.6: Classification and geometrical parameters of screw tips

3-2.6 Summary of geometrical screw characteristics

Within sections 3-2.1 to 3-2.5 the geometrical characteristics defining the five screw components “drive”, “head”, “shank”, “thread” and “tip” have been explained and discussed. Table 3.1 summarises the 11 main geometrical parameters of modern self-tapping timber screws. Furthermore, their influence on steel and timber properties in case of axial loading is evaluated, which can be seen as a preview of the corresponding sections 3-4, 5-2 and 5-4.

Table 3.1: *Overview of main geometrical screw parameters and their influence on steel and timber mechanical properties in case of axial loading*

component	geometrical parameters	influence on mechanical properties*	
		steel	timber
drive	wrench size	none	none
head	head diameter d_{head}	none	significant**
	heights of the head h_i	none	minor**
	head inclination angle ϑ	none	significant**
shank	shank length l_{sh}	significant	none
	shank diameter d_{sh}	significant	none
thread	outer thread diameter d	significant	significant
	inner thread diameter d_c	significant	minor
	pitch p	significant	minor
	flank inclination angle ν	significant	minor
	thread length l_{thread}	none	significant
tip	tip length l_{tip}	none	significant

* considering each currently produced parameter bandwidth, c. f. Pöll (2017)

** assumed but not treated in this thesis

3-3 PRODUCTION PROCESS OF SELF-TAPPING SCREWS

In order to obtain a deeper understanding concerning the product itself and its mechanical properties, significantly influenced by production-specific parameters, this section comprises a summarised description of modern self-tapping timber screws' production process. The main production steps discussed in subsections 3-3.1 to 3-3.5 are defined as follows:

- properties and pre-treatment of raw material
- forming the screw geometry
- screw hardening process
- adding protective coats
- final treatment

Worth mentioning, that the description is exemplarily for hardened carbon steel screws with rolled threads as majorly applied in practise.

3-3.1 Properties and pre-treatment of raw material

Since the (thread) geometry of self-tapping screws is a result of cold forming, steel wire rods, the applied raw material for screw production, should have suitable material properties for this process. Therefore the frequently used steel grades are denoted as “cold extrusion steels” and correspond to the declarations given in ON EN 10263-4 (2002). In general, they are low alloy carbon steels (base steels) with certain requirements concerning chemical composition, mechanical properties and post-processing. In Table 3.2 the alloying constituents for a sample of steel grade 1.5525 – 20MnB4 (applied for screw production by a specific manufacturer), determined by means of a heat analysis, are exemplarily given.

Table 3.2: *Alloying constituents and their contents for a sample of 1.5525, acc. to Koiner (2012);
in brackets: maximum values of alloying contents for 1.5525, acc. to ON EN 10263-4 (2002)*

const.	C	Si	Mn	P	S	Cr	Ni	Cu	Al
[%]	0.216 (0.230)	0.013 (0.300)	0.934 (1.200)	0.009 (0.030)	0.005 (0.030)	0.180 (0.300)	0.015	0.018 (0.250)	0.048
const.	Ti	Mo	V	W	Sn	B	N	Nb	O
[%]	0.052	0.006	0.006	0.000	0.002	0.004 (0.005)	0.006	0.000	-
const.	As	Sb	Zr	Pb	Co	Ca	Ta	H [ppm]	
[%]	0.003	0.000	-	0.000	0.003	0.003	0.000	0.000	

With regard to mechanical properties of the raw material, ON EN 10263-4 (2002) restricts the steel tensile strength f_t of steel 1.5525 to $\leq 680 \text{ N/mm}^2$ and Z , defined as its percentage reduction of area after fracture, to $\geq 55 \%$. Both properties were also determined by Koiner (2012) for this sample and are 551 N/mm^2 and 65.7% respectively, fulfilling the aforementioned requirements. According to www.metallograf.de (2015), further boundary conditions, concerning the post-processing of steel products made of raw material comparable to 1.5525, are as follows:

- steel hardening: $820 \div 860 \text{ }^\circ\text{C}$ (in oil or water)
- soft annealing: $650 \div 700 \text{ }^\circ\text{C}$
- normalising: $850 \div 880 \text{ }^\circ\text{C}$

Now focusing on the pre-treatment measurements of the raw material defined as a process part until forming the screw geometry: in a first step, wire rods delivered as coils with certain rod diameters d_{rod} are pickled (in acids or bases, under power) removing possible oxide (result of hot rolling the rods) and rust layers (result of outdoor storage). Thereby caused hydrogen depositions, disadvantageously in regard to HISCC, can be calcined by subsequently conducted recrystallization annealing, c. f. Toblier (2014). In a second step, steel wires are mechanically drawn (with drawing dies and paste) in order to reach a rod diameter suitable for the screw production. As already mentioned in section 3-2.3, the corresponding target values are in-between the outer and inner screw thread diameter. For instance, typical screw thread geometries with $d = 8 \text{ mm}$ are produced with $d_{\text{rod,fin}} = 5.80 \text{ mm}$. In order to increase the material's formability, which is in fact reduced by drawing, steel rods are subsequently stress-relief annealed (at roughly $650 \text{ }^\circ\text{C}$) before the screw geometry gets formed.

3-3.2 Forming the screw geometry

The (cold-)forming process of screw geometries is commonly carried out in two steps: first, the wire rods, cut with a defined length, are clamped at one end in order to stamp the screw head on the other end. As shown in Figure 3.7 (right), specific negative forms are therefore applied, already including the planned geometrical modifications (friction ribs, different head inclinations, etc.), as well as the screw drive. In a second step, thread and tip geometry are rolled on the steel rods. For this specific purpose, special rolling facilities have been developed. Worth mentioning, that these tools were produced as robust steels with roughly 700 HV with a three-dimensional surface and can be regarded as core components of the screw manufacture process. Thereby, "HV" stands for "hardness according to Vickers", see Smith and Sandland (1922). In order to enable the production of roughly $1.0 \div 1.5$ millions of screws by one tool set, without exceeding the geometrical tolerances declared in corresponding ETAs, their moulding process is quite complex, also time consuming and requires experience of the producer. In dependence of the aimed thread length, different kinds of rolling facilities are applied. Short threads with l_{thread} up to roughly

300 mm are formed by flat die rollers, while in case of bigger lengths a short section (including the screw tip if realisable) is again formed by this method serving as a start geometry for thread die rollers finishing this process. Specific tip geometries, which are not realisable by rolling (see section 3-2.5), are fabricated in an additional and final forming step.

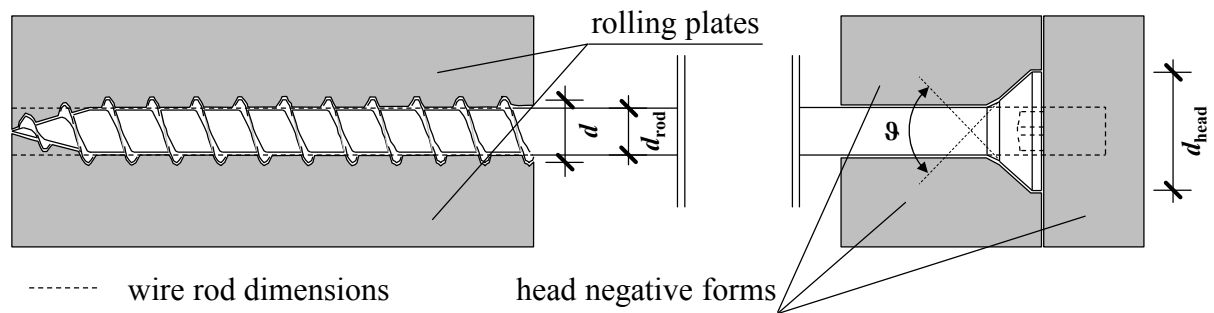


Figure 3.7: Forming the screw geometry; left: rolling the thread; right: stamping the head

With regard to mechanical properties of rolled screws, the cold-forming of the thread, tip and head geometry commonly leads to an increase of steel hardness (and thus strength), while viscosity and formability decrease. One reason is the impounding of crystalline dislocations at structural barriers (e. g. grain boundaries) as a consequence of the plastic material deformation, c. f. Maydl and Tritthart (2006). Nevertheless, the hardness of rolled screws (before hardening) barely exceeds 300 HV (see section 3-4.5) and is thus significantly lower than that of the forming tools.

3-3.3 Screw hardening process

After cold-forming the specific geometry, screws are hardened, which increases their tensile and torsional resistance by far. It is a core production process (besides forming), influencing screw steel properties in a major way, see also section 3-5.2. According to Maydl and Tritthart (2006) the hardening of steel products generally comprises four phases (see also Figure 3.8): First, the material is warmed up to roughly 900 °C, which is above the so-called “GSK”-line, separating the crystalline state of iron in the iron-carbon diagram between austenite (γ -iron, above GSK) and ferrite (α -iron) or mixed forms (both below GSK). In the second phase, the warmed material stays under constant temperature for a certain period of time, until complete austenitising occurs (all crystals are now γ -iron). This procedure is followed by an immediate cooling-down phase below 300 °C (transformation of γ - to α -iron, from austenite to martensite), realised by quenching the material in water or oil. Thereby, the carbon atoms are not able to diffuse out fast enough. Consequently, both, a carbon and an iron atom, exist in the centre of the cubic crystal lattice. This leads to inner lattice stress and thus to increased hardness, strength and also brittleness. The final (and optional) phase is denoted as “tempering”, in which the material is again warmed up to roughly 300 °C, reversing negative but also positive effects of hardening to some extent.

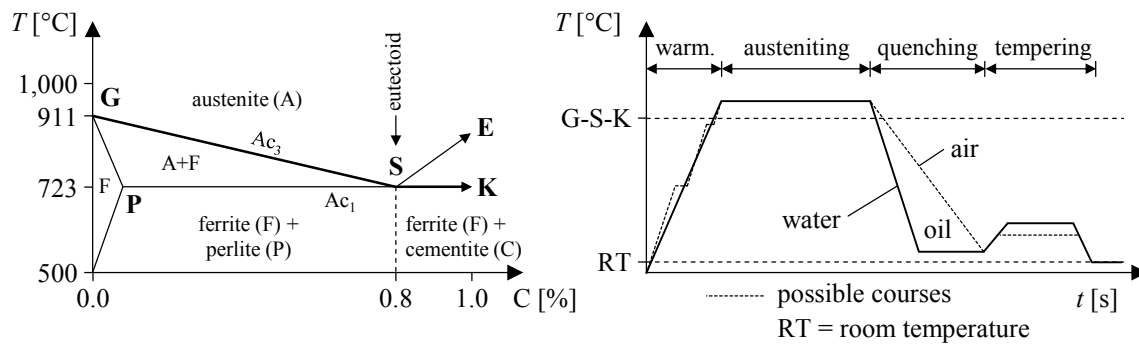


Figure 3.8: Left: extract of the iron-carbon diagram, including the G-S-K line; right: four phases of hardening in the temperature-time diagram; according to Weißbach (2012)

Concentrating on the screw production, hardening is commonly realised in continuous furnaces enabling continuous heat treatment in an inert gas atmosphere (denoted as “inert gas hardening”). The level of temperature thereby mainly depends on the requirements concerning the steel raw material. As mentioned in section 3-3.1, steel 1.5524 requires hardening at $820 \div 860 \text{ }^\circ\text{C}$ for instance. While both, austenitising time and quenching speed, base on experience and thus vary between different manufacturers, oil (instead of water) as a hardening substrate for the latter procedure is commonly used with temperatures below $100 \text{ }^\circ\text{C}$. In Figure 3.9, a time-temperature-diagram (TTD) of steel type 17B2 is given. This type is quite similar to 20MnB4 and also applied for screw production. The different illustrated curves represent the loss of temperature per time. In dependence of this quenching speed, different steel compositions (martensitic or bainite), hardness and consequently strength result and indicate the relevance of this production step on screw product properties.

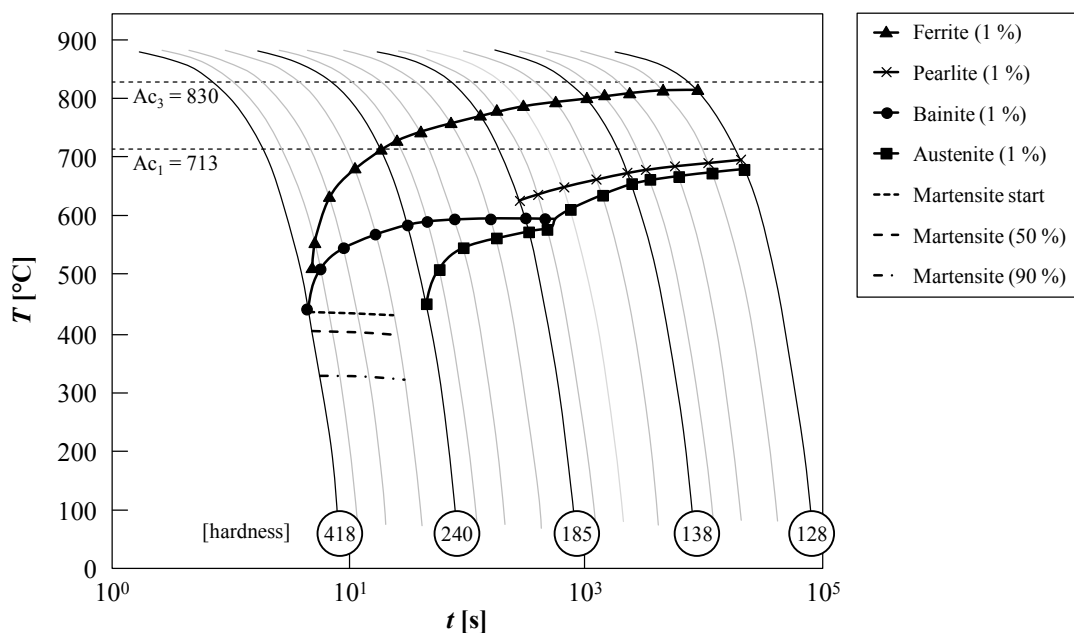


Figure 3.9: Example of a TTD for steel type 17B2; determined with JMatPro (2016)

In order to increase the torsional resistance of the screw, the so-called process of “carbonitriding” can be additionally applied. This procedure takes place at high temperatures (similar to conventional hardening) whereby the screw’s surface gets additionally enriched by carbon, which increases the mechanical properties (hardness, strength) of this outer thread zone. A quantitative evaluation of the corresponding impact is discussed in section 3-5.2.

3-3.4 Adding protective coats

In addition to geometrical forming and hardening, screws have to be subsequently protected against the environmental exposures for preserving durability over service life, as a basic requirement defined in ON EN 1990 (2013). The main reason for this measure is electrochemical corrosion, possibly impairing the functionality of a metallic material as a consequence of its reaction with the environment. With regard to self-tapping screws, the protection against corrosion is commonly realised by (a) metallurgical modification and (b) adding of a protective coat.

Case (a) corresponds to stainless steels with a certain composition of alloying constituents, especially chrome with mass content $\geq 12\%$, according to Maydl and Tritthart (2006) (defined as “parting limit”) and carbon with mass content $\leq 1.2\%$, according to Gläser et al. (2013), forming a passive oxide layer on the surface, which serves as a protective zone. Stainless steels, applied for screw production, correspond to groups 40 ÷ 49 according to ON EN 10088-1 (2005) and can be classified into martensitic, ferritic and austenitic steels (or mixed forms) with varying chrome, carbon and nickel contents and thus a varying performance regarding corrosion protection. With regard to currently valid ETAs related to self-tapping screws, most frequently used stainless steels are 1.4006 (martensitic), as well as 1.4401, 1.4567 and 1.4578 (all austenitic).

Case (b) is applied for carbon steel screws with insufficient corrosion protection by the raw material. As shown in Figure 3.10, a huge variety of different coatings, classified into metallic, non-metallic and organic ones, is therefore applied for screw production. Nevertheless, the vast majority is currently made with electro-galvanised zinc coatings. After the galvanisation, the screws are chromated/passivated by chromic acids (chromic oxides or chromic trioxides; defined as non-metallic coatings, see Figure 3.10) to achieve an additional protection.

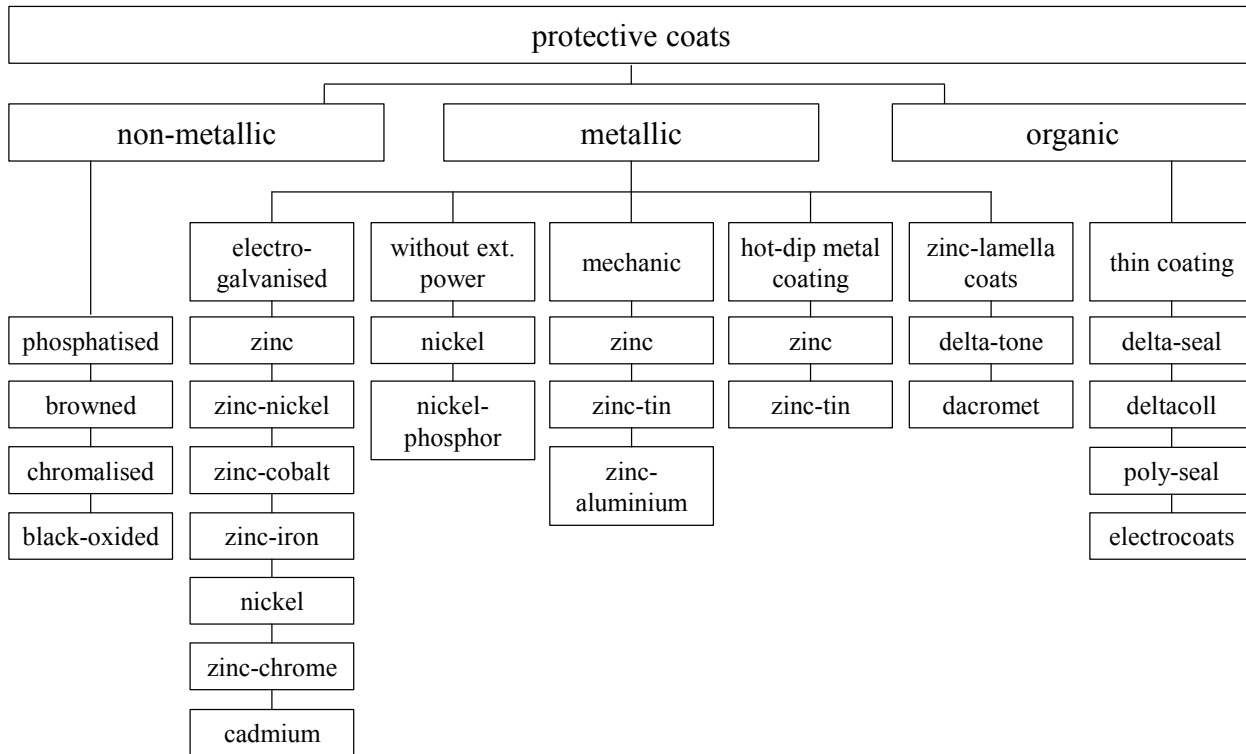


Figure 3.10: Overview and classification of protective coats applied for screw production; according to ABC-Verbindungsmitel (2008)

According to DIN 50962 (2013), process groups A, C and F have to be distinguished, indicating their colour (A = transparent to blue; C = yellow, red or olive to blue-green; F = black) as well as their efficiency (in alphabetic order). Currently, groups A and C are predominately applied for self-tapping screws, comprising blue and yellow chromates. The related coating thicknesses vary between 3 and 16 μm with 5.6 μm in average. In addition, zinc-nickel and zinc-lamella coatings with thicknesses between 4 ÷ 12 μm (6.3 μm in average) and 5 ÷ 20 μm (11.6 μm in average) are also frequently applied. In cases where carbon steel screws are used in climates with more harmful environmental exposures, hot-dip metal coatings with thicknesses of about 50 μm can be applied. Worth mentioning, an upper limit of coating thickness is given by the screw geometry, especially regarding its thread (problem with insertion and withdrawal) and drive (problem with fitting accuracy of the screw bit). In order to verify the aforementioned bandwidths of coating thickness, determined on the basis of currently valid ETAs, two fully threaded self-tapping screws with $d = 8 \text{ mm}$, $l_{\text{screw}} = 240 \text{ mm}$ and different coatings (yellow chromated, zinc-nickel) have been analysed by the Institute of Material Science, Joining and Forming at Graz University of Technology. The considered product corresponds to group A_s_II_08_240 as a part of the experimental campaign discussed in section 3-4.4.

Figure 3.11 consequently shows the distribution of coating thickness for both specimens along their threads, measured at cut cross-sections (three measurements per cross-section), exemplarily given in

Figure 3.12. In fact, both yellow chromated and zinc-nickel coating thicknesses result to 16 and 10 μm in average, and are thus closely located to the aforementioned upper limit found in ETAs. Furthermore, they significantly exceed the minimum thicknesses of 5 and 4 μm , declared in the specific manufacturer's assessment. With regard to their distribution along the thread, minima are found at the thread's centre, which may be caused by the galvanisation process leading to a coating concentration at both screw ends.

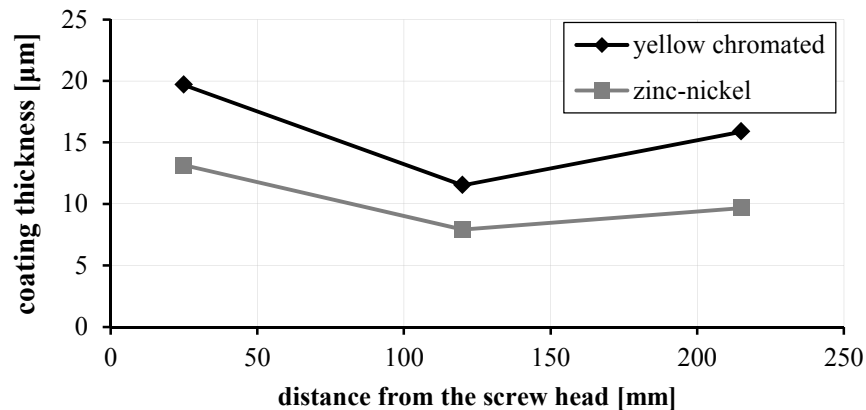


Figure 3.11: Distribution of coating thickness along the screw thread for varying protective measures; according to Toblier (2016)

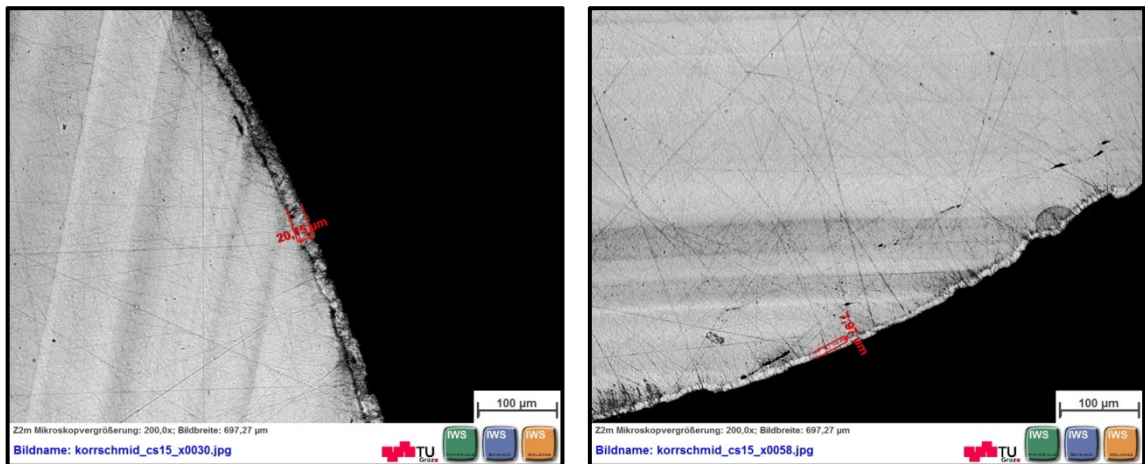


Figure 3.12: Micrographs of two cut screw thread cross-sections for determination of coating thickness

Since the electro-galvanisation discharges hydrogen (H) in the frame of the cathodic reaction, see Macherauch and Zoch (2011) and section 3-5.2, additional tempering at $T \approx 200$ $^{\circ}\text{C}$, applied before passivating according to DIN 50962 (2013), may calcine H-depositions and thus decrease the vulnerability of HISCC.

3-3.5 Final treatment

Within the final production step, the screws are mantled with an additional slide coating, decreasing their surface friction coefficient and thus their insertion moment. Nowadays, slide coatings commonly consist of water-based lubricants in form of high-molecular polymer compounds; see e. g. Fuchs Lubritech GMBH (n.d.).

3-4 GEOMETRICAL AND MECHANICAL PROPERTIES OF SELF-TAPPING SCREWS

3-4.1 Motivation

Nowadays, ETAs related to self-tapping screws declare mechanical properties, being necessary for design and application in form of their steel tensile strength f_{tens} (in [N]), their yield moment M_y (in [Nm]), as well as their torsional strength f_{tor} (in [Nm]). Presupposing ideal conditions, steel and therewith manufactured products, such as self-tapping timber screws, can be assumed as isotropic materials with an elastic-plastic stress-strain relationship, enabling the theoretical determination of all different design parameters (with a satisfying accuracy) through this mechanical constitution. Nevertheless, each of all aforementioned properties is experimentally determined on the basis of the test procedures specifically developed for the varying purpose, c. f. ON EN 14592 (2012), CUAP 06.03/08 (2010) or EAD 130118-00-0603 (2016) nowadays. The possible reasons, disabling their theoretical determination, are a certain complexity in terms of geometry, which especially concerns the threaded part of the screw, as well as material inhomogeneity, e. g. caused by thread rolling or screw hardening.

The prevalent aim of section 3-4 is to evaluate the possibility of a consistent theoretical description of the aforementioned design properties for the threaded part of the screw as a geometry deviating from an ideal cylinder. Thereby, the relationships between the product's yield and tensile strength with its tensile and torsional capacity, as well as its yield moment are derived and consequently compared with the results of specific test series and numerical simulations. The latter method is frequently used for analysing the loadbearing behaviour of timber engineered structures. A high sophisticated nonlinear modelling thereby demands stress-strain-relationships of all components applied in calculation and also includes those of self-tapping screws. A certain lack of knowledge, regarding the interrelationship between the screw thread's steel tensile and yield capacity, defined as f_{tens} and F_y , and their corresponding strengths f_u and f_y , currently disables an accurate derivation of the product's stress-strain-relationship by experimentally determined force-deformation diagrams. One possible approach how to increase the related predictability is part of section 3-4.

Subsequently, sections 3-4.2 and 3-4.3 comprise the mathematical description of the three-dimensional screw surface, as well as the determination of cross-sectional properties – both are necessary for the mechanical considerations, finally given in section 3-4.5. A comprehensive experimental programme for the verification of the corresponding theoretical assumptions is presented in section 3-4.4.

3-4.2 Mathematical description of the screw 3D surface

With regard to the mathematical description of a screw thread profile, examinations focusing on the profile of self-tapping timber screws are rare. The basic considerations, given in Hübner (2013a), are thus worth to be outlined. Therein, motivated by observations on screw threads cut perpendicular to the screw axis, Hübner (2013a) assumes the occurring cross-section as a combination of an inner circle (with $r_c = d_c / 2$) and an ellipse, the latter representing the thread's chamfer. Subsequently, Hübner (2013a) derived closed-form solutions for main cross-sectional properties, such as the cross-sectional area A_s and both moments of inertia I_y and I_z in dependence of the geometrical parameters d , d_c , p and v , as already introduced in section 3-2.4.

In contrast to Hübner (2013a), wherein this cut surface is approximated by suitable mathematical functions, own considerations aim on deriving the three-dimensional thread profile as a closed-form solution. Worth mentioning, a comparable approach has been derived by Rammer and Zelinka (2008) for analytically determining the surface area of threaded fasteners, applied for an optical determination of the corrosion rates, c. f. Rammer and Zelinka (2011).

As shown in Figure 3.13, the combination of two mathematical functions, namely a cone surface and a helicoid function, as already mentioned in section 3-2.4, is therefore applied.

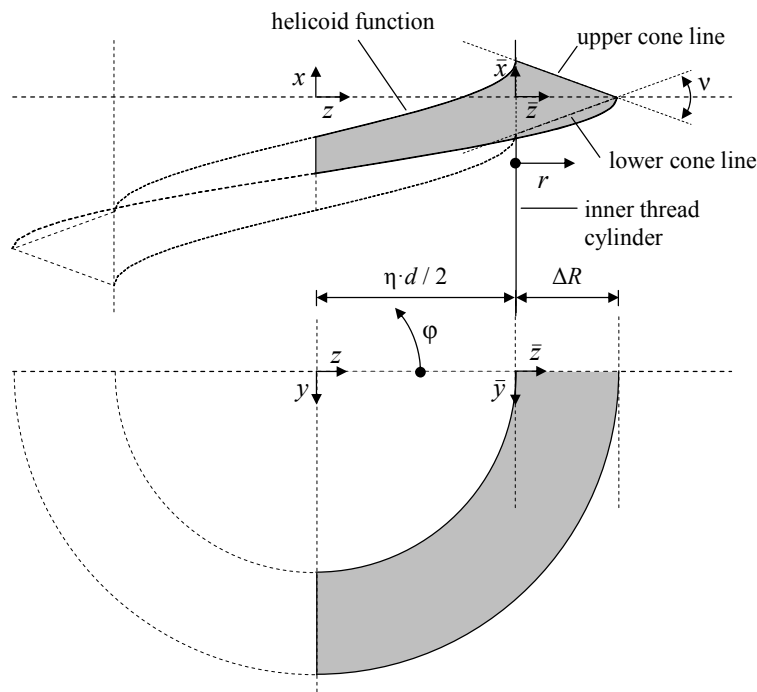


Figure 3.13: Illustration of mathematical functions describing the three-dimensional screw thread profile

Similar to Hübner (2013a), the parameters used for description are d , p , $\psi = v / 2$ and η , the latter defined as the ratio between the screw's inner and outer thread diameter, see eq. (3.1):

$$\eta = \frac{d_c}{d}. \quad (3.1)$$

The cone surface function is consequently expressed by the polar coordinates r and φ , applied in a local coordinate system defined by \bar{x} , \bar{y} and \bar{z} , see Figure 3.13. The upper (1) and lower (2) cone surface lines result as follows:

$$\begin{bmatrix} \bar{x}_1 \\ \bar{y}_1 \\ \bar{z}_1 \end{bmatrix} = \begin{bmatrix} [d \cdot (1 - \eta) / 2 - r] \cdot \tan \psi \\ -r \cdot \sin \varphi \\ r \cdot \cos \varphi \end{bmatrix} \text{ and } \begin{bmatrix} \bar{x}_2 \\ \bar{y}_2 \\ \bar{z}_2 \end{bmatrix} = \begin{bmatrix} -\bar{x}_1 \\ \bar{y}_1 \\ \bar{z}_1 \end{bmatrix}, \quad (3.2)$$

with

$$\bar{x}_1 = \Delta R \cdot \tan \psi - r \cdot \tan \psi = (\Delta R - r) \cdot \tan \psi = \left[\frac{d \cdot (1 - \eta)}{2} - r \right] \cdot \tan \psi, \quad (3.3)$$

$$\bar{x}_2 = -\Delta R \cdot \tan \psi + r \cdot \tan \psi = (r - \Delta R) \cdot \tan \psi = \left[r - \frac{d \cdot (1 - \eta)}{2} \right] \cdot \tan \psi, \quad (3.4)$$

and

$$\Delta R = \frac{d - d_c}{2} = \frac{d - \eta \cdot d}{2} = \frac{d \cdot (1 - \eta)}{2}, \quad (3.5)$$

with ΔR as the difference between inner r_c and outer thread radius $r \rightarrow d / 2$. The helicoid function as the transition curve between thread and inner thread cylinder can be described by

$$\begin{bmatrix} x \\ y \\ z \end{bmatrix} = \begin{bmatrix} p \cdot \varphi / (2\pi) \\ -r_c \cdot \sin \varphi \\ r_c \cdot \cos \varphi \end{bmatrix} = \begin{bmatrix} p \cdot \varphi / (2\pi) \\ -\eta \cdot d / 2 \cdot \sin \varphi \\ \eta \cdot d / 2 \cdot \cos \varphi \end{bmatrix}. \quad (3.6)$$

Consequently, the upper (1) and lower (2) thread surface function results by adding eq. (3.2) to eq. (3.6):

$$\begin{bmatrix} x_1 \\ y_1 \\ z_1 \end{bmatrix} = \begin{bmatrix} [d \cdot (1 - \eta) / 2 - r] \cdot \tan \psi \\ -r \cdot \sin \varphi \\ r \cdot \cos \varphi \end{bmatrix} + \begin{bmatrix} p \cdot \varphi / (2\pi) \\ -\eta \cdot d / 2 \cdot \sin \varphi \\ \eta \cdot d / 2 \cdot \cos \varphi \end{bmatrix}, \quad (3.7)$$

and

$$\begin{bmatrix} x_2 \\ y_2 \\ z_2 \end{bmatrix} = \begin{bmatrix} [r - d \cdot (1 - \eta) / 2] \cdot \tan \psi \\ -r \cdot \sin \varphi \\ r \cdot \cos \varphi \end{bmatrix} + \begin{bmatrix} p \cdot \varphi / (2\pi) \\ -\eta \cdot d / 2 \cdot \sin \varphi \\ \eta \cdot d / 2 \cdot \cos \varphi \end{bmatrix}. \quad (3.8)$$

Figure 3.14 shows one example of a screw thread profile, exemplarily determined with eq. (3.7) and (3.8) for a parameter set of $\{d, p, v, \eta\} = \{8.0 \text{ mm}, 3.8 \text{ mm}, 40^\circ, 0.65\}$. The inner (3) and outer (4) thread cylinder surfaces were thereby considered according to eq. (3.9), see

$$\begin{bmatrix} x_3 \\ y_3 \\ z_3 \end{bmatrix} = \begin{bmatrix} x \\ -\eta \cdot d / 2 \cdot \sin \varphi \\ \eta \cdot d / 2 \cdot \cos \varphi \end{bmatrix} \text{ and } \begin{bmatrix} x_4 \\ y_4 \\ z_4 \end{bmatrix} = \begin{bmatrix} x \\ -d / 2 \cdot \sin \varphi \\ d / 2 \cdot \cos \varphi \end{bmatrix}. \quad (3.9)$$

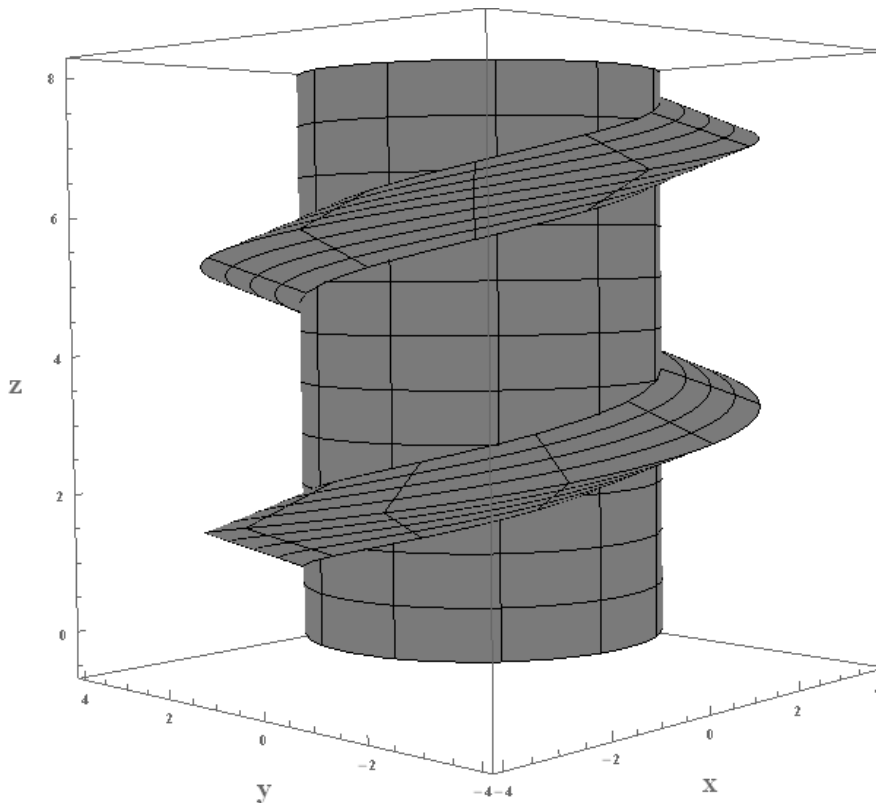


Figure 3.14: 3D illustration of an exemplarily determined screw thread profile

Describing the screw's cross-sectional shape, the three-dimensional functions given in eq. (3.7) and (3.8) are subsequently converted into two-dimensional ones. Thereby, x serves for the expression of r , gained section curves (upper = 1, lower = 2) are expressed in eq. (3.11):

$$r_{1,2} = \frac{d \cdot (1 - \eta)}{2} \mp \left(x - \frac{p \cdot \varphi}{2\pi} \right) \cdot \frac{1}{\tan \psi}, \quad (3.10)$$

and

$$\begin{bmatrix} y_{1,2} \\ z_{1,2} \end{bmatrix} = \begin{bmatrix} -\chi_{1,2} \cdot \sin \varphi \\ \chi_{1,2} \cdot \cos \varphi \end{bmatrix}, \text{ with } \chi_{1,2} = \frac{d}{2} \pm \left(\frac{p \cdot \varphi}{2\pi} - x \right) \cdot \frac{1}{\tan \psi}. \quad (3.11)$$

Consequently, the intersections (as functions of φ and x) between curves (1) and (2) with (3) and (4) are derived (equalising eq. (3.9) and (3.11)). Worth mentioning, these boundaries are the basis of further considerations given in section 3-4.3.

Intersection between upper and lower section curve (1, 2) and inner thread cylinder (3):

$$\begin{bmatrix} y_{1,2} \\ z_{1,2} \end{bmatrix} = \begin{bmatrix} y_3 \\ z_3 \end{bmatrix} \rightarrow \begin{bmatrix} -\chi_{1,2} \cdot \sin \varphi \\ \chi_{1,2} \cdot \cos \varphi \end{bmatrix} = \begin{bmatrix} -\frac{d \cdot \eta}{2} \cdot \sin \varphi \\ \frac{d \cdot \eta}{2} \cdot \cos \varphi \end{bmatrix}, \quad (3.12)$$

$$\varphi_{1,2} = \omega \cdot \pi \text{ and } \omega = \left[x \mp \frac{d}{2} \cdot (1 - \eta) \cdot \tan \psi \right] \cdot \frac{2}{p}. \quad (3.13)$$

Intersection between upper and lower section curve (1, 2) and outer thread cylinder (4):

$$\begin{bmatrix} y_{1,2} \\ z_{1,2} \end{bmatrix} = \begin{bmatrix} y_4 \\ z_4 \end{bmatrix} \rightarrow \begin{bmatrix} -\chi_{1,2} \cdot \sin \varphi \\ \chi_{1,2} \cdot \cos \varphi \end{bmatrix} = \begin{bmatrix} -\frac{d}{2} \cdot \sin \varphi \\ \frac{d}{2} \cdot \cos \varphi \end{bmatrix}, \text{ and} \quad (3.14)$$

$$\varphi_{1,2} = \frac{2\pi}{p} \cdot x. \quad (3.15)$$

Finally, Figure 3.15 shows one example of a screw cross-section exemplarily determined for the same parameter set as applied before ($\{d, p, \nu, \eta\} = \{8.0 \text{ mm}, 3.8 \text{ mm}, 40^\circ, 0.65\}$) and $x = p/2$. Thereby, the intersection angles φ given in eq. (3.13) and (3.15) result to:

$$(1,2) \text{ and } (3): \varphi_{1,2} = \left[\frac{3.8}{2} \mp \frac{8}{2} \cdot (1 - 0.65) \cdot \tan 20 \right] \cdot \frac{2\pi}{3.8} = [1 \mp 0.268] \pi = \{131.7, 228.3\}^\circ, \text{ and} \quad (3.16)$$

$$(1,2) \text{ and } (4): \varphi_{1,2} = \pi = 180^\circ. \quad (3.17)$$

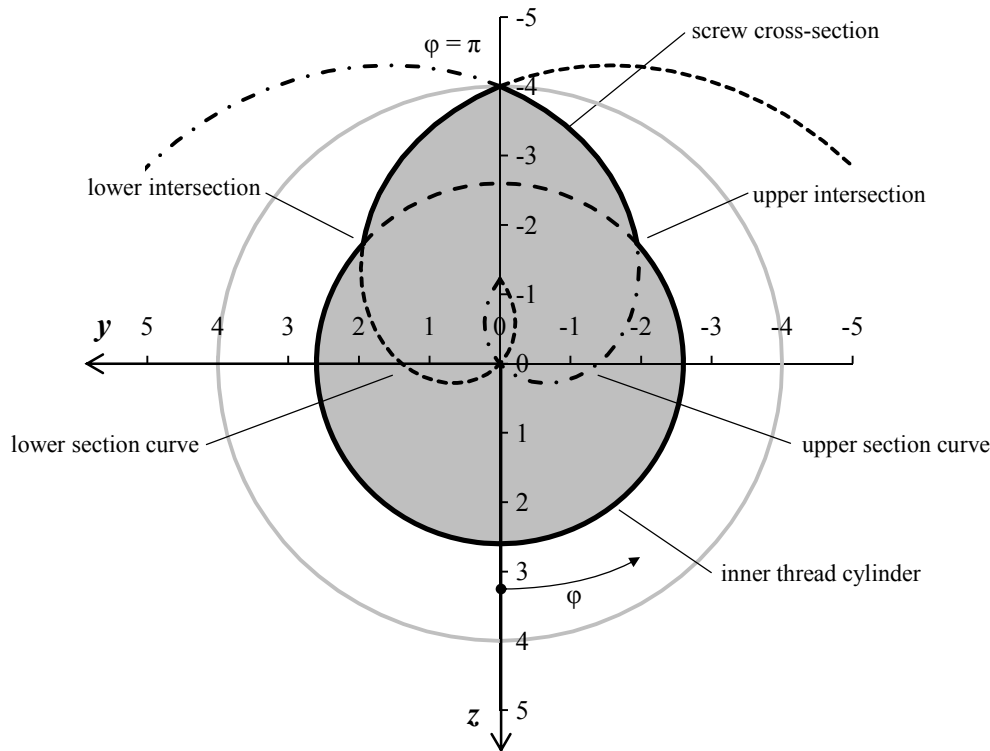


Figure 3.15: Cross-sectional shape of an example screw's threaded part at $x = p / 2$

3-4.3 Cross-sectional screw properties

3-4.3.1 Cross-sectional area

The first focus is on the determination of the screw's threaded part's cross-sectional area A_s . As shown in Figure 3.15, this can be realised by summing up the inner thread cylinder's area A_{dc} and that of the thread's chamfer $A_{1,2}$, defined by the upper and lower section curves, given in eq. (3.11). Since A_s stays constant along the screw axis, $x = p / 2$ is applied for determination. For reasons of symmetry, only one section curve has to be considered:

$$A_s = 2 \cdot (A_2 + A_{dc}) = 2 \cdot \left(\int_{\omega-\pi}^{\pi} \text{section curve} + \int_0^{\omega-\pi} \text{cylinder} \right). \quad (3.18)$$

Applying polar coordinates, the area under a function in form of $r = f(\varphi)$ can be determined according to eq. (3.19), see

$$A = \int_{\varphi_1}^{\varphi_2} \int_0^{r(\varphi)} r \, dr \, d\varphi = \int_{\varphi_1}^{\varphi_2} \frac{1}{2} [r(\varphi)]^2 \, d\varphi, \quad (3.19)$$

Following eq. (3.19), A_2 is determined considering $r(\varphi) = \chi(\varphi)$ according to eq. (3.11), see

$$A_2 = \int_{\omega-\pi}^{\pi} \int_0^{\chi(\varphi)} \chi d\chi d\varphi = \int_{\omega-\pi}^{\pi} \frac{1}{2} [\chi(\varphi)]^2 d\varphi = \int_{\omega-\pi}^{\pi} \frac{1}{2} \left[\frac{d}{2} + \left(\frac{p \cdot \varphi}{2\pi} - \frac{p}{2} \right) \cdot \frac{1}{\tan \psi} \right]^2 d\varphi, \quad (3.20)$$

$$A_2 = \frac{\pi \cdot \tan \psi}{24 \cdot p} \cdot \left[d^3 - (d + (\omega - 1) \cdot p \cdot \cot \psi)^3 \right]. \quad (3.21)$$

The same procedure is also applied for deriving A_{dc} :

$$A_{dc} = \int_0^{\omega \cdot \pi} \frac{1}{2} \left[\frac{\eta \cdot d}{2} \right]^2 d\varphi = \frac{\eta^2 \cdot d^2}{8} \cdot \omega \cdot \pi. \quad (3.22)$$

The cross-sectional area A_s at $x = p/2$ can subsequently be defined by summing up eq. (3.21) and eq. (3.22):

$$A_s = 2 \cdot (A_2 + A_{dc}) = \frac{\pi \cdot \tan \psi}{12 \cdot p} \cdot \left[d^3 - (d + (\omega - 1) \cdot p \cdot \cot \psi)^3 \right] + \frac{\eta^2 \cdot d^2}{4} \cdot \omega \cdot \pi. \quad (3.23)$$

Applying the aforementioned parameter set $\{d, p, v, \eta\} = \{8.0 \text{ mm}, 3.8 \text{ mm}, 40^\circ, 0.65\}$ in eq. (3.23), A_s results to 24.9 mm^2 and is about 117 % of the inner (21.2 mm^2) and about 49 % of the outer thread cylinder's area (50.3 mm^2).

3-4.3.2 Position of gravity centre

Second, the concentration is on the position of the cross-section's gravity centre, defined by the coordinates y_s and z_s . Again, case $x = p/2$ is selected, symmetry thus leads to $y_s = 0$. Applying polar coordinates and considering $r = f(\varphi)$, $z_{s,i}$ of any cross-section's partial area can subsequently be determined as follows:

$$z_{s,i} = \frac{\int_{\varphi_1}^{\varphi_2} \int_0^{r(\varphi)} [r(\varphi)]^2 \cos \varphi dr d\varphi}{\int_{\varphi_1}^{\varphi_2} \int_0^{r(\varphi)} r(\varphi) dr d\varphi} = \frac{\int_{\varphi_1}^{\varphi_2} \frac{1}{3} [r(\varphi)]^3 \cos \varphi d\varphi}{\int_{\varphi_1}^{\varphi_2} \frac{1}{2} [r(\varphi)]^2 d\varphi}. \quad (3.24)$$

With regard to the thread's chamfer area, the related coordinate $z_{s,2}$ results by applying eq. (3.24):

$$z_{s,2} = \frac{\int_{\omega-\pi}^{\pi} \frac{1}{3} \left[\frac{d}{2} + \left(\frac{p \cdot \varphi}{2\pi} - \frac{p}{2} \right) \cdot \frac{1}{\tan \psi} \right]^3 \cdot \cos \varphi d\varphi}{\int_{\omega-\pi}^{\pi} \frac{1}{2} \left[\frac{d}{2} + \left(\frac{p \cdot \varphi}{2\pi} - \frac{p}{2} \right) \cdot \frac{1}{\tan \psi} \right]^2 d\varphi}, \quad (3.25)$$

$$z_{s,2} = \frac{-p \cdot [a + b \cdot \cos(\omega\pi) + c \cdot \sin(\omega\pi)]}{\tan \psi \cdot \pi^4 \cdot [\tan^3 \psi \cdot d^3 - (\tan \psi \cdot d + (\omega - 1) \cdot p)^3]}, \text{ with} \quad (3.26)$$

$$a = -6 \cdot p^3 + 3 \cdot \tan^2 \psi \cdot d^2 \cdot p \cdot \pi^2, \quad (3.27)$$

$$b = 3p \cdot [-2p^2 + (\tan \psi \cdot d + (\omega - 1) \cdot p)^2 \cdot \pi^2], \text{ and} \quad (3.28)$$

$$c = [\tan \psi \cdot d + (\omega - 1) \cdot p] \cdot \pi \cdot [-6 \cdot p^2 + (\tan \psi \cdot d + (\omega - 1) \cdot p)^2 \cdot \pi^2]. \quad (3.29)$$

With regard to the inner thread cylinder's area, $z_{s,dc}$ results as follows:

$$z_{s,dc} = \frac{\int_0^{\omega\pi} \frac{1}{3} \left[\frac{\eta \cdot d}{2} \right]^3 \cdot \cos \varphi \, d\varphi}{\int_0^{\omega\pi} \frac{1}{2} \left[\frac{\eta \cdot d}{2} \right]^2 \, d\varphi} = \frac{\eta \cdot d \cdot \sin(\omega\pi)}{3 \cdot \omega \cdot \pi}. \quad (3.30)$$

Finally, z_s can be determined in form of

$$z_s = \frac{\sum A_i \cdot z_{s,i}}{\sum A_i} = \frac{A_2 \cdot z_{s,2} + A_{dc} \cdot z_{s,dc}}{0.50 \cdot A_s}. \quad (3.31)$$

Applying the known parameter set $\{d, p, v, \eta\} = \{8.0 \text{ mm}, 3.8 \text{ mm}, 40^\circ, 0.65\}$ in eq. (3.31), both coordinates $\{y_s, z_s\}$ result to $\{0.00, -0.43\}$ mm. Eccentricity $e = -z_s$, defined as the absolute distance between the threaded part's and that of the inner cylinder's gravity centre is thus about 7.9 % of the inner thread radius r_c . The location of this point $\{y_s, z_s\}$ varies in dependence of x ; this again given as helicoid function in eq. (3.32), see

$$\begin{bmatrix} x \\ y \\ z \end{bmatrix} = \begin{bmatrix} p \cdot \varphi / (2\pi) \\ e \cdot \sin \varphi \\ e \cdot \cos \varphi \end{bmatrix}. \quad (3.32)$$

The aforementioned subdivision into partial areas A_{dc} and A_2 , the positions of their gravity centres as well as that of the whole cross-section of a half screw's threaded part's profile at $x = p/2$ are illustrated in Figure 3.16.

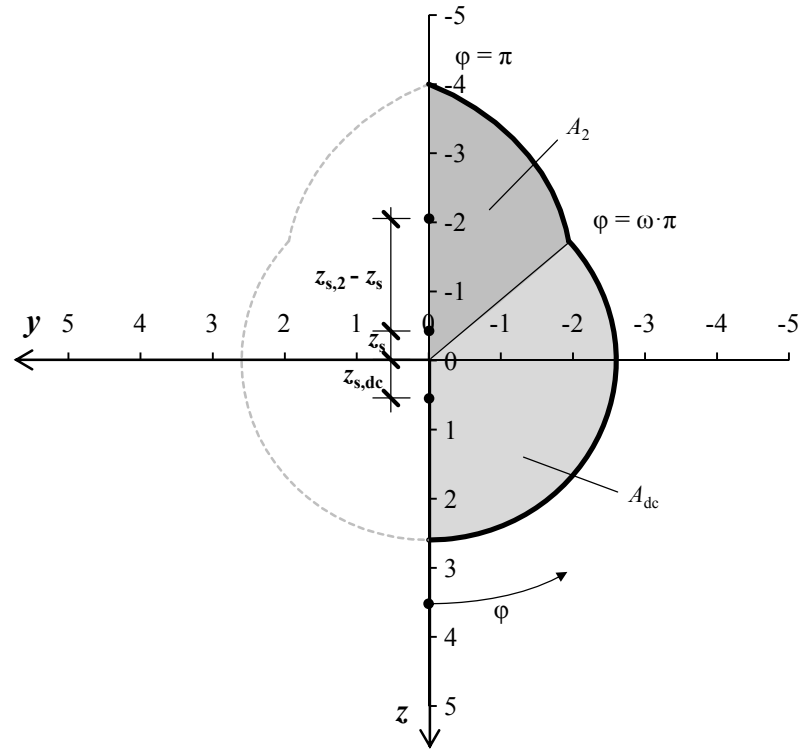


Figure 3.16: Partial areas and gravity centre positions for an example screw’s threaded part at $x = p / 2$

3-4.3.3 Moments of inertia

Subsequently, I_y an I_z , defined as the moments of inertia, are determined for the given profile. In general, both properties result by applying parallel axis theorem for combined cross-sections:

$$I_y = \sum \bar{I}_{y,i} - z_s^2 \cdot A_s \text{ and } I_z = \sum \bar{I}_{z,i} - y_s^2 \cdot A_s, \quad (3.33)$$

with $\bar{I}_{y,i}$ and $\bar{I}_{z,i}$ as the components’ moments of inertia referred to the coordinate origin illustrated in Figure 3.15. Applying polar coordinates and $r = f(\varphi)$, both $\bar{I}_{x,i}$ and $\bar{I}_{y,i}$ are generally determined as follows:

$$\bar{I}_y = \int_{\varphi_1}^{\varphi_2} \int_0^{r(\varphi)} ([r(\varphi)] \cos \varphi)^2 \cdot [r(\varphi)] dr d\varphi = \int_{\varphi_1}^{\varphi_2} \int_0^{r(\varphi)} [r(\varphi)]^3 \cos^2 \varphi dr d\varphi = \int_{\varphi_1}^{\varphi_2} \frac{1}{4} [r(\varphi)]^4 \cos^2 \varphi d\varphi, \quad (3.34)$$

and

$$\bar{I}_z = \int_{\varphi_1}^{\varphi_2} \int_0^{r(\varphi)} ([r(\varphi)] \sin \varphi)^2 \cdot [r(\varphi)] dr d\varphi = \int_{\varphi_1}^{\varphi_2} \int_0^{r(\varphi)} [r(\varphi)]^3 \sin^2 \varphi dr d\varphi = \int_{\varphi_1}^{\varphi_2} \frac{1}{4} [r(\varphi)]^4 \sin^2 \varphi d\varphi. \quad (3.35)$$

In case of the thread's chamfer $\bar{I}_{y,(1,2)}$ and $\bar{I}_{z,(1,2)}$ thus result to:

$$\bar{I}_{z,(1,2)} = \frac{-2 \cdot a + 10 \cdot b \cdot p \cdot \pi \cdot \cos(2\omega\pi) \cdot [\tan \psi \cdot d + \omega(\lambda - 1) \cdot p] + 5 \cdot c \cdot \sin(2\omega\pi)}{2560 \cdot \tan^4 \psi \cdot \pi^4}, \text{ with} \quad (3.36)$$

$$a = \begin{aligned} & 10 \cdot \tan^4 \psi \cdot d^4 \cdot (\omega - 1) \cdot \pi^5 + 20 \cdot \tan^2 \psi \cdot d^2 \cdot (\omega - 1)^3 \cdot p^2 \cdot \pi^5 + 2 \cdot (\omega - 1)^5 \cdot p^4 \cdot \pi^5 \\ & + 10 \cdot \tan^3 \psi \cdot d^3 \cdot p \cdot \pi^3 \cdot [1 + 2 \cdot (\omega - 1)^2 \cdot \pi^2] + 5 \cdot \tan \psi \cdot d \cdot p^3 \cdot \pi \cdot [-3 + 2 \cdot (\omega - 1)^4 \cdot \pi^4], \end{aligned} \quad (3.37)$$

$$b = 2 \cdot \tan^2 \psi \cdot d^2 \cdot \pi^2 + 4 \cdot \tan \psi \cdot d \cdot (\omega - 1) \cdot p \cdot \pi^2 + p^2 \cdot [-3 + 2 \cdot (\omega - 1)^2 \cdot \pi^2], \text{ and} \quad (3.38)$$

$$c = \begin{aligned} & 2 \cdot \tan^4 \psi \cdot d^4 \cdot \pi^4 + 8 \cdot \tan^3 \psi \cdot d^3 \cdot (\omega - 1) \cdot p \cdot \pi^4 \\ & + 4 \cdot \tan \psi \cdot d \cdot (\omega - 1) \cdot p^3 \cdot \pi^2 \cdot [-3 + 2 \cdot (\omega - 1)^2 \cdot \pi^2] \\ & + 6 \cdot \tan^2 \psi \cdot d^2 \cdot p^2 \cdot \pi^2 \cdot [-1 + 2 \cdot (\omega - 1)^2 \cdot \pi^2] \\ & + p^4 \cdot [3 - 6 \cdot (\omega - 1)^2 \cdot \pi^2 + 2 \cdot (\omega - 1)^4 \cdot \pi^4] \end{aligned} \quad (3.39)$$

$$\bar{I}_{y,(1,2)} = -\frac{2 \cdot a + 10 \cdot b \cdot p \cdot \pi \cdot \cos(2\omega\pi) \cdot [\tan \psi \cdot d + (\omega - 1) \cdot p] + 5 \cdot c \cdot \sin(2\omega\pi)}{2560 \cdot \tan^4 \psi \cdot \pi^4}, \text{ with} \quad (3.40)$$

$$a = \begin{aligned} & 10 \cdot \tan^4 \psi \cdot d^4 \cdot (\omega - 1) \cdot \pi^5 + 20 \cdot \tan^2 \psi \cdot d^2 \cdot (\omega - 1)^3 \cdot p^2 \cdot \pi^5 + 2 \cdot (\omega - 1)^5 \cdot p^4 \cdot \pi^5 \\ & + 10 \cdot \tan^3 \psi \cdot d^3 \cdot p \cdot \pi^3 \cdot [-1 + 2 \cdot (\omega - 1)^2 \cdot \pi^2] + 5 \cdot \tan \psi \cdot d \cdot p^3 \cdot \pi \cdot [3 + 2 \cdot (\omega - 1)^4 \cdot \pi^4], \end{aligned} \quad (3.41)$$

and b and c according to eq. (3.38) and eq. (3.39). In case of the inner thread cylinder, $\bar{I}_{y,dc}$ and $\bar{I}_{z,dc}$ are as follows:

$$I_{(y,z),dc} = \frac{1}{4} \left[\frac{\eta \cdot d}{2} \right]^4 \cdot \left[\frac{\omega \cdot \pi}{2} \pm \frac{1}{4} \sin(2\omega\pi) \right]. \quad (3.42)$$

For the known parameter set $\{d, p, v, \eta\} = \{8.0 \text{ mm}, 3.8 \text{ mm}, 40^\circ, 0.65\}$ and $x = p/2$ ($y_s = 0$), both moments of inertia I_y and I_z of the screw thread profile result as given in eq. (3.43), see

$$I_y = 2 \cdot (\bar{I}_{y,(1,2)} + \bar{I}_{y,dc}) - z_s^2 \cdot A_s = 63.4 \text{ mm}^4, \quad I_z = 2 \cdot (\bar{I}_{z,(1,2)} + \bar{I}_{z,dc}) = 39.0 \text{ mm}^4 \text{ and } \frac{I_y}{I_z} = 1.63. \quad (3.43)$$

Further assuming the structural component to be prismatic, the material as a homogeneous (e. g. constant hardness distribution as shown in Figure 3.44), with a linear-elastic stress-strain-relationship, Euler-

Bernoulli's beam theory and pure bending (moments $M_{(y,z)}$), maxima and minima of normal stresses $\sigma_{x,M(y,z),i}$ occur at the cross-section's edges according to eq. (3.44):

$$\sigma_{x,M(y,z),i} = \frac{M_{(y,z)}}{I_{(y,z)}} \cdot (z, y)_i = \frac{M_{(y,z)}}{W_{(y,z),i}}, \quad (3.44)$$

with $i = \{\max, \min\}$, $(z, y)_i$ as the distances from the cross-section's edges to its gravity centre and $W_{(y,z),i}$ as both section moduli. For the parameter set $\{d, p, v, \eta\} = \{8.0 \text{ mm}, 3.8 \text{ mm}, 40^\circ, 0.65\}$ and $x = p/2$ ($y_s = 0$), both section moduli result to $W_{y,i} = \{20.9, -17.8\} \text{ mm}^3$ and $W_{z,i} = \pm 15.0 \text{ mm}^3$.

In contrast to both moments of inertia I_y and I_z , I_T , defined as the cross-section's torsional moment of inertia, can only be determined in a closed form for a small number of specific cross-sectional types (e. g. circular cross-sections) and not for the given geometry. Consequently, the related values for I_T are estimated with an FE-based software package, written by Bogensperger (2002), for determining geometrical and mechanical properties of cross-sections with a general shape. Figure 3.17 subsequently shows two FE-meshes including up to 10,000 elements each, which have been generated by this application. In case of $\{d, p, v, \eta\} = \{8.0 \text{ mm}, 3.8 \text{ mm}, 40^\circ, 0.65\}$ and $x = p/2$ ($y_s = 0$), see Figure 3.17 (right), I_T exemplarily results to 92.8 mm^4 .

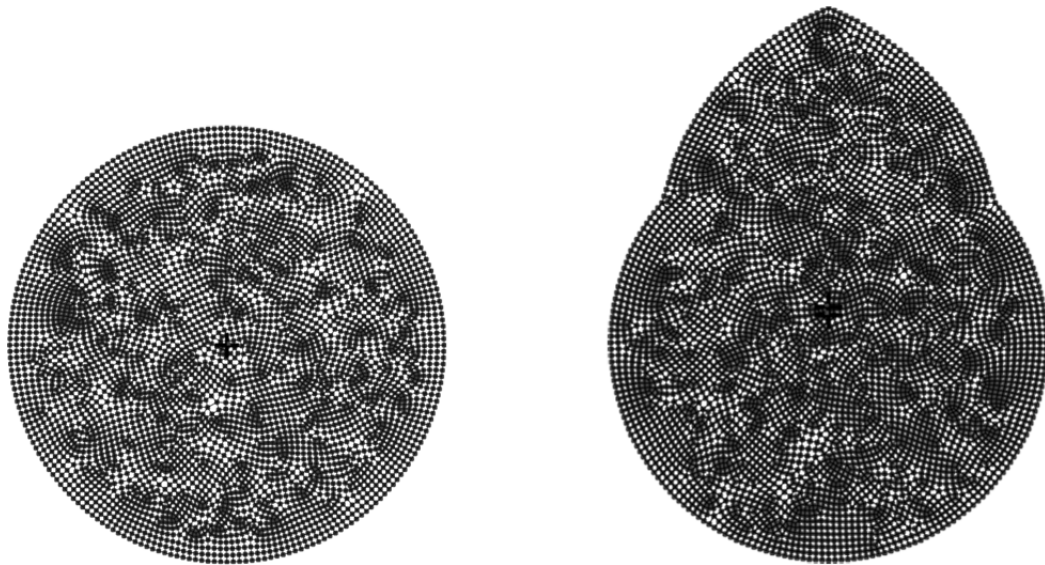


Figure 3.17: FE-meshes generated by the software package written by Bogensperger (2002); left: inner thread cylinder, $d_c = 5.2 \text{ mm}$; right: screw thread cross-section if $\{d, p, v, \eta\} = \{8.0 \text{ mm}, 3.8 \text{ mm}, 40^\circ, 0.65\}$

In order to verify the applicability of this FE-based approach, also $I_{T,dc}$ of a circular cross-section with $d_c = d \cdot \eta = 8.0 \cdot 0.65 = 5.20 \text{ mm}$ (Figure 3.17, left) has been determined and results to 71.6 mm^4 . The

closed-form solution of this geometry can be derived by the mechanical constitution, given in eq. (3.45), see:

$$I_{T,dc} = \frac{r_c^4 \pi}{2} = \frac{d_c^4 \pi}{32} = \frac{5.2^4 \pi}{32} = 71.8 \text{ mm}^4. \quad (3.45)$$

The corresponding difference between both solutions is about 0.25 % and thus regarded as negligible for further considerations. Considering the assumptions for material and geometry, as made before, the maximum shear stress due to uniform torsion of this circular cross-section is further determined by eq. (3.46), see

$$\tau_{\max,T,dc} = \frac{M_T}{I_{T,dc}} \cdot r_c, \quad (3.46)$$

with M_T as the torsional moment applied. In case of $d_c = 5.2 \text{ mm}$, I_T according to eq. (3.45) and $M_T = 1 \text{ Nmm}$, $\tau_{\max,T,dc}$ results to 0.0362 N/mm^2 . The package, written by Bogensperger (2002), also allows determining both shear stresses $\tau_{xy,i}$ and $\tau_{xz,i}$ in each FE-node as a consequence of the uniform torsion caused by $M_T = 1 \text{ Nmm}$. The numerical solution of $\tau_{\max,T}$ is thus equal to the maximum node stress $\tau_{T,i}$, determined by the Pythagorean theorem according to eq. (3.47), see

$$\tau_{T,i} = \sqrt{\tau_{xy,i}^2 + \tau_{xz,i}^2}. \quad (3.47)$$

For the given circular cross-section, $\tau_{\max,T,dc}$ results to 0.0365 N/mm^2 . The deviation to the closed-form solution is again below 1.00 %, the application of the FE-based approach is thus regarded as appropriate.

Figure 3.18 shows shear stress distributions due to the uniform torsion ($M_T = 1 \text{ Nmm}$) according to eq. (3.47) for both cross-sections illustrated in Figure 3.17. In contrast to the circular cross-section (Figure 3.18, left), where the expected linear shear stress distribution occurs, comparatively inhomogeneous torsional shear stresses can be observed for the threaded profile (Figure 3.18, right). Maxima are found at the transition zone between the inner thread cylinder and its chamfer ($\varphi = \omega \cdot \pi$), indicating a significant influence of this geometrical discontinuity.

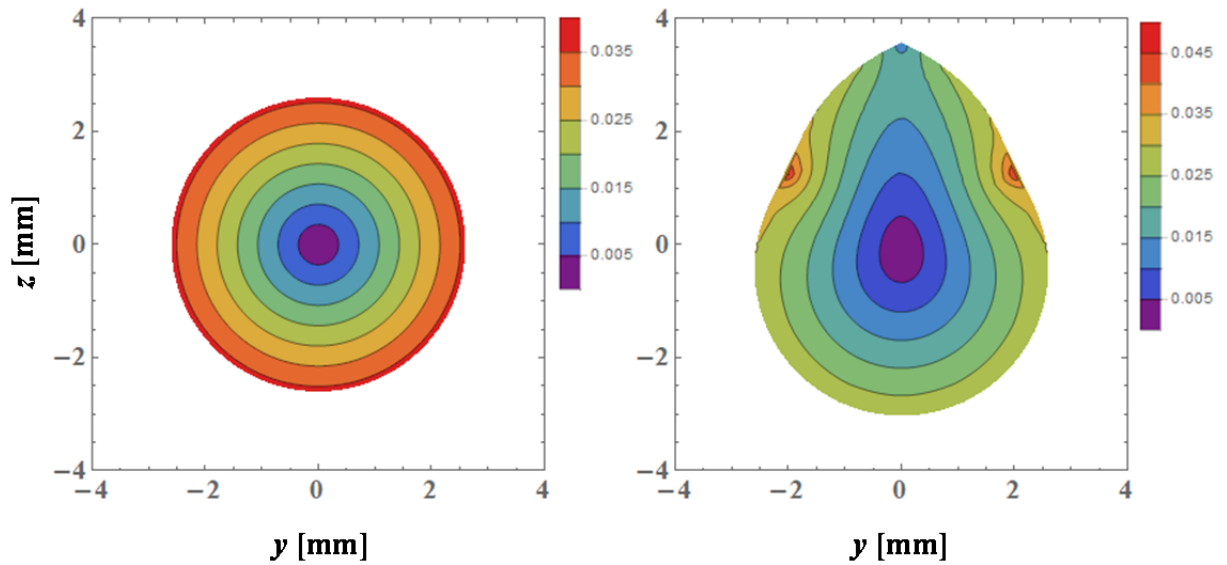


Figure 3.18: Shear stress distributions [N/mm^2] due to uniform torsion ($M_T = 1 \text{ Nmm}$) determined with the software application from Bogensperger (2002); left: inner thread cylinder, $d_c = 5.2 \text{ mm}$; right: screw thread cross-section in case of $\{d, p, v, \eta\} = \{8.0 \text{ mm}, 3.8 \text{ mm}, 40^\circ, 0.65\}$

In order to determine I_T for thread geometries, commonly applied in practice, corresponding values have been derived for a parameter bandwidth $d = \{8, 10, 12\} \text{ mm}$, $p = \{0.4 d, 0.7 d, 1.0 d\}$, $v = \{20, 40, 60\}^\circ$ and $\eta = \{0.50, 0.70, 0.90\}$. This variation bases on the geometrical boundary conditions, given in CUAP 06.03/08 (2010), as well as on the findings made by Pöll (2017), who determined minima and maxima of the screw thread properties, published in currently valid ETAs related to self-tapping screws. In Figure 3.19 and Figure 3.20, 3D illustrations and cross-sectional shapes of three screw thread geometries, considered within this parameter study, are given. Thereby, extremal types are shown in Figure 3.19 and Figure 3.20 (left and right), while Figure 3.19 and Figure 3.20 (middle) represent a parameter set similar to the thread geometries found in currently valid ETAs.

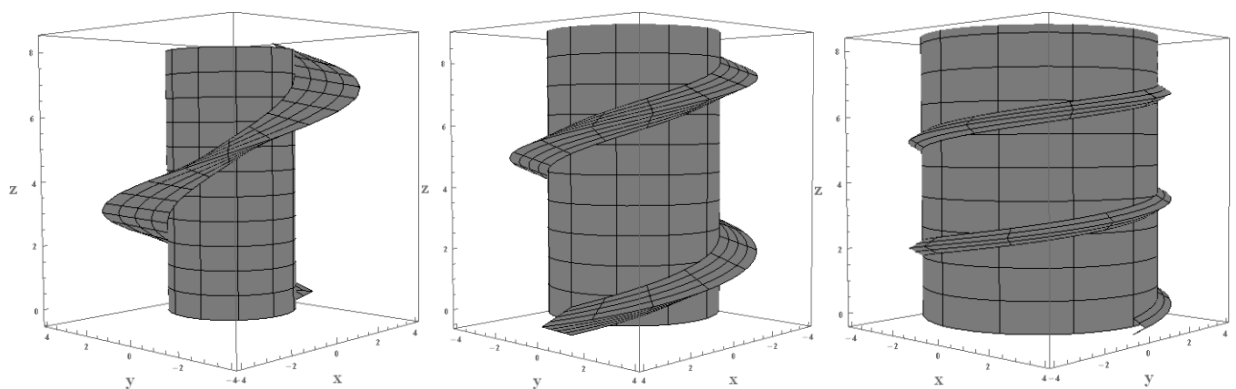


Figure 3.19: 3D illustration of thread geometries for three selected screw thread parameter sets, $d = 8 \text{ mm}$; left: $p = 8.0 \text{ mm}$, $v = 20^\circ$, $\eta = 0.50$; middle: $p = 5.6 \text{ mm}$, $v = 40^\circ$, $\eta = 0.70$; right: $p = 3.2 \text{ mm}$, $v = 60^\circ$, $\eta = 0.90$

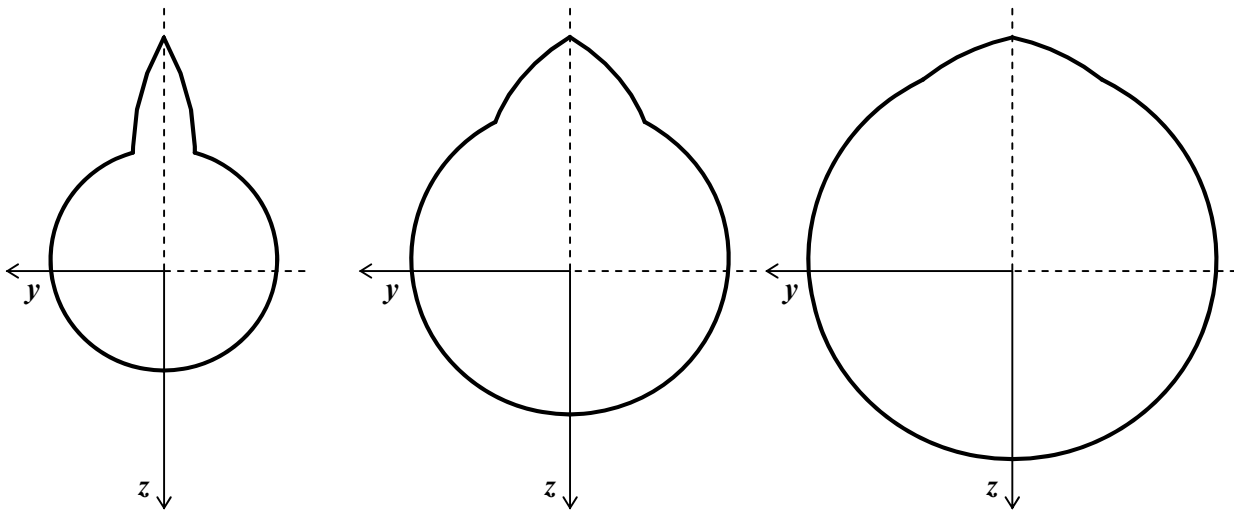


Figure 3.20: Illustration of thread cross-sections for three selected parameter sets, $d = 8$ mm;
 left: $p = 8.0$ mm, $v = 20^\circ$, $\eta = 0.50$; middle: $p = 5.6$ mm, $v = 40^\circ$, $\eta = 0.70$; right: $p = 3.2$ mm,
 $v = 60^\circ$, $\eta = 0.90$

The results of this parameter study in form of the ratios between numerically determined values of $I_{T,num}$ and $\tau_{max,T,num}$ (the latter according to eq. (3.47)) and the corresponding values of related inner thread cylinders are shown in Figure 3.21. Since the behaviour was found to be independent of d , only the case $d = 8$ mm is illustrated.

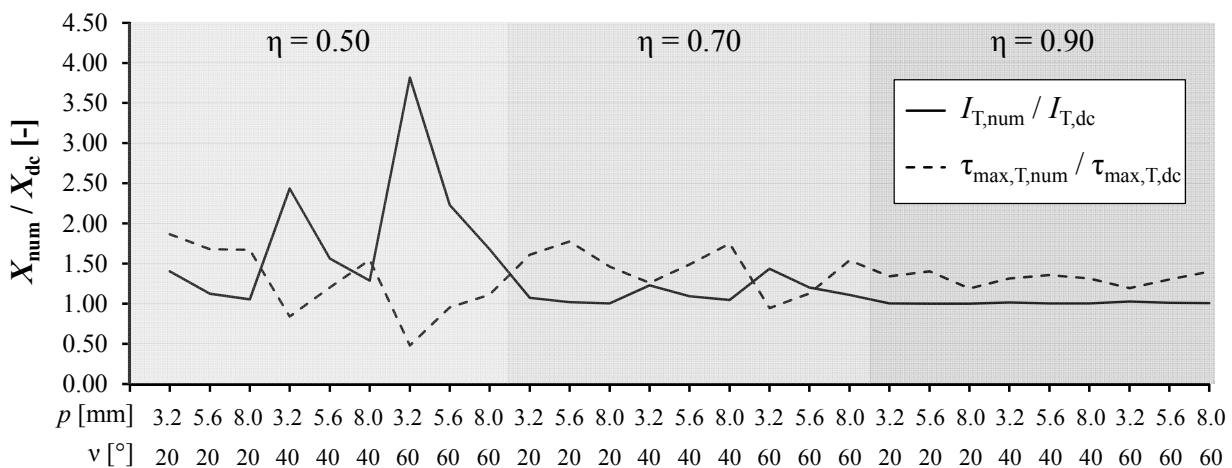


Figure 3.21: Ratios between cross-sectional screw thread torsional moments of inertia and maximum shear stresses due to uniform torsion and those of the inner thread's cylinder for varying parameters η , p and v , $d = 8$ mm

The major deviations between numerically determined $I_{T,num}$ and those of the inner thread cylinder are generally given for small p and large v . Consequently, it can be concluded that shape and size of the thread's chamfer govern the size of this property in a major way. Determined $I_{T,num}$ converging to $I_{T,dc}$ with increasing η additionally confirm this circumstance. Especially in case of $\eta \geq 0.90$ results for $I_{T,num}$

are more or less equal to $I_{T,dc}$. Such compact thread geometries allow the application of $I_{T,dc}$ instead of $I_{T,num}$. Considering the whole bandwidth of the parameters applied, an empirical relationship between $I_{T,num}$ and $\{I_{T,dc}, \eta$ and $\omega\}$, both latter representing the aforementioned influence of the thread's chamfer, can be formulated as follows:

$$I_{T,emp} = I_{T,dc} \cdot \omega^{(1.625\eta^2 - 0.04\eta - 1.479)}, \quad (3.48)$$

with ω according to eq. (3.13). In Figure 3.22 (left) numerically determined $I_{T,num}$ are compared with those estimated, according to eq. (3.48), for the parameter bandwidth of $\{d, p, v, \eta\}$, as explained before. Except of three cross-sections (all $\eta = 0.50$), where a difference of more than 10 % can be observed, $I_{T,emp}$ determined according to eq. (3.48) widely confirms the numerical results.

With regard to the ratio between $\tau_{max,T,num}$ and $\tau_{max,T,dc}$ at varying $\{p, v, \eta\}$, Figure 3.21 also outlines a dependency on these properties, which is similar, but quantitatively inverse, to that of $I_{T,num} / I_{T,dc}$. In contrast to the torsional moment of inertia, even at $\eta = 0.90$ a constant, but significant difference of about 30 % in average between both $\tau_{max,T,num}$ and $\tau_{max,T,dc}$ is given. In order to subsequently verify if $\tau_{max,T,num}$ can be approximated by the mechanical constitution, given in eq. (3.46) (with $M_T = 1$ Nmm, $I_{T,num,i}$ and $r = d / 2$ as input parameters), Figure 3.22 (right) compares $\tau_{max,T,num}$ and $\tau_{max,T,pred}$, the latter defined as the torsional shear stress, determined by this approach for the parameter bandwidth applied. Even though the torsional shear stresses $\tau_{max,T,pred}$ are quite equal to $\tau_{max,T,num}$ for the majority of the generated thread profiles, some significantly deviating results, which are in fact irrespective from geometrical thread properties, disable a reliable approximation of $\tau_{max,T,num}$. Both differences between $\tau_{max,T,num}$ and $\{\tau_{max,T,dc}, \tau_{max,T,pred}\}$, shown in Figure 3.21 and Figure 3.22 (right), are probably caused by the aforementioned inhomogeneous distribution of the torsional shear stress with singularities found at $\varphi = \omega \cdot \pi$, c. f. Figure 3.18 (right).

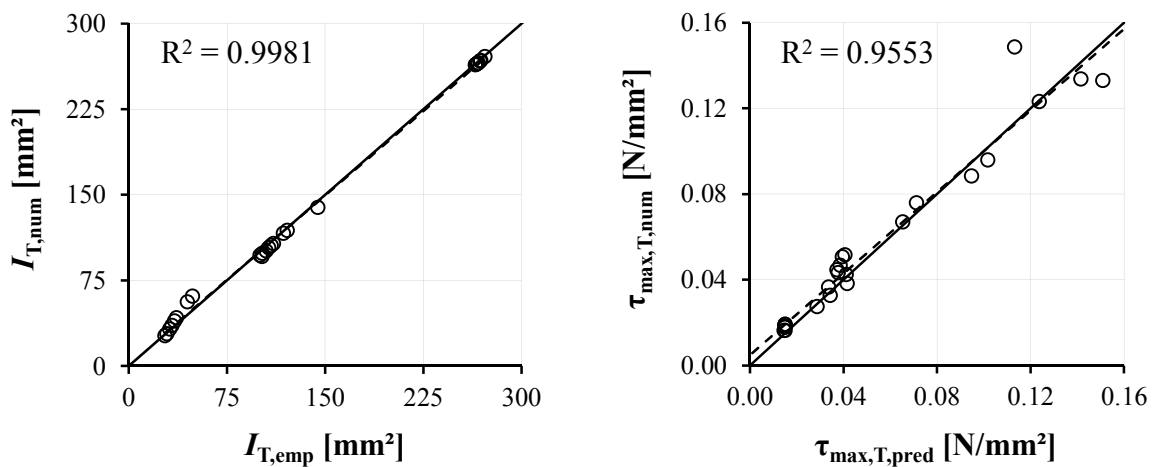


Figure 3.22: Comparison of approximated and numerically determined values of I_T (left) and $\tau_{max,T}$ (right)

Nevertheless, a correlation between $I_{T,num}$ and $\tau_{max,T,num}$ is given ($R = -0.82$), concluding that the approach in eq. (3.48) also serves as an indicator for evaluating the torsional shear stresses of this specific cross-sectional type.

Finally it is worth mentioning, that in the frame of this section only torsional shear stresses due to uniform torsion are considered. In contrast to an ideal cylinder, additional stresses due to non-uniform torsion (warping torsion) occur if a prismatic member with a cross-section, according to Figure 3.15, is loaded in pure torsion. A possible influence on mechanical screw properties is discussed in section 3-4.5.

3-4.3.4 Plastic cross-sectional screw properties

As mentioned in section 3-4.1, the stress-strain-relationship of hardened carbon steel screws is assumed as an elastic-ideal plastic, a qualitative comparison with the real and nonlinear relationship, as observed in tests, is illustrated in Figure 3.23.

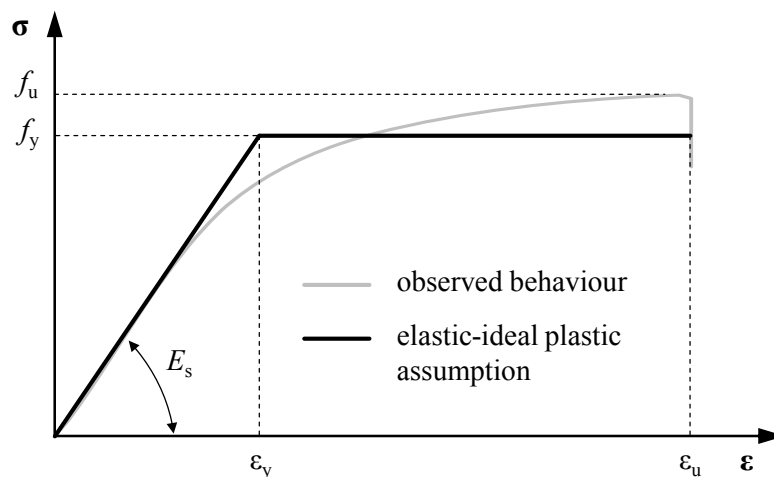


Figure 3.23: Observed and assumed stress-strain-relationship of a carbon steel screw loaded in tension

According to this assumption, normal bending stresses can be determined by eq. (3.44) until reaching the yield strength f_y at the cross-section's outer fibres (I). Further load increase is enabled by a plasticisation of the cross-section's inner fibres (II), finally restricted to the theoretical limit of full plasticity (III; all fibres: $\sigma_{x,M(y,z),i} = f_y$), c. f. Figure 3.24. The bending moment, bearable at state (III), is further denoted as the plastic moment $M_{pl,(y,z)}$. Figure 3.24 also illustrates the movement of the stress zero point from the gravity centre (at linear-elastic conditions) to the related (y_{half}, z_{half}) -coordinate of the point of equal cross-sectional areas **above** and **below** (in state of full plasticity). This, due to fulfil the force equilibrium ($N = 0$) according to eq. (3.49), see

$$N_a \stackrel{!}{=} N_b = \frac{A_s}{2} \cdot f_y, \quad (3.49)$$

with N_a and N_b as the plastic normal forces (above and below the stress zero point) caused by a bending moment $M_{(y,z)} = M_{pl,(y,z)}$.

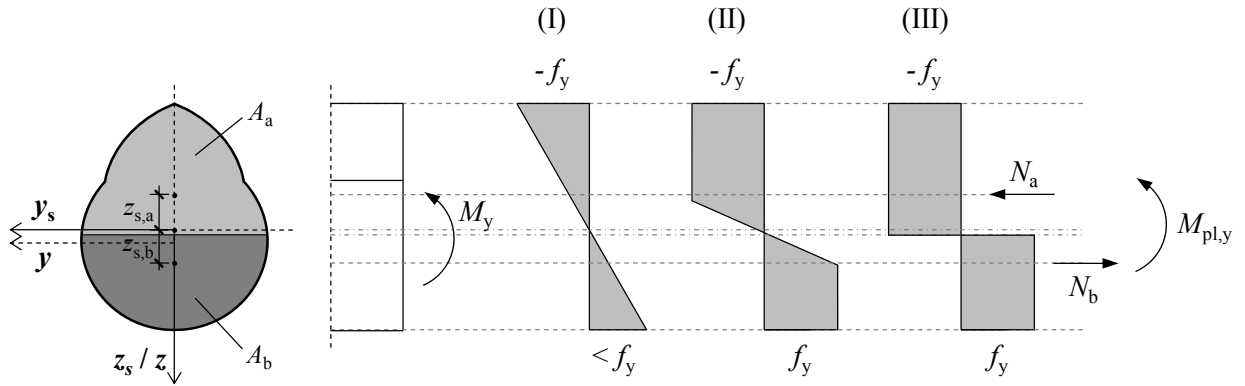


Figure 3.24: Different states of normal stresses due to pure bending (M_y) at the screw's threaded part's cross-section: (I) yield strength reached at outer fibre; (II) intermediate state of cross-section plasticisation; (III) theoretical limit state of full plasticity

Further concentrating on the determination of $M_{pl,(y,z)}$, a corresponding solution can be found in the moment equilibrium, see:

$$M_{(y,z)} \stackrel{!}{=} M_{pl,(y,z)} = N_a \cdot (z, y)_{s,a} + N_b \cdot (z, y)_{s,b} = \frac{A_s}{2} \cdot f_y \cdot [(z, y)_{s,a} + (z, y)_{s,b}], \quad (3.50)$$

with $(z, y)_{s,(a,b)}$, defined as the distance of both cross-sectional parts with $A_a = A_b = A_s / 2$ to its gravity centre (y_s, z_s) . In case of bending about the z -axis, cross-sectional symmetry enables the determination of $M_{pl,z}$ in closed form. Thereby, $|y_{s,l}| = |y_{s,r}|$ (indices l and r stand for left and right with regard to the z -axis) as the only parameter not determined so far, can be derived as follows:

$$y_s = \frac{\sum A_i \cdot y_{s,i}}{\sum A_i} = \frac{A_2 \cdot y_{s,2} + A_{dc} \cdot y_{s,dc}}{0.50 \cdot A_s}, \quad \text{with} \quad (3.51)$$

$$y_{s,i} = \frac{\int_{\varphi_1}^{\varphi_2} \int_0^{r(\varphi)} [r(\varphi)]^2 \sin \varphi \, dr \, d\varphi}{\int_{\varphi_1}^{\varphi_2} \int_0^{r(\varphi)} r(\varphi) \, dr \, d\varphi} = \frac{\int_{\varphi_1}^{\varphi_2} \frac{1}{3} [r(\varphi)]^3 \sin \varphi \, d\varphi}{\int_{\varphi_1}^{\varphi_2} \frac{1}{2} [r(\varphi)]^2 \, d\varphi}, \quad (3.52)$$

$$y_{s,2} = \frac{\int_{\omega-\pi}^{\pi} \frac{1}{3} \left[\frac{d}{2} + \left(\frac{p \cdot \varphi}{2\pi} - \frac{p}{2} \right) \cdot \frac{1}{\tan \psi} \right]^3 \cdot \sin \varphi \, d\varphi}{\int_{\omega-\pi}^{\pi} \frac{1}{2} \left[\frac{d}{2} + \left(\frac{p \cdot \varphi}{2\pi} - \frac{p}{2} \right) \cdot \frac{1}{\tan \psi} \right]^2 \, d\varphi}, \quad (3.53)$$

$$y_{s,2} = \frac{p \cdot [a + b \cdot \cos(\omega\pi) - c \cdot \sin(\omega\pi)]}{\tan \psi \cdot \pi^4 \cdot [\tan^3 \psi \cdot d^3 - (\tan \psi \cdot d + (\omega - 1) \cdot p)^3]}, \text{ with} \quad (3.54)$$

$$a = -6 \cdot \tan \psi \cdot d \cdot p^2 \cdot \pi + \tan^3 \psi \cdot d^3 \cdot \pi^3, \quad (3.55)$$

$$b = [\tan \psi \cdot d + (\omega - 1) \cdot p] \cdot \pi \cdot [-6p^2 + (\tan \psi \cdot d + (\omega - 1) \cdot p)^2 \cdot \pi^2], \text{ and} \quad (3.56)$$

$$c = 3p \cdot [-2p^2 + (\tan \psi \cdot d + (\omega - 1) \cdot p)^2 \cdot \pi^2]. \quad (3.57)$$

$$y_{s,dc} = \frac{\int_0^{\omega\pi} \frac{1}{3} \left[\frac{\eta \cdot d}{2} \right]^3 \cdot \sin \varphi \, d\varphi}{\int_0^{\omega\pi} \frac{1}{2} \left[\frac{\eta \cdot d}{2} \right]^2 \, d\varphi} = \frac{\eta \cdot d \cdot [1 - \cos(\omega\pi)]}{3 \cdot \omega \cdot \pi}. \quad (3.58)$$

With regard to bending about the y -axis ($M_{pl,y}$), an equal determination of $|z_{s,a}| = |z_{s,b}|$ is disabled by the discontinuity at $\omega \cdot \pi$. Consequently, the corresponding coordinates have to be determined by an iterative process, carried out with the software-package Wolfram Mathematica 10 (2014). Figure 3.25 outlines a triangular area with $A = A_{tri}$, necessary to be considered within the (numerical) determination of $\{z_{half}, z_{s,(a,b)}\}$.

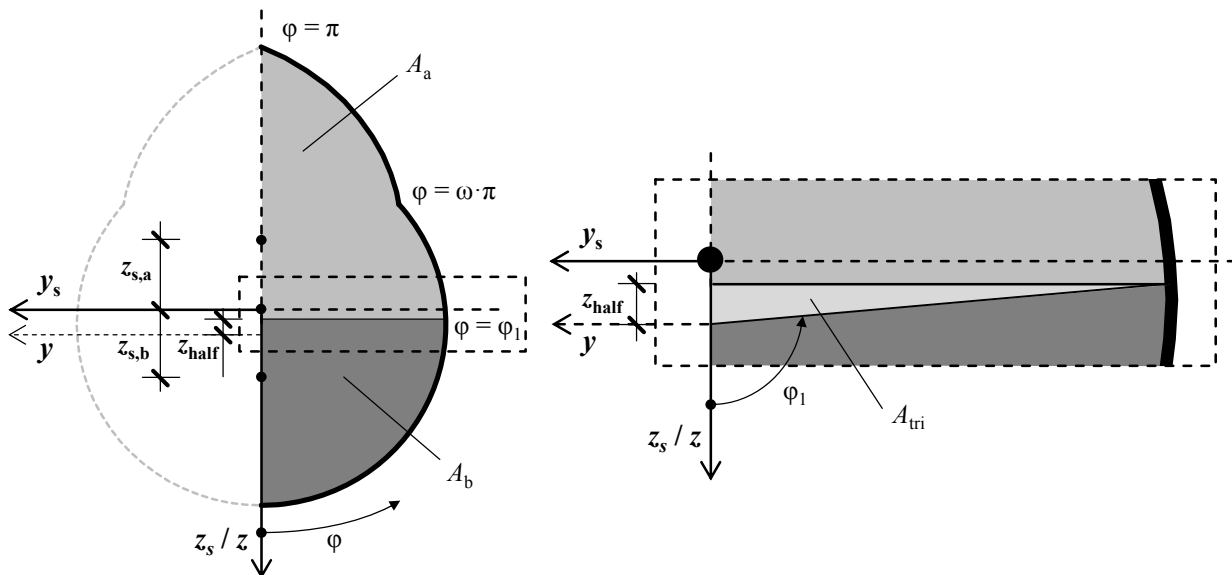


Figure 3.25: Extract and illustration of the triangular area with $A = A_{tri}$ to be considered for numerical determination of cross-sectional properties z_{half} and $z_{s,(a,b)}$ of the given screw thread profile

In case of $\{d, p, v, \eta\} = \{8.0 \text{ mm}, 3.8 \text{ mm}, 40^\circ, 0.65\}$ and $x = p / 2$ ($y_s = 0$), $\{y_{\text{half}}, z_{\text{half}}\}$, $\{y_{s,(l,r)}, z_{s,(a,b)}\}$, as well as $\{M_{pl,y}, M_{pl,z}, M_{pl,y} / M_{pl,z}\}$ result to $\{0.00, -0.35\} \text{ mm}$, $\{\pm 1.06; \mp 1.35\} \text{ mm}$ and $\{33.5 \cdot f_y, 26.3 \cdot f_y, 1.27\}$ respectively. Subsequently, the plastic section moduli $W_{pl,(y,z)}$ can be determined as the ratio between $M_{pl,(y,z)}$ and f_y and result to $\{W_{pl,y}, W_{pl,z}\} = \{33.5, 26.3\} \text{ mm}^3$. The ratio between $W_{(y,z)} = W_{el,(y,z)}$ and $W_{pl,(y,z)}$ is commonly denoted as the plastic shape factor $\alpha_{pl,M(y,z)}$ (here for pure bending) and describes the increase of the loadbearing resistance, comparing the ideal plastic material behaviour with a linear-elastic one. For the given thread geometry, $\{\alpha_{pl,My}, \alpha_{pl,Mz}\}$ consequently result to $\{1.60, 1.75\}$. These factors also significantly depend on geometrical thread parameters $\{d, p, v, \eta\}$ and the determination of $\alpha_{pl,My}$ is only possible by means of numerical methods, while in case of $\alpha_{pl,Mz}$, a closed-form solution is derivable by considering eq. (3.23) and eq. (3.51).

Now the focus lays on the screw's threaded part loaded by a normal force N . As illustrated in Figure 3.26, the position of N is assumed in the screw axis equal to the coordinate origin $\{y, z\}$. Consequently, the eccentricity z_s , between the screw axis and the threaded part's gravity centre, leads to a load interaction between N and an eccentric moment in form of $M_y = N \cdot z_s$.

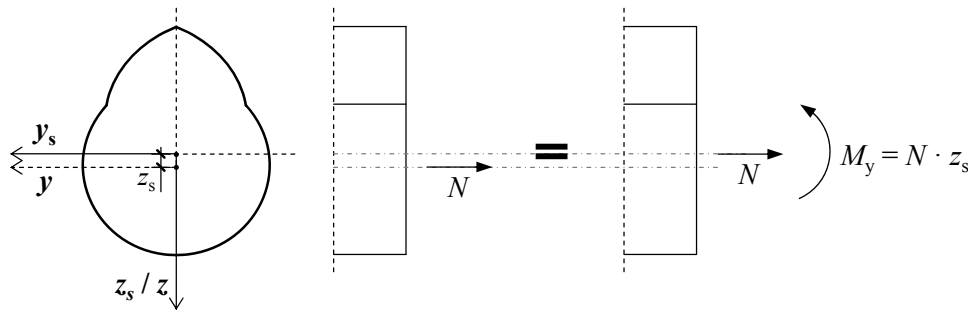


Figure 3.26: Internal forces of the screw's threaded part loaded in axial tension

In case of a linear-elastic material behaviour, maximum normal stresses occurring at the cross-section's edges can be determined by summing up both components $\sigma_{x,N,i}$ and $\sigma_{x,M,i}$, according to eq. (3.59), see

$$\sigma_{x,i} = \sigma_{x,N,i} + \sigma_{x,M,i} = \frac{N}{A_s} + \frac{M_y}{W_{y,i}} = N \cdot \left(\frac{1}{A_s} + \frac{z_s}{W_{y,i}} \right). \quad (3.59)$$

Again concentrating on stress state (I), the yield strength f_y is subsequently reached at the cross-section's lower edge (index 2) for the given geometry, c. f. Figure 3.27.

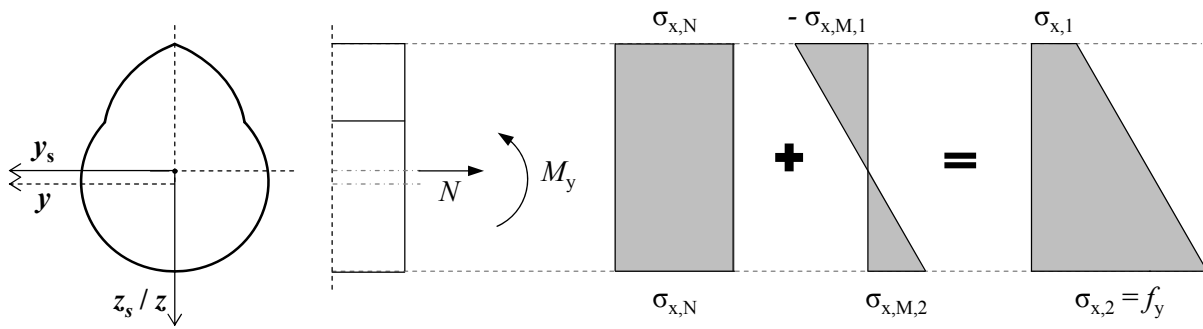


Figure 3.27: Stress distribution in the axially loaded screw's threaded part's cross-section with assumed linear-elastic material behaviour

With regard to stress state (III), normal stress interaction, equal to eq. (3.59), is not possible if an ideal plastic stress-strain relationship is assumed. A related solution is consequently derived by considering the force and moment equilibrium, as given in eq. (3.60) and eq. (3.61):

$$\sum N = 0 \rightarrow N = N_t + N_c = A_t \cdot f_y + A_c \cdot -f_y = f_y \cdot (A_t - A_c), \text{ and} \quad (3.60)$$

$$\sum M = 0 \rightarrow M_y = N \cdot z_s = M_t + M_c = N_t \cdot z_{s,t} + N_c \cdot z_{s,c} = f_y \cdot (A_t \cdot z_{s,t} - A_c \cdot z_{s,c}), \quad (3.61)$$

with A_i and $z_{s,i}$, $i = \{t, c\}$ as corresponding areas and distances to the cross-section's gravity centre illustrated in Figure 3.28.

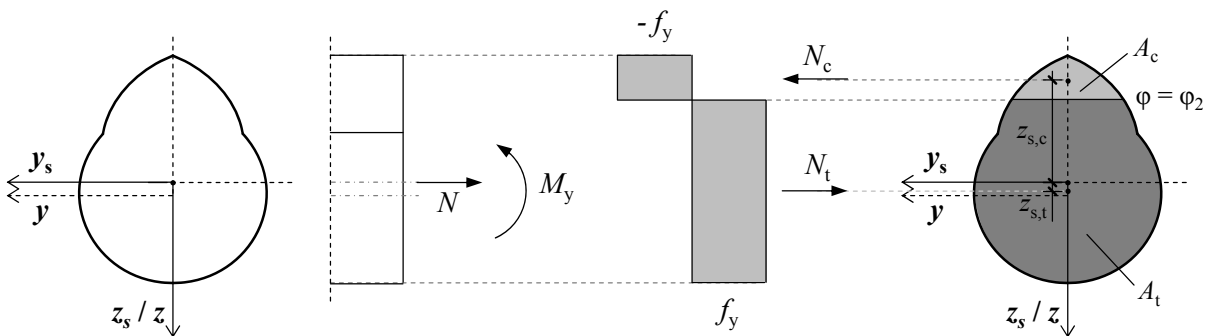


Figure 3.28: Stress distribution in the axially loaded screw's threaded part's cross-section with assumed ideal plastic material behaviour

For a given value of N , both f_y and φ_2 (the latter defined as angle related to the point of zero stress) remain as unknown variables, solvable by equalising eq. (3.60) and eq. (3.61). Again, Figure 3.29 outlines a triangular area with $A = A_{tri}$, to be considered within the numerical determination of φ_2 , $A_{(c,t)}$ and $z_{s,(c,t)}$.

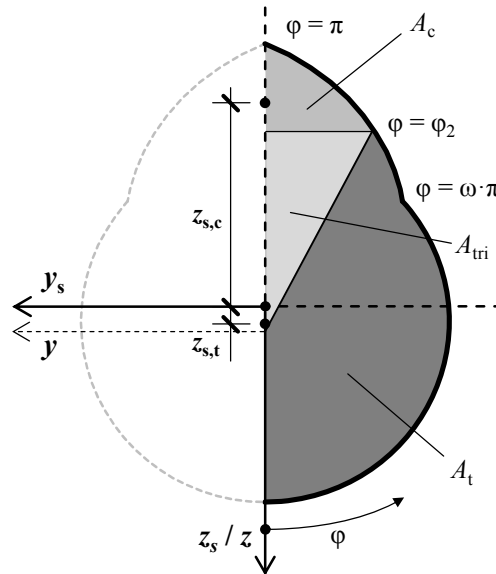


Figure 3.29: Illustration of the triangular area with $A = A_{tri}$ to be considered for numerical determination of cross-sectional properties φ_2 , $A_{(c,t)}$ and $z_{s,(c,t)}$ of the given screw thread profile

Subsequently, $A_{pl,N}$ as the cross-section’s area “reserved” for the normal force N is defined as follows:

$$A_{pl,N} = A_t - A_c, \tag{3.62}$$

which leads to

$$N = N_{pl} = f_y \cdot A_{pl,N}. \tag{3.63}$$

For the specific load situation, $\alpha_{pl,N}$ as the ratio between N_{pl} and N_{el} (bearable normal force according to eq. (3.59) if $\sigma_{x,2} = f_y$) can be determined according to eq. (3.64), see

$$\alpha_{pl,N} = \frac{N_{pl}}{N_{el}} = \frac{A_{pl,N}}{A_s} + \frac{A_{pl,N} \cdot |z_s|}{W_{y,i}}. \tag{3.64}$$

In case of $\{d, p, v, \eta\} = \{8.0 \text{ mm}, 3.8 \text{ mm}, 40^\circ, 0.65\}$ and $x = p/2$ ($y_s = 0$), φ_2 , $A_{pl,N}$ and $\alpha_{pl,N}$ result to 155.7° , 21.7 mm^2 and 1.32 respectively. Worth mentioning, $A_{pl,N}$ is quite equal to the inner thread cylinder’s area denoted as $A_{dc} = 21.2 \text{ mm}^2$, which is solvable in a closed form.

In order to verify the ratio between $A_{pl,N}$ and A_{dc} for typical thread geometries, the corresponding values have been derived for the same parameter bandwidth $d = \{8, 10, 12\} \text{ mm}$, $p = \{0.4 d, 0.7 d, 1.0 d\}$, $v = \{20, 40, 60\}^\circ$ and $\eta = \{0.50, 0.70, 0.90\}$ as applied for determining I_T and $\tau_{\max,T}$ in section 3-4.3.3. Figure 3.30 subsequently overviews the determined ratios between $A_{pl,N}$ and A_{dc} and furthermore between A_s and A_{dc} , as well as between $W_{pl,z}$ and $W_{pl,z,dc}$. Since results independent of d were found, only the case

$d = 8 \text{ mm}$ is illustrated. The determination of the inner thread cylinder's plastic section modulus $W_{pl,z,dc}$ was thereby done according to eq. (3.65), see

$$W_{pl,z,c} = \frac{d_c^3}{6}. \quad (3.65)$$

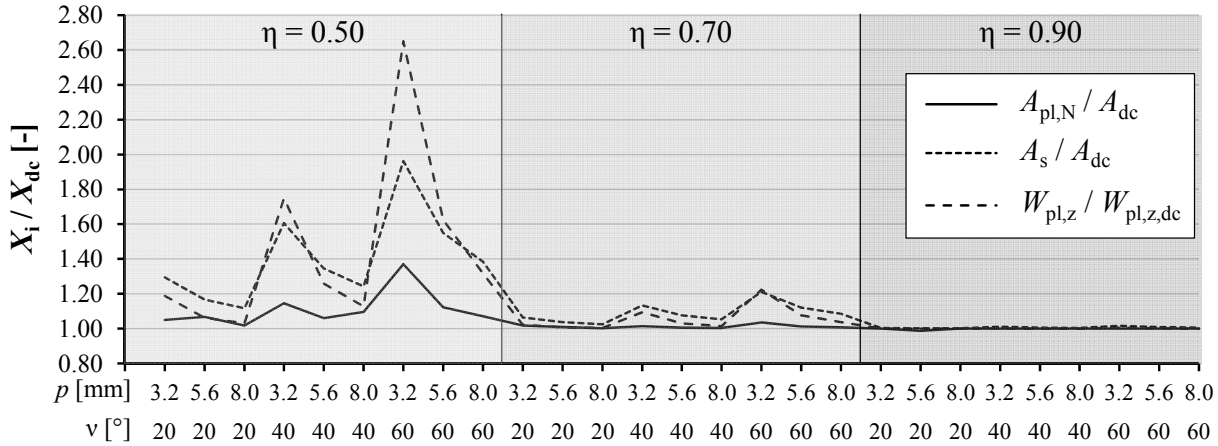


Figure 3.30: Selected ratios between cross-sectional screw thread properties and those of the inner thread's cylinder for varying parameters η , p and v ; $d = 8 \text{ mm}$

Similar to the behaviour of I_T , illustrated in Figure 3.21, the deviations between the size of plastic cross-sectional thread properties $A_{pl,N}$ and $W_{pl,z}$ and those of the inner thread cylinder are generally given for small p and large v , both also leading to significantly higher values of A_s if compared to A_{dc} . Furthermore, both trends of $A_{pl,N} / A_{dc}$ and $W_{pl,z} / W_{pl,z,dc}$ are differently pronounced but qualitatively similar to each other and similar to A_s / A_{dc} . The thread properties significantly converge to those of the inner thread cylinder with increasing η . Especially the results for $A_{pl,N}$ are more or less equal to A_{dc} in case of $\eta \geq 0.70$. Thus, such thread geometries allow the application of A_{dc} instead of $A_{pl,N}$. Again, an empirical relationship between $A_{pl,N}$ and $\{A_{dc}, \eta \text{ and } \omega\}$, both latter representing the aforementioned influence of the thread's chamfer, can be formulated as follows:

$$A_{pl,N,emp} = A_{dc} \cdot \omega^{\left(\frac{-0.015}{\eta^{3.95}}\right)}, \quad (3.66)$$

with ω according to eq. (3.13). Figure 3.31 consequently compares the numerically determined values of $A_{pl,N}$ with those estimated according to eq. (3.66) for the parameter bandwidth of $\{d, p, v, \eta\}$, as explained before. Therein, a high correspondence between both approaches can be observed, indicating that the empirical relationship is appropriate for predicting this property.

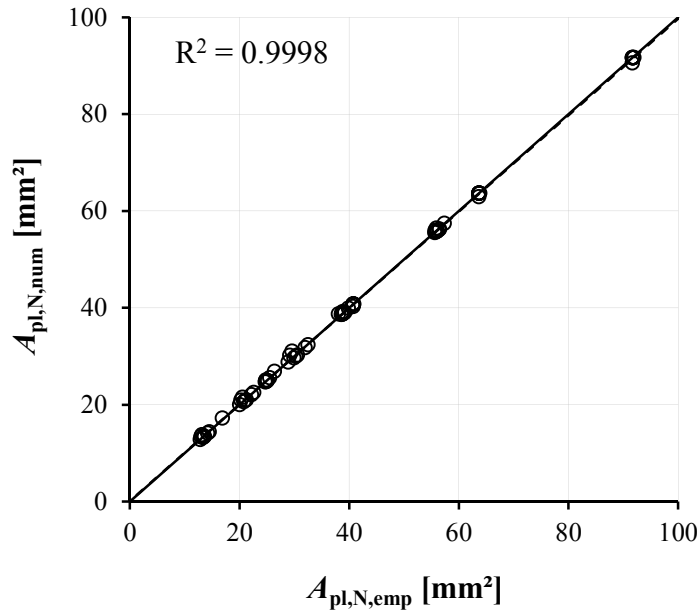


Figure 3.31: Comparison of empirically and numerically determined values of $A_{pl,N}$

Now concentrating on the plastic cross-sectional properties due to the uniform torsion, which comprise the plastic torsional section modulus $W_{T,pl}$ and the plastic torsional shape factor $\alpha_{pl,MT}$: the latter is again defined as the ratio between the torsional moments, bearable in case of an ideal-plastic and an linear-elastic material behaviour. Figure 3.32 compares the torsional shear stress distributions in states (I) and (III) for a circular cross-section, representing the inner thread cylinder's geometry. In case of $\tau_{max,T,dc} = \tau_{T,y}$ (yield shear stress), the corresponding maximum torsional moment in state (I) (Figure 3.32, left), $M_{T,el,dc}$ can be calculated on the basis of eq. (3.46) and results to

$$M_{T,el,dc} = \tau_{T,y} \cdot \frac{I_{T,dc}}{r_c} = \frac{1}{2} r_c^3 \cdot \pi \cdot \tau_{T,y}. \quad (3.67)$$

The maximum torsional moment bearable in case of full plasticity (Figure 3.32, right), is further determined according to eq. (3.68), see

$$M_{T,pl,dc} = \tau_{T,y} \cdot \int_A r dA = \tau_{T,y} \cdot \int_0^{2\pi} \int_0^{r_c} r^2 dr d\varphi = \frac{2}{3} r_c^3 \cdot \pi \cdot \tau_{T,y}. \quad (3.68)$$

The plastic shape factor $\alpha_{pl,MT,dc}$ for the inner thread cylinder subsequently results to

$$\alpha_{pl,MT,dc} = \frac{M_{T,pl,dc}}{M_{T,el,dc}} = \frac{\frac{2}{3} r_c^3 \cdot \pi \cdot \tau_{T,y}}{\frac{1}{2} r_c^3 \cdot \pi \cdot \tau_{T,y}} = \frac{4}{3}. \quad (3.69)$$

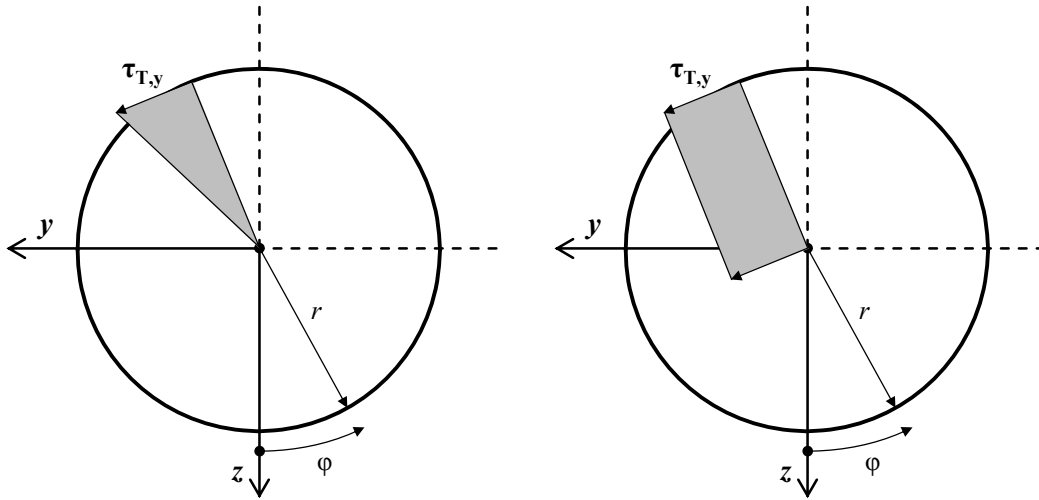


Figure 3.32: Comparison of torsional shear stress distributions due to uniform torsion for a circular cross-section; left: stress state (I); right: stress state (III)

With regard to the screw thread profile, the inhomogeneous torsional shear stress distribution, shown in Figure 3.18 (right), disabled the determination of an empirical relationship between I_T and $\tau_{\max,T,num}$ ($M_T = 1 \text{ Nmm}$), c. f. section 3-4.3.3. Consequently, the maximum torsional moment in state (I), $M_{T,el}$ can only be calculated as a single value of each parameter set $\{d, \eta, p, v\}$ according to eq. (3.70), see

$$M_{T,el,i} = \frac{\tau_{T,y}}{\tau_{\max,T,num,i}}. \quad (3.70)$$

The determination of $M_{T,pl}$ subsequently follows the constitution in eq. (3.68). In case of the pure torsion due to M_T , a structural member with general cross-sectional shape rotates about an axis located in the cross-section's shear centre, defined by $\{y_{\text{shear}}, z_{\text{shear}}\}$. In case of the given screw thread profile and in contrast to a circular cross-section, this point is neither equal to the coordinate origin nor to the cross-section's gravity centre. Assuming $x = p/2$, the symmetry again leads to $y_{\text{shear}} = 0$. The determination of z_{shear} , as the remaining property unknown, has been carried out by the FE-based approach, written by Bogensperger (2002), for the parameter bandwidth $d = \{8, 10, 12\} \text{ mm}$, $p = \{0.4 d, 0.7 d, 1.0 d\}$, $v = \{20, 40, 60\}^\circ$ and $\eta = \{0.50, 0.70, 0.90\}$. The results are further used for modifying eq. (3.68) as follows:

$$M_{T,pl} = 2 \cdot \tau_{T,y} \cdot \left(\int_0^{\omega\pi} \int_0^{r_{\text{shear}}} r_{\text{shear}}^2 dr_{\text{shear}} d\varphi + \int_{\omega\pi}^{\pi} \int_0^{\chi_{\text{shear}}} \chi_{\text{shear}}^2 d\chi_{\text{shear}} d\varphi \right), \quad (3.71)$$

with

$$\{r_{\text{shear}}, \chi_{\text{shear}}\} = \sqrt{\left(|z_{\text{shear}}| + \{r_c, \chi[\varphi]\} \cdot \cos \varphi \right)^2 + \left(\{r_c, \chi[\varphi]\} \cdot \sin \varphi \right)^2}, \quad (3.72)$$

and r_{shear} , χ_{shear} as both radii of the inner thread cylinder and the thread chamfer's section curve referred to $\{y_{\text{shear}}, z_{\text{shear}}\}$, see Figure 3.33, and $\chi[\varphi]$ according to eq. (3.11).

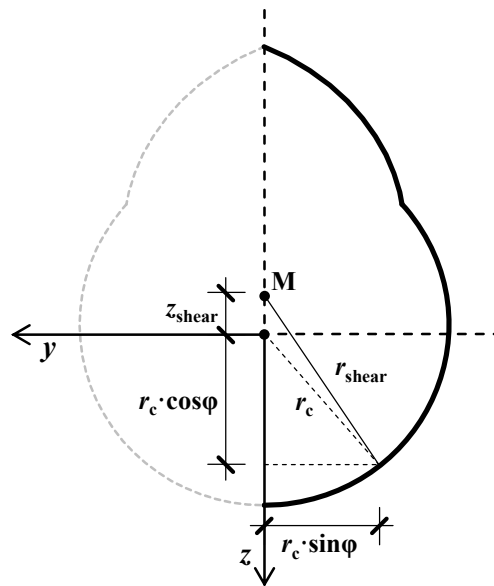


Figure 3.33: Relationship between r_{shear} and r_c for the given screw thread profile

Since the second integral of eq. (3.71) is not solvable in closed form, the corresponding values for $M_{T,\text{pl}}$ have subsequently been determined with the software-package Wolfram Mathematica 10 (2014). Figure 3.34 overviews the outcomes in form of ratios between the plastic section moduli $W_{\text{pl},T,\text{num}}$ and $W_{\text{pl},T,\text{dc}}$ (both by dividing eq. (3.68) and eq. (3.71) by $\tau_{T,y}$), as well as the related values of $\alpha_{\text{pl},\text{MT}}$, determined for the applied parameter bandwidth. Again, only the case $d = 8$ mm is illustrated, a clear influence of the thread's chamfer's shape and size can be observed. The ratio between $W_{\text{pl},T,\text{num}}$ and $W_{\text{pl},T,\text{dc}}$ has a similar course than that of $I_{T,\text{num}} / I_{T,\text{dc}}$ given in Figure 3.21, converging to 1.00 in case of $\eta \geq 0.90$. The behaviour of $\alpha_{\text{pl},\text{MT}}$ also significantly depends on $\{\eta, p, v\}$, especially in form of a pronounced decrease with increasing η . But even at $\eta = 0.90$, $\alpha_{\text{pl},\text{MT}}$ results to roughly 1.60 and is thus about 20 % higher than $\alpha_{\text{pl},\text{MT},\text{dc}}$ of the inner thread cylinder determined in eq. (3.69). A possible reason for this deviation is the occurrence of torsional stress peaks at $\varphi = \omega \cdot \pi$ in case of state (I), decreasing $M_{T,\text{el}}$ to a certain extent.

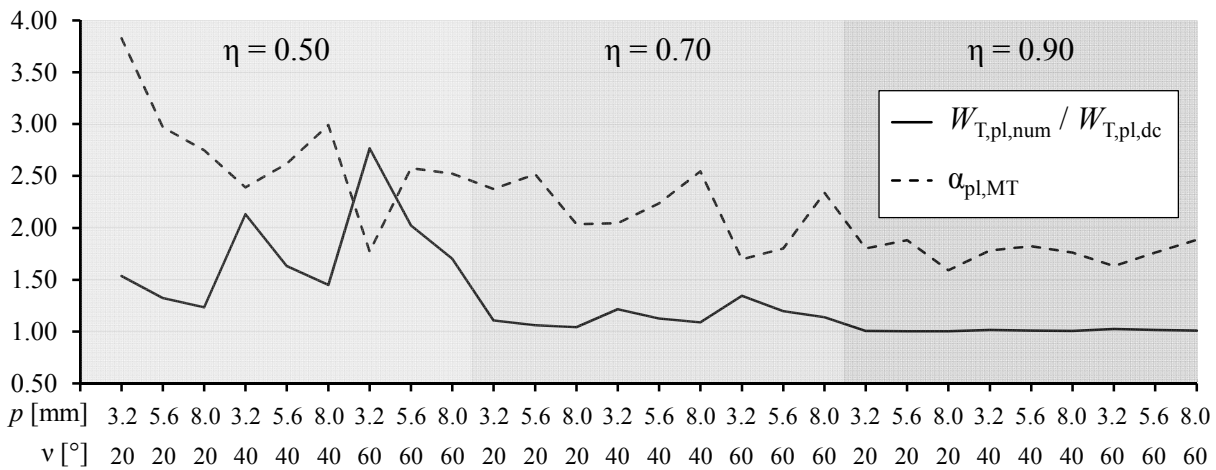


Figure 3.34: Ratios between plastic torsional section moduli of the screw thread profile and the inner thread cylinder and the distribution of the plastic torsional shape factor $\alpha_{pl,MT}$ due to uniform torsion for varying parameters η , p and v , $d = 8$ mm

In order to describe $W_{T,pl,emp}$ as a steady function in dependence of $\{d, \eta, p, v\}$, again an empirical approach similar to eq. (3.48) and eq. (3.66) has been derived and is shown in eq. (3.73). Thereby, the preterm as a linear function of η considers the regressive course of $\alpha_{pl,MT}$ with increasing η (outlined in Figure 3.21), but equalising $\alpha_{pl,MT,dc}$ in case of $\eta = 0.90$.

$$W_{T,pl,emp} = \left(-\frac{2}{3} \cdot \eta + 1.93 \right) \cdot W_{T,el,dc} \cdot \omega^{\left(\frac{-0.2108}{\eta^{1.7105}} \right)}. \quad (3.73)$$

Finally, Figure 3.35 compares the numerically determined values of $W_{T,pl}$, with those estimated according to eq. (3.73) for the parameter bandwidth of $\{d, p, v, \eta\}$, as explained before. Again, a high correspondence between both approaches can be observed, indicating that the empirical relationship is appropriate for predicting this property.

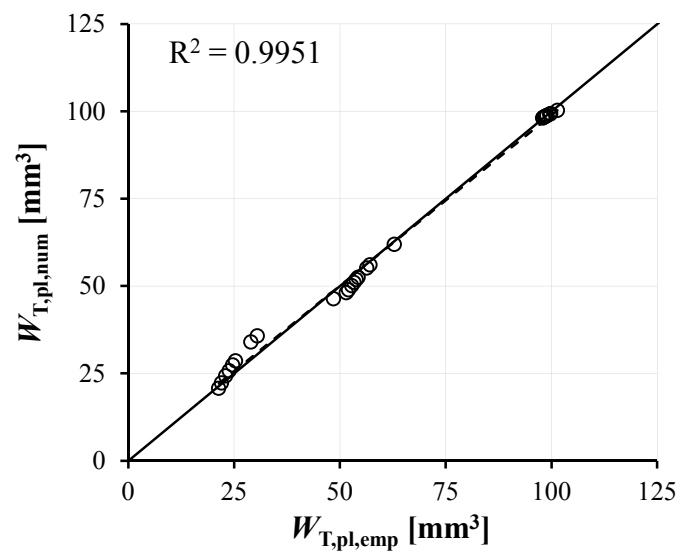


Figure 3.35: Comparison of empirically and numerically determined values of $W_{T,pl}$

3-4.4 Experimental programme

This subsection comprises an overview of the experimental programme, containing several test series for determining the mechanical product characteristics f_{tens} , f_{tor} and M_y of self-tapping screws. Further supplemental investigations, including hardness tests and microscopic scans (carried out at the Institute of Material Science, Joining and Forming at Graz University of Technology) are also summarised. The gained results are predominately used for the verification of theoretical considerations made in sections 3-4.3 and 3-4.5. Furthermore, specific test series serve as a reference for the experimental programme related to section 3-5.

3-4.4.1 Overview

As outlined in Table 3.3, screws from three different manufacturers, denoted as A, B and C, have been considered within the experimental programme. The parameter variation included the hardening procedure (classified from I to V, for explanation see Table 3.4), as well as the screw's outer thread diameter d_{nom} (nominal value, as published by the manufacturer). The corresponding bandwidth shall cover the typical screw application in form of high-stressed connections and reinforcements. Furthermore, manufacturer A also provided wire rods with $d_{\text{nom}} = 6$ mm as raw material applied for the production of test series A_s_I-V_08_240. It has to be pointed out, that all screws of this programme were fully threaded low-alloy carbon steel screws.

Table 3.3: Products selected for the experimental programme

product ID	manufacturer	product	hardening	nominal diameter d_{nom} [mm]	total length l_{screw} [mm]
A_s_I-V_08_240	A	screw	I-V	8	240
A_r_I-V_08_240	A	wire rod*	I-V	6	240
A_s_II_08_180	A	screw	II	8	180
A_s_II_08/10_500	A	screw	II	8, 10	500
A_s_II_08/10_1000	A	screw	II	8, 10	1,000
A_s_II_12_450	A	screw	II	12	450
B_s_II_08/10/12_300	B	screw	II	8, 10, 12	300
C_s_II_08_200	C	screw	II	8	200

* raw material for screw production

Table 3.4: *Classification of different hardening procedures applied*

hardening procedure	description
I	see type II, additionally carbonitrided
II	standard procedure of the specific manufacturer and type of screw
III	see type II, tempered after hardening
IV	see type III, additionally carbonitrided
V	unhardened

In addition, Table 3.5 and Table 3.6 contain type and number of tests conducted for determining the screw product characteristics, as well as those regarding further metallurgical investigations. The total programme contained 321 observations all in all.

Table 3.5: *Type and number of tests conducted within the experimental programme*

product ID	f_{tens}	f_{tor}	M_y	product ID	f_{tens}	f_{tor}	M_y
A_s_I_08_240	15	5	3	A_s_II_08_500	11	10	0
A_s_II_08_240	10	10	3	A_s_II_10_500	11	12	0
A_s_III_08_240	5	5	3	A_s_II_08_1000	0	0	12
A_s_IV_08_240	15	5	3	A_s_II_10_1000	0	0	12
A_s_V_08_240	5	0	3	A_s_II_12_450	12	12	14
A_r_I_08_240	3	0	1	A_s_II_08_180	5	0	0
A_r_II_08_240	1	0	1	B_s_II_08_300	13	10	3
A_r_III_08_240	2	0	1	B_s_II_10_300	6	10	3
A_r_IV_08_240	1	0	1	B_s_II_12_300	3	10	3
A_r_V_08_240	2	0	2	C_s_II_08_200	5	0	0
sum					125	89	68

Table 3.6: *Type and number of further investigations conducted at the Institute of Material Science, Joining and Forming at Graz University of Technology*

product ID	hardness acc. to Vickers (HV1)	macro-photography	stereo microscopy (SM)
A_s_I_08_240	1	2	2
A_s_II_08_240	7	6	5
A_s_III_08_240	1	0	4
A_s_IV_08_240	1	2	2
A_s_V_08_240	1	0	0
A_r_I_08_240	1	0	0
A_r_II_08_240	1	0	0
A_r_V_08_240	1	0	0
B_s_II_08_300	1	0	0
C_s_II_08_200	1	0	0
sum	16	10	13

3-4.4.2 Determination of main geometrical screw thread properties d , d_c and p

Similar to the procedure proposed in CUAP 06.03/08 (2010), the geometrical properties d , d_c and p , relevant for describing the screw thread geometry (see section 3-4.2), have been determined for the majority of investigated screws, see Table 3.7. Products, where the corresponding values have been taken out from related ETAs, are outlined therein. This especially concerns the flank inclination angle ν , which has not been measured at all.

Table 3.7: Geometrical properties (mean values) of products as parts of the experimental programme

product ID	d_{nom} [mm]	d [mm]	d_c [mm]	η [-]	ν^* [°]	p [mm]
A_s_I-V_08_240	8	8.00	5.15	0.64	40	3.66
A_r_I-V_08_240	8	5.76	-	-	-	-
A_s_II_08_180*	8	8.00	5.20	0.65	40	3.80
A_s_II_08_500	8	7.99	4.98	0.62	40	3.59
A_s_II_10_500	10	10.3	6.29	0.61	40	4.68
A_s_II_08_1000	8	8.07	5.05	0.63	40	3.59
A_s_II_10_1000	10	10.3	6.28	0.61	40	4.65
A_s_II_12_450	12	12.0	7.00	0.58	40	6.00
B_s_II_08_300	8	8.15	5.02	0.62	40	4.16
B_s_II_10_300	10	9.77	6.12	0.63	40	5.17
B_s_II_12_300	12	12.0	7.29	0.61	40	6.20
C_s_II_08_200*	8	8.00	5.00	0.63	40	3.70

* properties taken out of corresponding ETAs

3-4.4.3 Axial tensile test to determine f_{tens} and further mechanical properties F_y and D

Concentrating on the test configuration determining the product's axial loadbearing capacity f_{tens} , as denoted in ON EN 14592 (2012). Following the given regulations, a corresponding test set-up has to be arranged on the basis of ON EN 1383 (1999), which implies a fixed support at the end of the screw's threaded part and (hinged) head embedment in a steel plate with adequate dimensions. Consequently, this configuration allows the evaluation of both scenarios, "screw failure in tension" and "head tear-off", according to section 8.7.2 of ON EN 1995-1-1 (2015). As shown in Figure 3.36 (left), the aforementioned conditions have been realised in form of fixing the thread's end by clamping jaws and supporting the screw head with a cylindrical head adapter, especially manufactured for the specific (head-)geometry. The static system, given in Figure 3.36 (right), thus corresponds to a statically overdetermined, one-dimensional tensile bar. The load has thereby been applied monotonically by a vertical movement of the head's hinged support. The loading velocity varied between $0.3 \div 0.7$ mm/min (but stayed constant for each test) in order to reach the force maximum in the timeframe of 10 ± 5 s as proposed in ON EN 14592 (2012). All related experiments were performed on the test rig LIGNUM-UNI-275 (universal testing device, Zwick GmbH & Co. KG) at Graz University of Technology.

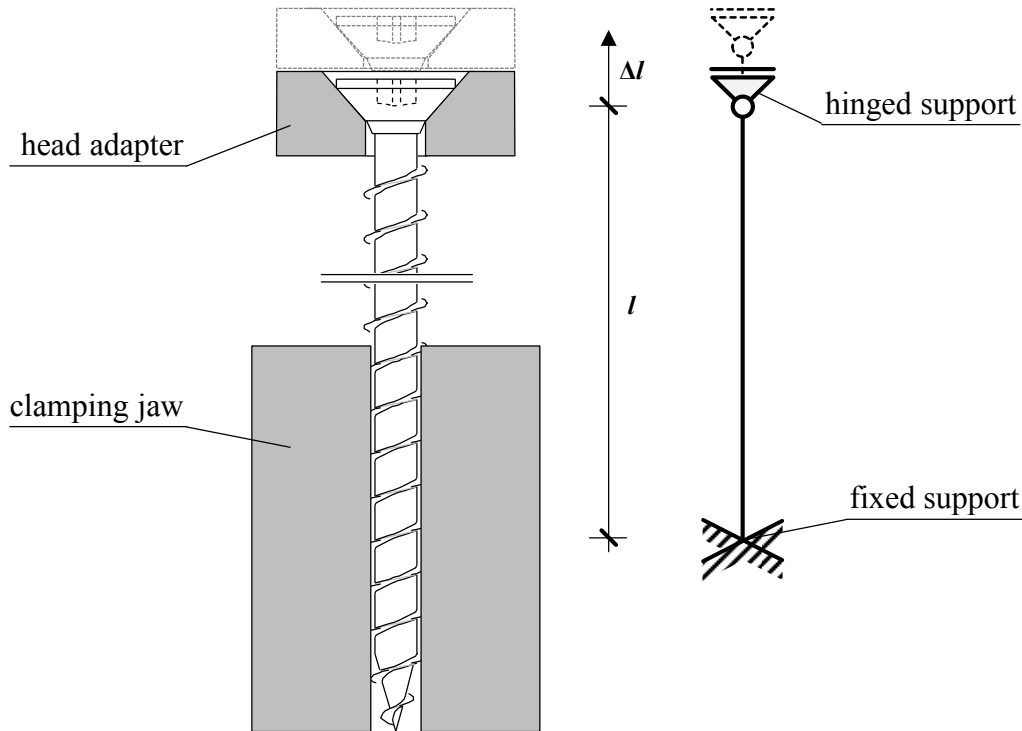


Figure 3.36: Screw axial tensile test according to ON EN 14592 (2012); left: schematic illustration of the test set-up; right: static system with load application in form of support movement

With regard to the data assessment, f_{tens} can be set equal to the maximum load recorded per test, F_{max} while the determination of F_y and D requires a more detailed explanation. In principle, various standards and publications, regarding the mentioned procedure, exist – a comprehensive review of corresponding literature is not part of this thesis, but can be found in Flatscher (2017). One applicable procedure bases on the standard ASTM E2126 (2002) and presupposes an elastic-ideal plastic material behaviour in form of the so-called equivalent energy elastic-plastic (EEEP) curve, which seems to be an adequate simplification for this type of (steel) product. Considering the boundary condition of equal areas A_i below both, the recorded and the ideal force-deformation relationship, F_y can be derived as follows:

$$F_y = K_{\text{ser}} \cdot \left(v_u - \sqrt{v_u^2 - \frac{2 \cdot A}{K_{\text{ser}}}} \right), \quad (3.74)$$

with v_u as the deformation at F_u , which is the force value of the last data point recorded but equal to or greater than $0.80 \cdot F_{\text{max}}$ and K_{ser} , here defined as the (spring) stiffness of the (assumed) linear-elastic part ($F = 0.1 \div 0.4 \cdot F_{\text{max}}$) of the experimentally determined force-deformation relationship, calculated by means of the linear regression analysis.

A simplification of the recorded curve by the ideal EEEP-curve is very similar to the procedure outlined in ON EN 12512 (2001), at least for those with pronounced linear conditions in their elastic and plastic

areas. Presupposing this circumstance for the results of the screw tensile tests, the main difference between both standards is a plastic gradient bigger than zero in case of ON EN 12512 (2001), while ASTM E2126 (2002) assumes a horizontal plastic plateau, as compared in Figure 3.37 (a) and (b).

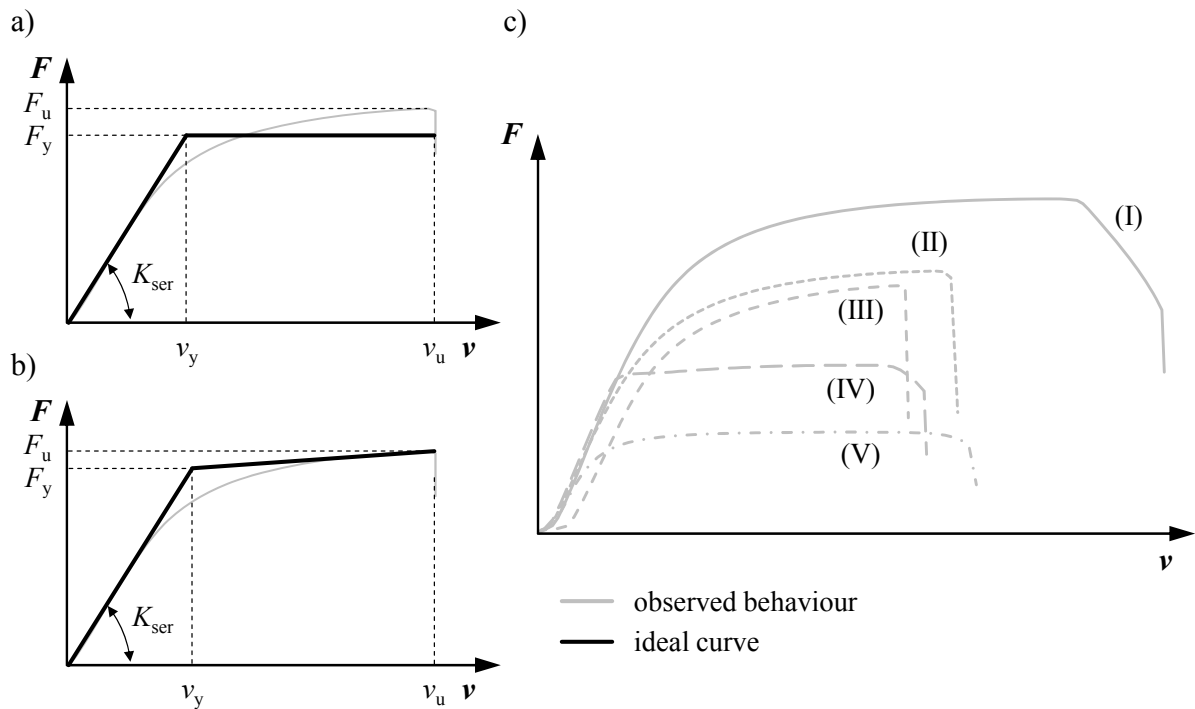


Figure 3.37: Determination of F_y and D for self-tapping screws loaded in tension; (a) according to ASTM E2126 (2002); (b) according to ON EN 12512 (2001); (c) illustration of five typical test curves observed

The maximum force of the ideal curve, according to ON EN 12512 (2001), is closely located to F_u and thus enables a more realistic description of the test curve's plastic area. Nevertheless, it was decided to determine F_y and consequently D , as the ratio between v_u and v_y in accordance to ASTM E2126 (2002). The main reason therefore is the clear definition of the area A below the test curve, allowing a more objective way of data assessment if compared to the (subjective) adjustment of the plastic gradient to the test curve recorded. Table 3.8 compares values of F_y and D of five representative screw tensile test curves (Figure 3.37, c), determined in accordance to both standards discussed. The differences between both procedures are below 5 %, indicating only a minor influence of the applied procedure, thus enabling the comparability with other sources using ON EN 12512 (2001) for data assessment.

Table 3.8: Comparison of properties F_y and D determined according to ON EN 12512 (2001) and ASTM E2126 (2002)

curve	ON EN 12512 (2001)		ASTM E2126 (2002)		$F_{y,2} / F_{y,1}$	D_2 / D_1
	$F_{y,1}$ [N]	D_1 [-]	$F_{y,2}$ [N]	D_2 [-]		
I	35,787	3.84	36,257	3.79	1.01	0.99
II	27,866	3.43	28,353	3.37	1.02	0.98
III	25,167	3.11	26,053	3.00	1.04	0.97
IV	18,786	4.18	18,904	4.15	1.01	0.99
V	11,182	4.82	10,954	4.92	0.98	1.02

1 = ON EN 12512 (2001), 2 = ASTM E2126 (2002)

Finally, it should be pointed out, that no local displacements were measured for the majority of tests listed in Table 3.5. Values v_i , applied for the determination of K_{ser} , F_y and D were those, recorded by the testing device (global way measurement). The corresponding influence on F_y and D is regarded as negligible, while the determined stiffness K_{ser} (also serving as indicator for E_s) was only considered for further comparisons, where l , defined as the free span length between both supports in Figure 3.36, has been kept constant.

3-4.4.4 Torsional test to determine f_{tor}

Tests to determine the product's torsional resistance f_{tor} have also been carried out in accordance to ON EN 14592 (2012), subsequently on the basis of ON EN ISO 10666 (2000). The only boundary conditions, which are given in this standard, are a fixed support at the thread's end, as well as an insertion device, which is able to measure the occurring torsional moments. The corresponding test set-up is illustrated in Figure 3.38 (left). Again, the end support is realised by clamping jaws, while the torsional moment is applied and recorded by an insertion engine. The static system is hereby assumed as an one-dimensional torsional bar, the load application as a support rotation about the product's x -axis, c. f. Figure 3.38 (right). In contrast to the explained axial tensile test, the data assessment solely included the torsional moment – the corresponding property f_{tor} was set equal to the maximum moment recorded.

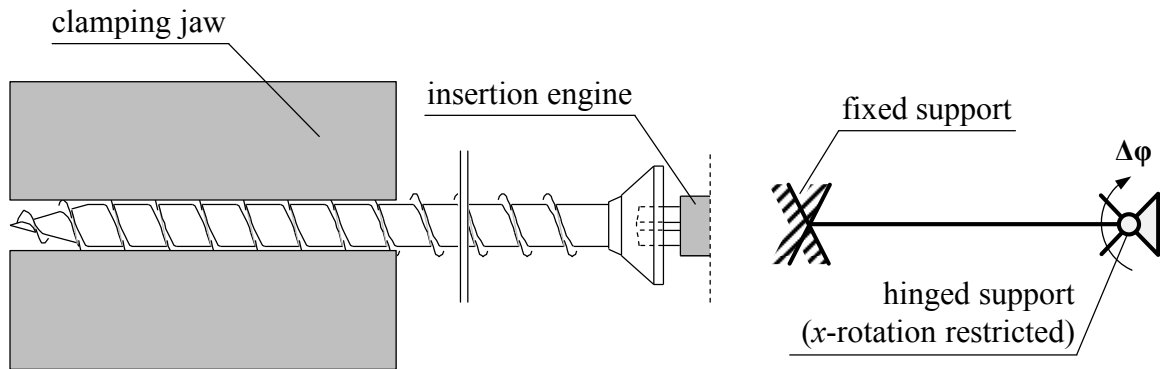


Figure 3.38: Screw torsional test according to ON EN 14592 (2012); left: schematic illustration of the test set-up; right: static system with load application in form of support rotation

3-4.4.5 Bending test to determine M_y

In contrast to the discussed test configurations, the set-up, applied at Graz University of Technology, for determining the fasteners' yield moment M_y , deviates from that proposed in ON EN 409 (2009), c. f. Figure 3.39. Worth mentioning, that for this purpose the related standard is referred by ON EN 14592 (2012), CUAP 06.03/08 (2010) and EAD 130118-00-0603 (2016). As shown in Figure 3.39, the screws cut with certain lengths and clamped by inner steel cylinders (dimensions vary in dependence of the fastener diameter) serve as the weakest part of this two-span beam system. Since the outer steel cylinder's moment of inertia is several times bigger than that of the screw cross-section, beam rotation $\Delta\varphi$ enforced by removing the dowel (right hinged support; movement seen as both support translation and rotation), solely occurs along the free span length l (commonly $3d$). The moment-rotation relationship M - φ , subsequently used for determining M_y , is gained by deriving M according to eq. (3.75) and φ by recording the beam rotation.

$$M = F \cdot a \cdot \left(1 - \frac{c}{b}\right), \quad (3.75)$$

with F as the force measured at the load cell, situated at the left hinged support, and a , b and c as the distances from the steel notch to the load cell, to the dowel and to the middle of the free span length l .

With regard to the data assessment, two values of M_y were determined for each test. One method thereby corresponds to the procedure applied for F_y , in form of a simplifying recorded M - φ relationship in accordance to ASTM E2126 (2002). The second approach bases on the considerations made in Blaß et al. (2000), who derived a reference relationship between M and φ by evaluating the test curves of steel dowels with varying diameters; see

$$M = M_{45} \cdot (0.866 + 0.00295 \cdot \varphi) \cdot \left[1 - \exp\left(\frac{-0.248 \cdot \varphi}{0.866}\right) \right], \quad (3.76)$$

with M_{45} as the moment recorded at a bending angle $\varphi = 45^\circ$. Consequently, M_y of this normalised M - φ relationship was determined for screws according to CUAP 06.03/08 (2010) at a plastic bending angle φ_{pl} defined in eq. (3.77) similar to the recommendation given in Steilner and Blaß (2014), see

$$\varphi_{pl} = \varphi_y + \frac{45}{d^{0.7}}, \quad (3.77)$$

with φ_y as the yield angle determined in accordance to ASTM E2126 (2002). For steel rods also tested in bending, the relationship given in ON EN 409 (2009) and eq. (3.78) was applied instead:

$$\varphi_{pl} = \varphi_1 \cdot \left(\frac{2.78 \cdot \rho_k}{f_u} \right)^{0.44} + \varphi_2, \quad (3.78)$$

with $\varphi_1 = 17.5^\circ$ as the basis rotation, $\rho_k = 350 \text{ kg/m}^3$ as the characteristic density of the timber product, wherein the fastener is located, assumed for solid timber with the strength class C24 according to ON EN 338 (2016), f_u as the tensile strength of the steel rod and φ_2 as an additional angle set to zero for this type of fastener.

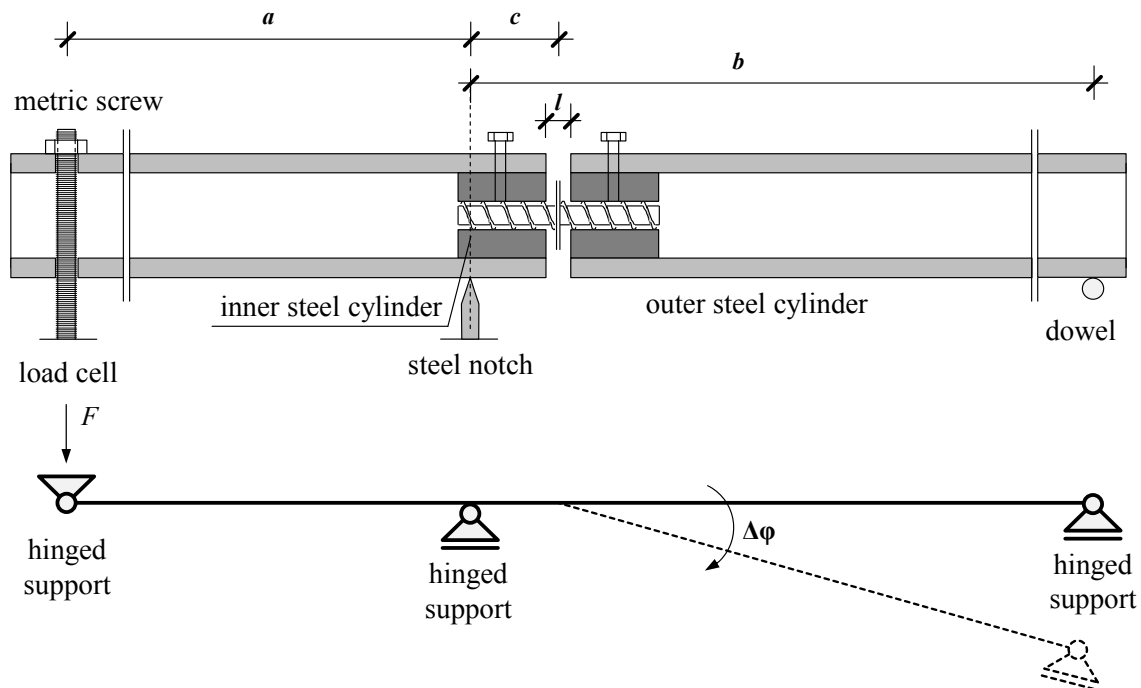


Figure 3.39: Screw bending test configuration applied at Graz University of Technology; above: schematic illustration of the test set-up; below: static system with load application in form of support translation and rotation

3-4.5 Mechanical screw properties

3-4.5.1 Introduction

Within this subsection, the theoretical assumptions concerning the mechanical modelling of screw product properties, made in section 3-4.3, and specific general relationships are verified with the test results gained from the experimental programme, which is explained in section 3-4.4. The cross-sectional properties, derived in section 3-4.3 and necessary for this verification, are given in Table 3.9 for the screw types considered within the experimental programme (c. f. Table 3.7). With regard to the elastic torsional section modulus, $W_{T,el}$, the corresponding values have been determined by the FE-based software package according to Bogensperger (2002), as a consequence of the stress peaks disabling an empirical estimation of this property, c. f. section 3-4.3.3. Since the screws referred to C_s_II_08_200 have not been tested in torsion, no related value was determined.

Table 3.9: Cross-sectional properties of screw types investigated in the experimental programme

product ID	general		tension		bending		torsion	
	A_s [mm ²]	z_s [mm]	$W_{el,y,min}$ [mm ³]	$A_{pl,N,emp}$ [mm ²]	$W_{el,z}$ [mm ³]	$W_{pl,z}$ [mm ³]	$W_{T,el,num}$ [mm ³]	$W_{T,pl,emp}$ [mm ³]
A_s_I-V_08_240	24.5	-0.47	17.7	21.2	14.6	25.6	21.2	46.2
A_s_II_08_180	24.9	-0.43	17.8	21.8	15.0	26.2	22.1	47.4
A_s_II_08_500	23.7	-0.52	17.1	20.0	13.8	24.0	18.0	43.2
A_s_II_10_500	38.5	-0.70	35.7	32.3	28.5	49.6	36.1	89.2
A_s_II_08_1000	24.6	-0.51	18.0	21.0	14.7	25.6	20.2	46.1
A_s_II_10_1000	38.6	-0.71	35.8	32.3	28.5	49.7	36.2	89.3
A_s_II_12_450	48.5	-0.89	51.2	39.9	39.4	68.9	46.9	124.2
B_s_II_08_300	24.1	-0.49	17.2	20.7	14.0	24.6	19.3	44.7
B_s_II_10_300	35.1	-0.54	29.8	30.6	24.8	43.6	30.7	79.2
B_s_II_12_300	51.1	-0.75	53.5	43.5	43.0	75.6	52.6	137.4
C_s_II_08_200	24.0	-0.49	17.3	20.6	14.1	24.7	-	44.5

Furthermore, the load configurations, applied for experimentally determining the mechanical screw properties f_{tens} and f_{tor} , have been simulated with the software package RFEM 5 (2012), by means of generating a three-dimensional full scale FE-model of one example screw thread with the reference geometry $\{d, p, v, \eta\} = \{8.0 \text{ mm}, 3.8 \text{ mm}, 40^\circ, 0.65\}$. As shown in Figure 3.40, the model consisting of altogether three thread turns is linked with two cylindrical parts at its ends. They shall homogenise the stress distribution between the screw and the location of loading and supporting.

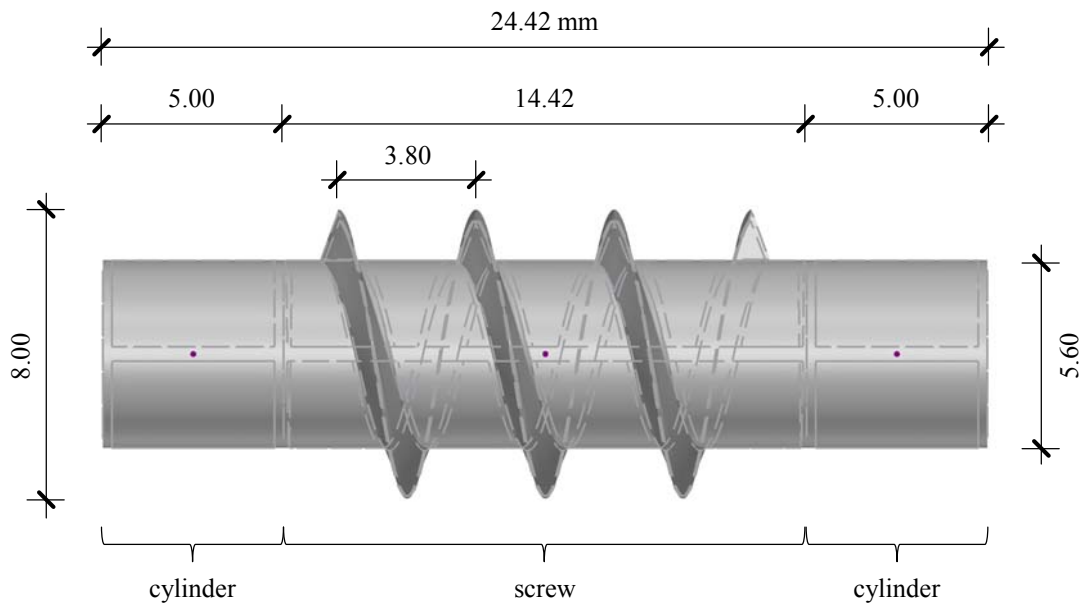


Figure 3.40: 3D full scale model of one example screw generated by the software package RFEM 5 (2012)

While for both cylindrical sections structural steel with a linear-elastic stress-strain relationship was applied as material, the corresponding behaviour of the threaded part was described by two elastic-plastic relationships, as shown in Figure 3.37 (a and b). The values assumed for stress and strain properties vary in dependence of the specific matter and are outlined in the following subsections. Worth mentioning, $E_s = 210,000 \text{ N/mm}^2$ and the von-Mises criterion for isotropic materials (interaction of volume stresses, see eq. (3.79), and strains) were applied for all considerations.

$$\sigma_v = \frac{1}{\sqrt{2}} \cdot \sqrt{(\sigma_x - \sigma_y)^2 + (\sigma_y - \sigma_z)^2 + (\sigma_x - \sigma_z)^2 + 6 \cdot (\tau_{xy}^2 + \tau_{xz}^2 + \tau_{yz}^2)}, \quad (3.79)$$

with σ_i and τ_{ij} , as normal and shear stresses in coordinate and plane directions $\{x, y, z\}$, and σ_v as the equivalent stress. With regard to FE-meshing, a combination of triangular and quadrangular 2D-elements as standard, provided by RFEM 5 (2012), has been applied, 3D-elements thus resulted to tetra-, penta- and hexahedrons. The model, shown in Figure 3.40, consists of up to 10^5 elements, each with a side length of 0.30 mm, found as minimum applicable to the specific situation.

3-4.5.2 Relationships between screw tensile properties and hardness

Firstly concentrating on the mechanical properties of self-tapping screws loaded in tension, the related test results in form of f_{tens} , F_y , their ratio f_{tens} / F_y and D as well as their corresponding coefficients of variation ($\text{CV}[X]$) are given in Table 3.10. Apart from product B_s_II_08_300, where two test results had to be excluded (production failure), the whole programme (outlined in Table 3.5) was considered for data assessment.

As shown in Table 3.4, hardening has been varied for screws denoted as A_s_I-V_08_240. With regard to the results related, procedures I and II led to significantly higher values for f_{tens} and F_y if compared to groups III and IV, which have been additionally tempered after hardening. The effect of carbonitriding (I and III) has no major impact on both properties, but decreases the ductility to some extent. The main reason therefore is an increase of brittleness in the cross-section's outer zones as a consequence of an enrichment of carbon in this area. Comparing unhardened (V) with hardened screws irrespective the specific procedure applied (I-IV), the major impact of this production step on product characteristics is demonstrated by significantly increasing the tensile capacities and yield loads, combined with a remarkable loss of ductility.

Focusing on screws with $d = 8$ mm, hardened by the standard procedure of the specific manufacturer (all II), remarkable differences regarding f_{tens} , F_y and D , not only between products of manufacturers A, B and C, but also in-between the different products of one manufacturer (see A_s_II_08_500 in case of f_{tens} and F_y) can be observed. While the former one has already been discussed in chapter 2 (section 2-2.5.5) and can be explained by differently adjusted hardening procedures, the latter mentioned and minor pronounced difference may also be caused by the surface discontinuities due to the forming process of the thread geometry (discussed in section 3-5.2 more in detail). Worth mentioning, that a negative relationship between f_{tens} and D , as a consequence of the varying hardening procedures by the manufacturers, can not be observed over all.

With regard to the deviation of the gained test results, expressed by $CV[X]$, the corresponding values for f_{tens} and F_y are consistently low and show no pronounced differences indicating a dependency on one of the aforementioned influencing parameters. The only exceptions are unhardened screws (A_s_V_08_240), where significantly higher coefficients of variation can be observed. The hardening is thus expected to homogenise the material. A remarkably higher CV for ductility if compared to that of f_{tens} and F_y can partially be explained by inaccuracies in determining this property.

Table 3.10: Mean values and coefficients of variation of screw tensile properties

product ID	n	f_{tens} [N]	CV[f_{tens}] [%]	F_y [N]	CV[F_y] [%]	f_{tens} / F_y [-]	D [-]	CV[D] [-]
A_s_I_08_240	15	29,000	0.56	26,402	0.75	1.10	3.00	4.01
A_s_II_08_240	10	30,455	0.45	27,966	1.01	1.09	3.45	5.13
A_s_III_08_240	5	19,859	0.44	19,464	0.93	1.02	2.48	8.30
A_s_IV_08_240	15	19,590	0.48	18,863	0.71	1.04	4.55	8.42
A_s_V_08_240	5	11,852	3.64	11,315	3.68	1.05	6.61	10.36
A_s_II_08_180	5	29,295	0.26	27,227	0.51	1.08	2.71	8.94
A_s_II_08_500	11	26,812	0.75	24,855	1.07	1.08	2.44	8.66
A_s_II_10_500	11	45,280	0.16	40,425	0.49	1.12	3.38	1.47
A_s_II_12_450	12	51,863	0.91	45,584	1.17	1.14	2.39	4.17
B_s_II_08_300	11	23,661	1.45	22,075	1.48	1.07	1.96	11.58
B_s_II_10_300	6	30,885	1.10	29,960	2.66	1.03	1.55	4.49
B_s_II_12_300	3	53,938	0.57	51,811	1.57	1.04	1.70	6.62
C_s_II_08_200	5	23,366	0.94	22,366	1.40	1.04	2.80	8.05

With regard to the derivations, conducted in section 3-4.3.4, the bearable normal force in state of full plasticity, N_{pl} , can be determined as a product of $A_{\text{pl,N}}$ and the yield strength of the material, f_y , see

$$N_{\text{pl}} = f_y \cdot A_{\text{pl,N}}, \quad (3.80)$$

Presupposing $N_{\text{pl}} = F_y$ (according to Table 3.10) and considering $A_{\text{pl,N,emp}}$, according to Table 3.9, eq.(3.80) enables approximating the yield strength of tensile tested self-tapping screws. The corresponding values of f_u , defined as the steel tensile strength related to f_{tens} , can be subsequently estimated by eq. (3.81), see

$$f_u = \frac{f_{\text{tens}}}{F_y} \cdot f_y. \quad (3.81)$$

The verification of both models, eq. (3.80) and eq. (3.81), is consequently enabled by comparing the corresponding results with those of the wire rods A_r_I-V_08_240, which served as a basis material for the production of A_s_I-V_08_240. They were hardened with the same configurations and therefore they should have the same strength properties. In contrast to the screw thread profile their circular cross-section enables a simple determination of $\{f_y, f_u\}$ as the ratios between $\{F_y, F_u\}$ and their cross-sectional area A_d with $d = 5.76$ mm (see Table 3.7). In Table 3.11 and Figure 3.41 the experimentally determined values of self-tapping screws' steel tensile and yield strength (results of wire rods) are compared with the

model predictions, determined according to eq. (3.80) and eq. (3.81). The model assumptions, made in section 3-4.3.4, base on simplifications regarding material behaviour and geometry (screw is assumed as prismatic beam). Nevertheless, the estimated values are closely located to the test results in case of groups I-IV, indicating an appropriate prediction of both mechanical properties by the aforementioned theoretical approaches. One reason for slightly underestimating all corresponding values are the surface discontinuities caused by thread rolling, which can decrease A_s and consequently $A_{pl,N}$ to some extent, c. f. section 3-5.2. With regard to A_s_V_08_240, the predicted values are significantly higher than the experimental results. A reason therefore is a difference between the hardness of screws and the wire rods of this group – the former significantly increased by cold work hardening due to thread rolling (see section 3-3.2).

Table 3.11: Comparison of experimentally determined and predicted values for f_u and f_y

product ID	$F_{u,exp}$ [N]	$f_{u,exp}$ [N/mm ²]	$f_{u,pred}$ [N/mm ²]	Δ [%]	$F_{y,exp}$ [N]	$f_{y,exp}$ [N/mm ²]	$f_{y,pred}$ [N/mm ²]	Δ [%]
A_s_I_08_240	36,426	1,398	1,368	-2.1	33,856	1,299	1,245	-4.1
A_s_II_08_240	38,817	1,490	1,437	-3.6	36,323	1,394	1,319	-5.4
A_s_III_08_240	25,531	980	937	-4.4	24,603	944	918	-2.8
A_s_IV_08_240	24,678	947	924	-2.4	23,882	916	890	-2.9
A_s_V_08_240	12,270	471	559	18.7	11,495	441	534	21.0

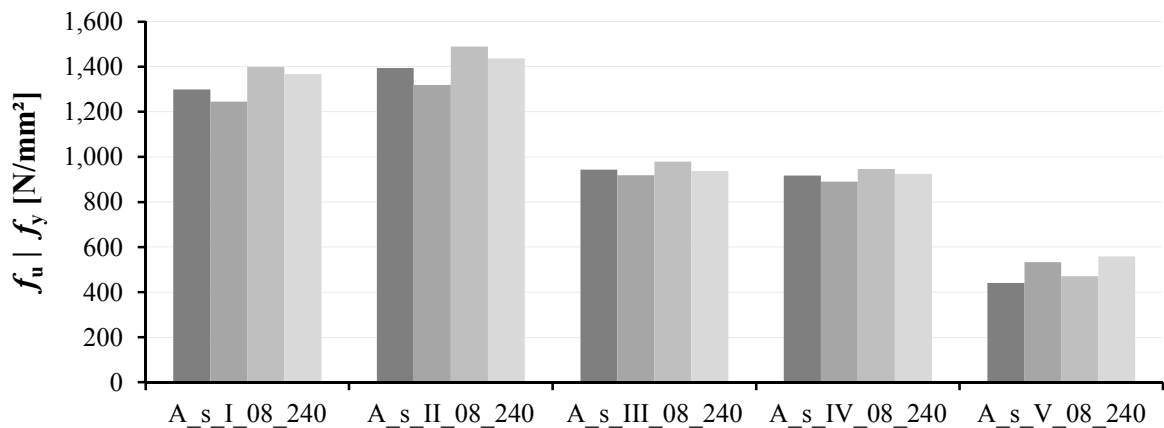


Figure 3.41: Comparison of experimentally determined and predicted values for f_u and f_y

In Figure 3.42, the normal stress (σ_x) distribution, due to an axially applied force F_y , determined by the constitution between $A_{pl,N}$, f_y and N_{pl} , derived in section 3-4.3.4, is compared with the one of the corresponding numerical simulation. Therefore, the defined material was linear-elastic/plastic (Figure 3.37, a) with constant plateau and $\max[\sigma_v] = f_y = 1,320$ N/mm². This is similar to the yield strength, predicted by eq. (3.80) for group A_s_II_08_240, c. f. Table 3.11. Since $A_{pl,N}$ for the reference cross-

section is slightly higher than that of A_s_II_08_240, $F_y = 28.75$ kN was applied instead of the experimentally determined value for this product group, c. f. Table 3.10.

It has to be pointed out, that both cross-sectional shapes in Figure 3.42 are quite equal. In general this confirms the mathematical description of the screw geometry given in section 3-4.2. Furthermore, both distributions are qualitatively similar in compressive stresses occurring at the thread's chamfer and tensile stresses in the inner thread cylinder's area. The analytical approach assumes full plasticity leading to an abrupt change of the stress sign at $\varphi = \varphi_2$. In contrast, the numerical simulation results in a more gradual relationship. With regard to the quantitative values, both stress distributions in the tensioned zone are widely comparable, while numerically determined compressive stresses are significantly lower than the analytical solution, see Figure 3.43 (left). The assumption of the screw's threaded part as a prismatic beam, in section 3-4.3, is seen as main reason causing this high deviation.

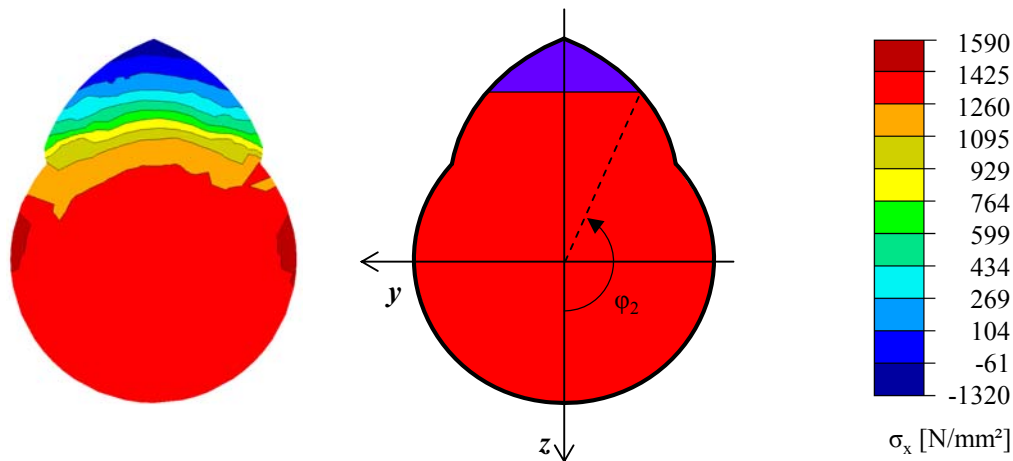


Figure 3.42: Comparison of analytically (middle) and numerically (left) determined normal stress distributions at the screw thread profile in case of $N = N_{p1}$ and $\{d, \eta, v, p\} = \{8.00 \text{ mm}, 0.65, 40^\circ, 3.80 \text{ mm}\}$

Figure 3.43 (right) compares the force-displacement curves determined by the FE-model for the aforementioned axial load situation with the analytical model predictions of f_{tens} and F_y . The material was thereby assumed to behave linear-elastic/plastic, one with constant plateau and $\max[\sigma_v] = f_y = 1,320$ N/mm² and the other with increasing plastic stresses from $f_y = 1,320$ N/mm² to $\max[\sigma_v] = f_u = 1,440$ N/mm², reached at $\epsilon_u = D \cdot \epsilon_y$. Again, both latter properties, f_u and D , were set equal to the related results of group A_s_II_08_240.

With regard to the location of both curves, slightly higher FE-results if compared to the analytical solutions can be observed. In case of the approach, considering plastic stress increase, the maximum bearable normal force results to $f_{\text{tens,num}} = 34.85$ kN. The difference to $f_{\text{tens,exp}}$ of group A_s_II_08_240 is about 14 %. So, the numerical simulation overestimates the real behaviour to a certain extent.

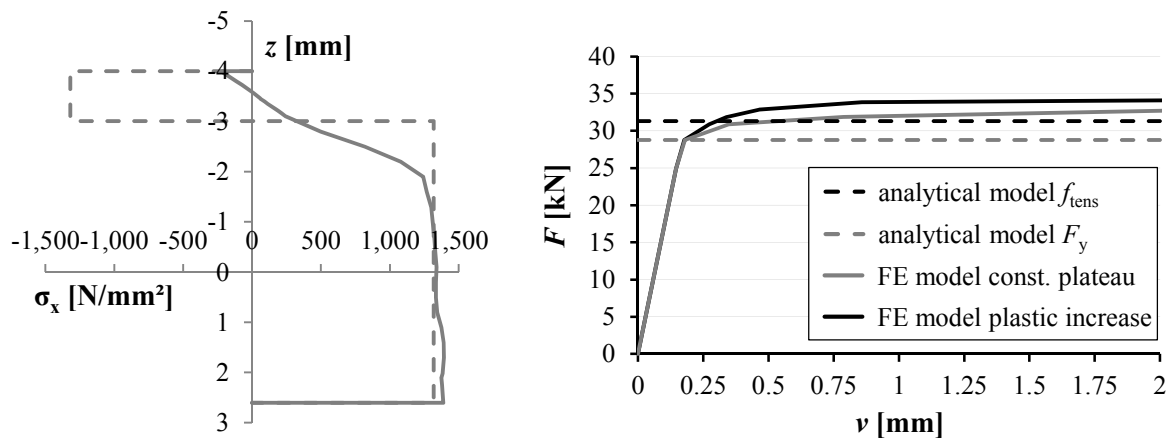


Figure 3.43: Left: analytically and numerically determined normal stress distributions at $y = 0$ and $N = N_{pi}$; right: numerically determined force-displacement curves for the screw thread loaded in tension

Now concentrating on steel hardness according to Vickers (HV1), as a property also determined within the experimental programme for selected types of screws, c. f. Table 3.6. For comparing hardness values and distributions in dependence of the hardening procedure applied, Toblier (2014) analysed one screw of each group A_s_I-IV_08_240 according to ON EN ISO 6507-1 (2004). In order to obtain knowledge concerning the variation of this property, as well as to identify the deviations between the screws from different manufacturers, hardness values and distributions of six screws related to A_s_II_08_240 and one screw/rod of each group (listed in Table 3.6, lines 5 ÷ 10) were determined at the Institute of Material Science, Joining and Forming at Graz University of Technology, within additional campaigns.

Thereby gained results are given in Table 3.12, while Figure 3.44 shows location and course of A_s_I-IV_08_240 over the screw thread profile. As expected and shown on the illustrations, tempering and carbonitriding have a significant impact on the steel hardness. Thereby, the influence of tempering can be observed in form of a constant negative shift of the (more or less) homogenous hardness distribution of sample A_s_II_08_240, hardened by the standard procedure of manufacturer A (without tempering and carbonitriding). In contrast, the carbonitriding has no effect on the profile's inner zones, but significantly modifies the surface hardness, leading to a progressive increase with an increasing distance to the cross-section's gravity centre.

Comparing the hardness values of A_s_I-IV_08_240 with the ones of A_s_V_08_240 (in Table 3.12), the expected and significant increase as a consequence of the hardening can be observed. Unfortunately, all measurements dedicated to Table 3.6, lines 5 ÷ 10 (A_s_V_08_240, B_s_II_08_300, C_s_II_08_300, A_r_I_08_240, A_r_II_08_240 and A_r_V_08_240) only comprised the hardness determination in the fasteners' inner zones, disabling the illustration of A_s_V_08_240 in Figure 3.44. This also explains the almost equal values found for A_s_V_08_240 (cold formed due to thread rolling) and A_r_V_08_240

(untreated) as well as the significant difference between A_s_I_08_240 and A_r_I_08_240. Especially with regard to A_s_II_08_240 vs. A_r_II_08_240, the aforementioned assumption, quite equal hardness for screws and rods, necessary for the comparison illustrated in Figure 3.41, can be confirmed.

With regard to the difference of the hardness between the screws from different manufacturers A, B and C (all II), considerably lower values for C_s_II_08_200 if compared to A_s_II_08_240 and B_s_II_08_240 are given. This is in fact surprising, since it contradicts the related results of f_{tens} (Table 3.10). One reason therefore may be a possibly different hardness distribution of the outer zones of B_s_II_08_240 and C_s_II_08_240, not determined within this experimental campaign.

Table 3.12: Hardness HV1 determined for the screws and rods listed in Table 3.6

product ID	mean[HV]	product ID	mean[HV]
A_s_I_08_240	592	A_r_I_08_240	466
A_s_II_08_240	452	A_r_II_08_240	474
A_s_III_08_240	382		
A_s_IV_08_240	300		
A_s_V_08_240	162	A_r_V_08_240	171
B_s_II_08_300	440		
C_s_II_08_200	353		

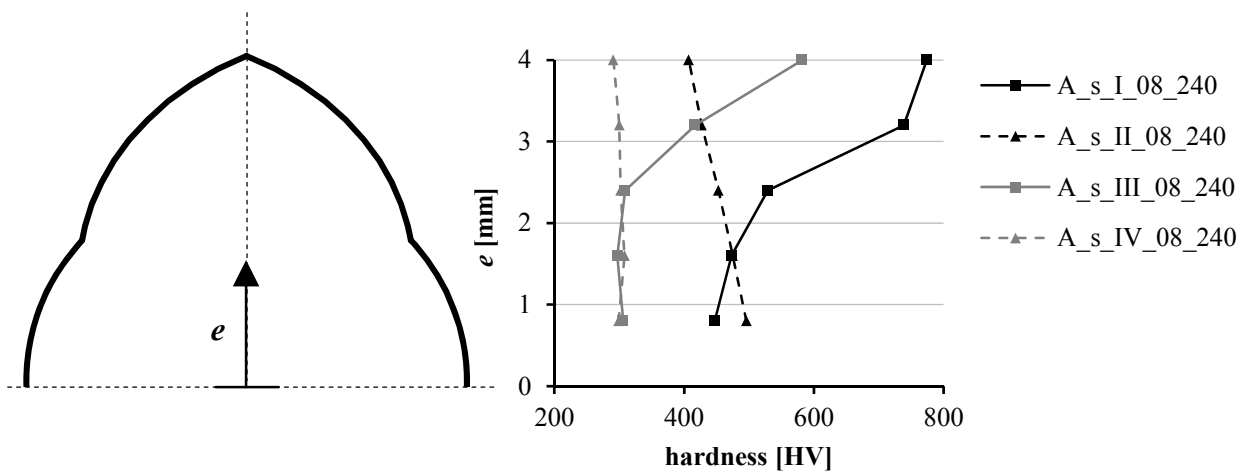


Figure 3.44: Varying hardness distributions over the screw thread profile determined by Toblier (2014) for product IDs A_s_I-IV_08_240

Now concentrating on the variability of hardness within the cross-section and between the different samples of one screw charge of product type A_s_II_08_240. The corresponding results are shown in Table 3.13 and Annex B-2.1, Figure B.3, the latter generally confirming the constant hardness distribution observed for this product group by Toblier (2014). Nevertheless it is worth mentioning, that the measured

values result between 341 HV and 515 HV, indicating a high variability of this property over the screw profile, which is also expressed by comparatively high coefficients of variation determined, see Table 3.13. With regard to the whole test series, where the average hardness of each profile has been considered, a comparatively smaller variability can be observed.

Table 3.13: *Main statistics of hardness HV1 of product ID A_s_II_08_240*

specimen	min[HV]	max[HV]	mean[HV]	CV[HV]
AL	349	491	415	11.4 %
7	341	443	394	7.91 %
11	357	515	440	12.4 %
12	359	468	416	9.19 %
20	331	439	391	10.4 %
28	351	477	393	11.6 %
mean			408	
CV			4.72 %	

The positive correlation between steel hardness and other mechanical properties is a well-known fact reported in literature, see e. g. ON EN ISO 18265 (2004), and can also be observed comparing the results of Table 3.10 and Table 3.12. Since the determination of hardness is a non-destructive test method, it can be applied for estimating the steel tensile strength, especially of those structural members, where direct (destructive) testing is hardly realisable. The translation between hardness and tensile strength is commonly carried out according to related standards, e. g. ON EN ISO 18265 (2004), wherein this relationship is provided for the specific steel product in a tabular form. In case of self-tapping screws, a conversation can be carried out according to Annex B of this standard, which includes a table for steels applied for quenching and tempering.

In case of product groups A_r_I_08_240, A_r_II_08_240 and A_r_V_08_240, both properties, tensile strength and hardness, are available enabling a verification of this relationship. Table 3.14 thus includes a comparison of experimentally determined tensile strengths, $f_{u,exp}$ with $f_{u,est}$, as those estimated according to ON EN ISO 18265 (2004) (note: for the unhardened rod A_r_V_08_240, Annex A was applied). With regard to A_r_I_08_240 and A_r_II_08_240, a negligible deviation between $f_{u,exp}$ and $f_{u,est}$ can be observed, while $f_{u,est}$ significantly overestimates the test result in case of A_r_V_08_240. Worth mentioning, that also the latter difference still lies within the scatter range of ± 85 N/mm² expressed in ON EN ISO 18265 (2004). Nevertheless, the results underline the statement given in this standard, that the hardness should only be seen as an indicator for the tensile strength and should not replace the direct (mechanical) test.

Table 3.14: Comparison of experimentally determined and estimated screw tensile strengths f_u of $A_r_I_{08_240}$, $A_r_{II_{08_240}}$ and $A_r_V_{08_240}$

product ID	$f_{u,exp}$ [N/mm ²]	HV	$f_{u,est}$ [N/mm ²]	Δ [%]
$A_r_I_{08_240}$	1,398	466	1,448	3.5
$A_r_{II_{08_240}}$	1,490	474	1,472	-1.2
$A_r_V_{08_240}$	471	171	548	14.1

3-4.5.3 Relationship between screw tensile and torsional properties

Now focusing on the mechanical behaviour of self-tapping screws loaded in torsion. The mean values and coefficients of variation determined for the tested screw products (see Table 3.5) are given in Table 3.15. The whole dataset has been considered for the assessment.

With regard to the varying hardening procedures, the effect of tempering (III and IV) has again a major negative influence on the achievable torsional strength. In contrast to the steel tensile properties, given in Table 3.10, the size of f_{tor} additionally depends on carbonitriding in form of an increase of roughly 10 % (I and III) if compared to screws, where this procedure was not applied (II and IV). The main reason therefore is strengthening the cross-section's surface zones (c. f. Figure 3.44), which gains more relevance as a consequence of an increasing influence of the cross-sectional dimensions on this mechanical property. Comparing the torsional strengths of product group II with $d_{nom} = 8$ mm, relative deviations between products of different manufacturers and also in-between products of one manufacturer are similar to those discussed in section 3-4.5.2 and probably caused by the same effects. The variability of the determined results is again comparatively low for the majority of the test series. The only exception is $B_s_{II_{12_300}}$, where a remarkably higher value for $CV[f_{tor}]$, in fact atypical for steel products, can be observed. Note: a visible production failure could not be detected, during the analysis of the corresponding specimen.

In Table 3.15, also the values of $f_{tor,el,pred}$ and $f_{tor,pl,pred}$ as torsional strengths predicted by applying mechanical constitutions, derived in section 3-4.3, are given. A corresponding determination was thereby carried out according to eq. (3.82) and eq. (3.83), see

$$f_{tor,el,pred} = W_{T,el,num} \cdot \tau_{T,y}, \quad (3.82)$$

$$f_{tor,pl,pred} = W_{T,pl,emp} \cdot \tau_{T,y}, \quad (3.83)$$

with $\tau_{T,y}$ defined as the torsional shear strength when σ_v according to eq. (3.79) is equal to f_y . In case of a one-dimensional and prismatic structural member, as assumed for the screw in section 3-4.3 and the pure uniform torsion, the components $\{\sigma_i, \tau_{ij}\}$ in eq. (3.79) result to $\{\sigma_i, \tau_{yz}\} = 0$, as well as

$$\tau_T = \tau = \sqrt{\tau_{xy}^2 + \tau_{xz}^2} . \quad (3.84)$$

Consequently, $\tau_{T,y}$ can be determined according to eq. (3.85), see

$$\tau_{T,y,\text{pred}} = \frac{f_{y,\text{pred}}}{\sqrt{3}} , \quad (3.85)$$

with $f_{y,\text{pred}}$ as the ratio between F_y according to Table 3.10 and $A_{pl,N}$ according to Table 3.9.

Focusing on the suitability of eq. (3.82) for estimating the experimentally determined $f_{\text{tor,exp}}$, major deviations between the latter mentioned and f_{tor} predicted by this linear-elastic model, are given. In fact, the test results are significantly underestimated by this approach. In contrast and irrespective of the varying parameters, the determined $f_{\text{tor,pl,pred}}$ correspond far better to the test results, see also Figure 3.45. The sole exception is product group B_s_II_10_300, a reason for the significant difference related is rather seen in the questionable reliability of test results, than in the model prediction.

Table 3.15: Comparison of experimentally determined and predicted values for f_{tor} (mean values)

product ID	n	$f_{\text{tor,exp}}$ [Nm]	CV[$f_{\text{tor,exp}}$] [%]	$f_{\text{tor,el,pred}}$ [Nm]	Δ [%]	$f_{\text{tor,pl,pred}}$ [Nm]	Δ [%]
A_s_I_08_240	5	35.73	0.48	15.24	-57.3	33.22	-7.0
A_s_II_08_240	10	32.85	1.47	16.15	-50.8	35.19	7.1
A_s_III_08_240	5	23.02	1.32	11.24	-51.2	24.49	6.4
A_s_IV_08_240	5	21.38	0.22	10.89	-49.1	23.73	11.0
A_s_II_08_500	10	28.71	0.95	12.92	-55.0	31.00	8.0
A_s_II_10_500	12	61.59	0.75	26.08	-57.6	64.45	4.6
A_s_II_12_450	12	85.53	0.98	30.94	-63.8	81.92	-4.2
B_s_II_08_300	10	26.88	3.04	11.88	-55.8	27.52	2.4
B_s_II_10_300	10	44.11	1.57	17.35	-60.7	44.77	1.5
B_s_II_12_300	10	79.19	13.83	36.17	-54.3	94.48	19.3

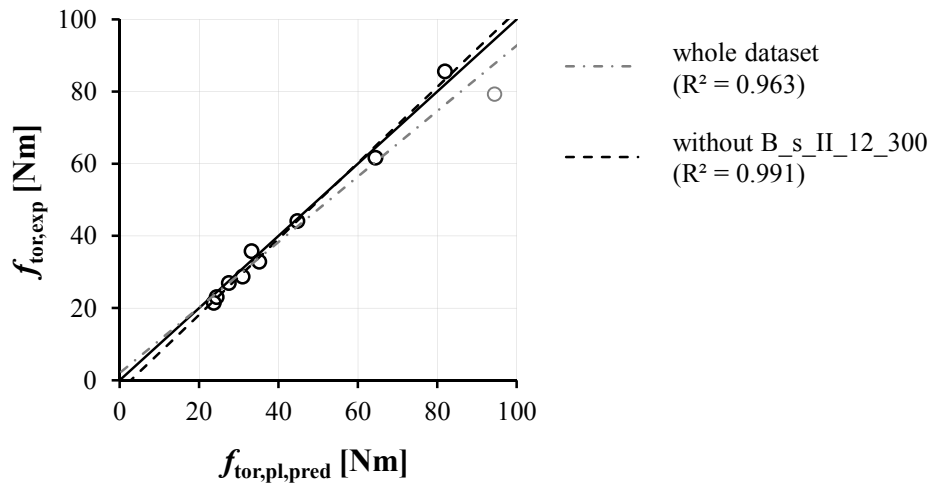


Figure 3.45: Comparison of experimentally determined and predicted values for f_{tor}

Due to the given model uncertainties (estimation of f_y by eq. (3.80), ideal plastic material behaviour, prismatic 1D beam vs. 3D structure, disregarding the non-uniform torsion, caused by the shape of the cross-sectional profile and the applied test configuration, which restricts free movement in x -direction, etc.), eq. (3.83) has to be only seen as an approximation to the real behaviour. Nevertheless, an appropriate prediction of the screw's threaded part's torsional strength can be achieved.

Figure 3.46 compares the moment-rotation curves, determined by the FE-model for the screw thread loaded in torsion with the analytical model prediction for f_{tor} according to eq. (3.83). Thereby, the material was assumed equal to section 3-4.5.2, simulating the screws related to group A_s_II_08_240. In contrast to tensile loading, the analytically determined value for f_{tor} is slightly higher than both numerical solutions, which result to $f_{tor,num} = 33.0$ Nm (const. plastic plateau) and $f_{tor,num} = 34.6$ Nm (plastic stress increase) respectively and are thus closer located to $f_{tor,exp}$, determined for this product group.

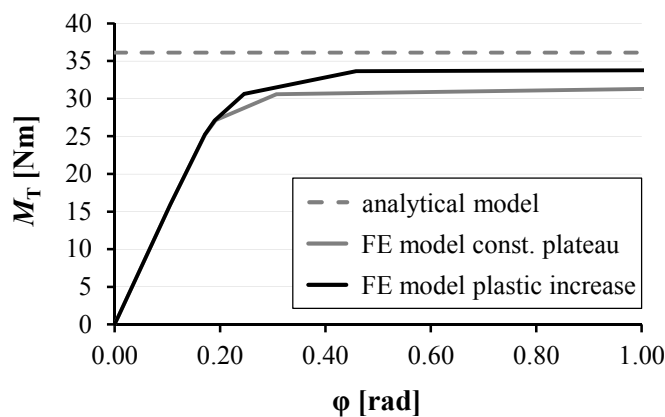


Figure 3.46: Numerically determined moment-rotation curves for the screw thread loaded in torsion

3-4.5.4 Relationship between screw tensile and bending properties

With regard to the yield moment of screw threads gained from the bending tests, as described in section 3-4.4.5, the corresponding statistical parameters of the experimental campaign (Table 3.5) are shown in Table 3.16. Altogether four screws related to product groups A_s_III_08_240 and B_s_II_12_300 failed in bending before a rotation angle $\varphi = 45^\circ$ has been reached. Consequently, the yield moments $M_{y,CUAP}$, according to the second method described in section 3-4.4.5, could not be determined for these specimen. In case of $M_{y,EEEP}$, according to ASTM E2126 (2002), which is independent from φ_{45} , the whole dataset was used for assessment.

Concentrating on the size of the mean values of both methods, the results are found in a similar range ($\Delta_{\max} = 6.0\%$), indicating that $M_{y,EEEP}$ according to ASTM E2126 (2002) is comparable to the standard procedure, currently applied for this purpose. Similar to the torsional moment, discussed in section 3-4.5.3, the hardening has a major impact on the size of the mechanical property – this again in form of significantly smaller M_y of tempered screws (III and IV) and higher M_y as a consequence of carbonitriding (I and III). The deviations between yield moments of different manufacturers A, B and C, as well as those between one manufacturer are also given and comparably pronounced than those found for the torsional moment in section 3-4.5.3. In contrast to tensile and torsional strength properties, the yield moments show a higher variability ($CV[M_{y,i}]$), irrespective the method applied for the determination. The overall maximum is again found for B_s_II_12_300, which can be additionally caused by the small number of tests.

Table 3.16: Mean values and coefficients of variation of screw bending properties

product ID	<i>n</i>	$M_{y,EEEP}$ [Nm]	$CV[M_{y,EEEP}]$ [%]	<i>n</i>	$M_{y,CUAP}$ [Nm]	$CV[M_{y,CUAP}]$ [%]	Δ [%]
A_s_I_08_240	3	33.7	2.17	3	32.6	1.81	3.5
A_s_II_08_240	3	30.3	1.55	3	30.6	1.27	-1.0
A_s_III_08_240*	3	25.0	3.74	0	-	-	-
A_s_IV_08_240	3	20.9	7.64	3	19.9	4.22	5.1
A_s_V_08_240	3	13.8	5.57	3	13.3	6.20	3.7
A_s_II_08_1000	12	32.1	6.02	12	32.1	4.84	-0.2
A_s_II_10_1000	12	57.8	3.48	12	56.8	2.26	1.7
A_s_II_12_450	14	83.0	2.76	14	79.6	2.93	4.3
B_s_II_08_300	3	27.6	1.06	3	26.6	1.51	3.5
B_s_II_10_300	3	45.1	2.19	3	42.6	1.30	6.0
B_s_II_12_300*	3	79.7	5.81	2	79.3	14.20	0.5

* screws failed in bending before φ_{45} has been reached.

In Table 3.17 and Figure 3.47, the deviations between experimentally determined yield moments $M_{y,EEEP}$ and $M_{y,CUAP}$ and those derived by eq. (3.86) and eq. (3.87) are illustrated. Equal to the torsional capacity, discussed in section 3-4.5.3, a linear-elastic and an ideal-plastic approach served for theoretically predicting this property.

$$M_{y,el,pred} = W_{el,z} \cdot f_{y,pred} \text{ , and} \quad (3.86)$$

$$M_{y,pl,pred} = W_{pl,z} \cdot f_{y,pred} \text{ ,} \quad (3.87)$$

with $f_{y,pred}$ as the ratio between F_y according to Table 3.10 and $A_{pl,N}$ according to Table 3.9.

Since in case of screws related to A_s_II_08/10_1000 no tensile test has been conducted, the corresponding values for $f_{y,pred}$ from A_s_II_08/10_500 have been applied instead. Evaluating the predictability of both theoretical approaches, given in eq. (3.86) and eq. (3.87), a significant underestimation of the linear-elastic solution can be observed, while the model presupposing ideal-plastic material conditions widely corresponds to the test results. Even though the deviations between model and experiment are slightly higher than those found for the torsional capacity (c. f. section 3-4.5.3), an adequate description of the overall data-trend is given, and in fact irrespective from the method of determining the experimental yield moment, c. f. Figure 3.47.

Table 3.17: Differences between experimentally and analytically determined yield moments

product ID	$M_{y,el,pred}$ [Nm]	Δ_{EEEP} [%]	Δ_{CUAP} [%]	$M_{y,pl,pred}$ [Nm]	Δ_{EEEP} [%]	Δ_{CUAP} [%]
A_s_I_08_240	18.2	-46.1	-44.2	31.9	-5.4	-2.1
A_s_II_08_240	19.3	-36.3	-37.0	33.8	11.6	10.5
A_s_III_08_240	13.4	-46.3	-	23.5	-5.9	-
A_s_IV_08_240	13.0	-37.9	-34.7	22.8	9.0	14.5
A_s_V_08_240	7.8	-43.7	-41.6	13.7	-1.2	2.5
A_s_II_08_1000	18.3	-43.1	-43.2	31.8	-0.9	-1.0
A_s_II_10_1000	35.7	-38.3	-37.2	62.2	7.7	9.5
A_s_II_12_450	45.0	-45.8	-43.5	78.7	-5.2	-1.2
B_s_II_08_300	14.9	-45.8	-43.9	26.2	-4.8	-1.4
B_s_II_10_300	24.3	-46.2	-43.0	42.7	-5.3	0.3
B_s_II_12_300	51.2	-35.7	-35.4	90.0	13.0	13.6

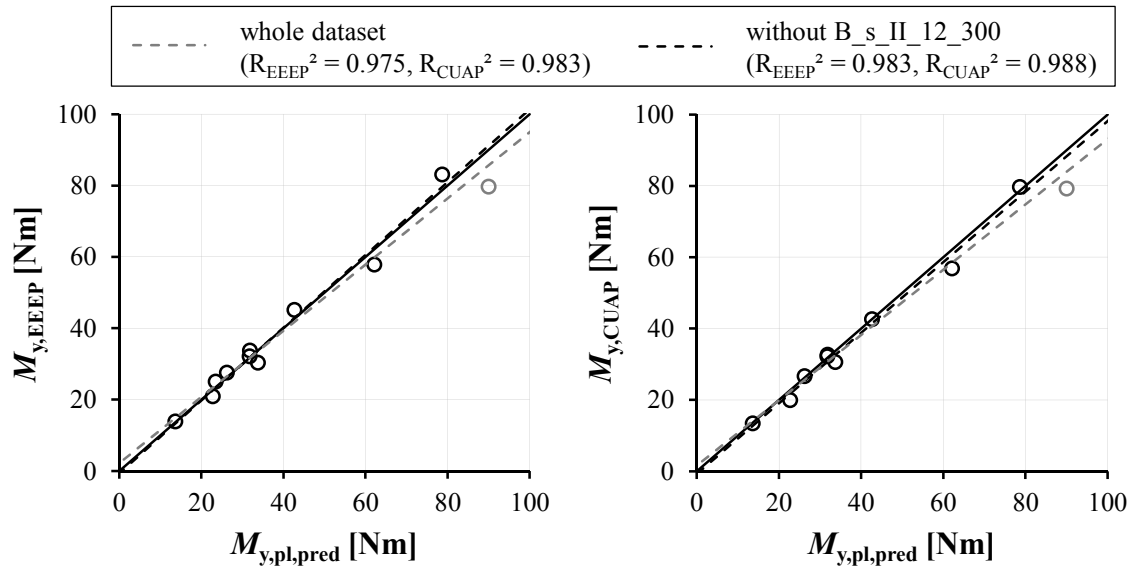


Figure 3.47: Comparison of experimentally determined and predicted values for M_y ; left: M_y determined according to ASTM E2126 (2002); right: M_y determined according to Blaß et al. (2000) and CUAP 06.03/08 (2010)

In addition to the screws tested in bending, also M_y of wire rods, serving as the base material for the production of groups A_s_I-V_08_240 has been determined within the experimental campaign. The corresponding results are shown in Table 3.18, indicating higher deviations between both assessment methods according to ASTM E2126 (2002) and ON EN 409 (2009) than observed for the screws in Table 3.16. With regard to the results, the influence of hardening again leads to significantly different M_y for groups I-V.

Furthermore, test results are compared with model predictions according to eq. (3.88), which have been derived by Blaß and Colling (2015) for determining the yield moment of dowels loaded in bending. In case of $f_u > 450 \text{ N/mm}^2$, $M_{y,pl,pred}$ is as follows:

$$M_{y,pl,pred} = \frac{0.9 \cdot f_u \cdot d^3}{6}, \quad (3.88)$$

with f_u as experimentally determined tensile strengths of the wire rods, according to Table 3.14. If compared to the model verification for screw tests, given in Table 3.17, higher deviations between theoretical predictions and test results can be observed. Possible reasons therefore are the small number of tests as well as the estimation of an effective yield strength f_y by $0.9 \cdot f_u$ in eq. (3.88), which underestimates the corresponding, experimentally determined properties to some extent, c. f. Table 3.14.

Table 3.18: Differences between experimentally and analytically determined yield moments of steel wire rods

product ID	n	$M_{y,EEEP}$ [Nm]	$M_{y,EN408}$ [Nm]	Δ [%]	$M_{y,pl,pred}$ [Nm]	Δ_{EEEEP} [%]	Δ_{EN408} [%]
A_r_I_08_240	1	47.5	47.1	0.9	40.1	-15.7	-14.9
A_r_II_08_240	1	45.0	43.5	3.5	42.7	-5.2	-1.8
A_r_III_08_240	1	33.9	31.0	9.2	28.1	-17.0	-9.4
A_r_IV_08_240	1	25.1	28.3	-11.4	27.1	8.2	-4.1
A_r_V_08_240*	2	13.1	14.2	-7.6	13.5	2.7	-5.2

* mean value of two test results

3-4.6 Concluding remarks to section 3-4

In section 3-4, the focus was set on geometrical and mechanical properties of self-tapping screws' threaded parts. Within a first step, their specific profile was described by a three dimensional mathematical approach basing on the main geometrical parameters $\{d, \eta, v \text{ and } p\}$. This subsequently enabled the derivation of corresponding cross-sectional properties, such as the cross-sectional area, the gravity centre's position as well as the moments of inertia.

Presupposing, that the material is homogeneous, behaves in an ideal-plastic way and the threaded part of the screw is a prismatic beam, the plastic section moduli for bending and torsion, as well as the plastic area in case of axial tension were determined and approximated by empirical constitutions – again in dependence of the aforementioned geometrical parameters. These analytical models – in fact representing the relationships between the main mechanical parameters of screws loaded in tension, torsion or bending – were subsequently verified by the corresponding test results gained from an experimental campaign, as well as by a numerical simulation of one example screw thread profile.

Even though the theoretical description bases on certain simplifications, an appropriate correspondence with experimentally determined properties could be widely achieved. This leads to the proposal of approximating the main mechanical properties $f_{tens}, f_y, f_u, f_{tor}$ and M_y of a self-tapping screw's threaded part by results gained from one representative screw tensile test combined with theoretical considerations, summarised in eq. (3.89) to eq. (3.100).

- Cross-sectional properties:

$$\eta = \frac{d_c}{d} \text{ and } \psi = v / 2, \quad (3.89)$$

$$\omega = \left[\frac{p}{2} - \frac{d}{2} \cdot (1 - \eta) \cdot \tan \psi \right] \cdot \frac{2}{p}, \quad (3.90)$$

$$A_s = \frac{\pi \cdot \tan \psi}{12 \cdot p} \cdot \left[d^3 - (d + (\omega - 1) \cdot p \cdot \cot \psi)^3 \right] + \frac{\eta^2 \cdot d^2}{4} \cdot \omega \cdot \pi, \text{ and} \quad (3.91)$$

$$A_{dc} = \frac{\eta^2 \cdot d^2}{4} \cdot \pi. \quad (3.92)$$

- Tensile properties:

$$f_{y,\text{pred}} = \frac{F_y}{A_{\text{pl},N}}, \text{ and} \quad (3.93)$$

$$f_{u,\text{pred}} = \frac{f_{\text{tens}}}{F_y} \cdot f_{y,\text{pred}}, \text{ with} \quad (3.94)$$

$$A_{\text{pl},N,\text{emp}} = A_{dc} \cdot \omega^{\left(\frac{-0.015}{\eta^{3.95}} \right)}, \quad (3.95)$$

- Torsional properties:

$$f_{\text{tor},\text{pl},\text{pred}} = W_{\text{T},\text{pl},\text{emp}} \cdot \frac{f_{y,\text{pred}}}{\sqrt{3}}, \text{ with} \quad (3.96)$$

$$W_{\text{T},\text{pl},\text{emp}} = \left(-\frac{2}{3} \cdot \eta + 1.93 \right) \cdot W_{\text{T},\text{el},\text{dc}} \cdot \omega^{\left(\frac{-0.2108}{\eta^{1.7105}} \right)}, \text{ and} \quad (3.97)$$

$$W_{\text{T},\text{el},\text{dc}} = \frac{\eta^3 \cdot d^3}{16} \cdot \pi. \quad (3.98)$$

- Bending properties:

$$M_{y,\text{pl},\text{pred}} = W_{\text{pl},z} \cdot f_{y,\text{pred}}, \text{ with} \quad (3.99)$$

$$W_{\text{pl},z} = A_s \cdot y_s, \quad (3.100)$$

and y_s according to eq. (3.51).

With regard to the theoretical derivations, conducted in this section, the following untreated topics are seen as an outlook for further considerations:

In section 3-4.3, the plastic cross-sectional properties have been determined in case of a screw, loaded in tension and leading to a load interaction between N and M , the latter as a product of N and z_s . Further concentration should be on the load interaction with M independent from N , realisable by approximating an N - M -relationship for the given screw thread, as e. g. provided in ON EN 1993-1-1 (2012), for steel profiles commonly used in practice. In addition, the influence of a shear force V on this relationship could also be included, subsequently enabling the plastic design of a screw e. g. inclined positioned in a tensile joint, as described in section 2-3.1.1.

Eqs. (3.93), (3.96) and (3.99) generally base on the ideal-plastic material conditions. As demonstrated in section 3-4.5, this enables an adequate approximation of mechanical screw properties, but not that of the whole load-displacement-curve in case of varying load situations. In fact, this could rather be realised by considering the elastic-plastic material behaviour and – if possible – by assuming the hardening in the plastic domain.

In contrast to the aforementioned assumption of a prismatic beam, the three dimensional thread surface consists of cross-sectional discontinuities in x -direction in form of the transition between inner thread cylinder and thread chamfer, see Figure 3.13. Stress singularities (normal and shear stresses) due to these geometrical notches are expected to influence the screw's loadbearing performance. Future investigations should concentrate on the impact of this local stress increase on the mechanical properties in case of varying material constitutions (linear elastic, ideal plastic, combination of both).

3-5 INFLUENCING PARAMETERS ON SCREW TENSILE CAPACITY

3-5.1 Introduction and overview

The product self-tapping screw regarding its geometrical properties, its production process, as well as the interrelationship of its main mechanical parameters f_{tens} , f_{tor} and M_y declared in related Technical Assessments have been discussed so far. Especially the latter has been theoretically derived for the quasi-static loading, furthermore taking precise thread geometry and environmental conditions not influencing the corresponding loadbearing behaviour into account.

This section is about self-tapping screws, produced and applied in situations deviating from the aforementioned ideal conditions. Thus, subsections 3-5.2 to 3-5.4 comprise the considerations regarding the influence of production process, time-dependent load situations and varying environments on their structural performance. The focus is thereby set on their steel tensile capacity as the major relevant product property for design, c. f. chapter 2. Since a pronounced correlation with torsional or bending properties is given, see section 3-4.5, related findings also serve, at least, as qualitative indicators for both latter mentioned load situations.

3-5.2 Production process

Within section 3-3, the production process of hardened carbon steel screws has been subdivided into five main steps. Type and treatment of raw material, as well as the final treatment of the screw, have not been experimentally varied in the frame of the investigations. Therefore, the following discussion is reduced to both core production steps, namely geometrical forming and hardening, as well as on the application of protective coats.

3-5.2.1 Influence of geometrical forming

In fact, the geometrical forming of screws influences their structural performance in different ways. First, as discussed in section 3-4, the thread geometry defined by the parameters $\{d, \eta, v \text{ and } p\}$ and seen as the result of this production step, has a major impact on the corresponding mechanical properties. For a screw with outer thread diameter $d = 8 \text{ mm}$, Figure 3.48 shows the influence of varying $\{\eta, v \text{ and } p\}$ on $A_{\text{pl,N}}$, which is the relevant plastic cross-sectional area for axial tension. Presupposing the relationship between $A_{\text{pl,N}}$ and the steel tensile capacity f_{tens} , is adequately described by eq. (3.93) to eq. (3.95), η as the ratio between inner and outer thread diameter governs the size of f_{tens} (Figure 3.48, left), while especially for $> \eta$ the impact of p is only minor pronounced. In case of a comparatively small $\eta = 0.65$, as value commonly found in practice, c. f. Pöll (2017), increasing f_{tens} with increasing $\psi = v / 2$ and decreasing p can be observed (Figure 3.48, right), the maximum can thus be achieved for small p and high ψ . Worth

mentioning, these effects influence the behaviour of f_{tor} and M_y in a similar or even more pronounced way, c. f. section 3-4.3 and 3-4.5.

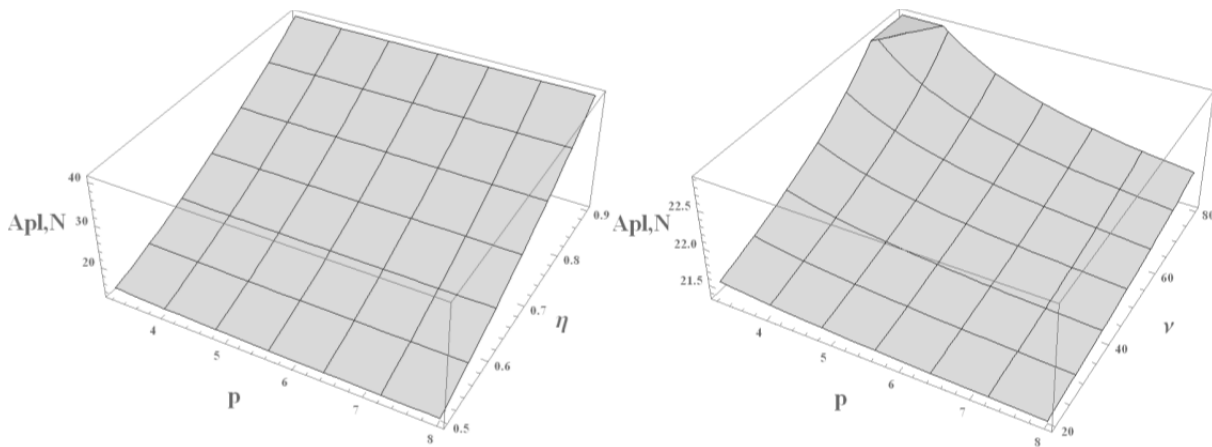


Figure 3.48: Influence of thread properties on plastic area $A_{pl,N}$ for $d = 8$ mm; left: $\nu = 40^\circ$; right: $\eta = 0.65$

Second, concentrating on thread rolling as a cold forming process, the corresponding modification of the crystalline structure leads to an increase of hardness and strength, combined with a significant decrease of ductility, c. f. section 3-4.5.2. In cases thread rolling is followed by heat treatment measures, such as hardening, as commonly applied for the production of low alloy carbon steel screws, the related impact is superposed and can thus be regarded as negligible (c. f. hardness distributions of A_s_I-V_08_240 and A_s_V_08_240 in Figure 3.44).

Third, as noted in section 3-4.5.2, rolled screw threads deviate from the ideal geometry derived in section 3-4.2. This is mainly caused by surface discontinuities in form of cracks or notches, especially when flat die rollers are applied for thread forming. As shown in Figure 3.49, their optical appearance, found for all screws examined irrespective the manufacturer occurs as some kind of flaking, located at the inner thread cylinder.



Figure 3.49: Photographs of self-tapping screws' threaded parts produced by manufacturers A, B and C

In order to receive an impression, regarding the character of these production inaccuracies, as well as to estimate the corresponding loss of cross-sectional geometry, micrographs of the screw thread's xz- (or xy-)plane from altogether 13 specimen were made by the Institute of Material Science, Joining and Forming at Graz University of Technology. Related examples of microscopic scans with varying scale are given in Figure 3.50 and Figure 3.51. Therein, not only cracks or notches at the inner thread cylinder (as expected on the basis of Figure 3.49), but also such located at the thread chamfer can be observed.

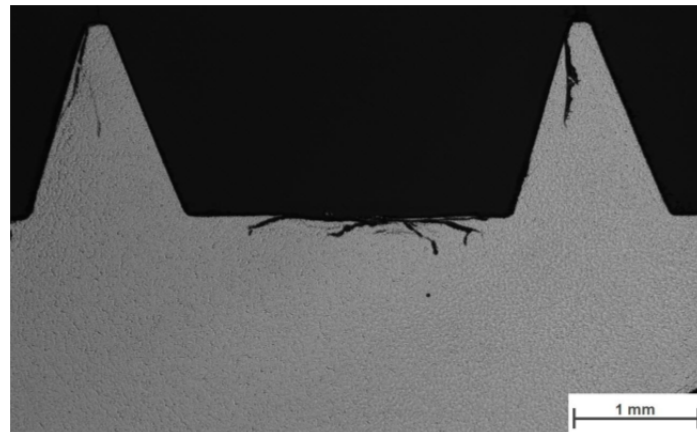


Figure 3.50: Micrograph (etched) of a self-tapping screw's threaded part related to product group *A_s_II_08_240*

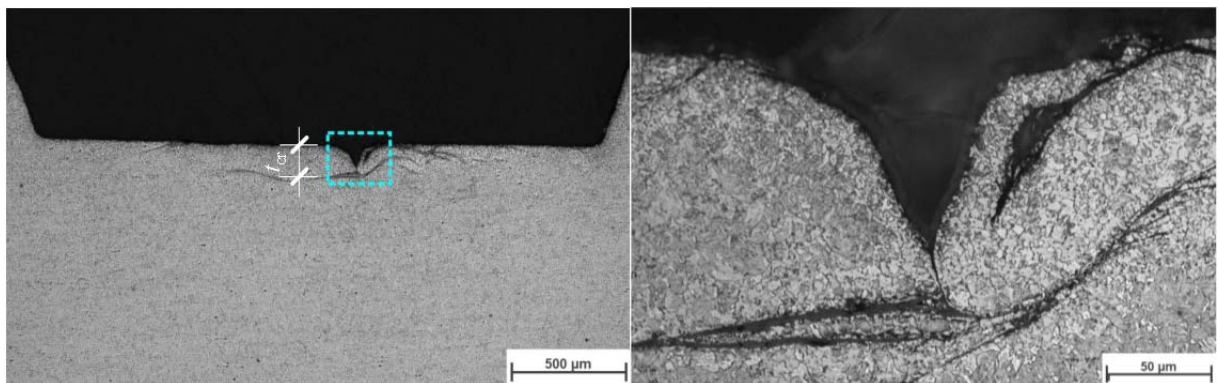


Figure 3.51: Further micrographs (etched) of a self-tapping screw's threaded part related to product group *A_s_II_08_240*

Subsequently, Table 3.19 includes the statistical parameters of measured t_{cr} , defined as a radial dispersion of these surface discontinuities, c. f. Figure 3.51 (left). Thereby, five specimen of group *A_s_II_08_240* have been considered. The average values for t_{cr} result to 0.674 mm and 0.271 mm for the thread chamfer and the inner thread cylinder, which thus are about 8 % and 3 % of the outer thread or 13 % and 5 % of the inner thread diameter. Assuming a reduction of d and d_c of 10 %, $A_{pl,N}$ for the reference thread geometry used in section 3-4.3 results to 17.6 mm², which is about 80 % of the value determined for ideal conditions. This difference indicates a significant influence of surface discontinuities on mechanical

properties, also contributing to the deviations between test results and model predictions observed in section 3-4.5. The additional effect of the stress singularities (e. g. Stellwag and Kaesche (1982) assume normal stresses σ_x occurring close to the crack's root in a dimension of $3 \cdot f_y$ in case of ideal plastic material behaviour) is ignored in this simplified comparison. Worth mentioning, the occurrence and the size of cracks and notches depend on the flat die rollers' condition, the tool wear is assumed decreasing t_{cr} to a significant extent.

Table 3.19: *Minima, maxima and mean values of t_{cr} determined at micrographs of screw threads related to product group A_s_II_08_240*

location	n	min[t_{cr}] [mm]	max[t_{cr}] [mm]	mean[t_{cr}] [mm]	CV[t_{cr}] [%]
thread chamfer	5	0.564	0.823	0.674	14.4
inner thread cylinder	5	0.198	0.343	0.271	23.6

In failure scenarios, where the type of loading and environment additionally influences the screw tensile capacity in a major way, the impact of surface discontinuities is even more pronounced and thus discussed in detail in the following sections.

3-5.2.2 Influence of screw hardening

As already explained in section 3-3.3, steel hardening influences mechanical properties in a major way; see also Maydl and Tritthart (2006), Macherauch and Zoch (2011) or Weißbach (2012). In general, yield and tensile strength are thereby increased by far, while ductility and formability significantly decrease. With special regard to self-tapping screws, the corresponding results of a parameter study, wherein the applied hardening procedure has been varied, are shown and discussed in section 3-4.5. The main outcomes are again summarised in form of Table 3.20, which qualitatively compares the effects of hardening in general, as well as those caused by additionally tempering and/or carbonitriding on mechanical screw properties f_u, f_y, D, f_{tor} and M_y .

Table 3.20: *Qualitative effect of different hardening methods on mechanical screw properties*

hardening method	f_u	f_y	D	f_{tor}	M_y
standard procedure*	>	>	<	>	>
add. tempering**	<	<	>	<	<
add. carbonitriding**	-	-	<	>	>

* referred to unhardened screws; ** referred to standard procedure

Subsequently focusing on the steel tensile failure, additionally influenced by loading and environment deviating from laboratory conditions, within quasi-static tensile tests are commonly carried out.

Concentrating on cyclic loading in tension without exceeding the specimen's yield strength (high-cycle-fatigue, c. f. section 3-5.3.1), the corresponding capacity is commonly reached at load levels far below the quasi-statically determined tensile capacity. In case of structural steel, the reason therefore is mainly the combination of crack formation and propagation. The latter proceeds with an increasing number of load cycles (N) and thus steadily reduces cross-sectional area. The steel failure consequently occurs in form of exceeding the net cross-section's tensile capacity, caused by reaching a critical value of $A_{pl,N}$, c. f. section 3-5.3.

Thereby the hardening influences the number of bearable load cycles and consequently the screw's endurance in different ways:

On the one hand, it increases yield and tensile strength of the material, which are positively correlated to the bearing capacity in case of $N > 1$. Thus, the impact of varying hardening procedures on quasi-statically determined product properties, as summarised in Table 3.20, is also valid for $> N$.

On the other hand, hardening decreases ductility and formability and thus negatively affects crack propagation. The latter is additionally strengthened for martensitic steel as a result of this production step, c. f. Radaj and Vormwald (2007). Therein, also a varying impact of hardening on notches, responsible for crack occurrence, is reported. In general, the high strengths negatively influence the related notch effects, while strength increase of the specimen's surface zones, as achieved by carbonitriding, may balance the corresponding stress increase occurring at the notch root.

Now focusing on the environmental exposures causing material corrosion, which negatively influences the bearing capacity of structural steel. Thereby, hardening has a major impact on such types of corrosion, which – in combination with outer loading (especially tensile stresses) – lead to an immediate and brittle failure mechanism. With regard to hardened low alloy carbon steel screws (a related form is denoted as hydrogen-induced stress corrosion cracking, HISSC) a comprehensive explanation of this phenomenon is given in section 3-5.4.

First, reported in literature, see e. g. Stellwag and Kaesche (1982), Kuron (2000), Illgner and Esser (2001), Kayser (2001), Kloos and Thomala (2007), DIN 50969-1 (2009) and Pohl and Kühn (2010), HISSC especially affects steel products with a high tensile strength and a reduced formability. With regard to a lower limit of f_u , if exceeded HISSC has to be considered, different values can be found in literature. Kuron (2000), as well as Pohl and Kühn (2010), therefore assume $f_{u,min} = 800 \text{ N/mm}^2$, while Illgner and Esser (2001), Kayser (2001) and DIN 50969-1 (2009) recommend a value of $f_{u,min} = 1,000 \text{ N/mm}^2$. Illustrating the impact of tensile strength on HISSC, Nürnberger (1995) reports the dependency of material endurance on hardness of steels, tested in HISSC-promoting atmospheres in form of eq. (3.101), see

$$HV250 : HV350 : HV450 : HV550 = 1265 : 60 : 6 : 1. \quad (3.101)$$

Second, similar to the impact of cyclic loading, the aforementioned negative effects of hardening on crack formation and propagation also increase the material's vulnerability to HISCC.

Third, the crystalline structure (body-centred cubic lattice) of martensitic steel, as a result of the screw hardening restricts the hydrogen solubility (< 1 ppm), but enables its movability leading to significantly higher hydrogen diffusion rates if compared to austenitic steel (face-centred cubic lattice), c. f. Gräfen and Kuron (1987), Nürnberger (1995) and Macherauch and Zoch (2011). Consequently, HISCC not only affects hardened carbon steel screws, but also martensitic stainless steel screws to a certain extent.

3-5.2.3 Application of protective coats

As discussed in section 3-3.4, protective coats, which are subsequently added after the hardening process, shall decelerate the corrosion process, caused by the environment the screw is applied in. Based on the declarations, found in currently valid ETAs, electro-galvanised zinc, as well as zinc-nickel coatings are frequently used. Since galvanisation and chromating commonly take place at temperatures at least below 100 °C, c. f. Orth (1974), a corresponding influence on mechanical steel properties determined at ideal conditions can be neglected. In Table 3.21, the mean values of experimentally determined tensile capacities f_{tens} are compared in dependence of the protective coating applied for the screws. Each subgroup, as part of the experimental campaign discussed in section 3-4.4.1, thereby contained $n = 5$ tests. As there are no differences of f_{tens} observable, the aforementioned fact can be confirmed.

Table 3.21: Comparison of steel tensile capacities in dependence of the applied coating

product ID	coating	mean[f_{tens}] in [N]
A_s_I_08_240	untreated	28,971
	yellow chromated	28,950
	zinc-nickel	29,078
A_s_II_08_240	untreated	30,476
	yellow chromated	30,434

With regard to hot-dip metal coating, also applied for self-tapping screws to a certain extent, the corresponding procedure demands temperatures of about 450 °C, c. f. Berns and Theisen (2006). This heat treatment measure consequently influences the mechanical screw properties: characteristic values of f_{tens} , f_{lor} and f_y , related to hot-dip galvanised screws, are about $80 \div 90$ % of those protected by standard coating, e. g. declared in ETA-11/0190 (2013).

The impact of HISCC, as comprehensively discussed in section 3-5.4, mainly depends on the quantity of hydrogen atoms diffusing into the metal's crystal lattice, where they occupy interstitials, or concentrate at

traps, increasing the lattice stresses to a significant extent, c. f. Gräfen and Kuron (1987). The galvanisation process majorly influences the occurrence of diffusible hydrogen at the phase interface of electrolyte and metal. Figure 3.52 schematically illustrates this process, taking place for instance in aqueous hydrogen chloride (HCl, also known as hydrochloric acid).

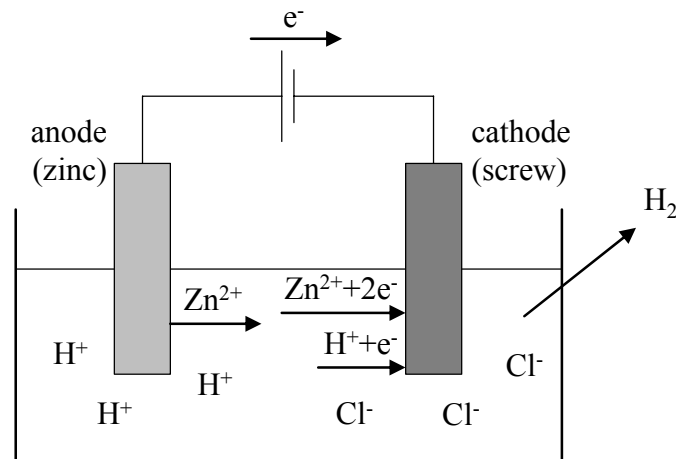


Figure 3.52: Schematic illustration of galvanisation process; according to Toblier (2014)

According to Orth (1974), H-ions (H^+) as contents of HCl thereby possibly move to the metal (screw) surface and react with flexible electrons (e^-) of the crystal lattice to atomic adsorbed hydrogen (H_{ad}), commonly denoted as the so-called Volmer reaction, see eq. (3.102):



Subsequently, free hydrogen molecules (H_2) are formed by molecular adsorbed hydrogen ($(H_2)_{ad}$) as a result of (a) the so-called Tafel reaction (eq. (3.103)) or (b) the so-called Hayrovsky reaction (eq. (3.104)), see



In general, H_2 , as a product of 2x-Volmer and 1x-Tafel or 1x-Volmer and 1x-Hayrovsky reaction, desorbs from the acid solution and thus does not affect the material at all (see Figure 3.52). In case of an iron (F_e) cathode, parts of H_{ad} possibly also diffuse into the metal (absorption, $H_{ad} \rightarrow H_{ab}$), which thus increases the vulnerability of HISCC. A schematic summary of this process is given in Figure 3.53.

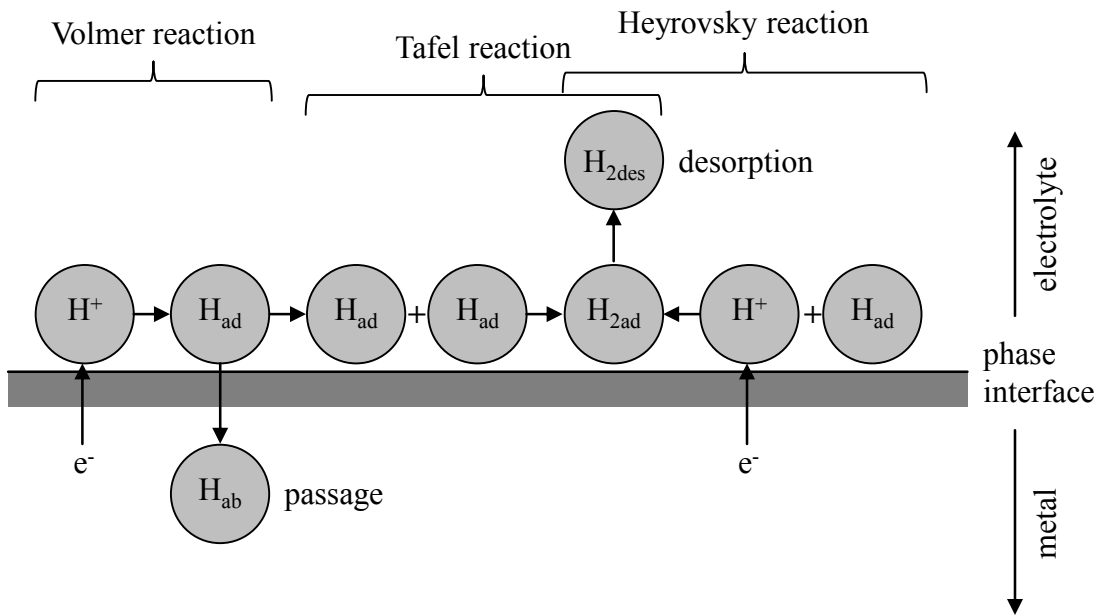


Figure 3.53: Schematic illustration of electrochemical hydrogen discharge; according to Landgrebe (1993)

In order to determine the extent of diffusible hydrogen, due to the galvanisation of self-tapping screws, product group A_s I-IV_08_240, introduced in section 3-4.4.1, has been supplied by manufacturer A with varying protective coats comprising yellow chromates and zinc-nickel, each with and without (standard case) additional tempering at $T \approx 200$ °C after galvanisation. Furthermore, one charge of screws has been blue chromated and also tempered. Subsequently, the corresponding quantity of H_{ad} has been determined by the company voestalpine STAHL GmbH performing carrier gas hot extraction (CGHE) – a related description of this method is e. g. given in Gruner (2002). Worth mentioning, that one part of this programme has been conducted in the frame of a student’s bachelor’s thesis, supervised by the Institute of Material Science, Joining and Forming at Graz University of Technology (in cooperation with the author of this thesis), c. f. Toblier (2014). Three measurements per screw were carried out, determining two values of H_{ad} in the coating and one in the steel, the latter realised by previously pickling the screw in hydrochloric acid. Table 3.22 and Figure 3.54 (error bars represent the standard deviation) consequently overview the corresponding test results in form of mean values and variabilities of H_{ad} in dependence of the coating applied. Two main facts have to be outlined in this context: first, the accuracy of CGHE is restricted to a margin of deviation of 0.1 ppm (equal to $\mu\text{g/g}$), c. f. Paatsch (2011). Second, corresponding results serve for relative comparisons, as a serious quantity of H_{ad} causing HISCC in the material is currently not assignable, c. f. Kayser (2001).

With regard to the results for yellow chromated and zinc-nickel coats (both not tempered), a remarkable difference in the quantity of H_{ad} can be observed. The diffusible hydrogen in zinc-nickel is about 56 % of that determined for yellow chromates, confirming findings made in the past, c. f. Gysen (2000), which assign zinc-nickel coats decreasing the vulnerability of HISCC if compared to other galvanisation

products. Focusing on tempering after galvanisation, a significant decrease of H_{ad} can be observed for yellow chromates, while H_{ad} of zinc-nickel coats stays more or less constant, indicating a variable impact of this measure. Since all blue chromated screws were additionally tempered, a comparison with the standard case is not possible. Nevertheless, a higher quantity of H_{ad} , especially if compared to additionally tempered yellow chromates, is given. With regard to H_{ad} determined in steel, a corresponding concentration is much lower than in all coating forms considered.

Table 3.22: Diffusible hydrogen contents determined for varying protective coats

protective coating	n [-]	mean[H_{ad}] [$\mu\text{g/g}$]	CV[H_{ad}] [%]
yellow chromated	6	2.39	16.6
yellow chromated (add. temp.)	3	0.80	10.6
zinc-nickel	9	1.34	17.2
zinc-nickel (add. temp.)	3	1.48	11.8
blue chromated (add. temp.)	3	1.80	32.6
steel	27	0.14	-

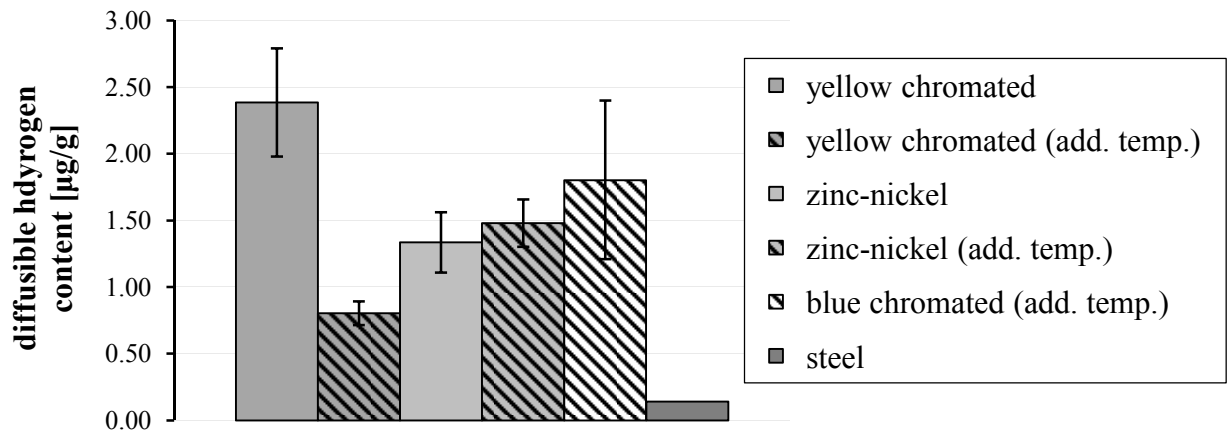


Figure 3.54: Diffusible hydrogen contents determined for varying protective coats

3-5.3 Loading

3-5.3.1 Introduction

The experimental determination of mechanical strength properties, declared in standards or assessments, is commonly conducted by so-called monotonic tests; see Figure 3.55 (left). A related test protocol, expressed as a load-time-relationship, is generally defined by a steady load increase (at least after exceeding 40 % of $F_{est} | F_{max}$) until reaching the specimen's corresponding bearing capacity F_{max} . Since they serve as input variables for the design of structures against “quasi-static” loads (assumed to have no relevance on fatigue effects during service life), the gained results are subsequently denoted as quasi-static properties. Furthermore, they are regarded as the maximum capacities of the specific structural member determined at ideal (laboratory) conditions.

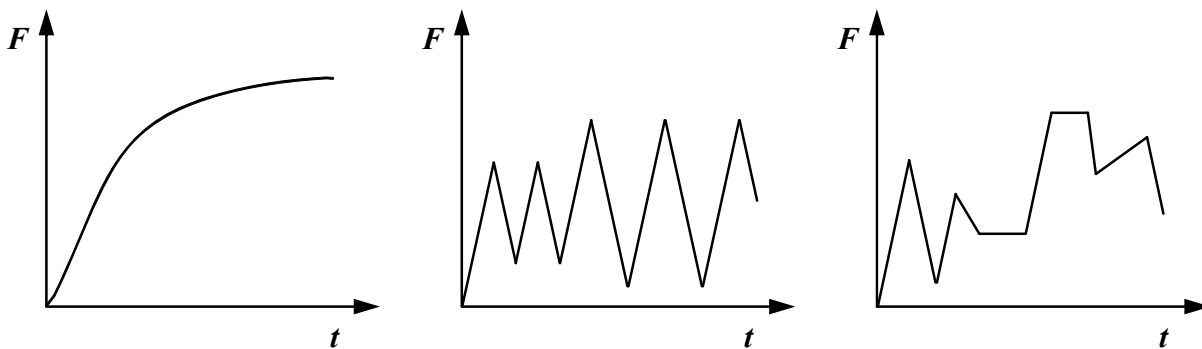


Figure 3.55: *Different load-time-relationships in the pulsating tensile domain: left: monotonic loading; middle: cyclic loading; right: random loading*

With regard to the load situations, deviating from the aforementioned monotonic character, especially a frequent and time-dependent load repetition, further defined as cyclic loading (see Figure 3.55, middle), leads to strength decrease and consequently to material failure, reached at load levels far below the quasi-statically determined bearing capacity. The first comprehensive investigations at least in German-speaking countries, c. f. Schütz (1993), concerning this phenomenon, commonly denoted as material fatigue can be addressed to Wöhler (1870), who gave a fundamental definition to be cited as:

“Rupture may be caused, not only by a steady load which exceeds the carrying strength, but also by repeated application of stresses, none of which are equal to this carrying strength. The differences of these stresses are measures of the disturbance of the continuity, in so far as by their increase the minimum stress which is still necessary for rupture diminishes.” – translated by Nicholas (2006)

In case of structural steel, as indicated in section 3-5.2.1, the disturbance of the continuity according to Wöhler (1870) is caused by crack formation located at defects, notches and changes of the cross-sectional geometry, which is followed by crack propagation due to load repetition until failure occurs; c. f. Bürgel

et al. (2014). In order to evaluate a specimen's or structural member's sensibility regarding this phenomenon, the experimental investigations are commonly carried out in form of the so-called Wöhler fatigue tests, as exemplarily illustrated in Figure 3.56 (left). The given load-time-relationship (in major cases under constant stress-controlled conditions) has a sinusoidal course describable by the strength parameters σ_{\max} and R , the latter as the ratio between σ_{\min} and σ_{\max} , as well as by f herein defined as loading frequency or inverse of one cycle's duration $t_{N=1}$. Further parameters σ_{\min} , σ_{mean} , $\Delta\sigma$ and σ_a as the minimum stress, the average stress, the stress difference and the alternating stress value can be expressed in dependence of σ_{\max} and R as follows:

$$\sigma_{\min} = R \cdot \sigma_{\max}, \quad (3.105)$$

$$\sigma_{\text{mean}} = \frac{\sigma_{\max} + \sigma_{\min}}{2} = \sigma_{\max} \cdot \frac{1+R}{2}, \quad (3.106)$$

$$\Delta\sigma = \sigma_{\max} - \sigma_{\min} = \sigma_{\max} \cdot (1-R), \text{ and} \quad (3.107)$$

$$\sigma_a = \frac{\Delta\sigma}{2} = \sigma_{\max} \cdot \frac{1-R}{2}. \quad (3.108)$$

The size of the stress ratio R furthermore describes the type of the Wöhler fatigue test. In case of $0 \leq R < 1$, loading corresponds to the pulsating tensile domain (all $\sigma \geq 0$, see Figure 3.56, left), which switches over to the alternating stress domain and to the pulsating compressive domain if $-\infty < R < 0$ and $1 < R \leq \mp\infty$ respectively.

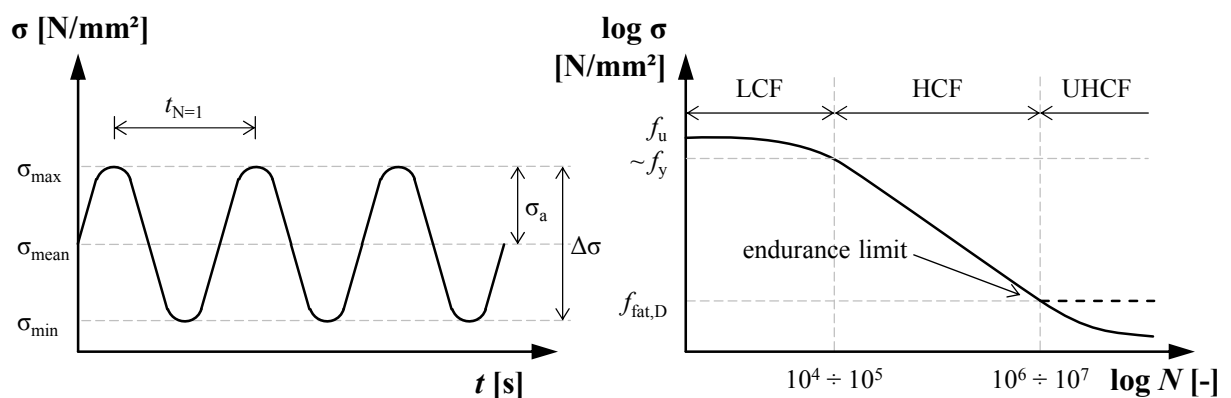


Figure 3.56: Left: load-time relationship of a typical Wöhler fatigue test in the pulsating tensile domain; right: S/N-diagram with classification of different fatigue domains; according to Radaj and Vormwald (2007) and Schäfer (2008)

As summarised in Radaj and Vormwald (2007), the sensibility of a specimen or structural member against loading, which is relevant for fatigue, depends on several parameters, far too much for a detailed treatment within this thesis. Beside those, already discussed in section 3-5.2, a further focus is restricted to R and N , both regarded as major parameters influencing the fatigue resistance at all. As previously mentioned, the size of R indicates the sign of stresses and thus that of σ_{mean} . According to Radaj and Vormwald (2007), as well as to Greiner and Unterweger (2009), bearable σ_{mean} and $\Delta\sigma$ are higher in case of loading, located in the pulsating compressive domain. Since self-tapping screws are majorly loaded in tension, comparatively more relevance is addressed to the value of R , varying between $0 \leq R < 1$.

Due to the fact, that corresponding investigations of axial loaded self-tapping timber screws have not been found so far, further theoretical assumptions base on bolts and rods with rolled or cut threads as applied in steel engineering and treated in ON EN 1993-1-9 (2013). For a verification in the case of axial loading in tension, $\Delta\sigma_C$ defined as the bearable stress difference at $N_C = 2 \cdot 10^6$ is thereby restricted to 50 N/mm^2 (“detail category 50”). Additionally considering eq. (3.107) and the stress limit $\sigma_{\text{max}} \rightarrow f_{\text{fat},N}$, the latter property can be expressed as follows:

$$f_{\text{fat},N} = \frac{\Delta\sigma_C}{(1-R)}. \quad (3.109)$$

The ratio between the component’s bearing capacity at N load cycles and that determined at quasi-static conditions (f_u), denoted as $k_{\text{fat},N}$, according to ON EN 1995-2 (2006), Annex A, is subsequently given in eq. (3.110) as function of R , see

$$k_{\text{fat},N} = \frac{f_{\text{fat},N}}{f_u} = \frac{\Delta\sigma_C}{f_u} \cdot \frac{1}{(1-R)} = \frac{1}{f_u} \cdot \frac{50}{(1-R)}. \quad (3.110)$$

Figure 3.57 illustrates the behaviour of $k_{\text{fat},N}$, according to eq. (3.110), in dependence of varying R for three selected steel tensile strengths f_u , which are chosen in a range similar to the values determined for self-tapping screws in section 3-4.5.2. Even though this comparison bases on a rough simplification (detail categories, according to ON EN 1993-1-9 (2013), ignore the positive influence of f_u on f_{fat} discussed in section 3-5.2.2, $k_{\text{fat},N}$ is restricted to ≤ 1.00), it may serve as an indicator for a pronounced and progressive dependency of fatigue resistance on the stress ratio R . Furthermore, comparatively small values of $k_{\text{fat},N}$ for at least $R \leq 0.80$ point out a poor performance of this fastener type in case of a time-dependent axial loading.

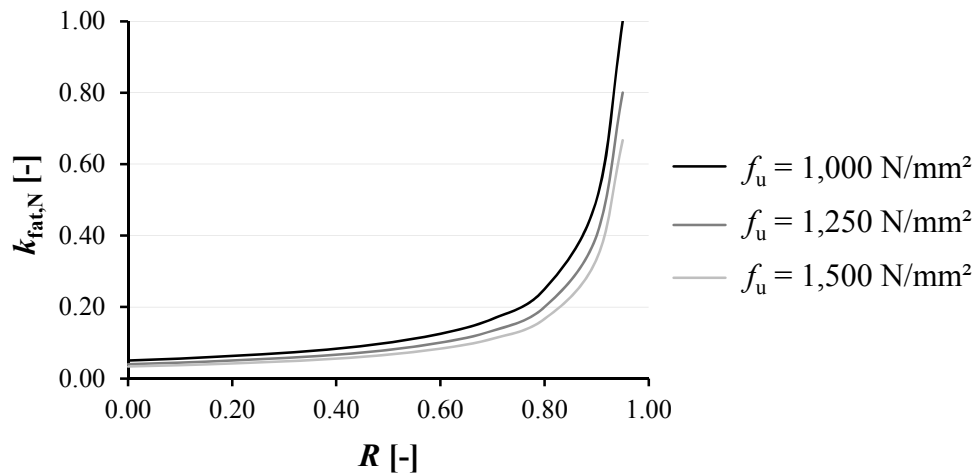


Figure 3.57: Behaviour of $k_{fat,N}$ in dependence of R for varying steel tensile strengths f_u

Now concentrating on the negative impact of N as the second main parameter being relevant for the fatigue related design: the corresponding dependency is commonly expressed in form of so-called S/ N -diagrams (also denoted as Wöhler-curves), as qualitatively illustrated in Figure 3.56 (right). The function, which is shown in this illustration, results by connecting experimentally determined load cycles N , bearable in case of varying load levels. Considering a logarithmic scaling, this relationship (for a constant value of R) can be separated in altogether three domains, each with an approximately linear course but different inclinations.

Between $10^0 < N \leq (10^4 \div 10^5)$ the corresponding behaviour is usually denoted as low-cycle-fatigue (LCF), c. f. Nicholas (2006) and Schäfer (2008), and characterised by a slight decrease of f_{fat} with increasing N . In general, LCF has to be considered for load levels close to the quasi-static bearing capacity occurring within a comparatively small number of cycles (e. g. earthquake scenarios). Since the transition to high-cycle-fatigue (HCF) is defined by loading above or below the component's yield capacity, the bandwidth of $10^4 \leq N \leq 10^5$ as the upper limit mainly depends on the ratio between ultimate and yield capacity, see Figure 3.56 (right) and Radaj and Vormwald (2007).

The domain addressed to HCF is further characterised by a comparatively more pronounced and steady decrease of f_{fat} with increasing N , until reaching an upper limit of $10^6 \leq N_D \leq 10^7$, also denoted as endurance limit and regarded as an essential property considered in fatigue design. One reason therefore is a strength value $f_{fat,D}$ related, which represents a (technical) lower limit bearable in case of $N \rightarrow \infty$. In contrast to the transition between LCF and HCF, the bandwidth of N_D is rather caused by specific material and environmental conditions applied, c. f. section 3-5.2.3 and Radaj and Vormwald (2007), than by the interrelationship of mechanical properties. The related standardisation, such as ON EN 1993-1-9 (2013) for instance, currently provides a value of $N_D = 5 \cdot 10^6$. Nevertheless, the corresponding design process considers $\Delta\sigma_C$, determined at $N_C = 2 \cdot 10^6$. Beside N_D , settled within this variable range, the course of the

linear function itself also serves as a relevant parameter for fatigue sensibility. According to Basquin (1910), the fatigue strength $f_{\text{fat},N}$ at any N within the HCF domain can be determined according to eq. (3.111), see

$$f_{\text{fat},N} = f_{\text{fat},D} \cdot \left(\frac{N_D}{N} \right)^{1/k_{\text{SN}}}, \quad (3.111)$$

with k_{SN} herein denoted as the inclination coefficient decreasing with increasing fatigue sensibility. As given in Table 3.23, k_{SN} serves as an indicator for the significant impact of notches or initial cracks on the size of $f_{\text{fat},D}$. In this context it has to be mentioned, that the detail categories, according to ON EN 1993-1-9 (2013), are provided with constant values of k_{SN} in form of $k = \{3, 5, \infty\}$ if $\{10^4 \leq N \leq N_D, N_D \leq N \leq 10^8, N > 10^8\}$, thus classified as moderate to significant notches, according to Table 3.23.

Table 3.23: Inclination coefficient k_{SN} in dependence of notches; according to Haibach (2002)

notch character	k_{SN}
unnotched specimen	15
moderate notch	5
significant notch, initial cracks	3

With regard to time-dependent loading exceeding N_D in Figure 3.56 (right), a further but minor pronounced decrease of f_{fat} with increasing N can be observed in major cases. Since, in contrast to LCF and HCF, a corresponding denotation varies in literature, see e. g. Nicholas (2006) and Schäfer (2008), it was decided to denote this domain as “ultra-high-cycle-fatigue (UHCF)” according to Schäfer (2008). As reported in Radaj and Vormwald (2007), it is currently not clear if a specific value of N exists, where – if exceeded – f_{fat} converges to a horizontal plateau. Consequently, and as previously indicated, N_D can be regarded as a *technical* endurance limit, set in order to keep the testing efforts within a tolerable range.

Specific assumptions made so far base on the performance of steel rods or bolts as fasteners frequently applied in steel engineering, according to ON EN 1993-1-9 (2013). The reasons therefore are geometrical similarities, due to their threaded shape, and that comprehensive knowledge exists regarding the time dependent loading, see e. g. Illgner and Esser (2001) or Kloos and Thomala (2007). Now concentrating on the situation for self-tapping timber screws, no investigations regarding their fatigue sensibility can be found. Since this circumstance also restricts their intended use to a significant extent, c. f. ETA-11/0190 (2013) or ETA-12/0114 (2012), it was decided to gain fundamental knowledge in this field, especially concerning the impact of both main parameters N and R on f_{fat} , related to axial loading in the pulsating tensile domain. Sections 3-5.3.2 and 3-5.3.3 consequently comprise the description of an experimental campaign on cyclically loaded self-tapping screws, serving as a basis for future model considerations.

Further focus is put on the time-dependent performance of single self-tapping screws determined by means of Wöhler fatigue tests, as given in Figure 3.56 (left). The corresponding results can be addressed to group “b”, according to Figure 3.58, and are thus regarded as the basic mechanical fatigue properties (“Wöhler strengths”). Their applicability in design process (group “g”) demands additional considerations in both fields of shape dependent strength (“b” → “c”) and damage accumulation (“c” → “g”) – not treated within this thesis.

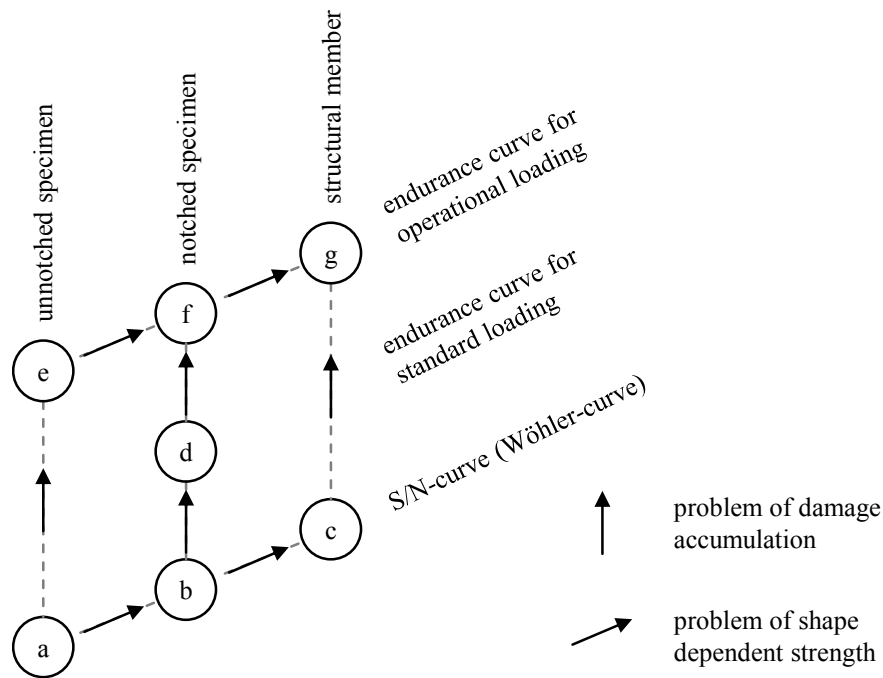


Figure 3.58: Classification of fatigue regarding specimen geometry and loading types; according to Haibach (2002)

3-5.3.2 Materials and methods

Table 3.24 subsequently overviews the experimental programme in form of Wöhler fatigue tests of axially loaded self-tapping screws, all dedicated to product group A_s_II_08_240, according to section 3-4.4. Corresponding geometrical (thread) properties, description of monotonic tensile tests and thereby gained results, serving as quasi-static reference values at $N = 10^0$, are thus found in Table 3.9, section 3-4.4.3 and Table 3.10.

All single test series addressed to cyclic loading (“c”, $N > 10^0$) in Table 3.24 were conducted with a sinusoidal (or sawtooth shaped) force-controlled loading protocol, according to Figure 3.56 (left), considering the constant values for f , σ_{\max} and R . The determination of stresses $\sigma_{\max,i}$ was done according to eq. (3.93) with $A_{pl,N} = 21.2 \text{ mm}^2$. The frequency variation in form of $f = 1 / t_{N=1} = 0.2 \div 90.0 \text{ Hz}$, given in Table 3.24, can be explained by different testing machines applied for determining N at varying stress levels $\sigma_{\max,i}$. As reported in Imsirovic (2014), who carried out the majority of the related tests within his

master's thesis (supervised by the author), the original aim was to execute the total programme (except $N = 10^0$) with a high-frequency (hf) pulsator, provided by the Institute of Technology and Testing of Construction Materials at Graz University of Technology (Note: one additional test series was executed by a hf-pulsator at Magna Steyr Fahrzeugtechnik AG & CO KG). The high frequency testing generally bases on the principle of an oscillating system (mass-spring-mass), which is stimulated in its resonant frequency (roughly 90 Hz for the situation given here, see Table 3.24), enabling a high amplification of the energy fed-in and thus an economic application of N in the HCL or UHCL domain, c. f. Russenberger Prüfmaschinen AG (2012).

Since the start of the oscillation demands a certain time span until the aimed value of $\Delta\sigma$ is applied, a comparatively small number of target cycles ($N = 10^0 \div 10^3$), reached at high load levels, cannot be realised with this method. Consequently, the corresponding load levels were performed by a hydraulic pulsator (also part of the testing facilities of the Institute of Technology and Testing of Construction Materials) and in addition, by the universal testing device LIGNUM-UNI-275, which also served for the quasi-static reference tests, c. f. section 3-4.4.3. According to Radaj and Vormwald (2007), the influence of the frequency on the behaviour of f_{fat} can be neglected if $1 < f < 10^3$ Hz, testing takes place at ideal laboratory conditions (20 °C, 65 % r. h., environment without corrosive impact) and $\sigma_{max} < f_y$. Since both load levels, dedicated to $N = 10^3$, can be classified into LCF (even close to the transition to HCF), the last requirement is not fulfilled. Thus, the results regarding this circumstance are also discussed in section 3-5.3.3.

Concentrating on N and R , as main parameters investigated, a corresponding variation is given in Table 3.24 in form of (a) $10^0 \leq N \leq 2 \cdot 10^6$, in case of constant $R = 0.56$ and (b) $0.10 \leq R \leq 0.90$, in case of $N_C = 2 \cdot 10^6$. The main aim was thus to cover (a) the S/N-diagram, shown in Figure 3.56 (right), until N_C as applied in ON EN 1993-1-9 (2013) for the verification, and (b) the almost total range of R , dedicated to the pulsating tensile domain. For $10^0 < N < 2 \cdot 10^6$, bearable N were determined at constant σ_{max} and R per test series further denoted as horizons. In case of N_C , a reverse situation is given (known N but unknown σ_{max} related), necessitating the application of the so-called staircase method, developed by Ransom and Mehl (1949), also recommended in DIN 969 (1997). This procedure comprises a stepwise increase or decrease of σ_{max} within one test series, each load step applied by considering the result of the previous test (failure before reaching $N_C \rightarrow$ stress decrease; no failure until $N_C \rightarrow$ stress increase). The corresponding determination of f_{fat} related to N_C , according to DIN 969 (1997), is explained in section 3-5.3.3.

In addition, it is worth mentioning that the test configuration of all screws investigated within this experimental campaign corresponds to the quasi-static tensile test, explained in section 3-4.4.3. This again enables the evaluation of both failure scenarios, “head tear-off” and “screw (thread) failure in tension”. Specifically modified adapters for the supporting of specimen are described in Imsirovic (2014).

Table 3.24: Overview of Wöhler fatigue tests carried out within the experimental programme

N^* [-]	n [-]	F_{\max} [kN]	σ_{\max} [N/mm ²]	R [-]	f [Hz]	type	domain	test rig
10^0	10	30.5	1,437	-	-	m	-	LIGNUM-UNI-275
10^3	5	30.3	1,429	0.56	0.2	c**	LCF	LIGNUM-UNI-275
10^3	5	28.0	1,321	0.56	8.0	c	LCF/HCF	hydraulic pulsator
10^4	6	16.0	755	0.56	90.0	c	HCF	hf-pulsator
10^5	5	9.6	453	0.56	90.0	c	HCF	hf-pulsator
$2 \cdot 10^6$	13	2.4 ÷ 3.4	113 ÷ 160	0.10	60.0	c	HCF	hf-pulsator
$2 \cdot 10^6$	7	5.0 ÷ 7.0	236 ÷ 330	0.56	90.0	c	HCF	hf-pulsator
$2 \cdot 10^6$	9	20.0 ÷ 22.0	943 ÷ 1,038	0.90	90.0	c	HCF	hf-pulsator

m = monotonic test; c = cyclic test; * scheduled value; ** sawtooth loading protocol

For a better understanding of the time-dependent failure mechanism, altogether six tested screws (one per each level of N at $R = 0.56$) were analysed by means of a fractographic scanning electron microscopy (SEM), conducted by the Institute of Material Science, Joining and Forming at Graz University of Technology. Related findings are also discussed in section 3-5.3.3.

3-5.3.3 Test results and discussion

In Table 3.25, the main statistics, in form of mean values and variabilities ($CV[N]$) as well as 5 %-quantiles (empirically determined and by assuming LND as given in eq. (3.112)) of bearable load cycles dedicated to the LCF and HCF domain in case of $R = 0.56$, are shown.

$$y_{0.05,LND} = \frac{\mu_Y \cdot \exp \left[\Phi^{-1}(0.05) \cdot \sqrt{\ln(CV[Y]^2 + 1)} \right]}{\sqrt{CV[Y]^2 + 1}}, \quad (3.112)$$

with μ_Y as the mean value of the lognormal distributed sample (approximated by the average value of test results) and $\Phi^{-1}(p)$ as the inverse standard normal distribution operator. Considering a logarithmic scaling, a pronounced and linear increase of both $\text{mean}[N]$ and $N_{0.05,i}$ with decreasing σ_{\max} can be observed, confirming the assumptions made in section 3-5.3.1. With regard to the variability of the test results, remarkably high values of $CV[N]$, as well as significant differences of this parameter between the investigated stress horizons are given. While the size of $CV[N]$ is assumed to be majorly influenced by the surface discontinuities, discussed in section 3-5.2.1, the latter mentioned circumstance indicates a questionable stability related, which is probably caused by the small number of tests conducted per each level of σ_{\max} . The course of both parameters $\text{mean}[N]$ and $N_{0.05,i}$ with varying σ_{\max} should thus be regarded

rather as an initial assessment, than as a generally valid relationship of axially loaded self-tapping screws' time-dependent loadbearing behaviour.

Table 3.25: Main statistics of cyclic screw test results in the LCF/HCF domain; basing on Imsirovic (2014)

horizon	σ_{\max} [N/mm ²]	R [-]	mean[N] [-]	CV[N] [%]	mean[$\log_{10}(N)$] [-]	$N_{0.05,empD}$ [-]	$N_{0.05,LND}$ [-]	$\log_{10}[N_{0.05,LND}]$ [-]
10^3	1,429	0.56	2,181	15.5	3.34	1,790	1,660	3.22
10^3	1,321	0.56	4,258	7.0	3.63	3,902	3,784	3.58
10^4	755	0.56	39,383	35.0	4.60	28,475	22,010	4.34
10^5	453	0.56	142,140	6.0	5.15	131,780	128,458	5.11

Now focusing σ_{\max} dedicated to $N_C = 2 \cdot 10^6$, the corresponding results are illustrated in Table 3.26 for varying $R = \{0.10, 0.56, 0.90\}$. The related strength level, further denoted as f_{fat} , has been determined according to DIN 969 (1997), see eq. (3.113) and eq. (3.114):

$$\text{med}[f_{fat}] = \text{med}[\sigma_{\max}] = \max[\sigma_{\max}] + \Delta\sigma \cdot \left(\frac{A}{C} \pm 0.5 \right), \text{ and} \quad (3.113)$$

$$\text{sd}[\sigma_{\max}] = 1.62 \cdot \Delta\sigma \cdot \left(\frac{C \cdot E - A^2}{C^2} + 0.029 \right), \quad (3.114)$$

with $\min(\sigma_{\max})$ as the minimum stress level of all staircases applied, $\Delta\sigma$ as step size (here: 24 N/mm²) and $\{A, C, E\}$ as the coefficients determined in Annex B-2.2, Table B.7 to Table B.9. The \pm sign in eq. (3.113) furthermore depends on comparing the sums of failed and survived specimen (“+” stands for more specimen failed, “-” stands for more specimen survived within one test series). It should be pointed out, that eq. (3.113) and eq. (3.114) base on a maximum-likelihood estimation (MLE), and have been derived by Dixon and Mood (1948), presupposing normal distributed values for f_{fat} . Table 3.26 thus comprises 5 %-quantiles of f_{fat} assuming ND and LND and determined by presupposing $\text{med}[f_{fat}] \rightarrow \text{mean}[f_{fat}]$. Since both values of $f_{fat,0.05,i}$ are almost equal, it was decided to apply $f_{fat,0.05,LND}$ for further considerations.

Table 3.26: Main statistics of f_{fat} dedicated to N_C

R [-]	N [-]	med[f_{fat}] [N/mm ²]	CV[f_{fat}] [%]	$f_{fat,0.05,ND}$ [N/mm ²]	$f_{fat,0.05,LND}$ [N/mm ²]
0.90	$2 \cdot 10^6$	1,008	2.7	963	964
0.56	$2 \cdot 10^6$	256	3.8	240	240
0.10	$2 \cdot 10^6$	143	9.3	121	122

Subsequently, the S/N-diagram, given in Figure 3.59, illustrates the experimentally determined values for N in dependence of σ_{\max} , considering the results from Table 3.25 and Table 3.26 in case of $R = 0.56$. Both models, included and aimed to cover the HCF domain for mean values and 5 %-quantiles, are equal to eq. (3.111) with index “C” instead of “D”. The inclination coefficient k_{SN} , as the only remaining unknown parameter, was determined by numerically solving the given least squares problem with the spreadsheet software Microsoft[®] Excel (2010). Doing so, k_{SN} results to 3.87 for both statistical levels indicating a tendency for the classification as a significant notch, according to Table 3.23. Since the position of both groups related to $N = 10^3$, carried out with comparatively small loading frequencies f , widely conforms to the overall data trend, an influence of f on N is not observable.

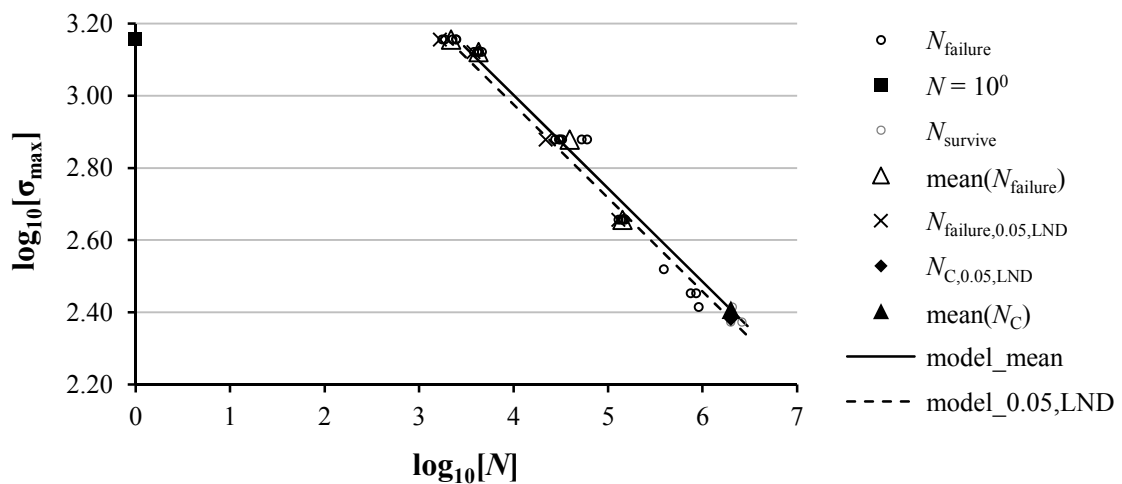


Figure 3.59: Bearable load cycles in dependence of N in case of $R = 0.56$

With regard to the impact of the stress ratio variation on the time-dependent loadbearing behaviour, a significant and progressive decrease of f_{fat} with decreasing R can be concluded, considering the results given in Table 3.26. Figure 3.60 subsequently compares the corresponding results in form of values for k_{fat} (5 %-quantiles) with the assumption for steel rods, according to EN 1993-1-9 (2013) (“detail category 50”), as well as with an own approach derived by varying $\Delta\sigma$ in eq. (3.110), achieving an adequate confirmation in case of $\Delta\sigma = 100 \text{ N/mm}^2$; see eq. (3.115):

$$k_{\text{fat},N} = \frac{1}{f_u} \cdot \frac{100}{(1-R)}. \quad (3.115)$$

Even though a similar behaviour in dependence of R can be observed, “detail category 50” obviously underestimates the experimentally determined relationship. Furthermore, the corresponding difference increases with increasing R up to a significant extent in case of $R = 0.90$.

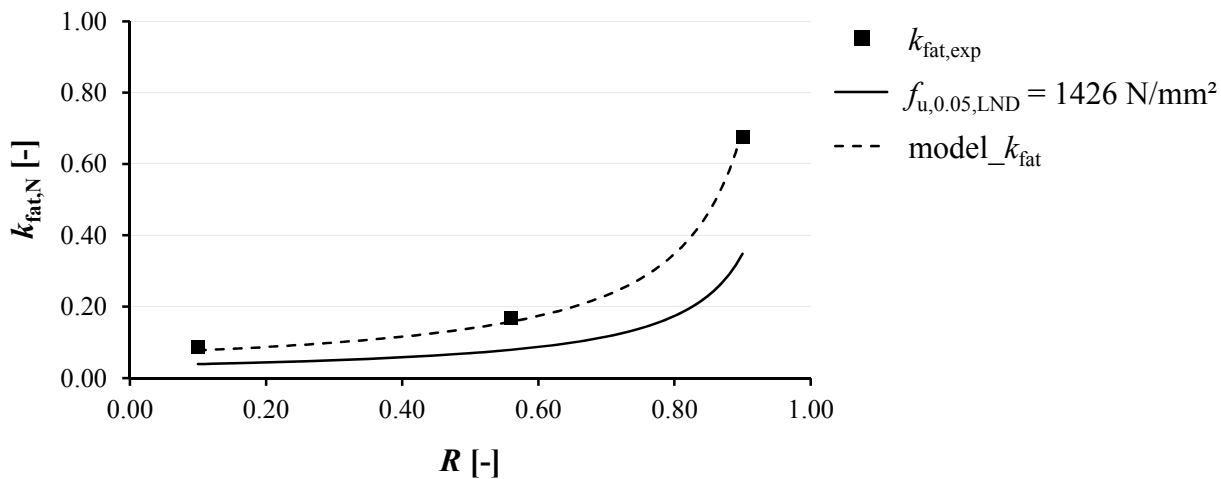


Figure 3.60: Comparison of experimentally determined values for k_{fat} with the model assumption and “detail category 50” according to ON EN 1993-1-9 (2013)

Now concentrating on the impressions gained from the fractographic SEM, performed by the Institute of Material Science, Joining and Forming at Graz University of Technology. Figure 3.61 to Figure 3.66 subsequently illustrate the corresponding microscopic scans conducted for the six screws, each dedicated to a stress horizon, outlined in Table 3.24 in case of $R = 0.56$. All specimen, being a part of this programme, were thereby analysed regarding their fracture pattern situated at the cross-section’s centre and edges. In case of $N = 10^0$, both related positions, given in Figure 3.61 (c, d), indicate a so-called “cup-and-cone” fracture, which occurs in form of spherical dimples in the microscopic view and allows a classification as a ductile failure mode in tension, c. f. Bürgel et al. (2014).

While a similar appearance can also be observed for cross-section’s centre positions, Figure 3.62 (d) to Figure 3.66 (d), related views dedicated to the edges indicate a pattern deviating from the aforementioned reference. In fact, they describe differently pronounced brittle fracture, as especially found for crack origins of fatigue dependent failure modes. Those initial areas, indicating the begin of the crack propagation, commonly have a semi-circular shape, c. f. Bürgel et al. (2014), which is clearly observable in the macroscopic views, given in Figure 3.62 to Figure 3.64 (a). In contrast to these images, related to $N = 10^3$ and 10^4 , which furthermore have a comparatively rugged macroscopic surface with radially oriented terrace-like structure, both made for $N \geq 10^5$ can be characterised by less crack origins and smooth fracture patterns, enabling a clear detection of the reduced cross-section’s area, failed by exceeding the remaining bearing capacity – see Figure 3.65 and Figure 3.66 (b). Worth mentioning, further characteristics of fatigue failure, such as striations or beach marks, typically found in the area of steady crack propagation, c. f. Bürgel et al. (2014), cannot be observed at all.

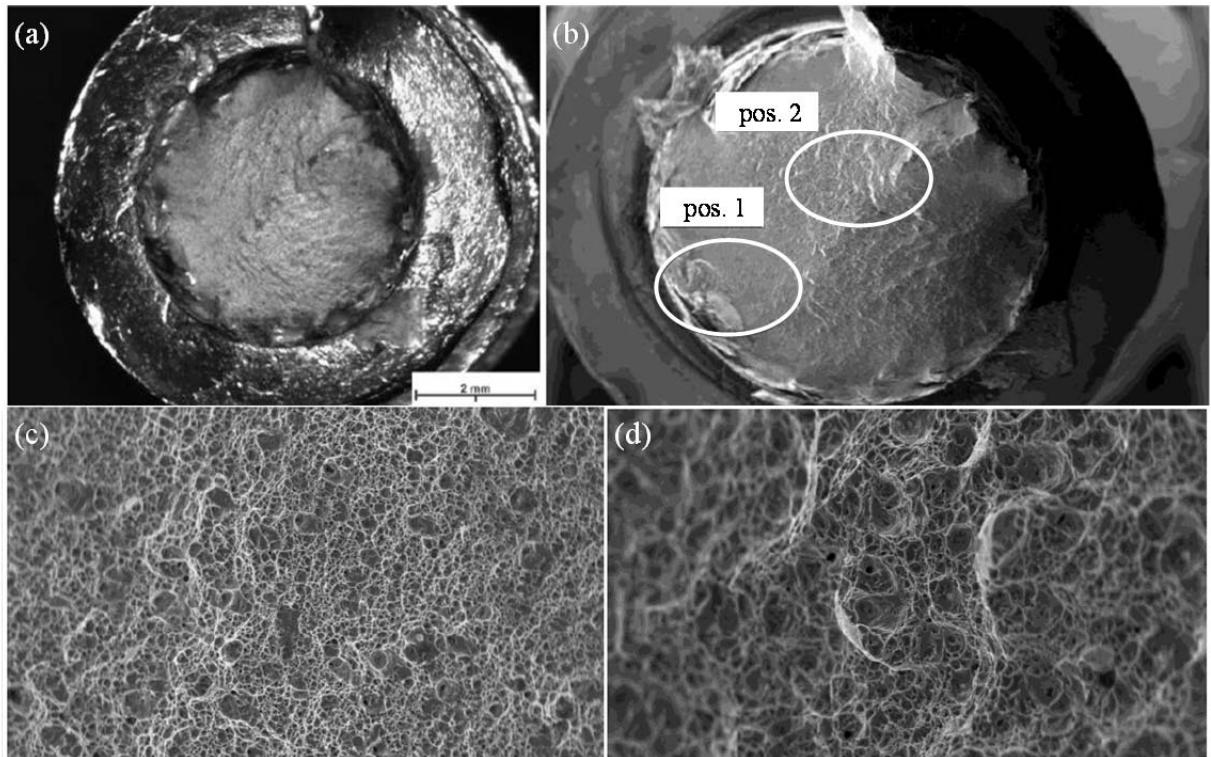


Figure 3.61: SEM images of the reference screw ($N = 10^0$); (a) photo of the fracture pattern; (b) microscopic scan with zoom positions; (c) zoom view of pos. 1; (d) zoom view of pos. 2; 500x magnification

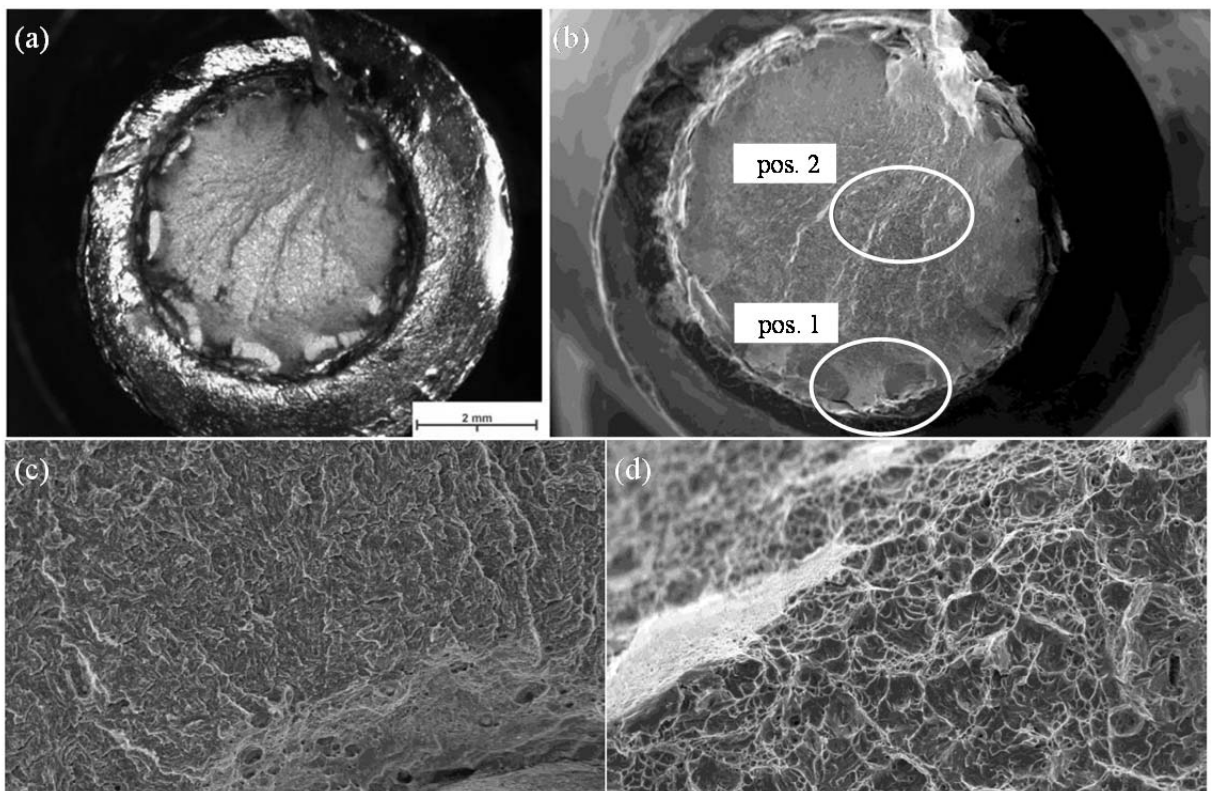


Figure 3.62: SEM images of a screw failed at $N = 1,766$; (a) photo of the fracture pattern; (b) microscopic scan with zoom positions; (c) zoom view of pos. 1; (d) zoom view of pos. 2; 500x magnification

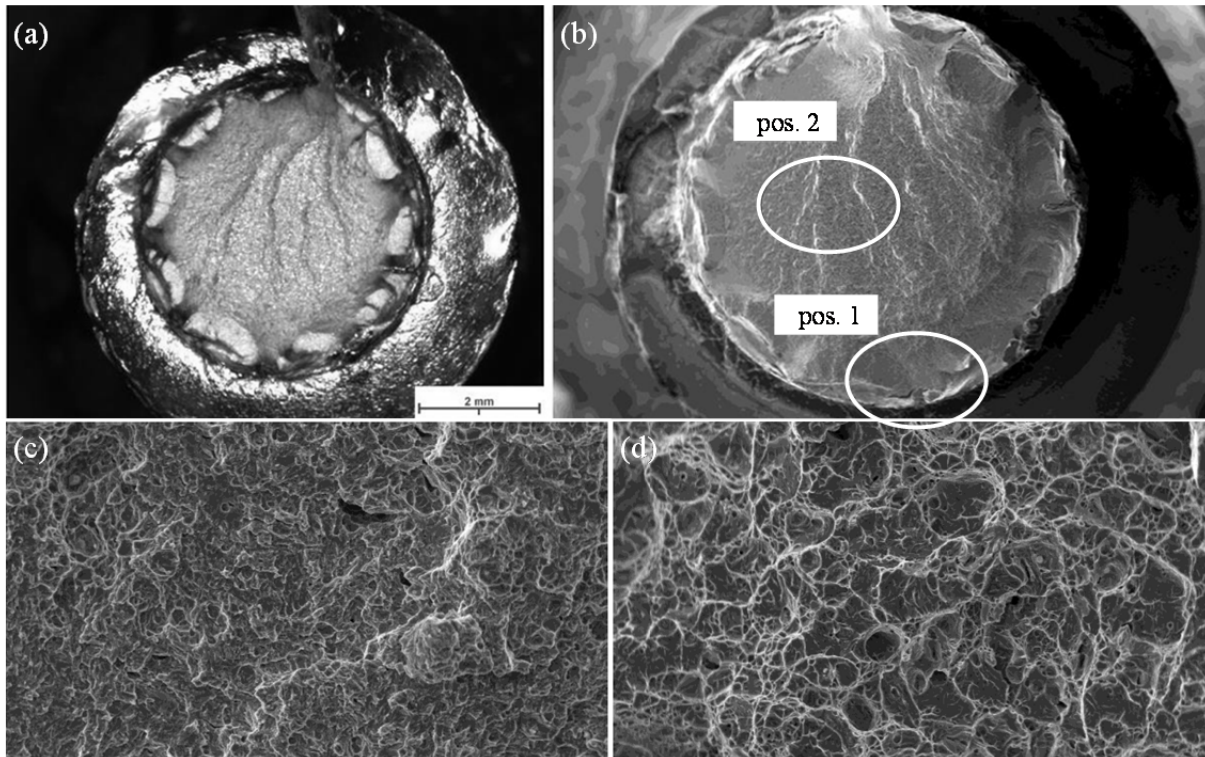


Figure 3.63: SEM images of a screw failed at $N = 4,340$; (a) photo of the fracture pattern; (b) microscopic scan with zoom positions; (c) zoom view of pos. 1; (d) zoom view of pos. 2; 500x magnification

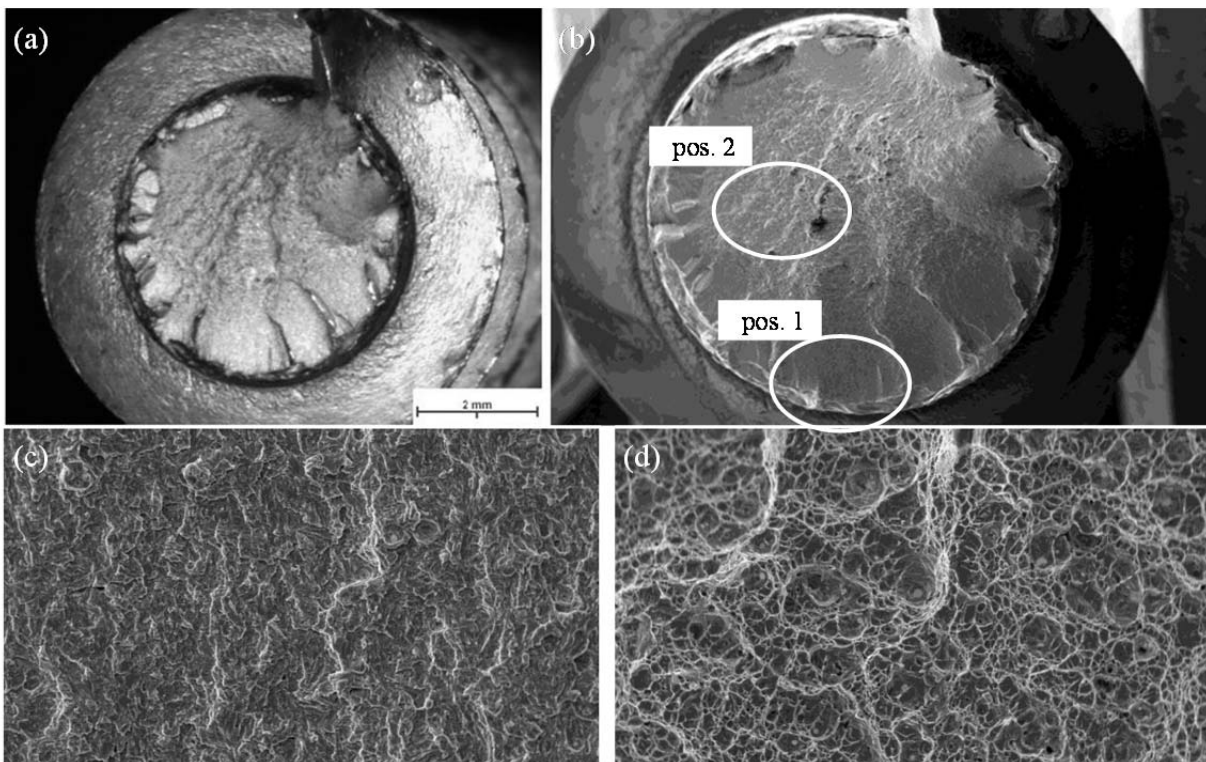


Figure 3.64: SEM images of a screw failed at $N = 31,500$; (a) photo of the fracture pattern; (b) microscopic scan with zoom positions; (c) zoom view of pos. 1; (d) zoom view of pos. 2; 500x magnification

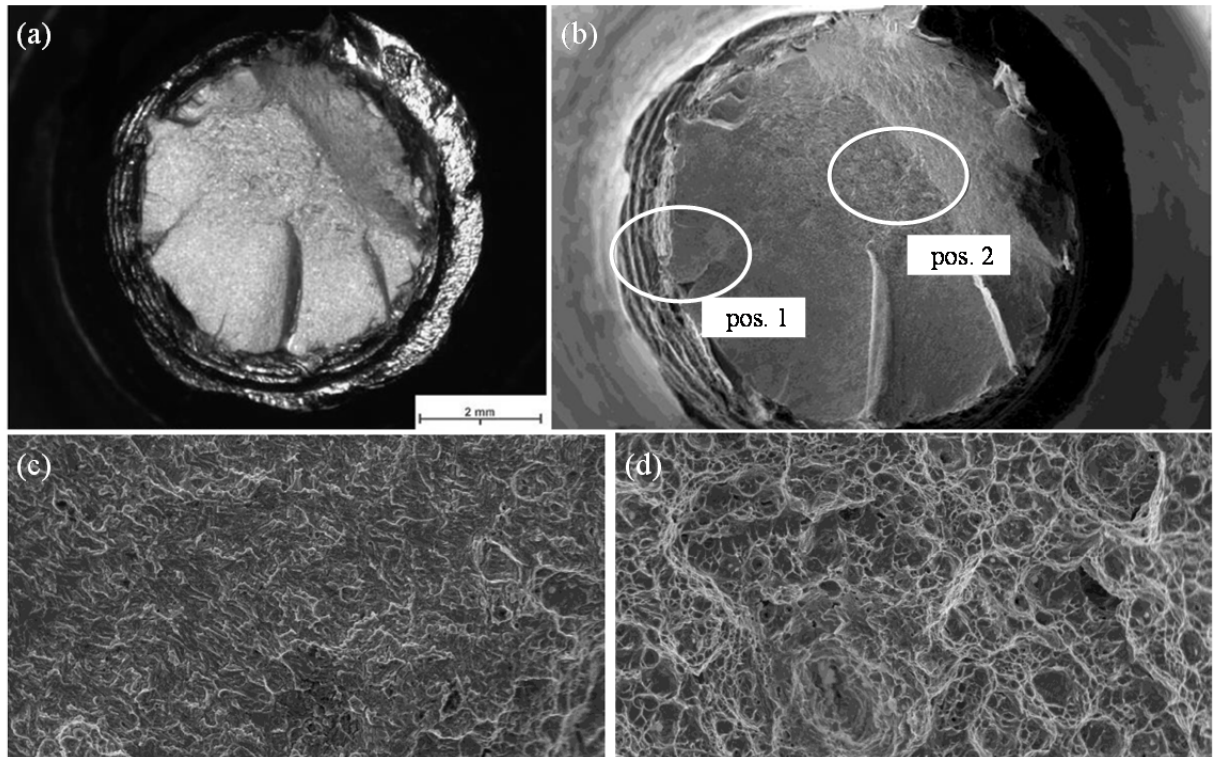


Figure 3.65: SEM images of a screw failed at $N = 144,500$; (a) photo of the fracture pattern; (b) microscopic scan with zoom positions; (c) zoom view of pos. 1; (d) zoom view of pos. 2; 500x magnification

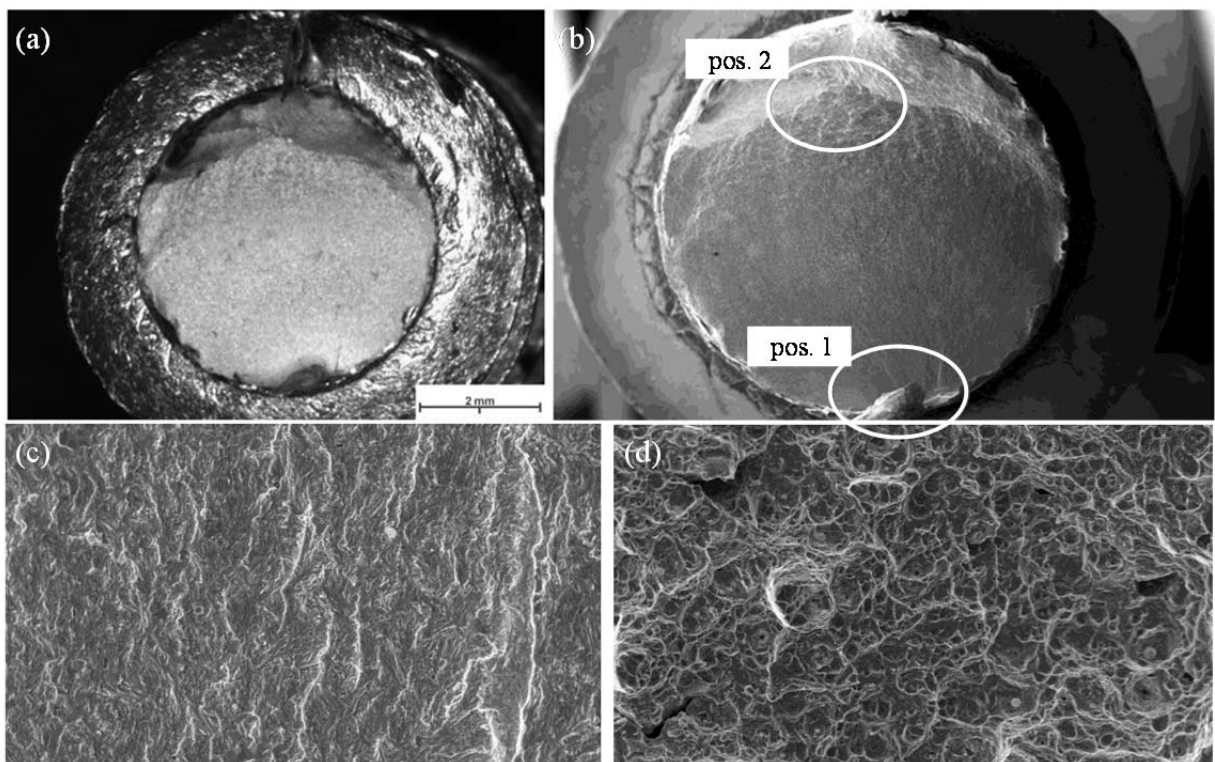


Figure 3.66: SEM images of a screw failed at $N = 2,088,700$; (a) photo of the fracture pattern; (b) microscopic scan with zoom positions; (c) zoom view of pos. 1; (d) zoom view of pos. 2; 500x magnification

Based on the observations made in Figure 3.62 to Figure 3.64, the stress level applied obviously influences the appearance of the fracture pattern, as well as the number of crack origins situated at the cross-sections' edges. A corresponding relationship between the latter mentioned and determined N for each screw is consequently given in Table 3.27, confirming this circumstance. Worth mentioning, the crack origins are assumed to be caused by the surface discontinuities, discussed in section 3-5.2.1, which are thus seen as a major parameter, significantly influencing the fatigue related loadbearing behaviour of self-tapping screws.

Table 3.27: Bearable N and positions of crack origins of screws analysed by SEM

specimen notation	AL	11	28	12	7	20
N [-]	10^0	1,766	4,340	31,500	144,500	2,088,700
pos. of crack origins [-]	-	8	11	3	2	1

3-5.4 Environment

3-5.4.1 General aspects concerning metal corrosion

Now concentrating on tensile loaded self-tapping screws exposed to environments deviating from ideal (laboratory) conditions as commonly defined by temperature and relative humidity (r. h.) in form of 20 °C and 65 % r. h. representing service class 1 according to ON EN 1995-1-1 (2015).

Especially the existence of water (H_2O) in combination with oxygen (O_2) or certain acid components (both result to aqueous solutions) thereby forms an electrolyte, which increases the tendency of base metal ions (with negative standard potential E_0 , e. g. such as iron (-0.44) or zinc (-0.76)) dissolving into the solution. This phenomenon is denoted as the electrochemical corrosion, c. f. Weißbach (2012), which consists of an anodic and a cathodic reaction. The pH of the electrolyte, defined as the negative of the base ten logarithm of the hydrogen ion activity, c. f. Robinson and Stokes (1959), governs this reaction process. In case of aerated water ($pH \geq 7$, neutral to alkaline), anodic and cathodic reactions can be described, according to eq. (3.116) to eq. (3.121), summarising the explanations given in Nürnberger (1995) and Weißbach (2012). The anodic reaction, also denoted as oxidation, thereby leads to the dissolution of the metal atoms (here: iron, Fe) into ions, combined with a loss of electrons, see



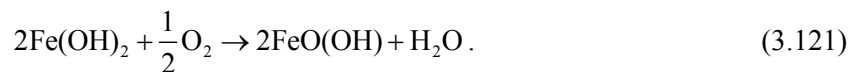
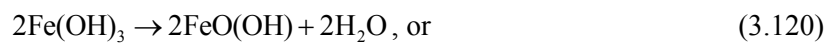
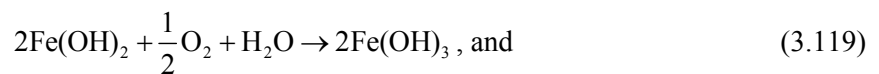
This process only perpetuates if thereby the lost electrons combine with oxidising components in the electrolyte (here oxygen, O_2) to hydroxyl ions OH^{-} as part of the cathodic reaction (reduction), see



In the next step, iron and hydroxyl ions are combined in the electrolyte to Fe(II)-hydroxide as a corrosion product of this so-called primary reaction, see



Subsequently, the rust (Fe(III)-oxide-hydroxide or FeO(OH)) formation occurs within a secondary reaction in form of



The process of anodic and cathodic reaction until forming Fe(II)-hydroxide (primary reaction) is illustrated in Figure 3.67.

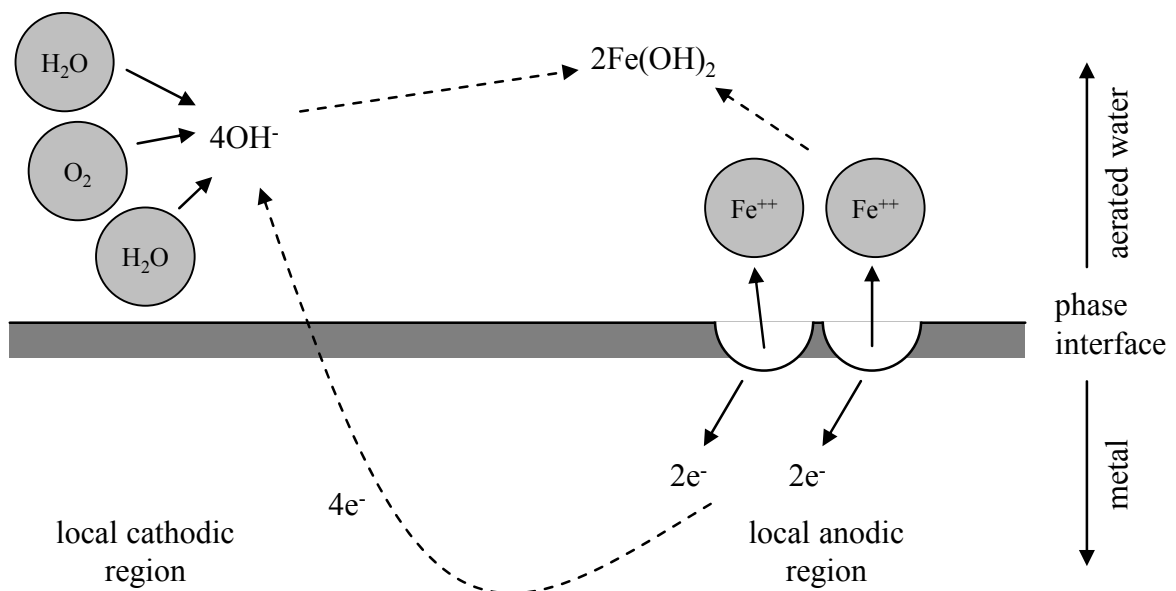
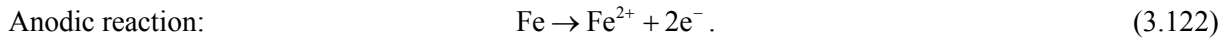
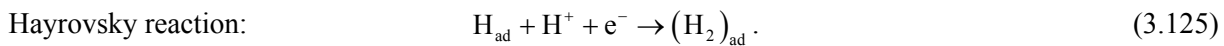
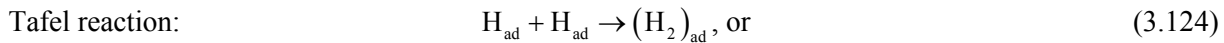
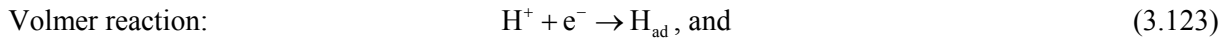


Figure 3.67: Schematic illustration of metal (steel) corrosion in aerated water (primary reaction); basing on Nürnberger (1995)

In case of aqueous and non-oxidising acids, such as hydrochloric acid (HCl) and $\text{pH} \leq 5$, a different process, also denoted as hydrogen corrosion (or acid corrosion), takes place, c. f. Nürnberger (1995) and eq. (3.122) to eq. (3.125):



The perpetuation is enabled at the local cathodic region occurring in form of a hydrogen discharge, as described in section 3-5.2.3 (Figure 3.53), see



Irrespective of the specific type of corrosion, their impact on the performance of self-tapping screws applied in engineered wood products (EWPs), can be expressed as the corrosion rate R_C [$\mu\text{m} \cdot \text{a}^{-1}$], defined by a loss of cross-sectional dimension per year. In fact, the size of R_C depends on many parameters comprehensively discussed in literature, corresponding summaries can be found in Gläser et al. (2013) or Zelinka (2014). In the frame of this thesis, the scope is reduced to summarising the influence of the main parameters, i. e. wood moisture content u , timber species' specific contents and their pH. The predominately negative effect of the chemical wood preservation on corrosion, see e. g. Zelinka et al. (2010), is thereby excluded.

Since both types of electrochemical processes, explained in eq. (3.116) to eq. (3.125), require the presence of water in the environment surrounding the metal fastener, the wood moisture content can be regarded as the major variable, controlling the corrosion of self-tapping screws applied in EWPs. Zelinka (2014) summarises the corresponding observations made in the past and defines a lower limit value of u causing corrosion, which varies between 15 % ÷ 18 %. One possible explanation is a percolation threshold of $u \approx 16$ %, where – if exceeded – a continuous path of conducting water (ion conduction) is given, c. f. Zelinka et al. (2008). Above the aforementioned bandwidth, increasing $u \geq 20$ % leads to significantly increasing R_C until reaching the timber's fibre saturation point (FSP, $u = 25 \div 30$ %), where it converges to a constant maximum plateau. The corresponding behaviour has been observed by Dennis et al. (1995) and subsequently used by Zelinka et al. (2011) for deriving an empirical estimation model of R_C in dependence of u , see eq. (3.126):

$$R_C = \frac{A}{1 + \exp[B \cdot (u_{\text{met}} - u)]}, \quad (3.126)$$

with A as the maximum corrosion rate at FSP (the asymptotic corrosion limit, also depending on further influencing parameters as previously mentioned), B as the curve inclination and u_{met} as the metric moisture content at which $R_C = A / 2$. Worth noting, that within their model considerations Zelinka et al.

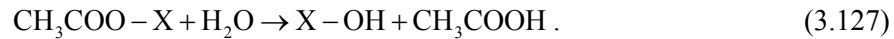
(2011) set both parameters $\{B, u_{\text{met}}\}$ to $\{0.83, 24\%\}$, which agreed well with experimental results determined by Dennis et al. (1995).

In addition to the wood moisture content, the pH of the timber species applied is an essential parameter influencing the size of R_C . Beside the fact, that the aqueous solutions' pH governs the type of corrosion process, see eq. (3.116) to eq. (3.125), it has furthermore a major impact on the course of R_C . As explained in Silverman (2003), the corrosion of carbon steel or zinc in neutral conditions ($5 < \text{pH} < 9$, aerated water) is mainly independent from pH, while in case of strongly acid conditions ($\text{pH} \leq 5$), a complex interaction between pH, the type and composition of acids in the solution and R_C has to be observed. With focus on timber material, a clear correlation is given, c. f. Farmer (1962), a corresponding relationship can be simplified by an exponential increase of R_C with decreasing pH, c. f. Zelinka and Stone (2011), who furthermore consider a constant plateau of R_C at $\text{pH} > 5$. Table 3.28 subsequently includes the pH-values of different timber species, summarised in Rückert (1986), which have been determined for specimen stored at "average" temperatures and relative humidity. In this context it is worth to point out, that Rückert (1986) and also Packman (1960) report, that the pH may significantly decrease (up to more than one unit) with increasing T and r. h.; especially the latter confirms the aforementioned dependency of R_C on u .

Table 3.28: Typical pH-values (aqueous extracts) of different timber species; extracted from Rückert (1986)

timber species	pH
oak	3.3 ÷ 3.9
beech	3.8 ÷ 5.2
Douglas fir	3.4 ÷ 4.4
larch	4.3 ÷ 4.7
pine	4.3 ÷ 5.1
birch	4.6 ÷ 5.3
spruce	4.8 ÷ 5.3

Now the focus is put on the wood acidity, predominately responsible for the corrosion in case of $\text{pH} \leq 5$, which corresponds more or less to all species given in Table 3.28. The main reason therefore is the existence of two acids, namely formic acid (HCOOH) and acetic acid (CH_3COOH) in timber material. Since the quantity of acetic acid was found to be much higher than that of formic acid, c. f. Balaban and Ucar (2003), further considerations are restricted to the latter mentioned. As reported in Packman (1960), volatile acetic acid is freed when acetyl groups, originally associated with hemicelluloses in form of acetates ($\text{CH}_3\text{COO-X}$; X represents the rest), get in contact with water, the corresponding process is denoted as hydrolysis and given in eq. (3.127), see



The quantity of volatile acetic acid in the aqueous solution mainly depends on the quantity of acetyl groups and the velocity of hydrolysis, the latter again majorly influenced by temperature and relative humidity, c. f. Rückert (1986). Summarising his conclusions, which in fact predominately base on data gained by Packman (1960), the complex interrelationship between acetyl content, hydrolysis velocity and acid content is subsequently expressed in Table 3.29 and Figure 3.68. Therein, the loss of acetyl content, as well as the increase of volatile acetic acid content caused by storing sawdust samples of four (herein) selected timber species under 48 °C and wet conditions, as determined by Packman (1960), is reported.

With regard to the data trend, illustrated in Figure 3.68, a degressive course of acid quantity in dependence of storage time and qualitatively irrespective from the timber species, can be observed. The maximum content, as well as the biggest inclination (which means velocity), is found for oak wood, the corresponding relationship to the other investigated species is quite similar to the different sizes of pH, given in Table 3.28. The same situation exists for acetyl contents of oak, compared to both coniferous woods in Table 3.29. A remarkable high value, determined for birch, contradicts a generally valid positive correlation between acetyl and acetic acid content and thus also between acetyl content and R_c . In this context it is furthermore worth mentioning, that the gained results were determined under extreme environmental conditions. Thus, Rückert (1986) concludes, that in case of practical conditions regarding temperature and relative humidity, the process of developing acetic acid in Figure 3.68 would last several years.

Table 3.29: Mean acetyl contents of four selected timber species, initial and after two years of storage at $T = 48 \text{ }^\circ\text{C}$ and wet climate (damp conditions); data from Packman (1960)

timber species	acetyl content [%]		loss [%]
	initial	after two years storage	
oak	2.59	0.13	95.0
birch	3.64	1.67	54.1
Douglas fir	1.10	0.38	64.5
Sitka spruce	1.23	0.38	69.1

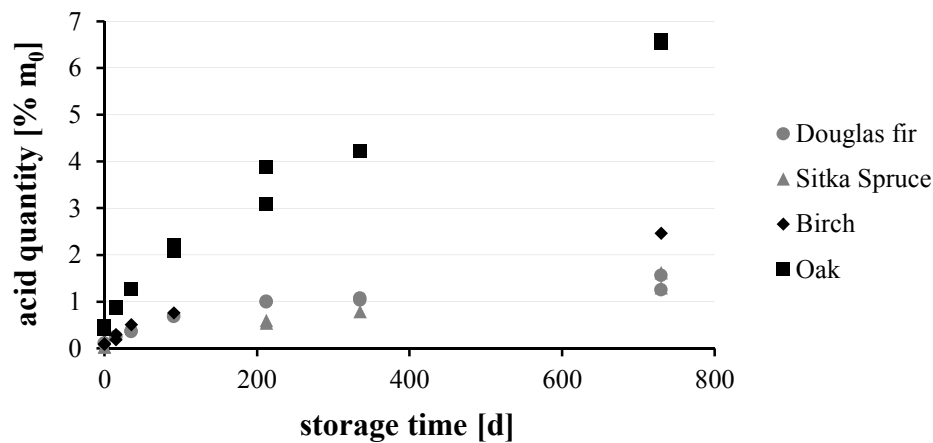


Figure 3.68: Quantity of acetic acid in dependence of storage time (days) at $T = 48\text{ }^{\circ}\text{C}$ and wet climate (damp conditions) for four timber species; data from Packman (1960)

Now focusing on the corrosion process of iron (or zinc) in an aqueous solution, consisting of acetic acid if compared to that caused by hydrochloric acid, as generally described in eq. (3.122) to eq. (3.125). One investigation was carried out by Tran et al. (2013), who conclude that acetic acid has a certain “buffering” effect, which is responsible for an accelerated corrosion under these conditions. This means, that CH_3COOH dissociates and only provides additional hydrogen ions (H^+) rather than acetic acid molecules are reduced at the phase interface between electrolyte and metal, see eq. (3.128):



Consequently, the cathodic reaction only comprises the reduction of hydrogen ions in form of 1x Volmer followed by 1x Heyrovsky, as proposed by Amri et al. (2011) for this situation, c. f. eq. (3.123) and eq. (3.125). Similar to the galvanisation process, described in section 3-5.2.3, parts of thereby formed H_{ad} possibly diffuse into the metal, thus additionally increase the vulnerability of HISCC.

Beside the impact of acetic acid on the corrosion of metal fasteners embedded in timber components, a possible role of further extractives, such as tannins (tannic acids) and therewith composed gallotannins (gallic acids), is controversially discussed in literature, c. f. Zelinka and Stone (2011). Especially in investigations, focusing on the durability of sawblades, c. f. Winkelmann et al. (2009), a pronounced negative effect of these components on corrosion is reported. According to Zelinka and Stone (2011), this might be caused by removing the Fe(III)-gallic acid formations – which may act as inhibitor, c. f. Krilov et al. (1993) – from the steel surface by a sawblade application creating friction and heat. In case of metal fasteners applied in timber products, a comparable mechanical exposure is not given at all. Additionally taking the outcomes published in Zelinka and Stone (2011) into account, who generally assign tannins

having an inhibitory effect in case of the latter situation (corrosion rate has a regressive course with increasing tannin concentration), they are not part of further considerations.

Now concentrating on the impact of corrosion on mechanical properties of metal fasteners embedded in EWP, which additionally depends on the specific type related. The corresponding classification in Figure 3.69 distinguishes between the corrosion, independently from mechanical stress, and such types, where an interrelationship with mechanical stress is given. In the former case, with regard to self-tapping screws, the corrosion (irrespective if uniform or non-uniform and independent from loading) leads to a loss of cross-sectional area and thus increases stress and strain in the reduced cross-section. This especially concerns such load situations causing linear stress distributions with maximum stresses located at the cross-section's edges, e. g. bending or torsion, c. f. Weißbach (2012). A related duration-of-load (DoL) approach (expressed by a loss of bearing resistance per time) of laterally loaded nailed connections is e. g. derived in Zelinka and Rammer (2012), who combine the European yield model, according to Johansen (1949), with the determined corrosion rates for the specific situation and with a hygrothermal simulation of the environment the joint is applied in. Even though a structural failure may occur, the corresponding process demands comparatively long time periods until reaching a significant reduction of the joint's bearing capacity.

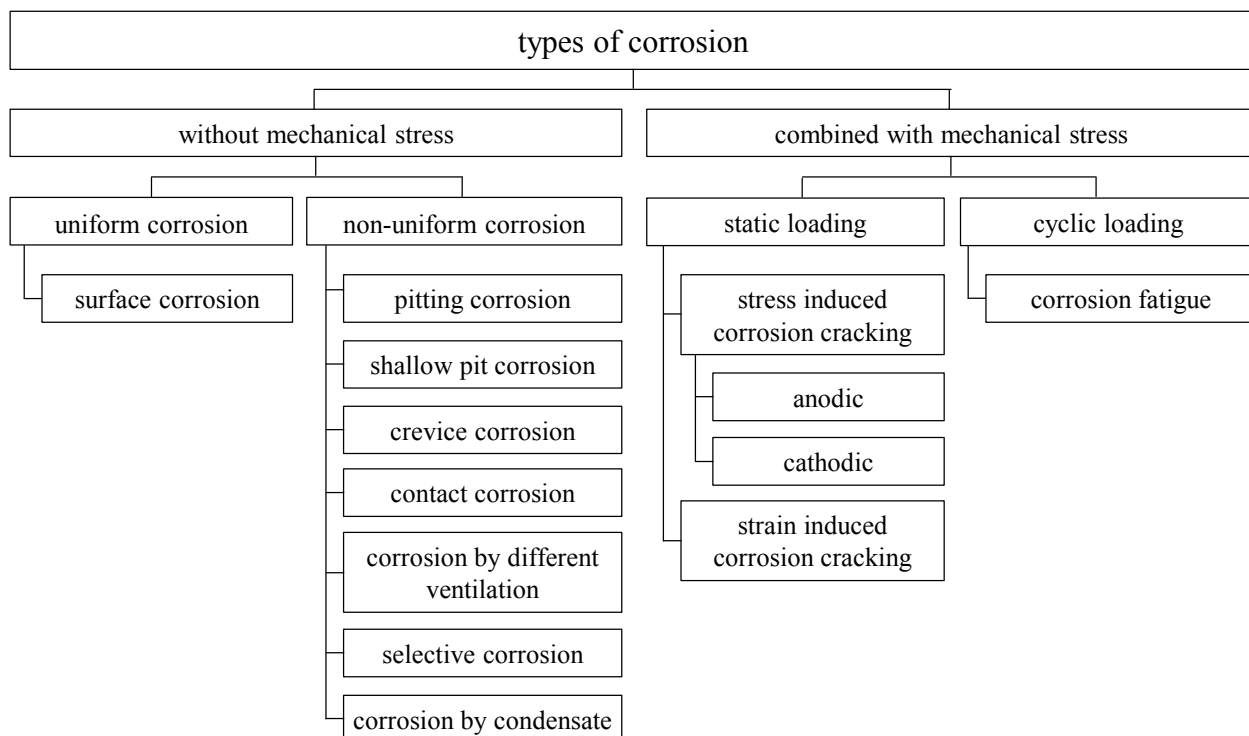


Figure 3.69: Classification of corrosion types; basing on Nürnberger (1995), Roos and Maile (2011) and Gläser et al. (2013)

The corrosion types occurring in combination with certain mechanical stress states are more relevant. The concomitance of environments and load situations, promoting corrosion and fatigue effective stresses, is commonly denoted as the corrosion fatigue, c. f. Radaj and Vormwald (2007). This phenomenon increases on the one hand R_C , as a consequence of vibration-induced extrusions and intrusions, harming the material's passive surface layer, and on the other hand the dispersion and number of surface discontinuities significantly influencing the component's endurance in case of cyclic loading, c. f. section 3-5.3. The main consequence reported in literature, c. f. Radaj and Vormwald (2007), Roos and Maile (2011) or Weißbach (2012), is the absence of a constant plateau in the S/N-diagram, expressed by a certain fatigue endurance limit $f_{fat,D}$, as described in section 3-5.3. Thus, the related ULS design process has to consider finite fatigue live limits determined for varying N .

Further focus is on the stress induced corrosion cracking (SCC) of quasi-statically loaded structural members as load situation, commonly found in the practical application of self-tapping screws. This phenomenon, which occurs as brittle and immediate failure mode (independent from service life), at load levels far below the characteristic (static) bearing capacity, is further subdivided into anodic and cathodic SCC, c. f. Figure 3.69.

Thereby, anodic SCC results as a combination of anions (Cl^- , O^{2-}), harming the material's passive surface layer (crack formation) and tensile stresses, being responsible for crack propagation and consequently fracture, c. f. Weißbach (2012). According to Orth (1974), it especially affects austenitic stainless steels and is thus not treated in detail. Its relevance, when designing timber constructions exposed to chloride atmospheres (e. g. indoor swimming pools, buildings situated near the coastline) with self-tapping screws commonly produced by stainless steels in such situations, is worth to be pointed out.

Cathodic SCC is an alternative (or old) notation of HISCC and especially affects martensitic steels, c. f. section 3-5.2.2. Its relevance for axially loaded self-tapping carbon steel screws is described in section 3-5.4.2 to 3-5.4.4.

3-5.4.2 The process of hydrogen-induced stress corrosion cracking (HISCC)

Figure 3.70 subsequently illustrates the fundamental requirements being necessary to cause HISCC of steel products, which are applied as structural components. Therein, they are subdivided into material properties, mechanical stress state and presence of hydrogen.

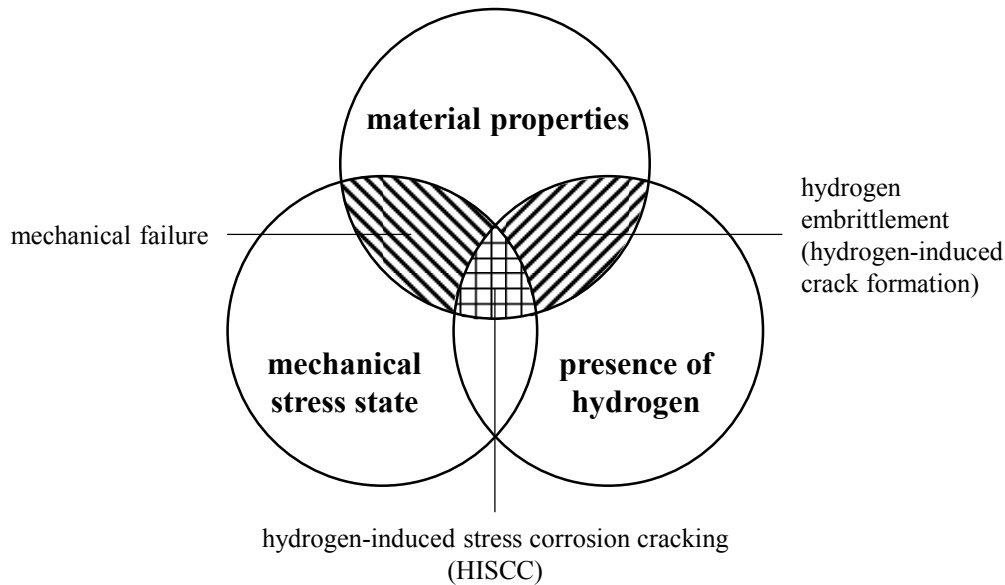


Figure 3.70: Requirements for HISCC; basing on Kloos et al. (1987)

With regard to material properties, as discussed in section 3-5.2, self-tapping carbon steel screws are made of martensitic steels with comparatively high values of tensile strength and hardness, and are especially vulnerable to HISCC. Furthermore, HISCC demands a mechanical stress state, where at least parts of the cross-section are stressed in tension, which is predominately given for the main fields the screws are commonly applied in, c. f. chapter 2. Finally, as indicated in the notation, it requires the presence of hydrogen (H) in the affected material. The related process is further denoted as hydrogen embrittlement and consists of three phases: adsorption, absorption and diffusion, c. f. Nürnberger (1995). Therein, the possible sources of absorbable hydrogen, such as steel production, welding, electrochemical corrosion, cathodic polarisation (galvanisation) or the existence of compressed gaseous hydrogen in the metal's environment are reported.

Further neglecting the content of H, due to steel production, both adsorption and absorption of hydrogen in the specific case of self-tapping screws applied in EWPs, are mainly caused by cathodic reactions such as galvanisation or corrosion in aqueous solutions with $\text{pH} < 7$. The corresponding hydrogen discharge, providing adsorbed H_{ad} , is comprehensively described in section 3-5.2.3 and section 3-5.4.1.

As mentioned in section 3-5.2.3, H_{ad} can be subsequently absorbed by the material ($\text{H}_{\text{ad}} \rightarrow \text{H}_{\text{ab}}$) or recombines to innocuous H_2 molecules (2x-Volmer and 1x-Tafel or 1x-Volmer and 1x-Hayrovsky) in form of a so-called concurrence reaction, c. f. Nürnberger (1995). The share of absorbed hydrogen H_{ab} , if compared to H_2 , thereby increases with an increasing content of promoters, as well as with decreasing pH and oxygen content. Amongst others, such promoters are: combinations of sulphur and phosphor, especially hydrogen sulphide H_2S , c. f. Kayser (2001).

The diffusion process regarded as the transport of diffusible and vulnerable hydrogen within the material, mainly depends on the metal's crystalline structure. As indicated in section 3-5.2.2, the body-centred cubic lattice of martensitic steel restricts hydrogen solubility (10^{-3} times less), but features diffusion rates about 10^3 to 10^6 times higher than those assumed for the face-centred cubic lattice of austenitic steel, c. f. Nürnberger (1995). Furthermore, the hydrogen transport depends on the existence of lattice inhomogeneity and traps (both decelerate diffusion), as well as on H composition (diffusion to areas with less H concentration), temperature gradient (diffusion to areas with increasing temperature), electrical potential gradient (diffusion in cathodic direction) and stress gradient (diffusion to areas with extended crystalline lattice caused by tensile stresses), c. f. Oriani (1993).

Especially the latter dependency, the so-called Gorsky-effect, c. f. Gorsky (1935), has major relevance if the hydrogen embrittlement is combined with (internal and external) mechanical tensile stresses thus leading to HISCC, see Figure 3.70. As e. g. reported in Gräfen and Kuron (1987), four main theories: the pressure theory according to Zapffe and Sims (1941), the adsorption hypothesis according to Petch and Stables (1952), the dislocation theory and the decohesion theory according to Troiano (1960) and Oriani (1972) are generally used for describing the corresponding failure mode. Although it is assumed, that none of them may exclusively explain this complex process, several authors assign the decohesion theory a major relevance, c. f. Stellwag and Kaesche (1982), Oriani (1993), Nürnberger (1995) and Kayser (2001).

Thereby, H_{ab} is assumed to decrease the cohesive forces between the iron (Fe) atoms in the extended crystal lattice, enabling an elastic separation of lattice bonding, which leads to crack formation, propagation and finally fracture. According to Stellwag and Kaesche (1982), this especially occurs at extremal stress conditions, as they are found at the transition between plastic and elastic zones close to surface discontinuities, such as cracks or notches, see section 3-5.2.1 and Figure 3.71. This again underlines the major relevance of material properties (occurrence and size of surface discontinuities, yield strength and ductility, both significantly influencing the stress distribution illustrated in Figure 3.71) regarding the vulnerability of HISCC.

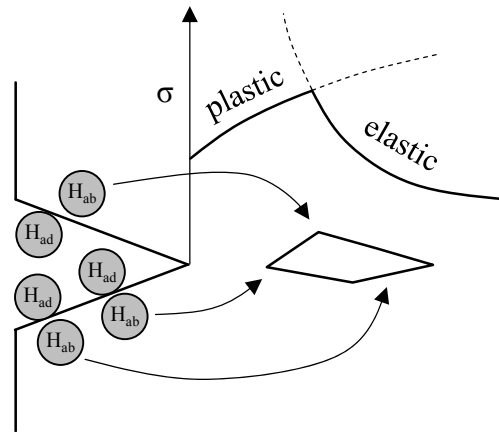


Figure 3.71: Crack formation close to surface discontinuities due to HISCC, according to Gräfen and Kuron (1987)

Figure 3.72 finally summarises the process of HISCC comprising hydrogen embrittlement (H discharge, adsorption, absorption and diffusion) and fracture mode, the latter presupposing the decohesion theory.

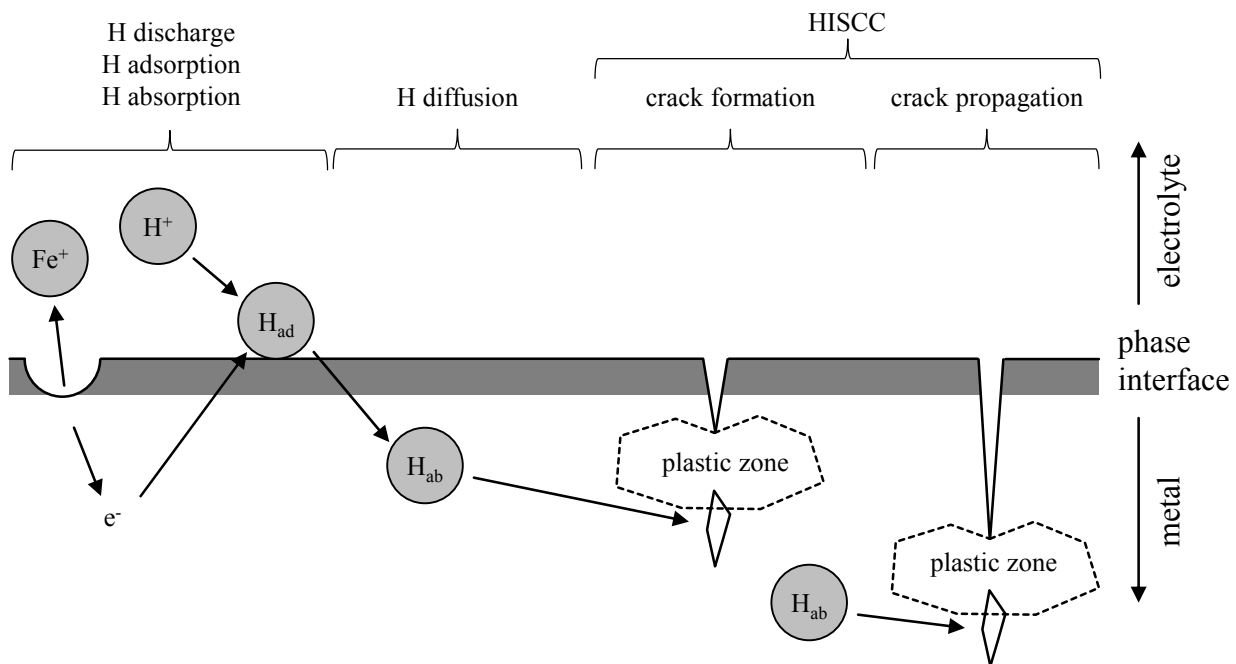


Figure 3.72: Process of HISCC considering decohesion theory; according to Nürnberger (1995)

The classification of HISCC is commonly conducted via analysing the ruptured cross-section of the affected specimen. According to Nürnberger (1995), brittle failure with fracture surface perpendicular to load direction and without contraction of cross-sectional area has to be observed in macroscopic view. In addition, crack origins are always located at the cross-section's edges. Examined under the microscope, for instance visualised by SEM, at least parts of the cross-section shall comprise an initial crack region with an intergranular fracture pattern (indicates brittle failure), consisting of gaping grain boundaries,

micropores and ductile hairlines also denoted as crow's feet, c. f. Nürnberger (1995) and Kayser (2001). Similar to the analysed specimen in section 3-5.3.3, the appearance of the residual fracture surface depends on the material's structural behaviour in the quasi-static tensile test. In case of self-tapping screws with mechanical properties, similar to those determined in section 3-4.5, a transgranular fracture pattern comprising spherical dimples, which indicate a ductile failure mode, can thus be expected for this area.

As indicated in section 3-5.4.1, SCC may occur as an immediate failure without prior warning and can be reached at load levels far below the component's tensile or yield strength, c. f. Nürnberger (1995). This process is influenced by the complex interrelationship of several material, mechanical and environmental parameters, c. f. Figure 3.70. Thus, an exact definition of an upper stress limit not be exceeded in practical application is hardly realisable. In general, the corresponding investigations aim on determining the vulnerability of a specific component regarding HISCC in form of a controlled parameter variation. The results are commonly expressed in form of DoL-curves, which are quite similar to the S/N-diagrams, discussed in section 3-5.3, c. f. Gräfen and Kuron (1987), Nürnberger (1995) or Pohl and Kühn (2010). Nevertheless, practical recommendations rather consist of prevention methods (e. g. limiting the steel hardness or strength, recommendation of heat treatment measures such as additional tempering after galvanisation, environmental modification, etc.) than of an endurance prediction.

Even though several boundary conditions of high-stressed timber connections or reinforcements, realised with predominately axially loaded self-tapping carbon steel screws, indicate a certain vulnerability regarding HISCC – there are no corresponding investigations published in this field. The only exception is a small amount of expert's reports on claims, where a related failure mode of comparatively small screws applied in secondary constructions has been observed, c. f. Reif (2014).

Motivated by this certain lack of knowledge, it was decided to carry out a fundamental research programme focusing on the influence of the aforementioned main parameters on the vulnerability of self-tapping carbon steel screws regarding HISCC. The corresponding investigations were conducted in cooperation with the Institute of Material Science, Joining and Forming at Graz University of Technology, in form of student projects (co-supervised by the author of this thesis), c. f. Toblier (2014), Hauptmann (2016) and Toblier (2016). The major outcomes are summarised in the following sections 3-5.4.3 and 3-5.4.4.

3-5.4.3 Materials and Methods

As summarised in sections 3-5.2.1, 3-5.2.2, 3-5.2.3, 3-5.4.1 and 3-5.4.2, the interrelationship of several mechanical, material and environmental parameters influences the occurrence of HISCC of carbon steels applied for structural purpose. Based on this literature survey, the experimental programme, conducted

within two long-term test campaigns at Graz University of Technology, contained a parameter variation which is discussed as follows:

Regarding the impact of material properties as a result of the screw production process, the variation considered both parameters, steel tensile strength and hardness. As mentioned in section 3-5.2.2, several authors define a lower limit of $f_u = 1,000 \text{ N/mm}^2$, if exceeded HISCC may occur in the structural application. Consequently, screws with two different strength levels, one below and one above this limit, have been applied within the programme. As shown in Table 3.30, the related specimen correspond to groups A_s_I_08_240 and A_s_IV_08_240 in case of test campaign I and to A_s_II_08_240 in case of test campaign II. The determination of the given reference mechanical properties can be found in section 3-4. Both groups, A_s_I_08_240 and A_s_II_08_240, have similar tensile strengths, but have significantly varying hardness distributions due to carbonitriding (c. f. Figure 3.44 and Table 3.31). This circumstance also enables a verification of the influence of the hardening procedure on the occurrence of HISCC. Since all considered fasteners are the outcome of one production cycle, where flat die rollers had been applied for thread forming, type and distribution of the surface discontinuities are expected being similar to those discussed in section 3-5.2.1.

Table 3.30: *Type, number and reference mechanical properties of the screw products applied in long-term test campaigns*

test campaign	product ID	n [-]	$F_{u,exp}$ [N]	$f_{u,pred}$ [N/mm ²]	mean[HV]
I	A_s_I_08_240	8	29,000	1,368	592
	A_s_IV_08_240	12	19,590	924	300
II	A_s_II_08_240	20	30,455	1,437	452

In section 3-5.4.2 the presence of diffusible hydrogen H_{ad} mainly caused by cathodic reactions, occurring in the frame of (a) galvanisation and (b) corrosion is discussed. Concentrating on (a), zinc-nickel coatings were observed, comprising a significantly smaller amount of H_{ad} if compared to screws with yellow chromates, c. f. section 3-5.2.3.

In order to verify an expected decrease of vulnerability regarding HISCC related, screws protected with both coatings have been considered within the experimental programme. Table 3.31 subsequently includes the number of fasteners (of each product group) assigned to yellow chromated (“yc”) and zinc-nickel (“zn”) coats. Worth mentioning, both types were not tempered after galvanisation. Since one part of the product group A_s_IV_08_240 could not be supplied by the manufacturer in this composition, blue chromated (“bc”) screws, additionally tempered after galvanisation, have been applied instead.

Table 3.31: *Hardening procedure and protective coating of the screw products applied in long-term test campaigns*

test campaign	product ID	n [-]	add. carbonitrided	add. tempered	coating	temp. after galvanisation
I	A_s_I_08_240	3	y	n	yc	n
	A_s_I_08_240	5	y	n	zn	n
	A_s_IV_08_240	6	n	y	bc	y
	A_s_IV_08_240	6	n	y	zn	n
II	A_s_II_08_240	11	n	n	yc	n
	A_s_II_08_240	9	n	n	zn	n

yc = yellow chromated, zn = zinc-nickel coated, bc = blue chromated

With regard to (b) conclusions, given in section 3-5.4.1, indicate that the corrosion rate R_C significantly increases with decreasing pH (below 5), representing the material's acidity as the main environmental source of H_{ad} . As summarised in Table 3.28, Figure 3.68 and Table 3.29, oak wood not only has the smallest pH, but also the highest amount of acetyl groups, hydrolysis velocity and acetic acid content and is thus supposed to develop the most aggressive environment, maximising the screws' vulnerability regarding HISCC. Consequently, the investigated timber species comprise oak and Norway spruce specimen, the latter representing the reference material screwed connections are commonly realised with, see Table 3.32.

Furthermore, the corrosion process demands wood moisture contents, exceeding a lower limit of $u = 15 \% \div 18 \%$, c. f. section 3-5.4.1. Consequently, the timber specimen, supplied by the manufacturers Hans J. Fischer Ges.m.b.H (oak) and HASSLACHER HOLDING GmbH (Norway spruce), were cut with the dimensions $w \times h \times l = 300 \times 80 \times 200 \text{ mm}^3$ and stored under certain climatic conditions until reaching values of u at least above 20 %.

Table 3.32: *Timber species applied in long-term test campaigns*

test campaign	product ID	<i>n</i> [-]	coating	timber species
I	A_s_I_08_240	3	yc	oak
	A_s_I_08_240	3	zn	oak
	A_s_I_08_240	2	zn	Norway spruce
	A_s_IV_08_240	3	bc	oak
	A_s_IV_08_240	3	bc	Norway spruce
	A_s_IV_08_240	3	zn	oak
	A_s_IV_08_240	3	zn	Norway spruce
II	A_s_II_08_240	7	yc	oak
	A_s_II_08_240	4	yc	Norway spruce
	A_s_II_08_240	6	zn	oak
	A_s_II_08_240	3	zn	Norway spruce

yc = yellow chromated, zn = zinc-nickel coated, bc = blue chromated

With regard to the climatic exposure, chosen for both long-term testing campaigns, two boundary conditions regarding temperature and relative humidity had to be considered:

On the one hand, the steady corrosion process demands moisture contents, never resulting below a lower limit of roughly 16 %, c. f. Zelinka et al. (2008). Such moisture contents occur at comparatively high relative humidity and low temperatures, as e. g. described in Schickhofer (2006a).

On the other hand, the hydrolysis velocity and thus an increasing presence of acetic acid are expected to be promoted by high temperatures.

Additionally, the performance of climatic chambers (wherein both test campaigns were conducted) had to be taken into account. In case of test campaign I, the corresponding facility, supplied by the Laboratory of Structural Engineering at Graz University of Technology, features maximum (constant) values of temperature and relative humidity in form of $T \approx 40 \text{ }^\circ\text{C}$ and r. h. $\approx 90 \text{ } \%$. Since this chamber could only be used for a period of 6 weeks, test campaign II has been subsequently conducted in a so-called fog chamber, supplied by the Institute of Technology and Testing of Construction Materials at Graz University of Technology. The installed climatic device enables achieving a theoretical upper limit of r. h. $\rightarrow 100 \text{ } \%$, which can only be reached at the room temperature of $T \approx 20 \text{ }^\circ\text{C}$. With increasing T (maximum is again about $40 \text{ }^\circ\text{C}$) a significant decrease of this upper limit is observable.

Considering all of the mentioned boundary conditions, it was decided to apply comparatively high temperatures varying between $30 \div 40 \text{ }^\circ\text{C}$, for promoting hydrolysis of acetic acid. The dry out of timber specimen below $u \approx 16 \text{ } \%$ has been prevented by maximising the relative humidity as far as possible and

additionally covering them with a transparent PE film acting as a water vapour barrier (especially necessary for test campaign II). The average values of temperature and relative humidity, steadily determined by a “Tinytag Plus 2 – TGP-4500” measuring device, are shown in Table 3.33. The monitoring of the moisture content was realised by the principle of electrical resistance (serving as an indicator for moisture content), using a system, comprising measurement screws (two per specimen), a moisture content sensor (“Gigamodul”) and a data logger (“Hygrofox”).

Table 3.33: Average values of temperature and relative humidity applied in long-term test campaigns

test campaign	duration	temperature	relative humidity
I	6 weeks	39.2 °C	91.1 %
II	24 weeks	33.7 °C	67.7 %

With regard to the mechanical stress state as the only parameter remaining the load chains, consisting of specimen pairs interlinked by the test screws (angle between screw axis and grain direction, $\alpha = 90^\circ$ in order to avoid DoL effects regarding withdrawal, c. f. section 5-5), were installed in the climatic chambers and exposed to dead loads in form of steel girders with F_{ax} of roughly 10 kN, see Figure 3.73. Worth mentioning, the oak wood samples were therefore pre-drilled with $d_{pD} = 6$ mm, c. f. ETA-11/0190 (2013), regarded as necessary in order to avoid steel failure in torsion when inserting the screws.

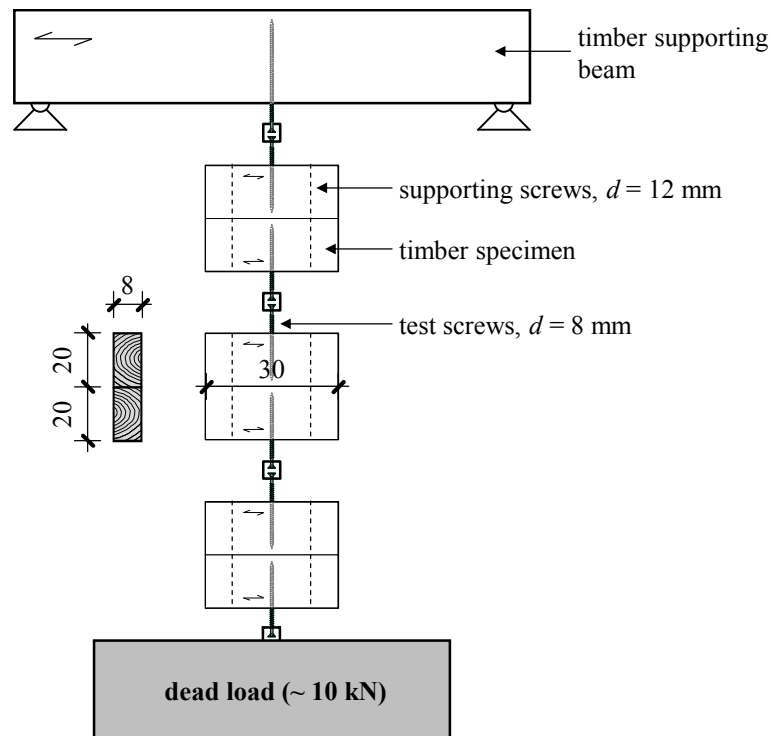


Figure 3.73: Schematic illustration of the long-term test configuration; dimensions in [cm]

Table 3.34 subsequently comprises tensile stress levels in form of η_σ , defined as the ratio between F_{ax} and f_{tens} (Table 3.30), occurring in the screw cross-sections as the result of this load situation. Due to constant dead loads, but varying f_{tens} for each product group, η_σ varies in a bandwidth of about 33 ÷ 51 % of the quasi-statically determined tensile capacity. Thus, this range overlaps with the ULS load level, commonly given in practical application, c. f. Flatscher (2017).

Table 3.34: *Approximate tensile stress levels for the screw types investigated*

test campaign	product group	η_σ [%]
I	A_s_I_08_240	34
	A_s_IV_08_240	51
II	A_s_II_08_240	33

In addition to temperature, relative humidity and moisture content, steadily measured as previously discussed, the data recording also contained the endurance (time to failure) of each screw applied within both test campaigns. In the frame of test campaign I, endurance monitoring was conducted by manual observations. Thus, the accuracy is restricted to 0.5 weeks. In case of test campaign II, a camera system taking pictures of all load chains every hour, was installed for this purpose. This increased the corresponding accuracy by far.

After finishing both time periods, given in Table 3.33, the quasi-static tensile capacity of screws remaining unbroken was determined according to section 0 in order to detect a possible pre-damage due to the already initialised crack formation as a consequence of HISCC. Those screws, which failed in the frame of long-term testing, and further ones, where a noticeable loadbearing behaviour has been observed in the quasi-static testing afterwards, were subsequently analysed by SEM conducted at the Institute of Material Science, Joining and Forming at Graz University of Technology, as well as by the voestalpine STAHL GmbH performing carrier gas hot extraction (CGHE).

In order to illustrate the influence of the acetic acid corrosion on screws' protective coats and cross-sections, macrophotos, as well as micrographs of the screw thread's xz- (or xy-)plane from selected specimen, have been made. With regard to the recorded moisture content distribution, the suitability of the aforementioned measurement system has been verified by means of performing the oven dry method according to ON EN 13183-1 (2004), determining u of the timber specimen (which means a prismatic section surrounding the screw hole) after finishing test campaign II.

3-5.4.4 Test results and discussion

The recorded climatic data in form of temperature, relative humidity and moisture content is subsequently given in Figure 3.74 and Figure 3.75 for test campaign I and in Figure 3.76 and Figure 3.77 for test

campaign II. As already mentioned in section 3-5.4.3, the climatic chamber, applied in the frame of test campaign I, enabled widely constant conditions regarding temperature and relative humidity, thus leading to a constant moisture content distribution resulting between $u = 16 \div 17 \%$. The only exception is a decrease of relative humidity (followed by a similar but delayed behaviour of moisture content) after testing for about ten days. This can be explained by an interruption of climate conditioning, due to replacing two screws by new ones – both were part of one load chain.

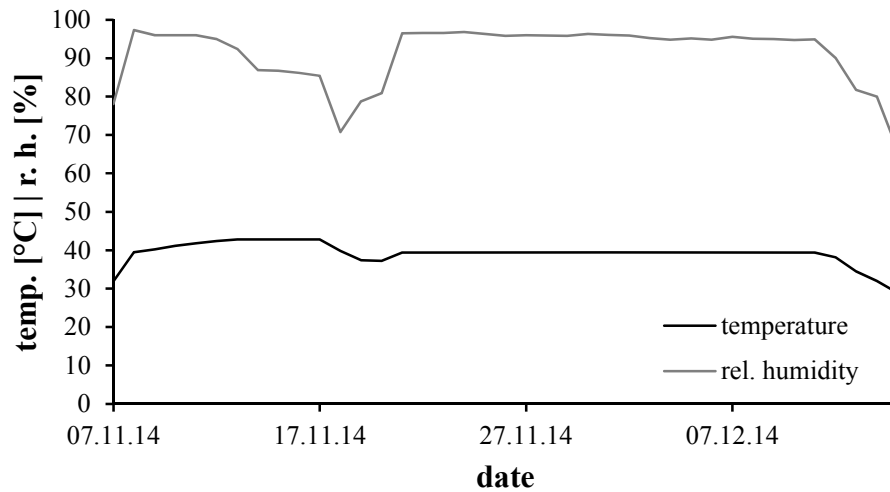


Figure 3.74: Distribution of temperature and relative humidity recorded in the frame of test campaign I

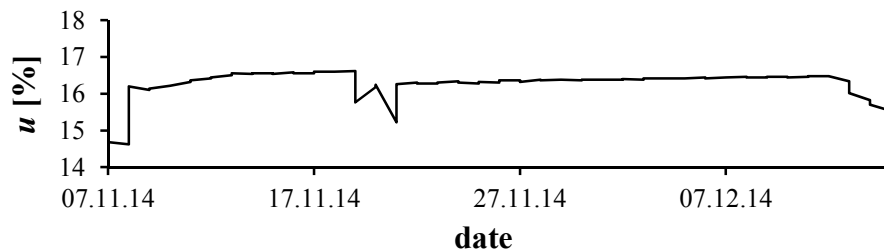


Figure 3.75: Distribution of moisture content recorded in the frame of test campaign I

In contrast to the first test campaign, the climatic distribution determined in the fog chamber, applied for test campaign II can be described as follows: as indicated in section 3-5.4.3, the climatic device, responsible for controlling the relative humidity, is very sensitive to temperature. As shown in Figure 3.76, a temperature change from 30 °C to 40 °C, conducted to increase corrosivity, led to a significant decrease of the relative humidity of about 50 %. Even though the timber specimen were covered with a vapour barrier, a minor pronounced (oak) to significant (Norway spruce) decrease of moisture content can be observed within the related period. In order to prevent u falling below 16 % while testing, it was decided to decrease the temperature again to 30 °C for the last five weeks.

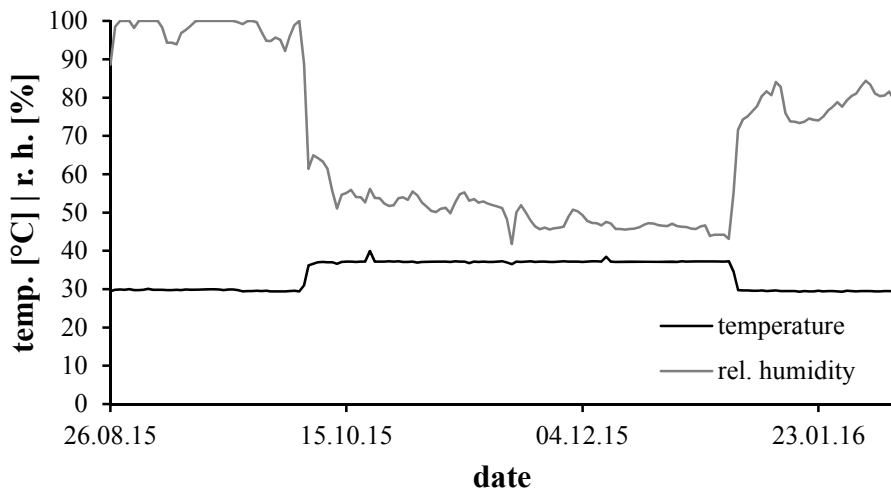


Figure 3.76: Distribution of temperature and relative humidity recorded in the frame of test campaign II

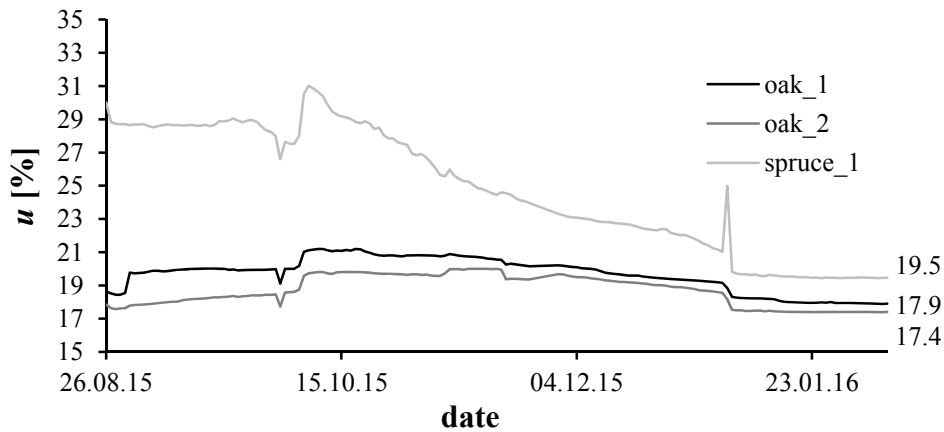


Figure 3.77: Distribution of moisture content recorded in the frame of test campaign II

Table 3.35 subsequently includes the moisture contents of the timber specimen (mean values of each load chain, dedicated to the measurement sensors in Figure 3.77), determined by performing the oven dry method after finishing test campaign II. Comparing them with the final values, given in Figure 3.77, a difference of about 2 % for oak wood has to be observed, while in case of Norway spruce the latter procedure widely confirms the long-term observation. The given deviations might be caused by inaccuracies in the sensor measurement (sensors were adjusted to spruce), as well as by the fact, that the moisture contents determined by the oven dry method are average values of the specimen's total cross-section. Since at least a slight decrease of moisture content can be observed for both sensors placed in oak wood (c. f. Figure 3.77), a moisture gradient in form of increasing u with an increasing distance to the sample surface and thus higher values of u close to the screw hole (equal to sensor location) can be expected.

Table 3.35: *Moisture contents of timber specimen corresponding to test campaign II, determined by oven dry method*

load chain dedicated to measurement sensor	n [-]	mean[u] [%]	CV[u] [%]
oak_1	6	15.6	2.9
oak_2	6	15.2	4.4
spruce_1	4	20.1	10.3

Now concentrating on the effect of corrosion on the tested screws as the major environmental source of H_{ad} . Figure 3.78 and Figure 3.79 comprise an extract of related macrophotos, taken after finishing both test campaigns (total documentation can be found in Annex B-2.1, Figure B.4 to Figure B.14).

With regard to those, as parts of test campaign I, a clear difference in the optical appearance of screws, situated in oak and Norway spruce specimen, has to be observed. While the latter mentioned (c and e) did not corrode anywhere, an advanced corrosion of screws inserted in oak wood is given, which underlines the aggressivity of this timber species, especially considering the comparatively short period of environmental exposure. As shown in Figure 3.78 (a, b, d), the corrosion products occurred in form of $FeO(OH)$ (rust-coloured), partially in combination with a black patina, which may be explained by the effect of tannins on steel corrosion, c. f. Zelinka and Stone (2011).



Figure 3.78: *Macrophotos of test campaign I: (a) yellow chromated in oak; (b) zinc-nickel in oak; (c) zinc-nickel in Norway spruce; (d) blue chromated in oak; (e) blue chromated in Norway spruce; according to Hauptmann (2016)*

The situation for the specimen used in test campaign II is as follows: an advanced corrosion process can be observed for both timber species, oak (a and b) and Norway spruce (c and d), the latter probably enabled (or accelerated) by a significantly longer period of exposure, as well as by higher moisture contents (see Figure 3.77) as they are expected for test campaign I – see Figure 3.79. Comparing the

optical appearance of screws inserted in oak wood in both test campaigns, the aforementioned black patina can be observed neither in Figure 3.79 (a and b) nor in Annex B-2.1, Figure B.11 and Figure B.12.



Figure 3.79: *Macrophotos of test campaign II: (a) yellow chromated in oak; (b) zinc-nickel in oak; (c) yellow chromated in Norway spruce; (d) zinc-nickel in Norway spruce*

Focusing on the suitability of galvanic protection applied to decelerate corrosion: based on the condition of screws inserted in oak in the frame of test campaign I, a total loss of the zinc coating, irrespective from the method applied, has to be expected. This is additionally confirmed by the microscopic scans, shown in Figure 3.80. Therein, the micrographs of the screw thread's xz- (or xy-)plane from specimen (zinc-nickel) inserted in oak (left) and Norway spruce (right) are compared. While an advanced corrosion, without a remaining coating, can be observed in the former case, the exemplarily determined coating thickness of about 9 μm in the latter one is quite equal to the corresponding reference value discussed in section 3-3.4, which indicates a much minor pronounced impact of the corrosion related.

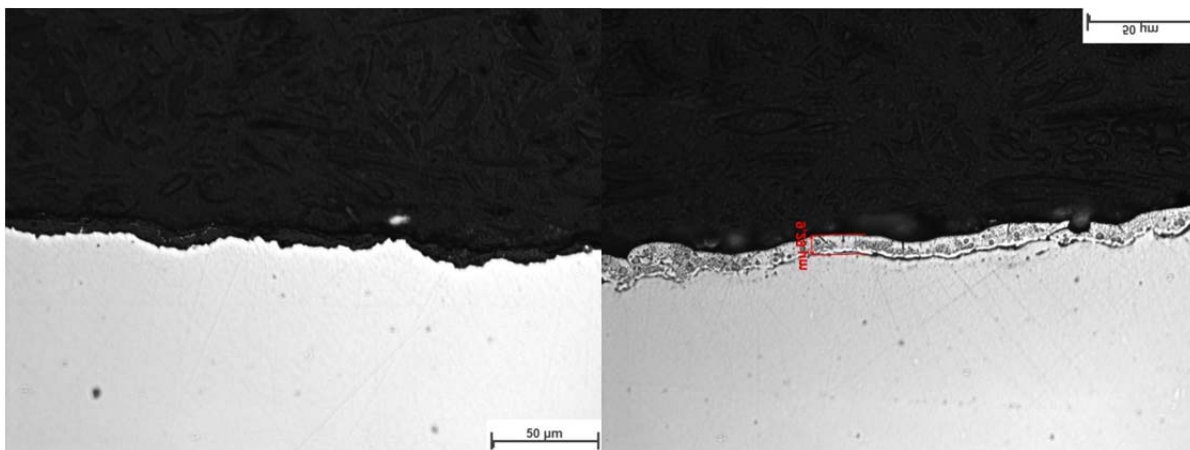


Figure 3.80: *Comparison of corrosion in oak (left) and Norway spruce (right); sample A_s_I_08_240 (zinc-nickel coating) as part of test campaign I; according to Hauptmann (2016)*

Figure 3.81 subsequently demonstrates the negative impact of surface discontinuities due to thread forming (see section 3-5.2.1) on the corrosion process. Since the corresponding notches or cracks are disadvantageously in regard to a homogenous dispersion of coating thickness due to the galvanisation,

c. f. Distelrath (2005), significantly higher values of R_C locally occur in these areas. The related effect is commonly denoted as crevice or pitting corrosion, c. f. Nürnberger (1995) and Figure 3.69.

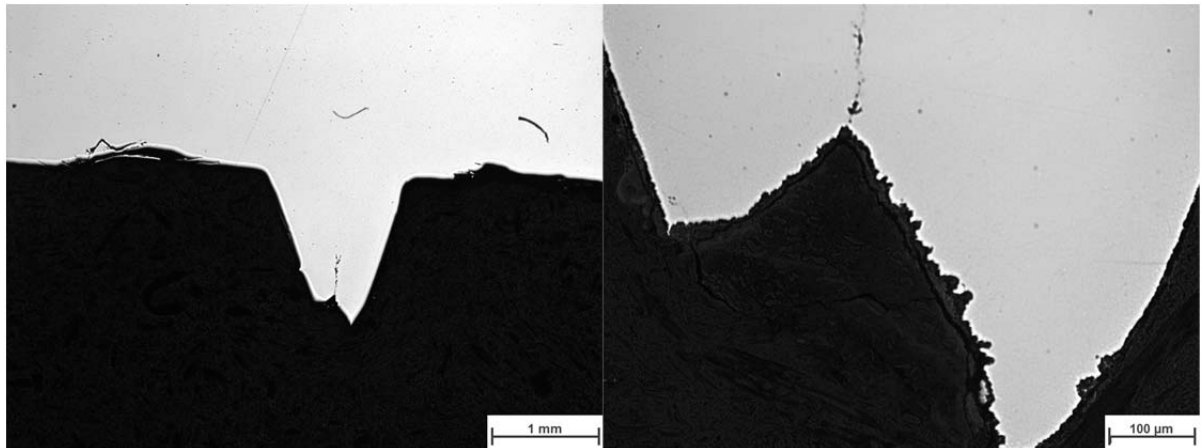


Figure 3.81: Micrograph of the advanced corrosion process, sample *A_s_I_08_240* (yellow chromated) in oak as part of test campaign I; according to Hauptmann (2016)

Summarising the results of test campaign II: all screws suffered to a significant extent from corrosion, especially those inserted in oak wood (this is similar to test campaign I), but also those placed in Norway spruce. The conclusion is, that the climatic exposure, leading to moisture contents steadily above roughly 16 %, fulfils the aimed purpose.

Now the concentration is on the consequences going along with all boundary conditions given for the occurrence of HISCC, c. f. sections 3-5.4.2 and 3-5.4.3. Table B.10 and Table B.11 in Annex B-2.2 comprise the endurance of all screws applied within both test campaigns, as well as the information if a specimen failed or survived the experiment. As given therein, four screws in total (two per each campaign, all yellow chromated) failed by exceeding their steel tensile capacity in the frame of long-term testing. Determining the steel tensile capacity by conducting a withdrawal test according to ON EN 1382 (1999), the corresponding failure commonly occurs outside the timber specimen. In contrast, all failures observed in this experiment occurred inside the timber specimen about 20 mm far from the surface, where the load has been introduced (which means where the head was situated), see Figure 3.82.



Figure 3.82: Opened timber specimen (oak) with *A_s_I_08_240* (yellow chromated) failed in the frame of test campaign I

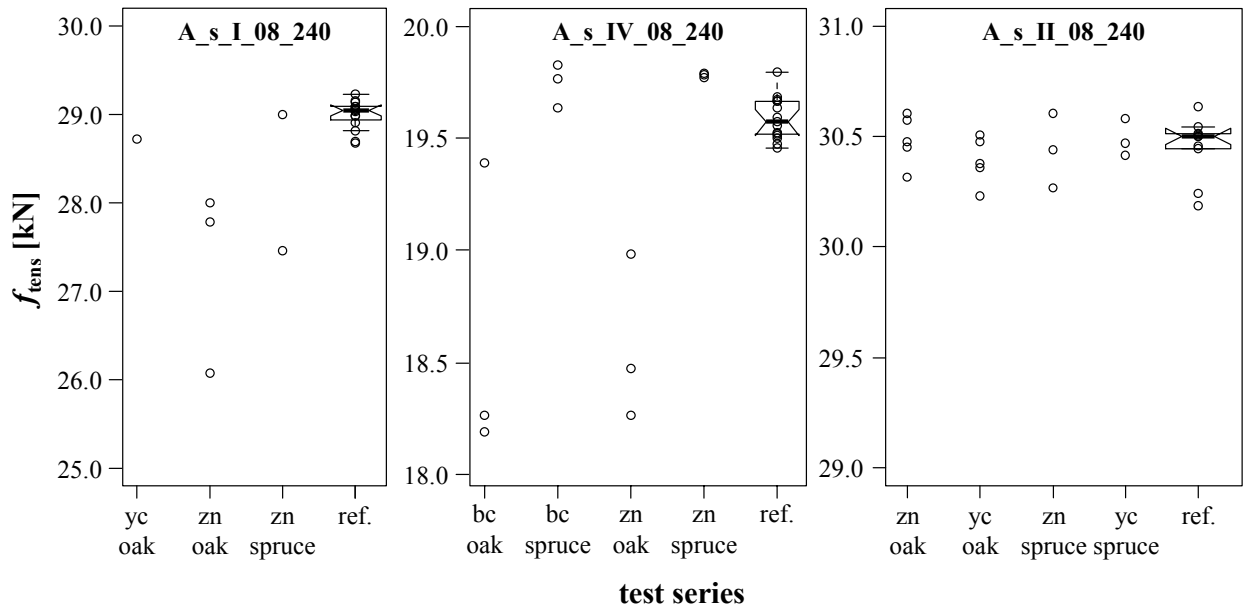
With regard to test campaign I, both fractured screws (*A_s_I_08_240*) were inserted in oak and survived only less than one week of exposure. In case of test campaign II, one screw (*A_s_II_08_240*), also

situated in oak, survived roughly two weeks. It is an interesting fact, that the second failure (A_s_II_08_240) in the frame of test campaign II was observed in Norway spruce (endurance about 2.5 months), which was not expected at all.

As mentioned in section 3-5.4.3, the steel tensile capacity of screws, which survived the climatic exposure was subsequently determined by quasi-static tests, described in section 3-4.4.3. Table 3.36 and Figure 3.83 include thereby gained properties, the latter in form of a combined scatterplot-/boxplot-diagram created by the software package R, see R Core Team (2016). Even though the given difference Δ_{ref} , referring to the values shown in Table 3.30, results in a comparatively small amount – certain screws as parts of test campaign I reached the tensile capacities remarkably below the bandwidth determined in the frame of the reference tests. Especially with regard to product group A_s_IV_08_240, an additional and clear dependency of the timber species, they were applied in, is observable. Apart from a possible occurrence of the advanced crack formation due to HISCC, further reasons for decreasing f_{tens} might be a loss of cross-sectional area due to corrosion, as well as pre-plasticisation (or preimpairment) due to removing the screws from the timber specimen. The fact, that almost all screws, which were placed in oak during test campaign I, failed in torsion when removing them (c. f. Annex B-2.1, Figure B.4 to Figure B.14), supports this hypothesis. Nevertheless, the corresponding samples of A_s_I_08_240 and A_s_IV_08_240 were also considered for subsequently conducting SEM.

Table 3.36: *Steel tensile capacities of screw products A_s_I_08_240, A_s_IV_08_240 and A_s_II_08_240 determined after long-term testing*

test campaign	product ID	n [-]	coating	timber species	mean[f_{tens}] [N]	Δ_{ref} [%]
I	A_s_I_08_240	1	yc	oak	28,731	-0.93
	A_s_I_08_240	3	zn	oak	27,287	-5.91
	A_s_I_08_240	2	zn	Norway spruce	28,229	-2.66
	A_s_IV_08_240	3	bc	oak	18,615	-4.98
	A_s_IV_08_240	3	bc	Norway spruce	19,745	0.79
	A_s_IV_08_240	3	zn	oak	18,574	-5.19
	A_s_IV_08_240	3	zn	Norway spruce	19,782	0.98
II	A_s_II_08_240	5	yc	oak	30,392	-0.21
	A_s_II_08_240	3	yc	Norway spruce	30,489	0.11
	A_s_II_08_240	5	zn	oak	30,485	0.10
	A_s_II_08_240	3	zn	Norway spruce	30,438	-0.06



indicate a brittle failure mode (probably caused by carbonitriding as applied for this product group), but not HISCC.

The situation for both screws A_s_I_08_240, analysed in Figure 3.87 and Figure 3.88, is contrary to the former described one. Figure 3.87 thereby includes SEM images representing one of the two yellow chromated samples, which failed after less than one week of climatic exposure (see Table B.10). Since their fractured surface was affected by corrosion (Figure 3.87, a), the corresponding products had to be chemically removed with a so-called “hexa-solution”, c. f. Hauptmann (2016). As discussed in Hauptmann (2016), unfortunately this procedure also attacks the cross-sectional surface restricting a failure interpretation to some extent (Figure 3.87, b). Nevertheless, the aforementioned intergranular fracture pattern can again be partially observed (Figure 3.87, c), but here in combination with gaping grain boundaries. More relevance is assigned to the zinc-nickel coated screw, shown in Figure 3.88. This specimen, as a part of the quasi-static tensile test series given in Table 3.36, failed far below the reference value at roughly 26 kN and was chosen for further analysis for this reason. As given in Figure 3.88 (d), all characteristics being necessary for the classification of HISCC occur, indicating the related crack formation at position 2. Taking into account, that both yellow chromated screws failed at a load level, which was roughly one third of their reference f_{tens} (c. f. Table 3.34), their failure behaviour, as well as that of the latter discussed zinc-nickel screw, can be classified as HISCC.

With regard to both screws of type A_s_II_08_240, which failed in the frame of test campaign II: the installed camera system enabled their removal from the climatic exposure immediately after the failure occurred, restricting the post-failure corrosion to a negligible extent. This circumstance simplified the related fractographical SEM by far and enabled a clear classification of HISCC, being responsible for the failure behaviour as shown in Figure 3.89 and Figure 3.90 (d). Interestingly, the dispersion of both affected areas (pos. 1 in Figure 3.89, b and pos. 2 in Figure 3.90, a) is far more pronounced than it was found for the samples as parts of test campaign I. This is probably caused by the comparatively longer endurance related.

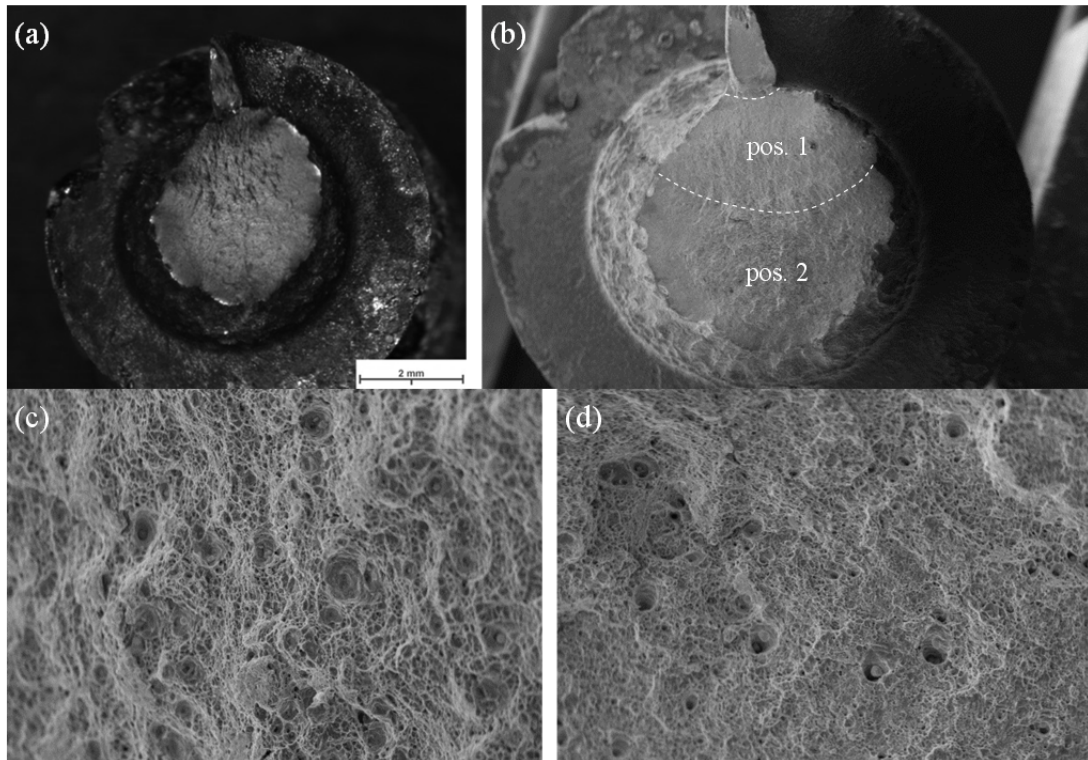


Figure 3.84: *A_s_IV_08_240 (bc) in oak; (a) fracture pattern; (b) SEM scan with zoom positions; (c) zoom view of pos. 1; (d) zoom view of pos. 2; 500x magnification; according to Hauptmann (2016)*

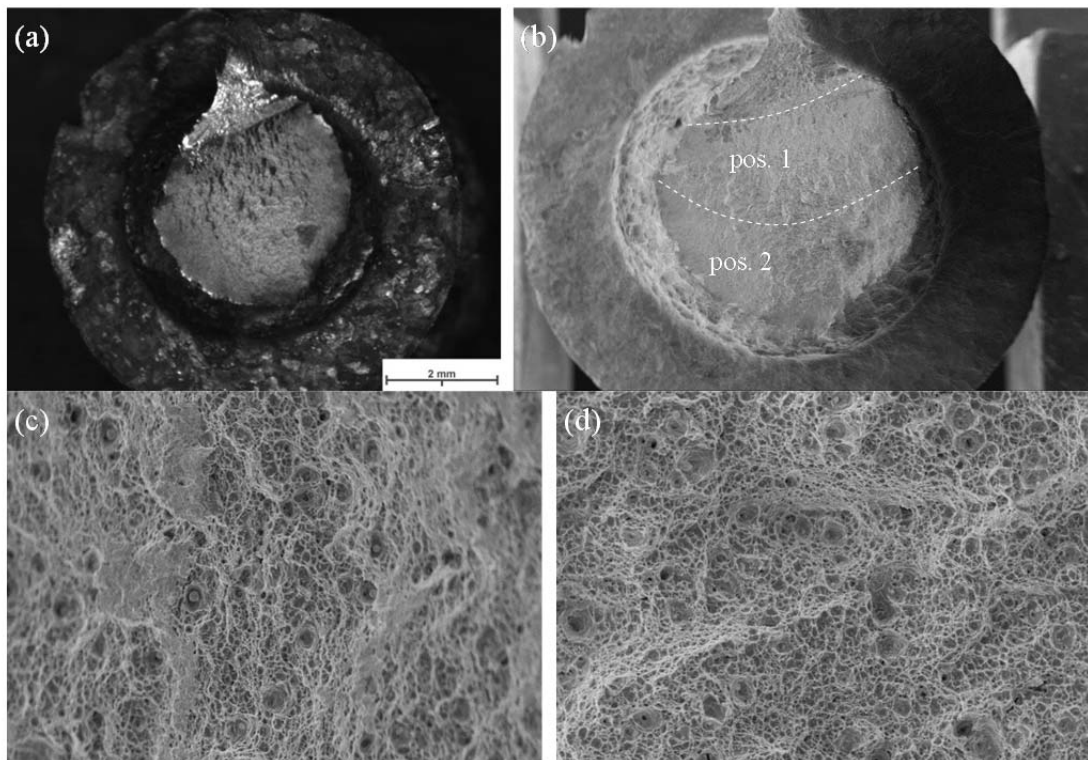


Figure 3.85: *A_s_IV_08_240 (zn) in oak; (a) fracture pattern; (b) SEM scan with zoom positions; (c) zoom view of pos. 1; (d) zoom view of pos. 2; 500x magnification; according to Hauptmann (2016)*

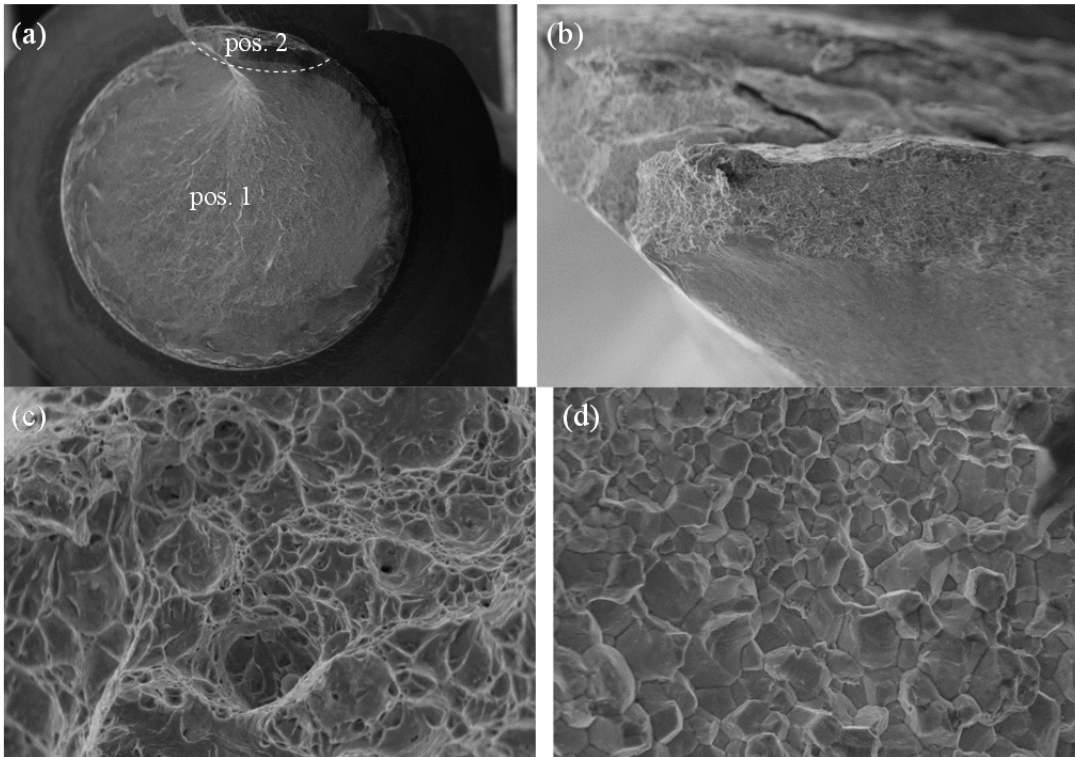


Figure 3.86: *A_s_I_08_240* (yc) reference; (a) SEM scan with zoom positions; (c) zoom view of pos. 1; (1000x) (b) and (d) zoom view of pos. 2; (100x/1000x magnification); according to Hauptmann (2016)

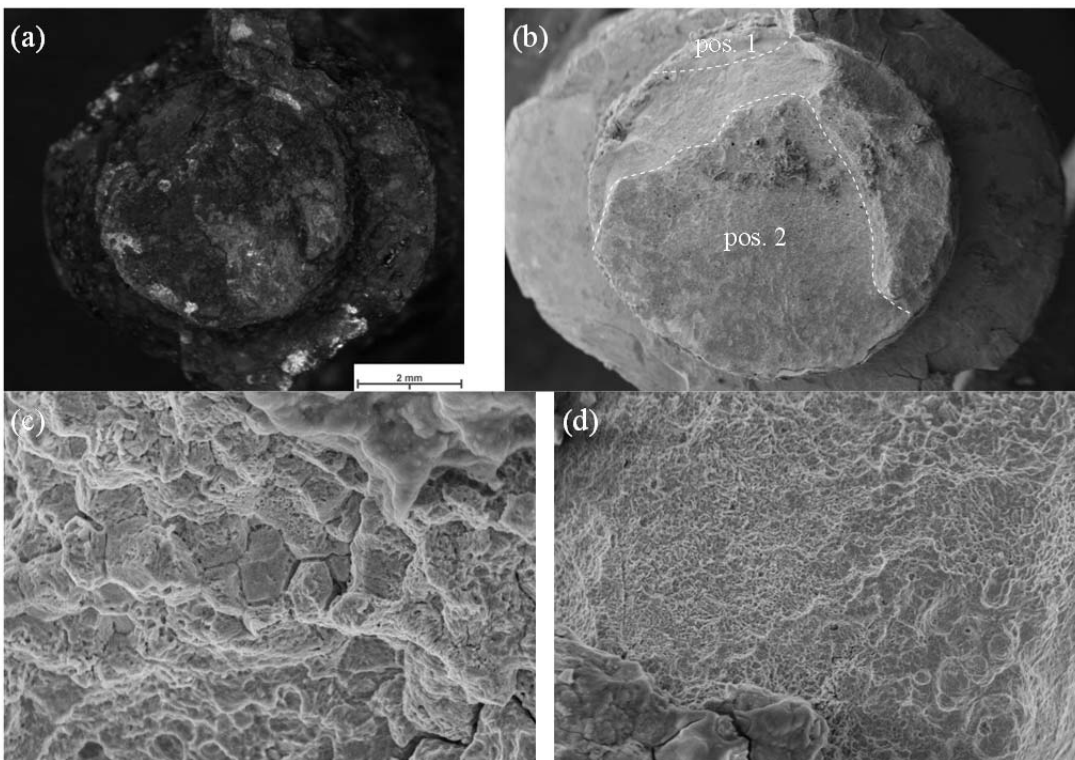


Figure 3.87: *A_s_I_08_240* (yc) in oak; (a) fracture pattern; (b) SEM scan with zoom positions; (c) zoom view of pos. 1 (1000x); (d) zoom view of pos. 2 (500x magnification); according to Hauptmann (2016)

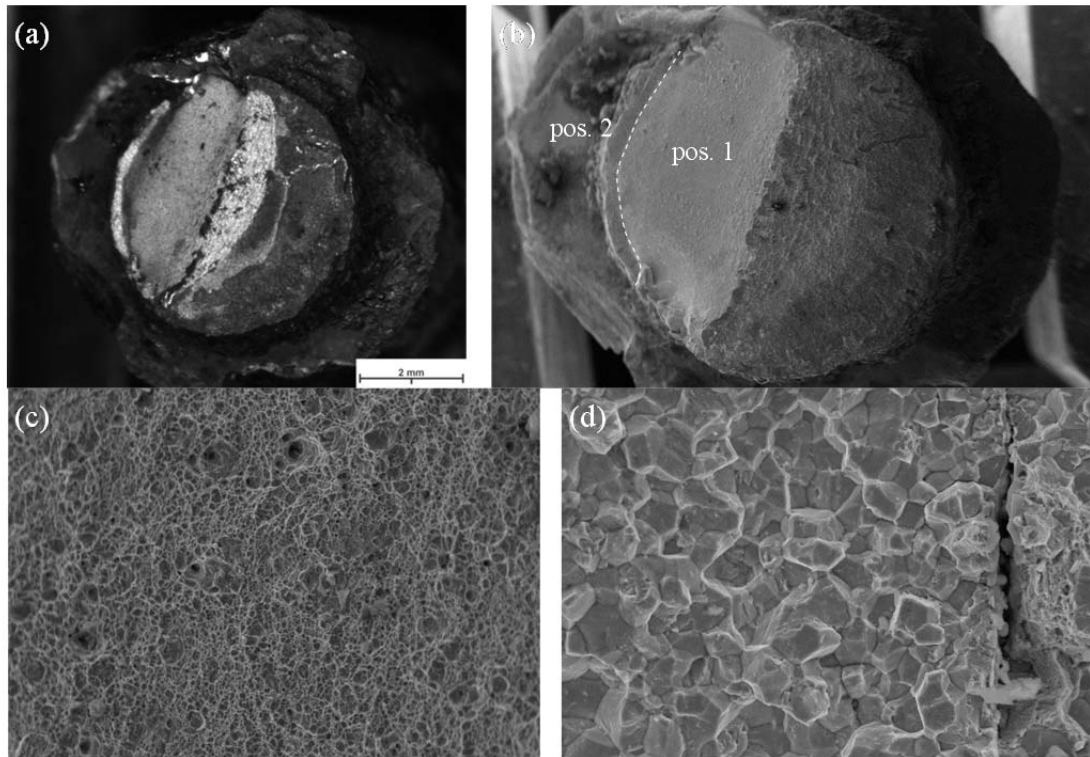


Figure 3.88: *A_s I_08_240 (zn) in oak; (a) fracture pattern; (b) SEM scan with zoom positions; (c) zoom view of pos. 1 (500x); (d) zoom view of pos. 2 (1000x magnification); according to Hauptmann (2016)*

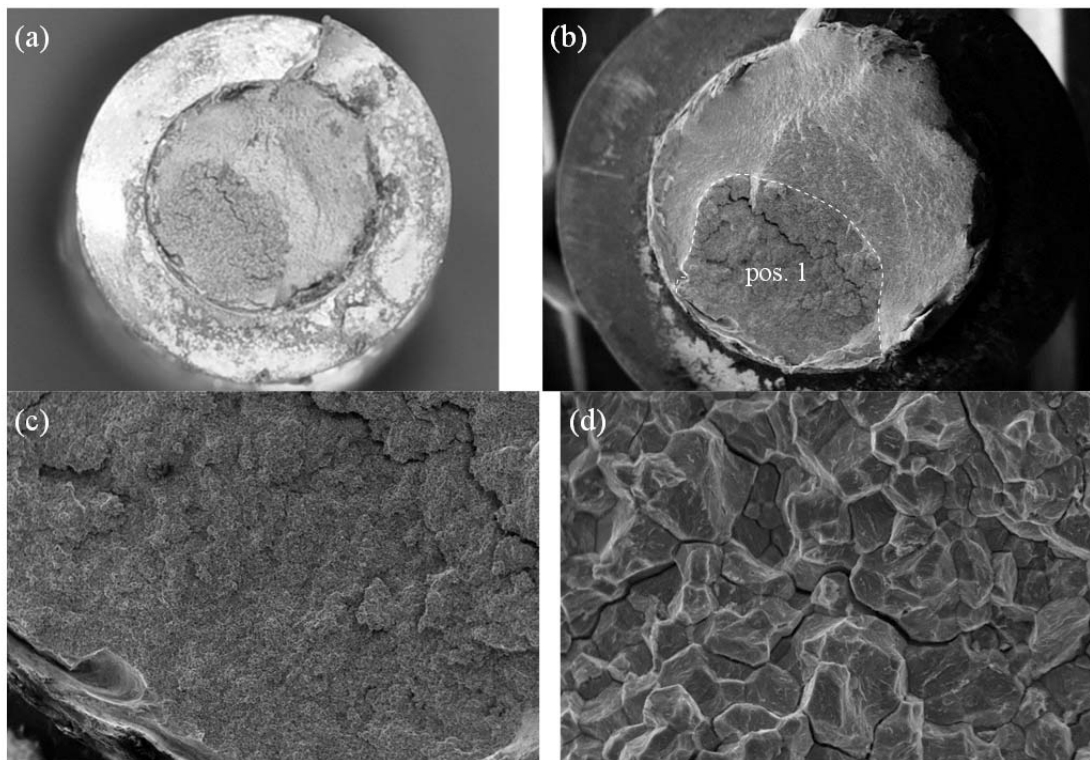


Figure 3.89: *A_s II_08_240 (yc) in oak; (a) fracture pattern; (b) SEM scan with zoom positions; (c) and (d) zoom view of pos. 1; 50x/1000x magnification; according to Toblier (2016)*

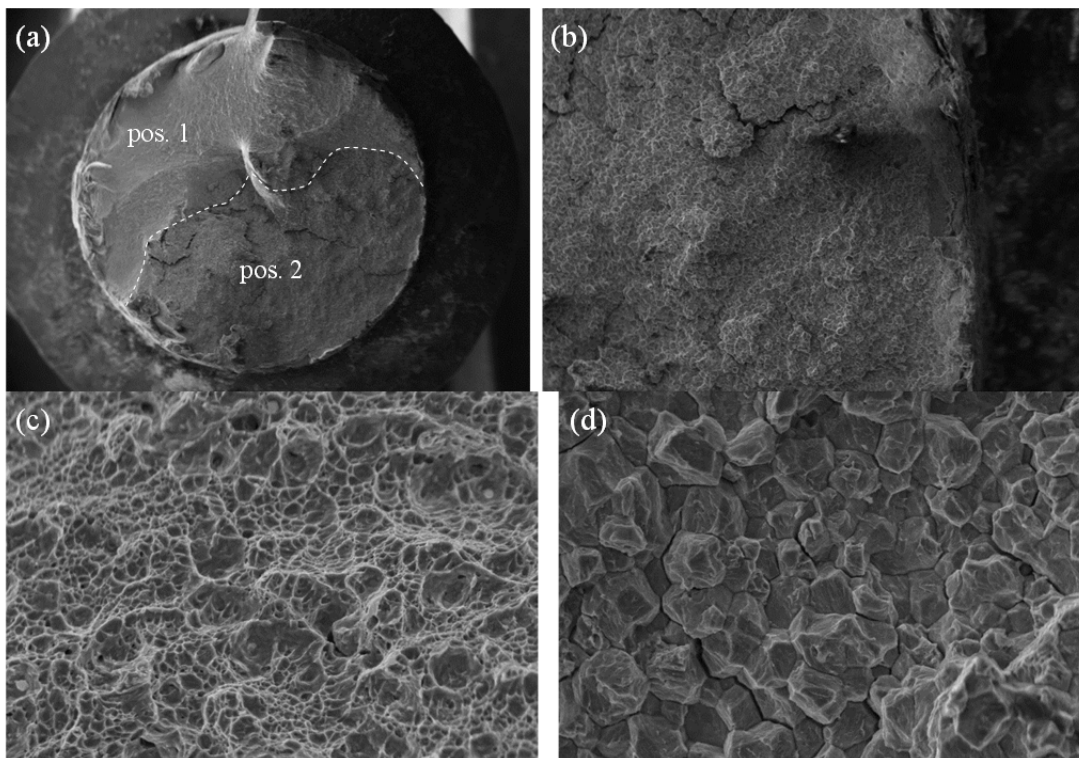


Figure 3.90: *A_s_II_08_240 (yc) in Norway spruce; (a) SEM scan with zoom positions; (c) zoom view of pos. 1; 1000x magnification; (b) and (d) zoom view of pos. 2; 50x/1000x magnification; according to Toblier (2016)*

Finally, the focus is on the outcomes gained from CGHE performed by the voestalpine STAHL GmbH. In case of test campaign I, the three aforementioned screws with a failure mode classified as HISCC were considered for this purpose. Since the focus is hereby on the presence of hydrogen in steel, the remaining protective coating, as well as any existing corrosion products, have been removed by pickling the specimen in HCl, c. f. Hauptmann (2016). The same was also applied for both screws of type *A_s_II_08_240*, which failed by HISCC during test campaign II. Furthermore, three additional samples of this programme were analysed by means of CGHE. This was mainly done to determine the diffusible hydrogen content in steel and protective coating after the full exposure period of roughly six months took place.

Figure 3.91 subsequently overviews the related quantities of diffusible hydrogen and compares them with the reference value for product group I, as determined by Toblier (2014). In fact, the results significantly vary in dependence of the considered screw type. In case of yellow chromated screws, which failed in the frame of long-term testing, both values are below the reference, the latter even below the accuracy limit of 0.10 ppm, c. f. section 3-5.2.3. In contrast, the value, determined for the zinc-nickel screw, which failed in the frame of post-tensile testing, exceeds the reference to a certain extent. Since the maximum

diffusible hydrogen content of the reference samples was determined to $0.60 \mu\text{g/g}$, the given difference can not be regarded as significant.

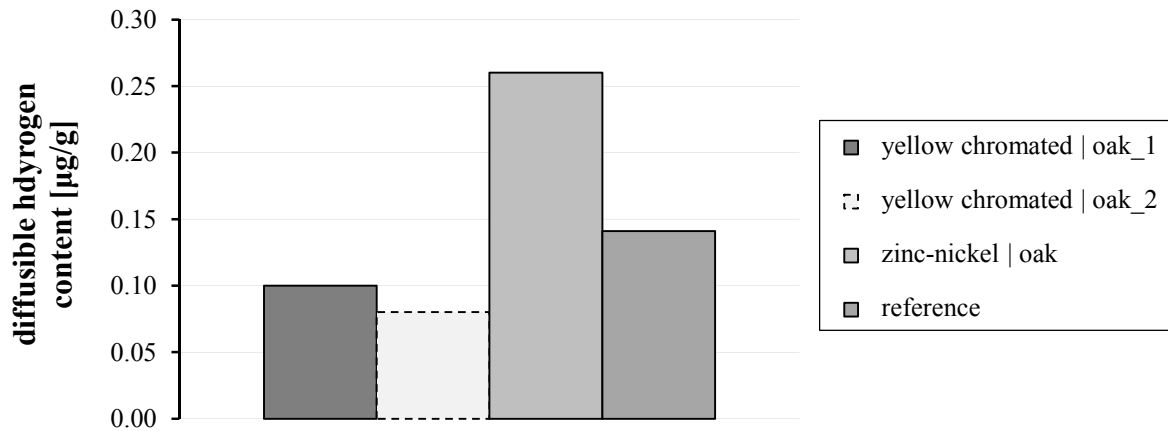


Figure 3.91: Diffusible hydrogen contents of three samples *A_s_I_08_240*, applied in oak, test campaign I (only steel)

In Figure 3.92 the corresponding results, dedicated to test campaign II, are illustrated. The main findings is brief: the diffusible hydrogen contents in the coatings result in a significantly higher magnitude than the ones, determined prior to the tests, shown in Figure 3.54. This underlines the effects of environmental exposure. It also concerns H_{ad} of the steel material, illustrated in Figure 3.92 (right), where a remarkable increase, if compared the ones shown in Figure 3.91, can be observed. H_{ad} of both samples, which failed by HISCC (abbreviated as “f” in Figure 3.92), is considerably lower than H_{ad} determined for all survived samples (coatings), as well as than $\max[H_{ad}]$, also dedicated to a survived sample (steel). Since related specimen failed during the long-term tests, duration of climatic exposure was much shorter than that of the survived ones, c. f. Annex B-2, Table B.11. This again confirms the impact of the environment on the behaviour of H_{ad} .

The given results are in-line with those of test campaign I, meaning that the magnitude of H_{ad} determined with CGHE does not serve as reasonable indicator for HISCC. This is mainly caused by the circumstance, that with CGHE the average of diffusible hydrogen of the total cross-section is determined, which disables the registration of local peaks, c. f. Hauptmann (2016).

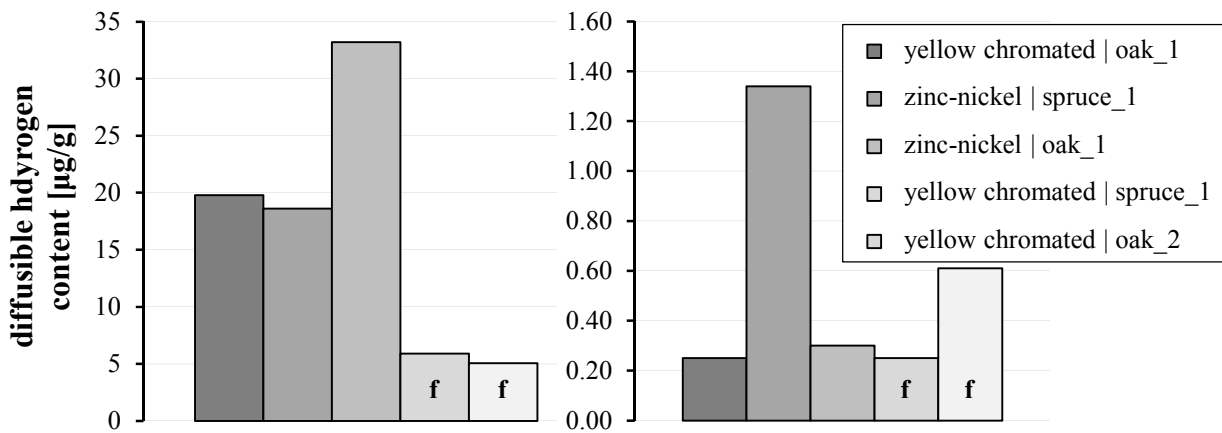


Figure 3.92: Diffusible hydrogen contents of five samples *A_s_II_08_240*, applied in oak and spruce, test campaign II (*f* = failed screws): left: protective coating, right: steel

3-5.5 Concluding remarks to section 3-5

The considerations, given in section 3-5, concentrated on the discussion about selected parameters influencing the tensile capacity of fully threaded and axially loaded self-tapping screws made of low-alloy carbon steel. The corresponding range thereby comprised (a) their production process, (b) selected load specifics as well as (c), the environment they are exposed to.

With regard to (a), steel tensile capacity f_{tens} of self-tapping screws can be controlled by geometrical and metallurgical modifications. In the former case, the thread geometry, expressed in form of $\{d, \eta, v \text{ and } p\}$ and applied for deriving cross-sectional properties in previous section 3-4, has a major impact on this property. For a constant d , especially η as ratio between d_c and d governs the size of f_{tens} , while the effect of both, v and p , is only minor pronounced. Furthermore, randomly dispersed surface discontinuities, occurring in form of cracks or notches at the inner thread cylinder and the thread chamfer, are supposed to influence the loadbearing behaviour to some extent. Further investigations should consider the effect of stress singularities, which dominate the related fracture process. In case of metallurgical modifications, the process of hardening, as described in section 3-3.3, including carbonitriding and tempering, majorly influences the achievable hardness distribution and thus the relevant parameters f_{tens} and D for classifying the screw's bearing behaviour when loaded in axial tension. At environments similar to laboratory conditions, the positive correlation between hardness and tensile capacity can be considered for creating a powerful fastener. The following example shall express the impact of both measures described before:

- (i) screw with $\{d, \eta, v \text{ and } p\} = \{8.0 \text{ mm}, 0.90, 40^\circ \text{ and } d/2 = 4.0 \text{ mm}\}$ and $f_u = 1,450 \text{ N/mm}^2$ (standard hardening of manufacturer A):

$$f_{\text{tens}} = A_{\text{pl},N,\text{emp}} \cdot f_u = 40.79 \cdot 1,450 = 59,146 \text{ N}, \quad (3.129)$$

with $\omega = 0.927$ and $A_{\text{dc}} = 40.72 \text{ mm}^2$.

- (ii) screw with $\{d, \eta, v \text{ and } p\} = \{8.0 \text{ mm}, 0.50, 40^\circ \text{ and } d/2 = 4.0 \text{ mm}\}$ and $f_u = 950 \text{ N/mm}^2$
(tempered after hardening):

$$f_{\text{tens}} = A_{\text{pl},N,\text{emp}} \cdot f_u = 13.95 \cdot 950 = 13,253 \text{ N}, \quad (3.130)$$

with $\omega = 0.636$ and $A_{\text{dc}} = 12.57 \text{ mm}^2$.

Considering the requirements of $\eta = 0.50 \div 0.90$, as given in CUAP 06.03/08 (2010), as well as the tensile strengths determined in section 3-4.5.2, a ratio between both determined values for f_{tens} results to 4.5 : 1, representing the bandwidth of the structural performance a $d = 8 \text{ mm}$ screw might vary in-between.

Concentrating on (b), the investigations, discussed in the frame of this section, focused on the influence of time-dependent loading on the screw's axial tensile capacity. Since this topic has barely been considered in literature, it was decided to determine the corresponding bearing behaviour at $N = 10^3 \div 10^6$, covering the range of high-cycle fatigue (HCF). The main fatigue related parameters, k_{SN} and $f_{\text{fat},C}$, result to 3.87 and 256 N/mm² respectively (for $R = 0.56$). Presupposing both, fastener type (group A_s_II_08_240) and loading protocol (sinusoidal, force-controlled with constant stress conditions), as a representative, the shape of the S/N-diagram thus corresponds to the behaviour of a sharp or significant notch, indicating, that the aforementioned surface discontinuities have a relevant influence on the fatigue performance of axially loaded self-tapping screws. The SEM observations, wherein the optical appearance of the fracture surface was found to differ remarkably in dependence of N , additionally underline this circumstance. Comparing the gained results for k_{fat} at varying R with a simplified model, which considers steel rods according to ON EN 1993-1-1 (2012), in the pulsating tensile domain, a similar behaviour of both fastener types can be observed. Following the principle, given in this standard, the screws may be assigned to "detail category 100". Since these investigations were restricted to a certain amount, they are regarded as initial measures for a consistent description of the fatigue-related loadbearing performance of self-tapping screws. The future research activities should concentrate on (i) single fatigue tests with screws, formed by thread die rollers (decrease surface discontinuities by far) and varying loading types (bending, shear and interaction with normal force), as well as on (ii), the relationship between the discussed results and such determined for connections with inclined positioned and predominately axially loaded groups of screws.

With regard to (c), the discussion in section 3-5.4 focused on the effect how electrochemical corrosion influences the mechanical properties of metal fasteners applied in EWPs. Thereby, especially the vulnerability of hydrogen-induced stress corrosion cracking (HISCC), leading to a brittle failure without prior warning of low-alloy carbon steel screws, has been treated in detail. Even though they fulfil several requirements (high hardness and tensile strength, initial cracks and notches, presence of hydrogen due to galvanisation and corrosion, tensile loading, etc.), which are necessary for HISCC – comparable investigations on self-tapping screws were not found in literature. The experimental programme, carried out in the frame of two long-term testing campaigns, thus aimed to gain some fundamental knowledge regarding this phenomenon.

The main outcomes in brief:

In the given climatic exposure, in form of a high temperature and moisture content, all in all five screws were observed failing in HISCC (or at least due to hydrogen induced crack formation). The corresponding classification was realised by SEM analysis, while carrier gas hot extraction (CGHE) was evaluated not being suitable for this purpose. All failed samples correspond to product groups I and II (see Table 3.4, representing extreme values of hardness and strength), which agrees with the major impact of both mechanical parameters regarding the vulnerability of HISCC, as found in literature. The screws dedicated to product group IV ($f_u < 1,000 \text{ N/mm}^2$) did not fail at all, confirm this circumstance.

Second, as initially expected, the application of oak wood creates an environment, not only being dangerous for the occurrence of HISCC, but also leading to an accelerated corrosion rate in general. Since in the frame of test campaign II, one failure also occurred in Norway spruce (at $u > 20 \%$), the vulnerability of HISCC can not be restricted to acetous timber species with low pH.

Third, all screws failing in the frame of long-term testing were yellow chromated, while those with zinc-nickel coating survived the climatic exposure at all. This indicates a qualitatively better protectability of zinc-nickel coatings against this failure mode.

It should be pointed out, that this test programme has to be seen as an initial step in this direction, without tending to be exhaustive. Nevertheless, the following recommendations for practical application are worth being outlined:

Due to their weak performance in form of a minor endurance (≤ 1 week), the carbonitrided screws with hardness distributions, given in Figure 3.44 (product group I), should not be applied for timber connections or reinforcements in general. Furthermore, in cases where moisture contents above $u = 16 \%$ are expected, the intended use shall be restricted to carbon steel screws with $f_u < 1,000 \text{ N/mm}^2$. As an alternative, stainless steel screws can be used for this purpose.

Further investigations in this field should expand long-term testing regarding all parameters varied, especially the project duration, the number of timber species, the screw types (different manufacturers, further coating forms, etc.), as well as the type of testing (more harmful conditions might possibly be realised by storing the screws in aqueous timber extracts vs. the application of a similar set-up as explained, but exposed to more practical climatic conditions e. g. realised by outdoor storage).

CHAPTER 4

DEFINITION AND LAY-UP OF SOLID TIMBER AND LAMINATED TIMBER PRODUCTS WITH FOCUS ON SCREW APPLICATION

4-1 INTRODUCTION

As summarised in chapter 2, section 2-5, self-tapping screws achieve their maximum efficiency when loaded in axial direction. Concentrating on therewith composed timber connections or reinforcement measures exposed to high stresses, the corresponding design process predominately comprises both failure modes, “withdrawal” and “steel failure in tension”. Since the latter mode is comprehensively discussed in chapter 3, the remaining chapters 4 to 6 focus on the withdrawal behaviour, defined as the composite interaction of the screw and the timber element where it is situated in.

The following sections of this introductory chapter concentrate on a general, brief definition and discussion regarding dimension, lay-up and main parameters of timber specimen, being relevant for the investigations on the single screw performance. Worth mentioning, that from now on the scope is reduced to solid timber and laminated timber products made of Norway spruce (*Picea abies*).

4-2 DEFINITION OF TIMBER SPECIMEN APPLIED FOR SCREW INVESTIGATIONS

Note: this paragraph summarises the related explanations given in Boding and Jayne (1982). As a naturally grown material, wood can generally be regarded as an organic, cellular substance, consisting of about 50 % carbon (C), 44 % oxygen (O), 6 % hydrogen (H) and both ash and nitrogen (N) with a mass content below 1 %. The therewith composed molecular groups are the basis of the cell wall components and extractives, the former being relevant for mechanical wood properties. The cell wall components can further be subdivided into carbohydrates (linear polymers or polysaccharides) and phenolics. The carbohydrates account for roughly 75 % of the wooden substance and consist of cellulose and hemicellulose, while the major share of phenolics is composed by the complex polymer lignin. Cellulose exists in form of discrete bundles, denoted as elementary fibrils, which are aggregated by a hydrogen bonding and lignin to microfibril clusters as the main components of a cell wall. The coniferous wood species are generally composed by two cell types, namely tracheids and parenchyma, given in a ratio of

about 90 % to 10 %. Both, occurring in arrays with a specific orientation (tracheids in longitudinal, parenchyma in form of wood rays in radial direction), assemble in geometrically high-structured lay-ups, subsequently denoted as annual rings.

The annual rings of coniferous woods consist of two regions with different optical appearance, namely earlywood (light-coloured) and latewood (dark-coloured), mainly characterised by their width a_w , defined as the normal distance from one ring limit to the other. In case of sawn timber made of Norway spruce, a_w was found roughly varying between 1 mm and 10 mm, c. f. Schickhofer and Augustin (2001) and Figure 4.3. Beside the number, the distribution and the width of annual rings, solid timber applied for structural purpose can be further characterised – amongst others – by the occurrence of knots (type, width and dispersion), fibre deviation, reaction wood, timber pith, resin (pitch pockets), cracks and finger joints, c. f. Meierhofer and Richter (1988).

Based on these considerations, wood can be regarded as a structured material, consisting of three main hierarchical levels, namely the nano level (from atoms and molecules to microfibril clusters), the micro level (including cell walls and cells) and the macro level (from annual ring to the tree), see Figure 4.1.

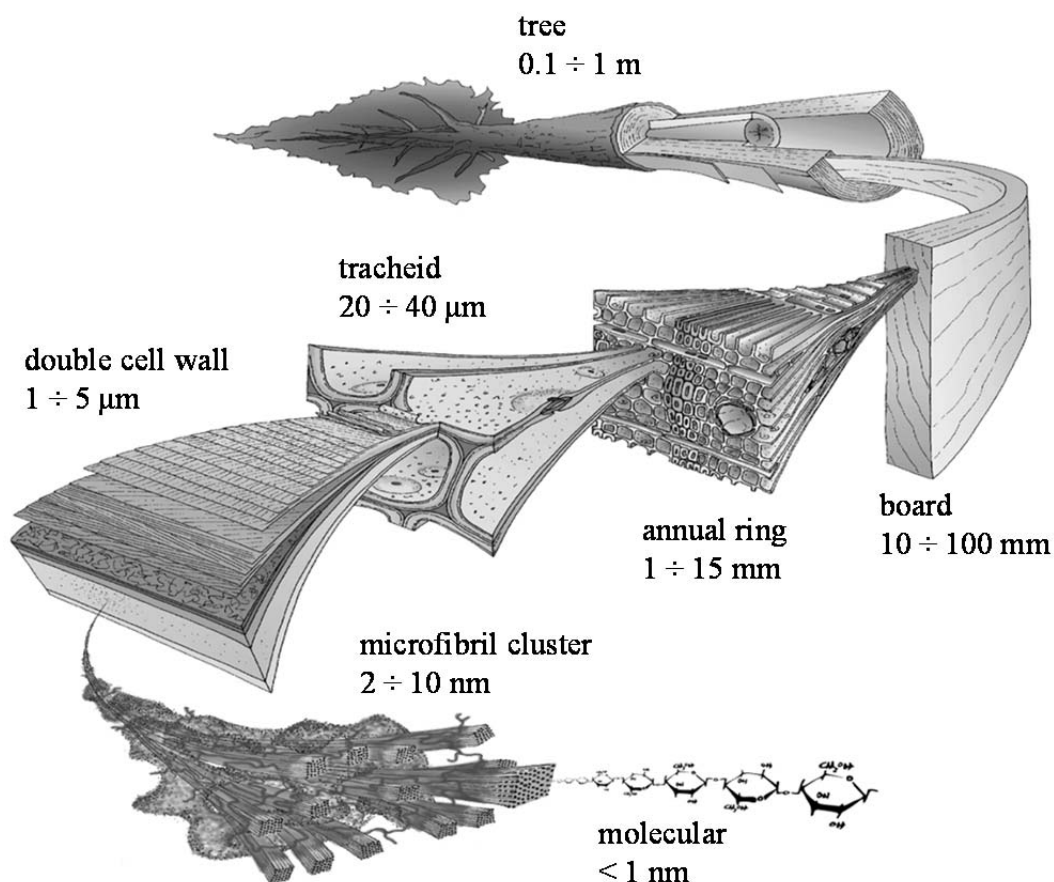


Figure 4.1: Schematic overview of the structural hierarchy of softwood; according to Harrington (2002)

Taking the dimension of self-tapping screws given in CUAP 06.03/08 (2010) or EAD 130118-00-0603 (2016) in form of $2.4 \text{ mm} \leq d \leq 24.0 \text{ mm}$ into account, as well as the level ranges illustrated in Figure 4.1, the application of the screws in timber can be assigned to the previously introduced macro level. Following the requirements given in ON EN 1382 (1999), as test standard commonly applied for determining the withdrawal capacity of axially loaded screws, c. f. ON EN 14592 (2012), CUAP 06.03/08 (2010) and EAD 130118-00-0603 (2016), timber specimen shall be chosen in accordance to ON EN 28970 (1991). Therein, the related material is described with constant quality and without local defects, which corresponds to the definition of the so-called “clear wood”, c. f. Schickhofer (2006a), and thus excludes the existence of the aforementioned growth and production characteristics of solid timber applied for structural purpose, c. f. Figure 4.2.

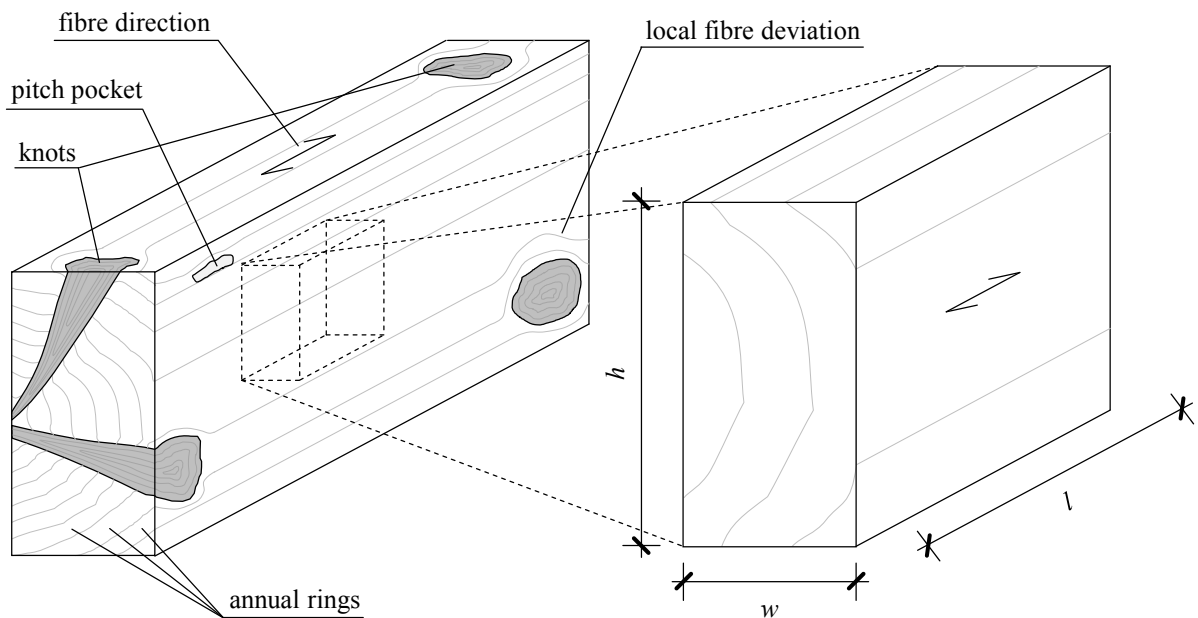


Figure 4.2: Definition of clear wood specimen applied for investigations on self-tapping screws

Beside the annual ring structure (orientation, number and width), the corresponding specimen, subsequently assumed as prismatic, are predominately defined by their geometrical dimensions w , h and l . The minimum requirements on $\{w, h \text{ and } l\}$, provided in ON EN 1382 (1999), depend on the outer thread diameter d , the insertion length of the fastener’s profiled section, l_p and the angle between the fastener’s axis and grain direction. In case of $2.4 \text{ mm} \leq d \leq 24.0 \text{ mm}$ and $l_p = 10 d$, the specimen volume V , according to eq. (4.1), results in a range of $V = 34.6 \cdot 10^3 \div 41.5 \cdot 10^6 \text{ mm}^3$.

$$V = w \cdot h \cdot l \quad (4.1)$$

Worth mentioning, that V thus partly exceeds typical clear wood sample dimensions, varying between $8.0 \cdot 10^3 \div 375.0 \cdot 10^3 \text{ mm}^3$, according to DIN 52185 (1976), DIN 52186 (1978) and DIN 52188 (1979)

by far. In addition to geometrical properties, timber specimen are commonly characterised by both physical parameters, density ρ (ratio between their mass m and V) and moisture content u , the latter according to eq. (4.2), see:

$$u = \frac{m_u - m_0}{m_0}, \quad (4.2)$$

with m_u and m_0 as the sample masses at given u and $u = 0\%$ (dry wood), e. g. determined by performing the oven dry method, according to ON EN 13183-1 (2004). In case of clear wood, a pronounced positive relationship between density and mechanical properties in form of strength and stiffness is given; see e. g. Augustin (2004). This matter, combined with its comparatively simple way of determination, are probably the main reasons, why density can be regarded as the major (timber) parameter being relevant for the design of fasteners in modern standardisation, c. f. ON EN 1995-1-1 (2015). Therefore the applied characteristic values are commonly referred to $u = 12\%$, which is defined as the equilibrium moisture content (at least for coniferous wood species) and reached at a constant climatic exposure in form of $T = 20\text{ }^\circ\text{C}$ and r. h. = 65 %, see ON EN 1995-1-1 (2015). Focusing on Norway spruce, ρ_{12} has been observed varying between $330 \div 680\text{ kg/m}^3$, c. f. Wagenführ (2007). Since the density of water is several numbers higher than of air, the timber density increases with increasing moisture content, the latter expressing the quantity of water in the material. According to DIN 52182 (1976), the corresponding relationship has a nonlinear progressive course (on a semi-logarithmic scale of u), which can be approximated in form of eq. (4.3) if $0 \leq u \leq 25\%$, see

$$\rho_u = \rho_0 \cdot \frac{100 + u}{100 + 0.85 \cdot \rho_0 \cdot u}, \quad (4.3)$$

with ρ_0 as the density determined at $u = 0\%$. A direct, and even more simplified, relationship between ρ_u and ρ_{12} , rather relevant for the laboratory investigations, since ρ_u can be determined immediately after finishing the experiment, is provided in ON EN 384 (2010) in form of eq. (4.4), see

$$\rho_{12} = \rho_u \cdot [1 - 0.5 \cdot (u - 0.12)]. \quad (4.4)$$

Further concentration is on the relationship between density and annual ring properties. Due to the occurrence of different cell wall dimensions in the earlywood and latewood regions, density is observed remarkably varying over an annual ring; see e. g. Persson (2000). Therein, he subdivides the behaviour into three sections, denoted as earlywood, transitionwood and latewood with the corresponding lengths l_e , l_t and l_l , as well as the average densities ρ_e , ρ_t and ρ_l for each region, c. f. Figure 4.3. While the earlywood and latewood regions are characterised by a linearly increasing ρ in radial direction, the course for the

transitionwood is therein approximated by an exponential function. Based on these assumptions, Persson (2000) recommends determining the average density of an annual ring according to eq. (4.5), see:

$$\rho = \rho_e + (\rho_t - \rho_e) \cdot s + (\rho_l - \rho_e) \cdot \frac{l_t}{a_w}, \quad (4.5)$$

with s as the ratio between l_t and a_w . Assuming $s = 0.2$, $\{\rho_e, \rho_t$ and $\rho_l\}$ to $\{300, 450$ and $1000\}$ kg/m^3 and l_t constantly to 0.2 mm, Persson (2000) achieves confirmation between the measured densities and those estimated by eq. (4.5), which thus solely depend on a_w in form of a regressive relationship.

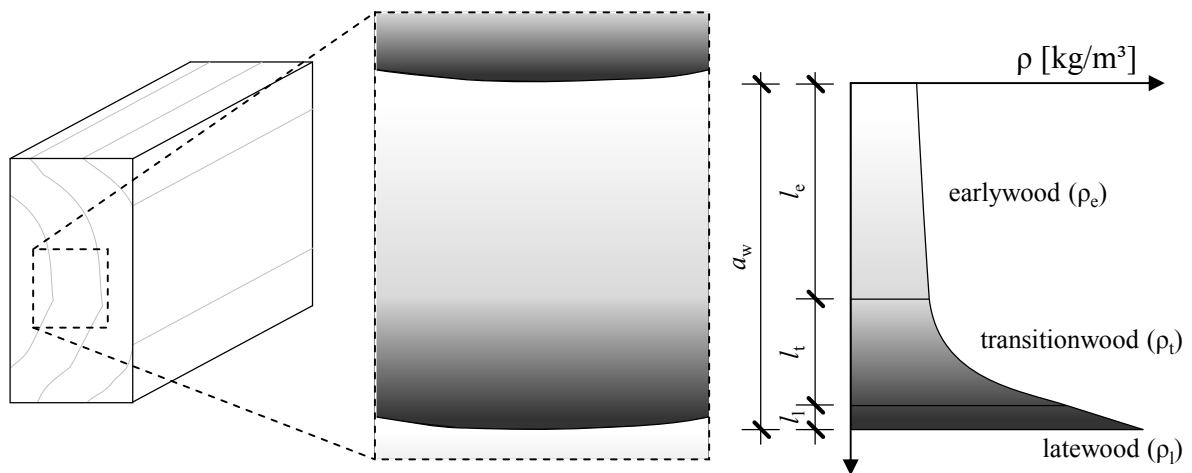


Figure 4.3: Density distribution over an annual ring with subdivision into three regions; according to Persson (2000)

A comparison with his approach and the results of own investigations as parts of an ongoing research project, an extract is already published in Müller et al. (2015), considering altogether 664 clear wood specimen, is subsequently illustrated in Figure 4.4. Since Persson (2000) applies ρ as the ratio of m_0 and V_{FSP} , the latter defined as the specimen volume at saturated conditions, the experimental results had to be determined as follows:

$$\rho = \frac{m_0}{V_{\text{FSP}}} = \frac{m_0}{V_u \cdot [1 + (FSP - u) \cdot \beta_v]}, \quad (4.6)$$

with V_u as the specimen volume at given u as well as $FSP = 25\%$ and $\beta_v = 0.40\% / \% u$ as the fibre saturation point and the volume elongation coefficient, both assumed in accordance to Wagenführ (2007). Although eq. (4.5) slightly overestimates the measured densities for the relevant range of $1 \text{ mm} \leq a_w \leq 6 \text{ mm}$, a similar trend between model expectation and experimental data can be observed.

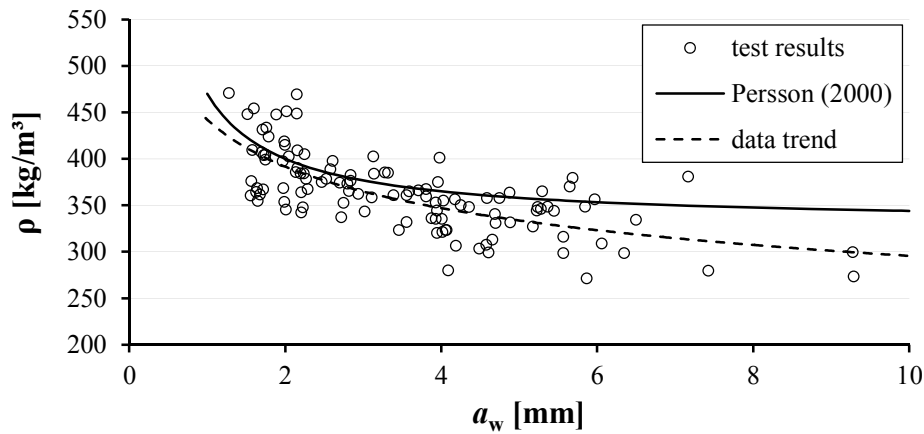


Figure 4.4: Comparison of the approach according to Persson (2000) with own test results

4-3 MAIN MECHANICAL CONSTITUTIONS OF CLEAR WOOD

The following discussion shall summarise the main mechanical constitutions, commonly assumed for the scale of timber specimen applied for investigations on self-tapping screws, as defined in section 4-2. Considering the basics of continuum mechanics, the generalised Hooke's law is one possibility for describing the mechanical behaviour of three-dimensional anisotropic solids. Presupposing material homogeneity and elasticity (occurring deformations are reversible), thermal equilibrium, no coupling between stress components, as well as a restriction to small deformations, c. f. Neuhaus (1981) and Boding and Jayne (1982), the linear relationship between stress and strain can generally be defined by this mathematical statement, as given in eq. (4.7) in tensorial form:

$$\varepsilon_{ij} = S_{ijkl} \cdot \sigma_{kl}, \quad (4.7)$$

with $\{i, j, k, l\}$ as a coordinate index, each varying from 1 to 3, ε_{ij} and σ_{kl} as the strain and stress components and S_{ijkl} as a compliance tensor, the latter including altogether $3^4 = 81$ parameters. For reasons of tensor symmetry and assuming the existence of an elastic potential, c. f. Neuhaus (1981), 21 independent terms, which are not equal to zero, remain. Further considering Voigt's notation, the compliance form of Hooke's law can thus be expressed by eq. (4.8), see:

$$\begin{bmatrix} \varepsilon_{11} \\ \varepsilon_{22} \\ \varepsilon_{33} \\ \gamma_{12} \\ \gamma_{13} \\ \gamma_{23} \end{bmatrix} = \begin{bmatrix} S_{11} & S_{12} & S_{13} & S_{14} & S_{15} & S_{16} \\ S_{21} & S_{22} & S_{23} & S_{24} & S_{25} & S_{26} \\ S_{31} & S_{32} & S_{33} & S_{34} & S_{35} & S_{36} \\ S_{41} & S_{42} & S_{43} & S_{44} & S_{45} & S_{46} \\ S_{51} & S_{52} & S_{53} & S_{54} & S_{55} & S_{56} \\ S_{61} & S_{62} & S_{63} & S_{64} & S_{65} & S_{66} \end{bmatrix} \cdot \begin{bmatrix} \sigma_{11} \\ \sigma_{22} \\ \sigma_{33} \\ \tau_{12} \\ \tau_{13} \\ \tau_{23} \end{bmatrix}, \text{ with} \quad (4.8)$$

$$s_{ik} = s_{ki}, \quad (4.9)$$

or in short form:

$$\boldsymbol{\varepsilon} = \boldsymbol{S} \cdot \boldsymbol{\sigma}. \quad (4.10)$$

Inversion of \boldsymbol{S} consequently leads to the stiffness form of this mathematical statement, see

$$\boldsymbol{\sigma} = \boldsymbol{C} \cdot \boldsymbol{\varepsilon}, \text{ with } \boldsymbol{C} = \boldsymbol{S}^{-1}, \quad (4.11)$$

with \boldsymbol{C} as stiffness matrix. Further concentrating on specific anisotropic materials, defined by three symmetry planes normal to each other, strains and stresses on both sides (+ and –) of such a symmetry plane are assumed, following the constitutions given in eq. (4.12). Thereby, normal strains and stresses on both sides result to be equal, while those dedicated to shear change their sign:

$$\begin{bmatrix} \varepsilon_{11}^+ \\ \varepsilon_{22}^+ \\ \varepsilon_{33}^+ \\ \gamma_{12}^+ \\ \gamma_{13}^+ \\ \gamma_{23}^+ \end{bmatrix} = \begin{bmatrix} \varepsilon_{11}^- \\ \varepsilon_{22}^- \\ \varepsilon_{33}^- \\ -\gamma_{12}^- \\ -\gamma_{13}^- \\ -\gamma_{23}^- \end{bmatrix} \quad \text{and} \quad \begin{bmatrix} \sigma_{11}^+ \\ \sigma_{22}^+ \\ \sigma_{33}^+ \\ \tau_{12}^+ \\ \tau_{13}^+ \\ \tau_{23}^+ \end{bmatrix} = \begin{bmatrix} \sigma_{11}^- \\ \sigma_{22}^- \\ \sigma_{33}^- \\ -\tau_{12}^- \\ -\tau_{13}^- \\ -\tau_{23}^- \end{bmatrix}. \quad (4.12)$$

Presupposing that the laws, given in eq. (4.10) or eq. (4.11), are fulfilled at the same time at both symmetry sides, it is e. g. demonstrated in Schickhofer (2006a), the number of independent components in \boldsymbol{S} or \boldsymbol{C} can be reduced to nine. Such materials can be characterised by an orthotropic mechanical behaviour:

$$\begin{bmatrix} \varepsilon_{11} \\ \varepsilon_{22} \\ \varepsilon_{33} \\ \gamma_{12} \\ \gamma_{13} \\ \gamma_{23} \end{bmatrix} = \begin{bmatrix} s_{11} & s_{12} & s_{13} & 0 & 0 & 0 \\ s_{21} & s_{22} & s_{23} & 0 & 0 & 0 \\ s_{31} & s_{32} & s_{33} & 0 & 0 & 0 \\ 0 & 0 & 0 & s_{44} & 0 & 0 \\ 0 & 0 & 0 & 0 & s_{55} & 0 \\ 0 & 0 & 0 & 0 & 0 & s_{66} \end{bmatrix} \cdot \begin{bmatrix} \sigma_{11} \\ \sigma_{22} \\ \sigma_{33} \\ \tau_{12} \\ \tau_{13} \\ \tau_{23} \end{bmatrix}. \quad (4.13)$$

Figure 4.5 subsequently illustrates an infinitesimal volume element, cut from a tree stem with ideally distributed and equidistant annual ring pattern. Introducing the polar coordinates, defined by the stem axis x , as well as both plane coordinates r and φ , the given volume element can be characterised by

$$dV = r \, dr \, d\varphi \, dx. \quad (4.14)$$

Furthermore taking the material homogeneity into account (inhomogeneously distributed mechanical properties over the annual rings in radial direction are thereby ignored), the corresponding mechanical behaviour of this element can be approximated by the aforementioned Hooke's law for orthotropic materials, given in eq. (4.13). In contrast to the general form $\{1, 2, 3\}$, as applied for previously introduced constitutions, the axis denotation is thereby commonly orientated to the (ideal) growth characteristics of a tree, defined by longitudinal (L , parallel to x and fibre direction), radial (R) and tangential (T).

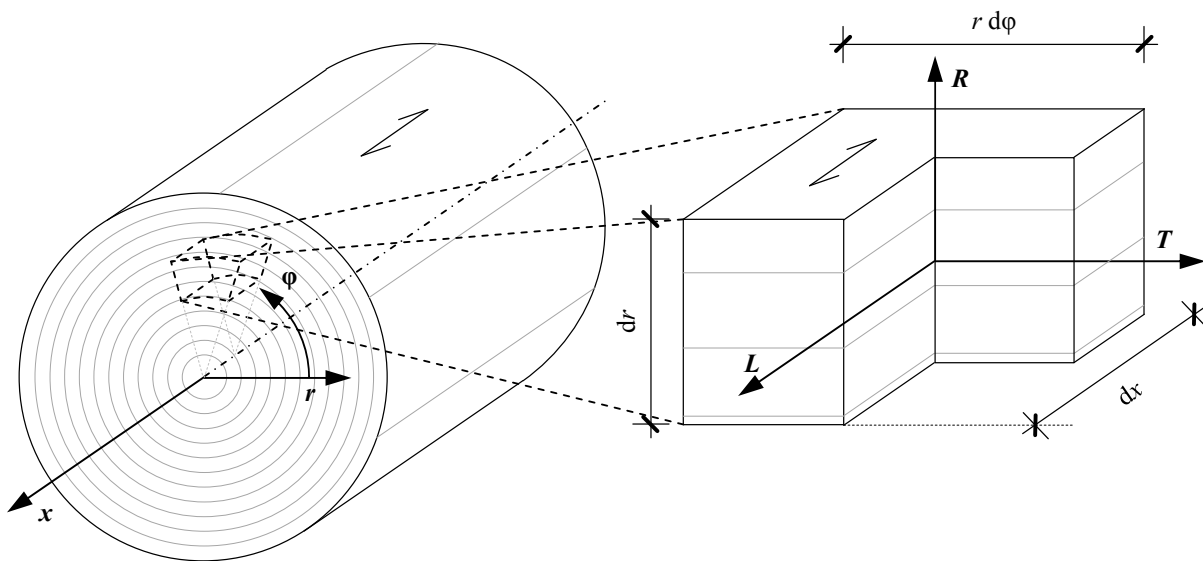


Figure 4.5: Symmetry planes L , R and T of an infinitesimal timber volume element

The compliance matrix of the infinitesimal timber volume element can thus be expressed in form of eq. (4.15), consisting of elastic moduli $\{E_L, E_R$ and $E_T\}$, shear moduli $\{G_{LR}, G_{LT}$ and $G_{RT}\}$ and Poisson's ratios $\{v_{RL}, v_{LR}, v_{TL}, v_{LT}, v_{RT}$ and $v_{TR}\}$, see:

$$\begin{bmatrix} \varepsilon_{LL} \\ \varepsilon_{RR} \\ \varepsilon_{TT} \\ \gamma_{LR} \\ \gamma_{LT} \\ \gamma_{RT} \end{bmatrix} = \begin{bmatrix} \frac{1}{E_L} & -\frac{v_{LR}}{E_R} & -\frac{v_{LT}}{E_T} & 0 & 0 & 0 \\ -\frac{v_{RL}}{E_L} & \frac{1}{E_R} & -\frac{v_{RT}}{E_T} & 0 & 0 & 0 \\ -\frac{v_{TL}}{E_L} & -\frac{v_{TR}}{E_R} & \frac{1}{E_T} & 0 & 0 & 0 \\ 0 & 0 & 0 & \frac{1}{G_{LR}} & 0 & 0 \\ 0 & 0 & 0 & 0 & \frac{1}{G_{LT}} & 0 \\ 0 & 0 & 0 & 0 & 0 & \frac{1}{G_{RT}} \end{bmatrix} \cdot \begin{bmatrix} \sigma_{LL} \\ \sigma_{RR} \\ \sigma_{TT} \\ \tau_{LR} \\ \tau_{LT} \\ \tau_{RT} \end{bmatrix} \quad (4.15)$$

Considering the aforementioned boundary conditions of orthotropic material behaviour (matrix symmetry including nine independent components), the given constitution has to fulfil the following requirements:

$$\frac{\nu_{LR}}{E_R} = \frac{\nu_{RL}}{E_L}, \quad \frac{\nu_{LT}}{E_T} = \frac{\nu_{TL}}{E_L} \quad \text{and} \quad \frac{\nu_{RT}}{E_T} = \frac{\nu_{TR}}{E_R}. \quad (4.16)$$

Furthermore, shear moduli G_{ij} are assumed equal to G_{ji} . The inversion of \mathbf{S} again leads to the stiffness form of this mathematical statement as expressed by eq. (4.17), see:

$$\begin{bmatrix} \sigma_{LL} \\ \sigma_{RR} \\ \sigma_{TT} \\ \tau_{LR} \\ \tau_{LT} \\ \tau_{RT} \end{bmatrix} = \begin{bmatrix} \frac{E_L(1-\nu_{TR}\nu_{RT})}{\Delta} & \frac{E_L(\nu_{LR}+\nu_{LT}\nu_{TR})}{\Delta} & \frac{E_L(\nu_{LT}+\nu_{LR}\nu_{RT})}{\Delta} & 0 & 0 & 0 \\ \frac{E_R(\nu_{RL}+\nu_{RT}\nu_{TL})}{\Delta} & \frac{E_R(1-\nu_{TL}\nu_{LT})}{\Delta} & \frac{E_R(\nu_{RT}+\nu_{LT}\nu_{RL})}{\Delta} & 0 & 0 & 0 \\ \frac{E_T(\nu_{TL}+\nu_{RL}\nu_{TR})}{\Delta} & \frac{E_T(\nu_{TR}+\nu_{LR}\nu_{TL})}{\Delta} & \frac{E_T(1-\nu_{LR}\nu_{RL})}{\Delta} & 0 & 0 & 0 \\ 0 & 0 & 0 & G_{LR} & 0 & 0 \\ 0 & 0 & 0 & 0 & G_{LT} & 0 \\ 0 & 0 & 0 & 0 & 0 & G_{RT} \end{bmatrix} \cdot \begin{bmatrix} \varepsilon_{LL} \\ \varepsilon_{RR} \\ \varepsilon_{TT} \\ \gamma_{LR} \\ \gamma_{LT} \\ \gamma_{RT} \end{bmatrix}, \quad (4.17)$$

with
$$\Delta = 1 - \nu_{LR}\nu_{RL} - \nu_{RT}\nu_{TR} - \nu_{LT}\nu_{TL} - \nu_{LR}\nu_{RT}\nu_{TL} - \nu_{RL}\nu_{TR}\nu_{LT}. \quad (4.18)$$

Since the majority of considerations, regarding the mechanical behaviour of clear wood, base on the constitutions given in eq. (4.15) or eq. (4.17), the corresponding properties (elastic and shear moduli, Poisson's ratios) have been comprehensively investigated in the past. Concentrating on spruce, Table 4.1 finally summarises their bandwidths at $u \approx 12\%$, as published in Persson (2000) based on data reported in Carrington (1923) and Hearmon (1948).

Table 4.1: Bandwidths of clear wood mechanical properties as summarised in Persson (2000)

mechanical property	dimension	min	max
E_{LL}	[N/mm ²]	13,500	16,700
E_{RR}	[N/mm ²]	700	900
E_{TT}	[N/mm ²]	400	650
G_{LR}	[N/mm ²]	620	720
G_{LT}	[N/mm ²]	500	850
G_{RT}	[N/mm ²]	29.0	39.0
ν_{RL}	[-]	0.018	0.030
ν_{TL}	[-]	0.013	0.021
ν_{TR}	[-]	0.240	0.330

4-4 DEFINITION AND LAY-UP OF LAMINATED TIMBER PRODUCTS

This subsection focuses on the definition of the structure and lay-up of laminated timber products. Worth mentioning, that the related scope is restricted to products composed by adhesively bonded, layered solid timber with a minimum layer thickness t_1 of 6 mm. Additionally considering the scope of application of self-tapping screws, as discussed in chapter 2, this especially concerns glued laminated timber (GLT) and glued solid timber according to ON EN 14080 (2013), as well as cross laminated timber (CLT), according to ON EN 16351 (2015). Further wood based products, such as particleboards, oriented strand boards (OSB), fibreboards or laminated veneer lumber (LVL), also covered by ETAs related to self-tapping screws, but not composed by solid timber layers, are excluded. Although, the following discussion focuses on products composed by timber boards with $t_1 = 6 \div 45$ mm, according to ON EN 14080 (2013), the definitions are also valid for those with lamellas exceeding the given upper limit of t_1 .

Figure 4.6 illustrates both relevant board-based layered timber products GLT and CLT, made of single lamellas in solid timber (ST). With regard to the layer dimensions, a prismatic shape with a rectangular cross section, defined by t_1 and the width of the layer, w_1 , is assumed. Furthermore, the fibre direction is supposed to be parallel to the layer's longitudinal axis. In fact, the main difference between the lay-up of both products is the orientation of their single layers. In case of GLT, the unidirectional layer orientation leads to its one-dimensional bar-shaped profile, while the orthogonal layer orientation of CLT enables the realisation of a two-dimensional laminar structural component.

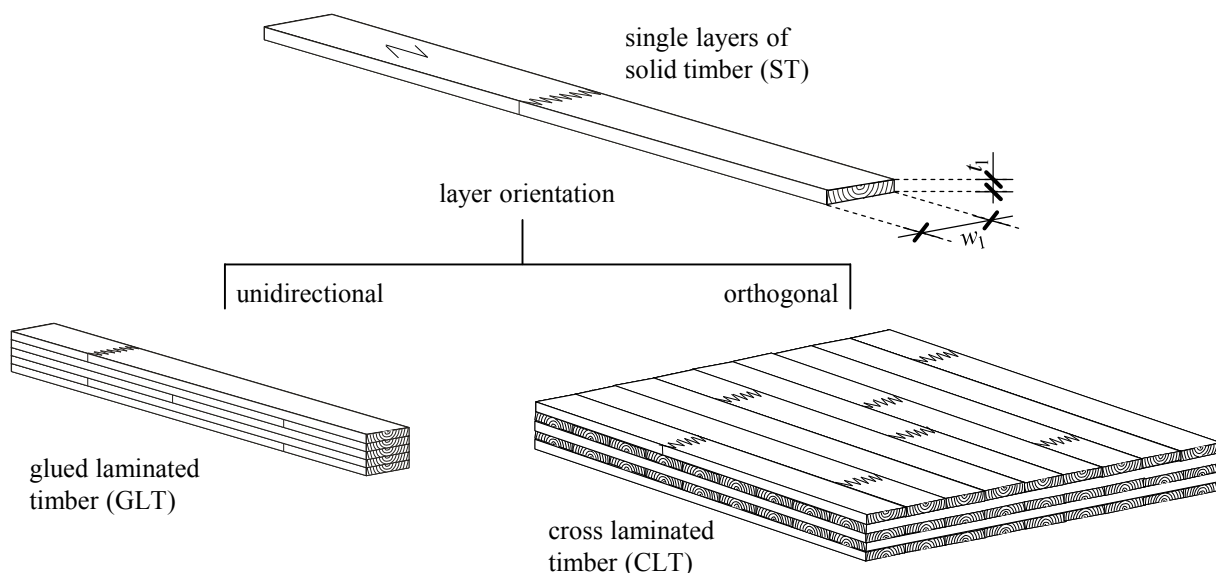


Figure 4.6: Definition of board-based layered timber products GLT and CLT

Within section 4-2, timber specimen, applied for screw investigations, have been defined with the dimensions $V = w \times h \times l$ and without growth and production characteristics, fulfilling the corresponding requirements given in ON EN 1382 (1999). Taking this dimensional restriction into account, the single screw application in laminated timber products can be assigned to the scale of layered clear wood. Figure 4.7 subsequently illustrates the main parameters of related timber specimen, whereby a differentiation is made between unidirectional (Figure 4.7, left) and orthogonal (Figure 4.7, right) layer orientation. Beside this information and the aforementioned layer thickness t_l , further relevant parameters are the number of layers within one specimen, N , as well as the occurrence of gaps or slots (here exclusively in orthogonal layered specimen), defined by their width, w_{gap} , and assumed with a rectangular base and a prismatic profile. Even though the latter can also be regarded as production characteristics, e. g. as a result of a CLT production without edge bonding or due to vacuum pressing, c. f. Brandner et al. (2016a), their relevant impact on screw withdrawal properties (c. f. chapter 5) necessitates their consideration in chapters 5 and 6. Worth mentioning, that according to ON EN 16351 (2015), w_{gap} is currently restricted to $\leq \{6.0, 4.0\}$ mm in case of gaps and slots.

Furthermore, Figure 4.7 classifies the surface areas of both types of layered clear wood specimen into side and narrow faces. This notation originally applied for CLT, c. f. Brandner et al. (2016a), has also been adopted for unidirectional layered elements in the frame of this thesis. Thereby, the side faces are regarded as oriented perpendicular to the layers' radial coordinate axis, as defined in section 4-3, and thus never include end-grain areas (oriented perpendicular to the layers' longitudinal axis), as well as base areas of gaps and slots. In contrary, narrow faces may include both, end-grain areas and those, which are predominately oriented perpendicular to the layers' tangential axis.

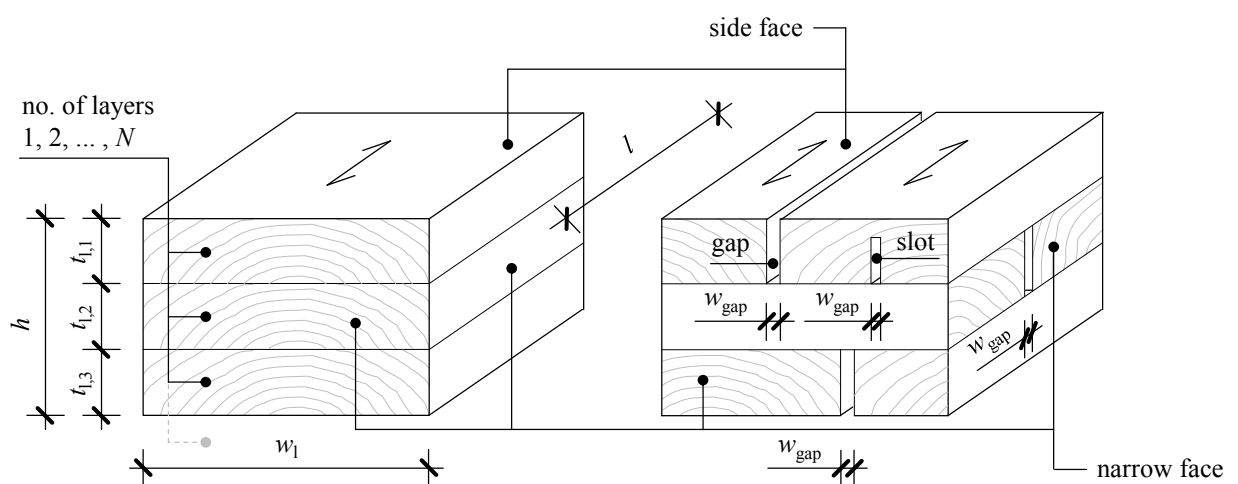


Figure 4.7: Relevant characteristics of unidirectional and orthogonal layered clear wood

CHAPTER 5

INFLUENCING PARAMETERS ON WITHDRAWAL PROPERTIES

5-1 INTRODUCTION AND OVERVIEW

In general, the withdrawal behaviour of self-tapping screws can be defined as an axial composite interaction between them and the timber member they are inserted in. The withdrawal failure, reached by exceeding the maximum bearing capacity related, has thus to be regarded as a local failure of the timber, surrounding the screw axis, c. f. section 5-1.1. Consequently, not only the size of the corresponding resistance R_{ax} , but also those of stiffness $K_{ser,ax}$ and ductility D , being necessary for specifying the load-displacement relationship of axially loaded self-tapping screws, significantly depend on the parameters influencing the timber's mechanical properties strength and stiffness.

Within this chapter, the focus is set on the impact of these and further selected parameters on withdrawal properties (especially the withdrawal resistance) of axially loaded self-tapping screws embedded in timber products, as defined in chapter 4. The corresponding considerations are separately discussed in the following sections 5-2 to 5-5, which are classified according to the illustration shown in section 5-1.4.

The given findings predominately base on comprehensive experimental investigations, carried out at Graz University of Technology within the last 10 years. They are compared – if available and reasonable – with those determined by other authors working in this field (c. f. section 5-1.3), as well as with gained relationships of basic mechanical properties. Discussions, given in section 5-4.6, 5-5.3 and 5-5.4, only base on experience from previously conducted investigations and thus have to be seen as a literature review. Even though own considerations did not focus on the parameters treated in these sections, it was decided to cover them in the frame of this chapter. The main reason therefore is their significant impact on the screw withdrawal properties, not only influencing the empirical modelling in chapter 6, but also the outlook regarding further works to be carried out in the future, gaining a more detailed knowledge regarding the loadbearing behaviour of this kind of fastener.

Although the presented results base on several different test programmes, the related experimental configurations and corresponding data assessment are quite comparable and thus generally introduced in section 5-1.2.

5-1.1 The definition of withdrawal failure

As mentioned before, the withdrawal failure of axially loaded self-tapping screws occurs by exceeding the resistance of the timber specimen they are inserted in. In section 4-3, the mechanical constitutions of the (local) timber region, surrounding the embedded screw axis, are approximated by an orthotropic material behaviour, defined by an R - T - L -coordinate system. Consequently, the timber failure specifics are supposed to depend on the position of the screw in regard to this axis system. For the practical application, this relationship is commonly expressed by α , as the angle between screw axis and grain direction, thus varying in a range of $0^\circ \leq \alpha \leq 90^\circ$. In case of $\alpha = 0^\circ$, the force interaction concerns both orthotropic planes, LR and LT , while in case of $\alpha = 90^\circ$, two further extremal alternatives have to be distinguished: one possibility thereby comprises the screw insertion in timber's radial direction, corresponding planes are RL and RT . The other possibility is a screw insertion in timber's tangential direction, which concerns both TL and TR planes. Considering this differentiation, the following discussion shall gain an impression regarding the specifics of a withdrawal failure in dependence of the screw positioning at $\alpha = \{0^\circ, 90^\circ\}$.

A related basis are the results of three representative withdrawal tests (configuration: see section 5-1.2), carried out with $d = 12$ mm screws (product B_s_II_12_300 according to section 3-4.4), which were inserted in test specimen made of solid timber. As illustrated in Figure 5.1, the corresponding screw insertion comprised the axis orientation in longitudinal ($\alpha = 0^\circ$, one test), as well as in radial direction ($\alpha = 90^\circ$, two tests). Enabling an observation of the failed specimen's cut views without separating them afterwards (which might disturb the fracture plane's optical appearance), they were cut in the specific plane directions (LT , RL and RT) prior to the tests. Furthermore, the specimen were pre-drilled with $d_{PD} = 7$ mm, in order to achieve a central screw positioning in the gaps. Clamping the specimen, the latter remained close during the tests. After tests were finished (immediately after reaching the maximum test force, F_{max}), the specimen were opened again for a screw extraction and image capturing the fracture pattern via a common copy unit.

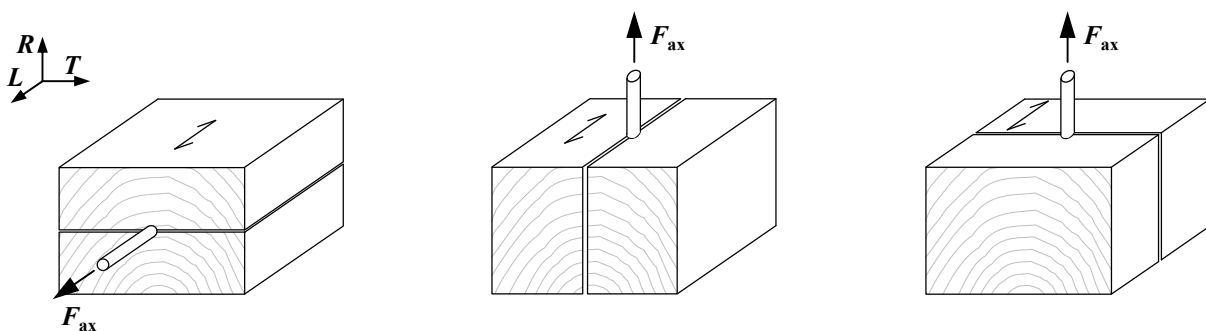


Figure 5.1: Schematic illustration of cut views made for the observation of withdrawal failure; left: LT -plane; middle: RL -plane; right: RT -plane

Figure 5.2 subsequently illustrates the scanned fracture surfaces in form of cut views of the *LT*- ($\alpha = 0^\circ$), *RL*- and *RT*-plane (both $\alpha = 90^\circ$), enabling an interpretation of the related withdrawal failure as follows:

In case of $\alpha = 0^\circ$ (Figure 5.2, left), the failure occurs by exceeding the timber specimen's local shear strength (combination of $f_{v,LR}$ and $f_{v,LT}$), in form of a crack formation, oriented parallel to the screw axis at the transition between the thread flank's end and the timber area around. A cylindrical fracture surface, defined by the product $d \cdot \pi \cdot l_{ef}$, can thus be assigned. Worth mentioning, the fracture solely concerns the timber material, situated in the area between the screw thread's inner and outer diameter (denoted as timber "consoles"), while the material surrounding the screw (optically) remains unaffected.

In case of $\alpha = 90^\circ$, the failure appearance remarkably differs in dependence of the observed cut view orientation. With regard to the fracture pattern dedicated to the orthotropic *RT*-plane given in Figure 5.2 (right), the crack formation oriented in radial (*R*) direction again occurs at the thread flank's end by exceeding the timber's rolling shear strength (here: $f_{v,RT}$) and is thus optically comparable to that found for $\alpha = 0^\circ$.

The situation for the fracture pattern situated in the *RL*-plane (Figure 5.2, middle) stands in contrast: cracks occur in the longitudinal direction and thus perpendicular to the screw axis and load direction. Similarities are found in Brandner et al. (2013), who also report crack formation in the longitudinal direction, when loading timber boards predominately perpendicular to grain (without a specification of radial or tangential force direction) for determining the material's related shear properties. Additionally taking a comparable evaluation given in Hübner (2013b) into account, the crack appearance is probably caused by an interaction of shear and tensile stresses perpendicular to grain due to local fibre bending. Furthermore, deviating from the observations related to *LT* and *RT*, crack occurrence and dispersion appear unsteadily along the screw axis (the crack formation is observed starting about $3d$ away from the screw axis in maximum cases) and are assumed to increase with decreasing distance to the timber surface where F_{ax} is introduced. A proper explanation therefore is given by considering the force distribution along the inserted screw thread also increasing with decreasing distance to the timber surface where the screw is pulled out, see e. g. Ringhofer and Schickhofer (2014b). While both fracture pattern, situated in the *LT*- and *RT*-plane, show timber failure, more or less restricted to the area between the screw thread's inner and outer diameter, the plastic timber deformation of a comparatively larger area around this zone can be observed in the *RL*-plane. Comparing the results of the scanned annual ringh structure before and after testing, the size of this area approximately results to $3 \div 4$ times of the product $d \cdot l_{ef}$, which expresses the projected area of the screw's outer thread surface.

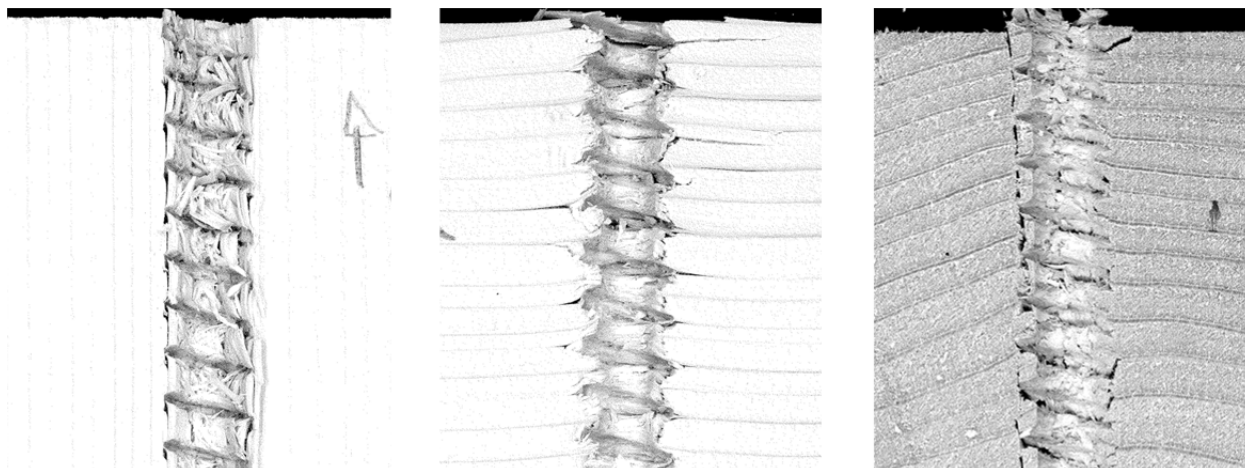


Figure 5.2: Photographs of cut views made for the observation of withdrawal failure; left: *LT-plane*; middle: *RL-plane*; right: *RT-plane*

Based on these considerations, the following conclusion can be drawn: as expected, the occurrence of local timber failure, when exceeding the axially loaded screw's withdrawal capacity, significantly depends on the position of the screw axis in regard to the *R-T-L*-coordinate system. In case of $\alpha = 0^\circ$, the timber's specific material structure leads to a shear failure in the longitudinal direction (combination of *LT*- and *LR*-shear planes), dedicated to the inserted screw thread's outer perimeter surface $d \cdot \pi \cdot l_{ef}$. In case of $\alpha = 90^\circ$, the observed behaviour is more complex and defined by a failure interaction of rolling shear (*RT*- or *TR*-plane) and shear perpendicular to grain (*RL*- or *TL*-plane) with remarkably different mechanical properties (for instance: the shear moduli ratios between those, with and without index *L*, vary between 13:1 and 30:1, according to Table 4.1), causing an inhomogeneous fracture appearance around the screw axis. The dispersion and the size of the stressed timber volume depends on the fibre orientation and can not be described by a cylindrical surface. Thus, the withdrawal strength f_{ax} , as the variable predominately focused on within this chapter and determined according to eq. (5.1), has to be regarded as an apparent timber property, deviating from the real clear wood strengths related to the stresses defined in eq. (4.15).

$$f_{ax} = \frac{F_{max}}{d \cdot \pi \cdot l_{ef}}, \quad (5.1)$$

with F_{max} as the force maximum of the corresponding load-displacement relationship.

5-1.2 General considerations regarding the experimental determination of withdrawal properties

5-1.2.1 Test execution and post-processing

Within this section 5-1.2, the experimental determination of the screw withdrawal properties f_{ax} , $K_{ser,ax}$ and D , as applied for the vast majority of the test series presented in sections 5-2 to 5-5, is explained and discussed. All tests related have been performed on two test rigs, namely the LIGNUM-UNI-275 (universal testing device, Zwick GmbH & Co. KG) and the Dyna Z-25FS (concrete adhesion tester), supplied by the Lignum Test Center (LTC) as a part of the Institute of Timber Engineering and Wood Technology at Graz University of Technology. In general, the experiments were conducted predominately in accordance to ON EN 1382 (1999) as the European test standard for determining the withdrawal capacity of timber fasteners. Note: the cited document is not valid any more, c. f. ON EN 1382 (2016). Since all withdrawal tests were performed before the latter version was published, ON EN 1382 (1999) still has to be regarded as the reference test standard for this chapter.

In fact, the corresponding procedure applied can be separated into the following steps: specimen preparation – testing – specimen post-processing – property determination – data assessment. Type and manufacturing of timber specimen significantly varied between the presented test series and are thus separately discussed in the frame of sections 5-2 to 5-5. Except a short introduction to the principle of “matched samples”, which was applied for the vast majority of the test campaigns to gain a similar density distribution of all subseries within one programme. In fact, this is necessary to avoid an unwanted impact of this parameter on the size and dispersion of withdrawal properties.

Assuming an experimental campaign with two varied parameters – one with two characteristics X and Y (for instance $\alpha = \{0, 90\}^\circ$) and the other with n characteristics (for instance various moisture contents, or outer thread diameters), as well as N solid timber beams (basis material) – specimen selection for each subseries defined by $\{X, Y\}_{\{A, \dots, N\}, \{1, \dots, n\}}$ was realised as illustrated in Figure 5.3. This sequential cutting procedure shall result in a density distribution equal for all different samples of $X_{N,n}$ and $Y_{N,n}$, as well as similar to that of the basis material. The boundary condition, which is necessary for this principle, is a widely negligible variation of clear wood densities within timber members as e. g. stated in Brandner et al. (2015) on the basis of data from Bratulic (2012) by a comparatively high value of the local density equi-correlation $r_{equi,LN} = 0.85$.

beam A	$X_{A,1}$	$Y_{A,1}$	$X_{A,2}$	$Y_{A,2}$	$X_{A,3}$	$Y_{A,3}$	$X_{A,4}$	$Y_{A,4}$...	$X_{A,n-1}$	$Y_{A,n-1}$	$X_{A,n}$	$Y_{A,n}$
beam B	$X_{B,1}$	$Y_{B,1}$	$X_{B,2}$	$Y_{B,2}$	$X_{B,3}$	$Y_{B,3}$	$X_{B,4}$	$Y_{B,4}$...	$X_{B,n-1}$	$Y_{B,n-1}$	$X_{B,n}$	$Y_{B,n}$
...													
beam N	$X_{N,1}$	$Y_{N,1}$	$X_{N,2}$	$Y_{N,2}$	$X_{N,3}$	$Y_{N,3}$	$X_{N,4}$	$Y_{N,4}$...	$X_{N,n-1}$	$Y_{N,n-1}$	$X_{N,n}$	$Y_{N,n}$

Figure 5.3: Schematic illustration of specimen selection applied for the majority of the test programmes discussed in this chapter

The principle of the test execution is subsequently shown in Figure 5.4 (left), illustrating a so-called push-pull configuration, as commonly applied for withdrawal tests of self-tapping screws. Thereby, the specimen with the already inserted screw is situated in the test rig by clipping the screw head to a cylindrical head adapter, shown in Figure 3.36 (left). Consequently, the realised hinged head support moves upwards until the specimen's surface is in contact with the steel supporting plate, serving as an abutment for loading in form of continuing with a monotonic head support movement. The load transmission from the supporting plate into the test device's abutment is realised by two steel counterplates and altogether eight steel rods. Restricting the focus on the screw and the local timber area around, the static system, given in Figure 5.4 (right), corresponds to a statically determined one-dimensional tensile bar with flexible supporting ($K_{\text{ser,ax}}$ and $K_{\text{ser,lat}}$) at its lower end, both spring parameters expressing the timber-screw composite interaction. Note: since the force introduction is supposed to be exclusively in the axial direction, further concentration is restricted to the spring parameter $K_{\text{ser,ax}}$.

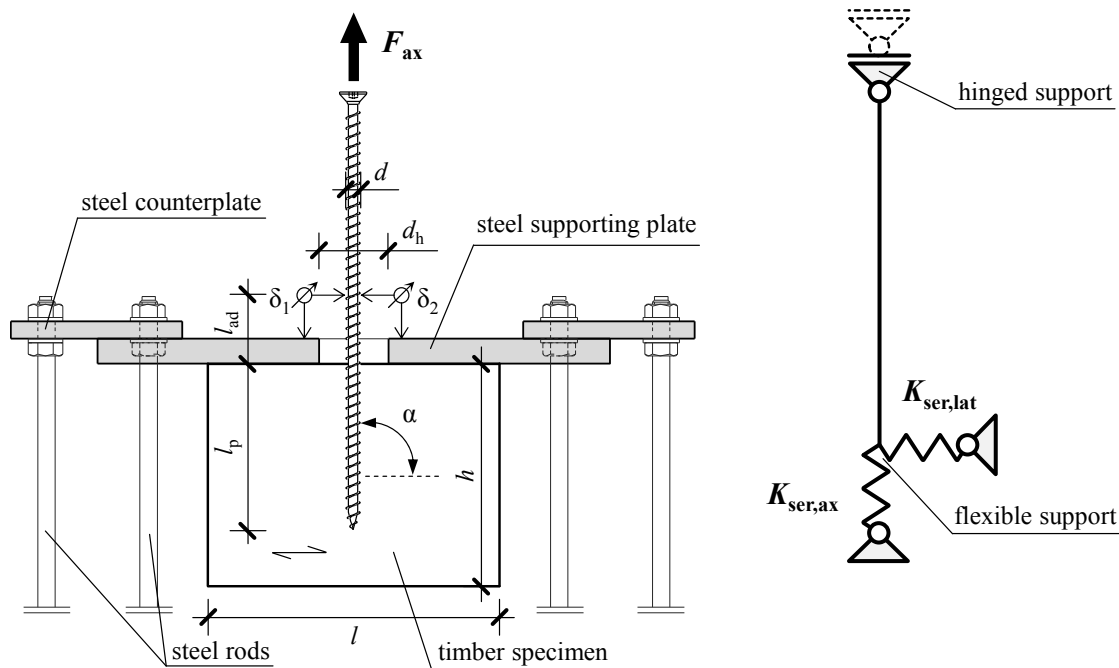


Figure 5.4: Screw withdrawal test according to ON EN 1382 (1999); left: schematic illustration of the push-pull test configuration; right: static system with a load application in form of support movement

The loading velocity, mainly depending on d , α and l_{ef} applied, was varied between approximately $0.5 \div 5.0$ mm/min (displacement-controlled in contrast to ON EN 1382 (1999); constant for each test) in order to reach the force maximum in the timeframe of 90 ± 30 s, as defined in ON EN 1382 (1999). In contrast to the procedure, for instance given in ON EN 26891 (1991), the load has been applied monotonically without any initial hysteresis until reaching the maximum force per test, F_{max} . In order to enable the determination of ductility D for the selected parameter variation, most of the tests were continued until at least $F_u = 0.80 \cdot F_{max}$ has been reached where $v(F_{max}) \leq v(F_u) \leq 30$ mm, c. f. ON EN 12512 (2001).

After finishing the experiments, the screws were removed from the timber specimen and (about) $4 d \times 4 d \times l_p$ clear wood samples were cut centrically around the screw hole for determining the density ρ_u by measuring the physical dimensions and moisture content u by performing the oven dry method according to ON EN 13183-1 (2004). Subsequently, the density ρ_{12} was determined according to eq. (4.4). In addition, the specimen were split centrically to evaluate possible influences on the withdrawal properties, caused by knots or other growth characteristics.

5-1.2.2 Withdrawal property determination

As mentioned in section 5-1.2.1, the evaluated mechanical properties are withdrawal strength (representing capacity), stiffness and ductility. While f_{ax} has been determined for each test, the scope of both latter mentioned $K_{ser,ax}$ and especially D is reduced to the most relevant influencing parameters found to govern the corresponding design process, c. f. sections 5-2 to 5-5. In case of the withdrawal strength, the determination is comparatively simple and was conducted according to eq. (5.1). Therein, l_{ef} as the effective insertion length of the screw thread, is used instead of l_p (inserted length of the screw's profiled part) as proposed in ON EN 1382 (1999). Both length parameters differ with regard to the consideration of the length of the screw tip, c. f. eq. (5.2) and Figure 5.5.

$$l_{ef} = l_p - l_{tip}, \quad (5.2)$$

with l_{tip} constantly set to $1.17d$ according to Pirnbacher et al. (2009) if the tip was situated in the timber member.

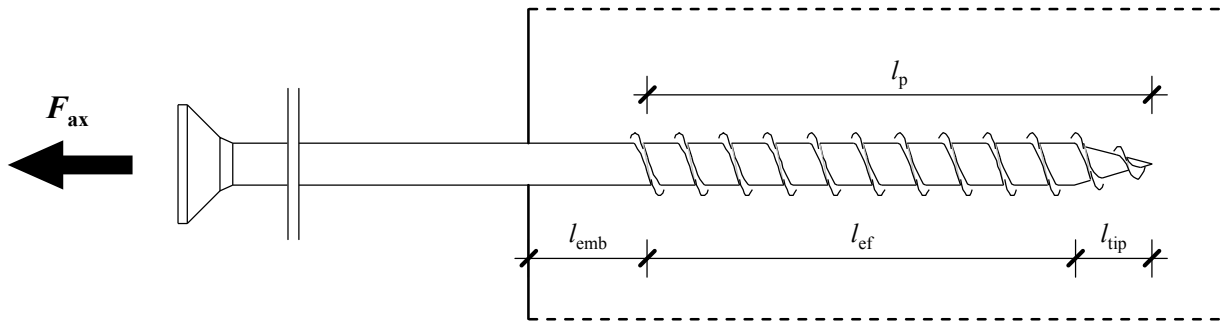


Figure 5.5: Screw insertion in timber specimen – definition of length parameters

In case of $K_{\text{ser,ax}}$ and D , nowadays several different methods are applied for determining these properties, see Flatscher (2017). Since no specific procedure is currently recommended for axially loaded self-tapping screws, it was decided adopting the procedure according to ASTM E2126 (2002), used for evaluating the steel failure in tension in section 3-4.4.3, also for the determination of withdrawal properties, see:

$$F_y = K_{\text{ser,ax}} \cdot \left(v_u - \sqrt{v_u^2 - \frac{2 \cdot A}{K_{\text{ser,ax}}}} \right). \quad (5.3)$$

The axial stiffness $K_{\text{ser,ax}}$, as component of eq. (5.3), was determined by means of a linear regression analysis, considering load and displacement recorded in the linear elastic part of the test curve. In contrast to section 3-4.4.3, as originally presented in Brandner et al. (2017), the corresponding domain was localised by plotting load increments $F_{i-1} - F_i$ against their related time steps of this way-controlled loading protocol. Figure 5.6 (right) exemplarily illustrates this relationship, including an apparent horizontal plateau, which serves as an indicator for the aforementioned linear-elastic zone. Furthermore, the displacement v was determined according to eq. (5.4), see:

$$v = \frac{\delta_1 - \delta_2}{2} - v(l_{\text{ad}}) = \frac{\delta_1 - \delta_2}{2} - \frac{\sigma_{\text{ax}}}{E_s} \cdot l_{\text{ad}}, \quad (5.4)$$

with δ_i as displacements, recorded by a local way measurement set-up in form of two LVDTs clamped on the screw shank (or thread), l_{ad} as the distance between their clamping points and the timber surface (see Figure 5.4, left), E_s as the screw's elastic modulus (constantly assumed as $E_s = 210,000 \text{ N/mm}^2$) and σ_{ax} as the axial stress, also assumed to be constant along l_{ad} and determined according to eq. (5.5) and (5.6):

screw shank along l_{ad} :

$$\sigma_{\text{ax}} = \frac{F_{\text{ax}}}{A_{\text{sh}}} = \frac{4 \cdot F_{\text{ax}}}{d_{\text{sh}}^2 \cdot \pi}, \quad (5.5)$$

screw thread along l_{ad} :

$$\sigma_{ax} = \frac{F_{ax}}{A_{pl,N,emp}}, \quad (5.6)$$

with $A_{pl,N,emp}$ according to eq. (3.95). It is worth mentioning, that the application of eq. (5.4) presupposes the screw being stressed in the linear-elastic domain of its force-displacement relationship. In cases, where this condition was not fulfilled (e. g. F_{max} close to f_{tens} , occurrence of steel failure in tension instead of withdrawal), the ductility D was not determined for the specific sample.

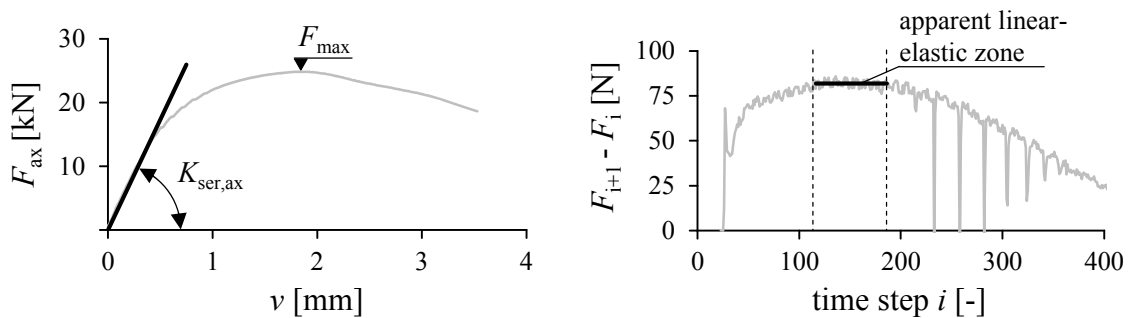


Figure 5.6: Left: typical test curve of an axially loaded screw; right: load increment vs. time step of this test curve, determined in accordance to Brandner et al. (2017)

5-1.2.3 Data assessment

The statistical assessment of the experimental data, predominately given in form of withdrawal properties, as well as timber density and moisture content, comprised outlier treatment, parameter determination and hypothesis testing. Thereby, the outlier treatment was done in two steps: first, tests, where screws penetrated or touched knots, were excluded from further considerations. Second, Tukey's criteria for statistical outliers (assuming lognormal distributed data, values outside the inter-quartil-range (IQR) ± 1.5 -times the IQR) has been performed on the logarithmised data sets and by means of box-plots, c. f. Figure 5.7. This concerned the related withdrawal properties, as well as the density ρ_{12} .

The logarithmising of data sets bases on the general hypothesis of lognormal-distributed (2pLND) densities and withdrawal properties, as assumed for all data presented in this chapter. In fact, there are two reasons for this commitment: (i) 2pLND constraints only positive data values, as they are common for physical and mechanical properties, such as strength, stiffness and density, c. f. Brandner (2013b), and (ii) standard ON EN 14358 (2007) as recommended in ON EN 14592 (2012), CUAP 06.03/08 (2010) or EAD 130118-00-0603 (2016) for determining the properties' characteristic 5 %-quantile values, as well as the recently published investigations related, c. f. Pirnbacher et al. (2009), Frese and Blaß (2009) and Hübner (2013b), also assume 2pLND for data assessment. Following Brandner (2013b), assigning a variable X being lognormal distributed generally presupposes that its (natural) logarithm is normal distributed (ND):

$$X = \ln(Y) \rightarrow X \sim \text{ND} \mid Y \sim 2\text{pLND}. \quad (5.7)$$

Density functions of X and Y consequently result to:

$$f_X(x) = \frac{1}{\sigma_X \cdot \sqrt{2 \cdot \pi}} \cdot \exp\left[-\frac{1}{2} \cdot \left(\frac{x - \mu_X}{\sigma_X}\right)^2\right], \text{ and} \quad (5.8)$$

$$f_Y(y) = \frac{1}{y \cdot \sigma_X \cdot \sqrt{2 \cdot \pi}} \cdot \exp\left[-\frac{1}{2} \cdot \left(\frac{\ln(y) - \mu_X}{\sigma_X}\right)^2\right], \quad (5.9)$$

with

$$\mu_X = E[X] = \int_{\forall x} x \cdot f_X(x) dx \rightarrow \hat{\mu}_X = \text{mean}[X] = \bar{X} = \frac{1}{n} \cdot \sum_{i=1}^n X_i, \text{ and} \quad (5.10)$$

$$\sigma_X^2 = \int_{\forall x} (x - \mu_X)^2 \cdot f_X(x) dx \mid \sigma_X = \sqrt{\sigma_X^2} \rightarrow \hat{\sigma}_X = \text{sd}[X] = S = \sqrt{\frac{1}{n-1} \cdot \sum_{i=1}^n (X_i - \bar{X})^2}, \quad (5.11)$$

$\{\mu_X, \sigma_X\}$ as the expectation and the standard deviation of X , which can be estimated from datasets via $\text{mean}[X]$ and $\text{sd}[X]$. The 5 %-quantile of X and Y can be subsequently determined as follows:

$$x_{05,\text{ND}} = \mu_X + \Phi^{-1}(0.05) \cdot \sigma_X = \mu_X \cdot (1 + \Phi^{-1}(0.05) \cdot \text{CV}[X]), \text{ and} \quad (5.12)$$

$$y_{05,\text{LND}} = \exp\left[\mu_X + \Phi^{-1}(0.05) \cdot \sigma_X\right], \quad (5.13)$$

with

$$\text{CV}[X] = \frac{\sigma_X}{\mu_X} \rightarrow \hat{\text{CV}}[X] = \frac{\text{sd}[X]}{\text{mean}[X]}, \quad (5.14)$$

as the coefficient of variation of X , again estimated from the experimental data. Note: for simplicity, in the frame of this thesis “ $\text{CV}[X]$ ” also stands for the estimated parameter. In addition, the following relationships between X and Y , as summarised in Brandner (2013b), are worth being expressed:

- for determination of parameters for $Y \sim 2\text{pLND}$:

$$\mu_X = \ln\left(\frac{\mu_Y^2}{\sqrt{\mu_Y^2 + \sigma_Y^2}}\right), \quad (5.15)$$

$$\sigma_X = \sqrt{\ln\left(\frac{\sigma_Y^2}{\mu_Y^2} + 1\right)} = \sqrt{\ln[\text{CV}(Y)^2 + 1]}, \text{ and} \quad (5.16)$$

$$y_{05,\text{LND}} = \frac{\mu_Y \cdot \exp\left[\Phi^{-1}(0.05) \cdot \sqrt{\ln(\text{CV}[Y]^2 + 1)}\right]}{\sqrt{\text{CV}[Y]^2 + 1}}. \quad (5.17)$$

- moments of $Y \sim 2\text{pLND}$:

$$\mu_Y = \exp\left(\mu_X + \frac{\sigma_X^2}{2}\right), \quad (5.18)$$

$$\sigma_Y = \mu_Y^2 \cdot \left[\exp(\sigma_X^2) - 1\right], \quad (5.19)$$

$$\text{med}[Y] = \tilde{Y} = \exp(\mu_X), \text{ and} \quad (5.20)$$

$$\text{CV}[Y] = \frac{\sigma_Y}{\mu_Y} = \sqrt{\exp(\sigma_X^2) - 1}. \quad (5.21)$$

In case of withdrawal properties and density, the subsequently determined statistics mainly comprised mean values, medians as well as coefficients of variations, calculated according to eq. (5.10), (5.11), (5.14) and (5.22). In case of moisture content, the assessment comprised also mean values and, in addition, maxima and minima.

$$\text{med}[X] = \tilde{X} = x_{50}. \quad (5.22)$$

As explained in section 5-2 to 5-5, specific test series include a certain number of tests, which were stopped before screws reached their maximum withdrawal capacity. The possible reasons are finishing the test at $F_{\text{ax}} < F_{\text{max}}$ or the occurrence of other failure modes, such as steel failure in tension or failure of the timber specimen (e. g. splitting by exceeding the material's tensile capacity perpendicular to grain). Consequently, the related datasets were regarded as right censored, necessitating an evaluation by means of the maximum-likelihood estimation technique for right censored data (rcMLE). Assuming lognormal-distributed test results, $X = f_{\text{ax},X} \sim 2\text{pLND}(\mathbf{x}|\boldsymbol{\theta})$, the parameters $\boldsymbol{\theta} = (\mu_Y, \sigma_Y)$ are estimated by maximising the log-likelihood function:

$$\ln\left[L(\hat{\boldsymbol{\theta}}|x_i)\right] = \max_{\boldsymbol{\theta}}\left[\ln\left[L(\boldsymbol{\theta}|x_i)\right]\right], \text{ with} \quad (5.23)$$

$$L(\hat{\theta}|x_i) = \prod_{i=1}^n f_{x_i}(x_i | \theta)^{d_i} \cdot [1 - F_{x_i}(x_i | \theta)]^{1-d_i}, \text{ and} \quad (5.24)$$

the indicator variable d_i equal to 1 (recorded F_{\max} due to withdrawal failure) or 0 (or not).

Finally, the inference was made by applying the frequentistic hypothesis testing by means of the software package R, c. f. R Core Team (2016), in order to verify, whether a varied parameter significantly influences the size of withdrawal properties, or not. This also concerned a comparison of the timber densities ρ_{12} of such test series, where it was tried to keep this parameter constant in order to reduce its additional influence on f_{ax} , $K_{ser,ax}$ or D . In general, inference was made by means of graphical illustrations in form of confidence intervals (CIs, if overlapping \rightarrow sign for non-significant deviation), as exemplarily shown in Figure 5.7. The given data example resulted by simulating a set of $n = 100$ samples, presupposing a standard normal distribution (SND), which is expressed by

$$X \sim \text{ND}(0,1). \quad (5.25)$$

Figure 5.7 (left) illustrates a typical scatterplot graphic with three main parameters: $\min[X]$, $\max[X]$ and $\text{mean}[X]$. The shown error bars, corresponding to the latter parameter, represent its 95 % confidence interval, thus covering the parameter's "real" location with a probability of at least 95 %, c. f. Stadlober and Schauer (2012). A related determination bases on the Student's t-Test, commonly applied for making the inference on the mean values of the assumed normal distributed datasets with unknown variance. Since data is assumed being 2pLND, the hypothesis testing was carried out for the logarithmised values, which necessitated – if required – a transformation of CIs back to the original domain of the random variable. The corresponding procedure is recommended in Olsson (2005) as follows:

$$\text{CI} = \exp \left[\bar{X} + \frac{S^2}{2} \pm t_{n-1, 1-\alpha/2} \cdot \sqrt{\frac{S^2}{n} + \frac{S^4}{2 \cdot (n-1)}} \right], \quad (5.26)$$

with $t_{n-1, \alpha}$ as the α -quantile of the Student t-distribution with $(n - 1)$ degrees of freedom. A further possibility, applied for making the inference is illustrated in Figure 5.7 (right) in form of a boxplot graphic. The main parameters are the dataset's median (according to eq. (5.22), expressed by a bold horizontal black line), the box bandwidth, denoted as IQR (range between the 75 %- and 25 %-quantile), and the plot boundaries, which are either the dataset's max/min-value (in case of $\max[X] \leq x_{75} + 1.5 \cdot \text{IQR}$ and $\min[X] \geq x_{25} - 1.5 \cdot \text{IQR}$) or $x_{\{75,25\}} \pm 1.5 \cdot \text{IQR}$. As mentioned before, the values beyond these borders were regarded as outliers, c. f. Figure 5.7 (right). The notches given therein express the 95 % confidence interval of the median and were determined according to McGill et al. (1978) as follows:

$$CI = \tilde{X} \pm 1.58 \cdot \frac{IQR}{\sqrt{n}} \tag{5.27}$$

Both, median and IQR, are empirically determined values, based on order statistics, which means that they do not require any assumption regarding the distribution model (except the condition that the distribution has to be continuous), c. f. Stadlober and Schauer (2012). Consequently, no transformation was necessary enabling an application of the test procedure, either in the original or in the logarithmic domain. In case of small n , the median values are known being less sensitive to the location of extremal data points than the mean values, which was taken especially for test series with $n < 20$ into account.

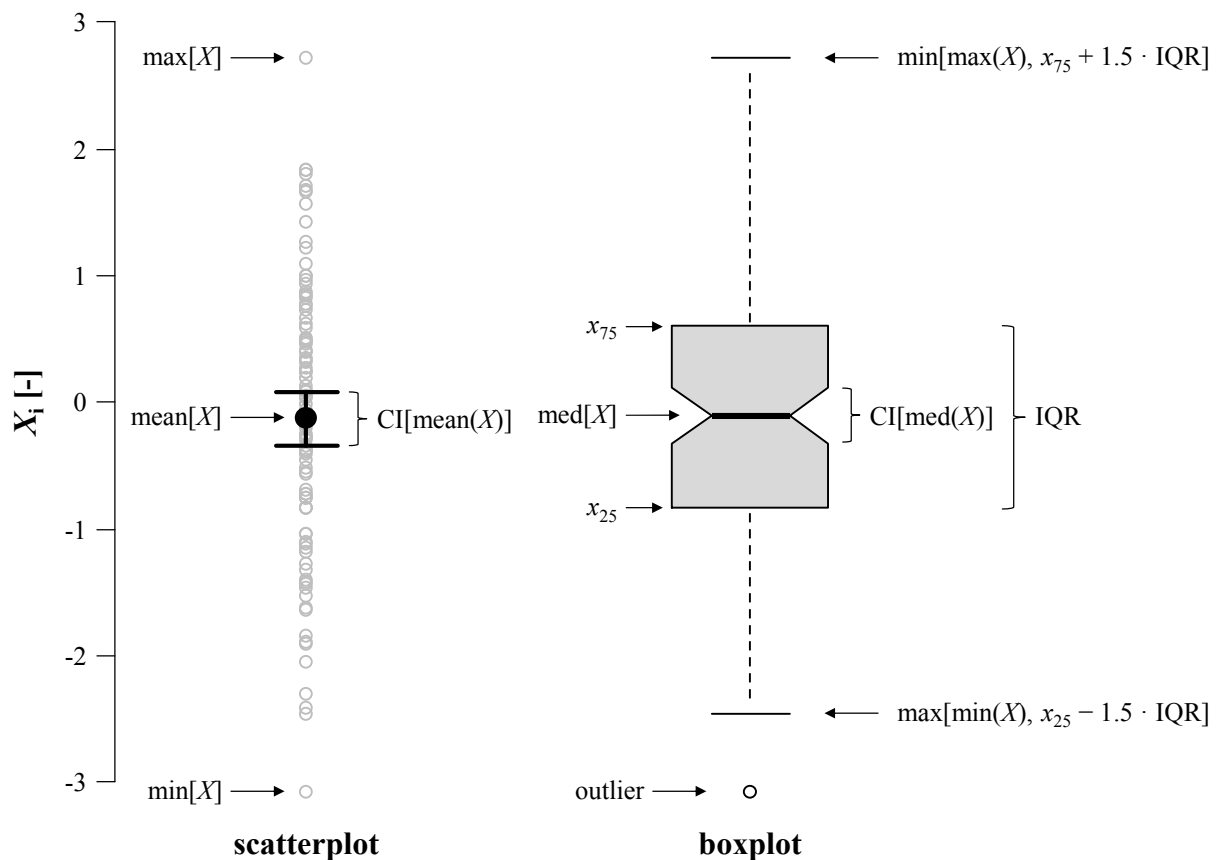


Figure 5.7: Definition of plot types predominately applied for the statistical assessment in this thesis; left: scatterplot; right: boxplot

Beside both main parameters, mean value and median, test series were also compared regarding the size of their dispersion, expressed by their coefficients of variation. Presupposing the random variable being ND (procedure was thus applied in the logarithmic domain), an approach published in Vangel (1996) was used for determining the corresponding CIs, see eq. (5.28):

$$CI = \left\{ CV[X] \cdot \left[\left(\frac{u_1 + 2}{n} - 1 \right) \cdot CV^2[X] + \frac{u_1}{n-1} \right]^{-1/2}, CV[X] \cdot \left[\left(\frac{u_2 + 2}{n} - 1 \right) \cdot CV^2[X] + \frac{u_2}{n-1} \right]^{-1/2} \right\}, \quad (5.28)$$

with

$$u_1 = F_{\chi^2}(n-1)^{-1}(1-\alpha/2), \quad u_2 = F_{\chi^2}(n-1)^{-1}(\alpha/2) \text{ and} \quad (5.29)$$

$$F_{\chi^2}(n-1), \quad (5.30)$$

as the cumulative distribution function of a central chi-squared distribution with $(n-1)$ degrees of freedom.

Furthermore, specific examinations necessitated a determination of the 95 % confidence interval for the (empirical) 5 %-quantile value. The corresponding realisation followed Stadlober and Schauer (2012), who provide the determination of the quantile's x_p confidence interval in general form as follows:

$$CI = \{X_{(k)}, X_{(l)}\}, \text{ with} \quad (5.31)$$

$$\text{rank}[X_{(k)}] = k = \left\lfloor n \cdot p + \frac{1}{2} - \sqrt{n \cdot p \cdot (1-p)} \cdot z_{1-\alpha/2} \right\rfloor, \text{ and} \quad (5.32)$$

$$\text{rank}[X_{(l)}] = l = \left\lceil n \cdot p + \frac{1}{2} + \sqrt{n \cdot p \cdot (1-p)} \cdot z_{1-\alpha/2} \right\rceil. \quad (5.33)$$

Thereby, z_α is the quantile of the standard normal distribution (SND), as defined in eq. (5.25).

In cases the withdrawal properties are found to be significantly influenced by other parameters, the corresponding relationship was partially evaluated by determining the linear correlation coefficient $r_{XY,PE}$ according to Pearson and/or $r_{XY,SP}$ based on order statistics according to Spearman, see

$$r_{XY,PE} = \frac{\sum_{i=1}^n (X_i - \bar{X}) \cdot (Y_i - \bar{Y})}{\sqrt{\sum_{i=1}^n (X_i - \bar{X})^2 \cdot \sum_{i=1}^n (Y_i - \bar{Y})^2}}, \text{ and} \quad (5.34)$$

$$r_{XY,SP} = \frac{\sum_{i=1}^n (\text{rank}[X_i] - \text{mean}[\text{rank}[X_i]]) \cdot (\text{rank}[Y_i] - \text{mean}[\text{rank}[Y_i]])}{\sqrt{\sum_{i=1}^n (\text{rank}[X_i] - \text{mean}[\text{rank}[X_i]])^2 \cdot \sum_{i=1}^n (\text{rank}[Y_i] - \text{mean}[\text{rank}[Y_i]])^2}}. \quad (5.35)$$

Following Stadlober and Schauer (2012), the gained values for $r_{XY,PE}$ and $r_{XY,SP}$ were classified into three domains,

- $0 \leq |\{r_{XY,PE}, r_{XY,SP}\}| < 0.5$ → low correlation,
- $0.5 \leq |\{r_{XY,PE}, r_{XY,SP}\}| < 0.8$ → medium correlation,
- $0.8 \leq |\{r_{XY,PE}, r_{XY,SP}\}| \leq 1.0$ → high correlation,

and, additionally tested, regarding the significance with the software package R, see R Core Team (2016).

5-1.3 A brief discussion of main literature sources

As mentioned before, the determined influence of parameters, illustrated in Figure 5.8, on withdrawal properties is subsequently compared with findings, made by other authors working in this field. In fact, this is predominately restricted to those wherein comparable parameter variations were carried out, resulting either in empirical relationships, aimed to demonstrate the impact of one specific parameter, or in empirical regression functions, derived for the general prediction of withdrawal properties. While the former are separately introduced in section 5-2 to 5-5, the latter contain at least more than one parameter and are discussed as follows:

With regard to the main property the withdrawal strength f_{ax} , the models published by Blaß et al. (2006), Pirnbacher et al. (2009), Frese and Blaß (2009) and Hübner (2013b) are worth being regarded as a reference within this chapter. As discussed in section 2-3.1, the model published by Blaß et al. (2006) is considered for withdrawal design, according to the European standard ON EN 1995-1-1 (2015) and seen as first the approach, specifically derived for modern self-tapping timber screws, see eq. (5.36) and (5.37):

$$f_{ax} = k_{ax} \cdot 0.60 \cdot d^{-0.5} \cdot l_{ef}^{-0.1} \cdot \rho^{0.8} \cdot \frac{1}{\pi}, \text{ with} \quad (5.36)$$

$$k_{ax} = \left(k_{90} \cdot \cos^2 \alpha + \sin^2 \alpha \right)^{-1} \text{ and } k_{90} = 1.20, \quad (5.37)$$

as k -parameters considering the influence of α on f_{ax} . Altogether, it bases on 1,212 withdrawal tests of axially loaded screws (supplied by five manufacturers) in solid timber made of Norway spruce (*Picea abies*) and covers parameter bandwidths in form of $d = \{6, 7.5, 8, 10, 12\}$ mm, $l_{ef} = \{3.33 \div 16\} d$, and $\alpha = \{0, 15, 30, 45, 60, 75, 90\}^\circ$. Two further models for determining f_{ax} were presented by Pirnbacher et al. (2009) and Frese and Blaß (2009) in the frame of the CIB-W18 conference in Dübendorf (Switzerland) 2009. The former one, basing on 7,779 screw withdrawal tests, conducted in solid timber and GLT (both in Norway spruce), is given in eq. (5.38) to (5.40), see

$$f_{ax} = k_{ax} \cdot (0.01353 \cdot \rho - 0.686787 \cdot d^{0.572} + 2.18888), \text{ with} \quad (5.38)$$

$$k_{ax} = (k_{90} \cdot \cos^{2.2} \alpha + \sin^{2.2} \alpha)^{-1} \text{ and } k_{90} = 1.30, \text{ or} \quad (5.39)$$

$$f_{ax} = 0.00538 \cdot \rho - 1.11935 \cdot d^{0.572} + 5.92460, \text{ if } \alpha = 0^\circ. \quad (5.40)$$

Thereby, the main influencing parameters have been varied within the following domains: $d = \{8, 10, 12\}$ mm, $\rho = \{300 \div 600\}$ kg/m³, $l_{ef} = \{4 \div 16\}$ d and $\alpha = \{0, 12.5, 25, 37.5, 45, 72.5, 90\}$ °. The latter approach considers 1,847 withdrawal tests in softwood, covers $d = \{4 \div 14\}$ mm, $\rho = \{325 \div 602\}$ kg/m³, $l_{ef} = \{18.8 \div 140\}$ mm, $\alpha = \{45 \div 90\}$ ° and is subsequently shown in eq. (5.41) and (5.42):

$$f_{ax} = k_{ax} \cdot 0.0857 \cdot \rho \cdot d^{-0.3423} \cdot \frac{1}{\pi}, \text{ with} \quad (5.41)$$

$$k_{ax} = \begin{cases} 1.00 & 45^\circ \leq \alpha \leq 90^\circ \\ \text{undef.} & 0^\circ \leq \alpha < 45^\circ \end{cases} \quad (5.42)$$

Even though the model from Hübner (2013b) was originally derived for screws, situated in timber products made of hardwood species (European ash, European beech and Black locust), a similar parameter treatment motivates to also consider his approach, given in eq. (5.43) and (5.44), for (relative) comparisons with own results. All in all, Hübner conducted 3,328 screw withdrawal tests, partially in solid timber and GLT, and thereby covers the (main) parameter bandwidths in form of $d = \{4 \div 20\}$ mm (including a threaded rod with $d = 20$ mm), $\rho = \{575 \div 915\}$ kg/m³, $l_{ef} = \{4 \div 7\}$ d and $\alpha = \{0, 15, 30, 45, 60, 75, 90\}$ °.

$$f_{ax} = k_{ax} \cdot 2.39 \cdot 10^{-3} \cdot \rho^{1.6} \cdot d^{-0.34} \cdot \frac{1}{\pi}, \text{ with} \quad (5.43)$$

$$k_{ax} = \begin{cases} 1.00 & 30^\circ \leq \alpha \leq 90^\circ \\ k_{90}^{-1} + \frac{1 - k_{90}^{-1}}{30} \cdot \alpha & 0^\circ \leq \alpha < 30^\circ \end{cases} \text{ and } k_{90} = 1.22. \quad (5.44)$$

With regard to eq. (5.36) to (5.44), the following remarks are worth being briefly discussed:

All models – except the one published by Pirnbacher et al. (2009), it can be defined as additive function – base on multiplicative approaches considering the impact of the main parameters d , ρ and l_{ef} by power functions with constant exponents. While the exponent of the outer thread diameter varies in a small range between -0.34 and -0.50 , the one, dedicated to the timber density, differs about the factor 2. This indicates a possibly significant influence of its investigated scope (maybe also caused by different timber

species) on the screw withdrawal strength. Furthermore, Blaß et al. (2006) exclusively consider a possible influence of l_{ef} on f_{ax} , while all later published models do not include this parameter. Concentrating on k_{ax} , therewith described influence of α on f_{ax} is either covered by a trigonometric approach, originally published by Hankinson (1921), or by a bilinear one with discontinuity at $\alpha = 30^\circ$ or 45° . Again, the model published by Pirnbacher et al. (2009) can be seen as an exception, since they provide a regression function especially derived for $\alpha = 0^\circ$.

Further concentrating on $K_{ser,ax}$, as the inserted screw thread's axial stiffness, comparatively minor efforts have been made so far for empirically describing this property in dependence of the relevant influencing parameters. In fact, two approaches, one also published in Blaß et al. (2006) and another one provided in the most approvals of a specific screw manufacturer as the holder of ETA-12/0063 (2013), are worth being introduced within this subsection. Note: both are also mentioned in section 2-2.5.5, eq. (2.26) and (2.27). As shown in eq. (5.45), similar to their approach for predicting f_{ax} , the model published by Blaß et al. (2006) for the withdrawal stiffness can be regarded as a multiplicative function, again treating the parameter impact by constant exponents. The corresponding bandwidths are identical with those mentioned for f_{ax} ; except the axis-to-grain angle α , which, according to Blaß et al. (2006), could not be considered for $K_{ser,ax}$ in eq. (5.45). Thus, the model solely covers screws inserted in solid timber at $\alpha = 90^\circ$.

$$K_{ser,ax} = 234 \cdot \rho^{0.2} \cdot d^{0.2} \cdot l_{ef}^{0.4} . \quad (5.45)$$

With regard to the approach according to ETA-12/0063 (2013), given in eq. (5.46), the corresponding parameter treatment significantly differs from the former one. This especially concerns the timber density ρ as the main material indicator, which is therein not considered at all. Furthermore, both d and l_{ef} are expressed with a linear influence in eq. (5.46), while eq. (5.45) constitutes a significant decrease of $K_{ser,ax}$ with increasing $\{d, l_{ef}\}$. Consequently, the model comparison, shown in Figure 2.25, results in remarkable different values for $K_{ser,ax}$ in dependence of the approach applied. Worth mentioning, that a possible influence of α on $K_{ser,ax}$ is again not considered in eq. (5.46) and thus currently not covered in the technical approvals related to self-tapping screws, c. f. section 2-2.5.5.

$$K_{ser,ax} = 25.0 \cdot d \cdot l_{ef} . \quad (5.46)$$

In contrast to f_{ax} and $K_{ser,ax}$, where at least two related approaches have been published for property determination, works focusing on the derivation of a similar model for the screw's ductility D can not be found at all.

5-1.4 Overview and classification of parameters influencing withdrawal properties

As previously introduced, the following sections 5-2 to 5-5 comprise a discussion regarding parameters influencing the withdrawal properties of axially loaded self-tapping screws inserted in timber products, as defined in chapter 4. Figure 5.8 subsequently illustrates a possible classification related, which has been originally published in Ringhofer et al. (2014a). It is also applied in this chapter. Therein, the parameters are separated into four main groups, comprising both the composite parts “screw” and “timber product”, as well as “application” and “loading”.

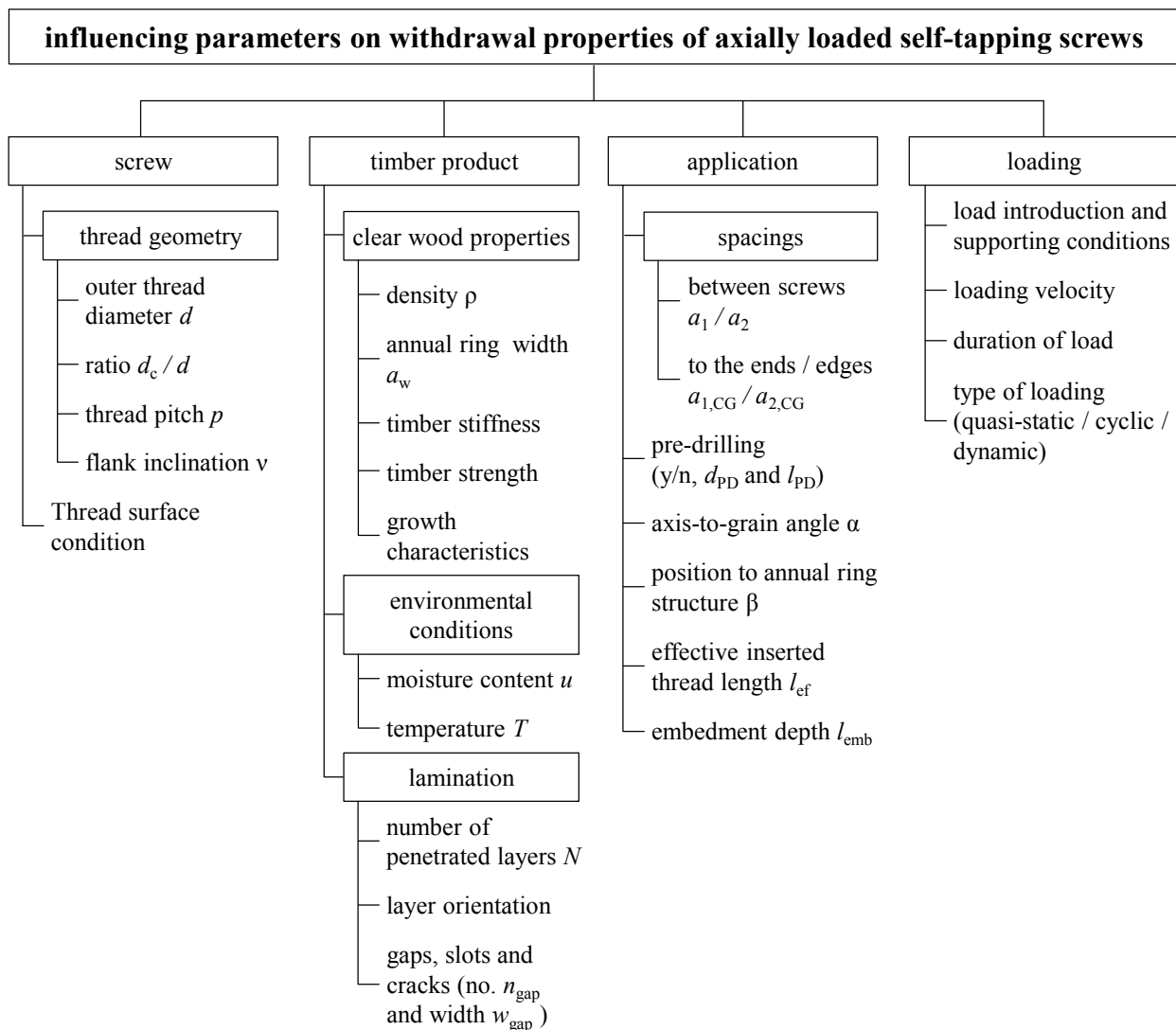


Figure 5.8: Overview and classification of influencing parameters on screw withdrawal properties; based on Ringhofer et al. (2014a)

5-2 SCREW

5-2.1 Thread geometry

5-2.1.1 Introduction

Since the screw thread is responsible for the composite interaction between the fastener and the timber volume around, its geometrical shape majorly influences the corresponding loadbearing behaviour. As comprehensively discussed (in section 3-2 and shown in Figure 5.8), the commonly applied screw threads can be generally described by their outer thread diameter d , the ratio between the inner and outer thread diameter $\eta = d_c / d$, the thread pitch p and the flank inclination angle v . With regard to the approaches discussed in section 5-1.3, as well as modern standardisation and technical approvals related, the outer thread diameter of the screws is persistently applied for representing the influence of these thread characteristics on withdrawal properties nowadays. Further thread parameters are in fact not considered at all.

The main reasons are probably the small bandwidths, in-between the latter mentioned vary nowadays, which especially concern both parameters η and v , c. f. Table 5.1. Therein, the corresponding ranges for nominal outer thread diameters $d = \{8, 10, 12\}$ mm, as they can be found in currently valid ETAs related to self-tapping screws, are given.

Table 5.1: Bandwidths of thread parameters η , p and v as given in currently valid ETAs (HiLo threads excluded); according to Pöll (2017)

thread parameter	nominal outer thread diameter d_{nom}		
	8 mm	10 mm	12 mm
η	0.60 ÷ 0.68	0.59 ÷ 0.66	0.57 ÷ 0.64
p	3.24 ÷ 7.15 mm	3.96 ÷ 8.25 mm	5.40 ÷ 7.50 mm
v		30 ° ÷ 50 °	

The works, focusing on the influence of thread characteristics $\{\eta, p$ and $v\}$ on withdrawal properties of modern self-tapping timber screws, are scarce. With regard to $K_{\text{ser,ax}}$ and D , no related investigations have been found so far. In case of the withdrawal capacity (or strength), two publications are worth being outlined:

Pirnbacher and Schickhofer (2007) report the results of about 400 screw withdrawal tests in solid timber at $\alpha = \{0, 45, 90\}$ °, conducted with five $d = 8$ mm self-tapping screws from five different manufacturers and one comparable wood screw with thread properties, according to DIN 7998 (1975). Apart from the latter mentioned product, where minor resistance was observed especially in case of $\alpha = 90$ °, the

withdrawal strength of all self-tapping screw products resulted in a similar range of $\pm 10\%$, indicating no significant impact of the specific thread geometry.

A more quantitative comparison, regarding the specific influence of both parameters p and η , was carried out by Frese and Blaß (2009). Creating a basis for modelling the withdrawal strength and capacity, as it is presented in section 5-1.3, they evaluated a corresponding parameter impact within a preliminary multiple regression analysis. The reported outcomes address no significant influence of the thread pitch p (where a bandwidth similar to those shown in Table 5.1 was considered) on withdrawal capacity. Since η was also not applied for the advanced modelling, compare eq. (5.41), it is assumed that there was not found a related influence.

With regard to the flank inclination angle v , neither Pirnbacher and Schickhofer (2007) nor Frese and Blaß (2009) concentrated on a corresponding effect on withdrawal properties. This can be explained by the circumstance, that only a small number of screws are produced with $v = 30^\circ$ or 50° – as the bandwidth's limits given in Table 5.1 – while, for the vast majority, a standard angle of 40° is applied, which currently disables a reasonable variation of this parameter.

Concluding the discussion far, taking own investigations into account, the focus of this section is reduced to the impact of the screw's outer thread diameter on withdrawal properties. Even though this seems appropriate for covering the current state-of-the-art of screw production, it is worth mentioning, that geometrical modifications, possibly conducted in the future, may require further thread parameters to be additionally considered in the corresponding design process.

Beside the approaches discussed in section 5-1.3, two further works, carried out by Pirnbacher et al. (2009) and Hübner (2013a), concentrated on the relationship between withdrawal strength and outer thread diameter d . Note: both are in fact the basis for eqs. (5.38), (5.40) and (5.43), thus covering the same parameter bandwidths as mentioned in section 5-1.3. Pirnbacher et al. (2009) recommend this relationship in form of a linear approach and alternatively as a power function, the latter as part of eqs. (5.38) and (5.40), expressed by a factor k_{diam} , see

$$f_{\text{ax,diam}} = k_{\text{diam}} \cdot f_{\text{ax,d=8mm}}, \text{ and} \quad (5.47)$$

$$k_{\text{diam}} = 1.322 - 0.0402 \cdot d, \text{ or} \quad (5.48)$$

$$k_{\text{diam}} = 2.44 \cdot d^{-0.428}, \quad (5.49)$$

with $f_{\text{ax,d=8mm}}$ as a reference withdrawal strength of screws with $d = 8$ mm. Pirnbacher et al. (2009) point out, that this relationship is irrespective from the timber product (they consider ST and GLT), the timber

density and the axis-to-grain angle. The latter conclusion is in contrast to the findings made by Hübner (2013a), who determined the diameter effect in dependence of α as follows:

$$f_{\text{ax},\alpha=0^\circ,\text{mean}} = 27.5 \cdot d^{-0.378}, \text{ and} \quad (5.50)$$

$$f_{\text{ax},\alpha=90^\circ,\text{mean}} = 27.3 \cdot d^{-0.291}, \quad (5.51)$$

and alternatively in form of an exponential approach:

$$f_{\text{ax},\alpha=0^\circ,\text{mean}} = 8.25 + 14.6 \cdot \exp(-0.152 \cdot d), \text{ and} \quad (5.52)$$

$$f_{\text{ax},\alpha=90^\circ,\text{mean}} = 6.63 + 14.3 \cdot \exp(-0.0624 \cdot d). \quad (5.53)$$

Comparatively lower power values for $\alpha = 0^\circ$ in both approaches indicate a more pronounced nonlinear influence of the outer thread diameter on withdrawal strength for this axis-to-grain-angle configuration.

Although all approaches quantitatively differ in size of the diameter influence, they agree in observing a regressive behaviour of f_{ax} with increasing d . A proper explanation therefore can be found in the so-called “size-effect” of mechanical timber properties. In Brandner et al. (2012), for instance, the loss of shear strength f_v with an increasing specimen dimension (stressed shear area or member depth) is similarly described by a power function with an exponent varying in a range of -0.13 to -0.41 .

5-2.1.2 Experimental programme

For determining an exclusive influence of the screw’s outer thread diameter d on withdrawal properties, additional impacts, e. g. caused by varying the timber densities or moisture contents between the test series, have to be excluded as far as possible. In the frame of a test campaign, conducted to investigate this diameter impact on withdrawal strength, this was realised by situating all different screws with varying d in one and the same specimen, each as a segment of altogether 54 solid timber beams in Norway spruce with cross-sectional dimensions $w \times h = 160 \times 240 \text{ mm}^2$. Thus, similar densities per specimen, as well as similar density distributions, could be expected. A corresponding illustration is given in Annex B-3.1, Figure B.15.

As discussed in section 5-1.1, the axial loadbearing behaviour of self-tapping screws mainly depends on the stressed shear planes related and significantly differs between $\alpha = 0^\circ$ and 90° . Thus, it was reasonable determining the influence of d on withdrawal strength for both axis-to-grain angles. Further boundary conditions, applied for this test campaign, are shown in Table 5.2, which especially includes the different screw products, covering a diameter range of $d = \{4, 6, 8, 12\} \text{ mm}$ (self-tapping screws) and $d = \{16, 18\} \text{ mm}$ (threaded rods). The latter were considered in order to gain additional information

concerning the loadbearing behaviour of this fastener type. Since the threaded rods are produced without tips, pre-drilling with d_{PD} , according to Z-9.1-777 (2010), was necessary. Both further boundary conditions l_{ef} and l_{emb} were constantly set to $\{\sim 10, 2\} d$.

Table 5.2: Thread characteristics and test conditions applied for the experimental campaign focusing on the diameter impact

thread characteristics					test conditions			
d_{nom}	d	η	p	v^*	l_p	l_{ef}	l_{emb}	d_{PD}
[mm]	[mm]	[-]	[mm]	[°]	[mm]	[mm]	[mm]	[mm]
4	3.93	0.64	1.86	40	42	37.3	8	-
6	5.98	0.64	2.55		72	65.0	12	-
8	7.94	0.68	5.57		99	89.6	16	-
12	11.6	0.62	6.57		144	130.0	24	-
16	15.6	0.75	6.02	61	192	192	32	12
20	19.6	0.76	6.92		200	200	40	16

* values taken from product information related

Worth mentioning, that all tests have been performed on the test rig LIGNUM-UNI-275 without local way measurement set-up, which disables a reasonable determination of $K_{ser,ax}$ and D . Further background information regarding test execution, post-processing, property determination and data assessment is summarised in section 5-1.2.

5-2.1.3 Results and discussion

Figure 5.9 and Figure 5.10 subsequently illustrate the main statistical parameters of timber density ρ_{12} and moisture content u (both determined according to eq. (4.2) and (4.4)) of small scale specimen in dependence of the outer thread diameter d (represents the nominal diameter d_{nom}) and axis-to-grain angle α . The related absolute values can be found in Annex B-3.2, Table B.12. Even though the average moisture contents exceed the equilibrium moisture content of 12 % to a certain extent, their location does not differ remarkably between the test series. Thus, a related impact on a relative comparison of withdrawal strengths can be excluded. The same situation is given for the determined densities varying around 400 kg/m^3 in average. The illustrated boxplot/scatterplot graphics indicate no significant deviations, neither for mean and median values, nor for the dataset's variability, as represented by the coefficient of variation.

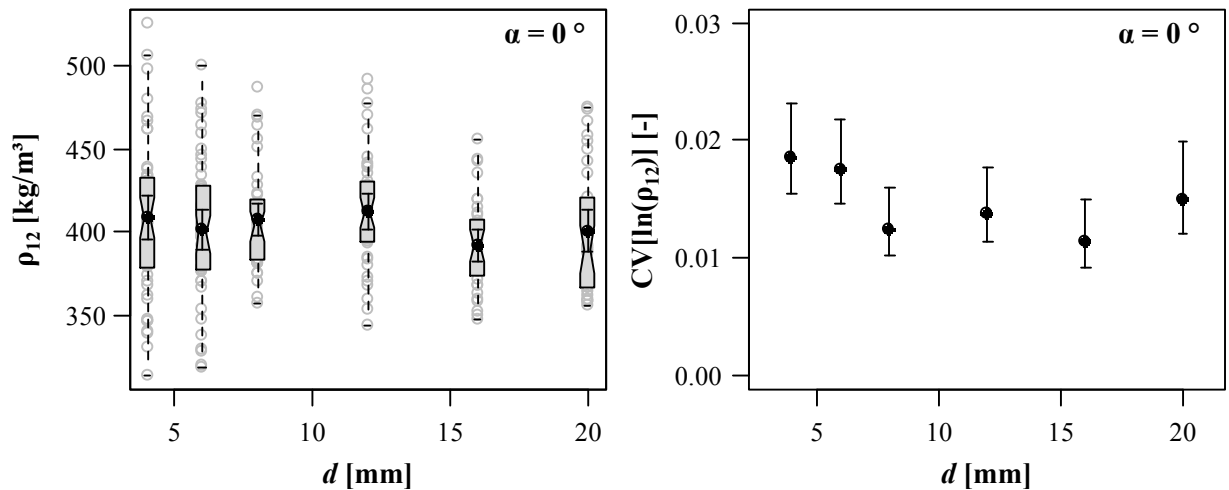


Figure 5.9: Left: Combined boxplot/scatterplot graphic of densities ρ_{12} ; right: CIs of $CV[\ln(\rho_{12})]$; $\alpha = 0^\circ$

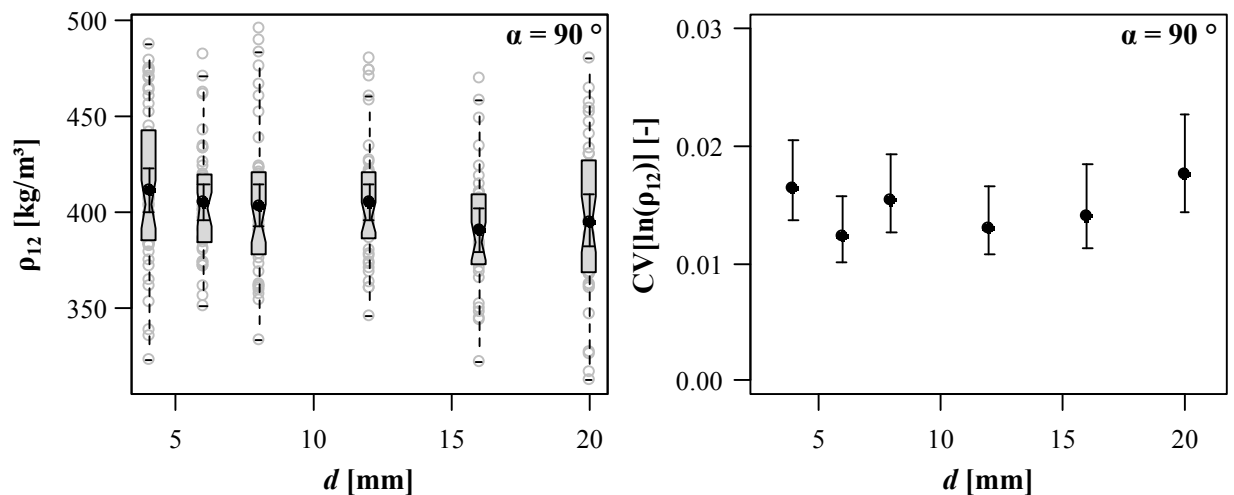


Figure 5.10: Left: combined boxplot/scatterplot graphic of densities ρ_{12} ; right: CIs of $CV[\ln(\rho_{12})]$; $\alpha = 90^\circ$

Now concentrating on the loadbearing performance of the screw products applied, the determined statistics of the withdrawal strengths f_{ax} are illustrated in Figure 5.11, as well as in Annex B-3.2, Table B.13 – again in dependence of the outer thread diameter d and the axis-to-grain angle α . With regard to the test results at $\alpha = 90^\circ$, a significant and regressive trend of f_{ax} with increasing d can be observed, converging to a constant horizontal plateau at $d \geq 12$ mm.

In case of the withdrawal strength determined at $\alpha = 0^\circ$, an even more pronounced nonlinear decrease of f_{ax} with increasing d is given for the self-tapping screws, while the results corresponding to the threaded rods with $d = \{16, 20\}$ mm indicate the opposite. This is in fact surprisingly, since an asymptotic behaviour, similar to $\alpha = 90^\circ$ and to the results gained by Hübner (2013a) for $\alpha = 0^\circ$, was expected prior to the tests. The possible reasons for this deviation may be the differences in thread geometry and test execution between self-tapping screws and threaded rods, as given in Table 5.2. While the latter influence

(especially pre-drilling) is separately discussed in section 5-4, the former is currently hardly verifiable, c. f. section 5-2.1.1. Consequently, this matter is worth to be focused on in future.

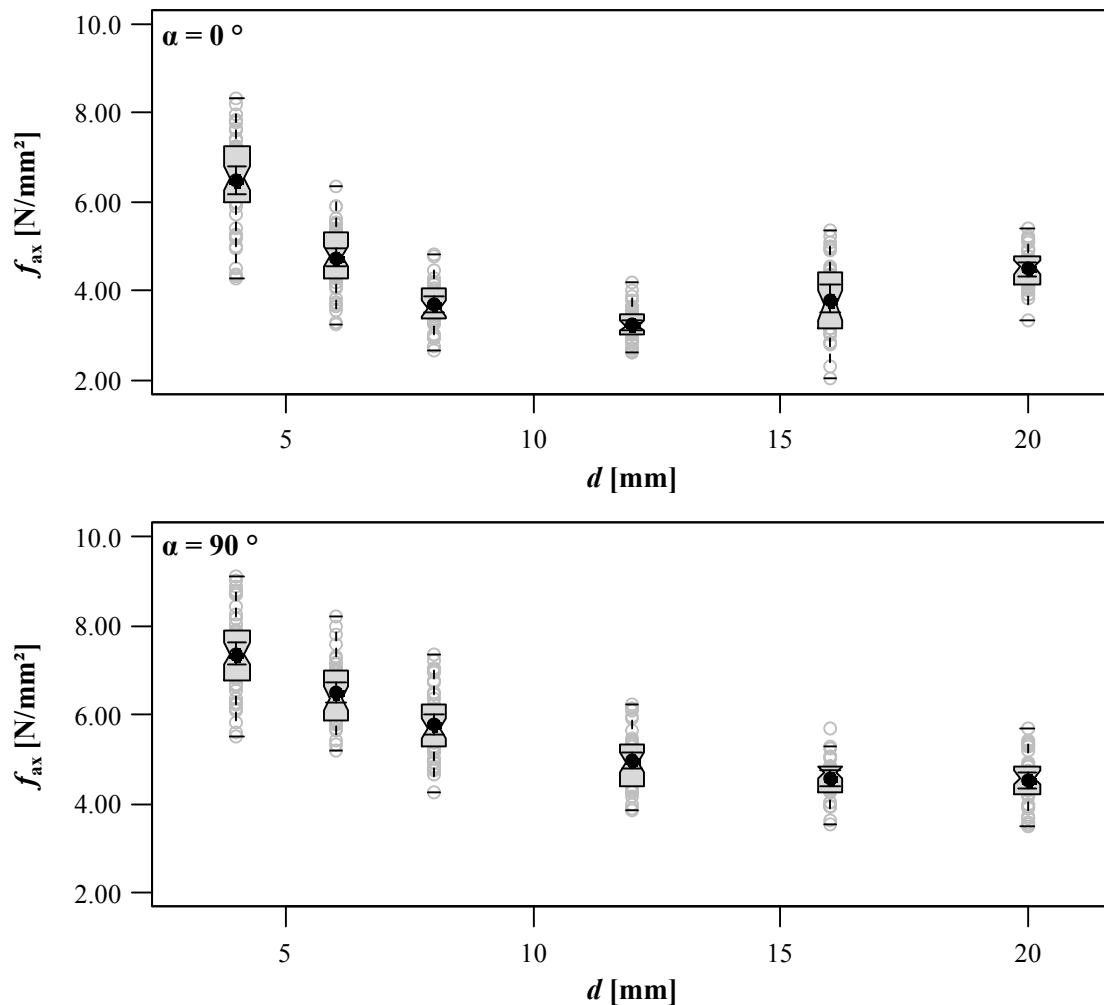


Figure 5.11: Combined boxplot/scatterplot diagram of withdrawal strength vs. outer thread diameter; above: $\alpha = 0^\circ$; below: $\alpha = 90^\circ$

Back to the results for self-tapping screws, the more pronounced decrease of f_{ax} with increasing d , in case of the parallel-to-grain insertion, indicates an influence of α on this relationship, corresponds to the findings made by Hübner (2013a) and is in contrast to those given in Pirnbacher et al. (2009). One possible explanation for this circumstance is the small bandwidth of $d = \{8, 10, 12\}$ mm, considered by Pirnbacher et al. (2009). This can be confirmed by more or less equal values of k_{90} (ratio between $f_{ax,\alpha=90^\circ,\text{mean}}$ and $f_{ax,\alpha=0^\circ,\text{mean}}$) for $d = \{8, 12\}$ mm, as given in Table 5.3.

Table 5.3: Experimentally determined ratios k_{90} in dependence of the outer thread diameter d

d	[mm]	4	6	8	12	16	20
k_{90}	[-]	1.14	1.37	1.57	1.53	1.20	1.01

With regard to the variability of the results of the withdrawal strength, the coefficients of variation determined for each dataset, illustrated in Figure B.16, indicate no clear influence of varying the outer thread diameters. This is additionally confirmed by Table 5.4, wherein the determined k_{CV} as the ratio between $CV[f_{ax}]$ and $CV[\rho_{12}]$ are shown in dependence of d and α .

Table 5.4: Experimentally determined ratios k_{CV} in dependence of outer thread diameter and axis-to-grain angle

α	d	[mm]	4	6	8	12	16	20
0 °	k_{CV}	[-]	1.43	1.41	1.80	1.37	3.31	1.14
90 °	k_{CV}	[-]	1.23	1.47	1.38	1.59	1.26	1.16

Further topics of interest are the consequences of an outer thread diameter variation on the relationship of withdrawal strength with other parameters, especially the axis-to-grain angle and the timber density, as both are considered in current model approaches, c. f. section 5-1.3. In case of α , restricting the focus to self-tapping screws, k_{90} ratios (given in Table 5.3) indicate an increasing difference between $f_{ax,\alpha=0^\circ}$ and $f_{ax,\alpha=90^\circ}$ with increasing d .

In case of ρ_{12} , in accordance to the approaches discussed in section 5-1.3, a corresponding evaluation can be realised by determining the power factor k_p for each subset as follows:

$$\ln(f_{ax}) = k_p \cdot \ln(\rho) + \Delta \rightarrow f_{ax} = \rho^{k_p} \cdot \exp(\Delta), \quad (5.54)$$

which presupposes a linear relationship (basing on a linear regression analysis) between both properties in the logarithmic domain and the assumption of $\{f_{ax}, \rho\} \rightarrow 2pLND$, as basically defined in section 5-1.2.3. Table 5.5 subsequently includes the corresponding values for k_p and $r_{XY,PE}$, the latter determined according to eq. (5.34). In fact, the clear differences in dependence of the axis-to-grain angle are given: focusing on parallel to grain insertion, k_p as well as $r_{XY,PE}$ linearly decrease with increasing d , meaning a loss of the relationship's proportionality and its strongness. With regard to $\alpha = 90^\circ$, an oppositional behaviour in form of a slight increase of k_p with increasing d , as well as more or less constant and comparatively high values of $r_{XY,PE}$, can be observed.

Concluding the comparisons made in Table 5.3 and Table 5.5, the varying relationships between f_{ax} and $\{\alpha, \rho\}$, as expressed by both factors k_{90} and k_p , clearly indicate an influence of the outer thread diameter, which necessitates a corresponding consideration for empirical modelling in chapter 6.

Table 5.5: Experimentally determined values for k_p and $r_{XY,PE}$ in dependence of outer thread diameter and axis-to-grain angle

α	d	[mm]	4	6	8	12	16	20
0°	k_p	[-]	0.91	0.85	0.57	0.46	1.33	0.42
	$r_{XY,PE}$	[-]	0.60	0.58	0.31	0.34	0.38	0.35
90°	k_p	[-]	1.11	1.28	1.28	1.33	1.07	1.00
	$r_{XY,PE}$	[-]	0.89	0.86	0.91	0.82	0.82	0.86

The focus of the last part of this section lays on the determination of a quantitative, empirical relationship between withdrawal strength and outer thread diameter on the basis of own test results. Taking their localisation, as given in Table B.13 and Figure 5.11, as well as the models discussed in in sections 5-1.3 and 5-2.1.1 into account, the corresponding approach includes a nonlinear relationship in form of a power function as expressed in eqs. (5.55) and (5.56) in dependence of the axis-to-grain angle α :

$$f_{ax,\alpha=i,\text{mean}} = A \cdot d^{k_{\text{diam}}}, \text{ which results to} \quad (5.55)$$

$$f_{ax,\alpha=0^\circ,\text{mean}} = 16.65 \cdot d^{-0.69}, \text{ and } f_{ax,\alpha=90^\circ,\text{mean}} = 12.22 \cdot d^{-0.36}. \quad (5.56)$$

Thereby, the model parameters A and k_{diam} were determined by means of the nonlinear least squares method for the average withdrawal strengths, achieving a comparatively high coefficient of determination $R^2 = \{0.976, 0.997\}$ in case of both $\alpha = \{0, 90\}^\circ$. Note: the aforementioned oppositional behaviour of $f_{ax,\alpha=0^\circ}$ at $d = \{16, 20\}$ mm necessitated restricting the model bandwidth to self-tapping screws in form of $d = 4 \div 12$ mm. With regard to $\alpha = 90^\circ$, the derived power factor k_{diam} agrees well with both approaches, published by Frese et al. (2010) and Hübner (2013b), given in eqs. (5.41) and (5.43). This may confirm the validity of the experimental programme. In case of $\alpha = 0^\circ$, a significantly higher absolute value of k_{diam} was determined, indicating a similar, but far more pronounced, interrelationship between withdrawal strength, outer thread diameter and axis-to-grain angle, as reported in Hübner (2013a).

Figure 5.12 subsequently compares the experimentally determined values of $f_{ax,\text{mean}}$ with the model predictions for varying the outer thread diameters. Concentrating on the threaded rods and as expected, the model extrapolation leads to a significant underestimation of test results in case of $\alpha = 0^\circ$, while those gained for perpendicular-to-grain insertion are widely confirmed.

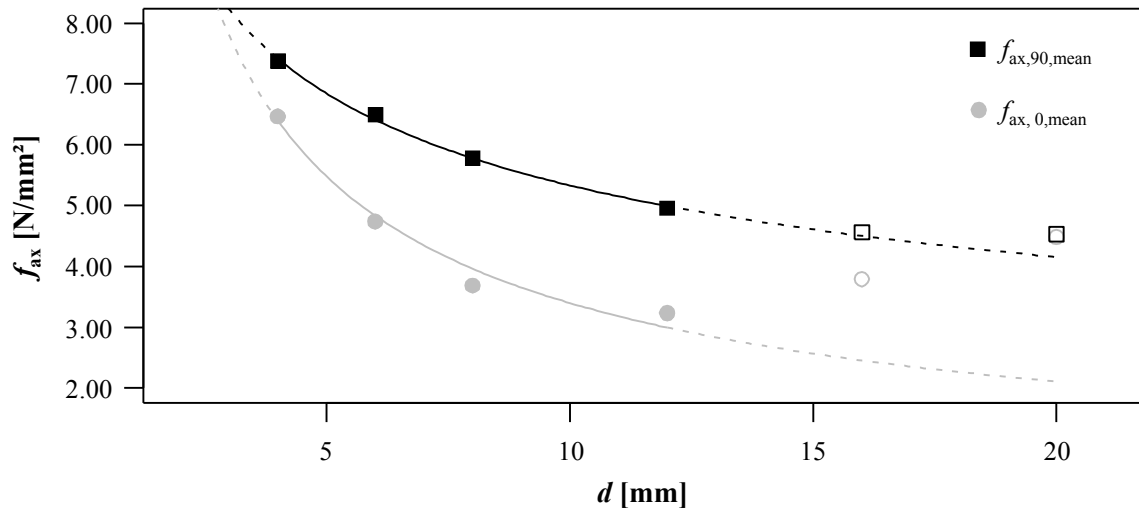


Figure 5.12: Comparison of experimentally determined withdrawal strength with model prediction at varying outer thread diameter d

Finally, it is worth outlining, that in contrast to the influence of d on f_{ax} (which is in fact comprehensively investigated) comparable efforts with regard to both further properties, $K_{ser,ax}$ and especially D , are missing. Nowadays, both approaches, given in eqs. (5.45) and (5.46), exclusively consider the outer thread diameter's impact on withdrawal stiffness, but differ in their treatment to a significant extent. For reasons of a corresponding model evaluation, in order to extend the scope of both functions (e. g. consideration of parallel-to-grain insertion), it is essential to concentrate on this relationship in the frame of future investigations.

5-2.2 Thread surface condition

The vast majority of self-tapping screws is produced with an additional slide coating, which decreases their surface friction coefficient to a significant extent, c. f. section 3-3.5. Furthermore, certain companies produce screw threads with thread surfaces, deviating from the ideal smooth geometry, discussed in section 3-4. This for instance concerns threads with ground serrations of a manufacturer as holder of ETA-12/0114 (2012).

While these measures are aimed and verified, optimising the screw installation process (decreasing the insertion moment or the risk of initial timber splitting failure, increasing the screwing-in velocity, etc.), the related effects on withdrawal properties have not been investigated so far and are thus seen as a topic for further investigations, possibly leading to new market developments in the frame of screw application.

5-3 TIMBER PRODUCT

5-3.1 Clear wood properties

5-3.1.1 Introduction

Summarising the discussion made in section 4-2, according to ON EN 1995-1-1 (2015), nowadays the timber density is regarded as the major parameter for the design of dowel-type fasteners in modern standardisation. The reasons therefore are a pronounced positive relationship between density and mechanical properties strength and stiffness (if the scope is restricted to clear wood dimensions), as well as a comparatively simple way of its determination.

Consequently, the prediction of both withdrawal properties, f_{ax} and $K_{ser,ax}$ (in case of D , no comparable approaches are given), of axially loaded self-tapping screws by means of empirical approaches predominately includes ρ as the material indicator, representing its mechanical constitution, c. f. section 5-1.3. Note: the sole exception is the model for determining $K_{ser,ax}$, given in eq. (5.46), which does not consider a timber related parameter at all. Furthermore, the density impact is majorly considered by a power function with exponent k_p , describing the relationship with withdrawal properties, meaning that in case of $k_p < 1.00$, (Blaß et al. (2006), a disproportionately small, in case of $k_p > 1.00$, Hübner (2013b), a disproportionately high, relationship is given. Furthermore, Pirnbacher et al. (2009), as well as Frese and Blaß (2009) constitute a proportional (linear) relationship, c. f. eqs. (5.38), (5.40) and (5.41). A second approach, provided in Frese and Blaß (2009), not discussed so far, also postulates a disproportionately small relationship between ρ and f_{ax} , see:

$$f_{ax} = \exp\left(2.359 - 0.04172 \cdot d + 2.039 \cdot 10^{-3} \cdot \rho\right) \cdot \frac{1}{\pi}. \quad (5.57)$$

Comparing the withdrawal strengths, according to eq. (5.57) with varying densities $\rho = 300 \div 600 \text{ kg/m}^3$, but constant d results in an exponent k_p of roughly 0.90. Beside the sources discussed in section 5-1.3, one further investigation, reported by Brandner et al. (2017), has to be outlined in this context, who determined k_p as 1.40, which bases on the specific test data they considered in their paper.

Since all approaches, including the density impact as a power function, recommend the exponent k_p as a constant value, they disregard the interrelationships with further relevant parameters, such as the outer thread diameter and the axis-to-grain angle. The only exception is the model, published by Pirnbacher et al. (2009), who provide two functions for predicting f_{ax} in dependence of α in form of eqs. (5.38) and (5.40). Figure 5.13 subsequently illustrates the courses of f_{ax} and the ratio k_{90} at varying timber density for different values of $\alpha = \{0, 90\}^\circ$ and $d = \{8, 10, 12\} \text{ mm}$, as calculated with this model. Due to differentiating the relationship between ρ and f_{ax} in dependence of α (parallel-to-grain insertion is less

influenced by the density) a nonlinear, degressive behaviour of k_{90} with increasing ρ occurs, which deviates from constant k_{90} , as presupposed by the other approaches discussed in section 5-1.3. Comparing k_{90} in dependence of d , the corresponding values are shifted, but equal in their course, indicating no specific treatment related, as concluded to be necessary in section 5-2.1.

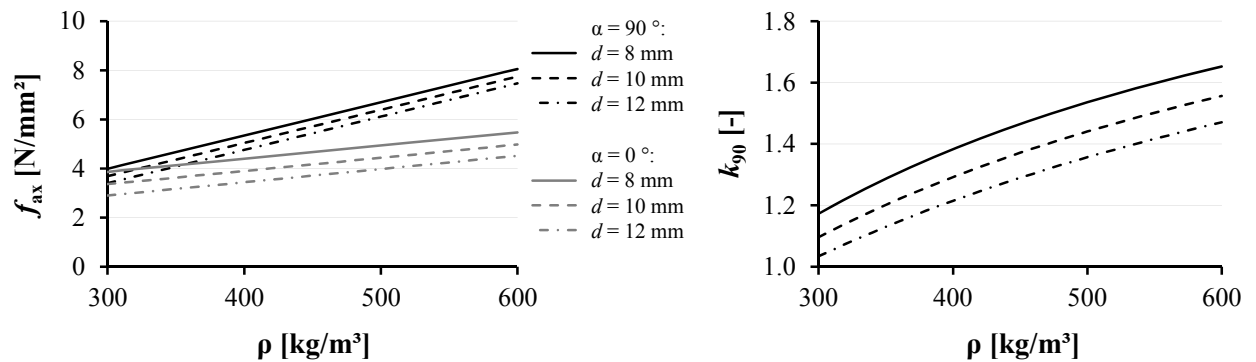


Figure 5.13: Left: withdrawal strength f_{ax} vs. density ρ ; right: ratios k_{90} vs. density ρ ; both in dependence of α and d ; predicted according to Pirnbacher et al. (2009)

With regard to the withdrawal stiffness $K_{ser,ax}$, Blaß et al. (2006) exclusively consider a density influence for empirically modelling this property, c. f. eq. (5.45), and postulate a comparatively minor pronounced relationship in form of $k_p = 0.2$. In contrary, Brandner et al. (2017) report a significantly different value of k_p in form of 1.42, indicating a disproportionately high relationship between both properties. Furthermore, a possible influence of d and α , on this parameter, is not considered in both sources.

Now concentrating on the impact of further clear wood properties in form of the annual ring width a_w , the timber strength and stiffness, as well as the growth characteristics (especially knots, pitch pockets and reaction wood) on self-tapping timber screws' withdrawal properties: first, related investigations, focusing on $K_{ser,ax}$ and D , have not been found at all. The further discussion is thus restricted to withdrawal strength. Second, if compared to timber density, comprehensive works determining the influence of these properties on f_{ax} (or F_{ax}) on a similar level are scarce, which partially necessitates an additional consideration of selected literature concerning other screw products.

Due to a negative relationship, but given correlation between density and annual ring width, as discussed in section 4-2, a corresponding influence of this parameter on withdrawal strength can be expected in form of decreasing f_{ax} with increasing a_w . In the past, certain student works, carried out at the Institute of Timber Engineering and Wood Technology, concentrated – amongst others – on this relationship and are thus worth being outlined. Gaich et al. (2008) conducted altogether 1,839 screw withdrawal tests in solid timber and GLT, varying $\alpha = \{0, 90\}^\circ$, $d = \{8, 10, 12\}$ mm and $l_p = 4d \div 16d$. Restricting the scope to ST and $\alpha = 90^\circ$, positive relationships between ρ and f_{ax} ($R^2 = 0.46 \div 0.84$), as well as negative

relationships between a_w and f_{ax} ($R^2 = 0.04 \div 0.61$) were observed, the latter with decreasing strongness when d increases. Two further studies were carried out by Gatternig (2010) and Plieschounig (2010), who determined the withdrawal strengths of $d = 6$ mm screws (n about 1,300) in solid timber with varying $\alpha = \{0, 45, 90\}^\circ$ and spacings $\{a_1, a_2, a_{1,CG}, a_{2,CG}\}$. Comparing the withdrawal capacities and density in case of $\alpha = 90^\circ$, both observed a pronounced positive relationship between them, while in case of a_w and F_{ax} only a poor negative tendency was found (note: both latter mentioned studies are comprehensively discussed in section 5-4). With regard to the withdrawal strength determined at $\alpha = 0^\circ$, neither Gaich et al. (2008) nor Plieschounig (2010) observed a meaningful relationship with the annual ring width a_w .

Concluding so far, the mentioned authors were able to observe a correlation between withdrawal strength and annual ring width, but determined a significantly deviating, as well as a steadily lower strongness of this relationship, as it was found for the density. A further aspect, indirectly dependent from a_w , is mentioned in Hübner (2013a): since the length of the earlywood zone, l_e is positively correlated to a_w , c. f. section 4-2, in case of parallel-to-grain insertion he assumes an increasing probability of screws with small d , fully inserted in the annual ring's earlywood zone, and thus smaller values for f_{ax} combined with a higher variability. Even though own investigations in form of ratios k_{CV} of $d = \{4, 6\}$ mm for $\alpha = 0^\circ$, as given in Table 5.4, do not indicate the latter assumed tendency, this matter is worth focusing on in the frame of future investigations.

As discussed in section 5-1.1, the screw withdrawal failure modes can be explained by exceeding local resistances of the timber member, defined as an orthotropic material with the R - T - L -coordinate system. Thus, concentrating on the relationship between withdrawal and timber strength and stiffness properties, is self-evident. Following the literature review on screw research given in Hübner (2013a), the investigations carried out by Eckelman (1975), with sheet metal screws ($d = 4.8$ mm) in varying Northern American timber species, are worth mentioned in this context, since he addresses the shear strength in longitudinal direction a higher correlation with F_{ax} , than it was found for the density. With regard to the relationship with timber stiffness, Divós et al. (1998) determined the withdrawal capacities of "special screws" ($d = 5.0$ mm, no exact definition given) in spruce softwood and compared them with shear moduli (assumption: combination of G_{LR} and G_{LT}), which were gained from the same material. Referring to this study, they report a high positive correlation between both properties in form of a coefficient of determination $R^2 = 0.68$. A proper explanation for this circumstance is seen in the high correlation between shear strength and modulus, as e. g. determined by Müller et al. (2004) for the LT - and LR -plane to $R^2 = 0.69$, while between density and shear strength or modulus comparatively smaller values ($R^2 = \{0.48, 0.58\}$) are given. Beside shear, investigations focusing on the relationship with other timber mechanical strength or stiffness properties, as given in eq. (4.15), were not found.

Even though the test specimen preparation aims to exclude local wood defects as far as possible, c. f. section 4-2, they are frequently observed in the frame of post-processing. This especially concerns knots, reaction wood, as well as pitch pockets possibly influencing the screw's axial loadbearing behaviour. Two master's thesis, authored by Plieschounig (2010) and Grabner (2013), are worth to be mentioned, since they include a comprehensive compilation of withdrawal strengths, determined in timber specimen with and without these local defects. Note: the database, given in Grabner (2013), comprises $n \approx 1,300$ tests with $d = \{8, 12\}$ mm screws, situated in the narrow faces of CLT elements, a detailed information is given in sections 5-3.4 and 5-4.3.

Comparing the withdrawal strengths with the densities by means of scatterplots, both report significantly higher values, as well as a deviating distribution of f_{ax} in cases, screws penetrated or even touched knots. This can be explained by a density difference of knots and clear wood in form of ρ_{knot} up to $2 \cdot \rho_{clearwood}$, c. f. Kaserer (2011). Although a quantitative consideration, regarding the knot diameter d_{knot} and the exact position with regard to the screw axis, is missing, Grabner (2013) found a lower limit of $d_{knot} \approx 5$ mm if exceeding there is a corresponding influence. Unlike the situation for pitch pockets and compression wood: neither Plieschounig (2010) nor Grabner (2013) observed a comparable influence on withdrawal strength and consequently considered the related data for statistical assessment, too.

5-3.1.2 Experimental programme

In order to verify the statements, discussed in section 5-3.1.1, an experimental campaign focusing on the relationship between screw withdrawal and clear wood properties was carried out. Especially with respect to the orthotropic R - T - L -coordinate system as the material law, basically assumed for timber in section 4-3. Beside the screw withdrawal tests (f_{ax} , $K_{ser,ax}$, D) in radial, tangential (both $\alpha = 90^\circ$) and longitudinal direction ($\alpha = 0^\circ$), a corresponding programme comprised further experiments for determining the selected mechanical timber properties in form of compressive strength $\{f_{c,L}, f_{c,R}, f_{c,T}\}$ and stiffness $\{E_L, E_R, E_T\}$, as well as shear stiffness $\{G_{LR}, G_{RL}, G_{LT}, G_{TL}, G_{RT}, G_{TR}\}$. Thus, all in all 21 properties were determined by means of five different test configurations.

Altogether 99 solid timber boards in Norway spruce, with average dimensions $w \times h \times l = 180 \times 47 \times 4000$ mm³, were therefore applied. In order to achieve a clear specimen annual ring and a fibre orientation in the R - T - L -direction, the related selection followed two main characteristics: (1) an annual ring orientation almost parallel to the board width and (2) a more or less constant annual ring width over the entire board's height. Furthermore, the boards were classified into three subgroups, according to their assumed average annual ring widths $a_w = \{2, 4, 6\}$ mm. The specimen preparation and the test execution related to the aforementioned properties is separately discussed as follows:

- screw withdrawal tests

Not to go beyond the scope of the test campaign, it was decided to carry out the screw withdrawal tests with one partially threaded screw ($d = 8$ mm, as representative outer thread diameter) with geometrical thread properties, as given in Table 5.6. Taking the aforementioned board dimensions and the main idea behind this programme to arrange an annual ring orientation with respect to the screw axis as exact as possible into account, a comparatively small value of $l_{ef} = 5 \cdot d$ (equal to the board height after formatting) was chosen. Furthermore, neither embedment, pre-drilling nor arranging the screw tip in the timber member was applied; l_p is thus equal to l_{ef} . Except the latter mentioned measure, the specimen preparation followed the dimensional requirements given in ON EN 1382 (1999); a corresponding illustration can be found in Annex B-3.1, Figure B.17.

Table 5.6: *Thread characteristics and test conditions applied for the experimental campaign focusing on the impact of clear wood properties*

thread characteristics					test conditions			
d_{nom}	d	η	p	v^*	l_p	l_{ef}	l_{emb}	d_{PD}
[mm]	[mm]	[-]	[mm]	[°]	[mm]	[mm]	[mm]	[mm]
8	8.06	0.67	5.57	40	40	40	0	0

Worth mentioning, that all tests have been performed on the test rig LIGNUM-UNI-275 with a local way measurement set-up, according to Figure 5.4, enabling the determination of $K_{ser,ax}$ and D . The further background information related to test execution, post-processing, property determination and data assessment is summarised in section 5-1.2.

- clear wood compression tests

The clear wood tests for determining the timber compression properties in form of strength and stiffness were carried out in accordance to ON EN 408 (2010), except certain requirements regarding prismatic specimen dimensions, which were modified following the idea of an almost ideally oriented annual ring pattern, especially with regard to both, radial and tangential, directions, c. f. Table 5.7.

Table 5.7: *Specimen dimensions applied for clear wood compression tests*

direction	h	l	w
[-]	[mm]	[mm]	[mm]
radial	40	40	40
tangential	40	40	40
longitudinal	160	40	40

Figure 5.14 subsequently illustrates the setup related to longitudinal (Figure 5.14, left) and radial as well as tangential (both Figure 5.14, right) compression tests. In the former mentioned case, two compact strain transducers were centrally situated at the specimen's side face, recording local displacements along a gauge length of 50 mm. In case of R - or T -direction, comparatively small specimen heights required a different measurement set-up in form of all in all four LVDTs installed at the corners of the upper steel plate, as applied for load introduction. The gauge length can thus be set equal to h . As shown in Figure 5.14, two teflon stripes were situated at the specimen's top and bottom for enabling horizontal timber elongation at load introduction and supporting. The former one was furthermore applied by monotonic vertical movement (longitudinal: 0.6 mm/min, radial: 0.2 mm/min, tangential: 0.4 mm/min); a related static system can be simplified as a statically underdetermined one-dimensional compressive column, c. f. Figure 5.14 (middle). Following the requirements, given in ON EN 408 (2010), a spherical hinge between upper steel plate and testing device to avoid an additional introduction of a bending moment was arranged. Note: after the application of a pre-force (longitudinal: ~ 550 N, radial and tangential: ~ 400 N), the hinge rotatability was restricted.

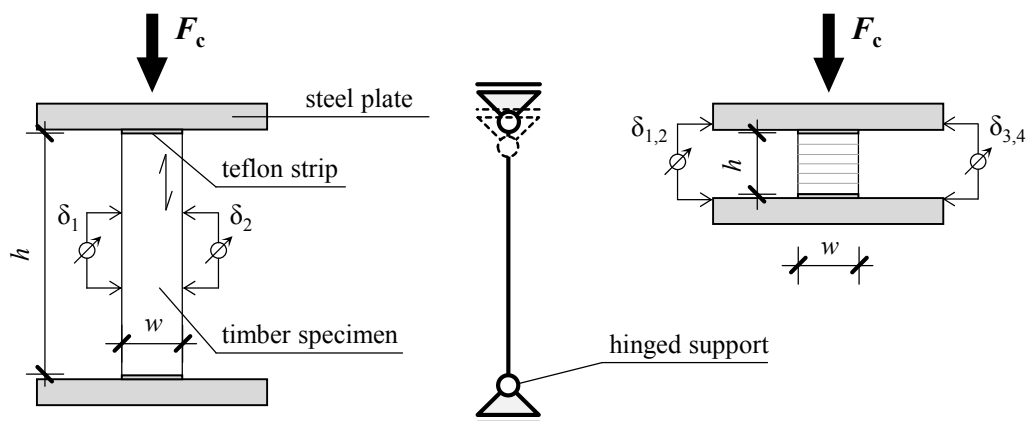


Figure 5.14: *Clear wood compression tests according to ON EN 408 (2010); left and right: schematic illustration of the test set-ups with load application in longitudinal and radial direction; middle: corresponding static system*

The mechanical property determination was equal to that of the withdrawal capacity and stiffness, as discussed in section 5-1.2 and thus deviates (in case of the moduli of elasticity) from recommendations given in ON EN 408 (2010). The sole exception is the procedure for determining $F_{c,90}$ (which means $F_{c,R}$ and $F_{c,T}$) as it was partially adopted from this standard (note: the force-displacement relationship's linear domain was here also defined by the method explained in section 5-1.2). The final data assessment was carried out according to section 5-1.2.

- clear wood shear tests

In contrast to both aforementioned campaigns, conducted at Graz University of Technology, the determination of shear moduli $\{G_{LR}, G_{RL}, G_{LT}, G_{TL}, G_{RT}, G_{TR}\}$ was part of a research programme executed at (and in cooperation with) the Institute of Wood Science and Technology at BOKU – University of Natural Resources and Applied Life Sciences. The corresponding experimental procedure and the post-processing were much more complex, compared to withdrawal and compression tests. Thus, the related discussion would exceed the scope of this section. A detailed information can be found in Müller et al. (2015).

Finally, it is worth mentioning that annual ring widths a_w of all specimen considered were determined with the software application GrowthRingLogger (2014) demanding scanned specimen surfaces as input data.

5-3.1.3 Results and discussion

Figure 5.15 subsequently overviews the distributions, confidence intervals and error bars of timber densities' $\{\rho_{12}, \rho_u\}$ statistical parameters in dependence of the test campaigns related to the specific property groups withdrawal, compression and shear. The supplemental information, regarding statistical parameters of timber density, moisture content u and annual ring width a_w , as well as the number of datasets per test series remaining for statistical assessment (after outlier treatment), n is given in Annex B-3.2, Table B.14 and Table B.15. Note: in case of shear tests, moisture content and annual ring width were not determined, since specimen are still intact and stored for future investigations.

Similar to the results discussed in section 5-2.1, average moisture contents exceed the equilibrium moisture content of 12 % to a small amount. Again they do not differ remarkably between the test series. Thus, a related (and unwanted) impact on the analysis of determined properties can be excluded. With regard to timber densities ρ_{12} and ρ_u , the graphics, illustrated in Figure 5.15, indicate no significant deviations between mean values, medians and variabilities of withdrawal, compression and shear test series. Values ρ_u dedicated to the latter campaign are slightly higher, since no moisture content correction was conducted in this case.

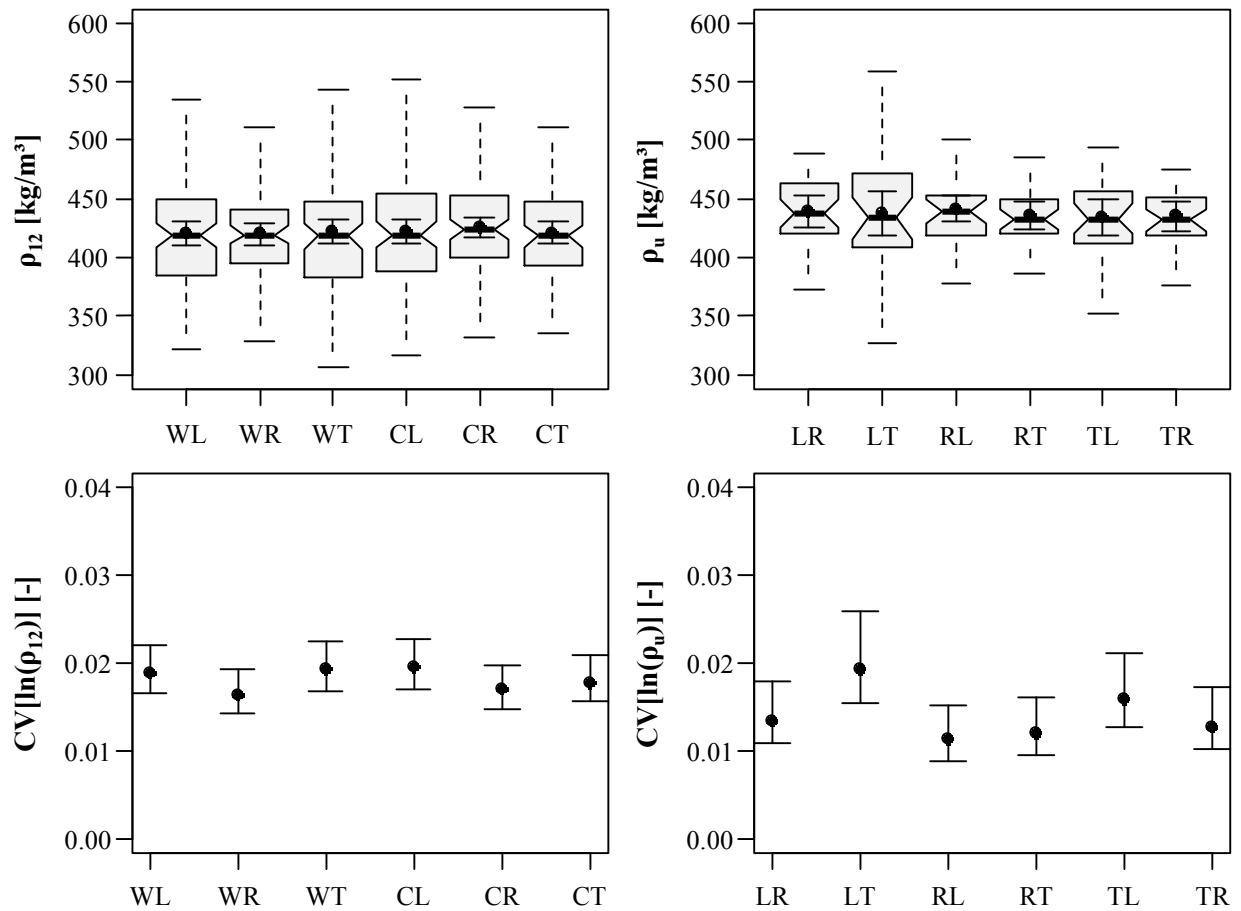


Figure 5.15: Above: Boxplot graphic of densities ρ_{12} (left) and ρ_u (right); below: CIs of $CV[\ln(\rho_{12})]$ (left) and $CV[\ln(\rho_u)]$ (right) in dependence of determined properties

Now concentrating on the assessment of withdrawal properties, Table 5.8, Figure 5.16 and Figure B.18 in Annex B-3 overview the related results in form of main statistical parameters for f_{ax} , $K_{ser,ax}$ and D in dependence of the screw axis orientation with respect to the R - T - L -coordinate system. Note: smaller numbers of datasets in case of $K_{ser,ax}$ and D if compared to f_{ax} are caused by inoperative local displacement measurements or by finishing the experiment before F_u , as defined in section 3-4.4, has been reached.

Similar to the literature findings, and those made in section 5-2.1.3, the average withdrawal strengths of screws with axis-to-grain angle of 90 ° (WR and WT) are significantly higher, than the value gained for parallel-to-grain insertion (WL). Comparing f_{ax} gained for both, tangential and radial, insertion, slightly but insignificantly higher values for the latter case are given. With regard to withdrawal stiffness, the same, but inverse and additionally minor pronounced, relationship between $K_{ser,ax}$ and α can be observed, while a behaviour equal to f_{ax} between radial and tangential insertion is given. In case of ductility D , two facts are worth being discussed more in detail: first, the average values result in a surprisingly high magnitude (irrespective the screw axis orientation), which is mainly caused by small yield deformations $\{v_{y,WL}, v_{y,WR}, v_{y,WT}\} = \{0.39, 0.63, 0.65\}$ mm due to the high withdrawal stiffness if compared to

$\{v_{u,WL}, v_{u,WR}, v_{u,WT}\} = \{2.32, 4.66, 4.14\}$ mm. Even though the given range allows a classification as a high ductility, according to SIA 265 (2012) or ON EN 1998-1 (2013) (note: the latter document presupposes D determined by cyclic tests), the absolute deformations are very small – with respect to other fastener types, c. f. Figure 2.1. Consequently, recognising a collapse scenario by a remarkable change of the optical appearance of the connection (or structural system), in form of high deformations, is barely possible, the determined values of the ductility are rather valuable for relative comparisons than for the fastener classification. Second, in contrast to both properties f_{ax} and $K_{ser,ax}$, Figure 5.16 (right) indicates no remarkable difference between D_{WL} and D_{WT} , while the average value determined for radial screw insertion is found to be significantly higher. A similar behaviour can be observed for variabilities, especially in form of $\ln(CV[X])$, as illustrated in Annex B-3.1, Figure B.18, which increase in the following order: radial – tangential – longitudinal. A possible explanation for this effect is the number of annual rings penetrated by the screw ($n_{aw,R} \gg \{n_{aw,T}, n_{aw,L}\}$), which may lead to a certain homogenisation effect in the nonlinear domain of the force-deformation relationship.

Table 5.8: Statistical parameters of withdrawal strength, stiffness and ductility of the experimental campaign focusing on the impact of clear wood properties

test	n	mean[f_{ax}]	CV[f_{ax}]	n	mean[$K_{ser,ax}$]	CV[$K_{ser,ax}$]	n	mean[D]	CV[D]
[-]	[-]	[N/mm ²]	[%]	[-]	[N/mm]	[%]	[-]	[-]	[%]
WL	92	3.68	14.2	91	8,845	21.2	78	6.03	23.5
WR	89	5.24	11.2	88	7,755	13.1	87	7.41	13.2
WT	94	5.09	14.8	94	7,458	19.7	83	6.50	15.3

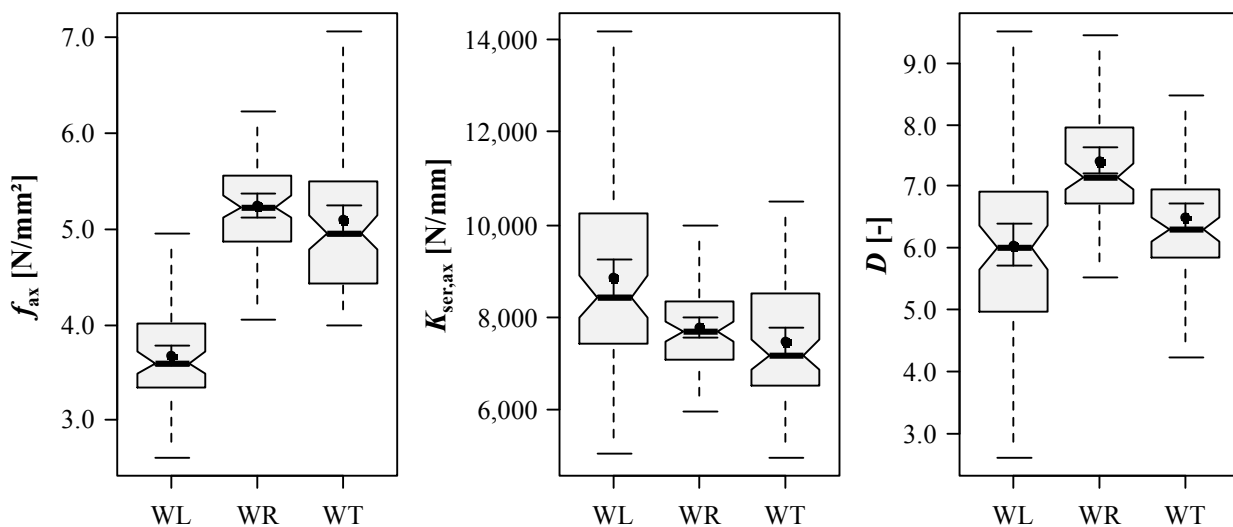


Figure 5.16: Boxplot diagrams of withdrawal strength (left), stiffness (middle) and ductility (right) vs. screw axis orientation

Now evaluating the relationship between logarithmised withdrawal strengths of screws inserted in longitudinal, radial and tangential direction. A matrix, including the related Pearson's correlation coefficients above and the Spearman's correlation coefficients below its main diagonal, is subsequently given in Table 5.9. Taking the determined values for $r_{XY,PE}$ and $r_{XY,SP}$, as well as the significance levels for $r_{XY,PE}$ into account, a pronounced dependency between the three properties can be observed. The highest values are found between both $\ln(f_{ax})$ in case of $\alpha = 90^\circ$, which indicates a similar distribution of the determined values in addition to the equal magnitudes of statistical parameters, shown in Figure 5.16.

Table 5.9: Correlation coefficients between logarithmic withdrawal strengths according to Pearson (black) and Spearman (grey)

	$\ln(f_{ax,WL})$	$\ln(f_{ax,WR})$	$\ln(f_{ax,WT})$
$\ln(f_{ax,WL})$	1.00	0.59 (***)	0.61 (***)
$\ln(f_{ax,WR})$	0.58	1.00	0.69 (***)
$\ln(f_{ax,WT})$	0.59	0.72	1.00

(***) $p < 0.001$ (high significant); (**) $p < 0.010$ (medium significant); (*) $p < 0.050$ (significant); (.) $p < 0.100$ (moderate significant)

Concentrating on the relationship between withdrawal and further clear wood properties, as determined in the frame of this test campaign. In order to avoid exceeding the scope of this section, the outcomes related to the compression and the shear tests (given in Annex B-3.2, Table B.16 and Table B.17), independently from the withdrawal properties, are not discussed in detail. They qualitatively confirm the relative differences between the clear wood properties, exemplarily shown in Table 4.1, but steadily result to a lower magnitude.

Subsequently, Table 5.10 to Table 5.12, as well as Figure 5.17 to Figure 5.27 (lines represent the models given in the tables) overview the dependencies of the withdrawal on the selected clear wood properties in form of the power parameters k_i , determined by means of a linear regression analysis of the logarithmised data, according to eq. (5.54). A related selection based on a correlation analysis of the properties dedicated to the same mechanical orientation. The corresponding matrices, whereof only those relationships with a pronounced correlation and high significance (***) were selected for further discussion, are shown in Annex B-3.2, Table B.18 to Table B.20, separately in dependence of the R - T - L -coordinate system.

Irrespective from the specific timber direction investigated, a pronounced correlation between withdrawal strength and stiffness, steadily above $r_{XY,PE} > 0.75$, can be observed, while the distributions of the ductility are independent from the aforementioned properties.

With regard to the timber's longitudinal direction and focusing on the withdrawal strength $f_{ax,WL}$ ($\alpha = 0^\circ$), beside $K_{ser,ax,WL}$ two parameters, namely ρ_{12} and G_{LR} , influencing this property to a significant extent were found. Each influence is in form of a disproportionately low ($k_i < 1.0$) relationship. Surprisingly, k_i , $r_{XY,PE}$ and s_e (the latter defined as the residual standard error, determined by the software package R), given in Table 5.10 as well as in the comparison shown in Figure 5.17 and Figure 5.18, attest the shear modulus G_{LR} a more pronounced impact on $f_{ax,WL}$, as it can be observed for the density ρ_{12} (note: k_p and $r_{XY,PE}$ are quite similar to the values given in Table 5.5 for $d = 8$ mm and $\alpha = 0^\circ$). This, in fact, corresponds to the analogies between shear and withdrawal properties, discussed in the introduction of this section.

In case of $K_{ser,ax,WL}$, apart from the withdrawal strength, density ρ_{12} was found exclusively influencing this property in a significant manner. Although, both values of k_p and $r_{XY,PE}$ are higher or at least equal to the relationship between density and withdrawal strength, the residual standard errors and the illustration given in Figure 5.18 (right) indicate a minor pronounced predictability of this property. A possible reason therefore is the lower accuracy in measuring and examining $K_{ser,ax}$ if compared to f_{ax} , which is derived from a force as an exactly defined upper limit of the load-displacement curve. Worth mentioning, that the correlations between withdrawal and clear wood stiffness properties, given in Table B.18, are steadily low and not significant. A corresponding analogy can thus not be confirmed.

In case of ductility D , no highly significant dependency on any other property was found at all.

Table 5.10: *Regression analyses of selected withdrawal vs. clear wood properties for longitudinal screw axis orientation*

$\ln(f_{ax,WL}) \sim$	k_i	δ	$r_{XY,PE}$	s_e
$\ln(\rho_{12})$	0.540 (***)	-1.97	0.44	0.127
$\ln(K_{ser,ax,WL})$	0.521 (***)	-3.43	0.77	0.010
$\ln(G_{LR})$	0.618 (***)	-2.59	0.61	0.121
$\ln(K_{ser,ax,WL}) \sim$	k_i	δ	$r_{XY,PE}$	s_e
$\ln(\rho_{12})$	0.775 (***)	4.39	0.43	0.189
$\ln(f_{ax,WL})$	1.141 (***)	7.59	0.77	0.133

(***) $p < 0.001$ (high significant); (**) $p < 0.010$ (medium significant); (*) $p < 0.050$ (significant); (.) $p < 0.100$ (moderate significant)

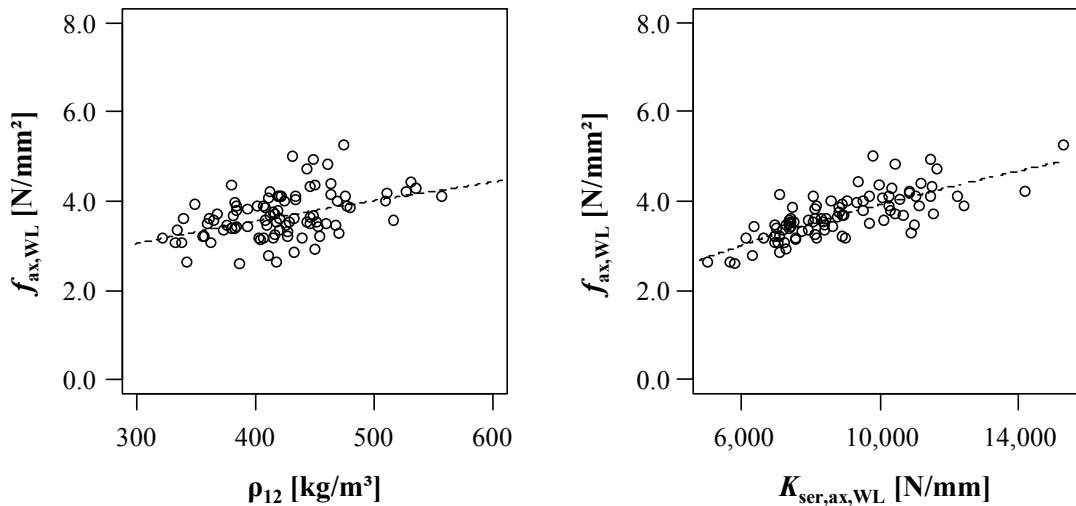


Figure 5.17: Comparison of selected withdrawal and clear wood properties for longitudinal screw axis orientation

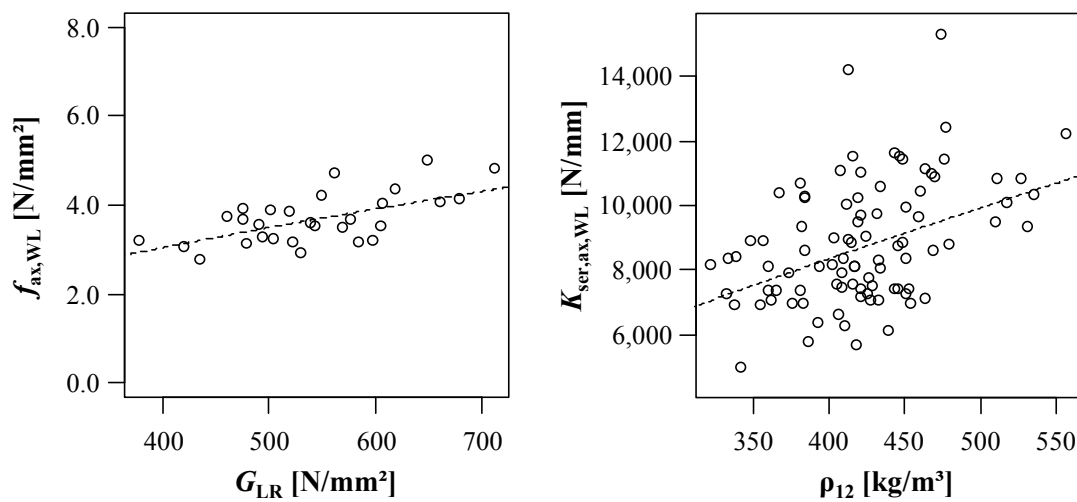


Figure 5.18: Comparison of selected withdrawal and clear wood properties for longitudinal screw axis orientation (continued)

If compared to the previously discussed longitudinal timber direction, the withdrawal properties gained for the radial screw axis orientation, shown in Table 5.11 and Figure 5.19 to Figure 5.22, were found to be more dependent on the examined clear wood properties. With regard to the withdrawal strength, beside the generally given relationship with stiffness (here: $K_{ser,ax,WR}$), a pronounced dependency on timber density ρ_{12} , compressive strength $f_{c,R}$ and again on G_{RT} , as one of both shear moduli related, can be observed. The corresponding exponent k_p results in a range, comparable to its treatment in the empirical approaches for spruce softwood, discussed in section 5-1.3, is thus lower than the value outlined in Table 5.5 for $d = 8$ mm and $\alpha = 90^\circ$.

In case of withdrawal stiffness, a similar and thus strong relationship with ρ_{12} , as it was found between $f_{ax,WR}$ and ρ_{12} , is given. Furthermore, in contrast to the longitudinal screw axis orientation, the relationships between $K_{ser,ax,WR}$ and clear wood properties, in form of a highly significant dependency on the modulus of elasticity, $E_{c,R}$, as well as a moderately significant dependency on the shear modulus G_{RT} can be observed, c. f. Table 5.11 and Table B.19. With regard to G_{RL} , neither a relationship with $f_{ax,WR}$ nor with $K_{ser,ax,WR}$ can be confirmed.

Concentrating on the ductility D , a steadily low, but highly significant, correlation with timber density and annual ring width is given. The corresponding exponents k_i indicate an increasing D with an increasing ρ_{12} and decreasing a_w . Taking both comparisons, illustrated in Figure 5.22, as well as the size of residual standard errors s_e into account, the related predictability is restricted to a certain extent.

Table 5.11: *Regression analyses of selected withdrawal vs. clear wood properties for radial screw axis orientation*

$\ln(f_{ax,WR}) \sim$	k_i	δ	$r_{XY,PE}$	s_e
$\ln(\rho_{12})$	0.821 (***)	-3.30	0.73	0.077
$\ln(K_{ser,ax,WR})$	0.659 (***)	-4.24	0.76	0.074
$\ln(f_{c,R})$	0.355 (***)	1.20	0.42	0.010
$\ln(G_{RT})$	0.224 (***)	0.95	0.65	0.063
$\ln(K_{ser,ax,WR}) \sim$	k_i	δ	$r_{XY,PE}$	s_e
$\ln(\rho_{12})$	0.834 (***)	3.91	0.65	0.099
$\ln(f_{ax,WR})$	0.866 (***)	7.52	0.76	0.085
$\ln(E_{c,R})$	0.271 (***)	7.23	0.39	0.117
$\ln(D_{WR}) \sim$	k_i	δ	$r_{XY,PE}$	s_e
$\ln(\rho_{12})$	0.455 (***)	-0.75	0.36	0.120
$\ln(a_w)$	-0.131 (***)	2.16	-0.44	0.115

(***) $p < 0.001$ (high significant); (**) $p < 0.010$ (medium significant); (*) $p < 0.050$ (significant); (.) $p < 0.100$ (moderate significant)

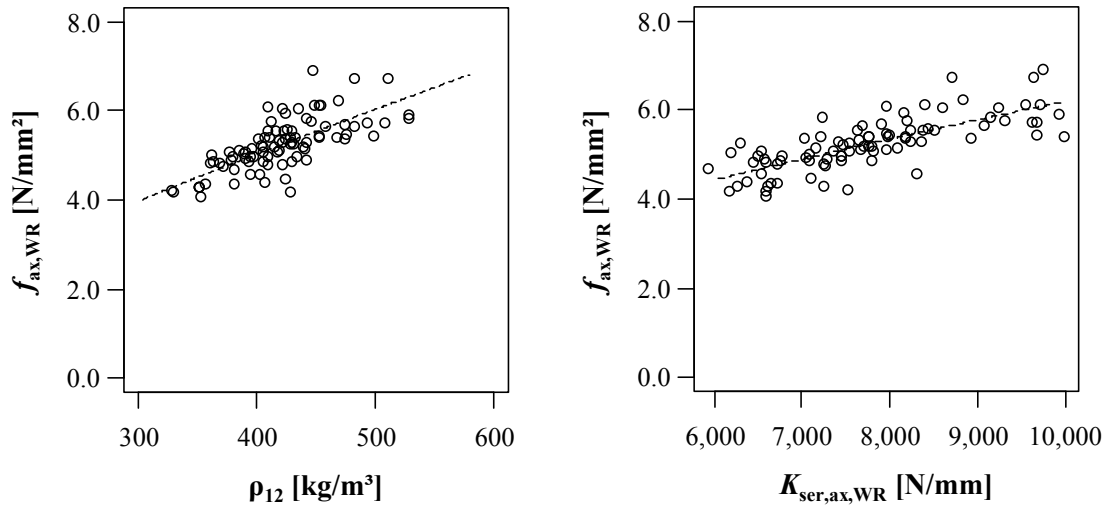


Figure 5.19: Comparison of selected withdrawal and clear wood properties for radial screw axis orientation

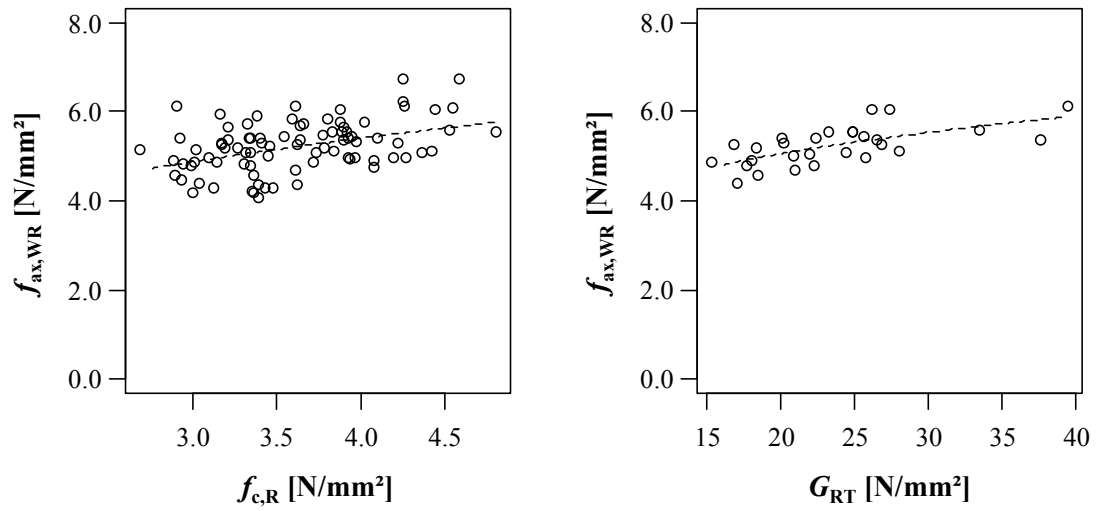


Figure 5.20: Comparison of selected withdrawal and clear wood properties for radial screw axis orientation (continued)

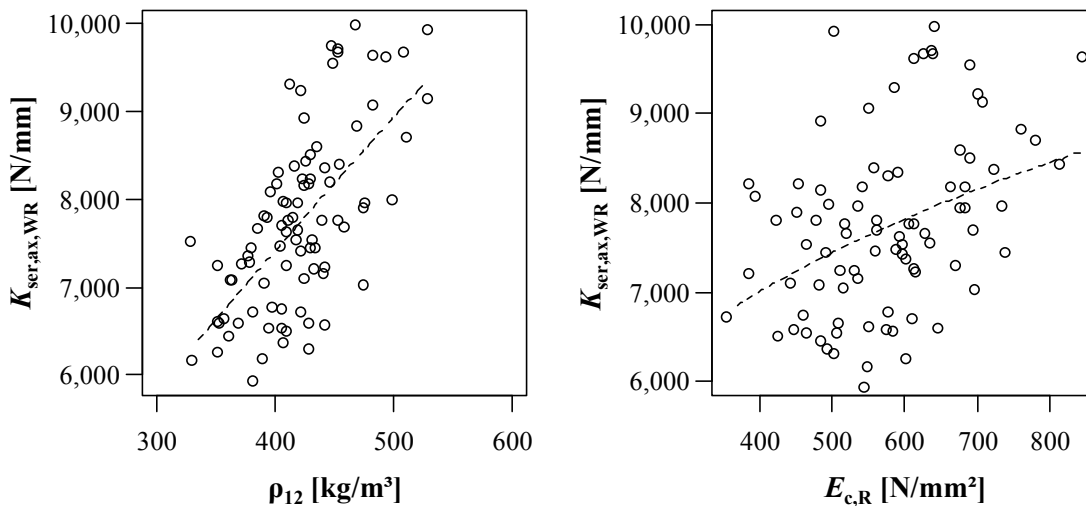


Figure 5.21: Comparison of selected withdrawal and clear wood properties for radial screw axis orientation (continued)

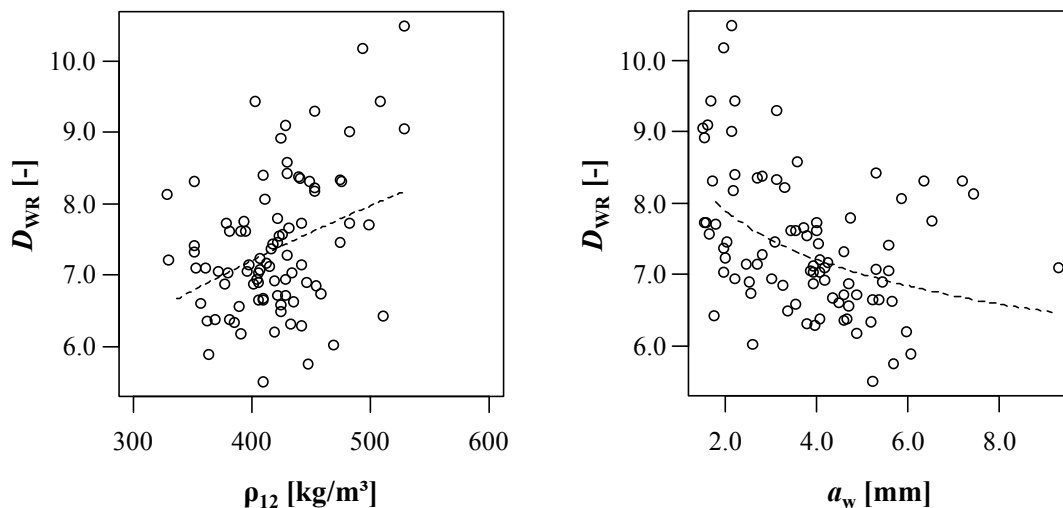


Figure 5.22: Comparison of selected withdrawal and clear wood properties for radial screw axis orientation (continued)

The corresponding relationships between withdrawal and clear wood properties, in case of the tangential screw axis orientation are subsequently illustrated in Table 5.12 and Figure 5.23 to Figure 5.27. Similar to the radial and longitudinal timber direction a clear relationship between $f_{ax,WT}$ and density ρ_{12} can be observed. In addition – in fact not only expected for this screw arrangement – $f_{ax,WT}$ also significantly depends on the size of the annual ring width a_w in form of decreasing $f_{ax,WT}$ with increasing a_w . Comparing the statistical parameters k_i , $r_{XY,PE}$ and s_e , the corresponding dependency is minor pronounced than that of $f_{ax,WT}$ on ρ_{12} . Concentrating on the mechanical clear wood properties and equal to the radial screw axis orientation, $f_{ax,WT}$ is furthermore positively correlated to the timber compressive strength $f_{c,T}$ (and also to $E_{c,T}$), while a dependency on any related shear modulus can not be found.

In case of the withdrawal stiffness $K_{\text{ser,ax,WT}}$, the same relationships with clear wood properties, as they are observed for the withdrawal strength, are given. While higher values of k_i in Table 5.12 indicate an even more pronounced dependency of this property, the related residual standard errors s_e , as well as the comparisons illustrated in Figure 5.26 and Figure 5.27, once again underline the challenging predictability of this property. Similar to longitudinal screw axis orientation, no significant relationship between ductility D and any examined clear wood property could be observed.

Table 5.12: Regression analyses of selected withdrawal vs. clear wood properties for tangential screw axis orientation

$\ln(f_{\text{ax,WT}}) \sim$	k_i	δ	$r_{\text{XY,PE}}$	s_e
$\ln(\rho_{12})$	1.006 (***)	-4.46	0.82	0.082
$\ln(a_w)$	-0.167 (***)	1.82	-0.53	0.122
$\ln(K_{\text{ser,ax,WT}})$	0.582 (***)	-3.56	0.78	0.091
$\ln(f_{c,T})$	0.568 (***)	0.77	0.72	0.098
$\ln(E_{c,T})$	0.362 (***)	-0.44	0.52	0.122
$\ln(K_{\text{ser,ax,WT}}) \sim$	k_i	δ	$r_{\text{XY,PE}}$	s_e
$\ln(\rho_{12})$	1.139 (***)	2.02	0.70	0.138
$\ln(a_w)$	-0.218 (***)	9.16	-0.51	0.165
$\ln(f_{\text{ax,WT}})$	1.037 (***)	7.22	0.78	0.121
$\ln(f_{c,T})$	0.614 (***)	7.99	0.59	0.152
$\ln(E_{c,T})$	0.499 (***)	6.07	0.54	0.159

(***) $p < 0.001$ (high significant); (**) $p < 0.010$ (medium significant); (*) $p < 0.050$ (significant); (.) $p < 0.100$ (moderate significant)

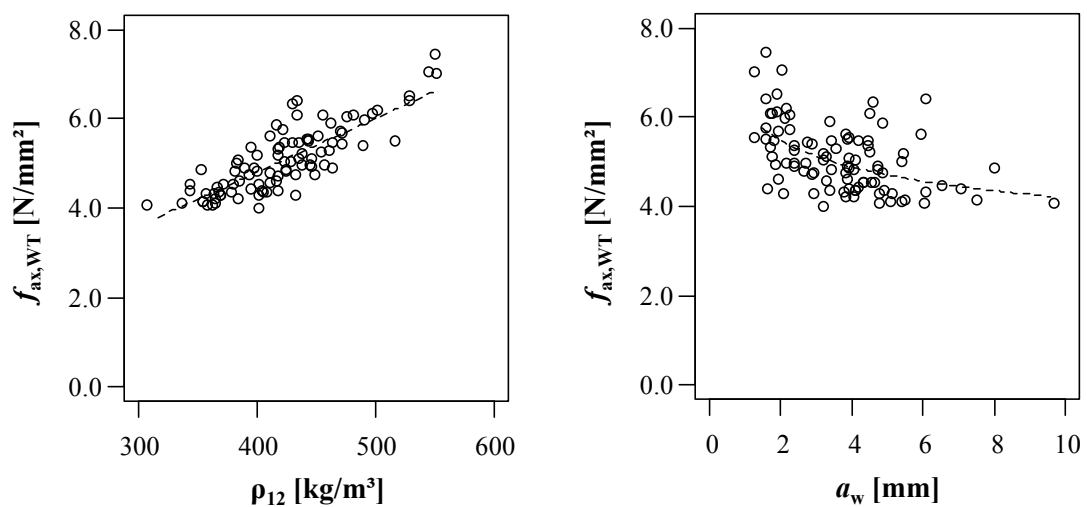


Figure 5.23: Comparison of selected withdrawal and clear wood properties for tangential screw axis orientation

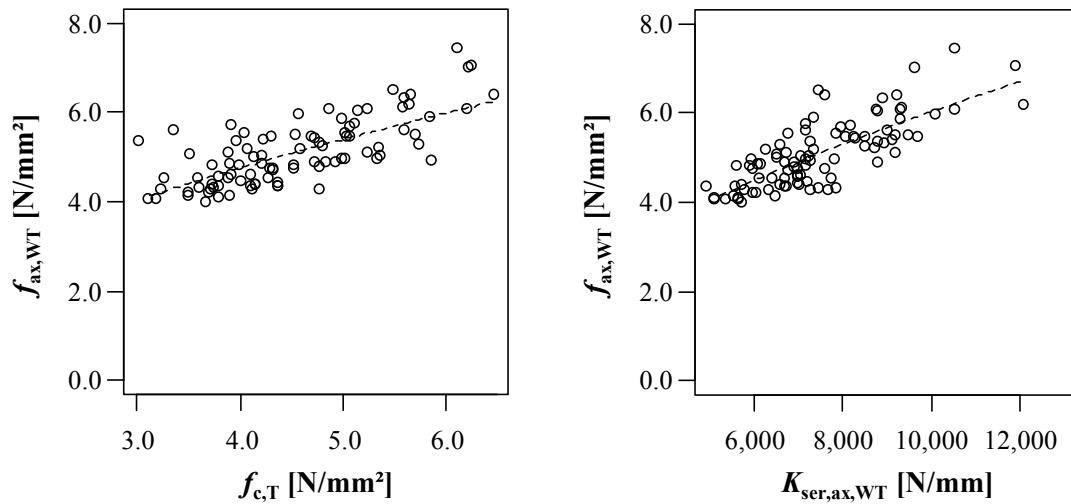


Figure 5.24: Comparison of selected withdrawal and clear wood properties for tangential screw axis orientation (continued)

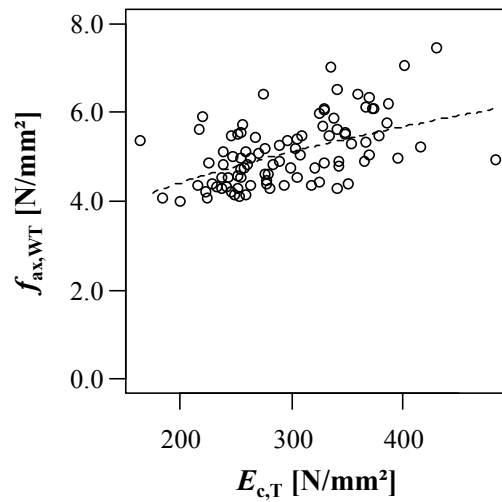


Figure 5.25: Comparison of selected withdrawal and clear wood properties for tangential screw axis orientation (continued)

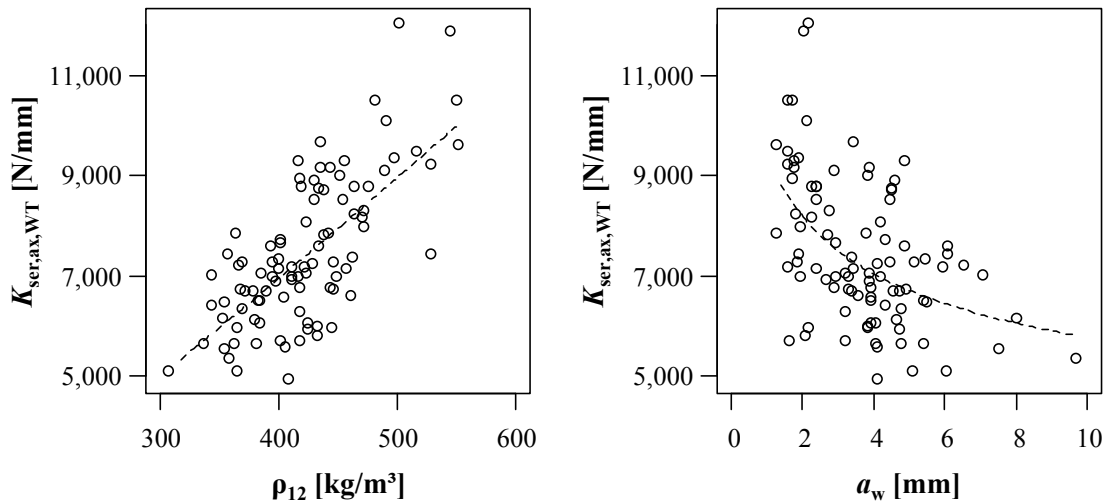


Figure 5.26: Comparison of selected withdrawal and clear wood properties for tangential screw axis orientation (continued)

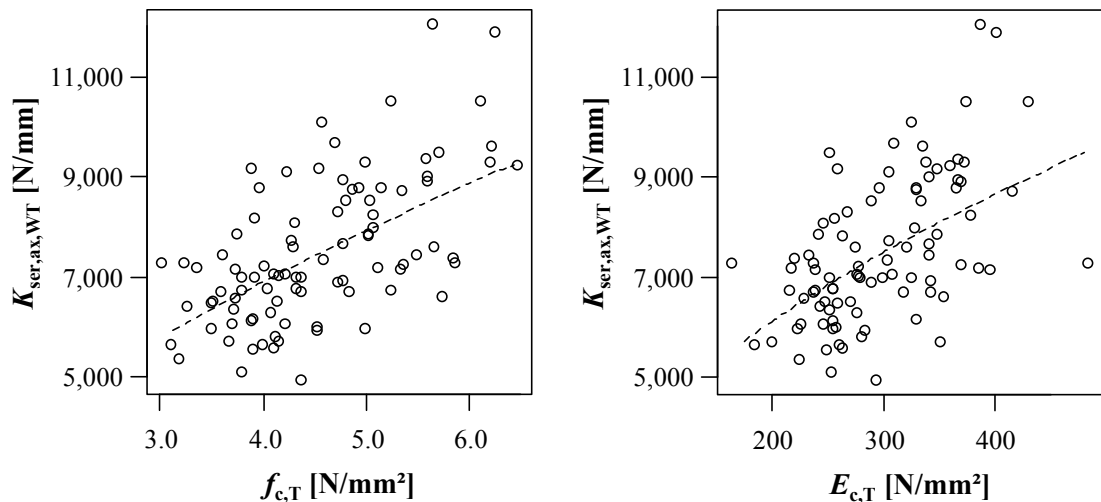


Figure 5.27: Comparison of selected withdrawal and clear wood properties for tangential screw axis orientation (continued)

Summarising the discussion, the timber density ρ_{12} can be concluded as exclusive parameter, steadily influencing withdrawal strength and stiffness. Furthermore, this is independent from the specific timber orientation considered. Therefore the density for empirical modelling of withdrawal strength and stiffness shall be considered in this thesis. With regard to the relationship between the annual ring width and the withdrawal properties, the literature findings in form of a minor pronounced influence for perpendicular-to-grain insertion (if compared to density) and no one for the parallel-to-grain insertion can be confirmed. Furthermore, the analogy between shear and withdrawal properties, given in literature, could partially be observed. Especially in case of a longitudinal screw axis orientation ($\alpha = 0^\circ$), where an even more pronounced relationship of withdrawal strength with G_{LR} than with ρ_{12} was found. It is surprising, that no highly significant dependency between $K_{ser,ax}$ and any shear property could be observed. With regard to

the perpendicular-to-grain insertion, f_{ax} and $K_{ser,ax}$ are additionally influenced by the clear wood compressive properties f_c and E_c , which especially concern the tangential screw axis orientation. For the parallel-to-grain insertion (longitudinal) no such dependency is given. Even though the relationships of both, withdrawal strength and stiffness, with clear wood properties were only partially found, they steadily correspond with the basic mechanical assumptions and are thus regarded as meaningful. In case of ductility D , no parameter was observed influencing this property in the same way for all considered timber orientations. Significant correlations with density and annual ring width for radial screw axis orientation were found. Nevertheless, the circumstance, that both signs of $r_{XY,PE}$ change with a changing timber direction, c. f. Table B.18 and Table B.20, disables an appropriate consideration for empirical modelling.

Subsequently concentrating on the interrelationship of withdrawal strength and stiffness with timber density ρ_{12} and axis-to-grain angle α , Pirnbacher et al. (2009) exclusively recommend a different treatment of the density impact in dependence of the position the screw is inserted in the timber member (α either 90° or 0°). Taking the determined values of k_p , as given in Table 5.10 to Table 5.12, into account, a steadily increase of the corresponding relationship's proportionality between longitudinal, radial and tangential screw axis orientation can be observed, which principally confirms their observations. This, also in form of Table 5.13, wherein the ratios k_{90} of $\{f_{ax}, K_{ser,ax}\}$ for $\{\text{radial, tangential}\}$ and longitudinal direction in dependence of the assumed annual ring group are given. For both, withdrawal strength and stiffness, k_{90} decreases with increasing a_w (thus a decreasing density), indicating a smaller difference between $f_{ax,\alpha=90^\circ}$ and $f_{ax,\alpha=0^\circ}$ for lower densities.

Table 5.13: Selected statistical parameters of ρ_{12} and a_w and experimentally determined ratios k_{90} for radial and tangential vs. longitudinal screw axis orientation; separated into annual ring groups

group		aw_2	aw_4	aw_6	total	
	mean[ρ_{12}] [*]	[kg/m ³]	458.7	410.6	386.6	420.9
	CV[ρ_{12}]	[%]	8.86	7.63	9.64	11.1
	mean[a_w] [*]	[mm]	2.10	4.04	5.56	3.78
	CV[a_w]	[%]	22.0	16.5	27.0	43.9
f_{ax}	$k_{90,LR}$	[-]	1.51	1.39	1.36	1.42
	$k_{90,LT}$	[-]	1.54	1.30	1.30	1.38
$K_{ser,ax}$	$k_{90,LR}$	[-]	0.91	0.86	0.86	0.88
	$k_{90,LT}$	[-]	0.93	0.79	0.79	0.84

* mean value of all withdrawal test specimen considered

5-3.2 Environmental conditions

Note: the major outcomes of this section have already been published in Ringhofer et al. (2014c).

5-3.2.1 Introduction

As basically introduced in section 4-2, the coniferous wood species, such as Norway spruce, reach their equilibrium moisture content $u \approx 12\%$ in environmental exposure in form of $20\text{ }^\circ\text{C}$ and 65% relative humidity. Not only timber density ρ , but also the mechanical properties, as exemplarily given in Table 4.1, are commonly referred to this generally defined percentage. The main reason therefore is their significant dependency on u , which according to Kollmann (1951), Kollmann (1959), Gerhards (1980), Rammer and McLean (1996), Keunecke et al. (2007) and Horvath et al. (2008) can be approximately described as follows:

Taking spruce softwood into account and starting from $u = 12\%$ as a reference, both timber strength ($2 \div 4\%$ per $\% u$) and stiffness properties ($1 \div 3\%$ per $\% u$) steadily decrease with an increasing moisture content until an upper limit of $u > 20\%$ (several authors also recommend FSP) is reached. Above this boarder, a gradient converging to a horizontal plateau can be observed; a significant influence related is not given any more above the threshold $u \gg \text{FSP}$. Below the equilibrium moisture content, with special focus on shear (where analogy to withdrawal properties was partially confirmed in section 5-3.1) still increasing properties down to $u \approx 5\%$, combined with a loss of strength and stiffness between $u \approx 0 \div 5\%$ (or especially in case of $u = 0\%$) were found so far.

In contrast to the situation for the timber properties in general (a comprehensive research focusing on their relationship with moisture content is still going on) the corresponding investigations concerning the related impact on the withdrawal properties is comparatively scarce. Additionally considering works, which were conducted with products differing from modern self-tapping timber screws, Table 5.14 summarises the dependencies of withdrawal strength f_{ax} on moisture content variation as published by Görlacher (1990), Jablonkay (1999), Pirnbacher et al. (2009) and Hübner (2013b). Thereby, the focus is set on the range of u , varying from $10 \div 12\%$ to $20 \div 30\%$ as a domain predominately considered for investigations. With regard to this comparison, some facts are worth to be discussed more in detail:

Apart from the findings made by Pirnbacher et al. (2009), all mentioned authors determined decreasing withdrawal strengths in a similar dimension, independent of the timber species considered, but slightly higher for parallel-to-grain than for perpendicular-to-grain insertion. The gained loss of f_{ax} with increasing u corresponds to the previously discussed level for timber strengths in general. In contrary, Pirnbacher et al. (2009) determined a far less pronounced decrease of f_{ax} with increasing u , recommending no relevant impact of this parameter at all. Furthermore, again except Pirnbacher et al. (2009), the range considered for the investigation is strongly restricted to the values of u , equal or higher than the

equilibrium moisture content; a comprehensive examination regarding the domain below $u < 12\%$ in fact can not be found.

Table 5.14: Literature observations regarding the behaviour of withdrawal strength f_{ax} in dependence of moisture content variation, according to Ringhofer et al. (2014c)

source	wood species	timber product	levels of u (no. values)	decrease of f_{ax} per % u above $u \approx 12\%$ (observed or proposed)
Görlacher (1990)	spruce	ST	3 11.5 %, 16 %, 22 %	$\sim 2.7\%$
Jablonek (1999)	spruce, douglas fir, beech	ST	2 10 %, 20 %	$\sim 3.3\%$ ($\alpha = 90^\circ$) $\sim 4.5\%$ ($\alpha = 0^\circ$) (both for spruce)
Pirnbacher et al. (2009)	spruce	ST, GLT	4 0 %, 9 %, 14 %, 19 %	$\sim 0.7\%$ ($\alpha = \{90^\circ, 0^\circ\}$)
Hübner (2013b)	ash	GLT	2 11 %, 28 %	$\sim 2.4\%$ ($\alpha = 90^\circ$) $\sim 2.7\%$ ($\alpha = 0^\circ$)

Concentrating on the test procedure, applied for determining the withdrawal strength, all investigations, outlined in Table 5.14, base on the same principle, as given in a stepwise form: the preparation of specimen ($u \approx 12\%$) (i) – climatic conditioning until the target value of u is reached (ii) – inserting the screw (iii) – withdrawal test (iv). In fact, this method simulates the case of the screw insertion in timber components with $u \neq 12\%$, presupposing that the moisture content will not change after assembling. In many practical situations, the connections are installed at the equilibrium moisture content, the environmental exposure and thus a change of u takes place afterwards.

Even though they solely cover the range between $u = 10 \div 12\%$ to $20 \div 30\%$ and differ in their conclusion, at least four reasonable investigations, regarding the influence of u on f_{ax} , could be considered for this discussion. In case of both further withdrawal properties $K_{ser,ax}$ and D , no comparable works have been found so far – the question regarding a corresponding impact of varying u , especially on $K_{ser,ax}$, remains.

Now focusing on a possible relationship between the withdrawal properties and the timber component's temperature at the time of the screw insertion. Pirnbacher et al. (2009) exclusively report the results of a corresponding parameter variation in form of $T = \{-20, 0, 20, 50\}^\circ\text{C}$, conducted in solid timber, as well as in GLT, at an axis-to-grain angle $\alpha = \{0, 90\}^\circ$. With regard to the parallel-to-grain insertion, no related impact of T on f_{ax} could be observed. In case of the perpendicular-to-grain insertion, the determined withdrawal strength indicates an oppositional behaviour in dependence of the timber product considered. This means, that for GLT specimen a slight increase of 0.15% of f_{ax} per degree Celsius, for ST specimen

a slight decrease with the same gradient, was observed. Examining the data, irrespective the timber product and axis-to-grain angle, Pirnbacher et al. (2009) conclude and recommend no relevant influence of T on the withdrawal strength overall. Beside these findings, they also outline their observations regarding an increasing number of timber splitting failure when installing the screws at low temperatures $T = \{-20, 0\}$ °C. Consequently, they recommend a related minimum value for the practical screw insertion in form of $T = 5$ °C. In case of further withdrawal properties $K_{\text{ser,ax}}$ and D , no comparable investigations were found at all. Obviously no related influence of temperature on withdrawal strength is given, the same situation can be assumed for withdrawal stiffness $K_{\text{ser,ax}}$. Consequently, the experimental campaign, regarding the impact of environmental conditions on withdrawal properties, is subsequently restricted to the moisture content variation.

5-3.2.2 Experimental programme

Within this subsection, two experimental campaigns, concerning the influence of the moisture content variation on withdrawal properties conducted at Graz University of Technology, are explained and discussed. The first one, the reference material solid timber (Norway spruce) has been applied for, was aimed to expand the state-of-knowledge, comprises a large bandwidth of moisture content levels, see Table 5.15, a varying procedure regarding the test execution {i, iii, ii, iv} vs. {i, ii, iii, iv}, as well as the axis-to-grain angles $\alpha = \{0^\circ, 90^\circ\}$. The corresponding specimen, illustrated in Annex B-3.1, Figure B.19 (left), were cut from solid timber beams with cross-sectional dimensions $w \times h = 160 \times 240$ mm². Note: in order to realise a similar density distribution for all moisture content groups within the test series, one specimen each was extracted per beam. The used screw product was also applied for the diameter variation, discussed in section 5-2.1 – the corresponding thread characteristics are again given in Table 5.16.

The second test programme, with a comparatively small extent, comprised the examinations regarding the behaviour of the withdrawal properties of screws, situated in the side face of the crosswise laminated timber product CLT ($\alpha = 90^\circ$), when moisture content varies. As illustrated in Figure B.19 (right), the three-layered CLT specimen were therefore applied, a related production was conducted at Graz University of Technology with PURBOND® HB110 adhesive and Norway spruce timber boards as the basis material. The thread characteristics of $d = 8$ mm screws, as well as the test conditions (screws were fully inserted through the specimen, pre-drilling with $d_{\text{PD}} = 5$ mm was applied) are given in Table 5.16.

Deviating from the previously discussed literature, the test execution of both campaigns was done as follows: the preparation of test specimen ($u \approx 12\%$) (i) – inserting the screw (iii) – climatic conditioning till target moisture content u was reached (ii) – withdrawal test (iv). In addition, one control group, denoted as “18pc” (see Table 5.15), was carried out in reversed order {i, ii, iii, iv}.

Table 5.15: *Planned moisture content groups in the frame of both test campaigns I and II*

test campaign	d [mm]	α [°]	groups
I	6	0	{00p, 06p, 09p, 12p, 15p, 18p, 21p} ^{**}
		90	{00p, 07p, 09p, 12p, 15p, 18p, 20p} [*] , 18pc ^{**}
II	8	90	{08p, 12p, 18p} ^{**}

conducted on: ^{*} Dyna Z-25FS | ^{**} LIGNUM-UNI-275

Table 5.16: *Thread characteristics and test conditions applied for the experimental campaigns focusing on moisture content variation*

test campaign	thread characteristics					test conditions			
	d_{nom} [mm]	d [mm]	η [-]	p [mm]	v^* [°]	l_p [mm]	l_{ef} [mm]	l_{emb} [mm]	d_{PD} [mm]
I	6	5.98	0.64	2.55	40	72.0	65.0	12.0	-
II	8	8.02	0.65	3.54		102.0	102.0	0.0	5.00

^{*} values taken from product information related

With regard to the test execution, the programme was partly conducted on Dyna Z-25FS, partly on the test rig LIGNUM-UNI-275, c. f. Table 5.15. In both cases no local way measurement set-up was applied. Nevertheless, a relative comparison of both properties, $K_{\text{ser,ax}}$ and D , in-between the test series – where boundary conditions, such as the axis-to-grain angle, the outer thread diameter, the specimen dimensions and the test configuration were kept constant – is possible. A further background information, regarding test execution, post-processing, property determination and data assessment is summarised in section 5-1.2.

5-3.2.3 Results and discussion

In Figure 5.28 and Figure 5.29 the confidence intervals and error bars of statistical parameters, dedicated to the timber density ρ_{12} (mean value, median and variability, the latter expressed by $\text{CV}[\ln(\rho_{12})]$), are given in dependence of the experimental programme, the axis-to-grain angle and the moisture content groups. The related statistical parameters, including realised moisture contents u for each subseries, can be found in Annex B-3.2, Table B.21 and Table B.22. With regard to the density distribution for each test series (note: experimental campaign I has to be separately considered in dependence of α), neither the determined values ρ_{12} (in Table B.21 and Table B.22), nor the graphical illustrations (given in Figure 5.28 and Figure 5.29) indicate a possible and unwanted influence of this parameter on the withdrawal properties. Deviating from the results, discussed so far in this chapter, the moisture contents u are significantly different; average values are closely located to the planned levels. Furthermore, moisture

contents related to both groups, “18p” and “18pc” (test campaign I, $\alpha = 90^\circ$), are more or less equal, enabling a comparison of withdrawal strength in dependence of the way of the test execution.

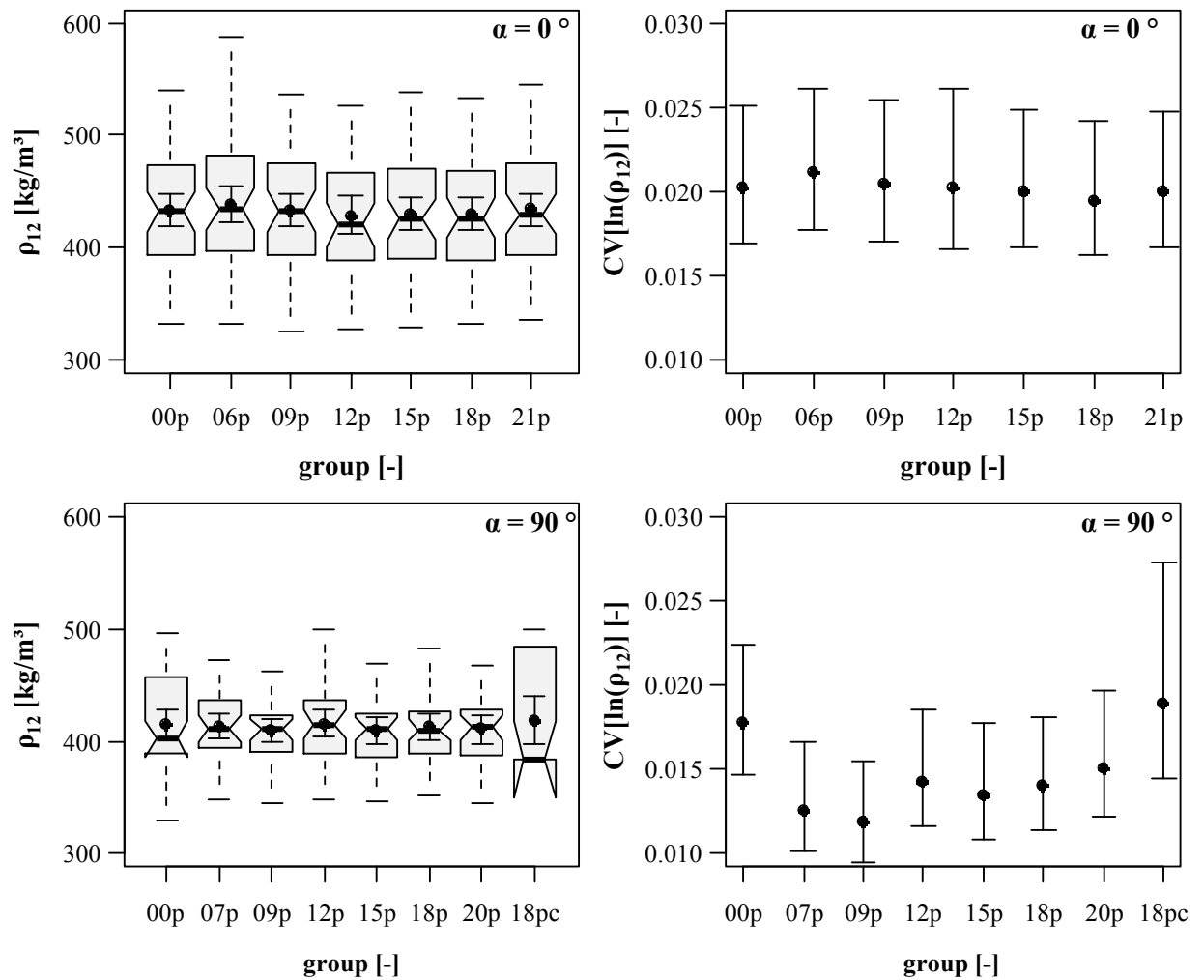


Figure 5.28: Left: boxplot graphic of densities ρ_{12} ; right: CIs of $CV[\ln(\rho_{12})]$ in dependence of moisture content groups; above: $\alpha = 0^\circ$; below: $\alpha = 90^\circ$, experimental campaign I

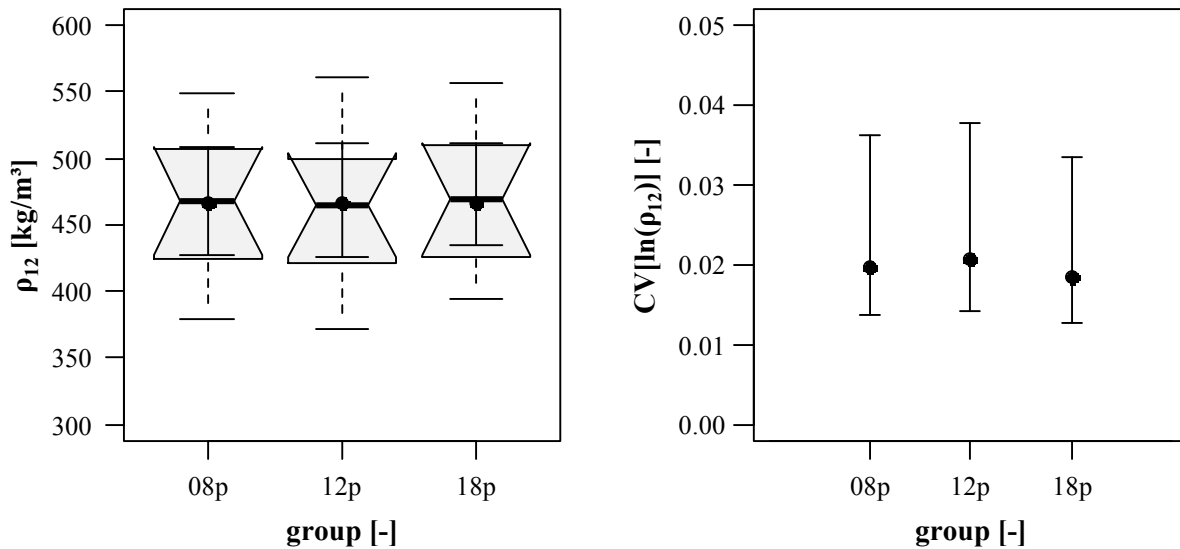


Figure 5.29: Left: boxplot graphic of densities ρ_{12} ; right: CIs of $CV[\ln(\rho_{12})]$ in dependence of moisture content groups; $\alpha = 90^\circ$, experimental campaign II

Figure 5.30 to Figure 5.33, as well as Annex B-3.2, Table B.23 to Table B.25, include the determined withdrawal properties, again in dependence of the axis-to-grain angle and the experimental programme.

Concentrating on withdrawal strength f_{ax} , the given behaviour in dependence of u can be separated into three main domains: (i) in case of moisture contents u between 0 % and ~ 7 %, f_{ax} increases with increasing u , (ii) in case of u between 8 % and 12 %, a more or less constant plateau is given, and (iii) from 12 % to ~ 20 % a significant and linear decrease of f_{ax} with increasing u can be observed. Worth mentioning, that the qualitative form of this behaviour is independent from α and the timber product applied, corresponds to the literature findings. In addition, the localisation of withdrawal strengths dedicated to both groups, “18p” and “18pc”, especially considering the boxplot/scatterplot diagram illustrated in Figure 5.30 (right), indicates, that the way of test execution ($\{i, iii, ii, iv\}$ vs. $\{i, ii, iii, iv\}$) does not influence the size of f_{ax} at all. With regard to the distribution of withdrawal strength in dependence of a moisture content variation, the coefficients of variation, given in Table B.23 to Table B.25, as well as the related error bars, illustrated in Annex B-3.1, Figure B.20 and Figure B.23 (left), do not differ significantly, a corresponding influence of u on $CV[f_{ax}]$ can thus be excluded.

Secondly, focusing on the withdrawal stiffness $K_{ser,ax}$, even though two groups, namely “09p” in case of $\alpha = 0^\circ$ and “18p” in case of $\alpha = 90^\circ$ (both experimental campaign I), significantly deviate from the general data trend, the determined values indicate a qualitatively similar behaviour with varying u as given for f_{ax} . Interestingly, comparing the coefficients of variation $CV[K_{ser,ax}]$, determined for $\alpha = 0^\circ$ and 90° , significantly different values can be observed. This is probably caused by the different inaccuracies

in determining this property, considering the globally measured displacements by the two test rigs applied.

Thirdly, with regard to ductility, especially for $\alpha = 0^\circ$ the load-displacement behaviour of several samples were characterised by an abrupt loss of the bearing resistance, immediately after F_{\max} was reached. Additionally observing a less pronounced nonlinear behaviour, before reaching F_{\max} in these cases, the corresponding values for D were determined to (or close to) 1.00 (which means $v_y = v_u$), c. f. Figure 5.32 (left). Apart from group “00p”, where comparatively more brittle failures occurred (oven dry samples are seen as responsible therefore), the related test data is independently distributed over all moisture content groups, thus a possible influence of u on the brittleness of withdrawal failure is not given. Furthermore, the determined ductility indicates neither similarities to the behaviour of f_{ax} or $K_{ser,ax}$ with varying u , nor such to both axis-to-grain angles considered in dependence of the moisture content variation. For instance, the results illustrated in Figure 5.32 (left, ST, $d = 6$ mm, $\alpha = 0^\circ$) and Figure 5.33 (right, CLT, $d = 8$ mm, $\alpha = 90^\circ$) do not seem to be influenced by varying u at all, while those given in Figure 5.32 (right, ST, $d = 6$ mm, $\alpha = 90^\circ$) steadily increase with increasing u , consequently showing the oppositional behaviour than it was found for f_{ax} or $K_{ser,ax}$ in comparable domains. A similar situation is given for the coefficient of variation: while a moisture dependent influence on $CV[D]$ in case of experimental programme I, $\alpha = 0^\circ$ and experimental programme II, $\alpha = 90^\circ$ cannot be observed, the related parameter steadily decreases with increasing u in case of the experimental programme I, $\alpha = 90^\circ$. Taking these circumstances into account, a generally valid and logical statement, regarding the behaviour of D in dependence of the moisture content variation, is not possible on the basis of the given test data.

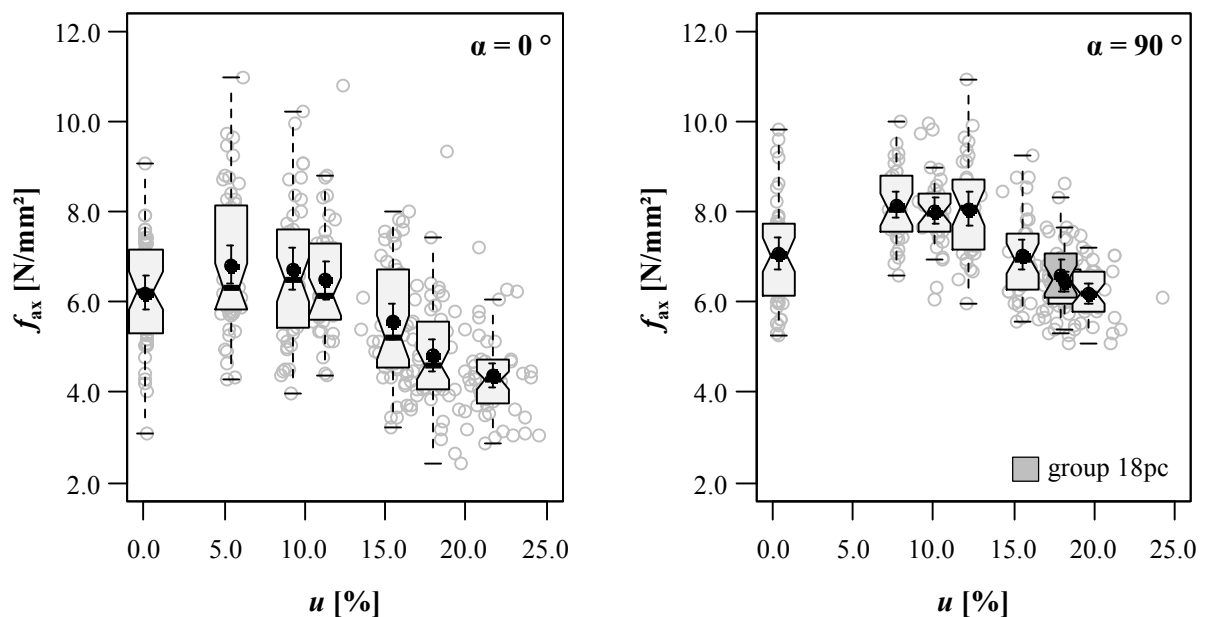


Figure 5.30: Combined boxplot/scatterplot diagrams of withdrawal strength vs. moisture content; left: $\alpha = 0^\circ$; right: $\alpha = 90^\circ$; experimental campaign I

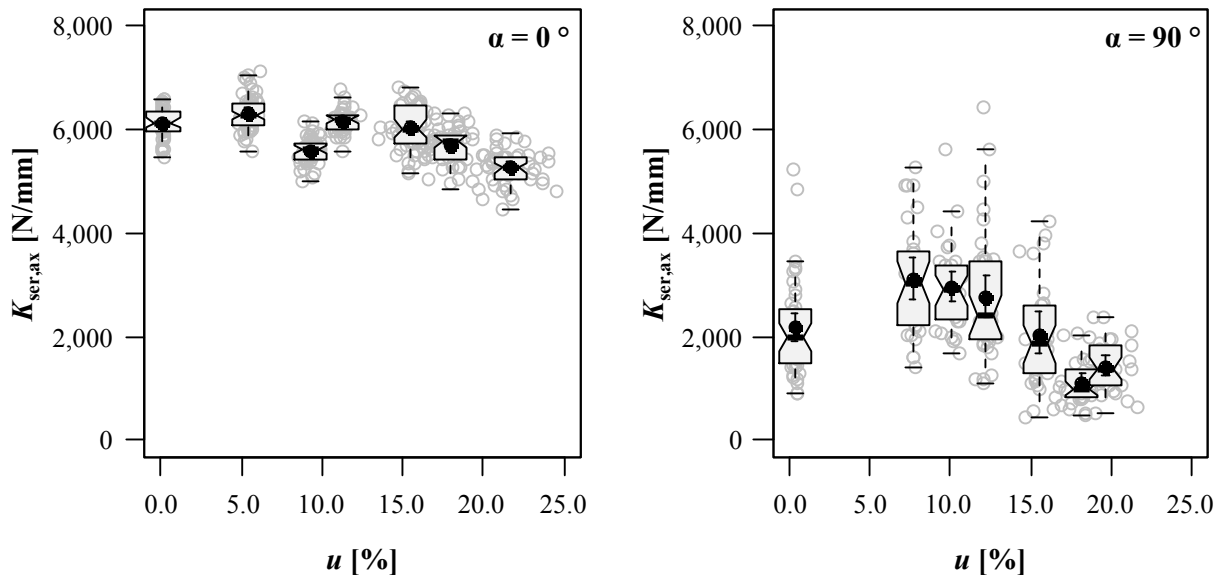


Figure 5.31: Combined boxplot/scatterplot diagrams of withdrawal stiffness vs. moisture content; left: $\alpha = 0^\circ$; right: $\alpha = 90^\circ$; experimental campaign I

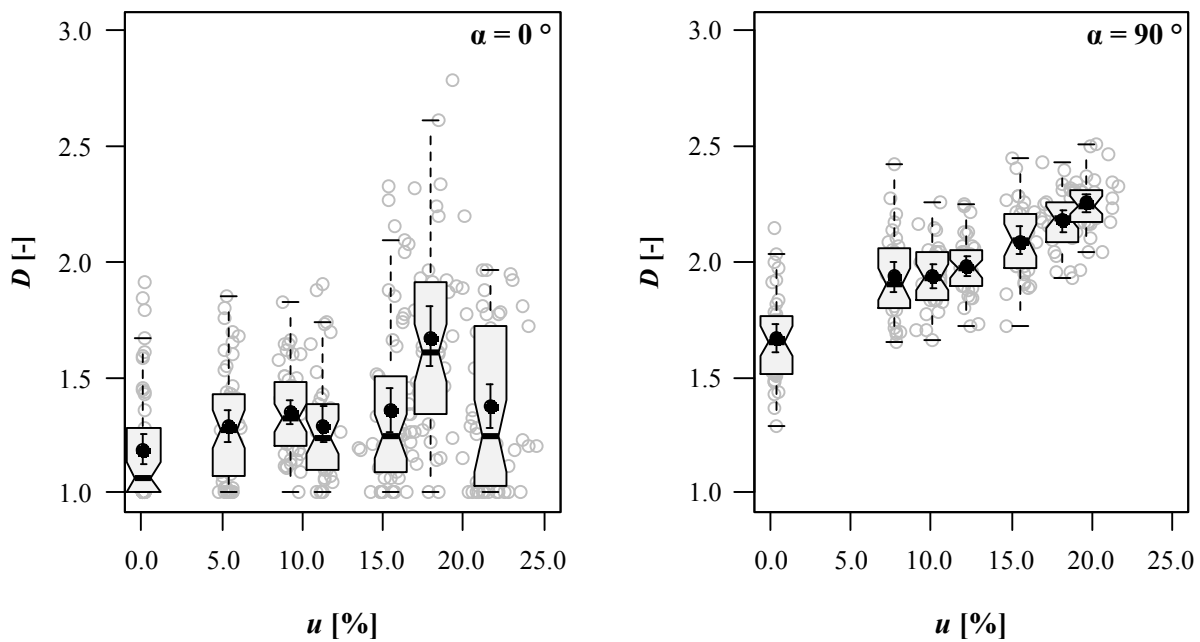


Figure 5.32: Combined boxplot/scatterplot diagrams of ductility vs. moisture content; left: $\alpha = 0^\circ$; right: $\alpha = 90^\circ$; experimental campaign I

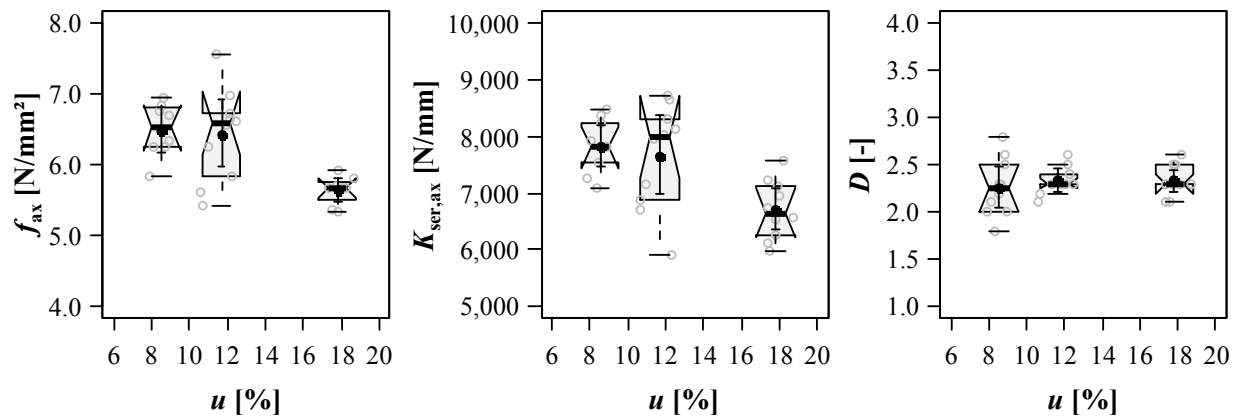


Figure 5.33: Combined boxplot/scatterplot diagrams of withdrawal strength (left), stiffness (middle) and ductility (right) vs. moisture content; $\alpha = 90^\circ$; experimental campaign II

Further concentrating on the relationship between withdrawal properties and density ρ_{12} in case of varying moisture contents: since in section 5-3.1 no dependency of ductility on density was observed, the focus is thereby restricted to f_{ax} and $K_{ser,ax}$. Table 5.17 and Table 5.18 subsequently comprise the determined exponents k_p and the correlation coefficients $r_{XY,PE}$ for f_{ax} and $K_{ser,ax}$, in dependence of the moisture content levels and axis-to-grain angle. With regard to withdrawal strength, the exponents result to be slightly lower than 1.00 in case of $\alpha = 0^\circ$, slightly higher in case of $\alpha = 90^\circ$ and are thus quite similar to those determined for $d = 6$ mm in Table 5.5. Even though certain peaks of k_p and $r_{XY,PE}$ can be observed for u varying between 12 % and 15 %, the given differences are regarded as too low for proving a specific moisture related influence on this relationship. Apart from the circumstance, that the corresponding exponents result in surprisingly low ($\alpha = 0^\circ$) and high ($\alpha = 90^\circ$) magnitudes, the relationship between withdrawal stiffness and density is also not really affected from varying u .

Table 5.17: Experimentally determined relationships between f_{ax} and ρ_{12} in dependence of moisture content level and axis-to-grain angle; experimental campaign I

α	group	[-]	00p	06p	09p	12p	15p	18p	21p
0°	k_p	[-]	0.93	0.97	1.02	1.09	1.28	1.12	0.99
	$r_{XY,PE}$	[-]	0.54	0.57	0.52	0.68	0.64	0.50	0.58
α	group	[-]	00p	07p	09p	12p	15p	18p	20p
90°	k_p	[-]	1.12	0.95	1.21	1.33	1.25	0.75	0.71
	$r_{XY,PE}$	[-]	0.75	0.69	0.79	0.85	0.76	0.61	0.64

Table 5.18: Experimentally determined relationships between $K_{ser,ax}$ and ρ_{12} in dependence of moisture content level and axis-to-grain angle; experimental campaign I

α	group	[-]	00p*	06p	09p	12p	15p	18p	21p
0°	k_p	[-]	0.15	0.25	0.24	0.16	0.41	0.41	0.30
	$r_{XY,PE}$	[-]	0.36	0.59	0.63	0.54	0.69	0.72	0.55
α	group	[-]	00p	07p*	09p	12p	15p	18p	20p
90°	k_p	[-]	3.01	2.36	2.79	4.07	4.34	3.25	3.25
	$r_{XY,PE}$	[-]	0.78	0.51	0.66	0.82	0.67	0.69	0.74

* no highly significant relationship

5-3.2.4 Modelling

The focus of the last part is on the determination of a quantitative, empirical relationship between the withdrawal properties f_{ax} and $K_{ser,ax}$ and the moisture content u . Following the considerations made in Ringhofer et al. (2014c), two approaches, namely (i) a simple bilinear model for moisture contents between 8 % and 20 % (seen as the relevant domain for a screw application), as well as (ii) a continuous function for the whole bandwidth of u , but exclusively derived for the withdrawal strength f_{ax} , are therefore applied.

With regard to (i), and the results given in Table B.23 to Table B.25, only minor and insignificant differences of f_{ax} and $K_{ser,ax}$ for moisture contents between 8 % and 12 % can be observed, the related behaviour can be approximated by a constant plateau with zero gradient. In case of u above 12 %, the given results significantly decrease with increasing u , allowing a simplification by a linear function with negative gradient k_{mc} , see eq. (5.58):

$$\eta_{mc} = \frac{X_u}{X_{ref}} = \begin{cases} 1.00 & \text{for } \{ 8\% \leq u \leq 12\% \\ 1.00 - k_{mc} \cdot (u - 12) & \text{for } \{ 12\% \leq u \leq 20\% \end{cases} \quad (5.58)$$

with $X = \{f_{ax}, K_{ser,ax}\}$ and η_{mc} as ratio between withdrawal properties at a specific u and a defined reference value. The determination of the gradients k_{mc} , in dependence of the axis-to-grain angle α and the withdrawal property X , was carried out by performing a simple linear regression analysis with the software package R, considering all moisture content groups above “09p”. As a reference, the mean values of the moisture content groups “12p” were therefore applied. With regard to the corresponding results, subsequently given in Table 5.19, certain outcomes are worth being discussed in detail:

First, the size and relationship between $\alpha = 0^\circ$ and 90° of the gradient, determined for the withdrawal strength, is quite similar to the results published by Görlacher (1990), Jablonkay (1999) and Hübner (2013b), as well as those of timber strength properties in general. This, in principle, confirms own test

results and again indicates, that the way of the test execution has no influence on the moisture dependent behaviour of withdrawal properties. Comparing both timber products investigated, k_{mc} determined for screws situated in CLT side face, is roughly 50 % of that in solid timber.

Second, the gradients determined for withdrawal stiffness in case of ST, $\alpha = 0^\circ$ and CLT, $\alpha = 90^\circ$ are similar to those for timber stiffness properties, while in case of ST, $\alpha = 90^\circ$ a surprisingly high value for k_{mc} is given. This is in fact caused by the values of $K_{ser,ax}$, dedicated to the moisture group “18p”, which are – as already discussed – significantly lower, than the general data trend in this domain, c. f. Figure 5.31 (right). The related value, determined independently from α , results in a domain regarded as reasonable for this property.

Table 5.19: *Determined gradients k_{mc} for the bilinear model approach, in dependence of timber product and axis-to-grain angle; based on Ringhofer et al. (2014c)*

test campaign	material	α [°]	gradient k_{mc} [-]	
			$X = f_{ax}$	$X = K_{ser,ax}$
I	ST	0	0.036	0.014
		90	0.031	0.071
		both	0.034	0.028
II	CLT	90	0.017	0.017

Comparing the general behaviour of the timber strength properties in dependence of the moisture content variation, as well as those published by the aforementioned authors and own findings given in Table 5.19 with the outcomes reported in Pirnbacher et al. (2009), a significant difference in the size of k_{mc} for withdrawal strength results. This circumstance led to a reassessment of the test data, which was considered by Pirnbacher et al. (2009) for the related linear regression analysis. As also applied for a part of experimental campaign I, Pirnbacher et al. (2009) performed all withdrawal tests on the Dyna Z-25FS device, which is characterised by a maximum displacement reachable, further denoted as $v_{max,setup}$. In cases, $v_{max,setup}$ is reached before the specimen failed in withdrawal with F_{max} and $v(F_{max})$, the device stopped the test and recorded the force $F_{max,measured}$ (at $v_{max,setup}$) as a limit value, c. f. Figure 5.34 (left).

This measurement error concerned a certain number of tests, dedicated to both groups with $u \approx \{9, 14\}$ % (see Table 5.14), where comparatively higher withdrawal loads and thus higher values for $v(F_{max})$ are expected. The corresponding datasets have consequently to be seen as right-censored, which means that the real withdrawal capacities are higher than the determined ones. As mentioned in section 5-1.2, a proper way of determining the main statistical parameters $mean[F_{ax}]$ and $sd[F_{ax}]$ of such datasets is the method of the maximum-likelihood estimation for right censored data (rcMLE). Figure 5.34 (right) illustrates uncorrected (boxplots, “data trend original”) and corrected (“data trend MLE”, determined by

eq. (5.23) and (5.24)) withdrawal test data, exemplarily for solid timber and $\alpha = 90^\circ$, indicating a significantly increasing gradient of a decreasing withdrawal capacity in the domain of $u = 14\% \div 19\%$, as a consequence of this measure.

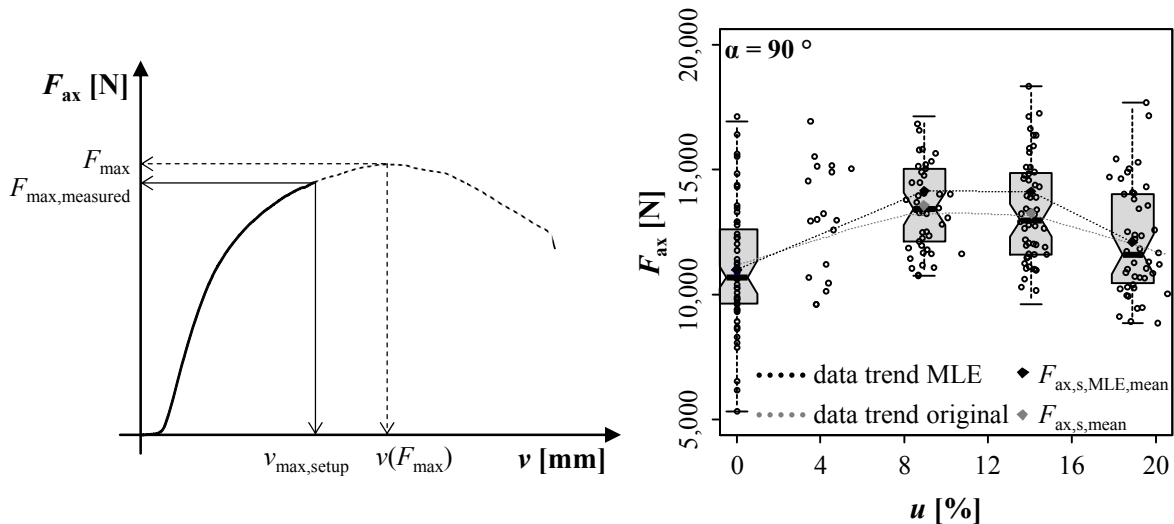


Figure 5.34: Left: measurement error of withdrawal capacity in the force-displacement relationship; right: comparison of results from Pirnbacher et al. (2009) with corrected values (ST, $\alpha = 90^\circ$); both according to Ringhofer et al. (2014c)

Table 5.20 subsequently comprises the values for k_{mc} , determined by Ringhofer et al. (2014c), with the aforementioned measure for all test series examined by Pirnbacher et al. (2009). Now the given results correspond to the ones published by the other authors, as well as to own findings, shown in Table 5.19. The gradient, dedicated to GLT and $\alpha = 90^\circ$, is again slightly smaller than the one determined for ST with the same axis-to-grain angle. This behaviour is similar to own outcomes (compare k_{mc} for ST and CLT in Table 5.19), and indicates a possibly minor pronounced impact of the moisture content variation on withdrawal properties of screws, situated in (the side face of) laminated timber products. Since both campaigns comprise either a relatively small number of tests (CLT, $\alpha = 90^\circ$) or estimated statistical parameters (Table 5.20), this effect should be studied more comprehensively in the future.

Table 5.20: Decrease of withdrawal strength f_{ax} with increasing moisture content considering corrected test data from Pirnbacher et al. (2009); according to Ringhofer et al. (2014c)

group	α [°]	gradient k_{mc} [-]
ST	0	0.027
	90	0.029
GLT	0	0.027
	90	0.025

With regard to (ii), a nonlinear continuous function of the withdrawal strength for the whole bandwidth of u considered in experimental campaign I, was determined by Ringhofer et al. (2014c). Therefore, a polynomial approach, originally developed by Glos (1978) for the description of the GLT compressive stress-strain relationship, was applied – see eq. (5.59):

$$\eta_{mc} = \frac{f_{ax,u}}{f_{ax,ref}} = \eta_0 + \frac{u + k_1 \cdot u^N}{k_2 + k_3 \cdot u + k_4 \cdot u^N} \text{ for } 0 \% < u \leq 20 \%, \quad (5.59)$$

with

$$k_1 = \frac{\eta_{fin}}{(N-1) \cdot k_{mc,start} \cdot u_{mean,pl}^N \cdot \left(1 - \frac{\eta_{fin}}{\eta_{pl}}\right)}, \quad k_2 = \frac{1}{k_{mc,start}}, \quad (5.60)$$

$$k_3 = \frac{k_1}{\eta_{pl}} - \frac{N}{N-1} \cdot \frac{1}{k_{mc,start} \cdot u_{mean,pl}}, \quad k_4 = \frac{k_1}{\eta_{fin}}, \quad \text{and} \quad (5.61)$$

$$\eta_0 = \frac{1}{n} \cdot \sum_{j=1}^n \frac{f_{ax,u=0,j}}{f_{ax,12,mean,i}}, \quad \eta_{pl} = \frac{1}{n} \cdot \sum_{j=1}^n \frac{f_{ax,pl,j}}{f_{ax,12,mean,i}}. \quad (5.62)$$

Hereby, $k_{mc,start}$ is regarded as the gradient of the referenced withdrawal strengths in the domain of $u = 0 \% \div 8 \%$, $u_{mean,pl}$ the mean moisture content of the test series between 8 % and 12 %, η_0 and η_{pl} as the referenced withdrawal strengths dedicated to 0 % and $u_{mean,pl}$, as well as η_{fin} as the referenced limit at FSP and N as a non-dimensional fitting exponent. Since the scope of the moisture contents, which was considered for investigation, does not include FSP, the corresponding value for η_{fin} was determined by extrapolating eq. (5.58) presupposing $u_{FSP} \rightarrow 28 \%$. All related model parameters, being necessary for the application of eq. (5.59), are subsequently given in Table 5.21 in dependence on α .

Table 5.21: *Input parameters of the nonlinear model; according to Ringhofer et al. (2014c)*

α [°]	η_0 [-]	k_1 [-]	k_2 [-]	k_3 [-]	k_4 [-]	N [-]
0	0.96	$-2.34 \cdot 10^{-6}$	53.6	5.44	$4.36 \cdot 10^{-6}$	5.94
90	0.88	$-3.42 \cdot 10^{-6}$	54.8	1.37	$9.13 \cdot 10^{-6}$	5.50
both	0.92	$-9.13 \cdot 10^{-6}$	55.5	1.99	$1.92 \cdot 10^{-5}$	5.30

Figure 5.35 finally compares the referenced mean withdrawal strengths, determined in the frame of experimental campaign I, with the course of the nonlinear model according to eq. (5.58) in case of $\alpha = \{0^\circ, 90^\circ, \text{both}\}$. With regard to the differences between test results and estimated values, a good predictive quality can be attested for the vast majority of test series considered.

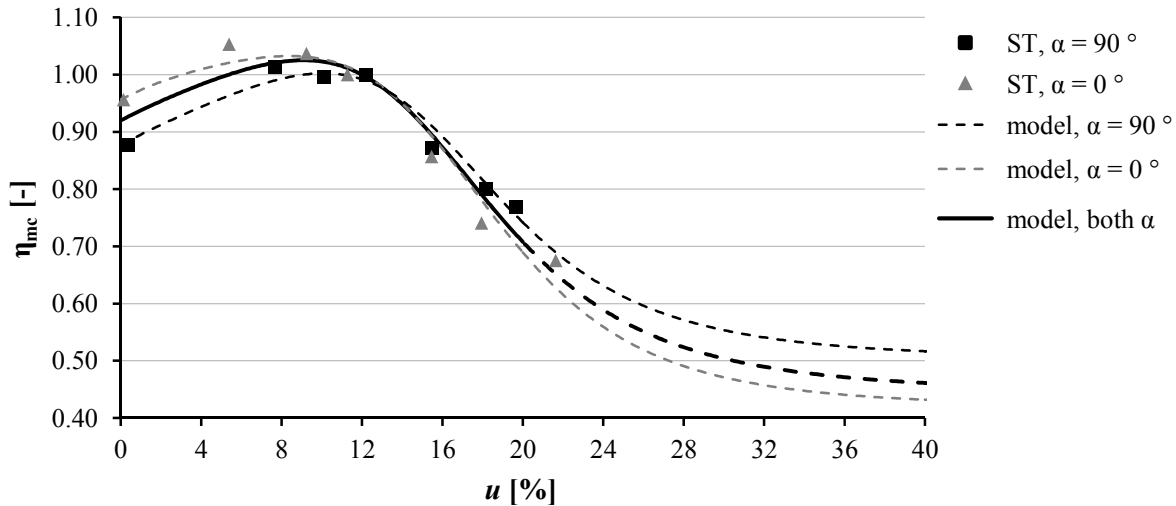


Figure 5.35: Comparison of the nonlinear model approach with test results of experimental campaign I

The moisture contents in timber components exposed to climatic conditions, especially dedicated to service class 2 according to ON EN 1995-1-1 (2015), are commonly characterised by a cyclic change in their magnitude, varying between $u = 12\%$ and 20% . Since the influence of the moisture content variation on withdrawal properties of self-tapping screws has been determined so far – exclusively for a static change of u – the possible additional effects due to the cyclic moisture content variation (simulating the real conditions) should be focused in future investigations.

The outcomes of a similar campaign, recently published by Silva et al. (2016) are worth to be mentioned. Summarising their efforts in testing $d = 8\text{ mm}$ screws, situated in GLT and CLT reference specimen (without gaps), before and afterwards a cyclic change of moisture content was applied (4 cycles from 30% r. h. to 90% r. h. at $T = 20\text{ }^\circ\text{C}$, 324 days of storage, $u_{\text{start}} = u_{\text{finish}} \approx 13 \div 14\%$), Silva et al. (2016) observed a slight decrease of $f_{ax, GLT}$, while the withdrawal strength of screws in CLT even increased. Based on these results, presupposing u_{start} and u_{finish} having the same magnitude, a certain tendency regarding the impact of a cyclic moisture content variation on the screw withdrawal strength is not given.

5-3.3 Lamination – general lay-up parameters

Note: the major outcomes of this section have already been published in Ringhofer et al. (2015b). The test results slightly deviate from the published ones, since a different form of outlier treatment is applied within this chapter.

5-3.3.1 Introduction and model approaches

So far, the vast majority of the investigations focused on the loadbearing behaviour of self-tapping screws situated in solid timber (as reference material). Within sections 5-3.3 and 5-3.4, the concentration lays on the specific lay-up of both laminated timber products GLT and CLT and the associated parameters possibly influencing the related withdrawal properties. Figure 5.36 again illustrates both products, as they are characterised by (i) general lay-up parameters such as the number of layers, N , their thickness t_i , as well as their orientation and (ii) certain specifics especially given for CLT in form of gaps or slots, commonly described by the gap width w_{gap} .

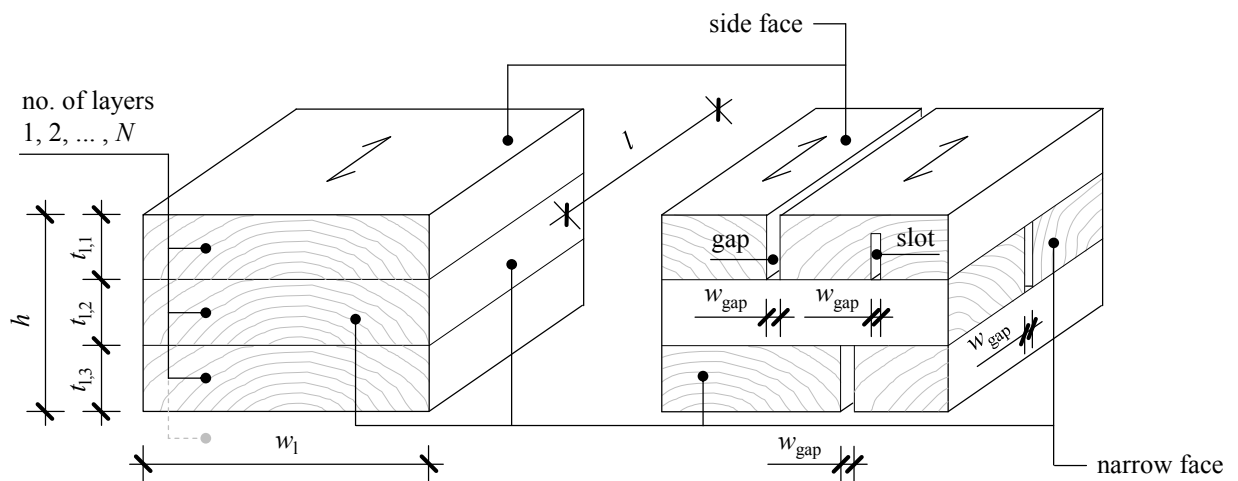


Figure 5.36: Relevant characteristics of unidirectional and orthogonal layered clear wood

With regard to (i), GLT and CLT are in principle timber products composed by a certain number of layers, exclusively considered as quasi-rigidly bonded together by adhesives within this section. Furthermore, as defined in section 4-4, the layer type is restricted to boards, consequently excluding products e. g. made of veneers, such as laminated veneer lumber (LVL). In case of homogeneous lay-ups, defined by an equal strength class of all single elements, the latter can be approximated as stochastically independent and identical distributed (iid). The composite interaction between the layers subsequently leads to a certain homogenisation effect, which concerns physical (density) and mechanical (strength, stiffness) properties and is characterised by a reduction of dispersion with increasing N .

The related quantification of this system effect is commonly described by the k -factor $k_{\text{sys}}(N)$, which expresses the ratio of a distribution characteristic C (e. g. the expectation $E[X] = \mu_X$, the variance $\text{Var}[X] = \sigma_X^2$ or the coefficient of variation $\text{CV}[X]$ of a random variable X) between N and $N = 1$ affected elements. Apart from the number of elements or layers, the size of k_{sys} also depends on the type of system action (serial vs. parallel), as well as on the property's dispersion, c. f. Brandner (2013b).

Amongst others, the aforementioned thesis, written by Brandner (2013b), is worth to be mentioned as a main source concentrating on system effects of timber strength and stiffness properties in general. Beside research activities, the system effects are also considered in the standardisation, e. g. in ON EN 1995-1-1 (2015) to cover the strength increase in dependence of the number of parallel acting components or in ON EN 14080 (2013), which takes a 10 % higher characteristic density of GLT if compared to the one of the single lamella into account. Especially the latter effect is important for further considerations and thus briefly discussed. Taking a system of N elements with iid densities $\rho_{1,i}$ ($i = 1 \div N$) into account, the density of the system ρ_N can be determined as the average of all single densities, see eq. (5.63):

$$\rho_N = \bar{\rho}_1 = \frac{1}{N} \cdot \sum_{i=1}^N \rho_{1,i}. \quad (5.63)$$

Further assuming the limit case of $N \rightarrow \infty$ and the Central Limit Theorem, ρ_N can be regarded as normal distributed (ND) and be defined by

$$E[\rho_N] = E[\rho_1] \text{ and } \text{Var}[\rho_N] = \frac{\text{Var}[\rho_1]}{N} \text{ or } \text{CV}[\rho_N] = \frac{\text{CV}[\rho_1]}{\sqrt{N}}. \quad (5.64)$$

Additionally considering eq. (5.12), the characteristic 5 % value of the system's density results to

$$\rho_{N,05} \approx \rho_{\text{mean}} \cdot \left(1 + \Phi^{-1}(0.05) \cdot \frac{\text{CV}[\rho_1]}{\sqrt{N}} \right). \quad (5.65)$$

Presupposing a common range for $\text{CV}[\rho_1] = 6 \div 10$ % with 8 % in average, c. f. Brandner (2013b), $\rho_1 \sim 2\text{pLND}$ and $N = 15$, which represents the standard GLT with $h = 600$ mm and $t_1 = 40$ mm, the ratio between $\rho_{N,05} = \rho_{\text{GLT},05}$ and $\rho_{1,05}$ (5 % quantile of the single layer density) results to $1.08 \div 1.13$, on average to 1.11, which is more or less equal to the aforementioned factor proposed in ON EN 14080 (2013).

Even though the empirical regression functions, derived for the screw withdrawal strength and discussed in section 5-1.3, base on the test results, predominately carried out in solid timber and commonly also applied for the screw insertion in GLT. Furthermore, as mentioned in sections 5-1.3 and 5-3.1, the timber density is exclusively used as a material indicator – not only representing strength and stiffness properties, but also timber product related specifics. With regard to the withdrawal strength of screws,

situated in GLT and ST, presupposing the same strength class of the basis material (this means GLT is made of lamellas with densities equal to that of ST), this circumstance thus results in equal mean values and significantly higher characteristic ones (5 % quantiles) in GLT if compared to ST, c. f. eq. (5.64) and (5.65). Thereby, this especially concerns the determination of a characteristic withdrawal strength according to design standards such as ON EN 1995-1-1 (2015) or related ETAs, there is no differentiation whether the screw is situated at $\alpha = 90^\circ$ in the GLT side face (penetrating N layers with homogenised density ρ_N) or in single lamella's narrow face (penetrating one layer with ρ_1). Concentrating on the screw insertion in CLT, one approach published by Uibel and Blaß (2007), on the basis of a comprehensive experimental campaign reported in Blaß and Uibel (2007), is worth to be outlined, see eq. (5.66):

$$R_{ax,k} = \frac{0.35 \cdot d^{0.8} \cdot I_{ef}^{0.9} \cdot \rho^{0.75}}{1.5 \cdot \cos^2 \varepsilon + \sin^2 \varepsilon} \rightarrow f_{ax,k} = \frac{0.35 \cdot d^{-0.2} \cdot I_{ef}^{-0.1} \cdot \rho^{0.75}}{1.5 \cdot \cos^2 \varepsilon + \sin^2 \varepsilon} \cdot \frac{1}{\pi}, \quad (5.66)$$

with ρ as the characteristic density of CLT (whole cross section, including N layers) and ε as an indicator where the screw is situated in ($\varepsilon = 90^\circ \rightarrow$ side face, N layers; $\varepsilon = 0^\circ \rightarrow$ narrow face, $N \approx 1$ layer). This, combined with the factor 1.5 in eq. (5.66), covers – beside further effects as discussed later – the varying densities due to different screw positioning (side vs. narrow face) and is thus in clear contrast to the commonly applied design practice of determining withdrawal capacity of screws, situated in GLT irrespective their specific position.

Summarising the discussion, the impact of timber products, deviating from ST on screw withdrawal properties, is currently covered by different densities related. This represents a certain homogenisation and thus the system effect, but exclusively for characteristic values, while on the mean level no differentiation is made at all, c. f. eq. (5.64). Not only a certain number of test results, dedicated to the experimental programme, which is discussed later, but also certain results reported by Blaß and Uibel (2007) (arrangement 1.2; $d = 8$ mm), indicate a positive influence of the number of penetrated layers N on screw withdrawal properties in average. For instance, the investigations made by Reichelt (2012) show, that $f_{ax,N,mean}$ significantly increases (7 ÷ 14 %), when screws are inserted through an increasing number of layers $N = \{3, 6, 20\}$ in GLT or CLT specimen. Since this effect cannot be covered by the density homogenisation, as given in eq. (5.64), something else must be responsible. Motivated by this lack of knowledge, Ringhofer et al. (2015b) derived a stochastic approach for covering the increase of average withdrawal strengths with increasing N , which is summarised as follows:

In fact, the main idea behind this model is the assumption, that in case of an axially loaded self-tapping screw, inserted in N layers, the one with the highest anchoring capacity governs its loadbearing behaviour. As demonstrated in section 5-3.1, at least for perpendicular-to-grain insertion, the timber density serves as the best indicator for this anchoring capacity in case of $N = 1$ (solid timber), thus the

layer with the highest anchoring capacity is presupposed, being equal to the one with the maximum density, see eq. (5.67):

$$f_{ax,N} \rightarrow f_{ax,N} \left(\max_i [\rho_{1,i}] \right), \text{ with } i = 1, \dots, N. \quad (5.67)$$

Beside the condition of $\{f_{ax}, \rho\} \sim 2p\text{LND}$ (see section 5-1.2), further assumptions are: the screw completely penetrates N layers of equal thickness and with iid material properties, an approximatively cylindrical stress distribution along the thread, a one-to-one relationship between the density and timber strength and stiffness properties, as well as brittle failure behaviour of screws without any possibility for load redistribution. Furthermore, the layer thickness has to be sufficient to fulfil all these conditions.

Since a distribution of extremes (maxima, c. f. eq. (5.67)) of lognormal distributed variables is not available in closed form, an approximation, originally developed by Brandner (2013b) is subsequently applied for describing the system effect in dependence of the number of layers penetrated by the screw, see eq. (5.68):

$$k_{\text{sys}}(N) = \frac{C_N}{C_1} = \frac{1}{[\ln(N) \cdot \beta_C + 1]^{\alpha_C}}, \quad (5.68)$$

with α_C and β_C as the model parameters determined for $C = E[X] = \mu_X$ and $\text{CV}[X]$ by virtual generation of $M = 10,000$ maxima for a given set of $N = 1, 2, \dots, 100$ realisations of the random variable X in the software package R. Thereby, the simulation considered three values for the timber density's coefficient of variation in form of $\text{CV}[\rho_1] = \{6, 8, 10\} \%$, see Table 5.22.

Table 5.22: Parameters α_C and β_C for $C = \{E[X], \text{CV}[X]\}$; according to Ringhofer et al. (2015b)

$\text{CV}[X_{2,1}] = \text{CV}[\rho_1] =$	6 %	8 %	10 %
α_{mean}	-0.1616	-0.2153	-0.2690
β_{mean}	0.3282	0.3267	0.3245
α_{CV}	0.8294	0.8289	0.8419
β_{CV}	0.3832	0.3811	0.3706

As demonstrated by the vast majority of the test results discussed so far, the variability of the withdrawal strength of screws situated in solid timber (which means $N = 1$), $f_{ax,1}$ appears to be somewhat higher than that of ρ_1 . Assuming, that this additional dispersion, further denoted as $\text{CV}[\varepsilon_1]$, is independent from N , the corresponding consideration can be qualitatively illustrated as follows:

$$\text{CV}[f_{ax,N}] = \text{CV}[\rho_N] + \text{CV}[\varepsilon_1]. \quad (5.69)$$

In case of $Y = \ln(X) \sim \text{ND}(\mu_y, \sigma_y)$, $X_2 = \rho \sim 2\text{pLND}$, both parameters μ_y and σ_y of $X_{1,N} = f_{ax,N} \sim 2\text{pLND}(\mu_{y,N}, \sigma_{y,N})$ are given as

$$\mu_{y_{1,N}} = \ln\left(\frac{\mu_{X_{1,N}}}{\sqrt{\text{CV}^2[X_{1,N}] + 1}}\right) = \ln\left(\frac{\mu_{X_{1,N}}}{\sqrt{(\text{CV}^2[X_{2,N}] + 1) \cdot K}}\right), \quad (5.70)$$

and

$$\sigma_{y_{1,N}} = \sqrt{\ln(\text{CV}^2[X_{1,N}] + 1)} = \sqrt{\ln(\text{CV}^2[X_{2,N}] + 1) + \ln(K)}, \quad (5.71)$$

with

$$K = \frac{\text{CV}^2[X_{1,1}] + 1}{\text{CV}^2[X_{2,1}] + 1} = \frac{k_{CV}^2 \cdot \text{CV}^2[X_{2,1}] + 1}{\text{CV}^2[X_{2,1}] + 1}, \text{ and } k_{CV} = \frac{\text{CV}[X_{1,1}]}{\text{CV}[X_{2,1}]} \quad (5.72)$$

Hereby, the k -factor k_{CV} as the ratio between $\text{CV}[f_{ax}]$ and $\text{CV}[\rho]$ in case of $N = 1$. Taking eq. (5.70) and (5.71) into account, the 5 %-quantile of f_{ax} , in dependence of N and $\text{CV}[\rho_1]$, can be subsequently determined as follows:

$$x_{1,N,0.05} = \exp\left[\mu_{y_{1,N}} + \Phi^{-1}(0.05) \cdot \sigma_{y_{1,N}}\right]. \quad (5.73)$$

Presupposing $k_{CV} = 1.50$, which is a value commonly observed in practice for the perpendicular-to-grain insertion, Figure 5.37 illustrates the behaviour of $C = \{f_{ax,mean}, f_{ax,0.05}\}$, in dependence of $N = 1 \div 20$ and $\text{CV}[\rho_1] = \{6, 8, 10\} \%$. Therein, the mean, as well as the 5 %-quantile value of withdrawal strength, can be observed increasing with increasing N in a degressive way. Referencing both parameters to each value given for $N = 1$, it can be shown, that the magnitude of this increase decreases with decreasing $\text{CV}[\rho_1]$, a smaller variability of density has thus a minor pronounced impact on the withdrawal strength of screws, situated in homogenised material. In fact, this approach composed by eqs. (5.68), (5.70), (5.71) and (5.73) is too complex for a manual calculation. Thus, Table 5.23 subsequently comprises the determined values for $k_{sys,mean}$ and $k_{sys,k}$ (ratio between $x_{1,N,0.05}$ and $x_{1,1,0.05}$) for a practically relevant bandwidth of N . Thereby, following the recommendations in Brandner (2013b), $\text{CV}[\rho_1]$ is constantly set to 8 %.

Table 5.23: Values for $k_{sys,mean}$ and $k_{sys,k}$ in dependence of N ; according to Ringhofer et al. (2015b)

N	1	2	3	4	5	6	7	8	9	10
$k_{sys,mean}$	1.00	1.05	1.07	1.09	1.10	1.11	1.12	1.12	1.13	1.13
$k_{sys,k}$	1.00	1.06	1.10	1.12	1.13	1.14	1.15	1.15	1.17	1.17

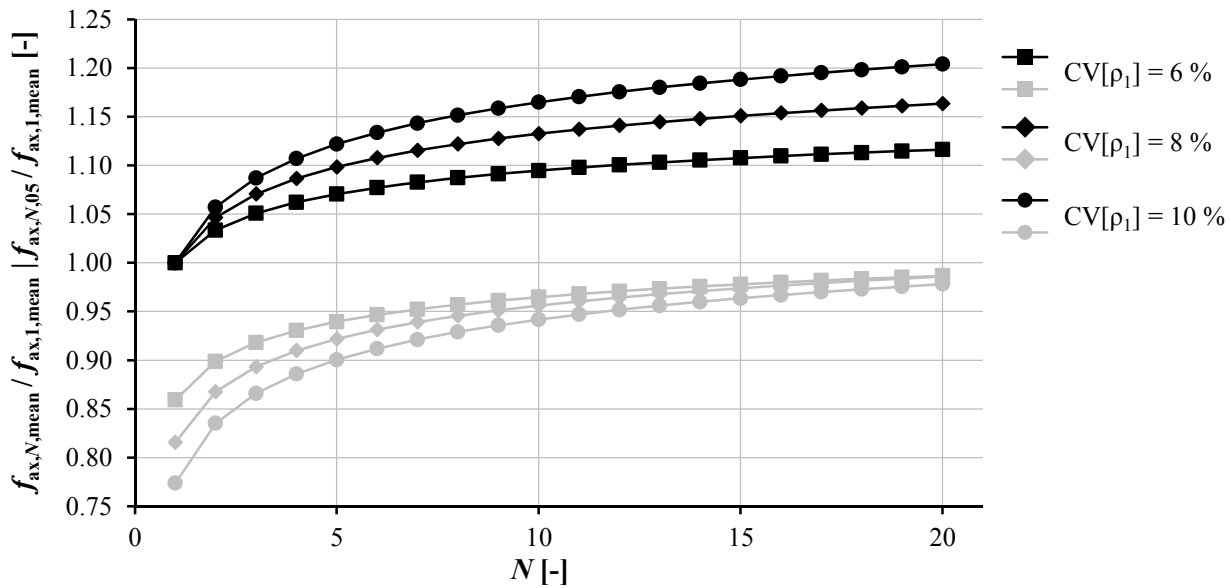


Figure 5.37: Behaviour of mean (black) and 5%-quantile (grey) values of $f_{ax,N}/f_{ax,1}$ in dependence of N and $CV[\rho_1]$ for $k_{CV} = 1.5$; according to Ringhofer et al. (2015b)

Taking the discussion made so far into account, N is considered as exclusively influencing the screw withdrawal properties, while the additional lay-up parameters, such as the layer thickness (ranging between $t_1 = 6 \div 45$ mm) and orientation are regarded as negligible. The main reason therefore are observations made in the frame of related experimental campaigns, as presented in the following subsection.

5-3.3.2 Experimental programme

The test programme, focusing on the impact of the number of penetrated layers N and their orientation (unidirectional vs. orthogonal oriented) on the screw withdrawal properties, was carried out in the frame of altogether four campaigns, subsequently denoted as {A, B, C, D} in Table 5.24. Worth mentioning, that all of them were conducted as parts of student's projects or master's theses at Graz University of Technology. For more detailed information see Reichelt (2012), Bratulic (2012) and Ringhofer et al. (2013). In general, all layered timber specimen considered were produced by the Institute of Timber Engineering and Wood Technology at Graz University of Technology. The basic material therefore were boards of Norway spruce (*Picea abies*), split up to small sections, randomly distributed, glued together and inserted into a hydraulic press. In case of series A \div C, the corresponding illustrations are given in Annex B-3.1, Figure B.24 to Figure B.26. The series D was also part of the investigations concerning the moisture content variation and its impact on the withdrawal properties, c. f. section 5-3.2, related timber specimen are thus illustrated in Figure B.19 (right). Here, the reference group with $u = 12\%$ is again considered for the assessment.

With regard to test series A, given in Table 5.24, the main idea behind this programme was not only to experimentally determine the impact of varying $N = \{3, 6, 20\}$ on withdrawal properties, but also that of the layer orientation (GLT vs. CLT), as well as a possible influence on these relationships if diameter $d = \{8, 12\}$ mm or pre-drilling (yes, no) are varied. Since the distribution of the basis material's density did not fulfil the requirements for a classification as ND or 2pLND, it was split up into two density groups with significantly different mean values but a similar variability, c. f. Reichelt (2012).

In the frame of series B, as the second comprehensive test programme concentrating on the layer effect, the aim was (a) to verify the outcomes of series A and (b), to determine the related impact if screws are inserted in inhomogeneous GLT lay-ups. As illustrated in Annex B-3.1, Figure B.25, three main subseries, denoted as B.0 (homogeneous lay-up as a reference), as well as B.1 and B.2 (varying number and positions of high density layers) were therefore considered. Equal to D, series C was originally conducted for a different purpose, the two subseries, included in Table 5.24, are thus an extract of a test programme, which is detailed discussed in section 5-4.3 and herein solely considered for the model verification.

Table 5.24: Overview of test series dedicated to the impact of general lay-up parameters

series	general information					test conditions			
	no. of subseries [-]	N [-]	t_1 [mm]	layer orientation [-]	d [mm]	d_{PD} [mm]	l_p [mm]	l_{ef} [mm]	l_{emb} [mm]
A	36	3, 6, 20	40, 20, 6	GLT, CLT	8, 8, 12	0, 5, 7	120	120	0
B	15	1, 2, 1, 10	15	GLT	10	0	15, 30, 15, 150	15, 30, 15, 150	0
C	2	5	12, 20	CLT	8, 12	0	60, 100	60, 100	0
D	1	3	34	CLT	8	5	102	102	0

With regard to the test conditions, given in Table 5.24, all series A ÷ D were conducted with screws inserted through the specimen, l_p is thus equal to l_{ef} . Furthermore, in addition to series A, also specimen of series D were pre-drilled in advance. Table 5.25 supplements the information concerning the test procedure in form of thread characteristics, dedicated to the screw types applied.

Table 5.25: *Thread characteristics applied for the experimental campaigns focusing on the impact of general lay-up parameters*

d_{nom} [mm]	d [mm]	η [-]	p [mm]	v^* [°]
8	8.02	0.65	3.54	
10	9.95	0.61	4.53	40
12	12.0	0.61	6.12	

* values taken from the product information related

Worth mentioning, that all tests have been performed on the test rig LIGNUM-UNI-275. In contrast to series {A, B, D}, which were carried out with the standard push-pull configuration, illustrated in Figure 5.4, for withdrawal tests of series C a so-called push-pile configuration with two $d = 8$ mm screws, reversely inserted in the specimen and acting as supporting, instead of the steel plate, was applied, c. f. Figure B.26 in Annex B-3.1. For enabling an exact position, both supporting screws were inserted after pre-drilling ($d_{\text{PD}} = 5$ mm). In addition, the whole programme was carried out without a local way measurement. Nevertheless, a relative comparison of both properties, $K_{\text{ser,ax}}$ and D , in-between series A, where boundary conditions, such as the axis-to-grain angle, the outer thread diameter, the specimen dimensions, as well as the test configuration were kept constant, seems possible. Further background information, regarding test execution, post-processing, property determination and data assessment is summarised in section 5-1.2.

5-3.3.3 Results and discussion

Distributions, confidence intervals and error bars of the statistical parameters for the small scale specimen densities ρ_{12} , dedicated to both experimental campaigns A and B, are subsequently illustrated in Figure 5.38 and Figure 5.41 in dependence of timber product, density group (in case of A) and number of penetrated layers N . The supplemental information is also including the determined density parameters for campaign C, as well as related moisture contents, given in Annex B-3.2, Table B.26 to Table B.28. The corresponding results for programme D can be found in Table B.22, line 2.

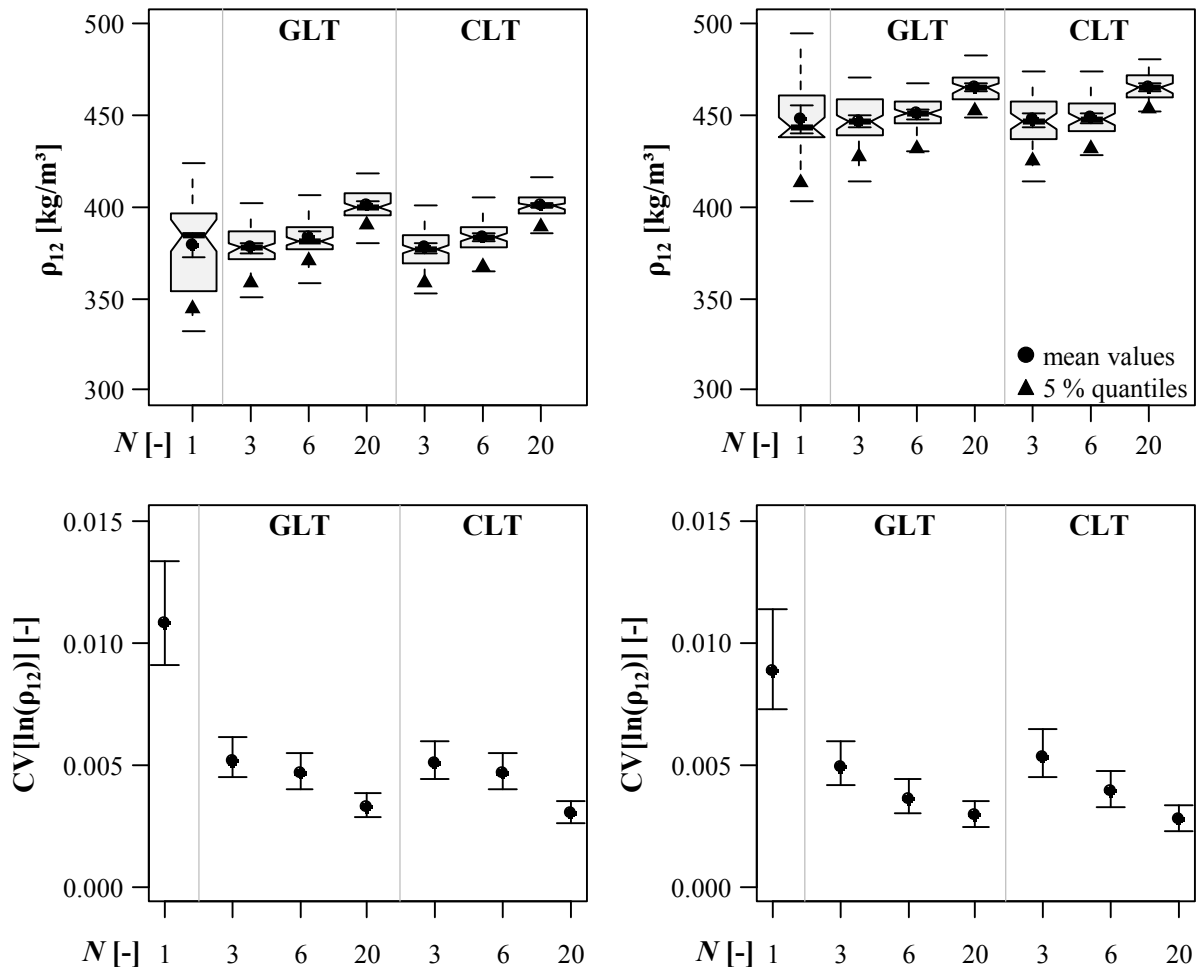


Figure 5.38: Above: boxplot graphic of densities ρ_{12} ; below: CIs of $CV[\ln(\rho_{12})]$ in dependence of timber product, density group and number of penetrated layers; left: group 1G; right: group 2G; series A

Apart from two extreme values, shown in Table B.26 and Table B.27 (each at line 1), the moisture content locations are similar and vary in a bandwidth of roughly $\pm 2\%$. A possible and unwanted influence of u on f_{ax} can thus be excluded. With regard to the density distribution, the test series A and B have to be separately discussed. Beginning with test programme A, irrespective from layer orientation and density group, a pronounced decrease of $CV[\rho_{12}]$, combined with an increase of the density's 5%-quantile $\rho_{12,05}$ with increasing N , is given. In addition, significantly higher average densities of specimen with $N = 20$ if compared to those with $N = \{1, 3, 6\}$ can be observed. The latter effect contradicts theoretical assumptions of the density homogenisation, as outlined in eq. (5.64) and (5.65), which presupposes the equality of mean values at varying N . Taking the ratio between the layer thickness $t_1 = \{40, 20, 6\}$ mm and the one of the adhesive films between the layers (about 0.1 mm) – which decreases from 400 to 60 with increasing N – into account, a therewith associated influence of the adhesive's weight on the specimen's density cannot be excluded for high values of N . Reichelt (2012) consequently recommends the related density correction of clear wood specimen in form of

$$m_{\text{corr}} = m - \Delta m(N - 1), \quad (5.74)$$

with m_{corr} as the specimen's corrected mass, m as its original mass and $\Delta m(N - 1)$ as the mass of all adhesive films in the specimen. Figure 5.39 and Figure 5.40 subsequently illustrate the distributions of the mean values and the 5 %-quantiles (error bars according to eq. (5.31) to (5.33)) of clear wood sample densities with and without the correction, given in eq. (5.74). Furthermore, the theoretical behaviour of $\rho_{12,05}$ in dependence of N , as approximated in eq. (5.65) (assumption of ND instead of 2pLND), is illustrated by the model bandwidths (grey areas), which take the 95 %-confidence interval of $\text{CV}[\rho_1]$ (values given in Table B.26), determined according to eq. (5.28), into account. Based on this comparison, a regressive behaviour of density corrected 5 %-values with increasing N can be observed, while mean values stay constant. Even though the model bandwidth slightly overestimates the given behaviour of $\rho_{12,05,\text{emp,corr}}$ for both density groups, the theoretical assumptions regarding the density homogenisation are principally confirmed. Furthermore, an unwanted influence of different locations of ρ_{12} , with varying N on withdrawal properties, can be excluded.

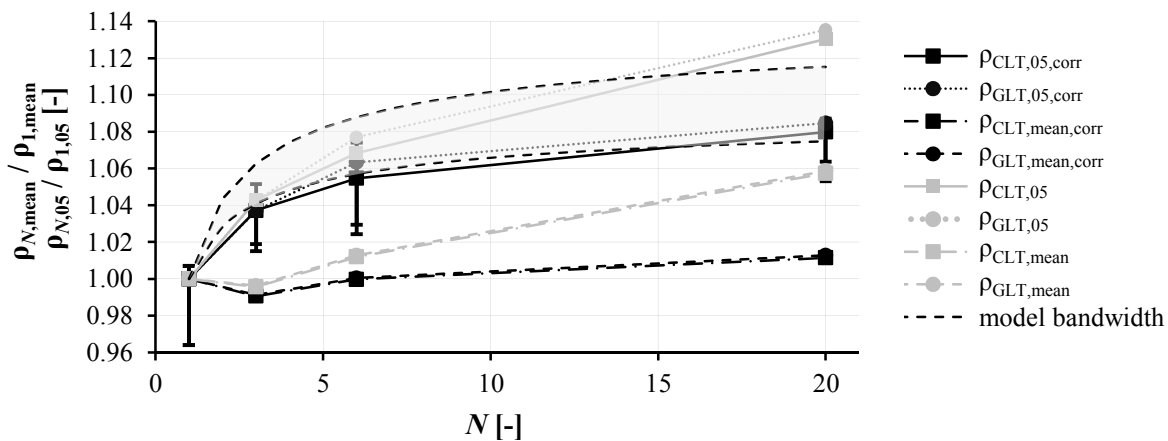


Figure 5.39: Corrected and uncorrected behaviour of timber density in dependence of N for density group 1G; according to Ringhofer et al. (2015b)

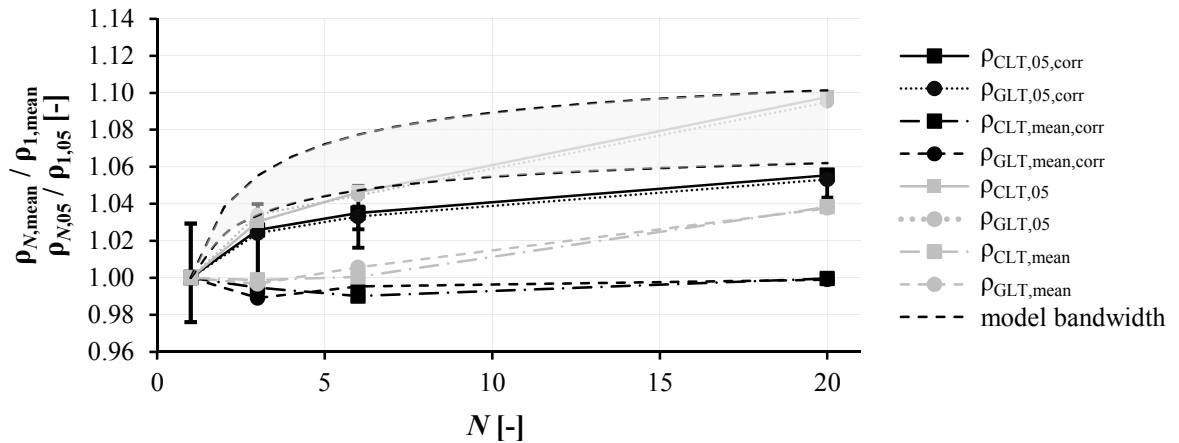


Figure 5.40: Corrected and uncorrected behaviour of timber density in dependence of N for density group 2G; according to Ringhofer et al. (2015b)

With regard to the densities ρ_{12} dedicated to the test programme B, given in Figure 5.41 and in Annex B-3.2, Table B.27, the following observations are worth being discussed: first, the significant difference of $CV[\rho_{12}]$ between $N = \{1, 2\}$ and $N = 10$, again confirms the theoretical considerations made in eq. (5.64). Second, comparing the results of groups B1 and B2, no remarkable deviations of the average densities are given. This is in fact surprisingly, since a different number of high density layers was applied for both inhomogeneous GLT lay-ups. Taking the related theoretical expectations (weighted average of $\rho_{12,mean}$ of subgroups B0.1 and B0.3) into account, c. f. Figure 5.41, B1-densities are found exceeding the target values to some extent. Nevertheless, the average values of ρ_{12} show only slight deviations in-between the specific subgroups B1.1 to B1.5. A corresponding influence on the withdrawal properties – at least on the mean value level – can therefore be neglected.

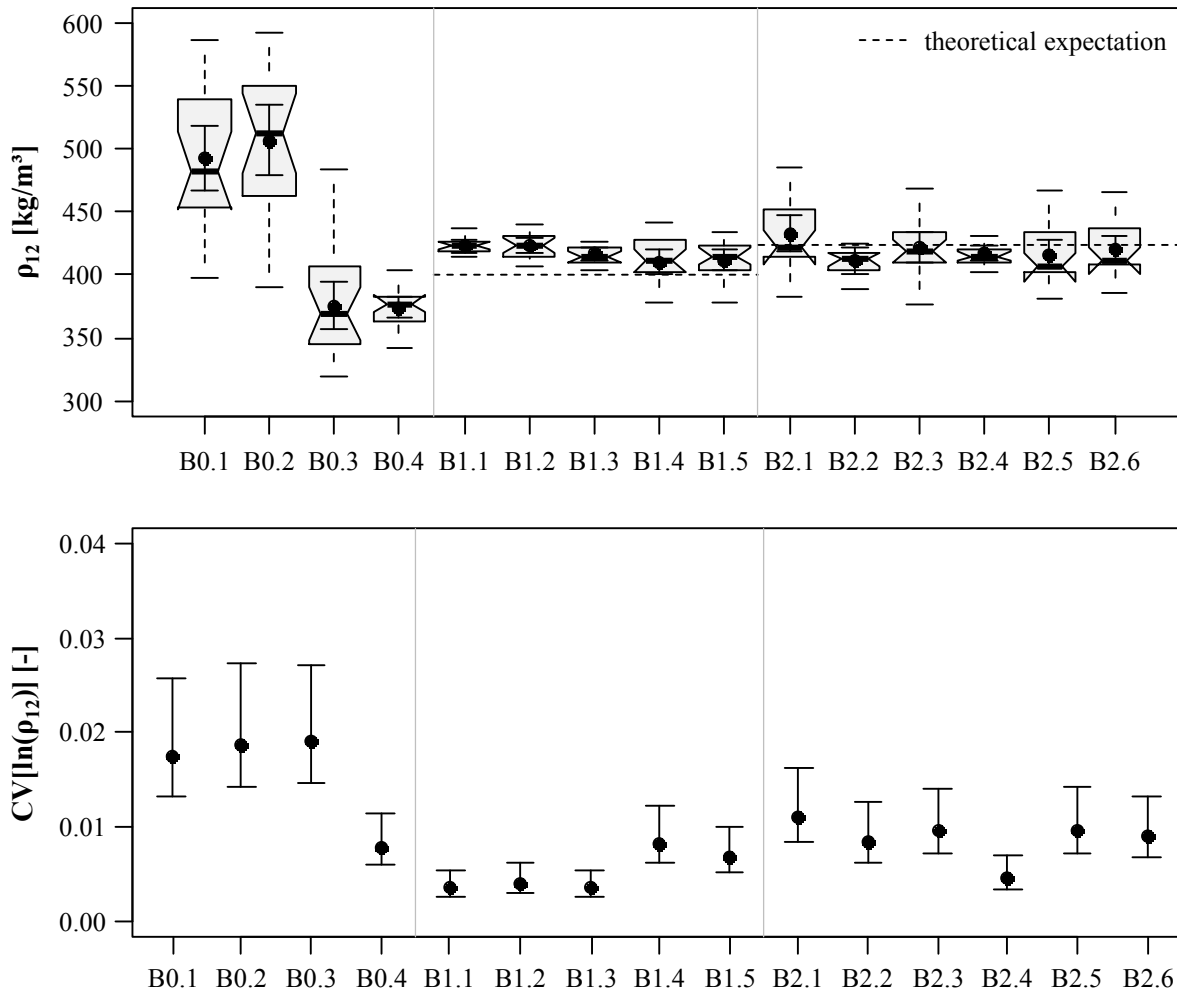


Figure 5.41: Above: boxplot graphic of densities ρ_{12} ; below: CIs of $CV[\ln(\rho_{12})]$ in dependence of the specific GLT lay-up; series B

Figure 5.42 to Figure 5.48, as well as Annex B-3.2, Table B.29 to Table B.32, subsequently include the determined withdrawal properties in dependence of the test programme and further parameters varied within the related campaigns, such as specimen lay-up, pre-drilling, outer thread diameter d and the number of penetrated layers N . A supplemental information regarding the properties' variability is given in Annex B-3.1, Figure B.27 to Figure B.33. Again, a separate discussion of the gained results of programme A and B seems to be appropriate:

With regard to A (note: from now on, there is no differentiation between density group 1G and 2G), starting with the withdrawal strength, a clear – considering the real distance between $N = \{3, 6, 20\}$ in Figure 5.42 and Figure 5.43 – regressive increase of f_{ax} with increasing N , not only for the 5 %-quantiles, but also for the mean values, can be observed. As highlighted before, the latter effect has to be seen as a main reason for the previously discussed theoretical modelling. Worth mentioning, that the given behaviour is not influenced to a certain extent by further varied parameters such as layer orientation, outer

thread diameter and pre-drilling. Beside the number of penetrated layers, also layer orientation is a relevant parameter for screw insertion in laminated timber members. Comparing the withdrawal strength determined in GLT and CLT specimen, slightly higher values for $f_{ax,mean}$ and $f_{ax,05}$ in case of CLT insertion are given. Restricting the focus on the values of N being relevant for a practical application, the given differences are insignificant. Thus, a special treatment of withdrawal strength in dependence of the layer orientation is excluded from further considerations. With regard to pre-drilling, the corresponding measure obviously leads to slightly smaller withdrawal strengths – a detailed discussion can be found in section 5-4.2.

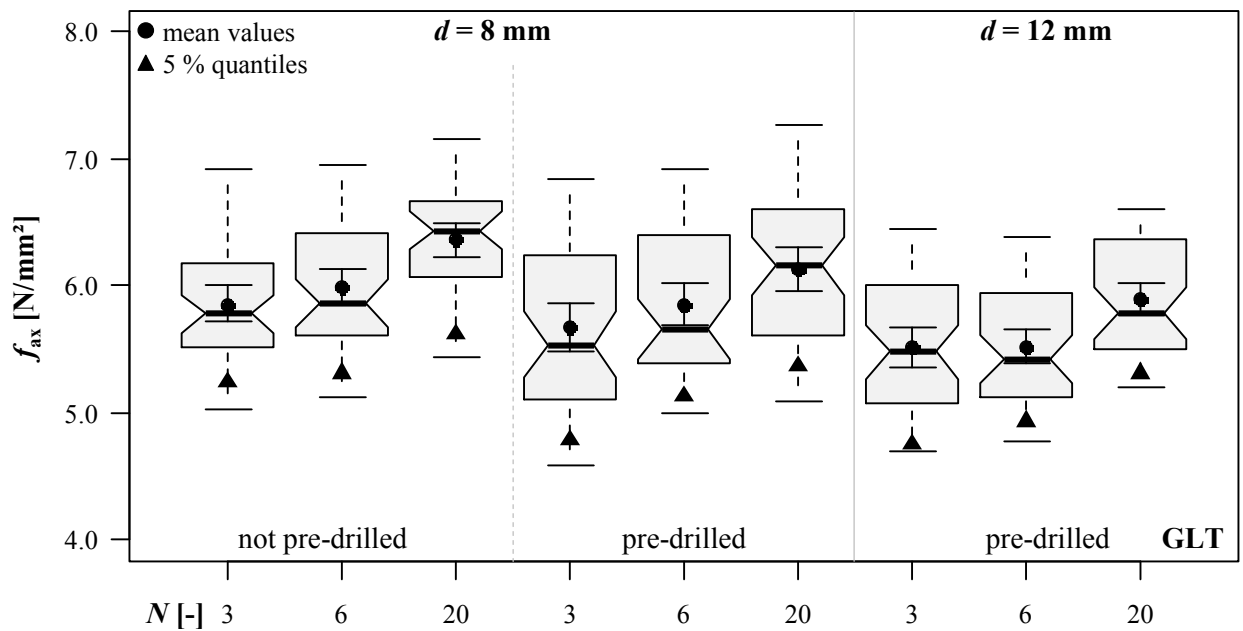


Figure 5.42: Boxplot diagrams of withdrawal strength vs. N in dependence of d and pre-drilling; test series A, GLT

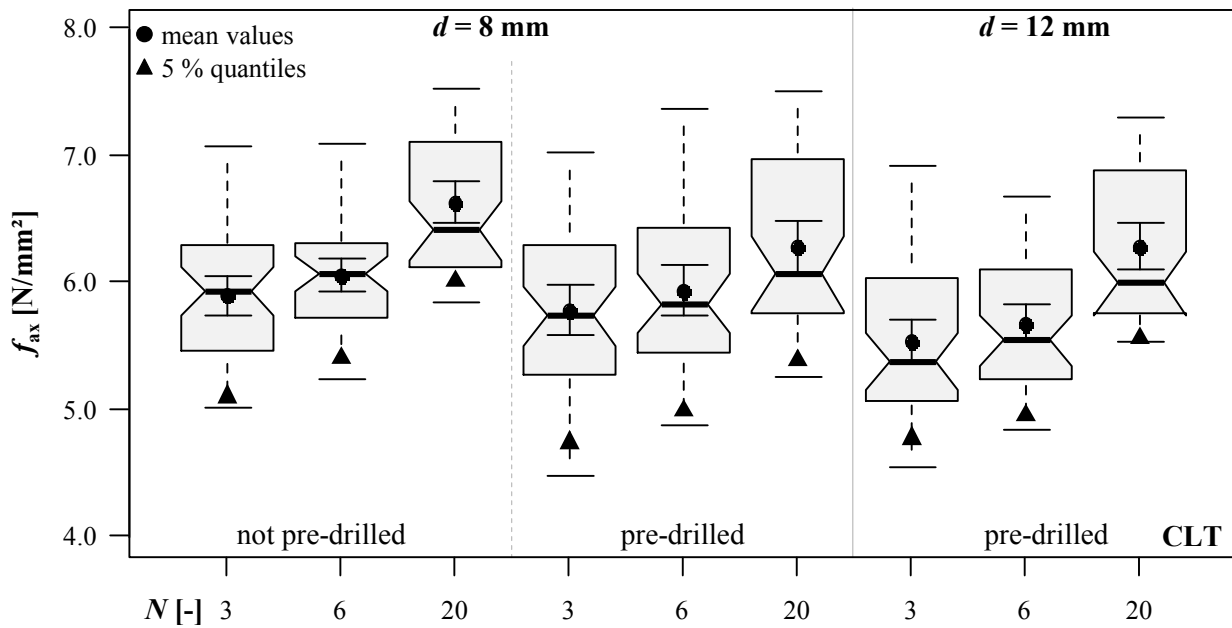


Figure 5.43: Boxplot diagrams of withdrawal strength vs. N in dependence of d and pre-drilling; test series A, CLT

Now focusing on withdrawal stiffness determined for all tests as parts of programme A. Overall and similar to the withdrawal strength, higher values of $K_{ser,ax}$ at higher N can be observed, which especially concerns the difference between $N = \{3, 6\}$ and $N = 20$. Nevertheless, the aforementioned regressive behaviour in dependence of the number of penetrated layers is comparatively less pronounced. A possible reason therefore may be the inaccuracy in determining $K_{ser,ax}$ (especially since no local displacements were recorded) if compared to withdrawal strength f_{ax} . With regard to the impact of layer orientation and pre-drilling, the conclusions made for the withdrawal strength (slightly higher values in case of CLT, smaller values as a consequence of pre-drilling) are also valid for the withdrawal stiffness.

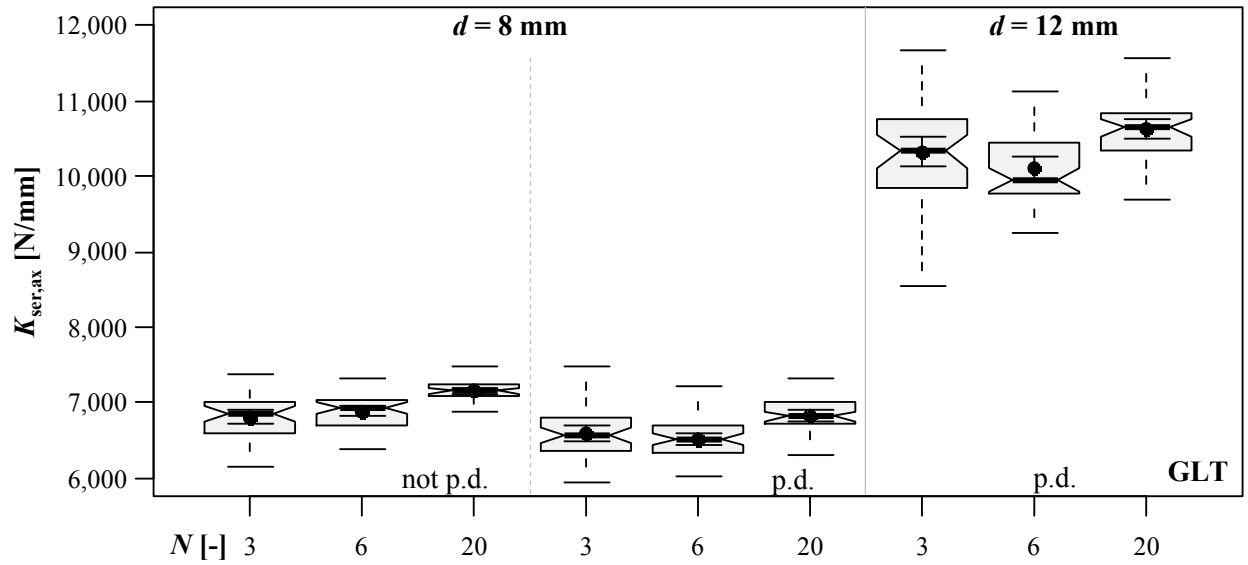


Figure 5.44: Boxplot diagrams of withdrawal stiffness vs. N in dependence of d and pre-drilling; test series A, GLT

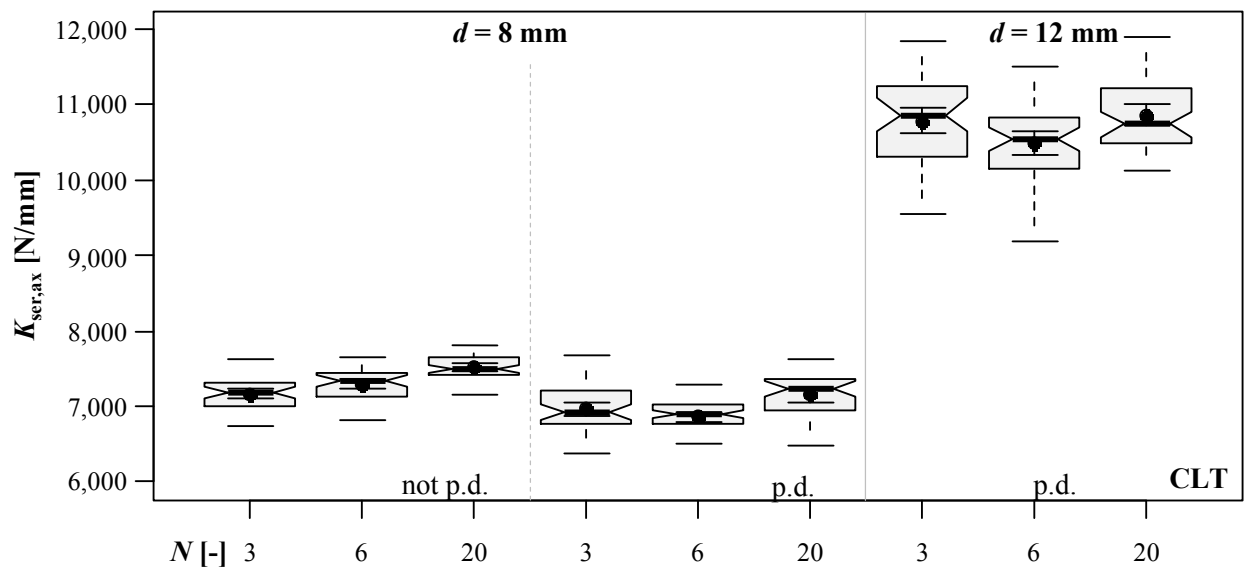


Figure 5.45: Boxplot diagrams of withdrawal stiffness vs. N in dependence of d and pre-drilling; test series A, CLT

Finally concentrating on the determined ductility D , as illustrated in Figure 5.46 and Figure 5.47: similar to the prior sections, either a behaviour oppositional to both other properties or no influence as a consequence of parameter variation can be observed. For instance, the values of D , dedicated to tests with pre-drilled specimen, are significantly higher than those where no pre-drilling was applied. Furthermore, apart from $N = 20$, $d = 8$ mm, not pre-drilled in CLT, the number of penetrated layers does not seem to influence ductility at all. The only exception is the impact of layer orientation, where again slightly higher values of D can be found for CLT if compared to GLT.

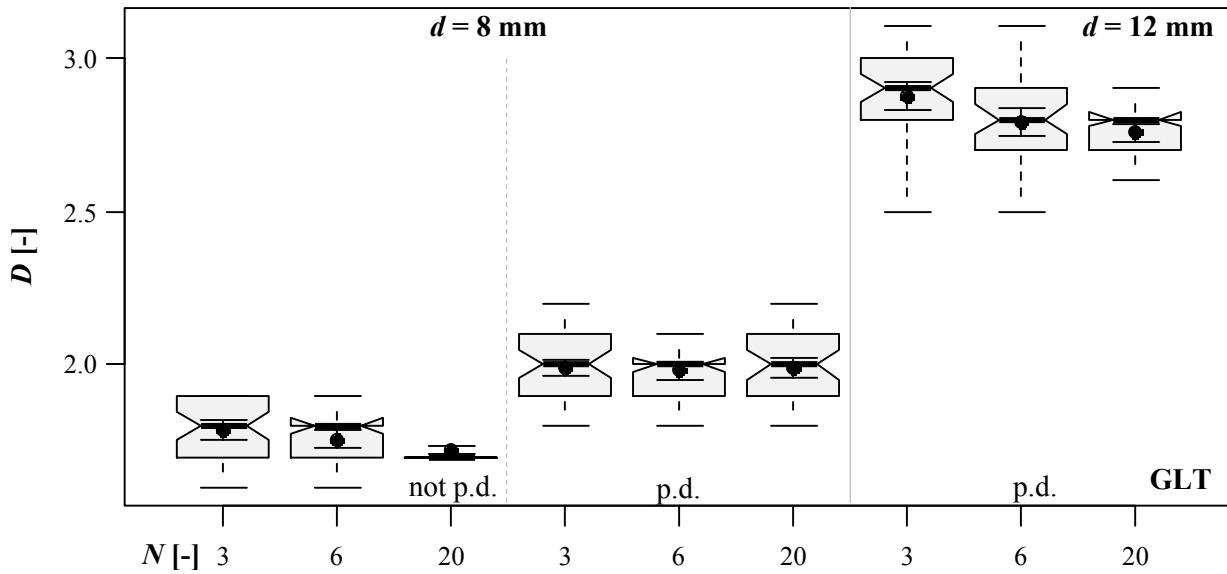


Figure 5.46: Boxplot diagrams of ductility vs. N in dependence of d and pre-drilling; test series A, GLT

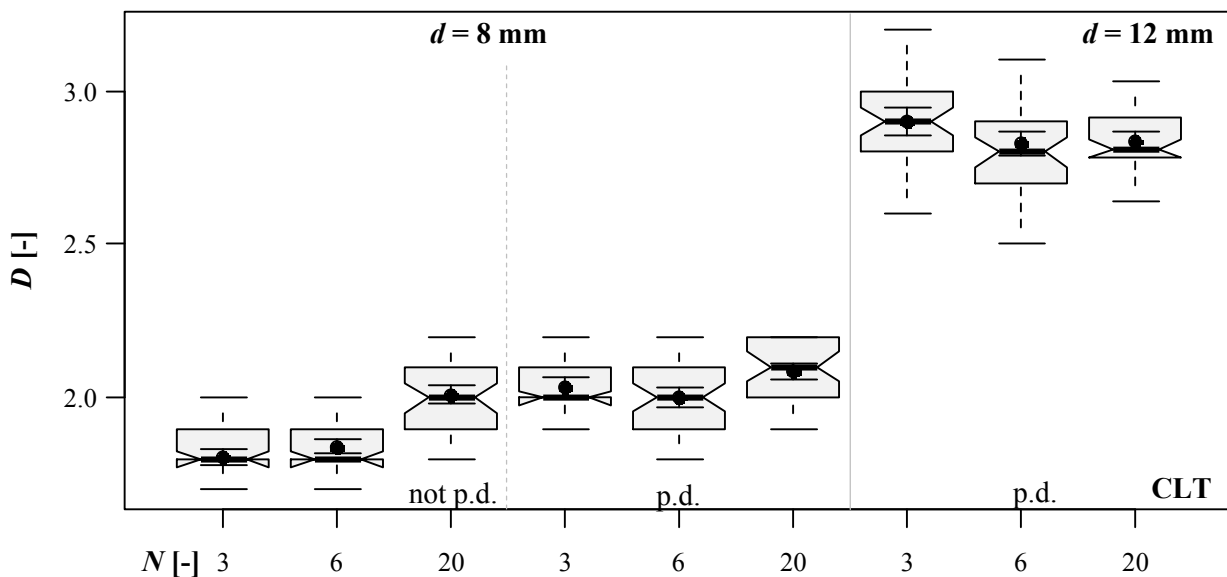


Figure 5.47: Boxplot diagrams of ductility vs. N in dependence of d and pre-drilling; test series A, CLT

The withdrawal strengths determined for test programme B are subsequently given in Figure 5.48 and Annex B-3.2, Table B.31 in dependence of N and the specific GLT lay-up. The two main conclusions are worth being discussed in detail: first, the results of group B0, comprising the examinations in homogeneous (reference) lay-ups, principally confirm the increase of $f_{ax,mean}$ and $f_{ax,05}$ with increasing N , compare subgroup B0.1 with B0.2, as well as B0.3 with B0.4. Second, the existence of high density layers in GLT lay-ups B1 and B2 generally leads to a (more or less pronounced) increase of f_{ax} if compared to the low density lay-up B0.4, while the specific position of these layers in the GLT specimen does not seem to affect the withdrawal strength at all. Even though the highest averages for f_{ax} are found

in subgroups dedicated to B2, the withdrawal strengths of both groups B1 and B2 result in a similar magnitude. This is probably caused by the minor difference of average densities related.

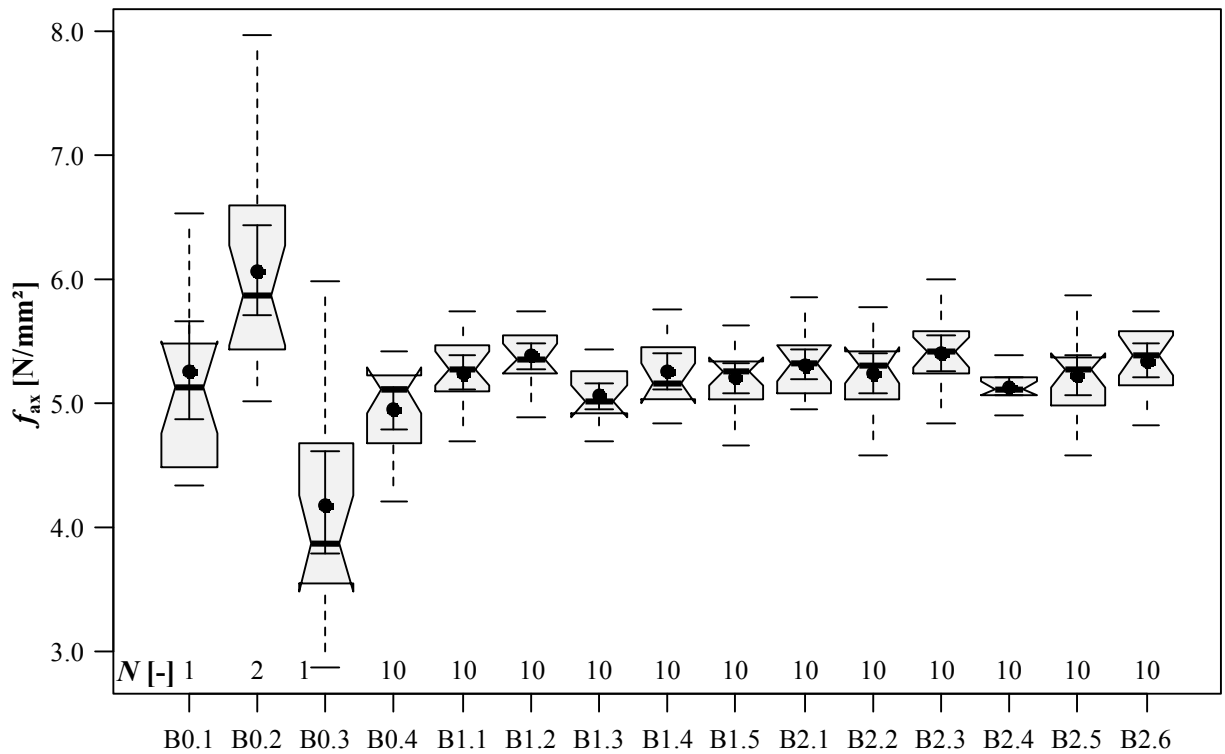


Figure 5.48: Boxplot diagrams of withdrawal strength vs. N in dependence of the specific GLT lay-up; test series B

5-3.3.4 Model verification

Within the last part of this section, the previously introduced stochastic model approach for covering the influence of N on f_{ax} is evaluated with the related experimental results. Taking a screw penetrating N layers into account, the corresponding system's mean withdrawal strength can be determined as follows:

$$f_{ax,N,\text{mean}} = f_{ax,1,\text{mean}} \cdot k_{\text{sys,mean}}(N), \quad (5.75)$$

with $k_{\text{sys,mean}}(N)$ according to Table 5.23. In case of the characteristic (5 %-quantile) values of the withdrawal strength, two possibilities for a determination are given. The first is similar to eq. (5.75) and bases on the experimentally determined characteristic (5 %-) withdrawal strength for $N=1$ as a reference value, see:

$$f_{ax,N,k} = f_{ax,1,k} \cdot k_{\text{sys,k}}(N), \quad (5.76)$$

again with $k_{\text{sys,k}}(N)$ according to Table 5.23. In contrast, the second possibility bases on the mean withdrawal strength for $N=1$ and includes the determination of $f_{ax,1,k}$ according to eq. (5.73), which

constitutes 2pLND and the ratio ξ between $CV[\rho_1]$ and $CV[f_{ax,1}]$, as expressed in eq. (5.72). Within this section it was decided to consider the latter procedure, comparing the experimentally determined withdrawal strengths with the model predictions. Beside further assumptions in form of $\xi = 1.50$ and $CV[\rho_1] = 8\%$, $f_{ax,1,mean}$ of test series, where no withdrawal tests in the reference material ($N = 1$) were examined (this concerns test campaigns A, C and D), the related value is approximated with the regression model published by Pirnbacher et al. (2009), c. f. eq. (5.38). Therefore, the average single layer densities ρ_{12} , in case of test series A and the ones, determined for the CLT lay-ups with $N = \{3, 5\}$, in case of test series C and D, are considered. For the inhomogeneous GLT lay-ups, as parts of series B1 and B2, which consist of two and four high density layers respectively, a “weighted” approach is applied in form of eq. (5.77), see:

$$f_{ax,N,mean} = \frac{N_{hd}}{N} \cdot f_{ax,1,mean,hd} \cdot k_{sys,mean}(N_{hd}) + \frac{N_{ld}}{N} \cdot f_{ax,1,mean,ld} \cdot k_{sys,mean}(N_{ld}), \quad (5.77)$$

where N_{hd} and N_{ld} are the number of high and low density layers in the specimen and $f_{ax,1,mean,hd}$ and $f_{ax,1,mean,ld}$ are both reference withdrawal strengths as results of series B0.1 and B0.3, c. f. Table B.31.

The comparison between the test results and the predicted values is subsequently given in Figure 5.49. Thereby, the statistical parameters of all in all 34 test series with $n_{tot} = 1,149$ results are considered. With regard to both illustrations, the following essential aspects are worth being discussed: the overall data trend, as represented by the partial regression lines, is well described. This especially concerns the mean values, shown in Figure 5.49 (left). In case of characteristic withdrawal strengths (Figure 5.49, right), the model estimations continuously underestimate the test results, leading to a slightly conservative, but qualitatively accurate, prediction. Even the prediction of the withdrawal strength in inhomogeneous GLT lay-ups results in smaller estimated than experimentally determined values, the application of eq. (5.77) seems to be appropriate for this purpose. Consequently, the theoretical model can be concluded as useful for determining the withdrawal strengths of axially loaded self-tapping screws, situated in at least more than one layer of laminated timber products.

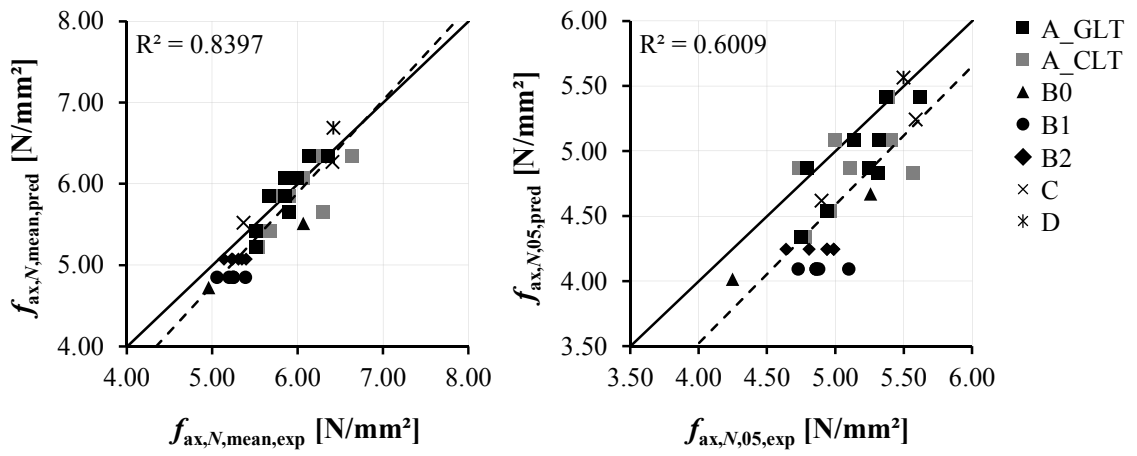


Figure 5.49: Experimental vs. predicted withdrawal strengths; left: mean values; right: 5 %-quantiles

5-3.4 Lamination – CLT production specifics

Note: a part of the test results this section bases on has already been published by Silva et al. (2014) and Brandner et al. (2017). As a co-author of these sources, the author of this thesis was responsible for the supervision of the related experimental programmes. The test results slightly deviate from the published ones since a different form of the outlier treatment is applied within this chapter.

5-3.4.1 Introduction and model approaches

Note: to simplify the following discussion, the screw axis is subsequently regarded as oriented perpendicular to the timber member's surface.

Concentrating on parameter type (ii), as outlined in Figure 5.36 (right), especially the production process of CLT, leading to its typical crosswise layered structure, necessitates a consideration of additional parameters, possibly influencing screw withdrawal properties. They are (a) the impact of screw insertion exactly in the transition of two neighbouring layers with different axis-to-grain angles ($\alpha_1 = 0 \div 90^\circ$, $\alpha_2 = 90 - \alpha_1$), (b) a varying ratio of screw outer thread diameter and layer thickness and (c) the existence, type and size of gaps or slots situated between (gaps) or within (slots) the layers. Since the corresponding effects are influenced by more than one parameter, it was decided to discuss topics (a) and (b) in section 5-4.3 (influence of α on withdrawal properties), while the following considerations exclusively concentrate on topic (c).

Beside the gap width w_{gap} as already discussed in section 4-4 and expressed in Figure 5.36 (right), further related parameters are the number of gaps penetrated by the screw, n_{gap} , as well as the gap type and the screw position with respect to the latter mentioned. The further discussion bases on Figure 5.50, which subsequently illustrates the selected possibilities of a screw insertion in the side and narrow face of CLT components.

In case of screws penetrating gaps in CLT narrow faces (Figure 5.50, right), n_{gap} can constantly be set to 1.0, while the gap type in combination with screw positioning may vary between “bed joints (BeJ)” (defined by $w_{\text{gap}} = 0 \text{ mm}$ and $\alpha = 0^\circ \mid 90^\circ$), “butt joints (BuJ)” (defined by $w_{\text{gap}} \geq 0 \text{ mm}$ and $\alpha = 0^\circ$) and “T-joints (TJ)” (defined by $w_{\text{gap}} \geq 0 \text{ mm}$ and $\alpha = 0^\circ \mid 90^\circ$). Worth mentioning, that Grabner (2013) originally introduced this denotation in analogy to the gap types defined for brickworks. Furthermore, the screw insertion in slots is quite equal to the one in gaps (butt joints or T-joints) but restricted to $\alpha = 0^\circ$. In case of screws situated or touching gaps in CLT side faces (Figure 5.50, left), n_{gap} varies between 1 and N , while the gap type, in combination with the screw positioning, exclusively occurs in form of “butt joints (BuJ)” – hereby defined by $w_{\text{gap}} \geq 0 \text{ mm}$ and $\alpha = 90^\circ$.

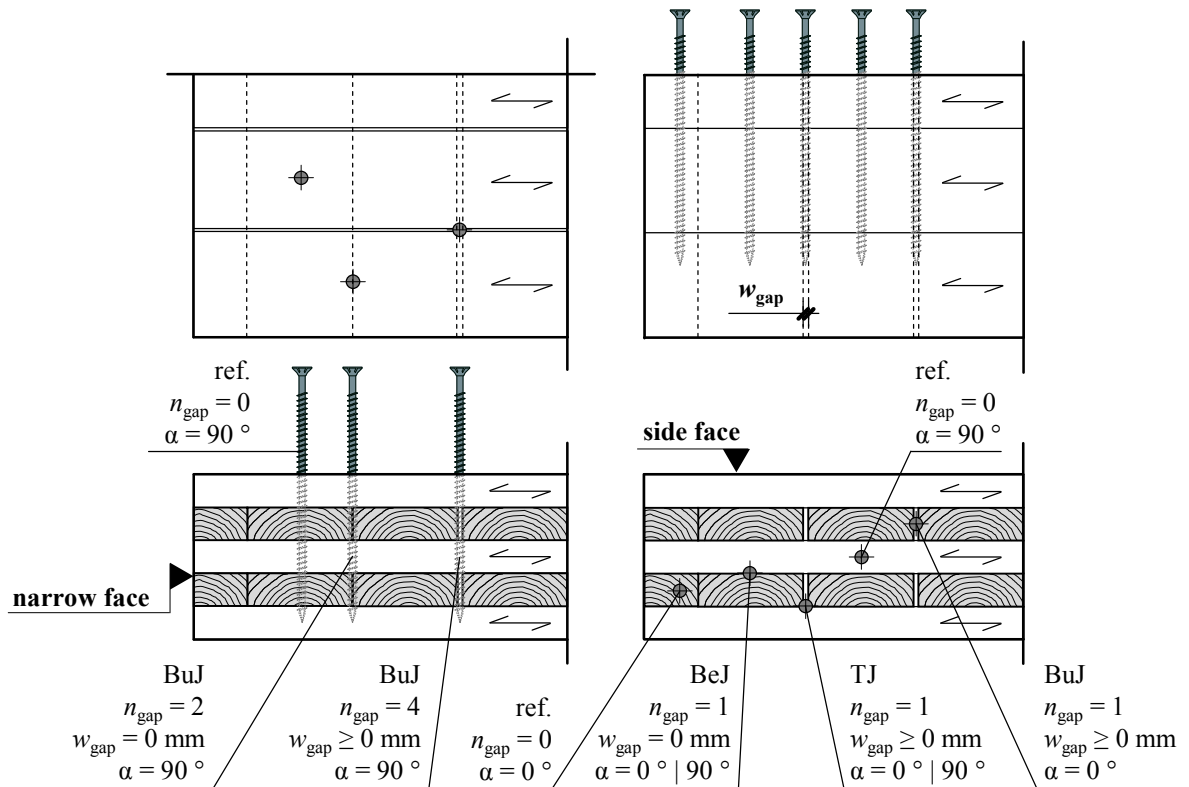


Figure 5.50: Screw insertion in CLT components with respect to specific product characteristics; left: side face insertion; right: narrow face insertion

Now the further focus is on the state-of-knowledge regarding the influence of these specifics on screw withdrawal properties. Apart from own investigations, as discussed in the following subsection, the paper presented by Uibel and Blaß (2007) on the basis of Blaß and Uibel (2007), is again worth to be highlighted. They were the first who concentrated on determining the withdrawal strengths of screws situated in CLT side and narrow faces. Beside the screw diameters, ranging between $d = 6 \div 12 \text{ mm}$, their parameter variation comprised $n_{\text{gap}} = \{1, 2, 3\}$ and gap type BuJ in CLT side face, as well as both BuJ and TJ in CLT narrow face, conducted with different CLT lay-ups.

Since the gap width w_{gap} was varied randomly from test to test, with $w_{\text{gap}} = 0.5 \div 2.0 \text{ mm}$ in average, a discussion of a quantified impact of w_{gap} in combination with n_{gap} and the gap type on the screw withdrawal strength is not possible. Nevertheless, the majority of the test results, given in Blaß and Uibel (2007), indicates a qualitatively decreasing f_{ax} with increasing n_{gap} (CLT side face), as well as smaller f_{ax} in cases, when the screws are situated in BuJ or TJ (CLT narrow face). As expected, the screws penetrating TJ perform slightly better than those placed in BuJ, since a certain part of the screw thread is arranged in a gap-free layer with $\alpha = 90^\circ$. Uibel and Blaß (2007) subsequently considered these findings in eq. (5.66) by the pre-factor 1.5, which – as already discussed – additionally takes the density difference between the screw insertion in CLT side and narrow face into account.

In fact, apart from the work carried out at Graz University of Technology and the one published by Uibel and Blaß (2007), no further related investigations have been found in literature. In addition and with regard to the behaviour of withdrawal stiffness and ductility of screws situated in gaps or slots of CLT elements, no comparable examinations are given at all. Motivated by this lack of knowledge, two research projects, focusing on the impact of gap insertion on withdrawal properties of self-tapping screws, have been carried out at Graz University of Technology within the last years. The most important outcomes related are presented in the following subsections.

In advance, a simple mechanical approach in form of a reduction k -factor k_{gap} , quantifying the influence of gap specifics on the screw withdrawal strength, is demonstrated as follows: taking the definition of f_{ax} , determined as ratio of withdrawal force and the thread surface area, into account, c. f. eq. (5.1), the loss of the bearing capacity, as a consequence of gap insertion, is subsequently expressed by the loss of the thread surface area, see

$$\text{BuJ:} \quad f_{\text{ax,CLT,gap}} = f_{\text{ax,CLT,ref}} \cdot \frac{n_{\text{gap}}}{N} \cdot \left(k_{\text{gap}} - 1 + \frac{N}{n_{\text{gap}}} \right), \text{ and} \quad (5.78)$$

$$\text{TJ:} \quad f_{\text{ax,CLT,gap}} = 0.50 \cdot f_{\text{ax,CLT,ref},\alpha=90^\circ} + 0.50 \cdot f_{\text{ax,CLT,ref},\alpha=0^\circ} \cdot \frac{n_{\text{gap}}}{N} \cdot \left(k_{\text{gap}} - 1 + \frac{N}{n_{\text{gap}}} \right), \text{ and} \quad (5.79)$$

$$k_{\text{gap}} = \frac{C_{\text{red}}}{C_{\text{tot}}} = \frac{\varphi}{\pi} \text{ and } \varphi = \pi - 2 \cdot \arcsin\left(\frac{w_{\text{gap}}}{d}\right) \quad (5.80)$$

In eq. (5.80) C_{red} and C_{tot} are the reduced and total screw outer thread circumference, φ the half opening angle of the threaded part, which is embedded in the timber component (Figure 5.51), and $f_{\text{ax,CLT,ref}}$ are the reference withdrawal properties of the screws positioned in an equal manner in CLT but without penetrating gaps. For instance, in case of CLT side face application this means a screw penetrating N layers of gap-free material, in case of CLT narrow face application it is a screw situated in one layer at $\alpha = 0^\circ$ for BuJ or partially at $\alpha = 0^\circ$ and 90° for TJ. In Figure 5.51 BuJ and TJ, both possibilities with $w_{\text{gap}} > 0$ mm, are schematically illustrated. Worth mentioning, that in case of TJ, the reduced circumference solely concerns the layer with $\alpha = 0^\circ$. Thus, the corresponding effect is reduced to 50 %, c. f. eq. (5.80). Note: eq. (5.79) assumes an equal contribution of $\alpha = 0^\circ$ and 90° shares for determining the withdrawal strength of screws, situated in BeJ – a detailed discussion is given in section 5-4.3.

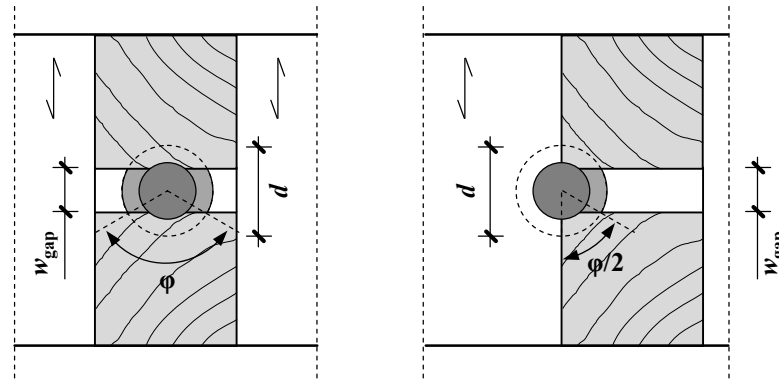


Figure 5.51: Screw insertion in gaps of CLT narrow face; left: BuJ; right: TJ

Finally Figure 5.52 illustrates the behaviour of k_{gap} for BuJ determined according to eq.(5.80) in dependence of outer thread diameter d and the gap width w_{gap} , both varying in practically relevant bandwidths, according to the corresponding technical documentations. In general, a progressive decrease of k_{gap} with increasing w_{gap} can be observed; furthermore the related impact decreases with increasing d .

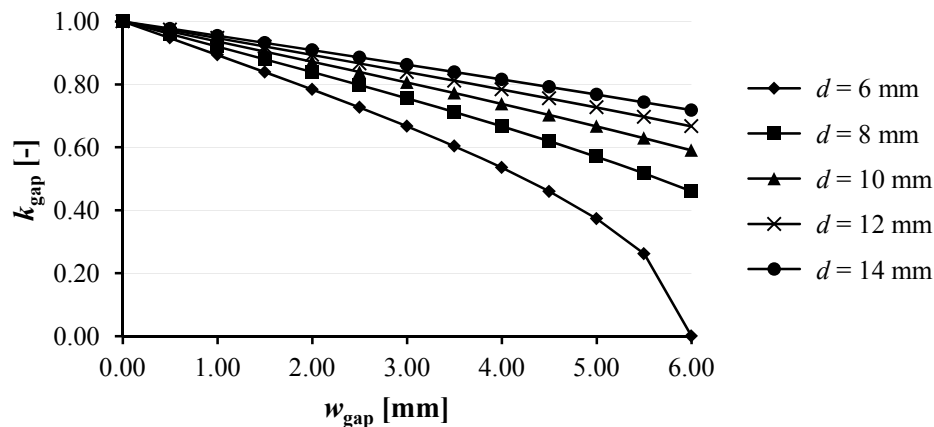


Figure 5.52: Behaviour of k_{gap} for screw insertion in BuJ in dependence of d and w_{gap} ($n_{\text{gap}} = N = 1$)

5-3.4.2 Experimental programme

As outlined in Table 5.27, the test programme, concentrating on the influence of gap specifics (n_{gap} , w_{gap} , gap type) on withdrawal properties of self-tapping screws situated in CLT side and narrow face, has been carried out in the frame of two experimental campaigns. Thereby, test campaign I, conducted by Grabner (2013), focused on the CLT narrow face screw insertion, while test campaign II, as part of an international research cooperation, c. f. Silva et al. (2014), was aimed to gain properties in case of screws situated in the CLT side face.

Again, all considered layered timber specimen were produced by the Institute of Timber Engineering and Wood Technology at Graz University of Technology. In fact, the production process is comparable to the one dedicated to the layer effect – related details can be found in Grabner (2013) and Silva et al. (2014).

The applied screw types are given in Table 5.6 for test campaign I, $d = 8$ mm, in Table 5.26 for test campaign I, $d = 12$ mm and in Table 5.25, line 1 in case of test campaign II.

Table 5.26: Thread characteristics of the $d = 12$ mm partially threaded screw applied for test campaign I

d_{nom} [mm]	d [mm]	η [-]	p [mm]	v^* [°]
12	11.6	0.62	6.57	40

With regard to the corresponding parameter variation, the investigation, which was carried out by Grabner (2013), considered all possible gap types in CLT narrow faces, c. f. Figure 5.51 with varying $w_{\text{gap}} = \{0, 2, 6\}$ mm and $d = \{8, 12\}$ mm. Worth mentioning, that the related upper limit of w_{gap} corresponds to the recommendation given in ON EN 16351 (2015). Furthermore, it was aimed to cover the different screw positions with respect to the CLT cross-section, realised by the screw insertion in CLT outer layers (top layers, TL), middle layers (ML) and cross layers (CL), c. f. Annex B-3.1, Figure B.34. Based on the findings made by Grabner (2013), considering the relationship between w_{gap} and d_{PD} , the variation of w_{gap} in the frame of test campaign II was reduced to $\{0, 4\}$ mm, while the number of penetrated gaps in the 3-layered CLT lay-up, illustrated in Annex B-3.1, Figure B.35, was varied from $n_{\text{gap}} = 1 \div 3$. To guarantee an exact screw positioning, with respect to the specific gap configuration, all specimen were pre-drilled in advance.

Table 5.27: Overview of test series dedicated to the impact of CLT production specifics

general information					test conditions				
series	no. of subseries	n_{gap}	w_{gap}	gap type	d_{nom}	d_{PD}	l_p	l_{ef}	l_{emb}
	[-]	[-]	[mm]	[-]	[mm]	[mm]	[mm]	[mm]	[mm]
I	32	1	ref, 0, 2, 6	ref, BeJ, BuJ, TJ	8	5	80	70.6	0
					12	7	120	106.0	0
II	9	1, 2, 3	ref, 0, 4	ref, BuJ	8	5	102	102	0

Worth mentioning, that all tests have been performed on the test rig LIGNUM-UNI-275, following the standard procedure, discussed in section 5-1.2. In case of test campaign I and $d = 8$ mm, local displacements were recorded, enabling a determination of both properties $K_{\text{ser,ax}}$ and D . In case of test campaign II, tests were carried out without a local way measurement. Nevertheless, a relative comparison of both parameters is also possible, since the related boundary conditions, such as axis-to-grain angle, outer thread diameter, specimen dimensions, as well as the test configuration were kept constant. Further background information regarding test execution, post-processing, property determination and data assessment is summarised in section 5-1.2.

5-3.4.3 Results and discussion

The boxplot and error bar graphics of the small scale specimen's timber density ρ_{12} , dedicated to both experimental campaigns I and II, are subsequently illustrated in Figure 5.53 to Figure 5.55, while the supplemental information regarding the related statistical parameters and moisture contents u are given in Annex B-3.2, Table B.33 to Table B.35.

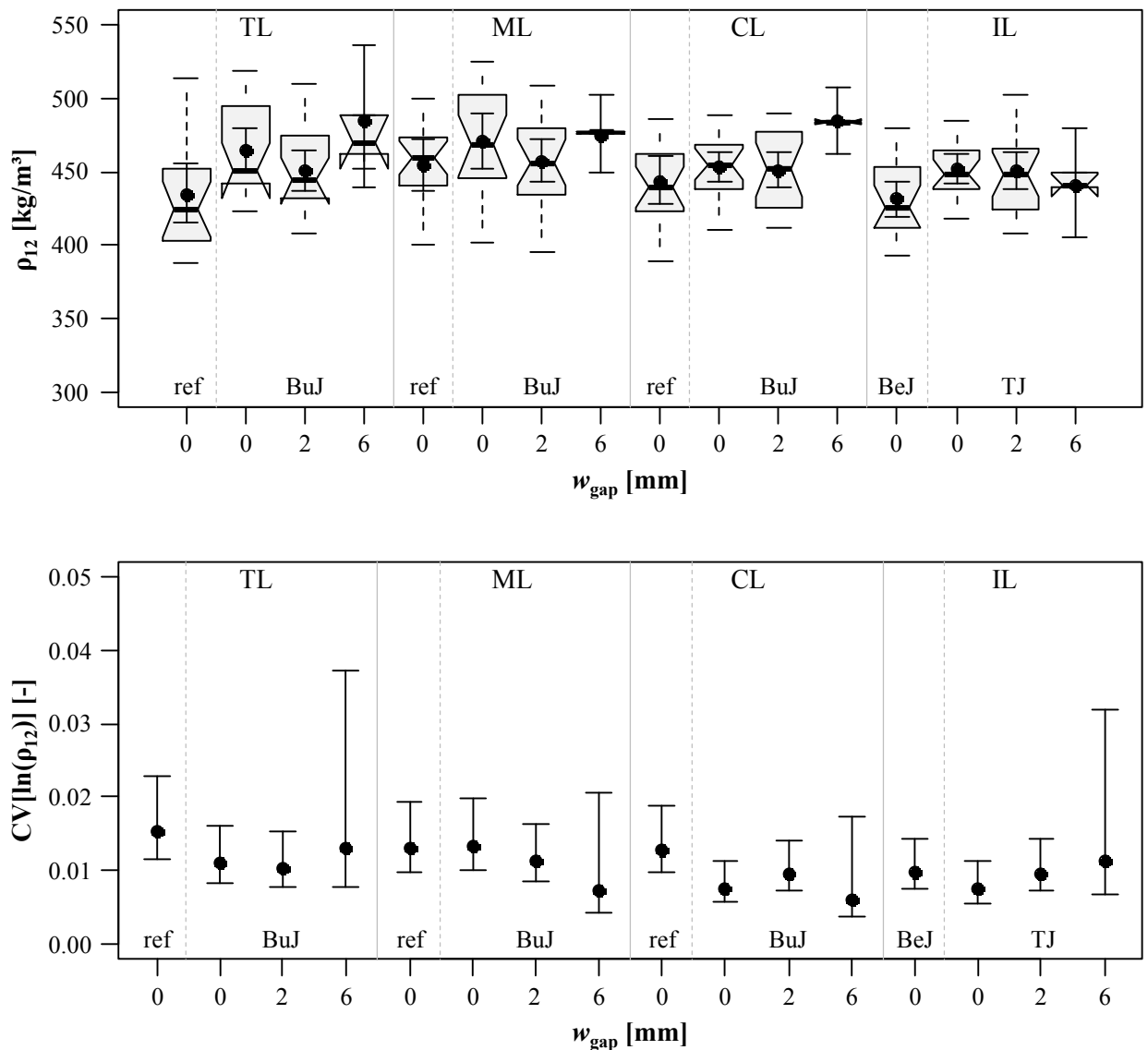


Figure 5.53: Above: boxplot graphic of densities ρ_{12} ; below: CIs of $CV[\ln(\rho_{12})]$ in dependence of gap type and width; test programme I, $d = 8 \text{ mm}$

All determined moisture contents are similar in average and vary in the target bandwidth of roughly $\pm 2 \%$, which excludes a possible influence on the withdrawal properties. With regard to the density, the results of test series I significantly vary in-between both subgroups as separated by $d = \{8, 12\} \text{ mm}$, c. f.

Figure 5.53 and Figure 5.54. To avoid an unwanted density-dependent influence on the withdrawal properties, the corresponding results of $X = \{f_{ax}, K_{ser,ax}\}$ were corrected as follows:

$$X_{corr,i} = X_i \cdot \frac{\rho_{ref}}{\rho_i}, \quad (5.81)$$

with ρ_{ref} as the reference density (here: $\rho_{ref} = 450 \text{ kg/m}^3$, rounded overall average of ρ_{12}) and ρ_i as the ρ_{12} -density associated to X_i . In case of the ductility no significant dependency on density was observed, c. f. section 5-3.1. Thus, no comparable treatment was performed for this property. In case of test series II, neither the determined values of ρ_{12} in Table B.35, nor the graphical illustrations, given in Figure 5.55, indicate a possible influence of this parameter on the withdrawal properties.

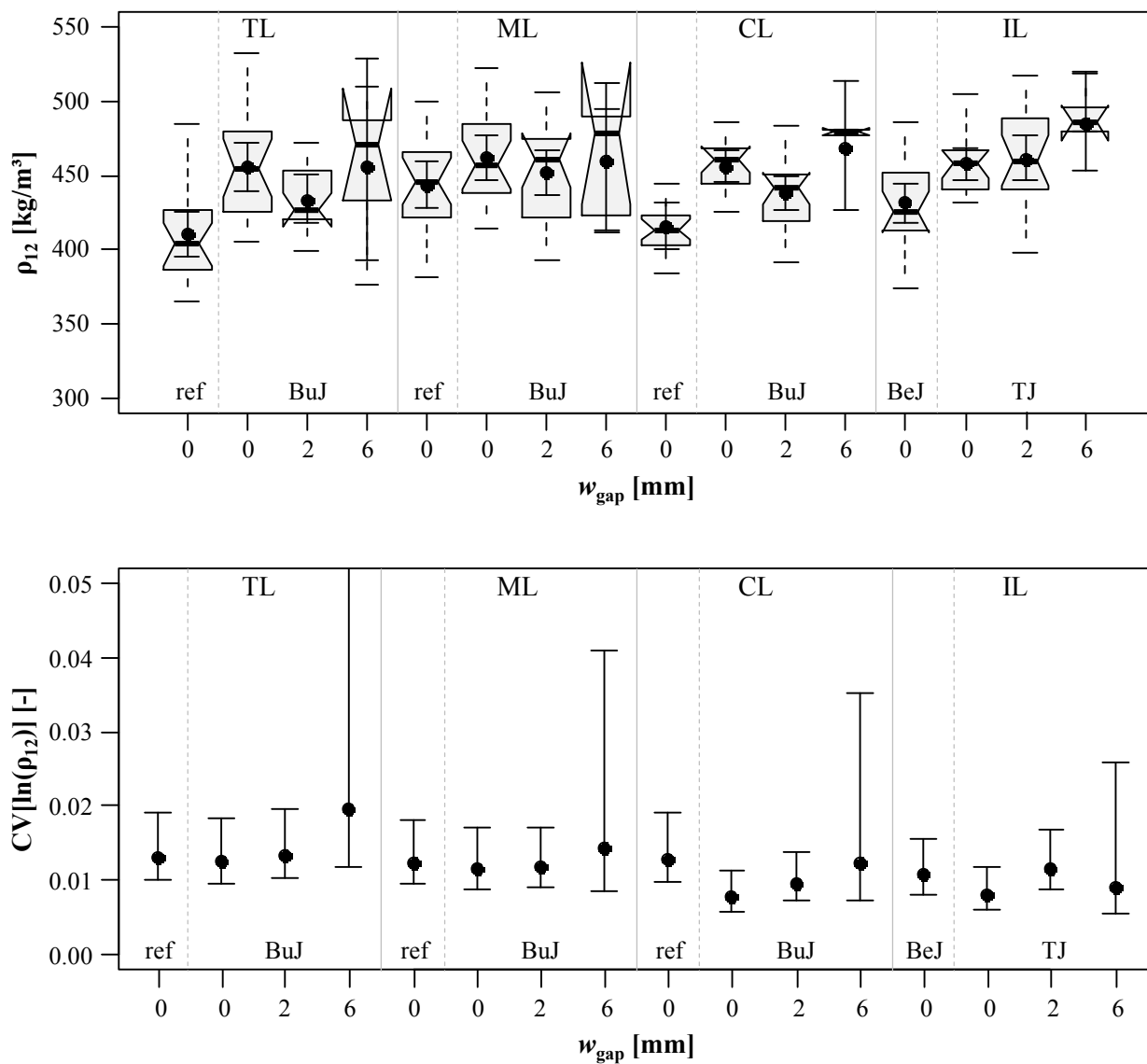


Figure 5.54: Above: boxplot graphic of densities ρ_{12} ; below: CIs of $CV[\ln(\rho_{12})]$ in dependence of gap type and width; test programme I, $d = 12 \text{ mm}$

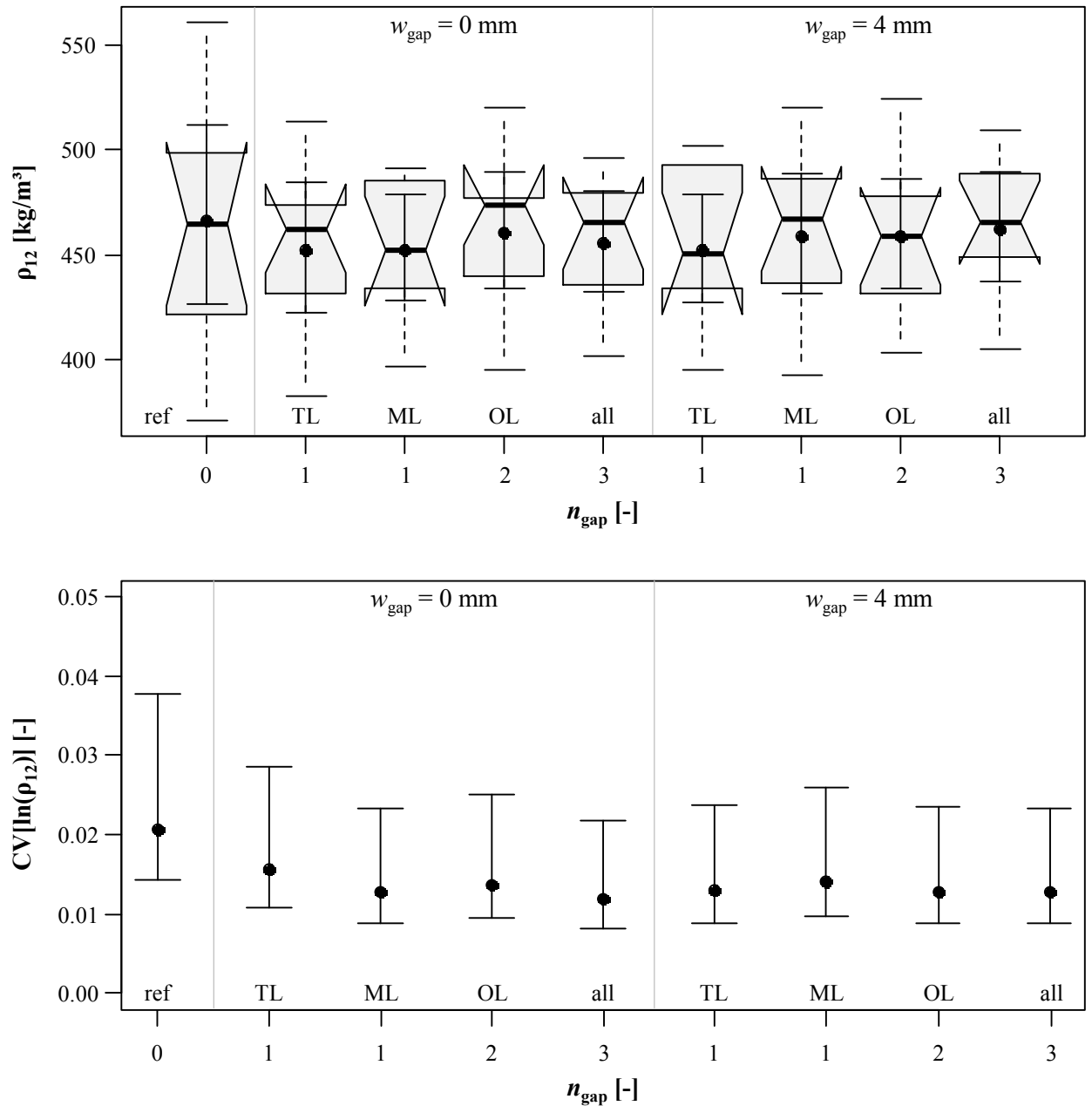


Figure 5.55: Above: boxplot graphic of densities ρ_{12} ; below: CIs of $CV[\ln(\rho_{12})]$ in dependence of w_{gap} and n_{gap} ; test programme II

Further concentration is on the withdrawal properties dedicated to test series I. Tests with $d = 8$ mm were performed with local displacement measurement devices, which enabled a determination of all properties f_{ax} , $K_{\text{ser,ax}}$ and D . The corresponding results are given in Figure 5.56 to Figure 5.58, as well as in Annex B-3.2, Table B.36. Furthermore, Figure B.36 to Figure B.38 in Annex B-3.1 comprise all supplemental information regarding their variability, as expressed by $CV[\ln(X)]$. Focusing on the behaviour of f_{ax} and $K_{\text{ser,ax}}$ in dependence of the screw position, the gap type and the width w_{gap} , all in all four main outcomes are worth being highlighted:

First, in case of BuJ, the screw positioning in the CLT narrow face (top, middle or cross layer) has no relevant impact on size and behaviour of both withdrawal properties at varying w_{gap} . Second, the screw insertion into intermediate layers (BeJ and TJ instead of ST and BuJ) leads to comparatively higher withdrawal strengths and to (more or less) equal withdrawal stiffness. Especially the behaviour of the latter property was not expected in advance. The impact of axis-to-grain angle interaction on withdrawal properties is discussed in section 5-4.3 in detail. Third, apart from gap type TL in Figure 5.56, closed gaps ($w_{\text{gap}} = 0 \text{ mm}$) do not influence the withdrawal properties at all. Fourth, a significant decrease of both withdrawal properties, f_{ax} and $K_{\text{ser,ax}}$ with increasing w_{gap} , is given. Surprisingly, this behaviour is independent from the gap type (BuJ vs. TJ), which was not expected, too. A possible explanation, as originally provided in Brandner et al. (2017), is the inaccuracy of inserting screws in TJ with $w_{\text{gap}} > 0 \text{ mm}$, even if the specimen were pre-drilled in advance. This especially concerns the test series with $w_{\text{gap}} = 6 \text{ mm}$, where an exclusive insertion in the gap at $\alpha = 0^\circ$ (BuJ), instead of an equal share of $\alpha = 0^\circ$ and 90° (TJ), is assumed.

With regard to the determined ductility D , in contrast to f_{ax} and $K_{\text{ser,ax}}$, the vast majority of the test results indicates no relevant impact of varying w_{gap} on this property. The only exception is a slight trend of decreasing D with increasing w_{gap} in case of TJ. As reported in section 5-3.1, higher values of D are given for $\alpha = 90^\circ$ if compared to $\alpha = 0^\circ$. This trend converging from $D(\alpha = 90^\circ | 0^\circ)$ to $D(\alpha = 0^\circ)$ may serve as an indicator, confirming the aforementioned explanation for the disproportional high decrease of $\{f_{\text{ax}}, K_{\text{ser,ax}}\}$ with increasing w_{gap} in case of the screw insertion in T-joints.

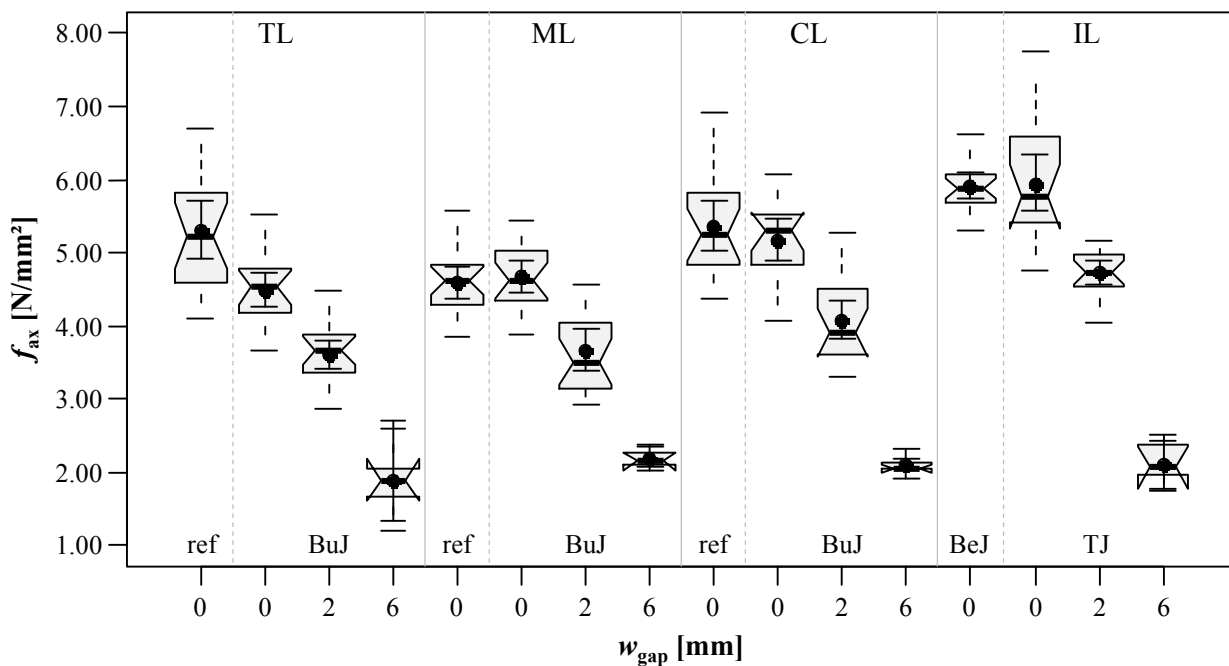


Figure 5.56: Boxplot diagrams of withdrawal strength vs. w_{gap} in dependence of screw position and gap type; test programme I, $d = 8 \text{ mm}$

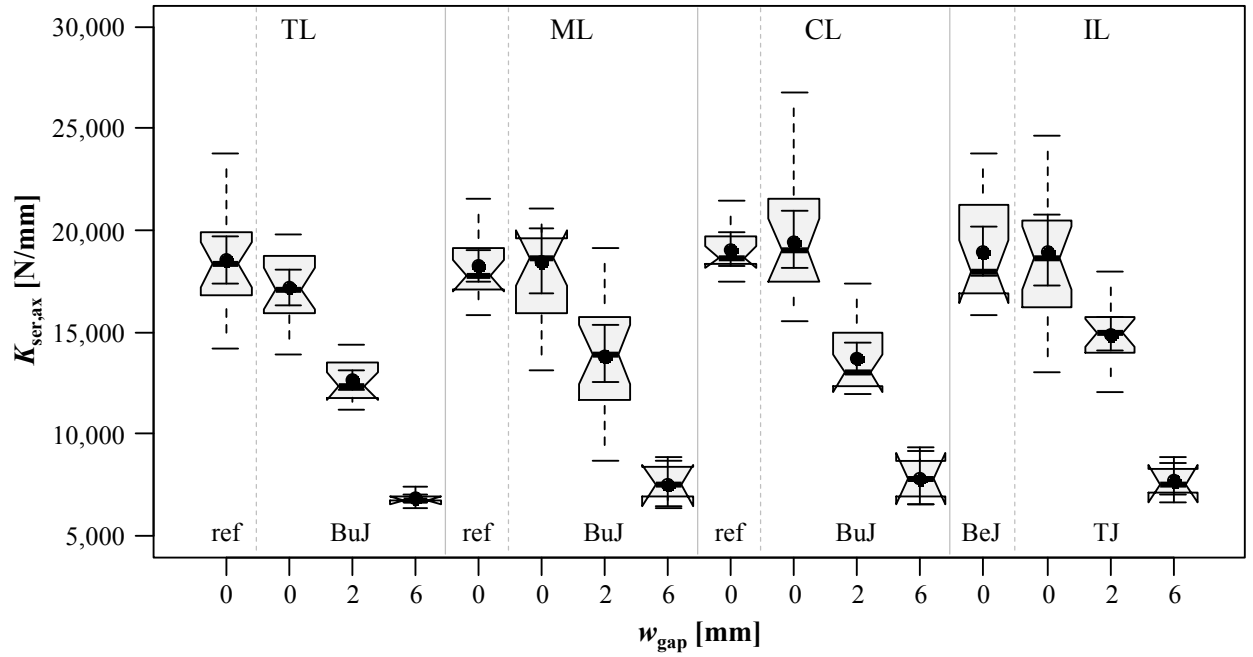


Figure 5.57: Boxplot diagrams of withdrawal stiffness vs. w_{gap} in dependence of screw position and gap type; test programme I, $d = 8 \text{ mm}$

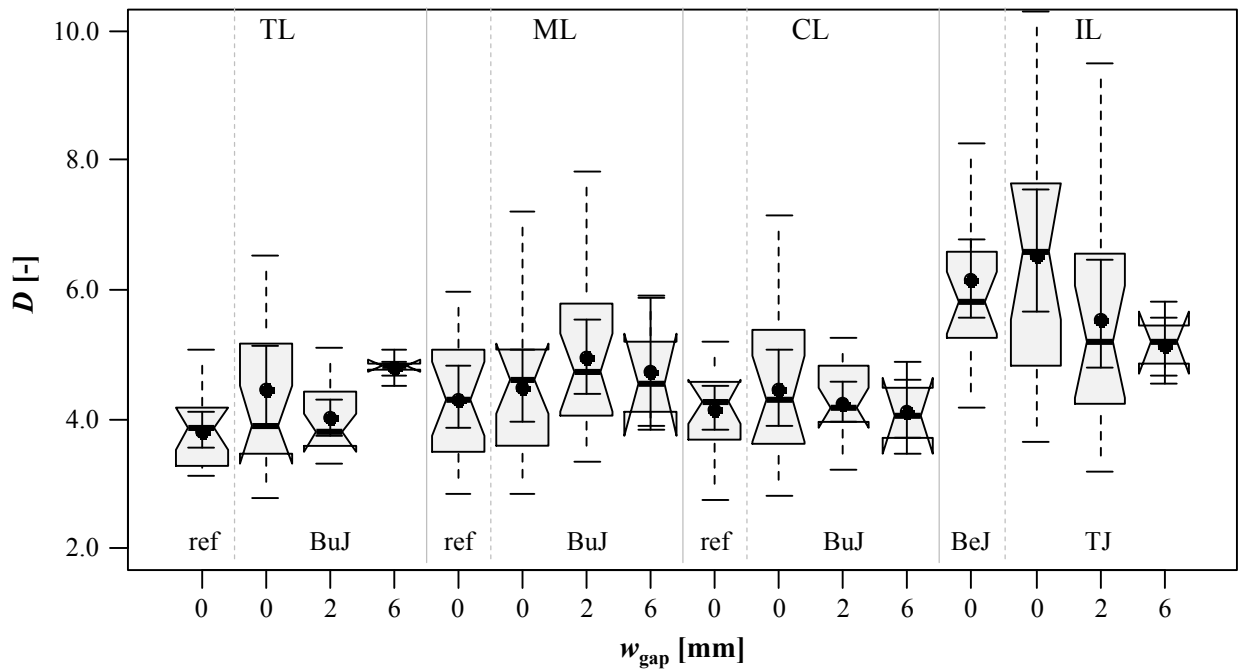


Figure 5.58: Boxplot diagrams of ductility vs. w_{gap} in dependence of screw position and gap type; test programme I, $d = 8 \text{ mm}$

In contrast to the previously discussed programme, tests with $d = 12$ mm were carried out without a local displacement measurement. Thus, the results given in Figure 5.59 and Annex B-3, Table B.37 and Figure B.39 solely comprise the withdrawal strength. In general, they confirm all conclusions made for f_{ax} of $d = 8$ mm screws.

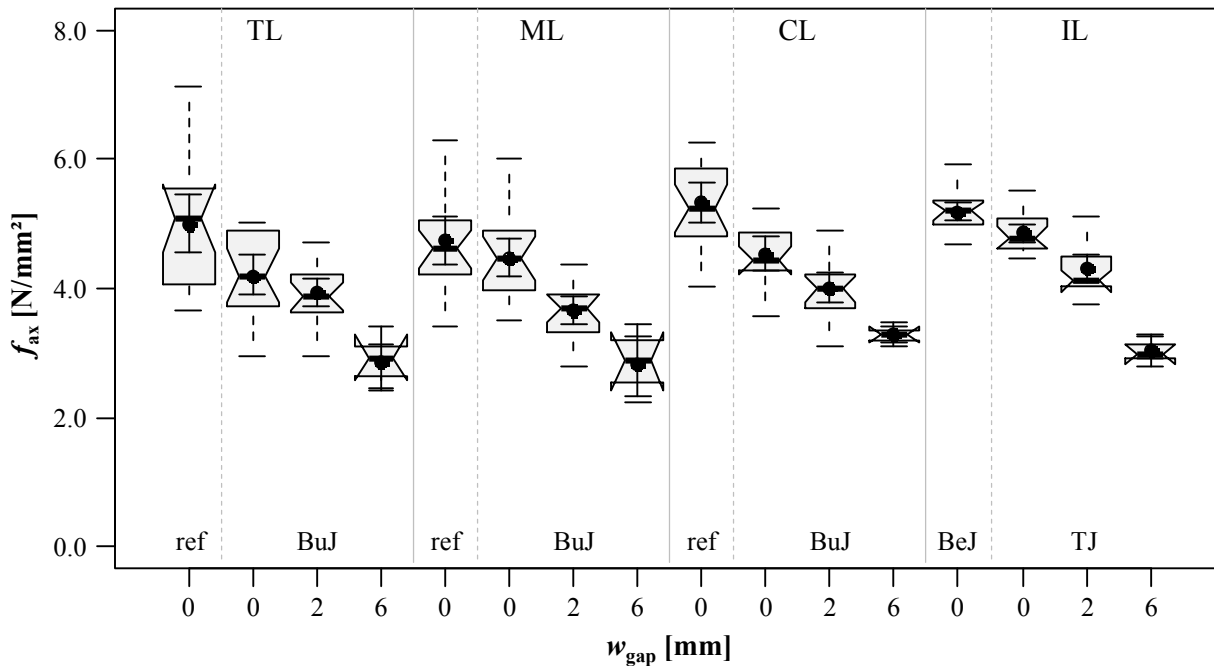


Figure 5.59: Boxplot diagrams of withdrawal strength vs. w_{gap} in dependence of screw position and gap type; test programme I, $d = 12$ mm

With regard to test programme II, the determined withdrawal properties are given in Figure 5.60 to Figure 5.62, as well as in Annex B-3, Table B.38 and Figure B.40 to Figure B.42 in dependence of width, number and position of gaps in the three-layered CLT specimen. Taking Figure 5.60 and Figure 5.61 into account, a similar behaviour of f_{ax} and $K_{ser,ax}$, in dependence of the aforementioned influencing parameters, can be observed. While the screw insertion in closed gaps, irrespective their number and position in the CLT lay-up, does not affect both withdrawal properties (in fact, the results are even higher than the reference), decreasing values for f_{ax} and $K_{ser,ax}$ with increasing n_{gap} and w_{gap} can be observed. Comparing groups TL and ML ($n_{gap} = 1$) in case of $w_{gap} = 4$ mm, no significant difference, as a consequence of different gap positions in the CLT lay-up, can be found. In case of ductility D , the gained results for $w_{gap} = 4$ mm indicate a somewhat mirrored behaviour of this property in dependence of the parameter variation. In contrary, the conclusions made for f_{ax} and $K_{ser,ax}$ of screws situated in closed gaps are also valid for the related ductility.

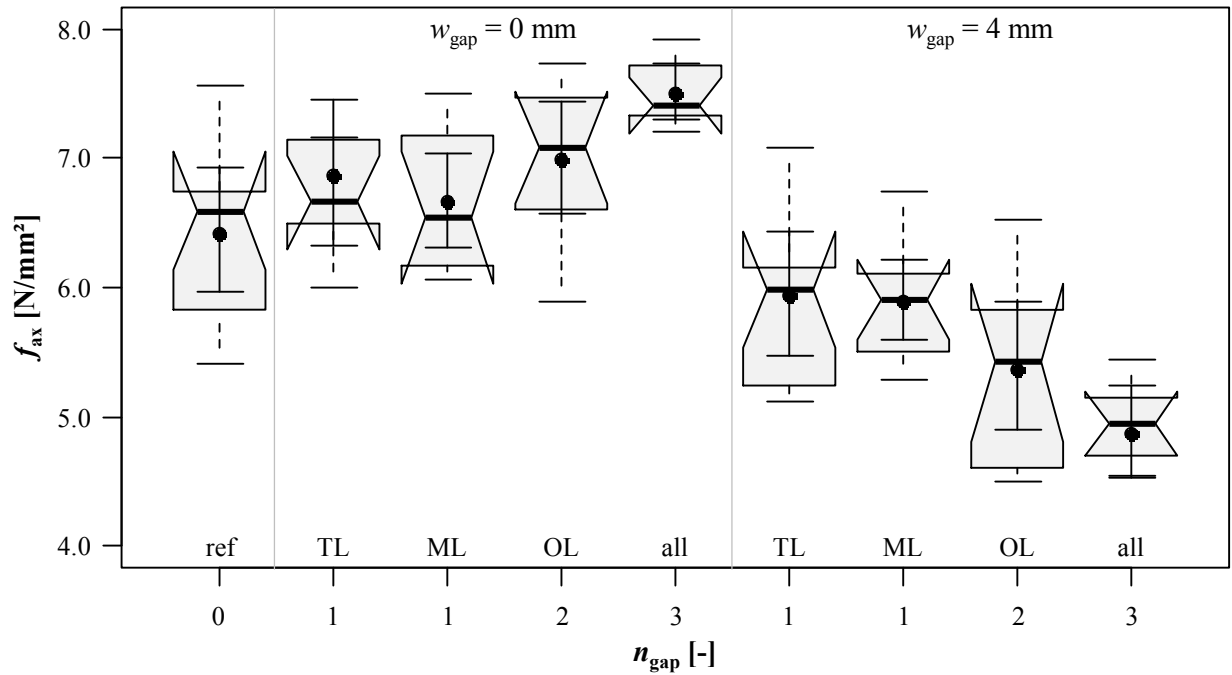


Figure 5.60: Boxplot diagrams of withdrawal strength vs. w_{gap} and n_{gap} ; test programme II

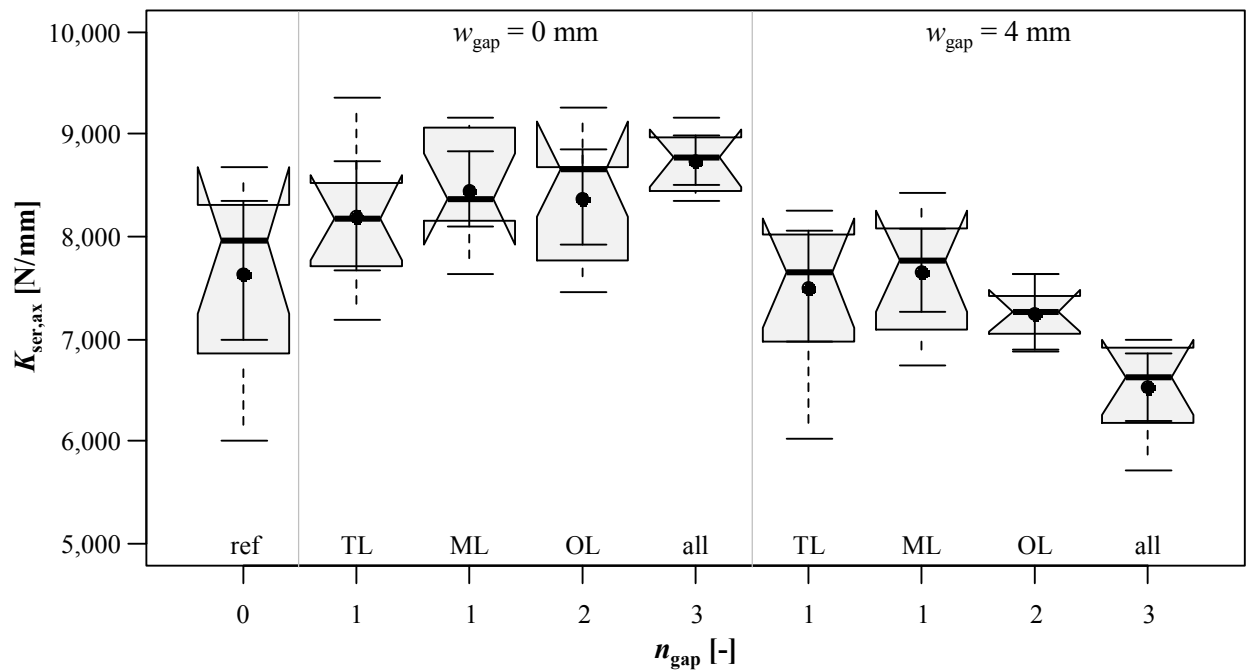


Figure 5.61: Boxplot diagrams of withdrawal stiffness vs. w_{gap} and n_{gap} ; test programme II

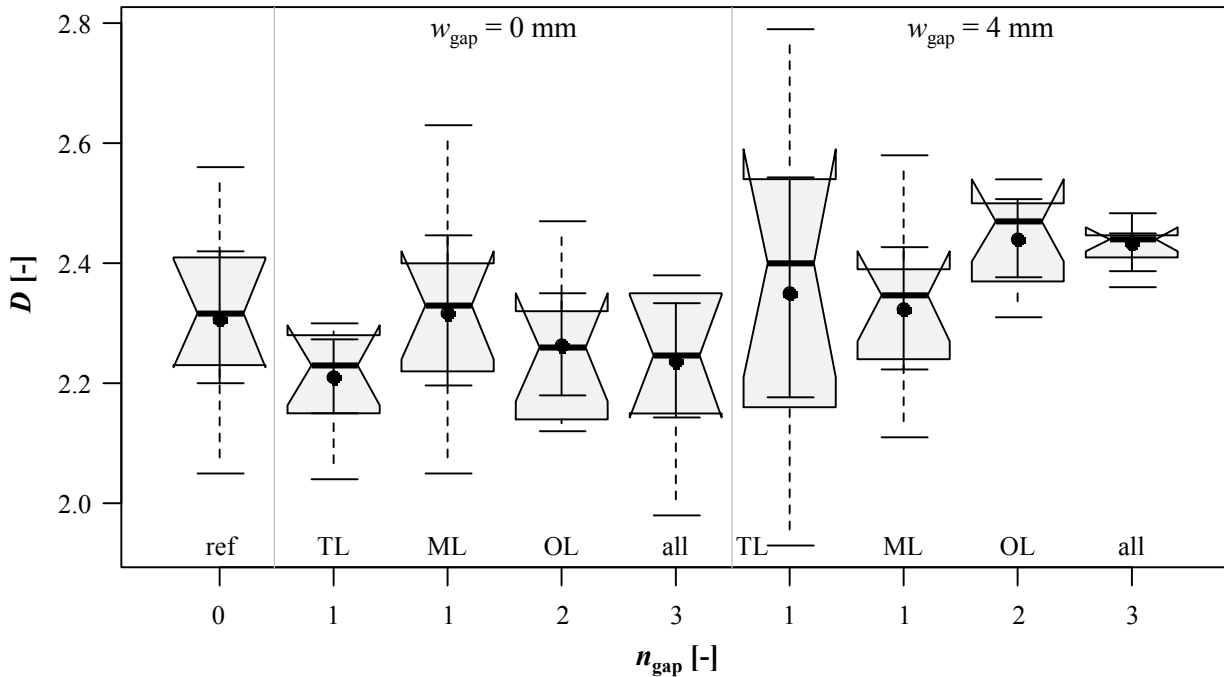


Figure 5.62: Boxplot diagrams of ductility vs. w_{gap} and n_{gap} ; test programme II

5-3.4.4 Model verification

Within the last part of this section, the previously introduced model approach, covering the impact of gap insertion (w_{gap} , n_{gap} and gap type) on withdrawal strength f_{ax} , as expressed in eqs. (5.78) to (5.80) is verified with the experimental results. In case of BuJ, independent from the CLT side or narrow face application, the reference test results, given in Table B.36 to Table B.38, represent $f_{\text{ax,CLT,ref}}$ according to eq. (5.78). In case of screws, situated in TJ, $f_{\text{ax,CLT,ref},\alpha=90^\circ}$ was not examined within the experimental campaigns. Taking the previously mentioned assumption of equally contributing shares of withdrawal strength at $\alpha = 0^\circ$ and 90° for determining BeJ, as expressed in eq. (5.79), into account, $f_{\text{ax,CLT,ref},\alpha=90^\circ}$ was estimated as follows for this purpose, see:

$$f_{\text{ax,CLT,ref},\alpha=90^\circ} = 2 \cdot f_{\text{ax,BeJ}} - f_{\text{ax,CLT,ref},\alpha=0^\circ} \quad (5.82)$$

Hereby, $f_{\text{ax,BeJ}}$ are the corresponding withdrawal strengths, given for BeJ insertion in Table B.36 and Table B.37, and $f_{\text{ax,CLT,ref},\alpha=0^\circ}$ the weighted average of all reference test results – irrespective of the screw position (TL, ML or CL) – but in dependence from outer thread diameter. The comparison between the test results and the predicted values is subsequently given in Figure 5.63. Thereby, the statistical parameters of all in all 32 test series with $n_{\text{tot}} = 383$ results (excluding reference series) are considered. In contrast to the impact of N on f_{ax} , the parameter variation (w_{gap} , n_{gap} , gap type) obviously does not affect the variability of the test results, c. f. Figure B.36, Figure B.39 and Figure B.40 in Annex B-3.1. Thus, the comparison is restricted to mean values.

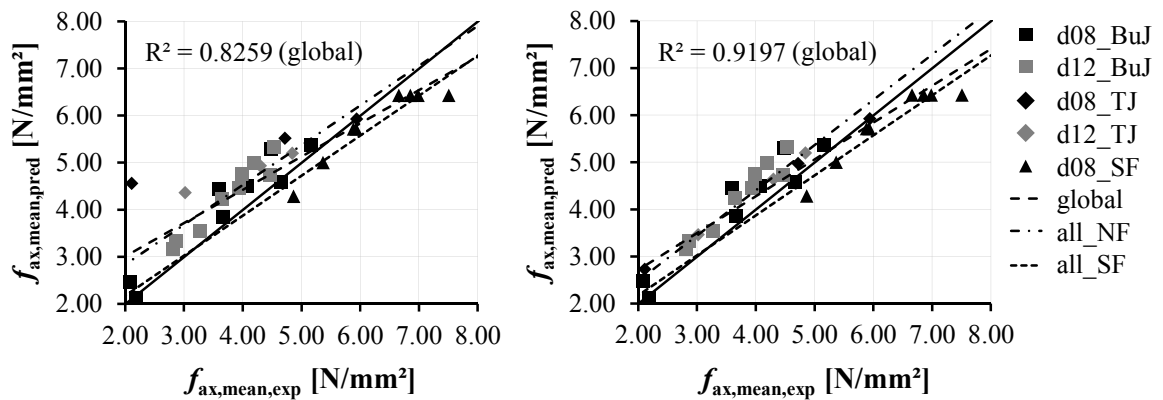


Figure 5.63: *Experimental vs. predicted withdrawal strengths; left: originally assumed TJ; right: TJ assumed as BuJ*

Concentrating on the position of $d = 8$ mm and 12 mm screws situated in T-joints, a significant overestimation of test results by model predictions can be observed, c. f. Figure 5.63 (left). In fact, this is caused by the aforementioned unexpectedly low values determined for this configuration. Consequently, in Figure 5.63 (right), the corresponding subgroups are treated as BuJ instead of TJ (application of eq. (5.78) instead of eq. (5.79)), leading to a far better compliance between estimated and experimentally determined values. Apart from these subgroups, both trend lines for CLT side and narrow face application in Figure 5.63 (right) attest the simple model approach a qualitatively high accuracy in predicting test results. Minor quantitative deviations are given (narrow face results slightly overestimated, side face results slightly underestimated) and are probably caused by the differences between the reference values and the values determined for closed gaps ($w_{\text{gap}} = 0$ mm), supposed as equal when applying eqs. (5.78) to (5.80).

5-4 APPLICATION

5-4.1 Spacings

5-4.1.1 Introduction

Taking the definition of withdrawal failure (as given in section 5-1.1) into account, the optical appearance of related crack formation indicates a certain size of stressed timber volume, which is necessary to achieve the screw's maximum possible value of the withdrawal capacity. As illustrated in Figure 5.2, the assumed orthotropic material behaviour, defined by the R - T - L -coordinate system and thus significantly depending on the axis-to-grain angle α , majorly influences the corresponding dimensions: in case of a parallel-to-grain insertion (longitudinal, $\alpha = 0^\circ$), the withdrawal failure appears at the screw's outer thread lateral surface and is thus limited to a small area around its axis. In case of a perpendicular-to-grain insertion (either radial, tangential or a combination of both, $\alpha = 90^\circ$), similarities are given for the associated rolling shear planes RT or TR , while those dedicated to longitudinal shear components, namely RL and TL , show a far more pronounced dispersion of crack formation in longitudinal direction.

Considering these observations, following first assumptions made in Ringhofer and Schickhofer (2014b), the timber volume stressed by shear, as a consequence of axial screw loading, is subsequently approximated by a nonlinear, three-dimensional body with elliptic surface, defined by $V = a \cdot b \cdot f(l_{ef}, \dots)$ and $\{a, b\}$ as major and minor semiaxes and $f(l_{ef}, \dots)$, as a function describing the nonlinear stress distribution along l_{ef} . The elliptic surface is in fact a raw simplification, not considering a probable geometrically deviating distribution of shear properties in dependence of φ , as the polar angle around the screw axis, and the axis-to-grain angle α , as e. g. demonstrated in Hübner (2013a). Nevertheless, in the frame of this first approach both elliptic parameters, a and b , are assumed to $3d$ and $1d$ in case of a perpendicular-to-grain insertion ($\alpha = 90^\circ$). While the minor semiaxis b remains constant, a shall decrease with decreasing α to $1d$ in case of a parallel-to-grain insertion ($\alpha = 0^\circ$, circle). The values a for angles varying in-between both limits are furthermore estimated by an approach according to Hankinson (1921) with an exponent of 2.5, as outlined in Hübner (2013a).

With regard to the application of screws in practise, assuming constant α and l_{ef} within one connection, the stressable timber volume per screw can be reduced, either by limited component dimensions or by a too compact fastener arrangement. Both are currently defined by minimum spacings between screws $\{a_1, a_2\}$, and those to the timber member's ends or edges $\{a_{1,CG}, a_{2,CG}\}$. Figure 5.64 shows these spacings exemplarily for the perpendicular-to-grain (Figure 5.64, left) and parallel-to-grain insertion (Figure 5.64, right).

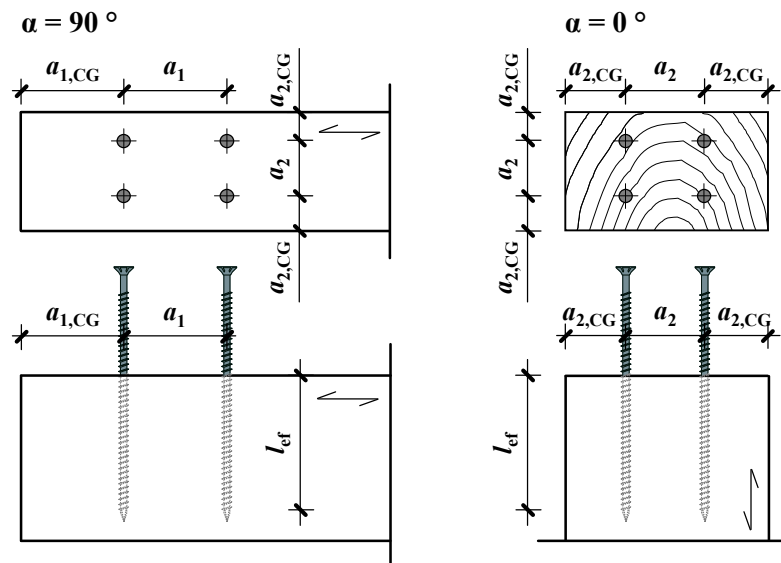


Figure 5.64: Definition of minimum spacings according to ON EN 1995-1-1 (2015);
left: $\alpha = 90^\circ$; right: $\alpha = 0^\circ$

Describing this loss of stressable timber volume per screw, as a consequence of insufficient spacings $\{a_1, a_2, a_{1,CG}$ and $a_{2,CG}\}$, the screw arrangement in form of a regular and rectangular pattern with constant a_1 and a_2 is subsequently presupposed. Figure 5.65 (left) illustrates this case for a screwed connection inserted perpendicular-to-grain. In Figure 5.65 (right), the surface of the reduced stressable timber volume of one single screw, A_{red} , is expressed by a grey shaded area, limited by the connecting lines between the coordinate points (x_i, y_i) as intersections with neighbouring ellipses or with the timber member's end or edge.

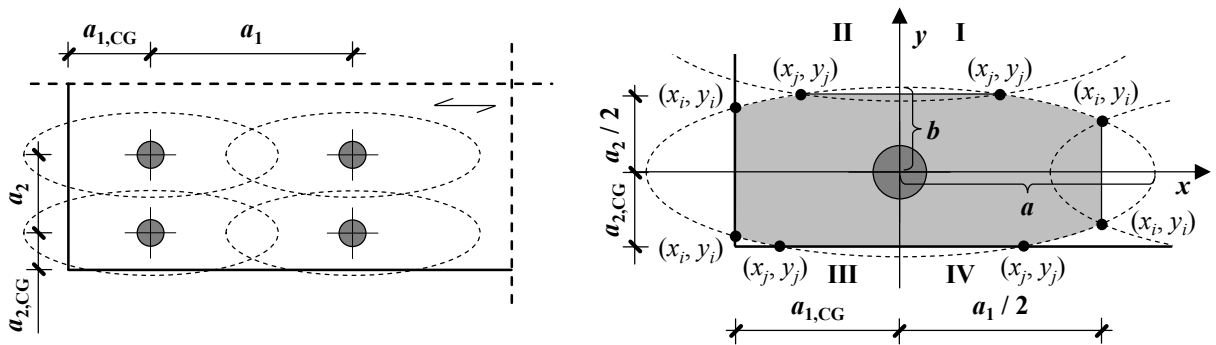


Figure 5.65: Left: top view of a screwed connection inserted at $\alpha = 90^\circ$; right: definition of the reduced stressable timber volume for the special case of an edge screw

Consequently, A_{red} is determined by summing up the reduced surfaces of each elliptic quadrant, $A_{red,i}$ (with $i = I \div IV$), c. f. Figure 5.65 (right) and eq. (5.83) to eq. (5.88). Note: if one or both spacings in x - and/or y - direction exceeds a and/or b , the corresponding terms have to be zeroized.

$$A_{\text{red}} = \sum_{i=1}^{\text{IV}} A_{\text{red},i}, \text{ with} \quad (5.83)$$

$$A_{\text{red},i} = \frac{\pi}{4} \cdot a \cdot b - \frac{1}{2} \cdot \left[a \cdot b \cdot \cos^{-1} \left(\frac{|x_i|}{a} \right) - |x_i| \cdot |y_i| \right] - \frac{1}{2} \cdot \left[a \cdot b \cdot \cos^{-1} \left(\frac{|y_j|}{b} \right) - |x_j| \cdot |y_j| \right], \text{ if} \quad (5.84)$$

$$|x_i| \geq |x_j|, \text{ else} \quad (5.85)$$

$$A_{\text{red},i} = |x_i| \cdot |y_j|, \text{ with} \quad (5.86)$$

$$|x_i| = \frac{a_1}{2} \text{ or } |x_i| = a_{1,\text{CG}} \text{ and } |y_i| = \frac{b}{a} \cdot \sqrt{a^2 - x_i^2}, \text{ and} \quad (5.87)$$

$$|y_j| = \frac{a_2}{2} \text{ or } |y_j| = a_{2,\text{CG}} \text{ and } |x_j| = \frac{a}{b} \cdot \sqrt{b^2 - y_j^2}. \quad (5.88)$$

Following the idea of considering the influence of a parameter variation on withdrawal properties by multiplicative (k -)factors, the impact of the reduced stressable timber volume, especially on withdrawal strength f_{ax} , is considered according to eq. (5.89), see

$$f_{\text{ax}} = k_{\text{red}} \cdot f_{\text{ax,ref}} \text{ with } k_{\text{red}} = \frac{A_{\text{red}}}{A_{\text{tot}}}, \text{ and} \quad (5.89)$$

$f_{\text{ax,ref}}$ as the reference withdrawal strength, determined at sufficient conditions regarding $\{a_1, a_2, a_{1,\text{CG}}$ and $a_{2,\text{CG}}\}$. Apart from the aforementioned theoretical work, done by Hübner (2013a), regarding the planar shear stress distribution around the screw axis and in dependence of α , a certain number of further investigations concentrating on this field, as published in Gehri (2009), Gatterinig (2010), Plieschounig (2010), Plüss (2014) and Grabner and Ringhofer (2014), are worth being discussed in brief: all corresponding programmes, summarised in Table 5.28, base on experimental campaigns determining the withdrawal strength of screws in dependence of varying spacings $\{a_1, a_2, a_{1,\text{CG}}$ and $a_{2,\text{CG}}\}$ and axis-to-grain angles $\alpha = \{0^\circ, 45^\circ, 90^\circ, 0^\circ|90^\circ, 45^\circ|90^\circ\}$, comparing the results with reference values given for sufficient conditions. As outlined, mainly spruce softwood and ST were applied. The outer thread diameters also show a small variation in the lower bandwidth of the practical application for high-stressed timber connections or reinforcements. The reason is, that related test set-ups have higher demands on specimen dimension and applied force if compared to single screw tests. The most authors stick to lower limits of $\{a_1, a_2, a_{1,\text{CG}}$ and $a_{2,\text{CG}}\}$ if exceeded no significant decrease of f_{ax} (if compared to the reference value) can be observed. The only exception is the approach made by Gehri (2009), who also proposes

empirically reducing withdrawal strength by a factor k_{red} if spacings are below the related threshold of $5 d$, c. f. section 2-3.1,

Furthermore, the majority of the related limits, given in Table 5.28, results in a similar range when the same configuration is applied. The sole exception is the recommendation for spacings dedicated to $\alpha = 0^\circ$ varying between $2.5 d \div 5 d$ in dependence of the considered source. With regard to the impact on f_{ax} if spacings are below the given thresholds, the results published in Gatternig (2010), Plieschounig (2010) and Grabner and Ringhofer (2014), indicate a more or less pronounced progressive decrease of withdrawal strength with decreasing spacings, especially in case of $\{a_1, a_{1,\text{CG}}, a_{2,\text{CG}}\}$ at $\alpha = \{45, 90\}^\circ$. Since they furthermore considered a large bandwidth of varying parameters, the related results are thus regarded as a valuable data for the model verification.

Table 5.28: Literature observations regarding the influence of spacings on withdrawal strength f_{ax} of self-tapping screws

source	wood species	timber product	α	spacings investigated	d	no. of screws n	proposed thresholds
Gehri (2009)	spruce	ST, GLT	0°	$a_2, a_{2,\text{CG}}$	10 mm	1, 4, 9, 16	$\{a_2, a_{2,\text{CG}}\} = 5 d$
Gatternig (2010)	spruce	ST	$0^\circ, 45^\circ, 90^\circ$	$a_{1,\text{CG}}, a_{2,\text{CG}}$	6 mm	1	$a_{1,\text{CG}} = 1 d,$ $a_{2,\text{CG}} = 0.5 d$
Plieschounig (2010)	spruce	ST	90°	a_1, a_2	6 mm	2	$a_1 = 7 d,$ $a_2 = 3 d$
Plüss (2014)	spruce	CLT narrow face*	$0^\circ, 45^\circ, 90^\circ,$ $0^\circ 90^\circ,$ $45^\circ 45^\circ$	a_1	8 mm	3	$a_{1,\alpha=0^\circ} = 2.5 d,$ $a_{1,\alpha=45^\circ} = 5 d,$ $a_{1,\alpha=90^\circ} = 7 d,$ $a_{1,\alpha=0^\circ 90^\circ} = 5 d,$ $a_{1,\alpha=45^\circ 45^\circ} = 5 d$
Grabner and Ringhofer (2014)	birch	ST	0°	$a_{2,\text{CG}}$	8 mm	1	$a_{2,\text{CG}} = 5 d$

* equal to ST in case of $\alpha = \{0, 45, 90\}^\circ$

In advance, the following subsections concentrate on the reassessment of test data gained by Gatternig (2010) and Plieschounig (2010). This was done for two reasons: first, the comparatively large amount of test results per parameter specification allows determining the interrelationship between withdrawal strength, spacing and timber density. Second – even though Plieschounig (2010) did not consider a local displacement measurement – his test configuration is regarded as appropriate for also determining the (relative) behaviour of the withdrawal properties $K_{\text{ser,ax}}$ and D in dependence of the spacing variation. The mentioned topics have not been investigated yet.

5-4.1.2 Reassessment of selected experimental programmes

Even though the author of this thesis was not involved in both investigations, the reassessment of test data from Gatternig (2010) and Plieschounig (2010) is described in a similar way, as the other experimental programmes presented in this chapter. Table 5.29 consequently includes all relevant information regarding both experimental campaigns. Concentrating on the spacings to the timber member's ends and edges, the test programme, carried out by Gatternig (2010), comprised a variation of $a_{2,CG}$ in dependence of the axis-to-grain angle $\alpha = \{0, 45, 90\}^\circ$, while in case of $a_{1,CG}$ an exclusively perpendicular-to-grain insertion was considered. With regard to in-between spacings, investigated by Plieschounig (2010), the axis-to-grain angle α was kept constant at $\alpha = 90^\circ$. Except one conducted as standard single screw withdrawal test for reference, Plieschounig (2010) performed all experiments as connection tests with $n = 2$ screws. Furthermore, he separated his programme in a radial and a tangential screw insertion. Since no related impact on withdrawal behaviour was observed, c. f. detailed discussion in section 5-4.4, the gained results are subsequently treated irrespectively from this variation.

The basic material for the specimen preparation of both campaigns were solid timber beams of Norway spruce (*Picea abies*) with cross-sectional dimensions of about $120 \times 180 \text{ mm}^2$, cut in single and widely knot-free sections and formatted to the target dimensions, as shown in Annex B-3.1, Figure B.43 to Figure B.46. In advance, beams were stored at standard conditions (20°C , 65 % r. h.) in order to reach the equilibrium moisture content u of $12 \pm 2\%$.

Table 5.29: Main information regarding the test campaigns carried out by Gatternig (2010) and Plieschounig (2010)

source	d [mm]	no. of screws	α [°]	spacings investigated	spacing specifications [d]
Gatternig (2010)	6	1	0	$a_{2,CG}$	0.5, 1, 2, 3, 4, 5, 7.5
			45	$a_{2,CG}$	0.5, 1, 2, 3, 4, 5
			90	$a_{1,CG} a_{2,CG}$	0.5, 1, 2, 3, 4, 5, 6, 7 0.5, 1, 2, 3, 4, 5
Plieschounig (2010)	6	2	90	a_1, a_2	2, 3, 4, 5, 6, 7, 14 2, 3, 4, 5 + ref*

* carried out as single screw test

In order to keep the maximum test load, as well as the specimen dimensions in tolerable amounts, Gatternig (2010) and Plieschounig (2010) applied $d = 6 \text{ mm}$ partially threaded screws, which solely differ from each other in their thread lengths, c. f. Table 5.30.

Table 5.30: Thread characteristics and test conditions applied for both experimental campaigns carried out by Gatternig (2010) and Plieschounig (2010)

source	thread characteristics*					test conditions			
	d_{nom} [mm]	d [mm]	η [-]	p [mm]	ν [°]	l_p [mm]	l_{ef} [mm]	l_{emb} [mm]	d_{PD} [mm]
Gatternig (2010)						64	57	12	-
Plieschounig (2010)	6	6.0	0.63	2.60	40	75	68	12	-
						63	63	12	-

* all values taken from product information related

With regard to the test execution, both programmes were conducted on the test rig LIGNUM-UNI-275 with the standard push-pull configuration, illustrated in Figure 5.4. Even though no local way measurement set-up was applied, Plieschounig's test configuration is – as previously mentioned – regarded as an appropriate method determining the relative behaviour of $K_{\text{ser,ax}}$ and D , as a consequence of the spacing variation. Worth mentioning, that in case of small values for $\{a_{1,\text{CG}}, a_{2,\text{CG}}\} = \{0.5, 1\}$ d , Gatternig (2010) clamped the majority of specimen during the test, in order to avoid screws tearing out from the end or edge (timber splitting caused by exceeding the tensile strength perpendicular to grain), as a consequence of a specimen misalignment. Since this fracture mode is seen as a configuration specific, only the results of tests with clamped specimen are considered for the data assessment. Further background information, regarding test execution, post-processing, property determination and data assessment is summarised in section 5-1.2.

5-4.1.3 Results and discussion

All statistical illustrations of timber density ρ_{12} of small scale specimen dedicated to both experimental campaigns, carried out by Gatternig (2010) and Plieschounig (2010), are subsequently given in Figure 5.66 to Figure 5.71, in dependence of the axis-to-grain angle and the spacing characteristics. In addition, the related statistical parameters, as well as the moisture contents u are given in Annex B-3.2, Table B.39 to Table B.41. With regard to moisture contents, corresponding to the variation of end and edge spacings, the averages are closely located to the equilibrium moisture content and vary in the planned bandwidth of roughly $\pm 2\%$. Even though the results gained for an in-between spacing variation exceed $u = 12\%$, as well as $\pm 2\%$ to some extent, c. f. Table B.41, the average values are nearly equal, which allows a moisture-independent comparison of the test results in this case too.

Concentrating on the location of timber densities ρ_{12} , data illustrated in Figure 5.66 to Figure 5.69, indicates no significant deviations necessitating the related density correction. In case of the test programme, conducted by Plieschounig (2010), the average density ρ_{12} determined for $a_1 = 14 d$

significantly differs from the other locations (especially for small a_1 and the series with $n = 1$ screw). Since this value is an important information for the model verification, it was decided to apply the density correction for the whole in-between spacing programme $X = \{f_{ax}, K_{ser,ax}\}$ in form of eq. (5.81), again with $\rho_{ref} = 450 \text{ kg/m}^3$ as a rounded overall average of ρ_{12} . With regard to the variability of density, the error bars dedicated to $CV[\rho_{12}]$, illustrated in the aforementioned figures, prove the equality for the majority of subseries. Again, $CV[\rho_{12}]$ of the series with $a_1 = 14 d$ has to be regarded as an outlier, possibly influencing the variability of the related withdrawal properties.

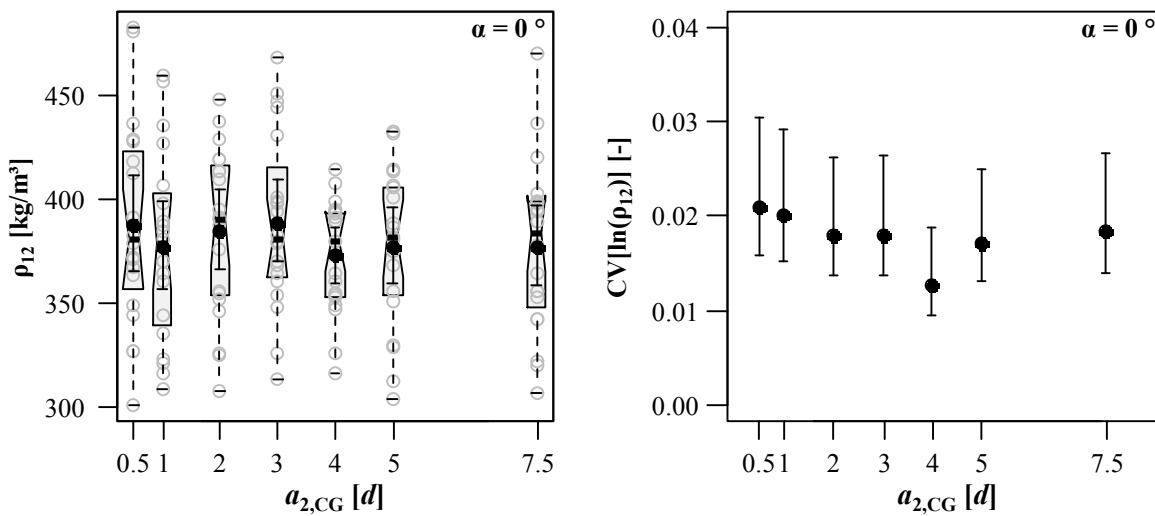


Figure 5.66: Left: combined boxplot/scatterplot graphic of densities ρ_{12} ; right: CIs of $CV[\ln(\rho_{12})]$ in dependence of spacing $a_{2,CG}$ for axis-to-grain angle $\alpha = 0^\circ$; test data from Gatterinig (2010)

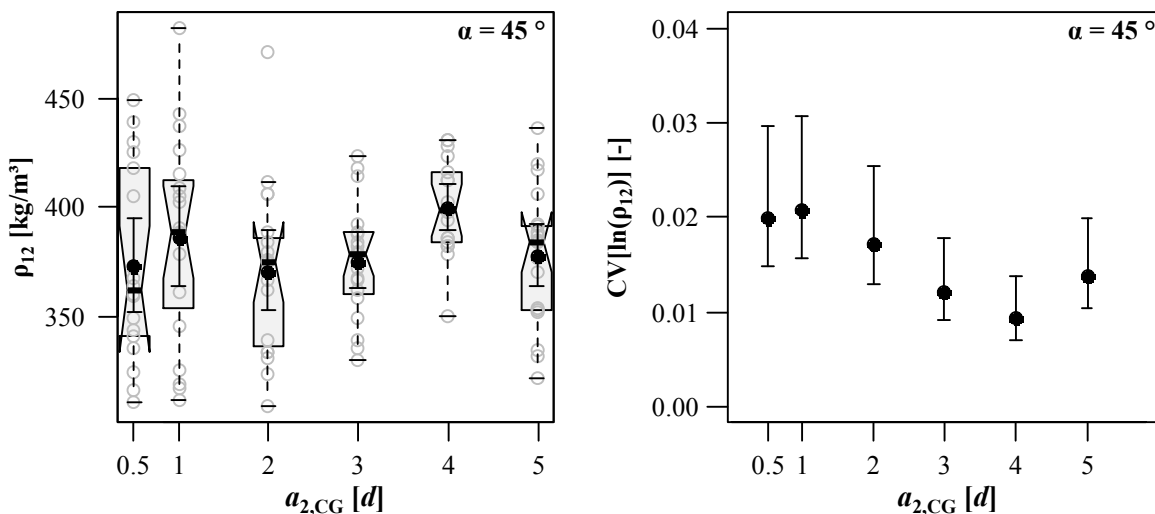


Figure 5.67: Left: combined boxplot/scatterplot graphic of densities ρ_{12} ; right: CIs of $CV[\ln(\rho_{12})]$ in dependence of spacing $a_{2,CG}$ for axis-to-grain angle $\alpha = 45^\circ$; test data from Gatterinig (2010)

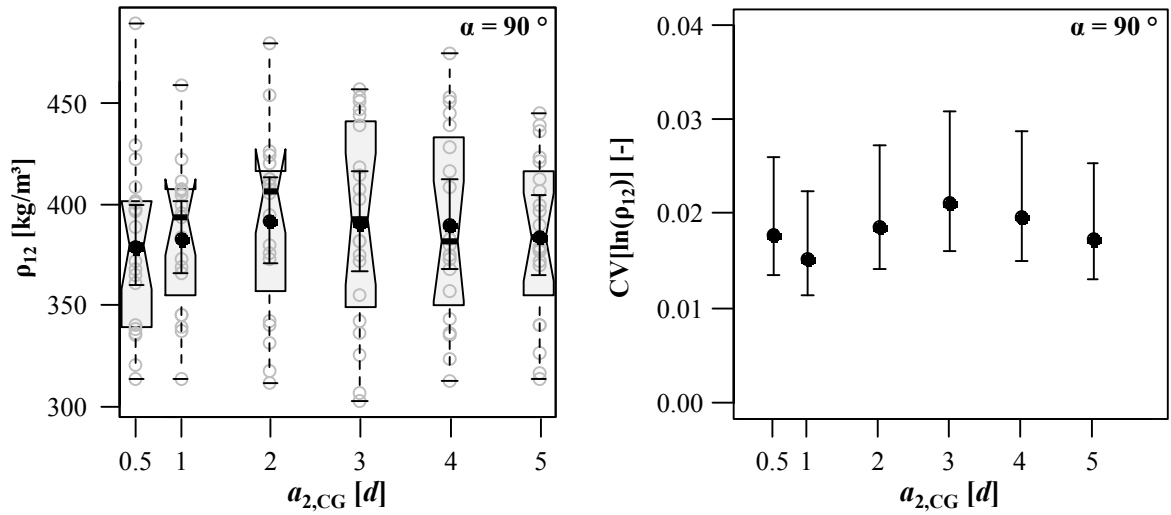


Figure 5.68: Left: combined boxplot/scatterplot graphic of densities ρ_{12} ; right: CIs of $CV[\ln(\rho_{12})]$ in dependence of spacing $a_{2,CG}$ for axis-to-grain angle $\alpha = 90^\circ$; test data from Gatterneg (2010)

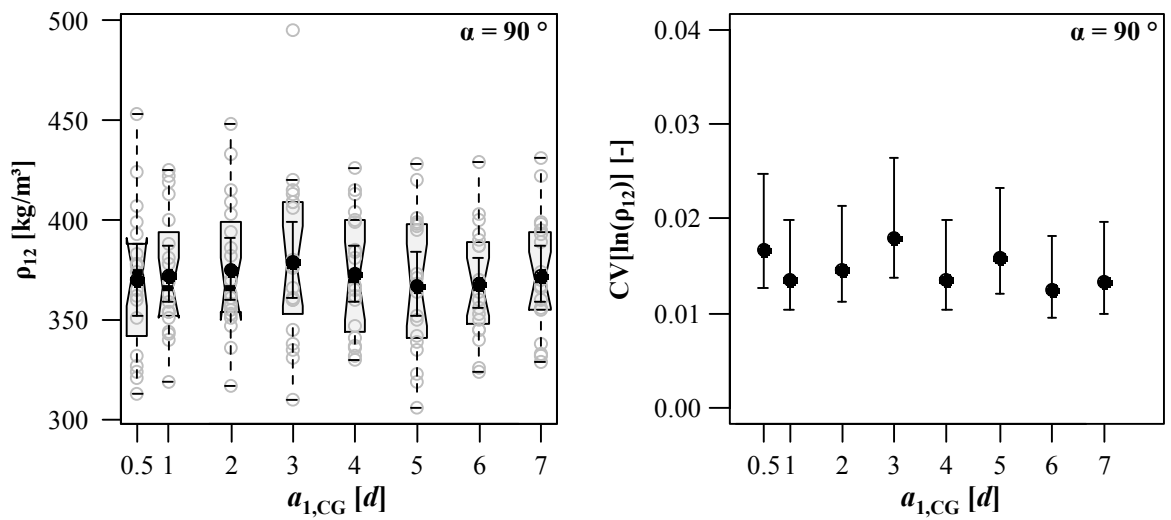


Figure 5.69: Left: combined boxplot/scatterplot graphic of densities ρ_{12} ; right: CIs of $CV[\ln(\rho_{12})]$ in dependence of spacing $a_{1,CG}$ for axis-to-grain angle $\alpha = 90^\circ$; test data from Gatterneg (2010)

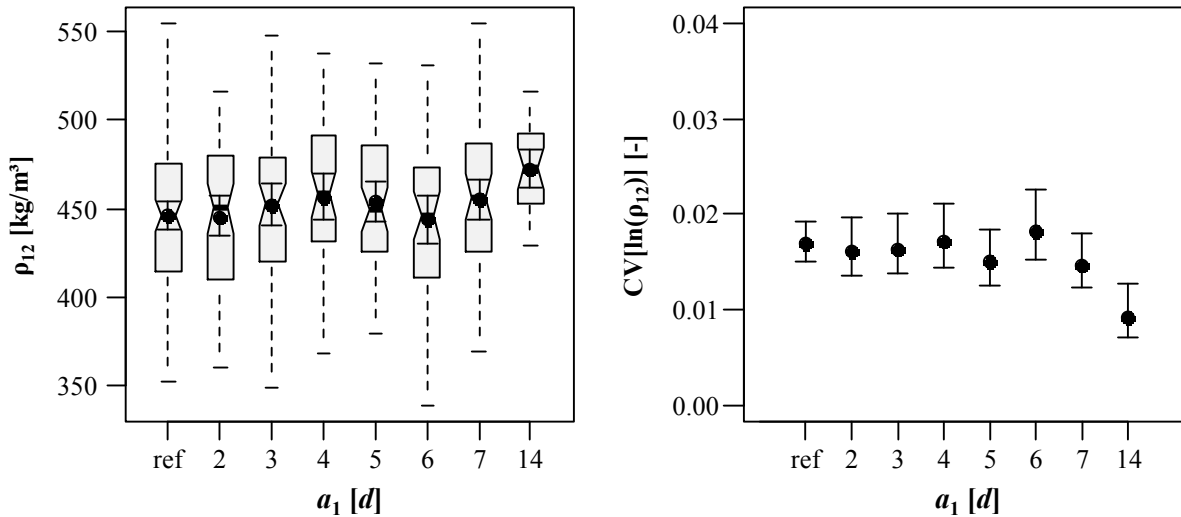


Figure 5.70: Left: boxplot diagram of densities ρ_{12} ; right: CIs of $CV[\ln(\rho_{12})]$ in dependence of spacing a_1 ; test data from Plieschounig (2010);

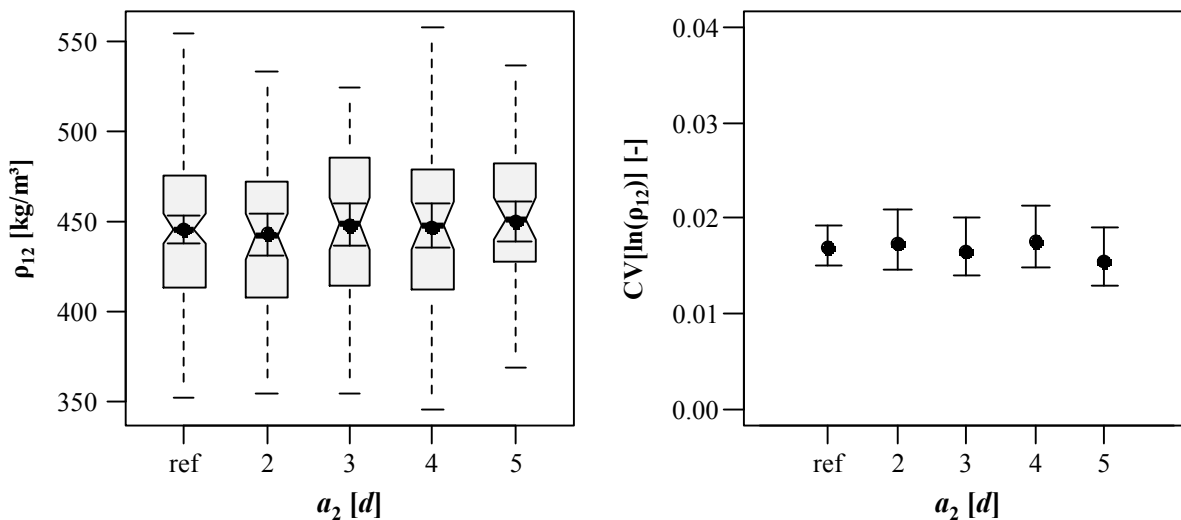


Figure 5.71: Left: boxplot diagram of densities ρ_{12} ; right: CIs of $CV[\ln(\rho_{12})]$ in dependence of spacing a_2 ; test data from Plieschounig (2010);

The main statistical data, regarding the withdrawal strength, dedicated to the test campaign from Gattermig (2010), is subsequently given in Figure 5.72, as well as in Annex B-3.2, Table B.42 and Table B.43. This is again in dependence of axis-to-grain angle, spacing type and variation. Furthermore, Figure B.47 and Figure B.48 in Annex B-3.1 illustrate the error bars of the related variabilities. As already mentioned, progressively decreasing withdrawal strengths with decreasing spacings can be observed for all configurations applied. In case of $a_{2,CG}$, this behaviour is more pronounced if the axis-to-grain angle increases from a parallel- to a perpendicular-to-grain insertion. Nevertheless, independent of α , significant differences of $\text{med}[f_{ax}]$ and $\text{mean}[f_{ax}]$ are only given for $a_{2,CG} = 0.5 d$, c. f. Gattermig (2010) and Figure 5.72. In case of $a_{1,CG}$, the related behaviour is even more pronounced, the withdrawal strength

f_{ax} of both subseries $a_{1,CG} = \{0.5, 1\}$ d significantly differs from those determined for bigger spacings. This in fact confirms the previously made assumption of an orthotropic material behaviour with a distinctive stress dispersion in longitudinal if compared to radial or tangential direction. Concentrating on the variability of the test results, the courses of $CV[\ln(f_{ax})]$ at varying spacings $\{a_{1,CG}, a_{2,CG}\}$ differ in dependence of spacing type and axis-to-grain angle, which are influenced by those of $CV[\ln(\rho_{12})]$ for the same configurations – compare Figure 5.66 to Figure 5.69 (each right) with Annex B-3.1, Figure B.47 and Figure B.48. Nevertheless, in case of $\alpha > 0^\circ$ a differently pronounced trend of increasing variabilities with decreasing spacings $\{a_{1,CG}, a_{2,CG}\}$ can be observed.

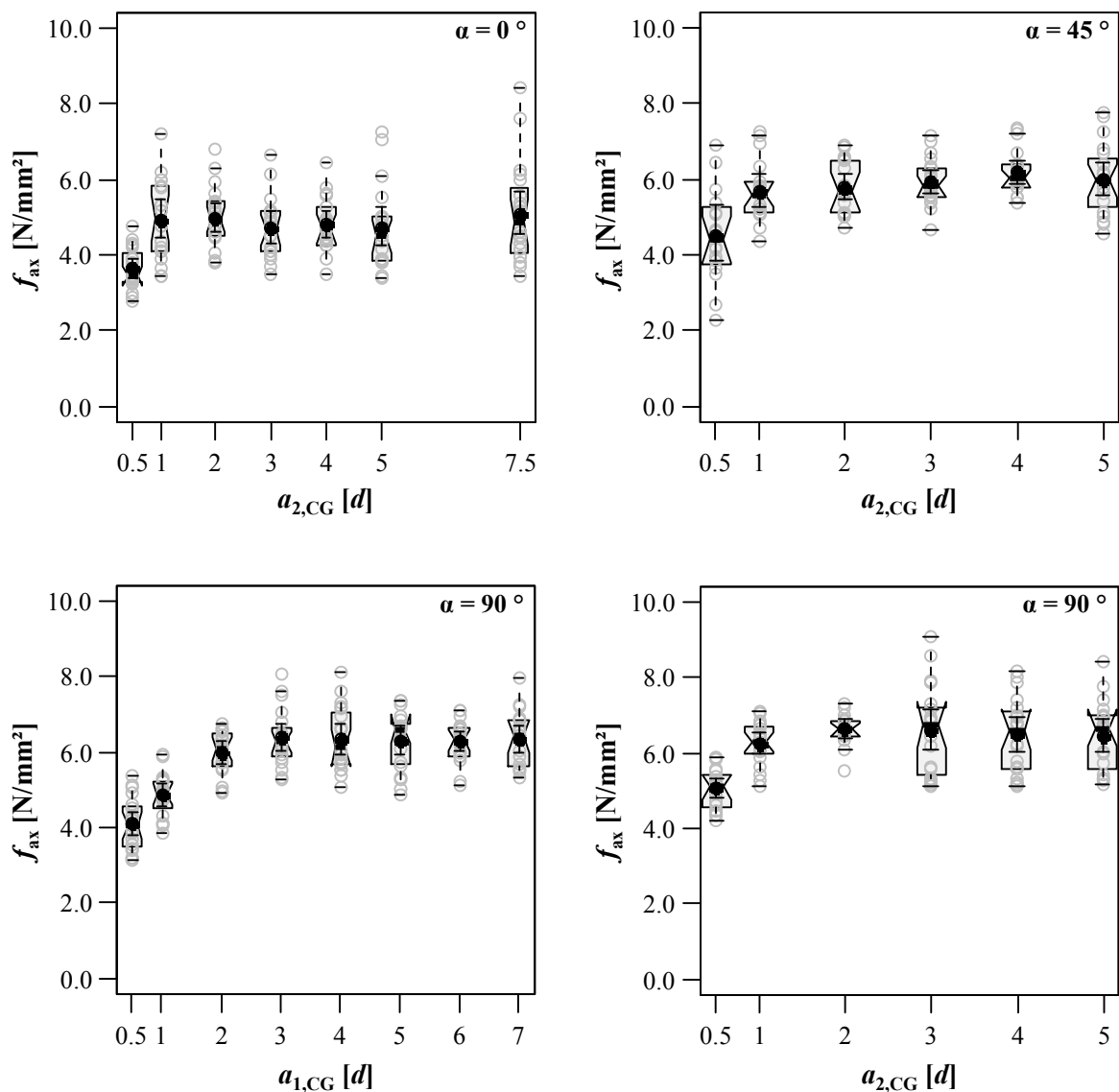


Figure 5.72: Combined boxplot/scatterplot diagrams of withdrawal strength vs. $a_{1,CG}$ and $a_{2,CG}$ in dependence of α ; test data from Gatterinig (2010)

Now concentrating on the experimental campaign carried out by Plieschounig (2010), determining the screw axial loadbearing behaviour at varying in-between spacings $\{a_1, a_2\}$, the corresponding results of

(partially) density-corrected withdrawal properties $\{f_{ax}, K_{ser,ax}, D\}$ are subsequently illustrated in form of Figure 5.73 to Figure 5.75 and Annex B-3.2, Table B.44. In addition, Figure B.49 to Figure B.51 comprise the error bars of the related variabilities. Worth mentioning, that the given values for f_{ax} (apart from the reference group with $n = 1$ screw) were determined by eq. (5.1), additionally dividing F_{max} by $n = 2$ screws. Since the results for further properties $K_{ser,ax}$ and D are exclusively applied for relative comparisons, no related modification was made.

With regard to the determined withdrawal strengths, a similar behaviour of f_{ax} at varying a_1 , as it was observed for the end-grain spacing $a_{1,CG}$ in form of a clear and progressive decrease with decreasing spacing dimensions – here already beginning at $a_1 = 5d \div 6d$ – is given. Furthermore, significant differences of both $med[f_{ax}]$ and $mean[f_{ax}]$ can be observed for $a_1 = \{2, 3\}d$. Since the value gained for $n = 1$ screw appears remarkably higher than the rest of the programme – the withdrawal strength at $a_1 = 14d$ is therefore considered as a reference. In case of varying a_2 , only f_{ax} gained for $a_2 = 2d$ results in a lower (but insignificantly different) value, while $a_2 > 2d$ obviously do not influence the withdrawal strength at all.

Comparing the variability of withdrawal strength at varying $\{a_1, a_2\}$ in Figure B.49, a pronounced regressive behaviour of $CV[\ln(f_{ax})]$ can be observed in case of a_1 . This clearly mirrors the given impact on the average values. The increase of variability with decreasing a_1 consequences an additional decrease of characteristic (5 %-) withdrawal strengths and is thus relevant if considering the influence of spacings in a design approach. In case of a_2 , a similar, but far less pronounced, trend of $CV[\ln(f_{ax})]$ is given, again mirroring the course of the average values related.

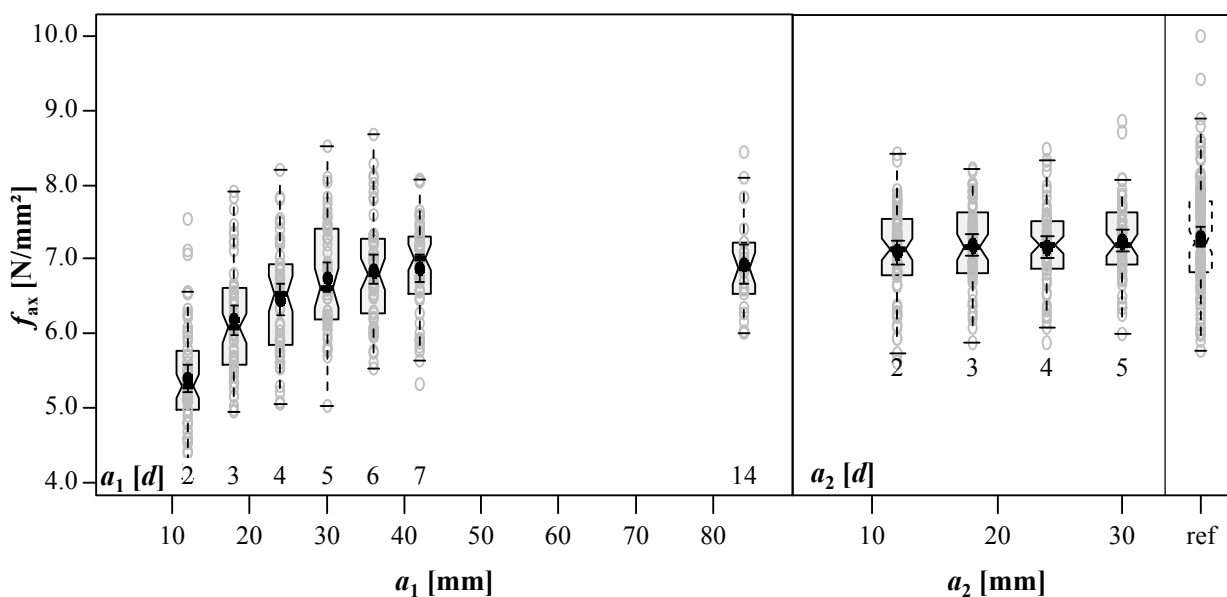


Figure 5.73: Combined boxplot/scatterplot diagram of withdrawal strength vs. spacing a_1 and a_2 ; test data from Plieschounig (2010)

Now focusing on the behaviour of the withdrawal stiffness $K_{\text{ser,ax}}$, possibly also influenced by the spacing variation: as subsequently illustrated in Figure 5.74, a generally similar but – in special case of a_1 – comparatively minor pronounced behaviour of $K_{\text{ser,ax}}$ in dependence of varying $\{a_1, a_2\}$, as it was found for the withdrawal strength, can be observed. This circumstance is in fact quite equal to other relationships for instance the influence of the moisture content variation or that of the lamination, c. f. sections 5-3.2 to 5-3.4. It is probably caused by the inaccuracy in determining this property, especially in case of considering global instead of local displacements – if compared to the applied procedure to gain withdrawal strengths. Furthermore, this also corresponds to the variability of $K_{\text{ser,ax}}$, illustrated in Figure B.50. Since the exact knowledge, concerning that topic, is seen as relevant for explaining the pronounced decrease of $K_{\text{ser,ax}}$ with an increasing number of screws within one connection, c. f. section 2-3.1, an experimental programme, including a local displacement measurement, should be considered in the frame of future investigations.

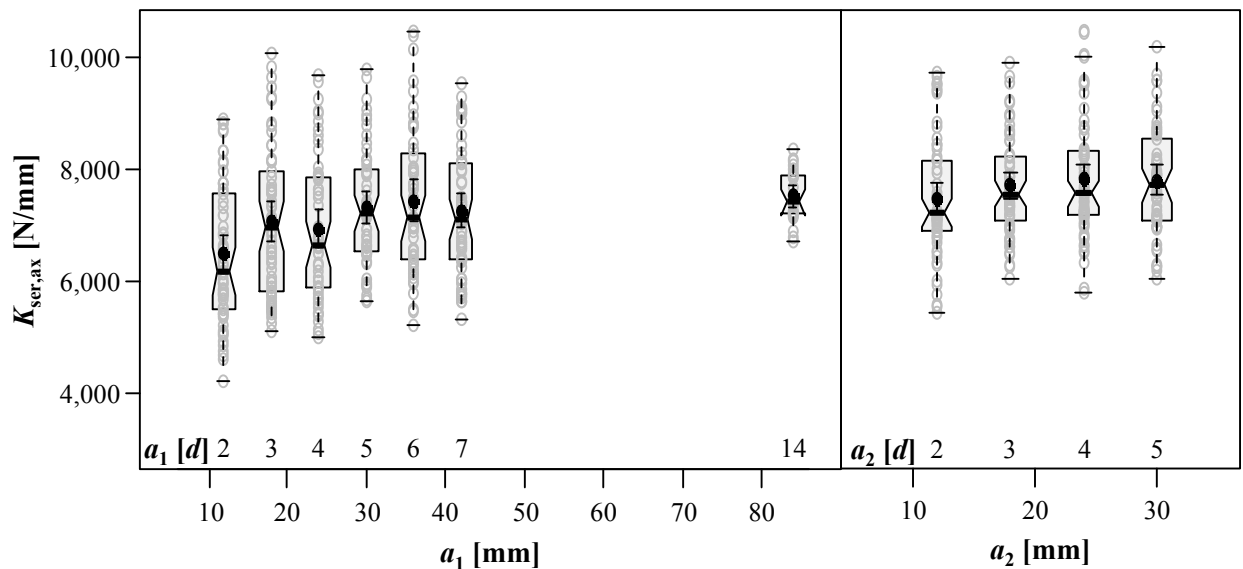


Figure 5.74: Combined boxplot/scatterplot diagram of withdrawal stiffness vs. spacing a_1 and a_2 ; test data from Plieschounig (2010)

Comparing the determined ductility D in dependence of $\{a_1, a_2\}$, as illustrated in Figure 5.75, two main observations are worth being briefly discussed: First, with regard to the influence of a_2 on D , no significant differences between the considered subseries are given. Second, the behaviour of D at varying a_1 is more or less oppositional to that of both properties f_{ax} and $K_{\text{ser,ax}}$, as discussed before. Surprisingly, the maximum results are achieved for the weakest resistances in case of $a_1 = 2d$, which is quite similar to the findings made in section 5-3.4, regarding the gap effect in CLT side faces, c. f. Figure 5.62, where $\max[D]$ is also found for the minimum values of f_{ax} and $K_{\text{ser,ax}}$.

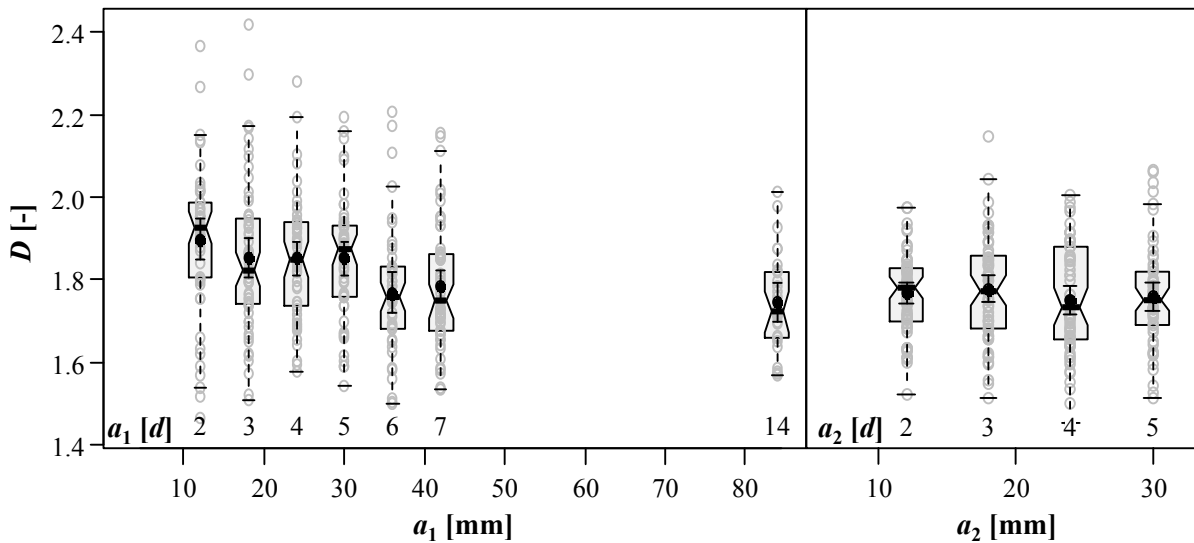


Figure 5.75: Combined boxplot/scatterplot diagram of ductility vs. spacing a_1 and a_2 ; test data from Plieschounig (2010)

As announced in the introduction of this subsection, one main reason for reassessing the test data, gained by Gatternig (2010) and Plieschounig (2010), was to investigate the interrelationship between withdrawal strength and timber density in case of varying spacings $\{a_1, a_2, a_{1,CG}, a_{2,CG}\}$. Table 5.31 subsequently comprises the corresponding results in form of k_p and $r_{XY,PE}$, determined according to eqs. (5.34) and (5.54) in dependence of axis-to-grain angle and spacing type. This excludes the subseries $a_1 = 14 d$, since the density distribution, c. f. Plieschounig (2010), and the number of tests significantly differ from the rest of this programme. With regard to spacings a_1 and $a_{1,CG}$ parallel and a_2 perpendicular to grain direction, the related distribution of the exponent k_p indicates no relevant influence of these parameters on the relationship between density and withdrawal strength. In case of the edge spacing $a_{2,CG}$, an equal situation is given for $\alpha = 45^\circ$, while for $\alpha = \{0, 90\}^\circ$, small values ($0.5 d$) lead to a remarkably smaller k_p and $r_{XY,PE}$, meaning a disproportionately low influence of ρ_{12} on f_{ax} , combined with a poor correlation for these subseries. It has to be pointed out, that both only represent an exception, even in their specific programmes. So it was decided to exclude this impact in the frame of further model considerations made in chapter 6.

Table 5.31: Experimentally determined values for k_p and $r_{XY,PE}$ in dependence of axis-to-grain angle, spacing type and characteristic

α	a_1	[d]	ref	-	2.0	3.0	4.0	5.0	6.0	7.0
90 °	k_p	[-]	0.58	-	0.57	0.63	0.81	0.79	0.76	0.52
	$r_{XY,PE}$	[-]	0.55	-	0.47	0.47	0.60	0.58	0.65	0.48
α	a_2	[d]	ref	-	2.0	3.0	4.0	5.0	-	-
90 °	k_p	[-]	0.58	-	0.87	0.90	0.63	0.86	-	-
	$r_{XY,PE}$	[-]	0.55	-	0.74	0.75	0.70	0.73	-	-
α	$a_{1,CG}$	[d]	0.5	1.0	2.0	3.0	4.0	5.0	6.0	7.0
90 °	k_p	[-]	1.46	1.23	0.66	1.14	1.31	1.20	0.96	1.24
	$r_{XY,PE}$	[-]	0.91	0.78	0.53	0.86	0.81	0.90	0.78	0.85
α	$a_{2,CG}$	[d]	0.5	1.0	2.0	3.0	4.0	5.0	7.0	7.5
0 °	k_p	[-]	0.24	1.21	1.05	0.97	0.86	1.24	-	1.55
	$r_{XY,PE}$	[-]	0.20	0.68	0.65	0.54	0.43	0.55	-	0.70
45 °	k_p	[-]	0.81	0.68	1.20	1.03	0.70	1.13	-	-
	$r_{XY,PE}$	[-]	0.31	0.55	0.87	0.70	0.41	0.61	-	-
90 °	k_p	[-]	0.36	0.63	0.70	1.24	1.16	1.24	-	-
	$r_{XY,PE}$	[-]	0.35	0.60	0.73	0.89	0.90	0.91	-	-

5-4.1.4 Model verification

The last part of this section comprises a verification of the model approach, illustrated in Figure 5.65 and eq. (5.83) to (5.89), in form of the k -factor k_{red} , covering the impact of a reduced stressable timber volume on the withdrawal strength f_{ax} . Therefore, not only the test results gained by Gattermig (2010) and Plieschounig (2010), but also those given in Plüss (2014) and Grabner and Ringhofer (2014) are considered. Both, experimentally determined and predicted values for $f_{ax,mean}$ according to eq. (5.89), in dependence of the axis-to-grain angle and the specific spacing setting applied, are summarised in Annex B-3.2, Table B.45 and Table B.46. With regard to $\Delta_{exp-pred}$ (referred to $f_{ax,mean,exp}$), apart from two exceptions of altogether 56 datasets, a maximum deviation between test result and model prediction below 10 % can be observed. In addition, a related comparison is subsequently illustrated in Figure 5.76, indicating an adequate agreement between both $f_{ax,mean,pred}$ and $f_{ax,mean,exp}$ for the whole bandwidth of the considered withdrawal strength.

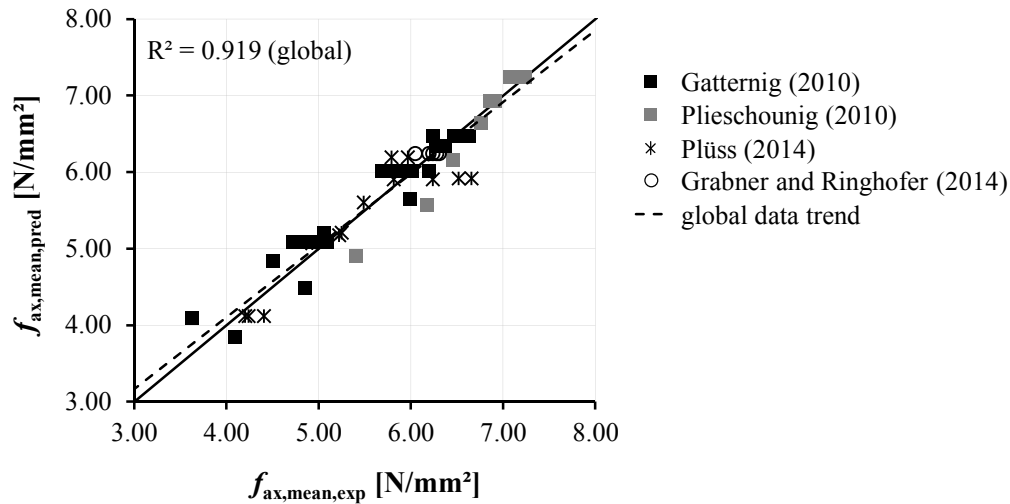


Figure 5.76: Experimental vs. predicted withdrawal strengths regarding the influence of spacings on f_{ax}

This verification also comprises the spacing configurations exceeding the upper limits of the elliptic parameters a and b . Thus, k_{red} is often equal to 1.00, which means in many cases a sole comparison of the given data with the reference value. In order to concentrate on the configurations with $\{a_1, a_2, a_{1,CG}, a_{2,CG}\}$ below both thresholds and to verify the course of the withdrawal strength with decreasing spacings, Figure B.52 to Figure B.54 in Annex B-3.1 compare the referenced test results (divided by each $f_{ax,ref}$, see Annex B-3.2, Table B.45 and Table B.46) with the model predictions in dependence of the spacing variation. Even though certain deviations between both $f_{ax,mean,pred}$ and $f_{ax,mean,exp}$ are given, the general data trend is again well represented by the model approach.

As mentioned before, representing the surface of the stressed timber volume by an elliptic form is a rough simplification, deviating from the real shear stress conditions in the area close to the screw axis. Taking a more realistic approach for describing this stress state into account, as e. g. proposed by Hübner (2013a), should be one of the next steps in the frame of future considerations. Within this thesis, the main aim of this section was (a) to show and discuss the effect of the spacing variation on the withdrawal properties and (b) to demonstrate the general applicability of a simplified model, describing this impact rather than concentrating on a detailed mechanical analysis.

Finally, it has to be mentioned, that a possible pre-damage of the timber matrix during the screw insertion causing crack formation due to tensile stresses perpendicular to grain, not only depends on the parameters, considered in the discussed programmes (e. g. d , ρ , position to annual ring structure, etc.), but also on further ones, such as the relationship between l_p and the thickness of the timber member, c. f. Uibel (2012), or the geometrical screw modifications (tips, thread properties, etc.), deviating from the fastener types herein applied, c. f. Pöll (2017). Thus, it would be valuable to increase the scope of corresponding investigations – if possible including a local displacement measurement – within one of the next steps.

5-4.2 Pre-drilling

5-4.2.1 Introduction

In fact, the vast majority of modern self-tapping timber screws is installed without pre-drilling nowadays, which is one of the main advantages of this fastener type. Nevertheless, certain cases of application, i. e. pre-processing of compact connections and reinforcements demand a high accuracy in screw positioning and may necessitate this additional preparation step. Thus, pre-drilling and its possible impact on the size and dispersion of the withdrawal properties, shall not be excluded from the considerations in this chapter. In general, as outlined in Figure 5.8, at least three parameters, namely the fact if applied – yes or no – as well as the length l_{PD} and the diameter d_{PD} of the borehole are relevant for describing this measure.

In those cases, where the screws are applied in pre-drilled timber members made of softwood, this is commonly realised with d_{PD} close to their inner thread diameter d_c as recommended in related technical approvals, c. f. ETA-11/0190 (2013), ETA-12/0114 (2012) or ETA-12/0373 (2012). The literature sources, including the impact of pre-drilling on withdrawal properties, consistently base on the experimental investigations restricted to this general agreement regarding d_{PD} . Thus, the exclusive impact of the fact if pre-drilling is applied on the withdrawal behaviour is herein considered as a comparison of screws in timber members, which were not pre-drilled in advance or d_{PD} close to d_c were used.

An extract of the related findings is subsequently summarised in Figure 5.77 in form of ratios between $f_{ax,mean,nPD}$ (no pre-drilling) and $f_{ax,mean,PD}$ (pre-drilling with $d_{PD} \approx d_c$) in dependence of the axis-to-grain angle, the number of penetrated layers and the timber product. In general, a remarkable difference between withdrawal strengths of screws, situated in pre-drilled or non-pre-drilled timber members, can not be observed for the vast majority of data series considered. In addition, the screw insertion into different laminated timber products obviously does not influence this behaviour. In case of the axis-to-grain angle, the ratio slightly tends to decrease with decreasing α , but can be regarded as negligible, since the related results vary in a tolerable bandwidth of $\pm 10\%$. Based on the findings, it can thus be concluded, that a significant impact of pre-drilling on the average withdrawal strength can not be expected at all – so far as the borehole diameters d_{PD} close to d_c are applied.

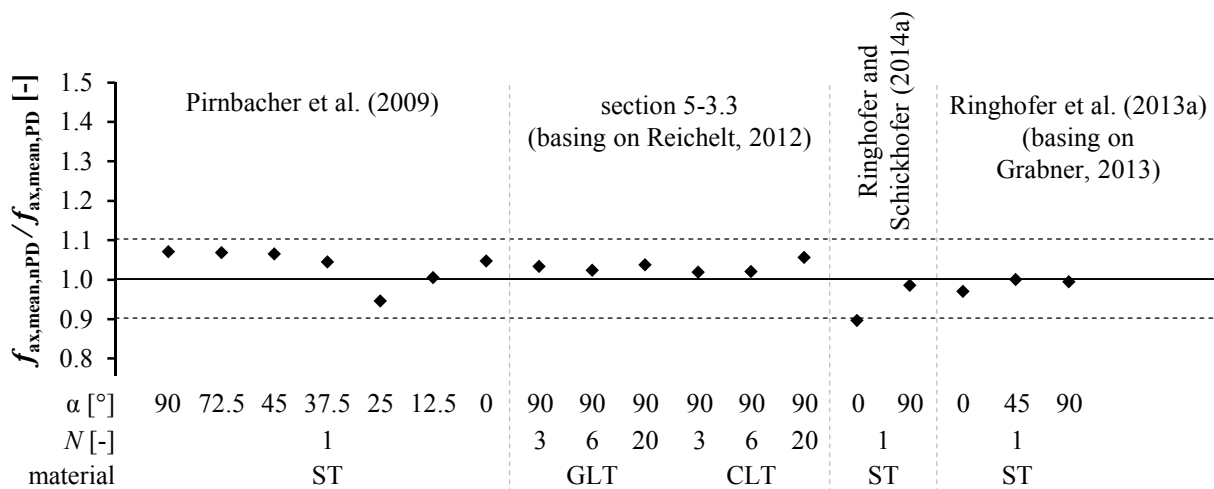


Figure 5.77: Ratios of withdrawal strengths of screws situated in pre-drilled vs. not pre-drilled specimen from selected literature sources; $d = 8 \text{ mm}$

Focusing on the variability of f_{ax} as a consequence of pre-drilling, which possibly influences the size of the characteristic (5 %-) withdrawal strength. Table 5.32 overviews the determined ratios k_{CV} (ratio between $CV[f_{ax}]$ and $CV[\rho_{12}]$), of those previously considered in literature sources, wherein the axis-to-grain angle was additionally varied. While the necessary information, regarding $CV[\rho_{12}]$ and $CV[f_{ax}]$, is available in Ringhofer et al. (2013a) and Ringhofer and Schickhofer (2014a), the test data presented in Pirnbacher et al. (2009) had to be re-assessed for this reason. Note: in order to avoid extending the content of this subsection the related experimental programme will not be discussed in this context. With regard to the courses of both k_{CV} in dependence of varying α , quite remarkable differences between values, gained from pre-drilled and not pre-drilled specimen have to be observed. Since they are more or less randomly distributed, a certain tendency (relevant for the consideration in design approaches) is in fact not given. This also corresponds to the ratios between $f_{ax,0.05,nPD}$ and $f_{ax,0.05,PD}$, presented in Pirnbacher et al. (2009), which result in average close to 1.00.

Table 5.32: Experimentally determined values for k_{CV} in dependence of pre-drilling; re-assessed data from Pirnbacher et al. (2009), Ringhofer et al. (2013a) and Ringhofer and Schickhofer (2014a)

source		Pirnbacher et al. (2009)								Ringhofer et al. (2013a)			Ringhofer and Schickhofer (2014a)	
	α	$[\circ]$	0	12.5	25	37.5	45	72.5	90	0	45	90	0	90
nPD*	k_{CV}	$[-]$	2.16	2.49	1.11	1.53	1.59	1.25	1.90	1.98	1.40	0.99	1.67	1.24
PD*	k_{CV}	$[-]$	1.96	1.67	1.82	1.44	1.42	1.72	1.45	1.53	1.43	2.16	1.52	1.57

* nPD = not pre-drilled, PD = pre-drilled

Another topic of interest is a possible influence of pre-drilling on the relationship between density and withdrawal strength. Therefore, Table 5.33 comprises the values for k_p and $r_{XY,PE}$ (determined according to eq. (5.54) and eq. (5.34)) of pre-drilled and non-pre-drilled specimen in dependence of the axis-to-grain angle variation. Since this comparison demands a certain number of tests within one subseries, the related scope is restricted to the test data from Pirnbacher et al. (2009) and Ringhofer and Schickhofer (2014a). The results from the latter source had to be re-assessed for this purpose. Note: the related programme was carried out for determining the influence of varying test configurations (loading and supporting conditions) on f_{ax} , detailed discussion is thus given in section 5-5.1. With regard to the behaviour of k_p and $r_{XY,PE}$ dedicated to pre-drilled and non-pre-drilled specimen, a more or less pronounced increase of both statistical parameters with increasing α can be observed, which again confirms the corresponding findings made in sections 5-2.1 and 5-3.1. Furthermore, apart from the series $\alpha = 90^\circ$ from Pirnbacher et al. (2009), considerably higher values for k_p , as well as for $r_{XY,PE}$, result as a consequence of pre-drilling. Based on this comparison, pre-drilling obviously leads to a more pronounced relationship between density and withdrawal strength.

Table 5.33: Experimentally determined values for k_p and $r_{XY,PE}$ in dependence of pre-drilling; re-assessed data from Pirnbacher et al. (2009) and Ringhofer and Schickhofer (2014a)

source		Pirnbacher et al. (2009)								Ringhofer and Schickhofer (2014a)	
	α	[°]	0	12.5	25	37.5	45	72.5	90	0	90
nPD*	k_p	[-]	-0.58	0.49	0.11	0.62	0.99	0.69	1.35	0.62	1.17
	$r_{XY,PE}$	[-]	-0.26	0.20	0.09	0.40	0.62	0.55	0.70	0.39	0.65
PD*	k_p	[-]	0.07	1.12	1.36	1.15	1.11	1.09	0.83	0.80	1.55
	$r_{XY,PE}$	[-]	0.03	0.68	0.75	0.80	0.78	0.65	0.56	0.43	0.90

* nPD = not pre-drilled, PD = pre-drilled

While several investigations for determining the impact of pre-drilling on withdrawal strength have been carried out so far, the knowledge regarding the further properties $K_{ser,ax}$ and D is comparatively scarce or missing at all. The corresponding results, given in Annex B-3.2, Table B.29 and Table B.30, indicate a certain loss of $K_{ser,ax}$, combined with a clear increase of ductility as a consequence of pre-drilling. Worth mentioning, that the related tests were carried out without a local displacement measurement and only comprise GLT and CLT at $\alpha = 90^\circ$. Nevertheless, the given behaviour of withdrawal stiffness is confirmed in Ringhofer et al. (2013a) for ST and $\alpha = \{0, 45, 90\}^\circ$. Since the property determination deviated from the procedure explained in section 5-1.2 – no ductility was examined – reassessment of this

programme is comprehensively discussed in the following subsections. Apart from the mentioned campaigns, no further related investigations were found in literature.

With regard to d_{PD} , exceeding the previously introduced boundary condition of $d_{PD} \approx d_c$ and a therewith associated impact on size and dispersion of withdrawal properties, no sources dealing with this parameter were found in literature. Motivated by this circumstance, a related experimental campaign was recently carried out at Graz University of Technology, c. f. Gasser (2017). The gained findings are presented in the following subsections. Unfortunately, the scope of this programme did not comprise a variation of l_{PD} as the third relevant parameter for describing the impact of pre-drilling. Since the knowledge, concerning the influence of the borehole's length on withdrawal properties, is also missing in literature, this remains as an open task for the future.

5-4.2.2 Experimental programme

As mentioned before, the results of two experimental campaigns, concentrating on the impact of pre-drilling on screw withdrawal properties, are subsequently presented and discussed. The first programme, also published in Ringhofer et al. (2013a), includes a variation of axis-to-grain angle α of pre-drilled and not pre-drilled specimen (but with constant $d_{PD} \approx d_c$), carried out by Grabner (2013). The main idea behind was to determine the impact of α on f_{ax} of screws, situated in the narrow face of CLT elements. Thus, the related experiments are comprehensively explained in section 5-4.3. The second programme, conducted by Gasser (2017), focusing on the impact of varying d_{PD} but with axis-to-grain angles stuck to $\alpha = \{0, 90\}^\circ$ shall be introduced as follows:

The basic material for this campaign were altogether 10 solid timber beams of Norway spruce with cross-sectional dimensions of about $w \times h = 140 \times 140 \text{ mm}^2$. Since the same $d = 8 \text{ mm}$ partially threaded screw was used, as considered in section 5-3.1 (thread characteristics see Table 5.6), the available thread length and the boundary condition to situate the screw tip outside the specimen necessitated a timber formatting to a target height of 60 mm. Further information, regarding specimen geometry and screw positioning, is shown in Annex B-3.1, Figure B.55. In order to realise a similar density distribution for all subseries considered, the principle of “matched samples”, as explained in section 5-1.2, was applied. Deviating from the majority of the test series, a strict time schedule did not allow a specimen storage in the climatic chamber until the equilibrium moisture content was reached. The related consequences are discussed in the following subsection. Additional information, regarding the parameter variation and the test conditions, is subsequently given in Table 5.34.

Table 5.34: *Varied parameters and test conditions applied for the experimental campaign focusing on the impact of d_{PD} on withdrawal properties*

varied parameters			test conditions		
d [mm]	α [°]	d_{PD} [mm]	l_p [mm]	l_{ef} [mm]	l_{emb} [mm]
8	0, 90	nPD*, 5.0, 5.5, 6.0, 6.5, 7.0, 7.5	60	60	0

* not pre-drilled

Worth mentioning, that all tests have been performed by Grabner (2013) and Gasser (2017) on the test rig LIGNUM-UNI-275 with a local way measurement set-up, enabling the determination of $K_{ser,ax}$ and D as absolute values. Further background information, regarding test execution, post-processing, property determination and data assessment, is summarised in section 5-1.2.

5-4.2.3 Results and discussion

Statistical parameters and distributions of small scale specimen's timber density ρ_{12} , dedicated to both experimental campaigns, are subsequently illustrated in Figure 5.78 to Figure 5.80 in dependence of the parameter variation given in Table 5.34. In addition, Annex B-3.2, Table B.47 and Table B.48 also include the statistical parameters of moisture content u related. Overall, the determined moisture contents vary in the aimed bandwidth of $\pm 2\%$. In case of the series, carried out by Grabner (2013), a prior climatic conditioning led to an average u , close to the equilibrium moisture content. In case of those conducted by Gasser (2017), as mentioned before, no climatic conditioning was applied. Thus, the average moisture contents result to be somewhat lower. Nevertheless, nearly equal average values within the series do not necessitate any moisture-dependent treatment of determined properties.

With regard to timber density, similar to the tests presented in section 5-3.4, the results gained by Grabner (2013) significantly vary in dependence of pre-drilling, c. f. Figure 5.78. Thus, both withdrawal properties f_{ax} and $K_{ser,ax}$ were corrected according to eq. (5.81) with an average density of 427 kg/m^3 . While this treatment was not necessary for the series carried out by Gasser (2017), a significant difference of the related variability can be observed for $\alpha = 90^\circ$, c. f. Figure 5.80, possibly causing an unwanted influence on the variability of the withdrawal properties.

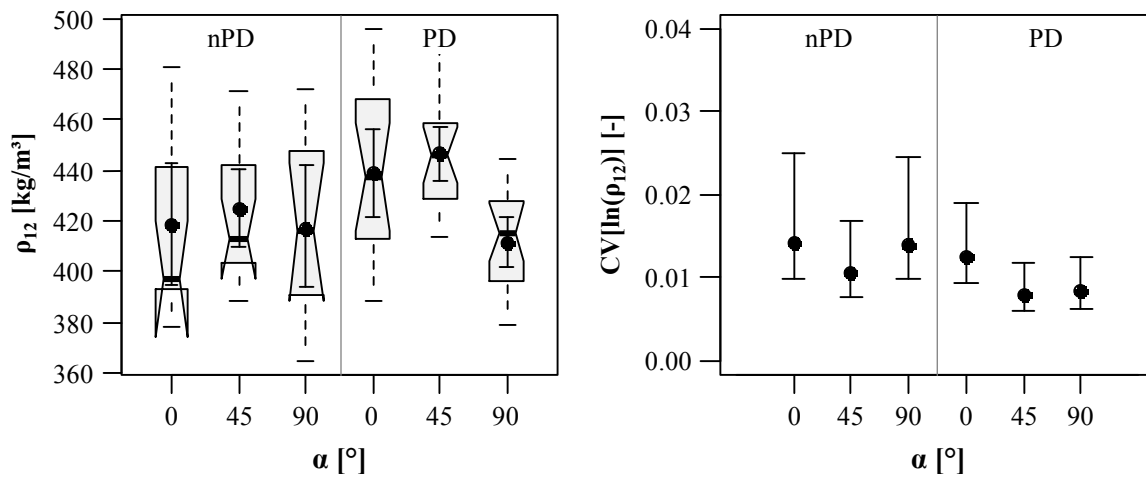


Figure 5.78: Left: boxplot diagram of densities ρ_{12} ; right: CIs of $CV[\ln(\rho_{12})]$ in dependence of pre-drilling and axis-to-grain angle α ; test data from Grabner (2013);

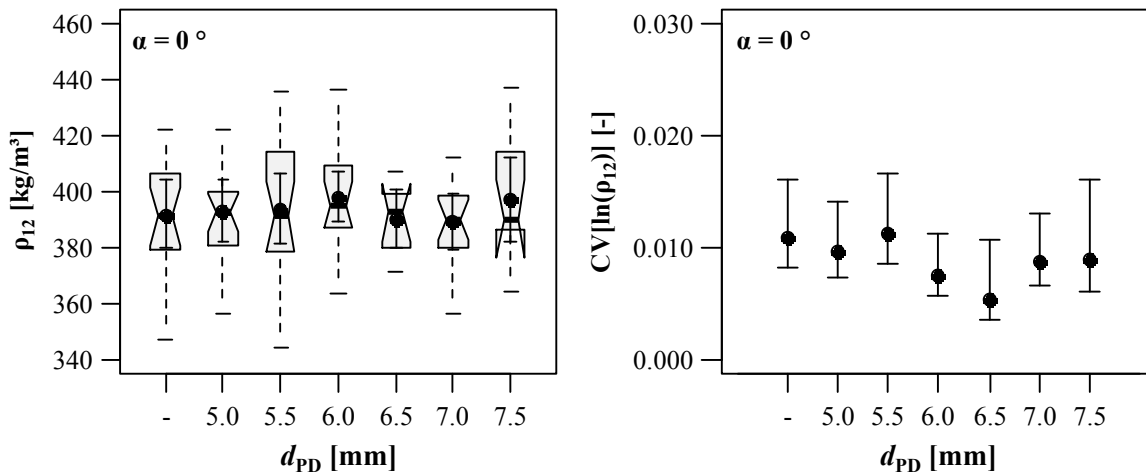


Figure 5.79: Left: boxplot diagram of densities ρ_{12} ; right: CIs of $CV[\ln(\rho_{12})]$ in dependence of d_{PD} for $\alpha = 0^\circ$; test data from Gasser (2017)

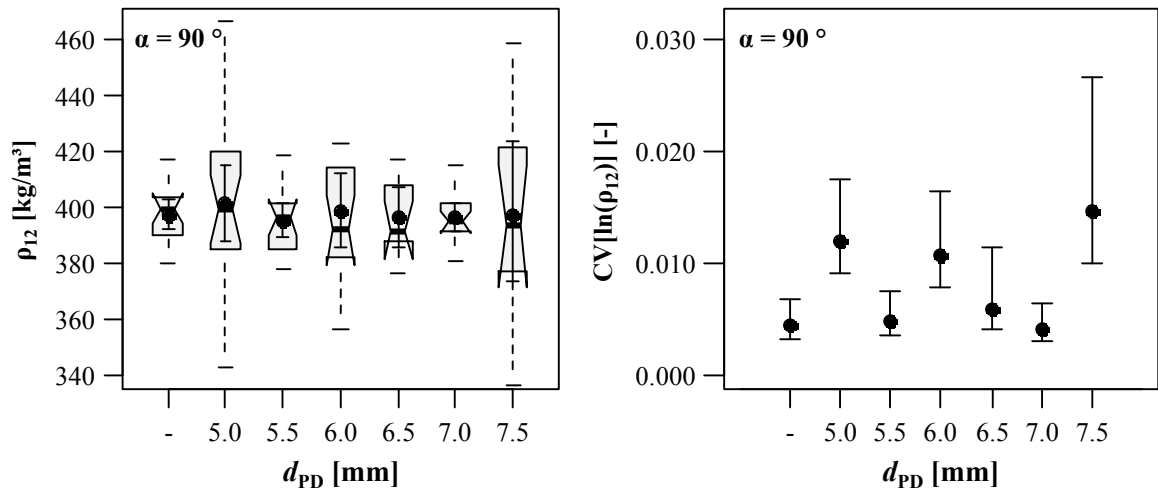


Figure 5.80: Left: boxplot diagram of densities ρ_{12} ; right: CIs of $CV[\ln(\rho_{12})]$ in dependence of d_{PD} for $\alpha = 90^\circ$; test data from Gasser (2017)

The confidence intervals and error bars of the main statistical parameters of the withdrawal properties are subsequently shown in Figure 5.81 to Figure 5.86, as well as in Annex B-3.2, Table B.49, Table B.50 and Figure B.56 to Figure B.58. Concentrating on the withdrawal strength of screws, situated in pre-drilled ($d_{PD} = 5$ mm) or non-pre-drilled timber members, the courses illustrated in Figure 5.81 again confirm, that the size of f_{ax} is not remarkably influenced by this preparation measure. With regard to the behaviour for d_{PD} at varying d_c , a bilinear relationship without any significant difference, up to a borehole diameter of $d_{PD} = 6$ mm ($\sim 1.11 \cdot d_c$), combined with a pronounced decrease for d_{PD} exceeding this threshold can be observed. Furthermore, the given performance of withdrawal strength does not qualitatively depend on the axis-to-grain angle α – compare Figure 5.82 (left vs. right). Since the variability of the timber density was found significantly varying in-between the subseries – a statement concerning that of withdrawal strength in dependence of d_{PD} is hardly definable. Nevertheless, at least for the parallel-to-grain insertion, a significant increase of $CV[\ln(f_{ax})]$ with increasing d_{PD} can be observed, c. f. Figure B.56, which expresses the uncertainty of the screw loadbearing behaviour for d_{PD} close to d .

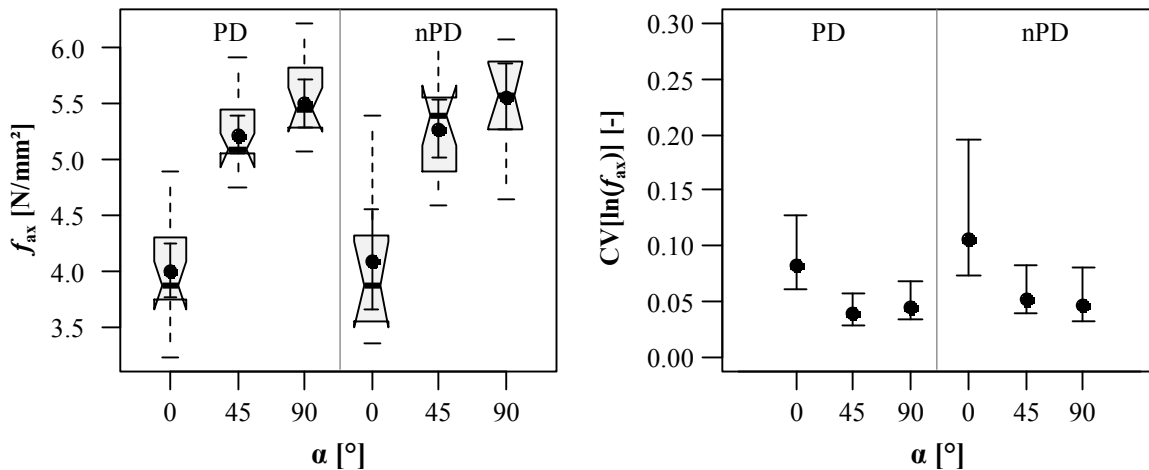


Figure 5.81: Left: boxplot diagram of withdrawal strength f_{ax} ; right: CIs of $CV[\ln(f_{ax})]$; both in dependence of axis-to-grain angle and pre-drilling, test data from Grabner (2013);

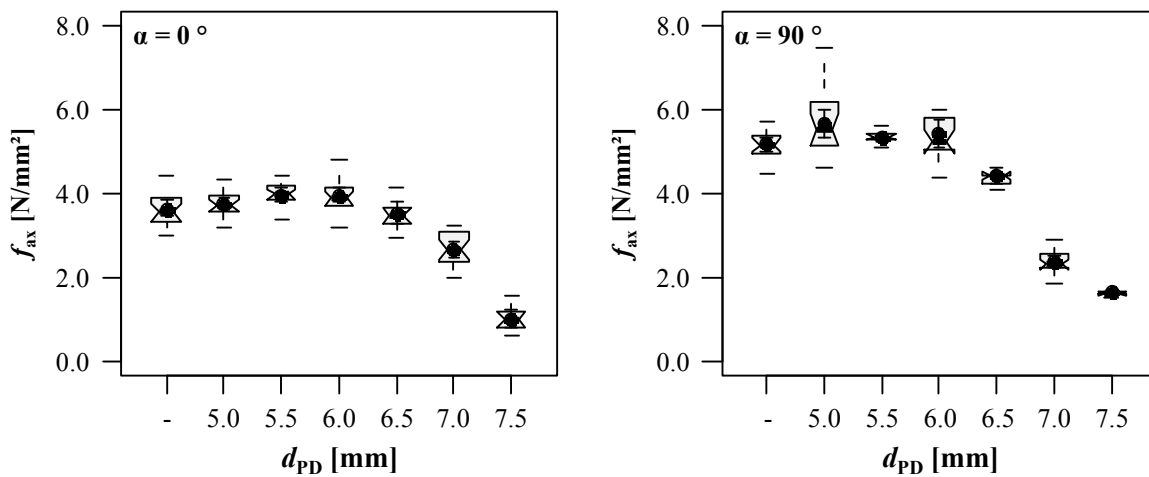


Figure 5.82: Boxplot diagrams of withdrawal strength f_{ax} vs. d_{PD} ; left: $\alpha = 0^\circ$; right: $\alpha = 90^\circ$; test data from Gasser (2017)

As already indicated in the introduction of this section and illustrated in Figure 5.83, the withdrawal stiffness of screws, situated in pre-drilled timber specimen, is moderately to significantly lower than of those inserted without pre-drilling. Similar to the withdrawal strength, the given difference between $K_{ser,ax,nPD}$ and $K_{ser,ax,PD}$ is independent from α , but results in a higher magnitude of roughly 20 %. A possible reason therefore could be an increase of the local timber stiffness properties, due to densifying the material when inserting the screws without pre-drilling in advance. The results gained from Gasser (2017), shown in Figure 5.84, generally confirm this circumstance. Furthermore, therein illustrated behaviour of $K_{ser,ax}$ with varying d_{PD} indicates the same relationships as they are observed for the withdrawal strength. This circumstance also corresponds to the variability of $K_{ser,ax}$, again increasing with increasing d_{PD} , c. f. Figure B.57.

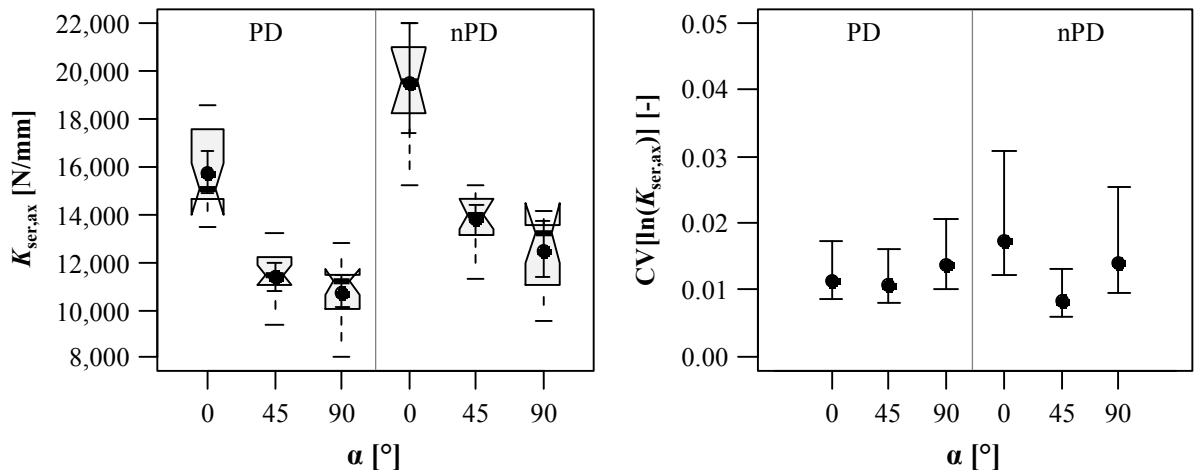


Figure 5.83: Left: boxplot diagram of withdrawal stiffness $K_{ser,ax}$; right: CIs of $CV[\ln(K_{ser,ax})]$; both in dependence of axis-to-grain angle and pre-drilling, test data from Grabner (2013)

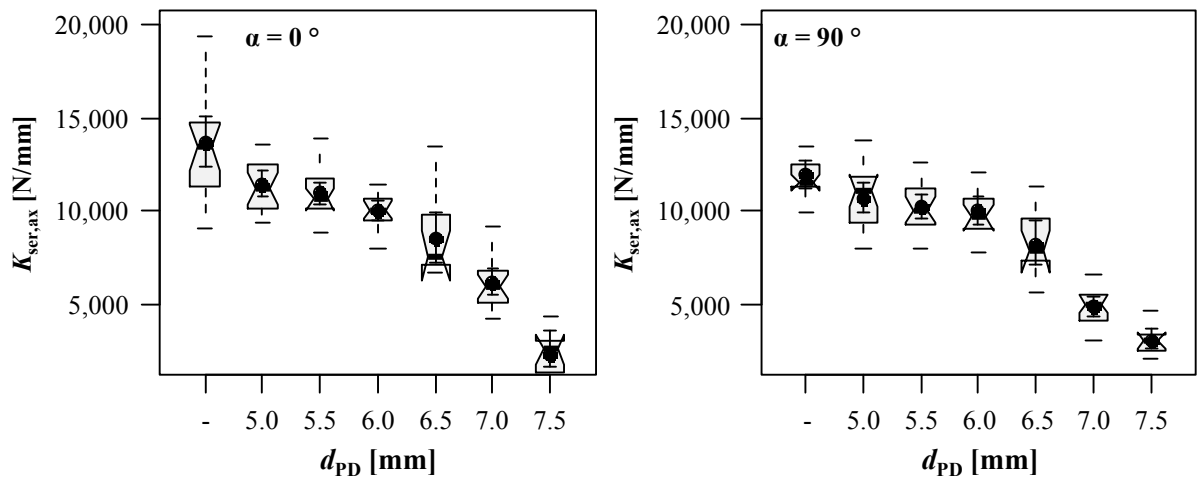


Figure 5.84: Boxplot diagrams of withdrawal stiffness $K_{ser,ax}$ vs. d_{PD} ; left: $\alpha = 0^\circ$; right: $\alpha = 90^\circ$; test data from Gasser (2017)

With regard to the ductility of axially loaded self-tapping screws, inserted in pre-drilled ($d_{PD} \approx d_c$) and non-pre-drilled timber members, the corresponding behaviour, shown in Figure 5.85, indicates a loss of D as a consequence of this preparation measure for the parallel- and perpendicular-to-grain insertion, while in case of $\alpha = 45^\circ$ the oppositional behaviour has to be observed. Nevertheless, absolute values, determined for non-pre-drilled specimen, result in a magnitude comparable to the one shown in Figure 5.16. Furthermore, the results, corresponding to the programme conducted by Gasser (2017), confirm the observation for $\alpha = \{0, 90\}^\circ$. Both are thus in contrast to the differences in D determined for screws, which were inserted in pre-drilled and non-pre-drilled timber members with varying N , c. f. Figure 5.46 and Figure 5.47. These circumstances again underline the challenge of describing the influence of certain parameters on this property. Focusing on the course of D , in case of varying d_{PD} , a clear ($\alpha = 0^\circ$) to a

minor pronounced ($\alpha = 90^\circ$) increase of ductility with increasing d_{PD} is given. Similar to the influence of gap insertion (section 5-3.4) and spacing variation (section 5-4.1), this clearly mirrors the behaviour of the other withdrawal properties f_{ax} and $K_{ser,ax}$.

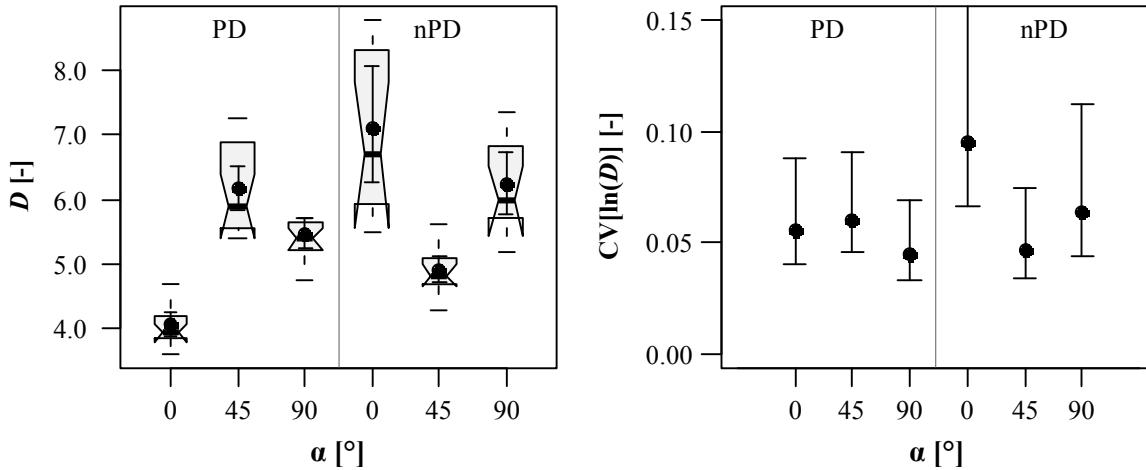


Figure 5.85: Left: boxplot diagram of ductility D ; right: CIs of $CV[\ln(D)]$; both in dependence of axis-to-grain angle and pre-drilling, test data from Grabner (2013)

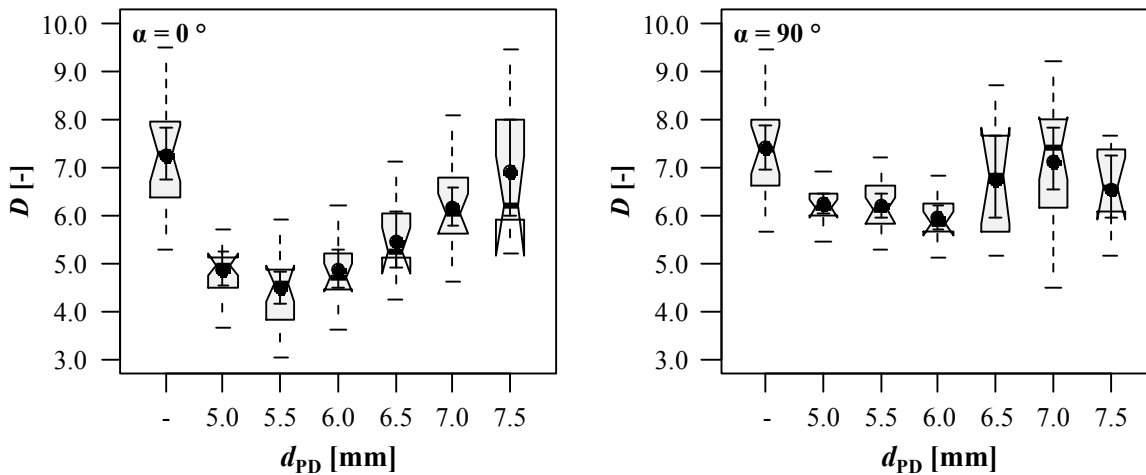


Figure 5.86: Boxplot diagrams of ductility D vs. d_{PD} ; left: $\alpha = 0^\circ$; right: $\alpha = 90^\circ$; test data from Gasser (2017)

As observed in Figure 5.82 and Figure 5.84, d_{PD} exceeding d_c lead to a significant decrease of both withdrawal properties, f_{ax} and $K_{ser,ax}$. Thus, the final part of this section concentrates on describing the given behaviour by simplified model approaches, enabling a possible consideration for design purposes. The first approach is independent from the test results and states, that a loss of bearing resistance (and stiffness) is caused by a loss of contact surface between the screw thread and the timber member as a consequence of d_{PD} varying between d_c and d , see Figure 5.87.

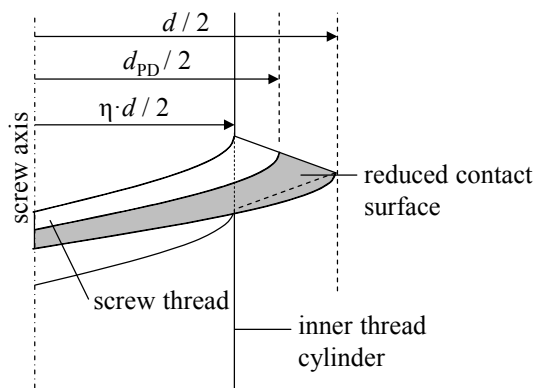


Figure 5.87: Schematic illustration of the reduced contact surface due to pre-drilling

Additionally assuming the force transmission, exclusively parallel to the screw axis and concentrating on one thread turn, the ratio between the reduced and the maximum possible contact surface solely depends on d , η and d_{PD} and can be expressed in form of a reduction (k -)factor as follows:

$$\eta_{PD} = \frac{X_{PD}}{X_{ref}} = \begin{cases} 1.00 \\ k_{PD} \end{cases} \text{ for } \begin{cases} d_{PD} \leq d_c \\ d_c < d_{PD} \leq d \end{cases}, \text{ with} \quad (5.90)$$

$$k_{PD} = \frac{A_{red}}{A_{tot}} = \frac{\frac{(d^2 - d_{PD}^2) \cdot \pi}{4}}{\frac{(d^2 - d_c^2) \cdot \pi}{4}} = \frac{1 - \left(\frac{d_{PD}}{d}\right)^2}{1 - \eta^2}. \quad (5.91)$$

The second approach bases on the observed behaviour of $X = \{f_{ax}, K_{ser,ax}\}$, in dependence of d_{PD} , being approximatively describable by a bilinear relationship with $1.10 \cdot d_c$ as threshold. If exceeded, a linear decrease of X is given, see eq. (5.92):

$$\eta_{PD} = \frac{X_{PD}}{X_{ref}} = \begin{cases} 1.00 \\ 1.00 - k_{PD} \cdot (d_{PD} - 1.1 \cdot d_c) \end{cases} \text{ for } \begin{cases} d_{PD} \leq 1.1 \cdot d_c \\ 1.1 \cdot d_c < d_{PD} \leq d \end{cases}, \text{ with} \quad (5.92)$$

$$k_{PD} = \frac{1}{d \cdot (1 - 1.1 \cdot \eta)}. \quad (5.93)$$

A comparison of both models, given in eq. (5.90) and eq. (5.92) with the test results of withdrawal strength and stiffness gained from Gasser (2017), is subsequently illustrated in Figure 5.88 and Figure 5.89, in dependence of the axis-to-grain angle. Therefore both properties were referenced to the average values for $d_{PD} = 5.0$ mm as outlined in Table B.50. In general, both approaches take the significant decrease of $\{f_{ax}, K_{ser,ax}\}$ with increasing d_{PD} into account, thus fulfilling the basic requirement for the related description. With regard to the model, considering the reduced contact surface according to

eq. (5.90), steady decreasing withdrawal properties for $d_{PD} > d_c$ lead to a significant underestimation of the test results. The situation for the bilinear approach stands in contrast: here, the chosen threshold of $1.10 \cdot d_c$, combined with the linear decrease of X above this boarder, enables a quite accurate property estimation for the majority of the subseries considered.

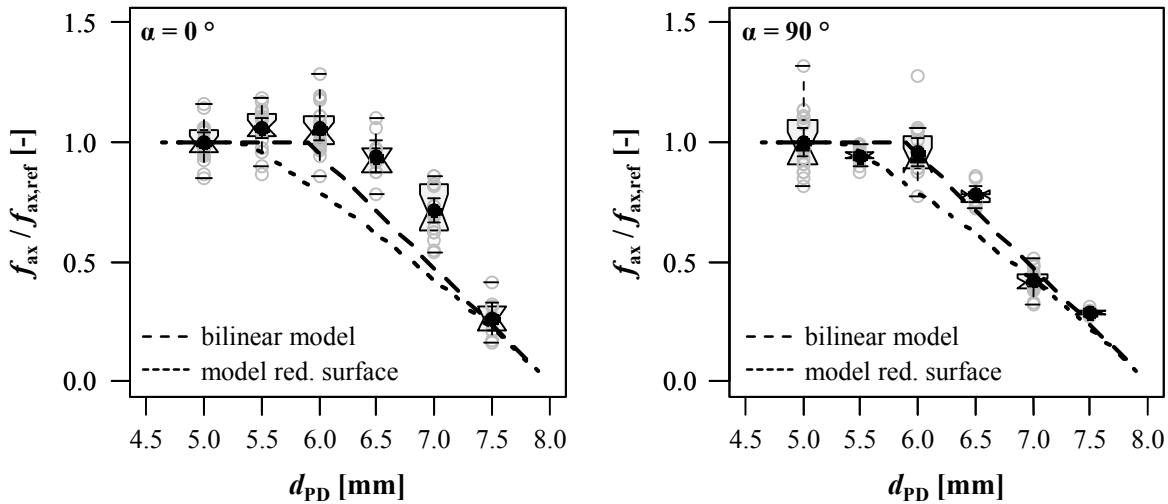


Figure 5.88: Comparison of test results with model predictions for withdrawal strength at varying d_{PD} , $d = 8 \text{ mm}$

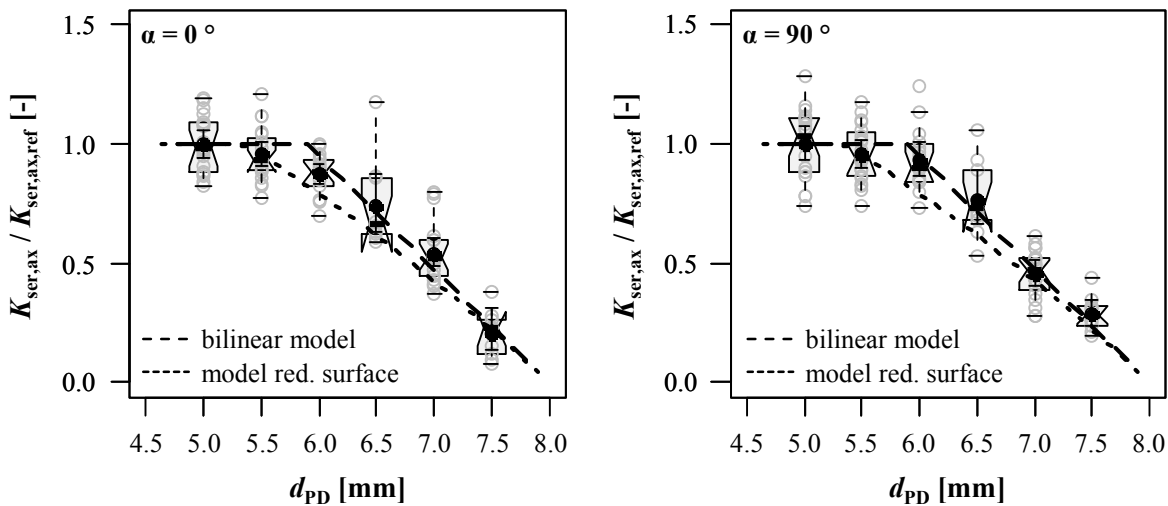


Figure 5.89: Comparison of test results with model predictions for withdrawal stiffness at varying d_{PD} , $d = 8 \text{ mm}$

5-4.3 Axis-to-grain angle α

5-4.3.1 Introduction

Following the definition of withdrawal failure, given in section 5-1.1, the orthotropic material behaviour of the timber member leads to a screw loadbearing performance, highly depending on the orientation of its axis with respect to the timber's *R-T-L*-coordinate system. This, especially when swapping the order of the associated longitudinal shear planes from $\{RL, TL\}$ to $\{LR, LT\}$, which means a change from perpendicular- to parallel-to-grain insertion. Additionally taking rather small bandwidths of outer thread diameters and timber densities, practically applied for high-stressed timber connections into account, the axis-to-grain angle α is probably the most relevant parameter dominating the size of withdrawal properties. Consequently, not only the vast majority of test series presented in this chapter, but also experimental programmes as the basis of model approaches, discussed in section 5-1.3, as well as test standard ON EN 1382 (1999) consider at least screw insertion at $\alpha = \{0, 90\}^\circ$, as the lower and upper bandwidth of the related parameter variation.

With regard to both mentioned limits, the consequences for the withdrawal properties (found in literature and discussed so far) are a pronounced decrease of the withdrawal strength f_{ax} , the inverse behaviour of the withdrawal stiffness $K_{ser,ax}$ and – rather a tendency than a fact – a slight decrease of the ductility D , when shifting the axis-to-grain angle from $\alpha = 90^\circ$ to 0° . This also concerns the variability of properties observed to be remarkably higher for the parallel- than for the perpendicular-to-grain insertion, which is seen to be relevant for the derivation of design approaches. Furthermore, restricting the scope to withdrawal strength, the parameter k_{90} as the ratio between $f_{ax,\alpha=90^\circ}$ and $f_{ax,\alpha=0^\circ}$ is significantly influenced by the major parameters outer thread diameter and timber density (k_{90} increases with increasing d and ρ), indicating an important interrelationship for advanced modelling. There are other influencing parameters with a differently pronounced impact on withdrawal properties in dependence of $\alpha = \{0, 90\}^\circ$ as moisture content u and the size of the stressed timber volume (spacings $\{a_1, a_2, a_{1,CG}, a_{2,CG}\}$), c. f. sections 5-3.2 and 5-4.1. In addition, a significant correlation between the withdrawal strength and the shear modulus was found for the parallel-to-grain insertion in section 5-3.1, while in case of a perpendicular-to-grain insertion, no comparable relationship could be observed. The latter circumstance shall again express the difference in the loadbearing behaviour of screws, situated at both axis-to-grain angles.

Now focusing on the impact on withdrawal properties if α varies between both limits. With regard to the behaviour of withdrawal strength, except from the model published in Frese and Blaß (2009), all approaches introduced in section 5-1.3 comprise a k_{ax} -factor as a function of k_{90} and α for covering the related influence on f_{ax} . As already mentioned in section 5-1.3, these functions are either trigonometric according to Hankinson (1921), or bilinear with a discontinuity at $\alpha = 30^\circ$ or 45° . The latter possibility is frequently recommended in technical approvals, too, c. f. for instance ETA-11/0190 (2013). In addition to

the varying values for k_{90} , proposed by the authors, different mathematical treatment consequences remarkable deviations in withdrawal strength. This especially for axis-to-grain angles below $\alpha = 60^\circ$, see Figure 5.90. The illustration not only includes the aforementioned approaches, but also one published in Brandner et al. (2017). The reason therefore is, that Brandner et al. (2017) describe the behaviour by a polynomial function of 3rd order, which was not applied so far for this purpose.

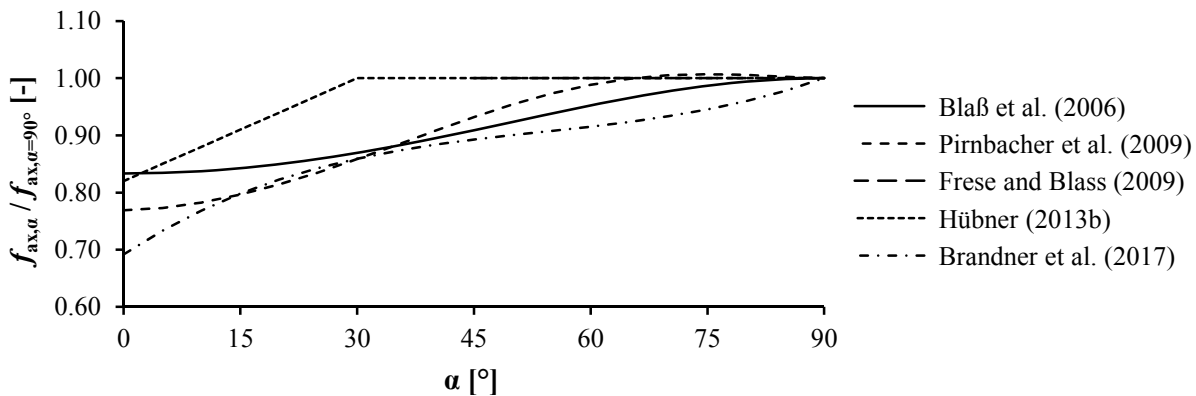


Figure 5.90: Comparison of k_{ax} -approaches proposed in literature sources discussed in section 5-1.3

Even though the comparison, given in Figure 5.90, indicates different opinions regarding the way withdrawal strength shall be influenced by the axis-to-grain angles, varying between $\alpha = \{0, 90\}^\circ$, the related recommendations base on comprehensive investigations made in the past. The situation for both withdrawal properties $K_{ser,ax}$ and D stands in contrast: as already mentioned in section 5-1.3, both currently applied models, presented in eqs. (5.45) and (5.46), do not consider any impact of α on the withdrawal stiffness. This is probably caused by a comparatively minor basic research carried out so far in this field. The paper published by Brandner et al. (2017) has to be outlined in this context, since they exclusively propose the related description in form of a bilinear approach with a discontinuity at $\alpha = 45^\circ$ and a linear increase of $K_{ser,ax}$ for α below this threshold. The related modelling based on an experimental campaign, carried out by Grabner (2013), comprising screw withdrawal tests in CLT narrow faces. Note: some parts of his programme have already been presented in section 5-3.4 and 5-4.2, mentioning that he considered local displacement measurement for a large part of his tests. This also enables determining the behaviour of D for axis-to-grain angles varying between $0^\circ < \alpha < 90^\circ$, which has not been examined in literature and is consequently part of the experimental programme introduced in the following subsections.

So far, the discussion regarding the impact of the axis-to-grain angle on withdrawal properties, based on a constant timber orientation around the screw's outer thread's lateral area, thus covering the application in solid timber or in one layer of laminated timber products. It is worth pointing out, that specifically the screw insertion in CLT side and narrow faces necessitates an additional consideration of alternating axis-

to-grain angles along the screw axis due to a crosswise layer orientation (CLT side face). Furthermore, the possibility of situating a screw directly in the transition of two neighbouring layers with different axis-to-grain angles (CLT narrow face, $\alpha_1 = 0 \div 90^\circ$, $\alpha_2 = 90 - \alpha_1$) – equally sharing the lateral area and thus the stressed timber volume – has to be taken into account. Their impact on all withdrawal properties $\{f_{ax}, K_{ser,ax}, D\}$, considered in this thesis has not been found in literature. Thus, related investigations, conducted as student works at Graz University of Technology, one explained in Ringhofer et al. (2013) and one as also part of the programme of Grabner (2013), are presented in the following subsections. This comprises a possible impact of the ratio between the screw outer thread diameter and the layer thickness in case of CLT narrow face insertion.

5-4.3.2 Experimental programme

As mentioned before, outlined in Table 5.35, the test programme concentrating on the influence of the axis-to-grain angle on screw withdrawal properties has been carried out in the frame of two experimental campaigns. In addition to an angle variation, also including the transition zones between two neighbouring layers, Grabner (2013) considered two outer thread diameters $d = \{8, 12\}$ mm (thread characteristics see Table 5.6 and Table 5.26), each positioned in two layers with $t_1 = \{20, 40\}$ mm and thus altogether four ratios of t_1 / d within his programme. Deviating from the common procedure of an in-house production, the 5-layered CLT specimen (Norway spruce), used for the tests and shown in Annex B-3.1, Figure B.59, were cut from panels supplied by a specific manufacturer. The related impact on the subseries' density distribution is discussed in the following subsection.

While Grabner (2013) concentrated on the screw insertion in CLT narrow faces, the second presented campaign comprised an axis-to-grain angle variation in a practically relevant bandwidth of $\alpha = \{30, 60, 90\}^\circ$ for screws situated in CLT side faces. Again, two outer thread diameters $d = \{8, 12\}$ mm (thread characteristics see Table 5.25, line 1 and 3), as well as 5-layered CLT elements were applied, c. f. Figure B.60. Note: both reference series, C 1.1 and C 2.1, are also considered in section 5-3.3 for the model verification. In contrast to programme I, the specimen production was conducted in the laboratory at Graz University of Technology, following the principle explained in section 5-1.2. Therefore, timber boards (Norway spruce) with dimensions of about $l \times w \times h = 4000 \times 200 \times 40$ mm³ were applied, related details regarding manufacture can be found in Ringhofer et al. (2013). Deviating from the vast majority of withdrawal tests discussed in this chapter, a pull-pile configuration was used for the test execution in order to situate the screws inclined to the specimen surface, which was necessary for simulating the practical application. A study, concerning the impact of this deviating test configuration on withdrawal properties, is presented in section 5-5.1. For reasons of accuracy, both $d = 8$ mm supporting screws were installed with pre-drilling ($d_{pD} = 5$ mm) the timber specimen in advance. Considering the boundary condition of determining all withdrawal properties at $N = 5$ penetrated layers with equal t_1 overall, the angle variation from $\alpha = 90^\circ$ to 30° doubles the length of the inserted screw thread l_{ef} . To examine a

possible influence related, two further subseries per d with constant l_{ef} but decreasing t_1 were conducted. In addition, the unequal value of N leads to a differing number of layers with alternating axis-to-grain angles per specimen, $N(\alpha = 90^\circ) = \{2, 3\}$. Thus, it was decided to test half of each subseries with two, and the others with three layers inserted perpendicular-to-grain.

Table 5.35: Overview of test series dedicated to the impact of axis-to-grain angle variation

series	general information					test conditions		
	no. of subseries [-]	α [°]	t_1 / d [-]	d_{nom} [mm]	d_{PD} [mm]	l_p [mm]	l_{ef} [mm]	l_{emb} [mm]
I	36*	0, 30, 45, 60, 90, 0 90, 45 45	2.5, 5.0	8	5	80	70.6	0
			1.7, 3.3	12	7	120	106.0	0
II	10	30, 60, 90	-	8	-	60, 69, 120, 58, 60	$= l_p$	0
				12	-	100, 115, 200, 98, 100	$= l_p$	0

* note: three subseries conducted without pre-drilling are excluded since a related discussion is given in section 5-4.2

Worth mentioning, that all tests have been performed on the test rig LIGNUM-UNI-275, following the standard procedure discussed in section 5-1.2. In case of test campaign I and $d = 8$ mm, local displacements were recorded enabling the determination of both properties, $K_{ser,ax}$ and D . In case of test campaign II, tests were carried out without a local way measurement. Furthermore, the pull-pile test configuration causes an unsteady impact on the load chain's flexibility. This in fact also disables a relative comparison of determined properties – the focus is thus restricted to the withdrawal strength. Further background information regarding test execution, post-processing, property determination and data assessment is summarised in section 5-1.2.

5-4.3.3 Results and discussion

For a better overview, the results from both experimental campaigns are separately discussed within this subsection. With regard to those gained from programme I, the main statistics of small scale specimen's timber densities ρ_{12} and moisture contents u (both determined according to eq. (4.2) and (4.4)) are subsequently given in Figure 5.91 and Figure 5.92, as well as in Annex B-3.2, Table B.51 and Table B.52. Note: the screw insertion, directly in the transition between two layers is further denoted as “intermediate layer” (IL).

Since all average moisture contents are closely located to the equilibrium value and their maximal deviations result between a target bandwidth of $\pm 2\%$ – a related treatment of withdrawal properties was not necessary. Focusing on density, especially the boxplot and error bar diagrams, illustrated in Figure

5.91 and Figure 5.92, show significant deviations of mean values and medians between the subseries, thus demanding a density correction of the withdrawal properties f_{ax} and $K_{ser,ax}$, according to eq. (5.81). Therefore, $\rho_{ref} = 450 \text{ kg/m}^3$ as a rounded overall average was applied. The corresponding variabilities of ρ_{12} – especially those dedicated to the screw insertion into cross layers (CL) – are also affected by this circumstance, possibly influencing those of the withdrawal properties.

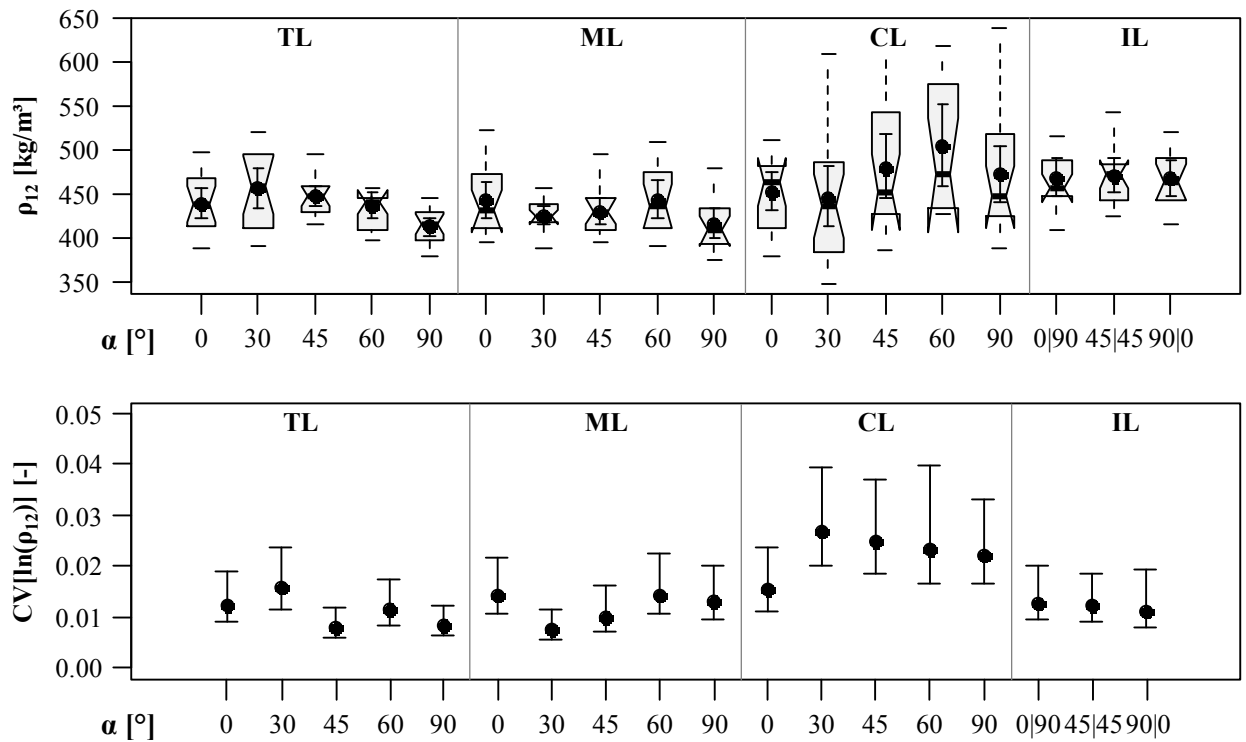


Figure 5.91: Above: boxplot graphic of densities ρ_{12} ; below: CIs of $CV[\ln(\rho_{12})]$; test programme I, $d = 8 \text{ mm}$;

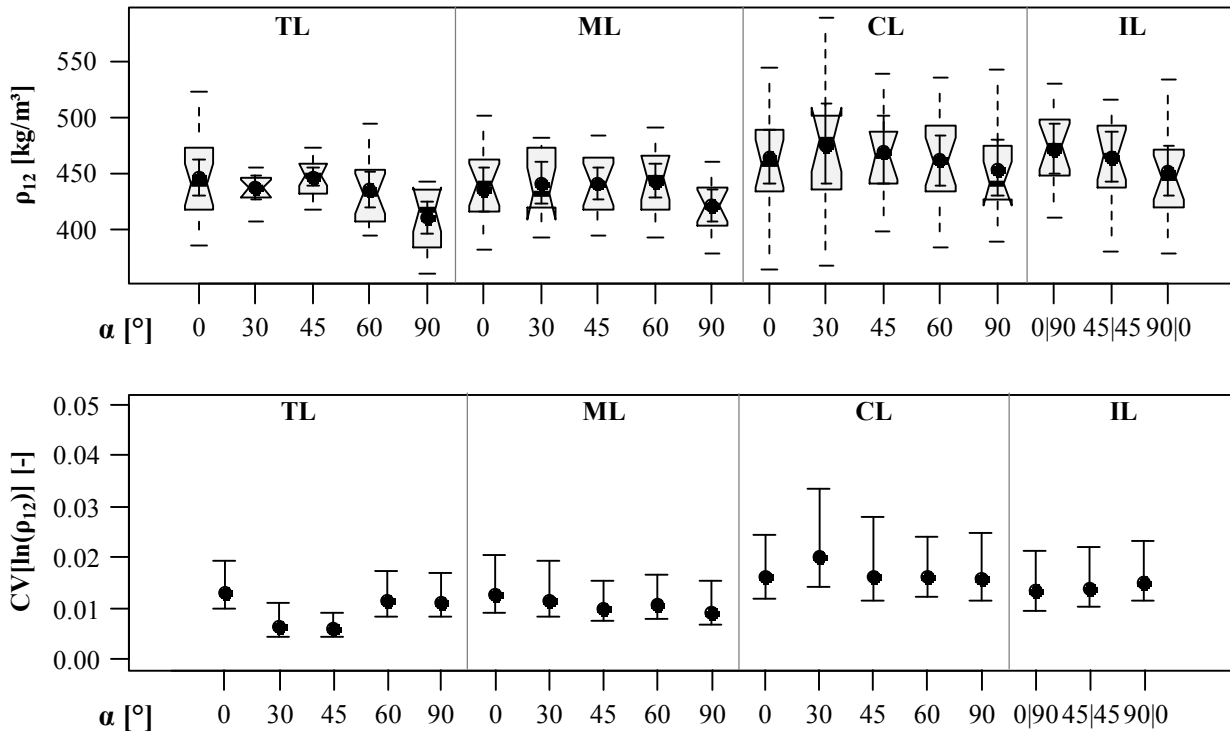


Figure 5.92: Above: boxplot graphic of densities ρ_{12} ; below: CIs of $CV[\ln(\rho_{12})]$; test programme I, $d = 12$ mm;

The behaviour of withdrawal properties $\{f_{ax}, K_{ser,ax}, D\}$, in dependence of the screw outer thread diameter, the axis-to-grain angle and the ratio t_1/d is consequently illustrated in Figure 5.93 to Figure 5.96. The absolute values of statistical parameters and variability are given in Annex B-3, Figure B.61 to Figure B.64 and Table B.53 to Table B.54. Firstly concentrating on the course of the withdrawal strength at a varying axis-to-grain angle, slightly, but steady decreasing values with decreasing α down to 30° , as well as a significant difference between f_{ax} , determined for this threshold and the parallel-to-grain insertion, can be observed. Furthermore, this behaviour obviously does not depend on both additionally varied parameters d and t_1/d . As already mentioned, Brandner et al. (2017) considered the given outcomes for deriving the polynomial approach, illustrated in Figure 5.90. In fact, the main reason for this decision was the localisation of subseries at $\alpha = \{30, 45, 60\}^\circ$, resulting in-between the estimation from a bilinear model (no difference between $\alpha = 45^\circ \div 90^\circ$) and the one according to Hankinson (1921) in case of equal limits at $\alpha = \{0, 90\}^\circ$. With regard to the behaviour of the withdrawal strength's variability, the courses illustrated in Figure B.61 and Figure B.64 (a) confirm no relevant impact of d and t_1/d and (b) indicate a mirrored relationship, as it was found for the average values in form of a clear bilinear trend with equal $CV[\ln(f_{ax})]$ between $\alpha = 30^\circ \div 90^\circ$, followed by a significant increase for the parallel-to-grain insertion. Furthermore, the deviations observed for $CV[\ln(\rho_{12})]$ between the cross layer insertion and the other subseries have no relevant impact on this course.

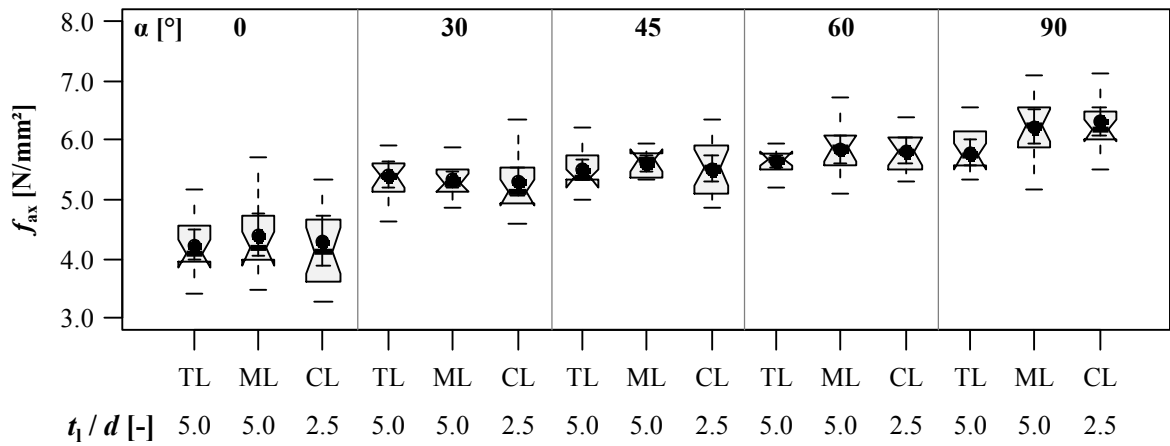


Figure 5.93: Boxplot diagram of withdrawal strength f_{ax} in dependence of axis-to-grain angle and ratio t_1/d ; test data from Grabner (2013); $d = 8$ mm

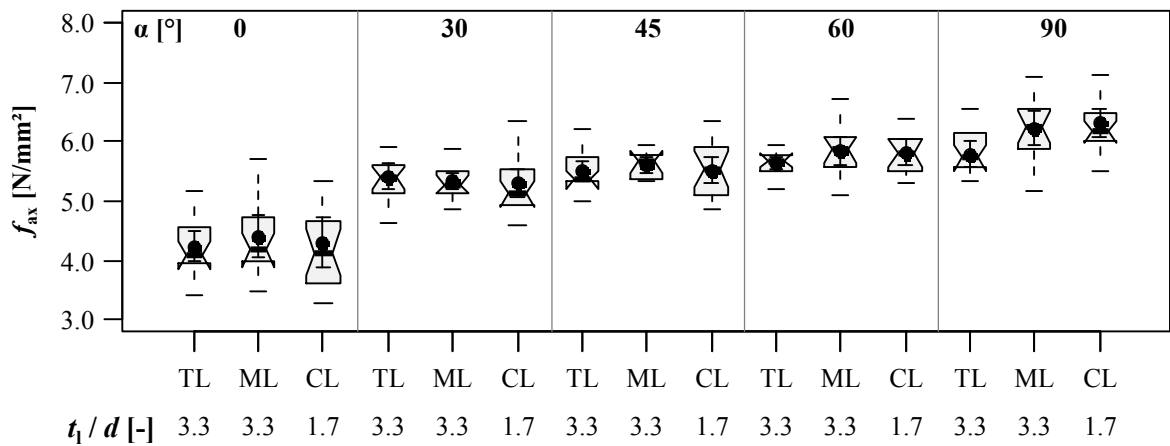


Figure 5.94: Boxplot diagram of withdrawal strength f_{ax} in dependence of axis-to-grain angle and ratio t_1/d ; test data from Grabner (2013); $d = 12$ mm

With regard to the same comparison for the withdrawal stiffness, the courses of $K_{ser,ax}$ at a varying axis-to-grain angle, illustrated in Figure 5.95, differ in their behaviour in dependence of the ratio t_1/d . For both subseries, dedicated to top and middle layer insertion, $t_1/d = 5.0$, more or less equal averages at each α , as well as a bilinear trend with constant $K_{ser,ax}$ between $\alpha = 45^\circ \div 90^\circ$, followed by an increasing stiffness at the angles below the lower threshold, can be observed. Note: as previously mentioned, Brandner et al. (2017) consequently derived a bilinear approach for the related description.

In case of those screws, inserted in cross layers with $t_1/d = 2.5$, the properties gained for a parallel- (decrease) and a perpendicular-to-grain (increase) insertion significantly deviate from those dedicated to “TL” and “ML” series. This is probably caused by a certain “locking” (or “unlocking”) effect, which means, that the neighbouring layers influence the timber-screw composite’s deformability for small ratios t_1/d . The results, regarding the impact of varying $a_{2,CG}$ on the withdrawal stiffness, illustrated in Figure

5.74 (note: exclusively for $\alpha = 90^\circ$), show a slight decrease of $K_{ser,ax}$ for $a_{2,CG}$ (comparable to $t_1 / d = 2.5$). This may indicate a similar behaviour as it is given here. The corresponding test series were carried out without a local displacement measurement – see section 5-4.1 – a verification of these observations could be a task for the future. In contrast to the withdrawal strength, the variability of $K_{ser,ax}$ appears to be influenced neither by the axis-to-grain angle nor by the t_1 / d variation, c. f. Figure B.62.

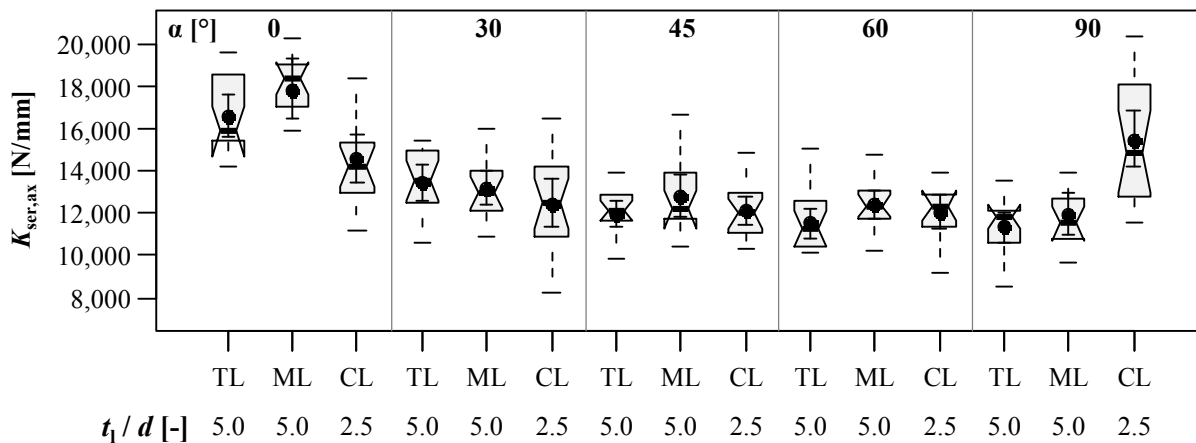


Figure 5.95: Boxplot diagram of withdrawal stiffness $K_{ser,ax}$ in dependence of axis-to-grain angle and ratio t_1 / d ; test data from Grabner (2013); $d = 8 \text{ mm}$

Figure 5.96 subsequently illustrates the behaviour of the ductility, gained from varying the axis-to-grain angles and the ratios t_1 / d . Confirming the conclusion made in the introduction of this subsection, the determined values for $\alpha = 0^\circ$ result to be significantly lower than those dedicated to $\alpha = 90^\circ$. Even though the results differ more in their magnitude, a behaviour of D in dependence of the axis-to-grain angle variation quite equal to the one of the withdrawal strength can be observed. This also corresponds to the course of the ductility's variability, illustrated in Figure B.63. In contrast to the majority of the test series discussed so far, a clear influence of α is obviously given for the ductility. With regard to the screw insertion in layers with different thicknesses, it is finally worth mentioning, that the impact of small values of t_1 / d (cross layer insertion) is rather oppositional than similar to the one observed for $K_{ser,ax}$.

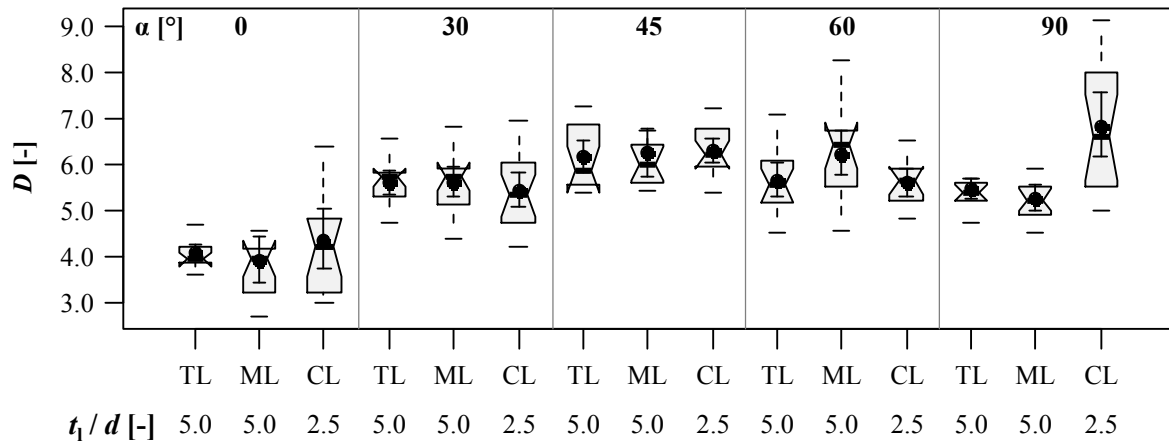


Figure 5.96: Boxplot diagram of ductility D in dependence of axis-to-grain angle and ratio t_1/d ; test data from Grabner (2013); $d = 8$ mm

Further concentrating on the behaviour of screw withdrawal properties, situated in intermediate layers: Figure 5.97 to Figure 5.100 compare the results gained for $\alpha = \{0|90, 45|45, 90|0\}^\circ$ with those determined for a full insertion into neighbouring layers (“TL” and “CL”). The same illustrations for related variabilities are given in Annex B-3.1, Figure B.65 and Figure B.66. With regard to the withdrawal strength, apart from the behaviour shown in Figure 5.97 (left), all remaining results for the intermediate layer insertion are more or less the average of those gained in the neighbouring layers. This is also confirmed by Plüss (2014) and means, that both lateral outer thread surface shares subjected to $\alpha_1 = 0 \div 90^\circ$ and $\alpha_2 = 90 - \alpha_1$ equally contribute to the screw bearing capacity. Note: this has already been presupposed for modelling in section 5-3.4.

Now focusing on the same comparison for $K_{ser,ax}$ and D , where a behaviour for both properties deviating from f_{ax} has to be observed. In case of $K_{ser,ax}$, the results gained for an intermediate layer insertion generally tend to those, which were determined for the screws situated in cross layers. Note: since the latter are obviously also influenced by their neighbouring layers, the given differences vary in a minor pronounced bandwidth if compared to the withdrawal strength. In case of ductility, the results for $\alpha = \{0|90, 90|0\}^\circ$ are equal to the perpendicular-to-grain insertion, indicating a rather docile loadbearing behaviour. With regard to the variabilities, the given dependencies are quite similar to those found for average values, additionally taking the results for $CV[\ln(X)]$ determined for screws situated in top, middle or cross layers at varying axis-to-grain angles into account.

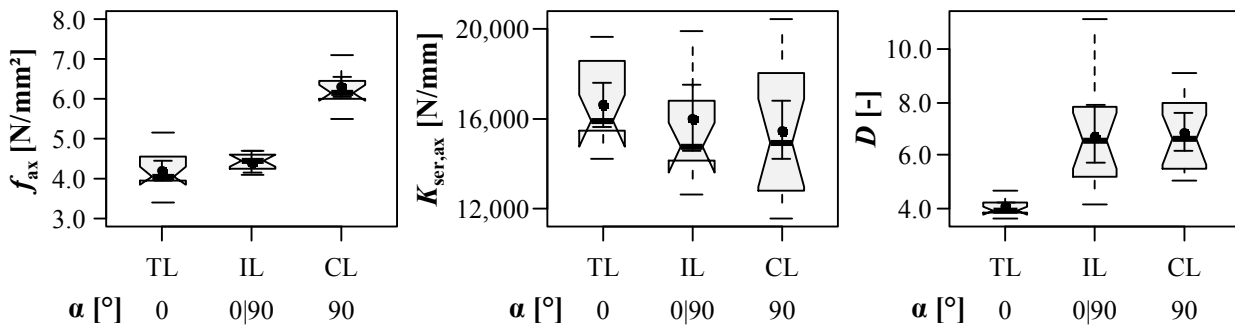


Figure 5.97: Boxplot diagrams of screw withdrawal properties when situated in intermediate layers; test data from Grabner (2013); $d = 8 \text{ mm}$, $\alpha = 0|90^\circ$

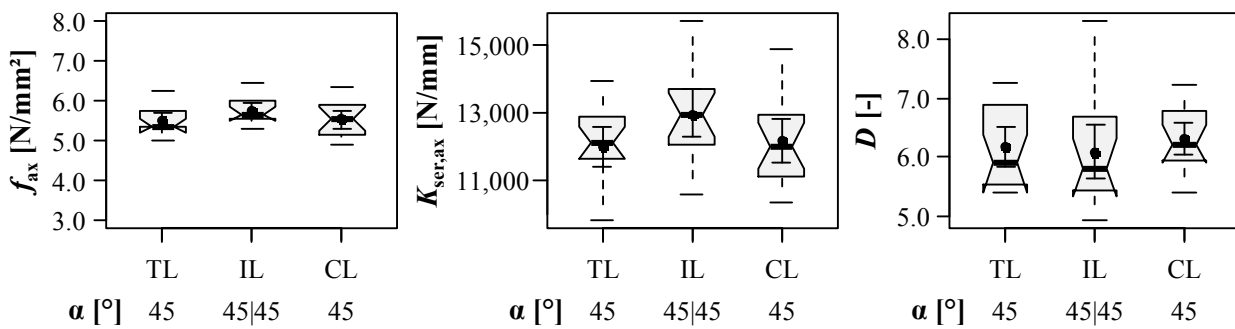


Figure 5.98: Boxplot diagrams of screw withdrawal properties when situated in intermediate layers; test data from Grabner (2013); $d = 8 \text{ mm}$, $\alpha = 45|45^\circ$

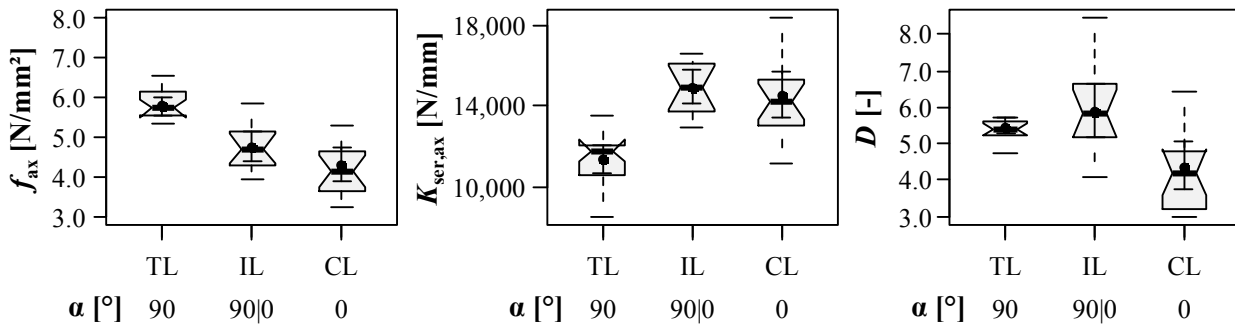


Figure 5.99: Boxplot diagrams of screw withdrawal properties when situated in intermediate layers; test data from Grabner (2013); $d = 8 \text{ mm}$, $\alpha = 90|0^\circ$

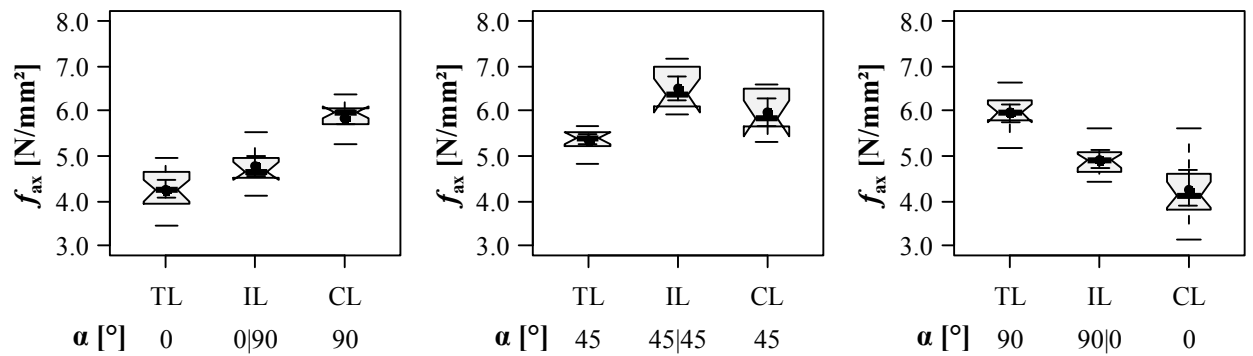


Figure 5.100: Boxplot diagrams of screw withdrawal strength f_{ax} when situated in intermediate layers; test data from Grabner (2013); $d = 12 \text{ mm}$

The final topic, dedicated to the experimental programme I, shall deal with the behaviour of k_p according to eq. (5.54) in dependence of the axis-to-grain angle variation. As stated, the values of k_p for the parallel-to-grain insertion result to be remarkably smaller than those related to the perpendicular-to-grain insertion. This means a loss of relationship between timber density and withdrawal strength, thus significantly influencing the property’s predictability. Table 5.36 consequently overviews the courses of k_p and $r_{XY,PE}$ gained for varying the axis-to-grain angles and the outer thread diameters. Note: since no impact of the ratio t_1 / d on the withdrawal strength was observed, c. f. Figure 5.93 and Figure 5.94, the test data was treated independently from this parameter in order to increase the number of observations for each characteristic. Furthermore, the results dedicated to the intermediate layer insertion are excluded. With regard to the behaviour of both statistical parameters k_p and $r_{XY,PE}$ in dependence of α , two main conclusions are worth to be drawn: First, irrespective from d , constant values for $\alpha = 30 \div 90^\circ$, as well as a remarkable decrease in case of the parallel-to-grain insertion are given. Second, the tendency of a remarkably decreasing k_p with increasing d especially for $\alpha = 0^\circ$ as already observed in section 5-2.1 can be confirmed.

Table 5.36: Experimentally determined values for k_p and $r_{XY,PE}$ in dependence of outer thread diameter and varying axis-to-grain angles

d [mm]	α	[°]	0	30	45	60	90
8	k_p	[-]	0.72	1.42	1.31	1.28	1.33
	$r_{XY,PE}$	[-]	0.38	0.94	0.92	0.94	0.88
12	k_p	[-]	0.26	1.06	1.29	1.31	0.99
	$r_{XY,PE}$	[-]	0.19	0.79	0.79	0.91	0.84

Now concentrating on the results dedicated to the experimental programme II; this campaign was carried out to investigate the influence of alternating axis-to-grain angles on withdrawal strength, which occur when inserting the screws inclined to the CLT side face’s surface. The main statistics of the timber

densities ρ_{12} are graphically illustrated in Figure 5.101, while Table B.55 in Annex B-3.2 comprises the absolute values related, including the moisture contents u . As aimed for this programme, both moisture contents and densities for all subseries are equal in their magnitude, vary in their target bandwidth (moisture contents) and show no unwanted differences in their variability (densities). Thus, a related correction of withdrawal strength is not necessary.

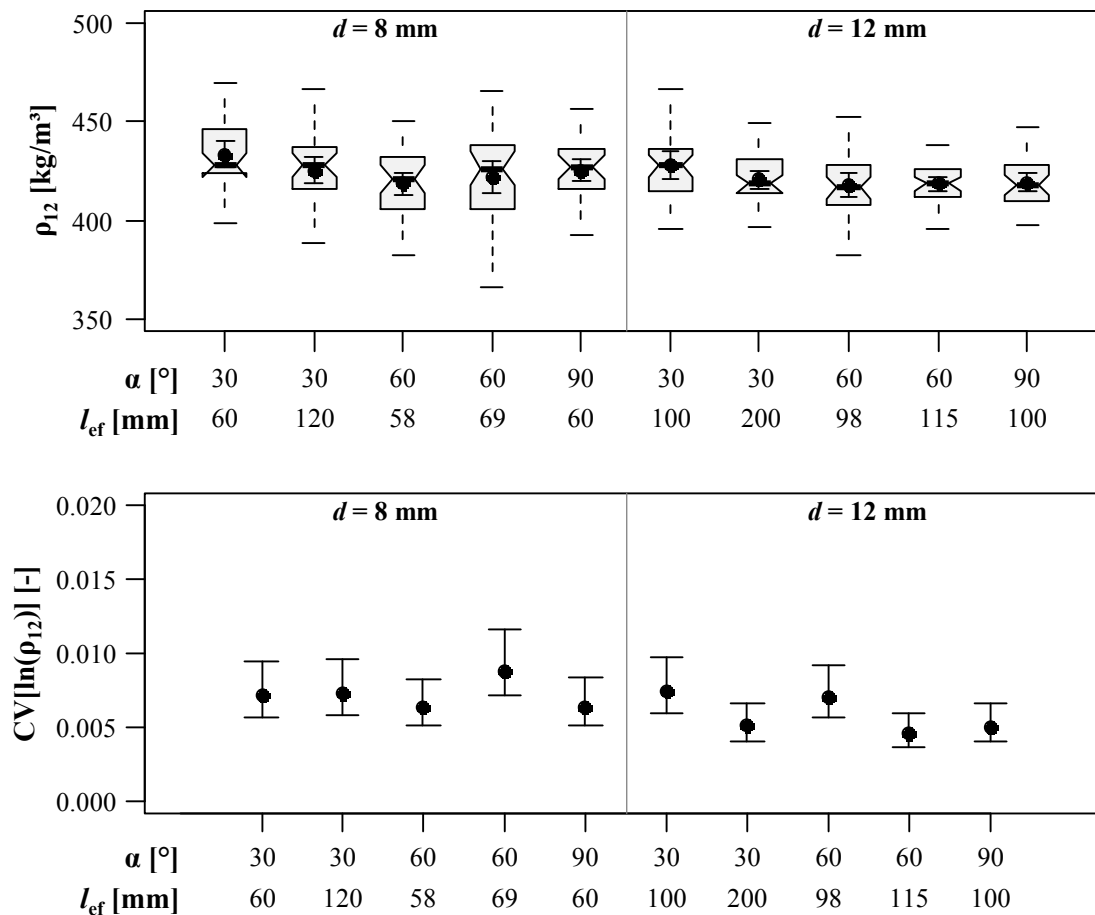


Figure 5.101: Above: boxplot graphic of densities ρ_{12} ; below: CIs of $CV[\ln(\rho_{12})]$; test programme II

The determined results for the withdrawal strength in dependence of outer thread diameter, axis-to-grain angle and effective inserted thread length are illustrated in Figure 5.102. In addition, the variabilities, as well as the absolute values of the statistical parameters can be found in Annex B-3, Figure B.67 and Table B.56. With regard to the given behaviour, three main observations are worth to be briefly discussed: first, steadily decreasing withdrawal strengths with decreasing α can be observed. The related loss of bearing resistance results in ratios similar to the ones observed for the results dedicated to programme I, c. f. Table B.53 and Table B.54 with Table B.56. This is in fact surprising, since grain direction of at least two layers per specimen was orientated perpendicular to the screw axis. Second, the relationship between withdrawal strength and axis-to-grain angle is not influenced by the additionally varied parameters d and l_{ef} . Third, the variability of the withdrawal strength is in case of $\alpha = 30^\circ$

significantly higher, than for the perpendicular-to-grain insertion, c. f. Figure B.67, which indicates an even more pronounced impact of the axis-to-grain angle, as it was found for screws situated in solid timber, see Figure B.61 and Figure B.64.

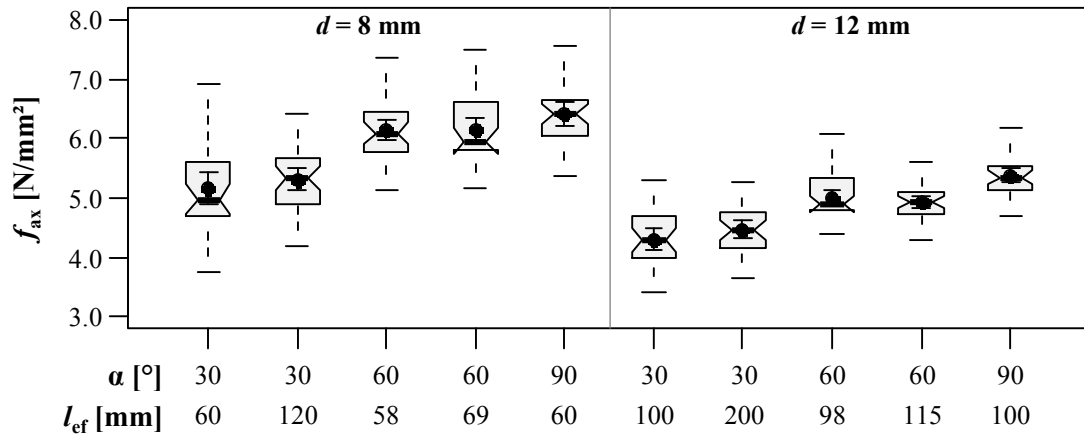


Figure 5.102: Boxplot diagram of screw withdrawal strength f_{ax} in dependence of outer thread diameter, axis-to-grain angle and effective insertion length; test programme II

Concluding the findings made so far, the grain direction of certain layers, oriented perpendicular to the screw axis, has obviously no positive influence on the withdrawal strength. The related tests were carried out with screws penetrating either two or three layers with $N(\alpha = 90^\circ)$. Figure 5.103 and Figure 5.104 consequently compare withdrawal strengths in dependence of d , α and $N(\alpha = 90^\circ) = \{2, 3\}$, but irrespective of l_{ef} (since there was not found any impact related). No influence of $N(\alpha = 90^\circ)$ on the course of f_{ax} with varying α can be observed, which again confirms this matter.

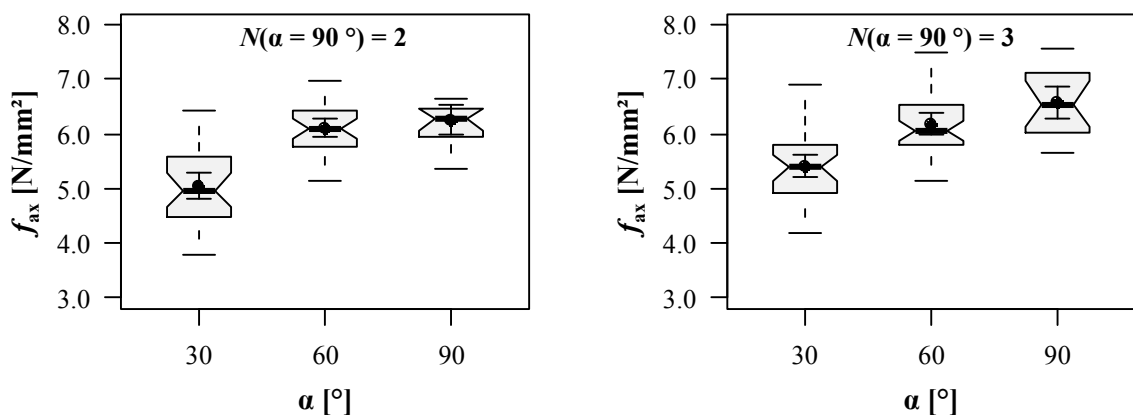


Figure 5.103: Boxplot diagram of screw withdrawal strength f_{ax} in dependence of $N(\alpha = 90^\circ)$ and axis-to-grain angle, $d = 8$ mm; test programme II

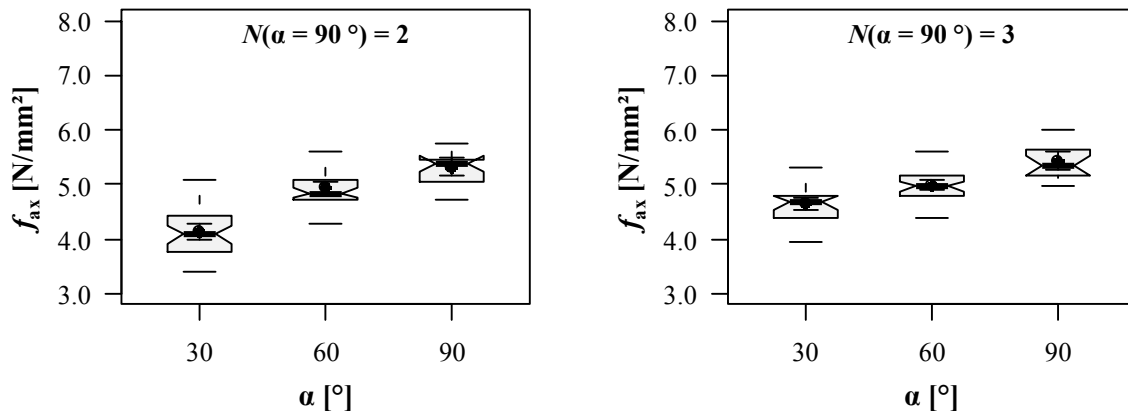


Figure 5.104: Boxplot diagram of screw withdrawal strength f_{ax} in dependence of $N(\alpha = 90^\circ)$ and axis-to-grain angle, $d = 12$ mm; test programme II

5-4.4 Position to annual ring structure

5-4.4.1 Introduction

As already discussed, a varying screw position within the timber's both orthotropic planes, associated to the longitudinal shear (including the index "L"), significantly influences the behaviour of all screw withdrawal properties considered. The focus of this section is to concentrate on a possible impact, when the screw axis position with respect to the remaining R - T shear plane is varied in case of a perpendicular-to-grain insertion. Similar to the former mentioned situation, as defined by the axis-to-grain angle α , the angle $\beta = \pi / 2 - \varphi$ (c. f. Figure 4.5) between the screw axis and the annual ring's tangent closest situated to the half inserted thread length ($l_{ef} / 2$), shall be introduced for the related description, c. f. Figure 5.105.

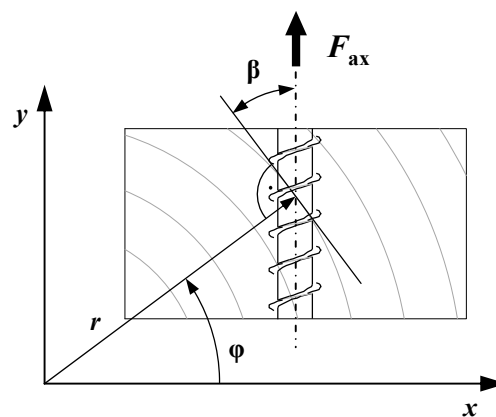


Figure 5.105: Definition of screw axis position with respect to annual ring orientation

Firstly concentrating on the properties determined for both limits of β ($\beta \rightarrow 0^\circ$, tangential insertion; $\beta \rightarrow 90^\circ$ radial insertion), neither the presented results in section 5-3.1, nor the investigations carried out in the past, namely by Cockrell (1933) and Koch and Dünisch (2008) for traditional screws, as well as by Gatternig (2010) and Plieschounig (2010) for $d = 6$ mm modern self-tapping timber screws, show a significant impact on the withdrawal strength f_{ax} . This also corresponds to the relationship between density and withdrawal strength, resulting in similar magnitude (exponent k_p) and quality, c. f. Table 5.11, Table 5.12, Figure 5.19 and Figure 5.23. With regard to both further properties $K_{ser,ax}$ and D (only considered in the frame of this thesis), the comparison, given in Figure 5.16, indicates no significant impact on the withdrawal stiffness (Figure 5.16, middle), while the determined ductility (Figure 5.16, right) was found to be higher for radial than for tangential axis orientation.

Focusing on the behaviour of withdrawal properties in case of β varying in-between both limits, the scope of the considered literature sources, quantitatively considering the measured values for β , is reduced to both investigations carried out by Gatternig (2010) and Plieschounig (2010). Again, no relevant influence of the screw axis position with respect to the annual ring orientation on the withdrawal strength was

found. In case of $K_{\text{ser,ax}}$ and D , comparable examinations are missing so far. Thus, it was decided to expand the amount of tests, planned for the impact of clear wood parameters on withdrawal properties, as presented in section 5-3.1, in form of two further subseries of screw withdrawal tests, carried out at $\beta \approx \{30, 60\}^\circ$. The results are discussed in the following subsections.

In advance, some theoretical considerations, regarding the mechanical behaviour of clear wood properties associated to the R - T -plane in case of varying β and a possible influence on the withdrawal properties, are worth being summarised. According to the assumptions made in chapter 4, the compliance matrix for this two-dimensional stress state is defined as follows:

$$\begin{bmatrix} \varepsilon_{\text{TT}} \\ \varepsilon_{\text{RR}} \\ \gamma_{\text{RT}} \end{bmatrix} = \begin{bmatrix} \frac{1}{E_{\text{T}}} & -\frac{\nu_{\text{TR}}}{E_{\text{R}}} & 0 \\ -\frac{\nu_{\text{RT}}}{E_{\text{T}}} & \frac{1}{E_{\text{R}}} & 0 \\ 0 & 0 & \frac{1}{G_{\text{RT}}} \end{bmatrix} \cdot \begin{bmatrix} \sigma_{\text{TT}} \\ \sigma_{\text{RR}} \\ \tau_{\text{RT}} \end{bmatrix} \rightarrow \begin{bmatrix} \varepsilon_{11} \\ \varepsilon_{22} \\ \gamma_{12} \end{bmatrix} = \begin{bmatrix} s_{11} & s_{12} & 0 \\ s_{12} & s_{22} & 0 \\ 0 & 0 & s_{33} \end{bmatrix} \cdot \begin{bmatrix} \sigma_{11} \\ \sigma_{22} \\ \tau_{12} \end{bmatrix}. \quad (5.94)$$

As described in Görlacher (2002), the influence of a varying annual ring orientation on the timber's compliance constants s_{ij} can be derived by a matrix transformation of the material law, given in eq. (5.94), see:

$$\begin{bmatrix} \overline{s_{11}} & \overline{s_{12}} & \overline{s_{13}} \\ \overline{s_{12}} & \overline{s_{22}} & \overline{s_{23}} \\ \overline{s_{13}} & \overline{s_{23}} & \overline{s_{33}} \end{bmatrix} = \left[\mathbf{M}_{\text{trans}} \cdot \begin{bmatrix} s_{11} & s_{12} & 0 \\ s_{12} & s_{22} & 0 \\ 0 & 0 & s_{33} \end{bmatrix}^{-1} \cdot \mathbf{M}_{\text{trans}}^T \right]^{-1}, \text{ with} \quad (5.95)$$

$$\mathbf{M}_{\text{trans}} = \begin{bmatrix} \cos^2 \beta & \sin^2 \beta & -2 \cdot \sin \beta \cdot \cos \beta \\ \sin^2 \beta & \cos^2 \beta & 2 \cdot \sin \beta \cdot \cos \beta \\ \sin \beta \cdot \cos \beta & -\sin \beta \cdot \cos \beta & \cos^2 \beta - \sin^2 \beta \end{bmatrix} \quad (5.96)$$

as the transformation matrix. With regard to the relationship between withdrawal and mechanical timber properties, determined in section 5-3.1, medium to significant dependencies were found between $\{f_{\text{ax}}, K_{\text{ser,ax}}\}$ and the timber's compressive moduli E_{R} and E_{T} , as well as the rolling shear modulus G_{RT} , c. f. Table B.19 and Table B.20. The application of eq. (5.95) subsequently enables determining both (apparent) stiffness parameters E and G in dependence of β as inverse of the corresponding compliance coefficients $\overline{s_{11}}$ and $\overline{s_{33}}$. Therefore, the input parameters s_{ij} resulted by inverting the related average mechanical properties given in Table B.16 and Table B.17. Furthermore, the Poisson's ratio ν_{TR} , as the only variable remaining unknown, was set equal to 0.24, which is the minimum value proposed in Table 4.1. Note: this decision was made since the determined clear wood properties rather correspond to

the minimum than to the maximum limits given in this table. The courses of both parameters E and G , each referred to E_T and G_{RT} resulting for $\beta = 0^\circ$, are shown in Figure 5.106, in dependence of the annual ring orientation. Based on this illustration, a significantly increasing shear modulus for β varying from $\{0, 90\}^\circ$ to 45° , combined with a decreasing elastic modulus can be observed. In the frame of the following subsections the given behaviour shall be applied for the evaluation of the behaviour of the withdrawal properties in case of a varying screw axis position with respect to the annual ring orientation.

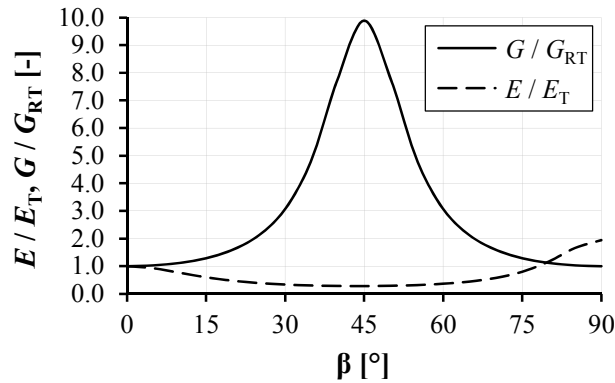


Figure 5.106: Behaviour of apparent elastic material properties E and G in dependence of β

5-4.4.2 Experimental programme

As mentioned before, the test programme was conducted as an expansion of the one presented in section 5-3.1. All background information related is thus to be found in this section, as well as in Annex B-3.1, Figure B.17. It is worth outlining, that the local displacement measurement was also applied for these subseries, enabling the determination of absolute values of $K_{ser,ax}$ and D .

5-4.4.3 Results and discussion

Statistical parameters of the timber density ρ_{12} , determined according to (4.4), comprising the averages and the variabilities of the small scale specimen, are subsequently illustrated in Figure 5.107. The related absolute values, as well as the determined moisture contents u , are additionally given in Annex B-3.2, Table B.57. Note: for a better overview, the results of WT ($\beta = 0^\circ$) and WR ($\beta = 90^\circ$) series, already presented in section 5-3.1, are herein repeated. Even though the moisture contents of both supplemental series with $\beta \approx \{30, 60\}^\circ$ are slightly smaller, than those dedicated to $\beta = \{0, 90\}^\circ$, the given differences are regarded as negligible with respect to a possible influence on the withdrawal properties related. Comparing the average densities, higher values for both groups with $\beta \approx \{30, 60\}^\circ$, than for radial and tangential insertion can be observed. Although differences are not significant, it was exceptionally decided to apply the density correction according to eq. (5.81) with $\rho_{ref} = 430 \text{ kg/m}^3$, excluding a possible impact on withdrawal strength and stiffness.

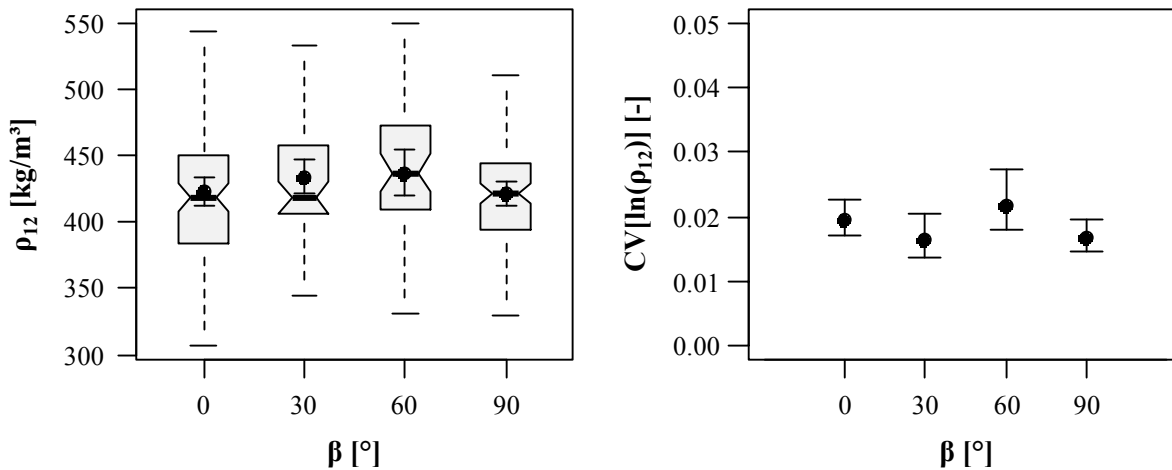


Figure 5.107: Left: boxplot graphic of densities ρ_{12} ; right: CIs of $CV[\ln(\rho_{12})]$, both in dependence of annual ring orientation

The results of the determined withdrawal properties and their variabilities, the latter expressed by $CV[\ln(X)]$, are subsequently illustrated in Figure 5.108 to Figure 5.110 in dependence of β . Note: the exact angles were only measured in case of $\beta = \{30, 60\}^\circ$, while for $\beta = \{0, 90\}^\circ$ nominal values are considered. A supplemental information can again be found in Annex B-3.2, Table B.58. Irrespective of the specific property, not expected in advance, steadily higher values for both subgroups with β , varying between radial and tangential insertion, can be observed. With regard to the withdrawal strength, the corresponding deviations are much minor pronounced if compared to $K_{\text{ser,ax}}$ or D . Nevertheless, mean and median values of f_{ax} dedicated to $\beta = \{30, 60\}^\circ$ significantly differ – especially to those determined for $\beta = 0^\circ$. This surprising outcome contradicts the literature findings and thus it has to be discussed more in detail:

On the one hand, concentrating on modern timber screws, Gatternig (2010) and Plieschounig (2010) situated their fasteners in solid timber specimen with random annual ring pattern differing along the fully inserted thread length, c. f. Annex B-3.1, Figure B.43 to Figure B.46. As explained in Plieschounig (2010), β was determined as the orientation of the annual ring, crossing the screw axis about $2d$ below the specimen surface and should thus be regarded rather as a blurred indicator for differing between radial and tangential insertion, than for steadily representing the exact orientation of all annual rings along the thread length. In contrary the situation for the presented test programme: the comparatively small value for l_{ef} , combined with a specimen preparation, which aimed to realise a quite exact and steady annual ring orientation, led to maximum deviations of β of about $\pm 5^\circ$. This especially concerns the tangential screw insertion, where a clear annual ring orientation in form of $\beta = 0^\circ$ is barely realisable for values of l_{ef} higher than those herein applied. Thus, the values e. g. gained by Plieschounig (2010) (for tangential screw insertion) are rather comparable to the subgroup with $\beta = 30^\circ$ than to the one with $\beta = 0^\circ$, which may serve as an explanation for the differently observed behaviour of the withdrawal strength in this limit

case. Summarising this discussion so far, a variation of the annual ring orientation, with respect to the screw axis, obviously leads to a decreasing f_{ax} in both limit cases, but especially for the tangential insertion. Since (a) positioning at $\beta = 0^\circ$ is barely realisable in practical application and (b) an exact and steady annual ring orientation along l_{ef} is hardly predictable, it was subsequently decided to exclude this effect from the advanced modelling in chapter 6.

On the other hand, with special regard to the withdrawal stiffness (since the deviations in dependence of β are far more pronounced, than for the withdrawal strength and a correlation with the aforementioned material stiffness parameters was observed in section 5-3.1, while in case of the ductility nothing was found), the given behaviour has a clear analogy to the one assumed for the apparent shear modulus G in Figure 5.106 in dependence of β . Worth mentioning, that the average $K_{ser,ax}$ ratio between $\beta = \{30, 60\}^\circ$ and $\beta = \{0, 90\}^\circ$ results to 1.34 as roughly the half of that derived for the shear modulus (3.07). Unfortunately, no related values of $K_{ser,ax}$ for $\beta = 45^\circ$ were determined within the test programme, which would have been helpful verifying this relationship. Comparing the withdrawal stiffness with the apparent modulus of elasticity E , similarities can only be observed for the difference between radial and tangential insertion (but far minor pronounced), while the course for in-between angles is in fact oppositional.

Concentrating on the behaviour of $CV[\ln(X)]$, given in Figure 5.108 to Figure 5.110 (right), apart from the significantly lower value for $CV[\ln(K_{ser,ax})]$, in case of the radial compared to the tangential insertion, the parameter variation obviously does not influence the variability of the withdrawal properties.

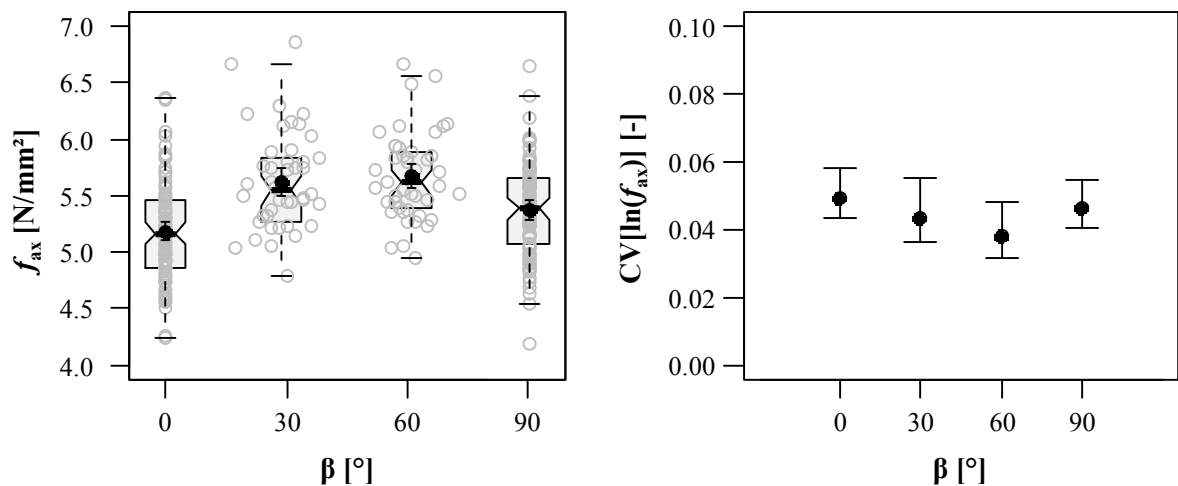


Figure 5.108: Left: combined boxplot/scatterplot graphic of density corrected withdrawal strengths f_{ax} ; right: CIs of $CV[\ln(f_{ax})]$, both in dependence of annual ring orientation

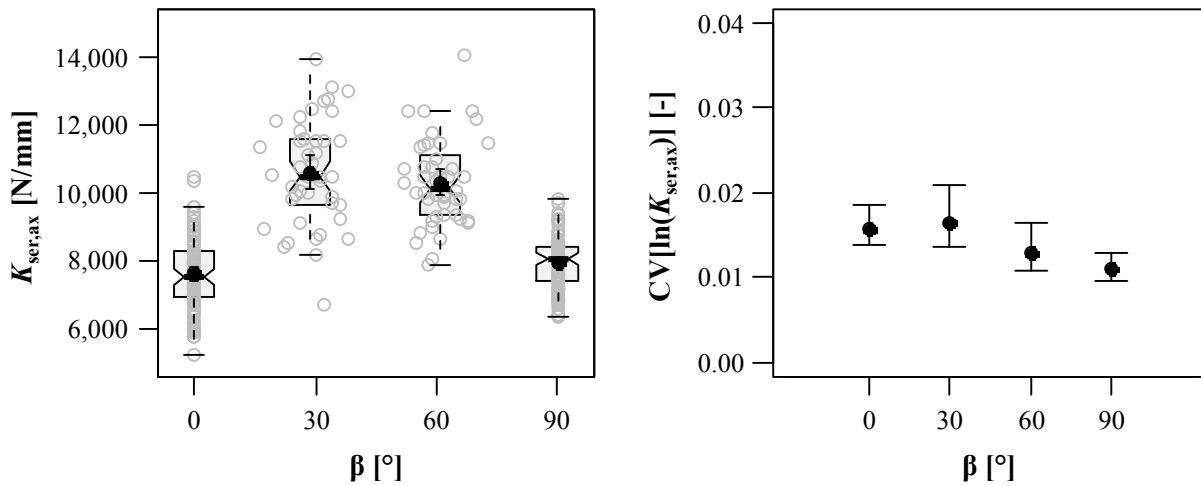


Figure 5.109: Left: combined boxplot/scatterplot graphic of density corrected withdrawal stiffness $K_{ser,ax}$; right: CIs of $CV[\ln(K_{ser,ax})]$, both in dependence of annual ring orientation

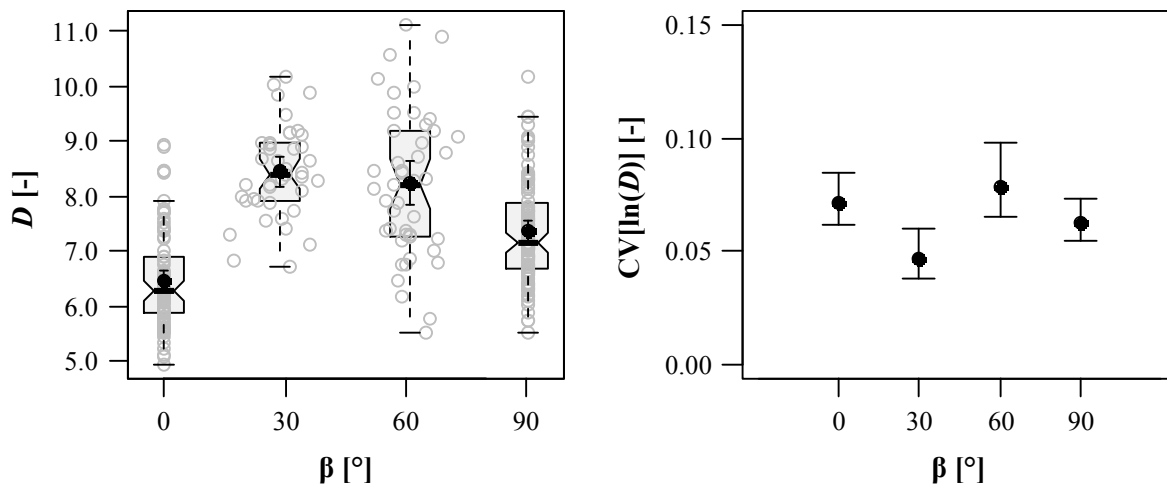


Figure 5.110: Left: combined boxplot/scatterplot graphic of ductility D ; right: CIs of $CV[\ln(D)]$, both in dependence of annual ring orientation

Table 5.37 subsequently includes the determined values for k_p and $r_{XY,PE}$, according to eq. (5.54) and eq. (5.34), as the final topic of this section. Even though a quite high variation in the exponent's magnitude is given, the experiences regarding the deviation of this parameter – compared with more or less equal correlations between $\ln(\rho_{12})$ and $\ln(f_{ax})$ for all subseries – exclude a corresponding consideration for advanced modelling.

Table 5.37: Experimentally determined values for k_p and $r_{XY,PE}$ in dependence of annual ring orientation

β	[°]	0	30	60	90
k_p	[-]	1.01	1.26	1.08	0.82
$r_{XY,PE}$	[-]	0.82	0.86	0.91	0.73

5-4.5 Effective inserted thread length l_{ef}

5-4.5.1 Introduction

With regard to the practical design of predominately axially loaded screwed connections, taking the typical restrictions for outer thread diameter (spacings, available fastener sizes, etc.), axis-to-grain angle (pre-defined connection type) and density (pre-defined timber product) into account, l_{ef} as the effective inserted length of the screw thread, not only governs the corresponding loadbearing performance, but also the type of failure the connection is limited by. This means, that “steel failure in tension”, as the failure mode dedicated to the maximum load-bearing capacity reachable per screw, is commonly achieved by providing screws with adequate effective thread lengths, c. f. section 2-1.2. This section focuses on a possible impact of this relevant design parameter on withdrawal properties $\{f_{ax}, K_{ser,ax}, D\}$.

Firstly concentrating on the withdrawal strength, considering the literature sources introduced in section 5-1.3, only the approach published by Blaß et al. (2006) comprises a thread length-dependent influence on f_{ax} in form of a power function with the exponent k_{lef} (own denotation) equal to -0.1 , which in fact indicates a negative, but minor pronounced relationship, between both parameters. All other authors exclude l_{ef} from predicting f_{ax} , presupposing the screw tip is either situated outside the timber member or its influence is already considered by correction (according to Pirnbacher et al. (2009) and Hübner (2013b) by $\{-1.17, -1.11\} d$, c. f. eq. (5.2)). Worth mentioning, that in all sources the slenderness $\lambda = l_{ef} / d$ is limited to 16. Higher values, which may provoke a nonlinear impact on withdrawal capacity (and thus an influence on f_{ax} deviating from zero) – as e. g. assumed by Hübner (2013a) – are barely treated in literature. Consequently, the related work, recently carried out by Stamatopoulos and Malo (2015), is worth being highlighted, even though they considered threaded rods with $d = 20$ mm instead of self-tapping screws. Amongst other topics, they experimentally determined the impact of slenderness values λ up to 22.5 (for parallel-to-grain insertion even up to 30; herein only test series without observing any steel failure are considered) on the withdrawal capacity. Irrespective of the axis-to-grain angle applied, $\alpha = \{0, 10, 20, 30, 60, 90\}^\circ$, they confirm the majority of aforementioned sources in form of no remarkable influence of a corresponding parameter variation on the withdrawal strength f_{ax} . This leads to the conclusion, that if any impact of l_{ef} on f_{ax} exists, it will occur at values for λ , where the screws consistently fail by exceeding their steel tensile strength and thus has no relevance for the practical design.

Further focus is on a possible impact of l_{ef} on the relationship between density and withdrawal strength, as expressed by the exponent k_p . The test data originally obtained by Gaich et al. (2008) (also serving as the basis of the investigations published in Pirnbacher et al. (2009) regarding the impact of l_{ef} on f_{ax}) is therefore considered. The related span of $\lambda = \{4, 8, 12, 14|15\}$, the number of observations per subseries, as well as additionally varied influencing parameters $d = \{8, 10, 12\}$ and $\alpha = \{0, 90\}^\circ$, enable a

reasonable comparison, given in Table 5.38. Worth mentioning, that only tests series conducted with solid timber (Norway spruce) were therefore considered. While the impact of α on the relationship between density and withdrawal strength can again be confirmed (k_p decreases with decreasing α), the results do not show any consistent trend or alteration of k_p in dependence of l_{ef} (or λ).

Table 5.38: Experimentally determined values for k_p in dependence of outer thread diameter, axis-to-grain angle and effective inserted thread length; re-assessed data (solid timber) from Gaich et al. (2008)

d [mm]	α [°]	λ [-]	4	8	12	14	15
8	0	k_p [-]	0.21	-0.01	0.25	-	0.62
	90	k_p [-]	1.21	1.28	1.23	-	1.19
10	0	k_p [-]	0.47	0.55	0.92	0.84	-
	90	k_p [-]	1.10	1.26	0.90	0.97	-
12	0	k_p [-]	0.60	0.77	0.31	-	0.50
	90	k_p [-]	1.04	1.17	1.06	-	0.68

Furthermore, Table 5.39 overviews the ratios k_{CV} , also gained from the database published in Gaich et al. (2008), again in dependence of outer thread diameter, axis-to-grain angle and slenderness. Irrespective of d and α , the results indicate no remarkable impact of the effective inserted thread length on the variability of the withdrawal strength, possibly influencing the determination of approaches predicting the characteristic values.

Table 5.39: Experimentally determined values for k_{CV} in dependence of outer thread diameter, axis-to-grain angle and effective inserted thread length; re-assessed data (solid timber) from Gaich et al. (2008)

d [mm]	α [°]	λ [-]	4	8	12	14	15
8	0	k_{CV} [-]	1.39	1.41	1.22	-	1.37
	90	k_{CV} [-]	1.65	1.52	1.42	-	1.33
10	0	k_{CV} [-]	1.18	1.15	1.21	0.98	-
	90	k_{CV} [-]	1.40	1.59	1.28	1.27	-
12	0	k_{CV} [-]	1.31	1.49	1.02	-	1.07
	90	k_{CV} [-]	1.33	1.27	1.20	-	1.01

With regard to the behaviour of the withdrawal stiffness $K_{ser,ax}$ in dependence of varying l_{ef} , the scope of investigations available in literature is scarce – if compared to the withdrawal strength. Both approaches introduced in section 5-1.3, currently being part of technical assessments, significantly differ in the way l_{ef} is taken into account. While the model published by Blaß et al. (2006), given in eq. (5.45), considers a

disproportionately small relationship between l_{ef} and $K_{ser,ax}$ in form of the exponent $k_{lef} = 0.4$, the second approach given in eq. (5.46) constitutes a linear relationship for this purpose. This circumstance is in fact mainly responsible for the high deviations between exemplarily predicted values for $K_{ser,ax}$, illustrated in Figure 2.25. Further examinations on withdrawal stiffness of threaded fasteners, as e. g. carried out by Blaß and Krüger (2010) (threaded rods with $d = \{16, 20\}$ mm, $\alpha = \{45, 90\}$ ° and $l_{ef} = \{200, 400\}$ mm) or again by Stamatopoulos and Malo (2016) (threaded rods with $d = 20$ mm, $\alpha = \{0, 10, 20, 30, 60, 90\}$ ° and $\lambda = \{5, 15, 23, 30\}$), even extend the bandwidth of possible solutions for describing the related behaviour. While Stamatopoulos and Malo (2016) widely confirm Blaß et al. (2006), the results published in Blaß and Krüger (2010) in fact indicate an oppositional behaviour in form of a disproportionately high relationship resulting in $k_{lef} > 1.0$. This leads to the conclusion, that a huge variety of different observations, regarding the influence of the effective inserted thread length on the withdrawal stiffness $K_{ser,ax}$ is given.

Similar to the impact of other parameters, discussed so far, no literature sources describing the relationship between l_{ef} and ductility D were found. This matter, combined with a poor amount of data regarding the withdrawal stiffness of self-tapping screws for high insertion lengths, were the motivation for an experimental campaign, recently carried out at Graz University of Technology. Materials, methods, as well as gained results and their discussion are part of the following subsections.

5-4.5.2 Experimental programme

The basic material for the campaign, focusing on the impact of different effective inserted thread lengths on the screw withdrawal properties, were altogether 18 solid timber beams of Norway spruce with cross-sectional dimensions of about $w \times h = 110 \times 310$ mm². As outlined in Table 5.40, the related parameter variation comprised five values for l_{ef} , varying from 40 mm to 310 mm, tested at different axis-to-grain angles $\alpha = \{0, 45, 90\}$ °. Since the whole programme was carried out with one screw type of $d = 8$ mm, the slenderness λ ranges from 5 to about 39 and thus exceeds previous works by far. Specimen with all varied parameter characteristics were cut out of each beam, which enables the realisation of a similar density distribution for all subseries included, c. f. section 5-1.2 and Annex B-3.1, Figure B.68. Similar to section 5-4.2, a strict time schedule did not allow a specimen storage in the climatic chamber until reaching the equilibrium moisture content. The related consequences are discussed in the following subsection. The $d = 8$ mm screw, especially produced for this test campaign, can be defined as a partially threaded screw with $\{l_{screw}, l_{sh}, l_{thread}\} = \{650, 300, 350\}$ mm but with thread properties similar to a fully threaded screw, c. f. Table 5.40. This screw type has on the one hand a thread length, long enough for covering the aforementioned slenderness range, and on the other hand the advantage to clamp both LVDTs on the (thread-free) screw shank enabling the determination of σ_{ax} according to eq. (5.5).

Table 5.40: Thread characteristics and test conditions applied for the experimental campaign focusing on the impact of the effective inserted thread length

thread characteristics						test conditions				
d_{nom}	d	η	p	v^*	α	l_p	l_{ef}	λ	l_{emb}	d_{PD}
[mm]	[mm]	[-]	[mm]	[°]	[°]	[mm]	[mm]	[-]	[mm]	[mm]
8	8.06	0.63	3.95	40	0, 45, 90	40, 80, 120, 240, 310	$= l_p$	5, 10, 15, 30, 39	0	0

Worth mentioning, that all tests have been performed on the test rig LIGNUM-UNI-275 with a local way measurement set-up enabling the determination of $K_{\text{ser,ax}}$ and D also for a comparison of absolute values. Further background information regarding test execution, post-processing, property determination and data assessment is summarised in section 5-1.2.

5-4.5.3 Results and discussion

The results of timber density ρ_{12} and moisture content u , both determined according to eq. (4.2) and (4.4), of the related small scale specimen are given in Annex B-3.2, Table B.59 in dependence of the axis-to-grain angle and the effective inserted thread length. Overall, the determined moisture contents vary in the aimed bandwidth of $\pm 2\%$. As mentioned before, no climatic conditioning prior to the tests was applied. The laboratory storage led to average moisture contents, resulting somewhat lower than the equilibrium moisture content. Nevertheless, nearly equal values for u_{mean} within the series did not necessitate any moisture-dependent treatment of the determined properties. With regard to the timber density, Figure 5.111 additionally illustrates the localisations of mean values, medians and variabilities ($\text{CV}[\ln(\rho_{12})]$) of all subseries' densities considered, proving the equality of the whole dataset, thus excluding a possible and unwanted influence on the withdrawal properties.

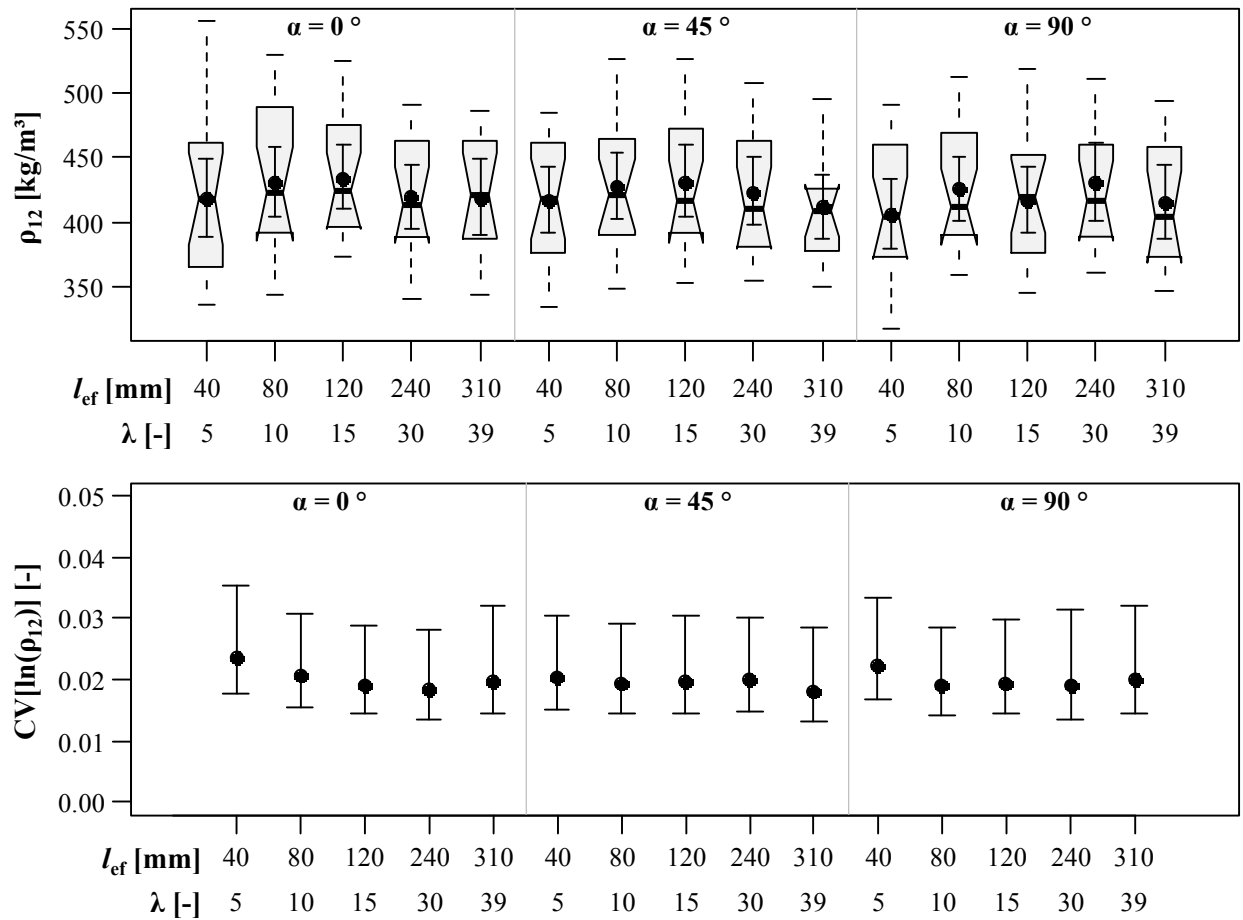


Figure 5.111: Above: boxplot graphic of densities ρ_{12} ; below: CIs of $CV[\ln(\rho_{12})]$, both in dependence of axis-to-grain angle and effective inserted thread length

The main statistical parameters of the related withdrawal properties are subsequently illustrated in Figure 5.112 to Figure 5.114 and outlined in Annex B-3.2, Table B.60, again in dependence of axis-to-grain angle α and slenderness λ . Statistical parameters of variabilities are additionally given in Annex B-3.1, Figure B.69 to Figure B.71.

With regard to the series carried out at $\alpha = \{45, 90\}^\circ$, all tests dedicated to $\lambda = \{30, 39\}$ failed by exceeding the screws' steel tensile capacity. This means, that only withdrawal strengths and ductility determined for $\lambda = \{5, 10, 15\}$ are subsequently considered for the discussion. In case of a parallel-to-grain insertion, parts of the subsets related to $\lambda = \{30, 39\}$ also failed in withdrawal ($n_{\lambda=30} = 13$, $n_{\lambda=39} = 7$). Thus, the right-censored data assessment according to eq. (5.23) and (5.24) was applied, enabling at least an estimation of average withdrawal strengths for the whole bandwidth of slenderness investigated. Since the determination of the withdrawal stiffness according to section 5-1.2 only concerns the linear-elastic part of the force-deformation relationship, the aforementioned restrictions were not applied for this property.

Now concentrating on the behaviour of the withdrawal strength at $\alpha = \{45, 90\}^\circ$ and λ , varying between 5 and 15, no significant impact of the effective inserted thread length on this property can be observed in Figure 5.112 (note: (i) since parts of the specimen showed steel failure in tension, σ_{\max} as the maximum axial stresses reached are illustrated instead of f_{ax} ; (ii) boxplots are only illustrated if all specimen of the subseries failed in withdrawal). In case of a parallel-to-grain insertion, the same situation is given for slenderness values up to 30, while f_{ax} estimated for $\lambda = 39$ by means of rcMLE results somewhat lower. Taking the general variation of mean and median withdrawal strengths over the whole database as well as the confidence interval for $\text{mean}[f_{\text{ax},\lambda=15}]$ overlapping with the estimation at $\lambda = 39$ into account, the given difference is too small for concluding a remarkable decrease of f_{ax} with increasing l_{ef} . Consequently, the given results agree with the common opinion, that the effective inserted thread length has no significant impact on the withdrawal strength at all. With regard to the variability of the withdrawal strength (illustrated in Annex B-3.1, Figure B.69) the given behaviour indicates no clear trend of $\text{CV}[\ln(f_{\text{ax}})]$ in dependence of λ and thus confirms the comparison shown in Table 5.39.

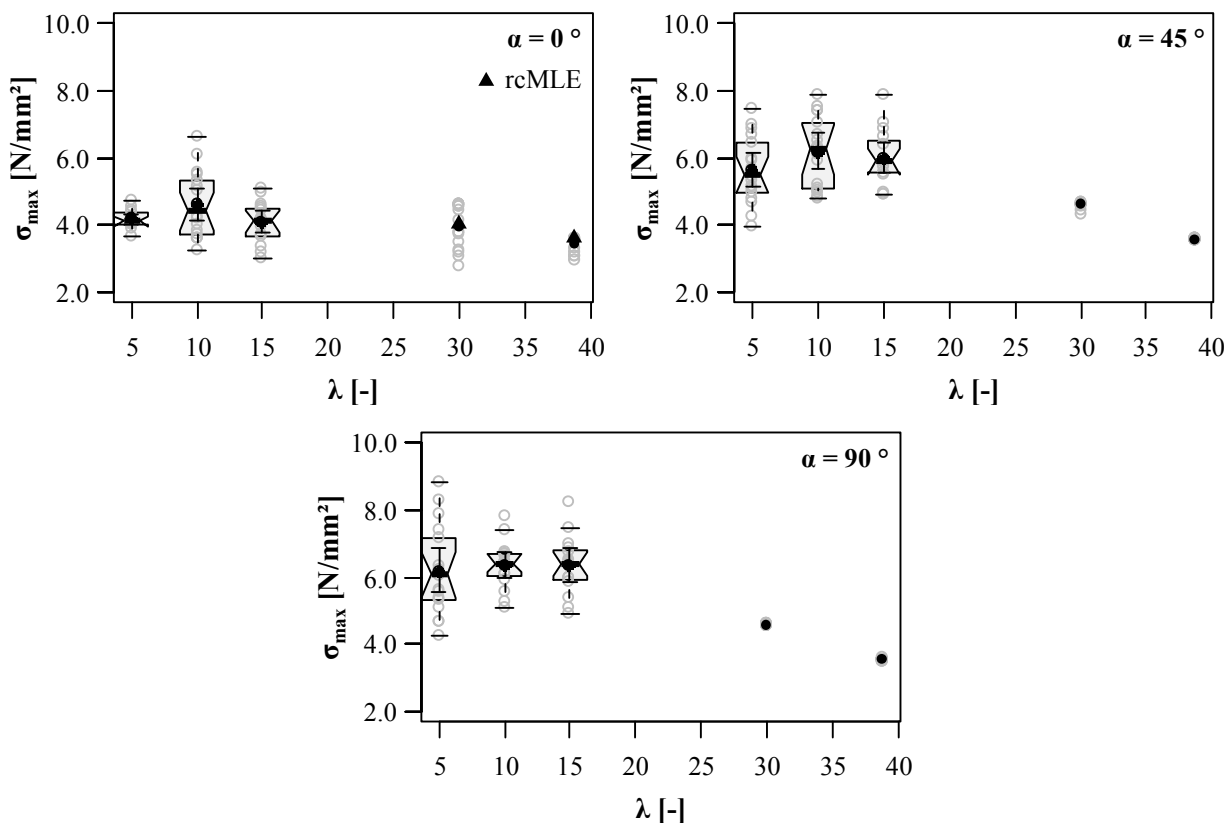


Figure 5.112: Combined boxplot/scatterplot graphics of maximum axial stresses reached in dependence of slenderness and axis-to-grain angle

In addition, Table 5.41 comprises the values for k_p and $r_{\text{XY,PE}}$ determined for all subseries, which exclusively include the test results of specimen failed by withdrawal. The given results again confirm,

that there is no specific trend observable, which indicates an impact of l_{ef} on the relationship between withdrawal strength and density.

Table 5.41: Experimentally determined values for k_p in dependence of axis-to-grain angle and effective inserted thread length (expressed by λ)

α [°]	λ [-]	5	10	15
0	k_p [-]	0.21	0.67	0.54
	$r_{XY,PE}$ [-]	0.37	0.40	0.40
45	k_p [-]	1.18	1.24	0.87
	$r_{XY,PE}$ [-]	0.82	0.88	0.81
90	k_p [-]	1.41	0.90	1.11
	$r_{XY,PE}$ [-]	0.91	0.74	0.85

Equal to the withdrawal strength, Figure 5.113 illustrates the gained values for the withdrawal stiffness $K_{ser,ax}$ in dependence of axis-to-grain angle and slenderness. Irrespective of the value of α applied, a strongly pronounced, degressive behaviour of $K_{ser,ax}$ with increasing λ (and thus l_{ef}) can be observed. For high values of $\lambda = \{30, 39\}$ the determined withdrawal stiffness converges to a constant plateau. This indicates, that an increase of effective inserted thread lengths, exceeding a certain upper limit of l_{ef} , does not influence the size of this property any more.

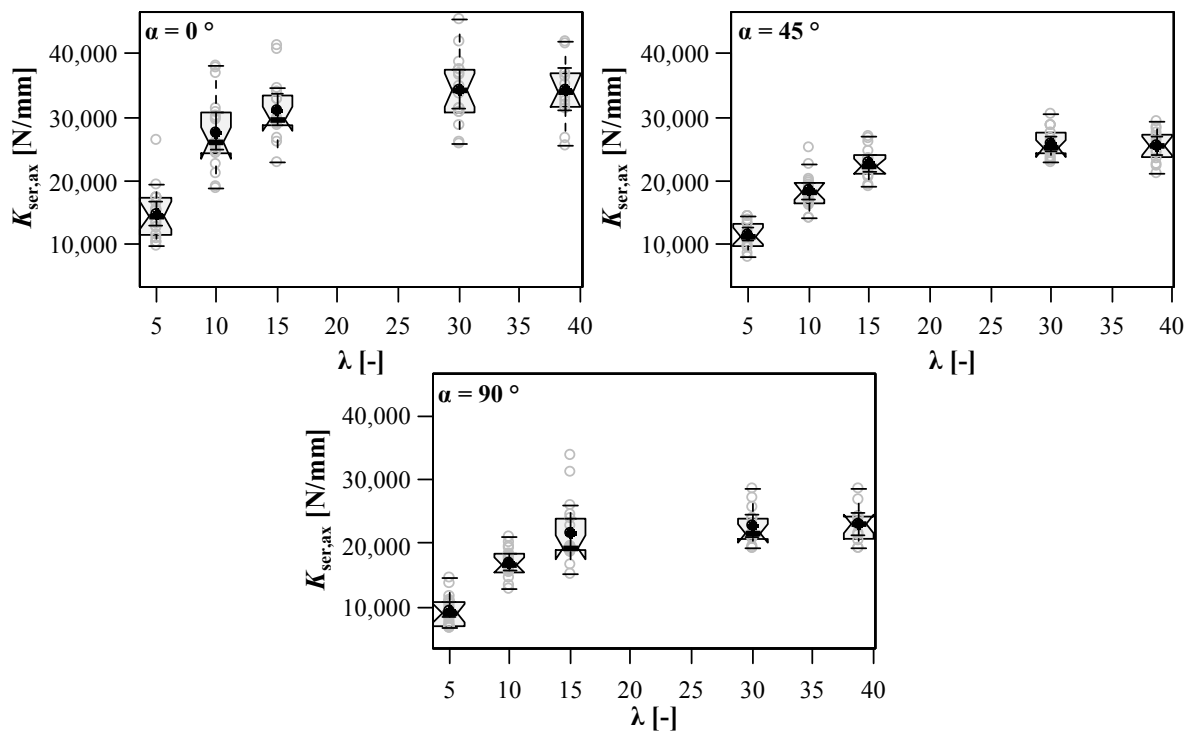


Figure 5.113: Combined boxplot/scatterplot graphics of withdrawal stiffness $K_{ser,ax}$ in dependence of slenderness and axis-to-grain angle

In order to quantify the impact of l_{ef} on $K_{ser,ax}$ in average, the exponent k_{lef} , introduced before, is determined by means of a nonlinear least squares method as also applied for k_{diam} in section 5-2.1, see eq. (5.97):

$$K_{ser,ax,\alpha,mean} = A \cdot l_{ef}^{k_{lef}}, \text{ with} \quad (5.97)$$

$A = \{6,544; 4,304; 3,813\}$ and $k_{lef} = \{0.30, 0.32, 0.32\}$ for varying $\alpha = \{0, 45, 90\}^\circ$. Comparing the given qualitative and quantitative results with previously discussed observations, and those published in literature sources, the following conclusions are:

First, the behaviour of the model parameter A in dependence of α corresponds to the findings made in section 5-4.3 in form of widely equal values for $K_{ser,ax}$ between $\alpha = 90^\circ$ and 45° , combined with a significant increase of withdrawal stiffness in case of a parallel-to-grain insertion.

Second, absolute values of $K_{ser,ax,mean}$ given in Annex B-3.2, Table B.60 result to be remarkably higher, than those determined for $d = 8$ mm and not pre-drilled screws with comparable values for l_{ef} in sections 5-3.1 and 5-4.2. Worth pointing out, that the latter mentioned campaigns were conducted with partially threaded screws, while the screw thread applied in this programme corresponds to that of a fully threaded screw. In addition, the results of $K_{ser,ax,\alpha=45}$, dedicated to a comparatively small test series reported in Ringhofer (2016), who also applied $d = 8$ mm fully threaded screws without pre-drilling for this purpose, are quite comparable to those given in Table B.60.

Since further parameters, such as the average density or the timber product and wood species applied, are either identical or do not vary to a significant extent, it seems, that the screw product is responsible for the differences in $K_{ser,ax}$. Comparing partially and fully threaded screw thread geometries, additionally neglecting differently pronounced screw tip features, the thread pitch p can be detected as the only parameter, which significantly differs between both thread types – compare e. g. Table 5.6 with Table 5.40. While a related influence of this parameter on the withdrawal strength f_{ax} is commonly regarded as insignificant, c. f. Frese and Blaß (2009), a comparable study focusing on its impact on withdrawal stiffness $K_{ser,ax}$ was not found in literature so far. Due to the high magnitude of given differences, a serious prediction of withdrawal stiffness, e. g. by an empirical regression model, demands a deeper focus on the impact of the screw thread geometry in the frame of future investigations.

Third, even though k_{lef} according to eq. (5.97) results to be somewhat lower, the gained results generally confirm the observations made by Blaß et al. (2006) and Stamatopoulos and Malo (2016) and are thus in strict contrast to the values published in Blaß and Krüger (2010), as well as to the approach given in eq. (5.46).

Fourth, the size of k_{lef} , determined in dependence of α , only varies in a small amount, confirming the qualitative observation, that its impact on withdrawal stiffness is irrespective of the axis-to-grain angle.

The final part of this section shall be addressed to the behaviour of ductility D in dependence of varying l_{ef} . This is illustrated in Figure 5.114 in dependence of the examined axis-to-grain angles. The related comparison solely comprises the span of withdrawal failure – slenderness λ is thus limited to 15. Apart from one subseries defined by $\lambda = 5$ and $\alpha = 45^\circ$, no significant differences of mean[D] or med[D] in-between the series with constant α can be observed. Even though the ductility, determined for perpendicular-to-grain insertion, partially results to be significantly higher than that dedicated to both other angles, the given differences vary in a small range and generally confirm the test results with comparable experimental set-ups.

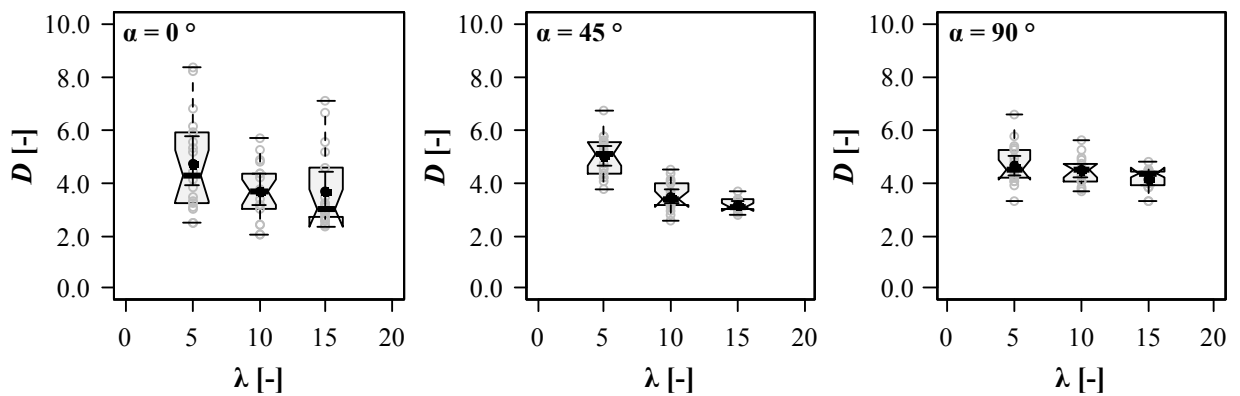


Figure 5.114: Combined boxplot/scatterplot graphics of ductility D in dependence of slenderness and axis-to-grain angle

5-4.6 Embedment length l_{emb}

Note: as mentioned in section 5-1, the discussion in this section only comprises a review of investigations conducted by other authors working in this field.

Specific detail solutions, such as steel-to-timber end-grain joints with self-tapping screws oriented parallel to grain direction, as e. g. illustrated in Figure 2.32, are nowadays realised by arranging the screw threads sunk into the timber member. The related parameter is further denoted as l_{emb} , already defined in Figure 5.5. In fact, the main reason for this measure is to prevent the splitting failure of the connection by moving its gravity centre of load introduction inwards, thus increasing the timber volume stressed by tension perpendicular-to-grain and consequently the related bearing capacity, c. f. Obermayr (2014), Grabner and Ringhofer (2014) or Meyer (2016). This subsection aims to answer the question if this parameter also influences the screw withdrawal behaviour, as defined by the properties $\{f_{ax}, K_{ser,ax}, D\}$. Worth mentioning, that the following discussion is reduced to short-time loading – a corresponding impact on the so-called duration-of-load (DoL) effect is treated in section 5-5.3.

In contrast to the majority of parameters discussed in this chapter, works focusing on a possible influence of l_{emb} , even on withdrawal strength f_{ax} , are scarce. The only exceptions found so far in literature, are: the paper published by Pirnbacher et al. (2009), as well as a student's project, carried out at Graz University of Technology, reported in Burgschwaiger (2010). With regard to the prior mentioned source, Pirnbacher et al. (2009) carried out withdrawal tests with a $d = 8$ mm partially threaded screw ($l_p = 100$ mm), situated in the side face of GLT members (Norway spruce, $N \geq 1$ and $\alpha = 90^\circ$) and l_{emb} as the only varying parameter in form of $l_{emb} = \{0, 15, 30, 100, 170, 240\}$ mm. Thereby, they could observe a significant increase in withdrawal strength if the embedment length increases from 0 mm to 15 mm ($\sim 2d$), followed by a steady, but insignificant, increase of f_{ax} for l_{emb} exceeding this threshold. Since the ratio between $f_{ax, l_{emb} \geq 15\text{mm}}$ and $f_{ax, l_{emb} = 0\text{mm}}$ results in a comparatively high magnitude between 1.13 to 1.18 in average, Pirnbacher et al. (2009) propose considering this effect for an empirical modelling in form of a multiplicative correction (k -)factor of f_{ax} as given in eq. (5.98), see

$$k_{emb} = 1.15, \text{ if } l_{emb} \geq 2d. \quad (5.98)$$

Furthermore, they explain this so-called “embedment effect” by means of a simple strut-and-tie model, as subsequently illustrated in Figure 5.115. Thereby, the load transmission from the screw thread into the timber member occurs in form of compressive diagonals (struts), which necessitate tensile bars (ties) for fulfilling the force equilibrium in each knot of this virtual system along the screw axis. In cases, the screw thread is sufficiently sunk into the timber member, c. f. eq. (5.98), this equilibrium is given for all knots considered, see Figure 5.115 (left), enabling a load transfer for the whole inserted screw thread. In cases where l_{emb} tends to zero, see Figure 5.115 (right), knots situated beyond the timber specimen do not fulfil

this condition any more, the related thread parts close to the surface are thus regarded as not participating in load transfer. Consequently, this critical thread length can be assumed depending on the outer thread diameter, but as a constant value with respect to the total thread length inserted – comparable to l_{tip} . As also concluded by Hübner (2013a), the size of the related impact on f_{ax} thus depends on l_p , a corresponding consideration should be treated similar to the tip correction, rather than as considered in eq. (5.98), see

$$l_{ef} = l_p - l_{tip} + l_{emb}, \text{ with } l_{emb} = \min \left\{ \begin{array}{l} l_{emb} \\ 2d \end{array} \right. \quad (5.99)$$

Since further studies with different values for l_p applied are missing, both constitutions in eq. (5.98) and (5.99) have to be verified in the frame of future investigations.

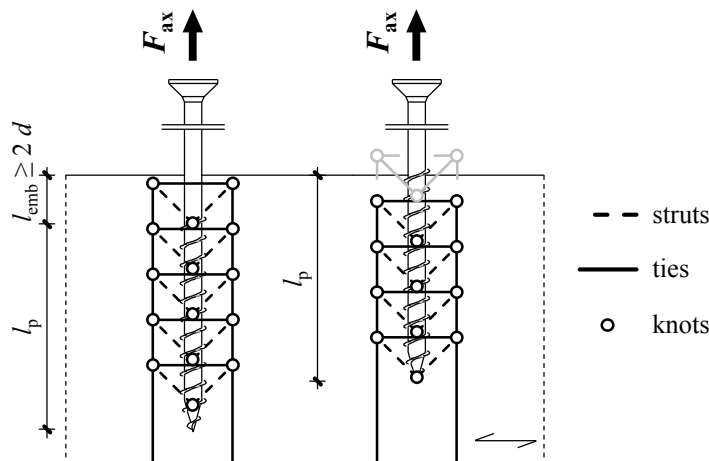


Figure 5.115: Explanation of the “embedment effect” in case of perpendicular-to-grain insertion by means of a strut-and-tie model according to Pirnbacher et al. (2009); left: embedded screw with sufficient l_{emb} , right: non-embedded screw with $l_{emb} = 0$ mm

Now concentrating on the influence of l_{emb} on withdrawal strength f_{ax} in cases, the axis-to-grain angle α deviates from a perpendicular-to-grain insertion. Within his student project, Burgschwaiger (2010) carried out an experimental campaign – similar to that presented in Pirnbacher et al. (2009) – in form of withdrawal tests of the same screw type, situated in solid timber specimen (again Norway spruce) in parallel-to-grain ($\alpha = 0^\circ$) and $l_{emb} = \{0, 4, 8, 12, 16, 24, 32, 80\}$ mm. Summarising his main conclusions, Burgschwaiger (2010) also determined a maximum increase of $\text{med}[f_{ax}]$ between $l_{emb} = 0$ mm and 12 mm in form of $k_{emb} = 1.13$. In strict contrast to Pirnbacher et al. (2009), two further conditions, necessary for stating a significant impact of this parameter on the withdrawal strength, are not fulfilled: first, the hypothesis testing proves no significant difference in the withdrawal strength, even for this upper limit of k_{emb} . Second, the average values of f_{ax} with increasing l_{emb} seem to be randomly distributed (e. g.

$\text{med}[f_{ax, l_{emb}=80\text{mm}}] < \text{med}[f_{ax, l_{emb}=0\text{mm}}]$!), rather than indicating a positive relationship between both variables.

This leads to the conclusion, that the relevance of the so-called “embedment effect” obviously depends on the axis-to-grain angle α . In fact, this may be caused by the different mechanical fracture behaviour for the perpendicular- and parallel-to-grain insertion, as previously demonstrated in section 5-1.1. In case of $\alpha = 0^\circ$, the crack formation occurs parallel to the screw axis at the transition between the thread flank’s end and the timber area around, c. f. Figure 5.2 (left), where the timber’s local resistance in shear is more or less responsible for. In case of $\alpha = 90^\circ$, cracks occur in the timber’s longitudinal direction (perpendicular to screw axis and load direction), indicating a far more pronounced affected timber area, as well as an interaction of shear and tensile stresses perpendicular to grain due to the local fibre bending, c. f. Figure 5.2 (middle). Especially both latter characteristics correspond to the strut-and-tie model, illustrated in Figure 5.115, while the failure at the parallel-to-grain insertion can be rather regarded as a local phenomenon.

Back to the experimentally determined impact of l_{emb} on the withdrawal properties: as reported in Pirnbacher et al. (2009), the related test series were conducted with specimen cut out of two GLT beams in total. This measure leads to comparable timber densities for all single tests, but deviates from the idea of specimen preparation introduced in section 5-1.2. Consequently, the distribution of the timber density does not represent real conditions, excluding a reasonable re-assessment of test data for determining the relationship between density and withdrawal strength (expressed by the exponent k_p) in dependence of l_{emb} . This restriction also concerns both further withdrawal properties $K_{ser,ax}$ and D , which cannot be determined from the campaigns carried out by Pirnbacher et al. (2009) and Burgschwaiger (2010), since the information regarding the test-setup applied is missing. Thus, the knowledge, especially regarding the behaviour of withdrawal stiffness $K_{ser,ax}$ in dependence of l_{emb} , is not given at all. Consequently, in addition to the aforementioned variation of the insertion length l_p (while l_{emb} also varies), this topic should be focused on in the frame of prospective investigations.

5-5 LOADING

5-5.1 Load introduction and supporting conditions

Note: the outcomes of this section have already been published in Ringhofer and Schickhofer (2014a). The statistical methods for determining significance, demonstrated in this paper, can be seen as template for the methodology applied in this chapter. Since the graphical assessment methods only deviate from the procedure explained in section 5-1.2 to a small extent and no additional property determination was applied, the results are consistently adopted from this source.

5-5.1.1 Introduction

Apart from one test campaign, presented in section 5-4.3, the vast majority of the experiments in this chapter was performed with a so-called push-pull test configuration, as schematically illustrated in Figure 5.4. This set-up is not only frequently applied at Graz University of Technology for this purpose, but also expected as a standard method, c. f. for instance Frese and Blaß (2009), Blaß and Krüger (2010), Ringhofer (2016) and Branco et al. (2016). Thereby, the screw is loaded in tension and – from a global point of view – the force transmission from the specimen’s area around the embedded screw axis to the supporting, which is located at the specimen’s side of the load introduction, occurs via compressive load paths – see Figure 5.116 (a). As implied in Figure 5.116 (b) to (d) comprising an extract of further possibilities, the loading and supporting conditions (push or pull), as well as the shape and direction of load paths (push/compression, pull/tension or pile/shear) may not only vary in the frame of the test execution, but also in practical application.

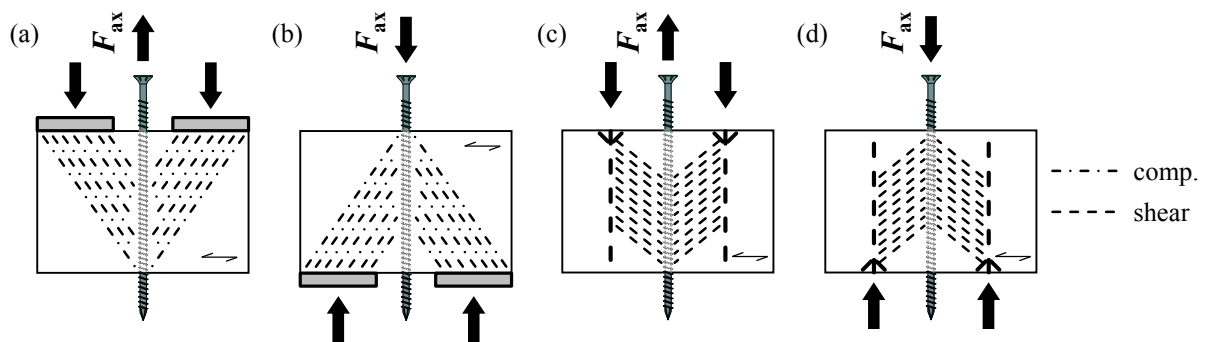


Figure 5.116: Examples of different loading and supporting conditions for screw withdrawal tests according to Gehri and Haas (2008); (a) and (c) loaded in tension, (b) and (d) loaded in compression

Thus, it is obvious, that one test set-up applied is hardly able to cover all different cases. Since works, which are focusing on the influence of varying loading and supporting conditions on the withdrawal behaviour of self-tapping screws were not found in literature at all, the aim of the test series, published in

Ringhofer and Schickhofer (2014a), subsequently presented in the following subsections, consequently was to identify a possible impact on the screw withdrawal capacity related.

In advance, some considerations, regarding the conception of the scope of this programme, shall be summarised in brief: first, presupposing that the screw threads have a symmetric flank inclination ($\psi = \nu / 2$), Bejtka (2005) reports in his dissertation, that both loading alternatives push (screw loaded in compression) and pull (screw loaded in tension) will lead to equal values for the withdrawal strength f_{ax} . This statement, in fact, reduced the varied test configurations to those, where the screw is loaded in tension. Second, ON EN 1382 (1999) recommends, that the distance between the supporting and the screw axis shall be at least $3d$. Since the investigations focusing on the impact of this parameter on the screw withdrawal properties were not found in literature, two out of four examined configurations comprised a related parameter variation. Third, ON EN 1382 (1999) additionally defines the fastener axis, being inserted perpendicular to the specimen surface (note: this angle is subsequently denoted as ϵ_{sur}). For instance, this condition was not fulfilled for the pull-pile configuration, applied for parts of the tests in section 5-4.3. Again no source dealing with this matter was found so far, it was also aimed to identify a possible influence of this parameter on the withdrawal strength.

5-5.1.2 Experimental programme

The experimental programme for determining the aforementioned effects was carried out in the frame of two campaigns, which are subsequently introduced. Following Ringhofer and Schickhofer (2014a), they are denoted as I and III (note: campaign II, also presented in this source, is separately discussed in section 5-5.2). As illustrated in Figure 5.117, the programme, dedicated to campaign I, is additionally subdivided into three parts: Ia, Ib and Ic. Taking the standard push-pull (i) configuration as a reference into account, the test series, corresponding to Ia, comprised a variation of further loading and supporting conditions in form of push-pile (ii, supporting screws loaded in compression, shear load paths occurring in the specimen), pull-pull (iii, supporting screws loaded in tension, tensile load paths occurring in the specimen) and pull-pile (iv, supporting screws loaded in tension, shear load paths occurring in the specimen). In the frame of subseries Ib (configuration i, diameter d_h of the supporting plate's hole) and Ic (configuration ii, parallel-to-grain distance a_s between tested screw and supporting screws) the aforementioned distance between the fastener axis and the supporting measure was varied. Worth mentioning, the withdrawal tests, dedicated to Ia and Ib, were conducted with both main axis-to-grain angles $\alpha = \{0, 90\}^\circ$, while in case of Ic, only the perpendicular-to-grain insertion was examined, c. f. Table 5.42. Therein, the parameter characteristics, as well as further test conditions, applied for campaigns I and III, are given (note: screw types are equal to those introduced in section 5-2.1, related thread properties are thus given in Table 5.2). A parameter variation of the latter campaign, again comprising a comparison of both (i) and (iv) test configurations, as well as two values for $\epsilon_{sur} = \{45, 90\}^\circ$

(main focus of this programme), conducted with an axis-to-grain angle $\alpha = 45^\circ$, is schematically illustrated in Figure 5.118.

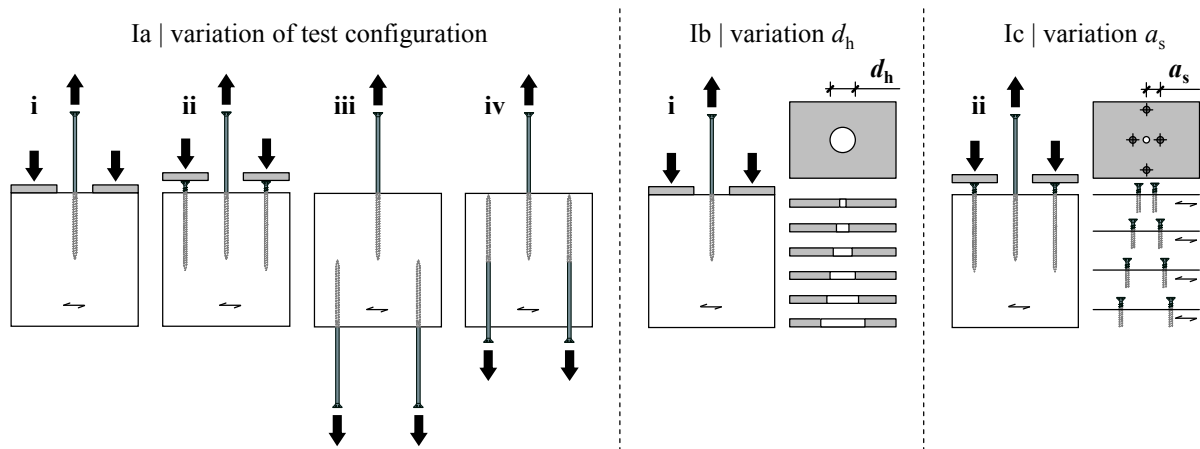


Figure 5.117: Schematic overview of campaign I parameter variation exemplarily for $\alpha = 90^\circ$; according to Ringhofer and Schickhofer (2014a); (i) push-pull, (ii) push-pile, (iii) pull-pull, (iv) pull-pile

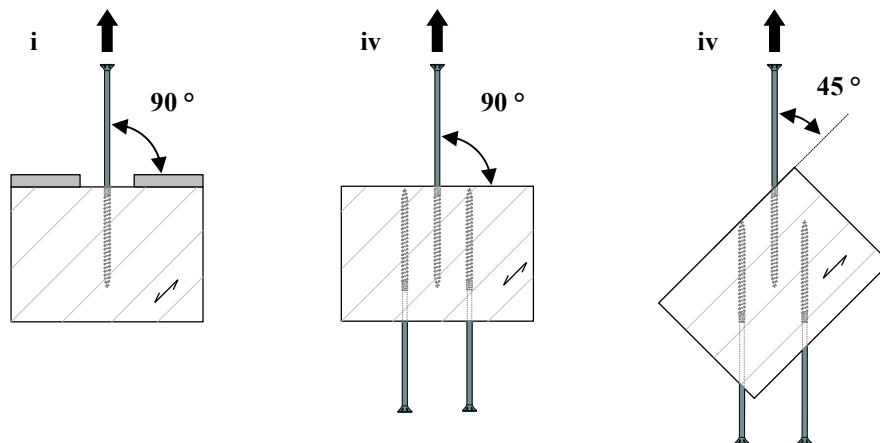


Figure 5.118: Schematic overview of campaign III parameter variation; according to Ringhofer and Schickhofer (2014a)

Table 5.42: Test conditions applied for the experimental campaign focusing on the impact of varying withdrawal test configurations

series	sub-series	d_{nom} [mm]	α [°]	ϵ_{sur} [°]	l_p [mm]	l_{ef} [mm]	l_{emb} [mm]	d_{PD} [mm]	d_h [d]	a_s [d]
I	Ia	8	0, 90	90	99	89.6	16	0, 6	5	5
	Ib	8	0, 90	90	99	89.6	16	6	2, 3, 4, 5, 6, 9	-
	Ic	8	90	90	99	89.6	16	6	-	2, 3, 4, 5
III		6	45	45, 90	114	107	0	0	9	6.7

The basic material for the campaign I specimen production were solid timber beams of Norway spruce with dimensions of about $h \times w \times l = 160 \times 240 \times 4000 \text{ mm}^3$, while in case of campaign III, specimen of unknown size were cut out of GLT beams (again Norway spruce). The selection and preparation of the specimen followed the principle introduced in section 5-1.2. The related dimensions, especially with regard to the position of tested and supporting screws, are illustrated in Annex B-3.1, Figure B.72 to Figure B.75. As given in Table 5.42 and Figure B.72, the impact of pre-drilling was also varied in the frame of campaign Ia (one screw tested with configuration i without pre-drilling), while for reasons of accuracy all remaining tests were carried out with specimen pre-drilled in advance. Since the consequence of this preparation measure has already been discussed in section 5-4.2, the following subsection exclusively includes the test results, when pre-drilling was applied. Campaign Ia- and Ic-specimen production and withdrawal testing immediately took place after the delivery of the timber material. Thus, no storage in the climatic chamber until reaching the equilibrium moisture content, took place. The related consequences are discussed in the following subsection.

Worth mentioning, all tests have been performed on the test rig LIGNUM-UNI-275, excluding a local way measurement with LVDTs. Since varying test configurations may differently contribute to the magnitude of global displacements recorded, the determination of $K_{\text{ser,ax}}$ and D is not reasonable, even for a relative comparison. Thus, the results exclusively comprise the withdrawal strengths f_{ax} . Supplemental information regarding test execution, post-processing, property determination and data assessment is summarised in Ringhofer and Schickhofer (2014a).

5-5.1.3 Results and discussion

Within this subsection, the results dedicated to the experimental campaigns I and III, as published in Ringhofer and Schickhofer (2014a), are separately discussed. In advance, the moisture contents, determined for each subseries and their impact on the withdrawal strength, shall be summarised in brief: as previously mentioned, the specimen, corresponding to Ia and Ic subseries, were tested without prior climatic conditioning. The average values for u_{mean} of $\{Ia_{\alpha=0^\circ}, Ia_{\alpha=90^\circ}, Ib, Ic, III\}$ result to $\{14.1, 14.5, 13.1, 13.4, 12.1\} \%$ and may exclude a reasonable overall comparison of (uncorrected) withdrawal strength. Since the moisture contents vary in the target bandwidth of $\pm 2 \%$ in-between each subseries, the aimed relative comparison of test results is possible.

Statistical parameters of withdrawal strengths, determined for varying loading and supporting conditions (i) ÷ (iv), are subsequently illustrated in Figure 5.119 in dependence of axis-to-grain angle α . In addition, Table B.61 and Figure B.76 in Annex B-3 comprise the main statistical parameters of density ρ_{12} and withdrawal strength and compare the gained variabilities of f_{ax} in form of $\text{CV}[\ln(f_{\text{ax}})]$. Note: due to the occurrence of tensile forces perpendicular-to-grain as a consequence of pull-pull testing at $\alpha = 90^\circ$, certain specimen dedicated to this subseries failed by exceeding the related tensile strength $f_{t,90}$ prior to the

withdrawal failure. Thus, this specific dataset has to be seen as right-censored, the determination of $f_{ax,mean}$ and $CV[f_{ax}]$ was conducted by means of rcMLE according to eq. (5.23) and (5.24). In contrast to the majority of investigations, the hypothesis testing of the density ρ_{12} for each subseries is missing. The average values and variabilities (expressed by $CV[\rho_{12}]$), given in Table B.61, indicate only minor deviations, a related impact on withdrawal strength ($f_{ax,mean}$ and $CV[f_{ax}]$) can thus be excluded. With regard to the magnitude of f_{ax} , in dependence of test configuration (i) ÷ (iv), neither for screws inserted parallel-to-grain, nor for those with a perpendicular-to-grain axis orientation, a significant difference can be observed. This also corresponds to the course of $CV[\ln(f_{ax})]$, indicating no significant deviation as a consequence of varying test configurations.

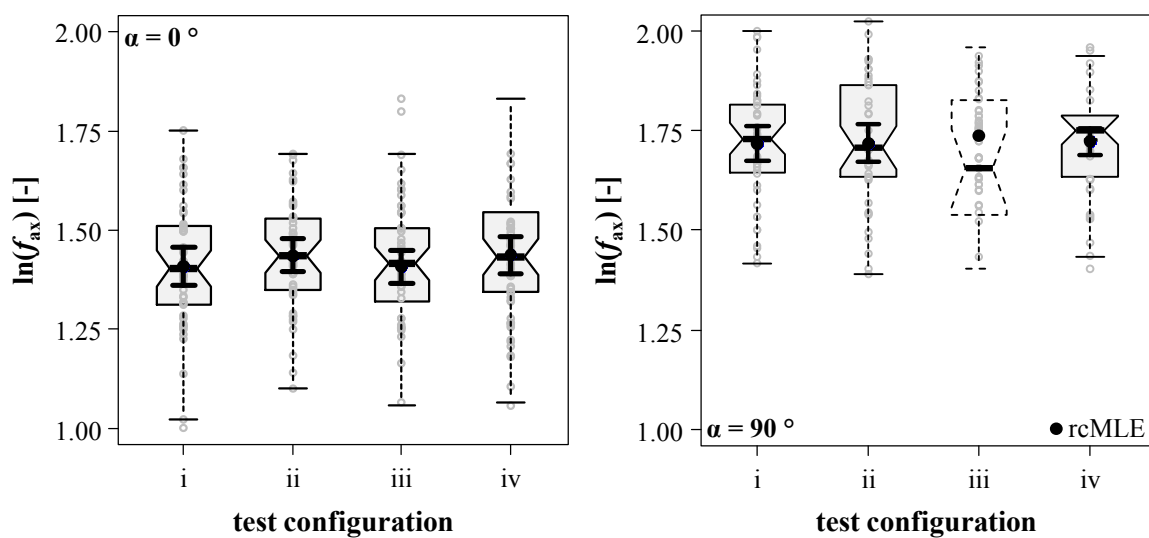


Figure 5.119: *Logarithmic withdrawal strength in dependence of axis-to-grain angle and test configuration; according to Ringhofer and Schickhofer (2014a)*

Now concentrating on the distance between screw axis and supporting in case of the standard push-pull test configuration (i): Figure 5.120 subsequently illustrates the logarithmic withdrawal strengths $\ln(f_{ax})$ in dependence of the axis-to-grain angle and the supporting plate's hole diameter d_h . The main statistical parameters of density ρ_{12} and withdrawal strength f_{ax} are given in Annex B-3.2, Table B.62, again excluding the necessity of applying a density correction for the test results.

In case of the perpendicular-to-grain insertion and equal to the varying test configurations, hypothesis testing, as well as the magnitudes of the withdrawal strength determined for each d_h , indicate no relevant impact of this parameter on the timber-screw composite resistance. In case of the parallel-to-grain insertion, a certain trend of decreasing values for f_{ax} with decreasing d_h , especially between $d_h = \{2, 3, 4\} d$ and $d_h = \{5, 6, 9\} d$ can be observed. This is in fact surprisingly since – from a mechanical point of view – rather an oppositional behaviour was expected. Following Ringhofer and Schickhofer (2014a), the experimental results were consequently evaluated by applying the approach from Pirnbacher et al. (2009)

(eq. (5.40), $\alpha = 0^\circ$) for a related property estimation. Therewith predicted withdrawal strengths, basing on ρ_{12} given in Table B.62, are also illustrated in Figure 5.120 and result exactly in-between both aforementioned groups, thus indicating no tendency to one of them. Additionally taking the insignificance of the given deviation into account, also for $\alpha = 0^\circ$, a relevant impact of d_h on f_{ax} can be excluded with a high reliability. With regard to the variability of the withdrawal strength, in dependence of d_h , again no related influence is given, c. f. Annex B-3.1, Figure B.77.

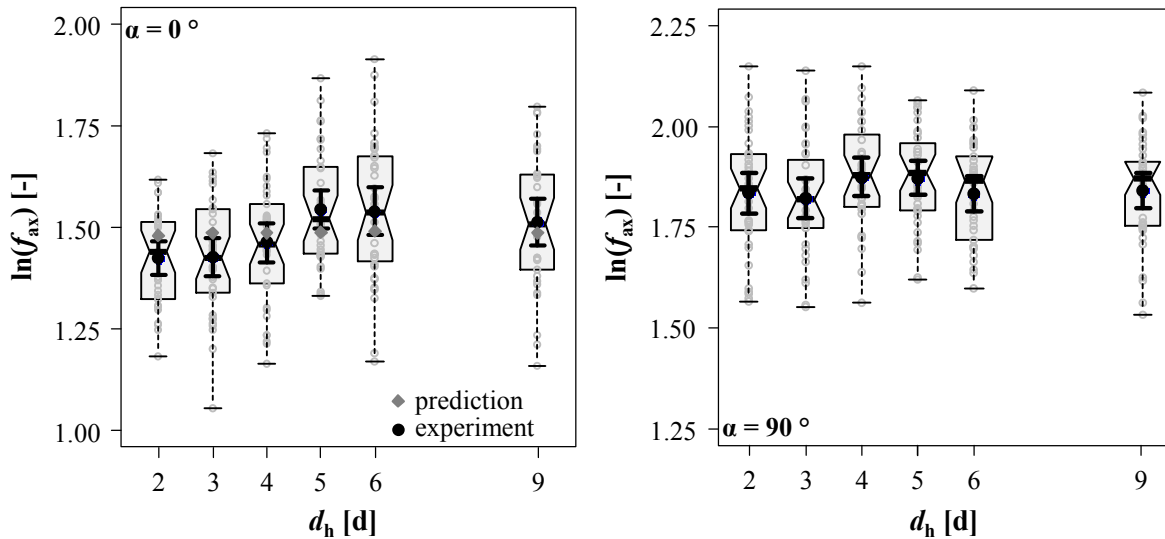


Figure 5.120: Logarithmic withdrawal strength in dependence of axis-to-grain angle and the supporting plate's hole diameter; according to Ringhofer and Schickhofer (2014a)

Figure 5.121 subsequently illustrates the behaviour of both, logarithmic withdrawal strength $\ln(f_{ax})$ and related variability $CV[\ln(f_{ax})]$, in dependence of the supporting screw's distance parallel to the grain direction, a_s for the push-pile test configuration (iv) applied. The supplemental information, regarding the statistical parameters of density ρ_{12} and withdrawal strength f_{ax} , is given in Annex B-3.2, Table B.63. As mentioned before, the scope of this campaign Ic was reduced to the perpendicular-to-grain insertion. First, the specimen preparation, according to section 5-1.2, led to similar densities (and also dispersions via $CV[\rho_{12}]$), again excluding a related impact on f_{ax} . Second, the given parameter variation obviously does not influence the variability of the withdrawal strength, c. f. Figure 5.121 (right). Third, more or less equal average values for the withdrawal strength can be observed for $a_s = \{3, 4, 5\} d$, while in case of $a_s = 2 d$, a pronounced decrease of f_{ax} is given. This loss of the bearing capacity, in fact, can be explained by an already harmed stressed timber volume – comparable to the findings made in section 5-4.1.

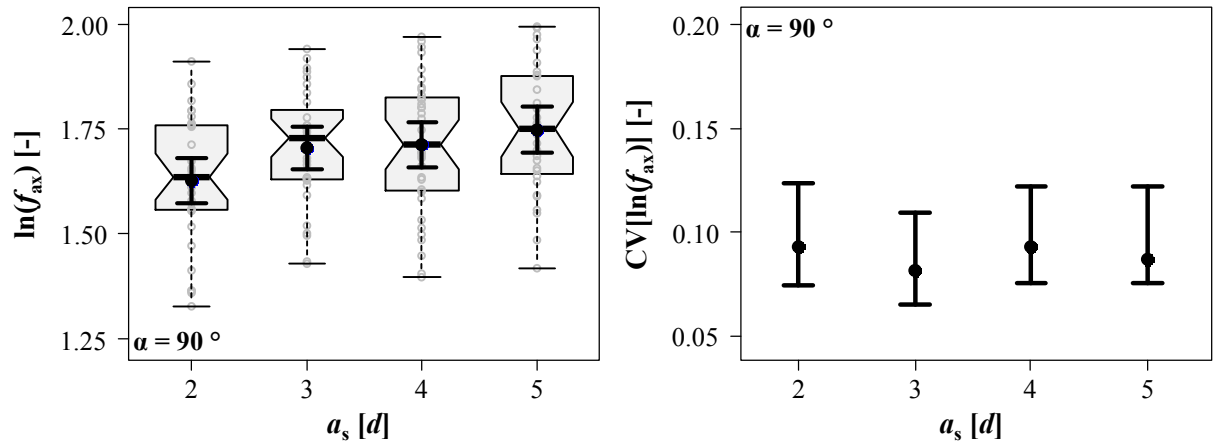


Figure 5.121: Left: logarithmic withdrawal strength, right: CIs of $CV[\ln(f_{ax})]$, both in dependence of the supporting screws' distance a_s ; according to Ringhofer and Schickhofer (2014a)

The final focus in this section is on the influence of varying the surface angle ϵ_{sur} on the screw withdrawal strength f_{ax} . As outlined in Annex B-3.2, Table B.64, the related programme comprised a comparatively small amount of tests and parameter characteristics. Since the variability of the density ρ_{12} shows a far more pronounced deviation, it was decided to exclude the one of withdrawal strength in dependence of ϵ_{sur} . Furthermore, the hypothesis testing of the withdrawal strength (results are illustrated in Figure 5.122) in dependence of test configuration (i vs. iv) and surface angle ϵ_{sur} , was carried out only for $med[f_{ax}]$ as a reasonable statistical parameter with respect to the given number of tests per subseries, c. f. section 5-1.2. Additionally taking slightly higher average values for ρ_{12} in case of test configuration (iv) into account, c. f. Table B.64, both varying parameters, the test configuration and the surface angle ϵ_{sur} , obviously do not influence the determined withdrawal strength to a significant extent.

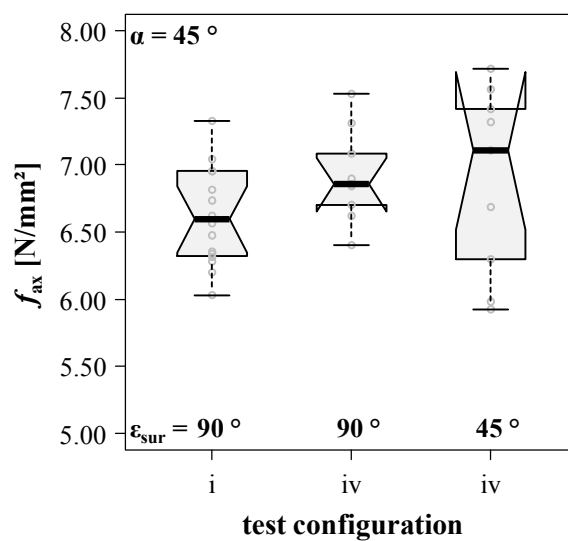


Figure 5.122: Withdrawal strength in dependence of test configuration and surface angle ϵ_{sur} ; according to Ringhofer and Schickhofer (2014a)

Summarising the findings, taking the basic discussion given in section 5-1.1 into account, the withdrawal failure of self-tapping screws has to be defined as a local phenomenon, influenced by the timber area, closely situated around the screw axis. Thus, a variation of global boundary conditions regarding load introduction, transmission and supporting has no relevant impact on size and dispersion of this property – irrespective the axis-to-grain angle applied. The sole restriction of this statement is given for supports, which influence the stressed timber volume along the screw axis as e. g. observed for $a_s = 2 d$. The standard test configuration, illustrated in Figure 5.4, can be regarded as sufficiently representing the real conditions for axially loaded self-tapping screws.

It is worth pointing out, that this conclusion may not correspond to both further withdrawal properties focused on in the frame of this chapter. This especially concerns the withdrawal stiffness $K_{ser,ax}$, which may be specifically influenced by the push-pull configuration, even if a local way measurement is applied. Consequently, a related study, to be carried out in the future, is seen as a vulnerable contribution to that topic.

5-5.2 Loading velocity

Note: the outcomes of this section have already been published in Ringhofer and Schickhofer (2014a). In contrast to section 5-5.1, the possibility of determining the additional withdrawal properties $K_{ser,ax}$ and D necessitated a re-assessment of test data. Therefore, the methodology, explained in section 5-1.2, was applied – the results thus slightly deviate from the published ones.

5-5.2.1 Introduction

Apart from the experimental campaign, presented in the frame of this section, all withdrawal tests were carried out fulfilling the requirement according to ON EN 1382 (1999), stating that the force maximum in a timeframe of 90 ± 30 s has to be reached, c. f. section 5-1.2. This duration is subsequently denoted as time-to-failure (t_{tf}).

Notes: first, replacement document ON EN 1382 (2016), as the currently valid test standard for determining the withdrawal capacity of self-tapping screws, postulates t_{tf} in form of 60 ± 15 s now (not applied for the tests, since they were conducted before this document has been published). Second, both ON EN 1382 (1999) and ON EN 1382 (2016) furthermore state a “constant rate of loading” (RoL), thus necessitating a force-controlled load application. For reasons of recording the post-failure behaviour, as e. g. necessary for determining the ductility D , deviating from this test standard but in accordance to ON EN 26891 (1991) (at least for load application above $0.70 \cdot F_{est}$), a displacement-controlled loading protocol was consistently applied for all withdrawal tests presented in this chapter, c. f. section 5-1.2. This is defined by a constant rate of slip (RoS), instead of a constant rate of loading. Considering these boundary conditions, regarding the test execution, the focus is subsequently restricted to displacement-controlled loads applied by means of a monotonic loading protocol in contrast to ON EN 26891 (1991) without any initial hysteresis. This excludes the impact impulse testing, as e. g. realised by pendulum impact hammers or drop weight impact testing machines.

Similar to the variation of different test configurations, discussed in section 5-5.1, the investigations concentrating on a possible influence of varying t_{tf} (or RoL) on withdrawal properties of axially loaded self-tapping screws are missing in literature. Consequently extending the scope to other screw types, one examination reported in Rosowsky and Reinhold (1999) is worth being highlighted, since they conducted the withdrawal tests of Northern American #8 screws (nominal thread diameter about 4 mm) situated in SPF (spruce-pine-fir) specimen and varied – amongst others – RoL in form of {2.5, 10, 25, 125, 250} mm/min. Even though their report does not include any information related, own experience with $d = 4$ mm screws (c. f. section 5-2.1) indicates, that the given parameter variation approximately covers a range of t_{tf} between ~ 0 s and 60 s. Even though they observed a comparatively high difference in average withdrawal capacities, determined for each subseries, the related deviations appear randomly and

do not indicate any impact of RoL on F_{ax} . Apart from this study, no further investigations, regarding any types of screws loaded in axial direction by varying RoL, were found in literature. Consequently, it was decided to identify a possible influence related by means of screw withdrawal tests. Materials, methods and test results, also published in Ringhofer and Schickhofer (2014a), are discussed in the following subsections.

5-5.2.2 Experimental programme

As mentioned in section 5-5.1, the test programme executed for evaluating a possible influence of RoL (or t_{tf}) on the screw withdrawal strength, was originally denoted as campaign II in Ringhofer and Schickhofer (2014a). The timber material applied for the specimen production was identical to that of campaign I, discussed in section 5-5.1. Following the principle of matched samples, introduced in section 5-1.2, the specimen of each solid timber beam comprised the whole range of varying RoL, in order to gain a similar density distribution for all subseries. The related dimensions, especially with respect to the screw positioning, are illustrated in Annex B-3.1, Figure B.78. Supplemental information regarding the test conditions is summarised in Table 5.43, pointing out, that only perpendicular-to-grain insertion was examined. The range of RoL lasting from 0.6 to 500 mm/min was chosen to cover, not only the immediate failure at t_{tf} close to 0 s, but also to examine the values for $t_{tf} \approx 300$ s, as recommended in ON EN 408 (2010) e. g. for experimentally determining the shear strength of structural timber.

The screw type applied was equal to that of campaign I (presented in section 5-5.1), the related thread properties are thus given in Table 5.2. Similar to campaigns Ia and Ic in section 5-5.1, the specimen production and withdrawal testing took place immediately after the delivery of the timber material. The related consequences (moisture content) are discussed in the following subsection.

Table 5.43: *Test conditions applied for the experimental campaign focusing on the impact of varying RoL on screw withdrawal properties*

series	d_{nom} [mm]	α [°]	l_p [mm]	l_{ef} [mm]	l_{emb} [mm]	d_{PD} [mm]	d_h [d]	RoL [mm/min]	(target) t_{tf} [s]
II	8	90	99	89.6	16	0	5	0.6, 1.5, 2.2, 4.0, 500	~0, 45, 90, 135, 300

All tests of this programme were performed on the test rig LIGNUM-UNI-275, according to Figure 5.4, but without measuring local displacements. Since the boundary conditions, such as axis-to-grain angle, outer thread diameter, specimen dimensions, as well as test configuration were kept constant, a relative comparison of both properties $K_{ser,ax}$ and D is possible and led to the re-assessment of test data. Further background information, regarding test execution, post-processing, property determination and statistical evaluation is thus summarised in section 5-1.2.

5-5.2.3 Results and discussion

Statistical parameters, dedicated to the timber density ρ_{12} of small scale specimen, are subsequently illustrated in Figure 5.123. Related quantitative test results, also those for moisture content u , are given in Annex B-3.2, Table B.65. As mentioned before, no climatic conditioning was applied in advance, the determined moisture content thus results at roughly 15 % in average, exceeding the equilibrium one to a remarkable extent. Nevertheless, $\text{mean}[u]$ of all subseries are similar and their extremal values result in a bandwidth of roughly $\pm 2\%$. Thus, a possible influence of moisture contents, differing in-between the test series, on a relative comparison of the withdrawal properties can be excluded. This boundary condition is also fulfilled for the timber density ρ_{12} : mean values, medians, as well as variabilities, the latter expressed by $\text{CV}[\ln(\rho_{12})]$, do not significantly deviate from each other.

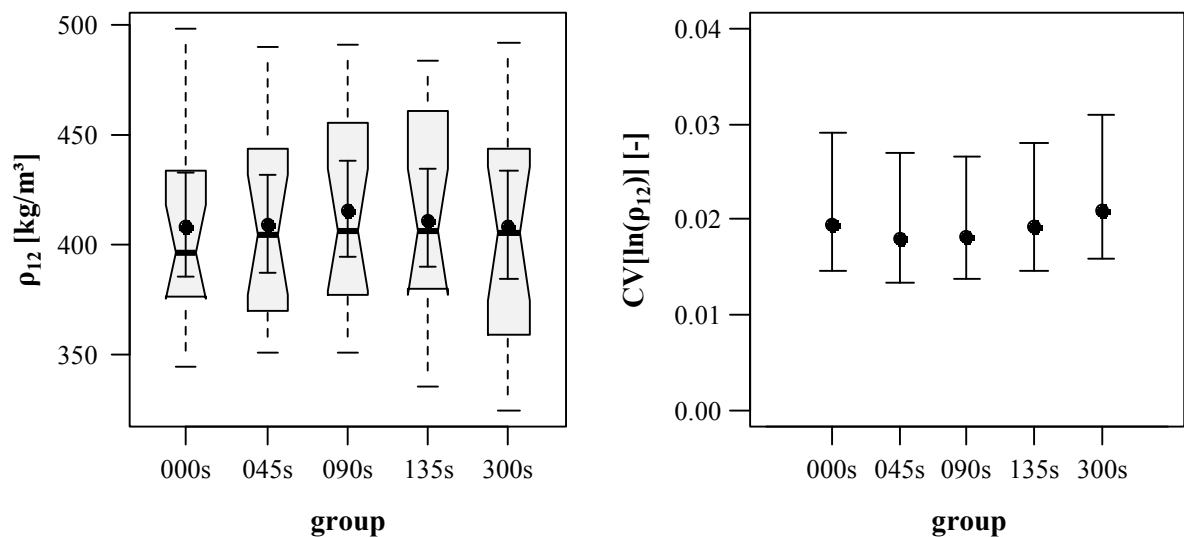


Figure 5.123: Left: boxplot graphic of densities ρ_{12} ; right: CIs of $\text{CV}[\ln(\rho_{12})]$, both in dependence of (target) time-to-failure groups

Concentrating on the withdrawal properties $\{f_{ax}, K_{ser,ax}, D\}$, the related test results are illustrated in Figure 5.124 to Figure 5.126 and quantitatively given in Annex B-3.2, Table B.67. Furthermore, Table B.66 comprises the reached average and the extremal values of t_{tf} per each subseries, differing from the target values only to a small extent. With regard to the behaviour of the withdrawal strength, in dependence of varied RoL or t_{tf} , no significant difference for the groups loaded with $\{0.6, 1.5, 2.2, 4.0\}$ mm/min is given, while both $f_{ax,mean}$ and $f_{ax,med}$ dedicated to RoL = 500 mm/min, result in a remarkably (but not significantly) higher magnitude.

Even though a slightly different procedure, regarding the outlier treatment, was applied by Ringhofer and Schickhofer (2014a), the behaviour of withdrawal strength in dependence of varying RoL was found being more or less equal to the course illustrated in Figure 5.124. In contrast to this paper, it was decided to exclude a discussion of an approach, which describes the related impact of RoL (or t_{tf}) by means of a

logarithmic (\log_{10}) relationship between both variables and which takes the observed increase at $ttf = \sim 0$ s into account. The main reason therefore is the absence of, at least, one additional data point, e. g. determined for $ttf = 10$ s or 1,000 s, enabling the verification of the linear course in the semi-logarithmic domain, as illustrated in Ringhofer and Schickhofer (2014a). Focusing on the current state-of-the-art, regarding withdrawal test execution, the main conclusion of this test campaign is, that a varying ttf , resulting at roughly $\log_{10}(ttf) = 1.5 \div 2.5$ (which respect to the range considered, this means $ttf = 45 \text{ s} \div 450 \text{ s}$), has no relevant impact on the withdrawal strength f_{ax} . Worth mentioning, the related variabilities in form of $CV[\ln(f_{ax})]$ for each subseries, compared in Figure 5.124 (right), do not significantly deviate from each other (even though a slight increase at (target) $ttf = \{135, 300\}$ s can be observed) – a RoL (or ttf) related impact on the dispersion of withdrawal strength needs not to be considered.

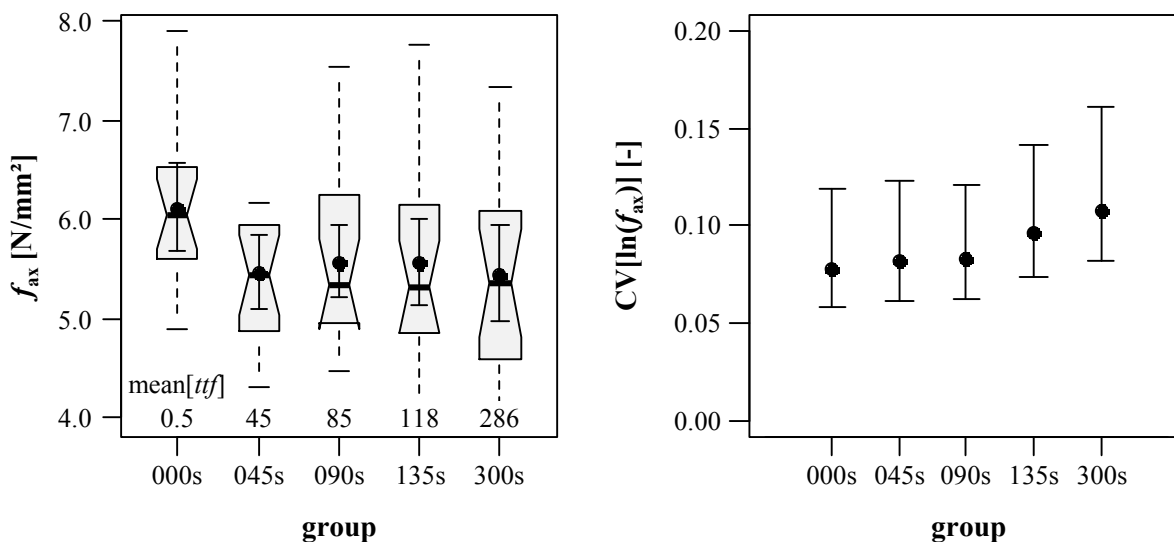


Figure 5.124: Left: boxplot graphic of withdrawal strength f_{ax} ; right: CIs of $CV[\ln(f_{ax})]$, both in dependence of time-to-failure (ttf)

Now focusing on the results of the withdrawal stiffness $K_{ser,ax}$ in dependence of varying loading rates (or ttf), as compared in Figure 5.125 (left), again a constant plateau for the groups loaded with $\{0.6, 1.5, 2.2, 4.0\}$ mm/min can be observed. In addition and in contrast to the withdrawal strength, both mean and median of $K_{ser,ax}$, dedicated to the data point with RoL = 500 mm/min, do not differ significantly to those of the other subseries. Based on this experimental campaign, it can thus be concluded, that the withdrawal stiffness is not affected by this parameter variation at all. This also corresponds to related variabilities, shown in Figure 5.125 (right).

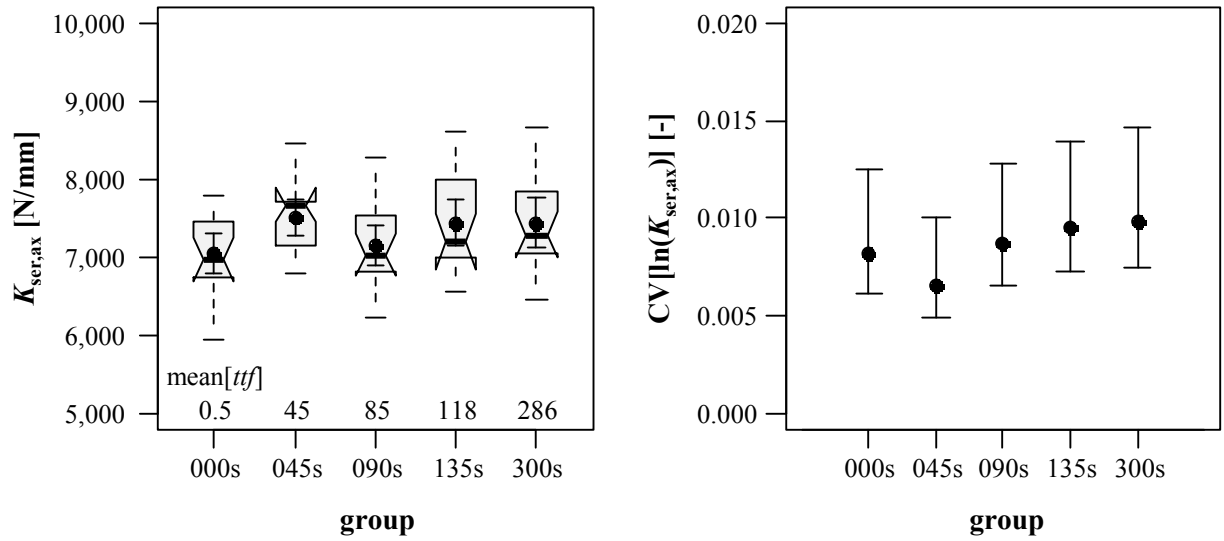


Figure 5.125: Left: boxplot graphic of withdrawal stiffness $K_{ser,ax}$; right: CIs of $CV[\ln(K_{ser,ax})]$, both in dependence of time-to-failure (ttf)

With regard to the determined ductility, illustrated in Figure 5.126 (left) in dependence of RoL (or ttf), a similar behaviour for all test series related to $\log_{10}(ttf) = 1.5 \div 2.5$, as it is observed for both withdrawal strength and stiffness in Figure 5.124 (left) and Figure 5.125 (left), is given. Interestingly, the results gained for the maximum loading rate considered, indicate an oppositional behaviour if compared to those of the withdrawal strength. This significant decrease of D with decreasing ttf bases on an increase of average yield displacements v_y (c. f. Figure 3.37, a; equal to the increase of f_{ax}) of this test series while average values of v_u remain the same. This leads to the conclusion, that immediate ttf close to 0 s obviously provokes a less pronounced post-failure behaviour and thus a smaller ductility.

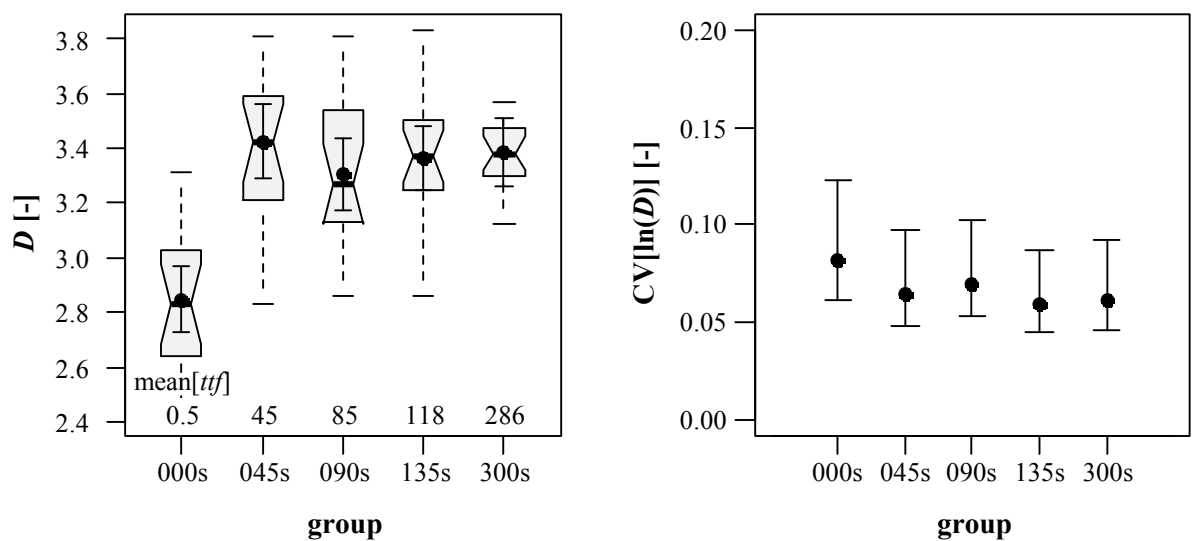


Figure 5.126: Left: boxplot graphic of ductility D ; right: CIs of $CV[\ln(D)]$, both in dependence of time-to-failure (ttf)

The final part of this subsection shall concentrate on a possible impact of RoL (or t_{tf}) on the relationship between density and withdrawal strength, as expressed by both parameters k_p and $r_{XY,PE}$. The related results – determined according to eq. (5.34) and (5.54) – are subsequently given in Table 5.44, in dependence of the aforementioned parameters. Taking the comparatively high variability of k_p and $r_{XY,PE}$ into account, the given magnitudes indicate no relevant influence to be considered for empirically modelling the screw withdrawal strength in the frame of chapter 6.

Table 5.44: Experimentally determined values for k_p and $r_{XY,PE}$ in dependence of the rate of loading

group	[-]	000s	045s	090s	135s	300s
RoL	[mm/min]	500	4.00	2.20	1.50	0.60
t_{tf}	[s]	0.5	45	85	118	286
k_p	[-]	1.18	1.16	1.19	1.28	1.32
$r_{XY,PE}$	[-]	0.90	0.91	0.93	0.90	0.91

Summarising the findings, a remarkable increase of withdrawal strength, combined with a significant decrease of ductility, was observed for the test series dedicated to a loading rate of 500 mm/min. Comparing the properties determined for the latter mentioned, no difference is given at all, which indicates no relevant impact of varying t_{tf} stated e. g. in ON EN 1382 (1999), ON EN 1382 (2016), ON EN 408 (2010) or in ON EN 26891 (1991) on the screw withdrawal properties. With respect to the withdrawal stiffness, even for an immediate failure close to 0 s, no deviation to the other results was found.

It is worth pointing out, that the scope of this investigation was reduced to specific conditions (only perpendicular-to-grain insertion, only displacement-controlled and monotonic loading protocol, no local displacement measurement, etc.). Even though an influence of additionally varied parameters on the given behaviour cannot be excluded, it is in fact not expected at all. More importance is assigned to a possible difference between the experimental results, conducted by means of impact impulse testing and those determined for $\max[\text{RoL}] = 500$ mm/min, examined in the frame of this campaign. Furthermore, a specific investigation, comprising one of both additional data points at target $t_{tf} = 10$ s or 1,000 s, would be worth carrying out for evaluating the $\log_{10}(t_{tf})$ model approach, published in Ringhofer and Schickhofer (2014a).

5-5.3 Duration of load

Note: as mentioned in section 5-1, the discussion in this section only comprises a review of investigations conducted by other authors working in this field.

The mechanical constitutions of wood approximately describable by Hooke's law for orthotropic materials, given in chapter 4, eq. (4.15), not only depend on size, sign and direction of loads applied, but also on further specific effects. One of them, representing the environmental (climatic) impact, is the variation of the moisture content u , as already comprehensively discussed in section 5-3.2. A further aspect of significant relevance, not introduced so far, is the so-called duration-of-load (DoL) effect:

Presupposing a quasi-static load application, it is well known, that timber strength properties significantly decrease with the stressed structure's endurance. The given dependency can be approximately described by a linear relationship in the semi-logarithmic domain (load reduction vs. $\log_{10}(\text{DoL})$), similar to the impact of RoL, discussed in section 5-5.2, originally derived at the Forest Products Laboratory in Madison, Wisconsin (US), c. f. for instance Wood (1960). The related consideration in ON EN 1995-1-1 (2015) comprises a reduction (k -)factor k_{mod} , which is independent from the specific strength property and takes not only the duration of different loading types into account (exceptional loads, snow and ice, wind, service loads, gravity loads, etc.), but also the environmental (climatic) conditions the structure is exposed to. Even though, the meanwhile enhanced approaches can be found in literature, c. f. for instance Hoffmeyer and Sorensen (2007), it can be shown, that the aforementioned original 'Madison Curve' coincides well with the standard's proposal, c. f. Schickhofer (2006b). Thus, it can still be regarded as a reference for further discussion.

The influence of the duration of load on the timber strength properties is commonly determined by executing experimental investigations, comprising a variation of loading magnitudes applied on a bearing system for time schedules for several years, c. f. for instance Wood (1960) or Hoffmeyer and Sorensen (2007). High efforts in testing facility are probably one reason, why a DoL-related influence on axially loaded self-tapping screws' withdrawal strength was scarcely treated in previous studies. One exception is, including quantitative test results, the report published by Pirnbacher and Schickhofer (2012), which is worth to be summarised in this context:

Therein, they illustrate the findings regarding a DoL test campaign of axially loaded, partially threaded $d = 8$ mm screws (thread properties see Table 5.2), situated in ST and GLT specimen (Norway spruce and partially pine) at $\alpha = \{0, 45, 90\}^\circ$. Apart from timber product and axis-to-grain angle, they varied the loading intensities (LI) (as a percentage of the prior determined short-time reference withdrawal capacities) within a range lasting from 48.5 % ÷ 118.3 % at environmental conditions, representing the service class 2 according to ON EN 1995-1-1 (2015). Thereby, the load levels assigned to the lower limit

(mean[LI] \approx 60 %) had been foreseen to examine the fasteners' creep behaviour and carried out as non-destructive tests, while higher levels (mean[LI] \approx {68, 85} %) should lead to a withdrawal failure after a certain period of time. Concentrating on the latter mentioned, the maximum recorded duration was 554 days (or about 1.5 years) until the testing facilities had to be dismantled. Within this schedule, all screws dedicated to mean[LI] \approx 85 % failed in withdrawal (max[DoL] = 132 days), while the campaign assigned to the lower level included a certain number of survivors (not considered in data assessment).

Based on determined times to failure at known loads applied for each screw and restricting the scope to $\alpha = \{45, 90\}^\circ$, Pirnbacher and Schickhofer (2012) confirmed the prior discussed approximately linear decrease of loadbearing capacity with increasing $\log_{10}(\text{DoL})$. Worth mentioning, the moisture contents of each timber specimen were not recorded over the whole timespan of loading (note: when executing this experimental campaign, it was assumed that moisture content variation has only a negligible influence on the screw withdrawal behaviour, c. f. Pirnbacher et al. (2009) and section 5-3.2). A differently pronounced impact of DoL and moisture content variation, on each test result can not be excluded with high reliability. From the author's point of view, a quantitative comparison of determined behaviour with previously published results of timber strength properties in general as well as with the regulation currently applied in standardisation (magnitudes of k_{mod} factor), is thus not reasonable.

With regard to the parallel-to-grain insertion, the related creep specimen exposed to comparatively small load intensities (mean[LI] \approx 60 %) and planned to survive the whole testing period, were observed failing immediately after load application (DoL = 30 min \div 12 hours). While a decrease of LI did not change this behaviour at all, Pirnbacher and Schickhofer (2012) observed a remarkable increase of related failure times (up to six months) for screws embedded in the timber specimen with $l_{\text{emb}} = 15$ mm. Both observations, a critical behaviour regarding DoL, as well as the recommendation to sink the screw thread with $l_{\text{emb}} = 2 \div 3 d$, both in case of $\alpha = 0^\circ$, not only influenced further investigations on self-tapping screws (c. f. conclusions made in Hübner (2013a) and Hübner (2013b) for parallel-to-grain insertion in hardwood species), but also the related standardisation, c. f. ON B 1995-1-1 (2015) and eq. (2.14), to a significant extent. Worth mentioning, since screws inserted parallel-to-grain already failed in the frame of non-destructive testing, Pirnbacher and Schickhofer (2012) desisted from increasing LI for determining the influence of DoL for this axis-to-grain angle configuration.

Now concentrating on the results gained for the prior mentioned non-destructive creep tests: Pirnbacher and Schickhofer (2012) recommend a value of k_{def} (accounts for an increased long-term deformation due to creep deformations), to be applied for connections with predominately axially loaded self-tapping screws, as bandwidth of 1.15 to 1.40 for service classes 1 and 2 conditions, according to ON EN 1995-1-1 (2015). Due to a comparatively small number of tests, a specific influence of further parameters (axis-to-

grain angle, timber product) on this relationship was not determined and remains as an open question for prospective investigations.

This, in fact, corresponds to the influence of DoL on screw withdrawal properties in general. Even though Pirnbacher and Schickhofer (2012) determined a relationship between f_{ax} and $\log_{10}(\text{DoL})$ for $\alpha = \{45, 90\}^\circ$, the given results need at least a data re-assessment (or a verification by means of additional test series) in order to count for both effects, DoL and moisture content variation, separately. In case of the parallel-to-grain insertion and irrespective of the screw embedment, the quantification of $f_{ax, \text{DoL}} / f_{ax, \text{ref}} = A \cdot \log_{10}(\text{DoL}) + B$ is missing at all. A related description is probably the most relevant (and open) topic in the field of axially loaded self-tapping screw failing in withdrawal. As mentioned before, the maximum loading endurance, reported in Pirnbacher and Schickhofer (2012), was about 550 days. Adopting their conclusion related, additional non-destructive creep tests of axially loaded self-tapping screws should be carried out for a longer time period to gain data for a more precise determination of k_{def} .

5-5.4 Type of loading

Note: as mentioned in section 5-1, the discussion in this section only comprises a review of investigations conducted by other authors working in this field.

ON EN 1382 (2016), as the currently valid test standard for determining the withdrawal capacity of self-tapping screws, recommends a test execution with a “constant rate of loading”. This not only indicates a load-controlled test set-up, but also a steady (monotonic) load increase until reaching the sample’s maximum bearing capacity. Since the vast majority of experiments, presented in this chapter, were conducted at least in accordance to the latter mentioned boundary condition, they are further denoted as monotonic withdrawal tests. Thereby gained results can be regarded as “quasi-static” properties, as they serve as input variables for the design of structures against “quasi-static” loads. Within this section, the current state-of-knowledge, regarding the impact of cyclic loading protocols, deviating from the aforementioned on screw withdrawal properties, shall be summarised in brief.

Firstly concentrating on the fatigue-relevant load application, assignable to the HCF-domain, illustrated in the S/N-diagram in Figure 3.56 (right). Comparable to structural steel, as discussed in section 3-5.3, it is well-known, that also timber material fails under repeated loading with magnitudes far below its specific quasi-static strength property, c. f. for instance Kreuzinger and Mohr (1994) (note: therein, a comprehensive literature survey, not only regarding the impact on strength properties of timber products, but also on, at that time frequently applied, connection capacities is given). Apart from N , as the number of cycles bearable until failure occurs, further main influencing parameters, discussed in this source, are sign and direction of loads (with respect to orthotropic material behaviour), as well as the stress ratio R , see eq. (3.105). As introduced in section 3-5.3, a related design process of timber engineered structures against such fatigue-relevant actions currently takes a reduction factor k_{fat} , applied for reducing the specific quasi-statically determined strength property, into account. According to ON EN 1995-2 (2006), Annex A, k_{fat} thereby mainly depends on the aforementioned parameters, not only covers the timber components, but also the laterally loaded connections made with dowels, bolts or nails.

Unfortunately, the comments regarding the treatment of k_{fat} for modern self-tapping timber screws’ withdrawal strength, are missing in this document. The main reason therefore is probably the fact, that (published) investigations focusing on this relationship were not found so far in literature. Conclusions made in Kreuzinger and Mohr (1994), who also summarise the observations on cyclically loaded small wood screws in furniture products, indicate that the fastener itself, stressed in axial direction, is assumed performing weaker in terms of fatigue-relevant load application, than the timber material surrounding it. Even though the investigations, presented in section 3-5.3, would consequently have more relevance for the corresponding design process, the knowledge regarding the withdrawal behaviour of axially-loaded

self-tapping screws, exposed to fatigue-relevant loading, would be a valuable contribution in that field. This especially concerns the determination of the effective inserted thread length's threshold, in dependence of N load cycles, where – if exceeded – steel tensile failure of the screw occurs.

Now concentrating on the cyclic load application, causing stress amplitudes close to the material's quasi-static strength properties assignable to the LCF-domain in Figure 3.56 (right): in contrast to the previously discussed topic, dealing with failure modes dedicated to fatigue, the knowledge gained in this field corresponds to the timber engineered structure's performance against seismic actions. As given in ON EN 1998-1 (2013), such timber connections, defined as the structure's dissipative zones, have to fulfil certain conditions regarding their bearing performance in case of cyclic loading. This mainly includes (a) specific values of ductility to be reached for a classification as DCM (medium capacity to dissipate energy, $D = 4$) and DCH (high capacity to dissipate energy, $D = 6$) and (b) a maximum loss of 20 % of bearing capacity during cyclic loading.

As also recommended in ON EN 1998-1 (2013), a related experimental verification shall be conducted according to test standard ON EN 12512 (2001). Therein, a cyclic loading protocol is described, including a specific number of cycles in the alternating stress domain ($R = -1$, $|F_{\min}| = F_{\max} = F(x \cdot v_y)$), defined by steady increasing values for $x = \{0.25, 0.50, 1.00, 2.00, 4.00, 6.00\}$ until failure occurs or the threshold $v_{\max} = 30$ mm is reached. Subsequently, the aforementioned properties, bearing resistance and ductility, can be determined (see discussion in section 3-4.4) by means of the recorded load-displacement relationship's envelope curve.

During the last years a certain number of investigations was carried out for determining the bearing behaviour of connections with self-tapping screws exposed to this kind of cyclic loading. As comprehensively discussed in section 2-3, related experimental campaigns mainly comprised tests of joint details situated in linear GLT members or laminar CLT components. Focusing on screws, stressed exclusively in axial direction (thus also excluding inclined positioning) and failing in withdrawal, the related amount of experience is reduced by far. One report was found, published by Flatscher et al. (2013), comprising the test results of two connection types (both out-of-plane wall-to-wall joints), which fulfil these boundary conditions and are thus comparable to the standard screw withdrawal tests this chapter concentrates on.

Table 5.45 subsequently compares the related withdrawal properties (F_{ax} , $K_{ser,ax}$, D , note: determination slightly deviated from the procedure introduced in section 5-1.2), gained by Flatscher et al. (2013), for monotonic and cyclic testing according to ON EN 26891 (1991) and ISO 16670 (2003) of the same joint configuration. As given therein, properties determined for both loading types only vary in a comparatively small bandwidth of roughly ± 10 %, indicating that this parameter has no remarkable

influence on the bearing behaviour of axially loaded self-tapping screws. The amount of additional parameters, such as the outer thread diameter or the axis-to-grain angle varied and the number of tests (monotonic: {3, 2}, cyclic: {6, 4}), are quite small. Thus, it is appropriate to concentrate on the impact of this type of cyclic loading on screw withdrawal properties in the frame of future investigations.

Table 5.45: *Screw withdrawal properties of two selected connection types in dependence of monotonic and cyclic loading; according to Flatscher et al. (2013)*

name	conditions		mean[F_{ax}]			mean[$K_{ser,ax}$]			mean[D]		
	d [mm]	α [°]	m [kN]	c [kN]	Δ [%]	m [kN/mm]	c [kN/mm]	Δ [%]	m [-]	c [-]	Δ [%]
_T41	8	90	20.8	23.1	11	17.6	18.3	4.0	3.5	3.7	5.7
_T42	8	0	10.8	9.50	12	20.8	20.8	0.0	3.3	3.4	3.0

m = monotonic test; c = cyclic test

5-6 SUMMARY AND CONCLUSIONS

The aim of this chapter is analysing, discussing and describing the relevance and the significance of selected parameters, influencing the withdrawal properties strength f_{ax} , stiffness $K_{ser,ax}$ and ductility D of axially loaded self-tapping screws, situated in solid timber and board-based, laminated timber products made with the softwood species Norway spruce (*Picea Abies*), as a reference material. As mentioned in the introduction, given in section 5-1, the main methodology therefore applied was an empirical analysis (supported by basic stochastic and mechanical approaches) of the relationship between the specific influencing parameter and the withdrawal property $\{f_{ax}, K_{ser,ax}, D\}$. This analysis based on the results of several experimental campaigns, conducted at Graz University of Technology, during the last years. For a rough quantification and summarising the facts and figures given in Annex B-3.2, Table B.12 to Table B.67, a related overview of all programmes considered in this chapter is subsequently given in Table 5.46.

Table 5.46: Summary of the experimental database serving as basis for analysing the impact on withdrawal properties in the frame of chapter 5

#	f_{ax}	$K_{ser,ax}$	D	other mechanical properties
no. of campaigns	23	13	13	1
no. of subseries	284	155	155	3
no. of tests	6,885	3,623	3,582	746

As generally defined in Figure 5.8, the related influencing parameters were separated into (i) screw, (ii) timber product, (iii) application and (iv) loading. The concluding remarks, highlighting the main outcomes of this chapter, are again classified by these four main parameter groups and given in the following subsections. This especially concerns withdrawal strength and stiffness, while findings, regarding the ductility, are separately discussed in section 5-6.5.

5-6.1 Screw

Taking the literature findings summarised in section 5-2.1, as well as the restriction to currently applied standard thread types, definable by $\{d, \eta, p, v\}$ and shown in Table 5.1, into account, the impact of the thread geometry on withdrawal properties was reduced to that of a varying outer thread diameter d . On the one hand, the results of a related experimental campaign confirm the already known relationship to withdrawal strength f_{ax} in form of a regressive behaviour with increasing d , describable by a power function with exponent k_{diam} , as expressed in eq. (5.56). A possible explanation therefore is the so-called “size-effect” of mechanical timber properties, meaning, for instance, that the associated shear strength decreases when the stressed timber volume increases. On the other hand, the experimental outcomes

indicate a significant impact of the axis-to-grain angle α on the relationship between outer thread diameter and withdrawal strength, which was found so far only for screws situated in hardwood species, c. f. Hübner (2013a). The related dependency will be considered for the empirical modelling in chapter 6.

Concentrating on further withdrawal properties $K_{\text{ser,ax}}$ and D , own experience, regarding a possible impact of d , is unfortunately missing, since no local displacement measurement set-up, enabling a related property determination, was applied for the tests. Restricting the discussion to withdrawal stiffness, the previously published findings, introduced in section 5-1.3, differ in the magnitude of this influence to a remarkable extent. Furthermore, the outcomes of the withdrawal tests of screws, with varying values of p , also indicate a significant impact of this geometrical thread parameter on $K_{\text{ser,ax}}$, c. f. section 5-4.5, while a possible influence of varying η was not examined at all. The given uncertainties are in fact one main reason, why it was decided to exclude the derivation of an approach for determining this property in the frame of this thesis. It has to be regarded as one of the most relevant topics to be focused on in future.

5-6.2 Timber product

With regard to the timber product the screws are inserted in, the discussion of the related impact was separated into (a) clear wood properties, (b) environmental conditions and (c) lamination.

Beginning with (a) and the experience with local wood defects made so far, only the presence of knots – penetrated or touched by the screw axis – was found, remarkably influencing withdrawal properties, while further characteristics, such as reaction wood or pitch pockets, do not influence the loadbearing performance at all. This main fact was considered for the data assessment in the frame of this chapter, only identifying (cut) samples with knots as outliers and excluding them from the statistical analysis.

Concentrating on the impact of the main physical clear wood properties density and annual ring width, defined in chapter 4: the results of the related experimental campaign generally confirmed the well-known and pronounced positive relationship between density and withdrawal properties strength and stiffness. In contrast to the current state-of-knowledge, the exponent k_p , as the main indicator of this relationship to withdrawal strength, was found significantly varying in dependence of the direction, the screw was inserted in the timber specimen. While in case of tangential or radial insertion (both $\alpha = 90^\circ$) no remarkable difference in its magnitude can be observed, the longitudinal insertion leads to a significant decrease of k_p , mirroring a loss of predictability (expressed by the correlation coefficient) – especially if this phenomenon (varying k_p in dependence of α) is not considered for empirical modelling. In case of withdrawal stiffness, this clear contrast between parallel- and perpendicular-to-grain insertion is not given at all. With regard to the dependency of withdrawal properties on annual ring width a_w , only for tangential screw insertion, a highly significant, but much less pronounced, relationship if compared to timber density, was found.

Apart from density and annual ring width, further clear wood relationships examined were those between withdrawal and timber mechanical strength and stiffness properties comprising $E_{c,i}$, $f_{c,i}$ and G_{XY} . The probably most relevant outcome of this study, originally conducted to gain input values for mechanical screw modelling, is the distinctive dependency of the withdrawal strength in longitudinal direction on related shear modulus G_{LR} (serving as best indicator for shear strength), which was found to be even higher, than that on timber density. Nevertheless, as no consistent relationship with any mechanical property, irrespective the specific material orientation, was observed, the density can still be regarded as the best indicator for both withdrawal properties, strength and stiffness, and can consequently be applied for empirical modelling of f_{ax} in chapter 6.

With regard to (b), the consequences of climatic conditioning, timber structures are exposed to, a sole change in the specimen's temperature was previously observed to have a negligible influence on screw withdrawal properties, c. f. Pirnbacher et al. (2009). Thus, the scope of the related discussion was restricted to the impact of varying moisture contents as main climatic indicator considered in modern standardisation. The corresponding investigations comprised a huge bandwidth of varied moisture contents in solid timber, lasting from oven-dry specimen ($u \approx 0\%$) to the transition between SC 2 and 3, according to ON EN 1995-1-1 (2015) ($u \approx 20\%$), a comprehensively smaller campaign with screws, situated in CLT side face, as well as re-assessment of test data from Pirnbacher et al. (2009), who conducted tests with solid timber and GLT specimen. Furthermore, the way of test execution was partially varied, c. f. section 5-3.2.

The main outcomes are as follows: irrespective of test procedure, axis-to-grain angle and timber product applied, similar to the behaviour of mechanical strength and stiffness properties in general, and partially confirming the previous studies conducted in this field, the influence of moisture content variation on withdrawal properties strength and stiffness can be separated into three domains: (i) in case of moisture contents u between 0% and $\sim 7\%$, $\{f_{ax}, K_{ser,ax}\}$ increase with increasing u , (ii) in case of u between 8% and 12% , a more or less constant plateau is given, and (iii) from 12% to $\sim 20\%$ a significant and linear decrease of both properties with increasing u was found. With special regard to the practical range of screw application, the observed behaviour in both domains (ii) and (iii) was subsequently described by an empirical bilinear approach, given in eq. (5.58), with gradients k_{mc} , outlined in Table 5.19 and Table 5.20. Furthermore, modelling included the derivation of a steady and nonlinear function for predicting the withdrawal strength f_{ax} , considering the whole bandwidth of u examined; c. f. eq. (5.59), Table 5.21 and Figure 5.35. Worth mentioning, that no relevant impact of moisture content variation on the relationship between density and withdrawal strength was found.

Concentrating on (c), the discussion on the impact of lamination (or: the difference between screw insertion in ST, GLT and CLT) was separated into general lay-up parameters, such as the number of

penetrated layers N , as well as layer orientation and screw insertion in gaps (as defined by their type, number and width). With regard to the general lay-up parameters, the layer orientation was experimentally verified, not influencing the screw withdrawal properties to a remarkable extent. The situation for screws penetrating $N > 1$ layers of GLT or CLT stands in contrast: here, a significant increase of withdrawal strength and stiffness with increasing N could be observed. Since this behaviour not only occurred for 5 %-quantiles, but also for average properties, the principle of density homogenisation can not be responsible. Thus, a related description based on a stochastic approach, presupposing, that the layer with the highest anchoring capacity ($\rightarrow \max[\rho_i]$) governs the screw loadbearing behaviour, c. f. eq. (5.68) to (5.73) and Table 5.22. The practical application of this system effect is recommended by considering a stochastically derived, multiplicative $k_{\text{sys}}(N)$ -factor, given in Table 5.23, in dependence of the statistical parameter considered (mean value, 5 %-quantile) and the number of layers penetrated by the screw. A successful verification of the model approach for withdrawal strength f_{ax} was subsequently conducted with the test results of several experimental campaigns, comprising a variation of N , d , pre-drilling, layer orientation and lay-up homogeneity.

Summarising the main outcomes, dedicated to the gap impact on withdrawal properties, a simple model approach, considering the decrease of withdrawal strength with increasing number of gaps n_{gap} and their width w_{gap} , as well as in dependence of the specific gap type by a loss of the inserted thread surface area, was derived and is given in eq. (5.78) to (5.80). The related verification comprised a comparison of predicted values with experimental results, gained from several campaigns, wherein the aforementioned parameters, as well as the outer thread diameter and the position of the screw in the CLT lay-up were varied. Further important observations are: no relevance if the screw is inserted in closed gaps ($w_{\text{gap}} = 0$ mm) and a behaviour of the withdrawal stiffness $K_{\text{ser,ax}}$ similar to f_{ax} in dependence of w_{gap} and n_{gap} .

5-6.3 Application

Similar to (ii), the impact of a varying screw application on withdrawal properties was separately discussed in sections 5-4.1 to 5-4.6 further denoted as (a) spacings, (b) pre-drilling, (c) axis-to-grain angle α , (d) position to annual ring structure, (e) effective inserted thread length l_{ef} and (f) embedment length l_{emb} .

Beginning with (a), based on the considerations made in section 5-1.1, as well as on several previous investigations related, a minimum timber volume, stressed by the screw and being necessary for achieving its full loadbearing resistance, was approximated by a nonlinear rotational body with elliptic surface, as defined by $\{a, b\} = \{f(\alpha) \mid f(90) = 3d \mid f(0) = 1d, 1d\}$. This approach, in form of a multiplicative reduction (k -)factor k_{red} and defined in eq. (5.83) to (5.89), shall express the dependency of

screw withdrawal strength f_{ax} on both spacing types (i) between two screws $\{a_1, a_2\}$ and (ii) to the timber's ends and edges $\{a_{1,CG}, a_{2,CG}\}$. For a related verification, especially the results gained from the theses authored by Gatternig (2010) and Plieschounig (2010), including a variation of $\{a_1, a_2, a_{1,CG}, a_{2,CG}\}$ and axis-to-grain angle α , were considered. Even though the given approach has to be seen as a simplification, only roughly approximates the timber's orthotropic material behaviour, a tolerable agreement with test results could be achieved, see Figure 5.76 and Annex B-3, Figure B.52 to Figure B.54, as well as Table B.45 and Table B.46. Nevertheless, this topic is worth being focused on in the frame of future investigations, comprising a more detailed mechanical modelling of the composite interaction between timber and screw. This especially concerns the behaviour of withdrawal stiffness at varying spacings. In addition, the majority of examined test series indicates no relevant impact of $\{a_1, a_2, a_{1,CG}, a_{2,CG}\}$ on the relationship between withdrawal strength and timber density.

With regard to (b), the scope of related investigations comprised the influence if pre-drilling (with d_{PD} close to d_c) is applied, as well as that of d_{PD} varying between d_c and d . In the prior case, both, the outcomes of previous studies, as well as those dedicated to the experimental campaigns presented in section 5-4.2, do not show up any relevant impact on withdrawal strength f_{ax} . Worth mentioning, this is independent from the timber product considered and the axis-to-grain angle applied; c. f. Figure 5.77. In case of withdrawal stiffness $K_{ser,ax}$, significantly higher values were determined for screws situated in non-pre-drilled specimen, which is probably caused by material densification. Concentrating on a varying d_{PD} and irrespective of parallel- or perpendicular-to-grain insertion, the observed behaviour can be explained by constant values of $\{f_{ax}, K_{ser,ax}\}$ in case of $d_c \leq d_{PD} \leq 1.10 \cdot d_c$, combined with linearly decreasing properties if d_{PD} exceeds this upper threshold. Consequently, a bilinear empirical model approach with gradient k_{PD} , given in eq. (5.93), was derived, which is able to describe this relationship quite accurately. A second model, explaining the loss of $\{f_{ax}, K_{ser,ax}\}$ by a loss of the thread's contact surface, c. f. eq. (5.90) and (5.91), leads to a qualitatively similar course, but remarkably underestimates the related test results.

Concentrating on (c), taking the big amount of previous works dedicated to this field into account, the focus was rather on quantifying the impact of varying axis-to-grain angles α on both k_p and $K_{ser,ax}$, than (again) examining their influence on withdrawal strength f_{ax} . Further topics, experimentally investigated, were the relationships between α and $\{f_{ax}, K_{ser,ax}\}$ in dependence of the position of the screw in the CLT-element (side face with alternating angles along the screw axis, narrow face with different layer positions and angle interaction). The main outcomes in brief: similar, but inverse to, withdrawal strength, the behaviour of withdrawal stiffness $K_{ser,ax}$ in dependence of α can be described by a bilinear approach with constant $K_{ser,ax}$ in case of $45^\circ \leq \alpha \leq 90^\circ$, combined with a linear increase for angles below the lower threshold. In case of the relationship between timber density and withdrawal strength, no relevant impact on k_p is given for $\alpha > 0^\circ$, while considerably lower k_p were again determined for parallel-to-grain

insertion, as well as for an increasing outer thread diameter. With regard to CLT side face insertion, deviating from prior expectations, the test results indicate a decrease of f_{ax} with decreasing α quite equal to solid timber, even though the grain direction of every second penetrated layer was oriented perpendicular to the screw axis. Thus, no differentiation to solid timber is made for empirical modelling in the frame of chapter 6. Finally, the results of the majority of subseries related indicate, that the screw insertion in the transition between two layers with different axis-to-grain angles leads to withdrawal strengths f_{ax} , as the averages of those determined for a full insertion in the neighbouring layers. This means, that the lateral outer thread surface shares, subjected to $\alpha_1 = 0 \div 90^\circ$ and $\alpha_2 = 90 - \alpha_1$, equally contribute to the screw loadbearing capacity.

Now focusing on (d) the influence of a varying position of the screw axis to the specimen's annual ring structure as described by the angle β : the test results of an experimental campaign, dedicated to this topic, indicate, that a strict tangential or radial insertion (extremal values of $\beta = \{0, 90\}^\circ$) leads to minimum average withdrawal strength and stiffness, while for screws situated at in-between angles somewhat higher properties could be observed. This especially concerns the withdrawal stiffness, the given difference results in being significant, which can be explained by a progressive behaviour of the apparent (rolling) shear modulus G for $\beta = 0 \mid 90^\circ \rightarrow 45^\circ$ in this R - T orthotropic material plane. In case of practical application, especially in solid timber, a varying angle β along the inserted screw thread "blurring" the observed effect can be expected. Thus, for modelling the withdrawal strength f_{ax} in the frame of chapter 6, this parameter is not considered. This also concerns the negligible impact of β on k_p .

With regard to (e), where the influence of the effective inserted thread length l_{ef} on screw withdrawal properties was examined, the results of a related experimental campaign, comprising a variation of $\lambda = l_{ef} / d$ (up to 39) at different axis-to-grain angles α , confirm the previous observations in form of (i) no relevant impact on f_{ax} and (ii) a degressive behaviour of $K_{ser,ax}$ with increasing l_{ef} . Worth mentioning and irrespective of α , for $\lambda \geq 30$ withdrawal stiffness was observed converging to a constant plateau. The related description was derived similar to the outer thread diameter as a multiplicative approach with exponent $k_{l_{ef}}$, c. f. eq. (5.97). Since, in addition, no impact of l_{ef} on the relationship between timber density and withdrawal strength was observed, this parameter is excluded from the considerations in chapter 6.

As mentioned, the discussion of the impact of the embedment length l_{emb} (f) on the withdrawal properties of self-tapping screws exclusively comprised a literature review of previous works focusing on this topic. Nevertheless, two relevant facts are worth being highlighted: First, the significant increase of f_{ax} if l_{emb} exceeds $2d$ depends on the axis-to-grain angle applied and should not be considered for a parallel-to-grain insertion. Second, since an additional influence of l_{ef} on the magnitude of this increase has to be

expected, c. f. Hübner (2013a), it should rather be considered as a length correction than as a multiplicative factor for the determination of f_{ax} , c. f. eq. (5.98) vs. eq. (5.99).

5-6.4 Loading

The discussion of this fourth parameter group comprised the influence of varying loading and supporting conditions (a), loading velocity (b), duration of load (c) and type of loading (d) on screw withdrawal properties.

Concentrating on (a), in section 5-5.1 the main outcomes of an experimental campaign regarding the impact of different test configurations, as originally published in Ringhofer and Schickhofer (2014a), were discussed and summarised. The most relevant findings in brief: irrespective the axis-to-grain angle $\alpha = \{0, 90\}^\circ$ applied, no significant differences of the average withdrawal strength and its dispersion were observed when loading the screw and supporting the specimen by a push-pull, push-pile, pull-pull or pull-pile configuration, presupposing that the dimensions of the specimen fulfil the requirements according to ON EN 1382 (1999). This also corresponds to varying ε_{sur} , d_h and a_s , defined as the angle between specimen surface and screw axis (pull-pile), the supporting plate's hole diameter (push-pull) and the parallel-to-grain distance between the test screw and the supporting screws (push-pile). The only exception was the smallest value for $a_s = 2d$ examined, leading to a considerably (but insignificantly) lower value of f_{ax} . One explanation is in this case the already reduced stressable timber volume, c. f. section 5-4.1. It can be concluded, that the withdrawal strength, determined with a push-pull configuration, is obviously representing the practically relevant bandwidth of the screw application. Since no local displacement measurement was applied for the related experiments, the behaviour of withdrawal stiffness in dependence of varying loading and supporting conditions remains unknown and will be focused in the future.

With regard to (b), the results of a comparatively smaller campaign, as originally conducted by Ringhofer and Schickhofer (2014a), indicate that the loading velocity (RoL), varied for a displacement-controlled withdrawal test without any initial hysteresis, has no impact on the withdrawal strength if the associated time-to-failure (t_{ff}) ranges between $\log_{10}(t_{ff}) = 1.5 \div 2.5$ (or: $t_{ff} = 45 \text{ s} \div 450 \text{ s}$), while t_{ff} close to 0 s lead to a remarkable increase of f_{ax} . In case of $K_{ser,ax}$, no difference in dependence of RoL (or t_{ff}) was observed at all.

Similar to the impact of the embedment length on screw withdrawal properties, a discussion of both, the so-called “duration-of-load-effect” (c) and the influence of different loading types (or protocols) (d), solely concerned a literature review. In case of (c) and as a consequence of the little experience made so far, a quantification of a time-to-failure model leading to specific k_{mod} -values for the withdrawal strength of self-tapping screws, especially when inserted parallel-to-grain, is probably the most important open

topic to be focused on in the frame of prospective investigations. In case of (d), this also concerns the withdrawal resistance of self-tapping screws for a fatigue-relevant load application, assignable to the HCF-domain. The situation for cyclic loading with force amplitudes close to F_{\max} , being necessary for evaluating the connection's suitability in case of earthquake actions, stands in contrast: even though related examinations are scarce, the findings published e. g. by Flatscher et al. (2013) clearly point out, that neither for the withdrawal resistance F_{ax} nor for the stiffness $K_{ser,ax}$ a significant impact, as a consequence of this deviating loading protocol, is given.

5-6.5 Final comments to the ductility of axially loaded self-tapping screws failing in withdrawal

As mentioned in the frame of this chapter, the ductility of axially loaded self-tapping screws failing in withdrawal was frequently observed, behaving inconsistently in dependence of the parameter variation. Even though a general statement regarding this property is thus hardly definable, the main findings shall be summarised as follows:

- Test results, where local displacement measurement was applied, indicate an absolute average magnitude of this property ranging from 4.0 to 8.5. Presupposing, that test execution and data assessment enable an adequate determination of D (note: no relevant difference between monotonic and cyclic testing was found in section 5-5.4), the given bandwidth would allow a classification as DCM to DCH, according to ON EN 1998-1 (2013). Once again, it should be outlined, that the determined values are rather valuable for a relative comparison than for a fastener classification, c. f. section 5-3.1.
- In case of radial insertion, significant relationships between ductility and timber density, as well as the annual ring width, were found, while for further main material orientations L and T , no dependencies of this property are given at all. Thus, a material indicator, expressing the impact of the timber product applied, is missing.
- The influencing parameters, provoking a behaviour qualitatively similar to withdrawal strength and mostly stiffness, are the axis-to-grain and the axis-to-annual ring orientation angles, α and β , as well as layer orientation.
- The influencing parameters, which cause an inverse behaviour of D , if compared to f_{ax} and $K_{ser,ax}$, are the minimum spacings between screws, the borehole diameter d_{pD} , the rate of loading and the number of penetrated gaps N_{gap} .
- Finally, the parameters, which have no influence on D , or where inconsistent behaviour was observed, are the moisture content variation, the circumstance if pre-drilling (with d_{pD} close to d_c) was applied, the number of penetrated layers N , the gap type and the width w_{gap} , as well as the effective inserted thread length l_{ef} .

Even though any further treatment for empirical modelling seems to be pointless, it was decided to consider the property “ductility” in the frame of this chapter. The main reason therefore is, that the given findings may serve as a basis for prospective investigations.

CHAPTER 6

EMPIRICAL MODELLING OF WITHDRAWAL STRENGTH

6-1 INTRODUCTION

Note: this chapter bases on considerations already published in Ringhofer et al. (2015c) and Ringhofer et al. (2015a).

Summarising the conclusions, dedicated to chapter 5 and given in section 5-6, several parameters were experimentally observed to significantly influence the magnitude of an axially loaded self-tapping screw's withdrawal strength f_{ax} . Apart from the outer thread diameter d , the timber density ρ and the axis-to-grain angle α , as they are already part of commonly applied approaches for this purpose, c. f. section 5-1.3, and representing the parameter groups “screw”, “timber product” and “application”, further relationships worth being considered for modelling are: the moisture content u , the number of penetrated layers N , the type, the number N_{gap} and the width w_{gap} of the gaps (in the CLT side and narrow faces), the sizes of the stressable timber volume and the pre-drilling diameter d_{PD} , as well as the embedment length l_{emb} .

Furthermore, the interrelationships between the timber density, the axis-to-grain angle and the outer thread diameter were found influencing the size of the density's exponent k_p , according to eq. (5.54), to a significant extent. This especially concerns the parallel-to-grain insertion and is worth also being considered for the empirical modelling in order to increase the related predictability. Following the idea of a multiplicative function, as majorly applied in the past, eq. (6.1) subsequently includes the own concept for modelling the withdrawal strength, as it is presented and discussed in the frame of this chapter, see:

$$f_{ax} = \eta_{mc} \cdot \eta_{PD} \cdot k_{red} \cdot k_{lemb} \cdot k_{ax}(k_{90}, \alpha, k_{gap}) \cdot k_{sys}(N) \cdot f_{ax,ref} \cdot \left(\frac{\rho}{\rho_{ref}} \right)^{k_p}, \text{ with} \quad (6.1)$$

$$k_{lemb} = f(\alpha, l_{emb}), \quad k_p = f(\alpha, d), \quad k_{ax} = k_{90} \cdot f(\alpha, k_{gap}), \text{ and} \quad (6.2)$$

$k_{sys}(N)$, according to Table 5.23, η_{mc} , η_{PD} , k_{red} , according to eq. (5.58), (5.89) and (5.92), k_{90} as ratio between the withdrawal strength for the perpendicular- and the parallel-to-grain insertion and k_{ax} , which describes the behaviour of the withdrawal strength at varying α and gap insertion. Worth mentioning, that

this approach bases on reference values for the withdrawal strength ($f_{ax,ref}$) and the single layer density (ρ_{ref}), especially considered to enable its applicability for design purposes, according to specific European Technical Assessments. Note: therein, these values ($f_{ax,ref}$ for ST | $N=1$, $\alpha=90^\circ$, commonly in dependence of d and referred to ρ_{ref} ; on the level of characteristic 5 %-quantiles) are given.

While the impact of varying spacings a_i , moisture contents u and pre-drilling was already derived in chapter 5, certain model components, such as the density exponent k_p , or k_{ax} , which considers the impact of varying α and gap insertion, consist of (a), more than one main variable, c. f. eq. (6.2), and (b), were not specified so far. The related description, basing on a test database introduced in section 6-2, is part of section 6-3. In advance, the test results, applied for deriving these components, are referenced to standard conditions for the withdrawal test execution, regarding sufficient spacings between two screws and to the timber member's ends and edges, the standard climatic conditions ($T=20^\circ\text{C}$, 65 % r. h. $\rightarrow u=12\%$), as well as the embedment of the screw thread.

The content of section 6-4 is the derivation of an approach to predict the reference withdrawal strength $f_{ax,ref}$ of a screw, inserted in solid timber ($N=1$) perpendicular to grain, as well as its comparison with previously published models (section 5-1.3). This, in fact, serves as a basis for the model verification, which is presented in section 6-5. The final content-related part of this chapter deals with the derivation, the discussion and the verification of an approach to predict the characteristic (5 %-)withdrawal strength, as it is required for the design of screwed connections or reinforcements.

6-2 OVERVIEW OF CONSIDERED TEST RESULTS AND PROPERTY CORRECTION

Table 6.1 subsequently includes the main information in form of the applied timber products, the use, the varied parameters, as well as the numbers of subseries and samples, the test database consists of. Worth mentioning, that the given results are not only applied to derive both model components, k_p and k_{ax} , in section 6-3, but also serve as a basis for the modelling, presented in sections 6-4 to 6-6. As illustrated therein, the determination of k_p and k_{ax} , as well as the one of the reference model exclusively base on the tests carried out with solid timber specimen, since the parameters, covering the effect of lamination, have already been described in chapter 5, section 5-3.3 and 5-3.4.

Comparing Table 6.1 with Table 5.46, certain differences of the number of the subseries and the tests can be observed. The smaller number of the subseries, given in Table 6.1, is caused by combining such test series, where no relevant impact of the analysed parameter was found in chapter 5. This especially concerns the test data dedicated to the variation of different loading and supporting conditions, presented in section 5-5.1, as well as all series, where either pre-drilling was applied or not. Worth mentioning, that the latter excludes such values of d_{pd} , which exceed d_c by far, as a significant influence is given in this

case, c. f. section 5-4.2. The difference of the total number of the tests has two reasons: first, the experimental campaigns carried out (or assessed) after the publication date of Ringhofer et al. (2015c) are not considered in the frame of this chapter. Since this only concerns the programmes, presented in sections 5-4.1 (varying a_i), 5-4.2 (varying d_{PD}) and 5-4.5 (varying l_{ef}), a relevant impact on both model parameters, k_p and k_{ax} , can be excluded. Second, to increase the amount of the data, specifically for α varying between parallel- and perpendicular-to-grain insertion and for verifying $k_{sys}(N)$ for the GLT side face insertion more in detail, the results of the test campaigns, published in Gaich et al. (2008), Pirnbacher et al. (2009), Pirnbacher and Schickhofer (2012) and Plüss (2014) are additionally considered. To avoid extending the scope of this chapter, it was decided to exclude a comprehensive description of the related materials and methods. Worth pointing out, that all boundary conditions, regarding the test execution, the post-processing and the data assessment, defined in section 5-1.2, are also fulfilled for these series.

Table 6.1: Overview of the test data base applied for component determination and model verification

material and orientation	use	varied parameters	no. of subseries	no. of tests
solid timber	modelling	$d, l_{ef}, \alpha, \rho, u, l_{emb}$	56	5,060
GLT	verification	$d, l_{ef}, \alpha, \rho, u, N$	9	1,631
CLT side face	verification	$d, l_{ef}, \alpha, \rho, u, N, w_{gap}, N_{gap}$	8	749
CLT narrow face	verification	d, α, ρ, w_{gap}	9	413

The supplemental information, regarding the range, each parameter outlined in Table 6.1 was varied in-between, is subsequently given in Table 6.2. The lower and upper limits represent the corresponding model boundaries to be considered when applying the approach this chapter concentrates on.

Table 6.2: Considered parameters and their range, according to Ringhofer et al. (2015c)

parameter	dimension	range
d	[mm]	4 6 8 10 12
l_{ef}	[d]	2.5 ÷ 15
α	[°]	0 12.5 25 30 37.5 45 60 72.5 90 45/45 0/90
ρ_{12}	[kg/m ³]	310 ÷ 621 (all Norway spruce)
u	[%]	8.20 ÷ 20.0
N	[-]	1 ÷ 20
w_{gap}	[mm]	0 2 4 6
N_{gap}	[-]	0 1 2 3

Taking the restriction to the tests conducted in solid timber for the derivation of the model components k_{ax} and k_p into account, as well as the circumstance, that the series focusing on the impact of the spacings a_i

and the borehole diameter d_{PD} are excluded, the remaining varied parameters, which additionally influence the screw withdrawal strength f_{ax} , are the moisture content u and the thread embedment l_{emb} . In order to avoid this unwanted impact related, the test data was referenced to standard conditions, c. f. section 6-1. Taking the outcomes presented in section 5-3.2 into account, the moisture-dependent property correction was applied as follows:

$$\eta_{mc} = \frac{f_{ax,u}}{f_{ax,ref}} = \begin{cases} 1.00 \\ 1.00 - k_{mc} \cdot (u - 12) \end{cases} \text{ for } \begin{cases} 8\% \leq u \leq 12\% \\ 12\% \leq u \leq 20\% \end{cases}, \quad (6.3)$$

with $k_{mc} = 0.034$, according to Table 5.19, and thus independent of the axis-to-grain angle α . With regard to the influence of the screw thread embedment on the withdrawal strength f_{ax} , the literature review, summarised in section 5-4.6, points out, that the related magnitude significantly depends on the axis-to-grain angle. Unfortunately, the verified knowledge is only given for parallel- and perpendicular-to-grain insertion, while the behaviour for the angles, varying in-between both thresholds, has not been examined yet. Assuming a linearly decreasing magnitude of k_{emb} with α decreasing from 90° to 0° , the property correction was consequently conducted according to eq. (6.4), see

$$\frac{f_{ax,emb}}{f_{ax,ref}} = \begin{cases} 1.00 \\ 1.05 + 1.11 \cdot 10^{-3} \cdot \alpha \end{cases} \text{ for } l_{emb} = \begin{cases} 0 \text{ mm} \\ 2d \end{cases}. \quad (6.4)$$

Note: in eq. (6.4), a minor impact of l_{emb} on f_{ax} is also assigned to parallel-to-grain insertion, resulting as an averaged increase of the withdrawal strength for all the test series conducted by Burgschwaiger (2010) with $l_{emb} > 0$ mm, if compared to the one, where no embedment was applied. This decision was made, even though the given difference was found being insignificant, c. f. section 5-4.6. Furthermore, eq. (6.4) only counts for two possible cases of the embedment, as for all concerned results the same value $l_{emb} = 2d$ was considered.

6-3 DISCUSSION OF MODEL COMPONENTS

6-3.1 Variable exponent k_p considering the density impact in case of $N = 1$

In fact, the huge bandwidth, the exponent k_p varies between the different approaches, introduced in section 5-1.3, already indicates a certain influence of additional parameters on the relationship between the timber density and the withdrawal strength. It furthermore served as a motivation for determining and discussing this additional property for the majority of the experimental campaigns dedicated to chapter 5. As summarised in section 5-6, the axis-to-grain angle and the outer thread diameter were observed significantly influencing the magnitude of k_p , while in case of all further investigated parameters, no

impact, worth being considered for modelling, was found. Within the following considerations, thus the focus is on steadily describing the given influence as a function expressed by $k_p = f(\alpha, d)$. Repeating the discussion in section 5-2.1 and assuming $\{\rho, f_{ax}\} \sim 2pLND$, the exponent k_p can be determined as the gradient of a linear regression model including the density and the withdrawal strength, see

$$\ln(f_{ax,12}) = k_p \cdot \ln(\rho_{12}) + \delta \rightarrow f_{ax,12} = \rho_{12}^{k_p} \cdot \exp(\delta), \quad (6.5)$$

with $\{\rho_{12}, f_{ax,12}\}$ as both variables referenced to standard climate, $u = 12\%$. The corresponding evaluation was already applied for several test series in chapter 5. Nevertheless, the moisture-dependent correction of the test data, as well as the combination of certain subseries (see section 6-2), necessitated a re-assessment of all 56 subseries (dedicated to solid timber in Table 6.1), regarding the exponent's k_p magnitude. In order to increase the number of the observations per parameter characteristic, the subseries with constant values for α and d (this concerned $d = \{8, 12\}$ mm and $\alpha = \{0, 45, 90\}^\circ$) were additionally combined to main series (MS) and evaluated according to eq. (6.5) too. The results of this data assessment, in form of determined k_p , are subsequently illustrated in Figure 6.1, in dependence of the axis-to-grain angle (Figure 6.1, left; $d = \{8, 12\}$ mm) and the outer thread diameter (Figure 6.1, right; $\alpha = \{0, 90\}^\circ$). Note: the error bars in Figure 6.1 represent the bandwidths of k_p , determined for the single subseries. The supplemental information of the main series' outcomes is given in Annex B-3, Figure B.79 to Figure B.82 and Table B.68.

Even though the values of k_p show a comparatively high variability, two main tendencies, observable in Figure 6.1, are worth being discussed in detail: in case of parallel-to-grain insertion, as already concluded in section 5-4.3, a less pronounced relationship between the density and the withdrawal strength is given. In case of the axis-to-grain angles α exceeding 0° , increasing k_p with increasing α up to roughly 30° , followed by a constant behaviour for all angles above this threshold, can be observed. This is, in fact, quite similar to the relationship between the axis-to-grain angle and the withdrawal strength f_{ax} itself, as e. g. considered for modelling by Hübner (2013b). With regard to a varying d at constant α , shown in Figure 6.1 (right), a widely linear decrease of k_p is given for the parallel-to-grain insertion, while the relationship between the density and the withdrawal strength of screws inserted perpendicular-to-grain seems not being influenced by the outer thread diameter at all.

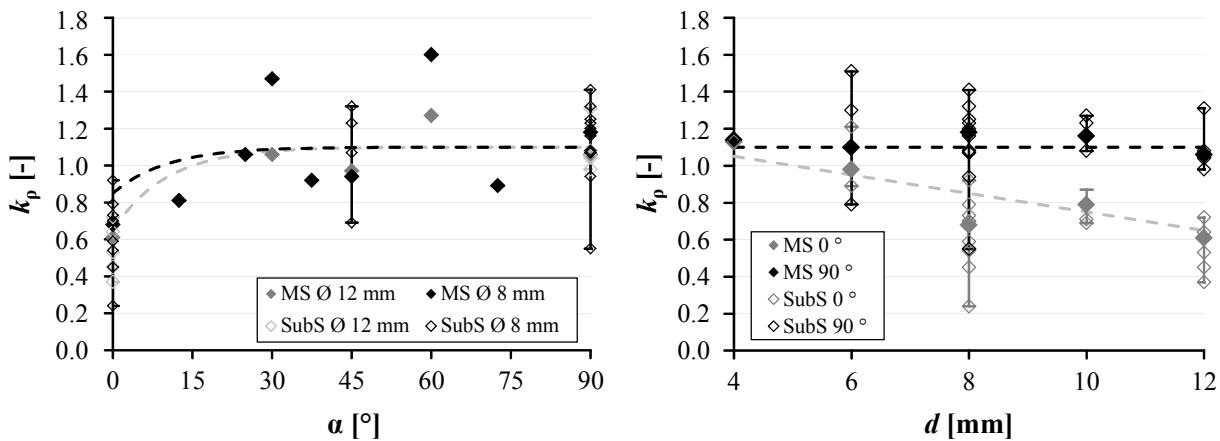


Figure 6.1: Exponent k_p vs. axis-to-grain angle α (left) and outer thread diameter d (right); MS = main series; SubS = single subseries; Mod = model; according to Ringhofer et al. (2015c)

Taking the discussed course of k_p in dependence of α and d into account, for the related description the following approach, comprising the linear decrease of k_p with increasing d for $\alpha = 0^\circ$, as well as the specifically nonlinear behaviour of k_p for varying α , was chosen:

$$k_p = \frac{a \cdot d + b}{\exp(\alpha/10)} + k_{p,90}, \quad (6.6)$$

with $\{a, b\} = \{-0.05, 0.15\}$ as the model constants and $k_{p,90} = 1.10$ as the density exponent in case of the perpendicular-to-grain insertion. The related determination was performed by means of a nonlinear least squares method with the spreadsheet software Microsoft[®] Excel (2010). It exclusively considered values of k_p dedicated to the main series (MS). Worth mentioning, that the black and grey dashed lines in Figure 6.1 represent the estimations according to eq. (6.6).

6-3.2 Function k_{ax} considering the influence of angle and gap variation

As outlined in eq. (6.2), k_{ax} as a function predominately considering the impact of the axis-to-grain angle variation on the withdrawal strength shall also cover the possibility of inserting the screws in gaps with different type and width w_{gap} , concerning the narrow faces of CLT elements. The main reason therefore is their occurrence exclusively in the layers with a fibre orientation perpendicular to the CLT surface and thus a dependency of the gap insertion on the axis-to-grain angle applied. Taking the main idea behind the approach, given in eq. (6.1), into account, k_{ax} should also comprise of multiplicative, independently treatable (and modifiable) components, the impacts of the axis-to-grain angle variation and the gap insertion were separately evaluated. The related discussion is given in the following subsections.

6-3.2.1 Withdrawal strength in dependence of α in gap-free material

Within a first step, the impact of varying axis-to-grain angles α on the screw withdrawal strength is analysed in the gap-free single-layer material solid timber. Thus, the related database consists of all series corresponding to Table 6.1, line 1. Since the timber density ρ_{12} significantly varies between those 56 subseries, the new approach for the density correction, derived in section 6-3.1, was applied for all single test results as follows:

$$f_{ax,corr,i} = f_{ax,i} \cdot \left(\frac{\rho_{ref}}{\rho_i} \right)^{k_p}, \quad (6.7)$$

with ρ_{ref} as the overall mean value of the density ρ_{12} , resulting to 427 kg/m³, and k_p , according to eq. (6.6). Figure 6.2 subsequently illustrates the density-corrected withdrawal strengths $f_{ax,norm}$ in dependence of the axis-to-grain angle, varying in form of $\alpha = \{0, 12.5, 25, 30, 37.5, 45, 60, 72.5, 90\}^\circ$. The main statistical parameters, also including empirical 5 %-quantiles, and such determined for $f_{ax} \sim 2pLND$ according to eq. (5.13), are additionally given in Table 6.3. Worth mentioning, that the results were referenced to $f_{ax,mean}$ and $f_{ax,05,i}$ for the perpendicular-grain-insertion, since the focus is exclusively on the relative dependency between the variables withdrawal strength and axis-to-grain angle. With regard to the behaviour of the average withdrawal strengths, shown in Figure 6.2, more or less constant values for $\alpha \geq 12.5^\circ$, combined with a significant decrease of f_{ax} in case of parallel-to-grain insertion, can be observed. The situation for the 5 %-quantiles (irrespective their way of determination, $f_{ax,norm,emp,05}$ vs. $f_{ax,norm,2pLND,05}$) stands in contrast: while the constant behaviour of $f_{ax,norm,05}$ can be confirmed for the bandwidth of $\alpha = 45 \div 90^\circ$, the given and almost linear decrease already begins at the lower limit mentioned. The main reason therefore is a steady increasing variability of the withdrawal strength for the angles below 45° , as expressed by $CV[f_{ax,norm}]$ in Table 6.3, seen as responsible for an increasing difference between $f_{ax,norm,mean}$ and $f_{ax,norm,05}$ in this range.

Table 6.3: *Main statistical parameters of density-corrected and normalised withdrawal strength $f_{ax, norm}$ in dependence of axis-to-grain angle α*

α [°]	no. of tests [-]	mean[$f_{ax, norm}$] [-]	CV[$f_{ax, norm}$] [%]	$f_{ax, norm, emp, 05}$ [-]	$f_{ax, norm, 2pLND, 05}$ [-]
0	1,756	0.74	21.7	0.64	0.64
12.5	90	0.95	18.9	0.85	0.85
25	85	0.96	13.3	0.88	0.95
30	62	0.87	7.48	0.94	0.96
37.5	81	1.02	13.1	1.00	1.02
45	378	1.01	13.7	1.02	1.01
60	65	0.92	5.90	1.03	1.05
72.5	81	1.08	10.8	1.07	1.12
90	2,462	1.00*	13.5	1.00*	1.00*

* reference values

As comprehensively discussed in section 5-4.3, several approaches, basing on a trigonometric function, according to Hankinson (1921), on a polynomic function of 3rd order, or on a bilinear model with discontinuities at $\alpha = \{30, 45\}^\circ$, are applied to cover the axis-to-grain angle's impact on the withdrawal strength. Taking the approach for predicting k_p in eq. (6.6) into account, an exponential relationship would be an additional possibility for the related description. In the frame of this thesis, it was decided to chose a bilinear model, on which the behaviour of $k_{ax, ST}$ (solid timber, $N = 1$, no gaps) depends; see eq. (6.8):

$$k_{ax, ST} = \begin{cases} 1.00 & \text{for } 45^\circ \leq \alpha \leq 90^\circ \\ c + \frac{1-c}{45} \cdot \alpha & \text{for } 0^\circ \leq \alpha \leq 45^\circ \end{cases} \quad (6.8)$$

with $c = k_{90}^{-1} = f_{ax, norm, \alpha=0^\circ} / f_{ax, norm, \alpha=90^\circ}$ and $k_{90} = \{1.35, 1.56\}$ as ratios for the average withdrawal strength and the 5 %-quantile respectively. In fact, there were two main reasons for this decision: first, the course of the 5 %-quantiles, given in Figure 6.2, indicates a clear bilinear relationship between both variables and seems to be well represented by the approach. Second, it was aimed to avoid deviating descriptions for both statistical parameter types, conceding underestimation of the test data ($f_{ax, norm, mean}$) for the axis-to-grain angles between 0° and 45° , c. f. Figure 6.2.

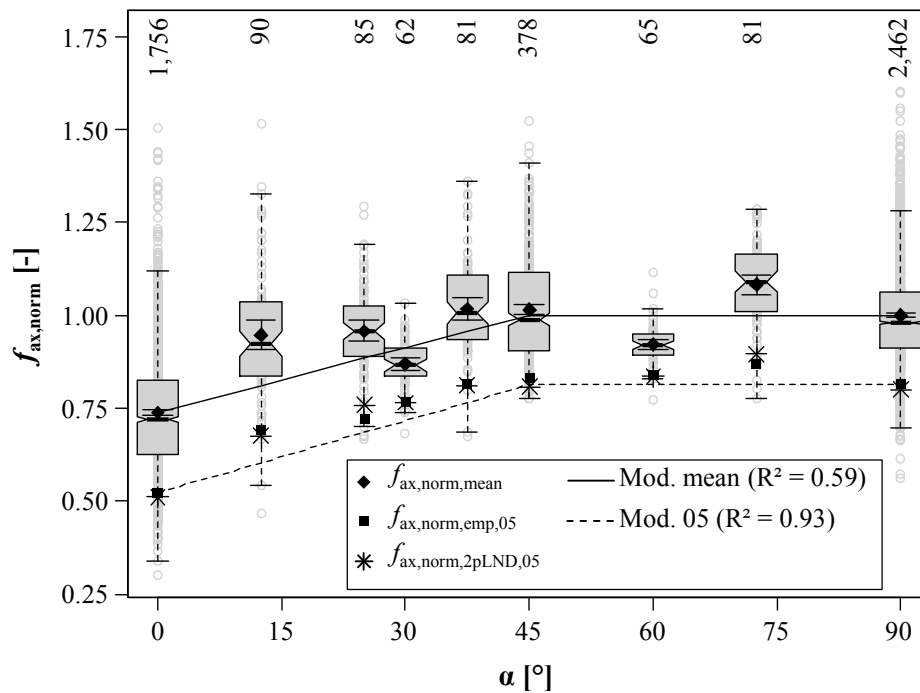


Figure 6.2: Behaviour of density-corrected and normalised withdrawal strength $f_{ax, norm}$ in dependence of axis-to-grain angle α ; according to Ringhofer et al. (2015c)

6-3.2.2 Parameter k_{gap} considering the influence of gap insertion

Note: this subsection briefly summarises the derivation of a probabilistic model for k_{gap} , as given in Ringhofer et al. (2015c). Furthermore, a more detailed description can be found in Brandner (2016).

For the practical screw application in the narrow face of CLT elements, both boundary conditions, the pre-drilling and the visible CLT specimen surface, enabling a widely exact situation of the screws in the specific gap types with varying widths w_{gap} for the tests presented in section 5-3.4, are not fulfilled. The main reason therefore is the typical case of inserting the fasteners through the CLT side face into its narrow face and thus a random positioning of them with respect to possible gaps in the layers oriented perpendicular to the CLT surface. This, in fact, served as a main motivation to describe the impact of the gaps on the screw withdrawal strength by means of a probabilistic approach. Thereby, a multi-modal density function $f_{X, CLT}(x)$ of the property $X = f_{ax}$, defined as the sum of the single density functions for the specific axis-to-grain angles, the gap types and the widths is applied as follows:

$$f_{X, CLT|w_{gap}}(x) = f_{X,0}(x) \cdot p_0 + f_{X,90}(x) \cdot p_{90} + f_{X, BuJ|w_{gap}}(x) \cdot p_{BuJ|w_{gap}} + f_{X, BeJ|w_{gap}}(x) \cdot p_{BeJ|w_{gap}} + f_{X, TJ|w_{gap}}(x) \cdot p_{TJ|w_{gap}}, \text{ with} \quad (6.9)$$

$$\sum p_i = 1, \quad (6.10)$$

as the specific probabilities of occurrence p_i , equal to the area ratios A_i / A_{tot} , which are illustrated in Figure 6.3.

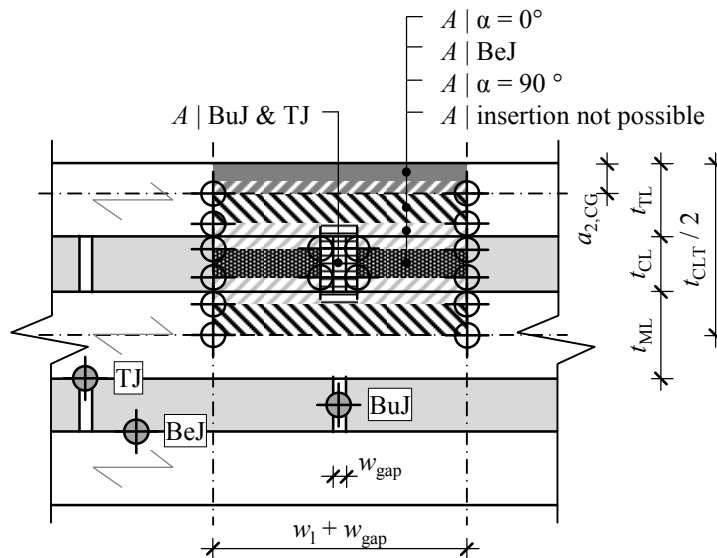


Figure 6.3: Definition of gap types and illustration of areas related to different axis-to-grain directions and gap types exemplarily for screw insertion normal to the CLT narrow face; according to Ringhofer et al. (2015c)

In Figure 6.3, not only the definition of the different gap types (BeJ = bed joint, BuJ = butt joint, TJ = T-joint), as introduced in section 5-3.4 (Figure 5.50), but also – on the basis of a 5-layered reference CLT element – the total area of the possible screw insertion A_{tot} as a product of $(w_{\text{CLT}} + w_{\text{gap}})$ and $(t_{\text{CLT}/2} - a_{2,\text{CG}})$, are shown. The latter takes the symmetrical lay-up, as well as a certain minimum spacing $a_{2,\text{CG}}$ to the element's edge, into account. Following Uibel and Blaß (2007), as basis of corresponding regulations in ON B 1995-1-1 (2015), Annex K, $a_{2,\text{CG}}$ was set to $5d$. Furthermore, the approach given in eq. (6.9) was simplified by assigning A_i of TJ to BuJ (insertion in TJ barely realisable, c. f. section 5-3.4) and A_i of BeJ to their neighbouring layers with $\alpha = 0^\circ$ (conservative approximation, c. f. section 5-4.3), see

$$f_{X,\text{CLT}|w_{\text{gap}}}(x) = f_{X,0}(x) \cdot p_0 + f_{X,90}(x) \cdot p_{90} + f_{X,\text{BuJ}|w_{\text{gap}}}(x) \cdot p_{\text{BuJ}|w_{\text{gap}}} \quad (6.11)$$

Now concentrating on the position of the screw with respect to an open gap $w_{\text{gap}} > 0$ mm (closed gaps were ignored $\rightarrow f_{\text{ax},w_{\text{gap}}=0\text{mm}} = f_{\text{ax},\alpha=0^\circ}$, c. f. section 5-3.4), Brandner (2016) demonstrates that the theoretically smallest reduced screw outer thread circumference C_{red} , according to eq. (5.80), occurs, when the screw only partially penetrates the gap, see Figure 6.4 (left). Since this position is hardly possible in practical application, an additional simplification takes a central gap insertion, as investigated in section 5-3.4 and illustrated in Figure 6.4 (right), into account.

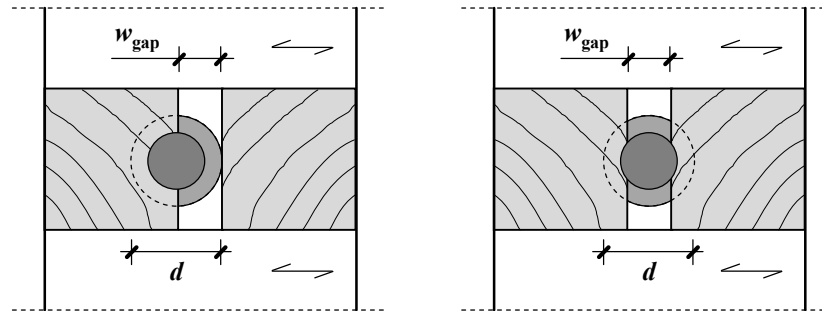


Figure 6.4: Left: screw position leading to the worst case value of C_{red} determined by Brandner (2016); right: central gap insertion experimentally investigated in section 5-3.4

Apart from the main parameters gap width and outer thread diameter, the crosswise and heterogeneous lay-up of CLT, definable by the number of layers, as well as by their width w_1 and the thickness of the single lamellas t_1 , c. f. Figure 4.7 (right), significantly influences each magnitude A_i and consequently the one of p_i in eq. (6.11). Within the next step, thus a representative set of different possibilities for the screw insertion perpendicular to the CLT surface was defined as follows:

- gap width $w_{gap} = \{0, 2, 4, 6\}$ mm
- outer thread diameter $d = \{8, 10, 12\}$ mm
- layer thickness $t_1 = \{20, 30, 40\}$ mm
- lamella width $w_1 = \{80, 160, 240\}$ mm
- number of layers $\{3, 5\}$
- top layer orientation with respect to the screw axis $\{0, 90\}^\circ$
- effective inserted thread length $l_{ef} = 15 d$
(note: necessary for axis-to-grain angles deviating from $\alpha = 0^\circ$)

Thereby, the aforementioned structural CLT parameters were combined to altogether 15 lay-ups, as they are available from four relevant European CLT manufacturers, c. f. Annex B-3.2, Table B.69. Based on a variation of all remaining parameters within these 15 different lay-ups, it can be concluded, that for 5-layered CLT elements with top layer orientation parallel to the screw axis and for 3-layered elements with top layer orientation perpendicular to screw axis, the screw positioning is only possible in the areas A_i assigned to $\alpha = 0^\circ$. This led to a further simplification of eq. (6.11), exclusively considering the parallel-to-grain insertion ($p_{90} \rightarrow 0$). The parameters influencing the both remaining probabilities p_0 and $p_{BuJ|w_{gap}}$ are the outer thread diameter, as well as the gap's and the lamella's width. The highest magnitudes of $p_{BuJ|w_{gap}}$ subsequently occur for those configurations with small lamellas and high values for d and w_{gap} and result to a maximum of 21 %. Conservatively adopting this worst case scenario for the modelling, eq. (6.12) generally counts for a probability of gap insertion in BuJ in form of 25 %, see

$$f_{X,CLT|w_{\text{gap}}}(x) = f_{X,0}(x) \cdot 0.75 + f_{X,BuJ|w_{\text{gap}}}(x) \cdot 0.25. \quad (6.12)$$

Additionally taking $f_{\text{ax}} \sim 2\text{pLND}$, $\text{CV}[f_{\text{ax},\alpha=0^\circ}] \approx 16\%$, a deterministic distribution of w_{gap} , as well as the worst case scenario with $d = 8\text{ mm}$ and $w_{\text{gap}} = 6\text{ mm}$, c. f. Brandner (2016), into account, k_{gap} , as the ratio between $f_{\text{ax,gap}}$ and $f_{\text{ax},\alpha=0^\circ}$, results to 86.4 % in average and to 89.0 % for the withdrawal strength's 5 %-quantile $f_{\text{ax},0.05}$. As illustrated in Brandner (2016), the behaviour of k_{gap} at axis-to-grain angles, varying from parallel-to-grain insertion to $\alpha = 45^\circ$, has a pronounced degressive course. Above this upper threshold, no relevant impact is given any more. Thus, the related consideration can be simply realised by multiplying the constant c in eq. (6.8) with $k_{\text{gap}} \rightarrow \{0.85, 0.90\}$ for determining $\{f_{\text{ax,mean}}, f_{\text{ax},0.05}\}$, see

$$k_{\text{ax}} = \begin{cases} 1.00 & \text{for } 45^\circ \leq \alpha \leq 90^\circ \\ c \cdot k_{\text{gap}} + \frac{1 - c \cdot k_{\text{gap}}}{45} \cdot \alpha & \text{for } 0^\circ \leq \alpha \leq 45^\circ \end{cases}. \quad (6.13)$$

In contrast to eq. (6.8), eq. (6.13) is applicable for the screw insertion in both laminated timber products GLT and CLT as well. Thereby, the screws, positioned at $\alpha > 45^\circ$, are supposed not being influenced by the gaps any more. This neglects the possibility of screws penetrating or touching gaps with $w_{\text{gap}} > 0\text{ mm}$, when being situated in the side face of the CLT elements. In fact, there is one main reason for ignoring the related impact (see section 5-3.4) for the modelling: in contrast to the CLT narrow face application, the timber surface, where the screw is drilled into, is visible in major cases. This allows avoiding the gap insertion, at least, in the product's top layer. Additionally taking an industrialised CLT manufacturing process (all boards with equal w_1 , an identical order of the boards in each layer) into account, the gap-free insertion can also be assumed in all layers with the same orientation. The related impact is reduced to $\{42.9, 40.0, 33.3\}\%$ (in case of $N = \{7, 5, 3\}$ penetrated layers), if compared to the one, given for a steady gap insertion along l_{ef} , and thus is not remarkable any more.

6-4 APPROACH FOR REFERENCE WITHDRAWAL STRENGTH

As outlined in eq. (6.1), the new prediction model for determining the withdrawal strength of the screws situated in solid timber and laminated timber products generally bases on the reference withdrawal strength $f_{\text{ax,ref}}$. The corresponding value shall represent the initial case of a screw, being inserted in solid timber ($N = 1$) perpendicular to grain ($\alpha = 90^\circ$). Additionally excluding the further separately treated influencing parameters (η_{mc} , η_{PD} , k_{red} , k_{lamb} , etc.), $f_{\text{ax,red}}$ exclusively depends on the timber density ρ and the outer thread diameter d and can be determined with one of the empirical regression functions, which were derived in the past, c. f. section 5-1.3.

A further possibility is to apply a new regression model for determining $f_{ax,ref}$ in order to minimise the inaccuracies of the reference value's magnitude as far as possible. For the related model derivation, the test data, outlined in Table 6.1, line 1, was restricted to perpendicular-to-grain insertion and referenced in terms of the moisture content (eq. (6.3)) and the thread embedment (eq. (6.4)). Thus, the remaining dataset comprised of about 2,500 realisations, as parts of 24 subseries. Similar to eq. (5.41), derived by Frese and Blaß (2009), the type of model, chosen for predicting $f_{ax,ref}$, can be defined as an empirical multiplicative power function, see

$$f_{ax,ref} = e \cdot \rho^{k_p} \cdot d^{k_{diam}} \quad \text{with } R^2 = 0.57 \text{ and} \quad (6.14)$$

$\{e, k_p, k_{diam}\} = \{0.014, 1.11, -0.33\}$ as the model components, determined with the software package R by means of a nonlinear regression analysis. The main reason for this decision was to conform with the dependencies of the withdrawal strength on the outer thread diameter and the timber density, as described by power functions with the exponents k_{diam} and k_p , see chapter 5.

Figure 6.5 (left) subsequently compares the experimentally determined withdrawal strengths $f_{ax,exp,i}$ (as content of the dataset applied for model derivation) with the values predicted according to eq. (6.14). In general, a comparatively high agreement, expressed by the coefficient of determination $R^2 = 0.57$, as well as by the locations of the test data and the regression line (Figure 6.5, left) is given. Nevertheless, as also illustrated by the qq-residual plot in Figure 6.5 (right), high values of the withdrawal strength seem to be underestimated by the new approach. This especially concerns the small outer thread diameters $d = \{4, 6\}$ mm, where the highest values of f_{ax} result, c. f. section 5-2.1. Due to a comparatively smaller number of test data for $d = \{4, 6\}$ mm, both diameters may be underrepresented and less weighted in the frame of the nonlinear-least-squares analysis. Consequently, the derivation of a different type of regression function (additive and/or in the logarithmic domain) for the same database will not lead to a remarkable improvement of the related predictive quality. As the main focus of this thesis is on the screws with outer thread diameters applied for engineering purposes ($d = \{8, 10, 12\}$ mm, where the approach leads to a quite accurate prediction), the (conservative) underestimation of f_{ax} for small outer thread diameters is regarded as tolerable.

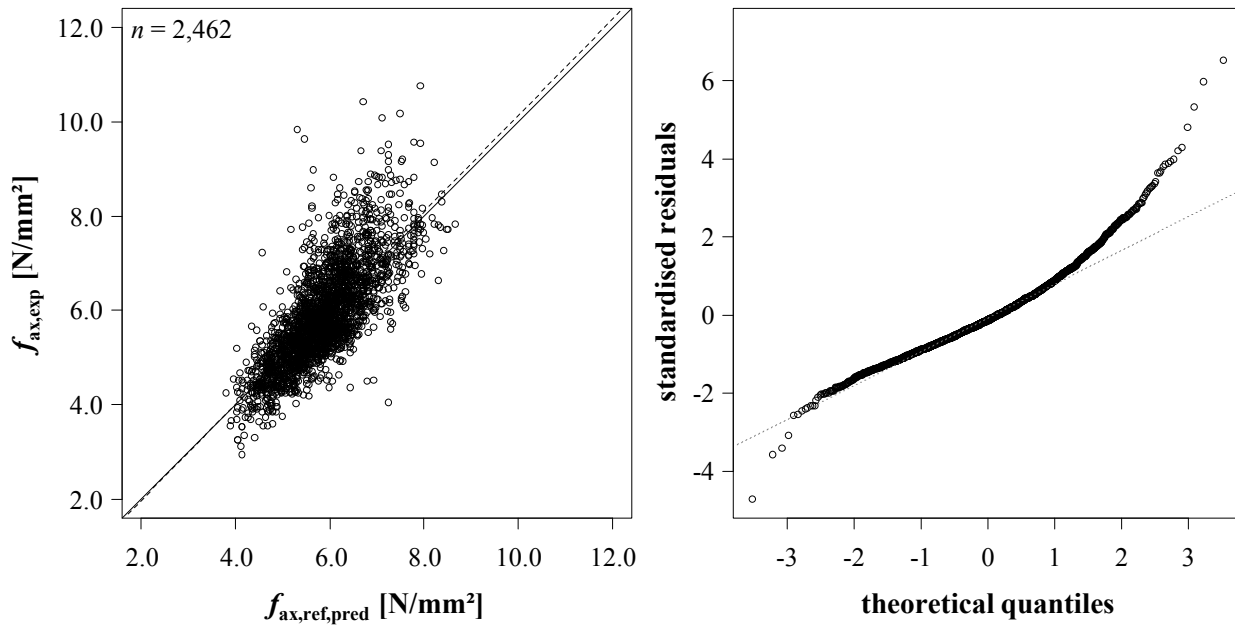


Figure 6.5: Left: experimentally determined vs. predicted reference withdrawal strength f_{ax} for perpendicular-to-grain insertion in solid timber; right: qq-residual plot

A comparison of withdrawal strengths $f_{ax,ref}$, determined according to eq. (6.14), with the ones, determined according to the approaches from Blaß et al. (2006) (eq. (5.36)), Pirmbacher et al. (2009) (eq. (5.38)) and Frese and Blaß (2009) (eq. (5.41) and (5.57)), is shown in Figure 6.6. It is referred to $f_{ax,ref}$ and in dependence of the outer thread diameter $d = 4 \div 12$ mm and the timber density $\rho = \{380, 420, 460\}$ kg/m³, the latter representing the solid timber strength classes C18, C24 and C30, according to ON EN 338 (2016). Apart from the model, published by Blaß et al. (2006), leading to remarkably higher withdrawal strengths for small outer thread diameters and densities, f_{ax} , determined with all remaining approaches are quite equal in their magnitude. Furthermore, $f_{ax,ref}$, determined according to eq. (6.14) for the practical relevant bandwidths of the density (\geq C24) and the outer thread diameter (\geq 8 mm), results to be slightly but consistently higher than the other predictions. The given observations indicate, not only a reasonable applicability of eq. (6.14), but also a certain increase of the efficiency regarding an economic design of the self-tapping screws.

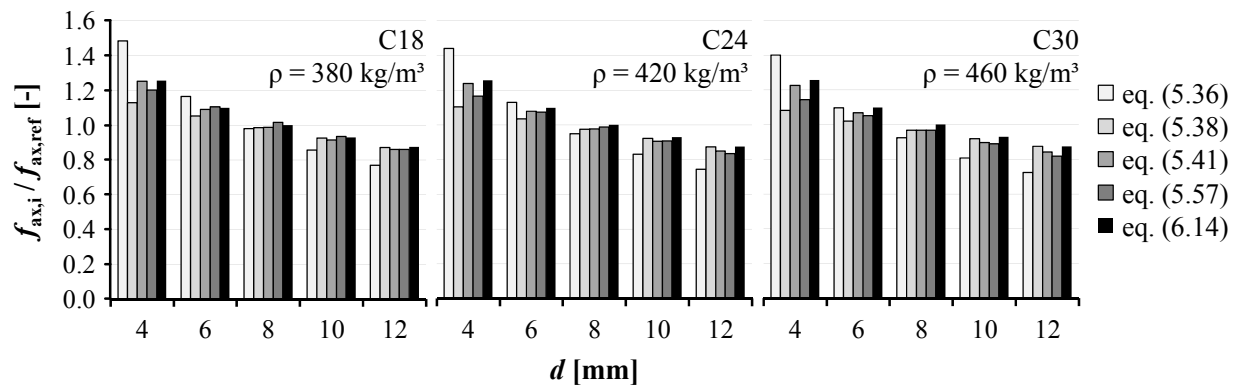


Figure 6.6: Comparison of the reference withdrawal strength model with previously published approaches in dependence of timber density and outer thread diameter

6-5 MODEL VERIFICATION

The aim of this section is to verify the suitability of the new approach, presented in eq. (6.1), for modelling the withdrawal strength of the axially loaded self-tapping screws in solid timber, GLT and CLT. The test data, which was therefore applied, comprises all realisations, summarised in Table 6.1, except those, which were used for deriving and verifying the reference withdrawal strength model in section 6-4 (solid timber, $\alpha = 90^\circ$). Equal to the data preparation for determining k_p and k_{ax} in section 6-3, as well as $f_{ax,ref}$ in section 6-4, the withdrawal test results were referenced in terms of the moisture content (eq. (6.3)) and the thread embedment (eq. (6.4)). Repeating, that the database does not consist of experiments with more than one screw, or insufficient spacings $a_{i,CG}$, or with d_{PD} exceeding d_c by far (thus no impact of k_{red} or η_{PD}), the main verified model components are the impact of the axis-to-grain angle and the gap variation (k_{ax}), the one of a multiple layer insertion (k_{sys}), as well as the influence of the timber density (k_p).

Figure 6.7 illustrates selected comparisons of the experimental data with the model predictions. The contents of Figure 6.7 (left) are all realisations dedicated to the tests in solid timber (apart from $\alpha = 90^\circ$, see Figure 6.5, left) with $\rho_{ref} = 427 \text{ kg/m}^3$, as the overall average density (referred to $u = 12\%$) of Table 6.1, line 1. With regard to the location of test data, the position of the partial regression lines, assigned to main axis-to-grain angles $\alpha = \{0, 45\}^\circ$, as well as the position of the overall regression line, a quite accurate agreement between the test results and the model estimations is given ($R^2 = 0.61$).

The comparison in Figure 6.7 (right) comprises the data given in Table 6.1, line 2 ÷ 4, thus the realisations of the withdrawal tests, conducted in GLT, as well as in the side and narrow faces of the CLT specimen ($\rho_{ref} = 436 \text{ kg/m}^3$). Worth mentioning, that the number of layers penetrated by the screw, as well as their position in gaps with defined w_{gap} was exactly known for the majority of the tests (note: in case of six

subseries, N was estimated by $l_{ef} / t_{i,GLT}$). This enabled the application of k_{sys} according to section 5-3.3, Table 5.23, line 1, as well as the one of k_{gap} , according to section 5-3.4, eq. (5.78) to (5.80). Even though the test data was not used for derivation of eq. (6.1), again a high agreement between the experimental results and the model predictions, as expressed by $R^2 = 0.66$, as well as by the position of the test data and the partial regression lines, can be observed.

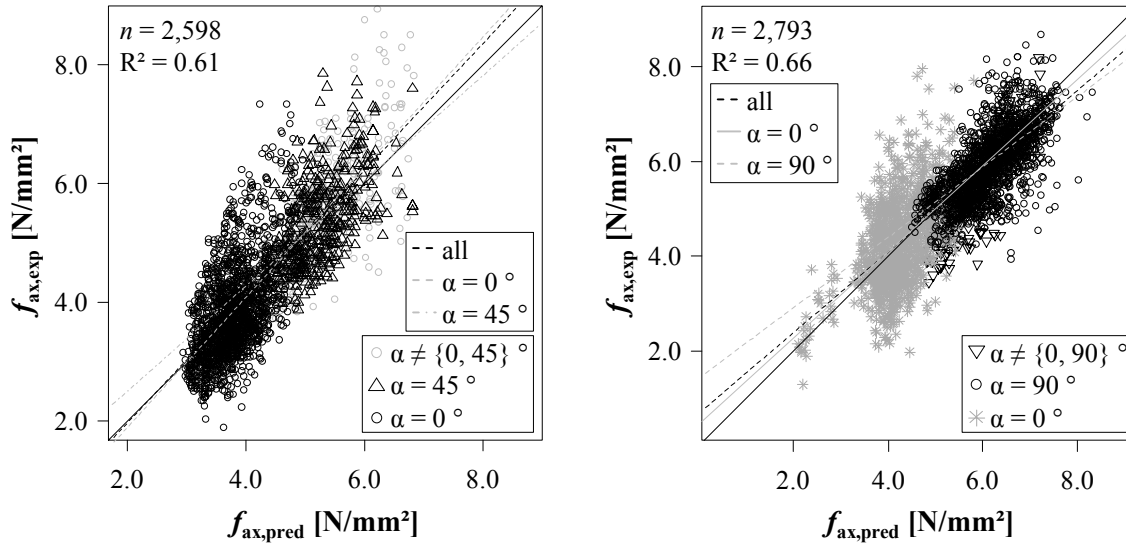


Figure 6.7: Experimentally determined vs. predicted withdrawal strength f_{ax} ; left: tests with solid timber at $\alpha \neq 90^\circ$; right: tests with GLT and CLT according to Ringhofer et al. (2015a)

Within the next step, eq. (6.1) is applied for determining the bearing resistance of screwed connections in CLT elements experimentally investigated by Bratulic et al. (2014a). Amongst other configurations, their programme comprised edge joints with force components perpendicular and parallel to the joint's gap orientation. As schematically illustrated in Figure 6.8, this leads to exclusively (cases a and b) or predominately (cases c and d) axial load conditions of the applied self-tapping screws. Since Bratulic et al. (2014a) consistently observed a withdrawal failure for all related tests, thus excluding other failure scenarios outlined in ON EN 1995-1-1 (2015), the joint's bearing resistance can be defined as the minimum of the screws' withdrawal resistance in the CLT's side or its narrow face. In case of (a) and (b), the related determination was conducted according to eq. (6.15), see:

$$R_{ax} = f_{ax} \cdot d \cdot \pi \cdot l_{ef}, \quad (6.15)$$

with f_{ax} , according to eq. (6.1), and l_{ef} without the tip length l_{tip} , according to eq. (5.2). In case of joint detail (d), the experimentally determined capacity R_X was converted into R_{ax} (per screw cross), according to Kevarinmäki (2002), in advance:

$$R_{ax} = \frac{R_x}{\cos \alpha}. \quad (6.16)$$

The same equation (sin instead of cos component) was applied for determining R_{ax} of configuration (c), thus neglecting the shear component R_v , derived by Jockwer et al. (2014), discussed in section 2-3.1 (see eq. (2.39)).

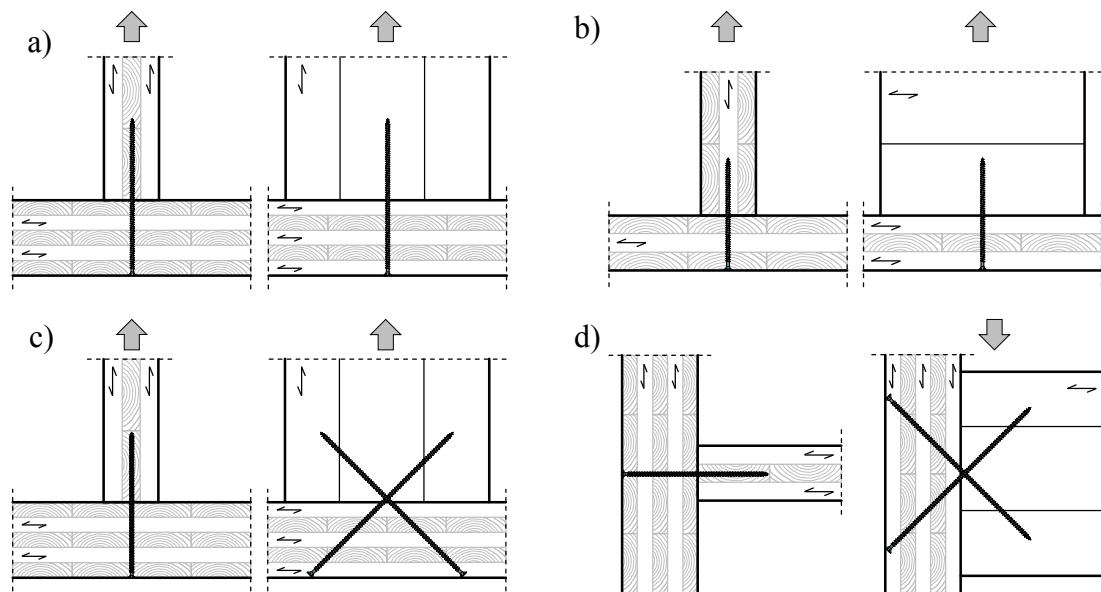


Figure 6.8: Overview of screwed CLT connections tested by Bratulic et al. (2014a): (a) and (b) exclusively axially loaded self-tapping screws; (c) and (d) predominately axially loaded self-tapping screws; according to Ringhofer et al. (2015a)

Table 6.4 finally illustrates the main characteristics of the connection tests (a) to (d), carried out by Bratulic et al. (2014a), being necessary for application of eq. (6.15), as well as the experimentally determined and predicted screw axial loadbearing capacities $R_{ax,exp}$ and $R_{ax,pred}$. The given differences between both forces, expressed by percentages Δ_i , again indicate a quite good agreement between the test result and the model estimation. The only exception, exceeding $\Delta = 10\%$, is the configuration (c), where the new approach obviously underestimates the experimentally determined bearing capacity to a certain extent. This is probably caused by ignoring the aforementioned additional force component R_v . Its share (as part of R_{90}) approximatively results to $R_v = 1.51$ kN (thus decreasing Δ to 6%), when assuming $M_y = 25$ Nm, $f_r = 2$ N/mm² and $f_{h,NF}$, the latter according to Uibel and Blaß (2007). This leads to the conclusion, that the new approach can be reasonably applied for determining the withdrawal resistance of exclusively or predominately axially loaded self-tapping screws as parts of CLT timber-to-timber joints.

Table 6.4: Main characteristics of connection tests done by Bratulic et al. (2014a) and comparison of experimental results with the new approach in eq. (6.1); according to Ringhofer et al. (2015a)

denotation Figure 6.8	n [-]	d [mm]	$l_{ef,SF}$ [mm]	$l_{ef,NF}$ [mm]	α_{SF} [°]	α_{NF} [°]	ρ_{SF} [kg/m ³]	ρ_{NF} [kg/m ³]	$R_{ax,exp}$ [kN]	$R_{ax,pred}$ [kN]	Δ^{**} [%]
(a)	3	8	134	137	90	90	445	441	20.8	20.9	0
(b)	2	8	98	93	90	0	416	439	10.8	10.4	4
(c)	3	8	190	151	45	45	445	393	32.6*	28.7*	12
(d)	2	8	198	143	45	45	435	439	30.0*	30.7*	-2

SF = side face, NF = narrow face; * resistance per screw cross, ** referred to $R_{ax,exp}$

6-6 DERIVATION AND VERIFICATION OF A CHARACTERISTIC APPROACH

The final content-related part of this chapter concentrates on the derivation and verification of an approach to determine the characteristic (5 %) withdrawal strength $f_{ax,k}$, as this variable is applied for design purposes in the ultimate limit state (ULS), according to ON EN 1990 (2013). The related basis is the prediction model for the average withdrawal strength f_{ax} , given in eq. (6.1), as well as the fundamental assumption of $Y = \{\rho, f_{ax}\}$ being lognormally distributed:

$$Y \sim 2pLND, \text{ and} \quad (6.17)$$

$$X = \ln(Y) \rightarrow X \sim ND. \quad (6.18)$$

Following the constitutions introduced in chapter 5, section 5-1.2, the 5 %-quantile of Y can be determined according to eq. (6.19), see:

$$y_{05,LND} = \mu_Y \cdot \frac{\exp\left[\Phi^{-1}(0.05) \cdot \sqrt{\ln(CV[Y]^2 + 1)}\right]}{\sqrt{CV[Y]^2 + 1}}. \quad (6.19)$$

As outlined in eq. (6.19), $y_{05,LND}$ not only depends on the magnitude of μ_Y , but also on the property's variability, as expressed by $CV[Y]$. For determining $y_{05,LND}$, independently from one specific observation, the general conditions $\{CV[\rho], CV[f_{ax}]\} = \{8\%, \xi \cdot CV[\rho] = 1.5 \cdot CV[\rho] = 12\%\}$, as also applied for modelling in section 5-3.3, are introduced. Both, $\rho_{05,LND}$ and $f_{ax,05,LND}$, result to $\{0.874, 0.816\} \cdot \{\rho_{mean}, f_{ax,mean}\}$ and the characteristic (5 %) withdrawal strength to

$$f_{ax,k} = \eta_{mc} \cdot \eta_{PD} \cdot k_{red} \cdot k_{lemb} \cdot k_{ax,k} \cdot k_{sys,k}(N) \cdot f_{ax,ref,k} \cdot \left(\frac{\rho_k}{\rho_{ref,k}}\right)^{k_p}, \text{ with} \quad (6.20)$$

$$f_{ax,ref,k} = 0.013 \cdot \rho_{ref,k}^{1.11} \cdot d^{-0.33}, \quad (6.21)$$

$$k_{ax,k} = \begin{cases} 1.00 & \text{for } 45^\circ \leq \alpha \leq 90^\circ \\ 0.64 \cdot k_{gap,k} + \frac{1 - 0.64 \cdot k_{gap,k}}{45} \cdot \alpha & \text{for } 0^\circ \leq \alpha \leq 45^\circ \end{cases}, \text{ and} \quad (6.22)$$

$$k_{gap,k} = \begin{cases} 0.90 & \text{CLT narrow face} \\ 1.00 & \text{other} \end{cases}, \quad (6.23)$$

or – in case of known gap characteristics – according to section 5-3.4, eq. (5.78) to (5.80), as well as $k_{sys,k}$ according to section 5-3.3, Table 5.23, line 2. The relationships between the remaining influencing parameters and the withdrawal strength, as covered by the model components $\{\eta_{mc}, \eta_{PD}, k_{red}, k_{lemb}, k_p\}$, were not found to remarkably influence the property's variability. Thus, the related eq. (5.89), (5.92), (6.3), (6.4) and (6.6) can be applied without any modification.

For verifying the characteristic approach, given in eq. (6.20), the empirical 5 %-quantiles of the withdrawal strength f_{ax} of all subseries, outlined in Table 6.1, were determined after referencing them again in terms of the moisture content (eq. (6.3)) and the thread embedment (eq. (6.4)). With regard to the prediction of the corresponding characteristic values, according to eq. (6.20), some boundary conditions are worth being summarised in brief:

First, equal to the verification of eq. (6.1) in section 6-5, the screw position with respect to the gaps was known for all tests conducted in the CLT narrow face. This again enabled the determination of k_{gap} , according to eq. (5.78) to (5.80). Apart from six subseries in GLT (N estimated by $l_{ef} / t_{i,GLT}$), this also concerned the number of the penetrated layers N for applying an exact value of k_{sys} .

Second, both characteristic densities, ρ_k and $\rho_{ref,k}$, in eq. (6.20) are referred to the single lamella when inserting the screw in a layered timber product. In case of several subseries, conducted in GLT and CLT side faces, only the small sample densities of the layered specimen, but no single layer densities are available. Consequently, instead of considering empirical 5 %-quantiles as characteristic values, both, ρ_k and $\rho_{ref,k} = 376 \text{ kg/m}^3$, of all subseries were determined according to eq. (6.19), assuming $\rho \sim 2pLND$ and $CV[\rho] = 8 \%$. Note: the latter is a commonly observable value for this property, c. f. Brandner (2013b).

Figure 6.9 subsequently compares the experimentally determined withdrawal strengths $f_{ax,05,exp}$ with $f_{ax,pred,k}$, as characteristic ones according to eq. (6.20). Thereby, each data point (in grey: series in solid timber, in black: series in GLT and CLT; the symbols differ, if N was known or it was estimated) represents one of altogether 82 test series, comprising in total about 8,000 realisations. With regard to their distribution and the courses of the related regression lines, a high agreement between the model

predictions and the test data can be concluded ($R^2 = 0.78$). Worth mentioning, that this is independent from the used material and further influencing parameters, such as the axis-to-grain angle. The only exceptions are four test series, marked as “outliers” in Figure 6.9. In fact, their overestimation is caused by unexpectedly high variabilities of the withdrawal strength and the density ($CV[X] \geq 20\%$), determined for these series. This significantly deviates from the assumption of $\{CV[\rho], CV[f_{ax}]\} = \{8\%, \xi \cdot CV[\rho] = 1.5 \cdot CV[\rho] = 12\%\}$. Applying the empirical 5%-quantile of ρ , instead of the aforementioned one, quite accurate prediction would be also achieved for these series.

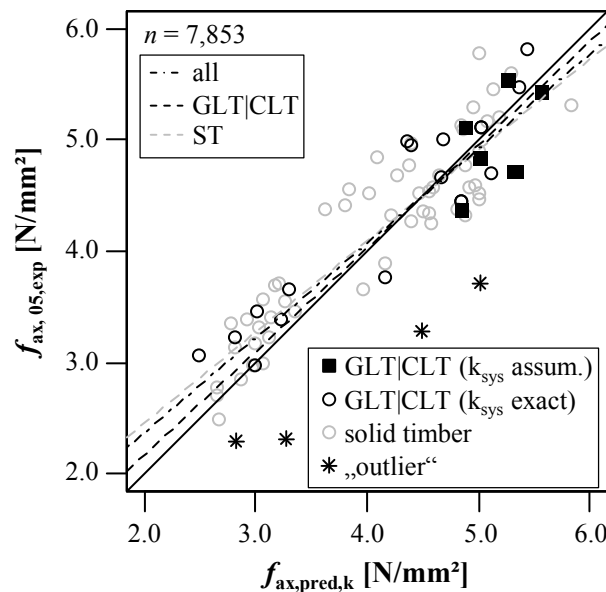


Figure 6.9: Comparison of empirical 5%-quantiles of all test series with characteristic (5%) withdrawal strengths determined by eq. (6.20); according to Ringhofer et al. (2015a)

6-7 SUMMARY AND CONCLUSION

In the frame of this chapter, the experience regarding the behaviour of axially loaded self-tapping screws failing in withdrawal was applied for deriving new approaches, which enable the prediction of the average withdrawal strength and its characteristic (5%-) value in dependence of several selected influencing parameters. This especially concerns the k -factors k_p and k_{ax} , covering the observed interrelationship between the timber density, the outer thread diameter and the axis-to-grain angle, as well as the impact of the latter mentioned on the screw withdrawal strength. Furthermore, a simple, empirical regression model, in form of a multiplicative power function for determining the reference withdrawal strength $f_{ax,ref}$ in solid timber ($N = 1, \alpha = 90^\circ$), was derived. The verification subsequently comprised a comparison of a comprehensive amount of test data ($n \approx 8,000$), gained for solid timber, GLT and CLT, with the predicted values. In addition, the same was done with the results of selected CLT connection tests, conducted by Bratulic et al. (2014a). Apart from minor relevant exceptions (e. g. underestimation of

$f_{ax,ref}$ for small $d = \{4, 6\}$ mm), the vast majority of the test results is well described by the new approaches, irrespective, if the data was used for the model derivation or not.

With regard to both models, given in eq. (6.1) and (6.20), and if compared to the previously published ones, the consideration of several additional k - and η -factors increases the complexity in practical application. Related simplifications are consequently a part of the recommendations for practise, summarised in chapter 7.

CHAPTER 7 SUMMARY, PRACTICAL RECOMMENDATIONS AND OUTLOOK

7-1 SUMMARY

Due to their economic installation without pre-drilling, their application for various different purposes, as well as their high efficiency – especially if stressed in axial direction – self-tapping screws are probably the most relevant fasteners in contemporary timber engineering. In fact, this was the main motivation for the present thesis, gaining a fundamental knowledge concerning the specifics of this kind of dowel-type fastener. Since each chapter (or major section) has already been comprehensively summarised at its end – see sections 2-5, 3-4.6, 3-5.5, 5-6 and 6-7 – only the most relevant findings shall be highlighted again:

The main idea behind chapter 2 was to concentrate not only on the current state-of-knowledge, but also on the development process leading to the present situation, regarding the application and the design of self-tapping screws for timber engineered structures. Restricting the scope to (predominately) axial load situations, this comprised a discussion of the past and present standardisation, the judicial background, as well as the regulation of self-tapping screws in Technical Approvals (TAs), serving as a basis for CE-labelling. Especially the latter documents were observed to be significantly influenced by research activities carried out in this field, which are subsequently summarised in dependence of the way, self-tapping screws are applied nowadays. The related content – separated into active application in form of connections vs. passive application in form of reinforcements – shall mirror their aforementioned major impact on timber engineering.

In the frame of chapter 3 the focus was on describing the product self-tapping screw itself. Consequently, its current geometrical characteristics – classified into “drive”, “head”, “shank”, “thread” and “tip”, as well as its most frequently applied production process, especially with regard to the main production steps “forming” and “hardening”, are explained and discussed. Assigning the screw thread a major relevance, the further concentration was to theoretically derive the relationship between the mechanical screw properties f_{tens} , f_{tor} and M_y by means of a prismatic 1D-member with a specific, parameterised cross-section as the result of 3D-modelling the screw thread surface. Further assuming Euler-Bernoulli’s beam theory, an ideal plastic material behaviour, as well as a constant hardness distribution over the entire profile, the related outcomes were simplified by empirical approaches taking the ratio between the inner and the outer thread diameter, the pitch, as well as the flank inclination angle into account. The successful verification of this approach with results of an experimental campaign not only varying the screw

manufacturer and the outer thread diameter but also the hardening procedure as one of the aforementioned core production steps is worth to be mentioned. So far, mechanical constitutions were evaluated presupposing ideal conditions regarding the screw thread geometry and the environmental exposure, as well as a quasi-static load application. Thus, the second relevant part of chapter 3 dealt with the impact on the screw's steel tensile capacity if these conditions are varied. This especially concerned cyclic (fatigue-relevant) loading and hydrogen-induced stress corrosion cracking (HISCC) as common phenomena treated in material science but neglected so far in terms of self-tapping screws applied in timber engineering.

Subsequently, the present thesis concentrated on the withdrawal of axially loaded single screws, representing their composite interaction with the timber component they are inserted into. Thus, chapter 4 aimed on defining this kind of material, approximately describable by an orthotropic (radial-anisotropic) material behaviour, as well as the specific scale – further denoted as layered clear wood – being considered for related modelling.

The content of chapter 5 is a summary and a discussion of the influence of several parameters – classified into “screw”, “timber product”, “application” and “loading” – on the axial loadbearing behaviour (expressed by the main properties strength f_{ax} , stiffness $K_{ser,ax}$ and ductility D) of self-tapping screws failing in withdrawal. This was mainly done on the basis of about 14,000 test results gained from experimental programmes carried out at the Institute of Timber Engineering and Wood Technology at Graz University of Technology within the last ten years. It should be pointed out, that the related considerations not only included the observations of specific effects or relationships, but also their description, consisting of (simplified) empirical, stochastic or mechanical approaches. The prediction of the withdrawal behaviour of screws at varying environmental conditions (moisture content), positioning in laminated timber products (number of penetrated layers, gaps, axis-to-grain angle, etc.) and forms of application (spacings, pre-drilling, etc.) is worth to be highlighted in this context.

Furthermore, the results presented in chapter 5 served as a basis for the empirical modelling of the withdrawal strength of axially loaded self-tapping screws situated in laminated timber products (ST as a reference, GLT, CLT) in chapter 6. Thereby, it was aimed to derive a universal approach enabling the related application irrespective the timber product used and the position the screw is inserted into. Amongst others, the described interrelationship between withdrawal strength, timber density, outer thread diameter and axis-to-grain angle (expressed by the power factor k_p) can be regarded as major parameter, improving the corresponding predictability. This not only for the average withdrawal strength, but also for its characteristic (5 %-) quantile as the relevant property for the design process in modern standardisation.

7-2 PRACTICAL RECOMMENDATIONS

The aforementioned model considerations for describing the mechanic relationship between the (steel) material properties (f_{tens} , f_{tor} , M_y) of the product self-tapping screw base on several simplifications. Nevertheless, the conformity with experimental results leads to the recommendation of eq. (3.89) to eq. (3.100) not only for the consideration in product development, but also for the implementation in design and product standardisation.

With regard to self-tapping screws exposed to axial, cyclic (fatigue-relevant) loading, presupposing a steel failure in tension, detail category “100” – in accordance to ON EN 1993-1-9 (2013) – can be assumed as a first approach for the related design process.

Even though examinations dealing with the occurrence of HISCC for axially loaded low-alloy carbon steel screws have to be seen as an initial step in this field, gained results indicate a certain vulnerability against this phenomenon in case of $f_u > 1,000 \text{ N/mm}^2$ and $u > 16 \%$. Consequently, it is recommended to avoid the application of carbon steel screws with high steel tensile strengths in such environmental conditions, which especially concerns the one in oak wood.

The results dedicated to the withdrawal stiffness $K_{\text{ser,ax}}$, presented in chapter 5, clearly point out that the significant deviations of the currently available approaches related to this property have a good reason. In contrast to withdrawal strength, the magnitude of $K_{\text{ser,ax}}$ obviously depends on parameters not considered so far for modelling, such as e. g. the thread pitch p or the axis-to-grain angle α . Thus, when considering this parameter for design purposes – as required in ON EN 1995-1-1 (2015) for instance – a much higher inaccuracy if compared to f_{ax} has to be taken into account.

Finally, with regard to axially (and quasi-statically) loaded self-tapping screws with $4 \text{ mm} \leq d \leq 12 \text{ mm}$, inserted in board-based, laminated timber products made of softwood at service class 1 conditions according to ON EN 1995-1-1 (2015) (otherwise a moisture content related correction as e. g. given in section 5-3.2 has to be applied), the characteristic withdrawal strength can be determined as follows:

$$f_{\text{ax,k}} = k_{\text{ax,k}} \cdot k_{\text{sys,k}}(N) \cdot f_{\text{ax,ref,k}} \cdot \left(\frac{\rho_k}{\rho_{\text{ref,k}}} \right)^{k_p}, \text{ with} \quad (7.1)$$

$$k_{\text{ax,k}} = \begin{cases} 1.00 & \text{for } 45^\circ \leq \alpha \leq 90^\circ \\ 0.64 \cdot k_{\text{gap,k}} + \frac{1 - 0.64 \cdot k_{\text{gap,k}}}{45} \cdot \alpha & \text{for } 0^\circ \leq \alpha \leq 45^\circ \end{cases}, \quad (7.2)$$

$$k_{\text{gap},k} = \begin{cases} 0.90 & \text{CLT narrow face} \\ 1.00 & \text{other} \end{cases}, \quad (7.3)$$

$$k_{\text{sys},k} = \begin{cases} 1.00 & \text{ST} \\ 1.10 & \text{CLT } N \geq 3, \\ 1.13 & \text{GLT} \end{cases}, \quad (7.4)$$

$$k_p = \begin{cases} 1.10 & 0^\circ < \alpha \leq 90^\circ \\ 1.25 - 0.05 \cdot d & \alpha = 0^\circ \end{cases}, \text{ or } k_p = \begin{cases} 1.10 & 0^\circ < \alpha \leq 90^\circ \\ 0.70 & \alpha = 0^\circ \end{cases}, \text{ and} \quad (7.5)$$

$f_{\text{ax,ref},k}$ as characteristic (5 %-) quantile withdrawal strength in case of ST ($N = 1$) and $\alpha = 90^\circ$, either as (d -dependent) value from a specific ETA or predicted with eq. (6.21). It is worth mentioning, that this approach presupposes sufficient spacings a_i between the screws and to the timber member's ends and edges, as well as – if pre-drilling is applied – d_{PD} close to d_c . So far, the screw withdrawal behaviour in case of $\alpha = 0^\circ$ and $t \rightarrow \infty$ has not been investigated yet to an adequate extent. Thus, it is additionally recommended to situate screws with an insertion angle of at least $\alpha = 15^\circ$.

7-3 OUTLOOK

In the frame of chapters 2 ÷ 6, several remaining investigations in the field of self-tapping screws worth being carried out are mentioned. The following list contains the probably most relevant ones, which should be focused on in the near future:

- With regard to the bearing capacity of self-tapping screws exposed to axial, cyclic (fatigue-relevant) loading, especially a possible influence of their inclined positioning in form of steel-to-timber butt joints on the behaviour of k_{fat} in dependence of R as derived in section 3-5.3 should be determined within an experimental campaign.
- Certain effects, such as geometrical thread properties or the applied test and measurement configuration, influence the magnitude of the withdrawal stiffness $K_{\text{ser,ax}}$ to an unknown extent and disabled an appropriate model determination in the frame of chapter 6. Thus, clarifying this lack of knowledge is envisaged within a next step.
- This also concerns the long-term resistance of axially loaded self-tapping screws failing in withdrawal. Especially the parallel-to-grain insertion, probably efficiently enabled by constructive measures as e. g. indicated in Pirnbacher and Schickhofer (2012), Hübner (2013b) and ON B 1995-1-1 (2014), has to be quantitatively verified in the frame of further experimental campaigns.
- In the present thesis, the scope of the timber density was restricted to the one of softwood species. Thus, further examinations on the interrelationship between withdrawal strength, timber density,

outer thread diameter and axis-to-grain angle also taking hardwood species into account would be valuable for extending the applicable model bandwidth the withdrawal strength can be determined within.

- In the frame of this thesis, to avoid the related scope, the modelling of withdrawal strength was restricted to simplified empirical, stochastic and mechanical approaches. In order to gain a better understanding of the timber-screw composite behaviour, especially the latter are worth being focused on in a next step.

ANNEX A REGISTER

A-1 References

- ABC-Verbindungsmittel (2008), Technische Informationen zu Korrosion, Korrosionsschutz, Materialien und Überzügen, Technical Report, ABC-Verbindungsmittel. (in German).
- Aicher, S. and Höfflin, L. (2009), Glulam beams with holes reinforced by steel bars, *in* 'Proceedings of the 42th CIB W18 Meeting', Dübendorf (Switzerland). paper CIB-W18/42-12-1.
- Amri, J., Gulbrandsen, E. and Nogueira, R. P. (2011), Role of acetic acid in CO₂ top of the line corrosion of carbon steel, *in* 'NACE International Corrosion Conference & Expo', pp. 1–22.
- Angst, V. (2012), Moisture Induced Stresses in Glulam - Effect of Cross Section Geometry and Screw Reinforcement, PhD thesis, NTNU Trondheim.
- Angst, V. and Malo, K. A. (2012), 'Effect of self-tapping screws on moisture induced stresses in glulam', *Engineering Structures* **45**, 299–306.
- ASTM E2126 (2002), 'Standard Test Methods for Cyclic (Reversed) Load Test for Shear Resistance of Walls for Buildings'.
- Augustin, M. (2004), Eine zusammenfassende Darstellung der Festigkeitssortierung von Schnittholz, Master's thesis, Institute of Timber Engineering and Wood Technology, Graz University of Technology. (in German).
- Augustin, M. (2009), Abtragung hoher Lasten mit Sherpa-Systemverbindern, *in* '15. Internationales Holzbau-Forum 09', Garmisch-Partenkirchen (Germany). (in German).
- Augustin, M. (2011), Prüftechnik und Modellbildung für HT NT-Systemverbinder, *in* '17. Internationales Holzbau-Forum 11', Garmisch-Partenkirchen (Germany). (in German).
- Augustin, M., Zimmer, S. E., Bogensperger, T. and Sleik, T. (2016), A contribution to the design of ribbed plates, *in* 'Proceedings of the 14th World Conference on Timber Engineering WCTE2016', Vienna (Austria).
- Austrian Standards (2015), 'Database ÖNORM Standards'. (in German). <https://shop.austrian-standards.at/> (2015-03-09)
- Balaban, M. and Ucar, G. (2003), 'Estimation of volatile acids in wood and bark', *Holz als Roh- und Werkstoff* **61**, 465–468.
- Basquin, O. H. (1910), The exponential law of endurance tests, *in* 'Proceedings ASTM 10', pp. 625–630.
- Bejtka, I. (2003), Querkzug- und Querdrukverstärkungen - Aktuelle Forschungsergebnisse, *in* 'Ingenieurholzbau - Karlsruher Tage', Karlsruhe (Germany). (in German).
- Bejtka, I. (2005), Verstärkung von Bauteilen aus Holz mit Vollgewindeschrauben, PhD thesis, Karlsruhe Institute of Technology. (in German).

- Bejtka, I. and Blaß, H. J. (2002), Joints with inclined screws, *in* ‘Proceedings of the 35th CIB W18 Meeting’, Kyoto (Japan). paper CIB-W18/35-7-5.
- Bejtka, I. and Blaß, H. J. (2005), Self-tapping screws as reinforcements in connection with dowel-type fasteners, *in* ‘Proceedings of the 38th CIB W18 Meeting’, Karlsruhe (Germany). paper CIB-W18/38-7-4.
- Bejtka, I. and Blaß, H. J. (2006), Self-tapping screws as reinforcements in beam supports, *in* ‘Proceedings of the 39th CIB W18 Meeting’, Florence (Italy). paper CIB-W18/39-7-2.
- Bernasconi, A. (2012), Überbauung Via Cenni Mailand - 4 Holzhochhäuser mit je 9 Geschossen, *in* ‘18. Internationales Holzbau-Forum 2012’, Garmisch-Partenkirchen (Germany). (in German).
- Berns, H. and Theisen, W. (2006), *Eisenwerkstoffe - Stahl und Gusseisen*, 3 edn, Springer Berlin Heidelberg New York. ISBN-10 3-540-29792-8 (in German).
- Blaß, H. J. (1998), ‘Aktuelle Forschung und Entwicklung im Holzbau zeigt große Zukunftspotentiale auf’, *Bauen mit Holz* **100**(10), 93–99. (in German).
- Blaß, H. J. (2000a), Neuere Entwicklungen im Bereich mechanischer Verbindungsmittel, *in* ‘HOLZ A R T 2000. Architecture - research - technology, 17. Dreiländer-Holztagung.’, Zürich (Switzerland). (in German).
- Blaß, H. J. (2000b), Verbindungen mit Nägeln und Schrauben - Bemessung nach E DIN 1052 und neuere Entwicklungen, *in* ‘Ingenieurholzbau - Karlsruher Tage’, Karlsruhe (Germany). (in German).
- Blaß, H. J. (2004), Innovative materials and connections for timber structures, *in* ‘COST E29 Symposium’, Florence (Italy).
- Blaß, H. J. (2007), Selbstbohrende Schrauben als hochwirksames Verbindungsmittel, *in* ‘6. Grazer Holzbau-Fachtagung "6. GraHFT'07"’, Graz (Austria). (in German).
- Blaß, H. J. (2010), Gutachterliche Stellungnahme zum Tragverhalten von SHERPA-XL/DXL Verbindern. (in German).
- Blaß, H. J. and Bejtka, I. (2001), Screws with continuous threads in timber connections, *in* S. Aicher, ed., ‘Joints in timber structures. Proceedings of the International RILEM Symposium’, number 22 *in* ‘RILEM publications’, Stuttgart (Germany), pp. 193–201.
- Blaß, H. J. and Bejtka, I. (2003a), Querzugverstärkungen in gefährdeten Bereichen mit selbstbohrenden Holzschrauben, Technical Report, Karlsruhe Institute of Technology. (in German).
- Blaß, H. J. and Bejtka, I. (2003b), ‘Verbindungen mit geneigt angeordneten Schrauben’, *Bauen mit Holz* **105**(10), 28–96. (in German).
- Blaß, H. J. and Bejtka, I. (2004a), Reinforcements perpendicular to the grain using self-tapping screws, *in* ‘Proceedings of the 8th World Conference on Timber Engineering WCTE2004’, Lahti (Finland).
- Blaß, H. J. and Bejtka, I. (2004b), ‘Selbstbohrende Holzschrauben und ihre Anwendungsmöglichkeiten’, *Holzbau Kalender* pp. 516–541. (in German).
- Blaß, H. J. and Bejtka, I. (2008), *Numerische Berechnung der Tragfähigkeit und der Steifigkeit von querzugverstärkten Verbindungen mit stiftförmigen Verbindungsmitteln*, number 10 *in* ‘Karlsruher Berichte zum Ingenieurholzbau’, Universitätsverlag Karlsruhe. (in German).

- Blaß, H. J., Bejtka, I. and Uibel, T. (2006), *Tragfähigkeit von Verbindungen mit selbstbohrenden Holzschrauben mit Vollgewinde*, number 4 in 'Karlsruher Berichte zum Ingenieurholzbau', Universitätsverlag Karlsruhe. (in German).
- Blaß, H. J., Bienhaus, A. and Kraemer, V. (2000), 'Ermittlung des Biege widerstandes stiftförmiger Verbindungsmittel', *Bauingenieur* **75**, 296–299. (in German).
- Blaß, H. J. and Colling, F. (2015), Load-carrying capacity of dowelled connections, in 'Proceedings of the 2nd INTER Meeting', Sibenik (Croatia). paper INTER/48-7-3.
- Blaß, H. J., Ehlbeck, J., Kreuzinger, H. and Steck, G. (2004), *Erläuterungen zu DIN 1052:2004-08*, DGfH INNOVATIONS- UND SERVICE GMBH. (in German).
- Blaß, H. J. and Krüger, O. (2010), *Schubverstärkung von Holz mit Holzschrauben und Gewindestangen*, number 15 in 'Karlsruher Berichte zum Ingenieurholzbau', Universitätsverlag Karlsruhe. (in German).
- Blaß, H. J. and Schädle, P. (2011), 'Ductility aspects of reinforced and non-reinforced timber joints', *Engineering Structures* **33**, 3018–3026.
- Blaß, H. J. and Schlager, M. (1996), 'Trag- und Verformungsverhalten von Holz-Beton-Verbundkonstruktionen Teil 1', *Bauen mit Holz* **98**(5), 392–399. (in German).
- Blaß, H. J., Schlager, M. and van der Linden, M. (1996), 'Trag- und Verformungsverhalten von Holz-Beton-Verbundkonstruktionen Teil 2', *Bauen mit Holz* **98**(6), 472–477. (in German).
- Blaß, H. J. and Schmid, M. (2001), Self-tapping screws as reinforcement perpendicular to the grain in timber connections, in S. Aicher, ed., 'Joints in timber structures. Proceedings of the International RILEM Symposium', number 22 in 'RILEM publications', Stuttgart (Germany), pp. 163–172.
- Blaß, H. J. and Uibel, T. (2007), *Tragfähigkeit von stiftförmigen Verbindungsmitteln in Brettsper Holz*, number 8 in 'Karlsruher Berichte zum Ingenieurholzbau', Universitätsverlag Karlsruhe. (in German).
- Blumer, H. (1979), *Spannungsberechnungen an anisotropen Kreisbogenscheiben und Sattelträgern konstanter Dicke*, PhD thesis, Karlsruhe Institute of Technology. (in German).
- Boding, J. and Jayne, B. A. (1982), *Mechanics of Wood and Wood Composites*, Krieger Publishing Company.
- Bogensperger, T. (2002), *Erweiterte Stabtheorie und der gevoutete Träger im Brückenbau*, PhD thesis, Graz University of Technology. (in German).
- Bogensperger, T. and Hude, F. (2007), Entwicklung einer hoch beanspruchbaren Verbindung für Haupt-Nebenträger-Anschlüsse, in '6. Grazer Holzbau-Fachtagung "6. GraHFT'07"', Graz (Austria). (in German).
- Bogensperger, T. and Jöbstl, R. (2015), Concentrated load introduction in CLT elements perpendicular to plane, in 'Proceedings of the 2nd INTER Meeting', Sibenik (Croatia). paper INTER/48-12-1.
- Branco, J., Sousa, H. S. and Lourenco, P. (2016), 'Experimental analysis of Maritime pine and Iroko single shear dowel-type connections', *Construction and Building Materials* **111**, 440–449.

- Brandl, L. (2015), Experimentelle Untersuchungen an zugbeanspruchten Schrägschraubverbindungen mit Bezug auf Versagen des Holzbauteils, Master's thesis, Institute of Timber Engineering and Wood Technology, Graz University of Technology.
- Brandner, R. (2013a), Production and Technology of Cross Laminated Timber (CLT): State-of-the-Art Report, in R. Harris, A. Ringhofer and G. Schickhofer, eds, 'Focus Solid Timber Solutions - European Conference on Cross Laminated Timber (CLT)', pp. 3–36.
- Brandner, R. (2013b), *Stochastic System Actions and Effects in Engineered Timber Products and Structures*, Vol. 2, Verlag der Technischen Universität Graz. ISBN 978-3-85125-263-7.
- Brandner, R. (2016), Group action of axially-loaded screws in the narrow face of cross laminated timber, in 'Proceedings of the 14th World Conference on Timber Engineering WCTE2016', Vienna (Austria).
- Brandner, R., Bogensperger, T. and Schickhofer, G. (2013), In plane shear strength of cross laminated timber (CLT): test configuration, quantification and influencing parameters, in 'Proceedings of the 46th CIB W18 Meeting', Vancouver (Canada). paper CIB-W18/46-12-2.
- Brandner, R., Bratulic, K. and Ringhofer, A. (2015), Serial Correlation of Withdrawal Properties from Axially-Loaded Self-Tapping Screws, in '12th International Conference on Applications of Statistics and Probability in Civil Engineering, ICASP12', Vancouver (Canada).
- Brandner, R., Flatscher, G., Ringhofer, A., Schickhofer, G. and Thiel, A. (2016a), 'Cross laminated timber (CLT): overview and development', *European Journal of Wood and Wood Products* **74**, 331–351.
- Brandner, R., Gattertnig, W. and Schickhofer, G. (2012), Determination of Shear Strength of Structural and Glued Laminated Timber, in 'Proceedings of the 45th CIB W18 Meeting', Växjö (Sweden). paper CIB-W18/45-12-2.
- Brandner, R., Ringhofer, A. and Grabner, M. (2017), 'Probabilistic Models for the Withdrawal Behavior of Single Self-Tapping Screws in the Narrow Face of Cross Laminated Timber (CLT)', *European Journal of Wood and Wood Products* pp. 1–41. (accepted for publication).
- Bratulic, K. (2012), Alteration of the withdrawal strength of self-tapping screws along the board and over the varying GLT cross section, Master's thesis, Institute of Timber Engineering and Wood Technology, Graz University of Technology.
- Bratulic, K., Flatscher, G. and Brandner, R. (2014), Monotonic and cyclic behaviour of joints with self-tapping screws in CLT structures, in 'Experimental Research with Timber, COST Action FP1004', Prague (Czech Republic).
- Bratulic, K., Flatscher, G., Brandner, R., Augustin, M. and Schickhofer, G. (2014a), Monotones und zyklisches Verhalten von Schraubenverbindungen in BSP-Strukturen, Technical Report, holz.bau forschung gmbh, Graz University of Technology. (in German).
- Bürgel, R., Richard, H. A. and Riemer, A. (2014), *Werkstoffmechanik - Bauteile sicher beurteilen und Werkstoffe richtig einsetzen*, 2 edn, Springer Vieweg. ISBN 978-3-658-03934-9 (in German).
- Brunauer, A. (2009), Messehalle 11 Frankfurt, in '15. Internationales Holzbau-Forum 09', Garmisch-Partenkirchen (Germany). (in German).

- Burgschwaiger, M. (2010), Einfluss der Einbindelänge auf die Ausziehfestigkeit von Teilgewindeschrauben, Technical Report, Institute of Timber Engineering and Wood Technology, Graz University of Technology. (in German).
- Carrington, H. (1923), ‘The elastic constants of spruce’, *Philosophical Magazine Series 6* **45**(269), 1055–1057.
- Chopra, A. K. (2007), *Dynamics of Structures - Theory and Applications to Earthquake Engineering*, Pearson Education Inc.
- Closen, M. and Lam, F. (2012), Performance of moment resisting self-tapping screw assembly under reverse cyclic load, in ‘Proceedings of the 12th World Conference on Timber Engineering WCTE2012’, Auckland (New Zealand).
- Cockrell, R. A. (1933), A study of the screw-holding properties of wood, Technical Report, New York State College of Forestry.
- Colling, F. (2001a), ‘Erhöhung der Querdruckfestigkeit von Holz - Teil 1’, *mikado* **10**, 66–69. (in German).
- Colling, F. (2001b), ‘Erhöhung der Querdruckfestigkeit von Holz - Teil 2’, *mikado* **11**, 62–66. (in German).
- Colling, F. (2012), *Holzbau - Grundlagen der Bemessung nach EC 5*, Vol. 3, Springer Vieweg. ISBN 978-3-658-14232-2 (in German).
- CUAP 06.03/08 (2010), *CUAP 06.03/08 - Common Understanding of Assessment Procedure - for European Technical Approval according to Article 9.2 - of the Construction Products Directive - Self-tapping screws for use in timber constructions.*
- Dalley, S. and Oleson, J. P. (2003), ‘Sennacherib, Archimedes, and the Water Screw: The Context of Invention in the Ancient World’, *Technology and Culture* **44**(1), 1–26.
- Danzer, M., Dietsch, P. and Winter, S. (2016), Reinforcement of round holes in glulam beams arranged eccentrically or in groups, in ‘Proceedings of the 14th World Conference on Timber Engineering WCTE2016’, Vienna (Austria).
- Danzig, I., Closen, M. and Tannert, T. (2014), High performance cross-laminated-timber shear connection with self-tapping screws assemblies, in ‘Proceedings of the 13th World Conference on Timber Engineering WCTE2014’, Quebec City (Canada).
- Delahunty, S., Chui, Y. H. and McCormick, M. (2014), Use of double-threaded self-tapping screws for in-situ repair of cracked timber connections, in ‘Proceedings of the 13th World Conference on Timber Engineering WCTE2014’, Quebec City (Canada).
- Dennis, J. K., Zou, C. and Short, N. R. (1995), ‘Corrosion behaviour of zinc and zinc alloy coated steel in preservative treated timber’, *Transactions of the Institute of Metal Finishing* **73**(3), 96–101.
- DIBt (2014), ‘Part II and III of the List of Technical Building Rules’, *DIBt Mitteilungen* **4**, 1–70.
- DIBt (2015a), ‘Construction Products List A, Construction Products List B, and List C’, *DIBt Mitteilungen* **2**, 1–193.
- DIBt (2015b), ‘National approvals (abZ) - Areas of approvals’. <https://www.dibt.de/en/Approvals/abZ-Zulassungsbereiche.html> (2015-04-10)

- DIBt (2015c), 'Procedure for drafting a European Assessment Document'.
https://www.dibt.de/en/Approvals/data/Grafik_Erarbeitung_ETB.pdf (2015-03-24)
- DIBt (2015d), 'Procedure for obtaining an approval'.
https://www.dibt.de/en/Approvals/data/Diagramm_ZulassAblauf_national.pdf (2015-03-24)
- Dietsch, P. (2012), Einsatz und Berechnung von Schubverstärkungen für Brettschichtholzbauteile, PhD thesis, Technical University of Munich. (in German).
- Dietsch, P. (2014), Einsatz und Berechnung von Schubverstärkungen für Brettschichtholzbauteile, in 'Ingenieurholzbau - Karlsruher Tage', Karlsruhe (Germany). (in German).
- Dietsch, P. and Brandner, R. (2015), 'Self-tapping screws and threaded rods as reinforcement for structural timber elements - A state-of-the-art report', *Construction and Building Materials* **0**(0), 1–12.
- Dietsch, P., Kreuzinger, H. and Winter, S. (2013), Design of shear reinforcement for timber beams, in 'Proceedings of the 46th CIB W18 Meeting', Vancouver (Canada). paper CIB-W18/46-7-9.
- Dietsch, P., Kreuzinger, H. and Winter, S. (2014), Effects of changes in moisture content in reinforced glulam beams, in 'Proceedings of the 13th World Conference on Timber Engineering WCTE2014', Quebec City (Canada).
- Dietsch, P., Mestek, P. and Winter, S. (2012), 'Analytischer Ansatz zur Erfassung von Tragfähigkeitssteigerungen infolge von Schubverstärkungen in Bauteilen aus Brettschichtholz und Brettsperrholz', *Bautechnik* **89**(6), 402–414. (in German).
- DIN 1052 (2004), 'Design of timber structures - General rules and rules for buildings'. (in German).
- DIN 1052 (2008), 'Design of timber structures - General rules and rules for buildings'. (in German).
- DIN 1052-10 (2012), 'Design of timber structures - Part 10: Additional provisions'. (in German).
- DIN 1052 C1 (2010), 'Corrigendum 1 - Design of timber structures - General rules and rules for buildings; Corrigendum to DIN 1052:2008-12'. (in German).
- DIN 1052 P1 (1988), 'Part 1: Timber structures; design and calculation'. (in German).
- DIN 1052 P2 (1988), 'Part 2: Timber structures; mechanical joints'. (in German).
- DIN 1052 P3 (1988), 'Part 3: Timber structures; buildings constructed from timber panels, design and construction'. (in German).
- DIN 18168-1 (2007), 'Ceiling linings and suspended ceilings with gypsum plasterboards - Part 1: Requirements for construction'. (in German).
- DIN 20000-6 (2013), 'Application of construction products in structures - Part 6: Fasteners and connectors according to EN 14592:2009-02 and EN 14545:2009-05'. (in German).
- DIN 20000-6 (2015), 'Application of construction products in structures - Part 6: Fasteners and connectors according to EN 14592 and EN 14545'. (in German).
- DIN 50962 (2013), 'Electrodeposited coatings - Chromated coatings of zinc alloys on iron and steel'. (in German).

- DIN 50969-1 (2009), ‘Prevention of hydrogen-induced brittle fracture of high-strength steel building elements - Part 1: Advice on the prevention’. (in German).
- DIN 52182 (1976), ‘Testing of wood; determination of density’. (in German).
- DIN 52185 (1976), ‘Testing of wood; compression test parallel to grain’. (in German).
- DIN 52186 (1978), ‘Testing of wood; bending test’. (in German).
- DIN 52188 (1979), ‘Testing of wood; determination of ultimate tensile stress parallel to grain’. (in German).
- DIN 571 (1986), ‘Hexagon head wood screws’. (in German).
- DIN 7998 (1975), ‘Thread and thread ends for wood screws’. (in German).
- DIN 96 (1986), ‘Slotted round head wood screws’. (in German).
- DIN 969 (1997), ‘Threaded fasteners - Axial load fatigue testing - Test methods and evaluation of results’. (in German).
- DIN 97 (1986), ‘Slotted countersunk (flat) head wood screws’. (in German).
- DIN EN 1995-1-1 (2010), ‘Eurocode 5: Design of timber structures; Part 1-1: General - Common rules and rules for buildings; German version EN 1995-1-1:2004 + AC:2006 + A1:2008’. (in German).
- DIN EN 1995-1-1/NA (2010), ‘National Annex - Nationally determined parameters - Eurocode 5: Design of timber structures; Part 1-1: General - Common rules and rules for buildings’. (in German).
- DIN EN 1995-1-1/NA (2013), ‘National Annex - Nationally determined parameters - Eurocode 5: Design of timber structures; Part 1-1: General - Common rules and rules for buildings’. (in German).
- DIN V ENV 1995-1-1 (1994), ‘Eurocode 5: Design of timber structures; Part 1-1: General rules and rules for buildings; German version ENV 1995-1-1:1993’. (in German).
- DIN V ENV 1995-1-1 NAD (1995), ‘National application document (NAD) - Guideline for application of DIN V ENV 1995-1-1 - Eurocode 5: General rules and rules for buildings’. (in German).
- Distelrath, N. (2005), Galvanisiergerechtes Konstruieren und Fertigen, *in* ‘Informationstagung Korrosionsschutz ohne Chrom-VI’, Velbert (Germany). (in German).
- Divós, F., Tanaka, T., Nagao, H. and Kato, H. (1998), ‘Determination of shear modulus on construction size timber’, *Wood Science and Technology* **32**, 393–402.
- Dixon, W. J. and Mood, A. M. (1948), ‘A Method for Obtaining and Analyzing Sensitivity Data’, *Journal of the American Statistical Association* **43**, 109–126.
- EAD 130118-00-0603 (2016), *EAD 130118-00-0603 - Screws for use in timber constructions*.
- Eckelman, C. A. (1975), ‘Screwholding performance in hardwoods and particleboard’, *Forest Products Journal* **25**(6), 30–35.
- Ed, D. and Hasselqvist, F. (2011), Timber compression strength perpendicular to the grain – testing of glulam beams with and without reinforcement, Master’s thesis, Lund University.

- Ehlbeck, J., Görlacher, R. and Werner, H. (1989), Determination of perpendicular-to-grain tensile stresses in joints with dowel-type fasteners - A draft proposal for design rules, in 'Proceedings of the 22nd CIB W18 Meeting', Berlin (Germany). paper CIB-W18A/22-7-2.
- EN 1995-1-1 (2004), 'Eurocode 5 - Design of timber structures - Part 1-1: General - Common rules and rules for buildings'.
- EN 1995-1-1:2004/A1 (2008), 'Eurocode 5 - Design of timber structures - Part 1-1: General - Common rules and rules for buildings'.
- ETA-11/0190 (2013), Adolf Würth GmbH & Co. KG: Würth self-tapping screws, European Technical Approval, DIBt.
- ETA-11/0295 (2013), Pitzl GmbH & Co. KG: Pitzl GmbH & Co. KG HVP Verbinder, European Technical Approval, ETA Danmark. (in German).
- ETA-11/0452 (2011), HECO-Schrauben GmbH & Co. KG: HECO-UNIX-plus and HECO-UNIX-top screws, European Technical Approval, DIBt. (in German).
- ETA-12/0063 (2013), SFS intec AG: SFS self-tapping screws WT, European Technical Approval, OIB. (in German).
- ETA-12/0114 (2012), SPAX International GmbH & Co. KG: SPAX self-tapping screws, European Technical Approval, ETA Danmark.
- ETA-12/0373 (2012), Schmid Schrauben Hainfeld GmbH: Schmid screws RAPID, STARDRIVE and SP, European Technical Approval, OIB. (in German).
- ETA-14/0354 (2015), Pollmeier Furnierwerkstoffe GmbH: Brettschichtholz aus Laubholz - Buchenfurnierschichtholz für tragende Zwecke, European Technical Approval, OIB. (in German).
- European Union (1989), 'Council Directive of 21 December 1988 on the approximation of laws, regulations and administrative provisions of the Member States relating to construction products', *Official Journal of the European Communities* **32**(L40).
- European Union (2009), 'Commission communication in the framework of the implementation of the Council Directive 89/106/EEC on the approximation of laws, regulations and administrative provisions of the Member States relating to construction products (1) (Publication of titles and references of harmonised standards under the directive)', *Official Journal of the European Union* **52**(C152).
- European Union (2011), 'Regulation (EU) No 305/2011 of the European Parliament and of the Council of 9 March 2011 laying down harmonised conditions for the marketing of construction products and repealing Council Directive 89/106/EEC', *Official Journal of the European Union* **54**(L88).
- European Union (2013), 'Commission communication in the framework of the implementation of the Council Directive 89/106/EEC of 21 December 1988 on the approximation of laws, regulations and administrative provisions of the Member States relating to construction products', *Official Journal of the European Union* **56**(C59).
- Farmer, R. H. (1962), 'Corrosion of Metals in Association with Wood', *Wood* **27**, 443–446.
- Federal State of Styria (2013), 'Gesetz vom 2. Juli 2013, mit dem die Bereitstellung von Bauprodukten auf dem Markt und deren Verwendung sowie die Marktüberwachung von Bauprodukten geregelt

- wird (Steiermärkisches Bauprodukte- und Marktüberwachungsgesetz 2013 – StBauMüG) und das Steiermärkische Baugesetz geändert wird. [XVI.GPStLT RV EZ 2049/1 AB EZ 2049/3]’, *Landesgesetzblatt für die Steiermark* **24**(83), 415–441. (in German).
- Fischer, J. (2015), ‘Schweizer Entsprechungen zu Eurocodes’, *TEC21* (11), 18–18. (in German).
- Flatscher, G. (2012), Versuchstechnische Betrachtung zyklisch beanspruchter Wandelemente in der Holz-Massivbauweise, in ‘18. Internationales Holzbau-Forum 2012’, Garmisch-Partenkirchen (Germany). (in German).
- Flatscher, G. (2017), Evaluation and approximation of timber connection properties for displacement-based simulation of CLT wall systems, PhD thesis, Institute of Timber Engineering and Wood Technology, Graz University of Technology.
- Flatscher, G. and Augustin, M. (2010), Nachweisführung für SHERPA-Verbindungen auf Basis des SHERPA-Handbuchs, in ‘16. Internationales Holzbau-Forum 10’, Garmisch-Partenkirchen (Germany). (in German).
- Flatscher, G., Bratulic, K., Brandner, R. and Schickhofer, G. (2013), Zusammenfassende und weiterführende Arbeiten zum Verhalten von BSP-Tragwerken bei der Beanspruchungssituation Erdbeben, Technical Report, holz.bau forschungs gmbh, Graz University of Technology. (in German).
- Flatscher, G., Bratulic, K. and Schickhofer, G. (2014a), ‘Experimental tests on cross-laminated timber joints and walls’, *Structures and Buildings* **0**(0), 1–10.
- Flatscher, G., Bratulic, K. and Schickhofer, G. (2014b), Screwed joints in cross laminated timber structures, in ‘Proceedings of the 13th World Conference on Timber Engineering WCTE2014’, Quebec City (Canada).
- Flatscher, G. and Schickhofer, G. (2014), Beschreibung der Last-Verschiebungskurven von Verbindungen im Holzbau, in ‘Forschungskolloquium, Holzbau Forschung und Praxis’, Stuttgart (Germany). (in German).
- Frangi, A. (2001), Brandverhalten von Holz-Beton-Verbunddecken, PhD thesis, ETH Zürich. (in German).
- Frese, M. and Blaß, H. J. (2009), Models for the calculation of the withdrawal capacity of self-tapping screws, in ‘Proceedings of the 42nd CIB W18 Meeting’, Dübendorf (Switzerland). paper CIB-W18/42-7-3.
- Frese, M., Fellmoser, P. and Blaß, H. J. (2010), ‘Modelle für die Berechnung der Ausziehfestigkeit von selbstbohrenden Holzschrauben’, *European Journal of Wood and Wood Products* **68**(4), 373–384. (in German).
- Fuchs Lubritech GMBH (n.d.), *gleitmo HMP Filme*, Fuchs Lubritech GMBH. Manual (in German).
- Gaich, A., Ringhofer, A. and Wallner, R. (2008), Auszieh widerstand selbstbohrender Holzschrauben in Abhängigkeit der Eindrehlänge - Experimentelle Untersuchungen an Brettschichtholz und Vollholz, Bachelor’s thesis, Institute of Timber Engineering and Wood Technology, Graz University of Technology. (in German).

- Gasparri, E., Lam, F. and Liu, Y. (2016), Compression perpendicular to grain behavior for the design of a prefabricated CLT facade horizontal joint, in 'Proceedings of the 14th World Conference on Timber Engineering WCTE2016', Vienna (Austria).
- Gasser, D. (2017), Einfluss des Vorbohrdurchmessers auf die Ausziehkenngößen axial beanspruchter selbstbohrender Holzschrauben, Technical Report, Institute of Timber Engineering and Wood Technology, Graz University of Technology. (in German).
- Gatternig, W. (2010), Untersuchung der Randabstände bei selbstbohrenden Holzschrauben, Technical Report, Institute of Timber Engineering and Wood Technology, Graz University of Technology. (in German).
- Gavric, I., Fragiaco, M. and Ceccotti, A. (2015), 'Cyclic behavior of typical screwed connections for cross-laminated (CLT) structures', *European Journal of Wood and Wood Products* **0**(0), 1–13.
- Gehri, E. (1993), Grundlagen der Verbindungstechnik, in 'SAH-Kurs 1993', (Switzerland). (in German).
- Gehri, E. (2007), Leistungsfähige Anschlüsse parallel zur Faser - Anforderungen und technische Lösungen, in '6. Grazer Holzbau-Fachtagung "6. GraHFT'07"', Graz (Austria). (in German).
- Gehri, E. (2009), Influence of fastener spacings on joint performance - experimental result and codification, in 'Proceedings of the 42th CIB W18 Meeting', Dübendorf (Switzerland). paper CIB-W18/42-7-8.
- Gehri, E. (2010), Schraubenverbindungen für Laubholzkonstruktionen, in '16. Internationales Holzbau-Forum 10', Garmisch-Partenkirchen (Germany). (in German).
- Gehri, E. and Haas, P. (2008), Schrauben auf Ausziehen senkrecht zur Faser - Einfluss der Prüfkfiguration, Technical Report. (in German).
- Gerhards, C. (1980), 'Effect of Moisture Content and Temperature on the Mechanical Properties of Wood - An Analysis of Immediate Effects', *Wood and Fiber Science* **14**(1), 4–36.
- Giongo, I., Piazza, M. and Tomasi, R. (2013), 'Investigation on the self tapping screws capability to induce internal stress in timber elements', *Advanced Materials Research* **778**, 601–611.
- Giongo, I., Schiro, G., Piazza, M. and Tomasi, R. (2016), Long-term out-of-plane testing of timber floors strengthened with innovative timber-to-timber solutions, in 'Proceedings of the 14th World Conference on Timber Engineering WCTE2016', Vienna (Austria).
- Glos, P. (1978), *Zur Bestimmung des Festigkeitsverhaltens von Brettschichtholz bei Druckbeanspruchung aus Werkstoff- und Einwirkungskenngrößen*, number 35 in 'Berichte zur Zuverlässigkeitsanalyse der Bauwerke', Technical University of Munich. (in German).
- Gläser, B., Rüter, N., Gerwin, A. and Schreiber, B. (2013), Informationsdienst Holz - spezial - Korrosion metallischer Verbindungsmittel in Holz und Holzwerkstoffen, Technical Report, Fraunhofer Institute for Wood Research. (in German).
- Gohlich, R. and Erochko, J. (2016), Development of a heavy timber moment-resisting frame with ductile steel links, in 'Proceedings of the 14th World Conference on Timber Engineering WCTE2016', Vienna (Austria).
- Gorsky, W. S. (1935), 'Theory of Elastic Aftereffect in Unordered Mixed Crystals', *Phys. Z. SU* **8**, 457–471.

- Grabner, M. (2013), Einflussparameter auf den Auszieh Widerstand selbstbohrender Holzschrauben in BSP-Schmalflächen, Master's thesis, Institute of Timber Engineering and Wood Technology, Graz University of Technology. (in German).
- Grabner, M. and Ringhofer, A. (2014), Untersuchungen zum Tragverhalten von leistungsfähigen Hirnholzanschlüssen in Laubholz, in '20. Internationales Holzbau-Forum 2014', Garmisch-Partenkirchen (Germany). (in German).
- Greiner, R. and Unterweger, H. (2009), *Stahlbau*, Graz University of Technology. (in German).
- Gräfen, H. and Kuron, D. (1987), 'Werkstoffverhalten in Wasserstoff', *Chem.-Ing.-Tech.* **59**, 555–563. (in German).
- Görlacher, R. (1990), 'Untersuchungen an altem Konstruktionsholz: Die Auszieh Widerstandsmessung', *Bauen mit Holz* **12**, 904–908. (in German).
- Görlacher, R. (2002), 'Ein Verfahren zur Ermittlung des Rollschubmoduls von Holz', *Holz als Roh- und Werkstoff* **60**(5), 317–322. (in German).
- GrowthRingLogger (2014), 'Growth Ring Logger'. Version: 1.00.
- Gruner, W. (2002), 'Trägergas-Heißgasextraktionsmethoden - Probleme bei der Sauerstoff-, Stickstoff-, Kohlenstoff- und Schwefel-Analytik', *Erzmetall* **55**(3), 151–157. (in German).
- Gustafsson, P. J. (1988), A study of strength of notched beams, in 'Proceedings of the 21st CIB W18 Meeting', Parksville, Vancouver Island (Canada). paper CIB-W18A/21-10-1.
- Gysen, B. (2000), Anwendung von Zink-Nickel-Legierungen als Kadiumersatz zum Korrosionsschutz hochfester Stähle, PhD thesis, TU Dortmund University. (in German).
- Haibach, E. (2002), *Betriebsfestigkeit - Verfahren und Daten zur Bauteilberechnung*, number 2, Springer Berlin. ISBN 978-3-540-29364-4 (in German).
- Hankinson, R. L. (1921), Investigation of crushing strength of spruce at various angles to the grain, in 'Air Service Information Circular 3', number 259. Materials Section Paper No. 130.
- Harrington, J. J. (2002), Hierarchical modelling of softwood hygro-elastic properties, PhD thesis, University of Canterbury.
- Hauptmann, R. (2016), Untersuchung der Wasserstoffversprödung von verzinkten, hochfesten Holzbauschrauben, Bachelor's thesis, Institute of Material Science, Joining and Forming, Graz University of Technology. (in German).
- Hübner, U. (2009), Auszieh Widerstand von Holzschrauben in Eschen-Brettschichtholz, in '15. Internationales Holzbau-Forum 09', Garmisch-Partenkirchen (Germany). (in German).
- Hübner, U. (2013a), Mechanische Kenngrößen von Buchen-, Eschen- und Robinienholz für lastabtragende Bauteile, PhD thesis, Institute of Timber Engineering and Wood Technology, Graz University of Technology. (in German).
- Hübner, U. (2013b), Withdrawal strength of self-tapping screws in hardwoods, in 'Proceedings of the 46th CIB W18 Meeting', Vancouver (Canada). paper CIB-W18/46-7-4.

- Hübner, U., Rasser, M. and Schickhofer, G. (2010), Withdrawal capacity of screws in european ash, *in* 'Proceedings of the 11th World Conference on Timber Engineering WCTE2010', Riva del Garda (Italy).
- Hearmon, R. F. S. (1948), The Elasticity of Wood and Plywood, Technical Report, Department of Scientific and Industrial Research, Forest Products Research.
- Henrici, D. (1984), Beitrag zur Spannungsermittlung in ausgeklinkten Biegeträgern aus Holz, PhD thesis, Technical University of Munich. (in German).
- Hoffmeyer, P. and Sorensen, J. D. (2007), 'Duration of load revisited', *Wood Science and Technology* **41**, 687–711.
- Hofmann, V., Gräfe, M., Werther, N. and Winter, S. (2016a), 'Fire resistance of primary beam - secondary beam connections in timber structures', *Journal of Structural Fire Engineering* **7**(2), 126–141.
- Hofmann, V., Gräfe, M., Werther, N. and Winter, S. (2016b), Fire resistance of primary beam - secondary beam connections with full thread screws, *in* 'Proceedings of the 14th World Conference on Timber Engineering WCTE2016', Vienna (Austria).
- Horvath, N., Molnar, S. and Niemz, P. (2008), 'Untersuchungen zum Einfluss der Holzfeuchte auf ausgewählte Eigenschaften von Fichte, Eiche und Rotbuche', *Holztechnologie* **49**(1), 10–15. (in German).
- Hossain, A., Danzig, I. and Tannert, T. (2016), 'Cross-Laminated Timber Shear Connections with Double-Angled Self-Tapping Screw Assemblies', *J. Struct. Eng.* **142**(11), 1–9.
- Hossain, A., Popovski, M. and Tannert, T. (2016), Shear connections with self-tapping-screws for cross-laminated-timber panels, *in* 'Proceedings of the 14th World Conference on Timber Engineering WCTE2016', Vienna (Austria).
- Hude, F. (2005), Verbindungssysteme für Queranschlüsse von Neben- an Hauptträger im Ingenieurholzbau, Master's thesis, Institute of Timber Engineering and Wood Technology, Graz University of Technology. (in German).
- Illgner, K. H. and Esser, J. (2001), *Schrauben Vademecum*, Textron Verbindungstechnik GmbH & Co. (in German).
- Imsirovic, A. (2014), Untersuchungen zur Zeitfestigkeit vorwiegend axial beanspruchter selbstbohrender Holzschrauben, Master's thesis, Institute of Timber Engineering and Wood Technology, Technische Universität Graz. (in German).
- IS-ARGEBAU (2012), 'Model Building Regulation - version november 2002 - modified on september 21, 2012'.
- IS-ARGEBAU (2014), 'Model List of Technical Building Rules'.
- IS-ARGEBAU (2015), 'Model List of Technical Building Rules'.
- ISO 16670 (2003), 'Timber structures - Joints made with mechanical fasteners - Quasi-static reversed-cyclic test method'.
- Jablonkay, P. (1999), Schrauben auf Ausziehen, Master's thesis, ETH Zürich. (in German).

- Jacob-Freitag, S. (2013), ‘Geschosswohnungsbau Mailand’, *mikado* **12**, 22–33. (in German).
- Jacquier, N. and Girhammar, U. A. (2014), ‘Tests on glulam-CLT shear connections with double-sided punched metal plate fasteners and inclined screws’, *Construction and Building Materials* **72**, 444–457.
- Jacquier, N. and Girhammar, U. A. (2015), ‘Evaluation of bending tests on composite glulam-CLT beams connected with double-sided punched metal plates and inclined screws’, *Construction and Building Materials* **95**, 762–773.
- Jöbstl, R. (2010), Zulassung ergänzt Norm – CE-Kennzeichnung für selbstbohrende Holzschrauben, in ‘16. Internationales Holzbau-Forum 10’, Garmisch-Partenkirchen (Germany). (in German).
- JMatPro (2016), ‘JMatPro the Materials Property Simulation Package’. Version: 9.0.
- Jönsson, J. and Thelandersson, S. (2005), Load carrying capacity of curved glulam beams reinforced with self-tapping screws, in ‘Proceedings of the 38th CIB W18 Meeting’, Karlsruhe (Germany). paper CIB-W18/38-7-3.
- Jockwer, R. (2014), Structural Behaviour of Glued Laminated Timber Beams with Unreinforced and Reinforced Notches, PhD thesis, ETH Zürich.
- Jockwer, R., Frangi, A., Steiger, R. and Serrano, E. (2013), Enhanced design approach for reinforced notched beams, in ‘Proceedings of the 46th CIB W18 Meeting’, Vancouver (Canada). paper CIB-W18/46-6-1.
- Jockwer, R. and Steiger, R. (2016), Performance of self-tapping screws and threaded steel rods in shear reinforcement of glulam beams, in ‘Proceedings of the 14th World Conference on Timber Engineering WCTE2016’, Vienna (Austria).
- Jockwer, R., Steiger, R. and Frangi, A. (2014), Design model for inclined screws under varying load to grain angles, in ‘Proceedings of the 1st INTER Meeting’, Bath (United Kingdom). paper INTER/47-7-5.
- Johansen, K. W. (1949), ‘Theory of timber connections’, *IABSE publications* **9**, 249–262.
- Jorissen, A. (1988), Double shear timber connections with dowel type fasteners, PhD thesis, Delft University of Technology.
- Karagiannis, V., Málaga-Chuquitaype, C. and Elghazouli, A. Y. (2017), ‘Behaviour of hybrid timber beam-to-tubular steel column moment connections’, *Engineering Structures* **131**, 243–263.
- Kasal, B., Guindos, P., Polocoser, T., Heiduschke, A., Urushadze, S. and Pospisil, S. (2014), ‘Heavy Laminated Timber Frames with Rigid Three-Dimensional Beam-to-Column Connections’, *Journal of Performance of Constructed Facilities* **28**(6), 1–11.
- Kaserer, D. (2011), Macromechanical characterisation of Norway spruce knot wood, Bachelor’s thesis, Institute of Wood Science and Technology, University of Natural Resources and Applied Life Sciences BOKU - Vienna.
- Kayser, K. (2001), Wasserstoffversprödung - Entstehung - Erkennung - Vermeidung, Technical Report, Klaus Kayser. (in German).

- Keunecke, D., Sonderegger, W., Pereteanu, K., Lüthi, T. and Niemz, P. (2007), ‘Determination of Young’s and shear moduli of common yew and Norway spruce by means of ultrasonic waves’, *Wood Science and Technology* **41**, 309–327.
- Kevarinmäki, A. (2002), Joints with inclined screws, in ‘Proceedings of the 35th CIB W18 Meeting’, Kyoto (Japan). paper CIB-W18/35-7-4.
- Kloos, K. H., Landgrebe, R. L. and Speckhardt, H. (1987), ‘Einfluß unterschiedlicher Wärmebehandlungsverfahren auf die wasserstoffinduzierte Sprödbruchbildung bei Vergütungsstählen für die Schraubenfertigung’, *Zeitschrift für Werkstofftechnik* **18**, 411–422. (in German).
- Kloos, K.-H. and Thomala, W. (2007), *Schraubenverbindungen - Grundlagen, Berechnung, Eigenschaften, Handhabung*, 5 edn, Springer Berlin Heidelberg New York. ISBN-13 978-3-540-21282-9 (in German).
- Küng, R. (1987), Verbunddecke Holz-Leichtbeton. Theoretische und experimentelle Untersuchung der Verbundkonstruktion aus Holz und Leichtbeton mit Holzschrauben als Verbindungsmittel., Technical Report, Graz University of Technology. (in German).
- Kobel, P. (2011), Modelling of Strengthened Connections for Large Span Truss Structures, Master’s thesis, Lund University.
- Koch, G. and Dünisch, O. (2008), *Juvenile wood in Robinie - Qualität von Robinienholz (Robinia pseudoacacia L.) und Folgerungen für Holzbearbeitung und Produktqualität*, Fraunhofer IRB Verlag, Stuttgart. ISBN 978-3-8167-7574-4.
- Koiner, W. (2012), Chemische Analyse des Werkstoffes 20MNB4 (Rundwalzdraht), Technical Report, voestalpine Austria Draht GmbH. (in German).
- Koj, C. and Trautz, M. (2014), ‘Mit Schrauben fügen und bewehren - Langzeitversuche an biegesteifen Rahmenecken im Außenklima’, *Bautechnik* **91**(1), 38–45. (in German).
- Koj, C. and Trautz, M. (2016), Long-term behaviour of timber connections with self-tapping screws in outdoor climate, in ‘Proceedings of the 14th World Conference on Timber Engineering WCTE2016’, Vienna (Austria).
- Kollmann, F. (1951), *Technologie des Holzes und der Holzwerkstoffe*, Vol. 1, 2 edn, Springer Berlin, Heidelberg. (in German).
- Kollmann, F. (1959), ‘Zur Frage der Querdruckfestigkeit von Holz’, *Holzforschung und Holzverwertung* **11**, 109–121. (in German).
- Kraler, A., Kögl, J. and Maderebner, R. (2014), Sherpa-CLT-connector for cross laminated timber (CLT) elements, in ‘Proceedings of the 13th World Conference on Timber Engineering WCTE2014’, Quebec City (Canada).
- Krenn, H. (2009), P06 connections - Verbindungstechnik im Ingenieurholzbau - Selbstbohrende Holzschrauben in hoch beanspruchten Bereichen, Technical Report, holz.bau forschungs gmbh, Graz University of Technology. (in German).
- Krenn, H. (2010), Der Einfluss der Gruppenwirkung von Schraubenverbindungen auf das Nachweisverfahren, in ‘16. Internationales Holzbau-Forum 10’, Garmisch-Partenkirchen (Germany). (in German).

- Krenn, H. and Schickhofer, G. (2007), Traglast von auf Zug beanspruchten Schraubenverbindungen mit Stahlblechen, in '6. Grazer Holzbau-Fachtagung "6. GraHFT'07"', Graz (Austria). (in German).
- Krenn, H. and Schickhofer, G. (2009), Joints with inclined screws and steel plates as outer members, in 'Proceedings of the 42nd CIB W18 Meeting', Dübendorf (Switzerland). paper CIB-W18/42-7-2.
- Kreuzinger, H. and Mohr, B. (1994), Holz und Holzverbindungen unter nicht vorwiegend ruhenden Einwirkungen, Technical Report, Technical University of Munich. (in German).
- Krilov, A., Holmgren, A., Gref, R. and Öhman, L.-O. (1993), 'Effects of Gallic Acid on Metals: An FT-IR Study of Complexes Between Gallic Acid and Sawblade Steel', *Holzforschung* **47**(3), 239–246.
- Kuron, D. (2000), *Wasserstoff und Korrosion*, 2 edn, Irene Kuron. (in German).
- Laggner, T. M. (2016), Prüftechnische Untersuchung kombiniert beanspruchter selbstbohrender Holzschrauben, Master's thesis, Institute of Timber Engineering and Wood Technology, Graz University of Technology. (in German).
- Laggner, T. M., Flatscher, G. and Schickhofer, G. (2016), Combined loading of self-tapping screws, in 'Proceedings of the 14th World Conference on Timber Engineering WCTE2016', Vienna (Austria).
- Lam, F., Schulte-Wrede, M., Yao, C. and GU, J. J. (2008), Moment resistance bolted timber connections with perpendicular to grain reinforcements, in 'Proceedings of the 10th World Conference on Timber Engineering WCTE2008', Miyazaki (Japan).
- Landgrebe, R. (1993), Wasserstoffinduzierte Sprödbruchbildung bei hochfesten Schrauben aus Vergütungsstählen, PhD thesis, TU Darmstadt. (in German).
- Lantos, G. (1969), 'Load distribution in a row of fasteners subjected to lateral load.', *Wood Science* **1**(3), 129–136.
- Lathuillière, D., Bléron, L., Bocquet, J.-F., Varacca, F. and Dubois, F. (2014), Reinforcement of the support areas of glued laminated timber structures, in 'Proceedings of the 13th World Conference on Timber Engineering WCTE2014', Quebec City (Canada).
- Lathuillière, D., Bléron, L., Descamps, T. and Bocquet, J.-F. (2015), 'Reinforcement of dowel type connections', *Construction and Building Materials* **97**, 48–54.
- Lederer, W., Bader, T. K., Unger, G. and Eberhardsteiner, J. (2016), 'Influence of different types of reinforcements on the embedment behavior of steel dowels in wood', *European Journal of Wood and Wood Products* **74**, 793–807.
- Loss, C. and Davison, B. (2017), 'Innovative composite steel-timber floors with prefabricated modular components', *Engineering Structures* **132**, 695–713.
- Macherauch, E. and Zoch, H.-W. (2011), *Praktikum in Werkstoffkunde*, Vol. 11, Vieweg+Teubner. ISBN 978-3-8348-0343-6 (in German).
- Mahlknecht, U. (2011), Untersuchung von rechtwinklig zur Faser eingebrachten, axial beanspruchten Schrauben im Vollholz und Brettsperrholz, Master's thesis, Institute of Timber Engineering and Wood Technology, Graz University of Technology. (in German).

- Mahlknecht, U. and Brandner, R. (2013), focus_sts 3.1.2_1 - Untersuchungen des mechanischen Verhaltens von Schrauben-Verbindungsmittelgruppen in VH, BSH und BSP, Technical Report, holz.bau forschung gmbh, Graz University of Technology. (in German).
- Mahlknecht, U., Brandner, R. and Augustin, M. (2016), Block shear failure mode of axially loaded groups of screws, in 'Proceedings of the 14th World Conference on Timber Engineering WCTE2016', Vienna (Austria).
- Mahlknecht, U., Brandner, R., Ringhofer, A. and Schickhofer, G. (2014), *Resistance and Failure Modes of Axially Loaded Groups of Screws*, number 9 in 'RILEM Bookseries', Springer Dordrecht Heidelberg New York London, chapter 27, pp. 289–300.
- Maydl, P. and Tritthart, J. (2006), *Baustofflehre GL Vorlesung*, Graz University of Technology. (in German).
- McGill, R., Tukey, J. W. and Larsen, W. A. (1978), 'Variations of Box Plots', *The American Statistician* **32**(1).
- Meierhofer, A. U. (1993), Tests on timber concrete composite structural elements (TCCS), in 'Proceedings of the 26th CIB W18 Meeting', Athens, Georgia (USA). paper CIB-W18/26-7-5.
- Meierhofer, U. and Richter, K. (1988), 'Sortierung und Qualität von Bauholz - Teil 1: Holzeigenschaften und Sortierung', *Schweizer Ingenieur und Architekt* **106**, 810–815. (in German).
- Mestek, P. (2011), Punktgestützte Flächentragwerke aus Brettsperrholz (BSP) - Schubbemessung unter Berücksichtigung von Schubverstärkungen, PhD thesis, Technical University of Munich. (in German).
- Mestek, P. and Winter, S. (2011), 'Punktstützung von BrettsperrholzBrettsperrholz - Schubverstärkung mit Vollgewindeschrauben', *Bauingenieur* **86**, 529–540. (in German).
- Meyer, N. (2016), Zugbeanspruchte Verbindungen in Buchenfurnierschichtholz, in R. Görlacher, ed., 'Karlsruher Tage 2016 - Holzbau: Forschung für die Praxis', KIT Scientific Publishing, Karlsruhe, Karlsruhe (Germany), p. 135. (in German).
- Microsoft® Excel (2010). Part of Microsoft Office Professional Plus 2010, Version 14.0.xx (64-Bit).
- Min-Juan, H. and Hui-Fen, L. (2015), 'Comparison of glulam post-to-beam connections reinforced by two different dowel-type fasteners', *Construction and Building Materials* **99**, 99–108.
- Min-Juan, H., Zhao, Y. and Ma, R. (2016), 'Experimental investigation on lateral performance of pre-stressed tube bolted connection with high initial stiffness', *Advances in Structural Engineering* **19**(5), 762–776.
- Müller, U., Ringhofer, A., Brandner, R. and Schickhofer, G. (2015), 'Homogeneous shear stress field of wood in an Arcan shear test configuration measured by means of electronic speckle pattern interferometry: description of the test setup', *Wood Science and Technology* **49**(6), 1123–1136.
- Müller, U., Sretenovic, A., Gindl, W., Grabner, M., Wimmer, R. and Teischinger, A. (2004), 'Effect of macro- and micro-structural variability on the shear behaviour of softwood', *IAWA Journal* **25**(2), 231–243.

- Mohammad, M., Salenikovich, A. and Quenneville, P. (2006), Investigations on the Effectiveness of Self-tapping Screws in Reinforcing Bolted Timber Connections, *in* 'Proceedings of the 9th World Conference on Timber Engineering WCTE2006', Portland (USA).
- Naderer, E., Franke, S. and Franke, B. (2016), Numerical simulation of reinforced timber structures perpendicular to the grain, *in* 'Proceedings of the 14th World Conference on Timber Engineering WCTE2016', Vienna (Austria).
- Neuhaus, F.-H. (1981), Elastizitätszahlen von Fichtenholz in Abhängigkeit von der Holzfeuchtigkeit, PhD thesis, Institute for Structural Engineering, Ruhr-Universität Bochum. (in German).
- Nicholas, T. (2006), *High Cycle Fatigue - A Mechanics of Materials Perspective*, Elsevier Science. ISBN-13 978-0080446912.
- Nürnberger, U. (1995), *Korrosion und Korrosionsschutz im Bauwesen - Band 1: Grundlagen, Betonbau*, Bauverlag GmbH, Wiesbaden und Berlin. ISBN 3-7625-3199-4 (in German).
- Obermayr, I. (2014), Leistungsfähige Hirnholz-Schrauben- und Klebeverbindungen für schlanke Birken-Laubholzkonstruktionen, Master's thesis, Institute of Timber Engineering and Wood Technology, Graz University of Technology. (in German).
- OIB (2013), '3. Novelle zur Baustoffliste ÖE (Sonderheft Nr. 13)', *OIB aktuell* **13**, 1–170. (in German).
- OIB (2015a), 'Building Products List ÖE'. <http://www.oib.or.at/de/news/baustoffliste-oe> (2015-03-30)
- OIB (2015b), 'ETA Database'. <http://www.oib.or.at/de/datenbanken/eta-expert> (2015-03-26)
- OIB (2015c), 'OIB Guidelines'. <http://www.oib.or.at/en/oib-guidelines> (2015-03-25)
- Olsson, U. (2005), 'Confidence Intervals for the Mean of a Log-Normal Distribution', *Journal of Statistics Education* **13**(1), 1–8. www.amstat.org/publications/jse/v13n1/olsson.html
- ON B 1995-1-1 (2006), 'Eurocode 5 - Design of timber structures - Part 1-1: General - Common rules and rules for buildings - National specifications concerning ÖNORM EN 1995-1-1 and national comments'. (in German).
- ON B 1995-1-1 (2009), 'Eurocode 5 - Design of timber structures - Part 1-1: General - Common rules and rules for buildings - National specifications, national comments and national supplements concerning ÖNORM EN 1995-1-1'. (in German).
- ON B 1995-1-1 (2014), 'Eurocode 5 - Design of timber structures - Part 1-1: General - Common rules and rules for buildings - National specifications for the implementation of ÖNORM EN 1995-1-1, national comments and national supplements'. (in German).
- ON B 1995-1-1 (2015), 'Eurocode 5 - Design of timber structures - Part 1-1: General - Common rules and rules for buildings - National specifications for the implementation of ÖNORM EN 1995-1-1, national comments and national supplements'. (in German).
- ON B 4100-2 (1981), 'Wooden Structures; load bearing - timber structures'. (in German).
- ON B 4100-2 (1997), 'Timber structures - Design and construction'. (in German).
- ON B 4100-2 (2003a), 'Timber structures - Part 2: Design and construction'. (in German).
- ON B 4100-2 (2003b), 'Timber structures - Part 2: Design and construction'. (in German).

- ON B 4100-2 (2004), 'Timber structures - Part 2: Design and construction'. (in German).
- ON B 4100-2 (2008), 'Timber structures - Part 2: Design and construction (Corrigendum)'. (in German).
- ON EN 10016-1 (1995), 'Non-alloy steel rod for drawing and/or cold rolling - Part 1: General requirements'. (in German).
- ON EN 10016-2 (1995), 'Non-alloy steel rod for drawing and/or cold rolling - Part 2: Specific requirements for general purposes rod'. (in German).
- ON EN 10016-3 (1995), 'Non-alloy steel rod for drawing and/or cold rolling - Part 3: Specific requirements for rimmed and rimmed substitute low carbon steel rod'. (in German).
- ON EN 10016-4 (1995), 'Non-alloy steel rod for drawing and/or cold rolling - Part 4: Specific requirements for rod for special applications'. (in German).
- ON EN 10083-1 (2006), 'Steels for quenching and tempering - Part 1: General technical delivery conditions'. (in German).
- ON EN 10083-2 (2006), 'Steels for quenching and tempering - Part 2: Technical delivery conditions for non alloy steels'. (in German).
- ON EN 10088-1 (2005), 'Stainless steels - Part 1: List of stainless steels'. (in German).
- ON EN 10088-2 (2005), 'Stainless steels - Part 2: Technical delivery conditions for sheet/plate and strip of corrosion resisting steels for general purposes'. (in German).
- ON EN 10263-4 (2002), 'Steel rod, bars and wire for cold heading and cold extrusion - Part 4: Technical delivery conditions for steels for quenching and tempering'. (in German).
- ON EN 12512 (2001), 'Timber Structures - Test methods - Cyclic tests of joints made with mechanical fasteners'. (in German).
- ON EN 13183-1 (2004), 'Moisture content of a piece of sawn timber - Part 1: Determination by oven dry method'. (in German).
- ON EN 1382 (1999), 'Timber structures - Test methods - Withdrawal capacity of timber fasteners'. (in German).
- ON EN 1382 (2016), 'Timber structures - Test methods - Withdrawal capacity of timber fasteners'. (in German).
- ON EN 1383 (1999), 'Timber structures - Test methods - Pull through resistance of timber fasteners'. (in German).
- ON EN 14080 (2013), 'Timber structures - Glued laminated timber and glued solid timber - Requirements'. (in German).
- ON EN 14081-1 (2016), 'Timber structures - Strength graded structural timber with rectangular cross section - Part 1: General requirements'. (in German).
- ON EN 14358 (2007), 'Timber structures - Calculation of characteristic 5-percentile values and acceptance criteris for a sample'. (in German).
- ON EN 14592 (2009), 'Timber structures - Dowel-type fasteners - Requirements'. (in German).

- ON EN 14592 (2012), 'Timber structures - Dowel-type fasteners - Requirements'. (in German).
- ON EN 16351 (2015), 'Timber structures - Cross laminated timber - Requirements'. (in German).
- ON EN 1990 (2013), 'Eurocode - Basis of structural design (consolidated version)'. (in German).
- ON EN 1993-1-1 (2012), 'Eurocode 3 - Design of steel structures - Part 1-1: General - Common rules and rules for buildings (consolidated version)'. (in German).
- ON EN 1993-1-9 (2013), 'Eurocode 3 - Design of steel structures - Part 1-9: Fatigue (consolidated version)'. (in German).
- ON EN 1995-1-1 (2006), 'Eurocode 5 - Design of timber structures - Part 1-1: General - Common rules and rules for buildings'. (in German).
- ON EN 1995-1-1 (2009), 'Eurocode 5 - Design of timber structures - Part 1-1: General - Common rules and rules for buildings (consolidated version)'. (in German).
- ON EN 1995-1-1 (2014), 'Eurocode 5 - Design of timber structures - Part 1-1: General - Common rules and rules for buildings (consolidated version)'. (in German).
- ON EN 1995-1-1 (2015), 'Eurocode 5 - Design of timber structures - Part 1-1: General - Common rules and rules for buildings (consolidated version)'. (in German).
- ON EN 1995-2 (2006), 'Eurocode 5 - Design of timber structures - Part 2: Bridges'. (in German).
- ON EN 1998-1 (2013), 'Eurocode 8 - Design of structures for earthquake resistance - Part 1: General rules, seismic actions and rules for buildings (consolidated version)'. (in German).
- ON EN 26891 (1991), 'Timber structures - Joints made with mechanical fasteners - General principles for the determination of strength and deformation characteristics'. (in German).
- ON EN 28970 (1991), 'Timber structures - Testing of joints made with mechanical fasteners - Requirements for wood density (ISO 8970:1989)'. (in German).
- ON EN 338 (2016), 'Structural timber - Strength classes'. (in German).
- ON EN 384 (2010), 'Structural timber - Determination of characteristic values of mechanical properties and density'. (in German).
- ON EN 408 (2010), 'Timber structures - Structural timber and glued laminated timber - Determination of some physical and mechanical properties'. (in German).
- ON EN 409 (2009), 'Timber structures - Test methods - Determination of the yield moment of dowel type fasteners'. (in German).
- ON EN ISO 10666 (2000), 'Drilling screws with tapping screw thread - Mechanical and functional properties'. (in German).
- ON EN ISO 18265 (2004), 'Metallic materials - Conversion of hardness values'. (in German).
- ON EN ISO 6507-1 (2004), 'Metallic materials - Vickers hardness test - Part 1: Test method'. (in German).

- ON ENV 1995-1-1 (1992), 'Eurocode 5 - Design of timber structures - Part 1-1: General rules and rules for buildings'. (in German).
- ON ENV 1995-1-1 (1995), 'Eurocode 5 - Design of timber structures - Part 1-1: General rules and rules for buildings'. (in German).
- ONR 21990 (2008), 'Eurocodes - Application in Austria'. (in German).
- Oriani, R. A. (1972), 'A mechanistic theory of hydrogen embrittlement of steels', *Berichte der Bunsengesellschaft für physikalische Chemie* **76**, 848–857.
- Oriani, R. A. (1993), The Physical and Metallurgical Aspects of Hydrogen in Metals, in 'ICCF4, Fourth International Conference on Cold Fusion', Lahaina, Maui (USA).
- Orth, H. (1974), *Korrosion und Korrosionsschutz*, Wissenschaftliche Verlagsgesellschaft mbh. ISBN 3-8047-0455-7 (in German).
- Oudjene, M., Tran, V.-D., Meghlat, E.-M. and Ait-Aider, H. (2016), Numerical models for self-tapping screws as reinforcement of timber structures and joints, in 'Proceedings of the 14th World Conference on Timber Engineering WCTE2016', Vienna (Austria).
- Paatsch, W. (2011), 'Wasserstoffbestimmung und Wasserstoffversprödung - Sinn und Nutzen', *Galvanotechnik* **1**, 48–55. (in German).
- Packman, D. F. (1960), 'The Acidity of Wood', *Holzforschung* **14**(6), 178–183.
- Persson, K. (2000), Micromechanical modelling of wood and fibre properties, PhD thesis, Lund University.
- Petch, N. J. and Stables, P. (1952), 'Delayed Fracture of Metals under Static Load', *Nature* **169**, 842–843.
- Piazza, M., Polastri, A. and Tomasi, R. (2011), 'Ductility of timber joints under static and cyclic loads', *Structures and Buildings* **164**(582), 79–90.
- Pirnbacher, G., Brandner, R. and Schickhofer, G. (2009), Base parameters of self-tapping screws, in 'Proceedings of the 42nd CIB W18 Meeting', Dübendorf (Switzerland). paper CIB-W18/42-7-1.
- Pirnbacher, G. and Schickhofer, G. (2007), Schrauben im Vergleich - eine empirische Betrachtung, in '6. Grazer Holzbau-Fachtagung "6. GraHFT'07"', Graz (Austria). (in German).
- Pirnbacher, G. and Schickhofer, G. (2012), Zeitabhängige Entwicklung der Traglast und des Kriechverhaltens von axial beanspruchten, selbstbohrenden Holzschrauben, Technical Report, holz.bau forschung gmbh, Graz University of Technology. (in German).
- Plieschounig, S. (2010), Ausziehverhalten axial beanspruchter Schraubengruppen, Master's thesis, Institute of Timber Engineering and Wood Technology, Graz University of Technology. (in German).
- Pöll, M. (2017), Entwicklung einer Hartlaubholzschraube: Optimierung der Gewindegeometrie für die Beanspruchung auf Herausziehen, Master's thesis, Institute of Timber Engineering and Wood Technology, Graz University of Technology. (in German).
- Plüss, Y. (2014), Prüftechnische Ermittlung des Tragverhaltens von Schraubengruppen in der BSP-Schmalfläche, Master's thesis, Institute of Timber Engineering and Wood Technology, Graz University of Technology. (in German).

- Plüss, Y. and Brandner, R. (2014), Untersuchungen zum Tragverhalten von axial beanspruchten Schraubengruppen in der Schmalseite von Brettsperrholz (BSP), in '20. Internationales Holzbau-Forum IHF 2014', Garmisch-Partenkirchen (Germany). (in German).
- Pohl, M. and Kühn, S. (2010), 'Spannungsrissskorrosion hochfester Stähle', *MP Materials Testing* **52**, 52–56. (in German).
- Polastri, A. and Angeli, A. (2014), An innovative connection system for CLT structures - Experimental - Numerical Analysis, in 'Proceedings of the 13th World Conference on Timber Engineering WCTE2014', Quebec City (Canada).
- Popovski, M. and Karacabeyli, E. (2011), Seismic performance of cross-laminated wood panels, in 'Proceedings of the 44th CIB W18 Meeting', Vancouver (Canada). paper CIB-W18/44-15-7.
- Prat-Vincent, F., Rogers, C. and Salenikovich, A. (2010), Evaluation of the performance of joist-to-header self tapping screw connections, in 'Proceedings of the 11th World Conference on Timber Engineering WCTE2010', Riva del Garda (Italy).
- prEN 1995-1-1 (1999), 'Eurocode 5 - Design of timber structures - Part 1-1: General rules and rules for buildings (FIRST DRAFT)'.
- Priestley, M. J. N., Calvi, G. M. and Kowalsky, M. J. (2007), *Displacement-Based Seismic Design of Structures*, IUSS Press.
- prSIA 118/265 (2015), 'General Conditions for Timber structures - Articles of Agreement to SIA 265'.
- R Core Team (2016), 'R: a language and environment for statistical computing'. Version: 3.0.2.
- Radaj, D. and Vormwald, M. (2007), *Ermüdungsfestigkeit - Grundlagen für Ingenieure*, Springer Berlin Heidelberg New York. ISBN 978-3-540-71458-3 (in German).
- Rammer, D. R. and McLean, D. I. (1996), Recent reasearch on the shear strength of wood beams, in 'Proceedings of the International Wood Engineering Conference', New Orleans (USA), pp. 2/96–2/103.
- Rammer, D. R. and Zelinka, S. L. (2008), 'Analytical Determination of the Surface Area of a Threaded Fastener', *Journal of Testing and Evaluation* **36**(1), 80–88.
- Rammer, D. R. and Zelinka, S. L. (2011), 'Method and apparatus for determining the surface area of a threaded fastener'. United States Patent No. US 8041150 B2.
- Ransom, J. T. and Mehl, R. F. (1949), 'The Statistical Nature of the Endurance Limit', *Metals Trans.* **185**, 364–365.
- Rückert, J. (1986), 'Korrosionsverhalten von Metallen in Verbindung mit Holz', *Werkstoffe und Korrosion* **37**, 336–339. (in German).
- Reichelt, B. (2012), Einfluss der Sperrwirkung auf den Auszieh widerstand selbstbohrender Holzschrauben - Eine vergleichende Betrachtung zwischen BSP und BSH, Master's thesis, Institute of Timber Engineering and Wood Technology, Graz University of Technology. (in German).
- Reif, S. (2014), Untersuchung der Wasserstoff-Versprödung von verzinkten, hochfesten Holzschrauben durch Korrosion in feuchtem Holz, Bachelor's thesis, Institute of Material Science, Joining and Forming, Graz University of Technology. (in German).

RFEM 5 (2012), 'RFEM'. Version: 5.06.1103.

Ringhofer, A. (2016), Stiffness Properties of Axially Loaded Self-Tapping Screws, Short Term Scientific Mission (STSM) Report of COST Action FP1402, Institute of Timber Engineering and Wood Technology, Graz University of Technology.

Ringhofer, A., Brandner, R., Flatscher, G. and Schickhofer, G. (2015a), 'Axial beanspruchte Holzschrauben in Vollholz, Brettschichtholz und Brettsperrholz', *Bautechnik* **92**(11), 770–782. (in German).

Ringhofer, A., Brandner, R., Grabner, M. and Schickhofer, G. (2014a), Die Ausziehfestigkeit selbstbohrender Holzschrauben in geschichteten Holzprodukten, in 'Forschungskolloquium, Holzbau Forschung und Praxis', Stuttgart (Germany). (in German).

Ringhofer, A., Brandner, R. and Schickhofer, G. (2014b), 'Entwicklung einer optimierten Schraubengeometrie für hochbeanspruchte Stahl-Holz-Verbindungen', *Bautechnik* **91**(1), 31–37. (in German).

Ringhofer, A., Brandner, R. and Schickhofer, G. (2015b), 'Withdrawal resistance of self-tapping screws in unidirectional and orthogonal layered timber products', *Materials and Structures* **48**(5), 1435–1447.

Ringhofer, A., Brandner, R. and Schickhofer, G. (2015c), A Universal Approach for Withdrawal Properties of Self-Tapping Screws in Solid Timber and Laminated Timber Products, in 'Proceedings of the 2nd INTER Meeting', Sibenik (Croatia). paper INTER/48-7-1.

Ringhofer, A., Ehrhart, T., Brandner, R. and Schickhofer, G. (2013), Prüftechnische Ermittlung weiterer Einflussparameter auf das Tragverhalten der Einzelschraube in der BSP-Seitenfläche, Technical Report, holz.bau forschung gmbh, Graz University of Technology. (in German).

Ringhofer, A., Grabner, M., Brandner, R. and Schickhofer, G. (2013a), Prüftechnische Ermittlung des Tragverhaltens der Einzelschraube in der BSP-Schmalfläche, Technical Report, holz.bau forschung gmbh, Graz University of Technology. (in German).

Ringhofer, A., Grabner, M., Silva, C. V., Branco, J. and Schickhofer, G. (2014c), 'The influence of moisture content variation on the withdrawal capacity of self-tapping screws', *Holztechnologie* **55**(3), 33–40.

Ringhofer, A. and Schickhofer, G. (2014a), Influencing Parameters on the Experimental Determination of the Withdrawal Capacity of Self-Tapping Screws, in 'Proceedings of the 13th World Conference on Timber Engineering WCTE2014', Quebec City (Canada).

Ringhofer, A. and Schickhofer, G. (2014b), *Investigations Concerning the Force Distribution along Axially Loaded Self-tapping Screws*, number 9 in 'RILEM Bookseries', Springer Dordrecht Heidelberg New York London, chapter 19, pp. 201–210.

Robinson, R. A. and Stokes, R. H. (1959), *Electrolyte Solutions*, 2 edn, Academic Press New York.

Roos, E. and Maile, K. (2011), *Werkstoffkunde für Ingenieure*, 4 edn, Springer Heidelberg Dordrecht London New York. ISBN 978-3-642-17463-6 (in German).

Rosowsky, D. V. and Reinhold, T. A. (1999), 'Rate-of-Load and Duration-of-Load Effects for Wood Fasteners', *Journal of Structural Engineering* **125**, 719–724.

- Russenberger Prüfmaschinen AG (2012), *RUMUL TESTRONIC - The original with the dynamic drive RUMUL MAGNODYN*, Russenberger Prüfmaschinen AG.
- Schäfer, H. J. (2008), Auswertealgorithmus auf der Basis einer Modifikation des Goniometrischen Modells zur stetigen Beschreibung der Wöhlerkurve vom Low-Cycle-Fatigue- bis in den Ultra-High-Cycle-Fatigue-Bereich, PhD thesis, RWTH Aachen University. (in German).
- Schickhofer, G. (2006a), *Holzbau - Der Roh- und Werkstoff Holz*, Graz University of Technology. (in German).
- Schickhofer, G. (2006b), *Holzbau - Nachweisführung für Konstruktionen aus Holz*, Graz University of Technology. (in German).
- Schickhofer, G. and Augustin, M. (2001), EU - Project INTELLIWOOD - Final Report, Technical Report, Institute of Timber Engineering and Wood Technology, Graz University of Technology.
- Schickhofer, G. and Obermayr, B. (1998), Development of an optimised test configuration to determine shear strength of glued laminated timber, in 'Proceedings of the 31st CIB W18 Meeting', Savolinnä (Finland). paper CIB-W18/31-21-1.
- Schmid, M. (2002), Anwendung der Bruchmechanik auf Verbindungen in Holz, PhD thesis, Karlsruhe Institute of Technology. (in German).
- Schmid Schrauben Hainfeld GmbH (2015), 'Components of the partially threaded screw StarDrive GPR'. http://www.schrauben.at/schraubenwelten/stardrive/stardrive_gpr (2017-02-17)
- Schoenmakers, J. C. M. (2010), Fracture and failure mechanisms in timber loaded perpendicular to the grain by mechanical connections, PhD thesis, Eindhoven University of Technology.
- Schütz, W. (1993), 'Zur Geschichte der Schwingfestigkeit', *Mat.-wiss. u. Werkstofftech.* **24**, 203–232. (in German).
- SIA (2015), 'comments to Eurocode (Swisscode) application in Switzerland'. (in German). <http://www.sia.ch/de/dienstleistungen/sia-norm/normenwerk/internationale-normen> (2015-03-19)
- SIA 118/265 (2004), 'General Conditions for Timber structures'. (in German).
- SIA 164 (1992), 'Timber structures'. (in German).
- SIA 265 (2003), 'Timber structures'. (in German).
- SIA 265 (2012), 'Timber structures'. (in German).
- SIA 265-C1 (2008), 'Timber structures (Corrigenda)'. (in German).
- SIA 265/1 (2003), 'Timber structures - Supplementary specifications'. (in German).
- SIA 265/1 (2009), 'Timber structures - Supplementary specifications'. (in German).
- SIA 265/1-C1 (2012), 'Timber structures - Supplementary specifications - Corrigenda C1'. (in German).
- Silva, C. V., Branco, J., Ringhofer, A., Lourenco, P. and Schickhofer, G. (2016), 'The influences of moisture content variation, number and width of gaps on the withdrawal resistance of self tapping screws inserted in cross laminated timber', *Construction and Building Materials* **125**, 1205–1215.

- Silva, C. V., Ringhofer, A., Branco, J., Lourenco, P. and Schickhofer, G. (2014), Influence of moisture content and gaps on the withdrawal resistance of self tapping screws in CLT, in '9º Congresso Nacional de Mecânica Experimental', Aveiro (Portugal).
- Silverman, D. C. (2003), Aqueous Corrosion, in S. D. Cramer and B. S. Covino, eds, 'Corrosion: Fundamentals, Testing, and Protection', Vol. 13A, ASM International, pp. 190–195.
- Smith, R. L. and Sandland, G. E. (1922), 'An Accurate Method of Determining the Hardness of Metals, with Particular Reference to Those of a High Degree of Hardness', *Proceedings of the Institution of Mechanical Engineers* **1**, 623–641.
- SN EN 14592+A1 (2012), 'Timber structures - Dowel-type fasteners - Requirements'. (in German).
- SN EN 1995-1-1/NA (2014), 'Eurocode 5: Design of timber structures; Part 1-1: General - Common rules and rules for buildings - National annex NA to SN EN 1995-1-1:2004'. (in German).
- Stadlober, E. and Schauer, J. (2012), *Statistik - Bakkalaureat Techn. Mathematik*, 6 edn, Institute of Statistics, Graz University of Technology. (in German).
- Stamatopoulos, H. and Malo, K. A. (2015), 'Withdrawal capacity of threaded rods embedded in timber elements', *Construction and Building Materials* **94**, 387–397.
- Stamatopoulos, H. and Malo, K. A. (2016), 'Withdrawal stiffness of threaded rods embedded in timber elements', *Construction and Building Materials* **116**, 263–272.
- Steilner, M. (2014), Querdruckvorspannung von Holz mit Vollgewindeschrauben - Relaxation und Anwendung, in 'Forschungskolloquium, Holzbau Forschung und Praxis', Stuttgart (Germany). (in German).
- Steilner, M. and Blaß, H. J. (2010), Selbstbohrende Holzschrauben mit veränderlicher Gewindesteigung, in 'Doktorandenkolloquium, Holzbau Forschung und Praxis', Stuttgart (Germany). (in German).
- Steilner, M. and Blaß, H. J. (2014), *A Method to Determine the Plastic Bending Angle of Dowel-Type Fasteners*, number 9 in 'RILEM Bookseries', Springer Dordrecht Heidelberg New York London, chapter 28, pp. 304–306.
- Stellwag, B. and Kaesche, H. (1982), 'Kinetik der wasserstoffinduzierten Spannungsrißkorrosion - Teil 1: Wesentliche Einflußgrößen des Bruchvorgangs im Hinblick auf hochfeste Stähle', *Werkstoffe und Korrosion* **33**, 274–280. (in German).
- Strassmann, B. (2005), 'Die Kunst des Anziehens', *Die Zeit* (14), 1–3. (in German).
- Swiss Federal Authorities (2010a), 'Swiss Federal Construction Products Law'. (in German).
- Swiss Federal Authorities (2010b), 'Swiss Federal Law on Technical Barriers to Trade'. (in German).
- Swiss Federal Authorities (2014a), 'Swiss Federal Construction Products Law'. (in German).
- Swiss Federal Authorities (2014b), 'Swiss Federal Construction Products Regulation'. (in German).
- Tannert, T. (2016), 'Improved performance of reinforced rounded dovetail joints', *Construction and Building Materials* **118**, 262–267.
- Tannert, T. and Lam, F. (2009), 'Self-tapping screws as reinforcement for rounded dovetail connections', *Structural control and health monitoring* **16**, 374–384.

- Toblier, L. (2014), Untersuchung der wasserstoffinduzierten Versprödung von verzinkten, hochfesten Holzschrauben, Bachelor's thesis, Institute of Material Science, Joining and Forming, Graz University of Technology. (in German).
- Toblier, L. (2016), Wasserstoffversprödung von Holzschrauben, Technical Report, Institute of Timber Engineering and Wood Technology and Institute of Material Science, Joining and Forming, Graz University of Technology. (in German).
- Tomasi, R., Crosatti, A. and Piazza, M. (2010), 'Theoretical and experimental analysis of timber-to-timber joints connected with inclined screws', *Construction and Building Materials* **24**, 1560–1571.
- Tomasi, R., Piazza, M., Angeli, A. and Mores, M. (2006), A new ductile approach design of joints assembled with screw connectors, in 'Proceedings of the 9th World Conference on Timber Engineering WCTE2006', Portland (USA).
- Tran, T., Brown, B., Nestic, S. and Tribollet, B. (2013), Investigation of the Mechanism for Acetic Acid Corrosion of Mild Steel, in 'NACE International Corrosion Conference & Expo', Orlando (USA), pp. 1–12.
- Trautz, M. and Koj, C. (2008), 'Mit Schrauben Bewehren', *Bautechnik* **85**(3), 190–196. (in German).
- Trautz, M. and Koj, C. (2009), 'Mit Schrauben Bewehren - Neue Ergebnisse', *Bautechnik* **86**(4), 228–238. (in German).
- Troiano, R. (1960), 'The role of hydrogen and other interstitials in the mechanical behaviour of metals', *Trans. ASM* **52**, 54–80.
- Uibel, T. (2012), Spaltverhalten von Holz beim Eindrehen von selbstbohrenden Holzschrauben, PhD thesis, Karlsruhe Institute of Technology. (in German).
- Uibel, T. and Blaß, H. J. (2006), Load carrying capacity of joints with dowel type fasteners in solid wood panels, in 'Proceedings of the 39th CIB W18 Meeting', Florence (Italy). paper CIB-W18/39-7-5.
- Uibel, T. and Blaß, H. J. (2007), Edge joints with dowel type fasteners in cross laminated timber, in 'Proceedings of the 40th CIB W18 Meeting', Bled (Slovenia). paper CIB-W18/40-7-2.
- Vangel, M. G. (1996), 'Confidence Intervals for a Normal Coefficient of Variation', *The American Statistician* **50**, 21–26.
- Volkersen, O. (1953), 'Die Schubkraftverteilung in Leim-, Niet- und Bolzenverbindungen', *Energie und Technik* pp. 68–154. (in German).
- VSM 12 800 (1942), 'Halbrundholzschrauben'. (in German).
- VSM 12 801 (1942), 'Senkholzschrauben'. (in German).
- VSM 12 802 (1942), 'Linsensenkholzschrauben'. (in German).
- VSM 12 803 (1942), 'Vierkantholzschrauben'. (in German).
- Wagenführ, R. (2007), *Holzatlas*, 6 edn, Carl Hanser Verlag München. (in German).

- Wallner, B. (2012), Versuchstechnische Evaluierung feuchteinduzierter Kräfte in Brettschichtholz verursacht durch das Einbringen von Schraubstangen, Master's thesis, Institute of Timber Engineering and Wood Technology, Graz University of Technology. (in German).
- Wang, M., Song, X., Gu, X., Zhang, Y. and Luo, L. (2015), 'Rotational Behavior of Bolted Beam-to-Column Connections with Locally Cross-Laminated Glulam', *J. Struct. Eng.* **141**(4), 1–7.
- Weißbach, W. (2012), *Werkstoffkunde - Strukturen, Eigenschaften, Prüfung*, 18 edn, Vieweg+Teubner. ISBN 978-3-8348-1587-3 (in German).
- Werner, H. (1993), Tragfähigkeit von Holz-Verbindungen mit stiftförmigen Verbindungsmitteln unter Berücksichtigung streuender Einflussgrößen, Technical Report, Karlsruhe Institute of Technology. (in German).
- Werther, N., Hofmann, V., Gräfe, M. and Winter, S. (2014), Fire resistance of primary beam - secondary beam connections in timber structures, in 'Proceedings of the 13th World Conference on Timber Engineering WCTE2014'.
- Wöhler, A. (1870), 'Über die Festigkeitsversuche mit Eisen und Stahl', *Zeitschrift für Bauwesen* **20**, 73–106. (in German).
- Winkelmann, H., Badisch, E., Roy, M. and Danninger, H. (2009), 'Corrosion mechanisms in the wood industry, especially caused by tannins', *Materials and Corrosion* **60**(1), 40–48.
- Wolfram Mathematica 10 (2014), 'Mathematica'. Version: 10.0.2.0.
- Wolfthaler, F. (2015), Entwicklung einer Messschraube und Anwendung auf das Bauwerksmonitoring und die Prüftechnik, Master's thesis, Institute of Timber Engineering and Wood Technology, Graz University of Technology. (in German).
- Wolfthaler, F. and Augustin, M. (2016), Development of a measurement screw and application for laboratory tests and building monitoring, in 'Proceedings of the 14th World Conference on Timber Engineering WCTE2016', Vienna (Austria).
- Wood, L. W. (1960), Relation of strength of wood to duration of load, Technical Report 1916, Forest Products Laboratory, Madison, Wisconsin.
- Wrzesniak, D. and Fragiaco, M. (2016), 'Cyclic behaviour of glulam shear walls with bolted connections', *European Journal of Wood and Wood Products* **74**, 393–405.
- Wu, Y., Song, X., Jiang, Y., Gu, X. and Wang, M. (2016), Experimental and numerical study on longitudinally cracked wood beams retrofitted by self-tapping screws, in 'Proceedings of the 14th World Conference on Timber Engineering WCTE2016', Vienna (Austria).
- www.metallograf.de (2015), 'Material number 1.5525 - 20MnB4'. <http://www.oib.or.at/en/oib-guidelines> (2015-03-25)
- Yagi, H., Shioya, S. and Tomiyoshi, E. (2016), Innovative hybrid timber structures in Japan: bending behaviour of T-shaped CLT-to-hybrid timber composite beam, in 'Proceedings of the 14th World Conference on Timber Engineering WCTE2016', Vienna (Austria).
- Yeh, M.-C., Lin, Y.-L. and Huang, G.-P. (2014), 'Investigation of the structural performance of glulam beam connections using self-tapping screws', *Journal of Wood Science* **60**, 39–48.

- Z-9.1-175 (1986), Adolf Würth GmbH & Co. KG: Würth ECOFAST-Holzschrauben und Würth WÜPOFAST-Holzschrauben als Holzverbindungsmittel, National Technical Approval, DIBt. (in German).
- Z-9.1-251 (2004), Industriegruppe Gipskartonplatten IGG im Bundesverband der Gips- und Gipsbauplattenindustrie e. V.: Schnellbauschrauben Typ TN, FN, Universalschraube FN und Blackstar als Verbindungsmittel von Grund- und Traglattung bei Unterdecken und Deckenbekleidungen und als Verankerungselemente in Holz für Aufhänger und Deckenbekleidungen, National Technical Approval, DIBt. (in German).
- Z-9.1-279 (2005), SFS intec GmbH & Co. KG: Doppelgewindeschrauben SFS TWIN UD für Dämmsysteme, National Technical Approval, DIBt. (in German).
- Z-9.1-342 (2010), SFS intec GmbH FasteningSystems: SFS-Verbundschrauben VB-48-7,5 als Verbindungsmittel für das Holz-Beton-Verbundsystem, National Technical Approval, DIBt. (in German).
- Z-9.1-427 (2000), Bierbach-Befestigungstechnik GmbH & Co. KG: BiRA-IngBAU-Schrauben als Holzverbindungsmittel, National Technical Approval, DIBt. (in German).
- Z-9.1-449 (2003), ABC Verbindungstechnik GmbH & Co. KG: SPAX-S Schrauben als Holzverbindungsmittel, National Technical Approval, DIBt. (in German).
- Z-9.1-453 (2000), Ludwig Hettich GmbH & Co.: HECO-fix-plus-Schrauben und HECO-Topix-Schrauben als Holzverbindungsmittel, National Technical Approval, DIBt. (in German).
- Z-9.1-472 (2006), SFS intec GmbH & Co. KG: SFS Befestiger WT-T-6,5, WT-T-8,2 und WR-T-8,9 als Holzverbindungsmittel, National Technical Approval, DIBt. (in German).
- Z-9.1-519 (2003), ABC Verbindungstechnik GmbH & Co. KG: SPAX-S Schrauben mit Vollgewinde als Holzverbindungsmittel, National Technical Approval, DIBt. (in German).
- Z-9.1-550 (2007), SIMPSON STRONG-TIE GmbH: ET Passverbinder als Holzverbindungsmittel, National Technical Approval, DIBt. (in German).
- Z-9.1-777 (2010), SFS intec GmbH: Gewindestangen mit Holzgewinde als Holzverbindungsmittel, National Technical Approval, DIBt. (in German).
- Z-9.1-845 (2014), Schmid Schrauben Hainfeld GmbH: Star-Drive und RAPID Schrauben als Verbindungsmittel für das Schmid Schrauben Holz-Beton-Verbundsystem, National Technical Approval, DIBt. (in German).
- Zapffe, C. A. and Sims, C. E. (1941), 'Hydrogen embrittlement, internal stress and defects in steels', *Trans. AIME* **145**, 225–259.
- Zelinka, S. L. (2014), Corrosion of Metals in Wood Products, in M. Aliofkhaezrai, ed., 'Developments in Corrosion Protection', InTech, chapter 23, pp. 567–592.
- Zelinka, S. L., Derome, D. and Glass, S. V. (2011), 'Combining hygrothermal and corrosion models to predict corrosion of metal fasteners embedded in wood', *Building and Environment* **46**, 2060–2068.
- Zelinka, S. L., Glass, S. V. and Donald (2008), 'A percolation model for electrical conduction in wood with implications for wood-water relations', *Wood and Fiber Science* **40**(4), 544–552.

- Zelinka, S. L. and Rammer, D. R. (2012), ‘Modeling the Effect of Nail Corrosion on the Lateral Strength of Joints’, *Forest Products Journal* **62**(3), 160–166.
- Zelinka, S. L., Sichel, R. J. and Stone, D. S. (2010), ‘Exposure testing of fasteners in preservative treated wood: Gravimetric corrosion rates and corrosion product analyses’, *Corrosion Science* **52**, 3943–3948.
- Zelinka, S. L. and Stone, D. S. (2011), ‘The effect of tannins and pH on the corrosion of steel in wood extracts’, *Materials and Corrosion* **62**(8), 739–744.
- Zhang, C., Chang, W.-S. and Harris, R. (2016), Investigation of thread configuration of self-tapping screws as reinforcement for dowel-type connection, in ‘Proceedings of the 14th World Conference on Timber Engineering WCTE2016’, Vienna (Austria).
- Zingerle, P., Maderebner, R. and Flach, M. (2016), System solutions for point-supported wooden flat slabs, in ‘Proceedings of the 14th World Conference on Timber Engineering WCTE2016’, Vienna (Austria).

ANNEX B ADDITIONAL INFORMATION

B-1 Supplementary material to chapter 2

Table B.1: Overview of NTAs analysed in section 2-2.5

number	issue date	expiration date	notified body	number	issue date	expiration date	notified body
Z-9.1-175	16.05.1986	30.04.1991	DIBt	Z-9.1-337	28.04.1997	30.04.2002	DIBt
Z-9.1-175	19.08.1992	31.07.1997	DIBt	Z-9.1-337	15.01.1999	30.04.2002	DIBt
Z-9.1-175	14.05.1998	30.04.2003	DIBt	Z-9.1-337	17.11.2000	30.04.2002	DIBt
Z-9.1-235	24.02.1991	31.01.1996	DIBt	Z-9.1-337	10.04.2002	30.04.2007	DIBt
Z-9.1-235	27.06.1997	31.07.2002	DIBt	Z-9.1-337	30.08.2002	30.04.2007	DIBt
Z-9.1-235	02.03.1999	31.07.2002	DIBt	Z-9.1-337	31.01.2003	30.04.2007	DIBt
Z-9.1-235	07.08.2001	31.07.2002	DIBt	Z-9.1-337	10.12.2004	30.04.2007	DIBt
Z-9.1-235	23.08.2002	31.07.2007	DIBt	Z-9.1-337	30.09.2005	30.04.2007	DIBt
Z-9.1-235	17.07.2003	31.07.2007	DIBt	Z-9.1-337	11.05.2007	30.04.2012	DIBt
Z-9.1-235	07.07.2005	31.07.2007	DIBt	Z-9.1-342	17.07.1998	30.06.2003	DIBt
Z-9.1-235	06.07.2007	31.07.2012	DIBt	Z-9.1-342	13.10.2003	30.06.2008	DIBt
Z-9.1-235	11.03.2011	31.07.2012	DIBt	Z-9.1-342	06.05.2010	31.05.2015	DIBt
Z-9.1-235	17.09.2012	01.08.2017	DIBt	Z-9.1-361	16.07.1998	30.06.2003	DIBt
Z-9.1-251	16.01.1992	31.12.1997	DIBt	Z-9.1-361	07.08.2001	30.06.2003	DIBt
Z-9.1-251	14.05.1998	30.04.2003	DIBt	Z-9.1-361	17.11.2003	30.06.2008	DIBt
Z-9.1-251	28.05.2004	31.05.2009	DIBt	Z-9.1-361	23.09.2004	30.06.2008	DIBt
Z-9.1-279	22.06.1995	30.06.2000	DIBt	Z-9.1-361	19.07.2008	30.06.2013	DIBt
Z-9.1-279	02.07.1996	30.06.2000	DIBt	Z-9.1-375	10.12.1998	30.11.2003	DIBt
Z-9.1-279	26.11.1996	30.06.2000	DIBt	Z-9.1-375	23.10.2003	30.11.2008	DIBt
Z-9.1-279	21.04.1998	30.06.2000	DIBt	Z-9.1-375	21.02.2009	28.02.2014	DIBt
Z-9.1-279	16.06.2000	30.06.2005	DIBt	Z-9.1-386	20.05.1998	31.05.2003	DIBt
Z-9.1-279	26.01.2004	30.05.2005	DIBt	Z-9.1-386	30.09.1998	31.05.2003	DIBt
Z-9.1-279	27.06.2005	30.06.2010	DIBt	Z-9.1-386	16.06.2003	31.05.2008	DIBt
Z-9.1-279	24.09.2008	30.06.2010	DIBt	Z-9.1-396	15.01.1999	30.01.2004	DIBt
Z-9.1-279	10.06.2010	30.06.2015	DIBt	Z-9.1-406	10.06.1997	31.05.2002	DIBt
Z-9.1-279	27.11.2012	30.06.2015	DIBt	Z-9.1-407	07.03.2001	31.03.2006	DIBt
Z-9.1-279	30.08.2013	30.06.2015	DIBt	Z-9.1-407	10.05.2006	31.03.2011	DIBt

Table B.2: Overview of NTAs analysed in section 2-2.5 (continued)

number	issue date	expiration date	notified body	number	issue date	expiration date	notified body
Z-9.1-407	05.10.2011	31.03.2012	DIBt	Z-9.1-453	23.04.2009	31.08.2009	DIBt
Z-9.1-426	15.01.1999	14.01.2004	DIBt	Z-9.1-453	30.09.2009	31.08.2014	DIBt
Z-9.1-426	07.08.2001	14.01.2004	DIBt	Z-9.1-471	06.03.2000	31.05.2005	DIBt
Z-9.1-426	23.09.2004	30.09.2009	DIBt	Z-9.1-471	10.04.2002	31.05.2005	DIBt
Z-9.1-426	09.10.2009	30.09.2014	DIBt	Z-9.1-471	10.12.2004	31.12.2009	DIBt
Z-9.1-427	06.09.2000	31.08.2005	DIBt	Z-9.1-471	29.01.2010	31.01.2015	DIBt
Z-9.1-427	10.07.2003	31.08.2005	DIBt	Z-9.1-472	22.05.2000	31.05.2005	DIBt
Z-9.1-427	11.01.2006	31.08.2010	DIBt	Z-9.1-472	30.03.2006	31.03.2011	DIBt
Z-9.1-435	17.12.1999	16.12.2004	DIBt	Z-9.1-472	21.03.2011	01.04.2016	DIBt
Z-9.1-435	23.08.2000	16.12.2004	DIBt	Z-9.1-484	19.01.2001	31.01.2006	DIBt
Z-9.1-435	11.07.2002	16.12.2004	DIBt	Z-9.1-484	09.11.2005	31.01.2011	DIBt
Z-9.1-435	02.02.2005	16.12.2009	DIBt	Z-9.1-484	10.03.2011	01.02.2016	DIBt
Z-9.1-435	16.12.2009	31.12.2014	DIBt	Z-9.1-497	16.01.2002	31.01.2007	DIBt
Z-9.1-435	31.12.2014	31.12.2019	DIBt	Z-9.1-497	01.02.2007	31.12.2008	DIBt
Z-9.1-445	23.08.2000	31.08.2005	DIBt	Z-9.1-497	24.01.2012	20.01.2017	DIBt
Z-9.1-445	13.10.2006	31.10.2011	DIBt	Z-9.1-509	17.11.2000	30.11.2005	DIBt
Z-9.1-445	16.03.2012	16.03.2017	DIBt	Z-9.1-509	10.04.2002	30.11.2005	DIBt
Z-9.1-445	27.02.2013	16.03.2017	DIBt	Z-9.1-509	21.06.2006	31.12.2011	DIBt
Z-9.1-445	18.07.2013	16.03.2017	DIBt	Z-9.1-509	29.05.2012	29.05.2014	DIBt
Z-9.1-449	02.03.1999	31.07.2002	DIBt	Z-9.1-509	09.07.2014	29.05.2019	DIBt
Z-9.1-449	02.12.1999	31.07.2002	DIBt	Z-9.1-511	17.11.2000	30.09.2005	DIBt
Z-9.1-449	07.08.2001	31.07.2002	DIBt	Z-9.1-511	22.03.2002	30.09.2005	DIBt
Z-9.1-449	23.08.2002	31.07.2007	DIBt	Z-9.1-511	09.12.2005	31.12.2010	DIBt
Z-9.1-449	14.10.2003	31.07.2007	DIBt	Z-9.1-511	11.03.2011	31.12.2015	DIBt
Z-9.1-449	27.03.2006	31.07.2007	DIBt	Z-9.1-514	01.08.2001	31.07.2006	DIBt
Z-9.1-449	05.07.2007	31.07.2012	DIBt	Z-9.1-514	11.07.2002	31.07.2006	DIBt
Z-9.1-449	03.02.2009	31.07.2012	DIBt	Z-9.1-514	20.10.2006	31.07.2011	DIBt
Z-9.1-449	11.03.2011	31.07.2012	DIBt	Z-9.1-514	28.03.2012	28.03.2017	DIBt
Z-9.1-449	31.07.2012	01.08.2017	DIBt	Z-9.1-519	17.04.2002	30.04.2007	DIBt
Z-9.1-453	02.09.1999	31.08.2004	DIBt	Z-9.1-519	14.10.2003	30.04.2007	DIBt
Z-9.1-453	06.09.2000	31.08.2004	DIBt	Z-9.1-519	27.03.2006	30.04.2007	DIBt
Z-9.1-453	02.12.2004	31.08.2009	DIBt	Z-9.1-519	30.06.2006	30.04.2007	DIBt
Z-9.1-453	12.10.2005	31.08.2009	DIBt	Z-9.1-519	07.05.2007	30.04.2012	DIBt

Table B.3: Overview of NTAs analysed in section 2-2.5 (continued)

number	issue date	expiration date	notified body	number	issue date	expiration date	notified body
Z-9.1-519	11.03.2011	30.04.2012	DIBt	Z-9.1-632	24.01.2010	24.10.2011	DIBt
Z-9.1-519	27.01.2012	31.01.2017	DIBt	Z-9.1-635	16.01.2006	15.01.2011	DIBt
Z-9.1-519	17.02.2014	01.08.2017	DIBt	Z-9.1-635	03.05.2010	15.11.2011	DIBt
Z-9.1-564	11.06.2003	30.06.2008	DIBt	Z-9.1-635	14.01.2011	16.01.2016	DIBt
Z-9.1-564	24.10.2005	30.06.2008	DIBt	Z-9.1-637	27.01.2006	31.08.2010	DIBt
Z-9.1-564	01.07.2008	30.06.2013	DIBt	Z-9.1-637	27.05.2010	31.08.2010	DIBt
Z-9.1-564	28.05.2014	28.05.2019	DIBt	Z-9.1-637	06.08.2010	31.08.2015	DIBt
Z-9.1-588	26.08.2004	31.08.2009	DIBt	Z-9.1-641	09.09.2005	30.11.2010	DIBt
Z-9.1-600	26.08.2004	31.08.2009	DIBt	Z-9.1-646	15.05.2006	31.03.2011	DIBt
Z-9.1-600	13.12.2005	31.08.2009	DIBt	Z-9.1-646	05.07.2011	01.04.2016	DIBt
Z-9.1-600	21.02.2009	28.02.2014	DIBt	Z-9.1-648	20.10.2006	31.10.2011	DIBt
Z-9.1-600	18.01.2010	28.02.2014	DIBt	Z-9.1-648	05.11.2012	05.11.2017	DIBt
Z-9.1-603	08.07.2005	31.07.2010	DIBt	Z-9.1-652	18.04.2008	30.04.2013	DIBt
Z-9.1-603	01.08.2010	01.08.2015	DIBt	Z-9.1-652	28.09.2011	30.04.2013	DIBt
Z-9.1-605	06.09.2004	31.08.2009	DIBt	Z-9.1-653	02.06.2006	31.05.2011	DIBt
Z-9.1-605	06.09.2009	30.11.2014	DIBt	Z-9.1-654	29.05.2006	31.05.2011	DIBt
Z-9.1-611	10.12.2004	31.12.2009	DIBt	Z-9.1-654	24.08.2011	01.06.2013	DIBt
Z-9.1-611	21.02.2009	28.02.2014	DIBt	Z-9.1-654	09.09.2013	01.06.2018	DIBt
Z-9.1-611	18.01.2010	28.02.2014	DIBt	Z-9.1-656	25.07.2007	30.06.2012	DIBt
Z-9.1-614	24.03.2006	31.03.2011	DIBt	Z-9.1-656	25.06.2012	01.07.2017	DIBt
Z-9.1-614	27.05.2009	30.06.2014	DIBt	Z-9.1-657	04.07.2006	31.07.2011	DIBt
Z-9.1-619	18.02.2005	31.12.2009	DIBt	Z-9.1-657	12.02.2007	31.07.2011	DIBt
Z-9.1-619	19.07.2009	31.12.2009	DIBt	Z-9.1-657	24.08.2011	01.06.2013	DIBt
Z-9.1-619	18.01.2010	31.12.2014	DIBt	Z-9.1-657	09.09.2013	01.06.2018	DIBt
Z-9.1-620	24.02.2005	28.02.2010	DIBt	Z-9.1-659	29.05.2006	31.05.2011	DIBt
Z-9.1-620	19.02.2007	28.02.2010	DIBt	Z-9.1-659	13.06.2008	31.05.2011	DIBt
Z-9.1-620	19.06.2009	28.02.2010	DIBt	Z-9.1-661	04.07.2006	31.07.2011	DIBt
Z-9.1-620	18.01.2010	28.02.2015	DIBt	Z-9.1-661	11.05.2007	31.07.2011	DIBt
Z-9.1-630	12.08.2005	31.08.2010	DIBt	Z-9.1-661	08.09.2009	31.07.2011	DIBt
Z-9.1-630	23.08.2010	23.08.2015	DIBt	Z-9.1-661	23.08.2010	31.07.2011	DIBt
Z-9.1-632	24.10.2005	23.10.2010	DIBt	Z-9.1-661	23.09.2011	01.08.2016	DIBt
Z-9.1-632	27.02.2006	23.10.2010	DIBt	Z-9.1-665	25.07.2007	30.06.2012	DIBt
Z-9.1-632	13.06.2008	23.10.2010	DIBt	Z-9.1-667	27.07.2007	31.07.2012	DIBt

Table B.4: *Overview of NTAs analysed in section 2-2.5 (continued)*

number	issue date	expiration date	notified body	number	issue date	expiration date	notified body
Z-9.1-667	23.09.2012	23.11.2017	DIBt	Z-9.1-701	02.06.2010	02.06.2015	DIBt
Z-9.1-670	21.05.2007	31.05.2012	DIBt	Z-9.1-703	26.06.2008	30.06.2013	DIBt
Z-9.1-676	09.07.2007	31.07.2012	DIBt	Z-9.1-703	28.10.2013	18.02.2016	DIBt
Z-9.1-676	20.07.2009	31.07.2012	DIBt	Z-9.1-710	20.06.2008	30.06.2013	DIBt
Z-9.1-676	31.07.2012	01.08.2017	DIBt	Z-9.1-723	26.10.2010	26.10.2015	DIBt
Z-9.1-681	26.03.2007	31.03.2012	DIBt	Z-9.1-724	14.01.2011	14.01.2016	DIBt
Z-9.1-681	26.11.2008	31.03.2012	DIBt	Z-9.1-729	22.09.2009	22.09.2014	DIBt
Z-9.1-681	10.08.2010	31.03.2012	DIBt	Z-9.1-731	14.07.2009	14.07.2014	DIBt
Z-9.1-681	16.05.2012	01.04.2017	DIBt	Z-9.1-731	05.05.2010	14.07.2014	DIBt
Z-9.1-684	18.07.2008	31.07.2011	DIBt	Z-9.1-734	24.06.2009	31.07.2014	DIBt
Z-9.1-684	03.06.2010	31.07.2011	DIBt	Z-9.1-764	09.06.2010	30.06.2015	DIBt
Z-9.1-684	23.09.2011	01.08.2016	DIBt	Z-9.1-799	18.01.2011	18.02.2016	DIBt
Z-9.1-687	17.12.2007	31.12.2012	DIBt	Z-9.1-799	05.12.2013	18.02.2016	DIBt
Z-9.1-687	25.01.2013	01.01.2018	DIBt	Z-9.1-803	09.07.2010	08.07.2015	DIBt
Z-9.1-693	31.05.2010	30.06.2015	DIBt	Z-9.1-804	19.05.2011	19.05.2016	DIBt
Z-9.1-694	10.03.2008	31.03.2013	DIBt	Z-9.1-817	10.10.2012	10.10.2017	DIBt
Z-9.1-695	10.10.2007	31.10.2012	DIBt	Z-9.1-845	10.04.2014	10.04.2019	DIBt

Table B.5: *Overview of ETAs analysed in section 2-2.5*

number	issue date	expiration date	notified body
ETA-11/0024	22.03.2011	22.03.2016	ETA Danmark
ETA-11/0024	26.06.2013	26.06.2018	ETA Danmark
ETA-11/0027	22.03.2011	22.03.2016	ETA Danmark
ETA-11/0027	08.05.2012	22.03.2016	ETA Danmark
ETA-11/0027	26.06.2013	26.06.2018	ETA Danmark
ETA-11/0030	05.04.2011	05.04.2016	ETA Danmark
ETA-11/0030	30.01.2012	05.04.2016	ETA Danmark
ETA-11/0030	17.07.2012	05.04.2016	ETA Danmark
ETA-11/0030	08.11.2012	05.04.2016	ETA Danmark
ETA-11/0106	28.02.2011	28.02.2016	DIBt
ETA-11/0106	15.08.2012	28.02.2016	DIBt
ETA-11/0190	05.09.2011	05.09.2016	DIBt
ETA-11/0190	03.06.2013	05.09.2016	DIBt
ETA-11/0190	27.06.2013	27.06.2018	DIBt
ETA-11/0270	13.09.2011	13.09.2016	ETA Danmark
ETA-11/0283	04.10.2011	04.10.2016	DIBt
ETA-11/0283	08.05.2013	08.05.2018	DIBt
ETA-11/0284	05.09.2011	05.09.2016	DIBt
ETA-11/0331	13.09.2011	22.03.2016	ETA Danmark
ETA-11/0331	26.06.2013	26.06.2018	ETA Danmark
ETA-11/0389	12.03.2012	12.03.2017	DIBt
ETA-11/0425	28.09.2011	22.03.2016	DIBt
ETA-11/0425	26.06.2013	26.06.2018	DIBt
ETA-11/0452	06.12.2011	06.12.2016	DIBt
ETA-12/0038	24.05.2012	24.05.2017	DIBt
ETA-12/0038	28.06.2013	24.05.2017	DIBt
ETA-12/0062	18.06.2012	17.06.2017	OIB
ETA-12/0063	18.06.2012	17.06.2017	OIB
ETA-12/0063	18.06.2013	17.06.2017	OIB
ETA-12/0073	07.02.2012	22.03.2016	ETA Danmark
ETA-12/0087	04.06.2012	04.06.2017	ETA Danmark
ETA-12/0087	16.04.2013	04.06.2017	ETA Danmark
ETA-12/0114	05.09.2012	17.07.2017	ETA Danmark
ETA-12/0114	26.06.2013	17.07.2017	ETA Danmark

Table B.6: Overview of ETAs analysed in section 2-2.5 (continued)

number	issue date	expiration date	notified body
ETA-12/0132	21.05.2012	21.05.2017	DIBt
ETA-12/0191	06.06.2012	22.03.2016	ETA Danmark
ETA-12/0191	26.06.2013	26.06.2018	ETA Danmark
ETA-12/0196	29.01.2013	16.07.2017	ETA Danmark
ETA-12/0197	17.07.2012	17.07.2017	ETA Danmark
ETA-12/0197	26.06.2013	17.07.2017	ETA Danmark
ETA-12/0198	24.05.2012	24.05.2017	DIBt
ETA-12/0276	06.09.2012	06.09.2017	DIBt
ETA-12/0280	07.08.2012	07.08.2017	DIBt
ETA-12/0280	18.06.2013	18.06.2018	DIBt
ETA-12/0354	07.09.2012	22.03.2016	ETA Danmark
ETA-12/0354	26.06.2013	26.06.2018	ETA Danmark
ETA-12/0373	05.11.2012	04.11.2017	OIB
ETA-12/0471	08.01.2013	08.01.2018	DIBt
ETA-12/0471	13.06.2013	08.01.2018	DIBt
ETA-12/0483	25.10.2012	28.02.2016	DIBt
ETA-12/0501	21.12.2012	05.04.2016	ETA Danmark
ETA-12/0501	23.11.2012	05.04.2016	ETA Danmark
ETA-12/0521	03.12.2012	03.12.2017	DIBt
ETA-12/0521	18.06.2013	18.06.2018	DIBt
ETA-13/0029	29.01.2013	16.07.2016	ETA Danmark
ETA-13/0090	28.05.2013	28.05.2018	ETA Danmark
ETA-13/0091	28.05.2013	28.05.2018	ETA Danmark
ETA-13/0393	20.06.2013	19.06.2018	ZUS
ETA-13/0536	27.06.2013	27.06.2018	DIBt
ETA-13/0674	18.06.2013	18.06.2018	DIBt
ETA-13/0699	13.06.2013	13.06.2018	DIBt
ETA-13/0796	28.06.2013	04.11.2017	OIB
ETA-13/0816	18.06.2013	18.06.2018	DIBt
ETA-13/0842	28.06.2013	04.11.2017	OIB
ETA-13/0899	26.06.2013	17.07.2017	ETA Danmark

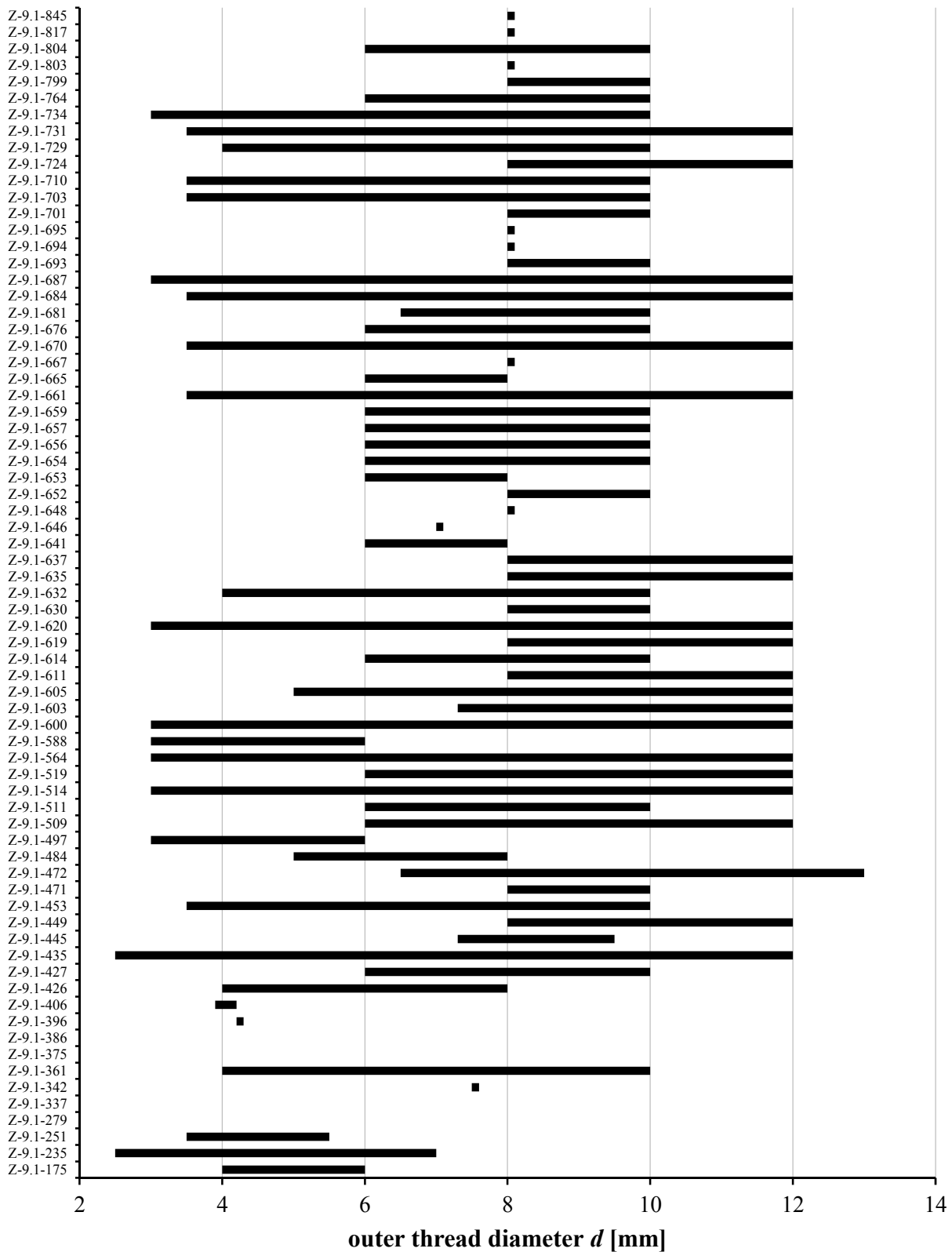


Figure B.1: Overview of the outer thread diameter bandwidth of all NTAs analysed

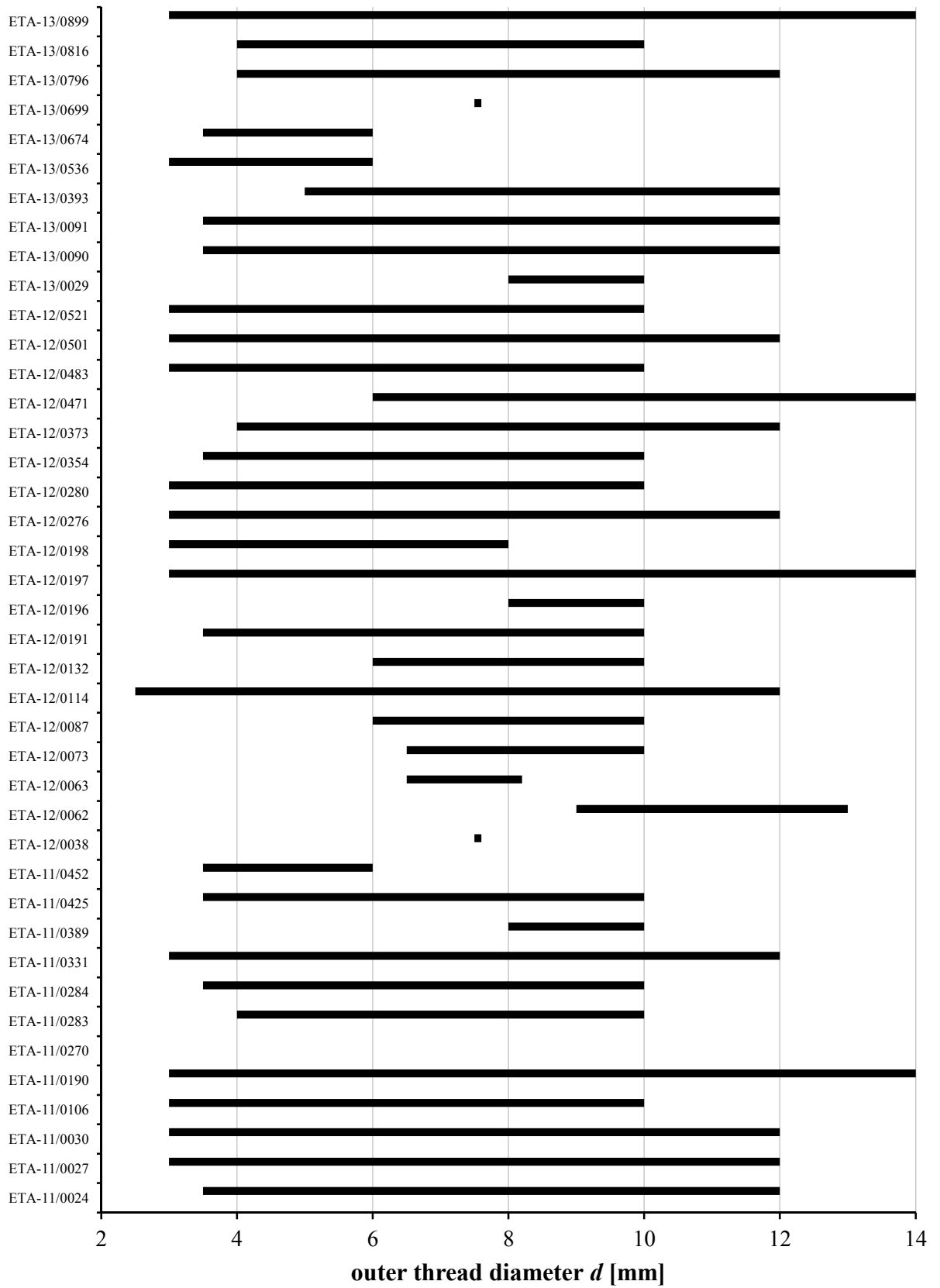


Figure B.2: Overview of the outer thread diameter bandwidth of all ETAs analysed

B-2 Supplementary material to chapter 3

B-2.1 Supplementary figures

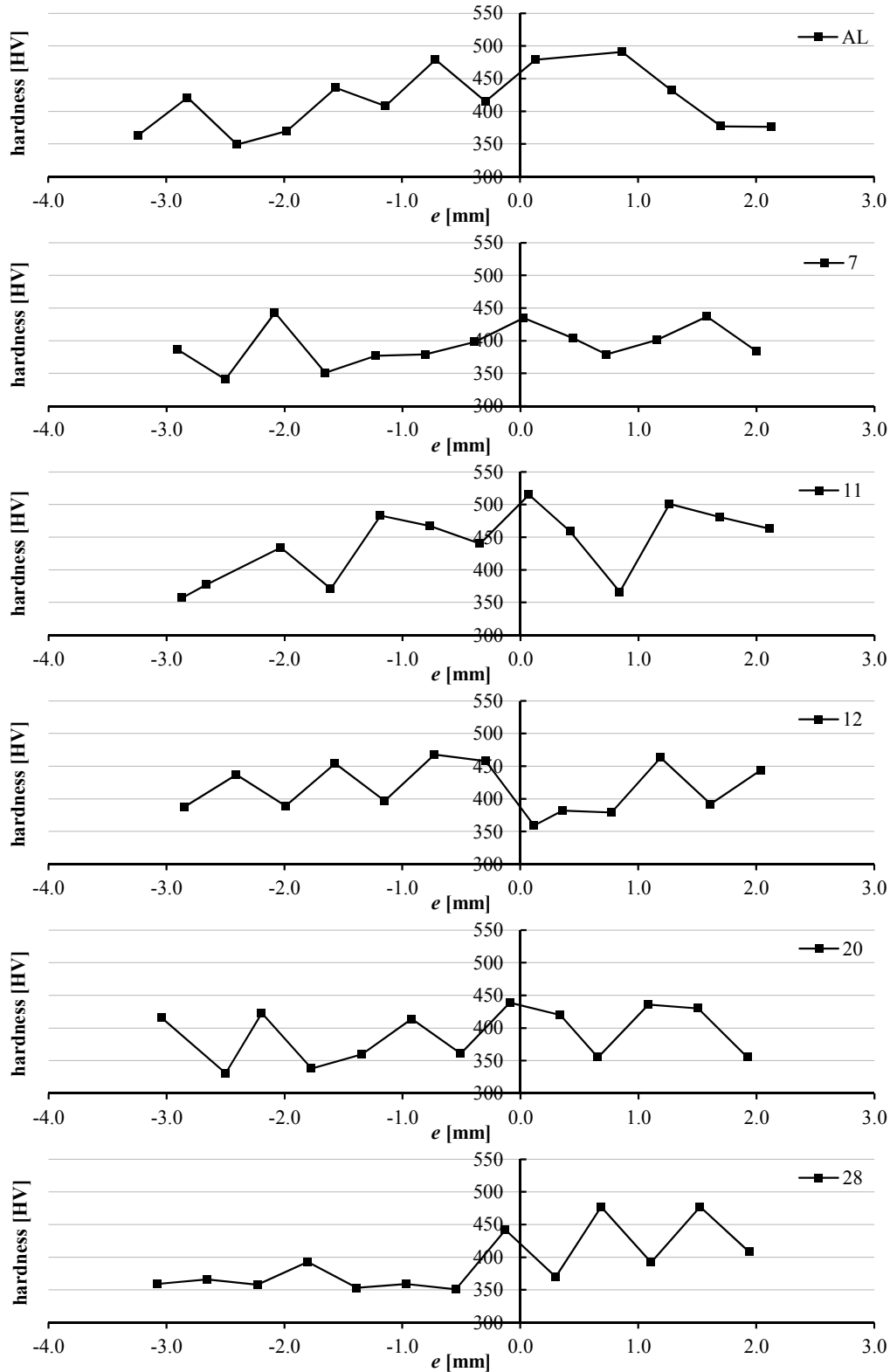


Figure B.3: Determined hardness distributions of screw product ID A_s_II_08_240

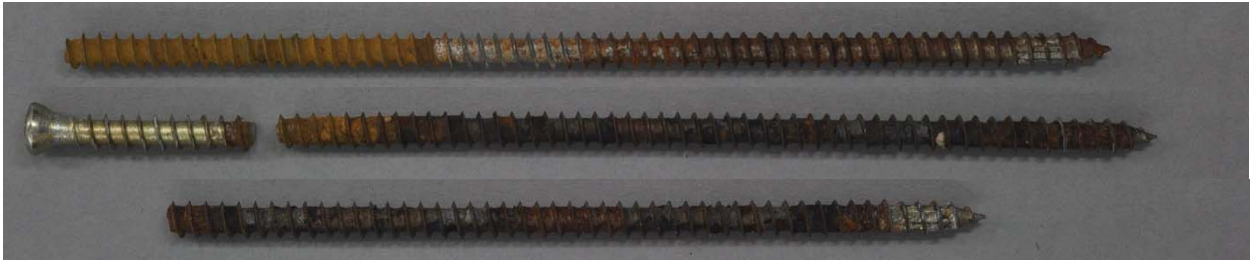


Figure B.4: *Macrophotos of A_s_I_08_240 (yellow chromated) applied in oak; test campaign I; according to Hauptmann (2016)*

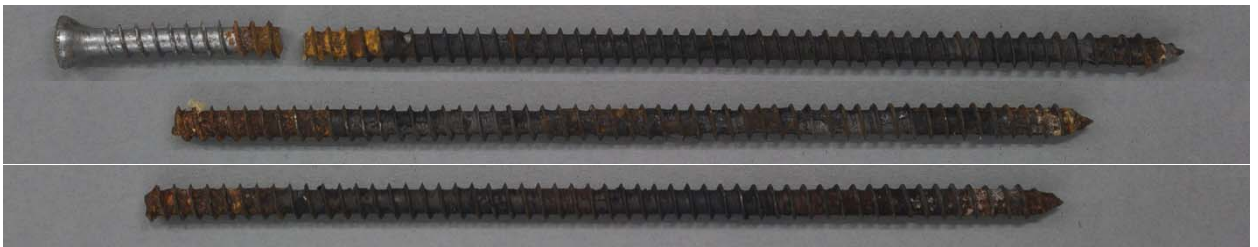


Figure B.5: *Macrophotos of A_s_I_08_240 (zinc-nickel) applied in oak; test campaign I; according to Hauptmann (2016)*



Figure B.6: *Macrophotos of A_s_I_08_240 (zinc-nickel) applied in Norway spruce; test campaign I; according to Hauptmann (2016)*



Figure B.7: *Macrophotos of A_s_IV_08_240 (blue chromated) applied in oak; test campaign I; according to Hauptmann (2016)*

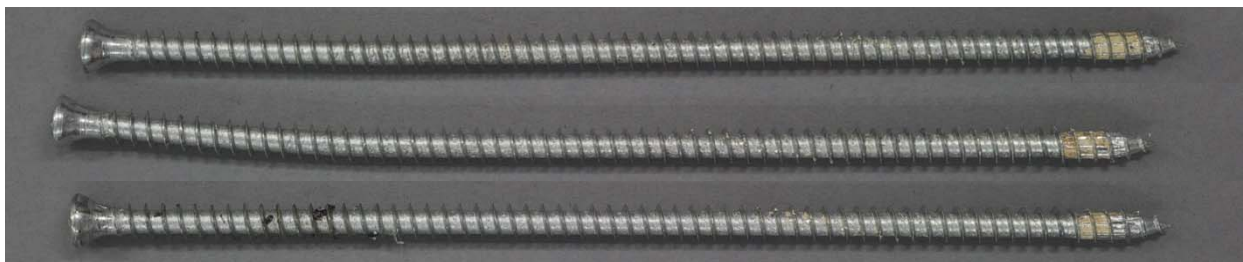


Figure B.8: *Macrophotos of A_s_IV_08_240 (blue chromated) applied in Norway spruce; test campaign I; according to Hauptmann (2016)*

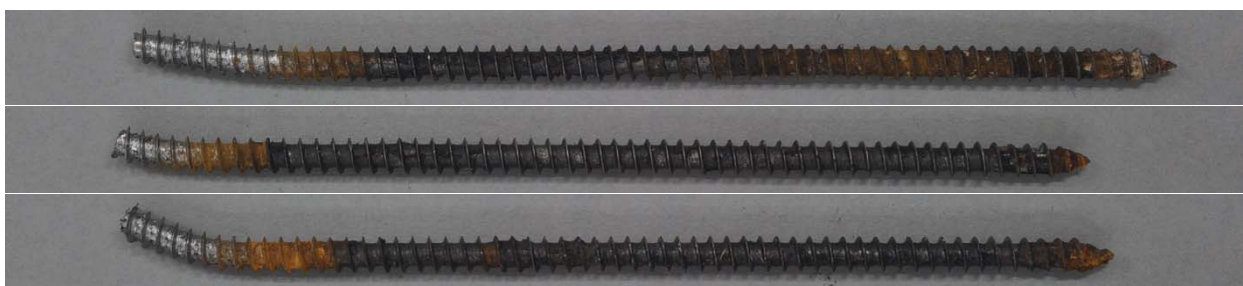


Figure B.9: *Macrophotos of A_s_IV_08_240 (zinc-nickel) applied in oak; test campaign I; according to Hauptmann (2016)*



Figure B.10: *Macrophotos of A_s_IV_08_240 (zinc-nickel) applied in Norway spruce; test campaign I; according to Hauptmann (2016)*



Figure B.11: *Macrophotos of A_s_II_08_240 (yellow chromated) applied in oak; test campaign II*



Figure B.12: *Macrophotos of A_s_II_08_240 (zinc-nickel) applied in oak; test campaign II*



Figure B.13: *Macrophoto of A_s_II_08_240 (yellow chromated) applied in Norway spruce; test campaign II*

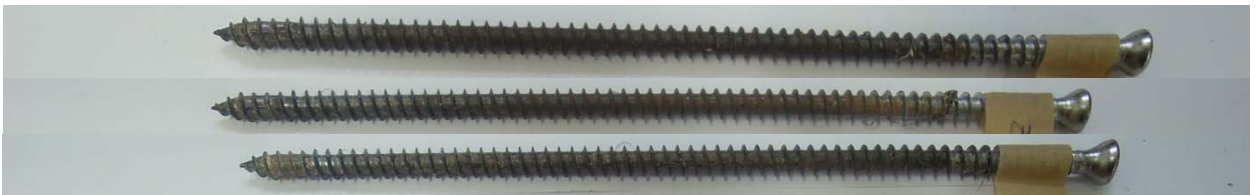


Figure B.14: *Macrophoto of A_s_II_08_240 (zinc-nickel) applied in Norway spruce; test campaign II*

B-2.2 Supplementary test results

Table B.7: Supplementary table to staircase method applied in section 3-5.3.3; $R = 0.10$

σ_{\max} [N/mm ²]	x = failure, o = survive						x	o	z	f	z · f	z ² · f	
160	x						x	2	0	4	2	8	32
149			x		x		o	2	1	3	2	6	18
137		x		o	x	o	o	2	3	2	2	4	8
125			o					0	1	1	0	0	0
113	o		o					0	2	0	0	0	0
							sum	6	7		6	18	58
											C	A	E

f = frequency of x or o (the lower sum counts), z = reference number beginning at $\min[\sigma_{\max}]$

Table B.8: Supplementary table to staircase method applied in section 3-5.3.3; $R = 0.56$

σ_{\max} [N/mm ²]	x = failure, o = survive						x	o	z	f	z · f	z ² · f	
330	x						1	0	4	0	0	0	
307							0	0	3	0	0	0	
283		x		x			2	0	2	0	0	0	
259			o		x		1	1	1	1	1	1	
236	o				o		0	2	0	2	0	0	
							sum	4	3		3	1	1
											C	A	E

f = frequency of x or o (the lower sum counts), z = reference number beginning at $\min[\sigma_{\max}]$

Table B.9: Supplementary table to staircase method applied in section 3-5.3.3; $R = 0.90$

σ_{\max} [N/mm ²]	x = failure, o = survive						x	o	z	f	z · f	z ² · f	
1,038	x			x			2	0	4	2	8	32	
1,014			o		x		o	1	2	3	1	3	9
991		o			x	o		1	2	2	1	2	4
967								0	0	1	0	0	0
943	o							0	1	0	0	0	0
							sum				4	13	45
											C	A	E

f = frequency of x or o (the lower sum counts), z = reference number beginning at $\min[\sigma_{\max}]$

Table B.10: Number of failed/survived specimen and related endurance of test campaign I; basing on Hauptmann (2016)

specimen	coating	timber species	load chain	failed (x) / survived (o)	endurance
A_s_I_08_240_1				o	3.5 weeks
A_s_I_08_240_2	yc	oak	1	x	≤ 1.0 week
A_s_I_08_240_3				x	≤ 1.0 week
A_s_I_08_240_1				o	5.0 weeks
A_s_I_08_240_2	zn	oak	2	o	5.0 weeks
A_s_I_08_240_3				o	5.0 weeks
A_s_I_08_240_1	zn	Norway spruce	1	o	3.5 weeks
A_s_I_08_240_2				o	3.5 weeks
A_s_IV_08_240_1				o	5.0 weeks
A_s_IV_08_240_2	bc	oak	2	o	5.0 weeks
A_s_IV_08_240_3				o	5.0 weeks
A_s_IV_08_240_1				o	6.0 weeks
A_s_IV_08_240_2	bc	Norway spruce	3	o	6.0 weeks
A_s_IV_08_240_3				o	6.0 weeks
A_s_IV_08_240_1				o	5.0 weeks
A_s_IV_08_240_2	zn	oak	2	o	5.0 weeks
A_s_IV_08_240_3				o	5.0 weeks
A_s_IV_08_240_1				o	6.0 weeks
A_s_IV_08_240_2	zn	Norway spruce	3	o	6.0 weeks
A_s_IV_08_240_3				o	6.0 weeks

yc = yellow chromated, zn = zinc-nickel coated, bc = blue chromated

Table B.11: *Number of failed/survived specimen and related endurance of test campaign II*

specimen	coating	timber species	load chain	failed (x) / survived (o)	endurance
A_s_II_08_240_1				o	168 days
A_s_II_08_240_2_1				x	11 days
A_s_II_08_240_2_2				o	157 days
A_s_II_08_240_3	yc	oak	1	o	168 days
A_s_II_08_240_4				o	168 days
A_s_II_08_240_5				o	168 days
A_s_II_08_240_6				o	168 days
A_s_II_08_240_1				o	169 days
A_s_II_08_240_2				o	169 days
A_s_II_08_240_3	zn	oak	2	o	169 days
A_s_II_08_240_4				o	169 days
A_s_II_08_240_5				o	169 days
A_s_II_08_240_6				o	169 days
A_s_II_08_240_1				o	149 days
A_s_II_08_240_3	yc	Norway spruce	3	o	149 days
A_s_II_08_240_5_1				x	69 days
A_s_II_08_240_5_2				o	73 days
A_s_II_08_240_2				o	149 days
A_s_II_08_240_4	zn	Norway spruce	3	o	149 days
A_s_II_08_240_6				o	149 days

yc = yellow chromated, zn = zinc-nickel coated, bc = blue chromated

B-3 Supplementary material to chapter 5

B-3.1 Supplementary figures

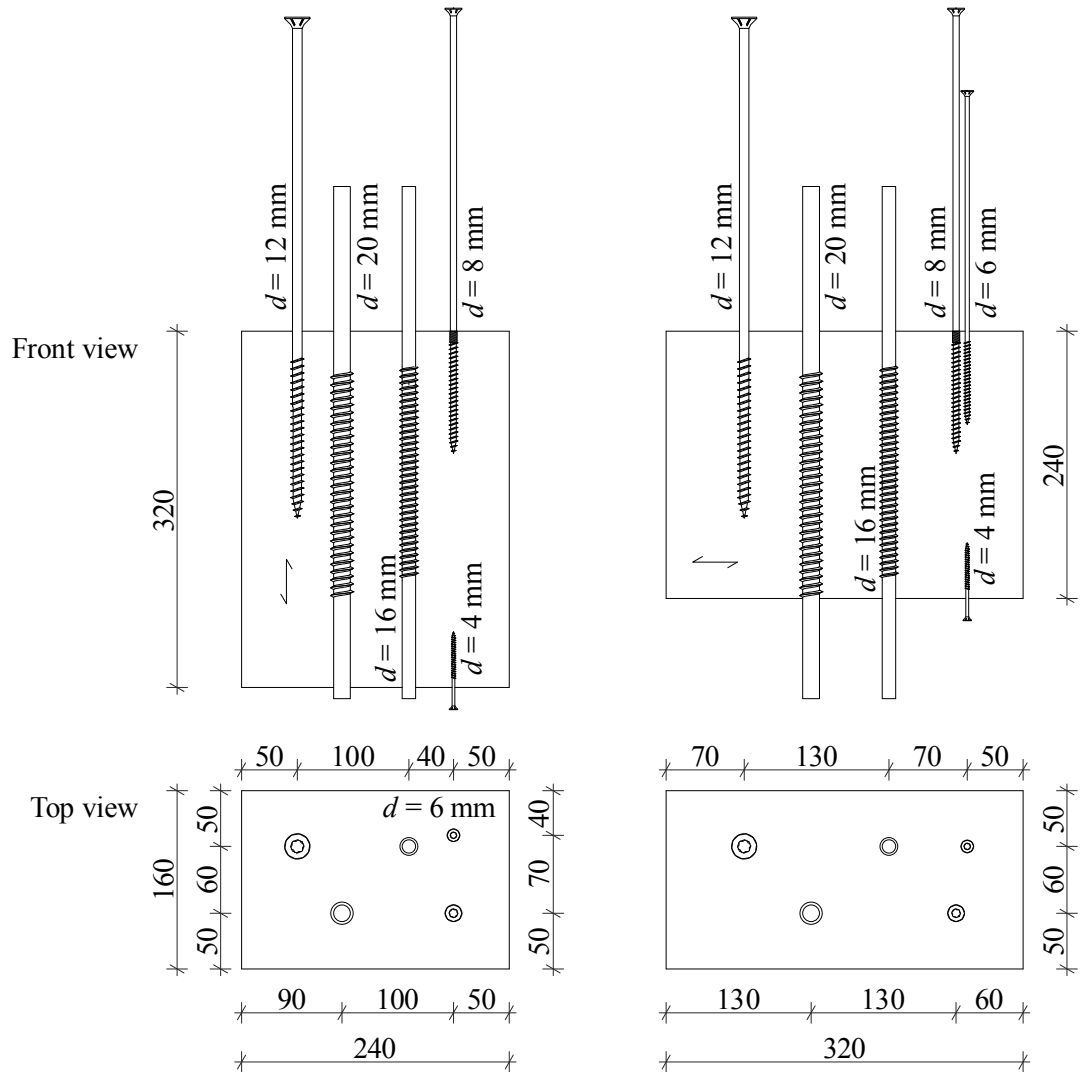


Figure B.15: Illustration of test specimen corresponding to section 5-2.1; left: $\alpha = 0^\circ$, right: $\alpha = 90^\circ$; all dimensions in [mm]

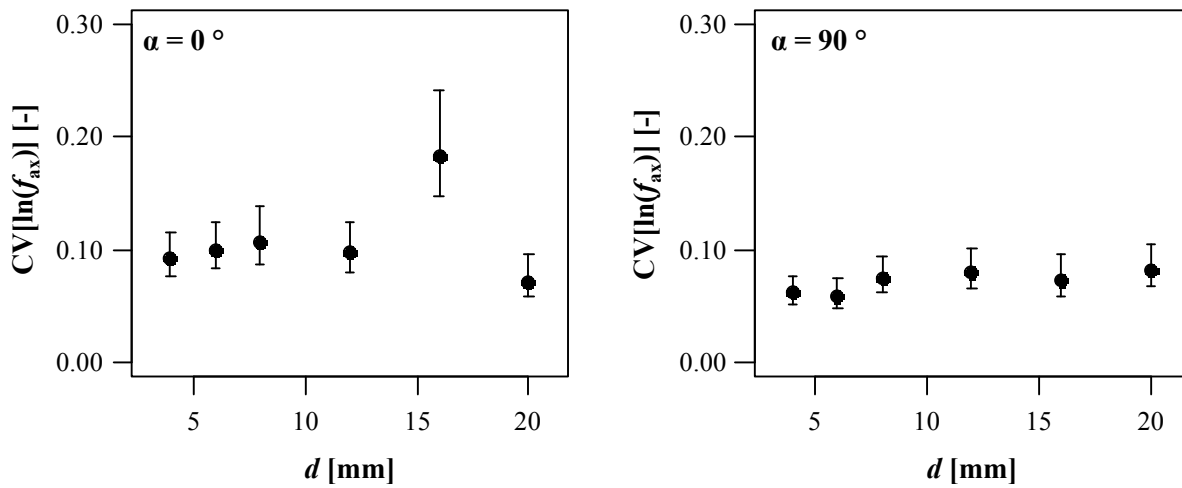


Figure B.16: CIs of $CV[\ln(f_{ax})]$, left: $\alpha = 0^\circ$; right: $\alpha = 90^\circ$; test specimen corresponding to section 5-2.1

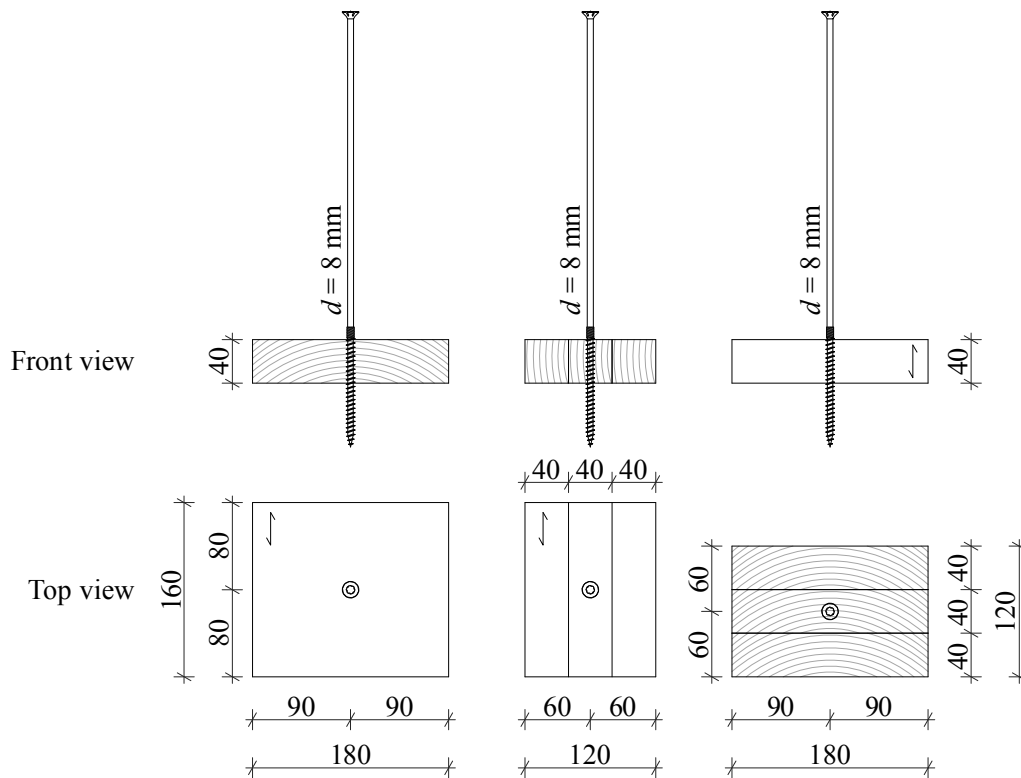


Figure B.17: Illustration of withdrawal test specimen corresponding to section 5-3.1; from left to right: radial, tangential, longitudinal direction; all dimensions in [mm]

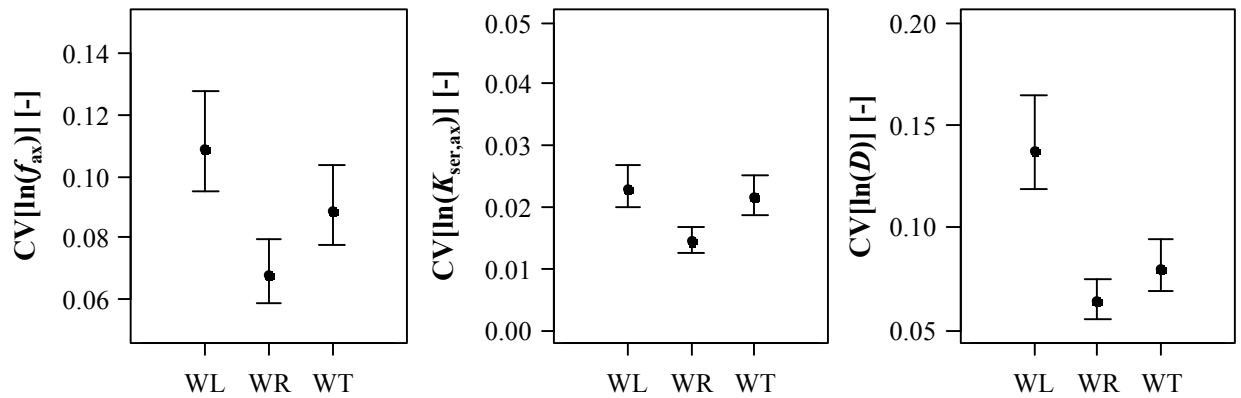


Figure B.18: CIs of $CV[\ln(f_{ax})]$ (left), $CV[\ln(K_{ser,ax})]$ (middle), $CV[\ln(D)]$ (right); test specimen corresponding to section 5-3.1

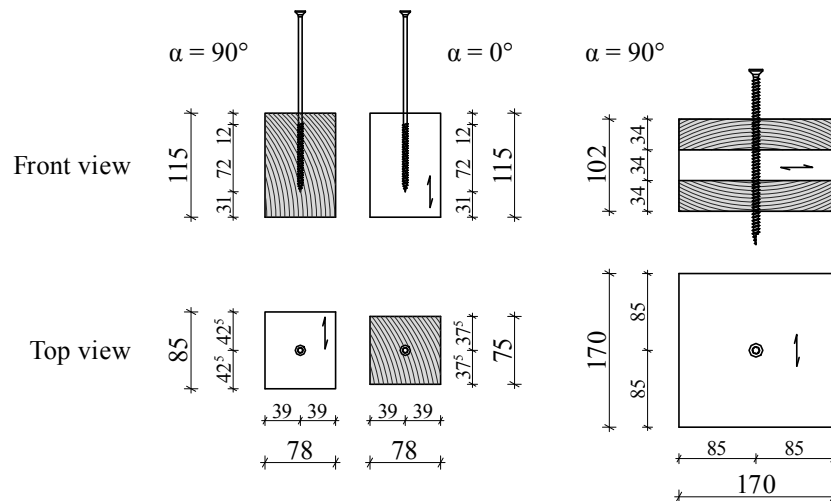


Figure B.19: Illustration of withdrawal test specimen corresponding to section 5-3.2; left: experimental campaign I; right: experimental campaign II; according to Ringhofer et al. (2014c); all dimensions in [mm]

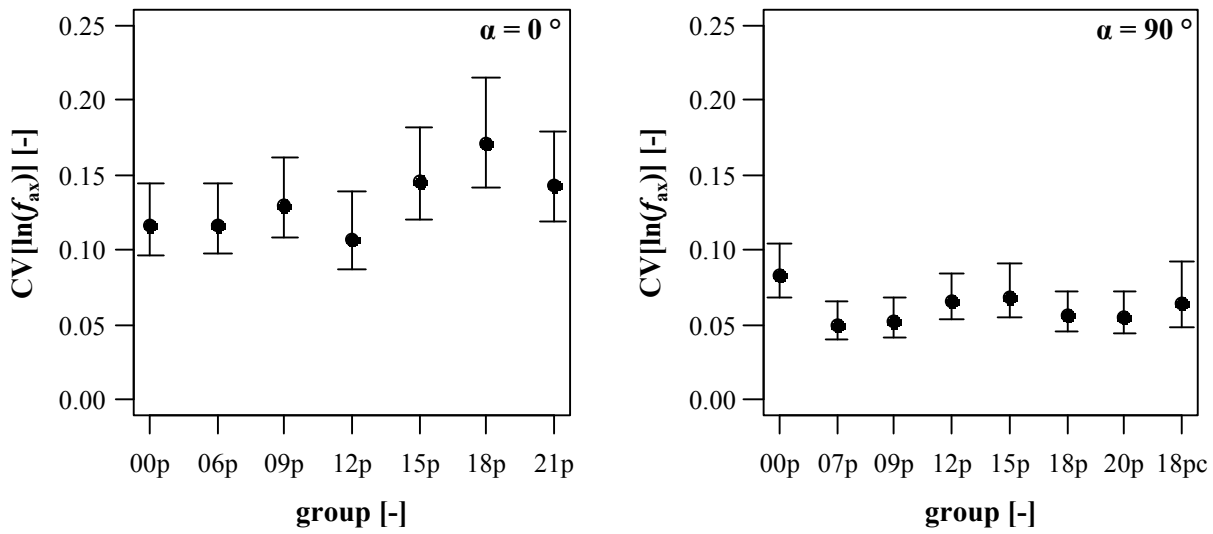


Figure B.20: CIs of $CV[\ln(f_{ax})]$ of test specimen corresponding to section 5-3.2; left: $\alpha = 0^\circ$; right: $\alpha = 90^\circ$, experimental campaign I

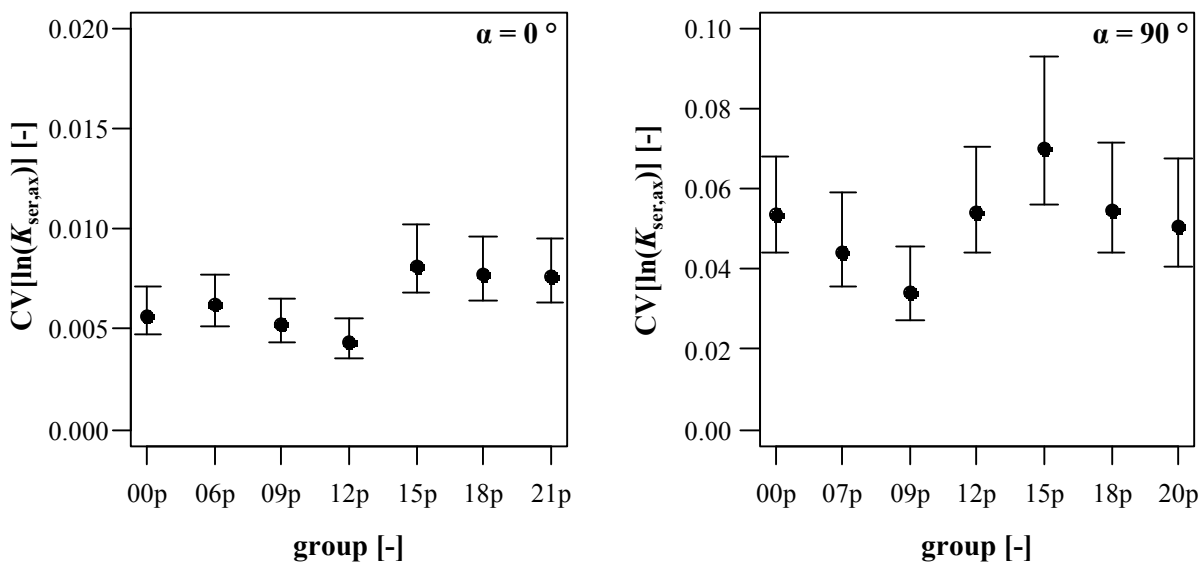


Figure B.21: CIs of $CV[\ln(K_{ser,ax})]$ of test specimen corresponding to section 5-3.2; left: $\alpha = 0^\circ$; right: $\alpha = 90^\circ$, experimental campaign I

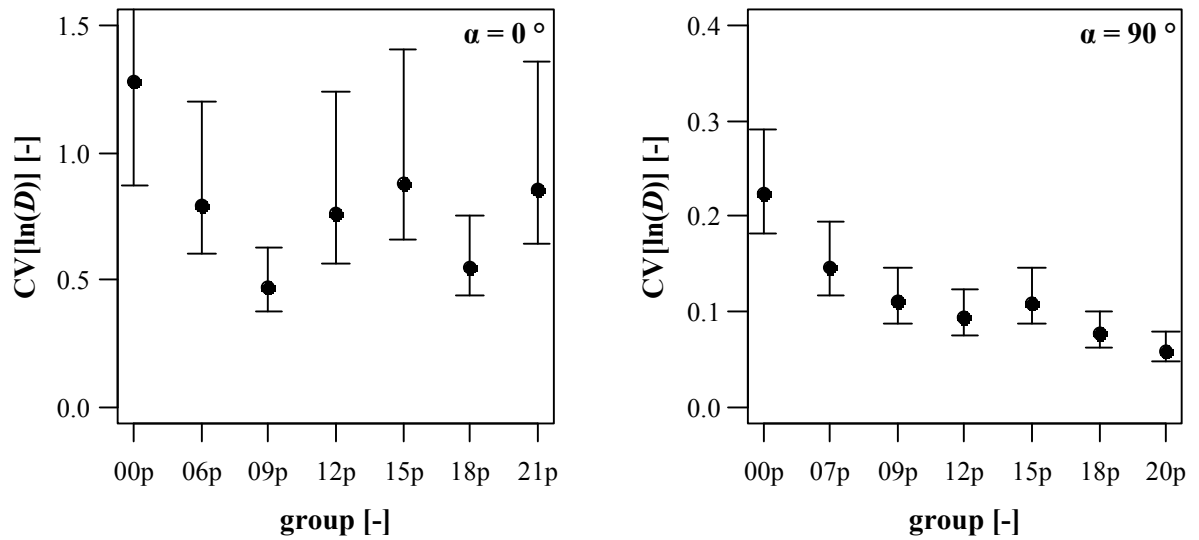


Figure B.22: CIs of $CV[\ln(D)]$ of test specimen corresponding to section 5-3.2; left: $\alpha = 0^\circ$; right: $\alpha = 90^\circ$, experimental campaign I

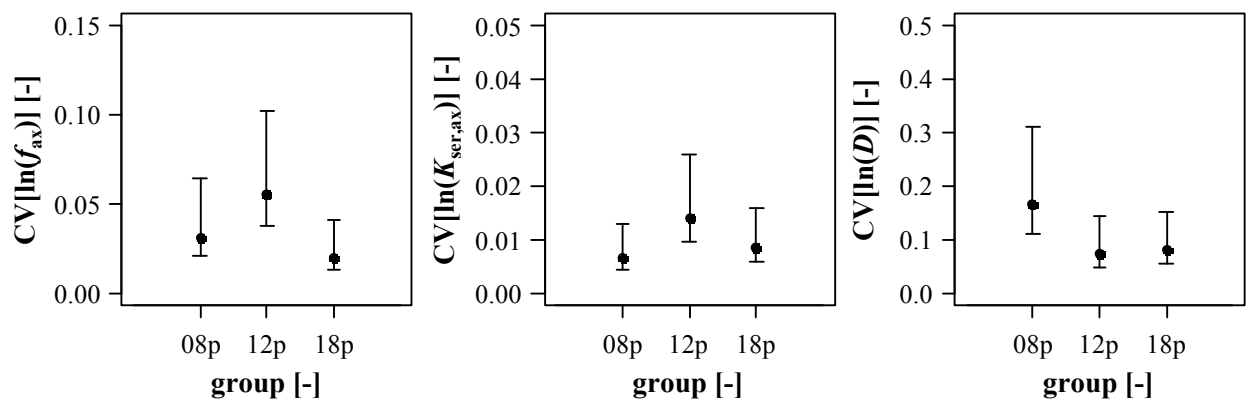


Figure B.23: CIs of $CV[\ln(f_{ax})]$ (left), $CV[\ln(K_{ser,ax})]$ (middle), $CV[\ln(D)]$ (right) of test specimen corresponding to section 5-3.2; $\alpha = 90^\circ$, experimental campaign II

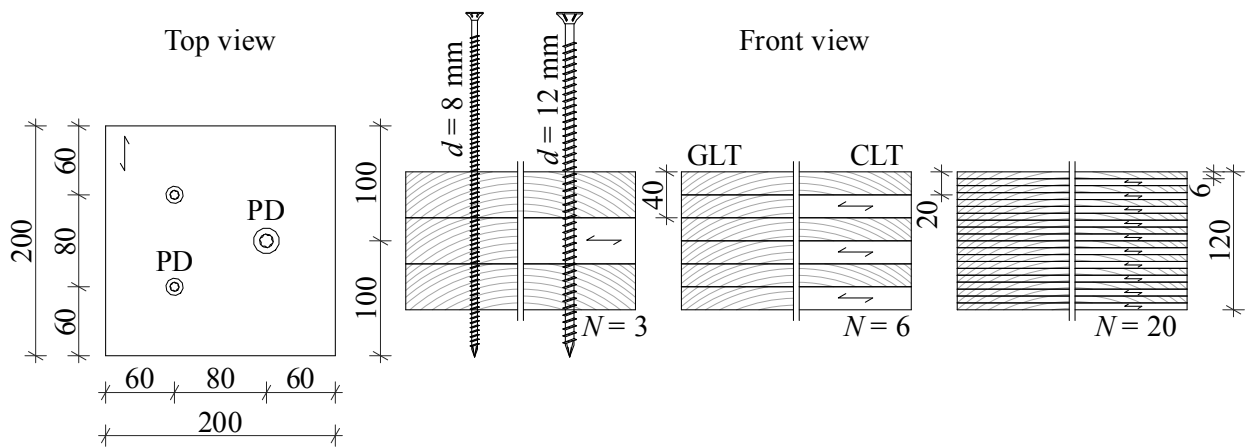


Figure B.24: Illustration of test specimen corresponding to section 5-3.3, test series A; all dimensions in [mm]

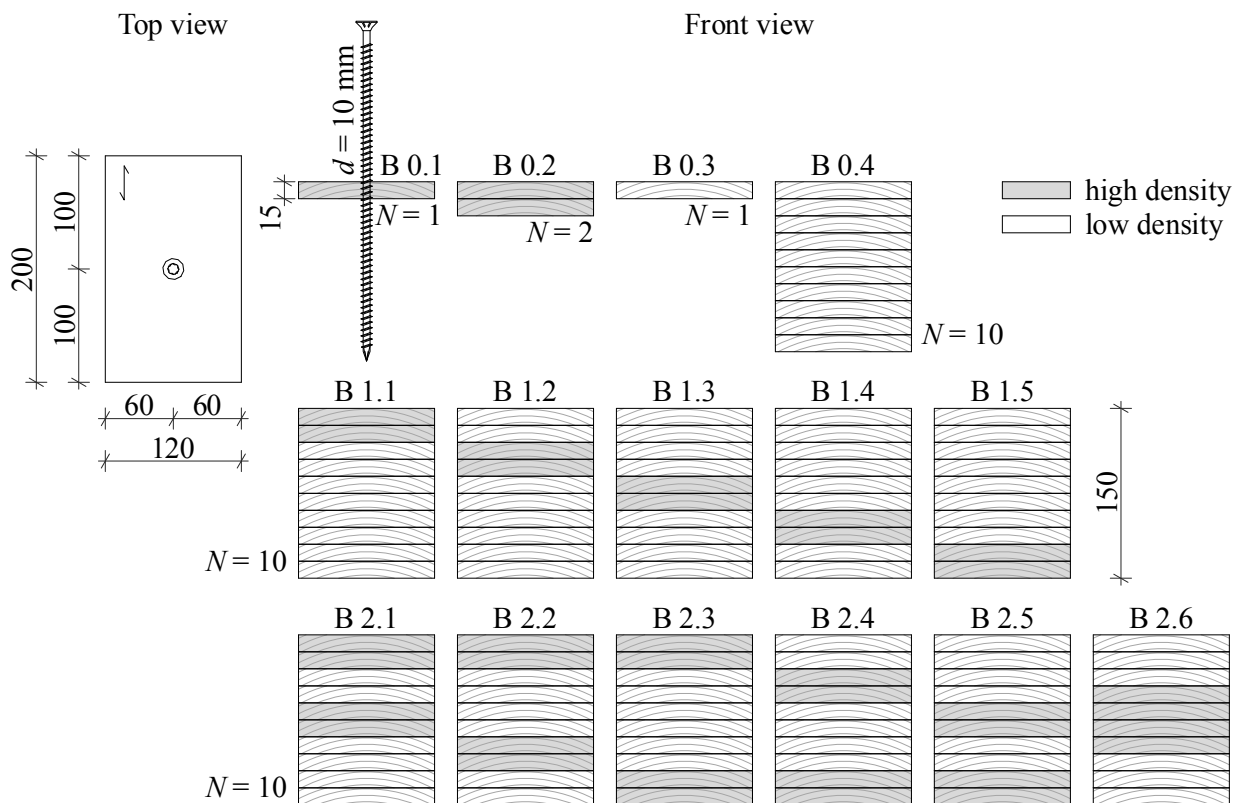


Figure B.25: Illustration of test specimen corresponding to section 5-3.3, test series B; all dimensions in [mm]

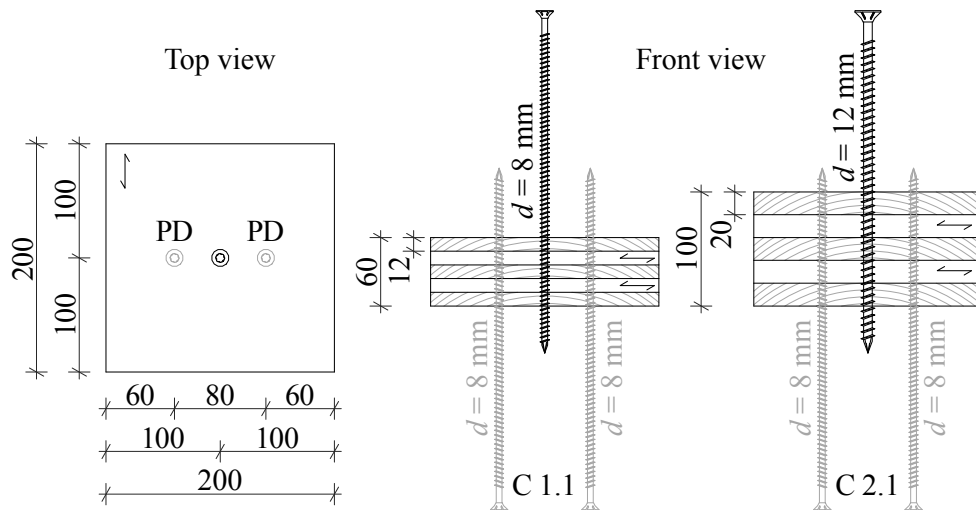


Figure B.26: Illustration of test specimen corresponding to section 5-3.3, test series C; all dimensions in [mm]

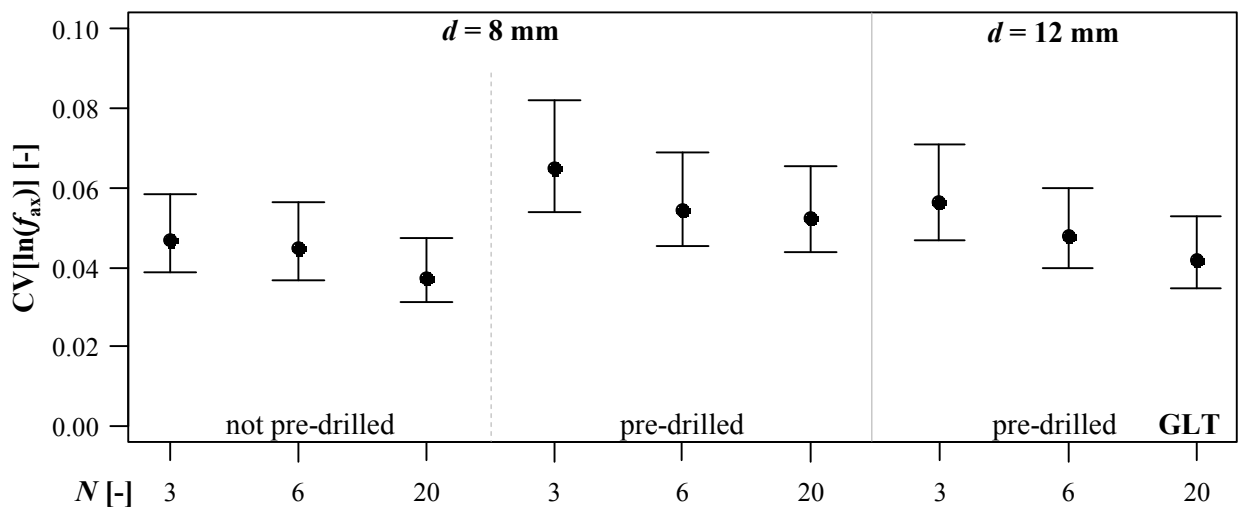


Figure B.27: CIs of $CV[\ln(f_{ax})]$ in dependence of N , d and pre-drilling; series A, GLT; test specimen corresponding to section 5-3.3

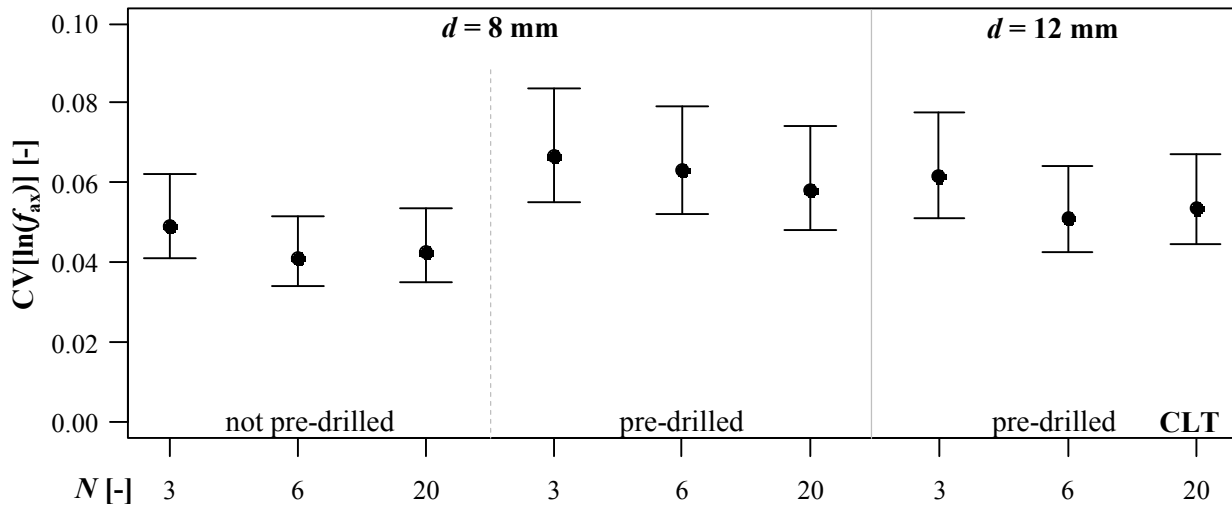


Figure B.28: CIs of $CV[\ln(f_{ax})]$ in dependence of N , d and pre-drilling; series A, CLT; test specimen corresponding to section 5-3.3

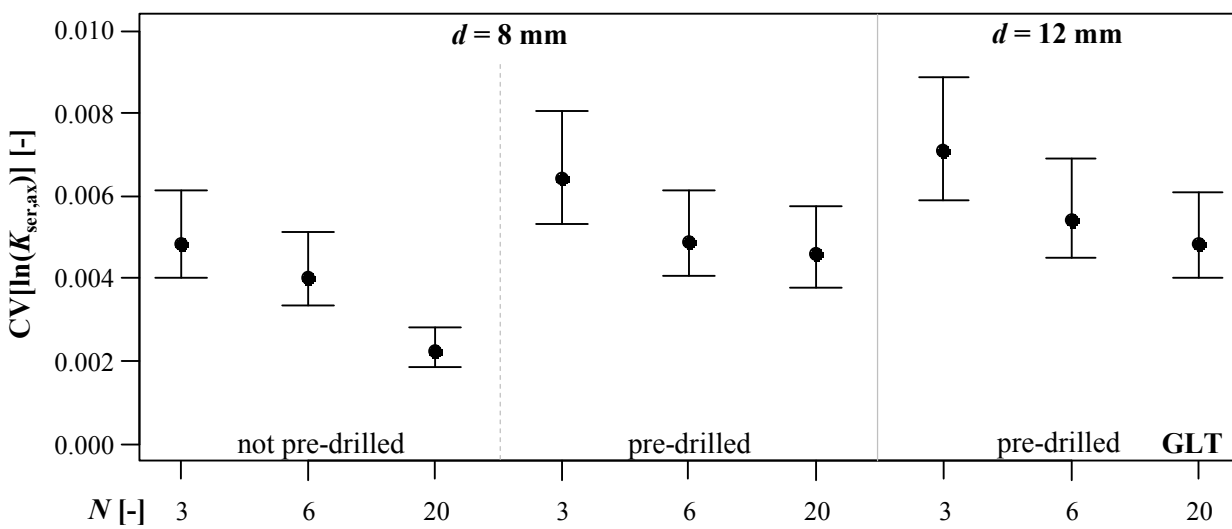


Figure B.29: CIs of $CV[\ln(K_{ser,ax})]$ in dependence of N , d and pre-drilling; series A, GLT; test specimen corresponding to section 5-3.3

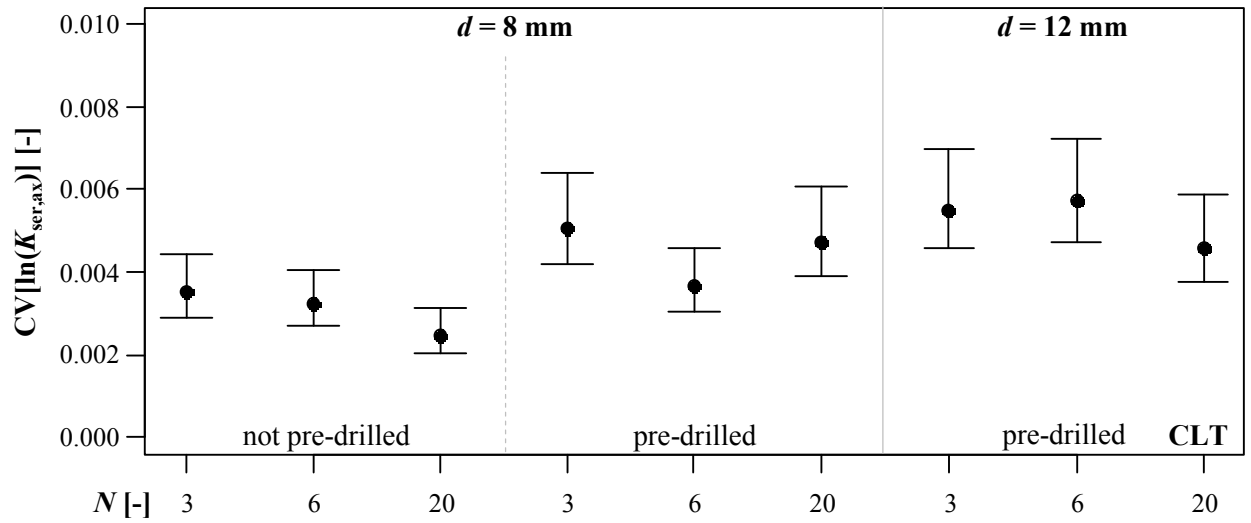


Figure B.30: CIs of $CV[\ln(K_{ser,ax})]$ in dependence of N , d and pre-drilling; series A, CLT; test specimen corresponding to section 5-3.3

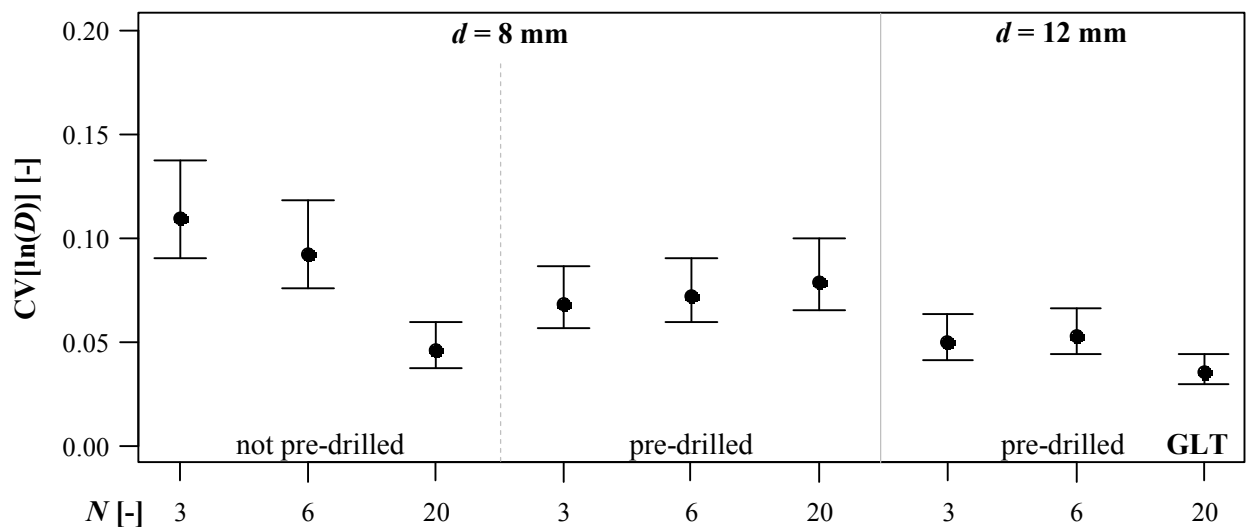


Figure B.31: CIs of $CV[\ln(D)]$ in dependence of N , d and pre-drilling; series A, GLT; test specimen corresponding to section 5-3.3

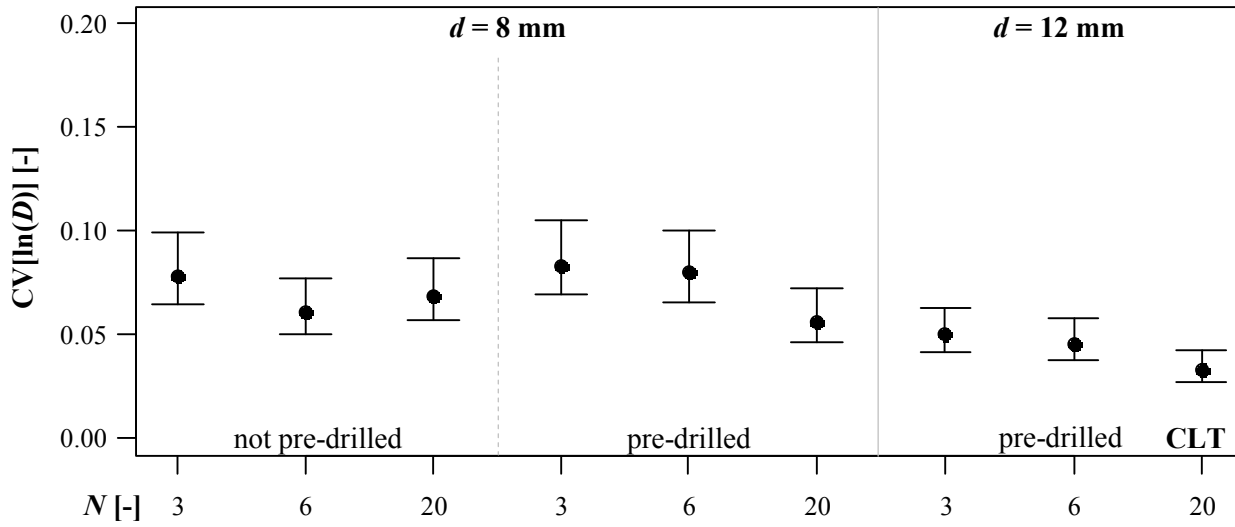


Figure B.32: CIs of $CV[\ln(D)]$ in dependence of N , d and pre-drilling; series A, CLT; test specimen corresponding to section 5-3.3

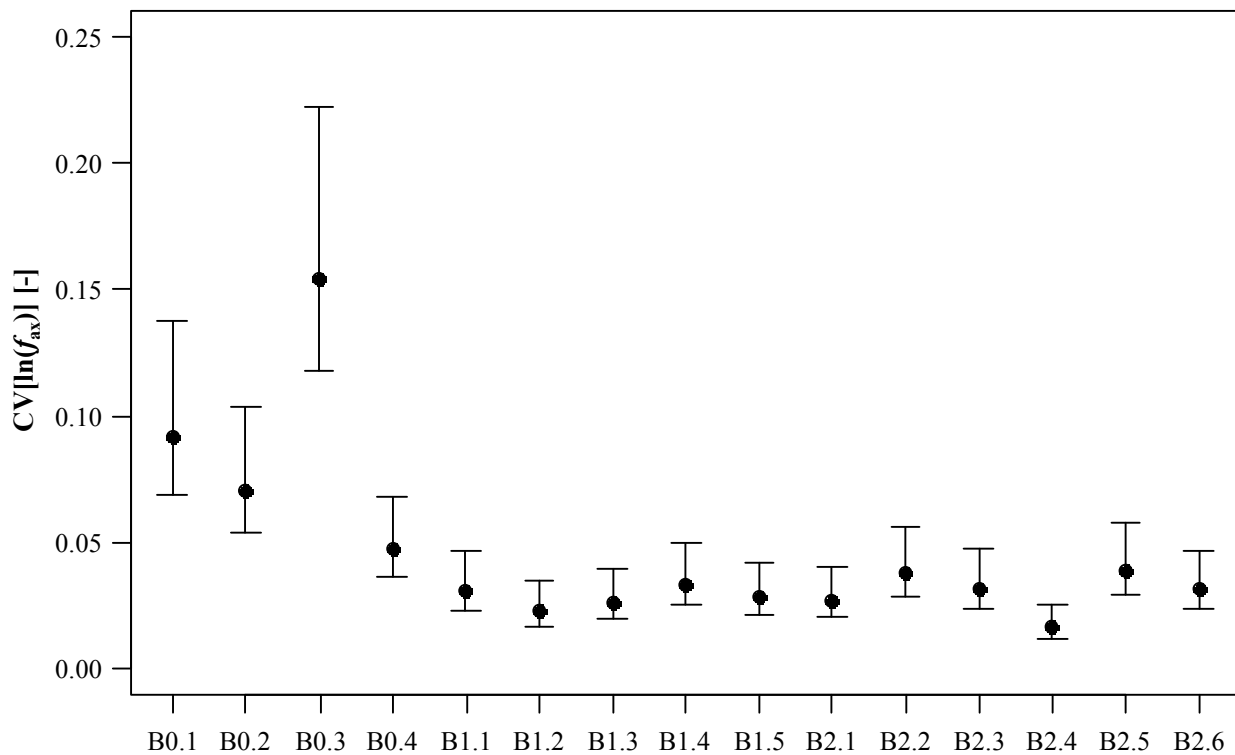


Figure B.33: CIs of $CV[\ln(f_{ax})]$ in dependence of the specific GLT lay-up; test specimen corresponding to section 5-3.3

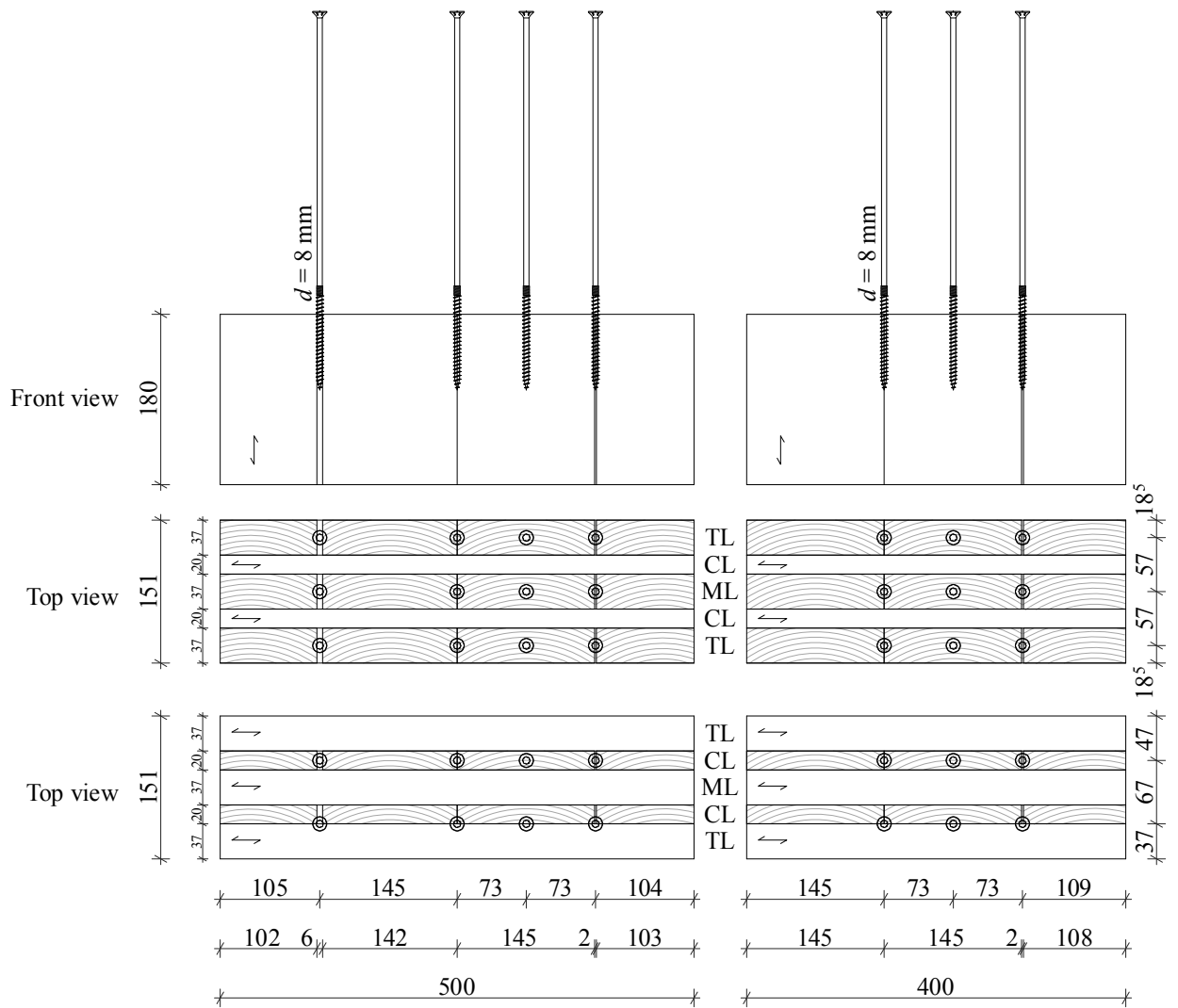


Figure B.34: Illustration of test specimen corresponding to section 5-3.4, test campaign I; exemplarily for $d = 8 \text{ mm}$; all dimensions in [mm]

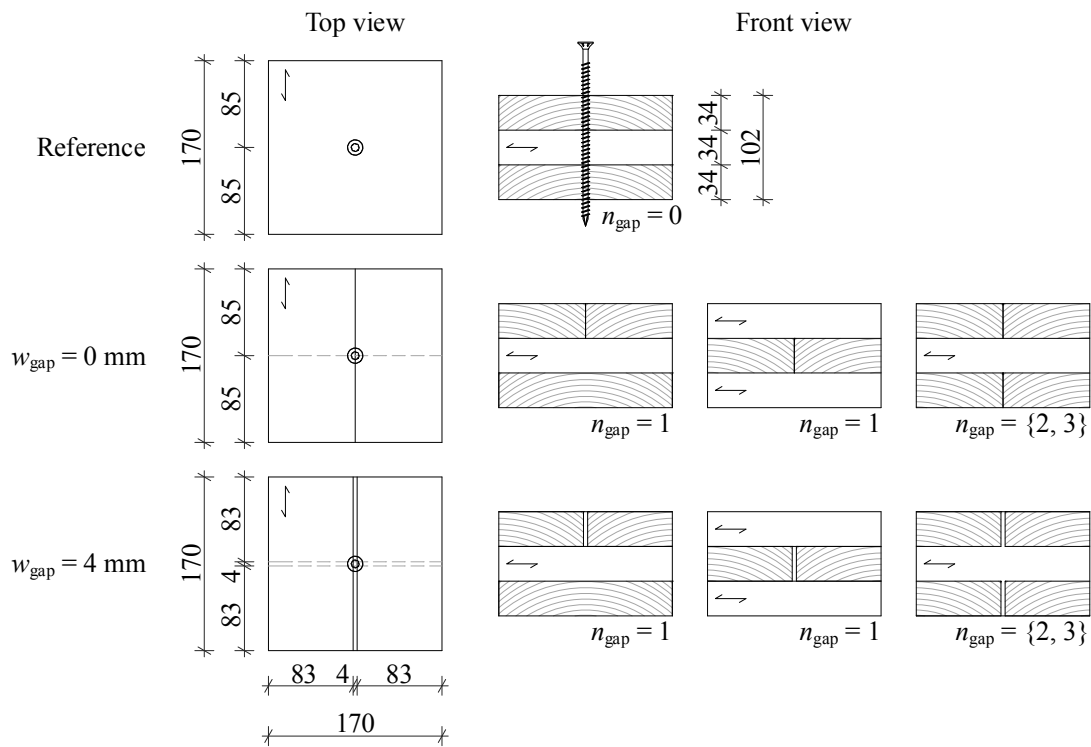


Figure B.35: Illustration of test specimen corresponding to section 5-3.4, test campaign II; all dimensions in [mm]

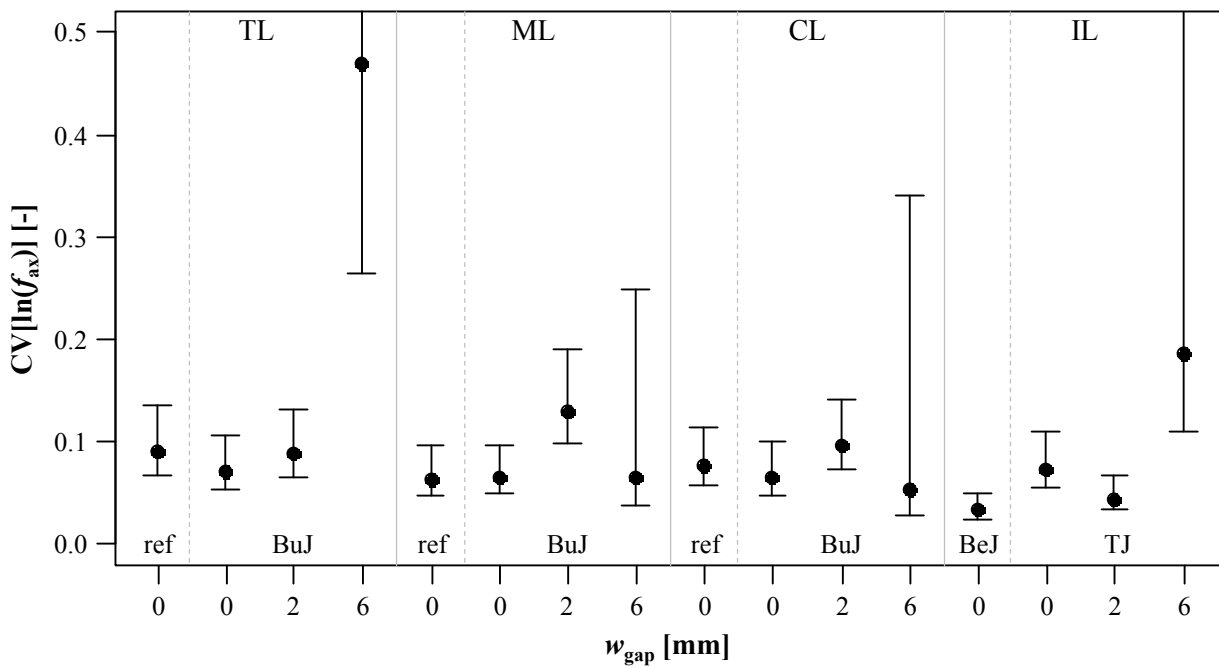


Figure B.36: CIs of $CV[\ln(f_{ax})]$; test programme I, $d = 8$ mm; test specimen corresponding to section 5-3.4

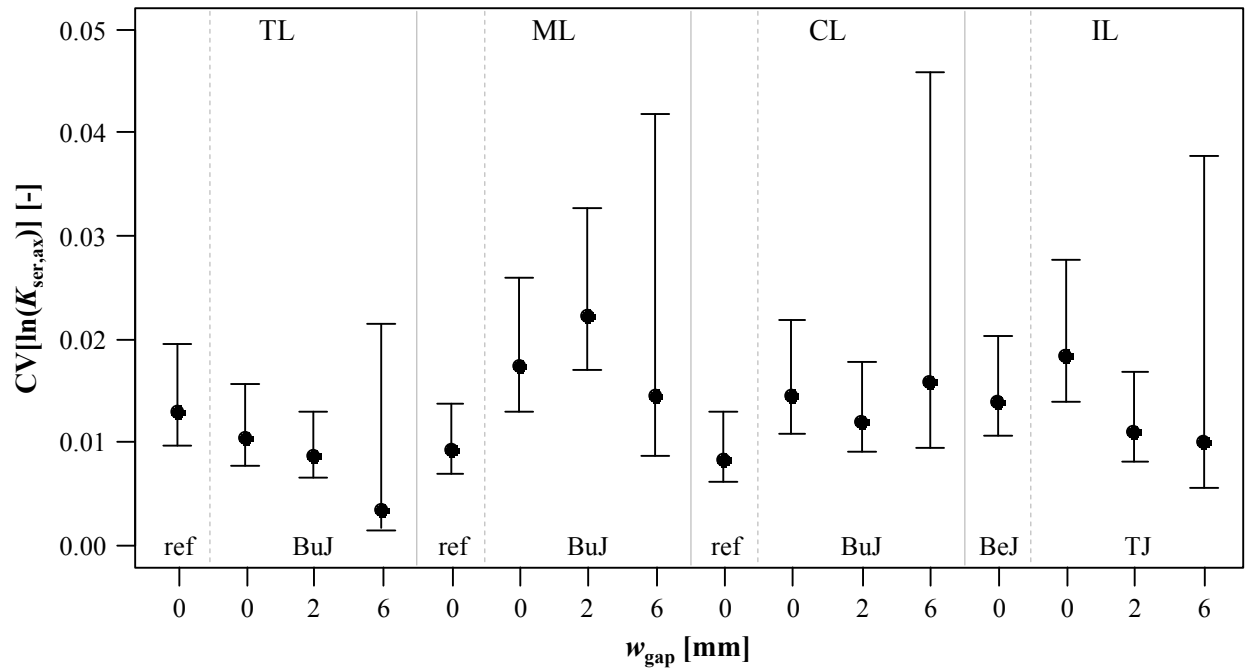


Figure B.37: Cls of $CV[\ln(K_{ser,ax})]$; test programme I, $d = 8$ mm; test specimen corresponding to section 5-3.4

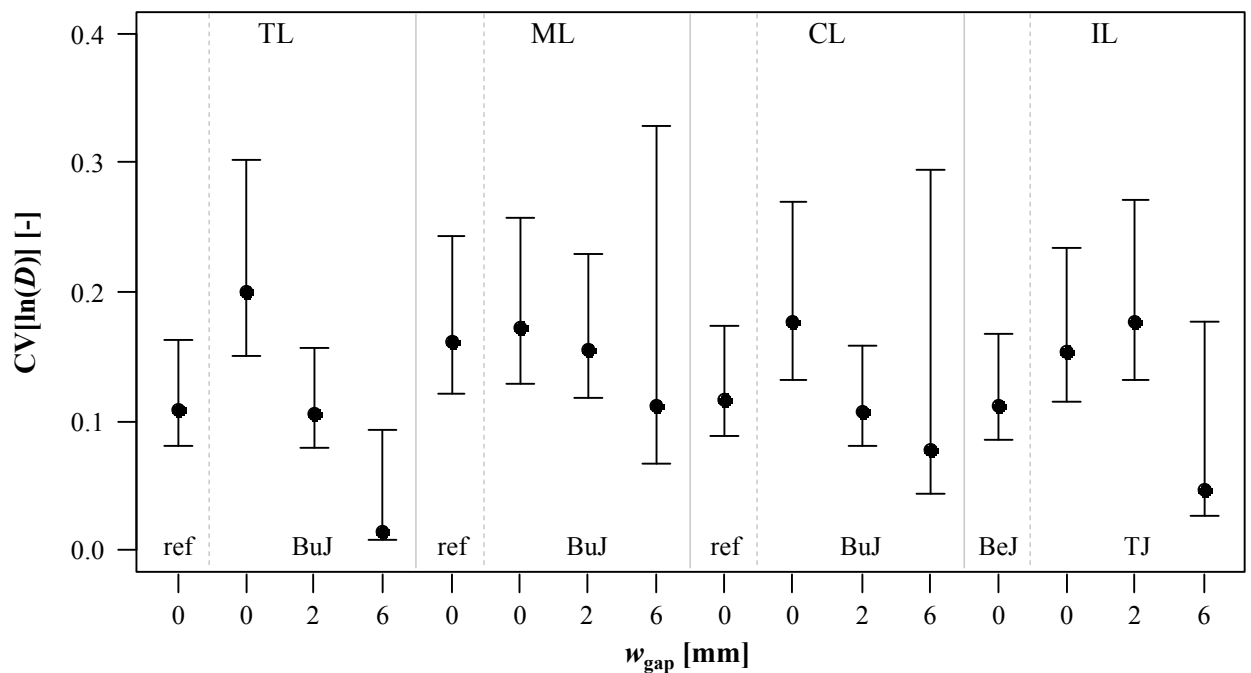


Figure B.38: Cls of $CV[\ln(D)]$; test programme I, $d = 8$ mm; test specimen corresponding to section 5-3.4

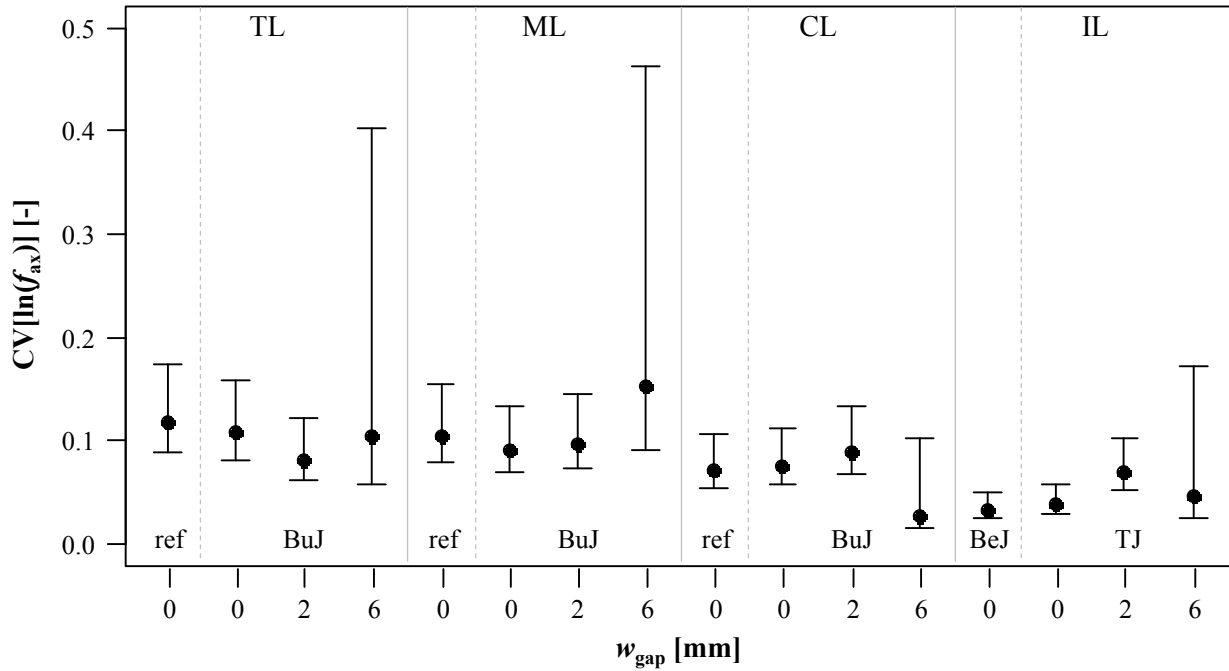


Figure B.39: Cls of $CV[\ln(f_{ax})]$; test programme I, $d = 12$ mm; test specimen corresponding to section 5-3.4

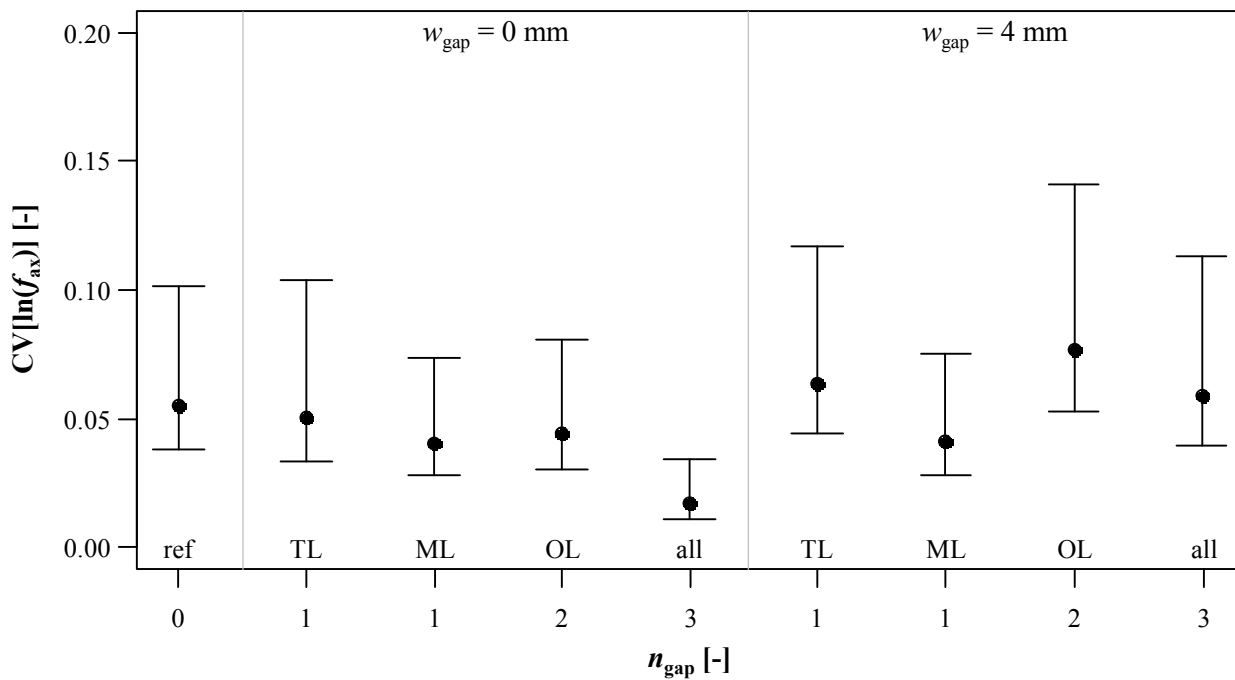


Figure B.40: Cls of $CV[\ln(f_{ax})]$; test programme II; test specimen corresponding to section 5-3.4

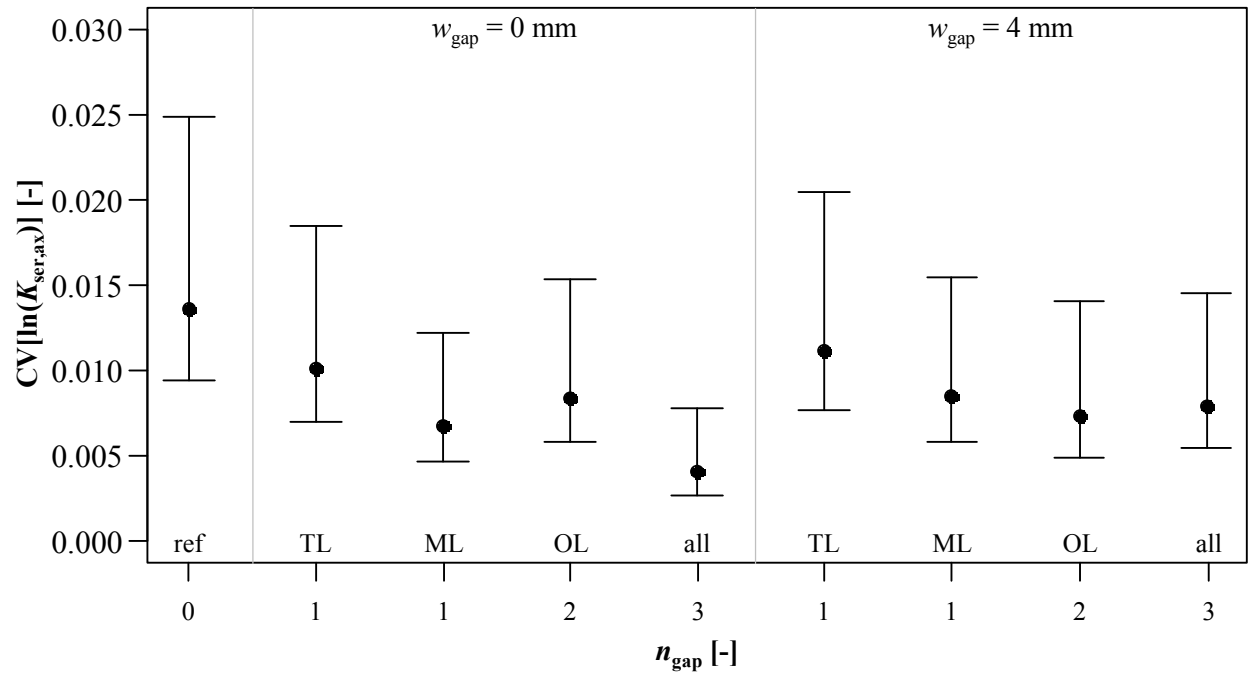


Figure B.41: Cls of $CV[\ln(K_{ser,ax})]$; test programme II; test specimen corresponding to section 5-3.4

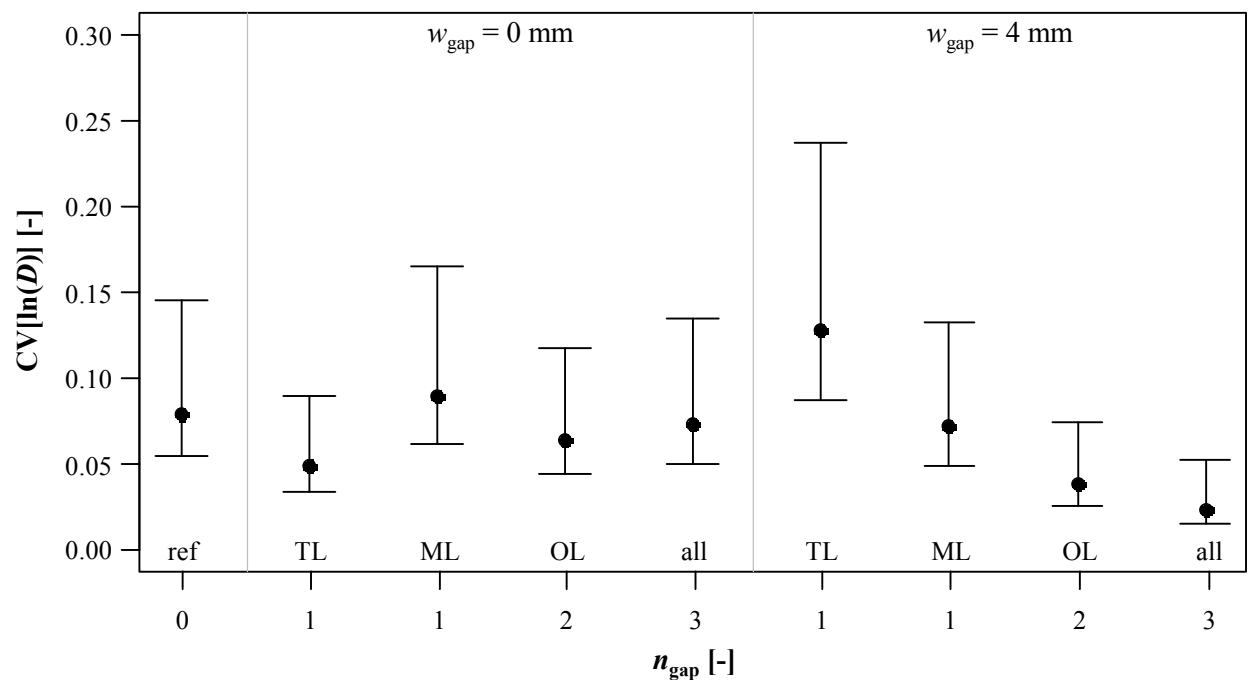


Figure B.42: Cls of $CV[\ln(D)]$; test programme II; test specimen corresponding to section 5-3.4

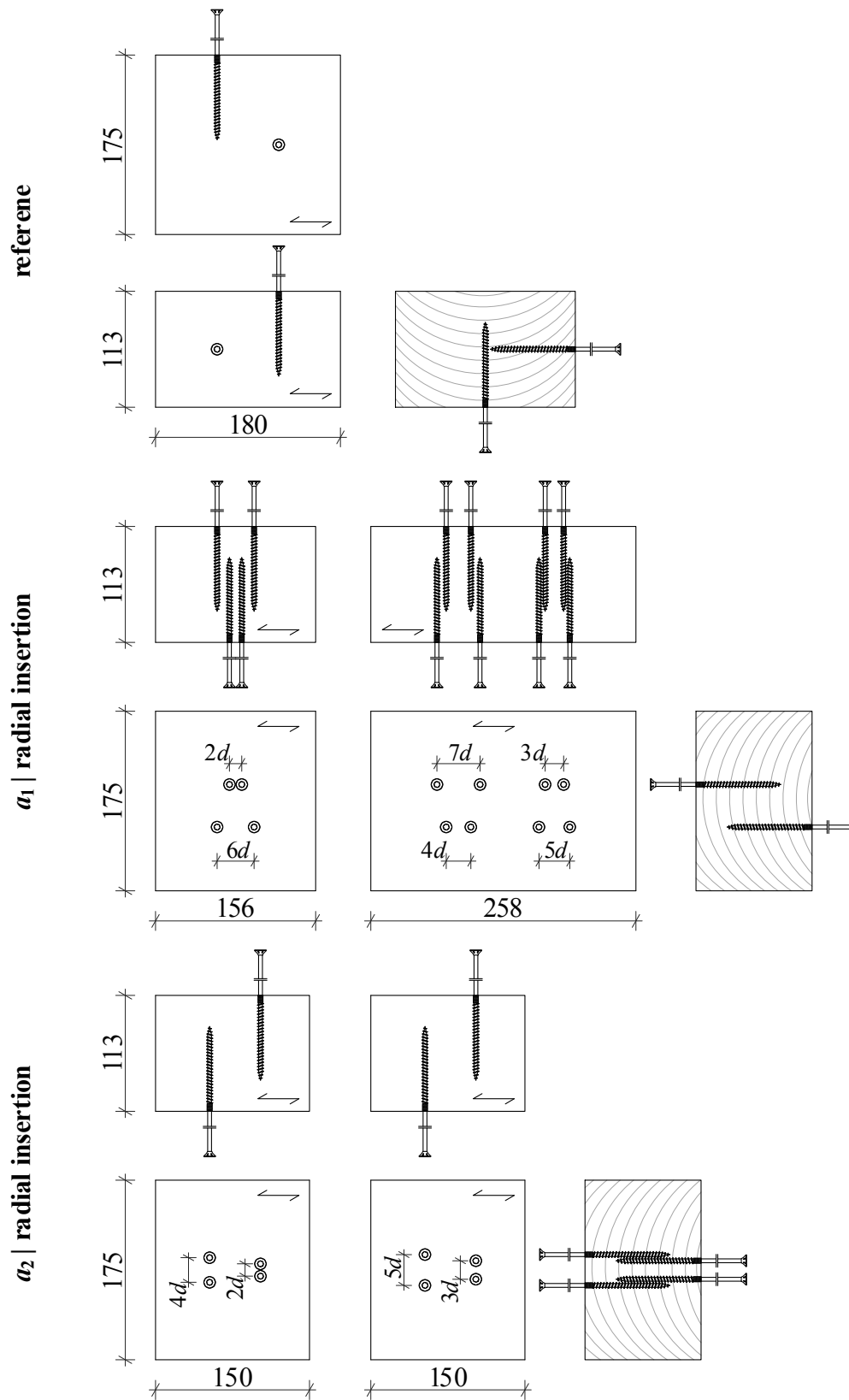


Figure B.43: Illustration of test specimen corresponding to section 5-4.1, according to Plieschounig (2010); all dimensions in [mm]

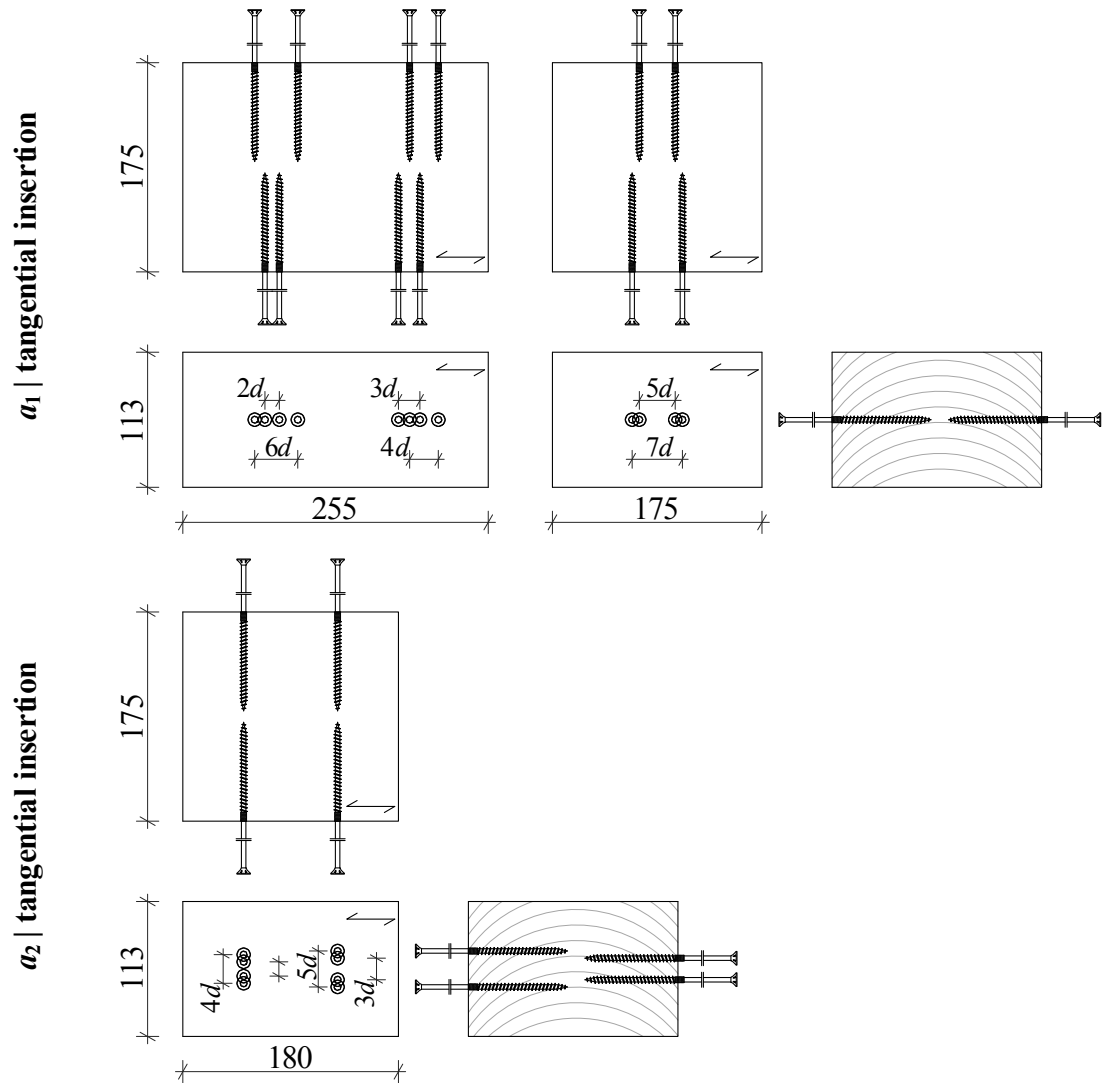


Figure B.44: Illustration of test specimen corresponding to section 5-4.1, according to Plieschounig (2010) (continued); all dimensions in [mm]

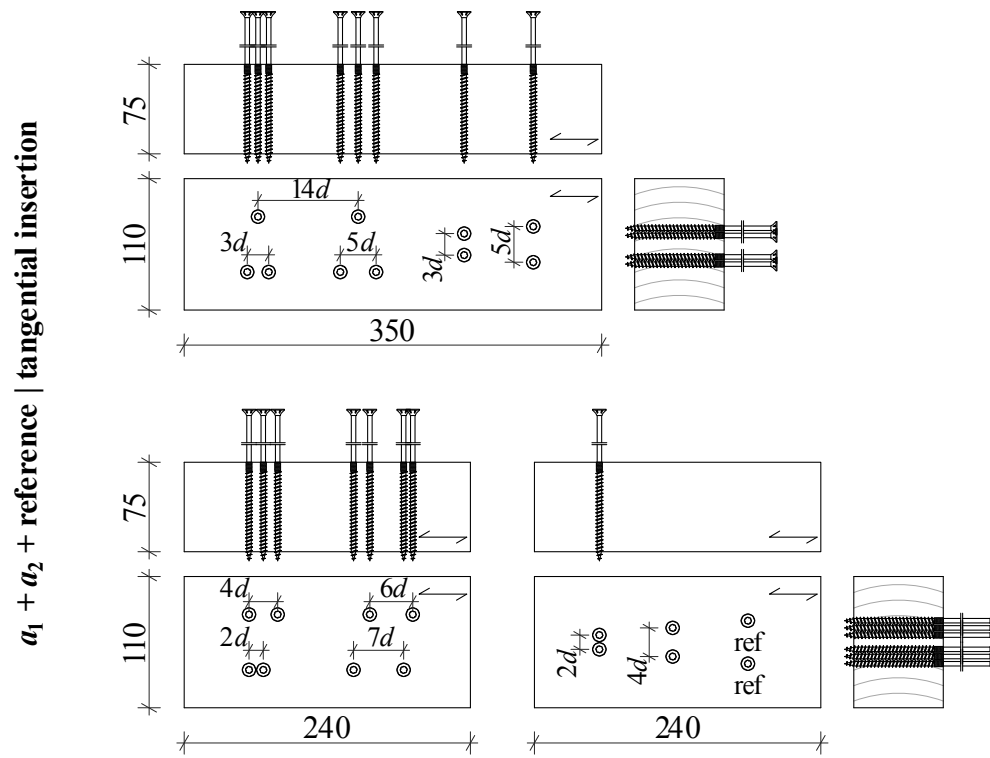


Figure B.45: Illustration of test specimen corresponding to section 5-4.1, according to Plieschounig (2010) (continued); all dimensions in [mm]

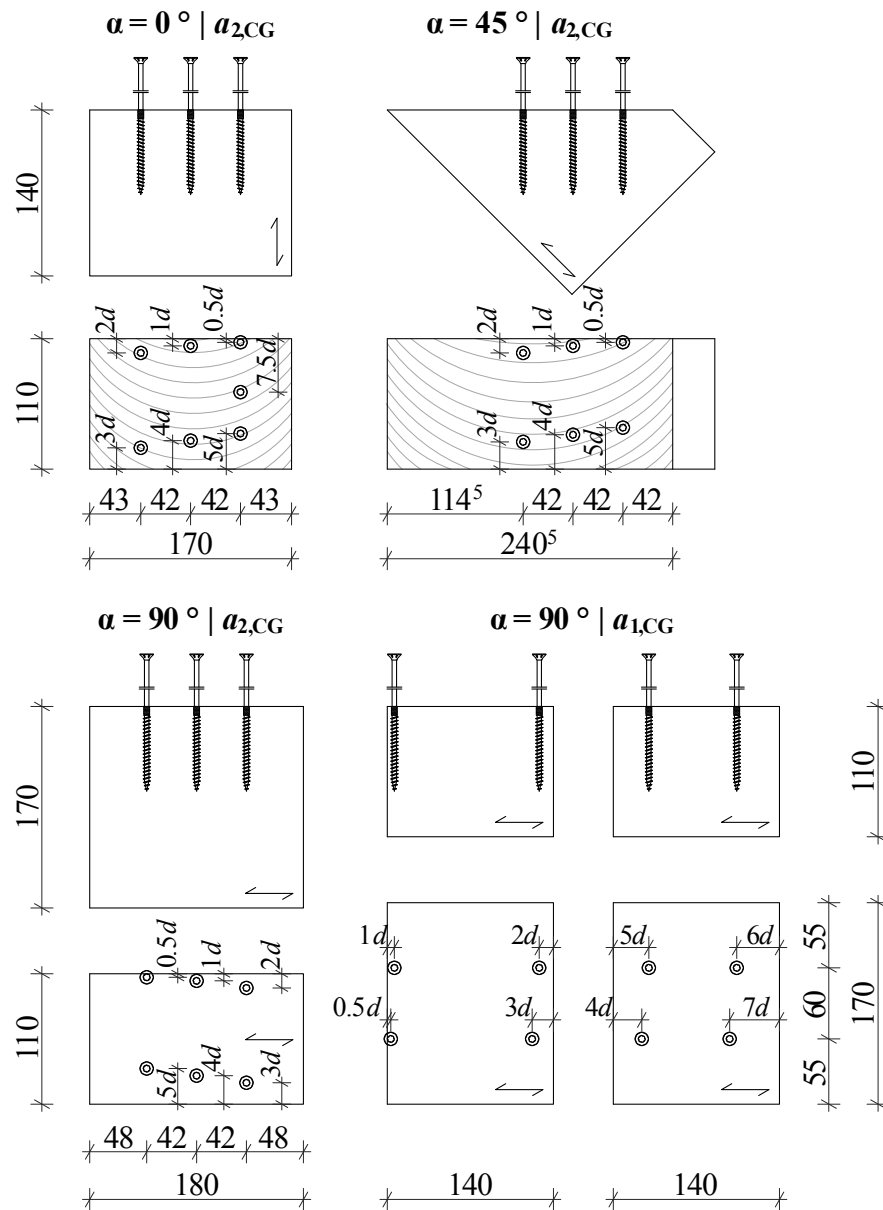


Figure B.46: Illustration of test specimen corresponding to section 5-4.1, according to Gatterrig (2010); all dimensions in [mm]

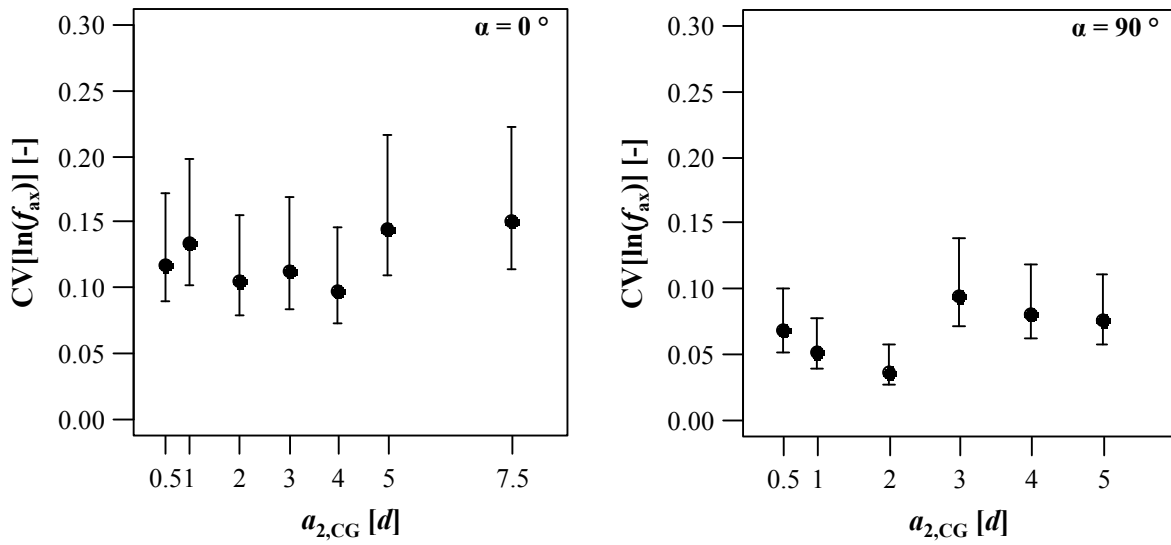


Figure B.47: CIs of $CV[\ln(f_{ax})]$ in dependence of spacing type and axis-to-grain angle; test specimen corresponding to section 5-4.1, test data from Gattermig (2010)

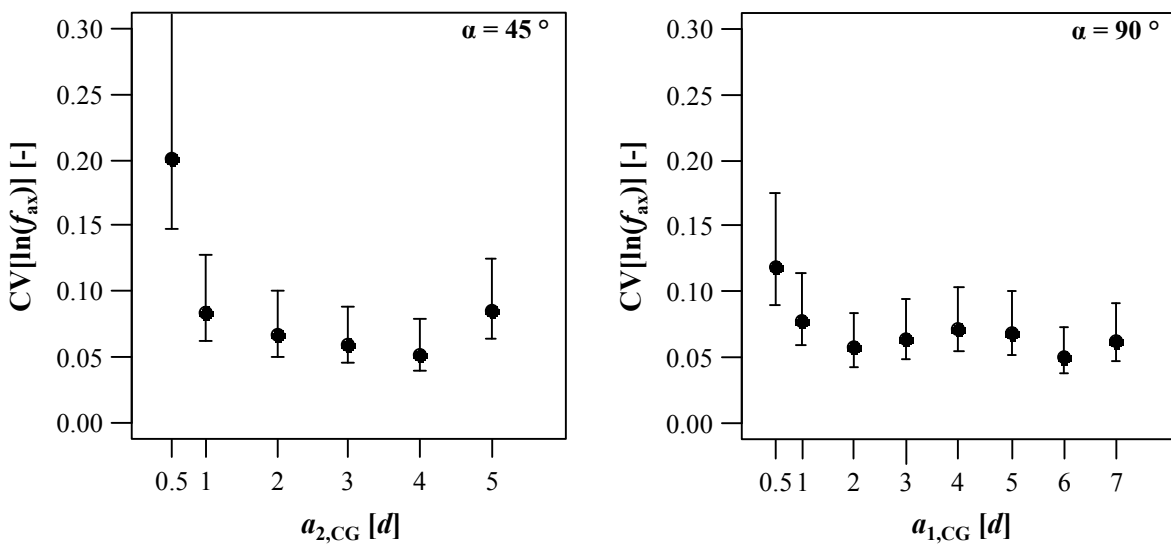


Figure B.48: CIs of $CV[\ln(f_{ax})]$ in dependence of spacing type and axis-to-grain angle; test specimen corresponding to section 5-4.1, test data from Gattermig (2010); (continued)

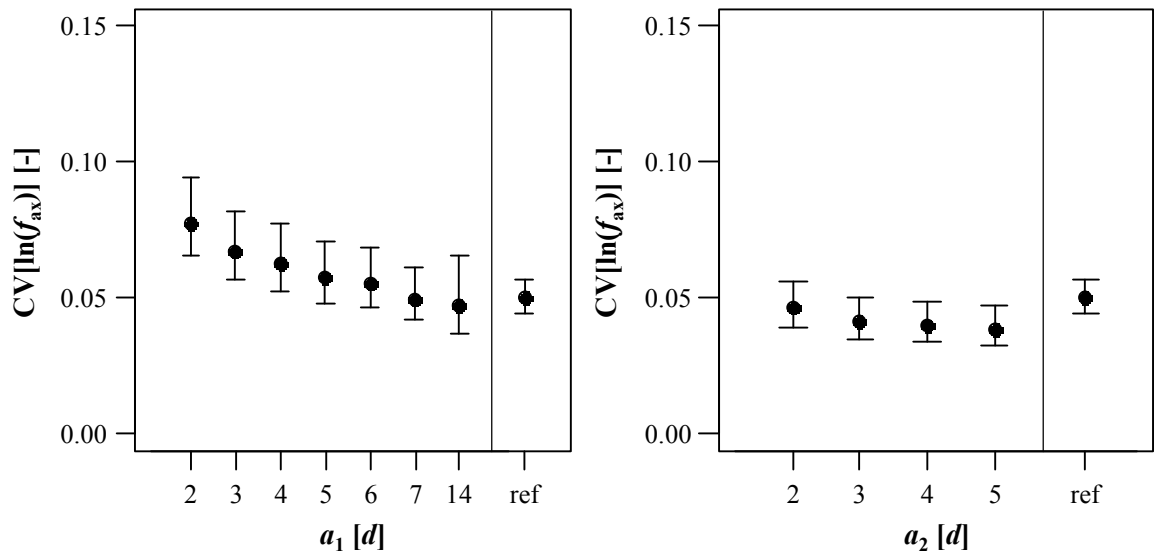


Figure B.49: CIs of $CV[\ln(f_{ax})]$ in dependence of spacing type a_1 and a_2 ; test specimen corresponding to section 5-4.1, test data from Plieschounig (2010)

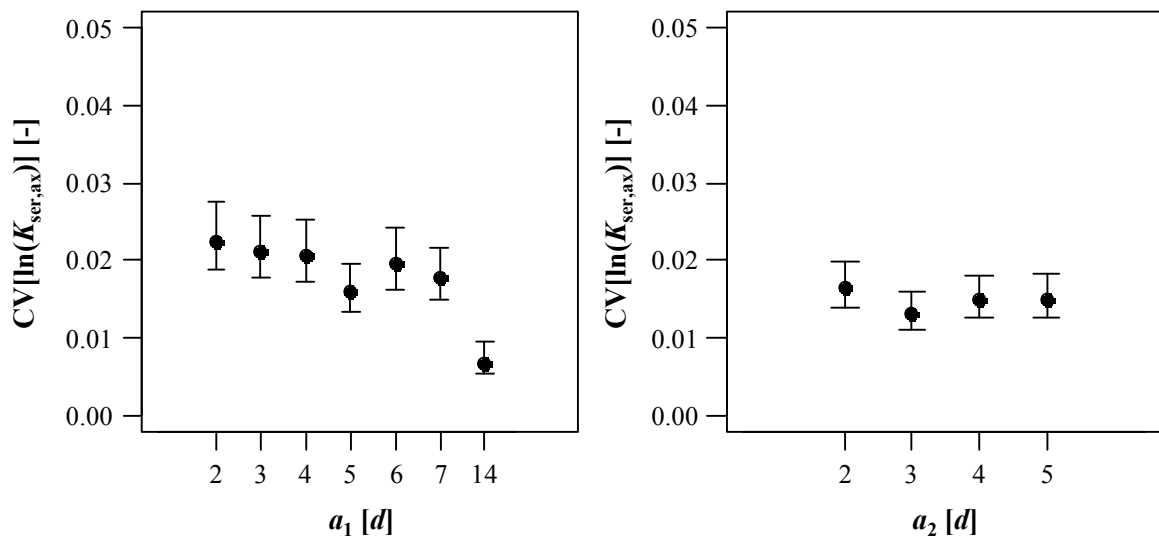


Figure B.50: CIs of $CV[\ln(K_{ser,ax})]$ in dependence of spacing type a_1 and a_2 ; test specimen corresponding to section 5-4.1, test data from Plieschounig (2010)

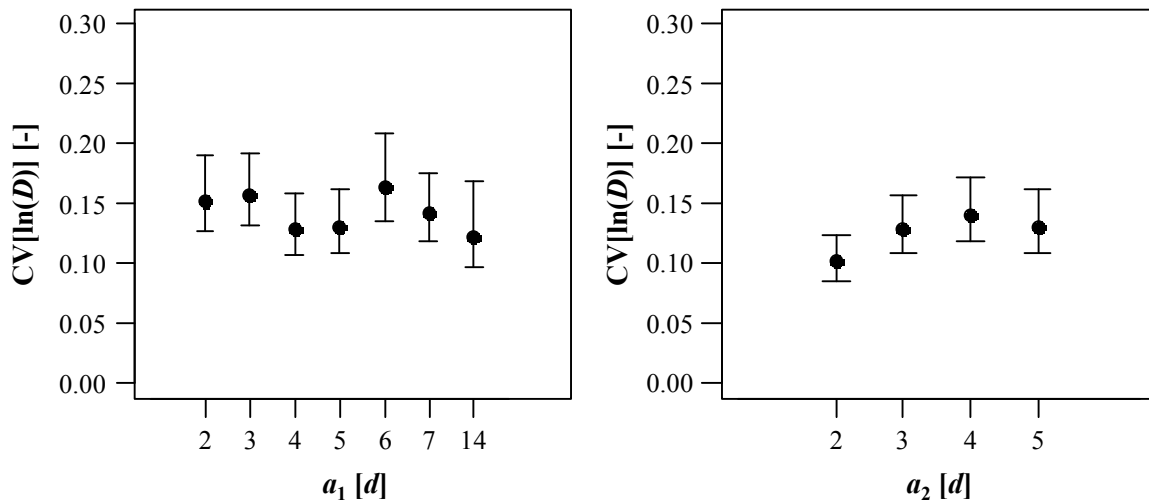


Figure B.51: CIs of $CV[\ln(D)]$ in dependence of spacing type a_1 and a_2 ; test specimen corresponding to section 5-4.1, test data from Plieschounig (2010)

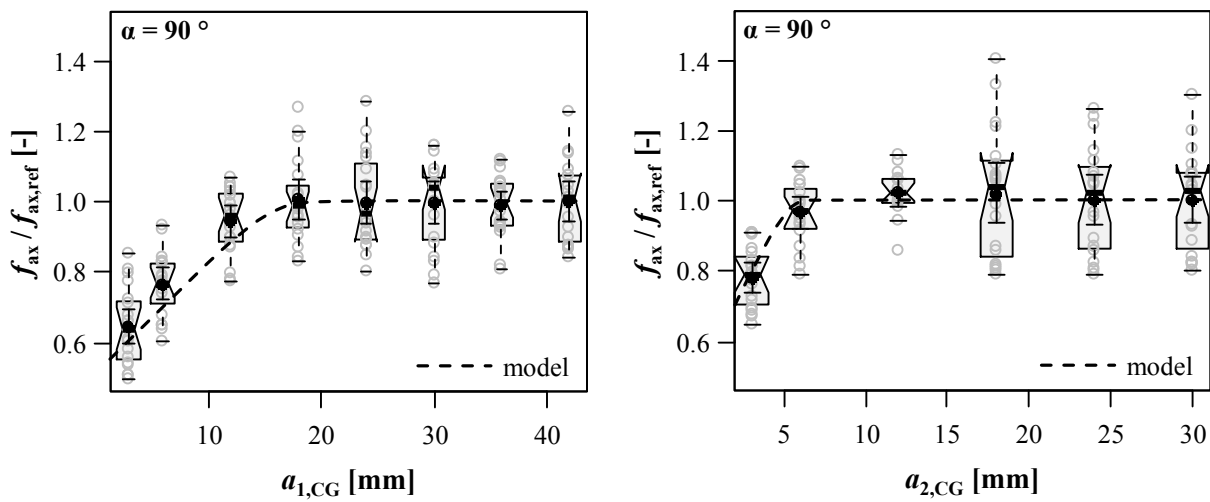


Figure B.52: Comparison of test results with model predictions for $a_{1,CG}$ and $a_{2,CG}$ at $\alpha = 90^\circ$; test data from Gatterinig (2010)

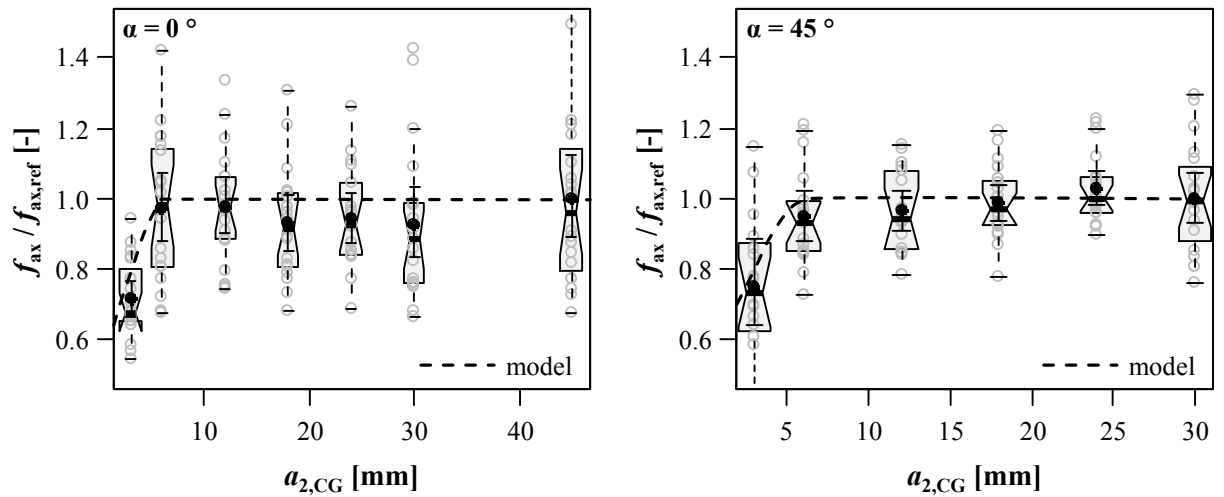


Figure B.53: Comparison of test results with model predictions for $a_{1,CG}$ and $\alpha = \{0, 45\}^\circ$; test data from Gatternig (2010)

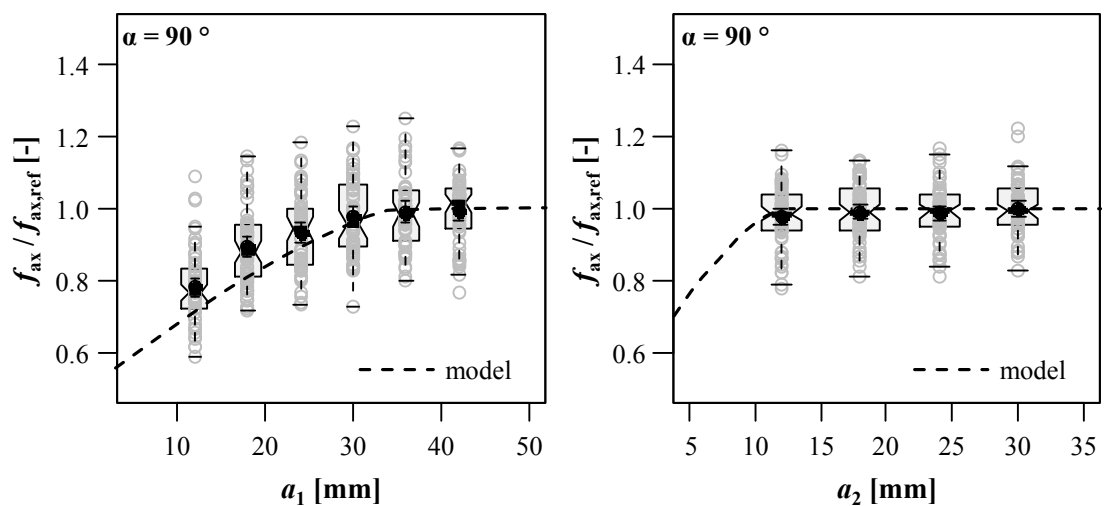


Figure B.54: Comparison of test results with model predictions for a_1 and a_2 at $\alpha = 90^\circ$; test data from Plieschounig (2010)

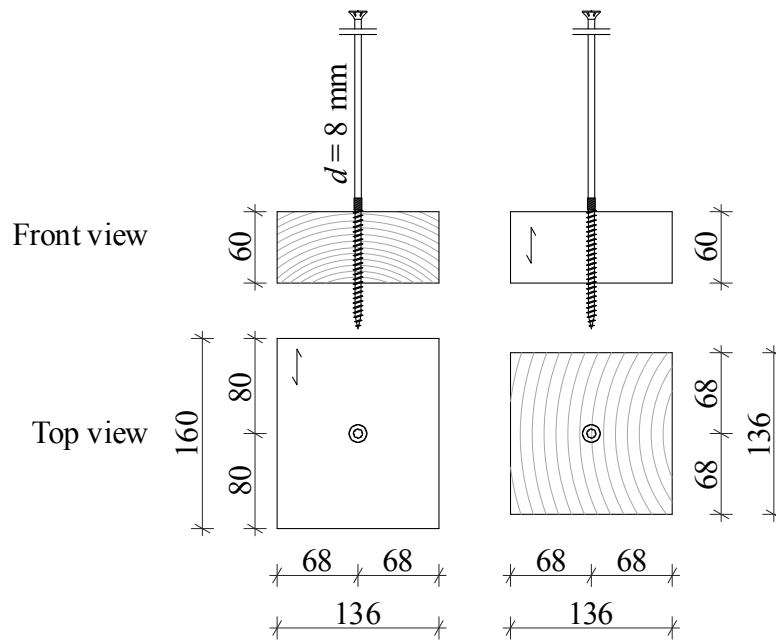


Figure B.55: Illustration of test specimen corresponding to section 5-4.2; left: $\alpha = 90^\circ$, right: $\alpha = 0^\circ$; all dimensions in [mm]

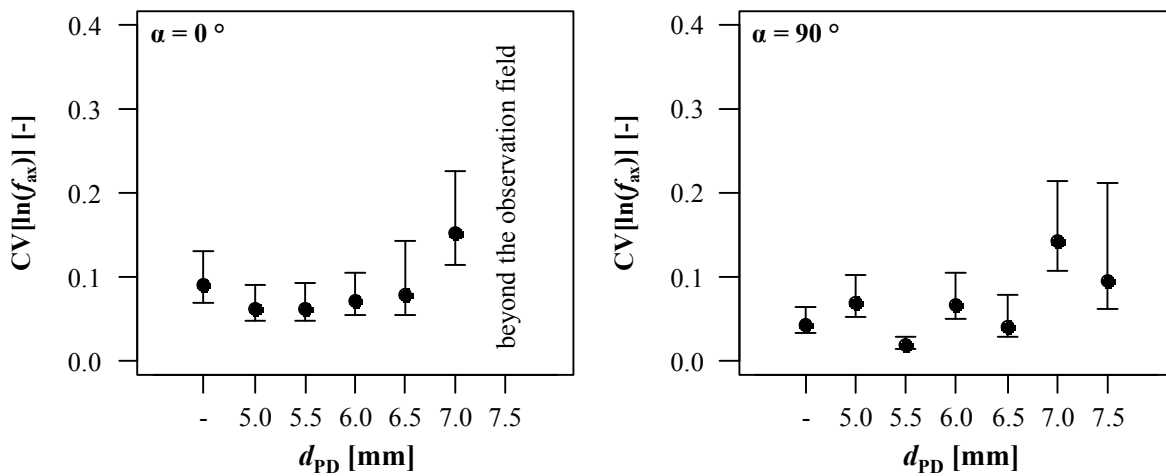


Figure B.56: CIs of $CV[\ln(f_{ax})]$; left: $\alpha = 0^\circ$; right: $\alpha = 90^\circ$; test specimen corresponding to section 5-4.2; test data from Gasser (2017)

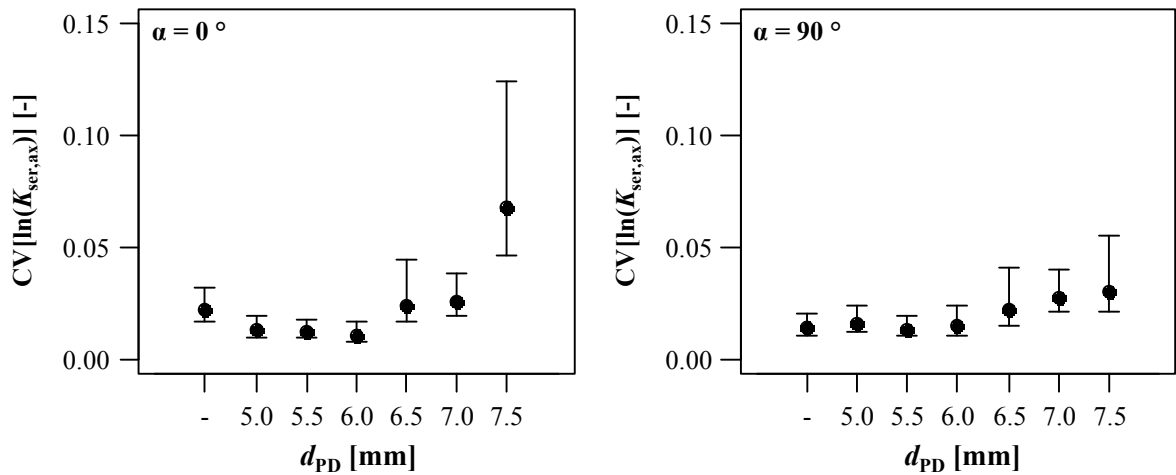


Figure B.57: CIs of $CV[\ln(K_{ser,ax})]$; left: $\alpha = 0^\circ$; right: $\alpha = 90^\circ$; test specimen corresponding to section 5-4.2; test data from Gasser (2017)

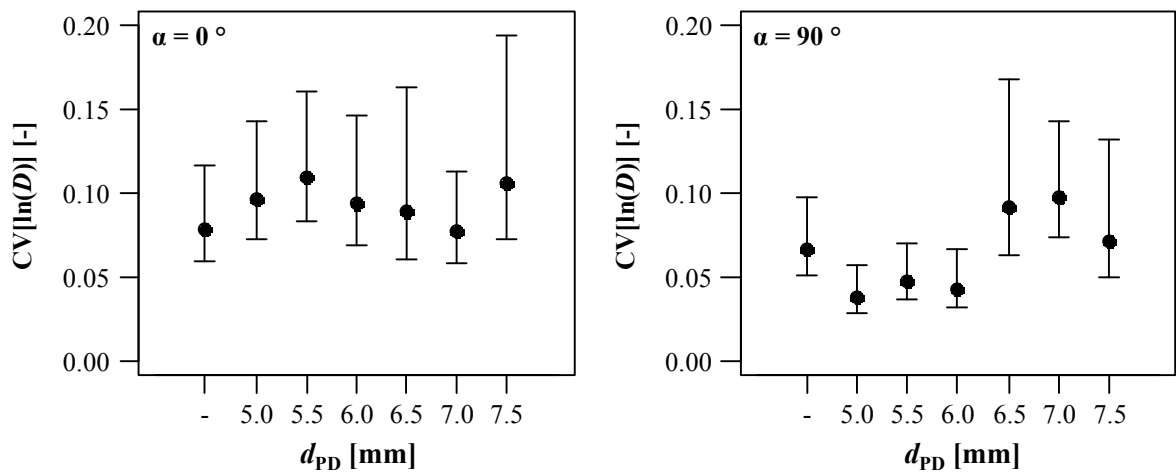


Figure B.58: CIs of $CV[\ln(D)]$; left: $\alpha = 0^\circ$; right: $\alpha = 90^\circ$; test specimen corresponding to section 5-4.2; test data from Gasser (2017)

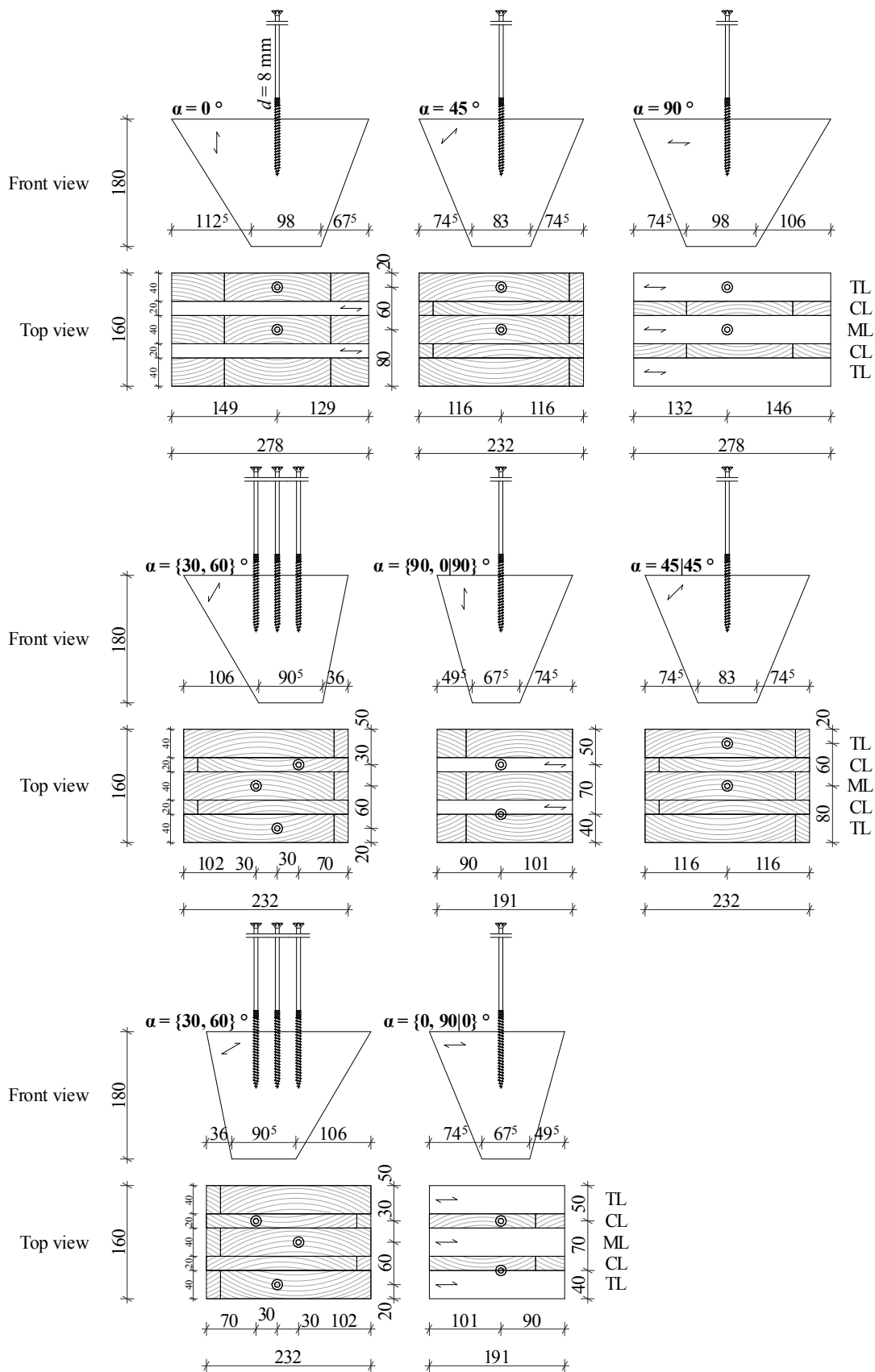


Figure B.59: Illustration of test specimen corresponding to section 5-4.3, test campaign I; exemplarily for $d = 8 \text{ mm}$; all dimensions in [mm]

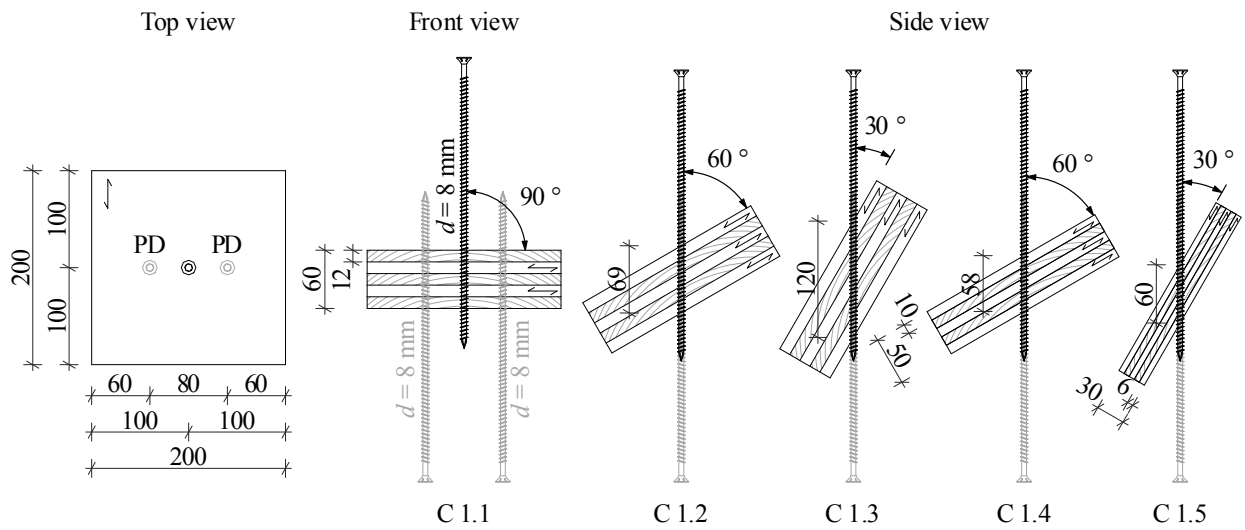


Figure B.60: Illustration of test specimen corresponding to section 5-4.3, test campaign II; exemplarily for $d = 8$ mm; all dimensions in [mm]

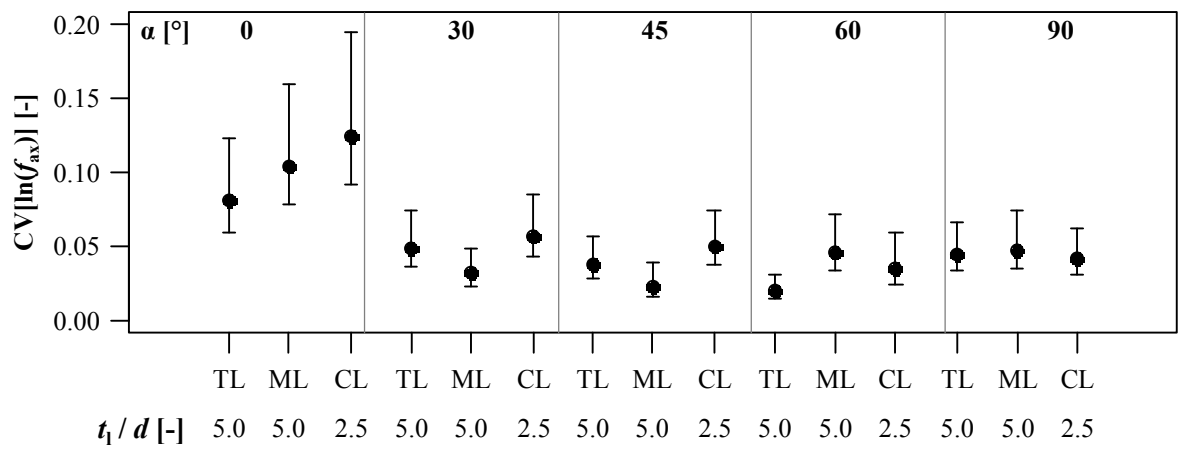


Figure B.61: Cls of $CV[\ln(f_{ax})]$ in dependence of axis-to-grain angle and ratio t_1/d ; test programme I, $d = 8$ mm; test specimen corresponding to section 5-4.3

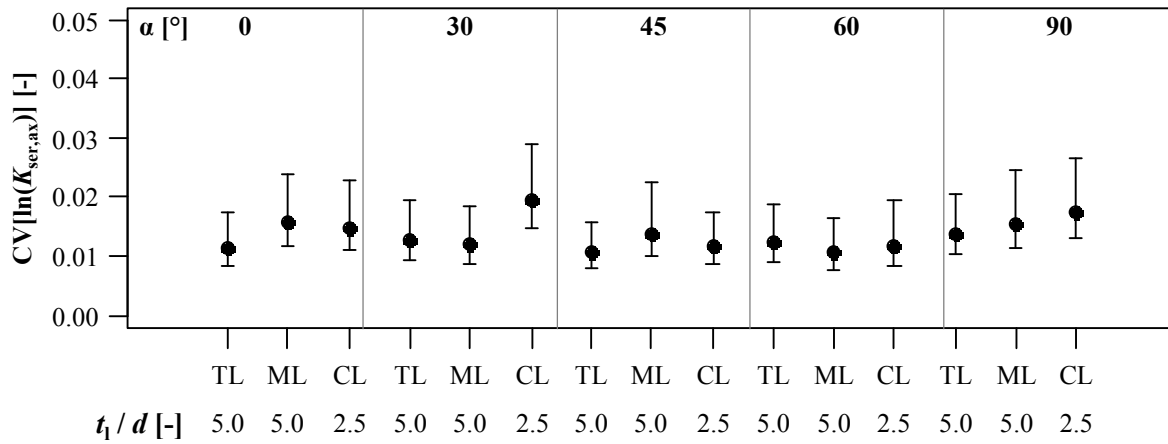


Figure B.62: CIs of $CV[\ln(K_{ser,ax})]$ in dependence of axis-to-grain angle and ratio t_1/d ; test programme I, $d = 8$ mm; test specimen corresponding to section 5-4.3

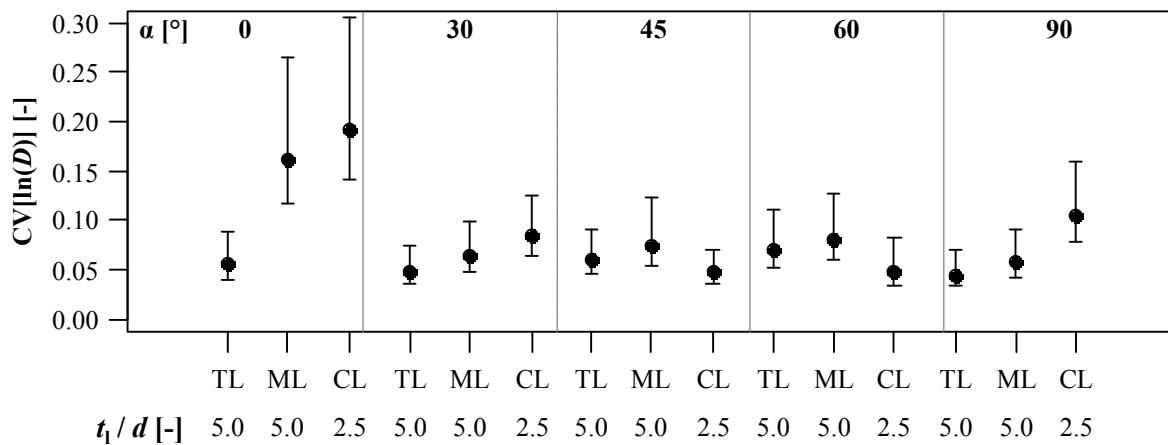


Figure B.63: CIs of $CV[\ln(D)]$ in dependence of axis-to-grain angle and ratio t_1/d ; test programme I, $d = 8$ mm; test specimen corresponding to section 5-4.3

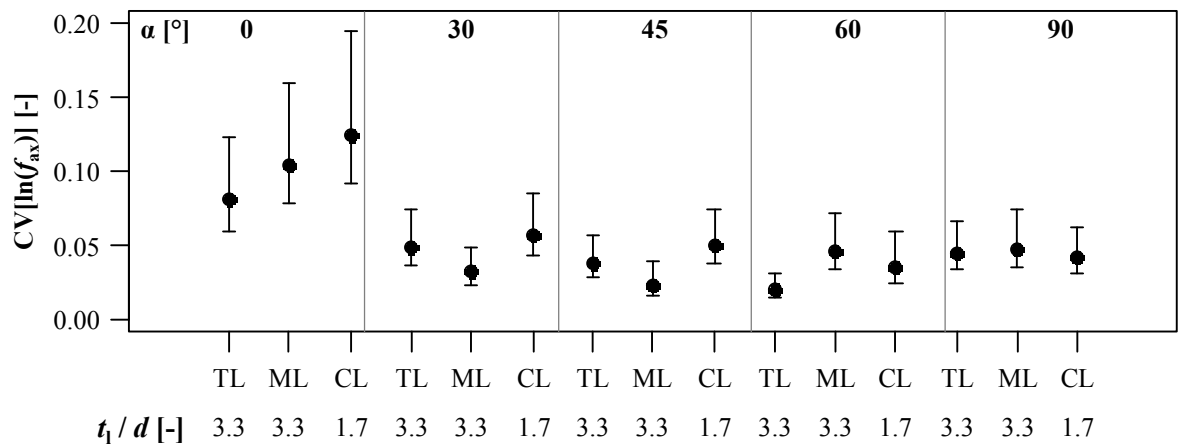


Figure B.64: CIs of $CV[\ln(f_{ax})]$ in dependence of axis-to-grain angle and ratio t_1 / d ; test programme I, $d = 12 \text{ mm}$; test specimen corresponding to section 5-4.3

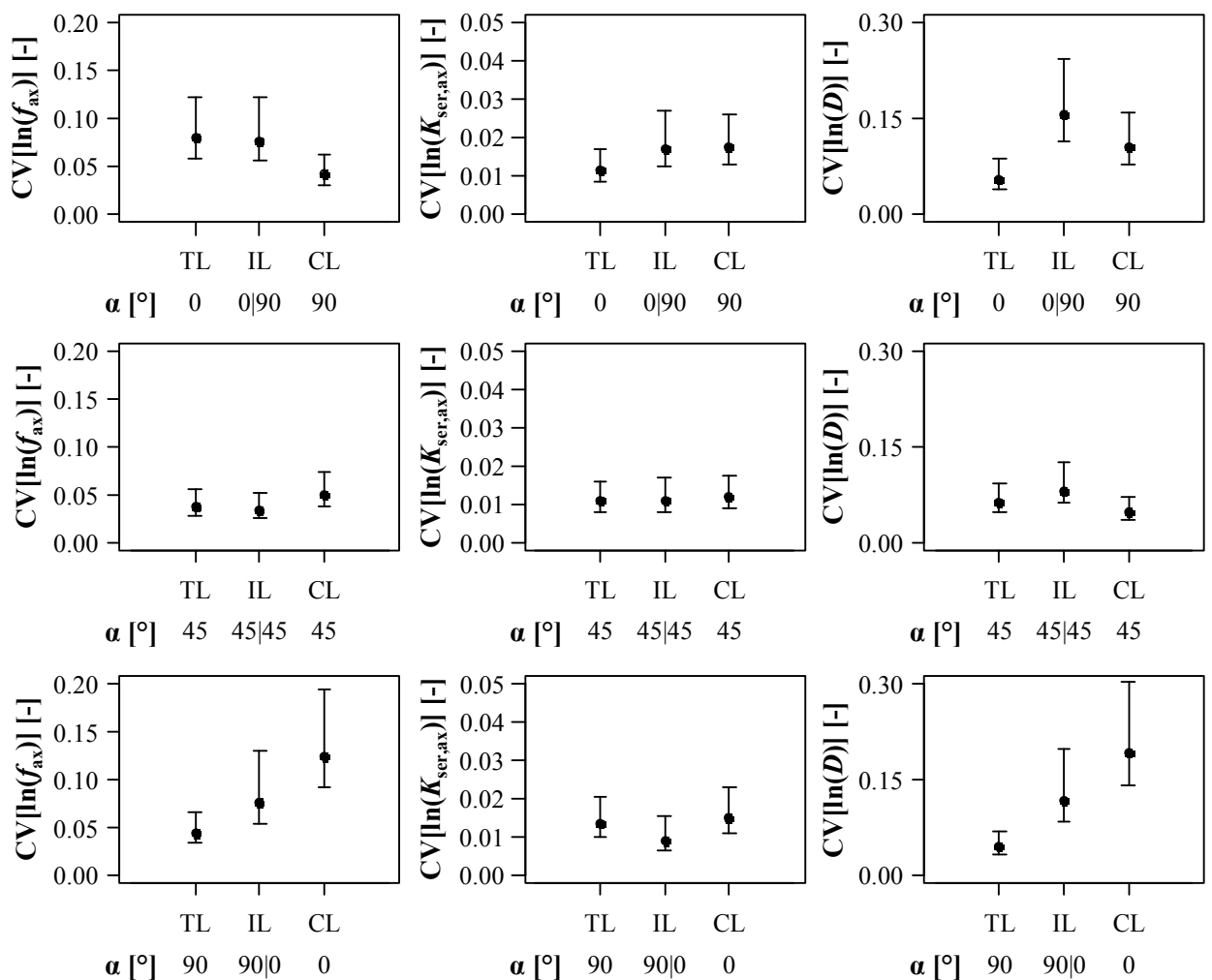


Figure B.65: CIs of $CV[\ln(X)]$ of screws situated in intermediate layers; test programme I, $d = 8 \text{ mm}$; test specimen corresponding to section 5-4.3

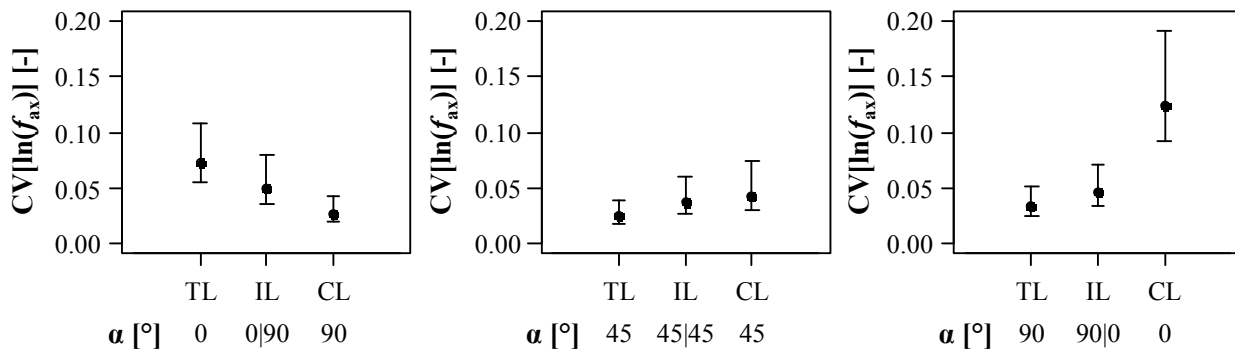


Figure B.66: CIs of $CV[\ln(f_{ax})]$ of screws situated in intermediate layers; test programme I, $d = 12$ mm; test specimen corresponding to section 5-4.3

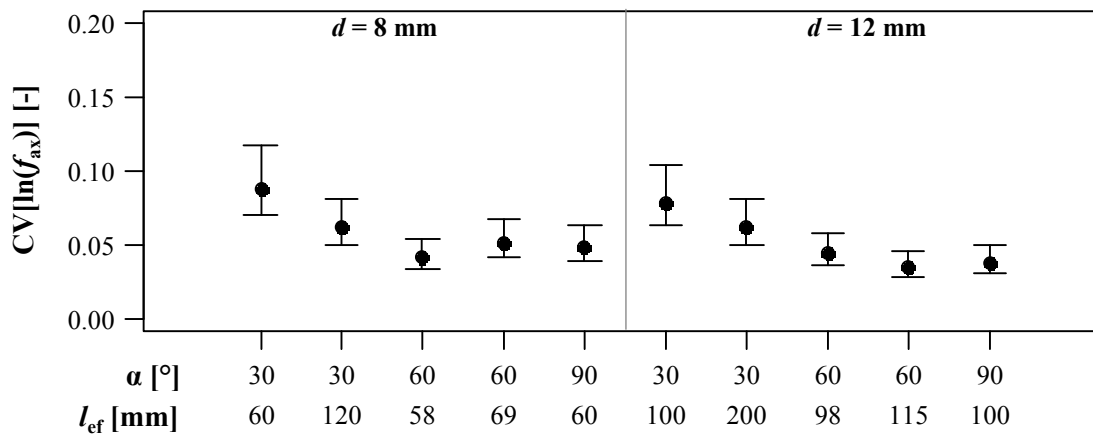


Figure B.67: CIs of $CV[\ln(f_{ax})]$ in dependence of axis-to-grain angle and effective insertion length; test programme II, test specimen corresponding to section 5-4.3

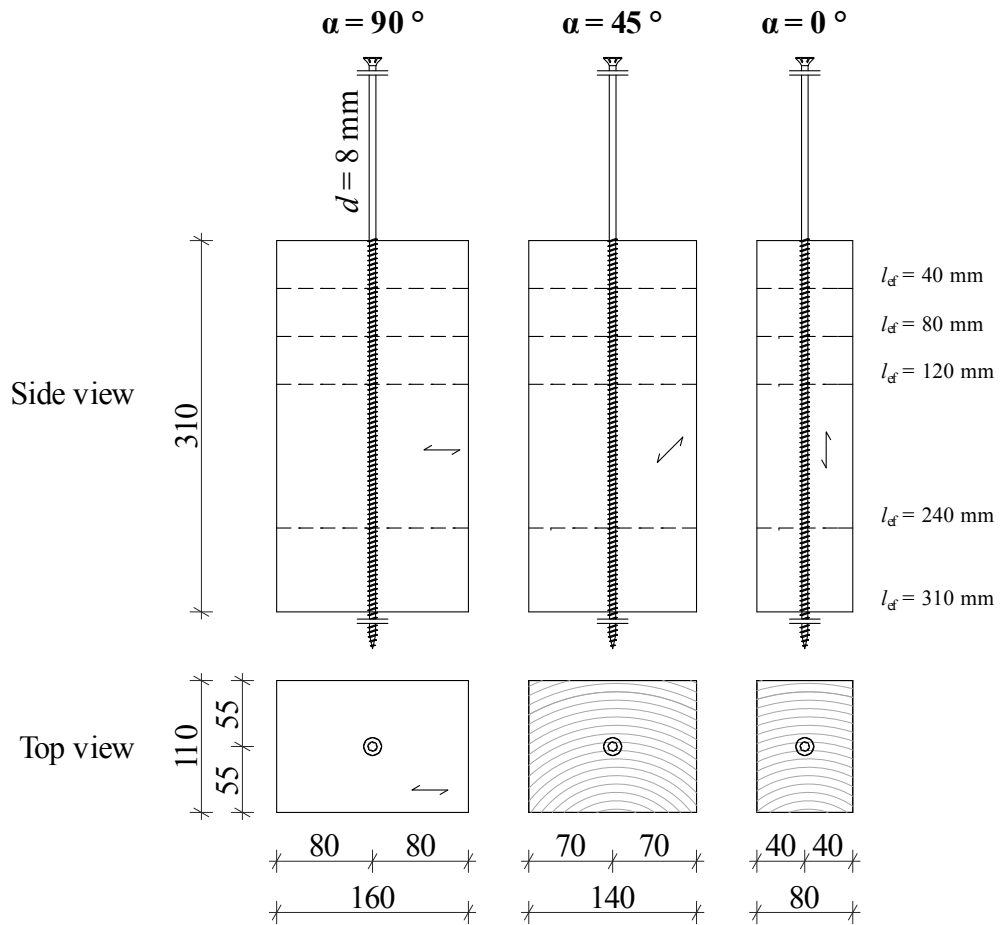


Figure B.68: Illustration of test specimen corresponding to section 5-4.5; all dimensions in [mm]

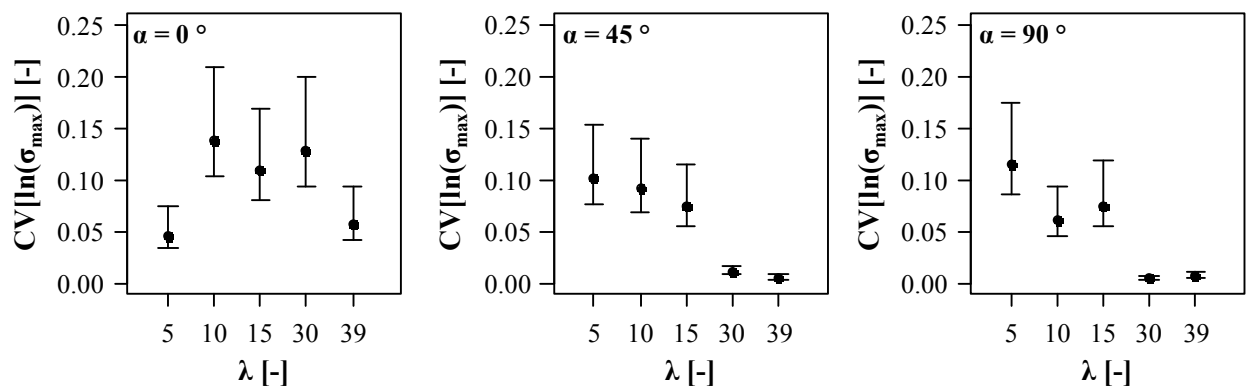


Figure B.69: CIs of $CV[\ln(\sigma_{max})]$ in dependence of axis-to-grain angle and slenderness; test specimen corresponding to section 5-4.5

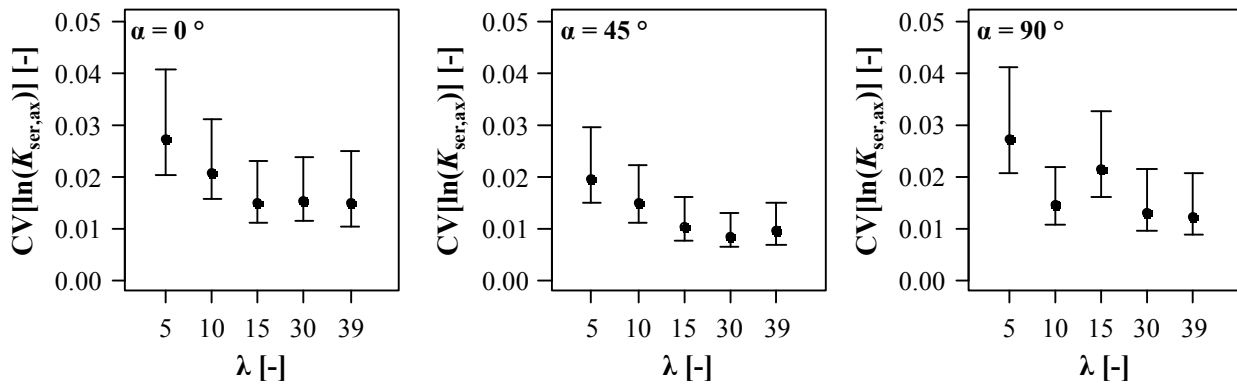


Figure B.70: CIs of $CV[\ln(K_{ser,ax})]$ in dependence of axis-to-grain angle and slenderness; test specimen corresponding to section 5-4.5

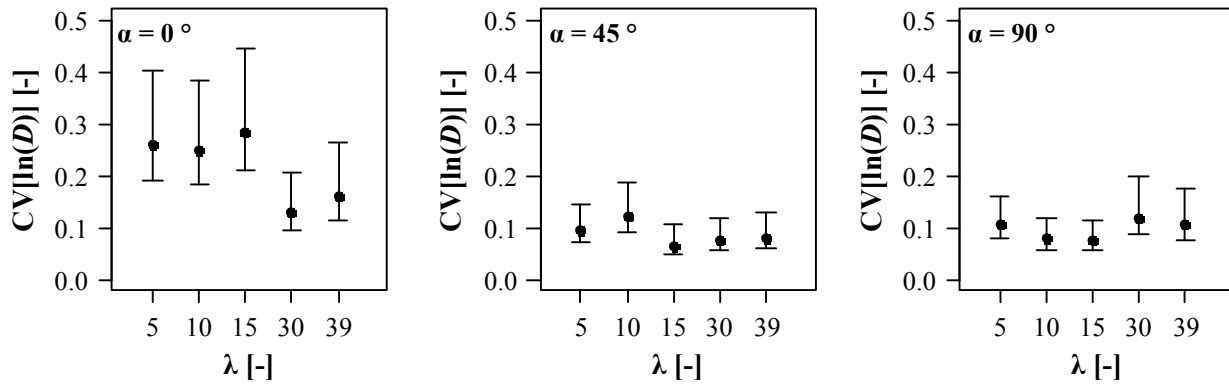


Figure B.71: CIs of $CV[\ln(D)]$ in dependence of axis-to-grain angle and slenderness; test specimen corresponding to section 5-4.5

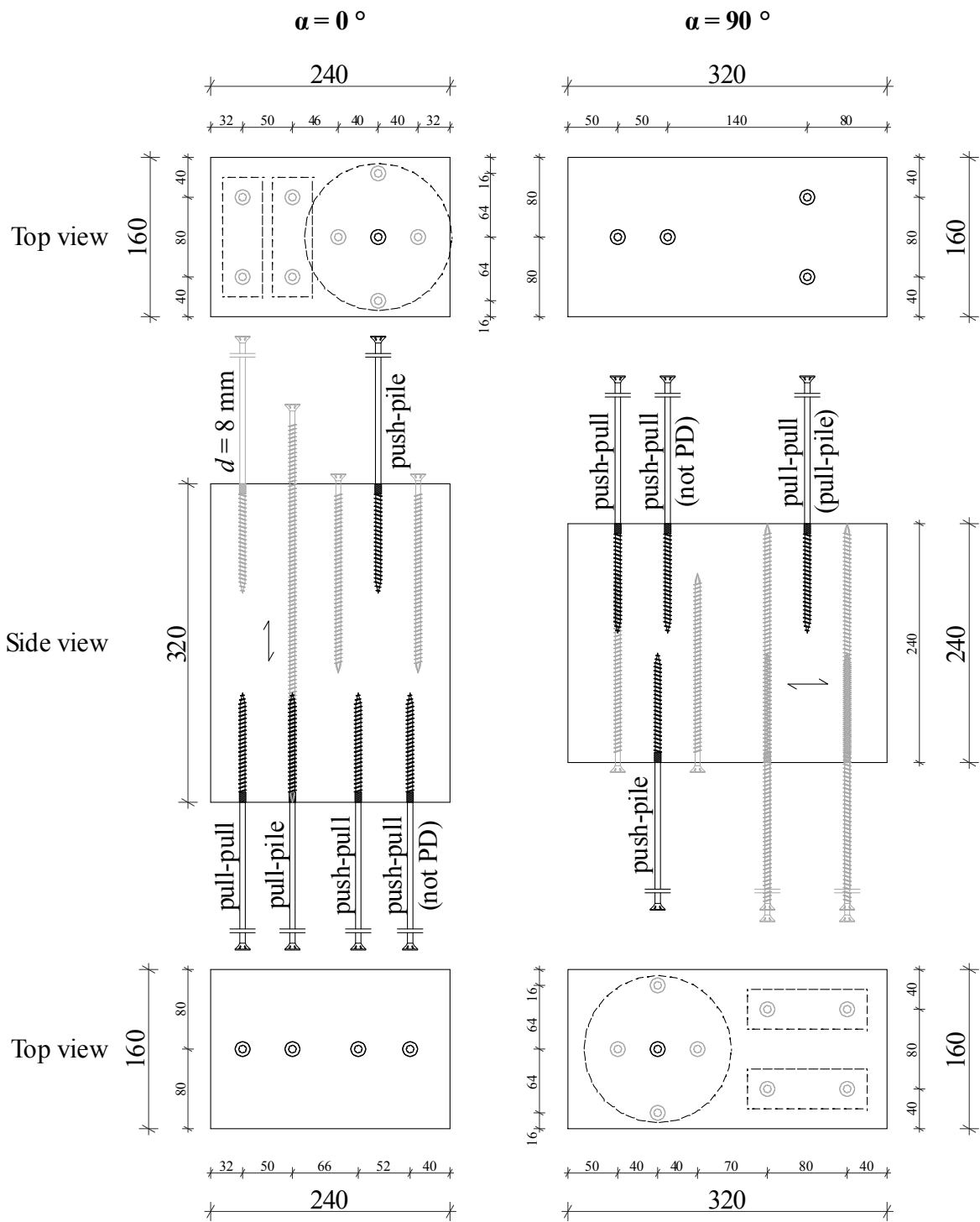


Figure B.72: Illustration of test specimen corresponding to section 5-5.1, variation of test configurations; all dimensions in [mm]

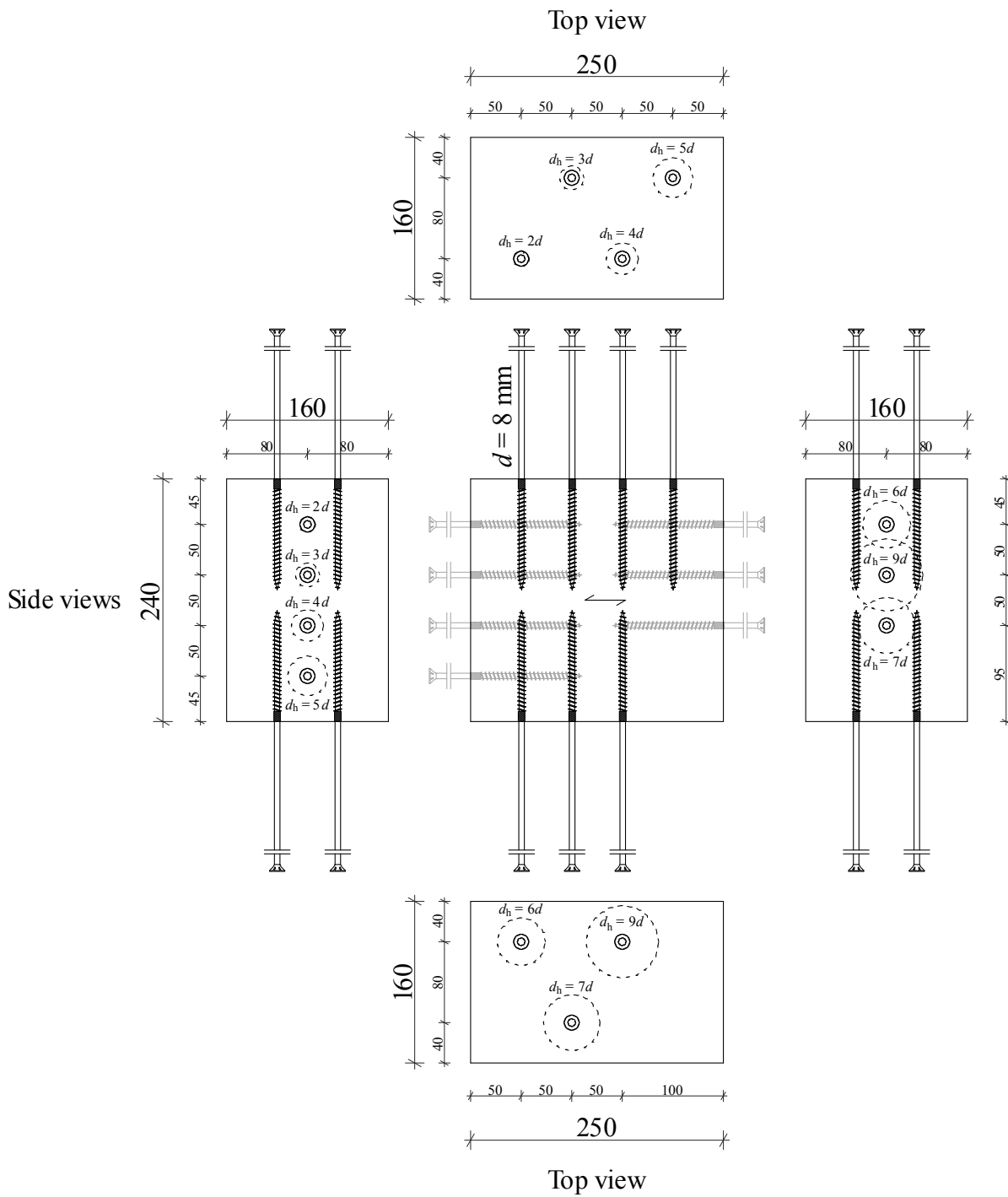


Figure B.73: Illustration of test specimen corresponding to section 5-5.1, variation of the supporting plate's d_h ; all dimensions in [mm]

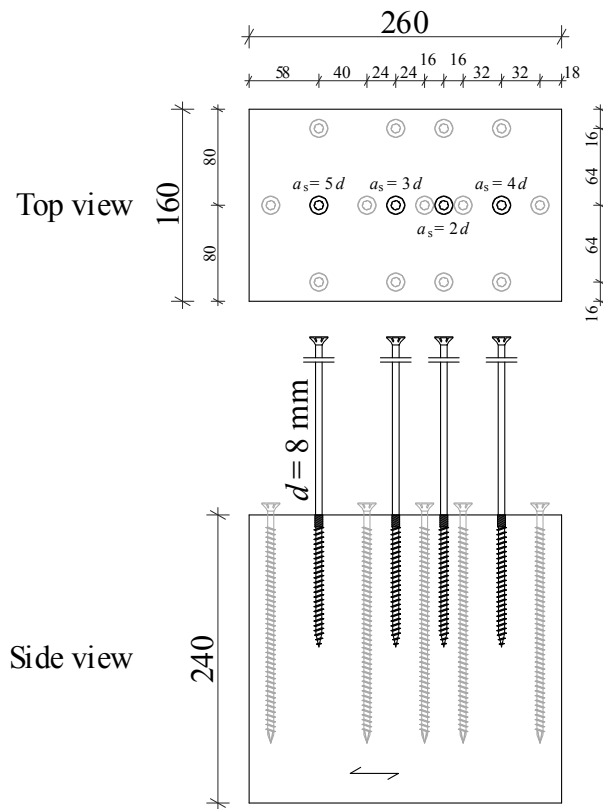


Figure B.74: Illustration of test specimen corresponding to section 5-5.1, variation of the supporting screw's a_s ; all dimensions in [mm]

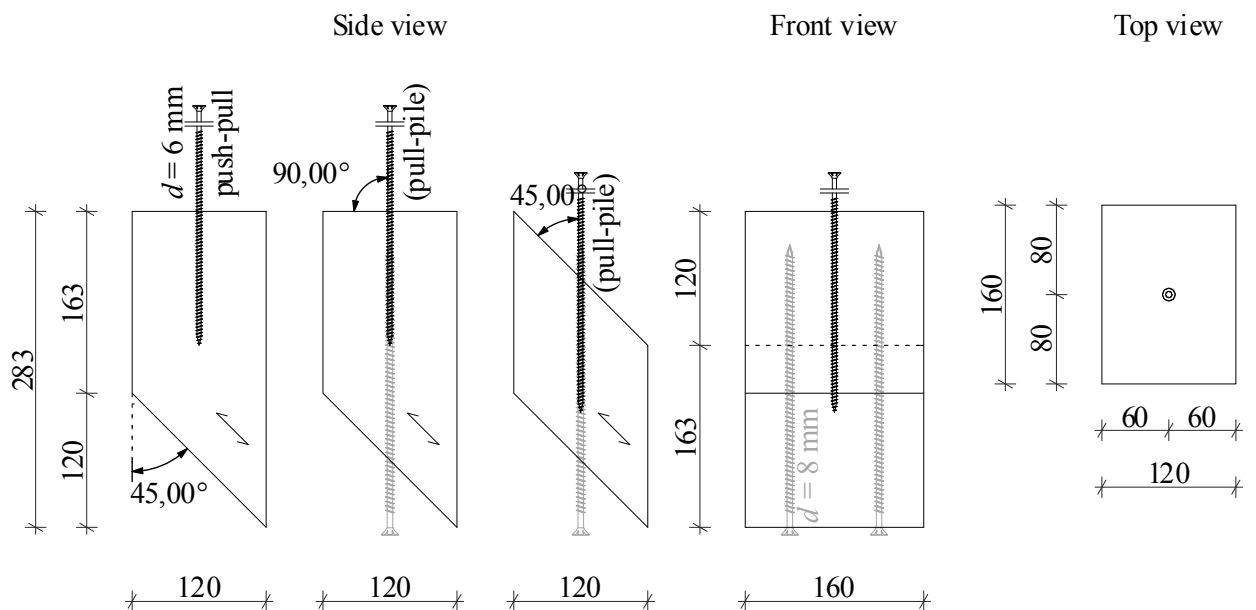


Figure B.75: Illustration of test specimen corresponding to section 5-5.1, variation of test configurations and surface angle ϵ_{sur} ; all dimensions in [mm]

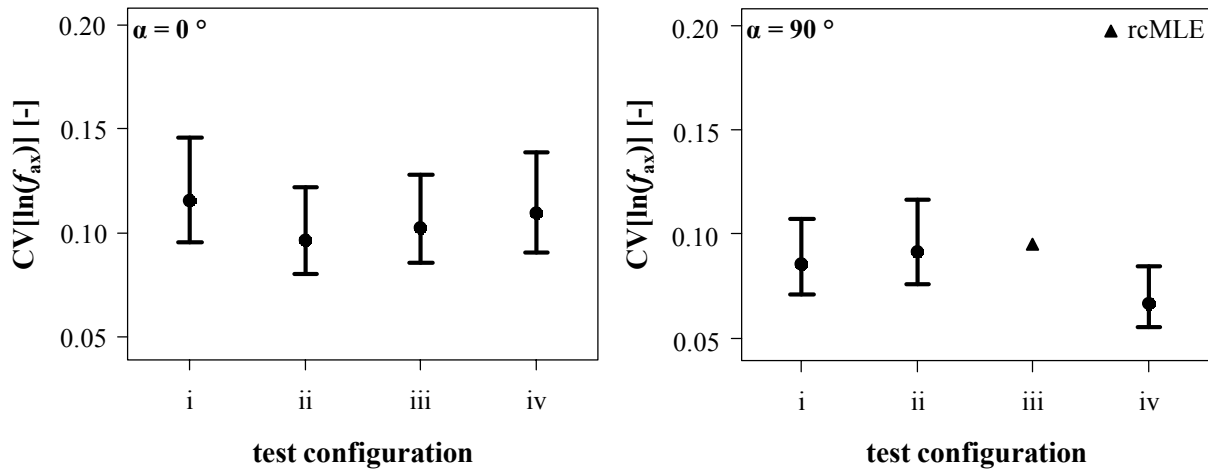


Figure B.76: CIs of $CV[\ln(f_{ax})]$ in dependence of axis-to-grain angle and test configuration; according to Ringhofer and Schickhofer (2014a)

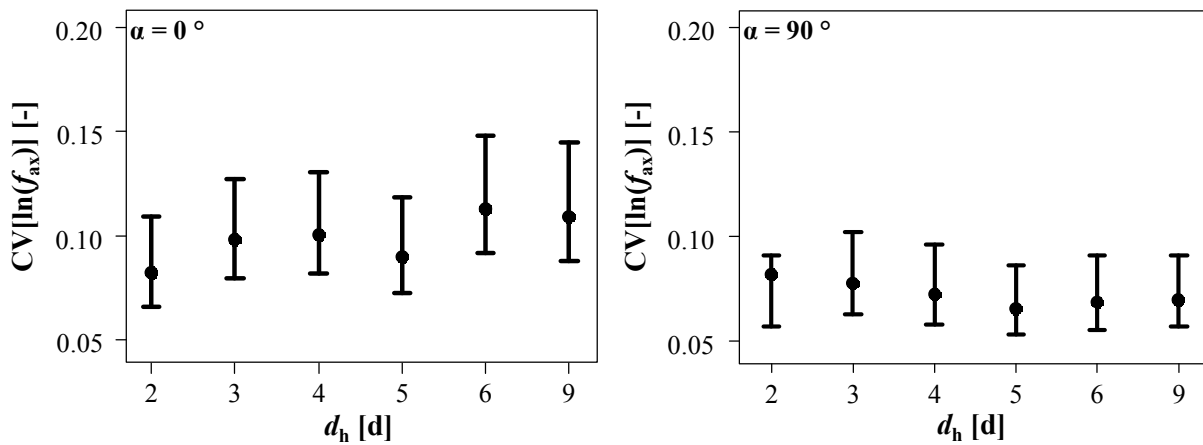


Figure B.77: CIs of $CV[\ln(f_{ax})]$ in dependence of axis-to-grain angle and d_h ; according to Ringhofer and Schickhofer (2014a)

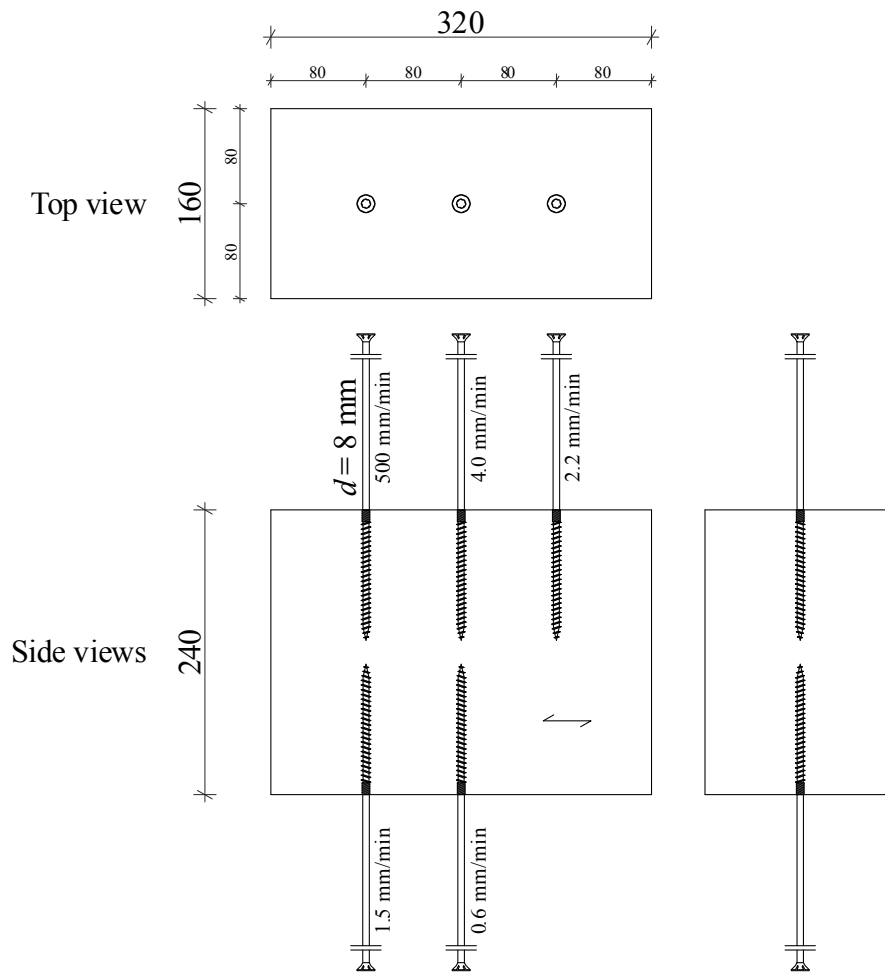


Figure B.78: Illustration of test specimen corresponding to section 5-5.2; all dimensions in [mm]

B-3.2 Supplementary test results

Table B.12: Statistical parameters of density and moisture content of the experimental campaign focusing on diameter impact; section 5-2.1

α	d [mm]	$\Sigma = 507$		ρ_{12}			u		
		n [-]	med[ρ_{12}] [kg/m ³]	mean[ρ_{12}] [kg/m ³]	CV[ρ_{12}] [%]	min[u] [%]	mean[u] [%]	max[u] [%]	
0°	4	50	408.7	408.5	11.2	12.6	13.8	14.5	
	6	50	398.8	401.0	10.4	11.2	13.8	14.7	
	8	39	403.7	407.1	7.62	13.3	14.2	14.7	
	12	41	411.3	412.4	8.35	13.2	14.3	14.8	
	16	35	392.0	392.0	6.89	-*	14.2*	-*	
	20	33	389.3	400.4	9.20	13.7	14.3	14.9	
90°	4	51	404.1	411.8	9.84	12.0	12.7	14.0	
	6	42	402.0	405.5	7.51	12.5	13.3	14.2	
	8	46	394.3	403.6	9.44	12.2	13.4	14.3	
	12	45	397.3	405.3	8.01	12.4	13.4	14.1	
	16	35	384.9	390.6	8.44	13.3	13.8	14.6	
	20	40	394.3	395.5	10.4	12.9	13.8	14.4	

* no moisture content determined for this subset, $u = 14.2\%$ applied as average value for density correction

Table B.13: Statistical parameters of withdrawal strength of the experimental campaign focusing on diameter impact; section 5-2.1

d [mm]	α	$\Sigma = 248$			$\Sigma = 259$				
		n [-]	med[f_{ax}] [N/mm ²]	mean[f_{ax}] [N/mm ²]	CV[f_{ax}] [%]	n [-]	med[f_{ax}] [N/mm ²]	mean[f_{ax}] [N/mm ²]	CV[f_{ax}] [%]
4	0°	50	6.53	6.47	16.0	51	7.38	7.38	12.1
6		50	4.77	4.74	14.8	42	6.37	6.50	11.1
8		39	3.61	3.69	13.7	46	5.68	5.78	13.0
12		41	3.20	3.24	11.4	45	4.92	4.96	12.7
16		35	3.68	3.79	22.8	35	4.71	4.57	10.7
20		33	4.53	4.48	10.5	40	4.58	4.53	12.1
	90°								

Table B.14: Statistical parameters of density, moisture content and annual ring width of the experimental campaign focusing on the impact of clear wood properties; section 5-3.1

test*	n	ρ_{12}			u			a_w		
		med[ρ_{12}]	mean[ρ_{12}]	CV[ρ_{12}]	min[u]	mean[u]	max[u]	med[a_w]	mean[a_w]	CV[a_w]
[-]	[-]	[kg/m ³]	[kg/m ³]	[%]	[%]	[%]	[%]	[mm]	[mm]	[%]
WL	92	418.9	421.0	11.5	12.3	13.4	14.2	3.82	3.87	46.6
WR	89	419.6	419.9	10.0	12.5	13.5	14.2	3.88	3.78	41.3
WT	94	418.3	421.9	11.8	12.3	13.5	14.3	3.82	3.69	43.7
CL	96	419.6	422.8	11.9	12.6	13.4	13.9	3.75	3.91	45.5
CR	91	423.6	425.5	10.3	11.5	12.8	13.8	3.68	3.78	43.5
CT	95	418.1	421.1	10.9	10.8	13.4	14.9	3.83	3.86	44.2

* {WL, WR, WT} = withdrawal test in longitudinal (L), radial (R) and tangential (T) direction
 {CL, CR, CT} = compression test in longitudinal (L), radial (R) and tangential (T) direction

Table B.15: Statistical parameters of density of the experimental campaign focusing on the impact of clear wood properties; section 5-3.1

test*	n	ρ_u		
		med[ρ_u]	mean[ρ_u]	CV[ρ_u]
[-]	[-]	[kg/m ³]	[kg/m ³]	[%]
LR	32	437.8	439.3	8.22
LT	32	433.5	437.2	11.8
RL	30	439.0	441.6	7.01
RT	29	433.1	435.3	7.39
TL	31	433.3	434.6	9.77
TR	30	432.1	435.4	8.13

* shear test in the XY-plane

Table B.16: Statistical parameters of compressive strength and stiffness of the experimental campaign focusing on the impact of clear wood properties; section 5-3.1

test	n	$f_{c,i}$			n	$E_{c,i}$		
		med[$f_{c,i}$]	mean[$f_{c,i}$]	CV[$f_{c,i}$]		med[$E_{c,i}$]	mean[$E_{c,i}$]	CV[$E_{c,i}$]
[-]	[-]	[N/mm ²]	[N/mm ²]	[%]	[-]	[N/mm ²]	[N/mm ²]	[%]
CL	96	36.8	36.7	18.0	95	12,333	12,301	23.9
CR	91	3.61	3.61	12.9	91	576.7	577.0	17.8
CT	95	4.36	4.52	18.1	95	288.5	297.1	20.3

Table B.17: Statistical parameters of shear stiffness of the experimental campaign focusing on the impact of clear wood properties; section 5-3.1

test	n	med[G_{ij}]	mean[G_{ij}]	CV[G_{ij}]	test	n	med[G_{ij}]	mean[G_{ij}]	CV[G_{ij}]
[-]	[-]	[N/mm ²]	[N/mm ²]	[%]	[-]	[-]	[N/mm ²]	[N/mm ²]	[%]
LR	31	530.3	532.6	16.1	RT	29	22.4	23.7	24.5
LT	32	553.4	550.3	28.0	TL	31	564.1	582.1	22.8
RL	30	568.8	584.4	13.8	TR	30	24.0	24.5	24.9

Table B.18: Correlation coefficients according to Pearson (black) and Spearman (grey) between logarithmic withdrawal and clear wood properties for longitudinal screw axis orientation; section 5-3.1

WL	$\ln(\rho_i)$	$\ln(a_w)$	$\ln(f_{ax})$	$\ln(K_{ser,ax})$	$\ln(D)$	$\ln(f_{c,L})$	$\ln(E_{c,L})$	$\ln(G_{LR})$	$\ln(G_{LT})$
$\ln(\rho_i)$	1.00	-0.69 (***)	0.44 (***)	0.43 (***)	-0.20	0.80 (***)	0.74 (***)	0.38 (*)	0.67 (***)
$\ln(a_w)$	-0.66	1.00	0.08	-0.09	0.12	-0.67 (***)	-0.65 (***)	-	-
$\ln(f_{ax})$	0.44	0.07	1.00	0.77 (***)	-0.05	0.17	0.12	0.61 (***)	0.14
$\ln(K_{ser,ax})$	0.41	-0.07	0.76	1.00	0.27 (*)	0.20 (.)	0.14	0.36 (.)	0.03
$\ln(D)$	-0.20	0.14	-0.12	0.23	1.00	-0.18	-0.30 (**)	-0.18	-0.17
$\ln(f_{c,L})$	0.81	-0.67	0.17	0.18	-0.16	1.00	0.82 (***)	0.18	0.50 (**)
$\ln(E_{c,L})$	0.73	-0.66	0.10	0.11	-0.28	0.83	1.00	0.16	0.40 (**)
$\ln(G_{LR})$	0.41	-	0.55	0.30	-0.16	0.11	0.03	1.00	0.37 (**)
$\ln(G_{LT})$	0.62	-	0.19	0.07	-0.19	0.40	0.25	0.40	1.00

(***) $p < 0.001$ (high significant); (**) $p < 0.010$ (medium significant); (*) $p < 0.050$ (significant); (.) $p < 0.100$ (moderate significant)

Table B.19: Correlation coefficients according to Pearson (black) and Spearman (grey) between logarithmic withdrawal and clear wood properties for radial screw axis orientation; section 5-3.1

WR	$\ln(\rho_i)$	$\ln(a_w)$	$\ln(f_{ax})$	$\ln(K_{ser,ax})$	$\ln(D)$	$\ln(f_{c,R})$	$\ln(E_{c,R})$	$\ln(G_{RL})$	$\ln(G_{RT})$
$\ln(\rho_i)$	1.00	-0.65 (***)	0.73 (***)	0.65 (***)	0.36 (***)	0.25 (*)	0.34 (***)	0.24	0.43 (**)
$\ln(a_w)$	-0.62	1.00	-0.24 (*)	-0.28 (**)	-0.44 (***)	-0.02	-0.22 (*)	-	-
$\ln(f_{ax})$	0.75	-0.25	1.00	0.76 (***)	-0.11	0.42 (***)	0.34 (**)	0.19	0.65 (***)
$\ln(K_{ser,ax})$	0.63	-0.27	0.79	1.00	0.30 (**)	0.34 (**)	0.39 (***)	0.30	0.54 (**)
$\ln(D)$	0.29	-0.41	-0.07	0.22	1.00	-0.20 (.)	0.04	-0.13	-0.01
$\ln(f_{c,R})$	0.24	0.01	0.39	0.34	0.18	1.00	0.49 (***)	0.37 (*)	0.61 (***)
$\ln(E_{c,R})$	0.39	-0.15	0.36	0.40	0.07	0.48	1.00	0.39 (*)	0.49 (**)
$\ln(G_{RL})$	0.30	-	0.20	0.28	-0.11	0.32	0.34	1.00	0.43 (*)
$\ln(G_{RT})$	0.35	-	0.64	0.54	-0.08	0.62	0.59	0.40	1.00

(***) $p < 0.001$ (high significant); (**) $p < 0.010$ (medium significant); (*) $p < 0.050$ (significant); (.) $p < 0.100$ (moderate significant)

Table B.20: *Correlation coefficients according to Pearson (black) and Spearman (grey) between logarithmic withdrawal and clear wood properties for tangential screw axis orientation; section 5-3.1*

WT	$\ln(\rho_i)$	$\ln(a_w)$	$\ln(f_{ax})$	$\ln(K_{ser,ax})$	$\ln(D)$	$\ln(f_{c,T})$	$\ln(E_{c,T})$	$\ln(G_{TL})$	$\ln(G_{TR})$
$\ln(\rho_i)$	1.00	-0.75 (***)	0.82 (***)	0.70 (***)	-0.07	0.85 (***)	0.61 (***)	0.58 (***)	0.00
$\ln(a_w)$	-0.75	1.00	-0.53 (***)	-0.51 (***)	0.04	-0.50 (***)	-0.40 (***)	-	-
$\ln(f_{ax})$	0.80	-0.49	1.00	0.78 (***)	-0.20 (.)	0.72 (***)	0.52 (***)	0.28	0.25
$\ln(K_{ser,ax})$	0.67	-0.47	0.77	1.00	0.34 (**)	0.59 (***)	0.54 (***)	0.11	0.14
$\ln(D)$	-0.06	0.00	-0.16	0.33	1.00	-0.12	-0.02	-0.28	0.00
$\ln(f_{c,T})$	0.84	-0.47	0.71	0.58	-0.10	1.00	0.79 (***)	0.63 (***)	0.52 (**)
$\ln(E_{c,T})$	0.61	-0.42	0.53	0.53	-0.01	0.76	1.00	0.55 (**)	0.28
$\ln(G_{TL})$	0.56	-	0.32	0.11	-0.31	0.61	0.51	1.00	0.30
$\ln(G_{TR})$	-0.04	-	0.22	0.14	0.00	0.50	0.23	0.27	1.00

(***) $p < 0.001$ (high significant); (**) $p < 0.010$ (medium significant); (*) $p < 0.050$ (significant); (.) $p < 0.100$ (moderate significant)

Table B.21: *Statistical parameters of density and moisture content of the experimental campaign focusing on the impact of moisture content variation on withdrawal properties; experimental campaign I; section 5-3.2*

α	group	$\Sigma = 618$ n	ρ_{12}			u		
			med[ρ_{12}] [kg/m ³]	mean[ρ_{12}] [kg/m ³]	CV[ρ_{12}] [%]	min[u] [%]	mean[u] [%]	max[u] [%]
0 °	00p	51	431.8	433.3	12.2	0.08	0.15	0.25
	06p	52	433.8	438.2	12.9	4.78	5.40	6.15
	09p	50	432.2	433.1	12.2	8.52	9.24	9.91
	12p	39	420.1	428.0	12.2	10.5	11.3	12.3
	15p	50	425.4	430.0	12.0	13.5	15.5	16.7
	18p	50	426.4	429.0	11.7	16.4	18.0	20.1
	21p	51	429.4	433.6	12.1	19.3	21.6	24.5
90 °	00p	45	402.4	415.0	10.7	0.22	0.36	0.59
	07p	33	411.8	419.2	7.51	7.18	7.68	8.06
	09p	34	410.5	409.4	6.99	9.12	10.1	10.8
	12p	37	415.2	415.3	8.63	11.5	12.2	13.0
	15p	33	411.1	409.7	8.12	14.3	15.5	16.2
	18p	37	410.1	413.0	8.76	15.9	18.2	20.2
	20p	35	412.1	410.7	9.31	16.7	19.7	21.6
18pc	21	384.2	418.2	11.8	16.9	18.0	21.2	

Table B.22: *Statistical parameters of density and moisture content of the experimental campaign focusing on the impact of moisture content variation on withdrawal properties; experimental campaign II; section 5-3.2*

α	group	$\Sigma = 30$ n	ρ_{12}			u		
			med[ρ_{12}] [kg/m ³]	mean[ρ_{12}] [kg/m ³]	CV[ρ_{12}] [%]	min[u] [%]	mean[u] [%]	max[u] [%]
90 °	08p	10	467.9	465.6	12.1	7.87	8.54	8.94
	12p	10	465.0	466.6	12.6	10.6	11.7	12.5
	18p	10	469.3	472.0	11.3	17.4	17.8	18.7

Table B.23: *Statistical parameters of withdrawal strength, stiffness and ductility of the experimental campaign focusing on the impact of moisture content variation on withdrawal properties; $\alpha = 0^\circ$; experimental campaign I; section 5-3.2*

group	n	mean[f_{ax}]	CV[f_{ax}]	n	mean[$K_{ser,ax}$]*	CV[$K_{ser,ax}$]	n	mean[D]*	CV[D]
[-]	[-]	[N/mm ²]	[%]	[-]	[N/mm]	[%]	[-]	[-]	[%]
00p	51	6.21	19.5	49	6,116	4.90	50	1.19	21.5
06p	52	6.83	22.5	50	6,328	5.47	50	1.28	19.0
09p	50	6.73	25.1	47	5,595	4.47	48	1.35	13.8
12p	39	6.49	20.8	37	6,166	3.76	37	1.30	19.4
15p	50	5.56	21.1	50	6,033	7.07	49	1.36	26.7
18p	50	4.81	26.5	49	5,685	6.58	49	1.67	28.2
21p	51	4.38	21.5	49	5,275	6.46	50	1.37	25.1

* Note: only for relative comparisons in-between test series!

Table B.24: *Statistical parameters of withdrawal strength, stiffness and ductility of the experimental campaign focusing on the impact of moisture content variation on withdrawal properties; $\alpha = 90^\circ$; experimental campaign I; section 5-3.2*

group	n	mean[f_{ax}]	CV[f_{ax}]	n	mean[$K_{ser,ax}$]*	CV[$K_{ser,ax}$]	n	mean[D]*	CV[D]
[-]	[-]	[N/mm ²]	[%]	[-]	[N/mm]	[%]	[-]	[-]	[%]
00p	45	7.08	16.3	43	2,164	43.4	40	1.67	11.4
07p	33	8.16	10.3	32	3,091	34.3	32	1.93	9.72
09p	34	8.03	10.8	31	2,952	28.3	32	1.94	7.26
12p	37	8.07	13.6	37	2,753	44.4	36	1.98	6.39
15p	33	7.03	16.7	33	2,018	48.5	32	2.09	7.98
18p	37	6.45	10.9	35	1,108	37.9	35	2.18	5.89
20p	35	6.20	9.82	32	1,416	34.0	31	2.26	4.87
18pc	21	6.58	12.0	-	-	-	-	-	-

* Note: only for relative comparisons in-between test series!

Table B.25: Statistical parameters of withdrawal strength, stiffness and ductility of the experimental campaign focusing on the impact of moisture content variation on withdrawal properties; $\alpha = 90^\circ$; experimental campaign II; section 5-3.2

group	n	mean[f_{ax}]	CV[f_{ax}]	n	mean[$K_{ser,ax}$]*	CV[$K_{ser,ax}$]	n	mean[D]*	CV[D]
[-]	[-]	[N/mm ²]	[%]	[-]	[N/mm]	[%]	[-]	[-]	[%]
08p	8	6.49	5.86	9	7,834	6.15	10	2.26	13.6
12p	10	6.42	10.2	10	7,641	12.2	9	2.33	6.43
18p	8	5.64	3.53	10	6,706	7.68	10	2.33	7.02

* Note: only for relative comparisons in-between test series!

Table B.26: Statistical parameters of density and moisture content of the experimental campaign focusing on the layer impact on withdrawal properties; series A; section 5-3.3

product	density group	N	n	ρ_{12}				u		
				med[ρ_{12}]	mean[ρ_{12}]	CV[ρ_{12}]	$\rho_{12,05,emp}$	min[u]	mean[u]	max[u]
[-]	[-]	[-]	[-]	[kg/m ³]	[kg/m ³]	[%]	[kg/m ³]	[%]	[%]	[%]
ST*	1G	1	54	384.6	379.1	6.36	344.0	6.24	12.3	13.9
	2G	1	41	443.3	448.2	5.48	416.2	12.1	12.8	13.4
GLT		3	79	377.8	377.7	3.05	358.7	11.6	12.3	13.1
	1G	6	81	381.7	383.9	2.79	370.5	11.8	12.3	12.7
		20	83	399.9	401.3	1.95	390.6	11.0	11.7	12.1
		3	63	446.6	446.7	2.97	427.3	12.3	12.7	13.2
	2G	6	59	451.1	450.7	2.19	431.5	12.3	12.8	13.4
		20	59	464.8	465.1	1.78	452.4	11.7	12.2	12.6
CLT		3	81	376.8	377.4	3.01	358.8	9.94	12.3	13.1
	1G	6	82	383.8	383.6	2.78	367.6	11.9	12.3	12.8
		20	82	400.5	400.8	1.79	388.9	11.1	11.6	12.1
		3	60	446.9	447.7	3.24	425.7	12.2	12.6	13.2
	2G	6	59	448.0	448.4	2.39	432.2	12.6	12.9	13.4
		20	54	464.8	465.4	1.68	453.5	11.5	12.2	12.8

* for series A, also clear wood densities of single board sections were determined

Table B.27: *Statistical parameters of density and moisture content of the experimental campaign focusing on the layer impact on withdrawal properties; series B; section 5-3.3*

group	subgroup	N	n	ρ_{12}			u		
				med[ρ_{12}]	mean[ρ_{12}]	CV[ρ_{12}]	min[u]	mean[u]	max[u]
[-]	[-]	[-]	[-]	[kg/m ³]	[kg/m ³]	[%]	[%]	[%]	[%]
B0	.1	1	19	482.7	492.2	10.8	12.3	13.5	16.3
	.2	2	20	512.7	506.2	11.4	12.8	13.4	13.9
	.3	1	22	369.4	375.5	11.6	11.4	13.0	14.3
	.4	10	20	377.1	373.9	4.57	12.1	12.6	13.9
B1	.1	10	16	423.3	422.8	2.12	12.3	12.7	13.1
	.2	10	16	423.4	423.5	2.43	12.5	12.8	13.3
	.3	10	16	414.1	416.7	2.12	12.4	12.8	13.1
	.4	10	19	411.8	410.2	4.89	12.5	13.0	14.1
	.5	10	19	414.8	411.8	3.97	12.2	12.7	13.7
B2	.1	10	19	422.0	433.0	6.74	12.0	12.8	13.2
	.2	10	17	412.5	410.8	5.01	12.4	12.7	13.0
	.3	10	19	418.8	422.1	5.79	12.4	12.8	13.1
	.4	10	16	414.8	417.3	2.75	12.6	12.9	13.3
	.5	10	19	406.4	416.6	5.85	12.3	12.9	13.3
	.6	10	19	411.2	420.3	5.47	12.3	12.7	13.3

Table B.28: *Statistical parameters of density and moisture content of the experimental campaign focusing on the layer impact on withdrawal properties; series C; section 5-3.3*

group	subgroup	N	n	ρ_{12}			u		
				med[ρ_{12}]	mean[ρ_{12}]	CV[ρ_{12}]	min[u]	mean[u]	max[u]
[-]	[-]	[-]	[-]	[kg/m ³]	[kg/m ³]	[%]	[%]	[%]	[%]
C	1.1	5	32	427.3	425.6	3.78	12.1	12.5	13.0
	2.1	5	36	418.1	419.5	3.05	12.1	12.4	12.9

Table B.29: Statistical parameters of withdrawal strength, stiffness and ductility of the experimental campaign focusing on the layer impact on withdrawal properties; test series A, GLT; section 5-3.3

d	[mm]		8		8		12			
N	[-]	3	6	20	3	60	20	3	6	20
PD*	[y/n]	n	n	n	y	y	y	y	y	y
n	[-]	47	44	45	47	45	48	47	47	46
mean[f_{ax}]	[N/mm ²]	5.86	5.99	6.36	5.67	5.85	6.13	5.51	5.52	5.90
CV[f_{ax}]	[%]	8.33	8.02	6.86	11.3	9.62	9.51	9.62	8.20	7.43
$f_{ax,05,emp}$	[N/mm ²]	5.25	5.32	5.62	4.79	5.14	5.37	4.75	4.94	5.31
n	[-]	46	43	44	48	47	46	47	43	48
mean[$K_{ser,ax}$]**	[N/mm]	6,810	6,894	7,161	6,602	6,524	6,830	10,329	10,120	10,628
CV[$K_{ser,ax}$]	[%]	4.25	3.56	1.98	5.71	4.31	3.99	6.48	5.06	4.50
n	[-]	47	43	37	47	47	45	44	46	48
mean[D]**	[-]	1.79	1.76	1.72	1.99	1.98	1.99	2.88	2.79	2.76
CV[D]	[%]	6.40	5.15	2.52	4.71	4.90	5.44	5.20	5.38	3.58

* = pre-drilling; ** note: only for relative comparison!

Table B.30: Statistical parameters of withdrawal strength, stiffness and ductility of the experimental campaign focusing on the layer impact on withdrawal properties; test series A, CLT; section 5-3.3

d	[mm]		8		8		12			
N	[-]	3	6	20	3	6	20	3	6	20
PD*	[y/n]	n	n	n	y	y	y	y	y	y
n	[-]	46	47	43	47	47	43	46	47	47
mean[f_{ax}]	[N/mm ²]	5.90	6.06	6.64	5.79	5.94	6.29	5.54	5.68	6.30
CV[f_{ax}]	[%]	8.71	7.37	8.03	11.5	11.2	10.8	10.7	8.86	9.93
$f_{ax,05,emp}$	[N/mm ²]	5.11	5.41	6.02	4.74	5.00	5.39	4.78	4.96	5.57
n	[-]	44	47	44	45	46	40	45	45	41
mean[$K_{ser,ax}$]**	[N/mm]	7,161	7,298	7,513	6,964	6,865	7,146	10,777	10,487	10,862
CV[$K_{ser,ax}$]	[%]	3.10	2.86	2.19	4.48	3.18	4.14	5.06	5.23	4.29
n	[-]	45	45	45	47	46	42	45	45	45
mean[D]**	[-]	1.80	1.84	2.01	2.03	2.00	2.09	2.90	2.83	2.84
CV[D]	[%]	4.57	3.75	4.77	5.91	5.52	4.12	5.27	4.73	3.50

* = pre-drilling; ** note: only for relative comparison!

Table B.31: *Statistical parameters of withdrawal strength of the experimental campaign focusing on the layer impact on withdrawal properties; series B; section 5-3.3*

group	subgroup	N	d	n	mean[f_{ax}]	CV[f_{ax}]	$f_{ax,05,emp}$
[-]	[-]	[-]	[mm]	[-]	[N/mm ²]	[%]	[N/mm ²]
B0	.1	1	10	18	5.25	16.0	4.40
	.2	2		20	6.07	13.2	5.26
	.3	1		22	4.18	22.4	3.07
	.4	10		21	4.96	7.27	4.25
B1	.1	10	10	18	5.25	5.07	4.86
	.2	10		17	5.39	3.78	5.10
	.3	10		18	5.06	4.26	4.73
	.4	10		19	5.25	5.57	4.88
	.5	10		19	5.20	4.59	4.86
B2	.1	10	10	18	5.31	4.53	4.99
	.2	10		19	5.24	6.22	4.64
	.3	10		18	5.40	5.33	4.99
	.4	10		16	5.14	2.71	4.94
	.5	10		19	5.23	6.41	4.81
	.6	10		19	5.35	5.25	4.94

Table B.32: *Statistical parameters of withdrawal strength of the experimental campaign focusing on the layer impact on withdrawal properties; series C and D; section 5-3.3*

group	subgroup	N	d	n	mean[f_{ax}]	CV[f_{ax}]	$f_{ax,05}$
[-]	[-]	[-]	[mm]	[-]	[N/mm ²]	[%]	[N/mm ²]
C	1.1	5	8	33	6.41	8.93	5.59
	2.1	5	12	36	5.37	6.36	4.90
D	-	3	8	10	6.42	10.2	5.50

Table B.33: Statistical parameters of density and moisture content of the experimental campaign focusing on the gap impact on withdrawal properties; test programme I, $d = 8$ mm; section 5-3.4

pos. *	type	w_{gap}	n	ρ_{12}			u		
				med[ρ_{12}]	mean[ρ_{12}]	CV[ρ_{12}]	min[u]	mean[u]	max[u]
[-]	[-]	[mm]	[-]	[kg/m ³]	[kg/m ³]	[%]	[%]	[%]	[%]
TL	ST	0	18	424.0	434.7	9.55	11.5	12.8	13.6
	BuJ	0	19	450.5	464.8	6.80	11.4	12.7	13.7
	BuJ	2	19	444.0	450.4	6.28	10.5	12.1	14.2
	BuJ	6	5	470.1	485.0	8.30	12.3	12.8	13.7
ML	ST	0	19	459.5	454.1	7.85	11.4	13.1	14.3
	BuJ	0	19	467.7	470.7	8.16	10.9	12.7	13.9
	BuJ	2	20	456.2	457.1	6.82	11.4	12.8	13.8
	BuJ	6	5	476.7	475.0	4.39	11.8	12.7	13.4
CL	ST	0	19	438.9	443.7	7.90	10.9	12.1	13.3
	BuJ	0	18	454.8	452.8	4.56	10.7	12.1	13.3
	BuJ	2	20	451.7	450.9	5.83	10.8	11.8	13.5
	BuJ	6	5	483.7	484.4	3.72	11.8	12.7	13.8
IL	BeJ	0	20	426.1	431.5	5.98	10.6	12.1	13.7
	TJ	0	18	448.7	452.0	4.60	9.88	11.6	13.9
	TJ	2	18	447.9	450.4	5.83	11.4	12.4	13.5
	TJ	6	5	440.6	440.7	6.66	12.0	12.7	13.9

* TL = top layer, CL = cross layer, ML = middle layer, IL = intermediate layer

Table B.34: Statistical parameters of density and moisture content of the experimental campaign focusing on the gap impact on withdrawal properties; test programme I, $d = 12$ mm; section 5-3.4

pos. *	type	w_{gap}	n	ρ_{12}			u		
				med[ρ_{12}]	mean[ρ_{12}]	CV[ρ_{12}]	min[u]	mean[u]	max[u]
[-]	[-]	[mm]	[-]	[kg/m ³]	[kg/m ³]	[%]	[%]	[%]	[%]
TL	ST	0	20	403.9	410.1	8.05	11.2	12.5	13.6
	BuJ	0	20	455.0	455.3	7.79	10.9	12.3	13.5
	BuJ	2	20	426.4	433.4	7.86	10.9	12.4	13.5
	BuJ	6	5	470.8	455.5	11.5	11.4	11.9	12.4
ML	ST	0	20	446.2	443.6	7.42	11.6	13.0	14.0
	BuJ	0	20	457.2	461.7	7.18	11.6	12.8	13.7
	BuJ	2	20	460.5	451.3	7.06	10.8	12.5	13.5
	BuJ	6	5	478.3	459.5	8.60	12.2	13.1	13.7
CL	ST	0	19	413.3	415.5	7.72	11.5	12.8	13.4
	BuJ	0	19	461.2	456.0	4.59	10.8	12.1	13.2
	BuJ	2	20	441.5	438.0	5.69	11.4	12.3	13.2
	BuJ	6	5	480.0	468.0	7.17	12.6	13.5	15.8
IL	BeJ	0	20	425.6	431.4	6.45	12.0	12.9	13.6
	TJ	0	20	457.9	457.8	4.99	11.3	12.3	13.3
	TJ	2	20	460.0	461.3	7.01	10.5	12.5	13.4
	TJ	6	5	485.4	485.1	5.53	12.0	12.8	13.4

* TL = top layer, CL = cross layer, ML = middle layer, IL = intermediate layer

Table B.35: Statistical parameters of density and moisture content of the experimental campaign focusing on the gap impact on withdrawal properties; test programme II; section 5-3.4

w_{gap}	n_{gap}	pos.*	n	ρ_{12}			u		
				med[ρ_{12}]	mean[ρ_{12}]	CV[ρ_{12}]	min[u]	mean[u]	max[u]
[mm]	[-]	[-]	[-]	[kg/m ³]	[kg/m ³]	[%]	[%]	[%]	[%]
0	0	ref.	10	465.0	466.6	12.6	10.6	11.7	12.5
	1	TL	10	462.6	452.1	9.39	10.4	11.0	11.5
	1	ML	10	452.0	452.5	7.64	10.4	11.2	12.0
	2	OL	10	473.7	461.0	8.29	10.4	11.1	12.0
	3	all	10	465.2	455.7	7.13	10.5	11.2	11.8
	1	TL	10	450.1	452.6	7.87	11.4	11.9	12.8
	1	ML	10	467.2	459.1	8.55	10.8	11.2	11.5
	2	OL	10	458.8	459.3	7.89	10.7	11.4	12.3
	3	all	10	465.8	462.5	7.66	10.7	11.3	12.0

* TL = top layer, ML = middle layer, OL = outer layers

Table B.36: *Statistical parameters of density corrected withdrawal properties of the experimental campaign focusing on the gap impact; test programme I, $d = 8$ mm; section 5-3.4*

pos.*	type	w_{gap}	f_{ax}			$K_{\text{ser,ax}}$			D		
			n	mean[f_{ax}]	CV[f_{ax}]	n	mean[$K_{\text{ser,ax}}$]	CV[$K_{\text{ser,ax}}$]	n	mean[D]	CV[D]
[-]	[-]	[mm]	[-]	[N/mm ²]	[%]	[-]	[N/mm]	[%]	[-]	[-]	[%]
TL	ref.	0	18	5.29	15.1	18	18,518	12.8	18	3.82	14.7
	BuJ	0	19	4.49	10.7	18	17,206	10.1	19	4.44	31.4
	BuJ	2	18	3.60	11.1	18	12,641	8.29	19	4.01	14.8
	BuJ	6	5	1.88	27.1	3	6,859	3.05	3	4.79	2.29
ML	ref.	0	18	4.58	9.67	19	18,226	9.34	19	4.31	22.8
	BuJ	0	19	4.66	10.1	18	18,422	18.1	19	4.48	25.3
	BuJ	2	20	3.67	17.7	20	13,831	20.7	20	4.94	24.9
	BuJ	6	4	2.18	5.22	5	7,572	12.9	5	4.72	17.5
CL	ref.	0	18	5.36	13.1	16	19,058	8.30	19	4.15	15.6
	BuJ	0	17	5.17	10.3	18	19,470	15.0	18	4.44	25.7
	BuJ	2	20	4.08	13.9	19	13,673	11.9	20	4.24	14.8
	BuJ	6	3	2.09	3.99	5	7,844	14.2	4	4.10	10.9
IL	BeJ	0	17	5.92	5.93	20	18,965	14.2	19	6.14	20.7
	TJ	0	18	5.94	13.2	18	18,961	18.2	18	6.52	27.9
	TJ	2	17	4.72	6.76	17	14,897	10.6	18	5.55	30.6
	TJ	6	5	2.11	13.5	4	7,707	9.16	4	5.15	7.62

* TL = top layer, CL = cross layer, ML = middle layer, IL = intermediate layer

Table B.37: *Statistical parameters of density corrected withdrawal strength of the experimental campaign focusing on the gap impact; test programme I, $d = 12$ mm; section 5-3.4*

pos.*	type	w_{gap}	n	mean[f_{ax}]	CV[f_{ax}]
[-]	[-]	[mm]	[-]	[N/mm ²]	[%]
TL	ref.	0	20	4.98	18.7
	BuJ	0	20	4.19	14.9
	BuJ	2	19	3.93	11.0
	BuJ	6	4	2.86	10.6
ML	ref.	0	20	4.73	16.7
	BuJ	0	20	4.47	13.8
	BuJ	2	19	3.65	12.2
	BuJ	6	5	2.82	15.2
CL	ref.	0	19	5.32	11.6
	BuJ	0	19	4.53	11.6
	BuJ	2	19	4.00	12.3
	BuJ	6	4	3.28	3.28
IL	BeJ	0	18	5.19	5.53
	TJ	0	19	4.85	6.36
	TJ	2	19	4.30	10.5
	TJ	6	4	3.02	5.21

* TL = top layer, CL = cross layer, ML = middle layer, IL = intermediate layer

Table B.38: Statistical parameters of withdrawal properties of the experimental campaign focusing on the gap impact; test programme II; section 5-3.4

w_{gap} [mm]	n_{gap} [-]	pos. * [-]	f_{ax}			$K_{\text{ser,ax}}$ **			D **		
			n [-]	mean[f_{ax}] [N/mm ²]	CV[f_{ax}] [%]	n [-]	mean[$K_{\text{ser,ax}}$] [N/mm]	CV[$K_{\text{ser,ax}}$] [%]	n [-]	mean[D] [-]	CV[D] [%]
0	0	ref.	10	6.42	10.2	10	7,637	11.7	10	2.31	6.54
0	1	TL	8	6.86	10.1	10	8,184	9.21	10	2.21	3.84
	1	ML	10	6.66	7.75	10	8,454	6.07	10	2.32	7.47
	2	OL	10	6.99	8.38	10	8,373	7.50	10	2.26	5.25
	3	all	8	7.51	3.46	9	8,743	3.68	10	2.24	5.77
4	1	TL	10	5.93	11.5	10	7,498	9.55	10	2.35	10.7
	1	ML	10	5.89	7.35	10	7,658	7.48	10	2.32	6.05
	2	OL	10	5.37	12.8	9	7,256	6.50	9	2.44	3.43
	3	all	9	4.87	8.88	10	6,526	6.83	7	2.43	2.15

* TL = top layer, ML = middle layer, OL = outer layers; ** only for relative comparison!

Table B.39: Statistical parameters of density and moisture content of the experimental campaign carried out by Gattermig (2010); $\alpha = \{0, 45\}^\circ$; section 5-4.1

α	$a_{1,\text{CG}}$ [d]	$a_{2,\text{CG}}$ [d]	$\Sigma = 529$			ρ_{12}		u	
			n [-]	med[ρ_{12}] [kg/m ³]	mean[ρ_{12}] [kg/m ³]	CV[ρ_{12}] [%]	min[u] [%]	mean[u] [%]	max[u] [%]
0°	-	0.5	20	381.1	387.9	12.5	11.3	12.2	13.6
	-	1.0	20	378.7	377.4	11.9	11.5	12.2	13.6
	-	2.0	20	390.8	385.0	10.4	11.4	12.3	13.6
	-	3.0	20	381.3	389.0	10.8	11.6	12.4	13.6
	-	4.0	19	379.9	372.8	7.39	11.4	12.5	13.6
	-	5.0	20	381.5	377.3	9.86	11.4	12.5	13.8
	-	7.5	20	383.8	377.4	10.9	11.4	12.5	13.8
45°	-	0.5	18	361.9	372.4	11.9	11.9	12.5	13.8
	-	1.0	19	388.3	385.6	12.2	11.8	12.8	14.3
	-	2.0	19	374.3	370.1	10.4	11.4	12.4	13.6
	-	3.0	19	378.2	374.8	7.10	11.7	12.6	13.8
	-	4.0	18	398.0	400.0	5.47	11.6	12.6	14.1
	-	5.0	20	383.6	377.7	8.02	11.3	12.6	13.8

Table B.40: Statistical parameters of density and moisture content of the experimental campaign carried out by Gatternig (2010); $\alpha = 90^\circ$; section 5-4.1

α	$\Sigma = 529$			ρ_{12}			u		
	$a_{1,CG}$ [d]	$a_{2,CG}$ [d]	n [-]	med[ρ_{12}] [kg/m ³]	mean[ρ_{12}] [kg/m ³]	CV[ρ_{12}] [%]	min[u] [%]	mean[u] [%]	max[u] [%]
90 °	-	0.5	20	374.5	373.7	10.7	11.2	12.0	12.8
	-	1.0	19	387.2	377.4	8.89	11.2	11.9	13.0
	-	2.0	20	399.3	385.1	10.9	11.2	11.9	12.8
	-	3.0	20	386.1	384.5	12.2	11.4	12.1	13.0
	-	4.0	20	375.9	383.3	11.7	11.3	12.0	13.1
	-	5.0	20	378.4	378.4	10.0	11.3	12.1	13.3
	0.5	-	19	373.9	369.6	9.97	11.5	12.7	13.6
	1.0	-	20	366.2	372.4	8.14	11.9	12.7	13.7
	2.0	-	20	365.8	375.4	8.83	12.0	12.8	13.9
	3.0	-	20	376.8	379.4	11.0	12.0	12.8	13.6
	4.0	-	20	369.6	372.9	8.04	11.9	12.7	13.4
	5.0	-	20	367.5	367.4	9.31	12.0	12.7	13.6
	6.0	-	20	366.2	368.2	7.43	12.2	12.7	13.5
	7.0	-	19	370.0	372.4	7.87	12.1	12.7	13.6

Table B.41: Statistical parameters of density and moisture content of the experimental campaign carried out by Plieschounig (2010); section 5-4.1

a_1	a_2	$\Sigma = 733$ n	ρ_{12}			u		
			med[ρ_{12}]	mean[ρ_{12}]	CV[ρ_{12}]	min[u]	mean[u]	max[u]
[d]	[d]	[-]	[kg/m ³]	[kg/m ³]	[%]	[%]	[%]	[%]
-	-	129	446.1	445.6	10.3	10.3	13.1	15.3
2	-	60	450.6	445.4	9.59	11.8	12.9	14.2
3	-	59	452.5	452.2	9.87	11.7	13.1	14.6
4	-	55	458.2	456.6	10.3	10.5	13.1	14.7
5	-	55	449.6	454.4	9.13	11.7	13.2	14.6
6	-	51	445.8	443.7	10.8	11.5	13.0	14.5
7	-	56	456.4	455.1	8.85	11.6	13.2	14.2
14	-	26	473.0	472.8	5.62	12.8	13.6	14.4
-	2	63	442.2	443.0	10.5	11.6	13.0	14.5
-	3	60	449.2	448.0	9.91	11.5	13.0	14.3
-	4	62	447.6	447.3	10.6	11.6	13.1	14.7
-	5	57	451.7	450.0	9.29	11.4	13.0	14.4

Table B.42: Statistical parameters of withdrawal strength of the experimental campaign carried out by Gatterinig (2010); $\alpha = \{0, 45\}^\circ$; section 5-4.1

α	$a_{2,CG}$	$\Sigma = 134$ n	f_{ax}			α	$a_{2,CG}$	$\Sigma = 108$ n	f_{ax}		
			med[f_{ax}]	mean[f_{ax}]	CV[f_{ax}]				med[f_{ax}]	mean[f_{ax}]	CV[f_{ax}]
	[d]	[-]	[N/mm ²]	[N/mm ²]	[%]		[d]	[-]	[N/mm ²]	[N/mm ²]	[%]
	0.5	20	3.45	3.63	15.2		0.5	16	4.41	4.51	27.7
	1.0	20	4.98	4.94	21.0		1.0	17	5.59	5.69	14.8
	2.0	19	4.94	4.97	16.7		2.0	18	5.66	5.80	11.7
0°	3.0	18	4.66	4.72	17.7	45°	3.0	19	5.82	5.93	10.5
	4.0	18	4.70	4.79	15.2		4.0	18	6.02	6.20	9.78
	5.0	19	4.49	4.72	23.7		5.0	20	5.97	6.01	15.2
	7.5	20	4.88	5.09	25.7		-	-	-	-	-

Table B.43: Statistical parameters of withdrawal strength of the experimental campaign carried out by Gatterinig (2010); $\alpha = 90^\circ$; section 5-4.1

α	$\Sigma = 156$					$\Sigma = 113$				
	$a_{1,CG}$	n	f_{ax}			$a_{2,CG}$	n	f_{ax}		
			med[f_{ax}]	mean[f_{ax}]	CV[f_{ax}]			med[f_{ax}]	mean[f_{ax}]	CV[f_{ax}]
[d]	[-]	[N/mm ²]	[N/mm ²]	[%]	[d]	[-]	[N/mm ²]	[N/mm ²]	[%]	
90°	0.5	20	4.06	4.09	16.7	0.5	19	5.11	5.06	10.9
	1.0	19	4.88	4.85	12.0	1.0	19	6.28	6.24	9.24
	2.0	19	6.11	5.99	9.83	2.0	15	6.64	6.63	6.71
	3.0	19	6.27	6.37	12.0	3.0	20	6.75	6.60	17.8
	4.0	20	6.13	6.33	13.3	4.0	20	6.62	6.49	15.0
	5.0	20	6.61	6.31	12.1	5.0	20	6.66	6.47	14.0
	6.0	20	6.33	6.27	8.80	-	-	-	-	-
	7.0	19	6.43	6.34	11.5	-	-	-	-	-

Table B.44: Statistical parameters of withdrawal properties of the experimental campaign carried out by Plieschounig (2010); section 5-4.1

a_1	a_2	f_{ax}			$K_{ser,ax}^*$			D^*		
		n	mean[f_{ax}]	CV[f_{ax}]	n	mean[$K_{ser,ax}$]	CV[$K_{ser,ax}$]	n	mean[D]	CV[D]
[d]	[d]	[-]	[N/mm ²]	[%]	[-]	[N/mm]	[%]	[-]	[-]	[%]
ref		128	7.30	10.0	129	5,371**	14.7	131	2.00**	8.85
2	-	60	5.40	13.3	57	6,477	19.7	53	1.90	9.44
3	-	59	6.18	12.4	58	7,062	18.9	60	1.85	9.82
4	-	55	6.46	11.6	55	6,918	18.4	54	1.85	7.96
5	-	55	6.76	10.9	55	7,317	14.3	54	1.85	7.98
6	-	51	6.86	10.7	51	7,428	17.7	45	1.77	9.37
7	-	56	6.88	9.32	56	7,240	15.7	54	1.78	8.31
14	-	25	6.92	9.28	25	7,515	6.06	27	1.74	6.90
-	2	63	7.08	8.83	61	7,475	14.7	60	1.76	5.72
-	3	59	7.18	8.03	60	7,693	11.8	60	1.78	7.38
-	4	61	7.15	7.79	62	7,803	13.7	61	1.75	7.77
-	5	57	7.24	7.72	57	7,800	13.6	54	1.76	7.42

* note: only for relative comparison!, ** not relevant since a test set-up with different supporting conditions was applied, c. f. Plieschounig (2010)

Table B.45: *Experimental vs. predicted withdrawal strengths regarding the influence of spacings on f_{ax} : section 5-4.1*

source	d [mm]	type	α [°]	a_i [d]	a_i [mm]	$f_{ax,mean,exp}$ [N/mm ²]	$f_{ax,ref}$ [N/mm ²]	k_{red} [-]	$f_{ax,mean,pred}$ [N/mm ²]	$\Delta_{exp-pred}$ [%]
Gatternig (2010)	6	$a_{2,CG}$	0	0.5	3	3.63	5.09	0.80	4.09	12.8
				1.0	6	4.94		1.00	5.09	3.04
				2.0	12	4.97		1.00	5.09	2.41
				3.0	18	4.72		1.00	5.09	7.84
				4.0	24	4.79		1.00	5.09	6.26
				5.0	30	4.72		1.00	5.09	7.84
				7.5	45	5.09		1.00	5.09	0.00
	6	$a_{2,CG}$	45	0.5	3	4.51	6.01	0.80	4.84	7.21
				1.0	6	5.69		1.00	6.01	5.62
				2.0	12	5.80		1.00	6.01	3.62
				3.0	18	5.93		1.00	6.01	1.35
				4.0	24	6.20		1.00	6.01	-3.06
				5.0	30	6.01		1.00	6.01	0.00
				6.0	36	6.01		1.00	6.01	0.00
	6	$a_{2,CG}$	90	0.5	3	5.06	6.47	0.80	5.21	2.87
				1.0	6	6.24		1.00	6.47	3.69
				2.0	12	6.63		1.00	6.47	-2.41
				3.0	18	6.60		1.00	6.47	-1.97
				4.0	24	6.49		1.00	6.47	-0.31
	5.0	30	6.47	1.00	6.47	0.00				

Table B.46: *Experimental vs. predicted withdrawal strengths regarding the influence of spacings on f_{ax}*
 (continued); section 5-4.1

source	d [mm]	type [-]	α [°]	a_i [d]	$f_{ax,mean,exp}$ [N/mm ²]	$f_{ax,ref}$ [N/mm ²]	k_{red} [-]	$f_{ax,mean,pred}$ [N/mm ²]	$\Delta_{exp-pred}$ [%]
Plieschounig (2010)	6	a_1	90	2.0	5.40	6.92	0.71	4.90	-9.24
				3.0	6.18		0.80	5.57	-9.92
				4.0	6.46		0.89	6.16	-4.61
				5.0	6.76		0.96	6.64	-1.71
				6.0	6.86		1.00	6.92	0.87
				7.0	6.88		1.00	6.92	0.58
				14.0	6.92		1.00	6.92	0.00
	6	a_2	90	2.0	7.08	7.24	1.00	7.24	2.26
				3.0	7.18		1.00	7.24	0.84
				4.0	7.15		1.00	7.24	1.26
5.0				7.24	1.00		7.24	0.00	
Plüss (2014)	8	a_1	90	5.0	5.49	5.91	0.95	5.60	2.08
				7.5	6.52		1.00	5.91	-9.25
				10.0	6.66		1.00	5.91	-11.2
	8	a_1	45	2.5	5.22	5.90	0.88	5.17	-0.97
				5.0	5.81		1.00	5.90	1.55
				10.0	6.24		1.00	5.90	-5.33
	8	a_1	0	2.5	4.20	4.12	1.00	4.12	-2.01
				5.0	4.40		1.00	4.12	-6.52
				10.0	4.24		1.00	4.12	-2.92
	8	a_1	45 45	5.0	5.96	6.19	1.00	6.19	3.78
7.5				5.79	1.00		6.19	6.91	
8	a_1	0 90	5.0	4.93	5.20	0.97	5.07	2.80	
			7.5	5.25		1.00	5.20	-0.86	
Grabner and Ringhofer (2014)	8	$a_{2,CG}$	0	1.25	6.05	6.24	1.00	6.24	3.14
				1.75	6.31		1.00	6.24	-1.11
				2.5	6.28		1.00	6.24	-0.64
				5.0	6.20		1.00	6.24	0.65
				10.0	6.24		1.00	6.24	0.00

Table B.47: Statistical parameters of density and moisture content of the experimental campaign carried out by Grabner (2013); $\alpha = \{0, 45, 90\}^\circ$; section 5-4.2

PD	α [°]	$\Sigma = 91$	ρ_{12}			u		
		n [-]	med[ρ_{12}] [kg/m ³]	mean[ρ_{12}] [kg/m ³]	CV[ρ_{12}] [%]	min[u] [%]	mean[u] [%]	max[u] [%]
yes	0	17	437.5	438.6	7.60	10.9	12.2	12.9
	45	18	446.2	446.5	4.89	11.9	12.5	13.2
	90	19	415.5	411.7	5.05	11.7	12.5	13.1
no	0	11	396.9	418.1	8.87	11.4	12.1	12.5
	45	15	412.9	424.9	6.50	11.3	12.3	12.8
	90	11	415.7	417.3	8.42	10.9	12.1	12.9

Table B.48: Statistical parameters of density and moisture content of the experimental campaign carried out by Gasser (2017); section 5-4.2

α	d_{PD} [mm]	$\Sigma = 214$	ρ_{12}			u		
		n [-]	med[ρ_{12}] [kg/m ³]	mean[ρ_{12}] [kg/m ³]	CV[ρ_{12}] [%]	min[u] [%]	mean[u] [%]	max[u] [%]
0 °	-	19	391.0	391.6	6.45	10.3	10.5	10.7
	5.0	19	392.4	393.0	5.77	9.97	10.5	10.7
	5.5	20	391.2	393.5	6.68	10.2	10.6	11.6
	6.0	18	395.2	398.0	4.51	10.2	10.5	10.8
	6.5	8	392.6	390.3	3.13	10.3	10.6	10.8
	7.0	18	390.0	389.2	5.14	10.3	10.5	10.7
	7.5	10	390.2	396.8	5.33	10.1	10.5	10.8
90 °	-	16	399.5	397.3	2.63	10.3	10.6	10.8
	5.0	20	399.3	401.0	7.12	10.2	10.6	10.9
	5.5	16	396.3	395.0	2.88	10.1	10.5	10.8
	6.0	16	391.7	398.6	6.56	10.3	10.5	11.0
	6.5	9	391.7	396.1	3.58	9.97	10.6	11.1
	7.0	15	394.6	396.3	2.41	10.2	10.5	10.9
	7.5	10	393.1	397.4	8.73	10.3	10.9	13.4

Table B.49: Statistical parameters of density corrected withdrawal properties of the experimental campaign carried out by Grabner (2013); section 5-4.2

PD	α	f_{ax}			$K_{ser,ax}$			D		
		n	mean[f_{ax}]	CV[f_{ax}]	n	mean[$K_{ser,ax}$]	CV[$K_{ser,ax}$]	n	mean[D]	CV[D]
	[°]	[-]	[N/mm ²]	[%]	[-]	[N/mm]	[%]	[-]	[-]	[%]
yes	0	17	4.01	11.6	17	15,733	11.3	15	4.07	7.96
	45	18	5.21	6.46	18	11,366	9.68	18	6.17	11.2
	90	18	5.49	7.59	18	10,748	12.2	16	5.47	7.76
no	0	10	4.09	15.6	11	19,539	16.7	11	7.10	18.4
	45	15	5.27	8.71	14	13,783	7.56	15	4.91	7.50
	90	11	5.55	7.63	10	12,460	12.5	11	6.23	11.6

Table B.50: Statistical parameters of withdrawal properties of the experimental campaign carried out by Gasser (2017); section 5-4.2

α	d_{PD}	f_{ax}			$K_{ser,ax}$			D		
		n	mean[f_{ax}]	CV[f_{ax}]	n	mean[$K_{ser,ax}$]	CV[$K_{ser,ax}$]	n	mean[D]	CV[D]
	[mm]	[-]	[N/mm ²]	[%]	[-]	[N/mm]	[%]	[-]	[-]	[%]
0 °	-	20	3.64	11.7	20	13,667	21.5	19	7.26	15.4
	5.0	19	3.74	8.08	18	11,423	12.0	19	4.87	15.2
	5.5	19	3.97	8.17	19	10,949	11.6	20	4.49	15.7
	6.0	19	3.96	9.74	17	9,978	9.80	16	4.88	15.2
	6.5	10	3.52	9.81	10	8,497	24.5	10	5.46	15.4
	7.0	19	2.67	14.4	19	6,194	23.7	20	6.17	13.9
	7.5	10	0.99	28.6	10	2,349	45.9	10	6.92	21.0
90 °	-	19	5.17	7.06	18	11,916	13.3	20	7.41	13.3
	5.0	20	5.66	12.3	20	10,691	14.7	19	6.23	7.10
	5.5	17	5.34	3.19	20	10,221	12.4	20	6.19	8.75
	6.0	16	5.41	11.9	15	10,009	14.2	16	5.95	7.64
	6.5	9	4.42	6.07	10	8,189	20.4	10	6.75	17.0
	7.0	19	2.39	12.1	20	4,879	21.5	20	7.14	17.6
	7.5	7	1.64	4.71	10	3,073	24.9	10	6.55	13.1

Table B.51: *Statistical parameters of density and moisture content of the experimental campaign focusing on the impact of axis-to-grain angle on withdrawal properties; test programme I, $d = 8$ mm; section 5-4.3*

pos. *	t_1 / d	α	n	ρ_{12}			u		
				med[ρ_{12}]	mean[ρ_{12}]	CV[ρ_{12}]	min[u]	mean[u]	max[u]
[-]	[-]	[°]	[-]	[kg/m ³]	[kg/m ³]	[%]	[%]	[%]	[%]
TL	5.0	0	17	437.5	438.6	7.60	10.9	12.2	12.9
		30	17	459.2	456.0	9.47	11.9	12.6	13.3
		45	18	446.2	446.5	4.89	11.9	12.5	13.2
		60	17	439.8	435.9	7.17	11.8	12.7	13.2
		90	19	415.5	411.7	5.05	11.7	12.5	13.1
ML	5.0	0	17	430.1	441.4	8.87	11.1	12.6	13.5
		30	16	423.1	424.7	4.48	12.3	12.9	13.5
		45	14	429.1	429.1	6.20	12.4	13.0	13.8
		60	16	435.4	442.5	8.92	12.2	13.0	13.7
		90	16	406.9	415.6	8.22	12.1	12.9	13.5
CL	2.5	0	16	463.2	451.7	9.12	11.0	12.0	12.6
		30	19	435.4	444.9	16.7	11.0	12.1	13.2
		45	18	451.6	478.6	15.9	11.1	11.9	12.6
		60	12	471.4	502.5	14.7	11.3	12.2	14.0
		90	18	446.4	471.0	14.3	11.3	11.9	12.4
IL	5.0 2.5	0 90	15	456.2	467.7	8.03	11.6	12.3	12.8
		45 45	17	471.8	470.0	7.68	11.5	12.2	12.7
		90 0	12	463.0	466.3	6.97	12.1	12.5	12.8

* TL = top layer, CL = cross layer, ML = middle layer, IL = intermediate layer

Table B.52: *Statistical parameters of density and moisture content of the experimental campaign focusing on the impact of axis-to-grain angle on withdrawal properties; test programme I, $d = 12$ mm; section 5-4.3*

pos. *	t_1 / d	α	n	ρ_{12}			u		
				med[ρ_{12}]	mean[ρ_{12}]	CV[ρ_{12}]	min[u]	mean[u]	max[u]
[-]	[-]	[°]	[-]	[kg/m ³]	[kg/m ³]	[%]	[%]	[%]	[%]
TL	3.3	0	20	440.9	446.5	8.10	11.7	12.4	13.2
		30	12	437.4	437.5	3.96	11.8	12.5	13.3
		45	18	449.3	447.2	3.72	12.0	12.4	13.2
		60	17	432.4	435.8	7.08	11.1	12.2	13.1
		90	17	418.1	410.4	6.58	10.8	12.4	13.2
ML	3.3	0	14	440.8	435.5	7.70	11.9	12.6	13.4
		30	13	432.9	442.0	7.04	12.0	12.9	13.5
		45	16	441.2	441.0	6.12	11.8	12.9	13.5
		60	16	447.0	443.7	6.53	12.1	12.5	13.1
		90	13	421.6	422.2	5.61	11.8	12.8	13.6
CL	1.7	0	17	459.4	464.5	9.74	10.9	11.7	13.3
		30	13	481.0	474.9	12.2	11.0	11.8	12.4
		45	12	466.7	469.9	10.2	11.1	11.8	13.3
		60	19	461.8	462.1	9.87	9.97	11.7	12.6
		90	15	442.4	454.7	9.88	10.7	11.7	12.7
IL	3.3 1.7	0 90	14	474.8	472.2	8.12	11.6	12.1	12.7
		45 45	15	466.9	464.5	8.40	11.4	12.1	12.7
		90 0	17	447.1	452.9	9.43	11.3	12.2	12.8

* TL = top layer, CL = cross layer, ML = middle layer, IL = intermediate layer

Table B.53: *Statistical parameters of density corrected withdrawal properties of the experimental campaign focusing on the impact of axis-to-grain angle variation; test programme I, $d = 8$ mm; section 5-4.3*

pos.*	t_1 / d	α	f_{ax}			$K_{ser,ax}$			D		
			n	mean[X]	CV[X]	n	mean[X]	CV[X]	n	mean[X]	CV[X]
[-]	[-]	[°]	[-]	[N/mm ²]	[%]	[-]	[N/mm]	[%]	[-]	[N/mm]	[%]
TL	5.0	0	17	4.22	11.6	17	16,581	11.3	15	4.07	7.96
		30	17	5.42	8.16	17	13,424	11.7	16	5.62	8.16
		45	18	5.50	6.46	18	11,978	9.68	18	6.17	11.2
		60	16	5.63	3.39	16	11,524	12.0	16	5.66	12.2
		90	18	5.78	7.58	18	11,327	12.2	16	5.47	7.76
ML	5.0	0	17	4.39	16.1	17	17,817	14.9	14	3.93	22.8
		30	16	5.34	5.28	16	13,191	11.5	17	5.61	10.9
		45	12	5.61	3.89	14	12,794	13.6	13	6.26	14.6
		60	16	5.83	8.02	16	12,413	10.0	16	6.25	17.8
		90	15	6.22	8.54	15	11,930	15.7	15	5.29	9.86
CL	2.5	0	16	4.29	18.9	16	14,535	14.6	16	4.34	29.2
		30	19	5.29	9.67	19	12,423	17.8	19	5.46	14.2
		45	18	5.52	8.42	18	12,147	11.1	18	6.32	8.71
		60	12	5.81	6.08	12	12,047	10.3	12	5.62	8.36
		90	18	6.31	7.88	18	15,424	17.1	18	6.86	20.0
IL	5.0 2.5	0 90	15	4.44	11.6	15	15,978	17.7	16	6.73	29.1
		45 45	17	5.73	6.02	16	12,950	10.3	17	6.09	15.2
		90 0	12	4.76	12.0	12	14,923	8.73	13	5.87	21.0

* TL = top layer, CL = cross layer, ML = middle layer, IL = intermediate layer

Table B.54: *Statistical parameters of density corrected withdrawal strength of the experimental campaign focusing on the impact of axis-to-grain angle variation; test programme I, $d = 12$ mm; section 5-4.3*

pos.*	t_1 / d	α	f_{ax}			
			n	med[f_{ax}]	mean[f_{ax}]	CV[f_{ax}]
[-]	[-]	[°]	[-]	[N/mm ²]	[N/mm ²]	[%]
TL	3.3	0	20	4.23	4.26	10.4
		30	12	5.21	5.23	8.61
		45	16	5.40	5.37	4.22
		60	16	5.67	5.64	3.77
		90	17	5.95	5.95	6.05
ML	3.3	0	11	4.46	4.37	12.1
		30	13	5.27	5.34	6.64
		45	16	5.68	5.67	7.16
		60	16	5.69	5.65	4.38
		90	13	6.14	6.12	5.05
CL	1.7	0	17	4.13	4.27	19.1
		30	13	5.65	5.67	4.06
		45	12	5.84	5.96	7.81
		60	19	5.95	5.96	6.45
		90	15	5.98	5.86	4.80
IL	3.3 1.7	0 90	14	4.66	4.76	7.81
		45 45	14	6.36	6.51	7.14
		90 0	17	4.90	4.93	7.61

* TL = top layer, CL = cross layer, ML = middle layer, IL = intermediate layer

Table B.55: *Statistical parameters of density and moisture content of the experimental campaign focusing on the impact of axis-to-grain angle on withdrawal properties; test programme II; section 5-4.3*

d [mm]	α [°]	l_{ef} [mm]	n [-]	ρ_{12}			u		
				med[ρ_{12}] [kg/m ³]	mean[ρ_{12}] [kg/m ³]	CV[ρ_{12}] [%]	min[u] [%]	mean[u] [%]	max[u] [%]
8	30	60	31	428.0	433.5	4.29	12.1	12.5	12.8
		120	33	428.3	425.6	4.33	11.9	12.5	12.8
	60	58	34	421.2	418.9	3.75	11.7	12.2	12.6
		69	34	426.7	422.1	5.21	9.40	12.4	12.9
	90	60	32	427.3	425.6	3.78	12.1	12.5	13.0
12	30	100	32	427.8	428.1	4.47	12.3	12.7	15.9
		200	36	418.9	420.7	3.03	12.3	12.6	13.1
	60	98	34	416.8	417.9	4.20	12.3	12.6	13.1
		115	36	418.8	418.6	2.70	12.3	12.6	13.0
	90	100	36	418.1	419.5	3.05	12.1	12.4	12.9

Table B.56: *Statistical parameters of withdrawal strength of the experimental campaign focusing on the impact of axis-to-grain angle on withdrawal properties; test programme II; section 5-4.3*

d [mm]	α [°]	l_{ef} [mm]	n [-]	f_{ax}		
				med[f_{ax}] [kg/m ³]	mean[f_{ax}] [kg/m ³]	CV[f_{ax}] [%]
8	30	60	31	4.98	5.16	14.5
		120	34	5.34	5.30	9.95
	60	58	34	6.09	6.14	7.44
		69	34	5.96	6.16	9.41
	90	60	33	6.42	6.41	8.93
12	30	100	32	4.29	4.30	11.3
		200	36	4.45	4.47	9.09
	60	98	35	4.90	5.00	7.27
		115	36	4.94	4.93	5.55
	90	100	36	5.35	5.37	6.36

Table B.57: *Statistical parameters of density and moisture content of the experimental campaign focusing on the influence of annual ring orientation on withdrawal properties; section 5-4.4*

test	β^*	n	ρ_{12}			u		
			med[ρ_{12}]	mean[ρ_{12}]	CV[ρ_{12}]	min[u]	mean[u]	max[u]
[-]	[°]	[-]	[kg/m ³]	[kg/m ³]	[%]	[%]	[%]	[%]
WR	90	89	419.6	419.9	10.0	12.5	13.5	14.2
WR T	60	47	437.0	437.0	12.9	12.4	12.9	13.4
WR T	30	47	418.6	433.6	10.1	11.7	12.8	13.5
WT	0	94	418.3	421.9	11.8	12.3	13.5	14.3

* nominal value

Table B.58: *Statistical parameters of density corrected withdrawal strength, stiffness and ductility of the experimental campaign focusing on the influence of annual ring orientation on withdrawal properties; section 5-4.4*

test	β^*	n	mean[f_{ax}]		n	mean[$K_{ser,ax}$]		n	mean[D]	
			CV[f_{ax}]	CV[$K_{ser,ax}$]		CV[D]				
[-]	[°]	[-]	[N/mm ²]	[%]	[-]	[N/mm]	[%]	[-]	[-]	[%]
WR	90	89	5.38	7.78	90	7,955	9.77	87	7.41	13.2
WR T	60	46	5.67	6.71	47	10,307	12.2	47	8.24	16.2
WR T	30	46	5.62	7.70	43	10,604	14.8	41	8.45	9.82
WT	0	94	5.19	8.21	95	7,615	14.1	83	6.50	15.3

* nominal value

Table B.59: *Statistical parameters of density and moisture content of the experimental campaign focusing on the influence of the effective inserted thread length on withdrawal properties; section 5-4.5*

α [°]	l_{ef} [mm]	n [-]	ρ_{12}			u		
			med[ρ_{12}] [kg/m ³]	mean[ρ_{12}] [kg/m ³]	CV[ρ_{12}] [%]	min[u] [%]	mean[u] [%]	max[u] [%]
0	40	18	417.8	418.1	14.4	11.0	11.3	11.9
	80	18	422.5	431.0	12.7	10.7	11.0	11.3
	120	18	424.6	434.4	12.0	10.8	11.1	11.5
	240	16	413.4	419.5	11.0	10.7	11.1	11.5
	310	14	421.7	418.4	11.8	11.0	11.2	11.6
45	40	18	418.4	416.6	12.0	10.1	10.9	11.2
	80	18	421.4	427.8	11.9	10.5	10.7	11.0
	120	16	416.6	430.9	11.9	10.7	11.1	13.3
	240	17	411.1	423.4	12.2	11.3	11.5	11.7
	310	15	408.6	411.9	11.1	11.2	11.4	11.7
90	40	18	403.8	405.9	13.1	10.7	11.0	11.4
	80	18	411.8	425.3	11.7	9.99	10.9	11.3
	120	17	420.2	416.8	11.8	10.7	11.1	11.6
	240	13	416.8	430.0	11.6	11.5	11.6	11.9
	310	14	404.4	414.5	12.1	11.1	11.4	11.6

Table B.60: Statistical parameters of withdrawal properties of the experimental campaign focusing on the influence of the effective inserted thread length on withdrawal properties; section 5-4.5

α	l_{ef}	f_{ax}			$K_{ser,ax}$			D		
		n	mean[f_{ax}]	CV[f_{ax}]	n	mean[$K_{ser,ax}$]	CV[$K_{ser,ax}$]	n	mean[D]	CV[D]
[°]	[mm]	[-]	[N/mm ²]	[%]	[-]	[N/mm]	[%]	[-]	[-]	[%]
0	40	14	4.17	6.58	18	14,741	27.7	18	4.72	39.0
	80	18	4.58	21.2	18	27,685	21.2	18	3.67	29.4
	120	16	4.08	14.7	16	31,122	15.7	18	3.67	40.3
	240	16	3.93* (4.05)***	16.5	16	34,269	15.9	16	4.02*	17.9
	310	14	3.39* (3.59)***	6.87	12	34,156	14.9	14	4.51*	22.2
45	40	18	5.62	17.3	18	11,562	17.9	18	4.99	15.2
	80	18	6.18	16.5	18	18,401	14.9	18	3.48	15.3
	120	16	5.99	13.5	16	22,775	10.5	14	3.17	7.60
	240	17	4.58**	1.70	17	25,872	8.74	17	3.42**	9.60
	310	15	3.55**	0.67	15	25,473	9.49	15	3.23**	9.09
90	40	18	6.16	21.1	18	9,418	25.8	18	4.66	16.6
	80	16	6.35	11.1	17	16,958	13.7	17	4.46	11.6
	120	15	6.34	13.8	17	21,518	23.2	16	4.16	9.96
	240	13	4.57**	0.66	13	22,677	13.4	13	3.32**	14.9
	310	14	3.53**	0.90	12	22,953	12.4	14	3.47**	12.8

* right censored data (partial steel failure in tension), ** all tests steel failure in tension, *** rcMLE value

Table B.61: *Statistical parameters of density and withdrawal strength of the experimental campaign Ia focusing on the influence of varying test configurations; according to Ringhofer and Schickhofer (2014a); section 5-5.1*

α [°]	test configuration	n [-]	mean[ρ_{12}] [kg/m ³]	CV[ρ_{12}] [%]	mean[f_{ax}] [N/mm ²]	CV[f_{ax}] [%]
0	i	46	408	10.8	4.15	16.4
	ii	46	407	9.68	4.24	14.0
	iii	51	422	10.8	4.13	14.5
	iv	46	416	11.0	4.26	15.9
90	i	47	402	9.36	5.62	14.7
	ii	44	405	9.62	5.65	15.9
	iii	51	415	14.9	5.77*	19.4*
	iv	45	410	7.79	5.63	11.5

* rcMLE value

Table B.62: *Statistical parameters of density and withdrawal strength of the experimental campaign Ib focusing on the influence of the supporting plate's hole diameter d_h ; according to Ringhofer and Schickhofer (2014a); section 5-5.1*

α [°]	d_h [d]	n [-]	mean[ρ_{12}] [kg/m ³]	CV[ρ_{12}] [%]	mean[f_{ax}] [N/mm ²]	CV[f_{ax}] [%]
0	2	33	398	10.5	4.18	11.8
	3	38	404	12.8	4.21	14.1
	4	38	403	10.6	4.36	14.8
	5	35	405	10.9	4.73	14.0
	6	36	407	10.7	4.73	17.5
	9	34	404	11.8	4.60	16.7
90	2	37	404	10.3	6.33	15.1
	3	35	406	9.02	6.25	14.2
	4	32	401	10.1	6.58	13.6
	5	35	409	9.59	6.55	12.3
	6	34	406	9.43	6.30	12.7
	9	37	404	9.44	6.36	12.9

Table B.63: Statistical parameters of density and withdrawal strength of the experimental campaign Ic focusing on the influence of the supporting screws' distance a_s ; according to Ringhofer and Schickhofer (2014a); section 5-5.1

α	a_s	n	mean[ρ_{12}]	CV[ρ_{12}]	mean[f_{ax}]	CV[f_{ax}]
[°]	[d]	[-]	[kg/m ³]	[%]	[N/mm ²]	[%]
90	2	33	396	9.99	5.15	15.2
	3	31	393	9.15	5.56	14.0
	4	36	393	9.87	5.61	16.0
	5	32	396	9.50	5.81	15.3

Table B.64: Statistical parameters of density and withdrawal strength of the experimental campaign III focusing on the influence of varying test configurations and surface angles ε_{sur} ; according to Ringhofer and Schickhofer (2014a); section 5-5.1

test configuration	ε_{sur}	n	mean[ρ_{12}]	CV[ρ_{12}]	mean[f_{ax}]	CV[f_{ax}]
[-]	[°]	[-]	[kg/m ³]	[%]	[N/mm ²]	[%]
i	90	16	430	2.80	6.62	16
iv	90	9	439	2.15	6.91	9
iv	45	9	448	7.01	6.89	9

Table B.65: Statistical parameters of density and moisture content of the experimental campaign II focusing on the influence of varying loading rates; section 5-5.2

group	n	ρ_{12}			u		
		med[ρ_{12}]	mean[ρ_{12}]	CV[ρ_{12}]	min[u]	mean[u]	max[u]
[-]	[-]	[kg/m ³]	[kg/m ³]	[%]	[%]	[%]	[%]
000s	18	396.4	407.9	11.9	12.5	15.0	17.4
045s	18	404.1	408.7	11.0	14.4	15.9	17.4
090s	20	406.3	415.4	11.0	14.0	15.4	16.8
135s	20	405.8	410.9	11.5	13.3	15.4	16.7
300s	19	404.9	407.7	12.5	14.0	15.6	17.2

Table B.66: *Statistical parameters of reached failure times dedicated to the groups of experimental campaign II focusing on the influence of varying loading rates; section 5-5.2*

group	<i>t_{tf}</i>		
	min[<i>t_{tf}</i>]	mean[<i>t_{tf}</i>]	max[<i>t_{tf}</i>]
[-]	[s]	[s]	[s]
000s	0.35	0.53	0.69
045s	37.3	45.0	55.2
090s	64.6	85.0	118
135s	96.0	118	135
300s	233	286	329

Table B.67: *Statistical parameters of withdrawal properties of the experimental campaign II focusing on the influence of varying loading rates; section 5-5.2*

group	<i>f_{ax}</i>			<i>K_{ser,ax}</i> *			<i>D</i> *		
	<i>n</i>	mean[<i>f_{ax}</i>]	CV[<i>f_{ax}</i>]	<i>n</i>	mean[<i>K_{ser,ax}</i>]	CV[<i>K_{ser,ax}</i>]	<i>n</i>	mean[<i>D</i>]	CV[<i>D</i>]
[-]	[-]	[N/mm ²]	[%]	[-]	[N/mm]	[%]	[-]	[-]	[%]
000s	17	6.10	14.2	17	7,041	7.18	18	2.85	8.52
045s	18	5.46	14.3	17	7,505	5.85	18	3.42	7.85
090s	20	5.56	14.5	19	7,142	7.72	20	3.31	8.35
135s	20	5.56	16.9	20	7,445	8.66	19	3.36	7.06
300s	19	5.43	18.2	19	7,444	8.94	18	3.38	7.44

* note: only for relative comparison

B-4 Supplementary material to chapter 6

B-4.1 Supplementary figures

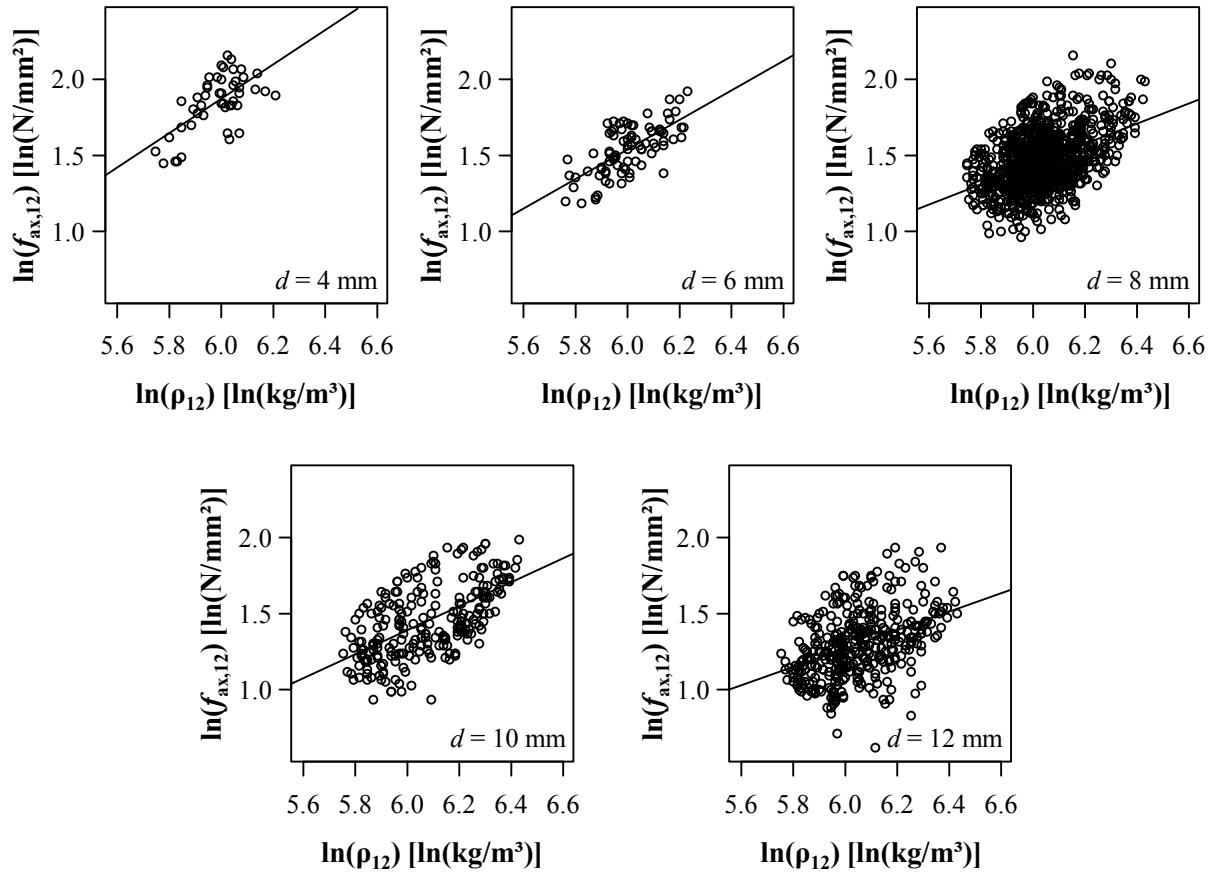


Figure B.79: Relationships between logarithmic withdrawal strength and density for main series in dependence of outer thread diameter; parallel-to-grain insertion, $\alpha = 0^\circ$; section 6-3.1

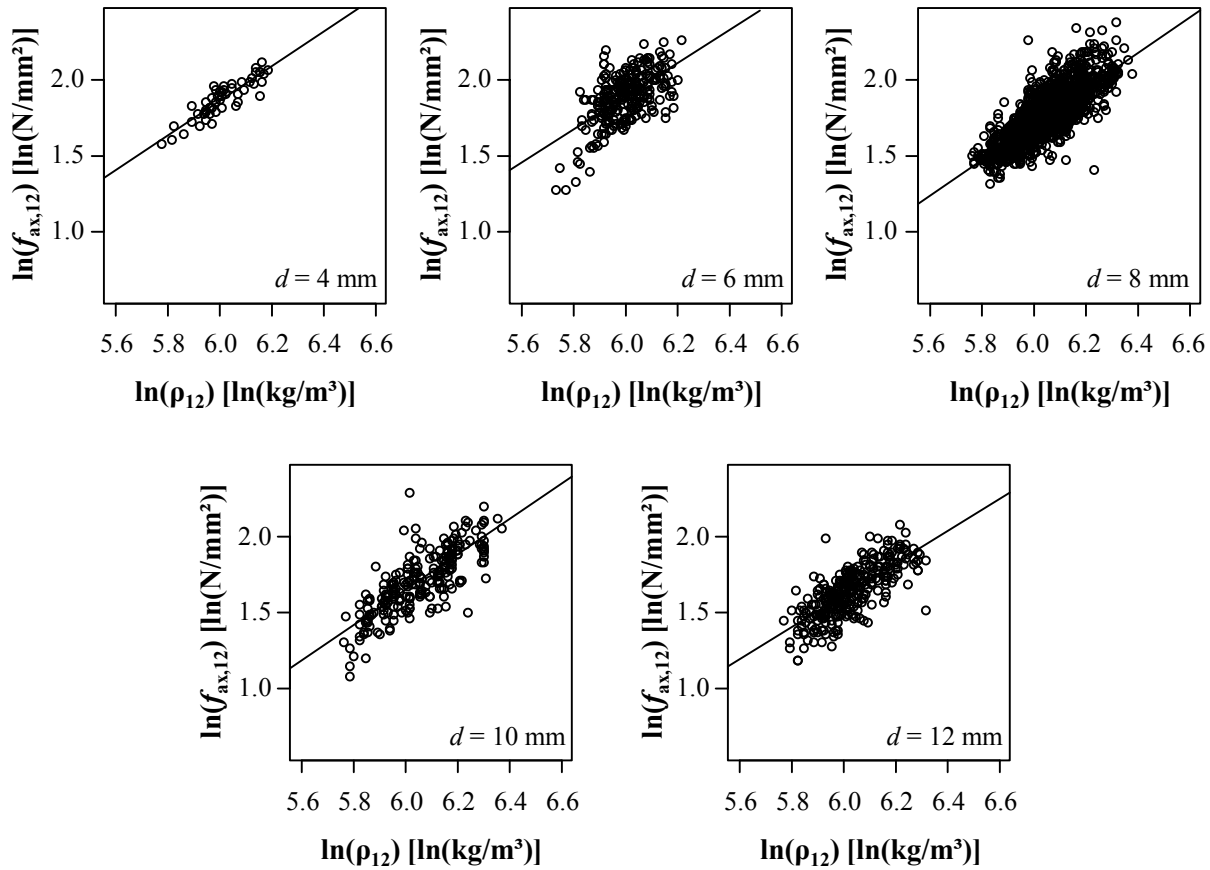


Figure B.80: Relationships between logarithmic withdrawal strength and density for main series in dependence of outer thread diameter; perpendicular-to-grain insertion, $\alpha = 90^\circ$; section 6-3.1

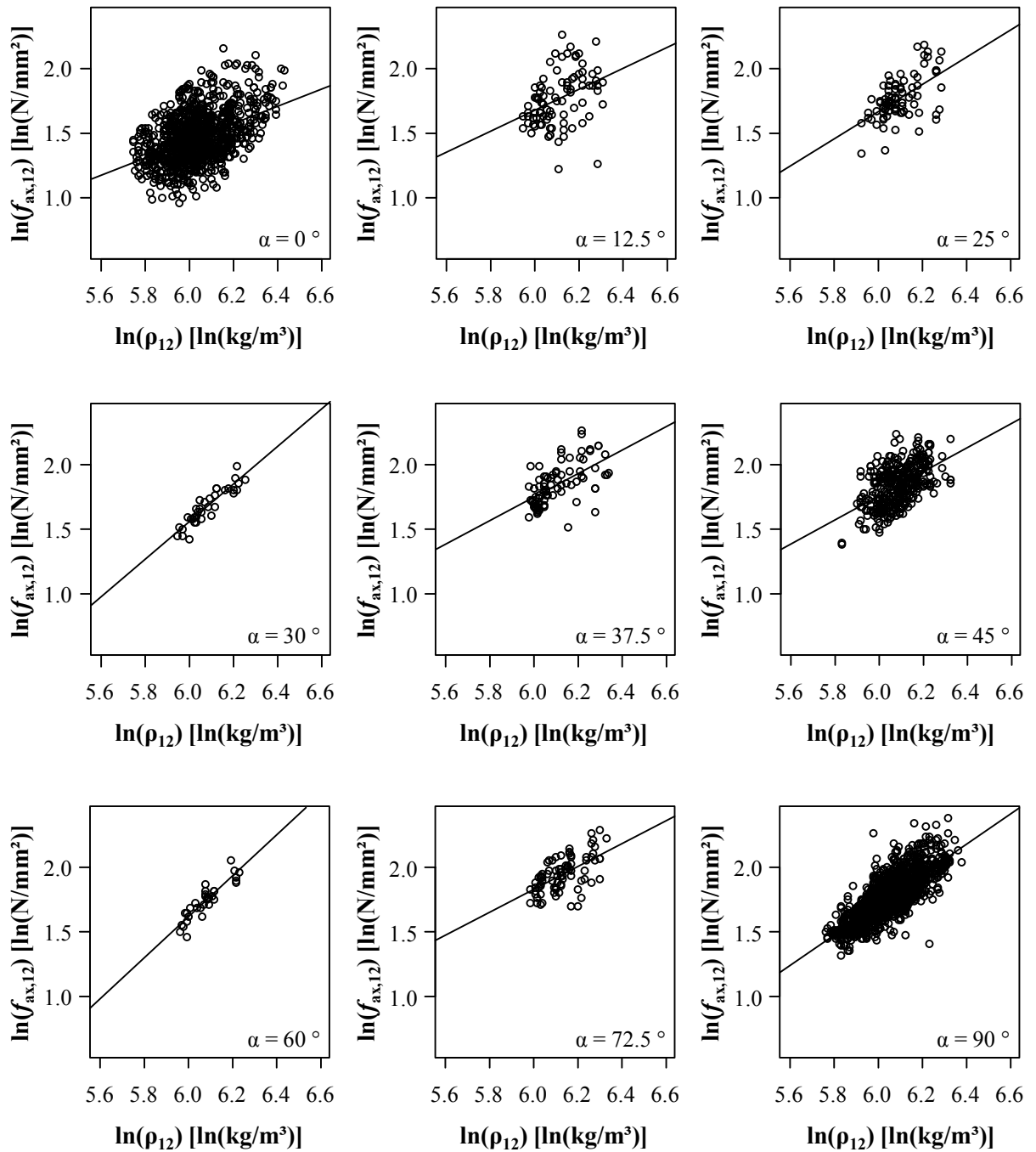


Figure B.81: Relationships between logarithmic withdrawal strength and density for main series in dependence of axis-to-grain angle α ; $d = 8$ mm; section 6-3.1

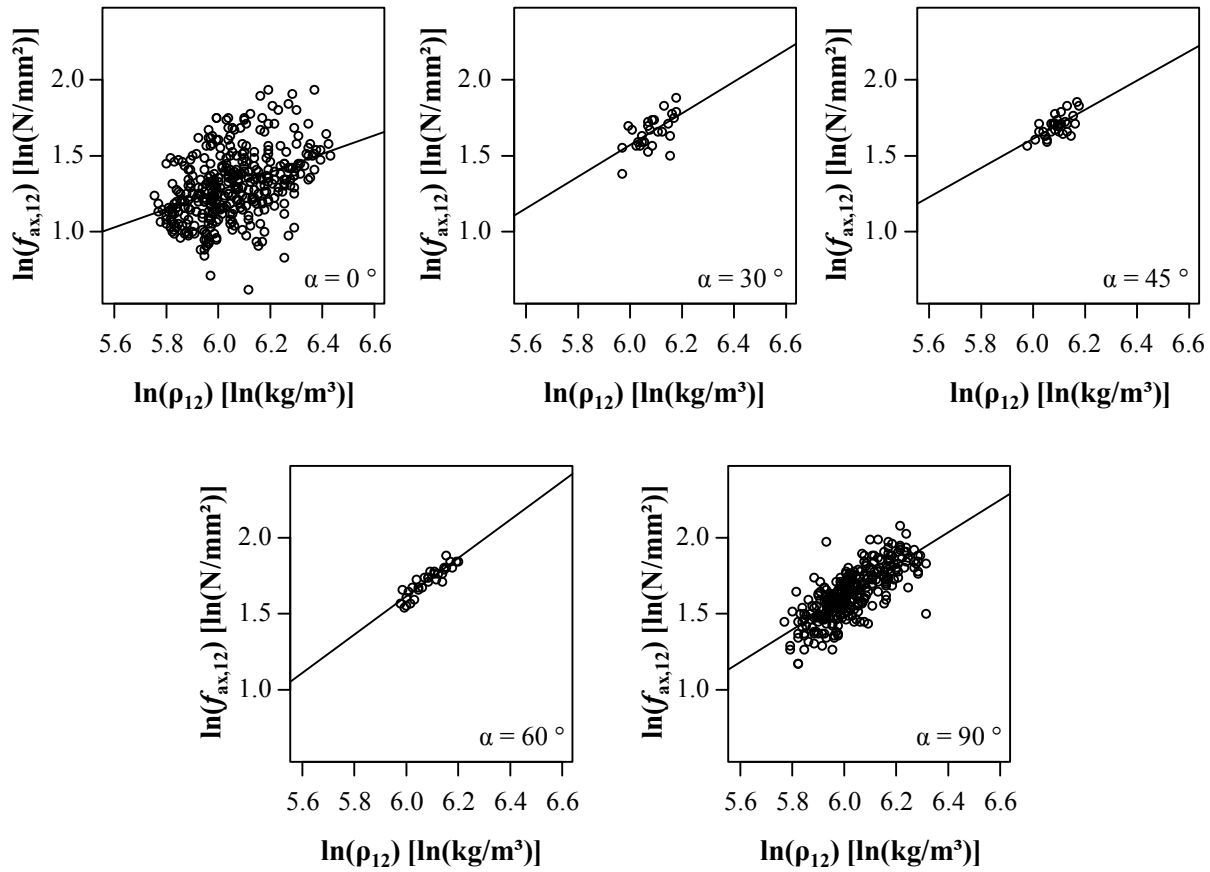


Figure B.82: Relationships between logarithmic withdrawal strength and density for main series in dependence of axis-to-grain angle α ; $d = 12$ mm; section 6-3.1

B-4.2 Supplementary test results

Table B.68: Determined exponents k_p for main series in dependence of axis-to-grain angle and outer thread diameter; section 6-3.1

d [mm]	α [°] (no. of tests)								
	0	12.5	25	30	37.5	45	60	72.5	90
4	1.13 (47)								1.14 (51)
6	0.98 (84)								1.10 (261)
8	0.68 (1,019)	0.81 (90)	1.06 (85)	1.47 (35)	0.92 (81)	0.94 (346)	1.60 (33)	0.89 (81)	1.18 (1,616)
10	0.79 (236)								1.16 (233)
12	0.61 (370)			1.06 (27)		0.97 (32)	1.27 (32)		1.06 (301)

Table B.69: Varied CLT lay-ups for determination of k_{gap} ; according to Brandner (2016); section 6-3.2

t_{CLT} [mm]	no. of layers [-]	layer thickness t_l (top to bottom) [mm]				
60	3	20	20	20		
80	3	30	20	30		
80	3	20	40	20		
90	3	30	30	30		
100	3	30	40	30		
120	3	40	40	40		
100	5	20	20	20	20	20
120	5	30	20	20	20	30
120	5	20	30	20	30	20
140	5	40	20	20	20	40
140	5	20	40	20	40	20
160	5	40	20	40	20	40
180	5	30	40	40	40	30
180	5	40	30	40	30	40
200	5	40	40	40	40	40